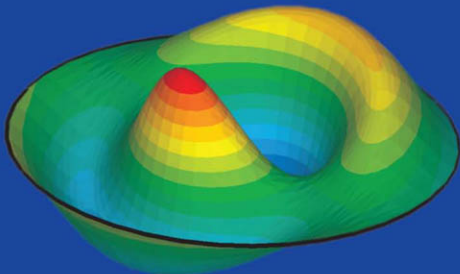


Applied Mechanics *of* Solids



Allan F. Bower



CRC Press
Taylor & Francis Group

Applied Mechanics *of* Solids

This page intentionally left blank

Applied Mechanics *of Solids*

Allan F. Bower



CRC Press
Taylor & Francis Group
Boca Raton London New York

CRC Press is an imprint of the
Taylor & Francis Group, an **informa** business

MATLAB® is a trademark of The MathWorks, Inc. and is used with permission. The MathWorks does not warrant the accuracy of the text or exercises in this book. This book's use or discussion of MATLAB® software or related products does not constitute endorsement or sponsorship by The MathWorks of a particular pedagogical approach or particular use of the MATLAB® software.

CRC Press
Taylor & Francis Group
6000 Broken Sound Parkway NW, Suite 300
Boca Raton, FL 33487-2742

© 2010 by Taylor and Francis Group, LLC
CRC Press is an imprint of Taylor & Francis Group, an Informa business

No claim to original U.S. Government works

Printed in the United States of America on acid-free paper
10 9 8 7 6 5 4 3 2 1

International Standard Book Number: 978-1-4398-0247-2 (Hardback)

This book contains information obtained from authentic and highly regarded sources. Reasonable efforts have been made to publish reliable data and information, but the author and publisher cannot assume responsibility for the validity of all materials or the consequences of their use. The authors and publishers have attempted to trace the copyright holders of all material reproduced in this publication and apologize to copyright holders if permission to publish in this form has not been obtained. If any copyright material has not been acknowledged please write and let us know so we may rectify in any future reprint.

Except as permitted under U.S. Copyright Law, no part of this book may be reprinted, reproduced, transmitted, or utilized in any form by any electronic, mechanical, or other means, now known or hereafter invented, including photocopying, microfilming, and recording, or in any information storage or retrieval system, without written permission from the publishers.

For permission to photocopy or use material electronically from this work, please access www.copyright.com (<http://www.copyright.com/>) or contact the Copyright Clearance Center, Inc. (CCC), 222 Rosewood Drive, Danvers, MA 01923, 978-750-8400. CCC is a not-for-profit organization that provides licenses and registration for a variety of users. For organizations that have been granted a photocopy license by the CCC, a separate system of payment has been arranged.

Trademark Notice: Product or corporate names may be trademarks or registered trademarks, and are used only for identification and explanation without intent to infringe.

Library of Congress Cataloging-in-Publication Data

Bower, Allan F.

Applied mechanics of solids / author, Allan F. Bower.

p. cm.

Includes bibliographical references and index.

ISBN 978-1-4398-0247-2 (hardcover : alk. paper)

1. Mechanics, Applied. 2. Solids. 3. Elasticity. 4. Strength of materials. I. Title.

TA405.B676 2010

620.1'05--dc22

2009026764

Visit the Taylor & Francis Web site at
<http://www.taylorandfrancis.com>

and the CRC Press Web site at
<http://www.crcpress.com>

Contents

Preface, xxiii

Author, xxv

CHAPTER 1 ■ Overview of Solid Mechanics	1
1.1 DEFINING A PROBLEM IN SOLID MECHANICS	2
1.1.1 Deciding What to Calculate	3
1.1.2 Defining the Geometry of the Solid	4
1.1.3 Defining Loading	5
1.1.4 Deciding What Physics to Include in the Model	6
1.1.5 Defining Material Behavior	7
1.1.6 A Representative Initial Value Problem in Solid Mechanics	10
1.1.7 Choosing a Method of Analysis	11
CHAPTER 2 ■ Governing Equations	13
2.1 MATHEMATICAL DESCRIPTION OF SHAPE CHANGES IN SOLIDS	13
2.1.1 Displacement and Velocity Fields	13
2.1.2 Displacement Gradient and Deformation Gradient Tensors	14
2.1.3 Deformation Gradient Resulting from Two Successive Deformations	18
2.1.4 The Jacobian of the Deformation Gradient	19
2.1.5 Lagrange Strain Tensor	20
2.1.6 Eulerian Strain Tensor	22
2.1.7 Infinitesimal Strain Tensor	22
2.1.8 Engineering Shear Strains	24
2.1.9 Decomposition of Infinitesimal Strain into Volumetric and Deviatoric Parts	24
2.1.10 Infinitesimal Rotation Tensor	25
2.1.11 Principal Values and Directions of the Infinitesimal Strain Tensor	26
2.1.12 Cauchy–Green Deformation Tensors	27

2.1.13	Rotation Tensor and Left and Right Stretch Tensors	27
2.1.14	Principal Stretches	29
2.1.15	Generalized Strain Measures	30
2.1.16	The Velocity Gradient	31
2.1.17	Stretch Rate and Spin Tensors	32
2.1.18	Infinitesimal Strain Rate and Rotation Rate	33
2.1.19	Other Deformation Rate Measures	33
2.1.20	Strain Equations of Compatibility for Infinitesimal Strains	34
2.2	MATHEMATICAL DESCRIPTION OF INTERNAL FORCES IN SOLIDS	38
2.2.1	Surface Traction and Internal Body Force	38
2.2.2	Traction Acting on Planes within a Solid	40
2.2.3	Cauchy (True) Stress Tensor	43
2.2.4	Other Stress Measures: Kirchhoff, Nominal, and Material Stress Tensors	44
2.2.5	Stress Measures for Infinitesimal Deformations	47
2.2.6	Principal Stresses and Directions	47
2.2.7	Hydrostatic, Deviatoric, and von Mises Effective Stress	48
2.2.8	Stresses near an External Surface or Edge: Boundary Conditions on Stresses	49
2.3	EQUATIONS OF MOTION AND EQUILIBRIUM FOR DEFORMABLE SOLIDS	49
2.3.1	Linear Momentum Balance in Terms of Cauchy Stress	49
2.3.2	Angular Momentum Balance in Terms of Cauchy Stress	51
2.3.3	Equations of Motion in Terms of Other Stress Measures	53
2.4	WORK DONE BY STRESSES: PRINCIPLE OF VIRTUAL WORK	54
2.4.1	Work Done by Cauchy Stresses	54
2.4.2	Rate of Mechanical Work in Terms of Other Stress Measures	56
2.4.3	Rate of Mechanical Work for Infinitesimal Deformations	57
2.4.4	The Principle of Virtual Work	58
2.4.5	The Virtual Work Equation in Terms of Other Stress Measures	61
2.4.6	The Virtual Work Equation for Infinitesimal Deformations	62
CHAPTER 3 ■ Constitutive Models: Relations between Stress and Strain		65
3.1	GENERAL REQUIREMENTS FOR CONSTITUTIVE EQUATIONS	66
3.1.1	Thermodynamic Restrictions	66
3.1.2	Objectivity	66
3.1.3	Drucker Stability	67

3.2	LINEAR ELASTIC MATERIAL BEHAVIOR	69
3.2.1	Isotropic, Linear Elastic Material Behavior	69
3.2.2	Stress–Strain Relations for Isotropic, Linear Elastic Materials: Young’s Modulus, Poisson’s Ratio, and the Thermal Expansion Coefficient	70
3.2.3	Reduced Stress–Strain Equations for Plane Deformation of Isotropic Solids	72
3.2.4	Representative Values for Density and Elastic Constants of Isotropic Solids	73
3.2.5	Other Elastic Constants: Bulk, Shear, and Lame Modulus	74
3.2.6	Physical Interpretation of Elastic Constants for Isotropic Solids	75
3.2.7	Strain Energy Density for Isotropic Solids	75
3.2.8	Stress–Strain Relation for a General Anisotropic Linear Elastic Material: Elastic Stiffness and Compliance Tensors	76
3.2.9	Physical Interpretation of the Anisotropic Elastic Constants	78
3.2.10	Strain Energy Density for Anisotropic, Linear Elastic Solids	79
3.2.11	Basis Change Formulas for Anisotropic Elastic Constants	79
3.2.12	The Effect of Material Symmetry on Stress–Strain Relations for Anisotropic Materials	81
3.2.13	Stress–Strain Relations for Linear Elastic Orthotropic Materials	82
3.2.14	Stress–Strain Relations for Linear Elastic Transversely Isotropic Material	83
3.2.15	Representative Values for Elastic Constants of Transversely Isotropic Hexagonal Close-Packed Crystals	85
3.2.16	Linear Elastic Stress–Strain Relations for Cubic Materials	85
3.2.17	Representative Values for Elastic Properties of Cubic Crystals and Compounds	87
3.3	HYPOElasticity: ELASTIC MATERIALS WITH A NONLINEAR STRESS–STRAIN RELATION UNDER SMALL DEFORMATION	87
3.4	GENERALIZED Hooke’s Law: ELASTIC MATERIALS SUBJECTED TO SMALL STRETCHES BUT LARGE ROTATIONS	91
3.5	HYPERELASTICITY: TIME-INDEPENDENT BEHAVIOR OF RUBBERS AND FOAMS SUBJECTED TO LARGE STRAINS	93
3.5.1	Deformation Measures Used in Finite Elasticity	95
3.5.2	Stress Measures Used in Finite Elasticity	96
3.5.3	Calculating Stress–Strain Relations from the Strain Energy Density	97
3.5.4	A Note on Perfectly Incompressible Materials	99

3.5.5	Specific Forms of the Strain Energy Density	100
3.5.6	Calibrating Nonlinear Elasticity Models	102
3.5.7	Representative Values of Material Properties for Rubbers	103
3.6	LINEAR VISCOELASTIC MATERIALS: TIME-DEPENDENT BEHAVIOR OF POLYMERS AT SMALL STRAINS	103
3.6.1	Features of the Small Strain Rate-Dependent Response of Polymers	104
3.6.2	General Constitutive Equations for Linear Viscoelastic Solids	109
3.6.3	Spring–Damper Approximations to the Relaxation Modulus	110
3.6.4	Prony Series Representation for the Relaxation Modulus	112
3.6.5	Calibrating the Constitutive Laws for Linear Viscoelastic Solids	112
3.6.6	Representative Values for Viscoelastic Properties of Polymers	113
3.7	SMALL STRAIN, RATE-INDEPENDENT PLASTICITY: METALS LOADED BEYOND YIELD	113
3.7.1	Features of the Inelastic Response of Metals	115
3.7.2	Decomposition of Strain into Elastic and Plastic Parts	118
3.7.3	Yield Criteria	118
3.7.4	Graphical Representation of the Yield Surface	119
3.7.5	Strain Hardening Laws	120
3.7.6	Plastic Flow Law	122
3.7.7	Elastic Unloading Condition	126
3.7.8	Complete Incremental Stress–Strain Relations for a Rate-Independent Elastic–Plastic Solid	126
3.7.9	Typical Values for Yield Stress of Polycrystalline Metals	129
3.7.10	Perspectives on Plastic Constitutive Equations: Principle of Maximum Plastic Resistance	129
3.7.11	Perspectives on Plastic Constitutive Equations: Drucker’s Postulate	131
3.7.12	Microscopic Perspectives on Plastic Flow in Metals	132
3.8	SMALL STRAIN VISCOPLASTICITY: CREEP AND HIGH STRAIN RATE DEFORMATION OF CRYSTALLINE SOLIDS	135
3.8.1	Features of Creep Behavior	135
3.8.2	Features of High Strain Rate Behavior	137
3.8.3	Small Strain, Viscoplastic Constitutive Equations	137
3.8.4	Representative Values of Parameters for Viscoplastic Models of Creeping Solids	142
3.8.5	Representative Values of Parameters for Viscoplastic Models of High Strain Rate Deformation	142

3.9	LARGE STRAIN, RATE-DEPENDENT PLASTICITY	143
3.9.1	Kinematics of Finite Strain Plasticity	143
3.9.2	Stress Measures for Finite Deformation Plasticity	145
3.9.3	Elastic Stress–Strain Relation for Finite Strain Plasticity	146
3.9.4	Plastic Constitutive Law for Finite Strain Viscoplasticity	147
3.10	LARGE STRAIN VISCOELASTICITY	148
3.10.1	Kinematics for Finite Strain Viscoelasticity	148
3.10.2	Stress Measures for Finite Strain Viscoelasticity	150
3.10.3	Relation among Stress, Deformation Measures, and Strain Energy Density	150
3.10.4	Strain Relaxation	151
3.10.5	Representative Values for Material Parameters in a Finite Strain Viscoelastic Model	152
3.11	CRITICAL STATE MODELS FOR SOILS	152
3.11.1	Features of the Behavior of Soils	152
3.11.2	Constitutive Equations for Cam-Clay	153
3.11.3	Application of the Critical State Equations to Simple 2D Loading	160
3.11.4	Typical Values of Material Properties for Soils	161
3.12	CONSTITUTIVE MODELS FOR METAL SINGLE CRYSTALS	161
3.12.1	Review of Some Important Concepts from Crystallography	162
3.12.2	Features of Plastic Flow in Single Crystals	166
3.12.3	Kinematic Descriptions Used in Constitutive Models of Single Crystals	171
3.12.4	Stress Measures Used in Crystal Plasticity	173
3.12.5	Elastic Stress–Strain Relation Used in Crystal Plasticity	174
3.12.6	Plastic Stress–Strain Relation Used in Crystal Plasticity	174
3.12.7	Representative Values for Plastic Properties of Single Crystals	176
3.13	CONSTITUTIVE MODELS FOR CONTACTING SURFACES AND INTERFACES IN SOLIDS	176
3.13.1	Cohesive Zone Models of Interfaces	176
3.13.2	Models of Contact and Friction between Surfaces	182
<hr/> CHAPTER 4 ■ Solutions to Simple Boundary and Initial Value Problems		193
4.1	AXIALLY AND SPHERICALLY SYMMETRIC SOLUTIONS TO QUASI-STATIC LINEAR ELASTIC PROBLEMS	193
4.1.1	Summary of Governing Equations of Linear Elasticity in Cartesian Components	193

x ■ Contents

4.1.2	Simplified Equations for Spherically Symmetric Linear Elasticity Problems	194
4.1.3	General Solution to the Spherically Symmetric Linear Elasticity Problem	197
4.1.4	Pressurized Hollow Sphere	197
4.1.5	Gravitating Sphere	199
4.1.6	Sphere with Steady-State Heat Flow	200
4.1.7	Simplified Equations for Axially Symmetric Linear Elasticity Problems	202
4.1.8	General Solution to the Axisymmetric Boundary Value Problem	205
4.1.9	Long (Generalized Plane Strain) Cylinder Subjected to Internal and External Pressure	206
4.1.10	Spinning Circular Plate	208
4.1.11	Stresses Induced by an Interference Fit between Two Cylinders	209
4.2	AXIALLY AND SPHERICALLY SYMMETRIC SOLUTIONS TO QUASI-STATIC ELASTIC-PLASTIC PROBLEMS	211
4.2.1	Summary of Governing Equations	212
4.2.2	Simplified Equations for Spherically Symmetric Problems	213
4.2.3	Elastic Perfectly Plastic Hollow Sphere Subjected to Monotonically Increasing Internal Pressure	215
4.2.4	Elastic Perfectly Plastic Hollow Sphere Subjected to Cyclic Internal Pressure	219
4.2.5	Simplified Equations for Plane Strain Axially Symmetric Elastic-Perfectly Plastic Solids	223
4.2.6	Long (Plane Strain) Cylinder Subjected to Internal Pressure	226
4.3	SPHERICALLY SYMMETRIC SOLUTION TO QUASI-STATIC LARGE STRAIN ELASTICITY PROBLEMS	229
4.3.1	Summary of Governing Equations of Finite Elasticity in Cartesian Components	229
4.3.2	Simplified Equations for Incompressible Spherically Symmetric Solids	230
4.3.3	Pressurized Hollow Sphere Made from an Incompressible Rubber	232
4.4	SIMPLE DYNAMIC SOLUTIONS FOR LINEAR ELASTIC MATERIALS	236
4.4.1	Surface Subjected to Time-Varying Normal Pressure	236
4.4.2	Surface Subjected to Time-Varying Shear Traction	239
4.4.3	One-Dimensional Bar Subjected to End Loading	239
4.4.4	Plane Waves in an Infinite Solid	240
4.4.5	Summary of Wave Speeds in Isotropic Elastic Solids	241

4.4.6	Reflection of Waves Traveling Normal to a Free Surface	242
4.4.7	Reflection and Transmission of Waves Normal to an Interface	243
4.4.8	Simple Example Involving Plane Wave Propagation: Plate Impact Experiment	245
CHAPTER 5 ■ Solutions for Linear Elastic Solids		249
5.1	GENERAL PRINCIPLES	250
5.1.1	Summary of the Governing Equations of Linear Elasticity	250
5.1.2	Alternative Form of the Governing Equations: Navier Equation	251
5.1.3	Superposition and Linearity of Solutions	251
5.1.4	Uniqueness and Existence of Solutions to the Linear Elasticity Equations	252
5.1.5	Saint-Venant's Principle	252
5.2	AIRY FUNCTION SOLUTION TO PLANE STRESS AND STRAIN STATIC LINEAR ELASTIC PROBLEMS	255
5.2.1	Airy Solution in Rectangular Coordinates	256
5.2.2	Demonstration That the Airy Solution Satisfies the Governing Equations	257
5.2.3	Airy Solution in Cylindrical-Polar Coordinates	259
5.2.4	Airy Function Solution to the End-Loaded Cantilever	260
5.2.5	2D Line Load Acting Perpendicular to the Surface of an Infinite Solid	262
5.2.6	2D Line Load Acting Parallel to the Surface of an Infinite Solid	264
5.2.7	Arbitrary Pressure Acting on a Flat Surface	265
5.2.8	Uniform Normal Pressure Acting on a Strip	266
5.2.9	Stresses near the Tip of a Crack	266
5.3	COMPLEX VARIABLE SOLUTION TO PLANE STRAIN STATIC LINEAR ELASTIC PROBLEMS	267
5.3.1	Complex Variable Solutions to Elasticity Problems	268
5.3.2	Demonstration That the Complex Variable Solution Satisfies the Governing Equations	270
5.3.3	Complex Variable Solution for a Line Force in an Infinite Solid (Plane Strain Deformation)	272
5.3.4	Complex Variable Solution for an Edge Dislocation in an Infinite Solid	274
5.3.5	Cylindrical Hole in an Infinite Solid under Remote Loading	277
5.3.6	Crack in an Infinite Elastic Solid under Remote Loading	278
5.3.7	Fields near the Tip of a Crack on Bimaterial Interface	280

5.3.8	Frictionless Rigid Flat Indenter in Contact with a Half-Space	283
5.3.9	Frictionless Parabolic (Cylindrical) Indenter in Contact with a Half-Space	284
5.3.10	Line Contact between Two Nonconformal Frictionless Elastic Solids	286
5.3.11	Sliding Contact between Two Rough Elastic Cylinders	287
5.3.12	Dislocation near the Surface of a Half-Space	289
5.4	SOLUTIONS TO 3D STATIC PROBLEMS IN LINEAR ELASTICITY	290
5.4.1	Papkovich Neuber Potential Representations for 3D Solutions for Isotropic Solids	290
5.4.2	Demonstration That the Papkovich Neuber Solution Satisfies the Governing Equations	291
5.4.3	Point Force in an Infinite Solid	292
5.4.4	Point Force Normal to the Surface of an Infinite Half-Space	293
5.4.5	Point Force Tangent to the Surface of an Infinite Half-Space	293
5.4.6	The Eshelby Inclusion Problem	294
5.4.7	Elastically Mismatched Ellipsoidal Inclusion in an Infinite Solid Subjected to Remote Stress	299
5.4.8	Spherical Cavity in an Infinite Solid Subjected to Remote Stress	300
5.4.9	Flat-Ended Cylindrical Indenter in Contact with an Elastic Half-Space	302
5.4.10	Frictionless Contact between Two Elastic Spheres	304
5.4.11	Contact Area, Pressure, Stiffness, and Elastic Limit for General Nonconformal Contacts	306
5.4.12	Load Displacement–Contact Area Relations for Arbitrarily Shaped Axisymmetric Contacts	308
5.5	SOLUTIONS TO GENERALIZED PLANE PROBLEMS FOR ANISOTROPIC LINEAR ELASTIC SOLIDS	310
5.5.1	Governing Equations of Elasticity for Anisotropic Solids	310
5.5.2	Stroh Representation for Fields in Anisotropic Solids	312
5.5.3	Demonstration That the Stroh Representation Satisfies the Governing Equations	314
5.5.4	Stroh Eigenvalues and Anisotropy Matrices for Cubic Materials	316
5.5.5	Degenerate Materials	317
5.5.6	Fundamental Elasticity Matrix	317
5.5.7	Orthogonal Properties of Stroh Matrices A and B	318
5.5.8	Barnett–Lothe Tensors and the Impedance Tensor	319

5.5.9	Useful Properties of Matrices in Anisotropic Elasticity	320
5.5.10	Basis Change Formulas for Matrices Used in Anisotropic Elasticity	321
5.5.11	Barnett–Lothe Integrals	323
5.5.12	Stroh Representation for a State of Uniform Stress	325
5.5.13	Line Load and Dislocation in an Infinite Anisotropic Solid	327
5.5.14	Line Load and Dislocation below the Surface of an Anisotropic Half-Space	329
5.6	SOLUTIONS TO DYNAMIC PROBLEMS FOR ISOTROPIC LINEAR ELASTIC SOLIDS	330
5.6.1	Love Potentials for Dynamic Solutions for Isotropic Solids	330
5.6.2	Pressure Suddenly Applied to the Surface of a Spherical Cavity in an Infinite Solid	331
5.6.3	Rayleigh Waves	333
5.6.4	Love Waves	335
5.6.5	Elastic Waves in Waveguides	337
5.7	ENERGY METHODS FOR SOLVING STATIC LINEAR ELASTICITY PROBLEMS	339
5.7.1	Definition of the Potential Energy of a Linear Elastic Solid under Static Loading	339
5.7.2	Principle of Stationary and Minimum Potential Energy	341
5.7.3	Uniaxial Compression of a Cylinder Solved by Energy Methods	344
5.7.4	Variational Derivation of the Beam Equations	346
5.7.5	Energy Methods for Calculating Stiffness	350
5.8	RECIPROCAL THEOREM AND APPLICATIONS	352
5.8.1	Statement and Proof of the Reciprocal Theorem	352
5.8.2	Simple Example Using the Reciprocal Theorem	353
5.8.3	Formulas Relating Internal and Boundary Values of Field Quantities	355
5.8.4	Classical Solutions for Displacement and Stress Induced by a 3D Dislocation Loop in an Infinite Solid	356
5.9	ENERGETICS OF DISLOCATIONS IN ELASTIC SOLIDS	359
5.9.1	Classical Solution for Potential Energy of an Isolated Dislocation Loop in an Infinite Solid	359
5.9.2	Nonsingular Dislocation Theory	362
5.9.3	Energy of a Dislocation Loop in a Stressed, Finite Elastic Solid	365
5.9.4	Energy of Two Interacting Dislocation Loops	369
5.9.5	Driving Force for Dislocation Motion: Peach–Kohler Formula	370

5.10 RAYLEIGH–RITZ METHOD FOR ESTIMATING NATURAL FREQUENCY OF AN ELASTIC SOLID	375
5.10.1 Mode Shapes and Natural Frequencies; Orthogonality of Mode Shapes and Rayleigh's Principle	375
5.10.2 Estimate of Natural Frequency of Vibration for a Beam Using Rayleigh–Ritz Method	379
CHAPTER 6 ■ Solutions for Plastic Solids	381
6.1 SLIP-LINE FIELD THEORY	381
6.1.1 Interpreting a Slip-Line Field	382
6.1.2 Derivation of the Slip-Line Field Method	386
6.1.3 Examples of Slip-Line Field Solutions to Boundary Value Problems	392
6.2 BOUNDING THEOREMS IN PLASTICITY AND THEIR APPLICATIONS	398
6.2.1 Definition of the Plastic Dissipation	399
6.2.2 Principle of Minimum Plastic Dissipation	401
6.2.3 Upper Bound Plastic Collapse Theorem	404
6.2.4 Examples of Applications of the Upper Bound Theorem	405
6.2.5 Lower Bound Plastic Collapse Theorem	410
6.2.6 Examples of Applications of the Lower Bound Plastic Collapse Theorem	411
6.2.7 Lower Bound Shakedown Theorem	412
6.2.8 Examples of Applications of the Lower Bound Shakedown Theorem	415
6.2.9 Upper Bound Shakedown Theorem	417
6.2.10 Examples of Applications of the Upper Bound Shakedown Theorem	419
CHAPTER 7 ■ Finite Element Analysis: An Introduction	423
7.1 A GUIDE TO USING FINITE ELEMENT SOFTWARE	423
7.1.1 Finite Element Mesh for a 2D or 3D Component	425
7.1.2 Nodes and Elements in a Mesh	428
7.1.3 Special Elements: Beams, Plates, Shells, and Truss Elements	432
7.1.4 Material Behavior	434
7.1.5 Boundary Conditions	435
7.1.6 Constraints	438

7.1.7	Contacting Surfaces and Interfaces	439
7.1.8	Initial Conditions and External Fields	441
7.1.9	Solution Procedures and Time Increments	441
7.1.10	Output	445
7.1.11	Units in Finite Element Computations	446
7.1.12	Using Dimensional Analysis to Simplify FEA	447
7.1.13	Simplifying FEA by Scaling the Governing Equations	449
7.1.14	Dimensional Analysis: Closing Remarks	451
7.2	A SIMPLE FINITE ELEMENT PROGRAM	451
7.2.1	Finite Element Mesh and Element Connectivity	452
7.2.2	Global Displacement Vector	453
7.2.3	Element Interpolation Functions	453
7.2.4	Element Strains, Stresses, and Strain Energy Density	454
7.2.5	Element Stiffness Matrix	455
7.2.6	Global Stiffness Matrix	456
7.2.7	Boundary Loading	459
7.2.8	Global Residual Force Vector	461
7.2.9	Minimizing the Potential Energy	461
7.2.10	Eliminating Prescribed Displacements	462
7.2.11	Solution	463
7.2.12	Postprocessing	463
7.2.13	Example FEA Code	464
<hr/> CHAPTER 8 ■ Finite Element Analysis: Theory and Implementation		467
8.1	GENERALIZED FEM FOR STATIC LINEAR ELASTICITY	468
8.1.1	Review of the Principle of Virtual Work	468
8.1.2	Integral (Weak) Form of the Governing Equations of Linear Elasticity	469
8.1.3	Interpolating the Displacement Field and the Virtual Velocity Field	470
8.1.4	Finite Element Equations	472
8.1.5	Simple 1D Implementation of the FEM	472
8.1.6	Summary of the 1D Finite Element Procedure	476
8.1.7	Example FEM Code and Solution	477
8.1.8	Extending the 1D FEM to 2D and 3D	480
8.1.9	Interpolation Functions for 2D Elements	481
8.1.10	Interpolation Functions for 3D Elements	481

8.1.11	Volume Integrals for Stiffness and Force in Terms of Normalized Coordinates	482
8.1.12	Numerical Integration Schemes for 2D and 3D Elements	485
8.1.13	Summary of Formulas for Element Stiffness and Force Matrices	486
8.1.14	Sample 2D/3D Linear Elastostatic FEM Code	486
8.2	THE FEM FOR DYNAMIC LINEAR ELASTICITY	490
8.2.1	Review of the Governing Equations of Dynamic Linear Elasticity	490
8.2.2	Expressing the Governing Equations Using the Principle of Virtual Work	491
8.2.3	Finite Element Equations of Motion for Linear Elastic Solids	491
8.2.4	Newmark Time Integration for Elastodynamics	493
8.2.5	1D Implementation of a Newmark Scheme	495
8.2.6	Example 1D Dynamic FEM Code and Solution	497
8.2.7	Lumped Mass Matrices	499
8.2.8	Example 2D and 3D Dynamic Linear Elastic Code and Solution	501
8.2.9	Modal Method of Time Integration	501
8.2.10	Natural Frequencies and Mode Shapes	502
8.2.11	Example 1D Code with Modal Dynamics	503
8.2.12	Example 2D and 3D FEM Code to Compute Mode Shapes and Natural Frequencies	505
8.3	FEM FOR NONLINEAR (HYPOELASTIC) MATERIALS	505
8.3.1	Summary of Governing Equations	505
8.3.2	Governing Equations in Terms of the Virtual Work Principle	507
8.3.3	Finite Element Equations	507
8.3.4	Solving the Finite Element Equations Using Newton–Raphson Iteration	509
8.3.5	Tangent Moduli for the Hypoelastic Solid	510
8.3.6	Summary of the Newton–Raphson Procedure for Hypoelastic Solids	511
8.3.7	What to Do if the Newton–Raphson Iterations Do Not Converge	511
8.3.8	Variations on Newton–Raphson Iteration	512
8.3.9	Example Hypoelastic FEM Code	512
8.4	FEM FOR LARGE DEFORMATIONS: HYPERELASTIC MATERIALS	514
8.4.1	Summary of Governing Equations	514
8.4.2	Governing Equations in Terms of the Principle of Virtual Work	515
8.4.3	Finite Element Equations	515

8.4.4	Solution Using Consistent Newton–Raphson Iteration	517
8.4.5	Tangent Stiffness for the Neo-Hookean Material	519
8.4.6	Evaluating the Boundary Traction Integrals	520
8.4.7	Example Hyperelastic Finite Element Code	521
8.5	THE FEM FOR VISCOPLASTICITY	522
8.5.1	Summary of Governing Equations	522
8.5.2	Governing Equations in Terms of the Virtual Work Principle	523
8.5.3	Finite Element Equations	524
8.5.4	Integrating the Plastic Stress–Strain Law	525
8.5.5	Material Tangent	527
8.5.6	Solution Using Consistent Newton–Raphson Iteration	528
8.5.7	Example Small Strain Plastic FEM Code	529
8.6	ADVANCED ELEMENT FORMULATIONS: INCOMPATIBLE MODES, REDUCED INTEGRATION, AND HYBRID ELEMENTS	530
8.6.1	Shear Locking and Incompatible Mode Elements	531
8.6.2	Volumetric Locking and Reduced Integration Elements	533
8.6.3	Hybrid Elements for Modeling Near-Incompressible Materials	541
8.7	LIST OF EXAMPLE FEA PROGRAMS AND INPUT FILES	544
<hr/> CHAPTER 9 ■ Modeling Material Failure		547
9.1	SUMMARY OF MECHANISMS OF FRACTURE AND FATIGUE UNDER STATIC AND CYCLIC LOADING	548
9.1.1	Failure under Monotonic Loading	548
9.1.2	Failure under Cyclic Loading	550
9.2	STRESS- AND STRAIN-BASED FRACTURE AND FATIGUE CRITERIA	553
9.2.1	Stress-Based Failure Criteria for Brittle Solids and Composites	553
9.2.2	Probabilistic Design Methods for Brittle Fracture (Weibull Statistics)	556
9.2.3	Static Fatigue Criterion for Brittle Materials	557
9.2.4	Constitutive Laws for Crushing Failure of Brittle Materials	558
9.2.5	Ductile Fracture Criteria	559
9.2.6	Ductile Failure by Strain Localization	562
9.2.7	Criteria for Failure by High Cycle Fatigue under Constant Amplitude Cyclic Loading	564
9.2.8	Criteria for Failure by Low Cycle Fatigue	565
9.2.9	Criteria for Failure under Variable Amplitude Cyclic Loading	566

9.3	MODELING FAILURE BY CRACK GROWTH: LINEAR ELASTIC FRACTURE MECHANICS	567
9.3.1	Crack Tip Fields in an Isotropic, Linear Elastic Solid	567
9.3.2	Assumptions and Application of Phenomenological Linear Elastic Fracture Mechanics	569
9.3.3	Calculating Stress Intensity Factors	572
9.3.4	Calculating Stress Intensity Factors Using FEA	578
9.3.5	Measuring Fracture Toughness	580
9.3.6	Typical Values for Fracture Toughness	581
9.3.7	Stable Tearing: K_r Curves and Crack Stability	581
9.3.8	Mixed-Mode Fracture Criteria	584
9.3.9	Static Fatigue Crack Growth	584
9.3.10	Cyclic Fatigue Crack Growth	586
9.3.11	Finding Cracks in Structures	587
9.4	ENERGY METHODS IN FRACTURE MECHANICS	588
9.4.1	Definition of Crack Tip Energy Release Rate for Cracks in Linear Elastic Solids	588
9.4.2	Energy Release Rate as a Fracture Criterion	589
9.4.3	Relation between Energy Release Rate and Stress Intensity Factor	589
9.4.4	Relation between Energy Release Rate and Compliance	591
9.4.5	Calculating Stress Intensity Factors Using Compliance	592
9.4.6	Integral Expressions for Energy Flux to a Crack Tip	593
9.4.7	Rice's J Integral	596
9.4.8	Calculating Energy Release Rates Using the J Integral	598
9.5	PLASTIC FRACTURE MECHANICS	599
9.5.1	Dugdale–Barenblatt Cohesive Zone Model of Yield at a Crack Tip	599
9.5.2	Hutchinson–Rice–Rosengren Crack Tip Fields for Stationary Crack in a Power Law Hardening Solid	601
9.5.3	Plastic Fracture Mechanics Based on J	605
9.6	LINEAR ELASTIC FRACTURE MECHANICS OF INTERFACES	607
9.6.1	Crack Tip Fields for a Crack on an Interface	607
9.6.2	Phenomenological Theory of Interface Fracture	610
9.6.3	Stress Intensity Factors for Some Interface Cracks	612
9.6.4	Crack Path Selection	613

CHAPTER 10 ■ Solutions for Rods, Beams, Membranes, Plates, and Shells	615
10.1 PRELIMINARIES: DYADIC NOTATION FOR VECTORS AND TENSORS	616
10.2 MOTION AND DEFORMATION OF SLENDER RODS	617
10.2.1 Variables Characterizing the Geometry of a Rod's Cross Section	617
10.2.2 Coordinate Systems and Variables Characterizing the Deformation of a Rod	618
10.2.3 Additional Deformation Measures and Useful Kinematic Relations	620
10.2.4 Approximating the Displacement, Velocity, and Acceleration in a Rod	624
10.2.5 Approximating the Deformation Gradient	625
10.2.6 Other Strain Measures	626
10.2.7 Kinematics of Rods That Are Bent and Twisted in the Unstressed State	628
10.2.8 Representation of Forces and Moments in Slender Rods	630
10.2.9 Equations of Motion and Boundary Conditions	631
10.2.10 Constitutive Equations Relating Forces to Deformation Measures in Elastic Rods	636
10.2.11 Strain Energy of an Elastic Rod	639
10.3 SIMPLIFIED VERSIONS OF THE GENERAL THEORY OF DEFORMABLE RODS	641
10.3.1 Stretched Flexible String with Small Transverse Deflections	641
10.3.2 Straight Elastic Beam with Small Deflections and No Axial Force (Euler–Bernoulli Beam Theory)	642
10.3.3 Straight Elastic Beam with Small Transverse Deflections and Significant Axial Force	643
10.4 EXACT SOLUTIONS TO SIMPLE PROBLEMS INVOLVING ELASTIC RODS	644
10.4.1 Free Vibration of a Straight Beam without Axial Force	645
10.4.2 Buckling of a Column Subjected to Gravitational Loading	648
10.4.3 Post-Buckled Shape of an Initially Straight Rod Subjected to End Thrust	650
10.4.4 Rod Bent and Twisted into a Helix	653
10.4.5 Helical Spring	655

10.5 MOTION AND DEFORMATION OF THIN SHELLS: GENERAL THEORY	657
10.5.1 Coordinate Systems and Variables Characterizing Deformation of Shells	657
10.5.2 Vectors and Tensor Components in Nonorthogonal Bases: Covariant and Contravariant Components	659
10.5.3 Additional Deformation Measures and Kinematic Relations	660
10.5.4 Approximating the Displacement and Velocity Field	664
10.5.5 Approximating the Deformation Gradient	665
10.5.6 Other Deformation Measures	666
10.5.7 Representation of Forces and Moments in Shells	667
10.5.8 Equations of Motion and Boundary Conditions	670
10.5.9 Constitutive Equations Relating Forces to Deformation Measures in Elastic Shells	678
10.5.10 Strain Energy and Kinetic Energy of an Elastic Shell	680
10.6 SIMPLIFIED VERSIONS OF GENERAL SHELL THEORY: FLAT PLATES AND MEMBRANES	681
10.6.1 Flat Plates with Small Out-of-Plane Deflections and Negligible In-Plane Loading	681
10.6.2 Flat Plates with Small Out-of-Plane Deflections and Significant In-Plane Loading	684
10.6.3 Flat Plates with Small In-Plane and Large Transverse Deflections (von Karman Theory)	686
10.6.4 Stretched, Flat Membrane with Small Out-of-Plane Deflections	688
10.6.5 Membrane Equations in Cylindrical-Polar Coordinates	689
10.7 SOLUTIONS TO SIMPLE PROBLEMS INVOLVING MEMBRANES, PLATES, AND SHELLS	692
10.7.1 Thin Circular Plate Bent by Pressure Applied to One Face	692
10.7.2 Vibration Modes and Natural Frequencies for a Circular Membrane	694
10.7.3 Estimate for the Fundamental Frequency of Vibration of a Simply Supported Rectangular Flat Plate	696
10.7.4 Bending Induced by Inelastic Strain in a Thin Film on a Substrate	697
10.7.5 Bending of a Circular Plate Caused by a Through-Thickness Temperature Gradient	700

10.7.6	Buckling of a Cylindrical Shell Subjected to Axial Loading	703
10.7.7	Torsion of an Open-Walled Circular Cylinder	705
10.7.8	Membrane Shell Theory Analysis of a Spherical Dome under Gravitational Loading	708
<hr/> <u>Appendix A: Review of Vectors and Matrices</u>		711
<hr/> <u>Appendix B: Introduction to Tensors and Their Properties</u>		729
<hr/> <u>Appendix C: Index Notation for Vector and Tensor Operations</u>		741
<hr/> <u>Appendix D: Vectors and Tensor Operations in Polar Coordinates</u>		749
<hr/> <u>Appendix E: Miscellaneous Derivations</u>		765
<hr/> <u>References</u>		771
<hr/> <u>Index</u>		775

This page intentionally left blank

Preface

Ronald Rivlin, a pioneer in the field of nonlinear elasticity, was asked once whether he intended to write a treatise on his field. “Why should I write a book?” he replied. “People write books to learn a subject. I already know it.”

This book is the result of a similar process. Some 15 years ago, I joined the faculty in the solid mechanics group in the Division of Engineering at Brown University. I am a proud graduate of an institution that considers inhaling the air once breathed by Isaac Newton to be more educational than taking graduate courses. Consequently, I started at Brown with lungs and head filled with erudite air but knowing far less about solid mechanics than the students in my classes. I have spent the intervening years attempting to remedy this situation, principally by eavesdropping on the conversations of my colleagues, who are all genuine and highly respected experts in solid mechanics. This book summarizes what I have learned.

Solid mechanics is a venerable field, with a history that spans nearly 200 years. It has been revolutionized within the past two decades by the advent of cheap and powerful computer software and hardware that can be used to solve virtually any problem. These changes have had two main consequences. First, courses in solid mechanics are replacing classical mathematical methods of analysis with computer simulations. Second, graduates from other disciplines, with little background in solid mechanics, are increasingly using highly sophisticated computer simulations to perform stress analysis and require an introduction to the subject.

This text is intended to meet this need. It includes a concise summary of all the main topics in classical solid mechanics but is written with a view to providing the background needed to solve problems using computer simulations. Practitioners must understand the fundamental principles on which these computer simulations are based, particularly constitutive equations and failure criteria, as well as the mathematical descriptions of deformation and internal forces that are used in these models. They need to know how to set up properly posed boundary and initial value problems: studying simple analytical solutions can be very helpful to see how this is done. In addition, computer simulations can all too easily make meaningless predictions if they are not used properly. People who use computer simulations can usually avoid these problems if they understand the algorithms that are implemented in the code and if they can identify physically meaningless predictions. An ability to read and learn from the classical literature on linear elasticity, plasticity, and structural mechanics is invaluable to develop the intuition required to identify such meaningless predictions.

The book could be used as the primary textbook for one or more courses on solid mechanics at the senior undergraduate or introductory graduate level and also provides a fairly complete reference for practicing engineers and scientists. It is not, however, intended as a “canned” course that an instructor would follow chapter by chapter; faculty teaching solid mechanics are invariably experts in the field, who have their own view on what should be taught and how. Instead, chapters, and even subsections within chapters, have been designed as self-contained modules to allow instructors to combine topics as they see fit. For example, I have used the text as the sole reference in (1) a senior year undergraduate course in solid mechanics for mechanical and civil engineers, and (2) classes in a two-semester sequence of graduate courses (for MSc and PhD students) on continuum mechanics and applied solid mechanics as part of Brown’s PhD program.

I have also used the book as the primary text (but supplemented by additional specialized texts) to teach plasticity, fracture mechanics, linear elasticity, and finite element programming.

This text began as a series of short lecture notes for my students and has inherited many of the features of these notes. In my experience, few people read textbooks. Instructors are too busy and already know the material, and students tend to flip through books in desperation looking for the answer to a problem. I have written the book with this situation in mind: chapters, and even individual sections within chapters, are as self-contained as possible. Often, the solution to a problem is presented before its derivation. I have also tried to present derivations in the step-by-step manner of a blackboard lecture. I hope this format will be useful not only to instructors and students, but also to practicing engineers and scientists who need a quick review of some aspect of solid mechanics.

A companion Web site is available at <http://solidmechanics.org> (note the .org extension, not .com). It includes a searchable electronic version of the text, over 400 practice problems, and demonstration of finite element codes in MAPLE® and MATLAB®.*

I am very grateful to readers who have pointed out errors on this Web site. Their efforts have reduced the number of errors in this book, but have not probably eliminated them altogether. Readers finding errors are encouraged to use the form provided on the Web site to correct them.

Allan F. Bower
Providence, RI

* MATLAB® is a registered trademark of The MathWorks, Inc. For product information, please contact:
The MathWorks, Inc.
3 Apple Hill Drive
Natick, MA 01760-2098 USA
Tel: (508) 647-7000
Fax: (508) 647-7001
E-mail: info@mathworks.com
Web: <http://www.mathworks.com>

Author

Allan Bower is a professor of engineering at Brown University, where he teaches in the undergraduate mechanical engineering program and the graduate program in mechanics of solids. He earned undergraduate and graduate degrees from the University of Cambridge and spent a short period on the faculty at Cambridge before joining Brown in 1992. His research involves developing and using computer simulations to model deformation and failure in materials. Applications of interest include modeling wear, plasticity, and contact fatigue between contacting surfaces; fracture in composites and ceramics; and mechanical failure processes in microelectronic circuits.

This page intentionally left blank

Overview of Solid Mechanics

Solid mechanics is a collection of physical laws, mathematical techniques, and computer algorithms that can be used to predict the behavior of a solid material that is subjected to mechanical or thermal loading. The field has a wide range of applications, including the following:

1. Geomechanics: Modeling the shape of planets, tectonics, and earthquake prediction
2. Civil engineering: Designing structures or soil foundations
3. Mechanical engineering: Designing load-bearing components for vehicles, engines, or turbines for power generation and transmission, as well as appliances
4. Manufacturing engineering: Designing processes (such as machining) for forming metals and polymers
5. Biomechanics: Designing implants and medical devices, as well as modeling stress driven phenomena controlling cellular and molecular processes
6. Materials science: Designing composites, alloy microstructures, thin films, and developing techniques for processing materials
7. Microelectronics: Designing failure-resistant packaging and interconnects for micro-electronic circuits
8. Nanotechnology: Modeling stress-driven self-assembly on surfaces, manufacturing processes such as nano-imprinting, and modeling atomic-force microscope/sample interactions

This chapter describes how solid mechanics can be used to solve practical problems. The remainder of the book contains a more detailed description of the physical laws that

2 ■ Applied Mechanics of Solids

govern deformation and failure in solids, as well as the mathematical and computational methods that are used to solve problems involving deformable solids:

- Chapter 2 covers the mathematical description of shape changes and internal forces in solids.
- Chapter 3 discusses constitutive laws that are used to relate shape changes to internal forces.
- Chapter 4 contains analytical solutions to a series of simple problems involving deformable solids.
- Chapter 5 provides a short summary of analytical techniques and solutions for linear elastic solids.
- Chapter 6 describes analytical techniques and solutions for plastically deforming solids.
- Chapter 7 gives an introduction to finite element analysis, focusing on using commercial software.
- Chapter 8 expands on the implementation of the finite element method.
- Chapter 9 describes how to use solid mechanics to model material failure.
- Chapter 10 discusses solids with special geometries (rods, beams, membranes, plates, and shells).

Solid mechanics is incomprehensible without some background in vectors, tensors, and index notation. These topics are reviewed briefly in the appendices.

1.1 DEFINING A PROBLEM IN SOLID MECHANICS

Regardless of the application, the general steps in setting up a problem in solid mechanics are always the same:

1. Decide on the goal of the problem and desired information.
2. Identify the geometry of the solid to be modeled.
3. Determine the loading applied to the solid.
4. Decide what physics must be included in the model.
5. Choose (and calibrate) a *constitutive law* that describes the behavior of the material.
6. Choose a method of analysis.
7. Solve the problem.

Each step in the process is discussed in more detail below.

1.1.1 Deciding What to Calculate

This question seems rather silly, but at some point in their careers, most engineers have been asked by their manager, “Why don’t you just set up a finite element model of our (crank-case, airframe, material, etc.) so we can stop it from (corroding, fatiguing, fracturing, etc.)?” If you find yourself in this situation, you are doomed. Models can certainly be helpful in preventing failure, but, unless you have a very clear idea of why the failure is occurring, you won’t know what to model.

Here is a list of things that can be calculated accurately using solid mechanics:

1. The deformed shape of a structure or component subjected to mechanical, thermal, or electrical loading
2. The forces required to cause a particular shape change
3. The stiffness of a structure or component
4. The internal forces (stresses) in a structure or component
5. The critical forces that lead to failure by structural instability (buckling)
6. Natural frequencies of vibration for a structure or component

In addition, solid mechanics can be used to model a variety of failure mechanisms. Failure predictions are more difficult, however, because the physics of failure can only be modeled using approximate constitutive equations. These mathematical relationships must be calibrated experimentally and do not always perfectly characterize the failure mechanism. Nevertheless, there are well-established procedures for each of the following:

1. Predicting the critical loads to cause fracture in a brittle or ductile solid containing a crack
2. Predicting the fatigue life of a component under cyclic loading
3. Predicting the rate of growth of a stress-corrosion crack in a component
4. Predicting the creep life of a component
5. Finding the length of a crack that a component can contain and still withstand fatigue or fracture
6. Predicting the wear rate of a surface under contact loading
7. Predicting the fretting or contact fatigue life of a surface

Solid mechanics is increasingly being used for applications other than structural and mechanical engineering design. These are active research areas, and some are better developed than others. Applications include the following:

1. Calculating the properties (e.g., elastic modulus, yield stress, stress-strain curve, fracture toughness, etc.) of a composite material in terms of those of its constituents

4 ■ Applied Mechanics of Solids

2. Predicting the influence of the microstructure (e.g., texture, grain structure, dispersoids, etc.) on the mechanical properties of metals such as modulus, yield stress, strain hardening, etc.
3. Modeling the physics of failure in materials, including fracture, fatigue, plasticity, and wear, and using the models to design failure resistant materials
4. Modeling materials processing, including casting and solidification, alloy heat treatments, and thin-film and surface-coating deposition (e.g., by sputtering, vapor deposition, or electroplating)
5. Modeling biological phenomena and processes, such as bone growth, cell mobility, cell wall/particle interactions, and bacterial mobility

1.1.2 Defining the Geometry of the Solid

Again, this step seems rather obvious: surely the shape of the solid is always known? True, but it is usually not obvious *how much* of the component to model and at what level of detail. For example, in a crash simulation, must the entire vehicle be modelled, or just the front part? Should the engine block be included? The driver? The cell phone that distracted the driver into crashing in the first place?

At the other extreme, it is often not obvious how much geometrical detail needs to be included in a computation. If you model a component, do you need to include every geometrical feature (such as bolt holes, cutouts, chamfers, etc.)? The following guidelines might be helpful:

1. For modeling brittle fracture, fatigue failure, or for calculating critical loads required to initiate plastic flow in a component, it is very important to model the geometry in great detail, because geometrical features can lead to stress concentrations that initiate damage.
2. For modeling creep damage, large-scale plastic deformation (e.g., metal forming) or vibration analysis, geometrical details are less important. Geometrical features with dimensions under 10% of the macroscopic cross section can generally be neglected.
3. Geometrical features often only influence *local* stresses: they do not have much influence far away. Saint Venant's principle, which will be discussed in more detail in Chapter 5, suggests that a geometrical feature with characteristic dimension L (e.g., the dimension of a hole in the solid) will influence stresses over a region with dimension around $3L$ surrounding the feature. In other words, if you are interested in the stress state at a particular point in an elastic solid, you don't need to worry about geometrical features that are far from the region of interest. Strictly speaking, Saint Venants' principle only applies to elastic solids, although it can usually also be applied to plastic solids that strain harden.

As a general rule, it is best to start with the simplest possible model and see what it predicts. If the simplest model answers your question, you're done. If not, the results can serve as a guide in refining the calculation.

1.1.3 Defining Loading

There are six ways that mechanical loads can be induced in a solid:

1. The boundaries can be subjected to a prescribed displacement or motion.
2. The boundaries can be subjected to a distribution of pressure normal to the surface or frictional traction tangent to the surface, as shown in Figure 1.1.
3. A boundary may be subjected to a combination of displacement and traction ("mixed") boundary conditions; for example, you could prescribe horizontal displacements, together with the vertical traction, at some point on the boundary.
4. The interior of the solid can be subjected to gravitational or electromagnetic body forces.
5. The solid can contact another solid or, in some cases, can contact itself.
6. Stresses can be induced by nonuniform thermal expansion in the solid or some other materials process such as phase transformation that causes the solid to change its shape.

When specifying boundary conditions, you must follow these rules:

1. In a three-dimensional (3D) analysis, you must specify three components of either displacement (u_1, u_2, u_3) or traction (t_1, t_2, t_3) (but not both) at each point on the boundary. You can mix these: so for example, you could prescribe (u_1, t_2, t_3) or (u_1, u_2, t_3) , but exactly three components must always be prescribed. This rule also applies to free surfaces, where the tractions are prescribed to be zero.
2. Similarly, in a two-dimensional (2D) analysis, you must prescribe two components of displacement or traction at each point on the boundary.
3. If you are solving a static problem with only tractions prescribed on the boundary, you must ensure that the total external force and moment acting on the solid sum to zero (otherwise, a static equilibrium solution cannot exist).

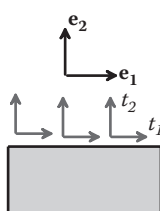


FIGURE 1.1 Tensions acting on the boundary of a solid.

6 ■ Applied Mechanics of Solids

In practice, it can be surprisingly difficult to find out exactly what the loading on your system looks like. For example, earthquake loading on a building can be modeled as a prescribed acceleration of the building's base, but what acceleration should you apply? Pressure loading usually arises from wind or fluid forces, but you might need to do some sophisticated calculations just to identify these forces. In the case of contact loading, you'll need to be able to estimate friction coefficients. For nanoscale or biological applications, you may also need to model attractive forces between the two contacting surfaces. Here, standards are helpful. For example, building codes regulate civil engineering structures, the National Highway Traffic Safety Administration specifies design requirements for vehicles, and so on.

You can also avoid the need to find exactly what loading a structure will experience in service by simply calculating the critical loads that will lead to failure or the fatigue life as a function of loading. In this case, some other unfortunate engineer will have to decide whether or not the failure loads are acceptable.

1.1.4 Deciding What Physics to Include in the Model

There are four decisions to make here:

1. Do you need to calculate additional field quantities, such as temperature, electric or magnetic fields, or mass/fluid diffusion through the solid? Temperature is the most common additional field quantity. Here are some rough guidelines that will help you to decide whether to account for heating effects.

The *stress induced by temperature variation* in a component can be estimated from the formula $\sigma = E(\alpha T)_{\max} - (\alpha T)_{\min}$, where E is the Young's modulus of the material, α is its thermal expansion coefficient, and T is temperature. The symbols $(\alpha T)_{\max}, (\alpha T)_{\min}$ denote the maximum and minimum values of the product αT in the component. You need to account for temperature variations if σ is a significant fraction of the stress induced by mechanical loading.

2. To decide whether you need to do a *transient heat conduction analysis*; note that the temperature rise at a distance r from a point source of heat of intensity \dot{Q} in an infinite solid is $\Delta T = \dot{Q} \operatorname{erfc}(r / 2\sqrt{\alpha t}) / (4\pi\kappa r)$, where $\operatorname{erfc}()$ denotes the complementary error function, κ is the material's thermal conductivity, and $\chi = \kappa / (\rho c_p)$ is its thermal diffusivity, with ρ the mass density and c_p the specific heat capacity. This equation suggests that a solid with dimension L will reach its steady-state temperature in time $t \approx 25L^2/\chi$. If the timescale of interest in your problem is significantly larger than this and heat flux is constant, you can use the steady-state temperature distribution. If not, you must account for transients.

Finally, to decide whether you need to account for *heat generated by plastic flow*, note that the rate of heat generation per unit volume is of order $\dot{q} = \sigma_y \dot{\varepsilon}^p$, where σ_y is the material yield stress, and $\dot{\varepsilon}^p$ is the plastic strain rate. The temperature rise attributable to rapid (adiabatic) plastic heating is thus of order $\Delta T = \sigma_y \Delta \varepsilon^p / (\rho c_p)$, where $\Delta \varepsilon^p$ is the strain increment applied to the material.

3. Do you need to do a *dynamic analysis* or a *static analysis*? Here are some rough guidelines that will help you to decide. The speed of a shear wave propagating through an elastic solid is $c = \sqrt{\mu/\rho}$, where ρ is the mass density of the solid, and μ is its shear modulus. The time taken for a wave to propagate across a component with size L is of order $t = L/c$. In many cases, stresses decay to their static values after about $10L/c$. If the loading applied to the component does not change significantly during this time period, a quasi-static computation (possibly including accelerations as body forces) should suffice.

The stress induced by acceleration (e.g., in a rotating component) is of order $L\rho a$, where L is the approximate size of the component, ρ is its mass density, and a is the magnitude of the acceleration. If this stress is negligible compared with other forces applied to the solid, it can be neglected. If not, it should be included (as a body force if wave propagation can be neglected).

4. Are you solving a *coupled fluid/solid interaction* problem? These situations arise in aeroelasticity (design of flexible aircraft wings or helicopter rotor blades, or very long bridges), offshore structures, pipelines, or fluid containers. In these applications, the fluid flow has a high Reynold's number (so fluid forces are dominated by inertial effects). Coupled problems are also very common in biomedical applications, such as blood flow or cellular mechanics. In these applications, the Reynold's number for the fluid flow is much lower, and fluid forces are dominated by viscous effects. Several analysis techniques are available for solving such coupled fluid/structure interaction problems but are beyond the scope of this book.

1.1.5 Defining Material Behavior

Choosing the right equations to describe material behavior is the most critical part of setting up a solid mechanics calculation. Using the wrong model, or inaccurate material properties, will always invalidate your predictions. Here are a few of your choices, with suggested applications:

- 1. Isotropic linear elasticity** (familiar in one dimension as $\sigma = E\varepsilon$): This constitutive law is useful for polycrystalline metals, ceramics, glasses, and polymers undergoing small deformations and subjected to low loads (less than the material yield stress). Only two material constants are required to characterize the material, and accurate values for these constants are readily available.
- 2. Anisotropic linear elasticity:** This model is similar to isotropic linear elasticity but models materials that are stiffer in some directions than others. It is useful for reinforced composites, wood, and single crystals of metals and ceramics. At least three, and up to 21, material properties must be determined to characterize an anisotropic material. Material data are accurate and readily available. Isotropic or anisotropic linear elasticity may be applied to the vast majority of engineering design calculations,

8 ■ Applied Mechanics of Solids

in which components cannot safely exceed yield. It can be used for deflection calculations, fatigue analysis, and vibration analysis.

3. **Hyperelasticity:** These models are used for rubber and foams, which can sustain huge, reversible shape changes. There are several models from which to choose. The simplest model is the incompressible neo-Hookean solid, which, in uniaxial stress, has a true stress-true strain relation given by $\sigma = C(\exp(2\epsilon) - 1/\exp(\epsilon))$. It has only a single material constant. More complex models have several parameters, and it may be difficult to find values of these parameters for your material in the published literature. Experimental calibration will almost certainly be required.
4. **Viscoelasticity:** This model is used for materials that exhibit a gradual increase in strain when loaded at constant stress (with stress rate-strain rate $\dot{\epsilon} = \dot{\sigma}/E + \eta\sigma$) or that show hysteresis during cyclic loading (with stress rate-strain rate of form $\dot{\sigma} = E\dot{\epsilon} + \lambda\dot{\epsilon}$). It is usually used to model polymeric materials, polymer-based composites, and biological tissue and can also model slow creep in amorphous solids such as glass. Constitutive equations contain at least three parameters and usually many more. Material behavior varies widely between materials and is highly temperature dependent. Experimental calibration will almost certainly be required to obtain accurate predictions.
5. **Rate-independent metal plasticity:** This model is used to calculate permanent deformation in metals loaded above their yield point. A wide range of models are available. The simplest is a *rigid perfectly plastic solid*, which changes its shape only if loaded above its yield stress, σ_y , and then deforms at constant stress. An *elastic perfectly plastic solid* deforms according to linear elastic equations when loaded below the yield stress but deforms at constant stress if yield is exceeded. These models can predict energy dissipation in a crash analysis or calculate tool forces in a metal-cutting operation, for example. Data for material yield stress are readily available but are sensitive to material processing and microstructure and so should be used with caution. More sophisticated models describe *strain hardening* in some way (the change in the yield stress of the solid with plastic deformation). These equations are used in modeling ductile fracture, low cycle fatigue (in which the material is repeatedly plastically deformed), and when predicting residual stresses and springback in metal forming operations. Finally, the most sophisticated plasticity models attempt to track the development of microstructure or damage in the metal. For example, the *Gurson* plasticity law models the nucleation and growth of voids in a metal and is widely used to simulate ductile fracture. Such models typically have a large number of parameters and can differ widely in their predictions. They must be very carefully chosen and calibrated to obtain accurate results.
6. **Viscoplasticity:** Similar in structure to metal plasticity, these models account for the tendency of the flow stress of a metal to increase when deformed at high strain rates. They are used in modeling high-speed machining, for example, or in applications involving explosive shock loading. Viscoplastic constitutive equations are also

used to model *creep*, the steady accumulation of plastic strain in a metal when loaded below its yield stress and subjected to high temperatures. The simplest viscoplastic constitutive law has only two parameters: uniaxial strain rate versus stress response of the form $\dot{\epsilon} = A\sigma^n$. More complex models account for elastic deformation and strain hardening. Data for the simple models is quite easy to find, but more sophisticated and accurate models must be calibrated experimentally.

7. **Crystal plasticity:** These models are used for calculating anisotropic plastic flow in a single crystal of a metal. They are mostly used in materials science calculations and in modeling some metal-forming processes. These models are still under development because material data are not easily found and are laborious and expensive to measure.
8. **Strain gradient plasticity:** This formulation was developed in the past 5–10 years to model the behavior of very small volumes of a metal (less than 100 μm). Typically, small volumes of metal are stronger than bulk samples. These models are still under development, are difficult to calibrate, and do not always work well.
9. **Discrete dislocation plasticity:** Currently used for research only, this technique models plastic flow in very small volumes of material by tracking the nucleation, motion, and annihilation of individual dislocations in the solid. Discrete dislocation plasticity models contain a large number of material parameters that are difficult to calibrate.
10. **Critical state plasticity (cam-clay):** This model is used for soils, whose behavior depends on moisture content. It is somewhat similar in structure to the metal plasticity model, except that the yield strength of a soil is highly pressure dependent (increases with compressive pressure). Simple models contain only three or four material parameters, which can be calibrated quite accurately.
11. **Pressure-dependent viscoplasticity:** This model is similar to critical state plasticity, in that they both account for changes in flow stress of a material with confining pressure. It is used to model granular materials and some polymers and composite materials (typically in modeling processes such as extrusion or drawing).
12. **Concrete models:** They are intended to model the crushing (in compression) or fracture (in tension) of concrete (obviously!). The mathematical structure resembles that of pressure-dependent plasticity.
13. **Atomistic models:** They replace traditional stress-strain laws with a direct calculation of stress-strain behavior using embedded atomic scale simulations. The atomic scale computations use empirical potentials to model atom interactions or may approximate the Schrodinger wave equation directly. Techniques include the “quasi-continuum” method and the coupled atomistic-discrete dislocation method. Their advantage is that they capture the physics of material behavior extremely accurately; their disadvantage is that they currently can only model extremely small material

10 ■ Applied Mechanics of Solids

volumes (approximately 20–100 nm). Atomistic models based on empirical potentials contain a large number of adjustable parameters; these are usually calibrated against known quantities such as elastic moduli and stacking fault energies and can also be computed using ab initio techniques. The accuracy of the predictions depends strongly on the accuracy of the potentials. Currently, these kinds of simulations are used mostly as a research tool for nanotechnology and materials design applications.

This list is by no means exhaustive; additional models are available for materials such as shape memory alloys, metallic glasses, and piezoelectric materials. These material models are intended primarily to approximate stress-strain behavior. Special constitutive equations have also been developed to model the behavior of contacting surfaces or interfaces between two solids (Coulomb friction is a simple example). In addition, if you need to model damage (fracture or fatigue), you may need to select and calibrate additional material models. For example, to model brittle fracture, you would need to know the fracture toughness of the material. To model the growth of a fatigue crack, you would probably use Paris' crack growth law $da/dt = C(\Delta K)^n$ and would need data for the Paris constant C and exponent n . There are several other stress- or strain-based fatigue laws in common use. These models are often curve fits to experimental data and are not based on any detailed physical understanding of the failure mechanism. They must therefore be used with caution, and material properties must be measured carefully.

1.1.6 A Representative Initial Value Problem in Solid Mechanics

The result of the decisions made in Sections 1.1.1 through 1.1.5 is a *boundary value problem* (for static problems) or *initial value problem* (for dynamic problems). This information consists of a set of partial differential equations, together with initial and boundary conditions, that must be solved for the displacement and stress fields, as well as any auxiliary fields (such as temperature) in the solid. To illustrate the structure of these equations, this section provides a list of the governing equations for a representative initial value problem.

As a representative example, we state the initial value problem that governs elastic wave propagation in a linear elastic solid. A representative problem is sketched in Figure 1.2.

Take the following:

1. The shape of the solid in its unloaded condition R
2. The mass density ρ , the Young's modulus E , and Poisson's ratio ν for the solid
3. The thermal expansion coefficient α for the solid and temperature distribution $T(x)$ in the solid (for simplicity, we assume that the temperature does not vary with time)

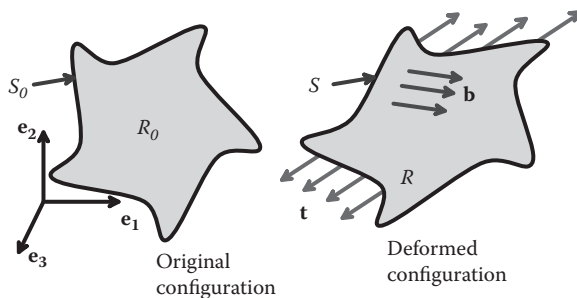


FIGURE 1.2 Schematic of a representative boundary value problem.

4. The initial displacement field in the solid $\mathbf{u}^0(\mathbf{x})$ and the initial velocity field $\mathbf{v}^0(\mathbf{x})$
5. A body force distribution $\mathbf{b}(\mathbf{x}, t)$ (force per unit volume) acting on the solid
6. Boundary conditions, specifying displacements $\mathbf{u}^*(\mathbf{x}, t)$ on a portion $\partial_1 R$ and tractions $\mathbf{t}^*(\mathbf{x}, t)$ on a portion $\partial_2 R$ of the boundary of R .

Then, calculate displacements u_i , strains ε_{ij} , and stresses σ_{ij} satisfying the governing equations of linear elastodynamics:

1. The strain-displacement (compatibility) equation $\varepsilon_{ij} = \frac{1}{2}(\partial u_i / \partial x_j + \partial u_j / \partial x_i)$.
2. The linear elastic stress-strain law $\sigma_{ij} = \frac{E}{1+\nu} \left(\varepsilon_{ij} + \frac{\nu}{1-2\nu} \varepsilon_{kk} \delta_{ij} \right) - \frac{Ev}{(1+\nu)(1-2\nu)} \alpha \Delta T \delta_{ij}$.
3. The equation of motion for a continuum ($\mathbf{F}=m\mathbf{a}$) $\partial \sigma_{ij} / \partial x_i + b_j = \rho \partial^2 u_j / \partial t^2$.
4. The fields must satisfy initial conditions $u_i(x_i, t=0) = u_i^0$ and $\frac{\partial u_i(x_i, t=0)}{\partial t} = v_i^0$, as well as boundary conditions $u_i = u_i^*(x_k, t)$ on $\partial_1 R$ and $\sigma_{ij} n_i = t_j^*(x_k, t)$ on $\partial_2 R$.

1.1.7 Choosing a Method of Analysis

Once you have set up the problem, you will need to solve the equations of motion (or equilibrium) for a continuum, together with the equations governing material behavior, to determine the stress and strain distributions in the solid. Several methods are available for this purpose.

Exact solutions. There is a good chance that you can find an exact solution for the following:

1. 2D (plane stress or plane strain) linear elastic solids, particularly under static loading. Solution techniques include integral transforms, stress function methods, and complex variable methods. Dynamic solutions are also possible but somewhat more difficult.

12 ■ Applied Mechanics of Solids

2. 2D viscoelastic solids.
3. 3D linear elasticity problems can be solved (usually using integral transforms) if they are simple enough.
4. 2D (plane strain) deformation of rigid plastic solids (using slip line fields).

Naturally, analytical solutions are most easily found for solids with a simple geometry (e.g., an infinite solid containing a crack, loading applied to a flat surface, etc.). In addition, special analytical techniques can be used for problems for which the solid's geometry can be approximated. Examples include membrane theory, shell and plate theory, beam theory, and truss analysis.

Even when you can't find an exact solution to the stress and strain fields in your solid, you can sometimes get the information you need using powerful mathematical theorems. For example, bounding theorems allow you to estimate the plastic collapse loads for a structure quickly and easily.

Numerical solutions. Computer simulations are used for most engineering design calculations in practice and include the following:

1. The finite element method (FEM): We will discuss this method in detail later in this book. It is the most widely used technique and can be used to solve almost any problem in solid mechanics, provided you understand how to model your material and have access to a fast enough computer.
2. Finite difference methods: They are somewhat similar to FEM but are much less widely used.
3. Boundary integral equation methods (or boundary element methods): These are more efficient computer techniques for linear elastic problems, but they are not as useful for problems involving nonlinear materials or geometry.
4. Free volume methods: They are used more in computational fluid dynamics than in solids but are useful for problems involving very large deformations, in which the solid flows much like a fluid.
5. Atomistic methods: They are used in nanotechnology applications to model material behavior at the atomic scale. *Molecular dynamic* techniques integrate the equations of motion (Newton's laws) for individual atoms, and *molecular statics* solve equilibrium equations to calculate atom positions. The forces between atoms are computed using empirical constitutive equations, or sometimes using approximations to quantum mechanics. These computations can only consider exceedingly small material volumes (up to a few million atoms) and short timescales (up to a few tens or hundreds of nanoseconds).

Governing Equations

The purpose of this chapter is to summarize the equations that govern the response of solids to mechanical or thermal loading. The following topics will be addressed in turn:

1. The mathematical description of shape changes in a solid
2. The mathematical description of internal forces in a solid
3. Equations of motion for deformable solids
4. Concepts of mechanical work and power for deformable solids and the important principle of virtual work.

2.1 MATHEMATICAL DESCRIPTION OF SHAPE CHANGES IN SOLIDS

In this section, we list the various mathematical formulas that are used to characterize shape changes in solids (and in fluids). The formulas might look scary at first, but they are mostly just definitions. You might find it helpful to refresh your memory on vectors and matrices (Appendix A) and to read the brief discussion of tensors (Appendix B) and index notation (Appendix C) before wading through this section.

As you work through the various definitions, you should bear in mind that shape changes near a point can always be characterized by six numbers. These could be the six independent components of the Lagrangian strain, Eulerian strain, the left or right stretch tensors, or your own favorite deformation measure. Given the complete set of six numbers for any one deformation measure, you can always calculate the components of other strain measures. The reason that so many different deformation measures exist is partly because different material models adopt different strain measures and partly because each measure is useful for describing a particular type of shape change.

2.1.1 Displacement and Velocity Fields

The displacement vector $\mathbf{u}(\mathbf{x},t)$ describes the motion of each point in the solid. To make this precise, visualize a solid deforming under external loads, as shown in Figure 2.1. Every

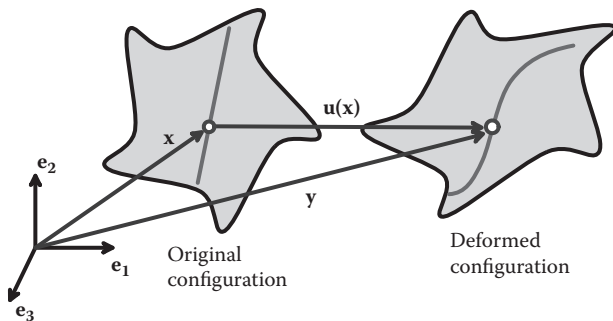


FIGURE 2.1 Deformation of a solid.

point in the solid moves as the load is applied: for example, a point at position \mathbf{x} in the undeformed solid might move to a new position \mathbf{y} at time t . The displacement vector is defined as

$$\mathbf{y} = \mathbf{x} + \mathbf{u}(\mathbf{x}, t).$$

We could also express this formula using *index notation*, which is discussed in detail in Appendix C, as

$$y_i = x_i + u_i(x_1, x_2, x_3, t).$$

Here, the subscript i has values 1, 2, or 3, and (for example) y_i represents the three Cartesian components of the vector \mathbf{y} .

The displacement field completely specifies the change in shape of the solid. The *velocity field* would describe its motion as

$$v_i(x_k, t) = \frac{\partial y_i}{\partial t} = \left. \frac{\partial u_i(x_k, t)}{\partial t} \right|_{x_k=\text{const}}.$$

Some examples of deformations are listed in Table 2.1.

2.1.2 Displacement Gradient and Deformation Gradient Tensors

These quantities are defined by the following:

- Displacement gradient tensor: $\mathbf{u} \otimes \nabla$ is a tensor with components $\frac{\partial u_i}{\partial x_k}$.
- Deformation gradient tensor:

$$\mathbf{F} = \mathbf{I} + \mathbf{u} \otimes \nabla \quad \text{or in Cartesian components} \quad F_{ik} = \delta_{ik} + \frac{\partial u_i}{\partial x_k},$$

TABLE 2.1 Examples of Some Simple Deformations

<p>Volume preserving uniaxial extension:</p> $y_1 = \lambda x_1$ $y_2 = x_2 / \sqrt{\lambda}$ $y_3 = x_3 / \sqrt{\lambda}$	
<p>Simple shear:</p> $y_1 = x_1 + \tan \theta x_2$ $y_2 = x_2$ $y_3 = x_3$	
<p>Rigid rotation through angle θ about e_3 axis:</p> $y_1 = x_1 \cos \theta - x_2 \sin \theta$ $y_2 = x_2 \cos \theta + x_1 \sin \theta$ $y_3 = x_3$	
<p>General rigid rotation about the origin:</p> $\mathbf{y} = \mathbf{R} \cdot \mathbf{x}$ or $y_i = R_{ij}x_j$ where \mathbf{R} must satisfy $\mathbf{R} \cdot \mathbf{R}^T = \mathbf{R}^T \cdot \mathbf{R} = \mathbf{I}$, $\det(\mathbf{R}) > 0$ (i.e., \mathbf{R} is proper orthogonal). \mathbf{I} is the identity tensor with components $\delta_{ik} = \begin{cases} 1, & i=k \\ 0, & i \neq k \end{cases}$	
<p>Alternatively, a rigid rotation through angle θ (with right-hand screw convention) about an axis through the origin that is parallel to a unit vector \mathbf{n} can be written as</p> $\mathbf{y} = \cos \theta \mathbf{x} + (1 - \cos \theta)(\mathbf{n} \cdot \mathbf{x})\mathbf{n} + \sin \theta (\mathbf{n} \times \mathbf{x}).$ <p>The components of \mathbf{R} are thus $R_{ij} = \cos \theta \delta_{ij} + \sin \theta \epsilon_{ijk} n_k$,</p> <p>where ϵ_{ijk} is the permutation symbol, satisfying $\epsilon_{ijk} = \begin{cases} 1 & i,j,k = 1,2,3; 2,3,1 \text{ or } 3,1,2 \\ -1 & i,j,k = 3,2,1; 2,1,3 \text{ or } 1,3,2 \\ 0 & \text{otherwise} \end{cases}$.</p>	
<p>General homogeneous deformation:</p> $y_1 = A_{11}x_1 + A_{12}x_2 + A_{13}x_3 + c_1$ $y_2 = A_{21}x_1 + A_{22}x_2 + A_{23}x_3 + c_2$ $y_3 = A_{31}x_1 + A_{32}x_2 + A_{33}x_3 + c_3$ <p>or</p> $\mathbf{y} = \mathbf{A} \cdot \mathbf{x} + \mathbf{c}$ $y_i = A_{ij}x_j + c_i$ where A_{ij} are constants. <p>The physical significance of a homogeneous deformation is that all straight lines in the solid remain straight under the deformation. Thus, every point in the solid experiences the same shape change. All the deformations listed above are examples of homogeneous deformations.</p>	

16 ■ Applied Mechanics of Solids

where \mathbf{I} is the identity tensor, with components described by the Kronecker delta symbol:

$$\delta_{ik} = \begin{cases} 1, & i=k \\ 0, & i \neq k \end{cases}$$

and ∇ represents the gradient operator. Formally, the gradient of a vector field $\mathbf{u}(\mathbf{x})$ is defined so that

$$[\mathbf{u} \otimes \nabla] \cdot \mathbf{n} = \lim_{\alpha \rightarrow 0} \frac{\mathbf{u}(\mathbf{x} + \alpha \mathbf{n}) - \mathbf{u}(\mathbf{x})}{\alpha}$$

(for more details, see Appendix B), but in practice the component formula $\partial u_i / \partial x_j$ is more useful.

Note also that

$$\mathbf{y} \otimes \nabla = (\mathbf{x} + \mathbf{u}(\mathbf{x})) \otimes \nabla = \mathbf{F}$$

$$\text{or } \frac{\partial y_i}{\partial x_j} = \frac{\partial}{\partial x_j} (x_i + u_i) = \delta_{ij} + \frac{\partial u_i}{\partial x_j} = F_{ij}$$

The rules of differentiation using index notation are described in more detail in Appendix C.

The concepts of displacement gradient and deformation gradient are introduced to quantify the change in shape of infinitesimal line elements in a solid body. To see this, imagine drawing a straight line on the undeformed configuration of a solid, as shown in Figure 2.2. The line would be mapped to a smooth curve on the deformed configuration. However, suppose we focus attention on a line segment $d\mathbf{x}$, much shorter than the radius of curvature of this curve, as shown. The segment would be straight in the undeformed configuration and would also be (almost) straight in the deformed configuration. Thus, no matter how complex a deformation we impose on a solid, infinitesimal line segments are

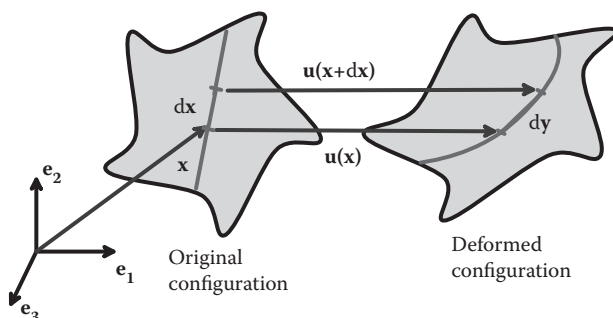


FIGURE 2.2 Deformation of an infinitesimal line element in a solid.

merely stretched and rotated by a deformation. The infinitesimal line segments $d\mathbf{x}$ and $d\mathbf{y}$ are related by

$$d\mathbf{y} = \mathbf{F} \cdot d\mathbf{x} \text{ or } dy_i = F_{ik} dx_k$$

Written out as a matrix equation, we have

$$\begin{bmatrix} dy_1 \\ dy_2 \\ dy_3 \end{bmatrix} = \begin{bmatrix} 1 + \frac{\partial u_1}{\partial x_1} & \frac{\partial u_1}{\partial x_2} & \frac{\partial u_1}{\partial x_3} \\ \frac{\partial u_2}{\partial x_1} & 1 + \frac{\partial u_2}{\partial x_2} & \frac{\partial u_2}{\partial x_3} \\ \frac{\partial u_3}{\partial x_1} & \frac{\partial u_3}{\partial x_2} & 1 + \frac{\partial u_3}{\partial x_3} \end{bmatrix} \begin{bmatrix} dx_1 \\ dx_2 \\ dx_3 \end{bmatrix}$$

To derive this result, consider an infinitesimal line element $d\mathbf{x}$ in a deforming solid. When the solid is deformed, this line element is stretched and rotated to a deformed line element $d\mathbf{y}$. If we know the displacement field in the solid, we can compute $d\mathbf{y} = [\mathbf{x} + d\mathbf{x} + \mathbf{u}(\mathbf{x} + d\mathbf{x})] - [\mathbf{x} + \mathbf{u}(\mathbf{x})]$ from the position vectors of its two end points

$$dy_i = x_i + dx_i + u_i(x_k + dx_k) - (x_i + u_i(x_k))$$

Expand $u_i(x_k + dx_k)$ as a Taylor series

$$u_i(x_k + dx_k) \approx u_i(x_k) + \frac{\partial u_i}{\partial x_k} dx_k$$

so that

$$dy_i = dx_i + \frac{\partial u_i}{\partial x_k} dx_k = \left(\delta_{ik} + \frac{\partial u_i}{\partial x_k} \right) dx_k$$

We identify the term in parentheses as the deformation gradient, so

$$dy_i = F_{ik} dx_k$$

The inverse of the deformation gradient \mathbf{F}^{-1} arises in many calculations. It is defined through

$$dx_i = F_{ik}^{-1} dy_k$$

or alternatively,

$$F_{ij}^{-1} = \frac{\partial x_i}{\partial y_j}.$$

2.1.3 Deformation Gradient Resulting from Two Successive Deformations

Suppose that two successive deformations are applied to a solid, as shown in Figure 2.3. Let

$$dy = \mathbf{F}^{(1)} \cdot d\mathbf{x} \quad d\mathbf{z} = \mathbf{F}^{(2)} \cdot dy \quad \text{or} \quad dy_i = F_{ij}^{(1)} dx_j \quad dz_i = F_{ij}^{(2)} dy_j$$

map infinitesimal line elements from the original configuration to the first deformed shape and from the first deformed shape to the second, respectively, with

$$\mathbf{F}^{(1)} = \mathbf{y} \otimes \nabla_{\mathbf{x}} \quad \mathbf{F}^{(2)} = \mathbf{z} \otimes \nabla_{\mathbf{y}} \quad \text{or} \quad F_{ij}^{(1)} = \frac{\partial y_i}{\partial x_j} \quad F_{ij}^{(2)} = \frac{\partial z_i}{\partial y_j}.$$

The deformation gradient that maps infinitesimal line elements from the original configuration directly to the second deformed shape then follows as

$$d\mathbf{z} = \mathbf{F} \cdot d\mathbf{x} \quad \text{with} \quad \mathbf{F} = \mathbf{F}^{(2)} \cdot \mathbf{F}^{(1)} \quad \text{or} \quad dz_i = F_{ij} dx_j \quad F_{ij} = F_{ik}^{(2)} F_{kj}^{(1)}.$$

Thus, the cumulative deformation gradient attributable to two successive deformations follows by multiplying their individual deformation gradients.

To see this, write the cumulative mapping as $z_i(y_j(x_k))$ and apply the chain rule

$$dz_i = \frac{\partial z_i}{\partial y_j} \frac{\partial y_j}{\partial x_k} dx_k.$$

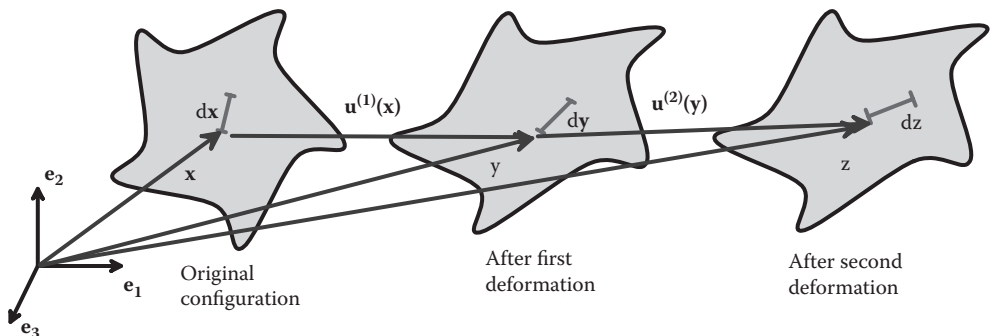


FIGURE 2.3 Solid subjected to two successive deformations.

2.1.4 The Jacobian of the Deformation Gradient

The Jacobian is defined as

$$J = \det(\mathbf{F}) = \det \left(\delta_{ij} + \frac{\partial u_i}{\partial x_j} \right).$$

It is a measure of the volume change produced by a deformation. To see this, consider the infinitesimal volume element with sides $d\mathbf{x}$, $d\mathbf{y}$, and $d\mathbf{z}$ shown in Figure 2.4. The original volume of the element is

$$dV_0 = d\mathbf{z} \cdot (d\mathbf{x} \times d\mathbf{y}) = \epsilon_{ijk} dz_i dx_j dy_k.$$

Here, ϵ_{ijk} is the permutation symbol. The element is mapped to a parallelepiped with sides $d\mathbf{r}$, $d\mathbf{v}$, and $d\mathbf{w}$ with volume given by

$$dV = \epsilon_{ijk} dw_i dr_j dv_k.$$

Recall that

$$dr_i = F_{il} dx_l, \quad dv_j = F_{jm} dy_m, \quad dw_k = F_{kn} dz_n$$

so that

$$dV = \epsilon_{ijk} F_{il} dx_l F_{jm} dy_m F_{kn} dz_n = \epsilon_{ijk} F_{il} F_{jm} F_{kn} dx_l dy_m dz_n.$$

Recall that

$$\epsilon_{ijk} A_{il} A_{jm} A_{kn} = \epsilon_{lmn} \det(\mathbf{A})$$

so that

$$dV = \det(\mathbf{F}) \epsilon_{lmn} dx_l dy_m dz_n = \det(\mathbf{F}) dV_0.$$

Hence,

$$\frac{dV}{dV_0} = \det(\mathbf{F}) = J.$$

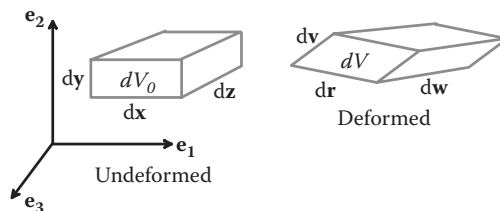


FIGURE 2.4 Deformation of an infinitesimal volume element in a solid.

20 ■ Applied Mechanics of Solids

Observe the following:

- For any physically admissible deformation, the volume of the deformed element must be positive (no matter how much you deform a solid, you can't make material disappear). Therefore, all physically admissible displacement fields must satisfy $J > 0$.
- If a material is *incompressible*, its volume remains constant. This requires $J = 1$.
- If the *mass density* of the material at a point in the undeformed solid is ρ_0 , its mass density in the deformed solid is $\rho = \rho_0 / J$.

When working with constitutive equations, it is occasionally necessary to evaluate derivatives of J with respect to the components of \mathbf{F} . The following result (which can be proved by, for example, expanding the Jacobian using index notation) is extremely useful:

$$\frac{\partial J}{\partial F_{ij}} = J F_{ji}^{-1}.$$

2.1.5 Lagrange Strain Tensor

The Lagrange strain tensor is defined as

$$\mathbf{E} = \frac{1}{2}(\mathbf{F}^T \cdot \mathbf{F} - \mathbf{I}) \quad \text{or} \quad E_{ij} = \frac{1}{2}(F_{ki}F_{kj} - \delta_{ij}).$$

The components of Lagrange strain can also be expressed in terms of the displacement gradient as

$$E_{ij} = \frac{1}{2} \left(\frac{\partial u_i}{\partial x_j} + \frac{\partial u_j}{\partial x_i} + \frac{\partial u_k}{\partial x_j} \frac{\partial u_k}{\partial x_i} \right).$$

The Lagrange strain tensor quantifies the changes in length of a material fiber and angles between pairs of fibers in a deformable solid. It is used in calculations in which large shape changes are expected.

To visualize the physical significance of \mathbf{E} , suppose we mark out an imaginary tensile specimen with (very short) length l_0 on our deforming solid, as shown in Figure 2.5. The orientation of the specimen is arbitrary and is specified by a unit vector \mathbf{m} , with components m_i . After deformation, the specimen increases in length to $l = l_0 + \delta l$. Define the strain of the specimen as

$$\epsilon_L(m_i) = \frac{l^2 - l_0^2}{2l_0^2} = \frac{\delta l}{l_0} + \frac{(\delta l)^2}{2l_0^2}.$$

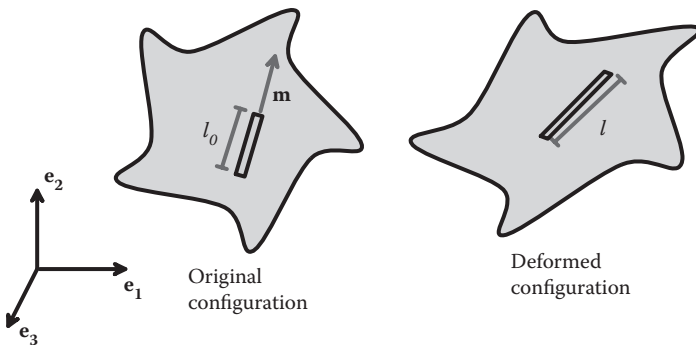


FIGURE 2.5 Deformation of a material fiber in a solid.

Note that this definition of strain is similar to the definition $\varepsilon = \delta l/l_0$ you are familiar with but contains an additional term. The additional term is negligible for small δl . Given the Lagrange strain components E_{ij} , the strain of the specimen may be computed from

$$\varepsilon_L(\mathbf{m}) = \mathbf{m} \cdot \mathbf{E} \cdot \mathbf{m} \text{ or } \varepsilon_L(m_i) = E_{ij}m_i m_j.$$

We proceed to derive this result. Note that

$$dx_i = l_0 m_i$$

is an infinitesimal vector with length and orientation of our undeformed specimen. From the preceding section, this vector is stretched and rotated to

$$dy_k = \left(\delta_{kj} + \frac{\partial u_k}{\partial x_j} \right) dx_j = \left(\delta_{kj} + \frac{\partial u_k}{\partial x_j} \right) l_0 m_j.$$

The length of the deformed specimen is equal to the length of dy , so we see that

$$\begin{aligned} l^2 &= dy_k dy_k = \left(\delta_{kj} + \frac{\partial u_k}{\partial x_j} \right) l_0 m_j \left(\delta_{ki} + \frac{\partial u_k}{\partial x_i} \right) l_0 m_i \\ &= \left(\delta_{ij} + \frac{\partial u_i}{\partial x_j} + \frac{\partial u_j}{\partial x_i} + \frac{\partial u_k}{\partial x_i} \frac{\partial u_k}{\partial x_j} \right) l_0^2 m_j m_i. \end{aligned}$$

Hence, the strain for our line element is

$$\varepsilon_L(m_i) = \frac{l^2 - l_0^2}{2l_0^2} = \frac{1}{2} \left(\frac{\partial u_i}{\partial x_j} + \frac{\partial u_j}{\partial x_i} + \frac{\partial u_k}{\partial x_j} \frac{\partial u_k}{\partial x_i} \right) m_i m_j,$$

giving the results stated.

2.1.6 Eulerian Strain Tensor

The Eulerian strain tensor is defined as

$$\mathbf{E}^* = \frac{1}{2}(\mathbf{I} - \mathbf{F}^{-T} \cdot \mathbf{F}^{-1}) \quad \text{or} \quad E_{ij}^* = \frac{1}{2}(\delta_{ij} - F_{ki}^{-1} F_{kj}^{-1}).$$

Its physical significance is similar to the Lagrange strain tensor, except that it enables you to compute the strain of an infinitesimal line element from its orientation *after* deformation. Specifically, suppose that \mathbf{n} denotes a unit vector parallel to the deformed material fiber, as shown in Figure 2.6. Then

$$\varepsilon_E(\mathbf{n}) = \frac{l^2 - l_0^2}{2l^2} = \mathbf{n} \cdot \mathbf{E}^* \cdot \mathbf{n} \quad \text{or} \quad \varepsilon_E(n_i) = E_{ij}^* n_i n_j.$$

The proof is left as an exercise.

2.1.7 Infinitesimal Strain Tensor

The infinitesimal strain tensor is defined as

$$\boldsymbol{\varepsilon} = \frac{1}{2}(\mathbf{u} \otimes \nabla + (\mathbf{u} \otimes \nabla)^T) \quad \text{or} \quad \varepsilon_{ij} = \frac{1}{2} \left(\frac{\partial u_i}{\partial x_j} + \frac{\partial u_j}{\partial x_i} \right),$$

where \mathbf{u} is the displacement vector. Written out in full,

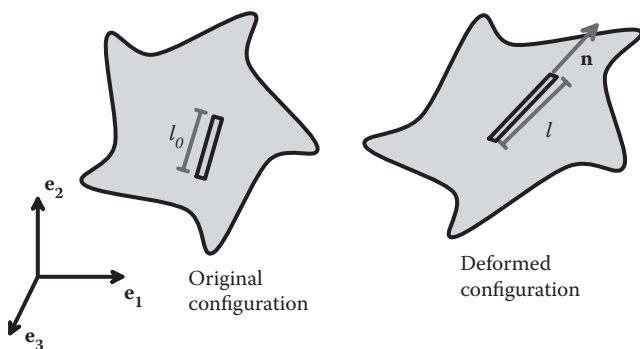


FIGURE 2.6 Deformation of a material fiber in a solid.

$$\boldsymbol{\varepsilon}_{ij} \equiv \begin{pmatrix} \frac{\partial u_1}{\partial x_1} & \frac{1}{2} \left(\frac{\partial u_1}{\partial x_2} + \frac{\partial u_2}{\partial x_1} \right) & \frac{1}{2} \left(\frac{\partial u_1}{\partial x_3} + \frac{\partial u_3}{\partial x_1} \right) \\ \frac{1}{2} \left(\frac{\partial u_2}{\partial x_1} + \frac{\partial u_1}{\partial x_2} \right) & \frac{\partial u_2}{\partial x_2} & \frac{1}{2} \left(\frac{\partial u_2}{\partial x_3} + \frac{\partial u_3}{\partial x_2} \right) \\ \frac{1}{2} \left(\frac{\partial u_3}{\partial x_1} + \frac{\partial u_1}{\partial x_3} \right) & \frac{1}{2} \left(\frac{\partial u_3}{\partial x_2} + \frac{\partial u_2}{\partial x_3} \right) & \frac{\partial u_3}{\partial x_3} \end{pmatrix}.$$

The infinitesimal strain tensor is an approximate deformation measure, which is only valid for small shape changes. It is more convenient than the Lagrange or Eulerian strain, because it is linear.

Specifically, suppose the deformation gradients are small, so that all $\delta u_i / \delta x_j \ll 1$. Then the Lagrange strain tensor is

$$E_{ij} = \frac{1}{2} \left(\frac{\partial u_i}{\partial x_j} + \frac{\partial u_j}{\partial x_i} + \frac{\partial u_k}{\partial x_j} + \frac{\partial u_k}{\partial x_i} \right) \approx \frac{1}{2} \left(\frac{\partial u_i}{\partial x_j} + \frac{\partial u_j}{\partial x_i} \right) \approx \boldsymbol{\varepsilon}_{ij},$$

so the infinitesimal strain approximates the Lagrange strain. You can show that it also approximates the Eulerian strain with the same accuracy.

The properties of the infinitesimal strain tensor include the following:

- For small strains, the engineering strain of an infinitesimal fiber aligned with a unit vector \mathbf{m} can be estimated as

$$\varepsilon_e(\mathbf{m}) = \frac{l - l_0}{l_0} \approx \varepsilon_{ij} m_i m_j.$$

- Note that

$$\text{trace}(\boldsymbol{\varepsilon}) \equiv \varepsilon_{kk} = \frac{\partial u_1}{\partial x_1} + \frac{\partial u_2}{\partial x_2} + \frac{\partial u_3}{\partial x_3} = \frac{dV - dV_0}{dV_0}.$$

For more details, see Section 2.1.9.

- The infinitesimal strain tensor is closely related to the strain matrix introduced in elementary strength of materials courses. For example, the physical significance of the (2D) strain matrix

$$\begin{bmatrix} \varepsilon_{11} & \gamma_{12} \\ \gamma_{21} & \varepsilon_{22} \end{bmatrix}$$

is illustrated in Figure 2.7.

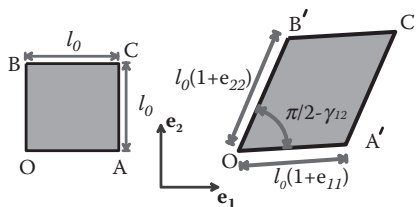


FIGURE 2.7 Plane deformation of an area element in a solid, showing definition of engineering strain measures.

To relate this to the infinitesimal strain tensor, let $\{\mathbf{e}_1, \mathbf{e}_2, \mathbf{e}_3\}$ be a Cartesian basis, with \mathbf{e}_1 parallel to x and \mathbf{e}_2 parallel to y as shown. Let ε_{ij} denote the components of the infinitesimal strain tensor in this basis. Then

$$\begin{aligned}\varepsilon_{11} &= \varepsilon_{xx} \\ \varepsilon_{22} &= \varepsilon_{yy} \\ \varepsilon_{12} = \varepsilon_{21} &= \gamma_{xy} / 2 = \gamma_{yx} / 2.\end{aligned}$$

2.1.8 Engineering Shear Strains

For a general strain tensor (which could be any of \mathbf{E} , \mathbf{E}^* or $\boldsymbol{\varepsilon}$, among others), the diagonal strain components ε_{11} , ε_{22} , ε_{33} are known as “direct” strains, whereas the off-diagonal terms $\varepsilon_{12} = \varepsilon_{21}$, $\varepsilon_{13} = \varepsilon_{31}$, $\varepsilon_{23} = \varepsilon_{32}$ are known as “shear” strains.

The shear strains are sometimes reported as “engineering shear strains,” which are related to the formal definition by a factor of 2, i.e.,

$$\gamma_{12} = 2\varepsilon_{12}, \quad \gamma_{13} = 2\varepsilon_{13}, \quad \gamma_{23} = 2\varepsilon_{23}.$$

This factor of 2 is an endless source of confusion. Whenever someone reports shear strain to you, be sure to check which definition they are using. In particular, many commercial finite element codes output engineering shear strains.

2.1.9 Decomposition of Infinitesimal Strain into Volumetric and Deviatoric Parts

The *volumetric infinitesimal strain* is defined as $\text{trace}(\boldsymbol{\varepsilon}) \equiv \varepsilon_{kk}$. The *deviatoric infinitesimal strain* is defined as

$$\mathbf{e} = \boldsymbol{\varepsilon} - \frac{1}{3} \mathbf{I} \text{trace}(\boldsymbol{\varepsilon}) \equiv e_{ij} = \varepsilon_{ij} - \frac{1}{3} \delta_{ij} \varepsilon_{kk}.$$

The volumetric strain is a measure of volume changes and, for small strains, is related to the Jacobian of the deformation gradient by $\varepsilon_{kk} \approx J - 1$. To see this, recall that

$$J = \det \begin{bmatrix} 1 + \frac{\partial u_1}{\partial x_1} & \frac{\partial u_1}{\partial x_2} & \frac{\partial u_1}{\partial x_3} \\ \frac{\partial u_2}{\partial x_1} & 1 + \frac{\partial u_2}{\partial x_2} & \frac{\partial u_2}{\partial x_3} \\ \frac{\partial u_3}{\partial x_1} & \frac{\partial u_3}{\partial x_2} & 1 + \frac{\partial u_3}{\partial x_3} \end{bmatrix} \approx \left(1 + \frac{\partial u_1}{\partial x_1}\right) \left(1 + \frac{\partial u_2}{\partial x_2}\right) \left(1 + \frac{\partial u_3}{\partial x_3}\right) \approx 1 + \frac{\partial u_1}{\partial x_1} + \frac{\partial u_2}{\partial x_2} + \frac{\partial u_3}{\partial x_3}.$$

The deviatoric strain is a measure of shear deformation (shear deformation involves no volume change).

2.1.10 Infinitesimal Rotation Tensor

The infinitesimal rotation tensor is defined as

$$\mathbf{w} = \frac{1}{2} (\mathbf{u} \nabla - (\mathbf{u} \nabla)^T) \quad \text{or} \quad w_{ij} = \frac{1}{2} \left(\frac{\partial u_i}{\partial x_j} - \frac{\partial u_j}{\partial x_i} \right).$$

Written out as a matrix, the components of w_{ij} are

$$w_{ij} \equiv \begin{bmatrix} 0 & \frac{1}{2} \left(\frac{\partial u_1}{\partial x_2} - \frac{\partial u_2}{\partial x_1} \right) & \frac{1}{2} \left(\frac{\partial u_1}{\partial x_3} - \frac{\partial u_3}{\partial x_1} \right) \\ \frac{1}{2} \left(\frac{\partial u_2}{\partial x_1} - \frac{\partial u_1}{\partial x_2} \right) & 0 & \frac{1}{2} \left(\frac{\partial u_2}{\partial x_3} - \frac{\partial u_3}{\partial x_2} \right) \\ \frac{1}{2} \left(\frac{\partial u_3}{\partial x_1} - \frac{\partial u_1}{\partial x_3} \right) & \frac{1}{2} \left(\frac{\partial u_3}{\partial x_2} - \frac{\partial u_2}{\partial x_3} \right) & 0 \end{bmatrix}.$$

Observe that w_{ij} is *skew symmetric*: $w_{ij} = -w_{ji}$.

A skew tensor represents a rotation through a small angle. Specifically, the operation $dy_i = (\delta_{ij} + w_{ij})dx_j$ rotates the infinitesimal line element dx_j through a small angle $\theta = \sqrt{w_{ij}w_{ji}}/2$ about an axis parallel to the unit vector $n_i = \epsilon_{ijk} w_{kj}/(2\theta)$. (A skew tensor also sometimes represents an angular velocity.) To visualize the significance of w_{ij} , consider the behavior of an imaginary, infinitesimal, tensile specimen embedded in a deforming solid. The specimen is stretched and then rotated through an angle ϕ about some axis \mathbf{q} (Figure 2.8). If the displacement gradients are small, then $\phi \ll 1$. The rotation of the specimen depends on its original orientation, represented by the unit vector \mathbf{m} . One can show (although one would rather not do all the algebra) that w_{ij} represents the average rotation, over all possible orientations of \mathbf{m} , of material fibers passing through a point.

As a final remark, we note that a general deformation can always be decomposed into an infinitesimal strain and rotation:

$$\frac{\partial u_i}{\partial x_j} = \frac{1}{2} \left(\frac{\partial u_i}{\partial x_j} + \frac{\partial u_j}{\partial x_i} \right) + \frac{1}{2} \left(\frac{\partial u_i}{\partial x_j} - \frac{\partial u_j}{\partial x_i} \right) = \epsilon_{ij} + w_{ij}.$$

Physically, this sum of ϵ_{ij} and w_{ij} can be regarded as representing two successive deformations: a small strain, followed by a rotation, in the sense that

$$dy_i = (\delta_{ik} + w_{ik})(\delta_{kj} + \epsilon_{kj})dx_j \approx dx_i + (\epsilon_{ij} + w_{ij})dx_j$$

first stretches the infinitesimal line element and then rotates it.

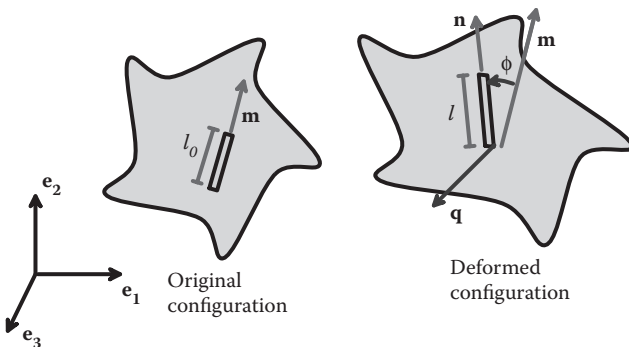


FIGURE 2.8 Rotation and extension of a material fiber in a solid.

2.1.11 Principal Values and Directions of the Infinitesimal Strain Tensor

The three principal values e_i and directions $\mathbf{n}^{(i)}$ of the infinitesimal strain tensor satisfy

$$\boldsymbol{\epsilon} \cdot \mathbf{n}^{(i)} = e_i \mathbf{n}^{(i)}$$

$$\text{or } \epsilon_{kl} n_l^{(i)} = e_i n_k^{(i)}$$

Clearly, e_i and $\mathbf{n}^{(i)}$ are the eigenvalues and eigenvectors of $\boldsymbol{\epsilon}$. There are three principal strains and three principal directions, which are always mutually perpendicular.

Their significance can be visualized as follows:

1. Note that the decomposition $\frac{\partial u_i}{\partial x_j} = \epsilon_{ij} + w_{ij}$ can be visualized as a small strain, followed by a small rigid rotation, as shown in Figure 2.9.
2. The formula $\boldsymbol{\epsilon} \cdot \mathbf{n}^{(i)} = e_i \mathbf{n}^{(i)}$ indicates that a vector \mathbf{n} is mapped to another, parallel vector by the strain.

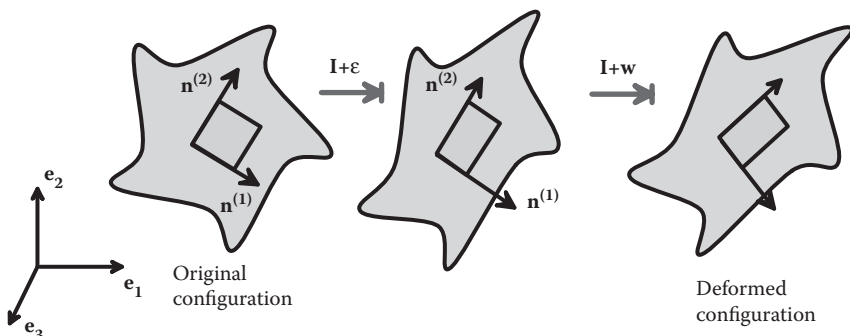


FIGURE 2.9 Decomposition of an infinitesimal strain into a stretch and a rotation.

3. Thus, if you draw a small cube with its faces perpendicular to $\mathbf{n}^{(i)}$ on the undeformed solid, this cube will be stretched perpendicular to each face, with a fractional increase in length $e_i = \delta l_i / l_0$. The faces remain perpendicular to $\mathbf{n}^{(i)}$ after deformation.
4. Finally, \mathbf{w} rotates the small cube through a small angle onto its configuration in the deformed solid.

2.1.12 Cauchy–Green Deformation Tensors

There are two Cauchy–Green deformation tensors, defined through the following:

- The right Cauchy–Green deformation tensor: $\mathbf{C} = \mathbf{F}^T \cdot \mathbf{F}$ $C_{ij} = F_{ki} F_{kj}$.
- The left Cauchy–Green deformation tensor: $\mathbf{B} = \mathbf{F} \cdot \mathbf{F}^T$ $B_{ij} = F_{ik} F_{jk}$.

They are called “left” and “right” tensors because of their relation to the “left” and “right” stretch tensors defined below. They can be regarded as quantifying the squared length of infinitesimal fibers in the deformed configuration by noting that, if a material fiber $d\mathbf{x} = l_0 \mathbf{m}$ in the undeformed solid is stretched and rotated to $d\mathbf{y} = l\mathbf{n}$ in the deformed solid, then

$$\frac{l^2}{l_0^2} = \mathbf{m} \cdot \mathbf{C} \cdot \mathbf{m} \quad \frac{l_0^2}{l^2} = \mathbf{n} \cdot \mathbf{B}^{-1} \cdot \mathbf{n}.$$

2.1.13 Rotation Tensor and Left and Right Stretch Tensors

The definitions of these quantities are as follows:

- The right stretch tensor:

$$\mathbf{U} = \mathbf{C}^{1/2} = (\mathbf{F}^T \cdot \mathbf{F})^{1/2} \quad U_{ij} = C_{ij}^{1/2}.$$

- The left stretch tensor:

$$\mathbf{V} = \mathbf{B}^{1/2} \quad V_{ij} = B_{ij}^{1/2}.$$

- The rotation tensor:

$$\mathbf{R} = \mathbf{F} \cdot \mathbf{U}^{-1} = \mathbf{V}^{-1} \cdot \mathbf{F} \quad R_{ij} = F_{ik} U_{kj}^{-1} = V_{ik}^{-1} F_{kj}.$$

To calculate these quantities, you need to remember how to calculate the square root of a matrix. For example, to calculate the square root of \mathbf{C} , you must do the following:

1. Calculate the eigenvalues of \mathbf{C} ; we will call these λ_n^2 , with $n = 1, 2, 3$. Because \mathbf{C} and \mathbf{B} are both symmetric and positive definite, the eigenvalues λ_n^2 are all

28 ■ Applied Mechanics of Solids

positive real numbers, and therefore their square roots λ_n are also positive real numbers.

2. Calculate the eigenvectors of \mathbf{C} and normalize them so they have unit magnitude. We will denote the eigenvectors by $\mathbf{c}^{(n)}$. They must be normalized to satisfy $\mathbf{c}^{(n)} \cdot \mathbf{c}^{(n)} = 1$.
3. Finally, calculate $\mathbf{C}^{1/2} = \sum_{n=1}^3 \lambda_n \mathbf{c}^{(n)} \otimes \mathbf{c}^{(n)}$, where \otimes denotes a dyadic product (see Appendix B). In components, this can be written $C_{ij}^{1/2} = \sum_{n=1}^3 \lambda_n c_i^{(n)} c_j^{(n)}$.
4. As an additional bonus, you can quickly compute the inverse square root (which is needed to find \mathbf{R}) as $\mathbf{C}^{-1/2} = \sum_{n=1}^3 \frac{1}{\lambda_n} \mathbf{c}^{(n)} \otimes \mathbf{c}^{(n)}$ or $C_{ij}^{-1/2} = \sum_{n=1}^3 \frac{1}{\lambda_n} c_i^{(n)} c_j^{(n)}$.

To see the physical significance of these tensors, observe the following:

1. The definition of the rotation tensor shows that

$$\begin{aligned}\mathbf{R} &= \mathbf{F} \cdot \mathbf{U}^{-1} \Leftrightarrow \mathbf{F} = \mathbf{R} \cdot \mathbf{U} \\ \mathbf{R} &= \mathbf{V}^{-1} \cdot \mathbf{F} \Leftrightarrow \mathbf{F} = \mathbf{V} \cdot \mathbf{R}.\end{aligned}$$

2. The multiplicative decomposition of a constant tensor $\mathbf{F} = \mathbf{R} \cdot \mathbf{U}$ can be regarded as a sequence of two homogeneous deformations: \mathbf{U} , followed by \mathbf{R} . Similarly, $\mathbf{F} = \mathbf{V} \cdot \mathbf{R}$ is \mathbf{R} followed by \mathbf{V} .
3. \mathbf{R} is proper orthogonal (it satisfies $\mathbf{R} \cdot \mathbf{R}^T = \mathbf{R}^T = \mathbf{I}$ and $\det(\mathbf{R}) = 1$) and therefore represents a rotation. To see this, note that \mathbf{U} is symmetric and therefore satisfies $\mathbf{U}^{-T} = \mathbf{U}^{-1}$, so that

$$\begin{aligned}\mathbf{R}^T \cdot \mathbf{R} &= (\mathbf{F} \cdot \mathbf{U}^{-1})^T \cdot (\mathbf{F} \cdot \mathbf{U}^{-1}) \\ &= \mathbf{U}^{-T} \cdot \mathbf{F}^T \cdot \mathbf{F} \cdot \mathbf{U}^{-1} \\ &= \mathbf{U}^{-1} \cdot \mathbf{U}^2 \cdot \mathbf{U}^{-1} = \mathbf{I}\end{aligned}$$

and $\det(\mathbf{R}) = \det(\mathbf{F})\det(\mathbf{U}^{-1}) = 1$.

4. \mathbf{U} can be expressed in the form

$$\mathbf{U} = \lambda_1 \mathbf{u}^{(1)} \otimes \mathbf{u}^{(1)} + \lambda_2 \mathbf{u}^{(2)} \otimes \mathbf{u}^{(2)} + \lambda_3 \mathbf{u}^{(3)} \otimes \mathbf{u}^{(3)}$$

where $\mathbf{u}^{(i)}$ are the three (mutually perpendicular) eigenvectors of \mathbf{U} . (By construction, these are identical to the eigenvectors of \mathbf{C} .) If we interpret $\mathbf{u}^{(i)}$ as basis vectors, we see that \mathbf{U} is *diagonal* in this basis and so corresponds to stretching parallel to each basis vector, as shown in Figure 2.10.

The decompositions $\mathbf{F} = \mathbf{R} \cdot \mathbf{U}$ and $\mathbf{F} = \mathbf{V} \cdot \mathbf{R}$ are known as the right and left polar decomposition of \mathbf{F} . (The right and left refer to the positions of \mathbf{U} and \mathbf{V} .) They show that every homogeneous deformation can be decomposed into a stretch followed by a rigid rotation or, equivalently, into a rigid rotation followed by a stretch. The decomposition is discussed in more detail in the next section.

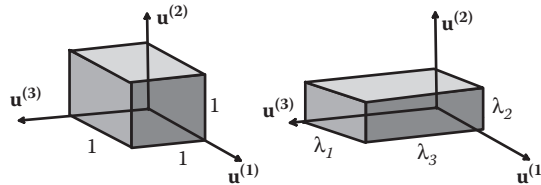


FIGURE 2.10 The deformation characterized by the right stretch tensor.

2.1.14 Principal Stretches

The principal stretches can be calculated from any one of the following (they all give the same answer):

1. The eigenvalues of the right stretch tensor \mathbf{U} .
2. The eigenvalues of the left stretch tensor \mathbf{V} .
3. The square root of the eigenvalues of the right Cauchy–Green tensor \mathbf{C} .
4. The square root of the eigenvalues of the left Cauchy–Green tensor \mathbf{B} .
5. The principal stretches are also related to the eigenvalues of the Lagrange and Eulerian strains. The details are left as an exercise.

There are two sets of principal stretch directions, associated with the undeformed and deformed solids.

1. The principal stretch directions in the *undeformed* solid are the (normalized) eigenvectors of \mathbf{U} or \mathbf{C} . Denote these by $\mathbf{u}^{(i)}$.
2. The principal stretch directions in the *deformed* solid are the (normalized) eigenvectors of \mathbf{V} or \mathbf{B} . Denote these by $\mathbf{v}^{(i)}$.

To visualize the physical significance of principal stretches and their directions, note that a deformation can be decomposed as $\mathbf{F} = \mathbf{R} \cdot \mathbf{U}$ into a sequence of a stretch followed by a rotation.

Note also the following:

1. The principal directions $\mathbf{u}^{(i)}$ are mutually perpendicular. You could draw a little cube on the undeformed solid with faces perpendicular to these directions, as shown in Figure 2.11.
2. The stretch \mathbf{U} will stretch the cube by an amount λ_i parallel to each $\mathbf{u}^{(i)}$. The faces of the stretched cube remain perpendicular to $\mathbf{u}^{(i)}$.
3. The rotation \mathbf{R} will rotate the stretched cube so that the directions $\mathbf{u}^{(i)}$ rotate to line up with $\mathbf{v}^{(i)}$.
4. The faces of the deformed cube are perpendicular to $\mathbf{v}^{(i)}$.

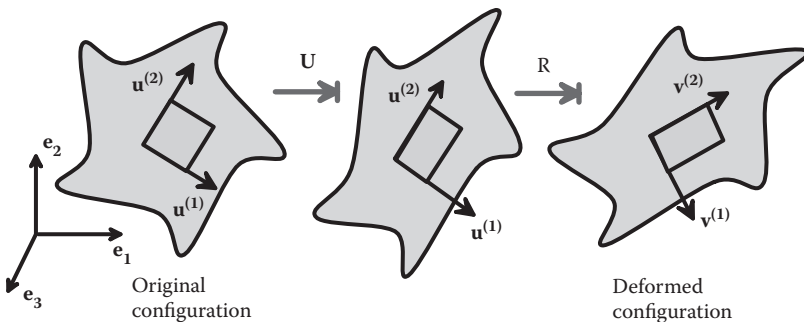


FIGURE 2.11 Decomposition of the deformation gradient into a stretch, followed by a rotation

The decomposition $\mathbf{F} = \mathbf{V} \cdot \mathbf{R}$ can be visualized in much the same way. In this case, the directions $\mathbf{u}^{(i)}$ are first rotated to coincide with $\mathbf{v}^{(i)}$. The cube is then stretched parallel to each $\mathbf{v}^{(i)}$ to produce the same shape change.

We could compare the undeformed and deformed cubes by placing them side by side, with the vectors $\mathbf{v}^{(i)}$ and $\mathbf{u}^{(i)}$ parallel, as shown in Figure 2.12.

2.1.15 Generalized Strain Measures

The polar decompositions $\mathbf{F} = \mathbf{V} \cdot \mathbf{R}$ and $\mathbf{F} = \mathbf{U} \cdot \mathbf{V}$ provide a way to define additional strain measures. Let λ_i denote the principal stretches and let $\mathbf{u}^{(i)}$ and $\mathbf{v}^{(i)}$ denote the normalized eigenvectors of \mathbf{U} and \mathbf{V} . Then one could define strain tensors through

$$\begin{aligned} \text{Lagrangian nominal strain: } & \sum_{i=1}^3 (\lambda_i - 1) \mathbf{u}^{(i)} \otimes \mathbf{u}^{(i)} \\ \text{Lagrangian logarithmic strain: } & \sum_{i=1}^3 \log(\lambda_i) \mathbf{u}^{(i)} \otimes \mathbf{u}^{(i)} \end{aligned}$$

The corresponding Eulerian strain measures are

$$\begin{aligned} \text{Eulerian nominal strain: } & \sum_{i=1}^3 (\lambda_i - 1) \mathbf{v}^{(i)} \otimes \mathbf{v}^{(i)} \\ \text{Eulerian logarithmic strain: } & \sum_{i=1}^3 \log(\lambda_i) \mathbf{v}^{(i)} \otimes \mathbf{v}^{(i)} \end{aligned}$$

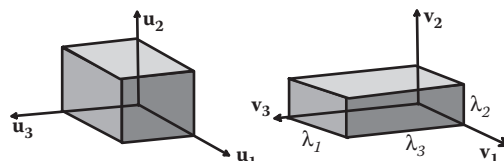


FIGURE 2.12 The deformation characterized by the left stretch tensor.

Another strain measure can be defined as

$$\text{Green's strain: } \mathbf{E}_G = \sum_{i=1}^3 \frac{1}{2} (\lambda_i^2 - 1) \mathbf{v}^{(i)} \otimes \mathbf{v}^{(i)}.$$

This can be computed directly from the deformation gradient as

$$\mathbf{E}_G = \frac{1}{2} (\mathbf{F} \cdot \mathbf{F}^T - \mathbf{I})$$

and is very similar to the Lagrangean strain tensor, except that its principal directions are rotated through the rigid rotation \mathbf{R} .

2.1.16 The Velocity Gradient

We now list several measures of the *rate* of deformation. The velocity gradient is the basic measure of deformation rate and is defined as

$$\mathbf{L} = \mathbf{v} \otimes \nabla_y \equiv L_{ij} = \frac{\partial v_i}{\partial y_j}.$$

It quantifies the relative velocities of two material particles at positions \mathbf{y} and $\mathbf{y} + d\mathbf{y}$ in the deformed solid, in the sense that

$$dv_i = v_i(\mathbf{y} + d\mathbf{y}) - v_i(\mathbf{y}) = \frac{\partial v_i}{\partial y_j} dy_j.$$

The velocity gradient can be expressed in terms of the deformation gradient and its time derivative as

$$\mathbf{v} \otimes \nabla_y = \dot{\mathbf{F}} \cdot \mathbf{F}^{-1} \quad \frac{\partial v_i}{\partial y_j} = \dot{F}_{ik} F_{kj}^{-1}.$$

To see this, note that

$$dv_i = \frac{d}{dt} dy_i = \frac{d}{dt} (F_{ij} dx_j) = \dot{F}_{ij} dx_j$$

and recall that $dy_j = F_{ji} dx_i \Rightarrow dx_j = F_{jk}^{-1} dy_k$, so that

$$dv_i = \dot{F}_{ij} F_{jk}^{-1} dy_k.$$

2.1.17 Stretch Rate and Spin Tensors

The stretch rate tensor is defined as $\mathbf{D} = (\mathbf{L} + \mathbf{L}^T)/2$, or, in index notation, $D_{ij} = (L_{ij} + L_{ji}) / 2$. The spin tensor is defined as $\mathbf{W} = (\mathbf{L} - \mathbf{L}^T)/2$ or $W_{ij} = (L_{ij} - L_{ji}) / 2$.

A general velocity gradient can be decomposed into the sum of stretch rate and spin, as

$$\mathbf{L} = \mathbf{D} + \mathbf{W} \quad L_{ij} = D_{ij} + W_{ij}.$$

The stretch rate quantifies the rate of stretching of a material fiber in the deformed solid, in the sense that

$$\frac{1}{l} \frac{dl}{dt} = \mathbf{n} \cdot \mathbf{D} \cdot \mathbf{n} = n_i D_{ij} n_j$$

is the rate of stretching of a material fiber with length l and orientation \mathbf{n} in the deformed solid, as shown in Figure 2.13. To see this, let $d\mathbf{y} = l\mathbf{n}$, so that

$$\frac{d}{dt} d\mathbf{y} = \frac{dl}{dt} \mathbf{n} + l \frac{d\mathbf{n}}{dt}.$$

By definition,

$$\frac{d}{dt} d\mathbf{y} = \frac{d}{dt} (\mathbf{F} \cdot d\mathbf{x}) = \dot{\mathbf{F}} \cdot d\mathbf{x} = \dot{\mathbf{F}} \cdot (\mathbf{F}^{-1} d\mathbf{y}) = \dot{\mathbf{F}} \cdot \mathbf{F}^{-1} \cdot d\mathbf{y} = \mathbf{L} \cdot d\mathbf{y} = (\mathbf{D} + \mathbf{W}) \cdot l\mathbf{n}.$$

Hence,

$$(\mathbf{D} + \mathbf{W}) \cdot l\mathbf{n} = \frac{dl}{dt} \mathbf{n} + l \frac{d\mathbf{n}}{dt}.$$

Finally, take the dot product of both sides with \mathbf{n} . Note that, because \mathbf{n} is a unit vector, $d\mathbf{n} / dt$ must be perpendicular to \mathbf{n} and therefore $\mathbf{n} \cdot d\mathbf{n} / dt = 0$. Note also that $\mathbf{n} \cdot \mathbf{W} \cdot \mathbf{n} = 0$, because \mathbf{W} is skew symmetric. It is easiest to show this using index notation:

$$n_i W_{ij} n_j = n_i (L_{ij} - L_{ji}) n_j / 2 = 0.$$

Therefore,

$$\mathbf{n} \cdot (\mathbf{D} + \mathbf{W}) \cdot l\mathbf{n} = \frac{dl}{dt} \mathbf{n} \cdot \mathbf{n} + l \mathbf{n} \cdot \frac{d\mathbf{n}}{dt} \Rightarrow \mathbf{n} \cdot \mathbf{D} \cdot l\mathbf{n} = \frac{dl}{dt}.$$

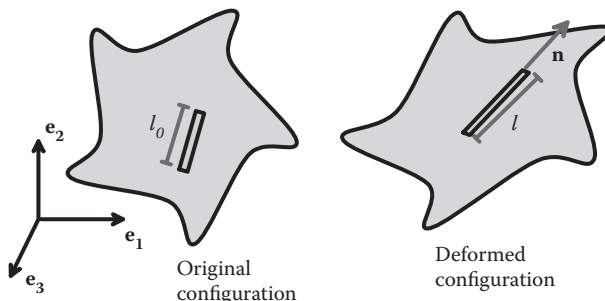


FIGURE 2.13 Deformation of a material fiber in a solid.

The spin tensor \mathbf{W} can be shown to provide a measure of the average angular velocity of all material fibers passing through a material point.

2.1.18 Infinitesimal Strain Rate and Rotation Rate

For *small strains*, the rate of deformation tensor can be approximated by the infinitesimal strain rate, whereas the spin can be approximated by the time derivative of the infinitesimal rotation tensor:

$$\frac{d}{dt} \boldsymbol{\epsilon} = \frac{d}{dt} \frac{1}{2} (\mathbf{u} \otimes \nabla + (\mathbf{u} \otimes \nabla)^T) \approx \mathbf{D} \quad \text{or} \quad \dot{\epsilon}_{ij} \approx D_{ij}$$

$$\frac{d}{dt} \mathbf{w} = \frac{d}{dt} \frac{1}{2} (\mathbf{u} \otimes \nabla - (\mathbf{u} \otimes \nabla)^T) \approx \mathbf{W} \quad \text{or} \quad \dot{w}_{ij} \approx W_{ij}.$$

Similarly, you can show that

$$\frac{d}{dt} \frac{\partial u_i}{\partial x_j} = \dot{F}_{ij} = \dot{\epsilon}_{ij} + \dot{w}_{ij} \approx L_{ij}.$$

2.1.19 Other Deformation Rate Measures

The rate of deformation tensor can be related to time derivatives of other strain measures. For example, the time derivative of the Lagrange strain tensor can be shown to be

$$\frac{d\mathbf{E}}{dt} = \mathbf{F}^T \cdot \mathbf{D} \cdot \mathbf{F} \quad \dot{E}_{ij} = F_{ki} D_{kl} F_{lj}.$$

Other useful results are as follows:

- For a pure rotation, $\dot{\mathbf{R}} \cdot \mathbf{R}^T + \mathbf{R} \cdot \dot{\mathbf{R}}^T = \mathbf{0}$ or, equivalently, $\dot{\mathbf{R}} \cdot \mathbf{R}^T = -(\dot{\mathbf{R}} \cdot \mathbf{R}^T)^T$. To see this, recall that $\mathbf{R} \cdot \mathbf{R}^T = \mathbf{I}$ and evaluate the time derivative.
- If the deformation gradient is decomposed into a stretch followed by a rotation as $\mathbf{F} = \mathbf{R} \cdot \mathbf{U}$, then $\mathbf{D} = \mathbf{R} \cdot (\dot{\mathbf{U}} \cdot \mathbf{U}^{-1} + \mathbf{U}^{-1} \cdot \dot{\mathbf{U}}) \cdot \mathbf{R}^T / 2$ and $\mathbf{W} = \dot{\mathbf{R}} \cdot \mathbf{R}^T + \mathbf{R} \cdot (\dot{\mathbf{U}} \cdot \mathbf{U}^{-1} - \mathbf{U}^{-1} \cdot \dot{\mathbf{U}}) \cdot \mathbf{R}^T / 2$.
- The trace of \mathbf{D} is a measure of rate of change of volume. To see this, note that

$$\frac{dJ}{dt} = \frac{dJ}{dF_{ij}} \frac{dF_{ij}}{dt} = J F_{ji}^{-1} \dot{F}_{ij} = J L_{ii} = J D_{ii}.$$

For small strains, the rate of change of Lagrangian strain \mathbf{E} is approximately equal to the rate of change of infinitesimal strain:

$$\frac{d\mathbf{E}}{dt} \approx \frac{d}{dt} \boldsymbol{\epsilon} \quad \dot{E}_{ij} \approx \frac{d}{dt} \epsilon_{ij}.$$

2.1.20 Strain Equations of Compatibility for Infinitesimal Strains

It is sometimes necessary to *invert* the relations between strain and displacement, that is to say, given the strain field, to compute the displacements. In this section, we outline how this is done, for the special case of *infinitesimal deformations*.

For infinitesimal motions, the relation between strain and displacement is

$$\epsilon_{ij} = \frac{1}{2} \left(\frac{\partial u_i}{\partial x_j} + \frac{\partial u_j}{\partial x_i} \right).$$

Given the six strain components ϵ_{ij} (six, because $\epsilon_{ij} = \epsilon_{ji}$), we want to determine the three displacement components u_i . First, note that we can never completely recover the displacement field that gives rise to a particular strain field. Any rigid motion produces no strain, so the displacements can only be completely determined if there is some additional information (besides the strain) that will tell us how much the solid has rotated and translated. However, integrating the strain field can tell us the displacement field to within an arbitrary rigid motion.

Second, we need to be sure that the strain-displacement relations can be integrated at all. The strain is a symmetric second-order tensor field, but not all symmetric second-order tensor fields can be strain fields. The strain-displacement relations amount to a system of six scalar differential equations for the three displacement components u_i .

To be integrable, the strains must satisfy the *compatibility conditions*, which may be expressed as

$$\epsilon_{ipm} \epsilon_{jqn} \frac{\partial^2 \epsilon_{mn}}{\partial x_p \partial x_q} = 0,$$

or, equivalently,

$$\frac{\partial^2 \epsilon_{ij}}{\partial x_k \partial x_l} + \frac{\partial^2 \epsilon_{kl}}{\partial x_i \partial x_j} - \frac{\partial^2 \epsilon_{il}}{\partial x_j \partial x_k} - \frac{\partial^2 \epsilon_{jk}}{\partial x_i \partial x_l} = 0,$$

or, once more equivalently,

$$\begin{aligned} \frac{\partial^2 \epsilon_{11}}{\partial x_2^2} + \frac{\partial^2 \epsilon_{22}}{\partial x_1^2} - 2 \frac{\partial^2 \epsilon_{12}}{\partial x_1 \partial x_2} &= 0 & \frac{\partial^2 \epsilon_{11}}{\partial x_2 \partial x_3} - \frac{\partial}{\partial x_1} \left(-\frac{\partial \epsilon_{23}}{\partial x_1} + \frac{\partial \epsilon_{31}}{\partial x_2} + \frac{\partial \epsilon_{12}}{\partial x_3} \right) &= 0 \\ \frac{\partial^2 \epsilon_{11}}{\partial x_3^2} + \frac{\partial^2 \epsilon_{33}}{\partial x_1^2} - 2 \frac{\partial^2 \epsilon_{13}}{\partial x_1 \partial x_3} &= 0 & \frac{\partial^2 \epsilon_{22}}{\partial x_3 \partial x_1} - \frac{\partial}{\partial x_2} \left(-\frac{\partial \epsilon_{31}}{\partial x_2} + \frac{\partial \epsilon_{12}}{\partial x_3} + \frac{\partial \epsilon_{23}}{\partial x_1} \right) &= 0 \\ \frac{\partial^2 \epsilon_{22}}{\partial x_3^2} + \frac{\partial^2 \epsilon_{33}}{\partial x_2^2} - 2 \frac{\partial^2 \epsilon_{23}}{\partial x_2 \partial x_3} &= 0 & \frac{\partial^2 \epsilon_{33}}{\partial x_1 \partial x_2} - \frac{\partial}{\partial x_3} \left(-\frac{\partial \epsilon_{12}}{\partial x_3} + \frac{\partial \epsilon_{23}}{\partial x_1} + \frac{\partial \epsilon_{31}}{\partial x_2} \right) &= 0. \end{aligned}$$

It is easy to show that all strain fields must satisfy these conditions; you simply need to substitute for the strains in terms of displacements and show that the appropriate equation is satisfied. For example,

$$\frac{\partial^2 \varepsilon_{11}}{\partial x_2^2} + \frac{\partial^2 \varepsilon_{22}}{\partial x_1^2} - 2 \frac{\partial^2 \varepsilon_{12}}{\partial x_1 \partial x_2} = \frac{\partial^4 u_1}{\partial x_1 \partial x_2^2} + \frac{\partial^4 u_2}{\partial x_2 \partial x_1^2} - 2 \frac{\partial^2}{\partial x_1 \partial x_2} \left(\frac{\partial u_1}{\partial x_2} + \frac{\partial u_2}{\partial x_1} \right) = 0$$

and similarly for the other expressions. Note that, for planar problems for which $\varepsilon_{13} = \varepsilon_{23} = 0$ and $\frac{d\varepsilon_{ij}}{dx_3} = 0$, all of these compatibility equations are satisfied trivially, with the exception of the first: $\frac{\partial^2 \varepsilon_{11}}{\partial x_2^2} + \frac{\partial^2 \varepsilon_{22}}{\partial x_1^2} - 2 \frac{\partial^2 \varepsilon_{12}}{\partial x_1 \partial x_2} = 0$. The following can be shown:

1. If the strains do not satisfy the equations of compatibility, then a displacement vector cannot be integrated from the strains.
2. If the strains satisfy the compatibility equations and the solid is *simply connected* (i.e., it contains no holes that go all the way through its thickness), then a displacement vector can be integrated from the strains.
3. If the solid is not simply connected, a displacement vector can be calculated, but it may not be *single valued*; i.e., you may get different solutions depending on how the path of integration encircles the holes.

Now, let us return to the question posed at the beginning of this section. Given the strains, how do we compute the displacements?

For two dimensions (plane stress or plane strain), the procedure is quite simple and is best illustrated by working through a specific case. As a representative example, we will use the strain field in a 2D (plane stress) cantilever beam with Young's modulus E and Poisson's ratio ν loaded at one end by a force P , as shown in Figure 2.14. The beam has a rectangular cross section with height $2a$ and out-of-plane width b . We will show later (Section 5.2.4) that the strain field in the beam is

$$\varepsilon_{11} = 2Cx_1x_2, \quad \varepsilon_{22} = -2\nu Cx_1x_2, \quad \varepsilon_{12} = (1+\nu)C(a^2 - x_2^2), \quad C = \frac{3P}{4Ea^3b}.$$

We first check that the strain is compatible. For 2D problems, this requires

$$\frac{\partial^2 \varepsilon_{11}}{\partial x_2^2} + \frac{\partial^2 \varepsilon_{22}}{\partial x_1^2} - 2 \frac{\partial^2 \varepsilon_{12}}{\partial x_1 \partial x_2} = 0,$$

which is clearly satisfied in this case.

For a 2D problem, we only need to determine $u_1(x_1, x_2)$ and $u_2(x_1, x_2)$ such that

$$\frac{\partial u_1}{\partial x_1} = \varepsilon_{11}, \quad \frac{\partial u_2}{\partial x_2} = \varepsilon_{22}, \quad \text{and} \quad \frac{\partial u_1}{\partial x_2} + \frac{\partial u_2}{\partial x_1} = 2\varepsilon_{12}.$$

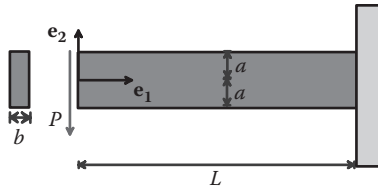


FIGURE 2.14 End-loaded cantilever beam.

The first two of these give

$$\varepsilon_{11} = \frac{\partial u_1}{\partial x_1} = 2Cx_1x_2 \quad \varepsilon_{22} = \frac{\partial u_2}{\partial x_2} = 2\nu Cx_1x_2.$$

We can integrate the first equation with respect to x_1 and the second equation with respect to x_2 to get

$$u_1 = Cx_1^2x_2 + f_1(x_2) \quad u_2 = -\nu Cx_1x_2^2 + f_2(x_1),$$

where $f_1(x_2)$ and $f_2(x_1)$ are two functions of x_2 and x_1 , respectively, which are yet to be determined. We can find these functions by substituting the formulas for $u_1(x_1, x_2)$ and $u_2(x_1, x_2)$ into the expression for shear strain

$$\begin{aligned} \varepsilon_{12} &= \frac{1}{2} \left(\frac{\partial u_1}{\partial x_2} + \frac{\partial u_2}{\partial x_1} \right) = (1+\nu)C(a^2 - x_2^2) \\ &\Rightarrow \frac{1}{2} \left(Cx_1^2 - \nu Cx_2^2 + \frac{df_1}{dx_2} + \frac{df_2}{dx_1} \right) = (1+\nu)C(a^2 - x_2^2). \end{aligned}$$

We can rewrite this as

$$\left(\frac{df_2}{dx_1} + Cx_1^2 \right) + \left(\frac{df_1}{dx_2} - \nu Cx_2^2 - 2(1+\nu)C(a^2 - x_2^2) \right) = 0.$$

The two terms in parentheses are functions of x_1 and x_2 , respectively. Because the left-hand side must vanish for all values of x_1 and x_2 , this means that

$$\begin{aligned} \left(\frac{df_2}{dx_1} + Cx_1^2 \right) &= \omega \\ \left(\frac{df_1}{dx_2} - \nu Cx_2^2 - 2(1+\nu)C(a^2 - x_2^2) \right) &= -\omega, \end{aligned}$$

where ω is an arbitrary constant. We can now integrate these expressions to see that

$$f_1 = (2(1+\nu)Ca^2 - \omega)x_2 - \frac{C}{3}(2+\nu)x_2^3 + c$$

$$f_2 = \omega x_1 - \frac{C}{3}x_1^3 + d,$$

where c and d are two more arbitrary constants. Finally, the displacement field follows as

$$u_1 = Cx_1^2 x_2 - \frac{C}{3}(2+\nu)x_2^3 + 2(1+\nu)Ca^2 x_2 - \omega x_2 + c$$

$$u_2 = -\nu Cx_1 x_2^2 - \frac{C}{3}x_1^3 + \omega x_1 + d.$$

The three arbitrary constants ω , c , and d can be seen to represent a small rigid rotation through angle ω about the x_3 axis, together with a displacement (c, d) parallel to (x_1, x_2) axes, respectively.

For a general, 3D field, a more formal procedure is required. Because the strains are the derivatives of the displacement field, so you might guess that we compute the displacements by integrating the strains. This is more or less correct. The general procedure is outlined below.

We first pick a point \mathbf{x}_0 in the solid and arbitrarily say that the displacement at \mathbf{x}_0 is zero and also take the rotation of the solid at \mathbf{x}_0 to be zero. Then, we can compute the displacements at any other point \mathbf{x} in the solid by integrating the strains along any convenient path, as shown in Figure 2.15. In a simply connected solid, it doesn't matter what path you pick.

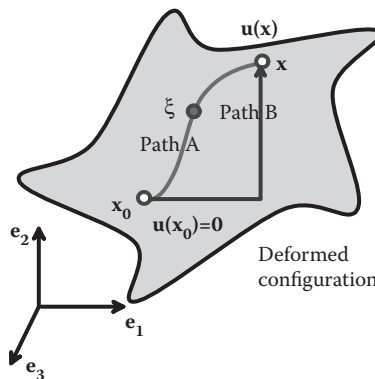


FIGURE 2.15 Two possible paths of integration used to determine the displacement corresponding to a strain.

Actually, you don't exactly integrate the strains; instead, you must evaluate the following integral

$$u_i(\mathbf{x}) = \int_{\mathbf{x}_0}^{\mathbf{x}} U_{ij}(\mathbf{x}, \xi) d\xi_j,$$

where

$$U_{ij}(\mathbf{x}, \xi) = \varepsilon_{ij}(\xi) + (x_k - \xi_k) \left[\frac{\partial \varepsilon_{ij}(\xi)}{\partial \xi_k} - \frac{\partial \varepsilon_{kj}(\xi)}{\partial \xi_i} \right].$$

Here, x_k are the components of the position vector at the point where we are computing the displacements, and ξ_j are the components of the position vector ξ of a point somewhere along the path of integration. The fact that the integral is path independent (in a simply connected solid) is guaranteed by the compatibility condition. Evaluating this integral in practice can be quite painful, but, fortunately, almost all cases in which we need to integrate strains to get displacement turn out to be two dimensional.

2.2 MATHEMATICAL DESCRIPTION OF INTERNAL FORCES IN SOLIDS

Our next objective is to outline the mathematical formulas that describe internal and external forces acting on a solid. Just as there are many different strain measures, there are several different definitions of internal force. We shall see that internal forces can be described as a second-order tensor, which must be symmetric. Thus, internal forces can always be quantified by a set of six numbers, and the various different definitions are all equivalent.

2.2.1 Surface Traction and Internal Body Force

Forces can be applied to a solid body in two ways, as illustrated in Figure 2.16.

1. A force can be applied to its boundary: examples include fluid pressure, wind loading, or forces arising from contact with another solid.

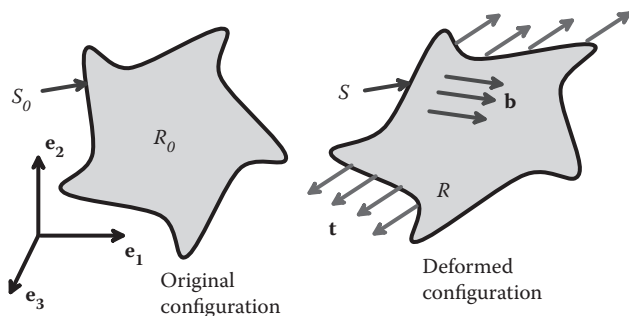


FIGURE 2.16 External tractions and internal body forces acting on a deformable solid.

2. The solid can be subjected to *body forces*, which act on the interior of the solid. Examples include gravitational loading, or electromagnetic forces.

These forces are quantified using the *surface traction vector* and the *body force vector*, respectively. These are defined as follows:

- The surface traction vector \mathbf{t} at a point on the surface represents the force acting on the surface per unit area of the deformed solid. Formally, let dA be an element of area on a surface. Suppose that dA is subjected to a force $d\mathbf{P}$, as shown in Figure 2.17. Then

$$\mathbf{t} = \lim_{dA \rightarrow 0} \frac{d\mathbf{P}}{dA}.$$

The resultant force acting on any portion S of the surface of the deformed solid is

$$\mathbf{P} = \int_S \mathbf{t} dA.$$

Surface traction, like “true stress,” should be thought of as acting on the deformed solid.

- The traction vector is often resolved into components acting normal and tangential to a surface, as shown in Figure 2.18. The normal component is referred to as the *normal traction*, and the tangential component is known as the *shear traction*. Formally, let \mathbf{n} denote a unit vector normal to the surface. Then

$$\mathbf{t}_n = (\mathbf{t} \cdot \mathbf{n})\mathbf{n} \quad \mathbf{t}_t = \mathbf{t} - \mathbf{t}_n.$$

- The body force vector denotes the external force acting on the interior of a solid, per unit mass. Formally, let dV denote an infinitesimal volume element within the

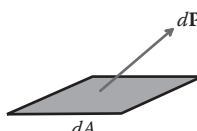


FIGURE 2.17 Force acting on an infinitesimal element on a surface.

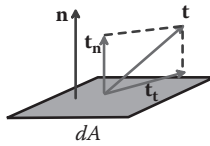


FIGURE 2.18 Decomposition of surface traction into normal and tangential components.

deformed solid, and let ρ denote the mass density (mass per unit deformed volume). Suppose that the element is subjected to a force $d\mathbf{P}$, as shown in Figure 2.19. Then

$$\mathbf{b} = \frac{1}{\rho} \lim_{dV \rightarrow 0} \frac{d\mathbf{P}}{dV}.$$

The resultant body force acting on any volume V within the deformed solid is

$$\mathbf{P} = \int_V \rho \mathbf{b} dV.$$

2.2.2 Traction Acting on Planes within a Solid

Every plane in the interior of a solid is subjected to a distribution of traction. To see this, consider a loaded, solid body in static equilibrium. Imagine cutting the solid in two, as illustrated in Figure 2.20. The two parts of the solid must each be in static equilibrium. This is possible only if forces act on the planes that were created by the cut. We quantify these forces by means of the *internal traction vector* $\mathbf{T}(n)$, which represents the force per unit area acting on an internal plane of a solid. The notation $\mathbf{T}(n)$ shows that the internal traction depends on the normal to the internal plane, denoted by n .

Formally, let dA be an element of area in the interior of the solid, with normal n . Suppose that the material on the underside of dA is subjected to a force $d\mathbf{P}^{(n)}$ across the plane dA , as shown in Figure 2.21. Then

$$\mathbf{T}(n) = \lim_{dA \rightarrow 0} \frac{d\mathbf{P}^{(n)}}{dA}.$$

Note that internal traction is the *force per unit area of the deformed solid*, like “true stress.” The traction vector has the following properties:

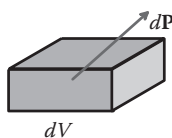


FIGURE 2.19 Body force acting on an infinitesimal volume element.

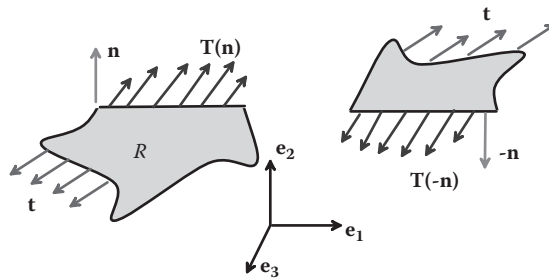


FIGURE 2.20 Tensions acting on internal planes within a solid.

- The *resultant force* acting on any internal volume V with boundary surface A (Figure 2.22) within a deformed solid is

$$\mathbf{P} = \int_A \mathbf{T}(\mathbf{n}) dA + \int_V \rho \mathbf{b} dV.$$

The first term is the resultant force acting on the internal surface A , and the second term is the resultant body force acting on the interior V .

- Newton's third law (every action has an equal and opposite reaction) requires that

$$\mathbf{T}(-\mathbf{n}) = -\mathbf{T}(\mathbf{n}).$$

To see this, note that the forces acting on planes separating two adjacent volume elements in a solid must be equal and opposite, as shown in Figure 2.23.

- Tensions acting on different planes passing through the same point are related to satisfy Newton's second law ($\mathbf{F} = m\mathbf{a}$). Specifically, let $\{\mathbf{e}_1, \mathbf{e}_2, \mathbf{e}_3\}$ be a Cartesian basis. Let $T_i(\mathbf{e}_1), T_i(\mathbf{e}_2), T_i(\mathbf{e}_3)$ denote the components of traction acting on planes with normal vectors in the $\mathbf{e}_1, \mathbf{e}_2$, and \mathbf{e}_3 directions, respectively. Then, the traction components $T_i(\mathbf{n})$ acting on a surface with normal \mathbf{n} are given by

$$T_i(\mathbf{n}) = T_i(\mathbf{e}_1)n_1 + T_i(\mathbf{e}_2)n_2 + T_i(\mathbf{e}_3)n_3,$$

where n_i are the components of \mathbf{n} .

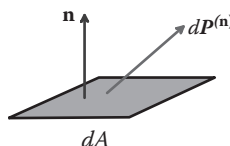


FIGURE 2.21 Force acting on an internal area element.

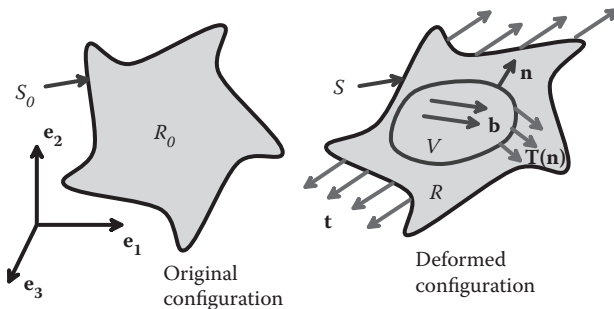


FIGURE 2.22 Tensions acting on an interior volume of a solid.

To see this, consider the forces acting on the infinitesimal tetrahedron shown in Figure 2.24. The base and sides of the tetrahedron have normals in the $-\mathbf{e}_2$, $-\mathbf{e}_1$, and $-\mathbf{e}_3$ directions. The fourth face has normal \mathbf{n} . Suppose the volume of the tetrahedron is dV and let dA_1 , dA_2 , dA_3 , and dA_n denote the areas of the faces. Assume that the material within the tetrahedron has mass density ρ and is subjected to a body force \mathbf{b} . Let \mathbf{a} denote the acceleration of the center of mass of the tetrahedron. Then, $\mathbf{F} = m\mathbf{a}$ for the tetrahedron requires that

$$\mathbf{T}(\mathbf{n})dA^{(n)} + \mathbf{T}(-\mathbf{e}_1)dA_1 + \mathbf{T}(-\mathbf{e}_2)dA_2 + \mathbf{T}(-\mathbf{e}_3)dA_3 + \rho\mathbf{b}dV = \rho dV\mathbf{a}.$$

Recall that $\mathbf{T}(-\mathbf{e}_i) = -\mathbf{T}(\mathbf{e}_i)$ and divide through by $dA^{(n)}$:

$$\mathbf{T}(\mathbf{n}) - \mathbf{T}(\mathbf{e}_1)\frac{dA_1}{dA^{(n)}} - \mathbf{T}(\mathbf{e}_2)\frac{dA_2}{dA^{(n)}} - \mathbf{T}(\mathbf{e}_3)\frac{dA_3}{dA^{(n)}} + \rho\mathbf{b}\frac{dV}{dA^{(n)}} = \rho\frac{dV}{dA^{(n)}}\mathbf{a}.$$

Finally, let $dA^{(n)} \rightarrow 0$. We can show (see Appendix E) that

$$\frac{dA_1}{dA^{(n)}} = n_1 \quad \frac{dA_2}{dA^{(n)}} = n_2 \quad \frac{dA_3}{dA^{(n)}} = n_3 \quad \lim_{dA^{(n)} \rightarrow 0} \frac{dV}{dA^{(n)}} = 0$$

so

$$\mathbf{T}(\mathbf{n}) = \mathbf{T}(\mathbf{e}_1)n_1 + \mathbf{T}(\mathbf{e}_2)n_2 + \mathbf{T}(\mathbf{e}_3)n_3$$

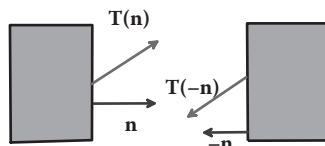


FIGURE 2.23 Equal and opposite tractions acting on adjacent internal surfaces.

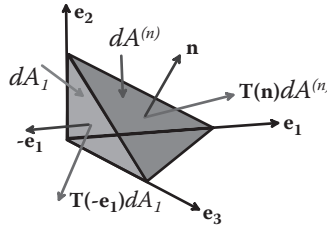


FIGURE 2.24 Tetrahedral infinitesimal volume element subjected to internal tractions.

or, using index notation,

$$T_i(\mathbf{n}) = T_i(\mathbf{e}_1)n_1 + T_i(\mathbf{e}_2)n_2 + T_i(\mathbf{e}_3)n_3.$$

The significance of this result is that the tractions acting on planes with normals in the \mathbf{e}_1 , \mathbf{e}_2 , and \mathbf{e}_3 directions completely characterize the internal forces that act at a point. Given these tractions, we can deduce the tractions acting on any other plane. This leads directly to the definition of the Cauchy stress tensor in the next section.

2.2.3 Cauchy (True) Stress Tensor

Consider a solid that deforms under external loading. Let $\{\mathbf{e}_1, \mathbf{e}_2, \mathbf{e}_3\}$ be a Cartesian basis. Let $T_i(\mathbf{e}_1)$, $T_i(\mathbf{e}_2)$, and $T_i(\mathbf{e}_3)$ denote the components of traction acting on planes with normals in the \mathbf{e}_1 , \mathbf{e}_2 , and \mathbf{e}_3 directions, respectively, as outlined in the preceding section. Define the components of the Cauchy stress tensor σ_{ij} by

$$\begin{aligned} \sigma_{ij} &= T_j(\mathbf{e}_i) \\ &\equiv \begin{cases} \sigma_{11} = T_1(\mathbf{e}_1) & \sigma_{12} = T_2(\mathbf{e}_1) & \sigma_{13} = T_3(\mathbf{e}_1) \\ \sigma_{21} = T_1(\mathbf{e}_2) & \sigma_{22} = T_2(\mathbf{e}_2) & \sigma_{23} = T_3(\mathbf{e}_2) \\ \sigma_{31} = T_1(\mathbf{e}_3) & \sigma_{32} = T_2(\mathbf{e}_3) & \sigma_{33} = T_3(\mathbf{e}_3). \end{cases} \end{aligned}$$

Then, the traction $T_i(\mathbf{n})$ acting on any plane with normal \mathbf{n} follows as

$$\mathbf{T}(\mathbf{n}) = \mathbf{n} \cdot \boldsymbol{\sigma} \quad \text{or} \quad T_i(\mathbf{n}) = n_j \sigma_{ji}.$$

To see this, recall the last result from the preceding section,

$$T_i(\mathbf{n}) = T_i(\mathbf{e}_1)n_1 + T_i(\mathbf{e}_2)n_2 + T_i(\mathbf{e}_3)n_3,$$

and substitute for $T_i(\mathbf{e}_j)$ in terms of the components of the Cauchy stress tensor

$$T_i(\mathbf{n}) = \sigma_{1i}n_1 + \sigma_{2i}n_2 + \sigma_{3i}n_3 = n_j \sigma_{ji}.$$

The Cauchy stress tensor completely characterizes the internal forces acting in a deformed solid. The physical significance of the components of the stress tensor is illustrated in Figure 2.25: σ_{ji} represents the i th component of traction acting on a plane with normal in the e_j direction. Note that Cauchy stress represents force per unit area of the deformed solid. In elementary strength of materials courses, it is called “true stress” for this reason.

HEALTH WARNING: Some texts define stress as the *transpose* of the definition used here, so that $T(\mathbf{n}) = \boldsymbol{\sigma} \cdot \mathbf{n}$ or $T_i(\mathbf{n}) = \sigma_{ji}n_j$. In this case, the first index for each stress component denotes the direction of traction, whereas the second denotes the normal to the plane. We will see later that Cauchy stress is always symmetric, so there is no confusion if you use the wrong definition. However, some stress measures are *not* symmetric (see below), and, in this case, you need to be careful to check which convention the author has chosen.

2.2.4 Other Stress Measures: Kirchhoff, Nominal, and Material Stress Tensors

Cauchy stress σ_{ji} (the actual force per unit area acting on an actual, deformed solid) is the most physical measure of internal force. Other definitions of stress often appear in constitutive equations, however.

The other stress measures regard forces as acting on the undeformed solid. Consequently, to define them, we must know not only what the deformed solid looks like, but also what it looked like before deformation. The deformation is described by a displacement vector $\mathbf{u}(\mathbf{x})$ and the associated deformation gradient

$$\mathbf{F} = \mathbf{I} + \mathbf{u} \otimes \nabla \quad F_{ij} = \delta_{ij} + \frac{\partial u_i}{\partial x_j}$$

as outlined in Section 2.1. In addition, let $J = \det(\mathbf{F})$. We then define the following stress measures:

- Kirchhoff stress: $\boldsymbol{\tau} = J\boldsymbol{\sigma} \quad \tau_{ij} = J\sigma_{ij}$.
- Nominal (first Piola–Kirchhoff) stress: $\mathbf{S} = J\mathbf{F}^{-1} \cdot \boldsymbol{\sigma} \quad S_{ij} = JF_{ik}^{-1}\sigma_{kj}$.
- Material (second Piola–Kirchhoff) stress: $\boldsymbol{\Sigma} = J\mathbf{F}^{-1} \cdot \boldsymbol{\sigma} \cdot \mathbf{F}^{-T} \quad \Sigma_{ij} = JF_{ik}^{-1}\sigma_{kl}F_{jl}^{-1}$.

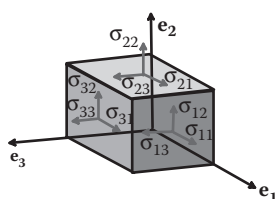


FIGURE 2.25 Infinitesimal volume element subjected to Cauchy stress components.

The inverse relations are also useful. The one for Kirchhoff stress is obvious; the others are

$$\boldsymbol{\sigma} = \frac{1}{J} \mathbf{F} \cdot \mathbf{S} \quad \sigma_{ij} = \frac{1}{J} F_{ik} S_{kj} \quad \boldsymbol{\sigma} = \frac{1}{J} \mathbf{F} \cdot \sum \mathbf{F}^T \quad \sigma_{ij} = \frac{1}{J} F_{ik} \sum_{kl} F_{jl}.$$

The Kirchoff stress has no obvious physical significance. The nominal stress tensor can be regarded as the internal force per unit undeformed area acting within a solid, as follows:

1. Visualize an element of area dA in the deformed solid, with normal \mathbf{n} , which is subjected to a force $d\mathbf{P}^{(n)}$ by the internal traction in the solid.
2. Suppose that the element of area dA has started out as an element of area dA_0 with normal \mathbf{n}_0 in the undeformed solid, as shown in Figure 2.26.
3. Then, the force $d\mathbf{P}^{(n)}$ is related to the nominal stress by $dP_j^{(n)} = dA_0 n_i^0 S_{ij}$.

To see this, note that one can show (see Appendix D) that

$$dA\mathbf{n} = J\mathbf{F}^{-T} \cdot dA_0\mathbf{n}_0 \quad dAn_i = JF_{ki}^{-1}n_k^0 dA_0$$

Recall that the Cauchy stress is defined so that

$$dP_i^{(n)} = dAn_j \sigma_{ji}.$$

Substituting for dAn_j and rearranging shows that

$$dP_i^{(n)} = JdA_0 n_k^0 (F_{kj}^{-1} \sigma_{ji}) = dA_0 n_k^0 S_{ki}.$$

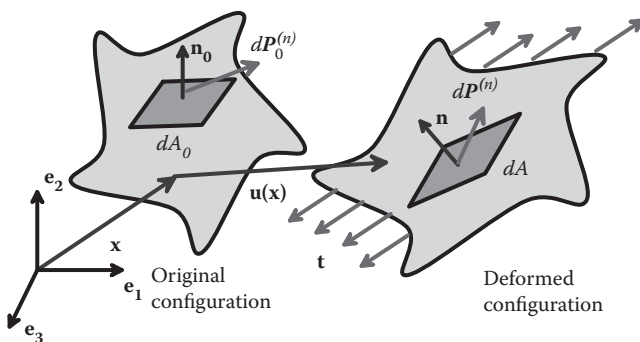


FIGURE 2.26 Deformation of an internal area element within a deformable solid.

The material stress tensor can also be visualized as force per unit undeformed area, except that the forces are regarded as acting within the undeformed solid rather than on the deformed solid:

1. The infinitesimal force $d\mathbf{P}^{(n)}$ is assumed to behave like an infinitesimal material fiber in the solid, in the sense that it is stretched and rotated just like a small vector $d\mathbf{x}$ in the solid.
2. This means that we can define a (fictitious) force in the reference configuration $d\mathbf{P}^{(n0)}$ that is related to $d\mathbf{P}^{(n)}$ by $\mathbf{F} \cdot d\mathbf{P}^{(n0)} = d\mathbf{P}^{(n)}$ or $F_{ij}dP_j^{(n0)} = dP_i^{(n)}$.
3. This fictitious force is related to material stress by $dP_i^{(n0)} = dA_0 n_j^0 \Sigma_{ji}$.

To see this, substitute into the expression relating $d\mathbf{P}^{(n)}$ to nominal stress to see that

$$F_{ik}dP_k^{(n0)} = dA_0 n_j^0 S_{ji}.$$

Finally, multiply through by F_{li}^{-1} , note that $F_{li}^{-1}F_{ik} = \delta_{lk}$, and rearrange to see that

$$dP_l^{(n0)} = dA_0 n_j^0 S_{ji} F_{li}^{-1} = dA_0 n_j^0 \Sigma_{jl},$$

where we have noted that $\Sigma_{jl} = S_{ji} F_{li}^{-1}$.

In practice, it is best not to try to attach too much physical significance to these stress measures. Cauchy stress is the best physical measure of internal force: it is the force per unit area acting inside the deformed solid. The other stress measures are best regarded as *generalized forces* (in the sense of Lagrangian mechanics), which are work conjugate to particular strain measures. This means that the stress measure multiplied by the time derivative of the strain measure tells you the rate of work done by the forces. When setting up any mechanics problem, we always work with conjugate measures of motion and forces.

Specifically, we shall show later that the rate of work \dot{W} done by stresses acting on a small material element with volume dV_0 in the undeformed solid (and volume dV in the deformed solid) can be computed as

$$\dot{W} = D_{ij}\sigma_{ij}dV = D_{ij}\tau_{ji}dV_0 = \dot{F}_{ij}S_{ji}dV_0 = \dot{E}_{ij}\Sigma_{ji}dV_0,$$

where D_{ij} is the stretch rate tensor, \dot{F}_{ij} is the rate of change of deformation gradient, and \dot{E}_{ij} is the rate of change of Lagrange strain tensor. Note that Cauchy stress (and also Kirchhoff stress) is not conjugate to any convenient strain measure; this is the main reason that nominal and material stresses need to be defined. The nominal stress is conjugate to the deformation gradient, whereas the material stress is conjugate to the Lagrange strain tensor.

2.2.5 Stress Measures for Infinitesimal Deformations

For a problem involving *infinitesimal deformation* (in which shape changes are characterized by the infinitesimal strain tensor and rotation tensor), all the stress measures defined in the preceding section are approximately equal:

$$\sigma_{ij} \approx \tau_{ij} \approx S_{ij} \approx \Sigma_{ij}.$$

To see this, write the deformation gradient as $F_{ij} = \delta_{ij} + \partial u_i / \partial x_j$; recall that $J = \det(\mathbf{F}) \approx 1 + \partial u_k / \partial x_k$, and finally assume that, for infinitesimal motions, $\partial u_i / \partial x_j \ll 1$. Substituting into the formulas relating Cauchy stress, nominal stress, and material stress, we see that

$$\sigma_{ij} = \frac{1}{J} F_{ik} S_{kj} \approx \frac{1}{1 + \partial u_p / \partial x_p} \left(\delta_{ip} + \frac{\partial u_i}{\partial x_p} \right) S_{pj} = S_{pj} + \dots \approx S_{pj}.$$

The same procedure will show that material stress and Cauchy stress are approximately equal, to within a term of order $\partial u_i / \partial x_j \ll 1$.

2.2.6 Principal Stresses and Directions

For any stress measure, the principal stresses σ_i and their directions $\mathbf{n}^{(i)}$, with $i = 1..3$ are defined such that

$$\mathbf{n}^{(i)} \cdot \boldsymbol{\sigma} = \sigma_i \mathbf{n}^{(i)} \quad \text{or} \quad n_j^{(i)} \sigma_{jk} = \sigma_i n_k^{(i)} \quad (\text{no sum on } i).$$

Clearly, (1) the *principal stresses* are the (left) eigenvalues of the stress tensor, and (2) the *principal stress directions* are the (left) eigenvectors of the stress tensor. The term “left” eigenvector and eigenvalue indicates that the vector multiplies the tensor on the left. We will see later that Cauchy stress and material stress are both symmetric. For a symmetric tensor, the left and right eigenvalues and vectors are the same.

Note that the eigenvectors of a symmetric tensor are orthogonal. Consequently, the principal Cauchy or material stresses can be visualized as tractions acting normal to the faces of a cube, as shown in Figure 2.27. The principal directions specify the orientation of this special cube.

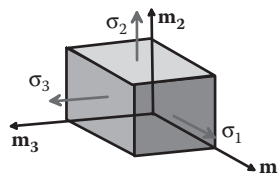


FIGURE 2.27 Infinitesimal volume element subjected to principal stresses.

One can also show that, if $\sigma_1 > \sigma_2 > \sigma_3$, then σ_1 is the largest normal traction acting on any plane passing through the point of interest, whereas σ_3 is the lowest. This is helpful in defining damage criteria for brittle materials, which fail when the stress acting normal to a material plane reaches a critical magnitude.

In the same vein, it can be shown that the largest shear stress acts on the plane with unit normal vector $\mathbf{m}_{\text{shear}} = -(\mathbf{m}_1 + \mathbf{m}_3)/\sqrt{2}$ (at 45° to the \mathbf{m}_1 and \mathbf{m}_3 axes as shown in Figure 2.28) and has magnitude $\tau_{\max} = \frac{1}{2}(\sigma_1 - \sigma_3)$. This observation is useful for defining yield criteria for metal polycrystals, which begin to deform plastically when the shear stress acting on a material plane reaches a critical value.

2.2.7 Hydrostatic, Deviatoric, and von Mises Effective Stress

Given the Cauchy stress tensor σ , the following may be defined:

- The *hydrostatic stress* is defined as $\sigma_h = \text{trace}(\sigma)/3 = \sigma_{kk}/3$.
- The *deviatoric stress tensor* is defined as $\sigma'_{ij} = \sigma_{ij} - \sigma_h \delta_{ij}$.
- The *von Mises effective stress* is defined as $\sigma_e = \sqrt{\frac{3}{2} \sigma'_{ij} \sigma'_{ij}}$.

The hydrostatic stress is a measure of the pressure exerted by a state of stress. Pressure acts so as to change the volume of a material element. The deviatoric stress is a measure of the shearing exerted by a state of stress. Shear stress tends to distort a solid, without changing its volume. The von Mises effective stress can be regarded as a uniaxial equivalent of a multiaxial stress state. It is used in many failure or yield criteria. Thus, if a material is known to fail in a uniaxial tensile test (with σ_{11} the only nonzero stress component) when $\sigma_{11} = \sigma_{\text{crit}}$, it will fail when $\sigma_e = \sigma_{\text{crit}}$ under multiaxial loading (with several $\sigma_{ij} \neq 0$).

The hydrostatic stress and von Mises stress can also be expressed in terms of principal stresses as

$$\sigma_h = (\sigma_1 + \sigma_2 + \sigma_3)/3$$

$$\sigma_e = \sqrt{\frac{1}{2} \{(\sigma_1 - \sigma_2)^2 + (\sigma_1 - \sigma_3)^2 + (\sigma_2 - \sigma_3)^2\}}.$$

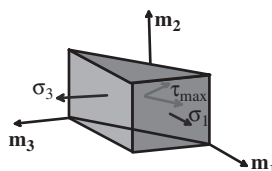


FIGURE 2.28 Volume element used to calculate maximum shear stress in a solid.

The hydrostatic and von Mises stresses are *invariants* of the stress tensor: they have the same value regardless of the basis chosen to define the stress components.

2.2.8 Stresses near an External Surface or Edge: Boundary Conditions on Stresses

Note that, at an external surface at which tractions are prescribed, some components of stress are known. Specifically, let \mathbf{n} denote a unit vector normal to the surface and let \mathbf{t} denote the traction (force per unit area) acting on the surface. Then the Cauchy stress at the surface must satisfy

$$n_i \sigma_{ij} = t_j.$$

For example, suppose that a surface with normal in the \mathbf{e}_2 direction is subjected to *no* loading, as shown in Figure 2.29. Then (noting that $n_i = \delta_{i2}$) it follows that $\sigma_{2i} = 0$. In addition, two of the principal stress directions must be parallel to the surface; the third (with zero stress) must be perpendicular to the surface.

The stress state at an edge is even simpler. Suppose that surfaces with normals in the \mathbf{e}_2 and \mathbf{e}_1 are traction free. Then $\sigma_{1i} = \sigma_{2i} = 0$, so that six stress components are known to be zero.

2.3 EQUATIONS OF MOTION AND EQUILIBRIUM FOR DEFORMABLE SOLIDS

In this section, we generalize Newton's laws of motion (conservation of linear and angular momentum) to a deformable solid.

2.3.1 Linear Momentum Balance in Terms of Cauchy Stress

Consider a solid that is deformed by external forces, as shown in Figure 2.30. Let σ_{ij} denote the Cauchy stress distribution within a deformed solid. Assume that the solid is subjected to a body force \mathbf{b}_i and let u_i , v_i and a_i denote the displacement, velocity, and acceleration of a material particle at position y_i in the deformed solid.

Newton's third law of motion ($\mathbf{F} = m\mathbf{a}$) can be expressed as

$$\nabla_y \cdot \boldsymbol{\sigma} + \rho \mathbf{b} = \rho \mathbf{a} \quad \text{or} \quad \frac{\partial \sigma_{ij}}{\partial y_i} + \rho b_j = \rho a_j.$$

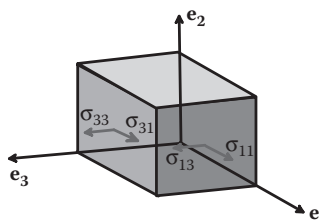


FIGURE 2.29 Stresses acting on a volume element just under a free surface.

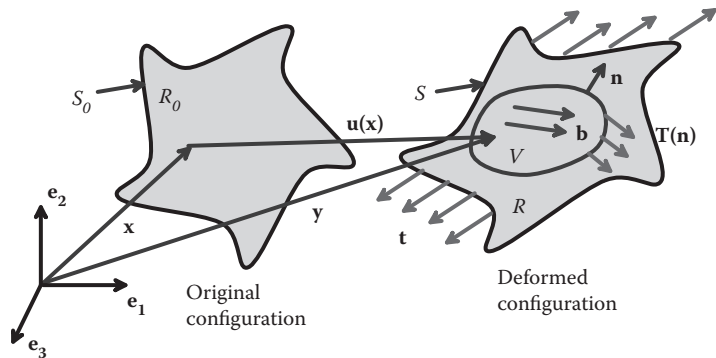


FIGURE 2.30 Tractions acting on an interior volume of a solid.

Written out in full,

$$\frac{\partial \sigma_{11}}{\partial y_1} + \frac{\partial \sigma_{21}}{\partial y_2} + \frac{\partial \sigma_{31}}{\partial y_3} + \rho b_1 = \rho a_1$$

$$\frac{\partial \sigma_{12}}{\partial y_1} + \frac{\partial \sigma_{22}}{\partial y_2} + \frac{\partial \sigma_{32}}{\partial y_3} + \rho b_2 = \rho a_2$$

$$\frac{\partial \sigma_{13}}{\partial y_1} + \frac{\partial \sigma_{23}}{\partial y_2} + \frac{\partial \sigma_{33}}{\partial y_3} + \rho b_3 = \rho a_3.$$

Note that the derivative is taken with respect to position in the actual, deformed solid. For the special (but rather common) case of a solid in static equilibrium in the absence of body forces,

$$\frac{\partial \sigma_{ij}}{\partial y_i} = 0.$$

Derivation: Recall that the resultant force acting on an arbitrary volume of material V within a solid is

$$P_i = \int_A T_i(\mathbf{n}) dA + \int_V \rho b_i dV,$$

where $\mathbf{T}(\mathbf{n})$ is the internal traction acting on the surface A with normal \mathbf{n} that bounds V . The linear momentum of the volume V is

$$\Lambda_i = \int_V \rho v_i dV,$$

where \mathbf{v} is the velocity vector of a material particle in the deformed solid. Express \mathbf{T} in terms of σ_{ij} and set $P_i = d\Lambda_i/dt$. Then

$$\int_A \sigma_{ji} n_j dA + \int_V \rho b_i dV = \frac{d}{dt} \left\{ \int_V \rho v_i dV \right\}.$$

Apply the divergence theorem to convert the first integral into a volume integral and note that one can show (see Appendix E) that

$$\frac{d}{dt} \left\{ \int_V \rho v_i dV \right\} = \int_V \rho a_i dV$$

so

$$\int_V \frac{\partial \sigma_{ji}}{\partial y_j} dV + \int_V \rho b_i dV = \int_V \rho a_i dV \Rightarrow \int_V \left(\frac{\partial \sigma_{ji}}{\partial y_j} + \rho b_i - \rho a_i \right) dV = 0.$$

Because this must hold for every volume of material within a solid, it follows that

$$\frac{\partial \sigma_{ji}}{\partial y_j} + \rho b_i = \rho a_i$$

as stated.

2.3.2 Angular Momentum Balance in Terms of Cauchy Stress

Conservation of angular momentum for a continuum requires that the Cauchy stress satisfy

$$\sigma_{ji} = \sigma_{ij}$$

i.e., the stress tensor must be symmetric.

Derivation: Write down the equation for balance of angular momentum for the region V within the deformed solid

$$\int_A \mathbf{y} \times \mathbf{T} dA + \int_V \mathbf{y} \times \rho \mathbf{b} dV = \frac{d}{dt} \left\{ \int_V \mathbf{y} \times \rho \mathbf{v} dV \right\}.$$

Here, the left-hand side is the resultant moment (about the origin) exerted by tractions and body forces acting on a general region within a solid. The right-hand side is the total angular momentum of the solid about the origin.

52 ■ Applied Mechanics of Solids

We can write the same expression using index notation

$$\int_A \epsilon_{ijk} y_j T_k dA + \int_V \epsilon_{ijk} y_j b_k \rho dV = \frac{d}{dt} \left\{ \int_V \epsilon_{ijk} y_j v_k \rho dV \right\}.$$

Express \mathbf{T} in terms of σ_{ij} and rewrite the first integral as a volume integral using the divergence theorem

$$\begin{aligned} \int_A \epsilon_{ijk} y_j T_k dA &= \int_A \epsilon_{ijk} y_j \sigma_{mk} n_m dA = \int_V \frac{\partial}{\partial y_m} (\epsilon_{ijk} y_j \sigma_{mk}) dV \\ &= \int_V \epsilon_{ijk} \left(\delta_{jm} \sigma_{mk} + y_j \frac{\partial \sigma_{mk}}{\partial y_m} \right) dV \end{aligned}$$

We may also show (see Appendix E) that

$$\frac{d}{dt} \left\{ \int_V \epsilon_{ijk} y_j v_k \rho dV \right\} = \int_V \epsilon_{ijk} y_j a_k \rho dV.$$

Substitute the last two results into the angular momentum balance equation to see that

$$\begin{aligned} \int_V \epsilon_{ijk} \left(\delta_{jm} \sigma_{mk} + y_j \frac{\partial \sigma_{mk}}{\partial y_m} \right) dV + \int_V \epsilon_{ijk} y_j b_k \rho dV &= \int_V \epsilon_{ijk} y_j a_k \rho dV \\ \Rightarrow \int_V \epsilon_{ijk} \delta_{jm} \sigma_{mk} dV &= - \int_V \epsilon_{ijk} y_j \left(\frac{\partial \sigma_{mk}}{\partial y_m} + \rho b_k - \rho a_k \right) dV. \end{aligned}$$

The integral on the right-hand side of this expression is zero, because the stresses must satisfy the linear momentum balance equation. Because this holds for any volume V , we conclude that

$$\begin{aligned} \epsilon_{ijk} \delta_{jm} \sigma_{mk} &= \epsilon_{ijk} \sigma_{jk} = 0 \\ \Rightarrow \epsilon_{imn} \epsilon_{ijk} \sigma_{jk} &= 0 \\ \Rightarrow (\delta_{jm} \delta_{kn} - \delta_{mk} \delta_{nj}) \sigma_{jk} &= 0 \\ \Rightarrow \sigma_{mn} - \sigma_{nm} &= 0, \end{aligned}$$

which is the result we wanted.

2.3.3 Equations of Motion in Terms of Other Stress Measures

In terms of nominal and material stress, the balance of linear momentum is

$$\nabla \cdot \mathbf{S} + \rho_0 \mathbf{b} = \rho_0 \mathbf{a} \quad \frac{\partial S_{ij}}{\partial x_i} + \rho_0 b_j = \rho_0 a_j$$

$$\nabla \cdot [\Sigma \cdot \mathbf{F}^T] + \rho_0 \mathbf{b} = \rho_0 \mathbf{a} \quad \frac{\partial (\Sigma_{ik} F_{jk})}{\partial x_i} + \rho_0 b_j = \rho_0 a_j.$$

Note that the derivatives are taken with respect to position in the undeformed solid.

The angular momentum balance equation is

$$\mathbf{F} \cdot \mathbf{S} = [\mathbf{F} \cdot \mathbf{S}]^T \quad \Sigma = \Sigma^T.$$

To derive these results, you can start with the integral form of the linear momentum balance in terms of Cauchy stress

$$\int_A \sigma_{ji} n_j dA + \int_V \rho b_i dV = \frac{d}{dt} \left\{ \int_V \rho v_i dV \right\}.$$

Recall (or see Appendix E for a reminder) that area elements in the deformed and undeformed solids are related through

$$dA_n = J F_{ki}^{-1} n_k^0 dA_0.$$

In addition, volume elements are related by $dV = J dV_0$. We can use these results to rewrite the integrals as integrals over a volume in the undeformed solid as

$$\int_{A_0} \sigma_{ji} J F_{kj}^{-1} n_k^0 dA_0 + \int_{V_0} \rho b_i J dV_0 = \frac{d}{dt} \left\{ \int_{V_0} \rho v_i J dV_0 \right\}.$$

Finally, recall that $S_{ij} = J F_{ik}^{-1} \sigma_{kj}$ and that $J\rho = \rho_0$ to see that

$$\int_{A_0} S_{ki} n_k^0 dA_0 + \int_{V_0} \rho_0 b_i dV_0 = \frac{d}{dt} \left\{ \int_{V_0} \rho_0 v_i dV_0 \right\}.$$

Apply the divergence theorem to the first term and rearrange

$$\int_V \left(\frac{\partial S_{ji}}{\partial x_j} + \rho_0 b_i - \rho_0 \frac{dv_i}{dt} \right) dV_0 = 0.$$

Once again, because this must hold for any material volume, we conclude that

$$\frac{\partial S_{ij}}{\partial x_i} + \rho_0 b_j = \rho_0 a_j.$$

The linear momentum balance equation in terms of material stress follows directly, by substituting into this equation for S_{ij} in terms of Σ_{ij} .

The angular momentum balance equation can be derived simply by substituting into the momentum balance equation in terms of Cauchy stress $\sigma_{ij} = \sigma_{ji}$.

2.4 WORK DONE BY STRESSES: PRINCIPLE OF VIRTUAL WORK

In this section, we derive formulas that enable you to calculate the work done by stresses acting on a solid. In addition, we prove the *principle of virtual work*, which is an alternative way of expressing the equations of motion and equilibrium derived in Section 2.3. The principle of virtual work is the starting point for finite element analysis and so is a particularly important result.

2.4.1 Work Done by Cauchy Stresses

Consider a solid with mass density ρ_0 in its initial configuration and density ρ in the deformed solid, as shown in Figure 2.31. Let σ_{ij} denote the Cauchy stress distribution within the solid. Assume that the solid is subjected to a body force b_i (per unit mass) and let u_i , v_i , and a_i denote the displacement, velocity, and acceleration of a material particle at position y_i in the deformed solid. In addition, let

$$D_{ij} = \frac{1}{2} \left(\frac{\partial v_i}{\partial y_j} + \frac{\partial v_j}{\partial y_i} \right)$$

denote the stretch rate in the solid.

The rate of work done by Cauchy stresses per unit deformed volume is then $\sigma_{ij} D_{ij}$. This energy is either dissipated as heat or stored as internal energy in the solid, depending on the material behavior.

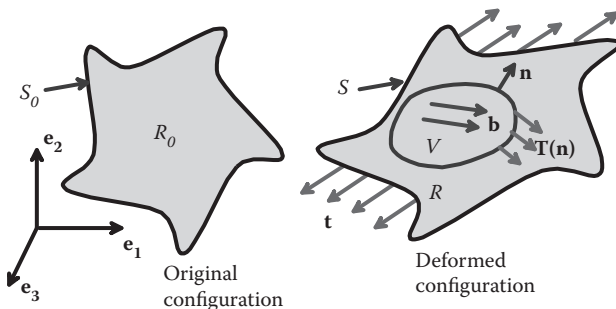


FIGURE 2.31 Tractions acting on an interior volume of a solid.

We shall show that the rate of work done by internal forces acting on any subvolume V bounded by a surface A in the deformed solid can be calculated from

$$\dot{r} = \int_A T_i(\mathbf{n}) v_i dA + \int_V \rho b_i v_i dV = \int_V \sigma_{ij} D_{ij} dV + \frac{d}{dt} \left\{ \int_V \frac{1}{2} \rho v_i v_i dV \right\}.$$

Here, the two terms on the left-hand side represent the rate of work done by tractions and body forces acting on the solid (rate of work done = force \times velocity). The first term on the right-hand side can be interpreted as the work done by Cauchy stresses; the second term is the rate of change of kinetic energy.

Derivation: Substitute for $T_i(\mathbf{n})$ in terms of Cauchy stress to see that

$$\dot{r} = \int_A T_i(\mathbf{n}) v_i dA + \int_V \rho b_i v_i dV = \int_A n_j \sigma_{ji} v_i dA + \int_V \rho b_i v_i dV.$$

Now, apply the divergence theorem to the first term on the right-hand side,

$$\dot{r} = \int_V \frac{\partial}{\partial y_j} (\sigma_{ji} v_i) dV + \int_V \rho b_i v_i dV.$$

Evaluate the derivative and collect together the terms involving body force and stress divergence,

$$\dot{r} = \int_V \left\{ \sigma_{ji} \frac{\partial v_i}{\partial y_j} + \left(\frac{\partial \sigma_{ji}}{\partial y_j} + \rho b_i \right) v_i \right\} dV.$$

Recall the equation of motion

$$\frac{\partial \sigma_{ji}}{\partial y_j} + \rho b_i = \rho a_i$$

and note that, because the stress is symmetric $\sigma_{ij} = \sigma_{ji}$,

$$\sigma_{ji} \frac{\partial v_i}{\partial y_j} = \frac{1}{2} (\sigma_{ij} + \sigma_{ji}) \frac{\partial v_i}{\partial y_j} = \frac{1}{2} \sigma_{ij} \left(\frac{\partial v_i}{\partial y_j} + \frac{\partial v_j}{\partial y_i} \right) = \sigma_{ij} D_{ij},$$

to see that

$$\dot{r} = \int_V \{\sigma_{ij} D_{ij} + \rho a_i v_i\} dV.$$

Finally, note that

$$\begin{aligned} \int_V \rho a_i v_i dV &= \int_{V_0} \rho_0 \frac{dv_i}{dt} v_i dV_0 = \int_{V_0} \rho_0 \frac{1}{2} \frac{d}{dt} (v_i v_i) dV_0 \\ &= \frac{d}{dt} \left(\int_{V_0} \frac{1}{2} \rho_0 (v_i v_i) dV_0 \right) = \frac{d}{dt} \left(\int_{V_0} \frac{1}{2} \rho_0 (v_i v_i) dV_0 \right) = \frac{d}{dt} \int_V \frac{1}{2} \rho (v_i v_i) dV. \end{aligned}$$

Finally, substitution leads to

$$\dot{r} = \int_A T_i(\mathbf{n}) v_i dA + \int_V \rho b_i v_i dV = \int_V \sigma_{ij} D_{ij} dV + \frac{d}{dt} \left\{ \int_V \frac{1}{2} \rho v_i v_i dV \right\}$$

as required.

2.4.2 Rate of Mechanical Work in Terms of Other Stress Measures

- The rate of work done per unit undeformed volume by Kirchhoff stress is $\tau_{ij} D_{ij}$.
- The rate of work done per unit undeformed volume by nominal stress is $S_{ij} \dot{F}_{ji}$.
- The rate of work done per unit undeformed volume by material stress is $\Sigma_{ij} \dot{E}_{ij}$.

This shows that nominal stress and deformation gradient are work conjugate, as are material stress and Lagrange strain.

In addition, the rate of work done on a volume V_0 of the undeformed solid can be expressed as

$$\begin{aligned} \dot{r} &= \int_A T_i(\mathbf{n}) v_i dA + \int_V \rho b_i v_i dV = \int_{V_0} \tau_{ij} D_{ij} dV_0 + \frac{d}{dt} \left\{ \int_{V_0} \frac{1}{2} \rho_0 v_i v_i dV_0 \right\} \\ \dot{r} &= \int_A T_i(\mathbf{n}) v_i dA + \int_V \rho b_i v_i dV = \int_{V_0} S_{ij} \dot{F}_{ji} dV_0 + \frac{d}{dt} \left\{ \int_{V_0} \frac{1}{2} \rho_0 v_i v_i dV_0 \right\} \\ \dot{r} &= \int_A T_i(\mathbf{n}) v_i dA + \int_V \rho b_i v_i dV = \int_{V_0} \Sigma_{ij} \dot{E}_{ij} dV_0 + \frac{d}{dt} \left\{ \int_{V_0} \frac{1}{2} \rho_0 v_i v_i dV_0 \right\}. \end{aligned}$$

Derivation: The proof of the first result (and the stress power of Kirchhoff stress) is straightforward and is left as an exercise. To show the second result, note that $T_i^{(n)}dA = n_j^0 S_{ji} dA_0$ and $dV = JdV_0$ to rewrite the integrals over the undeformed solid; then apply the divergence theorem to see that

$$\dot{r} = \int_{V_0} \frac{\partial}{\partial x_j} (S_{ji} v_i) dV_0 + \int_{V_0} \rho b_i v_i J dV_0.$$

Evaluate the derivative, recall that $J\rho = \rho_0$, and use the equation of motion

$$\frac{\partial S_{ij}}{\partial x_i} + \rho_0 b_j = \rho_0 \frac{dv_j}{dt}$$

to see that

$$\dot{r} = \int_{V_0} S_{ji} \frac{\partial v_i}{\partial x_j} dV_0 + \int_{V_0} \rho_0 \frac{dv_i}{dt} v_i dV_0.$$

Finally, note that $\partial v_i / \partial x_j = (\partial u_i / \partial x_j) = \dot{F}_{ij}$ and rewrite the second integral as a kinetic energy term as before to obtain the required result.

The third result follows by straightforward algebraic manipulations; note that, by definition,

$$S_{ij} \dot{F}_{ji} = \Sigma_{ik} F_{jk} \dot{F}_{ji}.$$

Because Σ_{ij} is symmetric, it follows that

$$\Sigma_{ik} F_{jk} \dot{F}_{ji} = \frac{1}{2} (\Sigma_{ik} + \Sigma_{ki}) F_{jk} \dot{F}_{ji} = \Sigma_{ik} \frac{1}{2} (F_{jk} \dot{F}_{ji} + F_{ji} \dot{F}_{jk}) = \Sigma_{ik} \dot{E}_{ik}.$$

2.4.3 Rate of Mechanical Work for Infinitesimal Deformations

For infinitesimal motions, all stress measures are equal, and all strain rate measures can be approximated by the infinitesimal strain tensor $\boldsymbol{\varepsilon}$. The rate of work done by stresses per unit volume of either deformed or undeformed solid (the difference is neglected) can be expressed as $\sigma_{ij} \dot{\varepsilon}_{ij}$, and the work done on a volume V_0 of the solid is

$$\dot{r} = \int_A T_i(\mathbf{n}) v_i dA + \int_V \rho b_i v_i dV = \int_{V_0} \sigma_{ij} \dot{\varepsilon}_{ij} dV_0 + \frac{d}{dt} \left\{ \int_{V_0} \frac{1}{2} \rho_0 v_i v_i dV_0 \right\}.$$

2.4.4 The Principle of Virtual Work

The principle of virtual work forms the basis for the finite element method and so will be discussed in detail in this section. Suppose that a deformable solid is subjected to loading that induces a displacement field $\mathbf{u}(\mathbf{x})$ and a velocity field $\mathbf{v}(\mathbf{x})$, as shown in Figure 2.32. The loading consists of a prescribed displacement on part of the boundary (denoted by S_1), together with a traction \mathbf{t} (which may be zero in places) applied to the rest of the boundary (denoted by S_2). The loading induces a Cauchy stress σ_{ij} . The stress field satisfies the angular momentum balance equation $\sigma_{ij} = \sigma_{ji}$.

The principle of virtual work is a different way of rewriting partial differential equation for linear moment balance

$$\frac{\partial \sigma_{ji}}{\partial y_i} + \rho b_i = \rho \frac{dv_i}{dt}$$

in an equivalent *integral* form, which is much better suited for computer solution.

To express the principle, we define a *kinematically admissible virtual velocity field* $\delta\mathbf{v}(\mathbf{y})$, satisfying $\delta\mathbf{v} = 0$ on S_1 . You can visualize this field as a small change in the velocity of the solid if you like, but it is really just an arbitrary differentiable vector field. The term “kinematically admissible” is just a complicated way of saying that the field is continuous, differentiable, and satisfies $\delta\mathbf{v} = 0$ on S_1 ; that is to say, if you perturb the velocity by $\delta\mathbf{v}(\mathbf{y})$, the boundary conditions on displacement are still satisfied.

In addition, we define an associated *virtual velocity gradient and virtual stretch rate* as

$$\delta L_{ij} = \frac{\partial \delta v_i}{\partial y_j} \quad \delta D_{ij} = \frac{1}{2} \left(\frac{\partial \delta v_i}{\partial y_j} + \frac{\partial \delta v_j}{\partial y_i} \right).$$

The principle of virtual work may be stated in two ways.

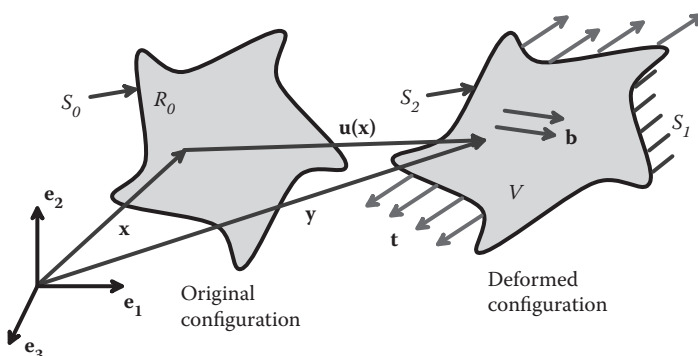


FIGURE 2.32 Deformation induced by external forces acting on a solid.

2.4.4.1 First Version of the Principle of Virtual Work

The first is not very interesting, but we will state it anyway. Suppose that the Cauchy stress satisfies the following:

1. The boundary condition $n_i \sigma_{ij} = t_j$ on S_2
2. The linear momentum balance equation

$$\frac{\partial \sigma_{ji}}{\partial y_j} + \rho b_i = \rho \frac{dv_i}{dt}.$$

Then the virtual work equation

$$\int_V \sigma_{ij} \delta D_{ij} dV + \int_V \rho \frac{dv_i}{dt} \delta v_i dV - \int_V \rho b_i \delta v_i dV - \int_{S_2} t_i \delta v_i dA = 0$$

is satisfied for all virtual velocity fields.

This result can be proven as follows. Observe that, because the Cauchy stress is symmetric,

$$\sigma_{ij} \delta D_{ij} = \frac{1}{2} \sigma_{ij} \left(\frac{\partial \delta v_i}{\partial y_j} + \frac{\partial \delta v_j}{\partial y_i} \right) = \frac{1}{2} \left(\sigma_{ji} \frac{\partial \delta v_i}{\partial y_j} + \sigma_{ij} \frac{\partial \delta v_j}{\partial y_i} \right) = \sigma_{ji} \frac{\partial \delta v_i}{\partial y_j}.$$

Next, note that

$$\sigma_{ji} \frac{\partial v_i}{\partial y_j} = \frac{\partial}{\partial y_j} (\sigma_{ji} \delta v_i) - \frac{\partial \sigma_{ji}}{\partial y_j} \delta v_i.$$

Finally, substituting the latter identity into the virtual work equation, applying the divergence theorem, using the linear momentum balance equation and boundary conditions on σ and $\delta v(y)$, we obtain the required result.

2.4.4.2 Second Version of the Principle of Virtual Work

The converse of this statement is much more interesting and useful. Suppose that σ_{ij} satisfies the virtual work equation

$$\int_V \sigma_{ij} \delta D_{ij} dV + \int_V \rho \frac{dv_i}{dt} \delta v_i dV - \int_V \rho b_i \delta v_i dV - \int_{S_2} t_i \delta v_i dA = 0$$

60 ■ Applied Mechanics of Solids

for all virtual velocity fields $\delta v(y)$. Then the stress field must satisfy the following:

1. The boundary condition $n_i \sigma_{ij} = t_j$ on S_2
2. The linear momentum balance equation

$$\frac{\partial \sigma_{ji}}{\partial y_j} + \rho b_i = \rho \frac{dv_i}{dt}.$$

The significance of this result is that it gives us an alternative way to solve for a stress field that satisfies the linear momentum balance equation, which avoids having to differentiate the stress. It is not easy to differentiate functions accurately in the computer, but it is easy to integrate them. The virtual work statement is the starting point for any finite element solution involving deformable solids.

To prove this result, follow the same preliminary steps as before, i.e.,

$$\begin{aligned}\sigma_{ij} \delta D_{ij} &= \frac{1}{2} \sigma_{ij} \left(\frac{\partial \delta v_i}{\partial y_j} + \frac{\partial \delta v_j}{\partial y_i} \right) = \frac{1}{2} \left(\sigma_{ji} \frac{\partial \delta v_i}{\partial y_j} + \sigma_{ij} \frac{\partial \delta v_j}{\partial y_i} \right) = \sigma_{ji} \frac{\partial \delta v_i}{\partial y_j} \\ \sigma_{ji} \frac{\partial v_i}{\partial y_j} &= \frac{\partial}{\partial y_j} (\sigma_{ji} \delta v_i) - \frac{\partial \sigma_{ji}}{\partial y_j} \delta v_i,\end{aligned}$$

and substitute into the virtual work equation

$$\int_V \left\{ \frac{\partial}{\partial y_j} (\sigma_{ji} \delta v_i) - \frac{\partial \sigma_{ji}}{\partial y_j} \delta v_i \right\} dV + \int_V \rho \frac{dv_i}{dt} \delta v_i dV - \int_V \rho b_i \delta v_i dV - \int_{S_2} t_i \delta v_i dA = 0.$$

Apply the divergence theorem to the first term in the first integral and recall that $\delta v = 0$ on S_1 to see that

$$-\int_V \left\{ \frac{\partial \sigma_{ji}}{\partial y_j} + \rho b_i - \rho \frac{dv_i}{dt} \right\} \delta v_i dV + \int_{S_2} (\sigma_{ji} n_j - t_i) \delta v_i dA = 0.$$

Because this must hold for all virtual velocity fields, we could choose

$$\delta v_i = f(y) \left\{ \frac{\partial \sigma_{ji}}{\partial y_j} + \rho b_i - \rho \frac{dv_i}{dt} \right\}$$

where $f(\mathbf{y}) = 0$ is an arbitrary function that is positive everywhere inside the solid but is equal to zero on S . For this choice, the virtual work equation reduces to

$$-\int_V f(\mathbf{y}) \left\{ \frac{\partial \sigma_{ji}}{\partial y_j} + \rho b_i - \rho \frac{dv_i}{dt} \right\} \left\{ \frac{\partial \sigma_{ki}}{\partial y_k} + \rho b_i - \rho \frac{dv_i}{dt} \right\} dV = 0,$$

and, because the integrand is positive everywhere, the only way the equation can be satisfied is if

$$\frac{\partial \sigma_{ji}}{\partial y_j} + \rho b_i = \rho \frac{dv_i}{dt}.$$

Given this, we can next choose a virtual velocity field that satisfies

$$\delta v_i = (\sigma_{ji} n_j - t_i)$$

on S_2 . For this choice (and noting that the volume integral is zero), the virtual work equation reduces to

$$+\int_{S_2} (\sigma_{ji} n_j - t_i)(\sigma_{ki} n_k - t_i) dA = 0.$$

Again, the integrand is positive everywhere (it is a perfect square) and so can vanish only if $\sigma_{ji} n_j = t_i$ as stated.

2.4.5 The Virtual Work Equation in Terms of Other Stress Measures

It is often convenient to implement the virtual work equation in a finite element code using different stress measures. To do so, we define the following:

1. The actual deformation gradient in the solid $F_{ij} = \delta_{ij} + \frac{\partial u_i}{\partial x_j}$
2. The virtual rate of change of deformation gradient $\delta \dot{F}_{ij} = \frac{\partial \delta v_i}{\partial y_k} F_{kj} = \frac{\partial \delta v_i}{\partial x_j}$
3. The virtual rate of change of Lagrange strain $\delta \dot{E}_{ij} = \frac{1}{2}(F_{ki} \delta \dot{F}_{kj} + \delta \dot{F}_{ki} F_{kj})$

In addition, we define (in the usual way)

1. Kirchhoff stress $\tau_{ij} = J \sigma_{ij}$
2. Nominal (first Piola–Kirchhoff) stress $S_{ij} = J F_{ik}^{-1} \sigma_{kj}$
3. Material (second Piola–Kirchhoff) stress $\Sigma_{ij} = J F_{ik}^{-1} \sigma_{ik} F_{jl}^{-1}$

In terms of these quantities, the virtual work equation may be expressed as

$$\begin{aligned} \int_{V_0} \tau_{ij} \delta D_{ij} dV_0 + \int_{V_0} \rho_0 \frac{dv_i}{dt} \delta v_i dV_0 - \int_{V_0} \rho_0 b_i \delta v_i dV_0 - \int_{S_2} t_i \delta v_i dA &= 0 \\ \int_{V_0} S_{ij} \delta \dot{F}_{ji} dV_0 + \int_{V_0} \rho_0 \frac{dv_i}{dt} \delta v_i dV_0 - \int_{V_0} \rho_0 b_i \delta v_i dV_0 - \int_{S_2} t_i \delta v_i dA &= 0 \\ \int_{V_0} \Sigma_{ij} \delta \dot{E}_{ij} dV_0 + \int_{V_0} \rho_0 \frac{dv_i}{dt} \delta v_i dV_0 - \int_{V_0} \rho_0 b_i \delta v_i dV_0 - \int_{S_2} t_i \delta v_i dA &= 0. \end{aligned}$$

Note that all the volume integrals are now taken over the undeformed solid; this is convenient for computer applications because the shape of the undeformed solid is known. The area integral is evaluated over the deformed solid, unfortunately. It can be expressed as an equivalent integral over the undeformed solid, but the result is messy and will be deferred until we actually need to do it.

2.4.6 The Virtual Work Equation for Infinitesimal Deformations

For infinitesimal motions, the Cauchy, nominal, and material stress tensors are equal, and the virtual stretch rate can be replaced by the virtual infinitesimal strain rate

$$\delta \dot{\epsilon}_{ij} = \frac{1}{2} \left(\frac{\partial \delta v_i}{\partial x_j} + \frac{\partial \delta v_j}{\partial x_i} \right).$$

There is no need to distinguish between the volume or surface area of the deformed and undeformed solid. The virtual work equation can thus be expressed as

$$\int_{V_0} \sigma_{ij} \delta \dot{\epsilon}_{ij} dV_0 + \int_{V_0} \rho_0 \frac{dv_i}{dt} \delta v_i dV_0 - \int_{V_0} \rho_0 b_i \delta v_i dV_0 - \int_{S_2} t_i \delta v_i dA_0 = 0$$

for all kinematically admissible velocity fields.

As a special case, this expression can be applied to a quasi-static state with $v_i = 0$. Then, for a stress state σ_{ij} satisfying the static equilibrium equation $d\sigma_{ij}/dx_i + \rho_0 b_j = 0$ and boundary conditions $\sigma_{ij} n_j = t_i$ on S_2 , the virtual work equation reduces to

$$\int_{V_0} \sigma_{ij} \delta \epsilon_{ij} dV_0 = \int_{V_0} \rho_0 b_i \delta u_i dV_0 + \int_{S_2} t_i \delta u_i dA,$$

in which δu_i are kinematically admissible displacements components ($\delta u_i = 0$ on S_2) and $\delta \varepsilon_{ij} = (\partial \delta u_i / \partial x_j + \partial \delta u_j / \partial x_i) / 2$. Conversely, if the stress state σ_{ij} satisfies

$$\int_{V_0} \sigma_{ij} \delta \varepsilon_{ij} dV_0 = \int_{V_0} \rho_0 b_i \delta u_i dV_0 + \int_{S_2} t_i \delta u_i dA$$

for every set of kinematically admissible virtual displacements, then the stress state σ_{ij} satisfies the static equilibrium equation $\partial \sigma_{ij} / \partial x_i + \rho_0 b_j = 0$ and boundary conditions $\sigma_{ij} n_j = t_i$ on S_2 .

This page intentionally left blank

Constitutive Models: Relations between Stress and Strain

The equations listed in Chapter 2 are universal: they apply to all deformable solids. They cannot be solved, however, unless the deformation measure can be related to the internal forces.

The *constitutive model* for a material is a set of equations relating stress to strain (and possibly strain history, strain rate, and other field quantities). Unlike the governing equations in the previous chapter, these equations cannot generally be calculated using fundamental physical laws (although people are trying to do these calculations). Instead, constitutive models are fit to experimental measurements.

Before discussing specific constitutive models, it is helpful to review the basic assumptions that we take for granted in developing stress-strain laws. They are listed below:

- A very small sample that is extracted from the solid has uniform properties.
- When the solid is deformed, initially straight lines in the solid are deformed into smooth curves (with continuous slope), as shown in Figure 3.1.
- This means that very short line segments (much shorter than the radius of curvature of the curves) are just stretched and rotated by the deformation. Consequently, the

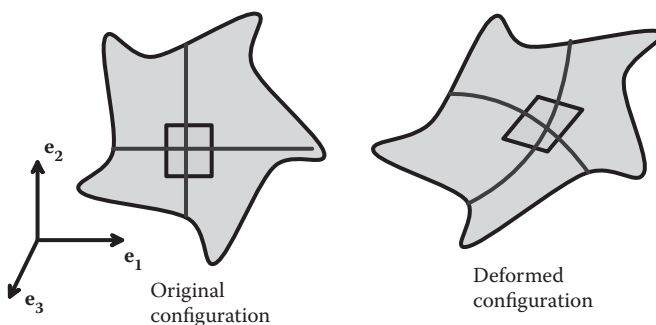


FIGURE 3.1 Deformation of an internal material element in a solid.

deformation of a sufficiently small volume element can be characterized by the deformation gradient.

- The stress at a point in the solid depends only on the change in shape of a vanishingly small volume element surrounding the point. It must therefore be a function of the deformation gradient or a strain measure that is derived from it.

If we accept the preceding assumptions, it means that we can measure the relationship between stress and strain by doing an experiment that induces a *uniform* strain in a suitable sample of the material. According to our assumptions, the stress should also be uniform and can be calculated from the forces acting on the specimen.

These are clearly approximations. Materials are not really uniform at small scales, whether you choose to look at the atomic scale or the microstructural scale. However, these features are usually much smaller than the solid part or component, and the material can be regarded as *statistically* uniform, in the sense that, if you cut two specimens with similar size out of the material, they will behave in the same way. A continuum model then describes the *average* stress and deformation in a region of the material that is larger than microstructural features but small compared with the dimensions of the part.

3.1 GENERAL REQUIREMENTS FOR CONSTITUTIVE EQUATIONS

You may be called on to develop a stress-strain law for a new material at some point in your career. If so, it is essential to make sure that the stress-strain law satisfies two conditions:

1. It must obey the laws of thermodynamics.
2. It must satisfy the condition of objectivity or material frame indifference.

In addition, it is a good idea to ensure that the material satisfies the Drucker stability criterion discussed in more detail below. Of course, your proposed law must conform to experimental measurements and, if possible, should be based on some understanding of the physical processes that govern the response of the solid.

3.1.1 Thermodynamic Restrictions

The laws of thermodynamics impose two restrictions on stress-strain laws:

1. The first law requires that the work done by stresses must either be stored as recoverable internal energy in the solid or be dissipated as heat (or a combination of both).
2. The second law requires that, if a sample of the material is subjected to a cycle of deformation that starts and ends with an identical strain and internal energy (at constant temperature or without heat exchange with the surroundings), the total work done must be positive or zero.

3.1.2 Objectivity

Strictly speaking, the term *objectivity* or *material frame independence* is the condition that the tensor-valued functions that relate stress to deformation measure must transform correctly

under a change of basis and change of origin for the coordinate system. A detailed mathematical derivation of the consequences of objectivity will not be given here [for more details, see Malvern 1969]. However, you can check whether a constitutive law is objective using the following simple (analytical) test:

1. Load the solid (quasi-statically) by subjecting its boundary to prescribed forces, to induce a Cauchy stress $\sigma_{ij}^{(0)}$ in the solid.
2. Subject both the solid, and the loads acting on the solid, to a quasi-static rigid rotation, characterized by a rotation tensor R_{ij} , as shown in Figure 3.2.
3. The constitutive law must predict that, after the rotation, the stress components change to new values given by $\sigma_{ij}^{(1)} = R_{ik}\sigma_{kl}^{(0)}R_{jl}$.

To see this, note that, because the loads rotate together with the solid, the components of traction acting normal and tangent to any interior material plane in the solid must remain constant. With this in mind,

1. Suppose that, just before the rotation is applied, $T_i^{(0)} = n_k^{(0)}\sigma_{ki}^{(0)}$ denotes the traction acting on an interior material plane with normal $n_i^{(0)}$.
2. The traction vector and the normal to the interior plane rotate with the solid and therefore have components $T_i^{(1)} = R_{ij}T_j^{(0)}$ and $n_i^{(1)} = R_{ij}n_j^{(0)}$ after rotation.
3. By definition, $T_i^{(1)} = n_j^{(1)}\sigma_{ji}^{(1)}$. From 2 above, we see therefore that $R_{ik}T_k^{(0)} = R_{kl}n_l^{(0)}\sigma_{ki}^{(1)}$.
4. Multiply both sides of this equation by R_{ip} and recall that $R_{ip}R_{ik} = \delta_{kp}$ to see that $T_p^{(0)} = n_l^{(0)}R_{kl}\sigma_{ki}^{(1)}R_{ip}$.
5. Comparing this with 1 above, we conclude that $R_{kl}\sigma_{ki}^{(1)}R_{ip} = \sigma_{lp}^{(0)}$. Finally, multiplying both sides of this equation by $R_{jn}R_{np}$, we conclude that $\sigma_{jn}^{(1)} = R_{jl}\sigma_{lp}^{(0)}R_{np}$, giving the required result.

3.1.3 Drucker Stability

For most practical applications, the constitutive equation must satisfy a condition known as the *Drucker stability criterion*, which can be expressed as follows. Consider a deform-

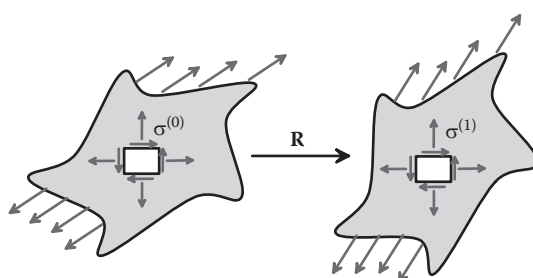


FIGURE 3.2 Loaded solid subjected to a rigid rotation.

able solid, subjected to boundary tractions t_i , which induce some displacement field u_i , as shown in Figure 3.3. Suppose that the tractions are increased to $t_i + \Delta t_i$, resulting in an additional displacement Δu_i . The material is said to be stable in the sense of Drucker if the work done by the tractions Δt_i through the displacements Δu_i is positive or zero for all Δt_i :

$$\Delta W = \int \left\{ \int_A \Delta t_i \frac{d\Delta u_i}{dt} \right\} dt \geq 0.$$

You can show that this condition is satisfied as long as the stress-strain relation obeys

$$\Delta \tau_{ij} \Delta \varepsilon_{ij} \geq 0,$$

where $\Delta \tau_{ij}$ is the change in Kirchhoff stress, and $\Delta \varepsilon_{ij} = (\partial \Delta u_i / \partial x_j + \partial \Delta u_j / \partial x_i)$ is an increment in strain resulting from an infinitesimal change in displacement Δu_i .

This is not a thermodynamic law (the work done by the *change* in tractions is not a physically meaningful quantity), and there is nothing to say that real materials have to satisfy Drucker stability. In fact, many materials show clear signs that they are *not* stable in the sense of Drucker. However, if you try to solve a boundary value problem for a material that violates the Drucker stability criterion, you are likely to run into trouble. The problem will probably not have a unique solution, and, in addition, you are likely to find that smooth curves on the undeformed solid develop *kinks* (and may not even be continuous) after the solid is deformed. This kind of deformation violates one of the fundamental assumptions underlying continuum constitutive equations.

A simple example of a stress-strain curve for material that is not stable in the sense of Drucker is shown in Figure 3.4. The stability criterion is violated wherever the stress

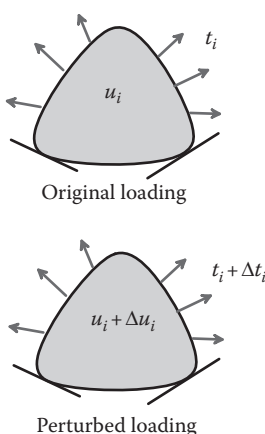


FIGURE 3.3 Deformation in a solid subjected to an increment in external forces.

decreases with strain in tension or increases with strain in compression. For the former, we see that $\Delta\sigma_{11} < 0$, whereas $\Delta\varepsilon_{11} > 0$; for the latter $\Delta\sigma_{11} > 0$, whereas $\Delta\varepsilon_{11} < 0$.

In the following chapter, we outline constitutive laws that were developed to approximate the behavior of a wide range of materials, including polycrystalline metals and nonmetals, elastomers, polymers, biological tissue, soils, and metal single crystals. A few additional material models, which account for material failure, are described in Chapter 9.

3.2 LINEAR ELASTIC MATERIAL BEHAVIOR

You are probably familiar with the behavior of linear elastic materials from introductory materials courses. Their main features are reviewed briefly below.

3.2.1 Isotropic, Linear Elastic Material Behavior

If you conduct a uniaxial tensile test on almost any material, and keep the stress levels sufficiently low, you will observe the following behavior:

- The specimen deforms reversibly: if you remove the loads, the solid returns to its original shape.
- The strain in the specimen depends only on the stress applied to it; it does not depend on the rate of loading or the history of loading.
- For most materials, the stress is a linear function of strain, as shown in Figure 3.5. Because the strains are small, this is true whatever stress measure is adopted (Cauchy stress or nominal stress) and is true whatever strain measure is adopted (Lagrange strain or infinitesimal strain).
- For most, but not all, materials, the material has no characteristic orientation. Thus, if you cut a tensile specimen out of a block of material, as shown in Figure 3.6, the stress-strain curve will be independent of the orientation of the specimen relative to the block of material. Such materials are said to be isotropic.
- If you heat a specimen of the material, increasing its temperature uniformly, it will generally change its shape slightly. If the material is isotropic (no preferred material orientation) and homogeneous, then the specimen will simply increase in size, without shape change.

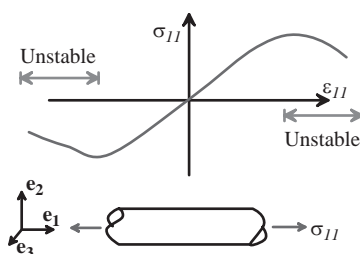


FIGURE 3.4 Unstable regions of a uniaxial stress-strain curve.

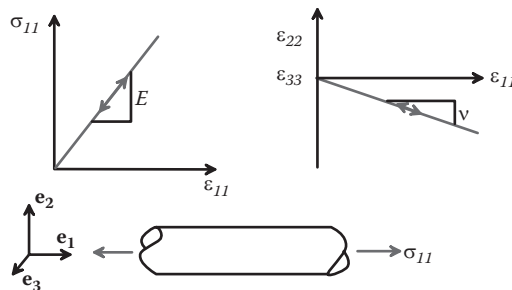


FIGURE 3.5 Stress-strain curves for a linear elastic solid.

3.2.2 Stress–Strain Relations for Isotropic, Linear Elastic Materials: Young's Modulus, Poisson's Ratio, and the Thermal Expansion Coefficient

Before writing down stress-strain relations, we need to decide what strain and stress measures we want to use. Because the model only works for small shape changes,

- Deformation is characterized using the infinitesimal strain tensor $\varepsilon_{ij} = (\partial u_i / \partial x_j + \partial u_j / \partial x_i) / 2$ defined in Section 2.1.7. This is convenient for calculations but has the disadvantage that linear elastic constitutive equations can only be used if the solid experiences small rotations, as well as small shape changes.
- All stress measures are taken to be equal. We can use the Cauchy stress σ_{ij} as the stress measure.

You probably already know the stress-strain relations for an isotropic, linear elastic solid. They are repeated below for convenience:

$$\begin{bmatrix} \varepsilon_{11} \\ \varepsilon_{22} \\ \varepsilon_{33} \\ 2\varepsilon_{23} \\ 2\varepsilon_{13} \\ 2\varepsilon_{12} \end{bmatrix} = \frac{1}{E} \begin{bmatrix} 1 & -\nu & -\nu & 0 & 0 & 0 \\ -\nu & 1 & -\nu & 0 & 0 & 0 \\ -\nu & -\nu & 1 & 0 & 0 & 0 \\ 0 & 0 & 0 & 2(1+\nu) & 0 & 0 \\ 0 & 0 & 0 & 0 & 2(1+\nu) & 0 \\ 0 & 0 & 0 & 0 & 0 & 2(1+\nu) \end{bmatrix} + \alpha \Delta T \begin{bmatrix} 1 \\ 1 \\ 1 \\ 0 \\ 0 \\ 0 \end{bmatrix}.$$

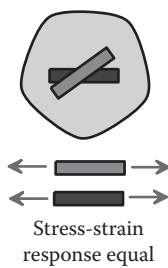


FIGURE 3.6 Specimens extracted from an isotropic material.

Here, E and ν are Young's modulus and Poisson's ratio, α is the coefficient of thermal expansion, and ΔT is the increase in temperature of the solid. The remaining relations can be deduced from the fact that both σ_{ij} and ε_{ij} are symmetric.

The inverse relationship can be expressed as

$$\begin{bmatrix} \sigma_{11} \\ \sigma_{22} \\ \sigma_{33} \\ \sigma_{23} \\ \sigma_{13} \\ \sigma_{12} \end{bmatrix} = \frac{E}{(1+\nu)(1-2\nu)} \begin{bmatrix} 1-\nu & \nu & \nu & 0 & 0 & 0 \\ \nu & 1-\nu & \nu & 0 & 0 & 0 \\ \nu & \nu & 1-\nu & 0 & 0 & 0 \\ 0 & 0 & 0 & \frac{(1-2\nu)}{2} & 0 & 0 \\ 0 & 0 & 0 & 0 & \frac{(1-2\nu)}{2} & 0 \\ 0 & 0 & 0 & 0 & 0 & \frac{(1-2\nu)}{2} \end{bmatrix} \begin{bmatrix} \varepsilon_{11} \\ \varepsilon_{22} \\ \varepsilon_{33} \\ 2\varepsilon_{23} \\ 2\varepsilon_{13} \\ 2\varepsilon_{12} \end{bmatrix} - \frac{E\alpha\Delta T}{1-2\nu} \begin{bmatrix} 1 \\ 1 \\ 1 \\ 0 \\ 0 \\ 0 \end{bmatrix}.$$

HEALTH WARNING: Note the factor of 2 in the strain vector. Most texts and most finite element codes use this factor of 2 but not all. In addition, shear strains and stresses are often listed in a different order in the strain and stress vectors. For isotropic materials, this makes no difference, but you need to be careful when listing material constants for anisotropic materials.

We can write this expression in a much more convenient form using index notation. Verify for yourself that the matrix expression above is equivalent to

$$\varepsilon_{ij} = \frac{1+\nu}{E} \sigma_{ij} - \frac{\nu}{E} \sigma_{kk} \delta_{ij} + \alpha \Delta T \delta_{ij}.$$

The inverse relation is

$$\sigma_{ij} = \frac{E}{1+\nu} \left\{ \varepsilon_{ij} + \frac{\nu}{1-2\nu} \varepsilon_{kk} \delta_{ij} \right\} - \frac{E\alpha\Delta T}{1-2\nu} \delta_{ij}.$$

The stress-strain relations are often expressed using the *elastic modulus tensor* C_{ijkl} or the *elastic compliance tensor* S_{ijkl} as

$$\sigma_{ij} = C_{ijkl} (\varepsilon_{kl} - \alpha \Delta T \delta_{kl}) \quad \varepsilon_{ij} = S_{ijkl} \sigma_{kl} + \alpha \Delta T \delta_{ij}.$$

In terms of elastic constants, C_{ijkl} and S_{ijkl} are

$$C_{ijkl} = \frac{E}{2(1+\nu)} (\delta_{il}\delta_{jk} + \delta_{ik}\delta_{jl}) + \frac{E\nu}{(1+\nu)(1-2\nu)} \delta_{ij}\delta_{kl}$$

$$S_{ijkl} = \frac{1+\nu}{2E} (\delta_{il}\delta_{jk} + \delta_{ik}\delta_{jl}) - \frac{\nu}{E} \delta_{ij}\delta_{kl}.$$

3.2.3 Reduced Stress–Strain Equations for Plane Deformation of Isotropic Solids

For *plane strain* or *plane stress* deformations, some strain or stress components are always zero (by definition) so the stress-strain laws can be simplified.

- For a plane strain deformation, $\varepsilon_{33} = \varepsilon_{23} = \varepsilon_{13} = 0$. The stress-strain laws are therefore

$$\begin{bmatrix} \varepsilon_{11} \\ \varepsilon_{22} \\ 2\varepsilon_{12} \end{bmatrix} = \frac{(1+\nu)}{E} \begin{bmatrix} 1-\nu & -\nu & 0 \\ -\nu & 1-\nu & 0 \\ 0 & 0 & 2 \end{bmatrix} \begin{bmatrix} \sigma_{11} \\ \sigma_{22} \\ \sigma_{12} \end{bmatrix} + (1+\nu)\alpha\Delta T \begin{bmatrix} 1 \\ 1 \\ 0 \end{bmatrix}$$

$$\begin{bmatrix} \sigma_{11} \\ \sigma_{22} \\ \sigma_{12} \end{bmatrix} = \frac{E}{(1+\nu)(1-2\nu)} \begin{bmatrix} 1-\nu & \nu & 0 \\ \nu & 1-\nu & 0 \\ 0 & 0 & \frac{1-2\nu}{2} \end{bmatrix} \begin{bmatrix} \varepsilon_{11} \\ \varepsilon_{22} \\ 2\varepsilon_{12} \end{bmatrix} - \frac{E\alpha\Delta T}{1-2\nu} \begin{bmatrix} 1 \\ 1 \\ 0 \end{bmatrix}$$

$$\sigma_{33} = \frac{Ev(\varepsilon_{11} + \varepsilon_{22})}{(1-2\nu)(1+\nu)} + \frac{E\alpha\Delta T}{1-2\nu}, \quad \sigma_{13} = \sigma_{23} = 0$$

In index notation,

$$\varepsilon_{\alpha\beta} = \frac{1+\nu}{E} \left\{ \sigma_{\alpha\beta} - \nu \sigma_{\gamma\gamma} \delta_{\alpha\beta} \right\} + (1+\nu)\alpha\Delta T \delta_{\alpha\beta} \quad \sigma_{\alpha\beta} = \frac{E}{1+\nu} \left\{ \varepsilon_{\alpha\beta} + \frac{\nu}{1-2\nu} \varepsilon_{\gamma\gamma} \delta_{\alpha\beta} \right\} - \frac{E\alpha\Delta T}{1-2\nu} \delta_{\alpha\beta}$$

where Greek subscripts α, β can have values 1 or 2.

- For a plane stress deformation, $\sigma_{33} = \sigma_{23} = \sigma_{13} = 0$, and the stress-strain relations are

$$\begin{bmatrix} \varepsilon_{11} \\ \varepsilon_{22} \\ 2\varepsilon_{12} \end{bmatrix} = \frac{1}{E} \begin{bmatrix} 1 & -\nu & 0 \\ -\nu & 1 & 0 \\ 0 & 0 & 2(1+\nu) \end{bmatrix} \begin{bmatrix} \sigma_{11} \\ \sigma_{22} \\ \sigma_{12} \end{bmatrix} + \alpha\Delta T \begin{bmatrix} 1 \\ 1 \\ 0 \end{bmatrix}$$

$$\begin{bmatrix} \sigma_{11} \\ \sigma_{22} \\ \sigma_{12} \end{bmatrix} = \frac{E}{(1-\nu^2)} \begin{bmatrix} 1 & \nu & 0 \\ \nu & 1 & 0 \\ 0 & 0 & (1-\nu)/2 \end{bmatrix} \begin{bmatrix} \varepsilon_{11} \\ \varepsilon_{22} \\ 2\varepsilon_{12} \end{bmatrix} - \frac{E\alpha\Delta T}{(1-\nu)} \begin{bmatrix} 1 \\ 1 \\ 0 \end{bmatrix}$$

$$\varepsilon_{33} = -\frac{\nu}{E} (\sigma_{11} + \sigma_{22}) + \alpha\Delta T$$

$$\varepsilon_{\alpha\beta} = \frac{1+\nu}{E} \left(\sigma_{\alpha\beta} - \frac{\nu}{1+\nu} \sigma_{\gamma\gamma} \delta_{\alpha\beta} \right) + \alpha\Delta T \delta_{\alpha\beta} \quad \sigma_{\alpha\beta} = \frac{E}{1+\nu} \left\{ \varepsilon_{\alpha\beta} + \frac{\nu}{1-\nu} \varepsilon_{\gamma\gamma} \delta_{\alpha\beta} \right\} - \frac{E\alpha\Delta T}{1-\nu} \delta_{\alpha\beta}.$$

3.2.4 Representative Values for Density and Elastic Constants of Isotropic Solids

Table 3.1 shows representative elastic constants for a range of different materials. The data are partly from Ashby and Jones [1997] and partly from manufacturers data sheets (web-based databases such as <http://www.matweb.com> are helpful sources of material data).

Note the units: values of E are given in GN/m^2 ; the G stands for giga and is short for 10^9 . The units for density are in Mgm^{-3} , which is megagrams. One megagram is 1000 kg.

TABLE 3.1 Elastic Constants for Isotropic Materials

Material	Mass Density ρ / Mgm^{-3}	Young's Modulus E / GNm^{-2}	Poisson's Ratio ν	Expansion Coefficient K^{-1}
Tungsten carbide	14–17	450–650	0.22	5×10^{-6}
Silicon carbide	2.5–3.2	450	0.22	4×10^{-6}
Tungsten	13.4	410	0.30	4×10^{-6}
Alumina	3.9	390	0.25	7×10^{-6}
Titanium carbide	4.9	380	0.19	13×10^{-6}
Silicon nitride	3.2	320–270	0.22	3×10^{-6}
Nickel	8.9	215	0.31	14×10^{-6}
CFRP	1.5–1.6	70–200	0.20	2×10^{-6}
Iron	7.9	196	0.30	13×10^{-6}
Low alloy steels	7.8	200–210	0.30	15×10^{-6}
Stainless steel	7.5–7.7	190–200	0.30	11×10^{-6}
Mild steel	7.8	196	0.30	15×10^{-6}
Copper	8.9	124	0.34	16×10^{-6}
Titanium	4.5	116	0.30	9×10^{-6}
Silicon	2.5–3.2	107	0.22	5×10^{-6}
Silica glass	2.6	94	0.16	0.5×10^{-6}
Aluminum and alloys	2.6–2.9	69–79	0.35	22×10^{-6}
Concrete	2.4–2.5	45–50	0.3	10×10^{-6}
GFRP	1.4–2.2	7–45	0.25	10×10^{-6}
Wood, parallel grain	0.4–0.8	9–16	0.2	40×10^{-6}
Polyimides	1.4	3–5	0.1–0.45	40×10^{-6}
Nylon	1.1 – 1.2	2–4	0.25	81×10^{-6}
PMMA	1.2	3.4	0.35–0.4	50×10^{-6}
Polycarbonate	1.2 – 1.3	2.6	0.36	65×10^{-6}
Natural rubbers	0.83–0.91	0.01–0.1	0.49	200×10^{-6}
PVC	1.3–1.6	0.003–0.01	0.41	70×10^{-6}

3.2.5 Other Elastic Constants: Bulk, Shear, and Lame Modulus

Young's modulus and Poisson's ratio are the most common properties used to characterize elastic solids, but other measures are also used. For example, we define the shear modulus, bulk modulus, and Lame modulus of an elastic solid as follows:

$$\text{Bulk Modulus } K = \frac{E}{3(1 - 2\nu)}$$

$$\text{Shear Modulus } \mu = \frac{E}{2(1 + \nu)}$$

$$\text{Lame Modulus } \lambda = \frac{\nu E}{(1 + \nu)(1 - 2\nu)}.$$

Table 3.2 relates all the possible combinations of moduli to all other possible combinations. Enjoy!

TABLE 3.2 Relations between Elastic Constants

Lame Modulus λ	Shear Modulus μ	Young's Modulus E	Poisson's Ratio ν	Bulk Modulus K
λ, μ		$\frac{(3\lambda + 2\nu)}{\lambda + 2\nu}$	$\frac{\lambda}{2(\lambda + 2\nu)}$	$\frac{3\lambda + 2\nu}{3}$
λ, E	Irrational		Irrational	Irrational
λ, ν	$\frac{\lambda(1 - 2\nu)}{2\nu}$	$\frac{\lambda(1 + \nu)(1 - 2\nu)}{\nu}$		$\frac{\lambda(1 + \nu)}{3\nu}$
λ, K	$\frac{3(K - \lambda)}{2}$	$\frac{9K(K - \lambda)}{3K - \lambda}$	$\frac{\lambda}{3K - \lambda}$	
μ, E	$\frac{(2\nu - E)}{E - 3}$		$\frac{E - 2\nu}{2}$	$\frac{E}{3(3\nu - E)}$
μ, ν	$\frac{2\nu}{1 - 2\nu}$	$2\nu(1 + \nu)$		$\frac{2\nu(1 + \nu)}{3(1 - 2\nu)}$
μ, K	$\frac{3K - 2\nu}{3}$	$\frac{9K}{3K + 2\nu}$	$\frac{3K - 2\nu}{2(3K + 2\nu)}$	
E, ν	$\frac{\nu E}{(1 + \nu)(1 - 2\nu)}$	$\frac{E}{2(1 + \nu)}$		$\frac{E}{3(1 - 2\nu)}$
E, K	$\frac{3K(3K - E)}{9K - E}$	$\frac{3EK}{9K - E}$		$\frac{3K - E}{6K}$
ν, K	$\frac{3K\nu}{(1 + \nu)}$	$\frac{3K(1 - 2\nu)}{2(1 + \nu)}$	$3K(1 - 2\nu)$	

3.2.6 Physical Interpretation of Elastic Constants for Isotropic Solids

It is important to have a feel for the physical significance of the various elastic constants. They can be interpreted as follows:

- Young's modulus E is the slope of the stress-strain curve in uniaxial tension. It has dimensions of stress (N/m^2) and is usually large, for steel, $E = 210 \times 10^9 N/m^2$. You can think of E as a measure of the stiffness of the solid. The larger the value of E , the stiffer the solid. For a stable material, the Young's modulus must satisfy $E > 0$.
- Poisson's ratio ν is the ratio of lateral to longitudinal strain in uniaxial tensile stress. It is dimensionless and typically ranges from 0.2 to 0.49 and is around 0.3 for most metals. For a stable material, Poisson's ratio is in the range of $-1 < \nu < 0.5$. It is a measure of the compressibility of the solid. If $\nu = 0.5$, the solid is incompressible; its volume remains constant, no matter how it is deformed. If $\nu = 0$, then stretching a specimen causes no lateral contraction. Some bizarre materials have $\nu < 0$; if you stretch a round bar of such a material, the bar increases in diameter!
- Thermal expansion coefficient quantifies the change in volume of a material if it is heated in the absence of stress. It has dimensions of $(\text{Kelvin})^{-1}$ and is usually very small. For steel, $\alpha \approx 6-10 \times 10^{-6} K^{-1}$.
- The bulk modulus quantifies the resistance of the solid to volume changes. It has a large value (usually bigger than E).
- The shear modulus quantifies its resistance to volume preserving shear deformations. Its value is usually somewhat smaller than E .

3.2.7 Strain Energy Density for Isotropic Solids

The following observations are the basis for defining the strain energy density of an elastic material:

- If you deform a block of material, you do work on it (or, in some cases, it may do work on you ...).
- In an elastic material, the work done during loading is stored as recoverable strain energy in the solid. If you unload the material, the specimen does work on you; when it reaches its initial configuration, you come out even.
- The work done to deform a specimen depends only on the state of strain at the end of the test. It is independent of the history of loading.

Based on these observations, we define the strain energy density of a solid as the work done per unit volume to deform a material from a stress-free reference state to a loaded state.

To write down an expression for the strain energy density, it is convenient to separate the strain into two parts:

$$\boldsymbol{\varepsilon}_{ij} = \boldsymbol{\varepsilon}_{ij}^e + \boldsymbol{\varepsilon}_{ij}^T$$

where, for an isotropic solid,

$$\varepsilon_{ij}^T = \alpha \Delta T \delta_{ij}$$

represents the strain attributable to thermal expansion (known as thermal strain), and

$$\varepsilon_{ij}^e = \frac{1 + \nu}{E} \sigma_{ij} - \frac{\nu}{E} \sigma_{kk} \delta_{ij}$$

is the strain attributable to mechanical loading (known as elastic strain). Work is done on the specimen only during mechanical loading. It is straightforward to show that the strain energy density is

$$U = \frac{1}{2} \sigma_{ij} \varepsilon_{ij}^e.$$

You can also rewrite this as

$$\begin{aligned} U &= \frac{1 + \nu}{2E} \sigma_{ij} \sigma_{ij} - \frac{\nu}{2E} \sigma_{kk} \sigma_{jj} \\ U &= \frac{E}{2(1 + \nu)} \varepsilon_{ij}^e \varepsilon_{ij}^e + \frac{Ev}{2(1 + \nu)(1 - 2\nu)} \varepsilon_{ij}^e \varepsilon_{kk}^e. \end{aligned}$$

Observe that

$$\varepsilon_{ij}^e = \frac{\partial U}{\partial \sigma_{ij}} \quad \sigma_{ij} = \frac{\partial U}{\partial \varepsilon_{ij}^e}.$$

3.2.8 Stress–Strain Relation for a General Anisotropic Linear Elastic Material: Elastic Stiffness and Compliance Tensors

The simple isotropic model described in the preceding section is unable to describe the response of some materials accurately, although the material may deform elastically. This is because some materials do have a characteristic orientation. For example, in a block of wood, the grain is oriented in a particular direction in the specimen. The block will be stiffer if it is loaded parallel to the grain than if it is loaded perpendicular to the grain. The same observation applies to fiber-reinforced composite materials. Generally, single crystal specimens of a material will also be anisotropic; this is important when modeling stress effects in small structures such as microelectronic circuits. Even polycrystalline metals may be anisotropic, because a preferred texture may form in the specimen during processing.

A more general stress-strain relation is needed to describe anisotropic solids. The most general linear stress-strain relation has the form

$$\sigma_{ij} = C_{ijkl} (\varepsilon_{kl} - \alpha_{kl} \Delta T).$$

Here, C_{ijkl} is a fourth-order tensor (horrors!), known as the elastic stiffness tensor, and $\alpha_{kl} = \alpha_{lk}$ is the thermal expansion coefficient tensor. The stress-strain relation is invertible:

$$\varepsilon_{ij} = S_{ijkl} \sigma_{kl} + \alpha_{ij} \Delta T,$$

where S_{ijkl} is known as the elastic compliance tensor.

At first sight, it appears that the stiffness tensor has 81 components. Imagine having to measure and keep track of 81 material properties! Fortunately, C_{ijkl} must have the following symmetries:

$$C_{ijkl} = C_{klij} = C_{jikl} = C_{ijlk}.$$

This reduces the number of material constants to 21. The compliance tensor has the same symmetries as C_{ijkl} . To see the origin of the symmetries of C_{ijkl} , note the following:

- The stress tensor is symmetric, which is only possible if $C_{ijkl} = C_{jikl}$.
- If a strain energy density exists for the material, the elastic stiffness tensor must satisfy $C_{ijkl} = C_{klij}$.
- The previous two symmetries imply $C_{ijkl} = C_{ijlk}$.

To see that $C_{ijkl} = C_{klij}$, note that, by definition

$$C_{ijkl} = \frac{\partial \sigma_{ij}}{\partial \varepsilon_{kl}}$$

and recall further that the stress is the derivative of the strain energy density with respect to strain

$$\sigma_{ij} = \frac{\partial U}{\partial \varepsilon_{ij}}.$$

Combining these,

$$C_{ijkl} = \frac{\partial^2 U}{\partial \varepsilon_{ij} \partial \varepsilon_{kl}}.$$

Now, note that

$$\frac{\partial^2 U}{\partial \varepsilon_{ij} \partial \varepsilon_{kl}} = \frac{\partial^2 U}{\partial \varepsilon_{kl} \partial \varepsilon_{ij}}$$

so that

$$C_{ijkl} = C_{klij}.$$

These symmetries allow us to write the stress-strain relations in a more compact matrix form as

$$\boldsymbol{\sigma} = \mathbf{C}(\boldsymbol{\epsilon} - \boldsymbol{\alpha}\Delta T)$$

$$\boldsymbol{\sigma} = \begin{bmatrix} \sigma_{11} \\ \sigma_{22} \\ \sigma_{33} \\ \sigma_{23} \\ \sigma_{13} \\ \sigma_{12} \end{bmatrix} \quad \mathbf{C} = \begin{bmatrix} c_{11} & c_{12} & c_{13} & c_{14} & c_{15} & c_{16} \\ c_{12} & c_{22} & c_{23} & c_{24} & c_{25} & c_{26} \\ c_{13} & c_{23} & c_{33} & c_{34} & c_{35} & c_{36} \\ c_{14} & c_{24} & c_{34} & c_{44} & c_{45} & c_{46} \\ c_{15} & c_{25} & c_{35} & c_{45} & c_{55} & c_{56} \\ c_{16} & c_{26} & c_{36} & c_{46} & c_{56} & c_{66} \end{bmatrix} \quad \boldsymbol{\epsilon} = \begin{bmatrix} \epsilon_{11} \\ \epsilon_{22} \\ \epsilon_{33} \\ 2\epsilon_{23} \\ 2\epsilon_{13} \\ 2\epsilon_{12} \end{bmatrix} \quad \boldsymbol{\alpha} = \begin{bmatrix} \alpha_{11} \\ \alpha_{22} \\ \alpha_{33} \\ 2\alpha_{23} \\ 2\alpha_{13} \\ 2\alpha_{12} \end{bmatrix},$$

where $c_{11} \equiv C_{1111}$, $c_{12} \equiv C_{1122} \equiv C_{2211}$, etc., are the *elastic stiffnesses* of the material. The inverse has the form

$$\boldsymbol{\epsilon} = \mathbf{S}\boldsymbol{\sigma} + \boldsymbol{\alpha}\Delta T$$

$$\mathbf{S} = \begin{bmatrix} s_{11} & s_{12} & s_{13} & s_{14} & s_{15} & s_{16} \\ s_{12} & s_{22} & s_{23} & s_{24} & s_{25} & s_{26} \\ s_{13} & s_{23} & s_{33} & s_{34} & s_{35} & s_{36} \\ s_{14} & s_{24} & s_{34} & s_{44} & s_{45} & s_{46} \\ s_{15} & s_{25} & s_{35} & s_{45} & s_{55} & s_{56} \\ s_{16} & s_{26} & s_{36} & s_{46} & s_{56} & s_{66} \end{bmatrix},$$

where $s_{11} = S_{1111}$, $s_{12} = S_{1122}$, etc. are the *elastic compliances* of the material. To satisfy Drucker stability, the eigenvalues of the elastic stiffness and compliance matrices must all be greater than zero.

HEALTH WARNING: The shear strain and shear stress components are not always listed in the order given when defining the elastic and compliance matrices. The conventions used here are common and are particularly convenient in analytical calculations involving anisotropic solids, but many sources use other conventions. Be careful to enter material data in the correct order when specifying properties for anisotropic solids.

3.2.9 Physical Interpretation of the Anisotropic Elastic Constants

It is easiest to interpret $s_{11}, s_{12}, \dots, s_{66}$ rather than $c_{11}, c_{12}, \dots, c_{66}$. Imagine applying a uniaxial stress, say σ_{11} , to an anisotropic specimen. In general, this would induce both extensional and shear deformation in the solid, as shown in Figure 3.7. The strain induced by the uniaxial stress would be

$$\begin{aligned} \epsilon_{11} &= s_{11}\sigma_{11}, & \epsilon_{22} &= s_{12}\sigma_{11}, & \epsilon_{33} &= s_{13}\sigma_{11} \\ \epsilon_{23} &= s_{14}\sigma_{11}, & \epsilon_{13} &= s_{15}\sigma_{11}, & \epsilon_{12} &= s_{16}\sigma_{11}. \end{aligned}$$

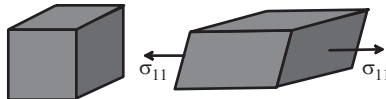


FIGURE 3.7 Shear deformation caused by uniaxial loading of an anisotropic solid.

All the constants have dimensions m^2/N . The constant s_{11} looks like a uniaxial compliance (like $1/E$), whereas the ratios s_{12}/s_{11} , s_{13}/s_{11} are generalized versions of Poisson's ratio: they quantify the lateral contraction of a uniaxial tensile specimen. The shear terms are new: in an isotropic material, no shear strain is induced by uniaxial tension.

3.2.10 Strain Energy Density for Anisotropic, Linear Elastic Solids

The strain energy density of an anisotropic material is

$$\begin{aligned} U &= \frac{1}{2} C_{ijkl} (\varepsilon_{ij} - \alpha_{ij} \Delta T) (\varepsilon_{kl} - \alpha_{kl} \Delta T) \\ &= \frac{1}{2} S_{ijkl} \sigma_{ij} \sigma_{kl}. \end{aligned}$$

3.2.11 Basis Change Formulas for Anisotropic Elastic Constants

The material constants c_{ij} or s_{ij} for a particular material are usually specified in a basis with coordinate axes aligned with particular symmetry planes (if any) in the material. When solving problems involving anisotropic materials, it is frequently necessary to transform these values to a coordinate system that is oriented in some convenient way relative to the boundaries of the solid. Because C_{ijkl} is a fourth-rank tensor, the basis change formulas are highly tedious, unfortunately.

Suppose that the components of the stiffness tensor are given in a basis $\{\mathbf{e}_1, \mathbf{e}_2, \mathbf{e}_3\}$, and we want to determine its components in a second basis, $\{\mathbf{m}_1, \mathbf{m}_2, \mathbf{m}_3\}$ (Figure 3.8). We define the usual transformation tensor Ω_{ij} with components $\Omega_{ij} = \mathbf{m}_i \cdot \mathbf{e}_j$ or in matrix form

$$[\Omega] = \begin{bmatrix} \mathbf{m}_1 \cdot \mathbf{e}_1 & \mathbf{m}_1 \cdot \mathbf{e}_2 & \mathbf{m}_1 \cdot \mathbf{e}_3 \\ \mathbf{m}_2 \cdot \mathbf{e}_1 & \mathbf{m}_2 \cdot \mathbf{e}_2 & \mathbf{m}_2 \cdot \mathbf{e}_3 \\ \mathbf{m}_3 \cdot \mathbf{e}_1 & \mathbf{m}_3 \cdot \mathbf{e}_2 & \mathbf{m}_3 \cdot \mathbf{e}_3 \end{bmatrix}.$$

This is an orthogonal matrix satisfying $\Omega \Omega^T = \Omega^T \Omega = \mathbf{I}$. In practice, the matrix can be computed in terms of the angles between the basis vectors. It is straightforward to show that stress, strain, thermal expansion, and elasticity tensors transform as

$$\begin{aligned} \sigma_{ij}^{(\mathbf{m})} &= \Omega_{ik} \sigma_{kl}^{(\mathbf{e})} \Omega_{jl} & \varepsilon_{ij}^{(\mathbf{m})} &= \Omega_{ik} \varepsilon_{kl}^{(\mathbf{e})} \Omega_{jl} & \alpha_{ij}^{(\mathbf{m})} &= \Omega_{ik} \alpha_{kl}^{(\mathbf{e})} \Omega_{jl} \\ C_{ijkl}^{(\mathbf{m})} &= \Omega_{ip} \Omega_{jq} C_{pqrs}^{(\mathbf{e})} \Omega_{kr} \Omega_{ls}. \end{aligned}$$

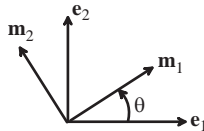


FIGURE 3.8 Basis vectors used to specify components of the elasticity tensor.

The basis change formula for the elasticity tensor can be expressed in matrix form as

$$\mathbf{C}^{(m)} = \mathbf{K} \mathbf{C}^{(e)} \mathbf{K}^T$$

where the basis change matrix \mathbf{K} is computed as

$$\mathbf{K} = \begin{bmatrix} \mathbf{K}^{(1)} & 2\mathbf{K}^{(2)} \\ \mathbf{K}^{(3)} & \mathbf{K}^{(4)} \end{bmatrix}$$

$$\left. \begin{array}{l} K_{ij}^{(1)} = \Omega_{ij}^2 \quad K_{ij}^{(2)} = \Omega_{i \bmod(j+1,3)} \Omega_{i \bmod(j+2,3)} \\ K_{ij}^{(3)} = \Omega_{\bmod(i+1,3)j} \Omega_{\bmod(i+2,3)j} \\ K_{ij}^{(4)} = \Omega_{\bmod(i+1,3)\bmod(j+1,3)} \Omega_{\bmod(i+2,3)\bmod(j+2,3)} \\ \quad + \Omega_{\bmod(i+1,3)\bmod(j+2,3)} \Omega_{\bmod(i+2,3)\bmod(j+1,3)} \end{array} \right\} i, j = 1..3$$

and the modulo function satisfies

$$\bmod(i, 3) = \begin{cases} i & i < 3 \\ i - 3 & i > 3 \end{cases}$$

Although these expressions look cumbersome, they are quite convenient for computer implementation.

The basis change for the compliance tensor follows as

$$\mathbf{S}^{(m)} = \mathbf{K}^{-T} \mathbf{S}^{(e)} \mathbf{K}^{-1},$$

where

$$\mathbf{K}^{-T} = \begin{bmatrix} \mathbf{K}^{(1)} & \mathbf{K}^{(2)} \\ 2\mathbf{K}^{(3)} & \mathbf{K}^{(4)} \end{bmatrix}.$$

The proof of these expressions is merely tiresome algebra and will not be given here. Ting [1996] has a nice clear discussion.

For the particular case of rotation through an angle θ in a counterclockwise sense about the $\mathbf{e}_1, \mathbf{e}_2, \mathbf{e}_3$ axes, respectively, the rotation matrix reduces to

$$\begin{bmatrix} 1 & 0 & 0 & 0 & 0 & 0 \\ 0 & c^2 & s^2 & 2cs & 0 & 0 \\ 0 & s^2 & c^2 & -2cs & 0 & 0 \\ 0 & -cs & cs & 0 & 0 & 0 \\ 0 & 0 & 0 & 0 & c & -s \\ 0 & 0 & 0 & 0 & s & c \end{bmatrix} \begin{bmatrix} c^2 & 0 & s^2 & 0 & 2cs & 0 \\ 0 & 1 & 0 & 0 & 0 & 0 \\ s^2 & 0 & c^2 & 0 & -2cs & 0 \\ 0 & 0 & 0 & c & 0 & -s \\ -cs & 0 & cs & 0 & c^2 - s^2 & 0 \\ 0 & 0 & 0 & s & 0 & c \end{bmatrix}$$

$$\begin{bmatrix} c^2 & s^2 & 0 & 0 & 0 & 2cs \\ s^2 & c^2 & 0 & 0 & 0 & -2cs \\ 0 & 0 & 1 & 0 & 0 & 0 \\ 0 & 0 & 0 & c & s & 0 \\ 0 & 0 & 0 & -s & c & 0 \\ -cs & cs & 0 & 0 & 0 & c^2 - s^2 \end{bmatrix},$$

where $c = \cos\theta$ $s = \sin\theta$. The inverse matrix \mathbf{K}^{-1} can be obtained simply by changing the sign of the angle θ in each rotation matrix. Clearly, applying the three rotations successively can produce an arbitrary orientation change.

For an isotropic material, the elastic stress-strain relations, the elasticity matrices, and thermal expansion coefficient are unaffected by basis changes.

3.2.12 The Effect of Material Symmetry on Stress–Strain Relations for Anisotropic Materials

A general anisotropic solid has 21 independent elastic constants. Note that, in general, tensile stress may induce shear strain, and shear stress may cause extension.

If a material has a symmetry plane, then applying stress normal or parallel to this plane, as shown in Figure 3.9, induces only extension in directions normal and parallel to the plane.

For example, suppose the material contains a single symmetry plane and let \mathbf{e}_1 be normal to this plane. Then the components of the elastic stiffness matrix $c_{15} = c_{16} = c_{25} = c_{26} = c_{35} = c_{36} = 0$

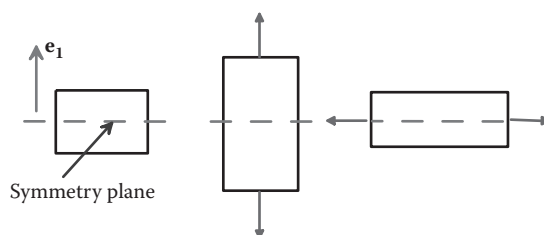


FIGURE 3.9 Loading applied to a solid containing a single symmetry plane.

$(C_{1112} = C_{1113} = C_{2212} = C_{2213} = C_{3312} = C_{3313} = 0)$ (symmetrical terms also vanish, of course). This leaves 13 independent constants. Similar restrictions on the thermal expansion coefficient can be determined using symmetry conditions. Details are left as an exercise.

In the following sections, we list the stress-strain relations for anisotropic materials with various numbers of symmetry planes.

3.2.13 Stress–Strain Relations for Linear Elastic Orthotropic Materials

An orthotropic material has three mutually perpendicular symmetry planes. This type of material has nine independent material constants. With basis vectors perpendicular to the symmetry planes, as shown in Figure 3.10, the elastic stiffness matrix has the form

$$\mathbf{C} = \begin{bmatrix} c_{11} & c_{12} & c_{13} & 0 & 0 & 0 \\ c_{21} & c_{22} & c_{23} & 0 & 0 & 0 \\ c_{31} & c_{32} & c_{33} & 0 & 0 & 0 \\ sym & & & c_{44} & 0 & 0 \\ & & & 0 & c_{55} & 0 \\ & & & 0 & 0 & c_{66} \end{bmatrix}.$$

This relationship is sometimes expressed in inverse form, in terms of generalized Young's moduli and Poisson's ratios (which have the same significance as Young's modulus and Poisson's ratio for uniaxial loading along the three basis vectors) as follows:

$$\mathbf{S} = \begin{bmatrix} 1/E_1 & -\nu_{21}/E_2 & -\nu_{31}/E_3 & 0 & 0 & 0 \\ -\nu_{12}/E_1 & 1/E_2 & -\nu_{32}/E_3 & 0 & 0 & 0 \\ -\nu_{13}/E_1 & -\nu_{23}/E_2 & 1/E_3 & 0 & 0 & 0 \\ 0 & 0 & 0 & 1/\nu_{23} & 0 & 0 \\ 0 & 0 & 0 & 0 & 1/\nu_{13} & 0 \\ 0 & 0 & 0 & 0 & 0 & 1/\nu_{12} \end{bmatrix}.$$

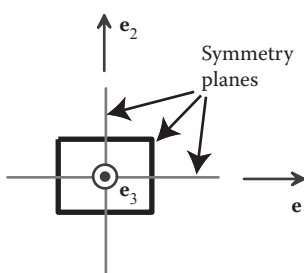


FIGURE 3.10 Symmetry planes in an orthotropic material.

Here the generalized Poisson's ratios are not symmetric but instead satisfy $\nu_{ij}/E_i = \nu_{ji}/E_j$ (no sums). This ensures that the stiffness matrix is symmetric.

The engineering constants are related to the components of the compliance tensor by

$$c_{11} = E_1(1 - \nu_{23}\nu_{32})\Upsilon \quad c_{22} = (1 - \nu_{13}\nu_{31})\Upsilon \quad c_{33} = c_{33}(1 - \nu_{12}\nu_{21})\Upsilon$$

$$c_{12} = E_1(\nu_{21} + \nu_{31}\nu_{23})\Upsilon = E_2(\nu_{12} + \nu_{32}\nu_{13})\Upsilon$$

$$c_{13} = E_1(\nu_{31} + \nu_{21}\nu_{32})\Upsilon = E_3(\nu_{13} + \nu_{12}\nu_{23})\Upsilon$$

$$c_{23} = E_2(\nu_{32} + \nu_{12}\nu_{31})\Upsilon = E_3(\nu_{23} + \nu_{21}\nu_{13})\Upsilon$$

$$c_{44} = c_{23} \quad c_{55} = c_{13} \quad c_{66} = c_{12}$$

$$\Upsilon = \frac{1}{1 - \nu_{12}\nu_{21} - \nu_{23}\nu_{32} - \nu_{31}\nu_{13} - 2\nu_{21}\nu_{32}\nu_{13}}$$

or in inverse form

$$E_1 = (c_{11}c_{22}c_{33} + 2c_{23}c_{12}c_{13} - c_{11}c_{23}^2 - c_{22}c_{13}^2 - c_{33}c_{12}^2) / (c_{22}c_{33} - c_{23}^2)$$

$$E_2 = (c_{11}c_{22}c_{33} + 2c_{23}c_{12}c_{13} - c_{11}c_{23}^2 - c_{22}c_{13}^2 - c_{33}c_{12}^2) / (c_{11}c_{33} - c_{13}^2)$$

$$E_3 = (c_{11}c_{22}c_{33} + 2c_{23}c_{12}c_{13} - c_{11}c_{23}^2 - c_{22}c_{13}^2 - c_{33}c_{12}^2) / (c_{11}c_{22} - c_{12}^2)$$

$$\nu_{21} = (c_{12}c_{33} - c_{13}c_{23}) / (c_{11}c_{33} - c_{13}^2) \quad \nu_{12} = (c_{12}c_{33} - c_{13}c_{23}) / (c_{22}c_{33} - c_{23}^2)$$

$$\nu_{31} = (c_{13}c_{22} - c_{12}c_{23}) / (c_{11}c_{22} - c_{12}^2) \quad \nu_{13} = (c_{22}c_{13} - c_{12}c_{23}) / (c_{22}c_{33} - c_{23}^2)$$

$$\nu_{23} = (c_{11}c_{23} - c_{12}c_{13}) / (c_{11}c_{33} - c_{13}^2) \quad \nu_{32} = (c_{11}c_{23} - c_{12}c_{13}) / (c_{11}c_{22} - c_{12}^2).$$

$$\mu_{23} = c_{44} \quad \mu_{13} = c_{55} \quad \mu_{12} = c_{66}$$

For an orthotropic material, thermal expansion cannot induce shear (in this basis), but the expansion in the three directions need not be equal. Consequently, the thermal expansion coefficient tensor has the form

$$\begin{bmatrix} \alpha_1 & 0 & 0 \\ 0 & \alpha_2 & 0 \\ 0 & 0 & \alpha_3 \end{bmatrix}.$$

3.2.14 Stress–Strain Relations for Linear Elastic Transversely Isotropic Material

A special case of an orthotropic solid is one that contains a plane of isotropy (this implies that the solid can be rotated with respect to the loading direction about one axis without measurable effect on the solid's response). Choose \mathbf{e}_3 perpendicular to this symmetry

plane. Then, transverse isotropy requires that $c_{22} = c_{11}$, $c_{23} = c_{13}$, $c_{55} = c_{44}$, $c_{66} = (c_{11} - c_{12})/2$, so that the stiffness matrix has the form

$$\mathbf{C} = \begin{bmatrix} c_{11} & c_{12} & c_{13} & 0 & 0 & 0 \\ c_{11} & c_{11} & c_{13} & 0 & 0 & 0 \\ & & c_{33} & 0 & 0 & 0 \\ sym & & & c_{44} & 0 & 0 \\ & & & 0 & c_{44} & 0 \\ & & & 0 & 0 & (c_{11} - c_{12}) / 2 \end{bmatrix}.$$

The engineering constants must satisfy

$$E_1 = E_2 = E_p \quad E_3 = E_t$$

$$\nu_{12} = \nu_{21} = \nu_p \quad \nu_{31} = \nu_{32} = \nu_{tp}$$

$$\nu_{13} = \nu_{23} = \nu_{pt}$$

and the compliance matrix has the form

$$\mathbf{S} = \begin{bmatrix} 1/E_p & -\nu_p/E_p & -\nu_{tp}/E_t & 0 & 0 & 0 \\ -\nu_p/E_p & 1/E_p & -\nu_{tp}/E_t & 0 & 0 & 0 \\ -\nu_{pt}/E_p & -\nu_{pt}/E_p & 1/E_t & 0 & 0 & 0 \\ 0 & 0 & 0 & 1/\mu_t & 0 & 0 \\ 0 & 0 & 0 & 0 & 1/\mu_t & 0 \\ 0 & 0 & 0 & 0 & 0 & 1/\mu_p \end{bmatrix},$$

where $\mu_p = E_p/2(1 + \nu_p)$. As before, the Poisson's ratios are not symmetric but satisfy $\nu_{tp}/E_t = \nu_{pt}/E_p$.

The engineering constants and stiffnesses are related by

$$c_{11} = c_{22} = E_p(1 - \nu_{pt}\nu_{tp})\Upsilon \quad c_{33} = E_t(1 - \nu_p^2)\Upsilon \quad c_{12} = E_p(\nu_p + \nu_{pt}\nu_{tp})\Upsilon$$

$$c_{13} = c_{23} = E_p(\nu_{tp} + \nu_p\nu_{tp})\Upsilon = E_t(\nu_{pt} + \nu_p\nu_{pt})\Upsilon \quad c_{44} = \quad c_{66} = \quad p$$

$$\Upsilon = \frac{1}{1 - \nu_p^2 - 2\nu_{pt}\nu_{tp} - 2\nu_p\nu_{pt}\nu_{tp}}$$

$$E_p = (c_{11}^2 c_{33} + 2c_{13}^2 c_{12} - 2c_{11} c_{13}^2 - c_{33} c_{12}^2) / (c_{11} c_{33} - c_{13}^2)$$

$$E_t = (c_{11}^2 c_{33} + 2c_{13}^2 c_{12} - 2c_{11} c_{13}^2 - c_{33} c_{12}^2) / (c_{11}^2 - c_{12}^2)$$

$$\nu_p = (c_{12}c_{33} - c_{13}^2) / (c_{11}c_{33} - c_{13}^2) \quad \nu_{tp} = (c_{13}c_{11} - c_{12}c_{13}) / (c_{11}^2 - c_{12}^2)$$

$$\nu_{pt} = (c_{11}c_{13} - c_{12}c_{13}) / (c_{11}c_{33} - c_{13}^2) \quad c_{23} = c_{44}, \quad c_{13} = c_{55}, \quad c_{12} = c_{66}.$$

For this material, the two thermal expansion coefficients in the symmetry plane must be equal, so the thermal expansion coefficient tensor has the form

$$\begin{bmatrix} \alpha_1 & 0 & 0 \\ 0 & \alpha_1 & 0 \\ 0 & 0 & \alpha_3 \end{bmatrix}.$$

3.2.15 Representative Values for Elastic Constants of Transversely Isotropic Hexagonal Close-Packed Crystals

Hexagonal close-packed crystals are an example of transversely isotropic materials. The \mathbf{e}_3 axis must be taken to be perpendicular to the basal (0001) plane of the crystal, as shown in Figure 3.11. Because the plane perpendicular to \mathbf{e}_3 is isotropic, the orientation of \mathbf{e}_1 and \mathbf{e}_2 is arbitrary.

A table of values of stiffnesses [reprinted from Freund and Suresh, 2003] is listed in Table 3.3. The engineering constants can be calculated and are listed in Table 3.4.

3.2.16 Linear Elastic Stress–Strain Relations for Cubic Materials

A huge number of materials have cubic symmetry: all the face-centered cubic (FCC) and body-centered cubic metals, for example. The constitutive law for such a material is particularly simple and can be parameterized by only three material constants. Pick basis vectors perpendicular to the symmetry planes, as shown in Figure 3.12.

TABLE 3.3 Elastic Constants for Hexagonal Crystals

	c_{11} (GNm ⁻²)	c_{33} (GNm ⁻²)	c_{44} (GNm ⁻²)	c_{12} (GNm ⁻²)	c_{13} (GNm ⁻²)
Be	292.3	336.4	162.5	26.7	14
C	1160	46.6	2.3	290	109
Cd	115.8	51.4	20.4	39.8	40.6
Co	307	358.1	78.3	165	103
Hf	181.1	196.9	55.7	77.2	66.1
Mg	59.7	61.7	16.4	26.2	21.7
Ti	162.4	180.7	46.7	92	69
Zn	161	61	38.3	34.2	50.1
Zr	143.4	164.8	32	72.8	65.3
ZnO	209.7	210.9	42.5	121.1	105.1

Source: Freund, L.B. and Suresh, S., *Thin Film Materials*. Cambridge, UK: Cambridge University Press, 2003.

TABLE 3.4 Engineering Constants for Hexagonal Crystals

	E_p (GNm $^{-2}$)	E_t (GNm $^{-2}$)	ν_p	ν_{tp}	ν_{pt}	μ_t (GNm $^{-2}$)	μ_p (GNm $^{-2}$)
Be	289.38	335.17	0.09	0.04	0.04	162.50	132.80
C	903.69	30.21	0.04	0.08	2.25	2.30	435.00
Cd	83.02	30.21	0.09	0.26	0.72	20.40	38.00
Co	211.30	313.15	0.49	0.22	0.15	78.30	71.00
Hf	139.87	163.07	0.35	0.26	0.22	55.70	51.95
Mg	45.45	50.74	0.36	0.25	0.23	16.40	16.75
Ti	104.37	143.27	0.48	0.27	0.20	46.70	35.20
Zn	119.45	35.28	-0.06	0.26	0.87	38.30	63.40
Zr	98.79	125.35	0.40	0.30	0.24	32.00	35.30
ZnO	127.30	144.12	0.44	0.32	0.28	42.50	44.30

Then

$$\begin{bmatrix} \sigma_{11} \\ \sigma_{22} \\ \sigma_{33} \\ \sigma_{23} \\ \sigma_{13} \\ \sigma_{12} \end{bmatrix} = \begin{bmatrix} c_{11} & c_{12} & c_{12} & 0 & 0 & 0 \\ & c_{11} & c_{12} & 0 & 0 & 0 \\ & & c_{11} & 0 & 0 & 0 \\ & & & c_{44} & 0 & 0 \\ & & & & 0 & c_{44} \\ & & & & 0 & 0 \end{bmatrix} \begin{bmatrix} \epsilon_{11} \\ \epsilon_{22} \\ \epsilon_{33} \\ 2\epsilon_{23} \\ 2\epsilon_{13} \\ 2\epsilon_{12} \end{bmatrix}$$

sym

or, in terms of engineering constants,

$$\begin{bmatrix} \epsilon_{11} \\ \epsilon_{22} \\ \epsilon_{33} \\ 2\epsilon_{23} \\ 2\epsilon_{13} \\ 2\epsilon_{12} \end{bmatrix} = \begin{bmatrix} 1/E & -\nu/E & -\nu/E & 0 & 0 & 0 \\ -\nu/E & 1/E & -\nu/E & 0 & 0 & 0 \\ -\nu/E & -\nu/E & 1/E & 0 & 0 & 0 \\ 0 & 0 & 0 & 1/ & 0 & 0 \\ 0 & 0 & 0 & 0 & 1/ & 0 \\ 0 & 0 & 0 & 0 & 0 & 1/ \end{bmatrix} \begin{bmatrix} \sigma_{11} \\ \sigma_{22} \\ \sigma_{33} \\ \sigma_{23} \\ \sigma_{13} \\ \sigma_{12} \end{bmatrix}.$$

This is virtually identical to the constitutive law for an isotropic solid, except that the shear modulus μ is not related to the Poisson's ratio and Young's modulus through the usual relation given in Section 3.1.6. In fact, the ratio

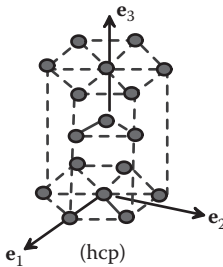


FIGURE 3.11 Atoms in a hexagonal close-packed solid.

$$A = \frac{2(1+\nu)}{E} = \frac{2c_{44}}{c_{11} - c_{12}}$$

provides a convenient measure of anisotropy. For $A = 1$, the material is isotropic. For this material, the thermal expansion coefficient matrix must be isotropic. The relationships between the elastic constants are

$$E = (c_{11}^2 + c_{12}c_{11} - 2c_{12}^2) / (c_{11} + c_{12}) \quad \nu = c_{12} / (c_{11} + c_{12}) \quad = c_{44}$$

$$c_{11} = E(1 - \nu) / (1 - \nu - 2\nu^2) \quad c_{12} = Ev / (1 - \nu - 2\nu^2).$$

3.2.17 Representative Values for Elastic Properties of Cubic Crystals and Compounds
 Table 3.5 lists values of elastic constants for various cubic crystals and compounds. The data for c_{11}, c_{44}, c_{12} were taken from Freund and Suresh [2003], whereas the elastic constants E, ν were calculated using the formulas in the preceding section.

3.3 HYPOELASTICITY: ELASTIC MATERIALS WITH A NONLINEAR STRESS–STRAIN RELATION UNDER SMALL DEFORMATION

Hypoelasticity is used to model materials that exhibit nonlinear, but reversible, stress-strain behavior even at small strains. Its most common application is in the so-called

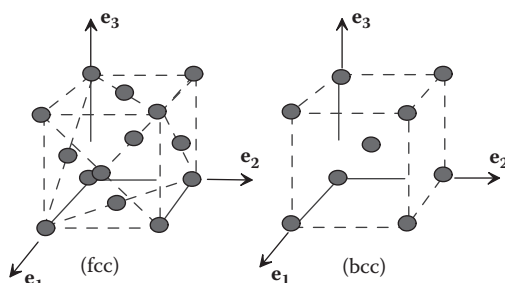


FIGURE 3.12 Atoms in face- and body-centered cubic materials.

88 ■ Applied Mechanics of Solids

TABLE 3.5 Elastic Constants for Cubic Crystals

Material	c_{11} (GNm $^{-2}$)	c_{44} (GNm $^{-2}$)	c_{12} (GNm $^{-2}$)	E (GNm $^{-2}$)	ν	μ (GNm $^{-2}$)	A
Ag	124.00	46.10	93.40	43.75	0.43	46.10	3.01
Al	107.30	28.30	60.90	63.20	0.36	28.30	1.22
Au	192.90	41.50	163.80	42.46	0.46	41.50	2.85
Cu	168.40	75.40	121.40	66.69	0.42	75.40	3.21
Ir	580.00	256.00	242.00	437.51	0.29	256.00	1.51
Ni	246.50	127.40	147.30	136.31	0.37	127.40	2.57
Pb	49.50	14.90	42.30	10.52	0.46	14.90	4.14
Pd	227.10	71.70	176.00	73.41	0.44	71.70	2.81
Pt	346.70	76.50	250.70	136.29	0.42	76.50	1.59
Cr	339.80	99.00	58.60	322.56	0.15	99.00	0.70
Fe	231.40	116.40	134.70	132.28	0.37	116.40	2.41
Mo	440.80	121.70	172.40	343.86	0.28	121.70	0.91
Nb	240.20	28.20	125.60	153.95	0.34	28.20	0.49
Ta	260.20	82.60	154.50	145.08	0.37	82.60	1.56
V	228.00	42.60	118.70	146.72	0.34	42.60	0.78
W	522.40	160.80	204.40	407.43	0.28	160.80	1.01
C	949.00	521.00	151.00	907.54	0.14	521.00	1.31
Ge	128.40	66.70	48.20	102.09	0.27	66.70	1.66
Si	166.20	79.80	64.40	130.23	0.28	79.80	1.57
GaAs	118.80	59.40	53.70	85.37	0.31	59.40	1.82
GaP	141.20	70.50	62.50	102.85	0.31	70.50	1.79
InP	102.20	46.00	57.60	60.68	0.36	46.00	2.06
LiF	114.00	63.60	47.70	85.86	0.29	63.60	1.92
MgO	287.60	151.40	87.40	246.86	0.23	151.40	1.51
TiC	500.00	175.00	113.00	458.34	0.18	175.00	0.90

“deformation theory of plasticity,” which is a crude approximation of the behavior of metals loaded beyond the elastic limit.

A hypoelastic material has the following properties:

- The solid has a preferred shape.
- The specimen deforms reversibly: if you remove the loads, the solid returns to its original shape.
- The strain in the specimen depends only on the stress applied to it; it does not depend on the rate of loading or the history of loading.

- The stress is a nonlinear function of strain, even when the strains are small, as shown in Figure 3.13. Because the strains are small, this is true whatever stress measure we adopt (Cauchy stress or nominal stress) and is true whatever strain measure we adopt (Lagrange strain or infinitesimal strain).
- We will assume here that the material is isotropic (i.e., the response of a material is independent of its orientation with respect to the loading direction). In principle, it would be possible to develop anisotropic hypoelastic models, but this is rarely done.

The stress-strain law is constructed as follows:

- Strains and rotations are assumed to be small. Consequently, deformation is characterized using the infinitesimal strain tensor ϵ_{ij} defined in Section 2.1.7. In addition, all stress measures are taken to be approximately equal. We can use the Cauchy stress σ_{ij} as the stress measure.
- When we develop constitutive equations for nonlinear elastic materials, it is usually best to find an equation for the *strain energy density* of the material as a function of the strain, instead of trying to write down stress-strain laws directly. This has several advantages: (1) we can work with a scalar function, and (2) the existence of a strain energy density guarantees that deformations of the material are perfectly reversible.
- If the material is isotropic, the strain energy density can only be a function of strain measures that do not depend on the direction of loading with respect to the material. One can show that this means that the strain energy can only be a function of *invariants* of the strain tensor, that is to say, combinations of strain components that have the same value in any basis (see Appendix B). The strain tensor always has three independent invariants: these could be the three principal strains, for example. In practice, it is usually more convenient to use the three fundamental scalar invariants:

$$I_1 = \epsilon_{kk} \quad I_2 = \frac{1}{2}(\epsilon_{ij}\epsilon_{ij} - \epsilon_{kk}\epsilon_{pp}/3) \quad I_3 = \det(\boldsymbol{\epsilon}) = \frac{1}{6}\epsilon_{ijk}\epsilon_{lmn}\epsilon_{li}\epsilon_{mj}\epsilon_{nk}.$$

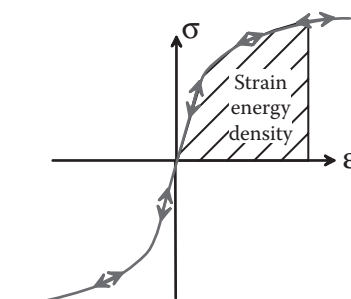


FIGURE 3.13 Stress-strain curve for a hypoelastic material.

Here, I_1 is a measure of the volume change associated with the strain, I_2 is a measure of the shearing caused by the strain, and I can't think of a good physical interpretation for I_3 . Fortunately, it doesn't often appear in constitutive equations.

Strain energy density: In principle, the strain energy density could be any sensible function $U(I_1, I_2, I_3)$. In most practical applications, nonlinear behavior is only observed when the material is subjected to shear deformation (characterized by I_2), whereas stress varies linearly with volume changes (characterized by I_1). This behavior can be characterized by a strain energy density,

$$U = \frac{1}{6} K I_1^2 + \frac{2n\sigma_0 \varepsilon_0}{n+1} \left(\frac{I_2}{\varepsilon_0^2} \right)^{(n+1)/2n},$$

where K , σ_0 , ε_0 , n are material properties (see below for a physical interpretation).

Stress-strain behavior: For this strain energy density function, the stress follows as

$$\sigma_{ij} = \frac{\partial U}{\partial \varepsilon_{ij}} = \frac{K}{3} \varepsilon_{kk} \delta_{ij} + \sigma_0 \left(\frac{I_2}{\varepsilon_0^2} \right)^{(1-n)/2n} \left(\frac{\varepsilon_{ij} - \varepsilon_{kk} \delta_{ij} / 3}{\varepsilon_0} \right).$$

The strain can also be calculated in terms of stress

$$\varepsilon_{ij} = \frac{1}{3K} \sigma_{kk} \delta_{ij} + \varepsilon_0 \left(\frac{J_2}{\sigma_0^2} \right)^{(n-1)/2} \left(\frac{\sigma_{ij} - \sigma_{kk} \delta_{ij} / 3}{\sigma_0} \right),$$

where $J_2 = (\sigma_{ij}\sigma_{ij} - \sigma_{kk}\sigma_{pp}/3)/2$ is the second invariant of the stress tensor. To interpret these results, note the following:

- If the solid is subjected to uniaxial tension (with stress $\sigma_{11} = \sigma$ and all other stress components zero), the nonzero strain components are

$$\varepsilon_{11} = \frac{\sigma}{3K} + \frac{2}{\sqrt{3}} \varepsilon_0 \left(\frac{\sigma}{\sqrt{3}\sigma_0} \right)^n \quad \varepsilon_{22} = \varepsilon_{33} = \frac{\sigma}{3K} - \frac{1}{\sqrt{3}} \varepsilon_0 \left(\frac{\sigma}{\sqrt{3}\sigma_0} \right)^n.$$

- If the solid is subjected to hydrostatic stress (with $\sigma_{11} = \sigma_{22} = \sigma_{33} = \sigma$ and all other stress components zero), the nonzero strain components are

$$\varepsilon_{11} = \varepsilon_{22} = \varepsilon_{33} = \frac{\sigma}{K}.$$

- If the solid is subjected to pure shear stress (with $\sigma_{12} = \sigma_{21} = \tau$ and all other stress components zero), the nonzero strains are

$$\varepsilon_{12} = \varepsilon_{21} = \varepsilon_0 \left(\frac{\tau}{\sigma_0} \right)^n.$$

Thus, the solid responds linearly to pressure loading, with a bulk modulus K . The relationship between shear stress and shear strain is a power law, with exponent n .

3.4 GENERALIZED HOOKE'S LAW: ELASTIC MATERIALS SUBJECTED TO SMALL STRETCHES BUT LARGE ROTATIONS

Recall that the stress-strain law for an anisotropic, linear elastic material (Section 3.1) has the form

$$\sigma_{ij} = C_{ijkl} \varepsilon_{kl},$$

where σ_{ij} is stress (any stress measure you like), $\varepsilon_{ij} = (\partial u_i / \partial x_j + \partial u_j / \partial x_i)/2$ is the infinitesimal strain, and C_{ijkl} is the tensor of elastic moduli. This stress-strain relation can only be used if the material is subjected to small deformations and small rotations. This is partly because the infinitesimal strain $\varepsilon_{ij} \neq 0$ for a finite rotation, so the law predicts that a non-zero stress is required to rotate a solid.

There are some situations in which a solid is subjected to small shape changes but large rotations. For example, Figure 3.14 shows a long slender beam bent into a circle by moments applied to its ends. The strains in the beam are of order h/R , where h is the thickness of the beam and R is its curvature. The ends of the beam have rotated through a full 90° , however. The linear elastic constitutive equations would not predict the correct stress in the beam.

It is easy to fix this problem: provided we choose a sensible (nonlinear) strain measure, together with the appropriate work-conjugate stress measure, we can still use a linear stress-strain relation. To make this precise, suppose that a solid is subjected to a displacement field $u_i(x_k)$, as shown in Figure 3.15. Define the following:

- The deformation gradient and its Jacobian:

$$F_{ij} = \delta_{ij} + \frac{\partial u_i}{\partial x_j} \quad J = \det(F).$$

- The Lagrange strain:

$$E_{ij} = \frac{1}{2}(F_{ki}F_{kj} - \delta_{ij}) = \frac{1}{2}\left(\frac{\partial u_i}{\partial x_j} + \frac{\partial u_j}{\partial x_i} + \frac{\partial u_k}{\partial x_i} \frac{\partial u_k}{\partial x_j}\right).$$

- The Eulerian strain: $E_{ij}^* = \frac{1}{2}(\delta_{ij} - F_{ki}^{-1}F_{kj}^{-1})$.

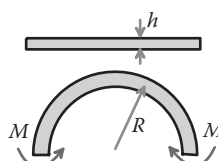


FIGURE 3.14 Slender beam bent by terminal couples.

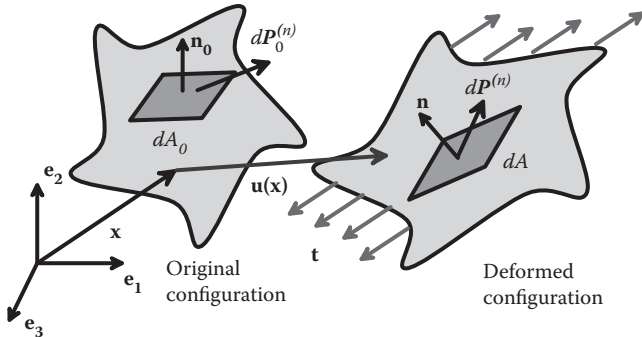


FIGURE 3.15 Deformation of an area element within a solid.

- The rotation tensor (for the best way to compute \mathbf{R} in practice, see Section 2.1.13):

$$R_{ij} = F_{ik} U_{kj}^{-1} \quad \mathbf{U} = (\mathbf{F}^T \cdot \mathbf{F})^{1/2}.$$

- The Cauchy (“true”) stress σ_{ij} , defined so that $n_i \sigma_{ij} = \lim_{dA \rightarrow 0} \frac{dP_j^{(n)}}{dA}$.
- The material stress (work conjugate to Lagrange strain): $\Sigma_{ij} = J F_{ik}^{-1} \sigma_{kl} F_{jl}^{-1}$.

The material stress–Lagrange strain relation can be expressed as

$$\Sigma_{ij} = C_{ijkl} E_{kl},$$

where C_{ijkl} is the tensor of elastic moduli for the material with orientation in the undeformed configuration. This is identical to the stress-strain relation for a linear elastic solid, except that the stress measure has been replaced by material stress, and the strain measure has been replaced by Lagrange strain. You can therefore use all the matrix representations and tables of data given in Section 3.1 to apply the constitutive equation. The Cauchy (true) stress can be computed from the material stress as

$$\sigma_{ij} = \frac{1}{J} F_{ik} \Sigma_{kl} F_{jl} \approx R_{ik} \Sigma_{kl} R_{jl}.$$

For the Cauchy stress–Eulerian strain relation, alternatively, the stress-strain relation can be expressed in terms of stress and deformation measures that characterize the deformed solid, as

$$\sigma_{ij} = C_{ijkl}^* E_{kl}^*,$$

where C_{ijkl}^* is the tensor of elastic moduli for the material with orientation of the deformed configuration. This tensor is related to C_{ijkl} by

$$C_{ijmn}^* = \frac{1}{J} F_{ip} F_{jq} C_{pqkl} F_{mk} F_{nl} \approx R_{ip} R_{jq} C_{pqkl} R_{mk} R_{nl}.$$

For the special case of an isotropic material with Young's modulus E and Poisson's ratio ν ,

$$\Sigma_{ij} = \frac{E}{1-\nu} \left\{ E_{ij} + \frac{\nu}{1-2\nu} E_{kk} \delta_{ij} \right\} \quad \sigma_{ij} = \frac{E}{1+\nu} \left\{ E_{ij}^* + \frac{\nu}{1-2\nu} E_{kk}^* \delta_{ij} \right\}.$$

3.5 HYPERELASTICITY: TIME-INDEPENDENT BEHAVIOR OF RUBBERS AND FOAMS SUBJECTED TO LARGE STRAINS

Hyperelastic constitutive laws are used to model materials that respond elastically when subjected to very large strains. They account for both nonlinear material behavior and large shape changes. The main applications of the theory are (1) to model the rubbery behavior of a polymeric material and (2) to model polymeric foams that can be subjected to large reversible shape changes (e.g., a sponge).

In general, the response of a typical polymer is strongly dependent on temperature, strain history, and loading rate. The behavior will be described in more detail in the next section, in which we present the theory of viscoelasticity. For now, we note that polymers have various regimens of mechanical behavior, referred to as "glassy," "viscoelastic," and "rubbery." The various regimens can be identified for a particular polymer by applying a sinusoidal variation of shear stress to the solid and measuring the resulting shear strain amplitude. A typical result is illustrated in Figure 3.16, which shows the apparent shear modulus (ratio of stress amplitude to strain amplitude) as a function of temperature.

At a critical temperature known as the *glass transition temperature*, a polymeric material undergoes a dramatic change in mechanical response. Below this temperature, it behaves like a glass, with a stiff response. Near the glass transition temperature, the stress depends strongly on the strain rate. At the glass transition temperature, there is a dramatic drop in modulus. Above this temperature, there is a regime in which the polymer shows rubbery behavior: the response is elastic, the stress does not depend strongly on strain rate or strain history, and the modulus increases with temperature. All polymers show these general trends, but the extent of each regime, and the detailed behavior within each regime, depend on the solid's molecular structure. Heavily cross-linked polymers (elastomers) are the most likely to show ideal rubbery behavior. Hyperelastic constitutive laws are intended to approximate this rubbery behavior.

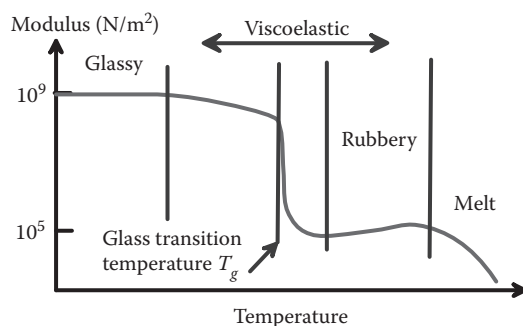


FIGURE 3.16 Modulus of a typical polymer as a function of temperature.

The features of the behavior of a solid rubber include the following:

1. The material is close to ideally elastic, i.e., (1) when deformed at constant temperature or adiabatically, stress is a function only of current strain and independent of history or rate of loading, and (2) the behavior is reversible, so no net work is done on the solid during a closed cycle of strain under adiabatic or isothermal conditions.
2. The material strongly resists volume changes. The bulk modulus (the ratio of volume change to hydrostatic component of stress) is comparable with that of metals or covalently bonded solids.
3. The material is very compliant in shear: shear modulus is of the order of 10^{-5} times that of most metals.
4. The material is isotropic: its stress-strain response is independent of material orientation.
5. The shear modulus is temperature dependent: the material becomes stiffer as it is heated, in sharp contrast to metals.
6. When stretched, the material gives off heat.

Polymeric foams (e.g., a sponge) share some of these properties:

1. They are close to reversible and show little rate or history dependence.
2. In contrast to rubbers, most foams are highly compressible; bulk and shear moduli are comparable.
3. Foams have a complicated true stress-true strain response, generally resembling sketch in Figure 3.17. The finite strain response of the foam in compression is quite different from that in tension because of buckling in the cell walls.
4. Foams can be anisotropic depending on their cell structure. Foams with a random cell structure are isotropic.

The literature on stress-strain relations for finite elasticity can be hard to follow, partly because nearly every paper uses a different notation and partly because there are many

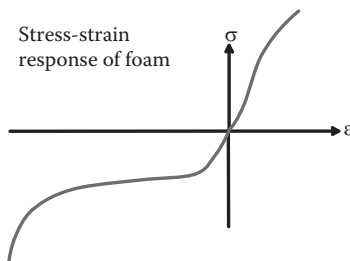


FIGURE 3.17 Stress-strain curve for a typical foam.

different ways to write down the same stress-strain law. You should find that most of the published literature is consistent with the framework given below, but it may take some work to show the equivalence.

All hyperelastic models are constructed as follows:

1. Define the stress-strain relation for the solid by specifying its strain energy density W as a function of deformation gradient tensor: $W = W(\mathbf{F})$. This ensures that the material is perfectly elastic and also means that we only need to work with a scalar function. The general form of the strain energy density is guided by experiment, and the formula for strain energy density always contains material properties that can be adjusted to describe a particular material.
2. The undeformed material is usually assumed to be isotropic, i.e., the behavior of the material is independent of the initial orientation of the material with respect to the loading. If the strain energy density is a function of the left Cauchy-Green deformation tensor $\mathbf{B} = \mathbf{F} \cdot \mathbf{F}^T$, the constitutive equation is automatically isotropic. If \mathbf{B} is used as the deformation measure, then the strain energy must be a function of the *invariants* of \mathbf{B} to ensure that the constitutive equation is objective (recall that the invariants of a tensor remain constant under a change of basis).
3. Formulas for stress in terms of strain are calculated by differentiating the strain energy density as outlined below.

3.5.1 Deformation Measures Used in Finite Elasticity

Suppose that a solid is subjected to a displacement field $u_i(x_k)$, as shown in Figure 3.18. Define the following:

- The deformation gradient and its Jacobian:

$$F_{ij} = \delta_{ij} + \frac{\partial u_i}{\partial x_j} \quad J = \det(\mathbf{F}).$$

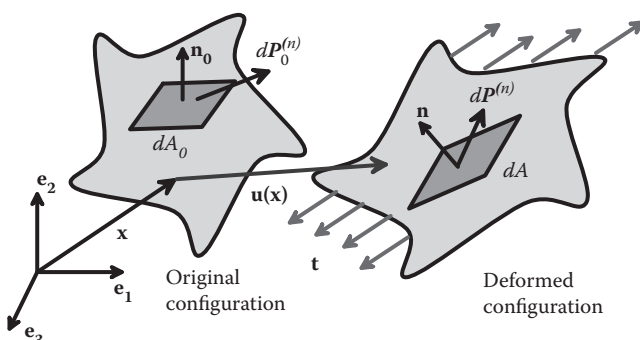


FIGURE 3.18 Deformable solid subjected to external forces.

- The left Cauchy–Green deformation tensor:

$$\mathbf{B} = \mathbf{F} \cdot \mathbf{F}^T \quad B_{ij} = F_{ik} F_{jk}.$$

- Invariants of \mathbf{B} (these are the conventional definitions):

$$I_1 = \text{trace}(\mathbf{B}) = B_{kk}$$

$$I_2 = \frac{1}{2} (I_1^2 - \mathbf{B} \cdot \mathbf{B}) = \frac{1}{2} (I_1^2 - B_{ik} B_{ki})$$

$$I_3 = \det \mathbf{B} = J^2$$

- An alternative set of invariants of \mathbf{B} more convenient for models of nearly incompressible materials (note that \bar{I}_1, \bar{I}_2 remain constant under a pure volume change):

$$\bar{I}_1 = \frac{I_1}{J^{2/3}} = \frac{B_{kk}}{J^{2/3}}$$

$$\bar{I}_2 = \frac{I_2}{J^{4/3}} = \frac{1}{2} \left(\bar{I}_1^2 - \frac{\mathbf{B} \cdot \mathbf{B}}{J^{4/3}} \right) = \frac{1}{2} \left(\bar{I}_1^2 - \frac{B_{ik} B_{ki}}{J^{4/3}} \right).$$

$$J = \sqrt{\det \mathbf{B}}$$

- Principal stretches and principal stretch directions, specified as follows:

- Let e_1, e_2, e_3 denote the three eigenvalues of \mathbf{B} . The principal stretches are

$$\lambda_1 = \sqrt{e_1}, \quad \lambda_2 = \sqrt{e_2}, \quad \lambda_3 = \sqrt{e_3}$$

- Let $\mathbf{b}_1, \mathbf{b}_2, \mathbf{b}_3$ denote three, mutually perpendicular *unit* eigenvectors of \mathbf{B} . These define the principal stretch directions. (Note: Because \mathbf{B} is symmetric, its eigenvectors are automatically mutually perpendicular as long as no two eigenvalues are the same. If two or all three eigenvalues are the same, the eigenvectors are not uniquely defined; in this case, any convenient mutually perpendicular set of eigenvectors can be used.)

- Recall that \mathbf{B} can be expressed in terms of its eigenvectors and eigenvalues as

$$\mathbf{B} = \lambda_1^2 \mathbf{b}^{(1)} \otimes \mathbf{b}^{(1)} + \lambda_2^2 \mathbf{b}^{(2)} \otimes \mathbf{b}^{(2)} + \lambda_3^2 \mathbf{b}^{(3)} \otimes \mathbf{b}^{(3)}.$$

3.5.2 Stress Measures Used in Finite Elasticity

Usually stress-strain laws are given as equations relating Cauchy stress (true stress) σ_{ij} to left Cauchy–Green deformation tensor. For some computations, it may be more convenient to use other stress measures. They are defined below, for convenience.

- The Cauchy (true) stress represents the force per unit deformed area in the solid and is defined by

$$n_i \sigma_{ij} = \lim_{dA \rightarrow 0} \frac{dP_j^{(n)}}{dA}.$$

- Kirchhoff stress is defined as $\tau = J\sigma \tau_{ij} = J\sigma_{ij}$.
- Nominal (first Piola–Kirchhoff) stress is defined as $\mathbf{S} = J\mathbf{F}^{-1} \cdot \boldsymbol{\sigma} \quad S_{ij} = JF_{ik}^{-1}\sigma_{kj}$
- Material (second Piola–Kirchhoff) stress is defined as.

$$\Sigma = J\mathbf{F}^{-1} \cdot \boldsymbol{\sigma} \cdot \mathbf{F}^{-T} \quad \Sigma_{ij} = JF_{ik}^{-1}\sigma_{kl}F_{jl}^{-1}.$$

3.5.3 Calculating Stress–Strain Relations from the Strain Energy Density

The constitutive law for an isotropic hyperelastic material is defined by an equation relating the strain energy density of the material to the deformation gradient or, for an isotropic solid, to the three invariants of the strain tensor:

$$W(\mathbf{F}) = U(I_1, I_2, I_3) = \bar{U}(\bar{I}_1, \bar{I}_2, J) = \tilde{U}(\lambda_1, \lambda_2, \lambda_3).$$

The stress-strain law must then be deduced by differentiating the strain energy density. This can involve some tedious algebra. Formulas are listed below for the stress-strain relations for each choice of strain invariant. The results are derived below:

- Strain energy density in terms of F_{ij} :

$$\sigma_{ij} = \frac{1}{J} F_{ik} \frac{\partial W}{\partial F_{jk}}.$$

- Strain energy density in terms of I_1, I_2, I_3 :

$$\sigma_{ij} \frac{2}{\sqrt{I_3}} \left[\left(\frac{\partial U}{\partial I_1} + I_1 \frac{\partial U}{\partial I_2} \right) B_{ij} - \frac{\partial U}{\partial I_2} B_{ik} B_{kj} \right] + 2\sqrt{I_3} \frac{\partial U}{\partial I_3} \delta_{ij}.$$

- Strain energy density in terms of \bar{I}_1, \bar{I}_2, J :

$$\sigma_{ij} = \frac{2}{J} \left[\frac{1}{J^{2/3}} \left(\frac{\partial \bar{U}}{\partial \bar{I}_1} + \bar{I}_1 \frac{\partial \bar{U}}{\partial \bar{I}_2} \right) B_{ij} - \left(\bar{I}_1 \frac{\partial \bar{U}}{\partial \bar{I}_1} + 2\bar{I}_2 \frac{\partial \bar{U}}{\partial \bar{I}_2} \right) \frac{\delta_{ij}}{3} - \frac{1}{J^{4/3}} \frac{\partial \bar{U}}{\partial \bar{I}_2} B_{ik} B_{kj} \right] + \frac{\partial \bar{U}}{\partial J} \delta_{ij}.$$

- Strain energy density in terms of $\lambda_1, \lambda_2, \lambda_3$:

$$\sigma_{ij} = \frac{\lambda_1}{\lambda_1 \lambda_2 \lambda_3} \frac{\partial \tilde{U}}{\partial \lambda_1} b_i^{(1)} b_j^{(1)} + \frac{\lambda_2}{\lambda_1 \lambda_2 \lambda_3} \frac{\partial \tilde{U}}{\partial \lambda_2} b_i^{(2)} b_j^{(2)} + \frac{\lambda_3}{\lambda_1 \lambda_2 \lambda_3} \frac{\partial \tilde{U}}{\partial \lambda_3} b_i^{(3)} b_j^{(3)}.$$

Derivations: We start by deriving the general formula for stress in terms of $W(\mathbf{F})$:

1. Note that, by definition, if the solid is subjected to some history of strain, the rate of change of the strain energy density $W(\mathbf{F})$ must equal the rate of mechanical work done on the material per unit reference volume.

2. Recall that the rate of work done per unit undeformed volume by body forces and surface tractions is expressed in terms of the nominal stress S_{ij} as $S_{ij}\dot{F}_{ij}$.

3. Therefore, for any deformation gradient F_{ij}

$$\frac{dW}{dt} = \frac{\partial W}{\partial F_{ij}} \frac{\partial F_{ij}}{\partial t} = S_{ji} \frac{\partial F_{ij}}{\partial t}.$$

This must hold for all possible \dot{F}_{ij} , so that

$$\frac{\partial W}{\partial F_{ij}} = S_{ji}.$$

4. Finally, the formula for Cauchy stress follows from the equation relating σ_{ij} to S_{ij} :

$$\sigma_{ij} = \frac{1}{J} F_{ik} S_{kj} = \frac{1}{J} F_{ik} \frac{\partial W}{\partial F_{jk}}.$$

For an isotropic material, it is necessary to find derivatives of the invariants with respect to the components of \mathbf{F} to compute the stress-strain function for a given strain energy density. It is straightforward but somewhat tedious to show that

$$\frac{\partial I_1}{\partial F_{ij}} = 2F_{ij}, \quad \frac{\partial I_2}{\partial F_{ij}} = 2(I_1 F_{ij} - B_{ik} F_{kj}), \quad \frac{\partial I_3}{\partial F_{ij}} = 2I_3 F_{ji}^{-1}$$

Then,

$$\frac{\partial W}{\partial F_{ij}} = \frac{\partial U}{\partial I_1} \frac{\partial I_1}{\partial F_{ij}} + \frac{\partial U}{\partial I_2} \frac{\partial I_2}{\partial F_{ij}} + \frac{\partial U}{\partial I_3} \frac{\partial I_3}{\partial F_{ij}} = 2 \left(\frac{\partial U}{\partial I_1} + I_1 \frac{\partial U}{\partial I_2} \right) F_{ij} - 2 \frac{\partial U}{\partial I_2} B_{ik} F_{kj} 2I_3 \frac{\partial U}{\partial I_3} F_{ji}^{-1}$$

and

$$\sigma_{ij} = \frac{1}{\sqrt{I_3}} F_{ik} \frac{\partial W}{\partial F_{jk}} = \frac{2}{\sqrt{I_3}} \left[\left(\frac{\partial U}{\partial I_1} + I_1 \frac{\partial U}{\partial I_2} \right) B_{ij} - \frac{\partial U}{\partial I_2} B_{ik} B_{kj} \right] + 2\sqrt{I_3} \frac{\partial U}{\partial I_3} \delta_{ij}.$$

When using a strain energy density of the form $\bar{U}(\bar{I}_1, \bar{I}_2, J)$, we will have to compute the derivatives of the invariants \bar{I}_1, \bar{I}_2 and J with respect to the components of \mathbf{F} to find

$$\frac{\partial W}{\partial F_{ij}} = \frac{\partial \bar{U}}{\partial \bar{I}_1} \frac{\partial \bar{I}_1}{\partial F_{ij}} + \frac{\partial \bar{U}}{\partial \bar{I}_2} \frac{\partial \bar{I}_2}{\partial F_{ij}} + \frac{\partial \bar{U}}{\partial J} \frac{\partial J}{\partial F_{ij}}$$

We find that

$$\frac{\partial J}{\partial F_{ij}} = J F_{ji}^{-1} \quad \frac{\partial \bar{I}_1}{\partial F_{ij}} = \frac{1}{J^{2/3}} \frac{\partial I_1}{\partial F_{ij}} - \frac{2I_1}{3J^{5/3}} \frac{\partial J}{\partial F_{ij}} = \frac{2}{J^{2/3}} \left(F_{ij} - \frac{I_1}{3} F_{ji}^{-1} \right) = \frac{2}{J^{2/3}} F_{ij} - \frac{2}{3} \bar{I}_1 F_{ji}^{-1}$$

$$\frac{\partial \bar{I}_2}{\partial F_{ij}} = \frac{1}{J^{4/3}} \frac{\partial I_2}{\partial F_{ij}} - \frac{4I_2}{3J^{7/3}} \frac{\partial J}{\partial F_{ij}} = \frac{2}{J^{4/3}} \left(I_1 F_{ij} - B_{ik} F_{kj} - \frac{2I_2}{3} F_{ji}^{-1} \right)$$

$$= \frac{2}{J^{2/3}} \bar{I}_1 F_{ij} - \frac{2}{J^{4/3}} B_{ik} F_{kj} - \frac{4\bar{I}_2}{3} F_{ji}^{-1}$$

Thus,

$$\begin{aligned}\sigma_{ij} &= \frac{1}{J} F_{ik} \frac{\partial W}{\partial F_{jk}} \\ &= \frac{2}{J^{5/3}} \left(\frac{\partial \bar{U}}{\partial \bar{I}_1} + \bar{I}_1 \frac{\partial \bar{U}}{\partial \bar{I}_2} \right) B_{ij} - \frac{2}{3J} \left(\bar{I}_1 \frac{\partial \bar{U}}{\partial \bar{I}_1} + 2\bar{I}_2 \frac{\partial \bar{U}}{\partial \bar{I}_2} \right) \delta_{ij} - \frac{2}{J^{7/3}} \frac{\partial \bar{U}}{\partial \bar{I}_2} B_{ik} B_{kj} + \frac{\partial \bar{U}}{\partial J} \delta_{ij}.\end{aligned}$$

Next, we derive the stress-strain relation in terms of a strain energy density $\tilde{U}(\lambda_1, \lambda_2, \lambda_3)$ that is expressed as a function of the principal strains. Note first that

$$\tilde{U}(\lambda_1, \lambda_2, \lambda_3) = U(I_1, I_2, I_3)$$

$$I_1 = \lambda_1^2 + \lambda_2^2 + \lambda_3^2, \quad I_2 = \lambda_1^2 \lambda_3^2 + \lambda_2^2 \lambda_3^2 + \lambda_1^2 \lambda_2^2, \quad I_3 = \lambda_1^2 \lambda_2^2 \lambda_3^2$$

so that the chain rule gives

$$\frac{\partial \tilde{U}}{\partial \lambda_i} = 2\lambda_i \left(\frac{\partial U}{\partial I_1} + (I_1 - \lambda_i^2) \frac{\partial U}{\partial I_2} + \frac{I_3}{\lambda_i^2} \frac{\partial U}{\partial I_3} \right), \quad (i=1,2,3).$$

Using this and the expression that relates the stress components to the derivatives of U ,

$$\sigma_{ij} = \frac{1}{\sqrt{I_3}} F_{ik} \frac{\partial W}{\partial F_{jk}} = \frac{2}{\sqrt{I_3}} \left[\left(\frac{\partial U}{\partial I_1} + I_1 \frac{\partial U}{\partial I_2} \right) B_{ij} - \frac{\partial U}{\partial I_2} B_{ik} B_{kj} \right] + 2\sqrt{I_3} \frac{\partial U}{\partial I_3} \delta_{ij},$$

we find that the principal stresses $\sigma_1, \sigma_2, \sigma_3$ are related to the corresponding principal stretches $\lambda_1, \lambda_2, \lambda_3$ (square roots of the eigenvalues of \mathbf{B}) through

$$\sigma_i = \frac{\lambda_i}{\lambda_1 \lambda_2 \lambda_3} \frac{\partial \tilde{U}}{\partial \lambda_i}, \quad (i = 1, 2, 3).$$

The spectral decomposition for \mathbf{B} in terms of its eigenvalues $\lambda_1^2, \lambda_2^2, \lambda_3^2$ and eigenvectors $\mathbf{b}^{(1)}, \mathbf{b}^{(2)}, \mathbf{b}^{(3)}$:

$$B_{ij} = \lambda_1^2 b_i^{(1)} b_j^{(1)} + \lambda_2^2 b_i^{(2)} b_j^{(2)} + \lambda_3^2 b_i^{(3)} b_j^{(3)}.$$

now allows the stress tensor to be written as

$$\sigma_{ij} = \frac{\lambda_1}{\lambda_1 \lambda_2 \lambda_3} \frac{\partial \tilde{U}}{\partial \lambda_1} b_i^{(1)} b_j^{(1)} + \frac{\lambda_2}{\lambda_1 \lambda_2 \lambda_3} \frac{\partial \tilde{U}}{\partial \lambda_2} b_i^{(2)} b_j^{(2)} + \frac{\lambda_3}{\lambda_1 \lambda_2 \lambda_3} \frac{\partial \tilde{U}}{\partial \lambda_3} b_i^{(3)} b_j^{(3)}.$$

3.5.4 A Note on Perfectly Incompressible Materials

The preceding formulas assume that the material has some (perhaps small) compressibility; that is to say, if you load it with hydrostatic pressure, its volume will change by a measurable amount. Most rubbers strongly resist volume changes, and, in hand calculations, it is sometimes convenient to approximate them as perfectly incompressible. The material model for incompressible materials is specified as follows:

- The deformation must satisfy $J = 1$ to preserve volume.
- The strain energy density is therefore only a function of two invariants; furthermore, both sets of invariants defined above are identical. We can use a strain energy density of the form $U(I_1, I_2)$.
- Because you can apply any pressure to an incompressible solid without changing its shape, the stress cannot be uniquely determined from the strains. Consequently, the stress-strain law only specifies the *deviatoric stress* $\bar{\sigma}_{ij} = \sigma_{ij} - \sigma_{kk}\delta_{ij} / 3$. In problems involving quasi-static loading, the hydrostatic stress $p = \sigma_{kk} / 3$ can usually be calculated, by solving the equilibrium equations (together with appropriate boundary conditions). Incompressible materials should not be used in a dynamic analysis, because the speed of elastic pressure waves is infinite.
- The formula for stress in terms of $U(I_1, I_2)$ has the form

$$\sigma_{ij} = 2 \left[\left(\frac{\partial U}{\partial I_1} + I_1 \frac{\partial U}{\partial I_2} \right) B_{ij} - \left(I_1 \frac{\partial U}{\partial I_1} + 2I_2 \frac{\partial U}{\partial I_2} \right) \frac{\delta_{ij}}{3} - \frac{\partial U}{\partial I_2} B_{ik} B_{kj} \right] + p \delta_{ij}.$$

The hydrostatic stress p is an unknown variable, which must be calculated by solving the boundary value problem.

3.5.5 Specific Forms of the Strain Energy Density

Specific forms of the strain energy density include the following:

Generalized neo-Hookean solid [adapted from Treloar 1948]:

$$\bar{U} = \frac{1}{2}(\bar{I}_1 - 3) + \frac{K_1}{2}(J - 1)^2,$$

where μ_1 and K_1 are material properties (for small deformations, μ_1 and K_1 are the shear modulus and bulk modulus of the solid, respectively). Elementary statistical mechanics treatments predict that $\mu_1 = NkT$, where N is the number of polymer chains per unit volume, k is the Boltzmann constant, and T is temperature. This is a rubber elasticity model, for rubbers with very limited compressibility, and should be used with $K_1 \gg \mu_1$. The stress-strain relation follows as:

$$\sigma_{ij} = \frac{1}{J^{5/3}} \left(B_{ij} - \frac{1}{3} B_{kk} \delta_{ij} \right) + K_1(J - 1) \delta_{ij}.$$

The fully incompressible limit can be obtained by setting $K_1(J - 1) = p/3$ in the stress-strain law.

Generalized Mooney–Rivlin solid [adapted from Mooney 1940]:

$$\bar{U} = \frac{1}{2}(\bar{I}_1 - 3) + \frac{2}{2}(\bar{I}_2 - 3) + \frac{K_1}{2}(J - 1)^2$$

where μ_1 , μ_2 , and K_1 are material properties. For small deformations, the shear modulus and bulk modulus of the solid are $\mu = \mu_1 + \mu_2$ and $K = K_1$. This is a rubber elasticity model and should be used with $K_1 \gg \mu_1$. The stress-strain relation follows as

$$\sigma_{ij} = \frac{1}{J^{5/3}} \left(B_{ij} - \frac{1}{3} B_{kk} \delta_{ij} \right) + \frac{2}{J^{7/3}} \left(B_{kk} B_{ij} - \frac{1}{3} [B_{kk}]^2 \delta_{ij} - B_{ik} B_{kj} + \frac{1}{3} B_{kn} B_{nk} \delta_{ij} \right) + K_1 (J - 1) \delta_{ij}.$$

Generalized polynomial rubber elasticity potential:

$$\bar{U} = \sum_{i+j=1}^N C_{ij} (\bar{I}_1 - 3)^i (\bar{I}_2 - 3)^j + \sum_{i=1}^N \frac{K_i}{2} (J - 1)^{2i},$$

where C_{ij} and K_i are material properties. For small strains, the shear modulus and bulk modulus follow as $\mu = 2(C_{01} + C_{10})$, $K = 2K_1$. This model is implemented in many finite element codes. Both the neo-Hookean solid and the Mooney–Rivlin solid are special cases of the law (with $N = 1$ and appropriate choices of C_{ij}). Values of $N > 2$ are rarely used, because it is difficult to fit such a large number of material properties to experimental data.

Ogden model [adapted from Ogden 1972a,b]:

$$\tilde{U} = \sum_{i=1}^N \frac{2}{\alpha_i^2} (\bar{\lambda}_1^{\alpha_i} + \bar{\lambda}_2^{\alpha_i} + \bar{\lambda}_3^{\alpha_i} - 3) + \frac{K_1}{2} (J - 1)^2,$$

where $\bar{\lambda}_i = \lambda_i / J^{1/3}$, and μ_i , α_i , K are material properties. For small strains, the shear modulus and bulk modulus follow as $\mu = \sum_{i=1}^N \mu_i$, $K = K_1$. This is a rubber elasticity model and is intended to be used with $K_1 \gg \mu_1$. The stress can be computed using the formulas in 3.5.3 but are too lengthy to write out in full here.

Arruda–Boyce eight-chain model [adapted from Arruda and Boyce 1992]:

$$\bar{U} = \left\{ \frac{1}{2} (\bar{I}_1 - 3) + \frac{1}{20\beta^2} (\bar{I}_1^2 - 9) + \frac{11}{1050\beta^4} (\bar{I}_1^3 - 27) + \dots \right\} + \frac{K}{2} (J - 1)^2,$$

where μ , β , K are material properties. For small deformations, μ , K are the shear and bulk modulus, respectively. This is a rubber elasticity model, so $K \gg \mu$. The potential was derived by calculating the entropy of a simple network of long-chain molecules, and the series is the result of a Taylor expansion of an inverse Langevin function. The reference provided lists more terms if you need them. The stress-strain law is

$$\sigma_{ij} = \frac{1}{J^{5/3}} \left(1 + \frac{B_{kk}}{5J^{2/3}\beta^2} + \frac{33(B_{kk})^2}{525\beta^4 J^{4/3}} + \dots \right) \left(B_{ij} - \frac{B_{kk}}{3} \delta_{ij} \right) + K_1 (J - 1) \delta_{ij}.$$

Ogden–Storakers hyperelastic foam [Storakers 1986]:

$$\tilde{U} = \sum_{i=1}^N \frac{2}{\alpha_i^2} \left(\lambda_1^{\alpha_i} + \lambda_2^{\alpha_i} + \lambda_3^{\alpha_i} - 3 \frac{1}{\beta_i} (J^{-\alpha_i \beta_i} - 1) \right),$$

where μ_i , α_i , β_i are material properties. For small strains, the shear modulus and bulk modulus follow as $\mu = \sum_{i=1}^N \mu_i$, $K = \sum_{i=1}^N 2 \mu_i (\beta_i + 1/3)$. This is a foam model and can model highly compressible materials. The shear and compression responses are coupled.

Blatz–Ko foam rubber [Blatz and Ko 1962]:

$$U(I_1, I_2, I_3) = \frac{1}{2} \left(\frac{I_1}{I_2} + 2\sqrt{I_3} \right),$$

where μ is a material parameter corresponding to the shear modulus at infinitesimal strains. Poisson's ratio for such a material is 0.25.

3.5.6 Calibrating Nonlinear Elasticity Models

To use any of these constitutive relations, you will need to determine values for the material constants. In some cases, this is quite simple (the incompressible neo-Hookean material only has one constant!); for models like the generalized polynomial or Ogden's, it is considerably more involved.

Conceptually, however, the procedure is straightforward. You can perform various types of test on a sample of the material, including simple tension, pure shear, equibiaxial tension, or volumetric compression. It is straightforward to calculate the predicted stress-strain behavior for the specimen for each constitutive law. The parameters can then be chosen to give the best fit to experimental behavior. Here are some guidelines on how best to do this:

1. When modeling the behavior of rubber under ambient pressure, you usually don't need to characterize response to volumetric compression in detail. For the rubber elasticity models listed above, you can take $K_1 \approx 10^5$ MPa. To fit the remaining parameters, you can assume the material is perfectly incompressible.
2. If rubber is subjected to large hydrostatic stress (>100 MPa), its volumetric and shear responses are strongly coupled. Compression increases the shear modulus, and high enough pressure can even induce a glass transition [Quested, Pae, Sheinbein, and Newman 1981]. To account for this, you would have to use one of the foam models: in the rubber models, the volumetric and shear responses are decoupled. You would also have to determine the material constants by testing the material under combined hydrostatic and shear loading.
3. For the simpler material models (e.g. the neo-Hookean solid, the Mooney–Rivlin material, or the Arruda–Boyce model, which contain only two material parameters in addition to the bulk modulus), you can estimate material parameters by fitting to the results of a uniaxial tension test. There are various ways to actually do the fit. You could match the small-strain shear modulus to experiment and then select the remaining parameter to fit the stress-strain curve at a larger stretch. Least-squared fits are also often used. However, models calibrated in this way do not always predict material behavior under multiaxial loading accurately.
4. A more accurate description of material response to multiaxial loading can be obtained by fitting the material parameters to multiaxial tests. To help in this exercise, the nominal stress (i.e., force/unit undeformed area) versus extension predicted by several constitutive laws are listed in Table 3.6 (assuming perfectly incompressible behavior, as suggested in 1 above). Specimen dimensions are illustrated in Figure 3.19.

3.5.7 Representative Values of Material Properties for Rubbers

The properties of rubber are strongly sensitive to its molecular structure, and, for accurate predictions, you will need to obtain experimental data for the particular material you plan to use. As a rough guide, the experimental data of Treloar [1944] for the behavior of vulcanized rubber under uniaxial tension, biaxial tension, and pure shear is shown in Figure 3.20. The solid lines in the figure show the predictions of the Ogden model (which gives the best fit to the data).

Material parameters fit to this data for several constitutive laws are listed in Table 3.7.

3.6 LINEAR VISCOELASTIC MATERIALS: TIME-DEPENDENT BEHAVIOR OF POLYMERS AT SMALL STRAINS

Amorphous polymers show complex time-dependent behavior when subjected to a history of stress or strain. Viscoelasticity theory was developed to approximate this behavior in polymers that are subjected to modest strains (less than 0.5%). Typical applications might

TABLE 3.6 Stress-Stretch Relations Predicted by Hyperelastic Constitutive Equations

	Uniaxial Tension	Biaxial Tension	Pure Shear
Invariants	$I_1 / L_1 = \lambda$	$I_1 / L_1 = I_2 / L_2 = \lambda$	$I_1 / L_1 = \lambda \quad I_2 / L_2 = 1$
	$I_2 / L_2 = I_3 / L_3 = \lambda^{-1/2}$	$I_3 / L_3 = \lambda^{-2}$	$I_3 / L_3 = \lambda^{-1}$
	$I_1 = \lambda^2 + 2\lambda^{-1}$	$I_1 = 2\lambda^2 + \lambda^{-4}$	$I_1 = 1 + \lambda^2 + \lambda^{-2}$
Neo-Hookean	$S_1 = -_1(\lambda - \lambda^{-2})$ $S_2 = S_3 = 0$	$S_1 = S_2 = -_1(\lambda - \lambda^{-5})$ $S_3 = 0$	$S_1 = -_1(\lambda - \lambda^{-3})$ $S_2 = -_1(\lambda^{-1} - \lambda^{-3})$ $S_3 = 0$
Mooney-Rivlin	$S_1 = -_1(\lambda - \lambda^{-2}) + -_2(1 - \lambda^{-3})$ $S_2 = S_3 = 0$	$S_1 = S_2 = -_1(\lambda - \lambda^{-5}) + -_2(\lambda^3 - \lambda^{-3})$ $S_3 = 0$	$S_1 = (-_1 + -_2)(\lambda - \lambda^{-3})$ $S_2 = -_1(1 - \lambda^{-1}) + -_2(\lambda^2 - 1)$ $S_3 = 0$
Arruda-Boyce	$S_1 = C(\lambda - \lambda^{-2})$ $S_2 = S_3 = 0$	$S_1 = S_2 = C(\lambda - \lambda^{-5})$ $S_3 = 0$	$S_1 = C(\lambda - \lambda^{-3})$ $S_2 = C(1 - \lambda^{-2})$
Ogden	$S_1 = \sum_n n(\lambda^{\alpha_n} - \lambda^{-\alpha_n/2}) / \lambda$ $S_2 = S_3 = 0$	$S_1 = S_2 = \sum_n n(\lambda^{\alpha_n} - \lambda^{-2\alpha_n}) / \lambda$ $S_3 = 0$	$S_1 = \sum_n n(\lambda^{\alpha_n} - \lambda^{-\alpha_n}) / \lambda$ $S_2 = \sum_n n(1 - \lambda^{-\alpha_n})$

$$C = \left(1 + \frac{I_1}{5\beta^2} + \frac{33I_1^2}{525\beta^4} \right)$$

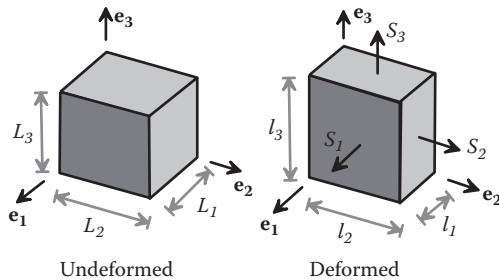


FIGURE 3.19 Homogeneous deformation of a hyperelastic solid.

be to model the energy dissipation during cyclic loading of a polymeric vibration damper or to model human tissue responding to an electric shaver.

3.6.1 Features of the Small-Strain Rate-Dependent Response of Polymers

The principal features of polymers (and some biological tissue) are summarized below:

1. Polymers strongly resist volume changes at all temperatures. The bulk modulus (the ratio of volume change to hydrostatic component of stress) is comparable to that of metals or covalently bonded solids.
2. The shear response of a polymer is strongly temperature dependent, as shown in Figure 3.21. At low temperatures (the glassy regimen), the shear modulus is high and comparable with that of metals. At a critical temperature (the glass transition), the

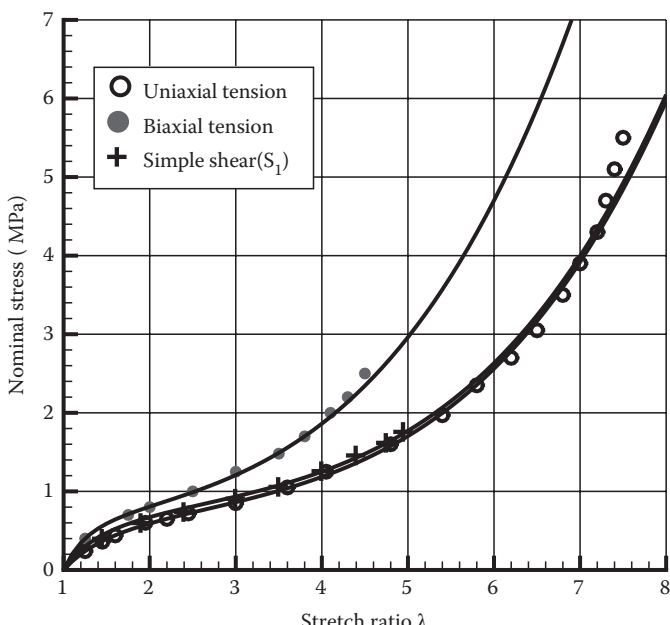


FIGURE 3.20 Comparison of predicted and measured stress-stretch curve for a rubber.

TABLE 3.7 Representative Material Properties for Vulcanized Rubber

Neo-Hookean	$\mu_1 = 0.4 \text{ MNm}^{-2}$
Mooney-Rivlin	$\mu_1 = 0.39 \text{ MNm}^{-2}, \mu_2 = 0.015 \text{ MNm}^{-2}$
Arruda-Boyce	$\mu_1 = 0.4 \text{ MNm}^{-2}, \beta = 10$
Ogden	$\mu_1 = 0.62 \text{ MNm}^{-2}, \alpha_1 = 1.3$ $\mu_2 = 0.00118 \text{ MNm}^{-2}, \alpha_2 = 5$ $\mu_3 = -0.00981 \text{ MNm}^{-2}, \alpha_3 = -2$

modulus drops. At temperatures well above the glass transition temperature (the rubbery regimen), the shear modulus can be as low as 10^{-5} times that of most metals.

- At temperatures near the glass transition, the shear modulus is strongly time (and load history) dependent; this behavior is discussed in more detail below. The time-dependent shear response can be measured in two ways: (1) by applying a step load to a sample or (2) by applying a harmonic (sinusoidal) load to the specimen.
- The time-dependent modulus of polymers is also temperature dependent. Reducing the temperature is qualitatively equivalent to increasing the strain rate. The equivalence of temperature and strain rate is discussed in more detail below.
- Most amorphous polymers are isotropic; their stress-strain response is independent of material orientation.

3.6.1.1 Time-Dependent Response to Step Loading

The time-dependent shear response can be measured in one of two ways:

- Take a specimen that is free of stress at time $t = 0$, apply a constant shear stress $\Delta\tau$ for $t > 0$, and measure the resulting shear strain ε as a function of time. The results are generally presented by plotting the *creep compliance* $J(t) = 2\varepsilon(t)/\Delta\tau$ as a function of time.
- Take a specimen that is free of stress at time $t = 0$, apply a constant shear strain $\Delta\varepsilon$ for $t > 0$, and measure the resulting shear stress $\tau(t)$ as a function of time. In this case, the results are presented by plotting the *relaxation modulus*: $G(t) = \tau(t)/2\Delta\varepsilon$.

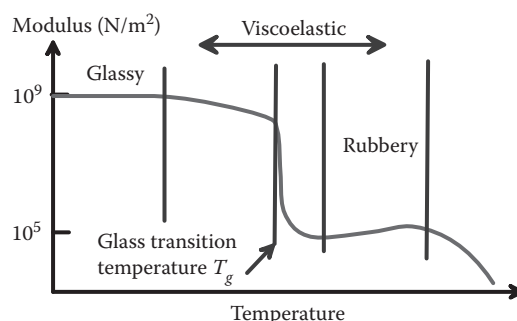


FIGURE 3.21 Variation of shear modulus of a typical polymer with temperature.

The results of such a test depend on the degree of cross-linking in the polymer. Heavily cross-linked materials show “retarded elastic” behavior, whereas un-cross-linked materials show steady-state creep. A detailed description of each type of behavior follows.

3.6.1.1.1 Retarded Elastic Behavior (Observed in Strongly Crosslinked Polymers)

The notable features of this behavior are shown in Figure 3.22:

1. There is always an instantaneous strain $\Delta\epsilon$ in response to a step change in stress $\Delta\tau$. The instantaneous compliance $J_g = 2\Delta\epsilon/\Delta\tau$ is low and only weakly dependent on temperature.
2. At temperatures significantly below the glass transition temperature, the solid is essentially elastic (there may be a very slow increase in compliance with time). At low temperatures, the compliance is low, comparable with J_g .
3. At temperatures significantly above the glass transition temperature, the solid is very compliant, and the compliance is a function of temperature. The specimen will show an initial transient response but will quite quickly settle to a constant strain. The time taken to reach steady state decreases with increasing temperature, and, for some materials, the transient may be short enough to be neglected. In this case, the material can be modeled using the hyperelastic constitutive law described in the preceding section.
4. For a range of temperatures both above and below the glass transition temperature, the solid shows a slow transient response.
5. The deformation is reversible: if the loading is removed, the specimen will eventually return to its original configuration, although in the transition regimen this may take a very long time.

3.6.1.1.2 Steady-State Creep Behavior (Observed in Uncrosslinked Polymers and Polymer Melts)

The notable features of this behavior are shown in Figure 3.23:

1. There is always an instantaneous strain in response to a step change in stress, exactly as in crosslinked polymers.

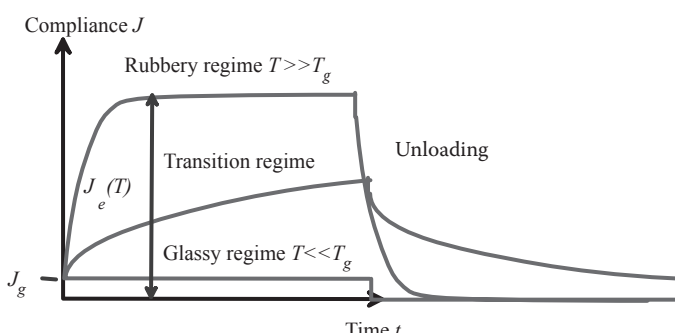


FIGURE 3.22 Time-dependent compliance of a typical crosslinked polymer.

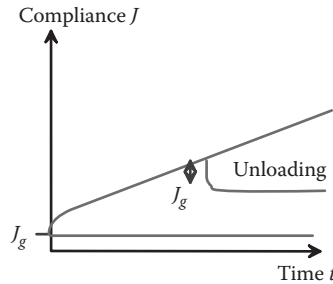


FIGURE 3.23 Time-dependent compliance of a typical uncrosslinked polymer.

2. At low temperatures (well below the glass transition temperature), the solid is essentially elastic (there may be a very slow rate of creep) and has a very low compliance, comparable with J_g .
3. At temperatures above the glass transition temperature, the solid is very compliant. It may show rubbery behavior for very low stresses, but, for most practical ranges of loading, the compliance will increase more or less linearly with time (especially for short time intervals). The rate of change of compliance is strongly temperature dependent, as discussed below.
4. Above the glass transition temperature, the deformation is irreversible: if the loading is removed, the specimen will not return to its original shape.

3.6.1.2 Response to Harmonic Loading

In addition to measuring the response of a material to a step change in load, one can subject it to cyclic strain, e.g., with strains that vary sinusoidally with time:

$$\varepsilon(t) = \varepsilon_0 \cos(\omega t) = \varepsilon_0 \operatorname{Re}[\exp(i\omega t)],$$

where $\operatorname{Re}(z)$ denotes the real part of a complex number z . The stress history will also be harmonic and could be expressed as $\tau = \tau_0 \operatorname{Re}[\exp(i\omega t)\exp(i\delta)]$, where τ_0 is the stress amplitude, and δ is a phase shift. Both τ_0 and δ depend on ω . One can define a complex modulus as

$$G^*(\omega, T) = \tau_0 \exp(i\delta)/2\varepsilon_0.$$

Experimental data is usually presented by plotting the real part $G'(\omega, T)$ of the complex modulus $G^*(\omega, T)$ against the inverse of frequency, where

$$G^* = G' + iG'' \quad G' = \tau_0 \cos(\delta)/\varepsilon_0 \quad G'' = \tau_0 \sin(\delta)/\varepsilon_0.$$

The variation of the modulus with frequency is illustrated in Figure 3.24.

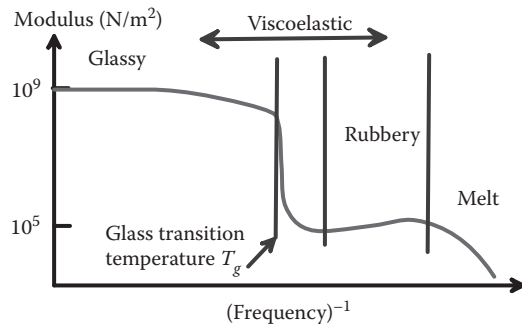


FIGURE 3.24 Harmonic modulus of a typical polymer as a function of frequency.

3.6.1.3 Williams–Landell–Ferry Time/Temperature Equivalence

You may have noticed that the figures showing the variation of modulus with temperature and frequency are remarkably similar. Of course these are just sketches, but in fact the connection between temperature and loading rate is more than just a qualitative trend. This can be demonstrated by means of the following experiment:

1. At temperature T_1 , subject a specimen to a step change in shear strain $\Delta\epsilon$ and measure the relaxation modulus $G(t; T_1) = \tau(t)/(2\Delta\epsilon)$.
2. Repeat the experiment at several progressively higher temperatures $T_2, T_3 \dots T_n$ to obtain a series of relaxation modulus curves $G(t; T_2), G(t; T_3) \dots$.
3. Plot $\log(G(t))$ versus $\log(t)$ for the raw data. The results will look like a complicated mess, something like Figure 3.25.
4. However, you will find that, if you simply shift the modulus curves for the higher temperatures to the right, you can make the data collapse onto a single master curve, as shown.
5. This observation can be expressed mathematically as $\log(G) = f\{\log(t) + \log[A(T; T_1)]\}$, where the function f represents the master curve, and $\log A(T; T_1)$ represents the horizontal shift

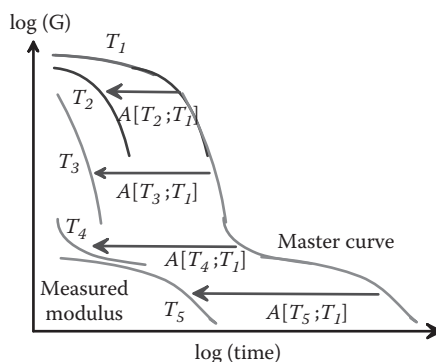


FIGURE 3.25 Scaling of the temperature-dependent relaxation modulus onto a master curve.

from temperature T_1 to T_2 . $A(T; T_1)$ is known as the Williams-Landell-Ferry (WLF) shift function.

6. If you measure $A(T; T_1)$ at a series of temperatures and plot $\log A(T; T_1)$ as a function of temperature T , you will find that the data can be well approximated by a function of the form $\log A(T; T_1) = -C_1(T - T_1)/(C_2 + (T - T_1))$. The scaling holds for any two temperatures, but of course C_1 and C_2 must depend on the choice of T_1 . In practice, it is convenient (and conventional) to use the glass transition temperature as the reference temperature. The scaling law can then be written as

$$A(T; T_g) = \exp \left\{ -\frac{C_1^g (T - T_g)}{C_2^g + (T - T_g)} \right\}.$$

The values of C_1^g and C_2^g vary slightly (but surprisingly little) from one polymer to another: typical ranges are $C_1^g \approx 10 - 40$ and $C_2^g \approx 50 - 100$ Kelvin. The expression works (again surprisingly) for T both above and below T_g , but of course the expression blows up if $T < T_g - C_2^g$. For temperatures below this critical value, the material is perfectly elastic (with constant elastic moduli).

7. Note that, because $A(T; T_1) = A(T_g; T_1)A(T; T_g)$, the constants C_1 , C_2 , T_1 and C_1^g , C_2^g , T_g are related by $C_1 = C_1^g C_2^g / (C_2^g + T_1 - T_g)$, $C_2 = C_2^g + T_1 - T_g$. This means that, if you measure a time-dependent modulus $G(t, T_1)$ at temperature T_1 and know the values of C_1^g , C_2^g , T_g for the material, you can immediately calculate the modulus at any other temperature as $G(t, T) = G(A(T; T_1)t, T_1)$, where

$$A(T; T_1) = \exp \left(\frac{-C_1^g C_2^g (T - T_1)}{[C_2^g + T_1 - T_g][C_2^g + T - T_g]} \right).$$

3.6.2 General Constitutive Equations for Linear Viscoelastic Solids

The general stress-strain law for a linear viscoelastic solid is constructed as follows:

- Assume that the material experiences small shape changes and rotations. The deformation can then be characterized using the infinitesimal strain tensor $\varepsilon_{ij} = (\partial u_i / \partial x_j + \partial u_j / \partial x_i) / 2$ defined in Section 2.1.7.
- For small strains, all stress measures are equal. We can use the Cauchy stress σ_{ij} as the stress measure.
- Assume that, for time $t < 0$, the solid is stress free, and $\varepsilon_{ij} = 0$.
- For small strains/stresses, we can assume that the stress and strain are related through linear equations. (This does not mean that stress is proportional to strain, of course; instead, stress, strain, and their rates are related by a time-dependent linear ODE, as discussed below.)
- Assume that the material is isotropic.

- In most practical applications, we can assume that material response to a pure volumetric strain ($\varepsilon_{11} = \varepsilon_{22} = \varepsilon_{33} = (V - V_0)/(3V_0)$ with all other $\varepsilon_{ij} = 0$) is perfectly elastic (with no time-dependent behavior). The volumetric strain will induce a state of hydrostatic tension $\sigma_{11} = \sigma_{22} = \sigma_{33} = \sigma$ with all other $\sigma_{ij} = 0$. The stress is related to the strain by $\sigma = K\delta V/V$, where K is the bulk modulus.
- Viscoelastic response is most commonly characterized by the shear relaxation modulus $G(t, T_1)$ measured at some reference temperature T_1 . (Recall that the shear relaxation modulus can be measured by subjecting a specimen to a step increase in shear strain $\Delta\varepsilon$ and measuring the resulting shear stress $\tau(t)$. The relaxation modulus follows as $G(t, T_1) = \tau(t)/(2\Delta\varepsilon)$.)
- The temperature dependence of the modulus is characterized by the WLF constants C_1^g , C_2^g and the glass transition temperature T_g through the WLF shift function defined in the preceding section.
- Because the stress is linearly related to strain, the stress history $\sigma_{ij}(t)$ resulting from an arbitrary strain history $\varepsilon_{ij}(t)$ can be computed by appropriately superposing the step response. The result is

$$\sigma_{ij}(t) = \int_0^t 2G(A(T; T_1)(t - \zeta), T_1) \left[\dot{\varepsilon}_{ij}(\zeta) - \frac{1}{3} \dot{\varepsilon}_{kk}(\zeta) \delta_{ij} \right] d\zeta + K\varepsilon_{kk}\delta_{ij}.$$

Here, the temperature T is assumed to be constant up to time t . It is not hard to extend the formula to account for time-varying temperatures, but the result looks messy and is difficult to visualize.

To apply this stress-strain relation in practice, it is necessary to find a convenient way to fit the relaxation modulus $G(t, T_1)$. Various approaches to doing this are described in the next two sections.

3.6.3 Spring–Damper Approximations to the Relaxation Modulus

Spring-damper models are often used as a simple, approximate model of the behavior of a viscoelastic solid. The sketches in Figure 3.26 illustrate the general idea: in each case, the force applied to the spring-dashpot system represents shear stress, whereas the extension represents shear strain. It is straightforward to show that they are related by

$$k\sigma + \eta \frac{d\sigma}{dt} = k\eta \frac{d\varepsilon}{dt} \quad \text{Maxwell}$$

$$\sigma = k\varepsilon + \eta \frac{d\varepsilon}{dt} \quad \text{Kelvin–Voigt}$$

$$k_1\sigma + \eta \frac{d\sigma}{dt} = k_1 k_2 \varepsilon + (k_1 + k_2)\eta \frac{d\varepsilon}{dt} \quad \text{3 Parameter.}$$

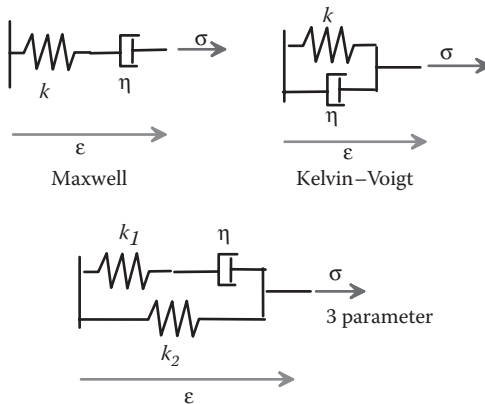


FIGURE 3.26 Spring-damper representations of polymer behavior.

For a material with time-independent bulk modulus K , these can be generalized to multi-axial loading as

$$e_{ij} = \varepsilon_{ij} - \varepsilon_{kk}\delta_{ij} \quad \sigma_{ij} = S_{ij} + K\varepsilon_{kk}\delta_{ij}$$

$$kS_{ij} + \eta \frac{dS_{ij}}{dt} = k\eta \frac{de_{ij}}{dt} \quad \text{Maxwell}$$

$$S_{ij} = ke_{ij} + \eta \frac{de_{ij}}{dt} \quad \text{Kelvin-Voigt}$$

$$k_1S_{ij} + \eta \frac{dS_{ij}}{dt} = k_1k_2e_{ij} + (k_1 + k_2)\eta \frac{de_{ij}}{dt} \quad \text{3 parameter.}$$

Qualitatively, these models describe the behavior of a typical polymer. The Kelvin-Voigt model gives retarded elastic behavior and represents a crosslinked polymer. The Maxwell model gives steady-state creep and would represent an uncrosslinked polymer. With an appropriate choice of k_1 and k_2 , the three-parameter model can describe both types of behavior.

For hand calculations, it is often more convenient to use the differential equations relating stress to strain than the integral form given in the preceding section. However, it is straightforward to calculate the relaxation modulus for the Maxwell and three-parameter models:

$$G(t) = ke^{-kt/\eta} \quad \text{Maxwell}$$

$$G(t) = k_2 + k_1e^{-k_1t/\eta} \quad \text{3 parameter.}$$

The Kelvin-Voigt model does not have a well-defined relaxation modulus.

3.6.4 Prony Series Representation for the Relaxation Modulus

The models described in the preceding section are too simple to give a good quantitative fit to any polymer over an extended period of time. We can make a more versatile model by connecting a bunch of Maxwell elements in series and adding a spring in parallel with the whole array. The relaxation modulus for this material has the form

$$G(t) = G_{\infty} + \sum_{i=1}^N G_i e^{-t/t_i},$$

where G_{∞} is the steady-state stiffness (represented by the parallel spring), and $G_i, t_i, i = 1 \dots N$ are the time constants and stiffnesses of the Maxwell elements. These parameters are used directly as the properties of the material. The sum of exponentials is known as the “Prony series.”

3.6.5 Calibrating the Constitutive Laws for Linear Viscoelastic Solids

Experimental data for the time-dependent behavior of polymers can be presented in several different ways:

1. The Young's modulus $E(t, T_i)$ or shear modulus $G(t, T_i)$ as a function of time t , at various temperatures T_i ;
2. The tensile compliance $C(t, T_i)$ or shear compliance $J(t, T_i)$ as a function of time, at various temperatures;
3. The complex modulus $G^*(\omega, T_i) = G'(\omega, T_i) + iG''(\omega, T_i)$, or, more usually, just the real part of the complex modulus $G'(\omega, T_i)$ as a function of frequency ω and temperature;
4. The complex compliance $J^*(\omega, T)$ or the real part of the complex compliance $J'(\omega, T)$ as a function of frequency and temperature.

The material parameters G_{∞}, G_i, t_i must be fit to this data. For each dataset, the first step is to combine data from tests at various temperatures into a master curve of $G(t, T)$, $G'(\omega, T)$, or $J(t, T), J'(\omega, T)$ at a single reference temperature, using the WLF scaling procedure described in Section 3.6.1. The parameters should then be chosen to give the best fit to this master curve. (A simple way to fit the parameters is to choose t_i to be spaced at exponentially increasing time intervals and then choose G_{∞}, G_i to minimize the square of the difference between the predicted and measured values $\log(G(t))$.)

To do the fit, it is helpful to find formulas for $G(t, T)$, or $G'(\omega, T)$, in terms of material properties. It is straightforward to show that

$$G(t, T) = G_{\infty} + \sum_{i=1}^N G_i \exp(-t / t_i)$$

$$G'(\omega, T) = G_{\infty} + \sum_{i=1}^N \frac{G_i \omega^2 t_i^2}{1 + \omega^2 t_i^2} \quad G''(\omega, T) = \sum_{i=1}^N \frac{G_i \omega t_i}{1 + \omega^2 t_i^2}.$$

It is slightly more cumbersome to fit the Prony series parameters to compliance measurements. The compliances can be expressed in terms of G_∞ , G_i , t_i as follows

$$J(t, T) = L^{-1} \left\{ \frac{1}{s^2} \left(\frac{G_\infty}{s} + \sum_{i=1}^N \frac{t_i G_i}{t_i s + 1} \right)^{-1} \right\},$$

$$J'(\omega, T) = \frac{G'(\omega, T)}{G'(\omega, T)^2 + G''(\omega, T)^2} \quad J''(\omega, T) = \frac{G''(\omega, T)}{G'(\omega, T)^2 + G''(\omega, T)^2},$$

where L^{-1} denotes an inverse Laplace transform (which can be calculated using a symbolic manipulation program), and G' , G'' were defined above.

If you are given experimental data for Young's modulus $E(t)$ or tensile compliance $C(t)$, you will need to estimate $G(t)$ or $J(t)$. Precise values cannot be found without knowing the bulk modulus or Poisson's ratio of the material, but, for most practical applications, you can assume that the bulk modulus is very large, in which case $G(t) = E(t)/3$ and $J(t) = 3C(t)$.

3.6.6 Representative Values for Viscoelastic Properties of Polymers

The properties of polymers are very sensitive to their molecular structure, so for accurate predictions, you will need to obtain data for the particular material you intend to use. As a rough guide to typical values, the master curve of $G(t, T_g)$ and the WLF shift function $A(T, T_g)$ for polyisobutylene have been calculated from the data in McCrum, Buckley, and Bucknall [1997] and are shown in Figure 3.27. The glass transition temperature for this material is $T_g = 193K$. The resulting WLF parameters, together with moduli and time constants for a seven-term Prony series fit to the data are listed in Table 3.8. The shear modulus predicted by the Prony series is shown on the modulus-versus-time plot for comparison with the experimental data.

3.7 SMALL STRAIN, RATE-INDEPENDENT PLASTICITY: METALS LOADED BEYOND YIELD

For many design calculations, the elastic constitutive equations outlined in Section 3.1 are sufficient, because large plastic strains are generally undesirable and will lead to failure. There are some applications, however, in which it is of interest to predict the behavior of solids subjected to large loads, sufficient to cause permanent plastic strains. Examples include the following:

- Modeling metal forming, machining, or other manufacturing processes
- Designing crash-resistant vehicles
- Plastic design of structures

Plasticity theory was developed to predict the behavior of metals under loads exceeding the plastic range, but the general framework of plasticity theory has since been adapted to other materials, including polymers and some types of soil (clay). Some concepts from metal plasticity are also used in modeling concrete and other brittle materials such as polycrystalline ceramics.

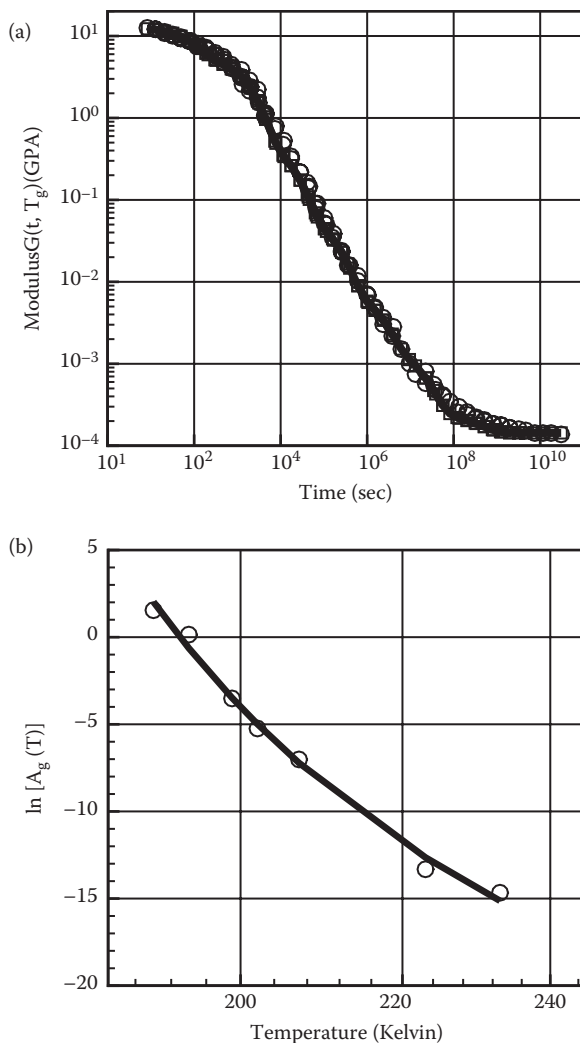


FIGURE 3.27 Relaxation behavior of polyisobutylene. (a) Modulus master-curve; (b) WLF shift function.

TABLE 3.8 Viscoelastic Properties of Polyisobutylene

WLF parameters: $C_1^g = 36.9$ $C_2^g = 57.6$ Kelvin $T_g = 193$ Kelvin

$G_\infty = 0.143 \text{ MNm}^{-2}$ $G_1 = 7.3 \text{ GNm}^{-2}$ $t_1 = 100 \text{ sec}$

$G_2 = 4.9 \text{ GNm}^{-2}$ $t_2 = 2000 \text{ sec}$ $G_3 = 0.48 \text{ GNm}^{-2}$ $t_3 = 2 \times 10^4 \text{ sec}$

$G_4 = 57 \text{ MNm}^{-2}$ $t_4 = 2 \times 10^5 \text{ sec}$ $G_5 = 6.4 \text{ MNm}^{-2}$ $t_5 = 2 \times 10^6 \text{ sec}$

$G_6 = 1.3 \text{ MNm}^{-2}$ $t_6 = 2 \times 10^7 \text{ sec}$ $G_7 = 0.1 \text{ MNm}^{-2}$ $t_7 = 4 \times 10^8 \text{ sec}$

3.7.1 Features of the Inelastic Response of Metals

We begin by reviewing the results of a typical tension/compression test on an annealed, ductile, polycrystalline metal specimen (e.g., copper or aluminum). Assume that the test is conducted at moderate temperature (less than half the melting point of the solid, e.g., room temperature) and at modest strains (less than 10%), at modest strain rates ($10^{-2} - 10 \text{ s}^{-1}$). The results of such a test are illustrated in Figure 3.28.

- For modest stresses (and strains), the solid responds elastically. This means the stress is proportional to the strain, and the deformation is reversible.
- If the stress exceeds a critical magnitude, the stress-strain curve ceases to be linear. It is often difficult to identify the critical stress accurately, because the stress-strain relation starts to curve rather gradually.
- If the critical stress is exceeded, the specimen is permanently changed in length on unloading.
- If the stress is removed from the specimen during a test, the stress-strain curve during unloading has a slope equal to that of the elastic part of the stress-strain curve. If the specimen is reloaded, it will initially follow the same curve, until the stress approaches its maximum value during previous loading. At this point, the stress-strain curve once again ceases to be linear, and the specimen is permanently deformed further.
- If the test is interrupted and the specimen is held at constant strain for a period of time, the stress will relax slowly. If the straining is resumed, the specimen will behave as though the solid were unloaded elastically. Similarly, if the specimen is subjected to a constant stress, it will generally continue to deform plastically, although the plastic strain increases very slowly. This phenomenon is known as creep.
- If the specimen is deformed in compression, the stress-strain curve is a mirror image of the tensile stress-strain curve. (Of course, this is only true for modest strains. For

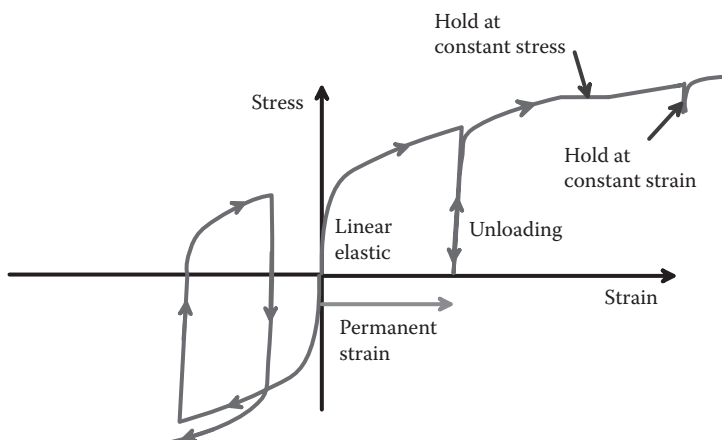


FIGURE 3.28 Typical stress-strain behavior of a ductile metal.

large strains, geometry changes will cause differences between the tension and compression tests.)

- If the specimen is first deformed in compression, then loaded in tension, it will generally start to deform plastically at a tensile stress that is lower than the yield stress of an annealed specimen. This phenomenon is known as the “Bauschinger effect.”
- Material response to cyclic loading can be extremely complex. One example is shown in the picture above; in this case, the material hardens cyclically. Other materials may soften.
- The detailed shape of the plastic stress-strain curve depends on the rate of loading, and also on temperature.

We also need to characterize the multiaxial response of an inelastic solid. This is a much more difficult experiment to do. Some of the nicest experiments were done by G. I. Taylor and collaborators in the early part of the past century. Their approach was to measure the response of thin-walled tubes under combined torsion, axial loading, and hydrostatic pressure. The main conclusions of these tests were as follows:

- The shape of the uniaxial stress-strain curve is insensitive to hydrostatic pressure. However, the ductility (strain to failure) can be increased by adding hydrostatic pressure, particularly under torsional loading.
- Plastic strains are volume preserving, i.e., the plastic strain rate must satisfy $\dot{\epsilon}_{kk} = 0$.
- During plastic loading, the principal components of the plastic strain rate tensor are parallel to the components of stress acting on the solid. This sounds obvious until you think about it. To understand what this means, imagine that you take a cylindrical shaft and pull it until it starts to deform plastically. Then, holding the axial stress fixed, apply a torque to the shaft. Experiments show that the shaft will initially stretch rather than rotate. The plastic strain increment is parallel to the stress acting on the shaft, not the stress increment. This is totally unlike elastic deformation.
- Under multiaxial loading, most annealed polycrystalline solids obey the *Levy–Mises flow rule*, which relates the principal components of strain rate during plastic loading to the principal stresses as follows:

$$\frac{\dot{\epsilon}_1 - \dot{\epsilon}_2}{\sigma_1 - \sigma_2} = \frac{\dot{\epsilon}_1 - \dot{\epsilon}_3}{\sigma_1 - \sigma_3} = \frac{\dot{\epsilon}_2 - \dot{\epsilon}_3}{\sigma_2 - \sigma_3}.$$

In this section, we will outline the simplest plastic constitutive equations that capture the most important features of metal plasticity. There are many different plastic constitutive laws, which are intended to be used in different applications. There are two broad classes:

1. Rate independent plasticity: used to model metals deformed at low temperatures (less than half the material’s melting point) and modest strain rates (of order 0.01–10/s). This is the focus of this section.

2. Rate-dependent plasticity, or viscoplasticity: used to model high-temperature creep (steady accumulation of plastic strain at constant stress) and also to model metals deformed at high strain rates (100/s or greater), where flow strength is sensitive to deformation rate. Viscoplasticity will be discussed in Section 3.8.

There are also various different models within these two broad categories. The models generally differ in two respects: (1) the yield criterion and (2) the strain hardening law. There is no completely general model that describes all the features that were just listed, so in any application, you will need to decide which aspect of material behavior is most important and then choose a model that accurately characterizes this behavior.

3.7.1.1 Key Ideas in Modeling Metal Plasticity

Five key concepts form the basis of almost all classical theories of plasticity. They are as follows:

1. The decomposition of strain into elastic and plastic parts;
2. Yield criteria, which predict whether the solid responds elastically or plastically;
3. Strain hardening rules, which control the way in which resistance to plastic flow increases with plastic straining;
4. The plastic flow rule, which determines the relationship between stress and plastic strain under multiaxial loading;
5. The elastic unloading criterion, which models the irreversible behavior of the solid.

These concepts will be described in more detail in the sections below.

For simplicity, we will at this stage restrict attention to infinitesimal deformations. Consequently, we adopt the infinitesimal strain tensor

$$\boldsymbol{\varepsilon}_{ij} = \frac{1}{2} \left(\frac{\partial u_i}{\partial x_j} + \frac{\partial u_j}{\partial x_i} \right)$$

as our deformation measure. We have no need to distinguish between the various stress measures and will use σ_{ij} to denote stress.

It is also important to note that the plastic strains in a solid depend on the load history. This means that the stress-strain laws are not just simple equations relating stress to strain. Instead, plastic strain laws must either relate the *strain rate* in the solid to the stress and stress rate or else specify the relationship between a small increment of plastic strain $d\varepsilon_{ij}^p$ in terms of strain, stress, and stress increment $d\sigma_{ij}$. In addition, plasticity problems are almost always solved using the finite element method. Consequently, numerical methods are used to integrate the plastic stress-strain equations.

3.7.2 Decomposition of Strain into Elastic and Plastic Parts

Experiments show that, under uniaxial loading, the strain at a given stress has two parts: a small recoverable elastic strain, and a large, irreversible plastic strain, as shown in Figure 3.29. In uniaxial tension, we would write

$$\varepsilon = \varepsilon^e + \varepsilon^p.$$

Experiments suggest that the reversible part is related to the stress through the usual linear elastic equations. Plasticity theory is concerned with characterizing the irreversible part.

For multiaxial loading, we generalize this by decomposing a general strain increment $d\varepsilon_{ij}$ into elastic and plastic parts, as

$$d\varepsilon_{ij} = d\varepsilon_{ij}^e + d\varepsilon_{ij}^p.$$

The elastic part of the strain is related to stress using the linear elastic equation (discussed in detail in Section 3.1)

$$C_{ijkl}d\varepsilon_{kl}^e = d\sigma_{ij}.$$

3.7.3 Yield Criteria

The yield criterion is used to determine the critical stress required to cause permanent deformation in a material. There are many different yield criteria; here we will just list the simplest ones. Let σ_{ij} be the stress acting on a solid and let $\sigma_1, \sigma_2, \sigma_3$ denote the principal values of stress. In addition, let Y denote the yield stress of the material in uniaxial tension. Then, define the following:

- von Mises yield criterion:

$$f(\sigma_{ij}, \bar{\varepsilon}^p) = \sqrt{\frac{1}{2}[(\sigma_1 - \sigma_2)^2 + (\sigma_1 - \sigma_3)^2 + (\sigma_2 - \sigma_3)^2]} - Y(\bar{\varepsilon}^p) = 0.$$

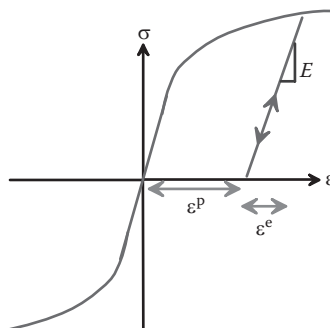


FIGURE 3.29 Decomposition of a uniaxial stress-strain curve into elastic and plastic parts.

- Tresca yield criterion:

$$f(\sigma_{ij}, \bar{\epsilon}^p) = \max\{|\sigma_1 - \sigma_2|, |\sigma_1 - \sigma_3|, |\sigma_2 - \sigma_3|\} - Y(\bar{\epsilon}^p) = 0.$$

In both cases, the criteria are defined so that the material deforms elastically for $f(\sigma_{ij}) < 0$ and plastically for $f(\sigma_{ij}) = 0$. The yield stress Y may increase during plastic straining, so we have shown that Y is a function of a measure of total plastic strain $\bar{\epsilon}^p$, to be defined in Section 3.7.5.

- An alternative form of von Mises criterion: for a general stress state, it is a nuisance having to compute the principal stresses to apply von Mises yield criterion. Fortunately, the criterion can be expressed directly in terms of the stress tensor

$$f(\sigma_{ij}, \bar{\epsilon}^p) = \sigma_e - Y(\bar{\epsilon}^p),$$

where

$$\sigma_e = \sqrt{\frac{3}{2} S_{ij} S_{ij}} \quad S_{ij} = \sigma_{ij} - \frac{1}{3} \sigma_{kk} \delta_{ij}$$

are the components of the von Mises effective stress and deviatoric stress tensor, respectively.

These yield criteria are based largely on the following experimental observations:

1. A hydrostatic stress (all principal stresses equal) will never cause yield, no matter how large the stress.
2. Most polycrystalline metals are isotropic. Because the yield criterion depends only on the magnitudes of the principal stresses, and not their directions, the yield criteria predict isotropic behavior.

Tests suggest that the von Mises yield criterion provides a slightly better fit to experiment than Tresca, but the difference between them is very small. Sometimes it simplifies calculations to use Tresca's criterion instead of von Mises.

3.7.4 Graphical Representation of the Yield Surface

Any arbitrary stress state can be plotted in “principal stress space,” with the three principal stresses as axes. The von Mises yield criterion is plotted in this way in Figure 3.30. The yield criterion is a cylinder, radius $Y/\sqrt{3}$, with its axis parallel to the line

$$\sigma_1 = \sigma_2 = \sigma_3.$$

If the state of stress falls within the cylinder, the material is below yield and responds elastically. If the state of stress lies on the surface of the cylinder, the material yields and deforms plastically. If the plastic deformation causes the material to strain harden, the radius of the cylinder increases. The stress state cannot lie outside the cylinder; this would lead to an infinite plastic strain.

Because the yield criterion $f(\sigma_{ij}) = 0$ defines a surface in stress space, it is often referred to as a *yield surface*. The yield surface is often drawn as it would appear when viewed down the

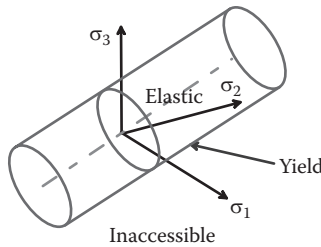


FIGURE 3.30 The von Mises yield surface.

axis of the cylinder, as shown in Figure 3.31a. The Tresca yield criterion can also be plotted in this way. It looks like a cylinder with a hexagonal cross section, as shown in Figure 3.31b.

3.7.5 Strain Hardening Laws

Experiments show that, if you plastically deform a solid, unload it, and then try to reload it so as to induce additional plastic flow, its resistance to plastic flow will have increased. This is known as strain hardening.

Obviously, we can model strain hardening by relating the size and shape of the yield surface to plastic strain in some appropriate way. There are many ways to do this. Here we describe the two simplest approaches.

3.7.5.1 Isotropic Hardening

Rather obviously, the easiest way to model strain hardening is to make the yield surface increase in size but remain the same shape, as a result of plastic straining, as shown in Figure 3.32.

This means that we must devise some appropriate relationship between Y and the plastic strain. To get a suitable scalar measure of plastic strain, we define the accumulated plastic strain magnitude

$$\bar{\varepsilon}^p \int \sqrt{\frac{2}{3} d\varepsilon_{ij}^p d\varepsilon_{ij}^p}$$

(The factor of 2/3 is introduced so that $\bar{\varepsilon}^p = \varepsilon_{11}^p$ in a uniaxial tensile test in which the specimen is stretched parallel to the \mathbf{e}_1 direction. To see this, note that plastic strains do not change volume, so that $d\varepsilon_{22} = d\varepsilon_{33} = -d\varepsilon_{11}/2$ and substitute into the formula.)

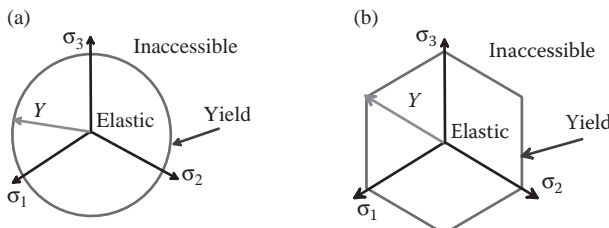


FIGURE 3.31 Axial views of yield surfaces. (a) von Mises; (b) Tresca.

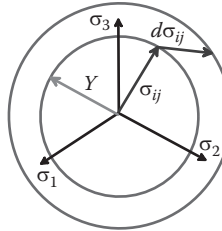


FIGURE 3.32 Evolution of a yield surface as a result of strain hardening.

Then we make Y a function of $\bar{\varepsilon}^p$. People often use power laws or piecewise linear approximations in practice. A few of the more common forms of hardening functions are as follows:

Perfectly plastic solid: $Y = \text{constant}$

Linear strain hardening solid: $Y(\bar{\varepsilon}^p) = Y_0 + h\bar{\varepsilon}^p$

Power-law hardening material: $Y = Y_0 + h(\bar{\varepsilon}^p)^{1/m}$.

In these formulas, Y_0 , h , and m are material properties. These functions are illustrated in Figure 3.33.

3.7.5.2 Kinematic Hardening

An isotropic hardening law is generally not useful in situations in which components are subjected to cyclic loading. It does not account for the Bauschinger effect and so predicts that, after a few cycles, the solid will just harden until it responds elastically.

To fix this, an alternative hardening law allows the yield surface to translate, without changing its shape. The idea is illustrated graphically in Figure 3.34. As you deform the material in tension, you drag the yield surface in the direction of increasing stress, thus modeling strain hardening. This *softens* the material in compression, however. So, this constitutive law can model cyclic plastic deformation. The stress-strain curves for isotropic and kinematic hardening materials are contrasted in Figure 3.35.

To account for the fact that the center of the yield locus is at a position α_{ij} in stress space, the von Mises yield criterion needs to be modified as follows:

$$f(\sigma_{ij}, \alpha_{ij}) = \sqrt{\frac{3}{2}(S_{ij} - \alpha_{ij})(S_{ij} - \alpha_{ij})} - Y = 0.$$

Here, Y is now a constant, and hardening is modeled by the motion of the yield surface. To do so, we need to relate α_{ij} to the plastic strain history somehow. There are many ways to

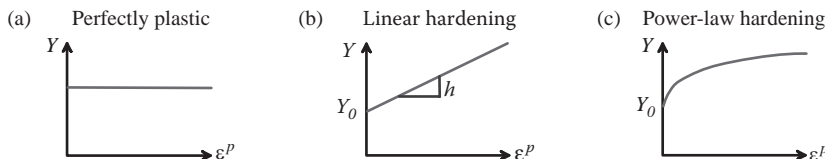


FIGURE 3.33 Simple hardening relations. (a) Perfectly plastic; (b) linear hardening; and (c) power-law hardening.

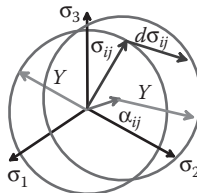


FIGURE 3.34 Evolution of a yield surface during kinematic hardening.

do this, which can model subtle features of the plastic response of solids under cyclic and nonproportional loading. The simplest approach is to set

$$d\alpha_{ij} = \frac{2}{3}cd\varepsilon_{ij}^p.$$

This hardening law predicts that the stress-plastic strain curve is a straight line with slope c . This is known as *linear kinematic hardening*.

A more sophisticated approach is to set

$$d\alpha_{ij} = \frac{2}{3}cd\varepsilon_{ij}^p - \gamma\alpha_{ij}d\bar{\varepsilon}^p,$$

where c and γ are material constants. It is not easy to visualize what this does; it turns out that this relation can model the tendency of a material to accumulate strain in the direction of mean stress under cyclic loading, as illustrated in Figure 3.36. It is known as the Armstrong–Frederick hardening law.

There are many other kinematic type hardening laws. New ones are still being developed.

3.7.6 Plastic Flow Law

To complete the plastic stress-strain relations, we need a way to predict the plastic strains induced by stressing the material beyond the yield point. Specifically, given

1. The current stress σ_{ij} applied to the material
2. The current yield stress (characterized by $Y(\bar{\varepsilon}^p)$ for isotropic hardening, or α_{ij} for kinematic hardening)

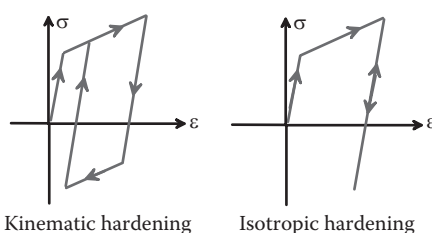


FIGURE 3.35 Comparison of stress-strain curves for kinematic and isotropic hardening.

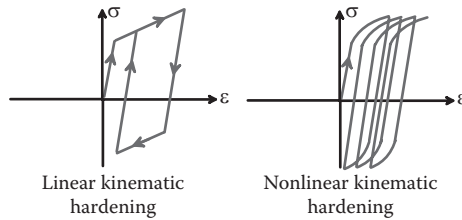


FIGURE 3.36 Stress-strain curves for kinematic hardening solids.

3. A small increase in stress $d\sigma_{ij}$ applied to the solid,

we want to determine the small change in plastic strain $d\bar{\varepsilon}^p$. The formulas are given below, for isotropic and kinematic hardening. These are just fits to experiment (specifically, to the Levy–Mises flow rule). The physical significance and reason for the structure of the equations will be discussed later.

The plastic strains are usually derived from the yield criterion f defined in Section 3.7.3 and so are slightly different for isotropic and kinematic hardening. A material that has its plastic flow law derived from f is said to have an “associated” flow law, i.e., the flow law is associated with f . The flow rules for isotropic and kinematic hardening solids are as follows.

3.7.6.1 Isotropic Hardening (von Mises Yield Criterion)

$$d\bar{\varepsilon}^p = d\bar{\varepsilon}^p \frac{\partial f}{\partial \sigma_{ij}} = d\bar{\varepsilon}^p \frac{3 S_{ij}}{2 Y},$$

where

$$f(\sigma_{ij}, \bar{\varepsilon}^p) = \sqrt{\frac{3}{2} S_{ij} S_{ij}} - Y(\bar{\varepsilon}^p) \quad S_{ij} = \sigma_{ij} - \frac{1}{3} \sigma_{kk} \delta_{ij}$$

denotes the von Mises yield criterion, and $d\bar{\varepsilon}^p$ is determined from the condition that the yield criterion must be satisfied at all times during plastic straining. This shows that

$$\begin{aligned} f(\sigma_{ij} + d\sigma_{ij}, \bar{\varepsilon}^p + d\bar{\varepsilon}^p) &= f(\sigma_{ij}, \bar{\varepsilon}^p) + \frac{\partial f}{\partial \sigma_{ij}} d\sigma_{ij} + \frac{\partial f}{\partial \bar{\varepsilon}^p} d\bar{\varepsilon}^p = 0 \\ &\Rightarrow \frac{\partial f}{\partial \sigma_{ij}} d\sigma_{ij} - \frac{\partial Y}{\partial \bar{\varepsilon}^p} d\bar{\varepsilon}^p = 0 \\ &\Rightarrow d\bar{\varepsilon}^p = \frac{1}{h} \frac{\partial f}{\partial \sigma_{ij}} d\sigma_{ij} = \frac{1}{h} \frac{3}{2} \frac{S_{ij} d\sigma_{ij}}{Y} \quad h = \frac{dY}{d\bar{\varepsilon}^p}. \end{aligned}$$

Here, $h = \partial Y / \partial \bar{\varepsilon}^p$ is the slope of the plastic stress-strain curve. The algebra involved in differentiating f with respect to stress is outlined below.

3.7.6.2 Linear Kinematic Hardening (*von Mises Yield Criterion*)

$$d\epsilon_{ij}^p = d\bar{\epsilon}^p \frac{\partial f}{\partial \sigma_{ij}} = d\bar{\epsilon}^p \frac{3(S_{ij} - \alpha_{ij})}{2Y},$$

where the yield criterion is now

$$f(\sigma_{ij}, \alpha_{ij}) = \sqrt{\frac{3}{2}(S_{ij} - \alpha_{ij})(S_{ij} - \alpha_{ij})} - Y \quad S_{ij} = \sigma_{ij} - \frac{1}{3}\sigma_{kk}\delta_{ij},$$

and as before, $d\bar{\epsilon}^p$ is determined from the condition that the yield criterion must be satisfied at all times during plastic straining. This shows that

$$f(\sigma_{ij} + d\sigma_{ij}, \alpha_{ij} + d\alpha_{ij}) = f(\sigma_{ij}, \alpha_{ij}) + \frac{\partial f}{\partial \sigma_{ij}} d\sigma_{ij} + \frac{\partial f}{\partial \alpha_{ij}} d\alpha_{ij} = 0.$$

Recall that, for linear kinematic hardening, the hardening law is

$$d\alpha_{ij} = \frac{2}{3}cd\epsilon_{ij}^p = cd\bar{\epsilon}^p \frac{(S_{ij} - \alpha_{ij})}{Y}.$$

Substituting into the Taylor expansion of the yield criterion and simplifying shows that

$$d\bar{\epsilon}^p = \frac{1}{c} \frac{3}{2} \frac{(S_{ij} - \alpha_{ij})d\sigma_{ij}}{Y}.$$

3.7.6.3 Comparison of Flow Law Formulas with the Levy–Mises Flow Rule

The Levy–Mises flow law (based on experimental observations) states that principal values of the plastic strain increment $d\epsilon_1, d\epsilon_2, d\epsilon_3$ induced by a stress increment are related to the principal stresses $\sigma_1, \sigma_2, \sigma_3$ by

$$\frac{d\epsilon_1 - d\epsilon_2}{\sigma_1 - \sigma_2} = \frac{d\epsilon_1 - d\epsilon_3}{\sigma_1 - \sigma_3} = \frac{d\epsilon_2 - d\epsilon_3}{\sigma_2 - \sigma_3}.$$

It is straightforward to show that this observation is consistent with the predictions of the flow law formulas given in this section. To see this, suppose that the principal axes of stress are parallel to the $\{\mathbf{e}_1, \mathbf{e}_2, \mathbf{e}_3\}$ directions. In this case, the only nonzero components of deviatoric stress are

$$S_{11} = \sigma_1 - (\sigma_1 + \sigma_2 + \sigma_3)/3 \quad S_{22} = \sigma_2 - (\sigma_1 + \sigma_2 + \sigma_3)/3 \quad S_{33} = \sigma_3 - (\sigma_1 + \sigma_2 + \sigma_3)/3.$$

The flow law

$$d\epsilon_{ij}^p = d\bar{\epsilon}^p \frac{\partial f}{\partial \sigma_{ij}} = d\bar{\epsilon}^p \frac{3}{2} \frac{S_{ij}}{Y}$$

gives

$$d\epsilon_1^p = d\epsilon_{11}^p = d\bar{\epsilon}^p \frac{3}{2} \frac{S_{11}}{Y} \quad d\epsilon_2^p = d\epsilon_{22}^p = d\bar{\epsilon}^p \frac{3}{2} \frac{S_{22}}{Y} \quad d\epsilon_3^p = d\epsilon_{33}^p = d\bar{\epsilon}^p \frac{3}{2} \frac{S_{33}}{Y}.$$

Thus, we see that

$$\begin{aligned} d\epsilon_1^p - d\epsilon_2^p &= d\bar{\epsilon}^p \frac{3}{2} \frac{S_{11} - S_{22}}{Y} = d\bar{\epsilon}^p \frac{3}{2} \frac{\sigma_1 - \sigma_2}{Y} \\ d\epsilon_1^p - d\epsilon_3^p &= d\bar{\epsilon}^p \frac{3}{2} \frac{S_{11} - S_{33}}{Y} = d\bar{\epsilon}^p \frac{3}{2} \frac{\sigma_1 - \sigma_3}{Y} \end{aligned}$$

with similar expressions for other components. Some trivial algebra then yields the Levy-Mises flow law.

3.7.6.4 Differentiating the Yield Criterion

Differentiating the yield criterion requires some sneaky index notation manipulations. Note that

$$\frac{\partial f}{\partial \sigma_{ij}} = \frac{3}{2} \frac{1}{2} \frac{1}{\sqrt{\frac{3}{2} S_{kl} S_{kl}}} 2S_{pq} \frac{\partial S_{pq}}{\partial \sigma_{ij}} = \frac{3}{2} \frac{1}{\sqrt{\frac{3}{2} S_{kl} S_{kl}}} S_{pq} \frac{\partial S_{pq}}{\partial \sigma_{ij}}.$$

Now, recall that

$$S_{ij} = \sigma_{ij} - \frac{1}{3} \sigma_{kk} \delta_{ij}$$

and further that

$$\frac{\partial \sigma_{ij}}{\partial \sigma_{kl}} = \delta_{ik} \delta_{jl}.$$

Hence,

$$\frac{\partial S_{pq}}{\partial \sigma_{ij}} = \delta_{ip} \delta_{jq} - \frac{1}{3} \delta_{ik} \delta_{jk} \delta_{pq}$$

and

$$S_{pq} \frac{\partial S_{pq}}{\partial \sigma_{ij}} = S_{pq} \left(\delta_{ip} \delta_{jq} - \frac{1}{3} \delta_{ik} \delta_{jk} \delta_{pq} \right) = S_{ij} - S_{pp} \delta_{ij}.$$

However, observe that

$$S_{pp} = \sigma_{pp} - \frac{1}{3} \sigma_{kk} \delta_{pp} = 0$$

so that

$$S_{pq} \frac{\partial S_{pq}}{\partial \sigma_{ij}} = S_{ij}$$

and finally

$$\frac{\partial f}{\partial \sigma_{ij}} = \frac{3}{2} \frac{S_{ij}}{\sqrt{\frac{3}{2} S_{kl} S_{kl}}} = \frac{3}{2} \frac{S_{ij}}{Y}.$$

3.7.7 Elastic Unloading Condition

There is one final issue to consider. Experiments show that plastic flow is irreversible, and always dissipates energy. If the increment in stress $d\sigma_{ij}$ is tangent to the yield surface, or brings the stress below yield, as shown in Figure 3.37, then there is no plastic strain. For an isotropically hardening solid, this unloading condition may be expressed as

$$S_{ij} d\sigma_{ij} < 0.$$

For kinematic hardening,

$$(S_{ij} - \alpha_{ij}) d\sigma_{ij} < 0.$$

In both cases, the solid deforms elastically (no plastic strain) if the condition is satisfied.

3.7.8 Complete Incremental Stress–Strain Relations for a Rate-Independent Elastic–Plastic Solid

We conclude by summarizing the complete elastic-plastic stress-strain relations for isotropic and kinematic hardening solids with von Mises yield surfaces.

3.7.8.1 Isotropically Hardening Elastic-Plastic Solid

The solid is characterized by its elastic constants E, v and by the yield stress $Y(\bar{\epsilon}^p)$ as a function of accumulated plastic strain $\bar{\epsilon}^p$ and its slope $h = \frac{dY}{d\bar{\epsilon}^p}$, as shown in Figure 3.38.

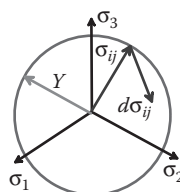


FIGURE 3.37 Stress trajectory during elastic unloading.

In this case, we have that

$$d\epsilon_{ij} = d\epsilon_{ij}^e + d\epsilon_{ij}^p$$

with

$$d\epsilon_{ij}^e = \frac{1+\nu}{E} \left(d\sigma_{ij} - \frac{\nu}{1+\nu} d\sigma_{kk} \delta_{ij} \right)$$

$$d\epsilon_{ij}^p = \begin{cases} 0 & \sqrt{\frac{3}{2} S_{ij} S_{ij}} - Y(\bar{\epsilon}^p) < 0 \\ \frac{1}{h} \frac{3}{2} \frac{\langle S_{kl} d\sigma_{kl} \rangle}{Y} \frac{3}{2} \frac{S_{ij}}{Y} & \sqrt{\frac{3}{2} S_{ij} S_{ij}} - Y(\bar{\epsilon}^p) = 0, \end{cases}$$

$$\text{where } \langle x \rangle = \begin{cases} x & x \geq 0 \\ 0 & x \leq 0. \end{cases}$$

These may be combined to

$$d\epsilon_{ij} = \begin{cases} \frac{1+\nu}{E} \left(d\sigma_{ij} - \frac{\nu}{1+\nu} d\sigma_{kk} \delta_{ij} \right) & \sqrt{\frac{3}{2} S_{ij} S_{ij}} - Y(\bar{\epsilon}^p) < 0 \\ \frac{1+\nu}{E} \left(d\sigma_{ij} - \frac{\nu}{1+\nu} d\sigma_{kk} \delta_{ij} \right) + \frac{1}{h} \frac{3}{2} \frac{\langle S_{kl} d\sigma_{kl} \rangle}{Y} \frac{3}{2} \frac{S_{ij}}{Y} & \sqrt{\frac{3}{2} S_{ij} S_{ij}} - Y(\bar{\epsilon}^p) = 0 \end{cases}.$$

It is sometimes necessary to invert these expressions. A straightforward but tedious series of index notation manipulations shows that

$$d\sigma_{ij} = \begin{cases} \frac{E}{1+\nu} \left(d\epsilon_{ij} + \frac{\nu}{1-2\nu} d\epsilon_{kk} \delta_{ij} \right) & \sqrt{\frac{3}{2} S_{ij} S_{ij}} - Y(\bar{\epsilon}^p) < 0 \\ \frac{E}{1+\nu} \left(d\epsilon_{ij} + \frac{\nu}{1-2\nu} d\epsilon_{kk} \delta_{ij} - \frac{3E}{3E+2(1+\nu)h} \frac{3}{2} \frac{\langle S_{kl} d\epsilon_{kl} \rangle}{Y} \frac{3}{2} \frac{S_{ij}}{Y} \right) & \sqrt{\frac{3}{2} S_{ij} S_{ij}} - Y(\bar{\epsilon}^p) = 0 \end{cases}.$$

This constitutive law is the most commonly used model of inelastic deformation. It has the following properties:

- It will correctly predict the conditions necessary to initiate yield under multiaxial loading.

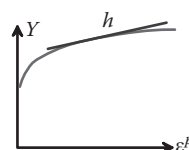


FIGURE 3.38 Definition of the hardening modulus.

- It will correctly predict the plastic strain rate under an arbitrary multiaxial stress state.
- It can model accurately any uniaxial stress-strain curve.

It has the following limitations:

- It is valid only for modest plastic strains (<10%).
- It will not predict creep behavior or strain rate sensitivity.
- It does not predict behavior under cyclic loading correctly.
- It will not predict plastic strains accurately if the principal axes of stress rotate significantly (more than about 30°) during inelastic deformation.

3.7.8.2 Linear Kinematically Hardening Solid

The solid is characterized by its elastic constants E , ν and by the initial yield stress Y and the strain hardening rate c . Then,

$$d\epsilon_{ij} = d\epsilon_{ij}^e + d\epsilon_{ij}^p$$

with

$$d\epsilon_{ij}^e = \frac{1+\nu}{E} \left(d\sigma_{ij} - \frac{\nu}{1+\nu} d\sigma_{kk} \delta_{ij} \right)$$

$$d\epsilon_{ij}^p = \begin{cases} 0 & \sqrt{\frac{3}{2}(S_{ij} - \alpha_{ij})(S_{ij} - \alpha_{ij})} - Y < 0 \\ \frac{1}{c} \frac{3}{2} \frac{\langle (S_{kl} - \alpha_{kl}) d\sigma_{kl} \rangle}{Y} \frac{3}{2} \frac{(S_{ij} - \alpha_{ij})}{Y} & \sqrt{\frac{3}{2}(S_{ij} - \alpha_{ij})(S_{ij} - \alpha_{ij})} - Y = 0 \end{cases},$$

$$\text{where } \langle x \rangle = \begin{cases} x & x \geq 0 \\ 0 & x \leq 0 \end{cases}.$$

Finally, the evolution equation for α_{ij} is

$$d\alpha_{ij} = \frac{3}{2} c d\epsilon_{ij}^p.$$

This constitutive equation is used primarily to model cyclic plastic deformation or plastic flow under nonproportional loading (in which principal axes of stress rotate significantly during plastic flow). It has the following limitations:

- It is valid only for modest plastic strains (<10%).
- It will not predict creep behavior or strain rate sensitivity.
- It does not predict the shape of the stress-strain curve accurately.

3.7.9 Typical Values for Yield Stress of Polycrystalline Metals

Unlike elastic constants, the plastic properties of metals are highly variable and are also very sensitive to alloying composition and microstructure (which can be influenced by heat treatment and mechanical working). Consequently, it is impossible to give accurate values for yield stresses or hardening rates for materials. Table 3.9 lists rough values for yield stresses of common materials [the data are from Ashby and Jones 1997]; these may provide a useful guide in preliminary calculations. If you need accurate data, you will have to measure the properties of the materials you plan to use yourself.

3.7.10 Perspectives on Plastic Constitutive Equations:

Principle of Maximum Plastic Resistance

The constitutive law outlined in the preceding section has an important property, known as the *principle of maximum plastic resistance*.

Statement of the principle: Let σ_{ij} be a stress state that causes plastic deformation, let $d\sigma_{ij}$ be a small change in σ_{ij} , and let $d\varepsilon_{ij}^p$ be the resulting strain increment. Now, let σ_{ij}^* be any other stress that can be imposed on the specimen that either does not reach yield or else just satisfies the yield criterion, i.e., $\sqrt{3S_{ij}^*S_{ij}^*/2} \leq Y$ with $S_{ij}^* = \sigma_{ij}^* - \sigma_{kk}^*\delta_{ij}$.

Then

$$(\sigma_{ij} - \sigma_{ij}^*) \frac{d\varepsilon_{ij}}{dt} \geq 0.$$

Interpretation: The principle of maximum plastic resistance is a mathematical statement of the following ideas:

1. The von Mises yield surface is convex.
2. The plastic strain rate is normal to the yield surface.

TABLE 3.9 Approximate Values for Yield Stress of a Few Materials

Material	Yield Stress σ_Y / MNm^{-2}	Material	Yield Stress σ_Y / MNm^{-2}
Tungsten carbide	6000	Mild steel	220
Silicon carbide	10 000	Copper	60
Tungsten	2000	Titanium	180–1320
Alumina	5000	Silica glass	7200
Titanium carbide	4000	Aluminum and alloys	40–200
Silicon nitride	8000	Polyimides	52–90
Nickel	70	Nylon	49–87
Iron	50	PMMA	60–110
Low alloy steels	500–1980	Polycarbonate	55
Stainless steel	286–500	PVC	45–48

It is best to illustrate these ideas graphically. In principal stress space, the product $\sigma_{ij}d\epsilon_{ij}^p$ is represented by the dot product of the stress and plastic strain rate vectors shown in Figure 3.39. The statement

$$(\sigma_{ij} - \sigma_{ij}^*)d\epsilon_{ij}^p \geq 0$$

is equivalent to the requirement that the angle between the vectors formed by $(\sigma_{ij} - \sigma_{ij}^*)$ and $d\epsilon_{ij}^p$ must be greater than 90° for all stresses and strain rates. This is only possible if the yield stress is convex and the strain rate is normal to the yield surface.

The principle of maximum plastic resistance is important because it is the basis for a number of very important theorems concerning plastic deformation in solids. For example, it can be shown that the stress field in a material that obeys the principle is always unique. In addition, the principle leads to clever techniques to estimate collapse loads for elastic-plastic solids and structures.

3.7.10.1 Proof of the Principle of Maximum Plastic Resistance

Our goal is to prove that $\sigma_{ij}d\epsilon_{ij}^p \geq \sigma_{ij}^*d\epsilon_{ij}^p$. The simplest way to do so is to show that $\sigma_{ij}d\epsilon_{ij}^p = Yd\bar{\epsilon}^p$, whereas $\sigma_{ij}^*d\epsilon_{ij}^p \leq Yd\bar{\epsilon}^p$, in which $d\bar{\epsilon}^p = \sqrt{2d\epsilon_{ij}^p d\epsilon_{ij}^p / 3}$ is the plastic strain magnitude, and Y is the yield stress. To this end,

1. Recall the plastic flow rule: $d\epsilon_{ij}^p = d\bar{\epsilon}^p \frac{\partial f}{\partial \sigma_{ij}} = d\bar{\epsilon}^p \frac{3}{2} \frac{S_{ij}}{Y}$.

2. Multiply both sides by stress:

$$\sigma_{ij}d\epsilon_{ij}^p = \sigma_{ij}d\bar{\epsilon}^p \frac{3}{2} \frac{S_{ij}}{Y} = (S_{ij} + \sigma_{kk}\delta_{ij}/3)d\bar{\epsilon}^p \frac{3}{2} \frac{S_{ij}}{Y} = d\bar{\epsilon}^p \frac{3}{2} \frac{S_{ij}S_{ij}}{Y},$$

where we have noted that $S_{kk}=0$.

3. Recall that S_{ij} causes yield and so must satisfy the yield condition $\sqrt{3S_{ij}S_{ij}/2} - Y = 0$. This shows that $\sigma_{ij}d\epsilon_{ij}^p = Yd\bar{\epsilon}^p$.

4. Now consider

$$\sigma_{ij}^*d\epsilon_{ij}^p = \sigma_{ij}^*d\bar{\epsilon}^p \frac{3}{2} \frac{S_{ij}}{Y} = d\bar{\epsilon}^p \frac{3}{2} \frac{S_{ij}^*S_{ij}}{Y}.$$

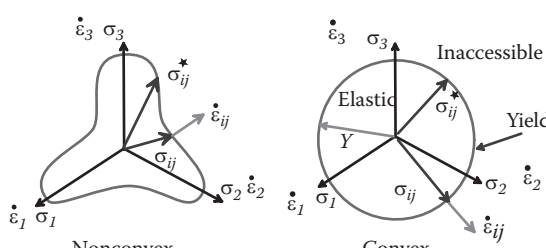


FIGURE 3.39 Comparison of nonconvex and convex yield surfaces.

5. Note that

$$\frac{3}{2}(S_{ij} - S_{ij}^*)(S_{ij} - S_{ij}^*) \geq 0 \Rightarrow \frac{3}{2}(S_{ij}S_{ij} + S_{ij}^*S_{ij}^* - 2S_{ij}S_{ij}^*) \geq 0.$$

6. Now, recall again that S_{ij} causes yield, whereas S_{ij}^* can be at or below yield. The yield criterion therefore requires that $3S_{ij}S_{ij}/2 = Y^2$. $3S_{ij}^*S_{ij}^*/2 \leq Y^2$. Substituting these inequalities into 5 above shows that $Y^2 \geq 3S_{ij}S_{ij}^*/2$. Finally, this shows

$$\sigma_{ij}^* d\epsilon_{ij}^P = d\bar{\epsilon}^P \frac{3}{2} \frac{S_{ij}^* S_{ij}}{Y} \leq Y d\bar{\epsilon}^P.$$

Thus, $\sigma_{ij} d\epsilon_{ij}^P \geq \sigma_{ij}^* d\epsilon_{ij}^P$, proving the principle.

3.7.11 Perspectives on Plastic Constitutive Equations: Drucker's Postulate

Constitutive models of inelastic behavior are based largely on experimental observations of plastic flow in laboratory specimens. Similar constitutive laws are used to describe very different materials, including metals, ceramics, glasses, soils, and polymers. The mechanisms of deformation in these materials are very different, so it is surprising that their response is similar.

One perspective on the structure of constitutive laws for inelastic solids was developed by Drucker in the 1950s. Drucker introduced the idea of a *stable plastic material*, as follows. Consider a deformable solid, subjected to boundary tractions t_i , which induce some displacement field u_i , as shown in Figure 3.40. Suppose that the tractions are increased to $t_i + \Delta t_i$, resulting in an additional displacement Δu_i . The material is said to be stable in the sense of Drucker if the work done by the tractions Δt_i through the displacements Δu_i is positive or zero for all Δt_i :

$$\Delta W = \int \left\{ \int_A \Delta t_i \frac{d\Delta u_i}{dt} \right\} dt \geq 0.$$

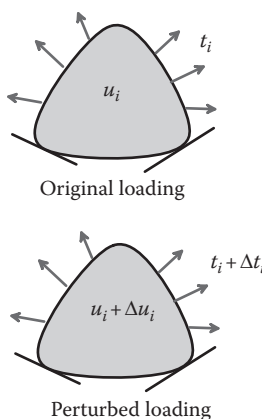


FIGURE 3.40 A plastically deforming solid subjected to incremental loading.

It can be shown that, for a plastic material to be stable in this sense, it must satisfy the following conditions:

- The yield surface $f(\sigma_{ij})$ must be convex.
- The plastic strain rate must be normal to the yield surface $d\bar{\varepsilon}_{ij}^p = d\bar{\varepsilon}^p \frac{\partial f}{\partial \sigma_{ij}}$.
- The rate of strain hardening must be positive or zero $\frac{dY}{d\bar{\varepsilon}^p} \geq 0$.

Furthermore, a material that is stable in the sense of Drucker must satisfy the principle of maximum plastic resistance.

This does not really explain *why* the constitutive law should have this structure, but materials that do not satisfy the Drucker stability criterion tend to be difficult to work with in calculations, so there is a strong incentive for choosing a constitutive law that meets the condition. It is not surprising, then, that the people developing constitutive laws ended up with a form that satisfies Drucker stability.

3.7.12 Microscopic Perspectives on Plastic Flow in Metals

It is possible to obtain some insight into the structure of the constitutive laws for metals by considering the micromechanisms responsible for plastic flow. Plastic flow in metals is caused by dislocation motion. Dislocations are line defects in crystalline solids; you can think of a dislocation as an extra plane of atoms inserted within a perfect crystal, as shown in Figure 3.41. When the crystal is subjected to stress, these defects move through the solid and rearrange the crystal lattice. For example, if the model crystal is subjected to a shear stress, the atoms rearrange so that the top part of the crystal is shifted to the right relative to the bottom part, as shown in Figure 3.42. Because the crystal lattice is distorted near a dislocation, only a modest shear stress is required to drive the dislocation through the solid, causing permanent plastic deformation.

Experiments and atomistic simulations suggest that dislocation motion obeys Schmidt's law: a dislocation moves through a crystal if the shear stress on its glide plane exceeds a critical magnitude τ_c . It can be shown that a material that deforms by dislocation glide and that obeys Schmidt's law will satisfy the principle of maximum plastic resistance. This, in turn, implies that the yield surface for the solid must be convex and the plastic strain rate must be normal to the yield surface.

The notion of a yield surface and convexity for a material that deforms by dislocation glide can be illustrated with a simple double-slip model. Consider a single crystal, which

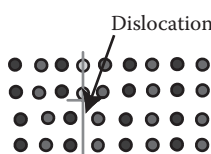


FIGURE 3.41 An edge dislocation in a crystal.

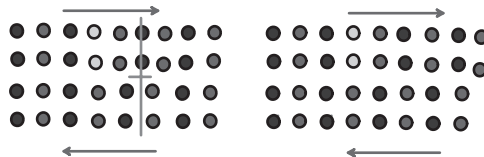


FIGURE 3.42 Plastic shearing caused by motion of an edge dislocation.

contains two dislocation glide planes oriented at 45° to the principal axes of stress as shown in Figure 3.43. Assume plane stress conditions, for simplicity.

Figure 3.44 shows side views of the two slip planes. As an exercise, you should verify that the shear stresses (tangential component of traction) acting on the two slip planes are

$$\tau = \pm \frac{1}{2}(\sigma_1 - \sigma_2)$$

$$\tau = \pm \frac{1}{2}\sigma_2.$$

The solid reaches yield if $\tau = \tau_c$. The resulting yield surface is sketched in Figure 3.45.

Observe that the yield surface is convex: this is a consequence of Schmidt's law. Now, suppose that slip is activated on one of the glide planes. Let t_i denote the tangent to the slip plane and let n_i denote the normal. To compute the strain produced by slip on a single slip system, consider the deformation of an infinitesimal line element dx under shear γ , as shown in Figure 3.46. The deformed line element is given by

$$d\mathbf{w} = d\mathbf{x} + \gamma(d\mathbf{x} \cdot \mathbf{n})\mathbf{t}$$

or, in index notation

$$dw_i = (\delta_{ij} + \gamma t_i n_j) dx_j.$$

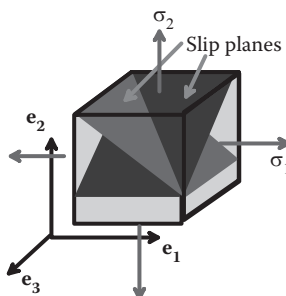


FIGURE 3.43 Crystal with two slip planes subjected to biaxial loading.

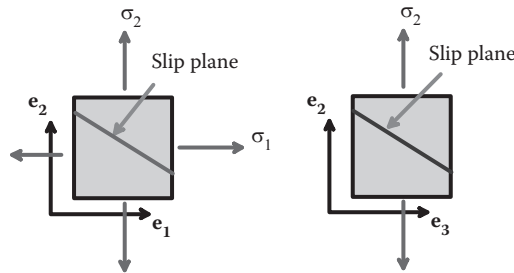


FIGURE 3.44 Side view of slip planes in a crystal.

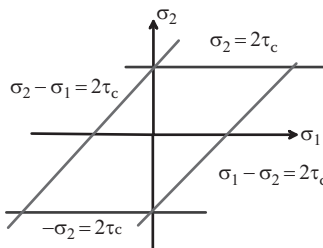


FIGURE 3.45 Yield surface for the crystal shown in Figures 3.43 and 3.44.

The deformation gradient follows as

$$F_{ij} = \delta_{ij} + \gamma t_i n_j,$$

and the Lagrange strain tensor is

$$E_{ij} = \frac{1}{2}(F_{ki}F_{jk} - \delta_{ij}) = \frac{1}{2}\gamma(t_i n_j + t_j n_i) + \frac{1}{2}\gamma^2 n_i n_j.$$

For small γ , we can approximate the Lagrange strain tensor by the infinitesimal strain tensor

$$\epsilon_{ij} = \frac{1}{2}\gamma(t_i n_j + t_j n_i).$$

Now, suppose that the stress satisfies

$$\sigma_2 - \sigma_1 = 2\tau_c,$$

as marked on the yield locus shown in Figure 3.47. This activates slip as shown in the figure. The normal and tangent to the appropriate slip plane are

$$\mathbf{t} = \left[\frac{-1}{\sqrt{2}}, \frac{1}{\sqrt{2}}, 0 \right] \quad \mathbf{n} = \left[\frac{1}{\sqrt{2}}, \frac{1}{\sqrt{2}}, 0 \right].$$

The strain rate therefore follows as

$$\left[\frac{d\epsilon_{ij}}{dt} \right] = \frac{d\gamma}{dt} \begin{bmatrix} -\frac{1}{2} & 0 & 0 \\ 0 & \frac{1}{2} & 0 \\ 0 & 0 & 0 \end{bmatrix}.$$

Thus, $\frac{d\epsilon_1}{dt} = -\frac{d\epsilon_2}{dt}$, showing that the plastic strain rate is normal to the yield locus (Figure 3.47). You could verify as an exercise that, if the stress reaches the other limiting surfaces of the yield locus, the resulting strain rate will be normal to the yield locus.

3.8 SMALL-STRAIN VISCOPLASTICITY: CREEP AND HIGH STRAIN RATE DEFORMATION OF CRYSTALLINE SOLIDS

Viscoplastic constitutive equations are used to model the behavior of polycrystalline materials (metals and ceramics) that are subjected to stress at high temperatures (greater than half the melting point of the solid), and also to model the behavior of metals that are deformed at high rates of strain (greater than 100 per second).

Viscoplasticity theory is a relatively simple extension of the rate-independent plasticity model discussed in Section 3.7. You may find it helpful to review this material before attempting to read this section.

3.8.1 Features of Creep Behavior

Creep tests conducted under uniaxial loading conditions yield the following results:

1. If a tensile specimen of a crystalline solid is subjected to a time-independent stress, it will progressively increase in length. A typical series of length-versus-time curves is illustrated in Figure 3.48.
2. The length-versus-time plot has three stages: a transient period of *primary creep*, in which the creep rate is high; a longer period of *secondary creep*, in which the extension rate is constant; and finally, a period of *tertiary creep*, in which the creep rate again increases. Most creep laws focus on modeling primary and secondary creep. In fact, it is often sufficient to model only secondary creep.

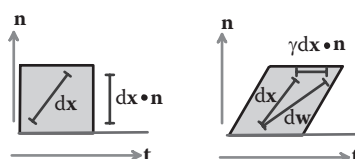


FIGURE 3.46 Deformation caused by shearing on a slip system.

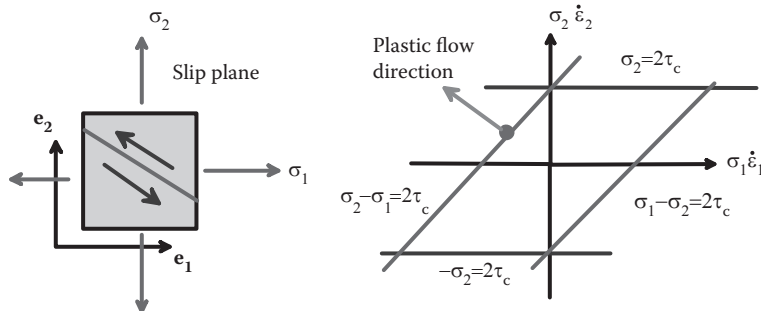


FIGURE 3.47 Direction of the plastic strain rate attributable to shearing on an active slip system.

3. The rate of extension increases with stress. A typical plot of secondary creep rate as a function of stress is shown in Figure 3.49. There are usually three regimes of behavior: each regime can be fit (over a range of stress) by a power-law with the form $\dot{\epsilon} \approx A\sigma^m$. At low stresses, $m \approx 1 - 2.5$, at intermediate stresses, $m \approx 2.5 - 7$, and at high stress, m increases rapidly and can exceed 10–20.
4. The rate of extension increases with temperature. At a fixed stress, the temperature dependence of strain rate can be fit by an equation of the form $\dot{\epsilon} = \dot{\epsilon}_0 \exp(-Q/kT)$, where Q is an activation energy, k is the Boltzmann constant, and T is temperature. Like the stress exponent m , the activation energy Q can transition from one value to another as the temperature and stress level is varied.
5. The various regimens for m and Q are associated with different mechanisms of creep. At low stress, creep occurs mostly by grain boundary sliding and diffusion. At higher stresses, it occurs as a result of thermally activated dislocation motion. Frost and Ashby [1982] plot charts that are helpful to get a rough idea of which mechanism is likely to be active in a particular application.

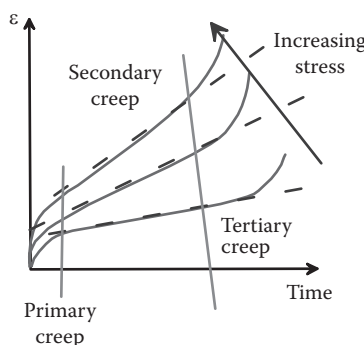


FIGURE 3.48 Typical strain-versus-time curves for high-temperature creep.

6. The creep behavior of a material is strongly sensitive to its microstructure (especially grain size and the size and distribution of precipitates) and composition.

Under proportional multiaxial loading, creep shows all the same characteristics as rate independent plasticity: (1) plastic strains are volume preserving; (2) creep rates are insensitive to hydrostatic pressure; (3) the principal strain rates are parallel to the principal stresses; and (4) plastic flow obeys the Levy–Mises flow rule. These features of behavior are discussed in more detail in Section 3.6.1.

3.8.2 Features of High-Strain Rate Behavior

Stress-strain curves for metals have been measured for strain rates as high as $10^7/\text{sec}$. The general form of the stress-strain curve is essentially identical to that measured at quasi-static strain rates (for an example, see Section 3.7.1), but the flow stress increases with strain rate. A schematic of typical stress-versus-strain rate curve for a ductile material such as aluminum or copper is shown in Figure 3.50. The flow stress rises slowly with strain rate up to a strain rate of about 10^6 and then begins to rise rapidly.

3.8.3 Small-Strain, Viscoplastic Constitutive Equations

Viscoplastic constitutive equations are almost identical to the rate-independent plastic equations in Section 3.7. The main concepts in viscoplasticity are as follows:

1. Strain rate decomposition into elastic and plastic components.
2. The elastic stress-strain law, which specifies the elastic part of the strain rate in terms of stress rate.
3. The plastic flow potential, which determines the magnitude of the plastic strain rate, given the stresses and the resistance of the material to flow.
4. State variables, which characterize the resistance of the material to flow (analogous to yield stress).

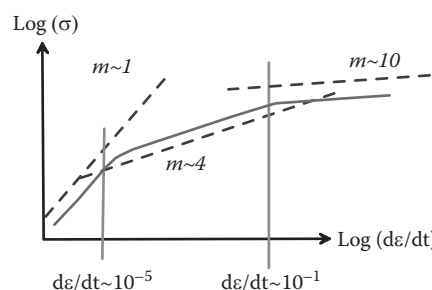


FIGURE 3.49 Typical steady-state stress-versus-strain rate response during creep.

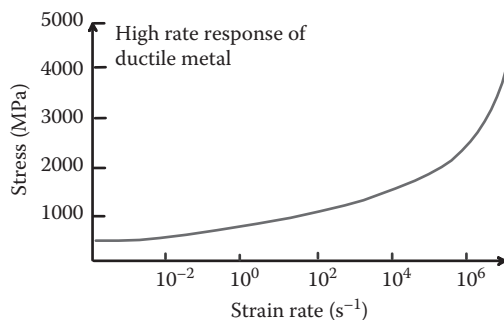


FIGURE 3.50 Typical stress-versus-strain rate during high rate deformation of a ductile metal.

5. The plastic flow rule, which specifies the components of plastic strain rate under multiaxial loading. Recall that, in rate-independent plasticity, the flow rule was expressed as the derivative of the yield surface with respect to stress. In viscoplasticity, the flow rule involves the derivative of the plastic flow potential.
6. Hardening laws, which specify the evolution of the state variables with plastic strain.

These are discussed in more detail below.

Strain rate decomposition: We assume infinitesimal deformation, so shape changes are characterized by

$$\dot{\varepsilon}_{ij} = (\partial u_i / \partial x_j + \partial u_j / \partial x_i) / 2.$$

The strain rate is decomposed into elastic and plastic parts as

$$\frac{d\dot{\varepsilon}_{ij}}{dt} = \frac{d\varepsilon_{ij}^e}{dt} + \frac{d\varepsilon_{ij}^p}{dt}$$

Elastic constitutive equations: The elastic strains are related to the stresses using the standard linear elastic stress-strain law. The elastic strain rate follows as

$$\frac{d\varepsilon_{ij}^e}{dt} = S_{ijkl} \frac{d\sigma_{kl}}{dt},$$

where S_{ijkl} are the components of the elastic compliance tensor. For the special case of an isotropic material with Young's modulus E and Poisson's ratio ν ,

$$\frac{d\varepsilon_{ij}^e}{dt} = \frac{1+\nu}{E} \frac{d\sigma_{ij}}{dt} - \frac{\nu}{E} \frac{d\sigma_{kk}}{dt} \delta_{ij}.$$

Plastic flow potential: The plastic flow potential specifies the magnitude of the plastic strain rate, as a function of stress and the resistance of the material to plastic flow. It is very similar to the yield surface for a rate-independent material. The plastic flow potential is constructed as follows.

1. Define the plastic strain rate magnitude as $\dot{\epsilon}_e = \sqrt{2\dot{\epsilon}_{ij}^p \dot{\epsilon}_{ij}^p / 3}$.
 2. Let σ_{ij} denote the stresses acting on the material and let $\sigma_1, \sigma_2, \sigma_3$ denote the principal stresses.
 3. Experiments show that the plastic strain rate is independent of hydrostatic pressure. The strain rate must be a function of only the deviatoric stress components, defined as
- $$S_{ij} = \sigma_{ij} - \sigma_{kk} \delta_{ij} / 3.$$
4. Assume that the material is isotropic. The strain rate can therefore only depend on the invariants of the deviatoric stress tensor. The deviatoric stress has only two non-zero invariants. It is convenient to choose

$$\sigma_e = \sqrt{\frac{3}{2} S_{ij} S_{ij}} \quad \sigma_{III} = \det(\mathbf{S}).$$

In practice, only the first of these (the von Mises effective stress) is used in most flow potentials.

5. The plastic flow potential can be represented graphically by plotting it as a function of the three principal stresses, exactly as the yield surface is shown graphically for a rate independent material. An example is shown in Figure 3.51. The lines show contours of constant plastic strain rate.
6. For Drucker stability, the contours of constant strain rate must be convex, and the plastic strain rate must increase with strain rate in the direction shown in Figure 3.51.
7. Just as the yield stress of a rate-independent material can increase with plastic strain, the resistance of a viscoplastic material to plastic straining can also increase with

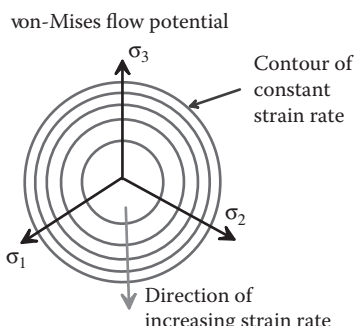


FIGURE 3.51 von Mises viscoplastic flow potential.

strain. The resistance to flow is characterized by one or more *material state variables*, which may evolve with plastic straining.

The most general form for the flow potential of an isotropic material is thus

$$\dot{\epsilon}_e = g(\sigma_e, \sigma_{III}, \text{State variables}),$$

where g must satisfy $g(\alpha\sigma_e, \alpha\sigma_{III}, \text{State vars}) \geq g(\sigma_e, \sigma_{III}, \text{State vars})$ for all $\alpha \geq 1$ (with state variables held fixed) and must also be a convex function of σ_e, σ_{III} .

3.8.3.1 Examples of Flow Potentials: von Mises Flow Potential with Power-Law Rate Sensitivity

Creep is often modeled using the a flow potential of the form

$$g(\sigma_e, \{\sigma_0^{(i)}\}) = \sum_{i=1}^N \dot{\epsilon}_0^{(i)} \exp(-Q_i/kT) \left(\frac{\sigma_e}{\sigma_0^{(i)}} \right)^{m_i},$$

where $\dot{\epsilon}_0^{(i)}$, Q_i , and m_i , $i = 1 \dots N$ are material properties (Q_i are the activation energies for the various mechanisms that contribute to creep), k is the Boltzmann constant, and T is temperature. The model is most often used with $N = 1$, but more terms are required to fit material behavior over a wide range of temperatures and strain rates. The potential has several state variables, $\sigma_0^{(i)}$. To model steady-state creep, you can take σ_0 to be constant; to model transient creep, σ_0 must increase with strain. An example of an evolution law for σ_0 is given below.

High strain rate deformation is also modeled using a power law von Mises flow potential. The following form is sometimes used:

$$g(\sigma_e, \sigma_0) = \begin{cases} 0 & 0 < \sigma_e / \sigma_0 < 1 \\ \dot{\epsilon}_0^{(1)} \left[(\sigma_e / \sigma_0)^{m_1} - 1 \right] & 1 < \sigma_e / \sigma_0 < \alpha, \\ \dot{\epsilon}_0^{(2)} \left[(\sigma_e / \sigma_0)^{m_2} - 1 \right] & \alpha < \sigma_e / \sigma_0 \end{cases}$$

where $\dot{\epsilon}_0^{(2)} = \dot{\epsilon}_0^{(1)}(\alpha^{m_1} - 1)/(\alpha^{m_2} - 1)$ and $\dot{\epsilon}_0^{(1)}, \alpha, m_1, m_2$ are material properties, whereas σ_0 is a strain-, strain rate-, and temperature-dependent state variable, which represents the quasi-static yield stress of the material and evolves with deformation as described below. In this equation, $m_2 < m_1$ so as to model the transition in strain rate sensitivity at high strain rates, whereas α controls the point at which the transition occurs.

Plastic flow rule: The plastic flow rule specifies the components of plastic strain rate resulting from a multiaxial state of stress. It is constructed so that the following applies:

1. The plastic strain rate satisfies the Levy–Mises plastic flow rule.
2. The viscoplastic stress-strain law satisfies the Drucker stability criterion.

3. The flow rule predicts a plastic strain magnitude consistent with the flow potential.

Both 1 and 2 are satisfied by

$$\dot{\epsilon}_{ij}^p = \sqrt{\frac{3}{2}} \frac{g(\sigma_e, \sigma_{III}, \text{State vars})}{[(\partial g / \partial \sigma_{kl})(\partial g / \partial \sigma_{kl})]} \frac{\partial g}{\partial \sigma_{ij}}.$$

If g depends on stress only through the von Mises effective stress, this expression can be simplified to

$$\dot{\epsilon}_{ij}^p = g(\sigma_e, \text{State vars}) \frac{3S_{ij}}{2\sigma_e}.$$

For the particular case of the power-law von Mises flow potential, this gives

$$\dot{\epsilon}_{ij}^p = \sum_{n=1}^N \dot{\epsilon}_0^{(n)} \exp(-Q_n / kT) \left(\frac{\sigma_e}{\sigma_0^{(n)}} \right)^{m_n} \frac{3S_{ij}}{2\sigma_e}.$$

Hardening rule: The hardening rule specifies the evolution of state variables with plastic straining. Many different forms of hardening rule are used (including kinematic hardening laws such as those discussed in Section 3.7.5). A simple example of an *isotropic* hardening law that is often used to model transient creep is

$$\sigma_0^{(i)} = Y_i \left(1 + \frac{\epsilon_e^{(i)}}{\epsilon_0^{(i)}} \right)^{1/n_i},$$

where $\epsilon_e^{(i)} = \int \dot{\epsilon}_0^{(i)} \exp(-Q_i / kT) (\sigma_e / \sigma_0^{(i)})^{m_i} dt$ is the accumulated strain associated with each mechanism of creep, and Y_i , $\epsilon_0^{(i)}$, and n_i are material constants. The law is usually used only with $N = 1$.

Similar hardening laws are used in constitutive equations for high strain rate deformation, but, in this case, the flow strength is made temperature dependent. The following formula is sometimes used:

$$\sigma_0 = Y [1 - \beta(T - T_0)] \left(1 + \frac{\epsilon_e}{\epsilon_0} \right)^{1/n},$$

where $\epsilon_e = \int \sqrt{3\dot{\epsilon}_{ij}^p \dot{\epsilon}_{ij}^p / 2} dt$ is the total accumulated strain, T is temperature, and Y , n , T_0 , β are material properties. More sophisticated hardening laws make the flow stress a function of strain rate [for more details, see Clifton 1990].

3.8.4 Representative Values of Parameters for Viscoplastic Models of Creeping Solids

Fitting material parameters to test data is conceptually straightforward: the flow potential has been constructed so that, for a uniaxial tension test with $\sigma_{11} = \sigma$, all other stress components zero, the uniaxial plastic strain rate is

$$\dot{\epsilon}_{11}^p = \sum_{n=1}^N \dot{\epsilon}_0^{(n)} \exp(-Q_n / kT) \left(\frac{\sigma}{\sigma_0^{(n)}} \right)^{m_n},$$

so the properties can be fit directly to the results of a series of uniaxial tensile tests conducted at different temperatures and applied stresses. To model steady-state creep, $\sigma_0^{(n)}$ can be taken to be constant. One or two terms in the series is usually sufficient to fit material behavior over a reasonable range of temperature and stress.

Creep rates are very sensitive to the microstructure and composition of a material, so for accurate predictions, you will need to find data for the particular material you plan to use. Frost and Ashby [1982] provide approximate expressions for creep rates of a wide range of materials, as well as references to experimental data. As a rough guide, approximate values for a one-term fit to creep data for polycrystalline aluminum alloys subjected to stresses in the range of 5–60 MPa are listed in Table 3.10.

3.8.5 Representative Values of Parameters for Viscoplastic Models of High Strain Rate Deformation

The material parameters in constitutive models for high strain rate deformation can also be fit to the results of a uniaxial tension or compression test. For the model described in Section 3.7.3, the steady-state uniaxial strain rate as a function of stress is

$$\dot{\epsilon} = \begin{cases} 0 & 0 < \sigma / \sigma_0 < 1 \\ \dot{\epsilon}_0^{(1)} \left[(\sigma / \sigma_0)^{m_1} - 1 \right] & 1 < \sigma / \sigma_0 < \alpha. \\ \dot{\epsilon}_0^{(2)} \left[(\sigma / \sigma_0)^{m_2} - 1 \right] & \alpha < \sigma / \sigma_0 \end{cases}$$

The material constants $m_1, m_2, \alpha, \dot{\epsilon}_0^{(1)}$ and the flow stress σ_0 can be determined from a series of uniaxial tension tests conducted at different temperatures and levels of applied stress, whereas $\dot{\epsilon}_0^{(2)}$ can be found from $\dot{\epsilon}_0^{(2)} = \dot{\epsilon}_0^{(1)}(\alpha^{m_1} - 1)/(\alpha^{m_2} - 1)$. If strain hardening can be neglected, σ_0 is a temperature-dependent constant, which could be approximated crudely as $\sigma_0 = Y(1 - \beta(T - T_0))$, where Y, β, T_0 are constants, and T is temperature. Viscoplastic properties of materials are very strongly dependent on their composition and microstructure, so for accurate predictions, you will need to find data for the actual material you intend to use. Clifton [1990] describes several experimental techniques for testing material at high strain rates, and the work contains references to experimental data. As a rough guide, parameter values for 1100-0 aluminum alloy (fit to data in Clifton's paper cited previously) are listed in Table 3.11. The value of β was estimated by assuming that the solid loses all strength at the melting point of aluminum (approximately 650°C).

TABLE 3.10 Approximate Creep Parameters for Polycrystalline Aluminum Alloys

$\dot{\epsilon}_0$ (sec $^{-1}$)	σ_0 (MNm $^{-2}$)	m	Q (J)
1.3×10^8	20	4	2.3×10^{-19}

3.9 LARGE STRAIN, RATE-DEPENDENT PLASTICITY

This section describes the constitutive equations that are used to model large, permanent deformations in polycrystalline solids. Representative applications include models of metal forming, crash simulations, and various military applications that are best left to the imagination. The constitutive equations are used mostly in numerical simulations. It is usually preferable to use rate-dependent, viscoplasticity models in computations, because they are less prone to instabilities than rate independent models. The rate-independent limit can always be approximated by using a high strain rate sensitivity.

The constitutive equations outlined in this section make use of many concepts from Sections 3.7 and 3.8, so you may find it convenient to read these sections before the material to follow.

3.9.1 Kinematics of Finite Strain Plasticity

Let x_i be the position of a material particle in the undeformed solid. Suppose that the solid is subjected to a displacement field $u_i(x_k)$, so that the point moves to $y_i = x_i + u_i$, as shown in Figure 3.52. Define the following:

- The deformation gradient and its Jacobian:

$$F_{ij} = \delta_{ij} + \frac{\partial u_i}{\partial x_j} \quad J = \det(\mathbf{F}).$$

- The velocity gradient:

$$L_{ij} = \frac{\partial \dot{u}_i}{\partial y_j} = \dot{F}_{ik} F_{kj}^{-1}.$$

- The stretch rate and spin:

$$D_{ij} = (L_{ij} + L_{ji})/2 \quad W_{ij} = (L_{ij} - L_{ji})/2.$$

TABLE 3.11 Approximate Constitutive Parameters for High Strain Rate Behavior of Aluminum Alloy

$\dot{\epsilon}_0^{(1)}$ (sec $^{-1}$)	$\dot{\epsilon}_0^{(2)}$ (sec $^{-1}$)	α	m_1	m_2	Y (MNm $^{-2}$)	β (K $^{-1}$)	T_0 (K)
100	$2.4 \cdot 10^7$	1.6	15	0.1	50	0.00157	298

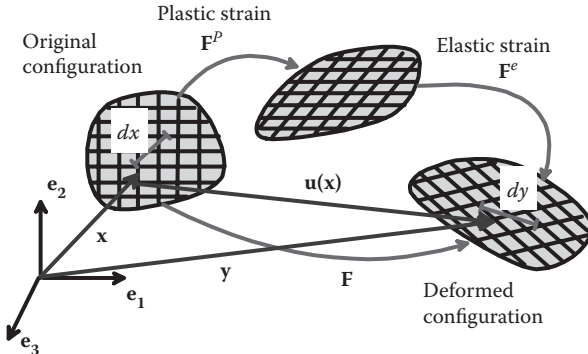


FIGURE 3.52 Decomposition of the deformation gradient into elastic and plastic parts.

- Recall that F_{ij} relates infinitesimal material fibers dy_i and dx_j in the deformed and undeformed solid, respectively, as

$$dy_i = F_{ij} dx_j.$$

- To decompose the deformation gradient into elastic and plastic parts, we borrow ideas from crystal plasticity. The plastic strain is assumed to shear the lattice, without stretching or rotating it. The elastic deformation rotates and stretches the lattice. We think of these two events occurring in sequence, with the plastic deformation first, and the stretch and rotation second, giving

$$dy_i = F_{ij} dx_j = F_{ik}^e F_{kj}^p dx_j.$$

- To decompose the velocity gradient into elastic and plastic parts, note that

$$L_{ij} = \dot{F}_{ik} F_{kj}^{-1} = \left(\dot{F}_{ik}^e F_{kl}^p + F_{ik}^e \dot{F}_{kl}^p \right) \left(F_{lm}^{p-1} F_{mj}^{e-1} \right) = \dot{F}_{ik}^e F_{kj}^{e-1} + F_{ik}^e \dot{F}_{kl}^p F_{lm}^{p-1} F_{mj}^{e-1}.$$

Thus, the velocity gradient contains two terms, one of which involves only measures of elastic deformation, whereas the other contains measures of plastic deformation. We use this to decompose \mathbf{L} into elastic and plastic parts:

$$L_{ij} = L_{ij}^e + L_{ij}^p \quad L_{ij}^e = \dot{F}_{ik}^e F_{kj}^{e-1} \quad L_{ij}^p = F_{ik}^e \dot{F}_{kl}^p F_{lm}^{p-1} F_{mj}^{e-1}.$$

- Define the elastic and plastic stretch rates and spin rates as

$$D_{ij}^e = (L_{ij}^e + L_{ji}^e) / 2 \quad W_{ij}^e = (L_{ij}^e - L_{ji}^e) / 2$$

$$D_{ij}^p = (L_{ij}^p + L_{ji}^p) / 2 \quad W_{ij}^p = (L_{ij}^p - L_{ji}^p) / 2.$$

Constitutive equations must specify relations between the stresses (as defined below) and the elastic and plastic parts of the deformation gradient. The equations are usually written in rate form, in which case the elastic and plastic stretch rates and spin are related to the stress rate.

3.9.2 Stress Measures for Finite Deformation Plasticity

Stress measures that appear in descriptions of finite strain plasticity are summarized below:

- The Cauchy (true) stress represents the force per unit deformed area in the solid and is defined by

$$n_i \sigma_{ij} = \lim_{dA \rightarrow 0} \frac{dP_j^{(n)}}{dA}.$$

- Kirchhoff stress is defined by $\tau_{ij} = J\sigma_{ij}$.
- Material stress for intermediate configuration is described by $\Sigma_{ij} = JF_{ik}^{e-1}\sigma_{kl}F_{jl}^{e-1}$.

Note that the material stress tensor is related to the Cauchy stress by a function of \mathbf{F}^e , not \mathbf{F} as in the usual definition. This stress should be interpreted physically as a material stress associated with the *intermediate* configuration, as shown in Figure 3.53. This stress measure is introduced because the elastic constitutive equations require an internal force measure that is work conjugate to an appropriate function of \mathbf{F}^e .

In addition, viscoplastic constitutive equations are often written in rate form (as in Section 3.7), relating stain rate to stress and (for the elastic part) stress rate. Stress rates are difficult to work with in finite strain problems. At first sight, it might appear that stress rate can be calculated by simply taking the time derivative of the stress components $d\sigma_{ij}/dt$, but in fact, this is not a useful measure of stress rate. To see this, imagine applying a uniaxial tensile stress to a material and then rotating the entire test apparatus (so the applied force and specimen rotate together). The time derivatives of the stress components are nonzero, but the material actually experiences a time-independent force per unit area. As shown below, the correct stress rate is the *Jaumann Rate with respect to the elastic spin*, defined as

$$\nabla_e^e = \frac{d\sigma_{ij}}{dt} - W_{ik}^e \sigma_{kj} + \sigma_{ik} W_{kj}^e.$$

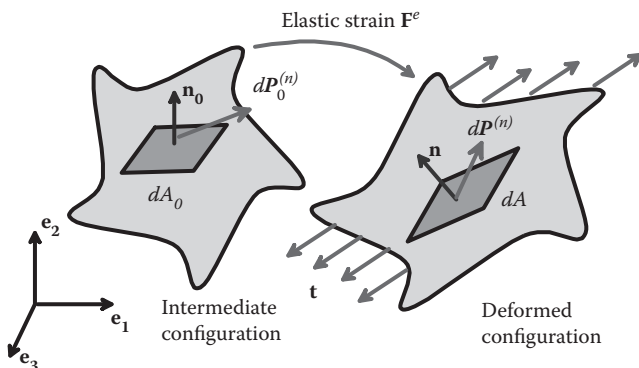


FIGURE 3.53 Deformation of an area element in a solid.

3.9.3 Elastic Stress–Strain Relation for Finite Strain Plasticity

Plastically deforming metals may experience large strains. The stresses remain modest, however, and are usually substantially lower than the elastic modulus of the solid. The elastic strains are small, but the material may experience large rotations. Under these conditions, the small-strain elastic constitutive equations of Section 3.1 cannot be used, and the simple generalized Hooke's law described in Section 3.3 must be used instead. This law relates the elastic part of the deformation gradient to stress, as follows:

1. Define the Lagrangean elastic strain as $E_{ij}^e = (F_{ki}^e F_{kj}^e - \delta_{ij})/2$.
2. Assume that the material stress is proportional to Lagrange strain, as $\Sigma_{ij} = C_{ijkl} E_{kl}^e$, where C_{ijkl} are the components of the elastic stiffness tensor (as defined and tabulated in Section 3.1), for the material with orientation in the undeformed configuration.
3. For the special case of an elastically isotropic material, with Young's modulus E and Poisson's ratio ν , the stress-strain law is

$$\Sigma_{ij} = \frac{E}{1 + \nu} \left\{ E_{ij}^e + \frac{\nu}{1 - 2\nu} E_{kk}^e \delta_{ij} \right\}.$$

4. The elastic stress-strain law is often expressed in rate form, as follows:

$$\dot{\tau}_{ij}^e \approx C_{ijkl}^e D_{kl}^e,$$

where $\dot{\tau}_{ij}^e$ is the Jaumann rate of Kirchhoff stress; $C_{ijkl}^e = F_{in}^e F_{jm}^e C_{nmpq} F_{kp}^e F_{lq}^e$ can be thought of as the components of the elastic compliance tensor for material with orientation in the deformed configuration, and D_{ij}^e is the elastic stretch rate. For the particular case of an isotropic material, the stress rate can be approximated further as

$$\dot{\tau}_{ij}^e \approx \frac{E}{1 + \nu} \left\{ D_{ij}^e + \frac{\nu}{1 - 2\nu} D_{kk}^e \delta_{ij} \right\}.$$

Derivation of the rate form of the elastic stress-strain law: Our goal is to derive the expression in item 4 above, starting from the stress-strain law in item 2. To this end, perform the following:

1. Take the time derivative of the constitutive equation: $\frac{d\Sigma_{ij}}{dt} = C_{ijkl} \frac{dE_{kl}^e}{dt}$.
2. Take the time derivative of the formula relating material and Kirchhoff stress

$$\tau_{ij} = F_{ik}^e \Sigma_{kl} F_{jl}^e$$

$$\Rightarrow \frac{d\tau_{ij}}{dt} = \frac{dF_{ik}^e}{dt} \Sigma_{kl} F_{jl}^e + F_{ik}^e \frac{d\Sigma_{kl}}{dt} F_{jl}^e + F_{ik}^e \Sigma_{kl} \frac{dF_{jl}^e}{dt}.$$

3. Substitute for material stress in terms of Kirchoff stress:

$$\frac{d\tau_{ij}}{dt} = \frac{dF_{ik}^e}{dt} F_{kl}^{e-1} \tau_{lj} + F_{ik}^e \frac{d\Sigma_{kl}}{dt} F_{jl}^e + \tau_{il} F_{lk}^{e-1} \frac{dF_{jk}^e}{dt}.$$

4. Recall that $\dot{F}_{ik}^e F_{kj}^{e-1} = L_{ij}^e = D_{ij}^e + W_{ij}^e$, observe that $W_{ij}^e = -W_{ji}^e$, $D_{ij}^e = D_{ji}^e$, and substitute from item 1

$$\frac{d\tau_{ij}}{dt} = (D_{ik}^e + W_{ik}^e) \tau_{kj} + F_{ik}^e C_{klmn} \frac{dE_{mn}^e}{dt} F_{jl}^e + \tau_{ik} (D_{kj}^e - W_{kj}^e).$$

5. Next, note that

$$\frac{dE_{mn}^e}{dt} = F_{pm}^e D_{pq}^e F_{qn}^e$$

so

$$\begin{aligned} \frac{d\tau_{ij}}{dt} &= (D_{ik}^e + W_{ik}^e) \tau_{kj} + F_{ik}^e F_{jl}^e C_{klmn} F_{pm}^e F_{qn}^e D_{pq}^e + \tau_{ik} (D_{kj}^e - W_{kj}^e) \\ &\Rightarrow \frac{d\tau_{ij}}{dt} + \tau_{ik} W_{kj}^e - W_{ik}^e \tau_{kj} = C_{ijpq}^e D_{pq}^e + D_{ik}^e \tau_{kj} + \tau_{ik} D_{kj}^e. \end{aligned}$$

6. Finally, assume that $\tau_{ik} D_{kj}^e \ll C_{ijpq}^e D_{pq}^e$ because the stresses are much less than the modulus. This shows that

$$\frac{\nabla_e}{\tau_{ij}} \approx C_{ijkl}^e D_{kl}^e.$$

3.9.4 Plastic Constitutive Law for Finite Strain Viscoplasticity

Next, we turn to developing an appropriate plastic constitutive law for finite deformations. The constitutive equations must specify a relationship between work-conjugate measures of stress and strain; recall that $\tau_{ij} L_{ij}$ is the rate of work done by stresses per unit reference volume. Consequently, the constitutive equations must relate \mathbf{D}^p , \mathbf{W}^p to $\boldsymbol{\tau}$ and its rate.

Usually, plastic constitutive laws for finite deformations are just simple extensions of small strain plasticity. For example, for a finite strain, rate-dependent, von Mises solid with isotropic hardening power-law hardening, we set

$$D_{ij}^p = \dot{\varepsilon}_0 \left(\frac{\tau_e}{\sigma_0} \right)^m \frac{3\tau'_{ij}}{2\tau_e} \quad W_{ij}^p = 0,$$

where $\tau'_{ij} = \tau_{ij} - \tau_{kk} \delta_{ij}$ and $\tau_e = \sqrt{3\tau'_{ij}\tau'_{ij}/2}$. The hardening rule is

$$\sigma_0 = Y \left(1 + \frac{\varepsilon_e}{\varepsilon_0} \right)^{1/n},$$

where $\varepsilon_0 = \int \dot{\varepsilon}_0 (\tau_e / \sigma_0)^m dt$.

Finite strain plasticity models disagree on the correct way to prescribe \mathbf{W}^p . Many theories simply set $\mathbf{W}^p = 0$. Simple models of polycrystals give some support for this assumption, but it may not be appropriate in materials that develop a significant texture. More complex models have also been developed. For isotropically hardening solids, predictions are relatively insensitive to the choice of \mathbf{W}^p , but any attempt to capture evolution of plastic anisotropy would need to specify \mathbf{W}^p carefully. Crystal plasticity-based models provide a way out of this difficulty, because they have a clearer (but not completely unambiguous) definition of the plastic spin.

3.10 LARGE STRAIN VISCOELASTICITY

This section describes constitutive equations that can be used to model large, irreversible deformations in polymers and also to model biological tissue that is subjected to large shape changes. Finite strain viscoelasticity is not as well developed as finite strain plasticity, and a number of different formulations exist. The model outlined here is based on Bergstrom and Boyce [1998].

The constitutive equation is intended to capture the following features of material behavior:

1. When the material is deformed very slowly (so that material behavior is fully reversible), it behaves like an ideal rubber, as described in Section 3.4.
2. When deformed very quickly (so that there is no time for inelastic mechanisms to operate), it again behaves like an ideal rubber but with different properties.
3. At intermediate rates, the solid exhibits a rate-dependent, hysteretic response.

In addition, we assume the following

- The material is isotropic.
- Material response to a pure volumetric strain ($\varepsilon_{11} = \varepsilon_{22} = \varepsilon_{33} = \delta V / V$ with all other $\varepsilon_{ij} = 0$) is perfectly elastic (with no time-dependent behavior).
- The material is nearly incompressible.
- Hydrostatic stress has no effect on the deviatoric response of the solid.

The constitutive equations outlined in this section make use of many concepts from Sections 3.5, 3.6, and 3.7, so you may find it convenient to read these sections before the material to follow.

3.10.1 Kinematics for Finite Strain Viscoelasticity

The description of shape changes in polymers follows closely the approach outlined in Section 3.9.1. Let x_i be the position of a material particle in the undeformed solid. Suppose

that the solid is subjected to a displacement field $u_i(x_k)$, so that the point moves to $y_i = x_i + u_i$ (Figure 3.54). Define the following:

- The deformation gradient and its Jacobian:

$$F_{ij} = \delta_{ij} + \frac{\partial u_i}{\partial x_j}$$

$$J = \det(\mathbf{F}).$$

- The velocity gradient:

$$L_{ij} = \frac{\partial \dot{u}_i}{\partial y_j} = \dot{F}_{ik} F_{kj}^{-1}.$$

- The deformation gradient is decomposed into elastic and plastic parts as

$$F_{ij} = F_{ik}^e F_{kj}^p.$$

- The velocity gradient is decomposed into elastic and plastic parts as

$$L_{ij} = L_{ij}^e + L_{ij}^p, \quad L_{ij}^e = \dot{F}_{ik}^e F_{kj}^{e-1}, \quad L_{ij}^p = F_{ik}^e \dot{F}_{kl}^p F_{lm}^{p-1} F_{mj}^{e-1}.$$

- Define the elastic and plastic stretch rates and spin rates as

$$D_{ij}^e = (L_{ij}^e + L_{ji}^e) / 2 \quad W_{ij}^e = (L_{ij}^e - L_{ji}^e) / 2$$

$$D_{ij}^p = (L_{ij}^p + L_{ji}^p) / 2 \quad W_{ij}^p = (L_{ij}^p - L_{ji}^p) / 2.$$

- Define the left Cauchy–Green deformation tensor for the total and elastic deformation gradients:

$$B_{ij} = F_{ik} F_{jk} \quad B_{ij}^e = F_{ik}^e F_{jk}^e.$$

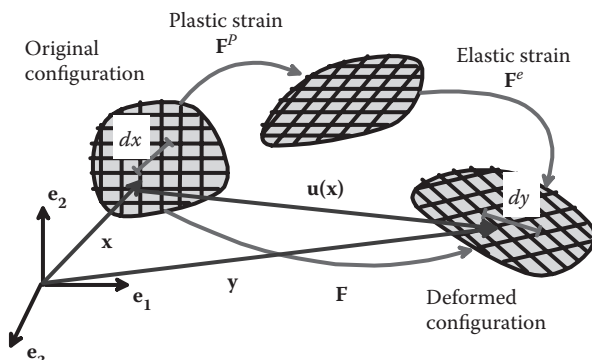


FIGURE 3.54 Decomposition of the deformation gradient into elastic and plastic parts.

- Define the invariants of \mathbf{B} and \mathbf{B}^e as

$$\begin{aligned}\bar{I}_1 &= \frac{B_{kk}}{J^{2/3}} & \bar{I}_2 &= \frac{1}{2} \left(\bar{I}_1^2 - \frac{B_{ik}B_{ki}}{J^{4/3}} \right) & \bar{I}_3 &= \det \mathbf{B} = J^2 \\ \bar{I}_1^e &= \frac{B_{kk}^e}{J_e^{2/3}} & \bar{I}_2^e &= \frac{1}{2} \left(\bar{I}_1^{e2} - \frac{B_{ik}^e B_{ki}^e}{J_e^{4/3}} \right) & \bar{I}_3^e &= \det \mathbf{B}^e = J_e^2.\end{aligned}$$

- Denote the principal stretches for \mathbf{B} and \mathbf{B}^e by λ_i, λ_i^e (these are the square roots of the eigenvalues of \mathbf{B} and \mathbf{B}^e) and principal stretch directions by $\mathbf{b}_i, \mathbf{b}_i^e$.

3.10.2 Stress Measures for Finite Strain Viscoelasticity

Usually stress-strain laws are given as equations relating Cauchy stress (true stress) σ_{ij} to left Cauchy–Green deformation tensor. For some computations, it may be more convenient to use other stress measures. They are defined below, for convenience.

- Cauchy (true) stress represents the force per unit deformed area in the solid and is defined by

$$n_i \sigma_{ij} = \lim_{dA \rightarrow 0} \frac{dP_j^{(n)}}{dA}.$$

- Kirchhoff stress is defined by $\tau_{ij} = J \sigma_{ij}$.

The constitutive model must specify relations between stress, the total deformation gradient \mathbf{F} , the elastic part of the deformation gradient \mathbf{F}^e , and the plastic part of the deformation gradient \mathbf{F}^p .

3.10.3 Relation among Stress, Deformation Measures, and Strain Energy Density

Just as for hyperelastic materials, the instantaneous stress in a hyperviscoelastic solid is calculated from a strain energy density function U . For viscoelastic materials, the strain energy density is separated into two parts:

$$U(\bar{I}_1, \bar{I}_2, J, \bar{I}_1^e, \bar{I}_2^e) = U_\infty(\bar{I}_1, \bar{I}_2, J) + U_T(\bar{I}_1^e, \bar{I}_2^e, J_e).$$

Here,

1. $U_\infty(\bar{I}_1, \bar{I}_2, J)$ specifies the strain energy density in the fully relaxed material. It represents the effect of a set of polymer chains in the solid that can only accommodate deformation by stretching to follow the total extension. $U_\infty = 0$ for a material that exhibits steady-state creep.
2. $U_T(\bar{I}_1^e, \bar{I}_2^e, J_e)$ is an additional, transient contribution to the total strain energy. This contribution gradually relaxes with time. It represents the effects of a set of polymer

chains that initially stretch with the solid but with time are able to relax toward their preferred configuration.

The stress is related to the energy density by

$$\begin{aligned}\sigma_{ij} = & \frac{2}{J} \left[\frac{1}{J^{2/3}} \left(\frac{\partial U_\infty}{\partial \bar{I}_1} + \bar{I}_1 \frac{\partial U_\infty}{\partial \bar{I}_2} \right) B_{ij} - \frac{\bar{I}_1}{3} \frac{\partial U_\infty}{\partial \bar{I}_1} \delta_{ij} - \frac{1}{J^{4/3}} \frac{\partial U_\infty}{\partial \bar{I}_2} B_{ik} B_{kj} \right] + \frac{\partial U_\infty}{\partial J} \delta_{ij} \\ & + \frac{2}{J_e} \left[\frac{1}{J_e^{2/3}} \left(\frac{\partial U_T}{\partial \bar{I}_1^e} + \bar{I}_1^e \frac{\partial U_T}{\partial \bar{I}_2^e} \right) B_{ij}^e - \frac{\bar{I}_1^e}{3} \frac{\partial U_T}{\partial \bar{I}_1^e} \delta_{ij} - \frac{1}{J_e^{4/3}} \frac{\partial U_T}{\partial \bar{I}_2^e} B_{ik}^e B_{kj}^e \right] + \frac{\partial U_T}{\partial J_e} \delta_{ij}.\end{aligned}$$

You can use any of the hyperelastic strain energy density potentials listed in Section 3.4 to describe a particular material. It is sensible to choose U_T , U_∞ to have the same functional form (but with different material constants). Note also that, because the inelastic strains are assumed to be volume preserving (see below), $J_e = J$, and therefore one can take $\partial U_T / \partial J_e = 0$ without loss of generality.

3.10.4 Strain Relaxation

The strain rate dependence and irreversibility of a viscoelastic material can be modeled using the framework described in Section 3.9 for finite strain viscoplasticity. The constitutive equations must specify the plastic stretch rate D_{ij}^p and plastic spin W_{ij}^p as a function of stress. The expressions given here follow Bergstrom and Boyce [1998].

Define the deviatoric Kirchhoff stress resulting from the elastic part of the deformation gradient F_{ij}^e as

$$\tau'_{ij} = 2 \left[\frac{1}{J_e^{2/3}} \left(\frac{\partial U_T}{\partial \bar{I}_1^e} + \bar{I}_1^e \frac{\partial U_T}{\partial \bar{I}_2^e} \right) B_{ij}^e - \frac{\bar{I}_1^e}{3} \frac{\partial U_T}{\partial \bar{I}_1^e} \delta_{ij} - \frac{1}{J_e^{4/3}} \frac{\partial U_T}{\partial \bar{I}_2^e} B_{ik}^e B_{kj}^e \right].$$

1. Define the effective stress:

$$\tau_e = \sqrt{3\tau'_{ij}\tau'_{ij}/2}.$$

2. The plastic strain rate is then

$$D_{ij}^p = \dot{\epsilon}_e(\tau_e, I_1^e, I_2^e, T) \frac{3\tau'_{ij}}{2\tau_e}.$$

3. Here, $\dot{\epsilon}_e$ is the magnitude of the plastic strain rate, which is a function of temperature T , the effective stress τ_e , and the elastic strain. This function must be calibrated experimentally. Bergstrom and Boyce [1998] suggest that the following function should describe approximately the relaxation dynamics of long-chain molecules:

$$\dot{\epsilon}_e = \dot{\epsilon}_0 \left(\sqrt{I_1^e} - \sqrt{3} \right)^n \left(\frac{\tau_e}{\tau_0} \right)^m.$$

where $C_1 > 0$, $-1 < n < 0$, $\tau_0 > 0$, and $m > 0$ are temperature-dependent material properties.

Additional constitutive equations must specify W_{ij}^P . This has not been studied in detail: usually we just take $W_{ij}^P = 0$.

3.10.5 Representative Values for Material Parameters in a Finite-Strain Viscoelastic Model

Bergstrom and Boyce [1998] give experimental data for the rate-dependent response of several rubbers and fit material properties to their data. They use the Arruda–Boyce [1992] potential for both U_∞ and U_T :

$$U_\infty = \infty \left\{ \frac{1}{2}(\bar{I}_1 - 3) + \frac{1}{20\beta_\infty^2}(\bar{I}_1^2 - 9) + \frac{11}{1050\beta_\infty^4}(\bar{I}_1^3 - 27) + \dots \right\} + \frac{K}{2}(J-1)^2$$

$$U_T = T \left\{ \frac{1}{2}(\bar{I}_1 - 3) + \frac{1}{20\beta_T^2}(\bar{I}_1^2 - 9) + \frac{11}{1050\beta_T^4}(\bar{I}_1^3 - 27) + \dots \right\}.$$

Material behavior is therefore characterized by values of the two shear moduli μ_T , μ_∞ , the bulk modulus K , the coefficients β_∞ , β_T , and the parameters $\dot{\varepsilon}_0$, n , τ_0 , and m , as outlined in the preceding section. Representative values for these parameters are listed in Table 3.12.

3.11 CRITICAL STATE MODELS FOR SOILS

Soils consist of a two-phase mixture of particles and water. They exhibit very complex behavior in response to stress, and a number of different constitutive theories are used to model them; in fact, entire books are devoted to critical state soil models. Here, we outline a basic soil model known as “Cam-clay,” developed at Cambridge University (Cambridge, UK). It uses many of the concepts that are used to model plastic deformation of metals, so you will find it helpful to review Sections 3.7 and 3.8 before reading this one.

3.11.1 Features of the Behavior of Soils

Experiments on soils reveal the following behavior:

1. Soils cannot withstand significant tensile stress: we, therefore, focus on their response to combined pressure and shear loading.
2. The behavior of a soil is very sensitive to its water content. Two types of experiment are conducted on soils: in a “drained” test, water is allowed to escape from the specimen as it is compressed (so the water pressure is zero); in an “undrained” test, the volume of the specimen (water + soil particles) is held fixed. In the latter test, the water pressure can be measured by means of a manometer connected to the pressurized cell.
3. Under combined pressure and shear loading, soil behaves like a frictional material. In a drained test, the solid can support shear stresses $\tau < Mp/\sqrt{3}$ without excessive

TABLE 3.12 Material Parameters for a Nitrile Rubber

μ_∞	0.29 MNm ⁻²
β_∞	6
μ_T	0.73 MNm ⁻²
β_T	4
K	100 MNm ⁻²
$\dot{\epsilon}_0$	7 sec ⁻¹
τ_0	1 MNm ⁻²
n	-0.6
m	5.0

Source: Bergstrom, J.S., Boyce, M.C., *J. Mech. Phys. Solids*, 46, 931, 1998.

deformation, where M is a material property (analogous to friction coefficient) and p is the applied hydrostatic pressure. If the shear stress reaches $\tau = Mp / \sqrt{3}$, the material collapses, usually by shearing along one or more discrete shear planes parallel to the maximum resolved shear stress. If the same test is conducted on an undrained specimen, shear occurs earlier, because the water supports part of the hydrostatic pressure. In this case, shear failure occurs when $\tau < M(p - p_w) / \sqrt{3}$, where p is the applied hydrostatic pressure, and p_w is the water pressure.

- If subjected to loads below those required to cause catastrophic collapse, soils show a complicated behavior that resembles that of a strain hardening metal, except that soils compact in response to combined shear and pressure, whereas metals do not. In addition, the strain hardening occurs only as a result of the compaction: shear strain does not increase the solid's strength. For example, Figure 3.55 shows the response of a soil sample to a test in which a specimen is subjected to a constant pressure, together with a steadily increasing shear stress. The soil accumulates a permanent shear strain and also compacts. The strength of the solid increases up to the limiting shear stress $\tau = M(p - p_w) / \sqrt{3}$, at which point the compaction reaches a steady state, and the specimen continues to deform at constant shear stress.

3.11.2 Constitutive Equations for Cam-Clay

The constitutive equations for Cam-clay are very similar to the rate-independent plastic equations in Section 3.6. The main concepts are as follows:

- Strain rate decomposition into elastic and plastic parts.
- Pressure decomposition into contributions from the water pressure (or “pore pressure”) and from the pressure supported by the soil particles. The pore pressure must be calculated by modeling fluid seepage through the soil.

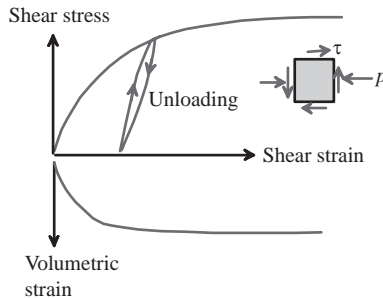


FIGURE 3.55 Typical stress-strain response of a soil.

3. The elastic stress-strain law, which specifies the elastic part of the strain in terms of stress.
4. A yield criterion, which determines the magnitude of the plastic strain rate, given the stresses and the resistance of the material to flow. Unlike metals, the yield criterion for a soil is a function of the hydrostatic stress, or pressure, in addition to shear stress. The yield criterion is expressed in terms of a state variable, which characterizes the resistance of the material to flow (analogous to yield stress).
5. A plastic flow rule that specifies the ratios of the plastic strain components under multiaxial stress.
6. A hardening law, which specifies how the state variable evolves with plastic straining.
7. The yield surface, flow rule, and hardening law also define a critical state criterion for the solid. The critical state criterion specifies the combination of stresses that lead to unconstrained collapse of the solid.

These are discussed in more detail below.

Strain rate decomposition: We assume small strains, so shape changes are characterized by $\varepsilon_{ij} = (\partial u_i / \partial x_j + \partial u_j / \partial x_i) / 2$. The strain is decomposed into elastic and plastic parts as

$$\varepsilon_{ij} = \varepsilon_{ij}^e + \varepsilon_{ij}^p.$$

Pressure decomposition: Assume that the soil is subjected to a stress σ_{ij} . The pressure is $p = -\sigma_{kk} / 3$ (note the negative sign). In general, part of this pressure is supported by the water in the soil, whereas the rest is supported by the soil particles themselves. The pressure is decomposed into two parts:

$$p = p_w + p_s$$

where p_s is the contribution to the pressure from the soil particles, and p_w is the contribution from the water.

When using the constitutive equation in a boundary value problem, the water pressure must be calculated as a separate problem, in addition to solving the usual mechanical field equations. Here, we outline briefly a simple approximate description of fluid seepage through a soil. More general treatments are also available, which include nonlinear versions of the flow law, finite strain effects, as well as the effects of fluid absorption by the soil particles to form a gel, the tendency of soil to absorb fluid due to capillarity, and the effects of partial soil saturation.

1. Fluid seepage through the soil is driven by gravity and fluid pressure variations. The driving force is quantified by the *piezometric head*, defined as

$$\phi = z + \frac{p_w}{\rho_w g},$$

where z is the height above some arbitrary datum, p_w is the fluid pressure (compressive pressure is positive), ρ_w is the fluid density, and g is the gravitational acceleration.

2. The volume of material flowing through unit area of solid in the x_i direction per unit time obeys *Darcy's law*:

$$q_i = -k \frac{\partial \phi}{\partial x_i},$$

where k is a material parameter, known as the *permeability* of the medium.

3. The fluid itself may be compressible, with bulk modulus K_w .
4. The fluid can be absorbed in cavities in the soil. The volume fraction of cavities n is defined as

$$n = \frac{dV_c}{dV},$$

where dV_c is the cavity volume in a volume of soil (including both cavities and soil particles) dV .

5. At time $t = 0$, the solid starts with some cavity volume fraction n_0 ; this volume fraction evolves as the solid is deformed. Usually the dominant contribution to the cavity volume change occurs as a result of plastic compaction of the soil (more sophisticated treatments include an elastic contribution). The cavity volume fraction after the solid is subjected to an infinitesimal plastic strain ε_{ij}^p is

$$n = n_0 + \varepsilon_{kk}^p.$$

6. At time $t = 0$, a fluid pressure p_{w0} acts on the solid, and for $t > 0$, the values of either fluid pressure or volumetric flow rate must be specified on the boundary of the solid.

7. Finally, the rate of change of fluid pressure follows from conservation of fluid volume as

$$\frac{n}{K_w} \frac{\partial p_w}{\partial t} = \frac{\partial q_i}{\partial x_i} + \frac{dn}{dt}.$$

Elastic constitutive equations: The elastic strains are related to the stresses using the standard linear elastic stress-strain law. The elastic strain is related to stress by

$$\sigma_{ij} = C_{ijkl} \epsilon_{kl}^e,$$

where C_{ijkl} are the components of the elastic compliance tensor. For the special case of an isotropic material with Young's modulus E and Poisson's ratio ν ,

$$\sigma_{ij} = \frac{E}{1 + \nu} \left\{ \epsilon_{ij} + \frac{\nu}{1 - 2\nu} \epsilon_{kk} \delta_{ij} \right\}.$$

Yield criterion and critical state surface: The yield criterion specifies the stresses that are required to cause plastic flow in the soil. The concept is identical to the yield criterion used in metal plasticity, except that, unlike metals, hydrostatic pressure can cause yield in a soil. The yield criterion is

$$f(\sigma_{ij}) = \left(\frac{p_s}{a} - 1 \right)^2 + \left(\frac{\sigma_e}{Ma} \right)^2 - 1 = 0,$$

where

1. $p_s = -\sigma_{kk}/3 - p_w$ is the pressure exerted by the stresses on the soil skeleton.
2. $\sigma_e = \sqrt{3S_{ij}S_{ij}/2}$, where $S_{ij} = \sigma_{ij} - \frac{1}{3}\sigma_{kk}\delta_{ij}$, is the von Mises effective stress.
3. M is a material property, whose physical significance was described in Section 3.11.1. Usually $M < 1$.
4. a is a state variable that quantifies the current yield strength of the soil. At time $t = 0$, the soil has some finite strength $a = a_0$, which subsequently evolves with plastic straining, as described below.

The yield criterion is sketched in principal stress space in Figure 3.56; it resembles a football (if you are American, or a rugby ball to the rest of the world) with its axis parallel to the line $\sigma_1 = \sigma_2 = \sigma_3$. The shape of the football depends on M ; for $M = 1$, it is a sphere, and for $M < 1$, it is stretched parallel to its axis. The size of the yield locus is determined by a .

The yield criterion, together with the hardening law, also define a critical state surface, which determines the stress in which unrestricted shear deformation can occur at constant shear

stress (i.e., with zero hardening). If the stresses lie inside the critical state surface (this is known as the “wet” side of critical state), the material shows stable strain hardening behavior. If the stresses lie outside the critical state surface (known as the “dry” side of the critical state), the material softens with plastic straining and so violates the Drucker stability condition. Under these conditions, the material is unstable, and plastic strain tends to localize into shear bands.

The critical state surface for Cam-clay is

$$g(\sigma_{ij}) = \sigma_e - Mp_s.$$

The material is stable for $g < 0$ and unstable for $g > 0$. The critical state surface is sketched in Figure 3.57: it is a cone, which cuts through the fattest part of the yield surface.

Flow law: The flow law specifies the plastic strain components under a multiaxial state of stress. Like metal plasticity, the Cam-clay model bases the flow law on the yield criterion, so that

$$d\epsilon_{ij}^p = d\lambda a \frac{\partial f}{\partial \sigma_{ij}} = d\lambda \left(-\frac{2}{3} \left[\frac{p_s}{a} - 1 \right] \delta_{ij} + 3 \frac{S_{ij}}{M^2 a} \right),$$

where $d\lambda$ is a dimensionless constant that depends on the increment of stress applied to the solid and is proportional to the plastic strain magnitude. The procedure to calculate $d\lambda$ is discussed in more detail below: if the stress state lies inside the critical state surface ($g(\sigma_{ij}) < 0$), then $d\lambda$ can be expressed in terms of the stress increment $d\sigma_{ij}$ and the fluid pressure increment dp_w applied to the solid as

$$d\lambda = \begin{cases} 0 & f(\sigma_{ij}) < 0 \\ \frac{-\frac{1}{3a} \left[\frac{p_s}{a} - 1 \right] (d\sigma_{kk} + 3dp_w) + \frac{3}{2} \frac{S_{ij} dS_{ij}}{(Ma)^2}}{2c \frac{p_s}{a} \left[\frac{p_s}{a} - 1 \right]} & f(\sigma_{ij}) = 0. \end{cases}$$

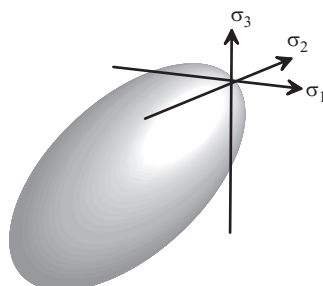


FIGURE 3.56 The Cam-clay yield surface.

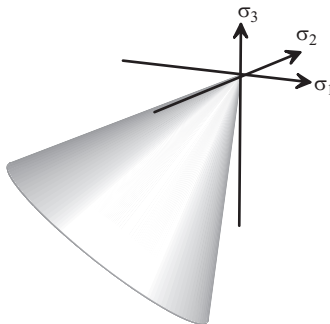


FIGURE 3.57 The Cam-clay critical state surface.

Here $\langle x \rangle = x$ for $x > 0$ and $\langle x \rangle = 0$ for $x < 0$, and c is a material property governing the hardening rate, as defined below. These expressions are valid only if the stress lies inside the critical state surface. If the stress lies on or outside the critical state surface $g(\sigma_{ij}) \geq 0$, then $d\lambda$ cannot be determined from the stress increment.

Hardening law: A soil becomes stronger if it is compacted to crush the soil particles together. This is described in the constitutive law by making the state variable a evolve with plastic straining in some appropriate way. A simple hardening law that captures the main features of experiments is

$$da = -cad\varepsilon_{kk}^p,$$

where c is a dimensionless material property, which determines the hardening rate. Notice that, in this law, hardening occurs only as a result of compaction and not as a result of shear deformation.

Calculating the plastic stress-strain relation: When using the constitutive equation, the formulas outlined in the preceding sections must be combined to predict the plastic strain $d\varepsilon_{ij}^p$ resulting from an increment in stress $d\sigma_{ij}$ and fluid pressure increment dp_w . This is done as follows:

1. Check the yield criterion. If $f < 0$, the plastic strain is zero $d\varepsilon_{ij}^p = 0$.
2. Check to see whether the stresses lie inside the critical state surface. If $g(\sigma_{ij}) < 0$, the material behaves like a stable, strain hardening plastic solid, and the plastic strain increment can be calculated by following steps 3–5 below.
3. Check for elastic unloading. The solid will unload elastically, with $d\varepsilon_{ij}^p = 0$, if the stress increment brings the stress below yield. This is the case whenever

$$\frac{\partial f}{\partial \sigma_{ij}} d\sigma_{ij} < 0 \Rightarrow \left(-\frac{2}{3a} \left[\frac{p_s}{a} - 1 \right] (d\sigma_{kk} + 3dp_w) + 3 \frac{S_{ij} dS_{ij}}{(Ma)^2} \right) < 0.$$

4. If plastic strain does occur, the yield criterion must be satisfied throughout plastic straining. This requires that

$$df = \frac{\partial f}{\partial \sigma_{ij}} d\sigma_{ij} + \frac{\partial f}{\partial a} da = 0.$$

It is straightforward to show that

$$\frac{\partial f}{\partial a} = \frac{-2p_s}{a^2} \left(\frac{p_s}{a} - 1 \right) - 2 \frac{\sigma_e^2}{M^2 a^3} = -\frac{2p_s}{a^2}.$$

5. The hardening law and plastic flow rule give

$$da = -cad\epsilon_{kk}^p = -cad\lambda \frac{\partial f}{\partial \sigma_{kk}} = 2cd\lambda \left[\frac{p_s}{a} - 1 \right].$$

6. Finally, combining steps 3–5 leads to

$$d\lambda = \frac{\left(-\frac{1}{3} \left[\frac{p_s}{a} - 1 \right] (d\sigma_{kk} + 3dp_w) + \frac{3}{2} \frac{S_{ij} dS_{ij}}{(Ma)^2} \right)}{2c \frac{p_s}{a} \left[\frac{p_s}{a} - 1 \right]}.$$

If the stress state is at yield $f(\sigma_{ij}) = 0$ and also lies on the critical state $g(\sigma_{ij}) = 0$, the material behaves like a perfectly plastic solid (with constant flow stress). In this case,

1. The solid unloads elastically, with $d\epsilon_{ij}^p = 0$ if

$$\frac{\partial f}{\partial \sigma_{ij}} d\sigma_{ij} < 0 \Rightarrow \left(-\frac{2}{3a} \left[\frac{p_s}{a} - 1 \right] (d\sigma_{kk} + 3dp_w) + 3 \frac{S_{ij} dS_{ij}}{(Ma)^2} \right) < 0.$$

2. If the solid deforms plastically, the stress state must satisfy

$$\frac{\partial f}{\partial \sigma_{ij}} d\sigma_{ij} = 0 \Rightarrow \left(-\frac{2}{3a} \left[\frac{p_s}{a} - 1 \right] (d\sigma_{kk} + 3dp_w) + 3 \frac{S_{ij} dS_{ij}}{(Ma)^2} \right) = 0.$$

In this case, the plastic strain cannot be determined from the stress increment: any $d\lambda > 0$ is admissible. In a situation in which the total strain of the solid is prescribed, the plastic strain increment can be determined by first solving for the elastic strain increment and subtracting it from the total strain.

If the stress lies outside the critical state $g(\sigma_{ij}) > 0$ and is at yield $f(\sigma_{ij}) = 0$, the material softens. In this case, it is impossible to distinguish unambiguously between elastic unloading and plastic flow accompanied by strain softening. The deformation in this regime usually consists of intense plastic shearing along one or more discrete shear bands, whereas the rest of the material unloads elastically. Boundary value problems with material behavior in the unstable regime are generally ill posed and cannot be solved uniquely. However,

attempting to load a soil past the critical state usually results in catastrophic collapse (such as a landslide), so detailed solutions to boundary value problems in this regime are not of much practical interest. The critical state surface can be used as a failure criterion to avoid collapse.

3.11.3 Application of the Critical State Equations to Simple 2D Loading

The constitutive equations for soils are complicated, and a simple 2D example helps to interpret them. To this end, consider a solid subjected to a 2D stress state of the form $\sigma_{ij} = -p\delta_{ij} + q(\delta_{i1}\delta_{j2} + \delta_{i2}\delta_{j1})$, as illustrated in Figure 3.58. Assume that the specimen is drained, so that the water pressure $p_w = 0$. In addition, assume that, at time $t = 0$, the solid has strength a_0 .

For this loading, the yield surface can be plotted in two dimensions, as a graph of the critical combinations of p and q that cause yield, as shown in Figure 3.59. The yield surface is an ellipse, with semi-axes a and Ma . The critical state surface is a straight line with slope M .

We can now examine the behavior of the solid as it is loaded. Consider first the response to a constant pressure on the wet side of critical state $p > a_0$, together with a steadily increasing shear stress q . In this case,

1. The solid first reaches yield when $(p/a_0 - 1)^2 + 3(q/Ma_0)^2 = 1$.
2. If the shear stress is raised beyond yield, the solid will deform plastically. Because the flow law is derived from the yield criterion, the plastic strain direction is normal to the yield surface. That is to say, if the solid experiences a plastic shear strain $d\gamma$ and volumetric strain dv , the vector $(dv, d\gamma)$ is normal to the yield surface, as shown in the figure.
3. On the wet side of critical state, the volumetric plastic strain component dv is always compressive. This means the solid compacts, and its strength increases (recall that $da = -cadv$ and $dv < 0$ during compaction).
4. As the yield surface expands, the volumetric strain component associated with an increase in shear stress dq decreases (remember that we assume a constant pressure).

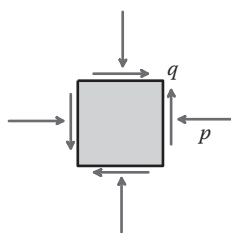


FIGURE 3.58 Material element in a soil subjected to pressure and shearing.

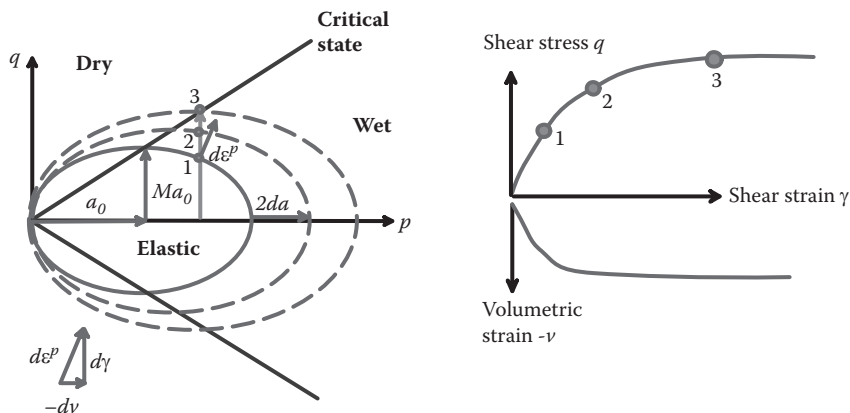


FIGURE 3.59 Evolution of yield surface and stress-strain response of a soil, with loading on the wet side of critical state.

The hardening rate therefore decreases with strain, until the stress reaches the critical state. At this point $dv = 0$, so there is no additional hardening.

Next, consider behavior on the dry side of critical state. In this case,

1. The solid first reaches yield when $(p/a_0 - 1)^2 + 3(q/Ma_0)^2 = 1$.
2. As before, the direction of the plastic strain is normal to the yield surface.
3. Notice that, on the dry side of critical state, the volumetric plastic strain component dv is always dilatational. This means that the strength of the solid decreases with plastic straining, as shown in Figure 3.60 (recall that $da = -cadv$ and $dv > 0$ during dilation).
4. The yield surface contracts during plastic straining, and this process continues until the stress reaches the critical state. At this point, the solid continues to deform at a constant shear stress.

3.11.4 Typical Values of Material Properties for Soils

Soil properties are highly variable, and, for accurate predictions, you will need to measure directly the properties of the soil you are intending to model. In addition, soil models that are used in practice are somewhat more sophisticated than the simplified version given here. As a rough guide, material properties estimated from data by Wood [1990] are listed in Table 3.13.

3.12 CONSTITUTIVE MODELS FOR METAL SINGLE CRYSTALS

Plastic flow in a single crystal is anisotropic and so cannot be modeled using the simple constitutive equations described in Section 3.7. Instead, a more complicated constitutive law is used that considers the slip activity in the crystal directly. The main application of the constitutive equation is to model the rotations of individual grains in a polycrystal and hence to predict the evolution of *texture* and to account for the effects of texture on the development of anisotropy in the solid.

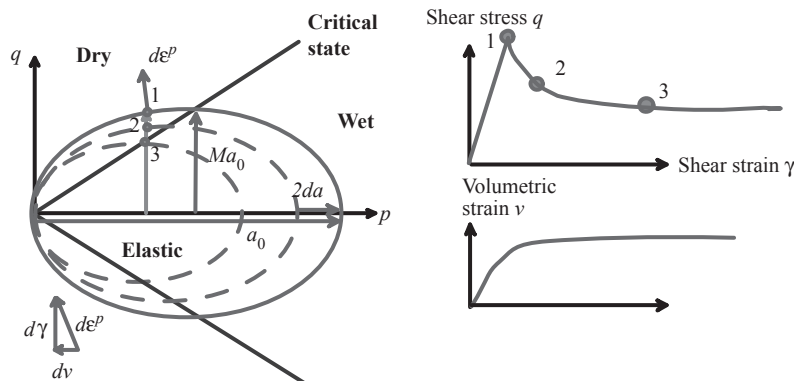


FIGURE 3.60 Evolution of yield surface and stress-strain response of a soil, with loading on the dry side of critical state.

3.12.1 Review of Some Important Concepts from Crystallography

Before describing the constitutive laws for plastically deforming crystals, we review briefly the various conventions that are used to describe crystallographic directions and orientations.

3.12.1.1 Common Crystal Structures

Most metal crystals of practical interest have face-centered cubic, body-centered cubic, or hexagonal crystal structures. These are illustrated in Figure 3.61. Crystal plasticity models exist for all three crystal structures, but FCC materials are the most extensively studied.

3.12.1.2 Miller index Notation for Crystallographic Planes and Directions

Planes and directions in a single crystal are referred to as follows. For a cubic crystal, we choose basis vec-tors $\{\mathbf{e}_1, \mathbf{e}_2, \mathbf{e}_3\}$ perpendicular to the faces of the basic cubic unit cell, as illustrated in Figure 3.61. Then,

1. The symbol $[l, m, n]$, where l, m, n are positive integers, denotes a direction parallel to a unit vector with components $(l\mathbf{e}_1 + m\mathbf{e}_2 + n\mathbf{e}_3) / \sqrt{l^2 + m^2 + n^2}$.
2. The symbol $[l, \bar{m}, n]$ denotes a direction parallel to the unit vector with components $(l\mathbf{e}_1 - m\mathbf{e}_2 + n\mathbf{e}_3) / \sqrt{l^2 + m^2 + n^2}$.

TABLE 3.13 Approximate Material Properties for Clay

Bulk Modulus K	Water Bulk Modulus K_w	Hardening Rate c	Critical State Constant M	Initial Strength a_0
2 GNm^{-2}	2.2 GNm^{-2}	5	0.8	0.2 MNm^{-2}

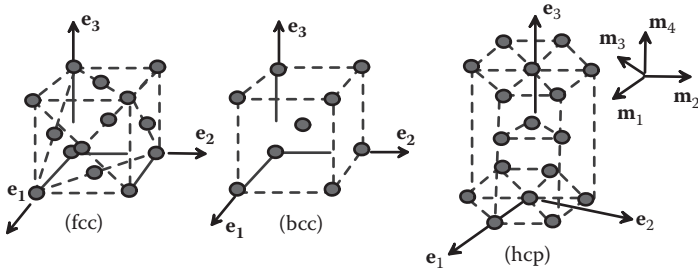


FIGURE 3.61 Crystal structures for common metals.

3. The symbol $\langle l, m, n \rangle$ denotes the family of $[l, m, n]$ directions that are identical because of the symmetry of the crystal. For example $\langle 111 \rangle$ in a cubic crystal includes all of

$$[111], [\bar{1}\bar{1}1], [1\bar{1}\bar{1}], [11\bar{1}], [\bar{1}\bar{1}\bar{1}], [\bar{1}1\bar{1}], [1\bar{1}\bar{1}], [\bar{1}\bar{1}\bar{1}].$$

4. The symbol (l, m, n) denotes a plane that is perpendicular to a unit vector with components $(l\mathbf{e}_1 + m\mathbf{e}_2 + n\mathbf{e}_3)/\sqrt{l^2 + m^2 + n^2}$.
5. The symbol (l, \bar{m}, n) denotes a plane that is perpendicular to a unit vector with components $(l\mathbf{e}_1 - m\mathbf{e}_2 + n\mathbf{e}_3)/\sqrt{l^2 + m^2 + n^2}$.
6. The symbol $\{l, m, n\}$ denotes the family of (l, m, n) planes that are crystallographically identical by symmetry.

For a hexagonal crystal, planes and directions are defined by introducing four auxiliary unit vectors \mathbf{m}_i , $i = 1 \dots 4$ as shown in Figure 3.61. The first three unit vectors lie in the basal plane and are oriented parallel to the three shortest distances between neighboring atoms. The fourth vector is perpendicular to the basal plane. These vectors are related to a Cartesian basis $\{\mathbf{e}_1, \mathbf{e}_2, \mathbf{e}_3\}$ by

$$\mathbf{m}_1 = \mathbf{e}_1 \quad \mathbf{m}_2 = (-\mathbf{e}_1 + \sqrt{3}\mathbf{e}_2)/2 \quad \mathbf{m}_3 = (-\mathbf{e}_1 - \sqrt{3}\mathbf{e}_3)/2 \quad \mathbf{m}_4 = \mathbf{e}_3.$$

Then,

- The symbol $[l, m, n, p]$, where l, m, n, p are positive integers, denotes a direction parallel to a unit vector $(l\mathbf{m}_1 + m\mathbf{m}_2 + n\mathbf{m}_3 + p\mathbf{m}_4)/\sqrt{l^2 + m^2 + n^2 + p^2}$.
- A bar over one of the indices, $[\bar{l}, m, n, p]$, changes the sign of the index, exactly as for cubic crystals.
- The symbol $\langle l, m, n, p \rangle$ denotes the family of $[l, m, n, p]$ directions that are crystallographically identical by symmetry.

4. The symbol (l, m, n, p) denotes a plane that is perpendicular to a unit vector with components $(l\mathbf{m}_1 + m\mathbf{m}_2 + n\mathbf{m}_3 + p\mathbf{m}_4) / \sqrt{l^2 + m^2 + n^2 - lm - ln - mn + p^2}$.
5. The symbol (l, \bar{m}, n, p) denotes a plane that is perpendicular to a unit vector with components $(l\mathbf{m}_1 - m\mathbf{m}_2 + n\mathbf{m}_3 + p\mathbf{m}_4) / \sqrt{l^2 + m^2 + n^2 - lm - ln - mn + p^2}$.
6. The symbol $\{l, m, n, p\}$ denotes the family of (l, m, n, p) planes that are crystallographically identical by symmetry.

3.12.1.3 Representing Crystallographic Directions and Orientations Using Stereographic Projections

Stereographic projection is a way to represent 3D orientations on a 2D plane. Figure 3.62 shows one way to interpret the projection:

1. The specimen is placed in the center of an imaginary sphere with unit radius, with some convenient material directions aligned with the $\{\mathbf{i}, \mathbf{j}, \mathbf{k}\}$ basis.
2. A direction of interest is represented by a unit vector $\mathbf{m} = xi + yj + zk$, which intersects the sphere at some point P on its surface.
3. A line is then drawn from P to the point where the \mathbf{k} axis intersects the sphere at Q.
4. The line PQ cuts through the equatorial plane of the sphere at some point R.
5. The vector $\overline{OR} \equiv \rho$ is the stereographic projection of the orientation \mathbf{m} .
6. The general conversion between the 2D projection and the 3D unit vector is easily shown to be

$$\rho = \frac{\mathbf{m} - (\mathbf{m} \cdot \mathbf{k})\mathbf{k}}{1 + \mathbf{m} \cdot \mathbf{k}} \quad \mathbf{m} = \frac{2\rho + \mathbf{k}(1 - \rho \cdot \rho)}{1 + \rho \cdot \rho}.$$

7. The symmetry of the crystal makes the $\pm \mathbf{m}$ directions equivalent. For this reason, projections usually only show vectors with a positive \mathbf{k} component (the projection of a vector with a negative \mathbf{k} component lies outside the sphere).

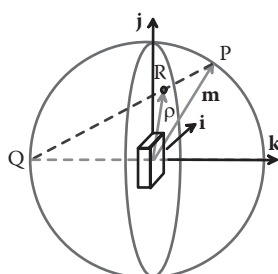


FIGURE 3.62 Illustration of the stereographic projection.

3.12.1.4 Pole Figures and Inverse Pole Figures

In crystal plasticity, the projection is used in two ways. In one approach, specific crystallographic directions are chosen to be aligned with the $\{i, j, k\}$ directions, and other directions of interest (which could be other crystallographic directions, or the direction of the loading axis in a tensile test, for example) are projected. This is known as an *inverse pole figure*.

For example, Figure 3.63 shows the standard projection for a cubic crystal. To interpret the figure, note the following:

1. The $[100]$, $[010]$, and $[001]$ directions are parallel to i , j , k , respectively. **HEALTH WARNING:** This is not the only choice of crystal orientation; you will often see the inverse pole figure with $[100]$ parallel to k , for example.
2. The points mark the projections of the specified crystallographic directions.
3. The lines mark the *traces* of the planes specified, that is to say, the projection of the line at which the plane intersects the surface of the unit sphere.
4. The figure also shows the standard triangle for a cubic crystal. Notice that the traces of the planes divide the plane into a set of 24 curvilinear triangles, each of which has $<100>$, $<110>$, and $<111>$ directions at its corners. These triangles are indistinguishable because of the symmetry of the crystal; you could interchange any two triangles by applying an appropriate rigid rotation to the crystal, without influencing the arrangement of atoms. This has important consequences: for example, when testing the response of a cubic crystal to uniaxial tension, you only need to run tests with the loading direction inside the standard triangle. For this reason, inverse pole figures often only display the standard triangle.

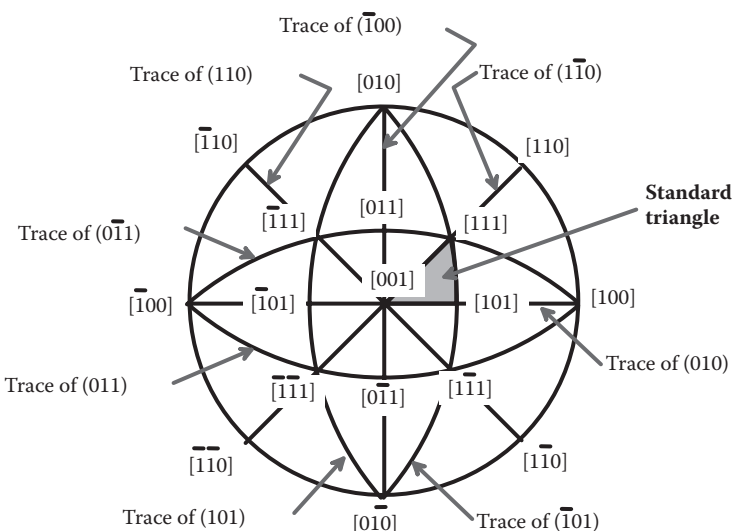


FIGURE 3.63 Stereographic projection of directions of interest in a cubic crystal.

A second application of the stereographic projection in crystal plasticity is to display *pole figures*. In this approach, specific physical directions are chosen to be aligned with the $\{i, j, k\}$ basis, and the orientations of crystallographic directions of interest are displayed on the projection.

For example, when a pole figure is plotted for a rolled sheet specimen, the rolling direction (denoted RD) is often chosen to be parallel to j , the direction transverse to the rolling direction in the plane of the sheet (denoted TD) is chosen to be parallel to i , and the direction perpendicular to the sheet (denoted ND) is chosen to be parallel to k . The sheet generally contains many grains, and each grain is a single crystal. The orientations of the grains are displayed on a pole figure by choosing some convenient crystallographic direction ($<100>$ or $<111>$ are common) and plotting the stereographic projection for each member of this family of crystallographic directions. In a cubic crystal, each grain contributes four points to the projection (there are eight $<100>$ directions but only four of them have positive k component). A typical $<100>$ pole figure for a rolled aluminum sheet after a 40% reduction is shown in Figure 3.64. The pole figure shows that grain orientations tend to cluster together, indicating that the sheet has developed a texture.

3.12.2 Features of Plastic Flow in Single Crystals

Plastic flow in a crystal is most often measured by conducting a tensile test with the loading axis parallel to a chosen crystallographic direction. The main results of these experiments are as follows:

1. For most orientations of the loading axis, the plastic flow initially consists of shearing parallel to one member of a family crystallographic planes in the crystal, in the direction of a vector s lying in that plane, as illustrated in Figure 3.64. The crystallographic plane on which shear occurs is called a *slip plane*. The shearing direction is known as the *slip direction*. Slip planes and directions for common crystals are listed in Table 3.14

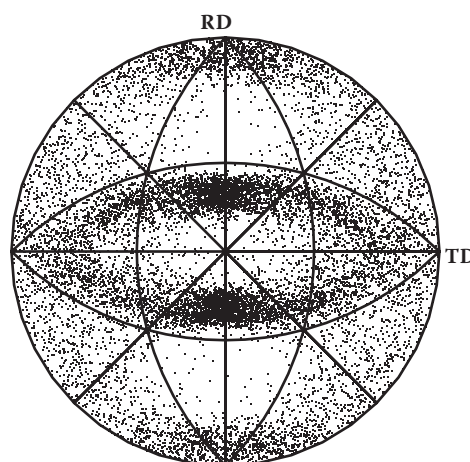


FIGURE 3.64 Typical pole figure showing texture induced by rolling a sheet of an FCC metal.

2. Crystals contain a large number of candidate slip systems. For example, an FCC crystal contains 12 possible slip systems. These are conventionally designated as listed in Table 3.15.
3. The slip systems in the undeformed crystal are identified by unit vectors \mathbf{m}^α normal to the slip plane, together with unit vectors \mathbf{s}^α parallel to the slip direction. Here $\alpha = 1 \dots N$, and N denotes the total number of slip systems (e.g., $N = 12$ for an FCC crystal). The crystal can rotate during deformation. In the deformed solid, the slip plane normals, and slip directions are denoted $\mathbf{m}^{*\alpha}$, $\mathbf{s}^{*\alpha}$.
4. In a tensile test on an annealed FCC single crystal, shearing occurs on the slip system that is subjected to the largest resolved shear stress. The resolved shear stress on the α th system can be computed from the Cauchy stress σ_{ij} acting on the solid as

$$\tau^\alpha = J\sigma_{ij}m_i^{*\alpha}s_j^{*\alpha},$$

where $J = dV/dV_0$ is the ratio of deformed to undeformed volume of the specimen ($J \approx 1$). For example, the inverse pole figure in Figure 3.66 shows the active slip system for all possible orientations of the tensile axis with respect to an FCC crystal (a bar over a slip system indicates a negative resolved shear stress). In materials with other crystal structures, some slip systems may be inherently stronger than others. In this case, slip occurs on the system with highest value of τ^α/g^α , where g^α denotes the strengths of the slip systems.

5. Slip on the critical system initiates when the resolved shear stress exceeds a critical magnitude (the strength of the slip system) $\tau^\alpha > g^\alpha$. The strength of the slip systems increases with plastic straining: this behavior will be discussed in more detail later.
6. For special orientations of the tensile axis, more than one slip system may be activated. For example, if an FCC crystal is loaded parallel to a $<100>$ direction, eight slip systems are subjected to the same resolved shear stress and so are active at the same time (the inverse pole figure in Figure 3.66 shows the active systems)
7. The deformation gradient resulting from a shear strain γ^α on the α th system is

$$F_{ij} = R_{ik}(\delta_{kj} + \gamma^\alpha s_k^\alpha m_j^\alpha),$$

TABLE 3.14 Slip Directions and Slip Planes for Common Crystal Structures

Structure	Slip Direction	Slip Plane
FCC	$<110>$	$\{111\}$
BCC	$<111>$	$\{110\}, \{112\}$
HCP	$<11\bar{2}0>$ $<11\bar{2}3>$	$(0001), \{1\bar{1}11\}$ $\{1\bar{1}01\}, \{1\bar{1}0\bar{1}\}$

TABLE 3.15 Slip Systems for an FCC Crystal

Slip Plane	Slip Direction	
	$[0\bar{1}\bar{1}]$	a_1
(111)	$[10\bar{1}]$	a_2
	$[\bar{1}10]$	a_3
	$[011]$	b_1
	$[\bar{1}0\bar{1}]$	b_2
	$[1\bar{1}0]$	b_3
	$[0\bar{1}1]$	c_1
(\bar{1}11)	$[\bar{1}0\bar{1}]$	c_2
	$[110]$	c_3
	$[011]$	d_1
	$[10\bar{1}]$	d_2
(1\bar{1}1)	$[\bar{1}\bar{1}0]$	d_3

where R_{ij} is a proper orthogonal tensor (i.e., $\det(\mathbf{R}) = 1$, $R_{ik}R_{jk} = \delta_{ij}$), representing a rigid rotation. The rotation is determined by the way the solid is loaded. For example, in a tensile test, R_{ij} is often calculated from the condition that the material fiber parallel to the loading axis (specified by a unit vector \mathbf{p}) does not rotate during deformation (Figure 3.67). This gives

$$R_{ij} = \delta_{ij} \cos \theta + 1(1 - \cos \theta)n_i n_j + \sin \theta \epsilon_{ijk} n_k$$

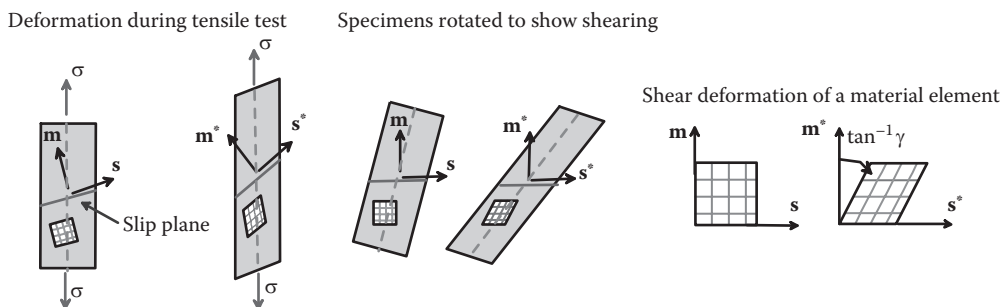


FIGURE 3.65 Deformation of a crystal occurring as a result of the slip on a single system during uniaxial loading.

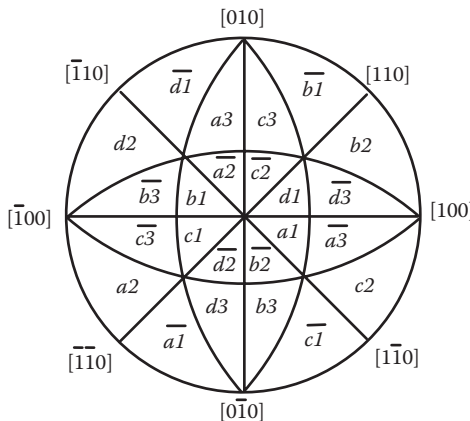


FIGURE 3.66 Active slip systems during uniaxial tensile loading of an FCC crystal.

where $n_i = \epsilon_{ijk} s_j p_k$, $\cos\theta = (1 + \gamma^\alpha p_i s_i^\alpha p_k m_k^\alpha) / C$, $\sin\theta = \gamma^\alpha (p_i m_i^\alpha) \sqrt{(1 - (p_i s_i^\alpha)^2) / C}$, and $C = \sqrt{1 + \gamma^{\alpha 2} (p_i m_i^\alpha)^2 + 2\gamma^\alpha p_i s_i^\alpha p_k m_k^\alpha}$. Other assumptions are also used to calculate \mathbf{R} .

- The crystal lattice is rotated by \mathbf{R} so that, after deformation, $s_i^* = R_{ij}s_j$ $m_i^* = R_{ij}m_j$ for all the slip systems.
 - The rate of deformation resulting from a shearing rate $\dot{\gamma}^\alpha$ on the α th system is

$$L_{ij} = \dot{F}_{ip} F_{pi}^{-1} = \dot{R}_{ik} R_{ik} + R_{ik} \dot{\gamma}^\alpha s_k^\alpha m_p^\alpha R_{ip} = \dot{R}_{ik} R_{ik} + \dot{\gamma}^\alpha s_i^{*\alpha} m_i^{*\alpha}.$$

This can be decomposed into a symmetric part, representing a stretching, together with a skew part, representing a spin, as

$$L_{ii} = D_{ii} + W_{ii} \quad \quad W_{ii} = \dot{R}_{ik} R_{ik} + \dot{\gamma}^\alpha (s_i^{*\alpha} m_i^{*\alpha} - s_i^{*\alpha} m_i^{*\alpha}) / 2 \quad \quad D_{ii} = \dot{\gamma}^\alpha (s_i^{*\alpha} m_i^{*\alpha} + s_i^{*\alpha} m_i^{*\alpha}) / 2.$$

Here, the first term in W_{ij} represents the rotation of the lattice, whereas the second term is the spin attributable to lattice shearing.

10. In a tensile test oriented for single slip, the crystal rotates so as to align the slip direction with the loading axis. This rotation is illustrated for an FCC crystal on the inverse pole figure in Figure 3.68. Eventually, the crystal rotates far enough to activate a second slip system. The exact point at which this occurs depends on how the crystal hardens; it usually occurs shortly before the loading axis moves out of the standard

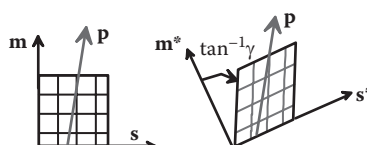


FIGURE 3.67 Rotation of a crystal lattice during uniaxial tensile loading

triangle. The rotation direction changes after the second slip system becomes active: eventually, the loading axis aligns with the $\langle 112 \rangle$ direction. This is a stable orientation, and the crystal continues to deform in double slip without additional rotation.

11. The resistance of each slip plane to shearing increases with plastic strain, caused by strain hardening. A typical stress-strain curve for a single crystal that is initially oriented for single slip is illustrated in Figure 3.69. The curve is divided into three characteristic regions. Stage I corresponds to the period while a single slip system is active and has a low hardening rate (resulting from self hardening). Stage II begins when a second slip system activates and has a higher hardening rate (resulting from both self and latent hardening). Stage III occurs at large strains, and the hardening rate decreases attributable to dynamic recovery. The hardening rates in Stages I and II are insensitive to temperature, but the Stage III hardening rate decreases with temperature.
12. Shearing on the α th system increases its own strength g^α : this is known as *self-hardening*. Shearing on the α th system also increases the strength of all the other slip systems g^β , $\beta \neq \alpha$: this is known as *latent hardening*. Self-hardening can be measured using single-slip tests. Latent hardening is often measured by first deforming the material in single slip and then reloading the specimen to activate a second slip system. Latent hardening is often quantified by the *latent hardening ratio*, which specifies the ratio of the strength of the second system to that of the first $q^{\alpha\beta} = g^\beta/g^\alpha$. The details of the hardening behavior of single crystals are very complex, and, at present, there is no consensus on how best to measure or characterize hardening.
13. Lattice rotation during a tensile test gives rise to a phenomenon known as “geometric softening,” which plays an important role in shear localization in single crystals. The term geometric softening refers to the fact that the crystal may rotate so as to increase the resolved shear stress on its active slip system and, therefore, lead to a decrease in the tensile flow stress of the crystal.

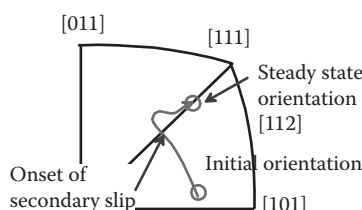


FIGURE 3.68 Inverse pole figure showing evolution of the tensile axis during uniaxial loading of an FCC crystal.

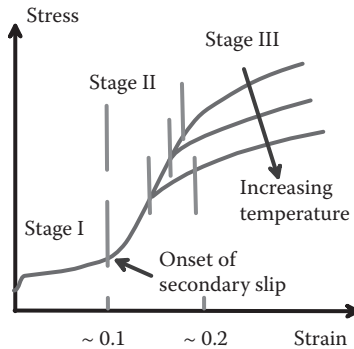


FIGURE 3.69 Typical stress-strain curves during uniaxial tensile loading of an FCC single crystal.

3.12.3 Kinematic Descriptions Used in Constitutive Models of Single Crystals

Let x_i be the position of a material particle in the undeformed crystal. Suppose that the solid is subjected to a displacement field $u_i(x_k)$, so that the point at x_i moves to $y_i = x_i + u_i$, as shown in Figure 3.70. Define the following:

- The deformation gradient and its Jacobian:

$$F_{ij} = \delta_{ij} + \frac{\partial u_i}{\partial x_j} \quad J = \det(F).$$

- The velocity gradient:

$$L_{ij} = \frac{\partial \dot{u}_i}{\partial y_j} = \dot{F}_{ik} F_{kj}^{-1}.$$

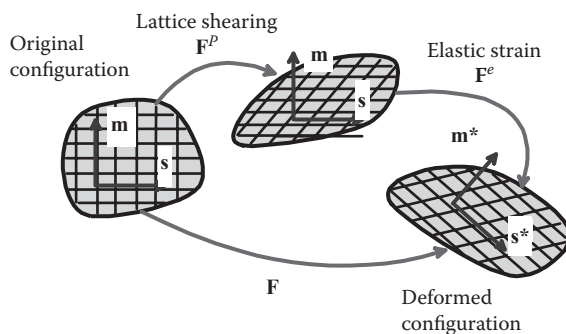


FIGURE 3.70 Decomposition of deformation in a crystal into elastic and plastic parts.

- The stretch rate and spin:

$$D_{ij} = (L_{ij} + L_{ji}) / 2 \quad W_{ij} = (L_{ij} - L_{ji}) / 2.$$

- Recall that F_{ij} relates infinitesimal material fibers dy_i and dx_i in the deformed and undeformed solid, respectively, as

$$dy_i = F_{ij} dx_j.$$

- To decompose the deformation gradient into elastic and plastic parts, we assume that deformation takes place in two stages. The plastic strain is assumed to shear the lattice, without stretching or rotating it. The elastic deformation rotates and stretches the lattice. We think of these two events occurring in sequence, with the plastic deformation first and the stretch and rotation second, giving

$$dy_i = F_{ij} dx_j = F_{ik}^e F_{kj}^p dx_j.$$

- To decompose the velocity gradient into elastic and plastic parts, note that

$$L_{ij} = \dot{F}_{ik} F_{kj}^{-1} = (\dot{F}_{ik}^e F_{kl}^p + F_{ik}^e \dot{F}_{kl}^p) (F_{lm}^{p-1} F_{mj}^{e-1}) = \dot{F}_{ik}^e F_{kj}^{e-1} + F_{ik}^e \dot{F}_{kl}^p F_{lm}^{p-1} F_{mj}^{e-1}.$$

Thus, the velocity gradient contains two terms, one of which involves only measures of elastic deformation, whereas the other contains measures of plastic deformation. We use this to decompose \mathbf{L} into elastic and plastic parts:

$$L_{ij} = L_{ij}^e + L_{ij}^p \quad L_{ij}^e = \dot{F}_{ik}^e F_{kj}^{e-1} \quad L_{ij}^p = F_{ik}^e \dot{F}_{kl}^p F_{lm}^{p-1} F_{mj}^{e-1}.$$

- Plastic flow in the crystal occurs by shearing a set of N slip systems. The slip systems are characterized by unit vectors parallel to slip directions s_i^α and slip plane normals m_i^α in the undeformed solid. The rate of shear on the α th system is denoted by $\dot{\gamma}^\alpha$. The velocity gradient attributable to this shearing is

$$\dot{F}_{ik}^p F_{kj}^{-1} = \sum_{\alpha=1}^N \dot{\gamma}^\alpha s_i^\alpha m_j^\alpha.$$

- It is convenient to define vectors that describe plastic shearing in the current configuration, as

$$s_i^{*\alpha} = F_{ik}^e s_k^\alpha \quad m_i^{*\alpha} = m_k^\alpha F_{ki}^{e-1}.$$

The former can be interpreted as the slip direction in the deformed solid (note that it is not a unit vector, however), whereas $m_i^{*\alpha}$ can be interpreted as the slip plane normal in the deformed solid.

- The plastic part of the velocity gradient can then be expressed in terms of the shearing rates as

$$L_{ij}^p = \sum_{\alpha=1}^N \dot{\gamma}^\alpha s_i^{*\alpha} m_j^{*\alpha}.$$

- The elastic and plastic parts of the velocity gradient can be decomposed into symmetric and skew symmetric parts, representing stretching and spin, respectively, as

$$\begin{aligned} D_{ij}^e &= (L_{ij}^e + L_{ji}^e) / 2 & W_{ij}^e &= (L_{ij}^e - L_{ji}^e) / 2 \\ D_{ij}^p &= (L_{ij}^p + L_{ji}^p) / 2 & W_{ij}^p &= (L_{ij}^p - L_{ji}^p) / 2. \end{aligned}$$

- The plastic stretching and spin can be expressed in terms of the lattice shearing as

$$D_{ij}^p = \sum_{\alpha=1}^N \dot{\gamma}^\alpha (s_i^{*\alpha} m_j^{*\alpha} + s_j^{*\alpha} m_i^{*\alpha}) / 2 \quad W_{ij}^p = \sum_{\alpha=1}^N \dot{\gamma}^\alpha (s_i^{*\alpha} m_j^{*\alpha} - s_j^{*\alpha} m_i^{*\alpha}) / 2.$$

3.12.4 Stress Measures Used in Crystal Plasticity

Stress measures that appear in descriptions of crystal plasticity are summarized below:

- The Cauchy (true) stress represents the force per unit deformed area in the solid and is defined by

$$n_i \sigma_{ij} = \lim_{dA \rightarrow 0} \frac{dP_j^{(n)}}{dA}.$$

- Kirchhoff stress is defined by $\tau_{ij} = J \sigma_{ij}$.
- Material stress for the intermediate configuration is defined by $\Sigma_{ij} = J F_{ik}^{e-1} \sigma_{kl} F_{jl}^{e-1}$.
- Resolved shear stress on a slip system is defined by $\tau^\alpha = J m_i^{*\alpha} \sigma_{ij} s_j^{*\alpha}$.
- Lattice Jaumann rate of Kirchhoff stress is defined by $\dot{\tau}_{ij} = \frac{d\tau_{ij}}{dt} - W_{ik}^e \tau_{kj} + \tau_{ik} W_{kj}^e$.

Note that the material stress should be interpreted as the force per unit area acting on the intermediate configuration, as shown in Figure 3.71, rather than on the undeformed configuration. For additional details, see Section 3.9.

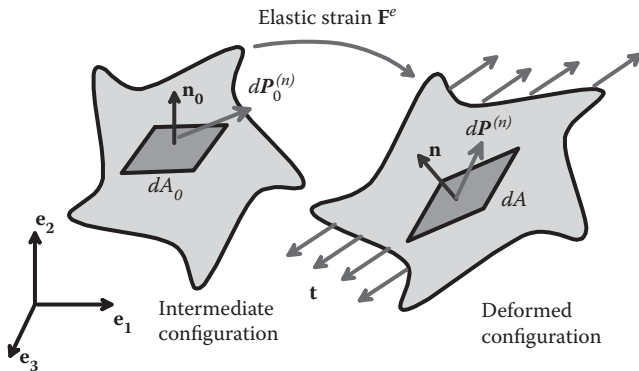


FIGURE 3.71 Deformation of an area element in a solid.

The constitutive equations must specify relationships between these stress measures and the deformation measures outlined in the preceding section. In particular, the constitutive equations must relate the following:

1. The elastic part of the deformation gradient to stress
2. The rate of shearing on each slip system to the resolved shear stress

3.12.5 Elastic Stress–Strain Relation Used in Crystal Plasticity

The relations between stress and the elastic part of the deformation gradient follow the procedure developed for finite strain plasticity in Section 3.8.3. Only the final results will be repeated here:

1. Define the Lagrangean elastic strain as $E_{ij} = (F_{ki}^e F_{kj}^e - \delta_{ij}) / 2$.
2. Assume that the material stress is proportional to Lagrange strain, as $\Sigma_{ij} = C_{ijkl} E_{kl}$, where C_{ijkl} are the components of the elastic stiffness tensor (as defined and tabulated in Section 3.1), for the material with orientation in the undeformed configuration.
3. The elastic stress-strain law is often expressed in rate form, as follows

$$\tau_{ij}^e \approx C_{ijkl}^e D_{kl}^e,$$

where τ_{ij}^e is the Jaumann rate of Kirchhoff stress with respect to axes that rotate with the crystal lattice; $C_{ijkl}^e = F_{in}^e F_{jm}^e C_{nmpq} F_{kp}^e F_{lq}^e$ can be thought of as the components of the elastic compliance tensor for material with orientation in the deformed configuration, and D_{ij}^e is the elastic stretch rate.

3.12.6 Plastic Stress–Strain Relation Used in Crystal Plasticity

The plastic constitutive equations specify the relationship between the stress on the crystal and slip rates $\dot{\gamma}^\alpha$ on each slip system. Here, we outline a simple and widely used approach to doing this, based on the work of Pierce, Asaro, and Needleman [1983]. This model is not

the best fit to experimental observations, however; in particular, more sophisticated equations are required to accurately describe latent hardening behavior.

Flow rule: There are many advantages to using a viscoplastic flow rule to predict the slip rates in a single crystal: this avoids having to use an iterative procedure to identify active slip systems and also helps to stabilize material behavior. The simplest such flow rule is

$$\dot{\gamma}^\alpha = \dot{\gamma}_0 \operatorname{sign}(\tau^\alpha) \left(\frac{|\tau^\alpha|}{g^\alpha} \right)^m,$$

where τ^α is the resolved shear stress on the slip system, g^α is its current strength (which evolves with plastic straining), and $\dot{\gamma}_0, m$ are material properties.

Hardening rule: The hardening rule must specify the relationship between the slip system strengths g^α and the plastic strain. At time $t = 0$, each slip system has the same initial strength g_0 . Thereafter, the slip systems increase in strength as a result of the plastic shearing according to

$$\dot{g}^\alpha = \sum_{\beta=1}^N h_{\alpha\beta} |\dot{\gamma}^\beta|,$$

where $h_{\alpha\beta}$ are strain-dependent hardening rates. The hardening rate is approximated as

$$h(\bar{\gamma}) = h_s + (h_s - h_0) \operatorname{sech}^2 \left\{ \left(\frac{h_0 - h_s}{g_s - g_0} \right) \bar{\gamma} \right\},$$

where $h_s, h_0, g_s, q_{\alpha\beta}$ are material properties, and $\bar{\gamma}$ is the total accumulated slip on all slip systems

$$\bar{\gamma} = \int_0^t \sum_{\alpha=1}^N |\dot{\gamma}^\alpha| dt.$$

The matrix $q_{\alpha\beta}$ controls the latent hardening rate: for an FCC crystal, it is usually taken to have the form

$$q_{\alpha\beta} = \begin{cases} 1 & \alpha, \beta \text{ coplanar} \\ q & \text{otherwise} \end{cases},$$

where q is a material property. The slip systems for an FCC crystal are listed in Table 3.15; for example, slip systems a_1, a_2, a_3 are coplanar, whereas a_1, b_1 are non-coplanar.

TABLE 3.16 Properties of a Copper Crystal

$\dot{\gamma}_0$	0.001 s ⁻¹
m	10–20
g_0	16 MNm ⁻²
g_s	70.4 MNm ⁻²
h_0	132 MNm ⁻²
h_s	8 MNm ⁻²
q	1.4

3.12.7 Representative Values for Plastic Properties of Single Crystals

Elastic properties of single crystals are listed in Sections 3.1.15 and 3.1.16. The plastic properties of single crystals are strongly sensitive to the material's crystal structure and composition. For accurate predictions, you will need to test the actual material you plan to use. As a rough guide, representative parameters for a copper single crystal [taken from Wu, Neale, and Van der Giessen 1996] are listed in Table 3.16.

3.13 CONSTITUTIVE MODELS FOR CONTACTING SURFACES AND INTERFACES IN SOLIDS

Many practical problems involve two contacting surfaces that roll or slide against one another: examples include machine elements, such as gears and bearings, machining and metal forming processes, or slip along a geological fault. In addition, models of deformation and failure in materials must often account for the nucleation and growth of cracks in the solid. In these applications, constitutive equations must be used to specify the forces transmitted across the interfaces or contacting surfaces as a function of their relative motion.

The simplest and most familiar such constitutive law is Coulomb friction, which relates the normal and tangential tractions acting across a contacting surface. More complex constitutive laws are also available, which can model very complex interactions between surfaces. In this section, we outline two general classes of interface law: (1) cohesive zone models, which are used to model interfaces in materials or adhesion between very clean (often nanoscale) surfaces; and (2) models that are intended to model contact and friction between two sliding surfaces.

3.13.1 Cohesive Zone Models of Interfaces

Cohesive zone models are usually used to model the nucleation and propagation of cracks along an interface between two solids and to model adhesion between two contacting surfaces. Figure 3.72 illustrates the problem to be solved. We assume the following:

- Two solids meet at a surface S.

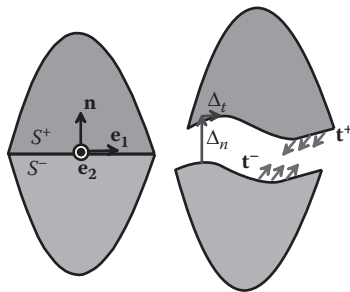


FIGURE 3.72 Separation of an interface between two solids.

- In the undeformed configuration, the interface is free of traction, and there is no overlap or separation between the solids along S .
- When the solid is loaded, forces are transmitted across the interface, while the two solids may separate, slide, or overlap at the interface. The notion that two solids may interpenetrate can be disturbing at first sight. However, the surface S where the solids meet does not represent a plane of atoms; it merely characterizes the equilibrium separation between the two solids when the interface is stress free. If the two solids overlap, this means that the atomic or material planes just adjacent to the interface move closer together.
- We shall assume that the relative displacement of the two solids across S is small compared with any characteristic dimension of the solid and also that the two contacting solids themselves experience small shape changes.

A *cohesive zone law* relates the relative motion of the two solids adjacent to S to the tractions transmitted across S . A large number of such constitutive equations have been developed, but there are two general classes. (1) The first consists of reversible force-displacement laws, in which the traction is simply a function of the relative distance between the two surfaces and independent of the history of loading. These are often used to model nucleation and growth of a crack on an interface that is subjected to monotonically increasing loading in which irreversibility plays no role and are also used to model interaction between surfaces of nanoscale structures, whose dimension can be comparable with the distance of action of long-range interatomic forces. (2) The second consists of irreversible force-displacement laws, which model failure processes that lead to the creation of new free surface in the solid. These could include separation of atomic planes attributable to cleavage, or more complex processes such as rupture by void nucleation and coalescence, or fatigue.

Kinematics: The relative motion of the two solids is characterized as follows:

1. Let \mathbf{n} denote a unit vector normal to the interface. The sense of \mathbf{n} is arbitrary (i.e., it can point up or down, as you prefer). Once \mathbf{n} has been chosen, however, we designate the two material surfaces adjacent to S by S^+ and S^- , with \mathbf{n} the outward normal to S^- .

2. Introduce two mutually perpendicular unit vectors \mathbf{e}_α that are tangent to the interface.
3. Let $\mathbf{u}^+(\mathbf{x})$ and $\mathbf{u}^-(\mathbf{x})$ denote the displacement of two material points that are just adjacent to a point \mathbf{x} on S in the undeformed solid.
4. Let $\Delta = \mathbf{u}^+ - \mathbf{u}^-$ denote the relative displacement of two initially coincident points. To specify constitutive equations, it is convenient to characterize the relative displacement using the three scalar Cartesian components ($\Delta_n, \Delta_1, \Delta_2$) of Δ in the basis $\{\mathbf{n}, \mathbf{e}_1, \mathbf{e}_2\}$. If the interface is isotropic (i.e., its response is independent of the direction of the relative tangential displacement between the surfaces), the behavior of the interface depends only on Δ_n and $\Delta_t = \sqrt{\Delta_1^2 + \Delta_2^2}$.

Kinetics: The forces acting between the two surfaces are characterized as follows:

1. Two points that are initially coincident in the undeformed interface are assumed to exert equal and opposite tractions on one another. Because the relative displacements of S^+ and S^- are assumed to be small and both solids are assumed to experience small shape changes, there is no need to distinguish between forces acting on the deformed and undeformed solids. Let $\mathbf{t}^-(\mathbf{x})$ and $\mathbf{t}^+(\mathbf{x})$ denote the force per unit area acting on S^- and S^+ , respectively.
2. Because $\mathbf{t}^+(\mathbf{x}) = -\mathbf{t}^-(\mathbf{x})$, the tractions can be characterized by the three scalar components (T_n, T_1, T_2) of \mathbf{t}^- in the basis $\{\mathbf{n}, \mathbf{e}_1, \mathbf{e}_2\}$.

The constitutive equations for the interface must relate (T_n, T_1, T_2) to $(\Delta_n, \Delta_1, \Delta_2)$.

Constitutive equations representing reversible separation between interfaces are the simplest cohesive zone laws. For these models, the tractions are a function only of the relative displacement of the material planes adjacent to the interface and are independent of the history or rate of loading. This means that the traction-displacement relation for the interface is reversible. The interface will heal if the two surfaces are brought back into contact after separation.

The constitutive equations relating (T_n, T_1, T_2) to $(\Delta_n, \Delta_1, \Delta_2)$ for a reversible interface are constructed as follows:

1. The traction-displacement relation is most conveniently characterized by a scalar interplanar potential $\Phi(\Delta_n, \Delta_1, \Delta_2)$ by setting

$$T_n = \frac{\partial \Phi}{\partial \Delta_n} \quad T_1 = \frac{\partial \Phi}{\partial \Delta_1} \quad T_2 = \frac{\partial \Phi}{\partial \Delta_2}.$$

The value of Φ represents the work done per unit area in separating the interface by Δ .

2. A number of different functions are used to approximate Φ . Here, we will just give one example [a simplified version of a potential developed by Xu and Needleman 1995]:

$$\Phi(\Delta_n, \Delta_t) = \phi_n - \phi_n \left(1 + \frac{\Delta_n}{\delta_n} \right) \exp \left(-\frac{\Delta_n}{\delta_n} \right) \exp \left(-\frac{\beta^2 \Delta_t^2}{\delta_n^2} \right).$$

Here, $\Delta_t^2 = \Delta_1^2 + \Delta_2^2$, whereas ϕ_n , δ_n , β are material properties. Their physical significance is discussed below.

3. Formulas relating (T_n, T_1, T_2) to $(\Delta_n, \Delta_1, \Delta_2)$ can be calculated by differentiating the potential. The result is

$$T_n = \sigma_{\max} \frac{\Delta_n}{\delta_n} \exp \left(1 - \frac{\Delta_n}{\delta_n} \right)$$

$$T_\alpha = 2\sigma_{\max} \left(\frac{\beta^2 \Delta_\alpha}{\delta_n} \right) \left(1 + \frac{\Delta_n}{\delta_n} \right) \exp \left(1 - \frac{\Delta_n}{\delta_n} \right) \exp \left(-\frac{\beta^2 \Delta_\alpha^2}{\delta_n^2} \right),$$

where $\sigma_{\max} = \phi_n / \delta_n \exp(1)$.

The traction-displacement relations are plotted in Figure 3.73. Under purely normal tensile loading, the interface has work of separation ϕ_n , and the normal traction reaches a value of σ_{\max} at an interface separation $\Delta_n = \delta_n$. Under purely shear loading, the tangential traction has a maximum value $\tau_{\max} = \beta \phi_n \sqrt{2} / (\delta_n \sqrt{\exp(1)})$ at a tangential shear displacement $\Delta_t = \delta_n / \sqrt{2}$.

Constitutive equations modeling irreversible separation between interfaces: Most interfaces do not heal when brought back into contact after separation. In applications in which interfaces are subjected to *cyclic* loading, more complicated constitutive equations

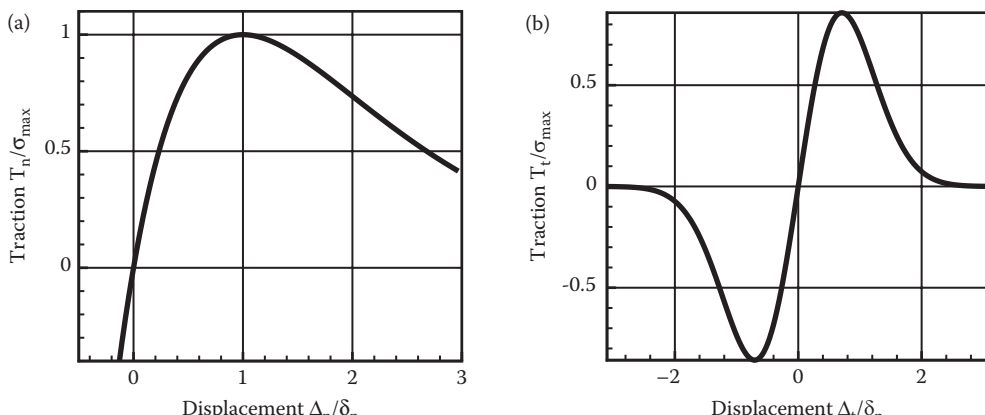


FIGURE 3.73 Traction-separation relations for a typical cohesive zone law. (a) Under normal loading; (b) under tangential loading.

must be used to account for this irreversible behavior. Again, a very large number of such constitutive equations have been developed: we will illustrate their general features using a model adapted from Ortiz and Pandolfi [1999] as a representative example.

The behavior of the interface can be illustrated using its response to a purely normal tensile traction, shown in the traction-separation law in Figure 3.74. The interface initially responds elastically, with a constant stiffness $k_0 = \sigma_{\max}/d_1$, so that $T_n = k_0\Delta_n$. As long as $\Delta_n \leq d_1$, the interface is reversible and undamaged. If the displacement exceeds $\Delta_n = d_1$, the interface begins to accumulate irreversible damage, which causes the stress to drop. At the same time, the damage reduces the stiffness of the interface so that, during unloading, the traction-displacement relation remains linear but with a reduced slope. Note that the total work of separation for the interface under tensile loading is $\phi_0 = \sigma_{\max}(d_1 + d_2)/2$. The constitutive equation is constructed as follows:

1. The material surfaces S^+ and S^- are completely prevented from overlapping, by enforcing the constraint $\Delta_n \geq 0$.
2. The magnitude of the relative displacement between S^+ and S^- is quantified by a scalar parameter $\lambda = \sqrt{\Delta_n^2 + \beta^2(\Delta_1^2 + \Delta_2^2)}$, where β is a material property, which controls the relative stiffness and strength of the interface under normal and shear loading.
3. Similarly, the magnitude of the traction can be quantified by an effective stress $\tau = \sqrt{T_n^2 + (T_1^2 + T_2^2) / \beta^2}$.
4. The tractions acting between S^+ and S^- are related to the relative displacement by an elastic potential $\Phi(\Delta_n, \Delta_1, \Delta_2, D)$ by setting

$$T_n = \frac{\partial \Phi}{\partial \Delta_n} \quad T_1 = \frac{\partial \Phi}{\partial \Delta_1} \quad T_2 = \frac{\partial \Phi}{\partial \Delta_2}.$$

Here, $0 \leq D \leq 1$ is a scalar parameter that quantifies the irreversible damage accumulated by the interface.

5. A linear traction-displacement relation is constructed by making Φ a quadratic function of λ , as follows

$$\Phi = k_0(1 - D)\lambda^2 / 2.$$

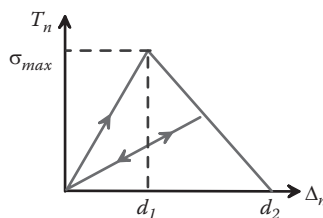


FIGURE 3.74 Traction-separation law for an irreversible cohesive zone law.

Here, k_0 is a material property that corresponds to the slope of the traction-displacement relation for the undamaged interface. It follows that the tractions are related to the displacements by

$$T_n = k_0(1 - D)\Delta_n \quad T_1 = \beta^2 k_0(1 - D)\Delta_1 \quad T_2 = \beta^2 k_0(1 - D)\Delta_2.$$

6. The constitutive law is completed by devising an appropriate equation governing the evolution of D . D remains constant if the traction on the interface is less than its current strength, if the interface is unloaded, or if D reaches 1. Otherwise, D must evolve so that the strength of the interface decreases linearly from its initial value σ_{\max} to zero as the effective displacement λ increases from $\lambda = d_1$ to $\lambda = d_2$. This requires

$$\frac{dD}{dt} = \begin{cases} 0 & \tau < \frac{(1 - D)(1 + d_1 / d_2)\sigma_{\max}}{1 - D + d_1 / d_2} \text{ or } d\lambda / dt < 0 \text{ or } D = 1 \\ \left((1 - D) + \frac{d_1}{d_2} \right) \frac{1}{\lambda} \frac{d\lambda}{dt} & \text{Otherwise.} \end{cases}$$

Representative values for properties of cohesive zones: The two constitutive laws contain the following parameters:

1. The reversible interface can be conveniently characterized by its strength, σ_{\max} , the total work of tensile separation ϕ_0 , and the parameter β that controls the ratio of shear to normal strength.
2. The irreversible interface can be characterized by its strength, σ_{\max} , the total work of tensile separation ϕ_0 , the parameter β , and the displacement d_1 at the instant of maximum stress.

It is difficult to give precise values for these material properties. This is partly because the constitutive equations are used to model a variety of physical processes that lead to failure and partly because there is no simple way to measure the values of the parameters. The following guidelines are usually followed:

1. If the cohesive zone is used to model atomic-scale cleavage in a brittle elastic material or adhesion between two elastic solids, then ϕ_0 is set equal to the fracture toughness of the interface (typically $\phi_0 \approx 1 \text{ Jm}^{-2}$) and the peak strength of the material $\sigma_{\max} \approx E/100$ where E is the Young's modulus. Available data suggest that interfaces are stronger in shear than in tension so β is usually taken to be slightly less than 1 ($\beta \approx 0.7$). Computations are usually not strongly sensitive to the shape of the cohesive zone, so d_1/d_2 can be taken to be approximately 1 in the irreversible model.
2. If the cohesive zone is intended to model both the plastic zone and the failure process at the tip of a crack in an otherwise elastic solid, then ϕ_0 is set equal to the fracture toughness of the solid (fracture toughness values are tabulated in Section 9.3.6),

whereas σ_{\max} is taken to be roughly three times the yield stress of the solid in uniaxial tension (yield stress values are tabulated in Section 3.7.9). Again, $\beta \approx 0.7$, whereas $d_1/d_2 \approx 1$ in the irreversible model.

3. Cohesive zones are sometimes used to model material separation at the tip of a crack in a plastic solid, together with an elastic-plastic constitutive equation for the two solids adjacent to the cohesive interface. In this case, it is not usually clear what process the cohesive zone represents. Experience shows that, if the strength σ_{\max} of the cohesive zone is taken to be too high (greater than approximately three times the yield stress of the plastic material), the crack will never propagate. If the strength of the cohesive zone is less than the yield stress, there is no plasticity. Consequently, $Y < \sigma_{\max} < 3Y$. It is difficult to interpret the meaning of ϕ_0 in these models, but fortunately simulations tend to be relatively insensitive to ϕ_0 . A value for ϕ_0 is usually estimated by choosing a sensible characteristic length (between 1 and 10 μm) for δ_n or d_1 and setting $\phi_n = \sigma_{\max} \delta_n \exp(1)$ for the reversible model or $\phi_0 = \sigma_{\max} (d_1/d_2)/2$ for the irreversible version.

3.13.2 Models of Contact and Friction between Surfaces

A friction experiment is conceptually very simple: two surfaces are pressed into contact by a controlled normal pressure p , and the specimens are loaded so as to induce a state of uniform shear traction T acting between the contacting surfaces (Figure 3.75). The experiment seeks to answer the following questions:

1. What is the critical combination of normal and tangential forces cause the surfaces to start to slide?
2. If the two surfaces do start to slip, what tangential force is required to *keep* them sliding?
3. If the surfaces are slipping, how does the tangential force vary with sliding velocity and normal pressure, and how does the surface respond to *changes* in sliding velocity and pressure?
4. How does friction depend on the contact area, the properties of the two contacting surfaces, surface roughness, environment, lubricant films, etc.?

The results of these experiments show the following for most engineering surfaces that make contact over a nominal area exceeding $100 \mu\text{m}^2$ or so:

- The critical tangential traction required to initiate sliding between two surfaces is proportional to the normal pressure. If the normal force is zero, the contact cannot support *any* tangential force. Doubling the normal force will double the critical tangential force that initiates slip.
- Surface roughness has a very modest effect on friction. Doubling the surface roughness might change the friction force by a few percentage.

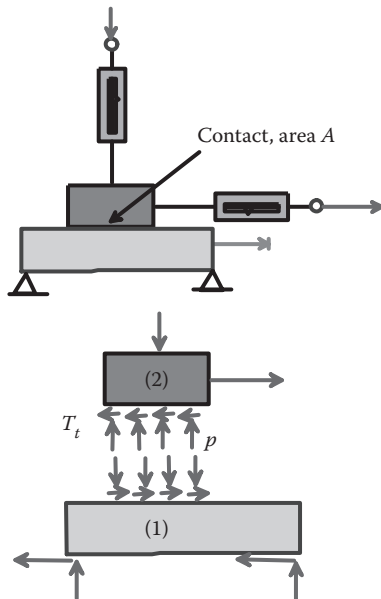


FIGURE 3.75 Simple friction experiment.

- Contaminants or lubricant on the two surfaces has a big effect on friction. Even a little moisture on the surfaces can reduce friction by 20–30%. If there is a thin layer of grease on the surfaces, it can cut friction by a factor of 10. If the contaminants are *removed*, friction forces can be huge, and the two surfaces can seize together completely.
- Friction forces depend quite strongly on what the two surfaces are made from. Some materials like to bond with each other (metals generally bond well to other metals, for example) and so have high friction forces. Some materials (e.g., Teflon) do not bond well to other materials. In this case, friction forces will be smaller.
- If the surfaces start to slide, the tangential force often (but not always) drops slightly. Thus, kinetic friction forces are often a little lower than static friction forces. Otherwise, kinetic friction forces behave just like static friction; they are proportional to the normal force, etc.
- The steady-state kinetic friction force usually (but not always) decreases slightly as the sliding speed increases. Increasing sliding speed by a factor of 10 might drop the friction force by a few percentage.
- The transient response to changes in sliding speed has been extensively studied in geological materials, motivated by the need to understand earthquakes. In these materials, increasing the sliding speed causes an instantaneous increase in shear traction, which then gradually decays to a lower steady-state value, as illustrated in Figure 3.76. If the sliding speed is reduced, there is an instantaneous drop in the friction force, which subsequently increases toward a steady state. The

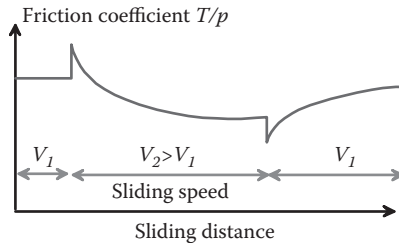


FIGURE 3.76 Transient variation of friction coefficient after changes in sliding velocity.

transients occur over a sliding distance of order 10–50 μm . This behavior has been observed in other materials (including metals) as well but is not universal; for example, Gearing, Moon, and Anand [2001] observe an increase in steady-state friction forces with sliding speed in sliding of aluminum against steel.

- The transient response to a change in contact pressure has not been studied as extensively as the response to changes in sliding speed. The data of Prakash [1998] indicates that, when the contact pressure is suddenly increased, the shear traction is initially unchanged and subsequently asymptotes toward a value proportional to the new contact pressure as the relative distance of sliding between the two surfaces increases, as illustrated in Figure 3.77.

These trends can be attributed to the effects of surface roughness. All surfaces are rough and, when brought into contact, meet only at highest points on the two surfaces, as shown in Figure 3.78. The true area of contact between the two surfaces is much less than the nominal contact area and increases roughly in proportion to the nominal contact pressure acting between the surfaces. The nominal tangential traction is proportional to the product of the true contact area and the shear strength of the contacting surfaces and is therefore approximately proportional to the nominal contact pressure.

There are some situations in which the true area of contact approaches the nominal contact area. Examples include (1) the tip of an atomic force microscope, which has roughness comparable with atomic scale dimensions, and (2) friction between the tool and work piece in metal forming applications. In these situations, the traction acting tangent to the surface is relatively insensitive to the contact pressure.

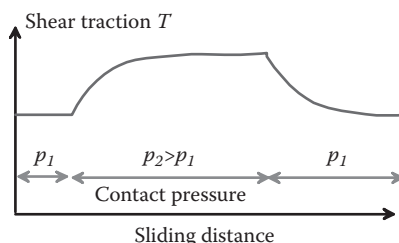


FIGURE 3.77 Transient variation of friction coefficient after changes in contact pressure.

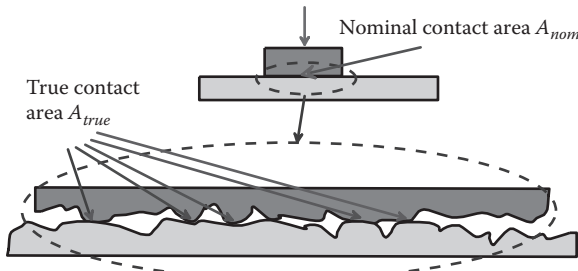


FIGURE 3.78 True and apparent area of contact between two rough surfaces.

Kinematics of surfaces in sliding contact: Constitutive laws for friction must account for large relative motion between the contacting surfaces. Consequently, the contact is best characterized by the relative position and motion of the two surfaces in the deformed configuration.

1. One of the two surfaces is arbitrarily designated the “master” surface and labeled S^- , as shown in Figure 3.79. The other surface is designated the “slave” and is labeled S^+ . Note that, in some friction models (e.g., the plasticity model described below), exchanging the master and slave surface will have a small influence on the behavior of the interface.
2. At a representative point y^- on S^- , we let \mathbf{n} denote a unit vector normal to S^- and introduce two mutually perpendicular unit vectors \mathbf{e}_α that are tangent to S^- . We take \mathbf{e}_1 to point along a characteristic material direction in S^- , i.e., if \mathbf{m}_1 is a unit vector tangent to S^- in the undeformed slave surface, $\mathbf{e}_1 = (\mathbf{F} \cdot \mathbf{m}_1)/|\mathbf{F} \cdot \mathbf{m}_1|$ in the deformed surface.
3. The gap between the two surfaces is characterized by the points on the two surfaces that lie along \mathbf{n} , i.e., $y^+ = y^- + \Delta_n \mathbf{n}$. The relative velocity of the two surfaces is defined as

$$\mathbf{v} = \frac{d}{dt}(y^+ - y^-) - \Delta_n \frac{d\mathbf{n}}{dt}.$$

4. It is convenient to separate the relative velocity into components normal and tangent to the surface $v_n = d\Delta_n/dt = \mathbf{v} \cdot \mathbf{n}$, $v_1 = \mathbf{v} \cdot \mathbf{e}_1$, $v_2 = \mathbf{v} \cdot \mathbf{e}_2$.

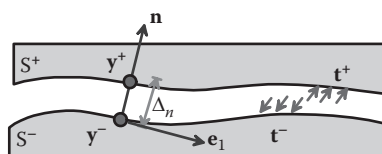


FIGURE 3.79 Geometry of two interacting surfaces.

5. In finite element computations, it is sometimes convenient to introduce a small elastic compliance for the interface. In this case, the relative velocity of the surfaces is divided into a reversible elastic part and an irreversible (plastic) part by defining

$$\mathbf{v} = \mathbf{v}^e + \mathbf{v}^p \quad v_n = v_n^e + v_n^p \quad v_\alpha = v_\alpha^e + v_\alpha^p \quad \alpha = 1, 2.$$

Kinetics of surfaces in sliding contact: The forces acting between the two surfaces are characterized as follows:

1. The points on the two surfaces at positions \mathbf{y}^+ and \mathbf{y}^- are assumed to exert equal and opposite tractions on one another. We let $\mathbf{t}^+(\mathbf{y}^+)$, $\mathbf{t}^-(\mathbf{y}^-)$ denote the tractions on S^+ and S^- , respectively.
2. Because $\mathbf{t}^+(\mathbf{y}^+) = -\mathbf{t}^-(\mathbf{y}^-)$, the tractions can be characterized by the three scalar components (T_n, T_1, T_2) of \mathbf{t}^- in the basis $\{\mathbf{n}, \mathbf{e}_1, \mathbf{e}_2\}$.

Constitutive equations for sliding friction must specify relationships between (Δ_n, v_i) and (T_n, T_1, T_2) . Various alternatives are summarized briefly below.

Coulomb friction: This is the most familiar friction law. For this model,

1. The interface separates, with an indeterminate Δ_n if $T_n > 0$.
2. The surfaces are prevented from interpenetrating $\Delta_n = 0$ if $T_n < 0$.
3. No slip occurs between the surfaces $v_i = 0$ if $\sqrt{T_1^2 + T_2^2} < |\mathbf{T}_n|$, where μ is the coefficient of friction.
4. The tangential traction is proportional to the normal pressure and opposes the direction of slip if the two surfaces slide $T_1 = |\mathbf{T}_n| v_1 / \sqrt{v_1^2 + v_2^2}$ $T_2 = |\mathbf{T}_n| v_2 / \sqrt{v_1^2 + v_2^2}$.

Table 3.17 lists rough values for friction coefficients for a few material pairs. These are rough guides only; friction coefficients for a given material can be highly variable (for example, friction for a steel/steel contact can vary anywhere between 0.001 and 3) and can even vary significantly with time or sliding distance during an experiment.

HEALTH WARNING: Descriptions of Coulomb friction in elementary mechanics and physics texts often distinguish between kinetic and static friction coefficients. It is not advisable to adopt this approach when posing a boundary value problem in continuum mechanics, because it is likely to make the problem ill posed (with either no solution or an infinite number of solutions). In fact, even with a single friction coefficient, the Coulomb friction model can be ill posed and should be used with caution.

TABLE 3.17 Friction Coefficients for Various Materials

Material	Approximate Friction Coefficient
Rubbers on dry surfaces	0.8–1.5
Clean metals in air	0.8–2
Clean metals in wet air	0.5–1.5
Soft metals (lead, bronze)	0.1
Ceramics (carbides, rocks)	0.05–0.5
Polymers on polymers	0.05–1.0
Grease or high temperature lubricant	0.05–0.2
Hydrodynamically lubricated surfaces (full oil film)	0.0001–0.0005

Coulomb friction with a shear cutoff: In metal-forming applications, contacting surfaces can be subjected to extremely high pressure, with the result that the true area of contact approaches the nominal area. Under these conditions, the shear traction is no longer proportional to the contact pressure. Behavior at high pressure is often approximated by truncating the shear traction at a critical value (usually taken to be somewhat lower than the shear yield strength of the softer of the two contacting surfaces). The modified friction has the following constitutive equations:

1. The interface separates, with an indeterminate Δ_n if $T_n > 0$.
2. The surfaces are prevented from interpenetrating $\Delta_n = 0$ if $T_n < 0$.
3. We introduce the shear resistance of the interface τ defined as

$$\tau = \begin{cases} |T_n| & |T_n| \leq \tau_0 \\ \tau_0 & |T_n| \geq \tau_0, \end{cases}$$

where τ_0 is the maximum shear stress that the interface can withstand.

4. No slip occurs between the surfaces $v_i = 0$ if $\sqrt{T_1^2 + T_2^2} < \tau$.
5. The tangential traction is proportional to the normal pressure and opposes the direction of slip if the two surfaces slide: $T_1 = \tau v_1 / \sqrt{v_1^2 + v_2^2}$ $T_2 = \tau v_2 / \sqrt{v_1^2 + v_2^2}$.

Rate and state variable models of friction: The variation of friction with sliding velocity and transient behavior after changes in contact pressure play an important role in controlling the stability of sliding on an interface. Several friction laws have been developed to describe this behavior and are widely used in geophysics applications. As a representative

example, we outline a constitutive law based loosely on work by Dieterich [1979], Ruina [1983], and Prakash [1998].

The transient behavior of sliding friction is modeled by introducing two *state variables* ω^\pm, p^\pm for each material point on S^\pm . The state variables evolve according to

$$\frac{d\omega}{dt} = (\nu_s - \omega) \left(\frac{\nu_s}{L_v} + \frac{1}{t_v} \right) \quad \frac{dp}{dt} = -(T_n + p) \left(\frac{\nu_s}{L_p} + \frac{1}{t_p} \right),$$

where $\nu_s = \sqrt{(\nu_1^p)^2 + (\nu_2^p)^2}$, (L_v, L_p) are material properties with units of length, and (t_v, t_p) are material properties with units of time. The two surfaces S^+ and S^- may have different properties. To interpret these equations, note the following:

1. Both ω and p evolve with time and the sliding distance.
2. If the surfaces slide at constant speed, then $\omega \rightarrow \nu_s$ in the steady state, whereas if the surfaces are subjected to a time-independent normal traction, $p \rightarrow -T_n$.
3. The two constants (t_v, t_p) control the timescale associated with this evolution for a static contact, whereas (L_v, L_p) control the distance required for ω and p to reach their steady-state values under a rapidly sliding contact.

HEALTH WARNING: Note the following. (1) State variables must be introduced to characterize both contacting surfaces, because coincident points on the two surfaces experience different histories of contact pressure and slip velocity. To see this, note that, as you slide your finger over the surface of a table, a point on your finger sees a constant contact pressure, whereas a point on the table experiences a cycle of loading. (2) The time derivatives of the state variables should be interpreted as the rate of change experienced by an observer traveling with a particular material particle in each surface.

The variation of steady-state friction coefficient with sliding velocity is modeled by introducing a friction coefficient that is a function of the state variables ω^\pm

$$(\bar{\omega}) = \mu_k + (\mu_s - \mu_k) \exp[-(\bar{\omega} / V_1)^n],$$

where $\bar{\omega} = (\omega^+ + \omega^-) / 2$ and μ_k, μ_s, V_1, n are all material properties. The constant μ_k represents the limiting value of the friction coefficient as sliding velocity approaches infinity (it can be interpreted as the kinetic friction coefficient), whereas μ_s is the steady-state value of friction coefficient for a static contact (and can be interpreted as the static friction coefficient). The two constants V_1 and n control the rate at which the friction transitions from one value to the other.

The friction law can be conveniently expressed as a relationship between the tractions and the relative velocity of the contact, as follows. For $\Delta_n > 0$, the surfaces are traction-free: $T_n = T_1 = T_2 = 0$. For $\Delta_n \leq 0$:

1. The elastic part of the relative velocity is related to the traction components by

$$v_n^e = \frac{1}{k_n} \frac{dT_n}{dt} \quad v_1^e = \frac{1}{k_t} \frac{dT_1}{dt} \quad v_2^e = \frac{1}{k_t} \frac{dT_2}{dt},$$

where k_n and k_t are two elastic stiffnesses. Note that these equations assume that the elastic distortion of the interface occurs on the slave surface (the time derivatives correspond to the traction rate experienced by an observer fixed to the slave surface).

2. The irreversible part of the normal component of velocity $v_n^p = 0$.
3. The irreversible part of the tangential component of velocity is calculated from

$$v_\alpha^p = \begin{cases} V_0 \left[\left(\frac{\bar{\omega}}{V_0} + 1 \right) \left(\frac{T_t}{\bar{p}} \right)^m - 1 \right] \frac{T_\alpha}{T_t} & T_t \geq \bar{p}, \\ 0 & T_t < \bar{p} \end{cases}$$

where $T_t = \sqrt{T_1^2 + T_2^2}$, $\bar{\omega} = (\omega^+ + \omega^-) / 2$, $\bar{p} = (p^+ + p^-) / 2$, and V_0, m are two constants that control the variation of shear stress to a step change in sliding velocity.

To interpret this equation, suppose that the interface is subjected to a constant (i.e., time independent) pressure and is constrained to slip at a rate v_s . The magnitude of the shear traction follows as

$$T_t = (\bar{\omega}) \bar{p} \left(\frac{v_s / V_0 + 1}{\bar{\omega} / V_0 + 1} \right)^{1/m}.$$

The steady-state value is $T_t = (v_s) \bar{p}$. After an instantaneous increase in sliding speed, the shear traction first jumps to a new, higher value and then progressively decreases to a lower steady-state value as $\bar{\omega}$ approaches the new value of sliding speed. Similarly, if the sliding speed is suddenly reduced, the shear stress first drops to a lower value, and subsequently increases gradually to a higher steady-state.

Representative values of material properties for state variable model of friction: The subtle features of friction captured by this constitutive equation are very sensitive to the materials involved, the surface finish, and the environment. Extensive tests are required to characterize a particular contacting pair. As a rough guide to the orders of magnitudes of the various material parameters, Table 3.18 lists estimates for parameters based on a discussion by Coker, Lykotrafitis, Needleman, and Rosakis [2005] of transient friction in Homalite.

Friction laws based on plasticity theory: The general framework of viscoplasticity can easily be adapted to construct friction laws that approximate the variation of friction with sliding speed and the evolution of friction with slip. Laws of this kind are often used in metal-forming simulations. Several such models exist but will not be described in detail here. Instead, we will illustrate the general idea by adapting the critical state theory of

TABLE 3.18 Representative Values of Parameters for a Simple State Variable Friction Law

k_n (GPa/m)	k_t (GPa/m)	μ_k	μ_s	V_1 (m/s)	n
300	100	0.5	0.6	26	1.2
L_p (μm)	t_p (s)	L_v (μm)	t_v (s)	V_0 (m/s)	m
20	∞	20	∞	100	5

The two contacting surfaces are assumed to have identical properties.

plasticity outlined in Section 3.11, together with the viscoplasticity law described in Section 3.8 to construct a friction law that captures the transient behavior of a sliding interface, as follows:

1. The normal traction must satisfy $T_n \leq 0$: if $T_n = 0$, the surfaces separate and $T_1 = T_2 = 0$.
2. The relative velocity of the two surfaces is divided into elastic and plastic parts:

$$v_n = v_n^e + v_n^p \quad v_\alpha = v_\alpha^e + v_\alpha^p \quad \alpha = 1, 2.$$

3. The elastic part of the relative velocity is related to the traction components by

$$v_n^e = \frac{1}{k_n} \frac{dT_n}{dt} \quad v_1^e = \frac{1}{k_t} \frac{dT_1}{dt} \quad v_2^e = \frac{1}{k_t} \frac{dT_2}{dt},$$

where k_n and k_t are two elastic stiffnesses. Note that these equations assume that the elastic distortion occurs on the slave surface (the time derivatives correspond to the traction rate experienced by an observer fixed to the slave surface).

4. Three state variables p^\pm, ω^\pm, s^\pm are introduced to track the history of contact pressure, sliding speed, and sliding distance on each of the two contacting surfaces. The state variables evolve according to

$$\frac{dp}{dt} = -cv_n^p \quad \frac{ds}{dt} = v_s \quad \frac{d\omega}{dt} = (v_s - \omega) \left(\frac{v_s}{L_v} + \frac{1}{t_v} \right),$$

where $v_s = \sqrt{v_1^2 + v_2^2}$ and c, L_v, t_v are material properties. Naturally, the two surfaces may have different values of c, L_v, t_v . The governing equations for the evolution of the state variables have been designed so that $p \rightarrow -T_n$ and $\omega \rightarrow v_s$ under conditions of steady sliding.

5. The variation of relative velocity between the surfaces with traction is approximated using a slip potential (similar to the viscoplastic potential described in Section 3.8), defined as

$$g(T_n, T_t) = \begin{cases} \frac{V_0 \tau_0}{m+1} \left[\left(1 + \frac{T_n}{\bar{p}} \right)^2 + \left(\frac{T_t}{\tau_0} \right)^2 - 1 \right]^{(m+1)/2} & \left(1 + \frac{T_n}{\bar{p}} \right)^2 + \left(\frac{T_t}{\tau_0} \right)^2 - 1 \geq 0 \\ 0 & \left(1 + \frac{T_n}{\bar{p}} \right)^2 + \left(\frac{T_t}{\tau_0} \right)^2 - 1 \leq 0 \end{cases},$$

where V_0 , m are material properties that control the response of the interface to an instantaneous change in traction, $\bar{p} = (p^+ + p^-) / 2$, and τ_0 is a representative shear strength that may be a function of one or more of the state variables, as discussed further below. The state variable \bar{p} plays the role of a in the critical state soil model outlined in Section 3.11.

6. The plastic part of the relative velocity between the surfaces is related to g through an associated flow law:

$$v_n^p = \frac{\partial g}{\partial T_n} \quad v_\alpha^p = \frac{\partial g}{\partial T_\alpha} \quad \alpha = 1, 2.$$

Evaluating the derivatives gives

$$v_n^p = \begin{cases} V_0 \frac{\tau_0}{\bar{p}} \left(1 + \frac{T_n}{\bar{p}} \right) \left[\left(1 + \frac{T_n}{\bar{p}} \right)^2 + \left(\frac{T_t}{\tau_0} \right)^2 - 1 \right]^{(m-1)/2} & \left(1 + \frac{T_n}{\bar{p}} \right)^2 + \left(\frac{T_t}{\tau_0} \right)^2 - 1 \geq 0 \\ 0 & \left(1 + \frac{T_n}{\bar{p}} \right)^2 + \left(\frac{T_t}{\tau_0} \right)^2 - 1 \leq 0 \end{cases}$$

$$v_\alpha^p = \begin{cases} V_0 \frac{T_\alpha}{\tau_0} \left[\left(1 + \frac{T_n}{\bar{p}} \right)^2 + \left(\frac{T_t}{\tau_0} \right)^2 - 1 \right]^{(m-1)/2} & \left(1 + \frac{T_n}{\bar{p}} \right)^2 + \left(\frac{T_t}{\tau_0} \right)^2 - 1 \geq 0 \\ 0 & \left(1 + \frac{T_n}{\bar{p}} \right)^2 + \left(\frac{T_t}{\tau_0} \right)^2 - 1 \leq 0 \end{cases}$$

7. Finally, the variation of the tangential force with contact pressure, sliding speed, and slip distance must be specified by an appropriate equation for $\tau_0(\bar{p}, \bar{\omega}, \bar{s})$. Any sensible function can be chosen, depending on the behavior that you would like to approximate. For example,

- Setting $\tau_0 = \bar{p}$ will produce Coulomb friction-like behavior, with a delayed response to changes in contact pressure. To see this, note that the model behaves like the critical state soil model discussed in Section 3.10, with “volumetric strain” replaced by the normal separation between the surfaces, and $\mu \equiv M$.
- Setting $\tau_0 = ((\tau_s - \tau_k) \exp(-(\bar{\omega}/V_1)^n)) \bar{p} / f(\bar{\omega}/V_0)$, where $f(y)$ is the root of the equation $y = x(x^2 - 1)^{(m-1)/2}$, will give a Coulomb-like friction law with a velocity-dependent friction coefficient similar to the rate- and state-variable model outlined previously.

There is very little to distinguish the rate- and state-variable model from the plasticity-based model. The plasticity model has some advantages for numerical simulations, because (1) the transition from stick to slip is gradual, (2) the plasticity model has a “soft” relationship between the normal displacement of the surfaces and the normal pressure, and (3) the plasticity model has an associated flow rule. All these tend to stabilize numerical computations.

This page intentionally left blank

Solutions to Simple Boundary and Initial Value Problems

In this chapter, we derive exact solutions to several problems involving deformable solids. The examples have been selected partly because they can easily be solved, partly because they illustrate clearly the role of the various governing equations and boundary conditions in controlling the solution, and partly because the solutions themselves are of some practical interest.

4.1 AXIALLY AND SPHERICALLY SYMMETRIC SOLUTIONS TO QUASI-STATIC LINEAR ELASTIC PROBLEMS

4.1.1 Summary of Governing Equations of Linear Elasticity in Cartesian Components

It is helpful to review briefly the equations we must solve to calculate deformation in an elastic material subjected to loading. A representative problem is sketched in Figure 4.1. We are given the following information:

1. The geometry of the solid
2. A constitutive law for the material (i.e., the linear elastic-stress-strain equations)
3. Body force density b_i (per unit mass) (if any)

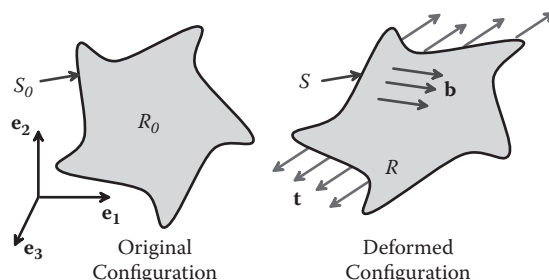


FIGURE 4.1 Typical boundary value problem for an elastic solid.

4. Temperature distribution ΔT (if any)
5. Prescribed boundary tractions t_i and/or boundary displacements u_i .

In addition, to simplify the problem, we make the following assumptions:

1. All displacements are small. This means that we can use the infinitesimal strain tensor to characterize deformation; we do not need to distinguish between stress measures, and we do not need to distinguish between deformed and undeformed configurations of the solid when writing equilibrium equations and boundary conditions.
2. The material is an isotropic, linear elastic solid, with Young's modulus E and Poisson's ratio ν , and mass density ρ_0 .

With these assumptions, we need to solve for the displacement field u_i , the strain field ε_{ij} , and the stress field σ_{ij} satisfying the following equations:

- Displacement-strain relation: $\varepsilon_{ij} = \frac{1}{2} \left(\frac{\partial u_i}{\partial x_j} + \frac{\partial u_j}{\partial x_i} \right)$.
- Stress-strain relation: $\sigma_{ij} = \frac{E}{1+\nu} \left\{ \varepsilon_{ij} + \frac{\nu}{1-2\nu} \varepsilon_{kk} \delta_{ij} \right\} - \frac{E\alpha\Delta T}{1-2\nu} \delta_{ij}$.
- Equilibrium equation: $\frac{\partial \sigma_{ij}}{\partial x_i} + \rho_0 b_j = 0$ (static problems only; you need the acceleration terms for dynamic problems).
- Traction boundary conditions: $\sigma_{ij} n_i = t_j$ on parts of the boundary where tractions are known.
- Displacement boundary conditions: $u_i = d_i$ on parts of the boundary where displacements are known.

4.1.2 Simplified Equations for Spherically Symmetric Linear Elasticity Problems

A representative spherically symmetric problem is illustrated in Figure 4.2. We consider a hollow, spherical solid that is subjected to spherically symmetric loading (i.e., internal body forces, as well as tractions or displacements applied to the surface, are independent of θ and φ and act in the radial direction only). If the temperature of the sphere is nonuniform, it must also be spherically symmetric (a function of R only).

The solution is most conveniently expressed using a spherical-polar coordinate system, illustrated in Figure 4.2. The general procedure for solving problems using spherical and cylindrical coordinates is complicated and is discussed in detail in Appendix D. In this section, we simply summarize the special form of these equations for spherically symmetric problems.

As usual, a point in the solid is identified by its spherical-polar coordinates (R, θ, φ) . All vectors and tensors are expressed as components in the basis $\{\mathbf{e}_R, \mathbf{e}_\theta, \mathbf{e}_\varphi\}$ shown in Figure 4.2. For a spherically symmetric problem, the position, displacement, and body force are

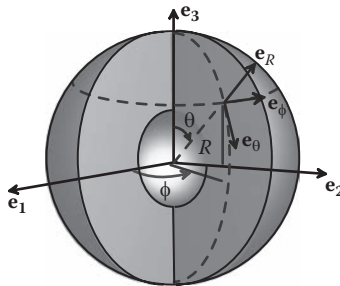


FIGURE 4.2 Coordinate system used for spherically symmetric problems.

- Position vector: $\mathbf{x} = R\mathbf{e}_R$
- Displacement vector: $\mathbf{u} = u(R)\mathbf{e}_R$
- Body force vector: $\mathbf{b} = \rho_0 b(R)\mathbf{e}_R$

Here, $u(R)$ and $b(R)$ are scalar functions. The stress and strain tensors (written as components in $\{\mathbf{e}_R, \mathbf{e}_\theta, \mathbf{e}_\phi\}$) have the form

$$\boldsymbol{\sigma} \equiv \begin{bmatrix} \sigma_{RR} & 0 & 0 \\ 0 & \sigma_{\theta\theta} & 0 \\ 0 & 0 & \sigma_{\phi\phi} \end{bmatrix} \quad \boldsymbol{\varepsilon} \equiv \begin{bmatrix} \varepsilon_{RR} & 0 & 0 \\ 0 & \varepsilon_{\theta\theta} & 0 \\ 0 & 0 & \varepsilon_{\phi\phi} \end{bmatrix}$$

and furthermore must satisfy $\sigma_{\theta\theta} = \sigma_{\phi\phi}$, $\varepsilon_{\theta\theta} = \varepsilon_{\phi\phi}$. The tensor components have exactly the same physical interpretation as they did when we used a fixed $\{\mathbf{e}_1, \mathbf{e}_2, \mathbf{e}_3\}$ basis, except that the subscripts (1,2,3) have been replaced by (R, θ, ϕ).

For spherical symmetry, the governing equations of linear elasticity reduce to the following:

- Strain displacement relations: $\varepsilon_{RR} = \frac{du}{dR}$, $\varepsilon_{\phi\phi} = \varepsilon_{\theta\theta} = \frac{u}{R}$.
- Stress-strain relations:

$$\sigma_{RR} = \frac{E}{(1+\nu)(1-2\nu)} \left\{ (1-\nu)\varepsilon_{RR} + \nu\varepsilon_{\theta\theta} + \nu\varepsilon_{\phi\phi} \right\} - \frac{E\alpha\Delta T}{1-2\nu}$$

$$\sigma_{\theta\theta} = \sigma_{\phi\phi} = \frac{E}{(1+\nu)(1-2\nu)} \left\{ \varepsilon_{\theta\theta} + \nu\varepsilon_{RR} \right\} - \frac{E\alpha\Delta T}{1-2\nu}.$$

- Equilibrium equations:

$$\frac{d\sigma_{RR}}{dR} + \frac{1}{R} (2\sigma_{RR} - \sigma_{\theta\theta} - \sigma_{\phi\phi}) + \rho_0 b_R = 0.$$

- Boundary conditions:

prescribed displacements, $u_R(a) = g_a$, $u_R(b) = g_b$;
 prescribed tractions, $\sigma_{RR}(a) = t_a$, $\sigma_{RR}(b) = t_b$.

These results can either be derived as a special case of the general 3D equations of linear elasticity in spherical coordinates or alternatively can be obtained directly from the formulas in Cartesian components. Here, we briefly outline the latter.

1. Note that we can find the components of $\{\mathbf{e}_R, \mathbf{e}_\theta, \mathbf{e}_\phi\}$ in the $\{\mathbf{e}_1, \mathbf{e}_2, \mathbf{e}_3\}$ basis as follows. First, note that \mathbf{e}_R is radial and can be written in terms of the position vector as $\mathbf{x}/|\mathbf{x}|$. Next, note $\mathbf{e}_\phi = \mathbf{e}_3 \times \mathbf{e}_R / |\mathbf{e}_3 \times \mathbf{e}_R|$ and $\mathbf{e}_\theta = \mathbf{e}_\phi \times \mathbf{e}_R / |\mathbf{e}_\phi \times \mathbf{e}_R|$. Using index notation, the components of the basis vectors $\{\mathbf{e}_R, \mathbf{e}_\theta, \mathbf{e}_\phi\}$ in $\{\mathbf{e}_1, \mathbf{e}_2, \mathbf{e}_3\}$ are therefore

$$\left\{ \frac{x_i}{R}, \frac{x_3 x_i - R^2 \delta_{i3}}{R^2 - x_3^2}, \frac{\epsilon_{ijk} R x_j}{R^2 - x_3^2} \right\}$$

where $R = |\mathbf{x}| = \sqrt{x_k x_k}$, δ_{ij} is the Kronecker delta and ϵ_{ijk} is the permutation symbol.

2. The components of the (radial) displacement vector in the $\{\mathbf{e}_1, \mathbf{e}_2, \mathbf{e}_3\}$ basis are $u_i = u(R)x_i/R$.
3. To proceed with the algebra, it is helpful to remember that $\partial x_i / \partial x_j = \delta_{ij}$, $\partial R / \partial x_j = x_j / R$, and $\partial R^{-1} / \partial x_j = -x_j / R^3$.
4. The components of the strain tensor in the $\{\mathbf{e}_1, \mathbf{e}_2, \mathbf{e}_3\}$ basis therefore follow as

$$\epsilon_{ij} = \frac{1}{2} \left(\frac{\partial u_i}{\partial x_j} + \frac{\partial u_j}{\partial x_i} \right) = \frac{du}{dR} \frac{x_i x_j}{R^2} + u(R) \left(\frac{\delta_{ij}}{R} - \frac{x_i x_j}{R^3} \right).$$

5. The strain components ϵ_{RR} , $\epsilon_{\theta\theta}$, $\epsilon_{\phi\phi}$ can then be found as $\epsilon_{RR} = \mathbf{e}_R \cdot \boldsymbol{\epsilon} \cdot \mathbf{e}_R$, $\epsilon_{\theta\theta} = \mathbf{e}_\theta \cdot \boldsymbol{\epsilon} \cdot \mathbf{e}_\theta$, and $\epsilon_{\phi\phi} = \mathbf{e}_\phi \cdot \boldsymbol{\epsilon} \cdot \mathbf{e}_\phi$. Substituting for the basis vectors and simplifying gives the strain-displacement relations. For example,

$$\epsilon_{RR} = \epsilon_{ij} \frac{x_i x_j}{R^2} = \frac{du}{dR} \frac{x_i x_i x_j x_j}{R^4} + u(R) \left(\frac{\delta_{ij}}{R} \frac{x_i x_j}{R^2} - \frac{x_i x_i x_j x_j}{R^5} \right) = \frac{du}{dR},$$

where we have noted $x_i x_i = R^2$. The remaining components are left as an exercise.

6. Finally, to derive the equilibrium equation, note that the stress tensor can be expressed as $\sigma = \sigma_{RR} \mathbf{e}_R \otimes \mathbf{e}_R + \sigma_{\theta\theta} \mathbf{e}_\theta \otimes \mathbf{e}_\theta + \sigma_{\phi\phi} \mathbf{e}_\phi \otimes \mathbf{e}_\phi$. Substituting for the basis vectors from item 1 above gives

$$\sigma_{ij} = \sigma_{RR} \frac{x_i x_j}{R^2} + \sigma_{\theta\theta} \frac{\epsilon_{ijk} R x_k}{R^2 - x_3^2} \frac{\epsilon_{jkn} R x_n}{R^2 - x_3^2} + \sigma_{\phi\phi} \left(\frac{x_3 x_i - R^2 \delta_{i3}}{R^2 - x_3^2} \right) \left(\frac{x_3 x_j - R^2 \delta_{j3}}{R^2 - x_3^2} \right).$$

7. Substitute the preceding result into the equilibrium equation

$$\frac{\partial \sigma_{ij}}{\partial x_i} + \rho_0 b(R) \frac{x_j}{R} = 0$$

and work through a good deal of tedious algebra to see that

$$\left(\frac{\partial \sigma_{RR}}{\partial R} + \frac{1}{R} (2\sigma_{RR} - \sigma_{\theta\theta} - \sigma_{\phi\phi}) + \rho_0 b(R) \right) \frac{x_j}{R} = 0.$$

4.1.3 General Solution to the Spherically Symmetric Linear Elasticity Problem

Our goal is to solve the equations given in Section 4.1.2 for the displacement, strain, and stress in the sphere. To do so, perform the following:

1. Substitute the strain-displacement relations into the stress-strain law to show that

$$\begin{bmatrix} \sigma_{RR} \\ \sigma_{\theta\theta} \end{bmatrix} = \frac{E}{(1+\nu)(1-2\nu)} \begin{bmatrix} 1-\nu & 2\nu \\ \nu & 1 \end{bmatrix} \begin{bmatrix} \frac{du}{dR} \\ \frac{u}{R} \end{bmatrix} - \frac{E\alpha\Delta T}{1-2\nu} \begin{bmatrix} 1 \\ 1 \end{bmatrix}.$$

2. Substitute this expression for the stress into the equilibrium equation and rearrange the result to see that

$$\frac{d^2u}{dR^2} + \frac{2}{R} \frac{du}{dR} - \frac{2u}{R^2} = \frac{d}{dR} \left\{ \frac{1}{R^2} \frac{d}{dR} (R^2 u) \right\} = \frac{\alpha(1+\nu)}{(1-\nu)} \frac{d\Delta T}{dR} - \frac{(1+\nu)(1-2\nu)}{E(1-\nu)} \rho_0 b(R).$$

Given the temperature distribution and body force, this equation can easily be integrated to calculate the displacement u . Two arbitrary constants of integration will appear when you do the integral—these must be determined from the *boundary conditions* at the inner and outer surface of the sphere. Specifically, the constants must be selected so that either the displacement or the radial stress have prescribed values on the inner and outer surface of the sphere. In the following sections, this procedure is used to derive solutions to various boundary value problems of practical interest.

4.1.4 Pressurized Hollow Sphere

A pressurized sphere is illustrated in Figure 4.3. Assume the following:

- No body forces act on the sphere.
- The sphere has uniform temperature.
- The inner surface $R = a$ is subjected to pressure p_a .

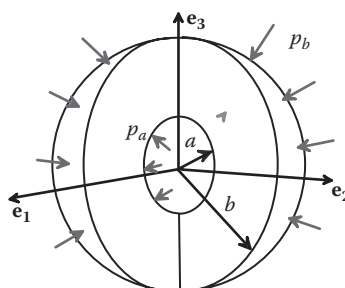


FIGURE 4.3 Spherical shell subjected to internal and external pressure.

- The outer surface $R = b$ is subjected to pressure p_b .
- The displacement, strain, and stress fields in the sphere are

$$\mathbf{u} = \frac{1}{2E(b^3 - a^3)R^2} \left\{ 2(p_a a^3 - p_b b^3)(1 - 2\nu)R^3 + (p_a - p_b)(1 + \nu)b^3 a^3 \right\} \mathbf{e}_R$$

$$\varepsilon_{RR} = \frac{1}{E(b^3 - a^3)R^3} \left\{ (p_a a^3 - p_b b^3)(1 - 2\nu)R^3 - (p_a - p_b)(1 + \nu)b^3 a^3 \right\}$$

$$\varepsilon_{\theta\theta} = \varepsilon_{\phi\phi} = \frac{1}{2E(b^3 - a^3)R^3} \left\{ 2(p_a a^3 - p_b b^3)(1 - 2\nu)R^3 + (p_a - p_b)(1 + \nu)b^3 a^3 \right\}$$

$$\sigma_{RR} = \frac{(p_a a^3 - p_b b^3)}{(b^3 - a^3)} - \frac{(p_a - p_b)b^3 a^3}{(b^3 - a^3)R^3} \quad \sigma_{\theta\theta} = \sigma_{\phi\phi} = \frac{(p_a a^3 - p_b b^3)}{(b^3 - a^3)} + \frac{(p_a - p_b)b^3 a^3}{2(b^3 - a^3)R^3}.$$

Derivation: The solution can be found by applying the procedure outlined in Section 4.1.3.

1. Note that the governing equation for u (Section 4.1.3) reduces to

$$\frac{d}{dR} \left\{ \frac{1}{R^2} \frac{d}{dR} (R^2 u) \right\} = 0.$$

2. Integrating twice gives

$$u = AR + \frac{B}{R^2},$$

where A and B are constants of integration to be determined.

3. The radial stress follows by substituting into the stress-displacement formulas

$$\sigma_{RR} = \frac{E}{(1+\nu)(1-2\nu)} \left\{ (1-\nu) \frac{du}{dR} + 2\nu \frac{u}{R} \right\} = \frac{E}{(1+\nu)(1-2\nu)} \left\{ (1+\nu)A - 2(1-2\nu) \frac{B}{R^3} \right\}.$$

4. To satisfy the boundary conditions, A and B must be chosen so that $\sigma_{RR}(R = a) = -p_a$ and $\sigma_{RR}(R = b) = -p_b$ (the stress is negative because the pressure is compressive). This gives two equations for A and B that are easily solved to find

$$A = \frac{(p_b b^3 - p_a a^3)(1-2\nu)}{(a^3 - b^3)E} \quad B = \frac{(p_b - p_a)(1+\nu)b^3 a^3}{2(a^3 - b^3)E}.$$

5. Finally, expressions for displacement, strain, and stress follow by substituting for A and B in the formula for u in item 2 and using the formulas for strain and stress in terms of u in Section 4.1.2.

4.1.5 Gravitating Sphere

A planet under its own gravitational attraction may be idealized (rather crudely) as a solid sphere with radius a , illustrated in Figure 4.4. The solid is subjected to the following loading:

- A body force $\mathbf{b} = -(gR/a)\mathbf{e}_R$ per unit mass, where g is the acceleration attributable to gravity at the surface of the sphere
- A uniform temperature distribution
- A traction-free surface at $R=a$

The displacement, strain, and stress in the sphere follow as

$$\begin{aligned}\mathbf{u} &= \frac{(1-2\nu)}{10aE(1-\nu)}\rho_0gR\{(1+\nu)R^2 - (3-\nu)a^2\}\mathbf{e}_R \\ \varepsilon_{RR} &= \frac{(1-2\nu)}{10aE(1-\nu)}\rho_0g\{3(1+\nu)R^2 - (3-\nu)a^2\} \\ \varepsilon_{\theta\theta} = \varepsilon_{\phi\phi} &= \frac{(1-2\nu)}{10aE(1-\nu)}\rho_0g\{(1+\nu)R^2 - (3-\nu)a^2\} \\ \sigma_{RR} &= \frac{\rho_0g(3-\nu)}{10a(1-\nu)}(R^2 - a^2) \quad \sigma_{\theta\theta} = \sigma_{\phi\phi} = \frac{\rho_0g}{10a(1-\nu)}\{(3\nu+1)R^2 - (3-\nu)a^2\}.\end{aligned}$$

Derivation

1. Begin by writing the governing equation for u given in Section 4.1.3 as

$$\frac{d}{dR}\left\{\frac{1}{R^2}\frac{d}{dR}(R^2u)\right\} = \frac{(1+\nu)(1-2\nu)}{E(1-\nu)}\frac{\rho_0gR}{a}.$$

2. Integrate

$$u = \frac{(1+\nu)(1-2\nu)}{E(1-\nu)}\frac{\rho_0gR^3}{10a} + AR + \frac{B}{R^2},$$

where A and B are constants of integration that must be determined from boundary conditions.

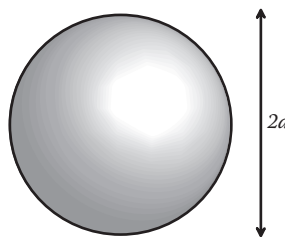


FIGURE 4.4 Spherical planet deforming under its own gravitational field.

3. The radial stress follows from the formulas in Section 4.1.3 as

$$\begin{aligned}\sigma_{RR} &= \frac{E}{(1+\nu)(1-2\nu)} \left\{ (1-\nu) \frac{du}{dR} + 2\nu \frac{u}{R} \right\} \\ &= \frac{\rho_0 g (3-\nu) R^2}{10a(1-\nu)} + \frac{E}{(1+\nu)(1-2\nu)} \left\{ (1+\nu) A - 2(1-2\nu) \frac{B}{R^3} \right\}.\end{aligned}$$

4. Finally, the constants A and B can be determined as follows: (1) the stress must be finite at $R \rightarrow 0$, which is only possible if $B = 0$; (2) the surface of the sphere is traction free, which requires $\sigma_{RR} = 0$ at $R = a$. Substituting the latter condition into the formula for stress in item 3 and solving for A gives

$$A = -\frac{(1-2\nu)(3-\nu)\rho_0 ga}{10E(1-\nu)}.$$

5. The final formulas for stress and strain follow by substituting the result of item 4 back into item 2 and using the formulas in Section 4.1.2.

4.1.6 Sphere with Steady-State Heat Flow

The deformation and stress in a sphere that is heated on the inside (or outside) and has reached its steady-state temperature distribution can be calculated as follows. A hollow sphere is shown in Figure 4.5. Assume the following:

- No body force acts on the sphere.
- The temperature distribution in the sphere is

$$T = \frac{T_b b - T_a a}{b - a} + \frac{(T_a - T_b)ab}{(b - a)R},$$

where T_a and T_b are the temperatures at the inner and outer surfaces. The total rate of heat loss from the sphere is $\dot{Q} = 4\pi k(T_a - T_b)ab/(b - a)$, where k is the thermal conductivity.

- The surfaces at $R = a$ and $R = b$ are traction free.

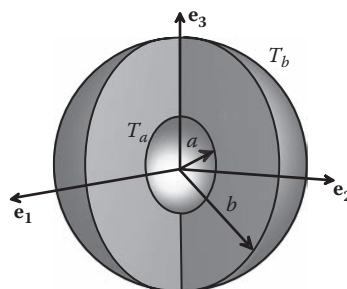


FIGURE 4.5 Spherical shell with prescribed internal and external temperatures.

The displacement, strain, and stress fields in the sphere follow as

$$\begin{aligned}
 u &= \frac{\alpha}{(1-\nu)} \frac{(T_a - T_b)a}{2(b^3 - a^3)} \left\{ (1+\nu)b(a^2 + ab + b^2) + 2(va^2 - a^2 - vab - vb^2)R - (1+\nu)\frac{a^2b^3}{R^2} \right\} + T_b\alpha R \\
 \varepsilon_{RR} &= \frac{\alpha}{(1-\nu)} \frac{(T_a - T_b)a}{2(b^3 - a^3)} \left\{ (va^2 - a^2 - vab - vb^2) + (1+\nu)\frac{a^2b^3}{R^3} \right\} + T_b\alpha \\
 \varepsilon_{\theta\theta} = \varepsilon_{\phi\phi} &= \frac{\alpha}{(1-\nu)} \frac{(T_a - T_b)a}{2(b^3 - a^3)R} \left\{ (1+\nu)b(a^2 + ab + b^2) + 2(va^2 - a^2 - vab - vb^2)R - (1+\nu)\frac{a^2b^3}{R^2} \right\} + T_b\alpha \\
 \sigma_{RR} &= \frac{E\alpha\nu}{(1-\nu)} \frac{(T_a - T_b)ab}{(b^3 - a^3)} (R - a)(R - b)(Ra + Rb + ab) \\
 \sigma_{\theta\theta} = \sigma_{\phi\phi} &= \frac{E\alpha}{2(1-\nu)} \frac{(T_a - T_b)ab}{(b^3 - a^3)} \left\{ 2(a + b) - \frac{a^2 + ab + b^2}{R} - \frac{a^2b^2}{R^3} \right\}.
 \end{aligned}$$

Derivation

1. The differential equation for u given in Section 4.1.3 reduces to

$$\frac{d}{dR} \left\{ \frac{1}{R^2} \frac{d}{dR} (R^2 u) \right\} = -\frac{\alpha(1+\nu)(T_a - T_b)ab}{(1-\nu)(b-a)R^2}.$$

2. Integrate

$$u = \frac{\alpha(1+\nu)(T_a - T_b)ab}{2(1-\nu)(b-a)} + AR + \frac{B}{R^2},$$

where A and B are constants of integration.

3. The radial stress follows from the formulas in Section 4.1.3 as

$$\begin{aligned}
 \sigma_{RR} &= \frac{E}{(1+\nu)(1-2\nu)} \left\{ (1-\nu) \frac{du}{dR} + 2\nu \frac{u}{R} \right\} - \frac{E\alpha\Delta T}{1-2\nu} \\
 &= \frac{E\nu\alpha}{(1-2\nu)(1-\nu)} \frac{(T_a - T_b)ab}{(b-a)R} + \frac{E}{(1+\nu)(1-2\nu)} \left\{ (1+\nu)A - 2(1-2\nu) \frac{B}{R^3} \right\} \\
 &\quad - \frac{E\alpha}{1-2\nu} \left\{ \frac{T_b b - T_a a}{b-a} + \frac{(T_a - T_b)ab}{(b-a)R} \right\}.
 \end{aligned}$$

4. The boundary conditions require that $\sigma_{RR} = 0$ at $R = a$ and $R = b$. Substituting these conditions into the result of step 3 gives two equations for A and B that can be solved to see that

$$A = \frac{(1-v)(T_b b^3 - T_a a^3) + (T_a - T_b)vab(a+b)}{(1-v)(a^3 - b^3)} \quad B = \frac{\alpha(T_a - T_b)(1+v)}{2(1-v)} \frac{a^3 b^3}{(b^3 - a^3)}.$$

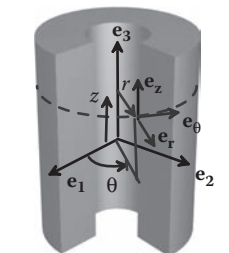
4.1.7 Simplified Equations for Axially Symmetric Linear Elasticity Problems

Two examples of axially symmetric problems are illustrated in Figure 4.6. In both cases, the solid is a circular cylinder that is subjected to axially symmetric loading (i.e., internal body forces, as well as tractions or displacements applied to the surface, are independent of θ and z and act in the radial direction only). If the temperature of the sphere is nonuniform, it must also be axially symmetric (a function of r only). Finally, the solid can spin with steady angular velocity about the e_3 axis.

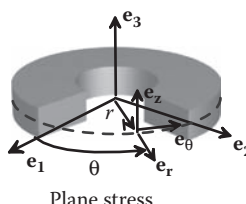
The two solids have different shapes. In the first case, the length of the cylinder is substantially greater than any cross-sectional dimension. In the second case, the length of the cylinder is much less than its outer radius.

The state of stress and strain in the cylinder depends on the loads applied to the ends of the cylinder. Specifically,

- If the cylinder is completely prevented from stretching in the e_3 direction, a state of plane strain exists in the solid. This is an exact solution to the 3D equations of elasticity, is valid for a cylinder with any length, and is accurate everywhere in the cylinder.



Plane strain, or
generalized plane strain



Plane stress

FIGURE 4.6 Coordinate system used for cylindrically symmetric problems.

- If the top and bottom surface of the short plate-like cylinder are free of traction, a state of plane stress exists in the solid. This is an approximate solution to the 3D equations of elasticity and is accurate only if the cylinder's length is much less than its diameter.
- If the top and bottom ends of the long cylinder are subjected to a prescribed force (or the ends are free of force), a state of *generalized plane strain* exists in the cylinder. This is an approximate solution that is accurate only away from the ends of a long cylinder. As a rule of thumb, the solution is applicable approximately three cylinder radii away from the ends.

The solution is most conveniently expressed using a cylindrical-polar coordinate system, illustrated in Figure 4.6. A point in the solid is identified by its spherical-polar coordinates (r, θ, z) . All vectors and tensors are expressed as components in the basis $\{\mathbf{e}_r, \mathbf{e}_\theta, \mathbf{e}_z\}$ shown in the figure. For an axially symmetric problem,

- Position vector: $\mathbf{x} = r\mathbf{e}_r + z\mathbf{e}_z$
- Displacement vector: $\mathbf{u} = u(r)\mathbf{e}_r + \varepsilon_{zz} z\mathbf{e}_z$
- Body force vector: $\mathbf{b} = \rho_0 b(r)\mathbf{e}_r$
- Acceleration vector: $\mathbf{a} = -\omega^2 r\mathbf{e}_r$

Here, $u(r)$ and $b(r)$ are scalar functions.

The stress and strain tensors (written as components in $\{\mathbf{e}_r, \mathbf{e}_\theta, \mathbf{e}_z\}$) have the form

$$\boldsymbol{\sigma} \equiv \begin{bmatrix} \sigma_{rr} & 0 & 0 \\ 0 & \sigma_{\theta\theta} & 0 \\ 0 & 0 & \sigma_{zz} \end{bmatrix} \quad \boldsymbol{\varepsilon} \equiv \begin{bmatrix} \varepsilon_{rr} & 0 & 0 \\ 0 & \varepsilon_{\theta\theta} & 0 \\ 0 & 0 & \varepsilon_{zz} \end{bmatrix}.$$

For axial symmetry, the governing equations of linear elasticity reduce to the following:

- Strain displacement relations: $\varepsilon_{rr} = \frac{du}{dr}$, $\varepsilon_{\theta\theta} = \frac{u}{r}$.
- Stress-strain relations (plane strain and generalized plane strain):

$$\begin{bmatrix} \sigma_{rr} \\ \sigma_{\theta\theta} \\ \sigma_{zz} \end{bmatrix} = \frac{E}{(1+\nu)(1-2\nu)} \begin{bmatrix} 1-\nu & \nu & \nu \\ \nu & 1-\nu & \nu \\ \nu & \nu & 1-\nu \end{bmatrix} \begin{bmatrix} \varepsilon_{rr} \\ \varepsilon_{\theta\theta} \\ \varepsilon_{zz} \end{bmatrix} - \frac{E\alpha\Delta T}{1-2\nu} \begin{bmatrix} 1 \\ 1 \\ 1 \end{bmatrix},$$

where $\varepsilon_{zz} = 0$ for plane strain and constant for generalized plane strain.

- Stress-strain relations (plane stress):

$$\begin{bmatrix} \sigma_{rr} \\ \sigma_{\theta\theta} \end{bmatrix} = \frac{E}{1-\nu^2} \begin{bmatrix} 1 & \nu \\ \nu & 1 \end{bmatrix} \begin{bmatrix} \epsilon_{rr} \\ \epsilon_{\theta\theta} \end{bmatrix} - \frac{E\alpha\Delta T}{1-\nu} \begin{bmatrix} 1 \\ 1 \end{bmatrix}$$

$$\sigma_{zz} = 0 \quad \epsilon_{zz} = \frac{\nu}{E}(\sigma_{rr} + \sigma_{\theta\theta}) + \alpha\Delta T.$$

- Equation of motion:

$$\frac{d\sigma_{rr}}{dr} + \frac{1}{r}(\sigma_{rr} - \sigma_{\theta\theta}) + \rho_0 b = -\rho_0 \omega^2 r.$$

- Boundary conditions:

prescribed displacements, $u_r(a) = g_a \quad u_r(b) = g_b$;

prescribed tractions, $\sigma_{rr}(a) = t_a \quad \sigma_{rr}(b) = t_b$;

plane strain solution, $\epsilon_{zz} = 0$;

generalized plane strain solution, with axial force F_z applied to cylinder,

$$\int_a^b 2\pi r \sigma_{zz} dr = F_z.$$

These results can either be derived as a special case of the general 3D equations of linear elasticity in spherical coordinates or alternatively can be obtained directly from the formulas in Cartesian components. Here, we briefly outline the latter.

1. Note that we can find the components of $\{\mathbf{e}_r, \mathbf{e}_\theta, \mathbf{e}_z\}$ in the $\{\mathbf{e}_1, \mathbf{e}_2, \mathbf{e}_3\}$ basis as follows. First, note that \mathbf{e}_r is radial; a radial unit vector can be written in terms of the position vector as $\mathbf{x}/|\mathbf{x}|$. Next, note $\mathbf{e}_\theta = \mathbf{e}_3 \times \mathbf{e}_r$ and $\mathbf{e}_z = \mathbf{e}_3$. Using index notation, the components of the basis vectors $\{\mathbf{e}_r, \mathbf{e}_\theta, \mathbf{e}_z\}$ in $\{\mathbf{e}_1, \mathbf{e}_2, \mathbf{e}_3\}$ are therefore

$$\left\{ \frac{x_\alpha}{r}, \epsilon_{i3\alpha} \frac{x_\alpha}{r}, \delta_{i3} \right\},$$

where $r = \sqrt{x_\alpha x_\alpha} = \sqrt{x_1^2 + x_2^2}$, and we use the convention that Greek subscripts range from 1 to 2.

2. The components of the (radial) displacement vector in the $\{\mathbf{e}_1, \mathbf{e}_2, \mathbf{e}_3\}$ basis are $u_\alpha = u(r)x_\alpha/r$.
3. To proceed with the algebra, it is helpful to remember that $\partial x_\alpha / \partial x_\beta = \delta_{\alpha\beta}$, $\partial r / \partial x_\alpha = x_\alpha / r$, and $\partial r^{-1} / \partial x_\alpha = -x_\alpha / r^3$.
4. The components of the strain tensor in the $\{\mathbf{e}_1, \mathbf{e}_2, \mathbf{e}_3\}$ basis therefore follow as

$$\epsilon_{\alpha\beta} = \frac{1}{2} \left(\frac{\partial u_\alpha}{\partial x_\beta} + \frac{\partial u_\beta}{\partial x_\alpha} \right) = \frac{du}{dr} \frac{x_\alpha x_\beta}{r^2} + u(r) \left(\frac{\delta_{\alpha\beta}}{r} - \frac{x_\alpha x_\beta}{r^3} \right) \quad \epsilon_{zz} = \epsilon_{33}.$$

5. The strain components ε_{rr} , $\varepsilon_{\theta\theta}$, ε_{zz} can then be found as $\varepsilon_{rr} = \mathbf{e}_r \cdot \boldsymbol{\varepsilon} \cdot \mathbf{e}_r$, $\varepsilon_{\theta\theta} = \mathbf{e}_\theta \cdot \boldsymbol{\varepsilon} \cdot \mathbf{e}_\theta$, and $\varepsilon_{zz} = \mathbf{e}_z \cdot \boldsymbol{\varepsilon} \cdot \mathbf{e}_z$. Substituting for the basis vectors and simplifying gives the strain-displacement relations. For example,

$$\varepsilon_{rr} = \varepsilon_{\alpha\beta} \frac{x_\alpha x_\beta}{r^2} = \frac{du}{dr} \frac{x_\alpha x_\alpha x_\beta x_\beta}{r^4} + u(r) \left(\frac{\delta_{\alpha\beta}}{r} \frac{x_\alpha x_\beta}{r^2} - \frac{x_\alpha x_\alpha x_\beta x_\beta}{r^5} \right) = \frac{du}{dr},$$

where we have noted $x_\alpha x_\alpha = r^2$. The remaining components are left as an exercise.

6. Finally, to derive the equilibrium equation, note that the stress tensor can be expressed as $\sigma = \sigma_{rr} \mathbf{e}_r \otimes \mathbf{e}_r + \sigma_{\theta\theta} \mathbf{e}_\theta \otimes \mathbf{e}_\theta + \sigma_{zz} \mathbf{e}_z \otimes \mathbf{e}_z$. Substituting for the basis vectors from item 1 above gives

$$\sigma_{\alpha\beta} = \sigma_{rr} \frac{x_\alpha x_\beta}{r^2} + \sigma_{\theta\theta} \epsilon_{\alpha 3\gamma} \frac{x_\gamma}{r} \epsilon_{\beta 3\kappa} \frac{x_\kappa}{r} \quad \sigma_{zz} = \sigma_{33}.$$

7. Substitute the preceding result into the equilibrium equation

$$\frac{\partial \sigma_{ij}}{\partial x_i} + \rho_0 b(r) \frac{x_j}{r} = 0$$

and crank through a good deal of tedious algebra to see that

$$\left(\frac{d\sigma_{rr}}{dr} + \frac{1}{r} (\sigma_{rr} - \sigma_{\theta\theta}) + \rho_0 b(r) \right) \frac{x_\alpha}{r} = 0.$$

4.1.8 General Solution to the Axisymmetric Boundary Value Problem

Our goal is to solve the equations given in Section 4.1.2 for the displacement, strain, and stress in the sphere. To do so, perform the following:

1. Substitute the strain-displacement relations into the stress-strain law to show that, for generalized plane strain,

$$\begin{bmatrix} \sigma_{rr} \\ \sigma_{\theta\theta} \\ \sigma_{zz} \end{bmatrix} = \frac{E}{(1+v)(1-2v)} \begin{bmatrix} 1-v & v & v \\ v & 1-v & v \\ v & v & 1-v \end{bmatrix} \begin{bmatrix} \frac{du}{dr} \\ \frac{u}{r} \\ \varepsilon_{zz} \end{bmatrix} - \frac{E\alpha\Delta T}{1-2v} \begin{bmatrix} 1 \\ 1 \\ 1 \end{bmatrix},$$

where ε_{zz} is constant. The equivalent expression for plane stress is

$$\begin{bmatrix} \sigma_{rr} \\ \sigma_{\theta\theta} \end{bmatrix} = \frac{E}{1-v^2} \begin{bmatrix} 1 & v \\ v & 1 \end{bmatrix} \begin{bmatrix} \frac{du}{dr} \\ \frac{u}{r} \end{bmatrix} - \frac{E\alpha\Delta T}{1-v} \begin{bmatrix} 1 \\ 1 \end{bmatrix}.$$

2. Substitute these expressions for the stress into the equilibrium equation and rearrange the result to see that, for generalized plane strain,

$$\frac{\partial^2 u}{\partial r^2} + \frac{1}{r} \frac{\partial u}{\partial r} - \frac{u}{r^2} = \frac{\partial}{\partial r} \left\{ \frac{1}{r} \frac{\partial}{\partial r} (ru) \right\} = \frac{\alpha(1+\nu)}{(1-\nu)} \frac{\partial \Delta T}{\partial r} - \frac{(1+\nu)(1-2\nu)}{E(1-\nu)} \rho_0 (b + \omega^2 r),$$

whereas for plane stress,

$$\frac{\partial^2 u}{\partial r^2} + \frac{1}{r} \frac{\partial u}{\partial r} - \frac{u}{r^2} = \frac{\partial}{\partial r} \left\{ \frac{1}{r} \frac{\partial}{\partial r} (ru) \right\} = \alpha(1+\nu) \frac{\partial \Delta T}{\partial r} - \frac{(1-\nu^2)}{E} \rho_0 (b + \omega^2 r).$$

Given the temperature distribution and body force, these equations can be integrated to calculate the displacement u . Two arbitrary constants of integration will appear when you do the integral; these must be determined from the boundary conditions at the inner and outer surface of the cylinder. Specifically, the constants must be selected so that either the displacement or the radial stress have prescribed values on the inner and outer surface of the sphere. Finally, for the generalized plane strain solution, the axial strain ε_{zz} must be determined, using the equation for the axial force acting on the ends of the cylinder.

In the following sections, this procedure is used to derive solutions to various boundary value problems of practical interest.

4.1.9 Long (Generalized Plane Strain) Cylinder Subjected to Internal and External Pressure

We consider a long hollow cylinder with internal radius a and external radius b as shown in Figure 4.7. Assume the following:

- No body forces act on the cylinder.
- The cylinder has zero angular velocity.
- The cylinder has uniform temperature.

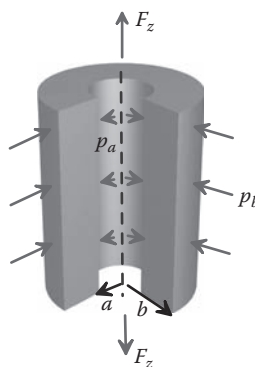


FIGURE 4.7 Cylindrical shell subjected to internal and external pressure and axial forces.

- The inner surface $r = a$ is subjected to pressure p_a .
- The outer surface $r = b$ is subjected to pressure p_b .
- For the plane strain solution, the cylinder does not stretch parallel to its axis. For the generalized plane strain solution, the ends of the cylinder are subjected to an axial force F_z as shown. In particular, for a *closed-ended* cylinder, the axial force exerted by the pressure inside the cylinder acting on the closed ends is $F_z = \pi(p_a a^2 - p_b b^2)$.

The displacement, strain, and stress fields in the cylinder are

$$\begin{aligned}\mathbf{u} &= \frac{(1+\nu)a^2b^2}{E(b^2-a^2)} \left\{ \frac{(p_a-p_b)}{r} + (1-2\nu) \frac{(p_a a^2 - p_b b^2)}{a^2 b^2} r \right\} \mathbf{e}_r - \nu \epsilon_{zz} r \mathbf{e}_r + \epsilon_{zz} z \mathbf{e}_z \\ \epsilon_{rr} &= \frac{(1+\nu)a^2b^2}{E(b^2-a^2)} \left\{ -\frac{(p_a-p_b)}{r^2} + (1-2\nu) \frac{(p_a a^2 - p_b b^2)}{a^2 b^2} \right\} - \nu \epsilon_{zz} \\ \epsilon_{\theta\theta} &= \frac{(1+\nu)a^2b^2}{E(b^2-a^2)} \left\{ \frac{(p_a-p_b)}{r^2} + (1-2\nu) \frac{(p_a a^2 - p_b b^2)}{a^2 b^2} \right\} - \nu \epsilon_{zz} \\ \sigma_{rr} &= \left\{ \frac{(p_a a^2 - p_b b^2)}{b^2 - a^2} - \frac{a^2 b^2}{(b^2 - a^2) r^2} (p_a - p_b) \right\} \\ \sigma_{\theta\theta} &= \left\{ \frac{(p_a a^2 - p_b b^2)}{b^2 - a^2} + \frac{a^2 b^2}{(b^2 - a^2) r^2} (p_a - p_b) \right\} \\ \sigma_{zz} &= 2\nu \frac{(p_a a^2 - p_b b^2)}{b^2 - a^2} + E \epsilon_{zz},\end{aligned}$$

where $\epsilon_{zz} = 0$ for plane strain, whereas

$$\epsilon_{zz} = \frac{F_z}{\pi E(b^2 - a^2)} - \frac{2\nu}{E} \frac{(p_a a^2 - p_b b^2)}{(b^2 - a^2)}$$

for generalized plane strain.

Derivation: These results can be derived as follows. The governing equation reduces to

$$\frac{\partial^2 u}{\partial r^2} + \frac{1}{r} \frac{\partial u}{\partial r} - \frac{u}{r^2} = \frac{\partial}{\partial r} \left\{ \frac{1}{r} \frac{\partial}{\partial r} (ru) \right\} = 0.$$

The equation can be integrated to see that

$$u = Ar + \frac{B}{r}.$$

The radial stress follows as

$$\sigma_{rr} = \frac{E}{(1+\nu)(1-2\nu)} \left\{ (1-\nu) \frac{\partial u}{\partial r} + \nu \frac{u}{r} \right\} = \frac{E}{(1+\nu)(1-2\nu)} \left\{ A - (1-2\nu) \frac{B}{r^2} \right\}.$$

The boundary conditions are $\sigma_{rr}(r=a) = -p_a$ $\sigma_{rr}(r=b) = -p_b$ (the stresses are negative because the pressure is compressive). This yields two equations for A and B that are easily solved to see that

$$A = \frac{(1+\nu)(1-2\nu)}{E} \frac{(p_a a^2 - p_b b^2)}{b^2 - a^2} \quad B = \frac{(1+\nu)}{E} \frac{a^2 b^2}{b^2 - a^2} (p_a - p_b).$$

The remaining results follow by elementary algebraic manipulations.

4.1.10 Spinning Circular Plate

We consider a thin solid plate with radius a that spins with angular speed ω about its axis, as shown in Figure 4.8. Assume the following:

- No body forces act on the disk.
- The disk has constant angular velocity.
- The disk has uniform temperature.
- The outer surface $r = a$ and the top and bottom faces of the disk are free of traction.
- The disk is sufficiently thin to ensure a state of plane stress in the disk.

$$\mathbf{u} = (1-\nu) \frac{\rho_0 \omega^2}{8E} \left\{ (3+\nu)a^2 r - (1+\nu)r^3 \right\} \mathbf{e}_r + z \boldsymbol{\varepsilon}_{zz} \mathbf{e}_z$$

$$\boldsymbol{\varepsilon}_{rr} = (1-\nu) \frac{\rho_0 \omega^2}{8E} \left\{ (3+\nu)a^2 - 3(1+\nu)r^2 \right\} \quad \boldsymbol{\varepsilon}_{\theta\theta} = (1-\nu) \frac{\rho_0 \omega^2}{8E} \left\{ (3+\nu)a^2 - (1+\nu)r^2 \right\}$$

$$\boldsymbol{\varepsilon}_{zz} = -\nu \frac{\rho_0 \omega^2}{8E} \left\{ 2(3+\nu)a^2 - (3\nu+2)r^2 \right\}$$

$$\sigma_{rr} = (3+\nu) \frac{\rho_0 \omega^2}{8} \left\{ a^2 - r^2 \right\}$$

$$\sigma_{\theta\theta} = \frac{\rho_0 \omega^2}{8} \left\{ (3+\nu)a^2 - (3\nu+1)r^2 \right\}.$$

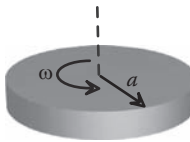


FIGURE 4.8 Thin disk spinning about its axis.

Derivation: To derive these results, recall that the governing equation is

$$\frac{\partial^2 u}{\partial r^2} + \frac{1}{r} \frac{\partial u}{\partial r} - \frac{u}{r^2} = \frac{\partial}{\partial r} \left\{ \frac{1}{r} \frac{\partial}{\partial r} (ru) \right\} = - \frac{(1-\nu^2)}{E} \rho_0 \omega^2 r.$$

The equation can be integrated to see that

$$u = Ar + \frac{B}{r} - \frac{(1-\nu^2)}{8E} \rho_0 \omega^2 r^3.$$

The radial stress follows as

$$\sigma_{rr} = \frac{E}{1-\nu^2} \left(\frac{du}{dr} + \nu \frac{u}{r} \right) = \frac{E}{1-\nu^2} \left\{ (1+\nu)A - (1-\nu) \frac{B}{r^2} - \frac{(1-\nu^2)\rho_0\omega^2}{8E} (3+\nu)r^2 \right\}.$$

The radial stress must be bounded at $r = 0$, which is only possible if $B = 0$. In addition, the radial stress must be zero at $r = a$, which requires that

$$A = \frac{\rho_0 \omega^2}{8E} \frac{(3+\nu)}{(1+\nu)} a^2.$$

The remaining results follow by straightforward algebra.

4.1.11 Stresses Induced by an Interference Fit between Two Cylinders

Interference fits are often used to secure a bushing or a bearing housing to a shaft. In this problem, we calculate the stress induced by such an interference fit.

Consider a hollow cylindrical bushing, with outer radius b and inner radius a . Suppose that a solid shaft with radius $a + \Delta$, with $\Delta/a \ll 1$, is inserted into the cylinder as shown in Figure 4.9 (in practice, this is done by heating the cylinder or cooling the shaft until they fit and then letting the system return to thermal equilibrium). Assume that

- No body forces act on the solids.
- The angular velocity is zero.
- The cylinders have uniform temperature.
- The shaft slides freely inside the bushing.
- The ends of the cylinder are free of force.

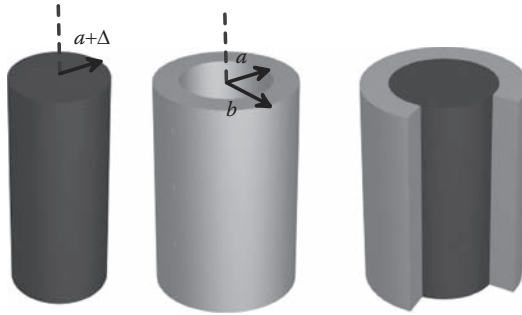


FIGURE 4.9 Interference fit between a solid shaft and a hollow cylinder.

- Both the shaft and cylinder have the same Young's modulus E and Poisson's ratio ν .
- The cylinder and shaft are sufficiently long to ensure that a state of generalized plane strain can be developed in each solid.

The displacements, strains, and stresses in the solid shaft ($r < a$) are

$$\mathbf{u} = -\frac{(1+\nu)(1-2\nu)\Delta(b^2-a^2)}{2ab^2}r\mathbf{e}_r - 2\nu^2 \frac{\Delta(b^2-a^2)}{2ab^2}r\mathbf{e}_r + 2\nu \frac{\Delta(b^2-a^2)}{2ab^2}z\mathbf{e}_z$$

$$\varepsilon_{rr} = \varepsilon_{\theta\theta} = -\frac{(1+\nu)(1-2\nu)\Delta(b^2-a^2)}{2ab^2} - 2\nu^2 \frac{\Delta(b^2-a^2)}{2ab^2}$$

$$\sigma_{rr} = \sigma_{\theta\theta} = -\frac{E\Delta(b^2-a^2)}{2ab^2} \quad \sigma_{zz} = 0.$$

In the hollow cylinder, they are

$$\mathbf{u} = \frac{(1+\nu)a\Delta}{r} \left\{ 1 + (1-2\nu) \frac{r^2}{b^2} \right\} \mathbf{e}_r - \nu^2 \frac{\Delta a}{b^2} r \mathbf{e}_r + 2\nu^2 \frac{\Delta a}{b^2} z \mathbf{e}_z$$

$$\varepsilon_{rr} = \frac{(1+\nu)a\Delta}{r^2} \left\{ -1 + (1-2\nu) \frac{r^2}{b^2} \right\} - \nu^2 \frac{\Delta a}{b^2}$$

$$\varepsilon_{\theta\theta} = \frac{(1+\nu)a\Delta}{r^2} \left\{ 1 + (1-2\nu) \frac{r^2}{b^2} \right\} - \nu^2 \frac{\Delta a}{b^2}$$

$$\sigma_{rr} = \frac{E\Delta a}{2b^2} \left\{ 1 - \frac{b^2}{r^2} \right\} \quad \sigma_{\theta\theta} = \frac{E\Delta a}{2b^2} \left\{ 1 + \frac{b^2}{r^2} \right\} \quad \sigma_{zz} = 0.$$

Derivation: These results can be derived using the solution to a pressurized cylinder given in Section 4.1.9. After the shaft is inserted into the tube, a pressure p acts to compress the shaft, and the same pressure pushes outward to expand the cylinder. Suppose that this pressure induces a radial displacement $u^s(r)$ in the solid cylinder and a radial displacement $u^c(r)$ in the hollow tube. To accommodate the interference, the displacements must satisfy

$$u^c(r=a) - u^s(r=a) = \Delta.$$

Evaluating the relevant displacements using the formulas in Section 4.1.9 gives

$$\begin{aligned} u^s(r=a) &= -\frac{(1-2\nu)(1+\nu)}{E}pa - \frac{2\nu^2}{E}pa \\ u^c(r=a) &= \frac{(1+\nu)a^2b^2}{E(b^2-a^2)} \left\{ \frac{p}{a} + (1-2\nu)\frac{pa}{b^2} \right\} + \frac{2\nu^2pa^3}{E(b^2-a^2)}. \end{aligned}$$

Here, we have assumed that the axial force acting on both the shaft and the tube must vanish separately, because they slide freely relative to one another. Solving these two equations for p shows that

$$p = \frac{E\Delta(b^2 - a^2)}{2ab^2}.$$

This pressure can then be substituted back into the formulas in Section 4.1.9 to evaluate the stresses.

4.2 AXIALLY AND SPHERICALLY SYMMETRIC SOLUTIONS TO QUASI-STATIC ELASTIC-PLASTIC PROBLEMS

In this section, we derive exact solutions to simple boundary value problems involving elastic-perfectly plastic solids. The solutions are of interest primarily because they illustrate important general features of solids that are loaded beyond yield. In particular, they illustrate the following concepts:

1. The elastic limit: This is the load required to initiate plastic flow in the solid.
2. The plastic collapse load: At this load, the displacements in the solid become infinite.
3. Residual stress: If a solid is loaded beyond the elastic limit and then unloaded, a system of self-equilibrated stress is established in the material.
4. Shakedown: If an elastic-plastic solid is subjected to cyclic loading and the maximum load during the cycle exceeds yield, then some plastic deformation must occur in the material during the first load cycle. However, residual stresses are introduced in the solid, which may prevent plastic flow during subsequent cycles of load. This process is

known as “shakedown,” and the maximum load for which it can occur is known as the “shakedown limit.” The shakedown limit is often substantially higher than the elastic limit, so the concept of shakedown can often be used to reduce the weight of a design.

5. Cyclic plasticity: For cyclic loads exceeding the shakedown limit, a region in the solid will be repeatedly plastically deformed.

4.2.1 Summary of Governing Equations

A representative problem is sketched in Figure 4.10. We are given the following information:

1. The geometry of the solid
2. Constitutive law for the material (i.e., the elastic-plastic stress-strain equations)
3. Body force density b_i (per unit mass) (if any)
4. Temperature distribution ΔT (if any)
5. Prescribed boundary tractions t_i and/or boundary displacements u_i

In addition, to simplify the problem, we make the following assumptions:

1. All displacements are small. This means that we can use the infinitesimal strain tensor to characterize deformation; we do not need to distinguish between stress measures, and we do not need to distinguish between deformed and undeformed configurations of the solid when writing equilibrium equations and boundary conditions.
2. The material is an isotropic, elastic-perfectly plastic solid, with Young's modulus E , Poisson's ratio ν , yield stress Y , and mass density ρ_0 .
3. We will neglect temperature changes.

With these assumptions, we need to solve for the displacement field u_i , the strain field ε_{ij} , and the stress field σ_{ij} satisfying the following equations:

- Displacement-strain relation:

$$\varepsilon_{ij} = \frac{1}{2} \left(\frac{\partial u_i}{\partial x_j} + \frac{\partial u_j}{\partial x_i} \right).$$

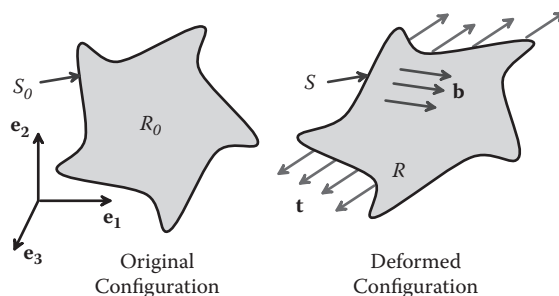


FIGURE 4.10 Typical boundary value problem for an elastic-plastic solid.

- Incremental stress-strain relation:

$$d\epsilon_{ij} = d\epsilon_{ij}^e + d\epsilon_{ij}^p$$

$$d\epsilon_{ij}^e = \frac{1+\nu}{E} \left(d\sigma_{ij} - \frac{\nu}{1+\nu} d\sigma_{kk} \delta_{ij} \right)$$

$$d\epsilon_{ij}^p = \begin{cases} 0 & \sqrt{\frac{3}{2} S_{ij} S_{ij}} < Y \\ d\bar{\epsilon}^p \frac{3 S_{ij}}{2 Y} & \sqrt{\frac{3}{2} S_{ij} S_{ij}} = Y \end{cases},$$

where $S_{ij} = \sigma_{ij} - \sigma_{kk} \delta_{ij} / 3$.

- Equilibrium equation: $\frac{\partial \sigma_{ij}}{\partial x_i} + \rho_0 b_j = 0$ (static problems only; you need the acceleration terms for dynamic problems).
- Traction boundary conditions: $\sigma_{ij} n_i = t_j$ on parts of the boundary where tractions are known.
- Displacement boundary conditions: $u_i = d_i$ on parts of the boundary where displacements are known.

4.2.2 Simplified Equations for Spherically Symmetric Problems

A representative spherically symmetric problem is illustrated in Figure 4.11. We consider a hollow, spherical solid that is subjected to spherically symmetric loading (i.e., internal body forces, as well as tractions or displacements applied to the surface, are independent of θ and ϕ and act in the radial direction only). If the temperature of the sphere is nonuniform, it must also be spherically symmetric (a function of r only).

The solution is most conveniently expressed using a spherical-polar coordinate system, illustrated in Figure 4.11. The general procedure for solving problems with spherical and cylindrical coordinates is complicated and is discussed in detail in Chapter 10 in the context

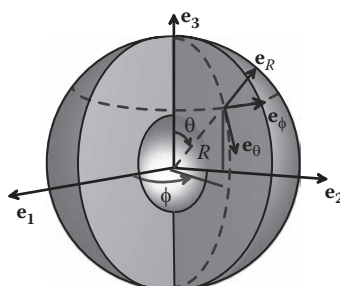


FIGURE 4.11 Coordinate system used for spherically symmetric problems.

of modeling deformation in shells. In this section, we summarize the special form of these equations for spherically symmetric problems.

As usual, a point in the solid is identified by its spherical-polar coordinates (r, θ, ϕ) . All vectors and tensors are expressed as components in the Cartesian basis $\{\mathbf{e}_r, \mathbf{e}_\theta, \mathbf{e}_\phi\}$ shown in the figure. For a spherically symmetric problem, we have the following:

- Position vector: $\mathbf{x} = r\mathbf{e}_r$.
- Displacement vector: $\mathbf{u} = u(r)\mathbf{e}_r$.
- Body force vector: $\mathbf{b} = \rho_0 b(r)\mathbf{e}_r$.

Here, $u(r)$ and $b(r)$ are scalar functions. The stress and strain tensors (written as components in $\{\mathbf{e}_r, \mathbf{e}_\theta, \mathbf{e}_\phi\}$) have the form

$$\boldsymbol{\sigma} \equiv \begin{bmatrix} \sigma_{rr} & 0 & 0 \\ 0 & \sigma_{\theta\theta} & 0 \\ 0 & 0 & \sigma_{\phi\phi} \end{bmatrix} \quad \boldsymbol{\varepsilon} \equiv \begin{bmatrix} \varepsilon_{rr} & 0 & 0 \\ 0 & \varepsilon_{\theta\theta} & 0 \\ 0 & 0 & \varepsilon_{\phi\phi} \end{bmatrix}$$

and furthermore must satisfy $\sigma_{\theta\theta} = \sigma_{\phi\phi}$, $\varepsilon_{\theta\theta} = \varepsilon_{\phi\phi}$. The tensor components have exactly the same physical interpretation as they did when we used a fixed $\{\mathbf{e}_1, \mathbf{e}_2, \mathbf{e}_3\}$ basis, except that the subscripts (1,2,3) have been replaced by (r, θ, z) .

For spherical symmetry, the governing equations reduce to the following:

- Strain-displacement relations: $\varepsilon_{rr} = \frac{du}{dr}$ $\varepsilon_{\phi\phi} = \varepsilon_{\theta\theta} = \frac{u}{r}$.
- Stress-strain relations:

in elastic region(s),

$$\begin{aligned} \sigma_{rr} &= \frac{E}{(1+\nu)(1-2\nu)} \left\{ (1-\nu)\varepsilon_{rr} + \nu\varepsilon_{\theta\theta} + \nu\varepsilon_{\phi\phi} \right\} \\ \sigma_{\theta\theta} = \sigma_{\phi\phi} &= \frac{E}{(1+\nu)(1-2\nu)} \left\{ \varepsilon_{\theta\theta} + \nu\varepsilon_{rr} \right\} \\ |\sigma_{\theta\theta} - \sigma_{rr}| &< Y; \end{aligned}$$

in plastic region(s),

$$\text{yield criterion: } |\sigma_{\theta\theta} - \sigma_{rr}| = Y$$

$$\text{strain partition: } d\varepsilon_{rr} = d\varepsilon_{rr}^p + d\varepsilon_{rr}^e \quad d\varepsilon_{\phi\phi} = d\varepsilon_{\phi\phi}^p + d\varepsilon_{\phi\phi}^e \quad d\varepsilon_{\theta\theta} = d\varepsilon_{\theta\theta}^p + d\varepsilon_{\theta\theta}^e$$

elastic strain:

$$d\varepsilon_{rr}^e = d\sigma_{rr}/E - \nu(d\sigma_{\theta\theta} + d\sigma_{\phi\phi})/E$$

$$d\varepsilon_{\theta\theta}^e = d\varepsilon_{\phi\phi}^e = d\sigma_{\theta\theta}(1-\nu)/E - \nu d\sigma_{rr}/E$$

flow rule:

$$\begin{aligned} d\varepsilon_{rr}^p &= d\bar{\varepsilon}^p (\sigma_{rr} - \sigma_{\theta\theta})/Y \\ d\varepsilon_{\theta\theta}^p &= d\varepsilon_{\phi\phi}^p = d\bar{\varepsilon}^p (\sigma_{\theta\theta} - \sigma_{rr})/(2Y). \end{aligned}$$

- Equilibrium equations: $\frac{d\sigma_{rr}}{dr} + \frac{1}{r}(2\sigma_{rr} - \sigma_{\theta\theta} - \sigma_{\phi\phi}) + \rho_0 b_r = 0.$
- Boundary conditions:

prescribed displacements, $u_r(a) = g_a \quad u_r(b) = g_b;$
 prescribed tractions, $\sigma_{rr}(a) = t_a \quad \sigma_{rr}(b) = t_b.$

The equilibrium and strain-displacement equations can be derived following the procedure outlined in Section 4.1.2. The stress-strain relations are derived by substituting the strain components into the general constitutive equation and simplifying the result.

Unlike the elastic solution discussed in Section 4.1, there is no clean, direct, and general method for integrating these equations. Instead, solutions must be found using a combination of physical intuition and some algebraic tricks, as illustrated in the sections below.

4.2.3 Elastic Perfectly Plastic Hollow Sphere Subjected to Monotonically Increasing Internal Pressure

A pressurized spherical thick-walled sphere is illustrated in Figure 4.12. Assume the following:

- The sphere is stress free before it is loaded.
- No body forces act on the sphere.
- The sphere has uniform temperature.
- The inner surface $r = a$ is subjected to (monotonically increasing) pressure $p_a.$
- The outer surface $r = b$ is traction free.
- Strains are infinitesimal.

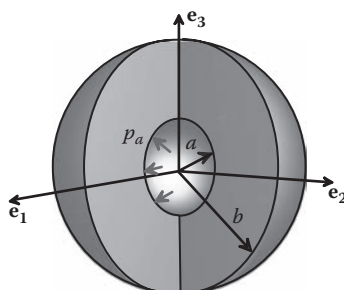


FIGURE 4.12 Spherical shell subjected to internal pressure.

Solution

1. Preliminaries:

- The sphere first reaches yield (at $r = a$) at an internal pressure $p_a/Y = 2(1 - a^3/b^3)/3$.
- For pressures in the range $2(1 - a^3/b^3)/3 < p_a/Y < 2\log(b/a)$ the region between $r = a$ and $r = c$ deforms plastically, whereas the region between $c < r < b$ remains elastic, in which c satisfies the equation $p_a/Y = 2\log(c/a) + \frac{2}{3}(1 - c^3/b^3)$.
- At a pressure $p_a/Y = 2\log(b/a)$, the entire sphere is plastic. At this point, the sphere collapses, and the displacements become infinitely large.

2. Solution in the plastic region $a < r < c$:

$$\mathbf{u} = \frac{(1-2\nu)}{E} r \{2Y\log(r/a) - p_a\} \mathbf{e}_r + \frac{Y(1-\nu)c^3}{Er^2} \mathbf{e}_r$$

$$\sigma_{rr} = 2Y\log(r/a) - p_a \quad \sigma_{\theta\theta} = \sigma_{\phi\phi} = 2Y\log(r/a) - p_a + Y.$$

3. Solution in the elastic region $c < r < b$:

$$\mathbf{u} = \frac{Yc^3}{3Eb^3r^2} \{2(1-2\nu)r^3 + (1+\nu)b^3\} \mathbf{e}_r$$

$$\sigma_{rr} = \frac{2Yc^3}{3b^3} \left(1 - \frac{b^3}{r^3}\right) \quad \sigma_{\theta\theta} = \sigma_{\phi\phi} = \frac{2Yc^3}{3b^3} \left(1 + \frac{b^3}{2r^3}\right).$$

These results are plotted in Figure 4.13. Displacements are shown for $\nu = 0.3$.

Derivation: By substituting the stresses for the elastic solution given in Section 4.1.4 into the von Mises yield criterion, we see that a pressurized elastic sphere first reaches yield at $r = a$. If the pressure is increased beyond yield, we anticipate that a region $a < r < c$ will deform plastically, whereas a region $c < r < b$ remains elastic. We must find separate solutions in the plastic and elastic regimes.

In the plastic regime $a < r < c$:

- We anticipate that $\sigma_{rr} < 0$ $\sigma_{\theta\theta} = \sigma_{\phi\phi} > 0$. The yield criterion then gives $\sigma_{\theta\theta} - \sigma_{rr} = Y$.
- Substituting this result into the equilibrium equation given in Section 4.2.2 shows that

$$\frac{d\sigma_{rr}}{dr} + \frac{1}{r} (2\sigma_{rr} - \sigma_{\theta\theta} - \sigma_{\phi\phi}) = 0 \Rightarrow \frac{d\sigma_{rr}}{dr} - 2\frac{Y}{r} = 0.$$

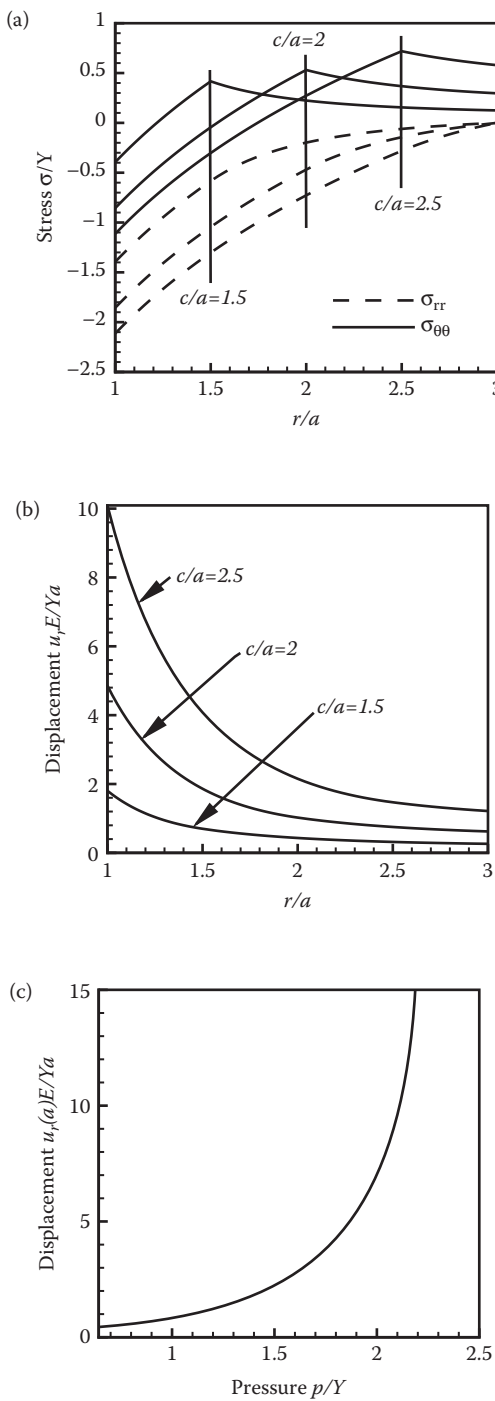


FIGURE 4.13 Stress and displacement fields for a pressurized elastic-plastic spherical shell. Stress (a) and displacement (b) distributions for various positions of the elastic-plastic boundary c/a ; (c) variation of internal displacement with applied pressure. Displacements are shown for $\nu = 0.3$.

3. Integrating and using the boundary condition $\sigma_{rr} = -p_a$ at $r = a$ together with the yield condition in item 1 gives

$$\sigma_{rr} = 2Y \log(r/a) - p_a \quad \sigma_{\theta\theta} = \sigma_{\phi\phi} = 2Y \log(r/a) - p_a + Y.$$

4. Because the pressure is monotonically increasing, the incremental stress-strain relations for the elastic-plastic region given in Section 4.2.2 can be integrated. The elastic strains follow as

$$\varepsilon_{rr}^e = (\sigma_{rr} - 2\nu\sigma_{\theta\theta})/E \quad \varepsilon_{\phi\phi}^e = \varepsilon_{\theta\theta}^e = ((1-\nu)\sigma_{\theta\theta} - \nu\sigma_{rr})/E.$$

5. The plastic strains satisfy $\varepsilon_{rr}^p + 2\varepsilon_{\theta\theta}^p = 0$. Consequently, using the strain partition formula, the results of item 4 and the strain-displacement relation shows that

$$\begin{aligned} \varepsilon_{rr} + 2\varepsilon_{\theta\theta} &= \varepsilon_{rr}^e + 2\varepsilon_{\theta\theta}^e = \frac{(1-2\nu)}{E}(\sigma_{rr} + 2\sigma_{\theta\theta}) \\ \Rightarrow \frac{du}{dr} + \frac{2u}{r} &= \frac{1}{r^2} \frac{d}{dr}(r^2 u) = \frac{(1-2\nu)}{E}(6Y \log(r/a) - 3p_a + 2Y). \end{aligned}$$

6. Integrating gives

$$u = \frac{(1-2\nu)}{E} r \{ 2Y \log(r/a) - p_a \} + C/r^2,$$

where C is a constant of integration.

7. The constant of integration can be found by noting that the radial displacements in the elastic and plastic regimens must be equal at $r = c$. Using the expression for the elastic displacement field below and solving for C gives

$$C = \frac{3(1-\nu)c^3b^3}{2E(b^3 - c^3)} \{ p_a - 2Y \log(c/a) \}.$$

This result can be simplified by noting that $p_a - 2Y \log(c/a) = 2Y(1 - c^3/b^3)/3$ from the expression for the location of the elastic-plastic boundary given below.

In the elastic region, the solution can be found directly from the solution to the internally pressurized elastic sphere given in Section 4.1.4. From step 3 in the solution for the plastic regimen, we see that the radial pressure at $r = c$ is $p_c = -\sigma_{rr} = p_a - 2Y \log(c/a)$. We can simplify the solution by noting $p_a - 2Y \log(c/a) = 2Y(1 - c^3/b^3)/3$ from the expression for the location of the elastic-plastic boundary. Substituting into the expressions for stress and displacement shows that

$$\sigma_{rr} = \frac{p_c c^3}{(b^3 - c^3)} \left(1 - \frac{b^3}{r^3} \right) \quad \sigma_{\theta\theta} = \sigma_{\phi\phi} = \frac{p_c c^3}{(b^3 - c^3)} \left(1 + \frac{b^3}{2r^3} \right)$$

$$\mathbf{u} = \frac{p_c c^3}{2E(b^3 - c^3)r^2} \{2(1 - 2\nu)r^3 + (1 + \nu)b^3\} \mathbf{e}_r.$$

The elastic-plastic boundary is located by the condition that the stress in the elastic region must just reach yield at $r = c$ (so there is a smooth transition into the plastic region). The yield condition is $\sigma_{\theta\theta} - \sigma_{rr} = Y$, so substituting the expressions for stress in the elastic region and simplifying yields

$$\sigma_{\theta\theta} - \sigma_{rr} = \frac{3(p_a - 2Y \log(c/a))b^3}{2(b^3 - c^3)} = Y \quad \Leftrightarrow \quad \frac{p_a}{Y} = 2 \log(c/a) + \frac{2}{3}(1 - c^3/b^3).$$

If p_a , Y , a , and b are specified, this equation can be solved (numerically) for c . For graphing purposes, it is preferable to choose c and then calculate the corresponding value of p_a .

4.2.4 Elastic Perfectly Plastic Hollow Sphere Subjected to Cyclic Internal Pressure

Figure 4.14 illustrates a thick-walled internally pressurized sphere. Assume the following:

- The sphere is stress free before it is loaded.
- No body forces act on the sphere.
- The sphere has uniform temperature.
- The outer surface $r = b$ is traction free.

Suppose that the inner surface of the sphere $r = a$ is repeatedly subjected to pressure p_a and then unloaded to zero pressure.

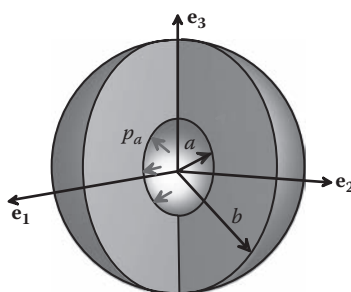


FIGURE 4.14 Elastic-plastic spherical shell subjected to cyclic internal pressure.

Solution: The nature of the solution depends on the magnitude of the internal pressure as follows:

- If the maximum pressure p_a applied to the sphere does not exceed the elastic limit (i.e., $p_a/Y < 2(1 - a^3/b^3)/3$), the solid remains elastic throughout the loading cycle. In this case, the sphere is stress free after unloading and remains elastic throughout all subsequent load cycles.
- For pressures in the range $2(1 - a^3/b^3)/3 < p_a/Y < 2\log(b/a)$, the region between $r = a$ and $r = c$ deforms plastically during the first application of pressure, whereas the region between $c < r < b$ remains elastic, in which c satisfies the equation $p_a/Y = 2\log(c/a) + \frac{2}{3}(1 - c^3/b^3)$. In this case, the solid is permanently deformed. After unloading, its internal and external radii are slightly increased, and the sphere is in a state of *residual stress*.
- If the maximum internal pressure satisfies $2(1 - a^3/b^3)/3 < p_a/Y < 4(1 - a^3/b^3)/3$, the cylinder deforms plastically during the first application of pressure. It then deforms elastically (no yield) while the pressure is removed. During subsequent pressure cycles between zero and the maximum pressure, the cylinder deforms elastically. Residual stresses introduced during the first loading cycle are protective and prevent additional plasticity. This behavior is known as shakedown, and the maximum load for which it can occur ($p_a/Y = 4(1 - a^3/b^3)/3$) is known as the shakedown limit.
- If the maximum internal pressure reaches the shakedown limit $p_a/Y = 4(1 - a^3/b^3)/3$, the residual stress just reaches yield at $r = a$ when the pressure is reduced to zero after the first loading cycle.
- For internal pressures $p_a/Y > 4(1 - a^3/b^3)/3$, a plastic zone forms between $a < r < d$ as the pressure is reduced to zero, where d satisfies the equation $p_a = 4Y(1 - d^3/b^3)/3 + 4Y\log(d/a)$. During subsequent cycles of loading, the region $a < r < d$ is repeatedly plastically deformed, stretching in the hoop direction during increasing pressure and compressing as the pressure is reduced to zero. The region between $d < r < c$ deforms plastically during the first cycle of pressure but remains elastic for all subsequent cycles. This is a “shakedown region.” The remainder of the sphere experiences elastic cycles of strain.

In the preceding discussion, we have assumed that the cylinder is thick enough to support an arbitrarily large pressure. The internal pressure cannot exceed the collapse load $p_a/Y = 2\log(b/a)$, so some regimens are inaccessible for thinner-walled spheres.

The stress fields at maximum and minimum load for these various ranges of applied load are listed below. The displacements can be computed, but the formulas are too long to record here.

The residual stress distributions (after unloading to zero pressure) are shown in Figure 4.15, for a sphere with $b/a = 3$. The solution for $c/a = 1.25$ is below the shakedown limit; the other two solutions are for pressures exceeding the shakedown limit. The region of cyclic plasticity can be seen from the discontinuity in the hoop stress curves. Note that the residual stresses are predominantly compressive. For this reason, bolt holes, pressure vessels, and gun barrels are often purposely pressurized above the elastic limit so as to introduce a compressive stress near the loaded surface. This protects the component against fatigue, because fatigue cracks do not propagate under compressive loading.

Solution for pressures below the elastic limit $p_a/Y < 2(1 - a^3/b^3)/3$: The displacement, strain, and stress field at maximum load are given by the elastic solution in Section 4.1.4.

Solution for pressures between the elastic and shakedown limits $p_a/Y < 4(1 - a^3/b^3)/3$

- At maximum pressure, the displacement and stress fields are given by the elastic-plastic solution in Section 4.2.3.
- At zero pressure, the solutions are as follows:

1. Solution for $a < r < c$:

$$\sigma_{rr} = 2Y \log\left(\frac{r}{a}\right) - p_a - \frac{p_a a^3}{(b^3 - a^3)} \left(1 - \frac{b^3}{r^3}\right)$$

$$\sigma_{\theta\theta} = \sigma_{\phi\phi} = 2Y \log\left(\frac{r}{a}\right) - p_a + Y - \frac{p_a a^3}{(b^3 - a^3)} \left(1 + \frac{b^3}{2r^3}\right).$$

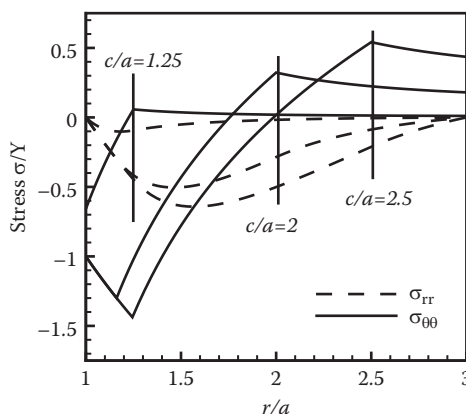


FIGURE 4.15 Residual stress distributions after unloading a pressurized elastic-plastic shell, for various positions of the elastic/plastic boundary c/a .

2. Solution for $c < r < b$:

$$\sigma_{rr} = \frac{2Yc^3}{3b^3} \left(1 - \frac{b^3}{r^3} \right) - \frac{p_a a^3}{(b^3 - a^3)} \left(1 - \frac{b^3}{r^3} \right)$$

$$\sigma_{\theta\theta} = \sigma_{\phi\phi} = \frac{2Yc^3}{3b^3} \left(1 + \frac{b^3}{2r^3} \right) - \frac{p_a a^3}{(b^3 - a^3)} \left(1 + \frac{b^3}{2r^3} \right).$$

Solution for pressures exceeding the shakedown limit $p_a/Y > 4(1 - a^3/b^3)/3$

- At maximum pressure, the displacement, strain, and stress fields are given in Section 4.2.3.
- At zero pressure, the solutions are as follows:

1. Solution for cyclic plastic region $a < r < d$:

$$\sigma_{rr} = -2Y \log(r/a) \quad \sigma_{\theta\theta} = \sigma_{\phi\phi} = -2Y \log(r/a) - Y.$$

2. Solution for shakedown region $d < r < c$:

$$\sigma_{rr} = 2Y \log(r/a) - p_a - \frac{4Yd^3}{3b^3} \left(1 - \frac{b^3}{r^3} \right)$$

$$\sigma_{\theta\theta} = \sigma_{\phi\phi} = 2Y \log(r/a) - p_a + Y - \frac{4Yd^3}{3b^3} \left(1 + \frac{b^3}{2r^3} \right)$$

3. Solution for the elastic region $c < r < b$:

$$\sigma_{rr} = \frac{2Yc^3}{3b^3} \left(1 - \frac{b^3}{r^3} \right) - \frac{4Yd^3}{3b^3} \left(1 - \frac{b^3}{r^3} \right) \quad \sigma_{\theta\theta} = \sigma_{\phi\phi} = \frac{2Yc^3}{3b^3} \left(1 + \frac{b^3}{2r^3} \right) - \frac{4Yd^3}{3b^3} \left(1 + \frac{b^3}{2r^3} \right).$$

Derivation of stress after unloading in the cyclic plastic regime $a < r < d$

1. We anticipate that $\sigma_{rr} > 0$, $\sigma_{\theta\theta} < 0$. The yield criterion then gives

$$\sigma_{\theta\theta} - \sigma_{rr} = -Y.$$

2. Substituting this result into the equilibrium equation shows that

$$\frac{d\sigma_{rr}}{dr} + 2\frac{Y}{r} = 0.$$

3. Integrating and using the boundary condition $\sigma_{rr} = 0$ at $r = a$ together with the yield condition in step 1 gives

$$\sigma_{rr} = -2Y \log(r/a) \quad \sigma_{\theta\theta} = \sigma_{\phi\phi} = -2Y \log(r/a) - Y.$$

Derivation of stress after unloading in the shakedown regime $d < r < c$

1. In this region, the stress at maximum load are given by the expressions for $r < c$ in 4.2.3, i.e.,

$$\sigma_{rr} = 2Y \log(r/a) - p_a \quad \sigma_{\theta\theta} = \sigma_{\phi\phi} = 2Y \log(r/a) - p_a + Y.$$

The solid then unloads elastically while the pressure is removed.

2. The change in stress during unloading can be calculated quickly by regarding the region $d < r < b$ as a spherical shell with internal radius d and external radius b , subjected to radial pressure at $r = d$. At maximum load, the pressure at $r = d$ is $p_a - 2Y \log(d/a)$; after unloading, the pressure follows from the solution for the cyclic plastic regime as $2Y \log(d/a)$. The change in pressure at $r = d$ during unloading is thus $\Delta p = 4Y \log(d/a) - p_a$.
3. The change in pressure during unloading can also be expressed as $\Delta p = -4Y(1 - b^3/d^3)/3$ using the governing equation for d shown below. We then can simply add the (elastic) stress and displacement induced by this pressure change to the displacement and stress at maximum load, to obtain the solution given above.

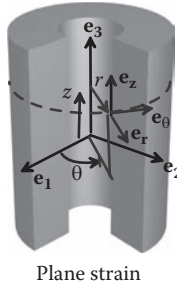
Boundary of the cyclic plastic zone: The boundary of the cyclic plastic zone is determined by the condition that the stress in the shakedown regime must just reach yield at $r = d$ when the pressure reaches zero. This gives

$$\sigma_{\theta\theta} - \sigma_{rr} = -Y \Rightarrow p_a = 4Y(1 - d^3/b^3)/3 + 4Y \log(d/a).$$

Derivation of solution in the elastic region $c < r < b$: The solution in this region is derived in the same way as the solution for the shakedown region, except that the displacement and stress at maximum load are given by solutions for $c < r < b$.

4.2.5 Simplified Equations for Plane Strain Axially Symmetric Elastic-Perfectly Plastic Solids

An axially symmetric solid is illustrated in Figure 4.16. The solid is a circular cylinder that is subjected to axially symmetric loading (i.e., internal body forces, as well as tractions or displacements applied to the surface, are independent of θ and z and act in the radial direction only). Temperature changes will be neglected, to simplify calculations. However, the solid can spin with steady angular velocity about the e_3 axis.



Plane strain

FIGURE 4.16 Coordinate system used for cylindrically symmetric problems.

We will assume that the cylinder is completely prevented from stretching in the \mathbf{e}_3 direction, so that a state of plane strain exists in the solid.

The solution is most conveniently expressed using a cylindrical-polar coordinate system, illustrated in Figure 4.16. A point in the solid is identified by its cylindrical-polar coordinates (r, θ, z) . All vectors and tensors are expressed as components in the basis $\{\mathbf{e}_r, \mathbf{e}_\theta, \mathbf{e}_z\}$ shown in the figure. For an axially symmetric problem, the following applies:

- Position vector: $\mathbf{x} = r\mathbf{e}_r + z\mathbf{e}_z$
- Displacement vector: $\mathbf{u} = u(r)\mathbf{e}_r$
- Body force vector: $\mathbf{b} = \rho_0 b(r)\mathbf{e}_r$
- Acceleration vector: $\mathbf{a} = -\omega^2 r\mathbf{e}_r$

Here, $u(r)$ and $b(r)$ are scalar functions. The stress and strain tensors (written as components in $\{\mathbf{e}_r, \mathbf{e}_\theta, \mathbf{e}_z\}$) have the form

$$\boldsymbol{\sigma} \equiv \begin{bmatrix} \sigma_{rr} & 0 & 0 \\ 0 & \sigma_{\theta\theta} & 0 \\ 0 & 0 & \sigma_{zz} \end{bmatrix} \quad \boldsymbol{\varepsilon} \equiv \begin{bmatrix} \varepsilon_{rr} & 0 & 0 \\ 0 & \varepsilon_{\theta\theta} & 0 \\ 0 & 0 & \varepsilon_{zz} \end{bmatrix}.$$

For axial symmetry, the governing equations reduce to the following

- Strain-displacement relations: $\varepsilon_{rr} = \frac{du}{dr}$, $\varepsilon_{\theta\theta} = \frac{u}{r}$, $\varepsilon_{zz} = 0$.
- Stress-strain relations (plane strain and generalized plane strain):

in elastic region(s),

$$\begin{bmatrix} \sigma_{rr} \\ \sigma_{\theta\theta} \\ \sigma_{zz} \end{bmatrix} = \frac{E}{(1+\nu)(1-2\nu)} \begin{bmatrix} 1-\nu & \nu & \nu \\ \nu & 1-\nu & \nu \\ \nu & \nu & 1-\nu \end{bmatrix} \begin{bmatrix} \varepsilon_{rr} \\ \varepsilon_{\theta\theta} \\ \varepsilon_{zz} \end{bmatrix}$$

$$\sqrt{\{(\sigma_{\theta\theta} - \sigma_{rr})^2 + (\sigma_{\theta\theta} - \sigma_{zz})^2 + (\sigma_{rr} - \sigma_{zz})^2\}/2} < Y.$$

in plastic region(s),

yield criterion:

$$\sqrt{\{(\sigma_{\theta\theta} - \sigma_{rr})^2 + (\sigma_{\theta\theta} - \sigma_{zz})^2 + (\sigma_{rr} - \sigma_{zz})^2\}/2} = Y;$$

strain partition:

$$d\varepsilon_{rr} = d\varepsilon_{rr}^p + d\varepsilon_{rr}^e \quad d\varepsilon_{\theta\theta} = d\varepsilon_{\theta\theta}^p + d\varepsilon_{\theta\theta}^e \quad d\varepsilon_{\theta\theta} = d\varepsilon_{\theta\theta}^p + d\varepsilon_{\theta\theta}^e;$$

elastic strain:

$$d\varepsilon_{rr}^e = d\sigma_{rr}/E - v(d\sigma_{\theta\theta} + d\sigma_{zz})/E$$

$$d\varepsilon_{\theta\theta}^e = d\sigma_{\theta\theta}/E - v(d\sigma_{rr} + d\sigma_{zz})/E$$

$$d\varepsilon_{zz}^e = d\sigma_{zz}/E - v(d\sigma_{rr} + d\sigma_{\theta\theta})/E;$$

flow rule:

$$d\varepsilon_{rr}^p = d\bar{\varepsilon}^p \frac{\sigma_{rr} - (\sigma_{\theta\theta} + \sigma_{zz})/2}{Y}$$

$$d\varepsilon_{\theta\theta}^p = d\bar{\varepsilon}^p \frac{\sigma_{\theta\theta} - (\sigma_{rr} + \sigma_{zz})/2}{Y}$$

$$d\varepsilon_{zz}^p = d\bar{\varepsilon}^p \frac{\sigma_{zz} - (\sigma_{rr} + \sigma_{\theta\theta})/2}{Y}.$$

- Equation of motion:

$$\frac{d\sigma_{rr}}{dr} + \frac{1}{r}(\sigma_{rr} - \sigma_{\theta\theta}) + \rho_0 b_r = -\rho_0 \omega^2 r.$$

- Boundary conditions:

prescribed displacements, $u_r(a) = g_a \quad u_r(b) = g_b$;

prescribed tractions, $\sigma_{rr}(a) = t_a \quad \sigma_{rr}(b) = t_b$.

The equilibrium and strain-displacement equations can be derived following the procedure outlined in Section 4.1.2. The stress-strain relations are derived by substituting the strain components into the general constitutive equation and simplifying the result.

Unlike the elastic solution in Section 4.1, there is no clean, direct, and general method for integrating these equations. Instead, solutions must be found using a combination of physical intuition and some algebraic tricks, as illustrated in the sections below.

4.2.6 Long (Plane Strain) Cylinder Subjected to Internal Pressure

We consider a long hollow cylinder with internal radius a and external radius b as shown in Figure 4.17. Assume the following:

- No body forces act on the cylinder.
- The cylinder has zero angular velocity.
- The sphere has uniform temperature.
- The inner surface $r = a$ is subjected to pressure p_a .
- The outer surface $r = b$ is free of pressure.
- The cylinder does not stretch parallel to its axis.

The solution given below is approximate, because it assumes that both elastic and plastic axial strains vanish separately (when in fact only the sum of elastic and plastic strains should be zero).

Solution

1. Preliminaries:

- The cylinder first reaches yield (at $r = a$) at an internal pressure:

$$\sqrt{3}p_a/Y \approx \left(1 - a^2/b^2\right).$$

- For pressures in the range $\left(1 - a^2/b^2\right) < \sqrt{3}p_a/Y < 2\log(b/a)$, the region between $r = a$ and $r = c$ deforms plastically, whereas the region between $c < r < b$ remains elastic, in which c satisfies the equation $\sqrt{3}p_a/Y = 2\log(c/a) + 1 - c^2/b^2$.
- At a pressure $p_a/Y = (2/\sqrt{3})\log(b/a)$, the entire cylinder is plastic. At this point, the sphere collapses; the displacements become infinitely large.



FIGURE 4.17 Internally pressurized thick-walled elastic-plastic cylinder.

2. Solution in the plastic region $a < r < c$:

$$u = \frac{(1-2\nu)(1+\nu)}{E} 2r \left\{ \left(2Y/\sqrt{3} \right) \log(r/a) - p_a \right\} + \frac{(1+\nu)Yc^2 \left(2(1-\nu)b^2 + (1-2\nu)(b^2 - c^2) \right)}{\sqrt{3}Eb^2r}$$

$$\sigma_{rr} = \left(2Y/\sqrt{3} \right) \log(r/a) - p_a \quad \sigma_{\theta\theta} = \left(2Y/\sqrt{3} \right) \log(r/a) - p_a + 2Y/\sqrt{3}.$$

3. Solution in the elastic region $c < r < b$:

$$u_r = \frac{(1+\nu)c^2Y}{E\sqrt{3}} \left\{ \frac{1}{r} + (1-2\nu) \frac{r}{b^2} \right\}$$

$$\sigma_{rr} = \frac{Yc^2}{\sqrt{3}b^2} \left\{ 1 - \frac{b^2}{r^2} \right\} \quad \sigma_{\theta\theta} = \frac{Yc^2}{\sqrt{3}b^2} \left\{ 1 + \frac{b^2}{r^2} \right\}.$$

The stress and displacement fields are plotted in Figure 4.18, for various positions of the elastic-plastic boundary. The results are for $b/a = 3$, and the displacement is shown for a solid with $\nu = 0.3$.

Derivation: By substituting the stresses for the elastic solution given in Section 4.1.4 into the von Mises yield criterion, we see that a pressurized elastic cylinder first reaches yield at $r = a$. If the pressure is increased beyond yield, a region $a < r < c$ will deform plastically, whereas a region $c < r < b$ remains elastic. We must find separate solutions in the plastic and elastic regimes.

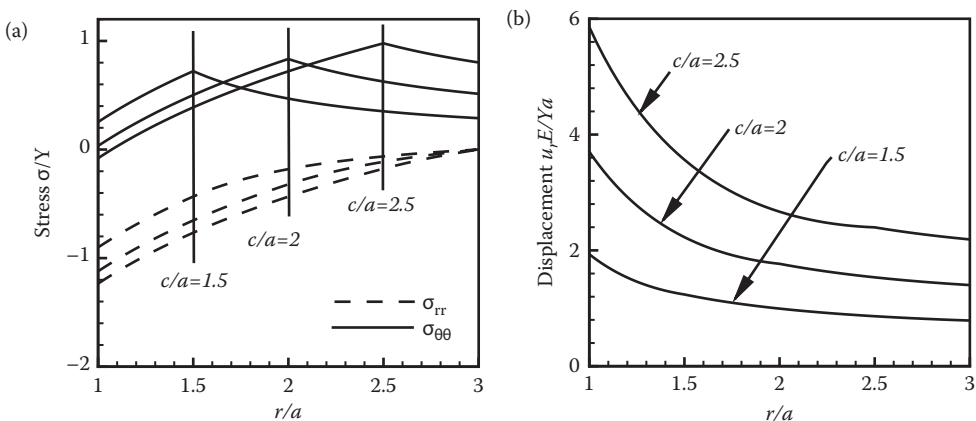


FIGURE 4.18 Stress and displacement fields for a pressurized elastic-plastic cylinder. Stress (a) and displacement (b) distributions for various positions of the elastic-plastic boundary c/a .

In the plastic regime $a < r < c$:

- To simplify the calculation, we assume that $d\varepsilon_{zz}^p = d\varepsilon_{zz}^e = 0$. This turns out to be exact for $\nu = 1/2$ but is approximate for other values of Poisson's ratio. The plastic flow rule shows that $d\varepsilon_{zz}^p = d\bar{\varepsilon}^p \frac{\sigma_{zz} - (\sigma_{rr} + \sigma_{\theta\theta})/2}{Y}$, in which case $d\varepsilon_{zz}^p = 0$ requires that $\sigma_{zz} = (\sigma_{rr} + \sigma_{\theta\theta})/2$.
- We anticipate that $\sigma_{rr} < 0$, $\sigma_{\theta\theta} > 0$. Substituting the result of item 1 into the yield criterion then gives $\sigma_{\theta\theta} - \sigma_{rr} = 2Y\sqrt{3}$.
- Substituting this result into the equilibrium equation shows that

$$\frac{d\sigma_{rr}}{dr} - \frac{2Y}{\sqrt{3}r} = 0.$$

- Integrating and using the boundary condition $\sigma_{rr} = -p_a$ at $r = a$ together with the yield condition 2 gives

$$\sigma_{rr} = (2Y/\sqrt{3})\log(r/a) - p_a \quad \sigma_{\theta\theta} = (2Y/\sqrt{3})\log(r/a) - p_a + 2Y/\sqrt{3}.$$

- The elastic strains follow as

$$\varepsilon_{rr}^e = (\sigma_{rr} - \nu\sigma_{\theta\theta} - \nu\sigma_{zz})/E \quad \varepsilon_{\theta\theta}^e = (\sigma_{\theta\theta} - \nu\sigma_{rr} - \nu\sigma_{zz})/E.$$

- With assumption 1, the flow rule shows that plastic strains satisfy $\varepsilon_{rr}^p + \varepsilon_{\theta\theta}^p = 0$. Consequently, using the strain partition formula and the strain-displacement relation shows that

$$\begin{aligned} \varepsilon_{rr} + \varepsilon_{\theta\theta} &= \frac{du}{dr} + \frac{u}{r} = \frac{1}{r} \frac{d}{dr}(ru) = \frac{(1-2\nu)(1+\nu)}{E} \{\sigma_{rr} + \sigma_{\theta\theta}\} \\ &= \frac{(1-2\nu)(1+\nu)}{E} 2(2Y[\log(r/a) + 1]/\sqrt{3} - p_a). \end{aligned}$$

- Integrating gives

$$u = \frac{(1-2\nu)(1+\nu)}{E} 2r \left\{ (2Y/\sqrt{3})\log(r/a) - p_a \right\} + C/r,$$

where C is a constant of integration

- The constant of integration can be found by noting that the radial displacements in the elastic and plastic regimes must be equal at $r = c$. Using the expression for the elastic displacement field below and solving for C gives

$$C = \frac{(1+\nu)c^2 \left(2(1-\nu)b^2 + (1-2\nu)(b^2 - c^2) \right)}{E(b^2 - c^2)} \left\{ p_a - (2Y/\sqrt{3})\log(c/a) \right\}.$$

This result can be simplified by noting that $p_a - (2Y/\sqrt{3})\log(c/a) = Y(1 - c^2/b^2)/\sqrt{3}$ from the expression for the location of the elastic-plastic boundary given below.

In the elastic regime, the solution can be found directly from the solution to the internally pressurized elastic cylinder given in Section 4.1.9. From step 4 in the solution for the plastic regime, we see that the radial pressure at $r = c$ is $p_c = -\sigma_{rr} = p_a - (2Y/\sqrt{3})\log(c/a)$. We can simplify the solution by noting $p_a - (2Y/\sqrt{3})\log(c/a) = Y(1 - c^2/b^2)/\sqrt{3}$ from the expression for the location of the elastic-plastic boundary. Substituting into the expressions for stress and displacement in Section 4.1.9 shows that

$$\begin{aligned}\sigma_{rr} &= \frac{p_c c^2}{b^2 - c^2} \left\{ 1 - \frac{b^2}{r^2} \right\} \quad \sigma_{\theta\theta} = \frac{p_c c^2}{b^2 - c^2} \left\{ 1 + \frac{b^2}{r^2} \right\} \quad \sigma_{zz} = 2\nu \frac{pc^2}{b^2 - c^2} \\ u_r &= \frac{(1+\nu)c^2 b^2 p_c}{E(b^2 - c^2)} \left\{ \frac{1}{r} + (1-2\nu) \frac{r}{b^2} \right\}.\end{aligned}$$

Finally, the elastic-plastic boundary is located by the condition that the stress in the elastic region must just reach yield at $r = c$ (so there is a smooth transition into the plastic region). The yield condition is $\sigma_{\theta\theta} - \sigma_{rr} = 2Y/\sqrt{3}$, so substituting the expressions for stress in the elastic region and simplifying yields

$$\begin{aligned}\sigma_{\theta\theta} - \sigma_{rr} &= \frac{2(p_a - (2Y/\sqrt{3})\log(c/a))b^2}{(b^2 - c^2)} = 2Y/\sqrt{3} \\ \Leftrightarrow \sqrt{3} \frac{p_a}{Y} &= 2\log(c/a) + (1 - c^2/b^2).\end{aligned}$$

If p_a , Y , a , and b are specified, this equation can be solved (numerically) for c . For graphing purposes, it is preferable to choose c and then calculate the corresponding value of p_a .

4.3 SPHERICALLY SYMMETRIC SOLUTION TO QUASI-STATIC LARGE STRAIN ELASTICITY PROBLEMS

4.3.1 Summary of Governing Equations of Finite Elasticity in Cartesian Components
This section is intended to illustrate the nature of solutions to elasticity problems with large shape changes.

A representative problem is sketched in Figure 4.19. We are given the following information:

1. The geometry of the solid
2. A constitutive law for the material (i.e., the hyperelastic strain energy potential)

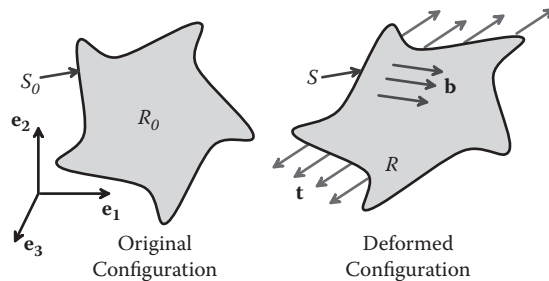


FIGURE 4.19 Typical boundary value problem for an elastic solid experiencing large deformations.

3. The body force density b_i (per unit mass) (if any)
4. Prescribed boundary tractions t_i and/or boundary displacements u_i

To simplify the problem, we will assume the following:

- The solid is stress free in its undeformed configuration.
- Temperature changes during deformation are neglected.
- The solid is incompressible.

With these assumptions, we want to calculate the displacement field u_i , the left Cauchy-Green deformation tensor B_{ij} and the stress field σ_{ij} satisfying the following equations:

- Displacement-strain relation: $B_{ij} = F_{ik}F_{jk}$ $F_{ij} = \delta_{ij} + \frac{\partial u_i}{\partial x_j}$.
- Incompressibility condition: $J = \det(\mathbf{F}) = 1$.
- Stress-strain relation:

$$\sigma_{ij} = 2 \left[\left(\frac{\partial U}{\partial I_1} + I_1 \frac{\partial U}{\partial I_2} \right) B_{ij} - \left(I_1 \frac{\partial U}{\partial I_1} + 2I_2 \frac{\partial U}{\partial I_2} \right) \frac{\delta_{ij}}{3} - \frac{\partial U}{\partial I_2} B_{ik} B_{kj} \right] + p \frac{\delta_{ij}}{3},$$

where σ_{ij} is the Cauchy stress tensor, $U(I_1, I_2)$ is the strain energy potential for the elastic solid, p is the hydrostatic part of the stress (which must be determined as part of the solution), and $I_1 = B_{kk}$ $I_2 = (I_1^2 - B_{ik}B_{ki})/2$.

- Equilibrium equation: $\frac{\partial \sigma_{ij}}{\partial y_i} + \rho b_j = 0$.
- Traction boundary conditions: $\sigma_{ij} n_i = t_j$ on parts of the boundary where tractions are known.
- Displacement boundary conditions: $u_i = d_i$ on parts of the boundary where displacements are known.

4.3.2 Simplified Equations for Incompressible Spherically Symmetric Solids

A representative spherically symmetric problem is illustrated in Figure 4.20. We consider a hollow, spherical solid that is subjected to spherically symmetric loading (i.e., internal

body forces, as well as tractions or displacements applied to the surface, are independent of θ and ϕ and act in the radial direction only).

The solution is most conveniently expressed using a spherical-polar coordinate system, illustrated in Figure 4.20. For a finite deformation problem, we need a way to characterize the position of material particles in both the undeformed and deformed solid. To do this, we let (R, Θ, Φ) identify a material particle in the undeformed solid. The coordinates of the same point in the deformed solid are identified by a new set of spherical-polar coordinates (r, θ, ϕ) . One way to describe the deformation would be to specify each of the deformed coordinates (r, θ, ϕ) in terms of the reference coordinates (R, Θ, Φ) . For a spherically symmetric deformation, points only move radially, so that

$$r = f(R) \quad \theta = \Theta \quad \phi = \Phi.$$

In finite deformation problems, vectors and tensors can be expressed as components in a basis $\{\mathbf{e}_R, \mathbf{e}_\Theta, \mathbf{e}_\Phi\}$ associated with the position of material points in the undeformed solid or, if more convenient, in a basis $\{\mathbf{e}_r, \mathbf{e}_\theta, \mathbf{e}_\phi\}$ associated with material points in the deformed solid. For spherically symmetric deformations, the two bases are identical; consequently, we can write the following:

- Position vector in the undeformed solid: $\mathbf{x} = R\mathbf{e}_r$
- Position vector in the deformed solid: $\mathbf{y} = r\mathbf{e}_r = f(R)\mathbf{e}_r$
- Displacement vector: $\mathbf{u} = \mathbf{y} - \mathbf{x} = r\mathbf{e}_r - R\mathbf{e}_r = (f(R) - R)\mathbf{e}_r$

The stress, deformation gradient, and deformation tensors (written as components in $\{\mathbf{e}_r, \mathbf{e}_\theta, \mathbf{e}_\phi\}$) have the form

$$\boldsymbol{\sigma} \equiv \begin{bmatrix} \sigma_{rr} & 0 & 0 \\ 0 & \sigma_{\theta\theta} & 0 \\ 0 & 0 & \sigma_{\phi\phi} \end{bmatrix} \quad \mathbf{F} \equiv \begin{bmatrix} F_{rr} & 0 & 0 \\ 0 & F_{\theta\theta} & 0 \\ 0 & 0 & F_{\phi\phi} \end{bmatrix} \quad \mathbf{B} \equiv \begin{bmatrix} B_{rr} & 0 & 0 \\ 0 & B_{\theta\theta} & 0 \\ 0 & 0 & B_{\phi\phi} \end{bmatrix}$$

and furthermore must satisfy $\sigma_{\theta\theta} = \sigma_{\phi\phi}$, $F_{rr} = F_{\theta\theta}$, $B_{\theta\theta} = B_{\phi\phi}$.

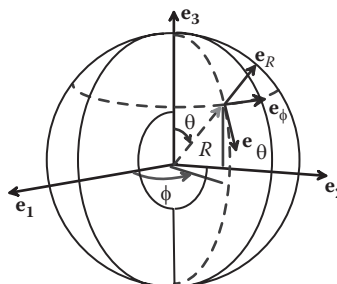


FIGURE 4.20 Coordinate system used for spherically symmetric problems.

For spherical symmetry, the governing equations reduce to the following:

- Strain-displacement relations:

$$F_{rr} = \frac{df}{dR} \quad F_{\phi\phi} = F_{\theta\theta} = \frac{f(R)}{R} \quad B_{rr} = \left(\frac{df}{dR} \right)^2 \quad B_{\phi\phi} = B_{\theta\theta} = \left(\frac{f(R)}{R} \right)^2.$$

- Incompressibility condition: $\left(\frac{df}{dR} \right) \left(\frac{f(R)}{R} \right)^2 = 1$.

- Stress-strain relations:

$$\sigma_{rr} = 2 \left[\left(\frac{\partial U}{\partial I_1} + I_1 \frac{\partial U}{\partial I_2} \right) B_{rr} - \frac{I_1}{3} \frac{\partial U}{\partial I_1} - \frac{2I_2}{3} \frac{\partial U}{\partial I_2} - \frac{\partial U}{\partial I_2} B_{rr}^2 \right] + p$$

$$\sigma_{\theta\theta} = \sigma_{\phi\phi} = 2 \left[\left(\frac{\partial U}{\partial I_1} + I_1 \frac{\partial U}{\partial I_2} \right) B_{\theta\theta} - \frac{I_1}{3} \frac{\partial U}{\partial I_1} - \frac{2I_2}{3} \frac{\partial U}{\partial I_2} - \frac{\partial U}{\partial I_2} B_{\theta\theta}^2 \right] + p.$$

- Equilibrium equations: $\frac{d\sigma_{rr}}{dr} + \frac{1}{r}(2\sigma_{rr} - \sigma_{\theta\theta} - \sigma_{\phi\phi}) + \rho_0 b_r = 0$.

- Boundary conditions:

prescribed displacements, $u_r(a) = g_a \quad u_r(b) = g_b$;
prescribed tractions: $\sigma_{rr}(a) = t_a \quad \sigma_{rr}(b) = t_b$.

4.3.3 Pressurized Hollow Sphere Made from an Incompressible Rubber

As an example, consider a pressurized hollow rubber shell, as shown in Figure 4.21. Assume the following:

- Before deformation, the sphere has inner radius A and outer radius B .
- After deformation, the sphere has inner radius a and outer radius b .
- The solid is made from an incompressible Mooney–Rivlin solid, with strain energy potential:

$$U = \frac{1}{2}(I_1 - 3) + \frac{2}{2}(I_2 - 3).$$

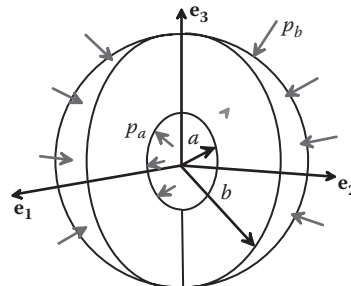


FIGURE 4.21 Spherical hyperelastic shell subjected to internal and external pressure.

- No body forces act on the sphere.
- The inner surface $r = a$ is subjected to pressure p_a .
- The outer surface $r = b$ is subjected to pressure p_b .

The deformed radii a, b of the inner and outer surfaces of the spherical shell are related to the pressure by

$$\frac{p_a - p_b}{1} = 2\left(\frac{1}{\beta} - \frac{1}{\alpha}\right) + \frac{1}{2}\left(\frac{1}{\beta^4} - \frac{1}{\alpha^4}\right) - \frac{2}{1}\left(\beta - \alpha\right) + \frac{2}{1}\left(\frac{1}{\beta^2} - \frac{1}{\alpha^2}\right),$$

where $\alpha = a/A$, $\beta = b/B$, and α, β are related by

$$\frac{B^3}{A^3} = \frac{1 - \alpha^3}{1 - \beta^3}.$$

Provided the pressure is not too large (see below), the preceding two equations can be solved for α and β given the pressure and properties of the shell (for graphing purposes, it is better to assume a value for α , calculate the corresponding β , and then determine the pressure).

The position r of a material particle after deformation is related to its position R before deformation by

$$\frac{r}{A} = \left(\frac{R^3}{A^3} + \alpha^3 - 1 \right)^{1/3} \quad \frac{R}{A} = \left(\frac{r^3}{A^3} - \alpha^3 + 1 \right)^{1/3}.$$

The deformation tensor distribution in the sphere is

$$B_{rr} = (R/r)^4 \quad B_{\theta\theta} = B_{\phi\phi} = (r/R)^2.$$

The Cauchy stress in the sphere is

$$\begin{aligned} \sigma_{rr} &= -_1\left(\frac{2R}{r} + \frac{R^4}{2r^4}\right) - _2\left(\frac{2r}{R} - \frac{R^2}{r^2}\right) + C \\ \sigma_{\theta\theta} &= -_1\left(\frac{2R}{r} - \frac{R^4}{2r^4} + \frac{r^2}{R^2}\right) - _2\left(\frac{2r}{R} - \frac{r^4}{R^4}\right) + C \\ C &= -\frac{1}{2}\left(\frac{2}{\alpha} + \frac{1}{2\alpha^4} + \frac{2}{\beta} + \frac{1}{2\beta^4}\right) + \frac{1}{2}\left(2\alpha - \frac{1}{\alpha^2} + 2\beta - \frac{1}{\beta^2}\right) - \frac{p_a + p_b}{2}. \end{aligned}$$

The variation of the internal radius of the spherical shell with applied pressure is plotted in Figure 4.22, for $_2/_1 = 0.04$ (a representative value for a typical rubber). For comparison,

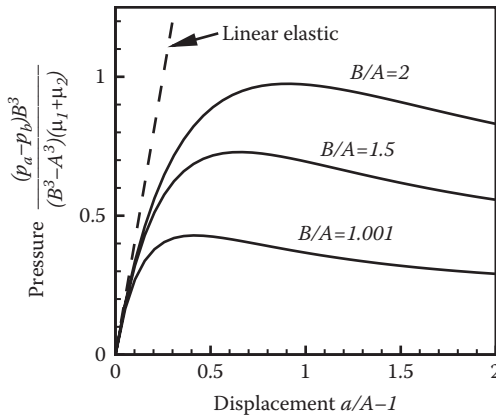


FIGURE 4.22 Variation of internal pressure with displacement for an internally pressurized hyperelastic spherical shell.

the linear elastic solution (obtained by setting $E = 3(\mu_1 + \mu_2)$ and $\nu = 1/2$ in the formulas given in Section 4.1.4) is also shown. Note the following:

1. The small strain solution is accurate for $u/A < 0.05$.
2. The relationship between pressure and displacement is nonlinear in the large deformation regimen.
3. As the internal radius of the sphere increases, the pressure reaches a maximum and thereafter decreases (this will be familiar behavior to anyone who has inflated a balloon). This is because the wall thickness of the shell decreases as the sphere expands.

The stress distribution for various displacements in the shell is plotted in Figure 4.23, for $p_b = 0$, $\mu_2/\mu_1 = 0.04$, and $B/A = 3$. The radial stress remains close to the linear elastic solution even in the large deformation regimen. The hoop stress distribution is significantly altered as the deformation increases, however.

Derivation

1. Integrate the incompressibility condition from the inner radius of the sphere to some arbitrary point R :

$$\int_{f(A)}^{f(R)} [f(R)]^2 df = \int_A^R R^2 dR \Rightarrow f(R)^3 - f(A)^3 = R^3 - A^3.$$

2. Note that $f(R) = r$ by definition, and $f(A) = a$ because the point at $R = A$ moves to $r = a$ after deformation. This gives the relationship between the position r of a point in the deformed solid and its position R before deformation:

$$r = f(R) = \sqrt[3]{R^3 + a^3 - A^3} \quad R = f^{-1}(r) = \sqrt[3]{r^3 + A^3 - a^3}.$$

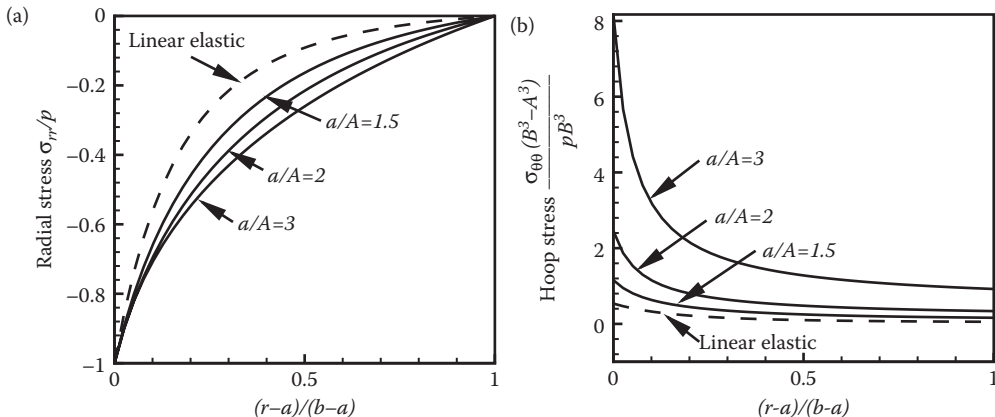


FIGURE 4.23 Stress distributions in a pressurized hyperelastic spherical shell. a, radial stress; b, hoop stress.

3. The components of the left Cauchy–Green tensor follow as $B_{rr} = (R/r)^4$, $B_{\theta\theta} = B_{\phi\phi} = (r/R)^2$.

4. The stresses follow from the stress-strain equation as

$$\sigma_{rr} = \frac{2}{3}(-_1 + _2 B_{\theta\theta})(B_{rr} - B_{\theta\theta}) + p \quad \sigma_{\theta\theta} = \sigma_{\phi\phi} = \frac{1}{3}(-_1 + _2 B_{\theta\theta})(B_{\theta\theta} - B_{rr}) + p.$$

5. Substituting these stresses into the equilibrium equation leads to the following differential equation for σ_{rr} :

$$\frac{d\sigma_{rr}}{dr} + \frac{2}{r}(-_1 + _2 B_{\theta\theta})(B_{rr} - B_{\theta\theta}) = 0.$$

6. After substituting for B_{rr} and $B_{\theta\theta}$ and expressing R in terms of r , this equation can be integrated and simplified to see that

$$\sigma_{rr} = -_1 \frac{R(4r^3 + R^3)}{2r^4} - _2 \frac{(2r^3 - R^3)}{r^2 R} + C.$$

7. The boundary conditions require that $\sigma_{rr} = -p_a$ on $(r = a, R = A)$, whereas $\sigma_{rr} = -p_b$ on $(r = b, R = B)$, which requires

$$-p_a = -_1 \left(\frac{2}{\alpha} + \frac{1}{2\alpha^4} \right) - _2 \left(2\beta - \frac{1}{\beta^2} \right) + C$$

$$-p_b = -_1 \left(\frac{2}{\beta} + \frac{1}{2\beta^4} \right) - _2 \left(2\beta - \frac{1}{\beta^2} \right) + C,$$

where $\alpha = a/A$ and $\beta = b/B$. The expression that relates α and β to the pressure follows by subtracting the first equation from the second. Adding the two equations gives the expression for C .

8. Finally, the hoop stress follows by noting that, from item 4,

$$\sigma_{\theta\theta} - \sigma_{rr} = (-_1 + _2B_{\theta\theta}) (B_{\theta\theta} - B_{rr}).$$

4.4 SIMPLE DYNAMIC SOLUTIONS FOR LINEAR ELASTIC MATERIALS

In this section, we summarize and derive the solutions to various elementary problems in dynamic linear elasticity.

4.4.1 Surface Subjected to Time-Varying Normal Pressure

An isotropic, linear elastic half-space with shear modulus E , Poisson's ratio ν , and mass density ρ_0 occupies the region $x_2 > 0$. The solid is at rest and stress free at time $t = 0$. For $t > 0$, it is subjected to a uniform pressure $p(t)$ on $x_2 = 0$ as shown in Figure 4.24.

Solution: The displacement and stress fields in the solid (as a function of time and position) are

$$u_2(x_2, t) = \begin{cases} \frac{c_L (1+\nu)(1-2\nu)}{E(1-\nu)} \int_0^{t-x_2/c_L} p(\tau) d\tau & x_2 < tc_L \\ 0 & x_2 > tc_L \end{cases}$$

$$\sigma_{22} = \begin{cases} -p(t - x_2/c_L) & x_2 < tc_L \\ 0 & x_2 > tc_L \end{cases},$$

where $c_L = \sqrt{E(1-\nu)/\rho_0(1+\nu)(1-2\nu)}$ is the speed of longitudinal wave propagation through the solid. All other displacement and stress components are zero. For the particular case of a constant (i.e., time independent) pressure, magnitude σ_0 , applied to the surface

$$u_2(x_2, t) = \begin{cases} \frac{(1-2\nu)(1+\nu)}{(1-\nu)} \frac{\sigma_0}{E} (c_L t - x_2) & x_2 < c_L t \\ 0 & x_2 > c_L t \end{cases}$$

$$\sigma_{22} = \begin{cases} -\sigma_0 & x_2 < c_L t \\ 0 & x_2 > c_L t \end{cases}.$$

Evidently, a stress pulse equal in magnitude to the surface pressure propagates vertically through the half-space with speed c_L .

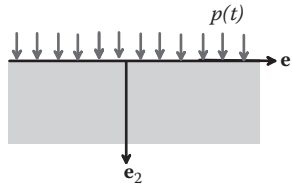


FIGURE 4.24 Surface subjected to time-varying pressure.

Notice that the velocity of the solid is constant in the region $0 < x_2 < tc_L$, and the velocity is related to the pressure by

$$v_2 = c_L \frac{(1 - 2\nu)(1 + \nu)}{(1 - \nu)} \frac{\sigma_0}{E} = \frac{\rho_0}{c_L} \sigma_0.$$

Derivation: The solution can be derived as follows. The governing equations are as follows:

- Strain-displacement relation: $\epsilon_{ij} = (\partial u_i / \partial x_j + \partial u_j / \partial x_i) / 2$.
- Elastic stress-strain equations: $\sigma_{ij} = E \left\{ \epsilon_{ij} + \nu \epsilon_{kk} \delta_{ij} / (1 - 2\nu) \right\} / (1 + \nu)$.
- Linear momentum balance equation: $\partial \sigma_{ij} / \partial x_i = \rho_0 \partial^2 u_j / \partial t^2$.

Now,

1. Symmetry considerations indicate that the displacement field must have the form

$$u_1 = u_3 = 0 \quad u_2 = u(x_2, t).$$

Substituting this equation into the strain-displacement equations shows that the only nonzero component of strain is $\epsilon_{22} = \partial u / \partial x_2$.

2. The stress-strain law then shows that

$$\sigma_{22} = \frac{E(1-\nu)}{(1+\nu)(1-2\nu)} \frac{\partial u}{\partial x_2}.$$

In addition, the shear stresses are all zero (because the shear strains are zero), and, whereas σ_{11} , σ_{22} are nonzero, they are independent of x_1 and x_3 .

3. The only nonzero linear momentum balance equation is therefore

$$\partial \sigma_{22} / \partial x_2 = \rho_0 \partial^2 u / \partial t^2.$$

Substituting for stress from item 2 yields

$$\frac{\partial^2 u}{\partial x_2^2} = \frac{1}{c_L^2} \frac{\partial^2 u}{\partial t^2},$$

where

$$c_L^2 = \frac{E(1-\nu)}{\rho_0(1+\nu)(1-2\nu)}.$$

4. This is a one-dimensional (1D) wave equation with general solution

$$u(x_2, t) = f(t - x_2/c_L) + g(t + x_2/c_L),$$

where f and g are two functions that must be chosen to satisfy boundary and initial conditions.

5. The initial conditions are

$$\left. \begin{aligned} u(x_2, 0) &= f(-x_2/c_L) + g(x_2/c_L) = 0 \\ \frac{\partial u}{\partial t} &= f'(-x_2/c_L) + g'(x_2/c_L) = 0 \end{aligned} \right\} x_2 \geq 0,$$

where the prime denotes differentiation with respect to its argument. Solving these equations (differentiate the first equation and then solve for f' , g' and integrate) shows that

$$f(-x_2/c_L) = -g(x_2/c_L) = A,$$

where A is some constant.

6. Observe that $t + x_2/c_L \geq 0$ for $t > 0$, so that $g(t + x_2/c_L) = -A$. Substituting this result back into the solution in item 4 gives $u(x_2, t) = f(t - x_2/c_L) - A$.

7. Next, use the boundary condition $\sigma_{22} = -p(t)$ at $x_2 = 0$ to see that

$$\begin{aligned} \sigma_{22} &= \frac{E(1-\nu)}{(1+\nu)(1-2\nu)} \frac{\partial u}{\partial x_2} = -p(t) \Rightarrow \frac{E(1-\nu)}{(1+\nu)(1-2\nu)} \left(\frac{-1}{c_L} \right) f'(t) = -p(t) \\ &\Rightarrow f(t - x_2/c_L) = \frac{c_L(1+\nu)(1-2\nu)}{E(1-\nu)} \int_0^{t-x_2/c_L} p(\tau) d\tau + B, \end{aligned}$$

where B is a constant of integration.

8. Finally, B can be determined by setting $t = 0$ in the result of step 7 and recalling from step 5 that $f(-x_2/c_L) = A$. This shows that $B = -A$ and so

$$u_2(x_2, t) = \frac{c_L(1+\nu)(1-2\nu)}{E(1-\nu)} \int_0^{t-x_2/c_L} p(\tau) d\tau$$

$$\sigma_{22} = -p(t - x_2/c_L)$$

as stated.

4.4.2 Surface Subjected to Time-Varying Shear Traction

An isotropic, linear elastic half-space with shear modulus E , Poisson's ratio ν , and mass density ρ_0 occupies the region $x_2 > 0$, as shown in Figure 4.25. The solid is at rest and stress free at time $t = 0$. For $t > 0$, it is subjected to a uniform antiplane shear traction $p(t)$ on $x_2 = 0$. Calculate the displacement, stress, and strain fields in the solid.

It is straightforward to show that, in this case,

$$u_3(x_2, t) = \frac{2(1+\nu)c_s}{E} \int_0^{t-x_2/c_s} p(\tau) d\tau$$

$$\sigma_{32} = -p(t - x_2/c_s),$$

where $c_s^2 = \frac{E}{2(1+\nu)\rho_0}$ is the speed of shear waves propagating through the solid. The details are left as an exercise.

4.4.3 One-Dimensional Bar Subjected to End Loading

This solution is a cheat, because it does not satisfy the full 3D equations of elasticity, but it turns out to be quite accurate.

A long thin rod occupies the region $x_1 > 0$, as shown in Figure 4.26. It is made from a homogeneous, isotropic, linear elastic material with Young's modulus E and mass density ρ_0 . At time $t < 0$, it is at rest and free of stress. At time $t = 0$, it is subjected to a pressure $p(t)$ at one end. Calculate the displacement and stress fields in the solid.

We cheat by modeling this as a 1D problem. We assume that σ_{11} is the only nonzero stress component, in which case the constitutive law and balance of linear momentum require that

$$\sigma_{11} = E \frac{\partial u_1}{\partial x_1} \quad \frac{\partial \sigma_{11}}{\partial x_1} = \rho_0 \frac{\partial^2 u_1}{\partial t^2} a$$

$$\Rightarrow \frac{\partial^2 u_1}{\partial x_1^2} = \frac{1}{c_B^2} \frac{\partial^2 u_1}{\partial t^2},$$

where $c_B^2 = E/\rho_0$ is the wave speed. This equation is exact for $\nu = 0$ but cannot be correct in general, because transverse motion is neglected. In practice, waves are repeatedly reflected off the sides of the bar, which behaves as a wave guide (for more discussion of wave guides, see Section 5.6.5).

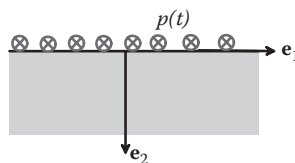


FIGURE 4.25 Surface subjected to time-varying tangential traction.



FIGURE 4.26 One-dimensional bar subjected to time-varying pressure on one end.

It is straightforward to solve the equation to see that

$$u_1(x_2, t) = \frac{c_B}{E} \int_0^{t - x_1/c_B} p(\tau) d\tau$$

$$\sigma_{11} = -p(t - x_1/c_B).$$

4.4.4 Plane Waves in an Infinite Solid

A plane wave that travels in direction \mathbf{p} at speed c has a displacement field of the form

$$u_i = a_i f(ct - x_k p_k),$$

where \mathbf{p} is a unit vector. Again, to visualize this motion, consider the special case

$$\mathbf{u} = \begin{cases} 0 & ct < x_k p_k \\ u_i = a_i (ct - x_k p_k) / c & ct \geq x_k p_k. \end{cases}$$

In this solution, the wave has a planar front, with normal vector \mathbf{p} . The wave travels in direction \mathbf{p} at speed c . Ahead of the front, the solid is at rest. Behind it, the solid has velocity \mathbf{a} . For $\mathbf{a} \cdot \mathbf{p} = 0$, the particle velocity is perpendicular to the wave velocity. For $\mathbf{a} = \alpha \mathbf{p}$, the particle velocity is parallel to the wave velocity. These two cases are like the shear and longitudinal waves discussed in the preceding sections.

We seek plane wave solutions of the Cauchy–Navier equation of motion

$$C_{ijkl} \frac{\partial^2 u_k}{\partial x_j \partial x_l} = \rho_0 \frac{\partial^2 u_i}{\partial t^2}.$$

Substituting a plane wave solution for \mathbf{u} we see that

$$A_{ik} a_k f(ct - x_j p_j) = \rho_0 a_i c^2 f(ct - x_j p_j),$$

where

$$A_{jk} = C_{ijkl} p_i p_l$$

is a symmetric, positive definite tensor known as the “acoustic tensor.” Plane wave solutions to the Cauchy–Navier equation must therefore satisfy

$$(A_{ik} - \rho_0 c^2 \delta_{ik}) a_k = 0.$$

This requires

$$\det(A_{ik} - \rho_0 c^2 \delta_{ik}) = 0.$$

Evidently, for any wave propagation direction, there are three wave speeds and three corresponding displacement directions that follow from the eigenvalues and eigenvectors of A_{ij}/ρ_0 . For the special case of an isotropic solid,

$$C_{ijkl} = (\delta_{il}\delta_{jk} + \delta_{ik}\delta_{jl}) + \frac{2\nu}{1-2\nu} \delta_{ij}\delta_{kl},$$

where ν is the shear modulus and ν is the Poisson's ratio of the solid. The acoustic tensor follows as

$$A_{ik} = p_l p_l \delta_{ik} + \frac{1}{1-2\nu} p_i p_k$$

so that

$$(-\rho_0 c^2) a_k + \frac{1}{1-2\nu} p_i a_i p_k = 0.$$

By inspection, there are two eigenvectors that satisfy this equation:

1. $a_i p_i = 0 \Rightarrow c^2 = c_s^2 = \rho_0 / (1-2\nu)$ (shear wave, or S-wave)
2. $a_i = \eta p_i \Rightarrow c^2 = c_L^2 = 2(1-\nu)/\rho_0(1-2\nu)$ (longitudinal, or P-wave).

The two wave speeds are evidently those we found in our 1D calculation previously. So there are two types of plane wave in an isotropic solid. The S-wave travels at speed c_s , and material particles are displaced perpendicular to the direction of motion of the wave. The P-wave travels at speed c_L , and material particles are displaced parallel to the direction of motion of the wave.

4.4.5 Summary of Wave Speeds in Isotropic Elastic Solids

It is worth summarizing the three wave speeds calculated in the preceding sections. Recall that

$$c_L^2 = \frac{E(1-\nu)}{\rho_0(1+\nu)(1-2\nu)} = \frac{2(1-\nu)}{\rho_0(1-2\nu)} \quad c_s^2 = \frac{E}{2(1+\nu)\rho_0} = \frac{1}{\rho_0} \quad c_B^2 = \frac{E}{\rho_0}.$$

It is straightforward to show that, for all positive definite materials (those with positive definite strain energy density, a thermodynamic constraint), $c_L > c_s$. For most real materials, $c_L > c_B > c_s$.

There are also special kinds of waves (called Rayleigh and Stoneley waves) that travel near the surface of a solid or near the interface between two dissimilar solids, respectively. These waves have their own speeds. Rayleigh waves are discussed in more detail in Section 5.5.3.

4.4.6 Reflection of Waves Traveling Normal to a Free Surface

Suppose that a longitudinal wave with stress state and displacement

$$u_1(x_1, t) = -\frac{c_L}{E} \frac{(1+\nu)(1-2\nu)}{(1-\nu)} \int_0^{t-x_1/c_L} f(\tau) d\tau$$

$$u_2 = u_3 = 0$$

$$\sigma_{11} = f(t - x_1/c_L)$$

is incident on a free surface at $x_1 = a$, as shown in Figure 4.27. Our objective is to calculate the state of stress in the solid as a function of time, accounting for the stress-free surface.

To visualize the wave, imagine that it is a front, such as would be generated by applying a constant uniform pressure at $x_1 = 0$ at time $t = 0$. The material ahead of the front is at rest and stress free, whereas behind the front, material has a constant stress and velocity. At time $t = a/c_L$, the front would reach the free surface and be reflected. Let the horizontal stress associated with the reflected wave be

$$\sigma_{11} = g(t + x_1/c_L)$$

(we need a + in the argument because the wave travels to the left and has negative velocity). For the stress to vanish at the free surface, we must have

$$f(t - a/c_L) + g(t + a/c_L) = 0,$$

so,

$$g(t + x_1/c_L) = -f(t - a/c_L + (x_1 - a)/c_L)$$

and the full solution consists of both incident and reflected waves:

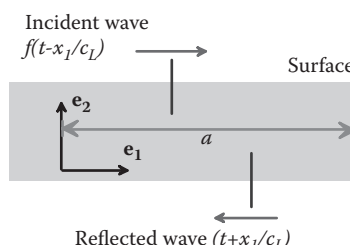


FIGURE 4.27 Reflection of a longitudinal wave at a free surface.

$$u_1(x_1, t) = -\frac{c_L}{E} \frac{(1+\nu)(1-2\nu)}{1-\nu} \left\{ \int_0^{t-x_1/c_L} f(\tau) d\tau + \int_0^{t-a/c_L + (x_1-a)/c_L} f(\tau) d\tau \right\}$$

$$u_2 = u_3 = 0$$

$$\sigma_{11} = f(t - x_1/c_L) - f(t - a/c_L + (x_1 - a)/c_L).$$

As a specific example, consider a plane, constant-stress wave that is incident on a free surface. The histories of stress and velocity in the solid are illustrated in Figure 4.28. In this case,

1. Behind the incident stress wave, the stress is constant, with magnitude σ_0 . The velocity of the solid is constant and related to the stress by $v_1 = -\rho\sigma_0/c_L$.
2. At time, $t = a/c_L$ the stress wave reaches the free surface. At this time, an equal and opposite stress pulse $-\sigma_0$ is reflected from the free surface and propagates away from the surface.
3. Behind the reflected wave, the solid is stress free and the solid has constant velocity $v_1 = -2\rho\sigma_0/c_L$.

4.4.7 Reflection and Transmission of Waves Normal to an Interface

The problem to be solved is illustrated in Figure 4.29. The material on the left has mass density ρ_0 and elastic properties that give a longitudinal wave speed c_L . The corresponding properties for the material on the right are ρ_B , c_L^B . Suppose that a longitudinal wave with displacement and stress state and displacement

$$u_1(x_1, t) = -\frac{c_L}{E} \frac{(1+\nu)(1-2\nu)}{1-\nu} \int_0^{t-x_1/c_L} f(\tau) d\tau$$

$$u_2 = u_3 = 0$$

$$\sigma_{11} = f(t - x_1/c_L)$$

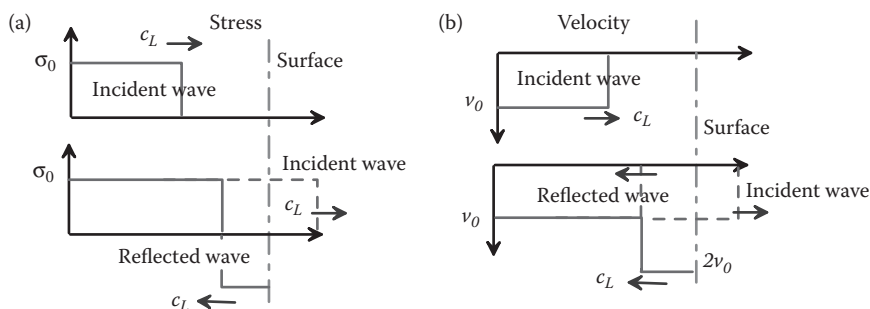


FIGURE 4.28 Solutions for reflection of a wave at a free surface. (a) Stress; (b) velocity.

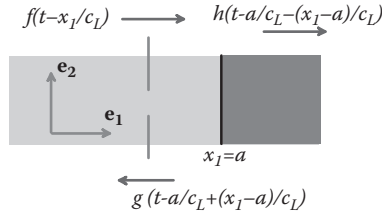


FIGURE 4.29 Reflection and transmission of a longitudinal wave at a bimaterial interface.

is incident on a bimaterial interface at $x_1 = a$. Calculate the state of stress in the solid as a function of time, accounting for the interface.

As before, waves will be reflected at the bimaterial interface. This time, however, some of the energy will be reflected, whereas some will be transmitted into the adjacent solid. Guided by the solution to the preceding problem, we assume that the stress associated with the reflected and transmitted waves have the form

$$\begin{aligned}\sigma_{11} &= g\left(t - a/c_L + (x_1 - a)/c_L\right) \\ \sigma_{11} &= h\left(t - a/c_L - (x_1 - a)/c_L^B\right).\end{aligned}$$

The functions g and h must be chosen to satisfy stress and displacement continuity at the interface. Stress continuity requires the following:

$$f\left(t - a/c_L\right) + g\left(t - a/c_L\right) = h\left(t - a/c_L\right).$$

To satisfy displacement continuity, we make the acceleration continuous

$$\begin{aligned}\rho_0 \frac{\partial^2 u_1}{\partial t^2} &= \frac{\partial \sigma_{11}}{\partial x_1} \\ \Rightarrow -\frac{f'\left(t - a/c_L\right)}{\rho_0 c_L} + \frac{g'\left(t - a/c_L\right)}{\rho_0 c_L} &= -\frac{h'\left(t - a/c_L^B\right)}{\rho_B c_L^B},\end{aligned}$$

which may be integrated to give

$$-\frac{f\left(t - a/c_L\right)}{\rho_0 c_L} + \frac{g\left(t - a/c_L\right)}{\rho_0 c_L} = -\frac{h\left(t - a/c_L^B\right)}{\rho_B c_L^B} + C,$$

where C is a constant of integration. Setting $t = 0$ shows that C must vanish, because $f = g = h = 0$ at $t = 0$. The conditions of stress and displacement continuity may now be solved for g and h to see the following:

$$\text{reflected wave: } \sigma_{11}^{(r)} = \beta_r f\left(t - a/c_L + (x_1 - a)/c_L\right),$$

$$\text{transmitted wave: } \sigma_{11}^{(t)} = \beta_t f\left(t - a/c_L - (x_1 - a)/c_L^B\right),$$

where the coefficients of reflection and transmission are given by

$$\beta_r = \frac{\rho_B c_L^B - \rho_0 c_L}{\rho_B c_L^B + \rho_0 c_L} \quad \beta_t = \frac{2\rho_B c_L^B}{\rho_B c_L^B + \rho_0 c_L}.$$

Results for a shear wave approaching the interface follow immediately from the preceding calculation, by simply setting $c_L = c_S$.

4.4.8 Simple Example Involving Plane Wave Propagation: Plate Impact Experiment

A plate impact experiment is used to measure the plastic properties of materials at high rates of strain. In typical experiment, a large, elastic flyer plate is fired (e.g., by a gas gun) at a stationary target plate. The specimen is a thin film of material that is usually deposited on the surface of the flyer plate. When the flyer plate impacts the target, plane pressure and shear waves begin to propagate through both plates, as shown in Figure 4.30. The experiment is designed so that the target and flyer plates remain elastic, whereas the thin film specimen deforms plastically. A laser interferometer is used to monitor the velocity of the back face of the target plate: these measurements enable the history of stress and strain in the film to be reconstructed.

A full analysis of the plate impact experiment will not be attempted here; instead, we illustrate the general procedure for modeling plane wave propagation in the plate impact experiment using a simple example. Suppose the following:

- Two elastic plates with Young's modulus E , Poisson's ratio ν and density ρ are caused to collide, as shown in Figure 4.31.
- As a representative example, we suppose that the target has thickness h , whereas the projectile has thickness $2h$, as shown in Figure 4.31. The thickness of both flyer and target are assumed to be much smaller than any other relevant dimension (so wave reflection off lateral boundaries can be neglected).
- For simplicity, we assume that the faces of flyer and target are perpendicular to the direction of motion. This means that the particle velocity in both flyer and target remains perpendicular to their surfaces throughout.

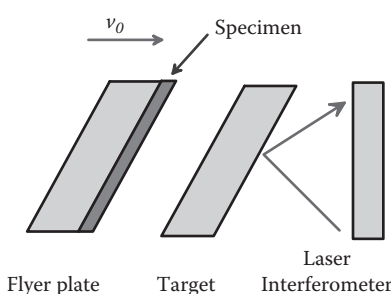


FIGURE 4.30 The pressure-shear plate impact experiment.

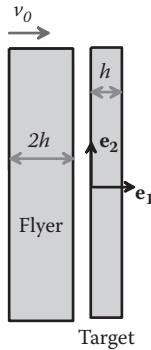


FIGURE 4.31 Normal impact between a flyer and a target plate.

- Just before impact, the projectile has a uniform velocity v_0 , whereas the target is stationary.
- At impact, plane pressure waves are initiated at the impact surface and propagate (in opposite directions) through both target and projectile. Our objective is to calculate the history of stress and velocity in both plates.

The resulting stress and motion in the plate is most conveniently displayed on “ $(x - t)$ diagrams” as shown in Figure 4.32. The graphs can be used to deduce the velocity and stress in both flyer and target at any position x and time t in both plates. The solution consists of triangular regions (of time and position) of constant velocity and stress, separated by lines with slope equal to the longitudinal wave speed c_L in the two plates (these lines are called “characteristics”). Note that the stress and velocity have constant discontinuities across each characteristic. Figure 4.32 illustrates the following sequence of events:

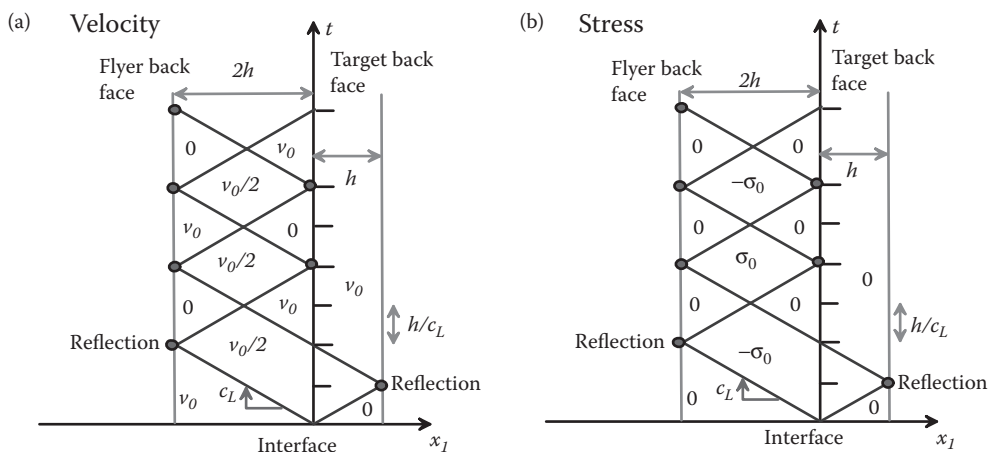


FIGURE 4.32 Characteristic diagrams for wave propagation during normal impact between a flyer and target plate, showing histories of velocity (a) and stress (b).

1. Just after impact, plane pressure waves propagate in opposite directions through the flyer and target. Behind the traveling wave fronts, both plates have velocity $v_1 = v_0/2$ and are subjected to a stress state $\sigma_{11} = \sigma_{22} = \sigma_{33} = -\sigma_0$, where $\sigma_0 = v_0 c_L / 2\rho$.
2. At time $t = h/c_L$, the wave propagating in the target plate reaches the free surfaces on the back side of the target. The wave is reflected from the free surface. Behind this reflected wave, the target is stress free and has velocity v_0 . The target thereafter continues to travel at constant speed and remains free of stress indefinitely.
3. At time $t = 2h/c_L$, there are two simultaneous events. (1) The plane wave in the flyer is reflected off the back surface; behind the reflected wave, the flyer is stress free and has zero velocity. (2) The reflected wave in the target reaches the interface. Because the interface is in compression and the stress merely drops to zero behind the reflected wave, it passes freely through the interface without reflection.
4. At time $t = 3h/c_L$, the two reflected waves in the flyer meet at the midpoint of the flyer. Thereafter, the region between the two reflected waves in the flyer becomes tensile. In addition, the flyer plate has speed $v_0/2$ between the two wavefronts.
5. At time $t = 4h/c_L$, the reflected wave from the back surface of the flyer reaches the interface. The stress is tensile behind this wave front and, because the interface between flyer and target cannot support tension, it behaves like a free surface, and the wave is reflected off the interface back into the flyer. At the same time, the reflected wave from the target reaches the back face of the flyer and is reflected for a second time.
6. Thereafter, the target continues to propagate with constant velocity v_0 , whereas the flyer contains two plane waves that are repeatedly reflected from its two surfaces. These waves effectively cause the flyer to vibrate, while traveling with average speed $v_0/2$.

Derivation: The solution can be constructed using the simple 1D solutions given in Sections 4.4.1 and 4.4.6. For example, to find the stress and velocity associated with the waves generated by the initial impact, note the following:

1. At the moment of impact, both flyer and target are subjected to a sudden pressure. Wave motion in both solids can be analyzed using the solution given in Section 4.4.1.
2. Let Δv_f , Δv_t denote the change in velocity of the flyer and target, respectively, as a result of impact.
3. Let $\sigma_{11} = \sigma_f$ and $\sigma_{11} = \sigma_t$ denote the horizontal stress component behind the wavefronts in the flyer and target just after impact.
4. From Section 4.4.1, we know that the velocity change and stress are related by

$$\Delta v_f = -\rho \sigma_f / c_L \quad \Delta v_t = -\rho \sigma_t / c_L.$$

5. The target and flyer must have the same velocity at the impact surface. Therefore,
 $v_0 - \Delta v_f = \Delta v_t$.
6. The horizontal stress must be equal in both solids at the impact surface. Therefore,
 $\sigma_f = \sigma_t$.
7. The four equations in steps 4–6 can be solved to yield $\Delta v_f = \Delta v_t = v_0/2$, $\sigma_f = \sigma_t = -\sigma_0$,
with $\sigma_0 = v_0 c_L / 2\rho$.

The changes in stress and velocity that occur at each reflection can then be deduced using the results at the end of Section 4.4.6. Alternatively, the $(x - t)$ diagrams can be constructed directly, by first drawing all the characteristic lines and then deducing the velocity and stress in each sector of the diagram by noting that (1) the change in stress and velocity across each line must be constant, (2) the overall momentum of the solid must be conserved, and (3) the total energy of the solid must be conserved.

Solutions for Linear Elastic Solids

In the preceding chapter, we solved some simple linear elastic boundary value problems. The problems were trivial, however, in that the stress, strain, and displacement fields were axially or spherically symmetric. Most problems of practical interest involve fully 3D stress and displacement fields.

It is extremely difficult to solve general boundary value problems. However, some of the best mathematicians over the past 200 years have turned their attention to this matter and have developed several very elegant techniques. None of these are completely general, but solutions derived using these techniques have provided invaluable insight into the behavior of deformable solids.

Sadly, these days any fool with a personal computer and a finite element package can solve virtually any linear elastic boundary value problem, so you will not be able to make a living calculating exact elasticity solutions. Nevertheless, some exact solutions are of fundamental practical importance. Examples include contact problems, solutions for cracks, stress concentrations, thermal stress problems, and problems involving defects such as dislocations in solids. It is worth seeing how such solutions were derived.

In addition, there are some very powerful theorems in linear elasticity (such as the principle of minimum potential energy and the reciprocal theorem) that can be used to calculate quantities of interest without necessarily having to solve all the governing equations.

In this chapter, we present a very brief survey of the field of linear elasticity. Specifically,

1. We will outline some important general features of solutions to boundary and initial value problems.
2. We will discuss some solution techniques and present solutions to selected boundary value problems of interest.

3. We will discuss energy methods for solving problems involving linear elastic solids, including the principle of minimum potential energy, the reciprocal theorem, and the Rayleigh–Ritz method for estimating natural frequencies of vibrating elastic solids.

5.1 GENERAL PRINCIPLES

5.1.1 Summary of the Governing Equations of Linear Elasticity

Static problems: We already listed the governing equations of linear elasticity in our discussion of simple axisymmetric problems. They are repeated here for convenience.

A representative problem is sketched in Figure 5.1. We are given the following:

1. The shape of the solid in its unloaded condition R
2. The initial stress field in the solid (we will take this to be zero)
3. The elastic constants for the solid C_{ijkl} and its mass density ρ_0
4. The thermal expansion coefficients α_{ij} for the solid and temperature change from the initial configuration ΔT
5. A body force distribution \mathbf{b} (per unit mass) acting on the solid
6. Boundary conditions, specifying displacements $\mathbf{u}^*(\mathbf{x})$ on a portion $\partial_1 R$ or tractions on a portion $\partial_2 R$ of the boundary of R

With this information, our goal is to calculate displacements, strains, and stresses satisfying the governing equations of linear elastostatics:

$$\begin{aligned}\varepsilon_{ij} &= \frac{1}{2} \left(\frac{\partial u_i}{\partial x_j} + \frac{\partial u_j}{\partial x_i} \right) & \sigma_{ij} &= C_{ijkl} (\varepsilon_{kl} - \alpha_{kl} \Delta T) & \frac{\partial \sigma_{ij}}{\partial x_i} + \rho_0 b_j &= 0 \\ u_i = u_i^* &\quad \text{on } \partial_1 R & \sigma_{ij} n_i = t_j^* &\quad \text{on } \partial_2 R.\end{aligned}$$

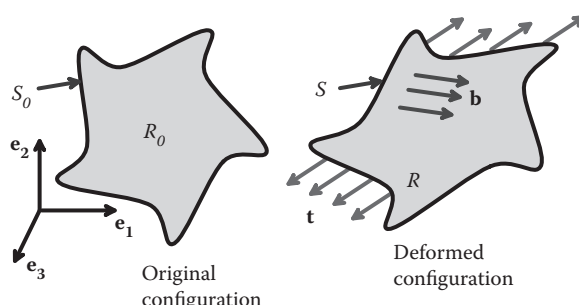


FIGURE 5.1 A representative boundary value problem for an elastic solid.

Dynamic problems: Dynamic problems are essentially identical, except that the boundary conditions must be specified as functions of time, and the initial displacement and velocity field must be specified. In this case, the governing equations are

$$\boldsymbol{\varepsilon}_{ij} = \frac{1}{2} \left(\frac{\partial u_i}{\partial x_j} + \frac{\partial u_j}{\partial x_i} \right) \quad \sigma_{ij} = C_{ijkl} (\varepsilon_{kl} - \alpha_{kl} \Delta T) \quad \frac{\partial \sigma_{ij}}{\partial x_i} + \rho_0 b_j = \rho_0 \frac{\partial^2 u_j}{\partial t^2}$$

$$u_i = u_i^*(t) \quad \text{on } \partial_1 R \quad \sigma_{ij} n_i = t_j^*(t) \quad \text{on } \partial_2 R.$$

5.1.2 Alternative Form of the Governing Equations: Navier Equation

The governing equations can be simplified by eliminating stress and strain from the governing equations and solving directly for the displacements. In this case, the linear momentum balance equation (in terms of displacement) reduces to

$$C_{ijkl} \frac{\partial}{\partial x_i} \left(\frac{\partial u_k}{\partial x_l} - \alpha_{kl} \Delta T \right) + \rho_0 b_j = \rho_0 \frac{\partial^2 u_j}{\partial t^2}.$$

For the special case of an isotropic solid with shear modulus μ and Poisson's ratio ν and uniform temperature $\Delta T = 0$, this equation reduces to

$$\frac{1}{1 - 2\nu} \frac{\partial^2 u_k}{\partial x_k \partial x_i} + \frac{\partial^2 u_i}{\partial x_k \partial x_k} + \rho_0 \frac{b_i}{b_i} = \rho_0 \frac{\partial^2 u_i}{\partial t^2}.$$

These are known as the Navier (or Cauchy–Navier) equations of elasticity. The boundary conditions remain as given in the preceding section.

5.1.3 Superposition and Linearity of Solutions

The governing equations of elasticity are *linear*. This has two important consequences:

1. The stresses, strains, and displacements in a solid are directly proportional to the loads (or displacements) applied to the solid.
2. If you can find two sets of displacements, strains, and stresses that satisfy the governing equations, you can add them to create more solutions.

These principles can be illustrated clearly using some of the simple solutions derived in Section 4.1. For example, examine the solution to the pressurized sphere illustrated in Figure 5.2. As an example, the radial stress induced by pressure p_a on the interior and zero pressure on the exterior surface is

$$\sigma_{rr} = \frac{(p_a a^3)}{(b^3 - a^3)} \left(1 - \frac{b^3}{r^2} \right).$$

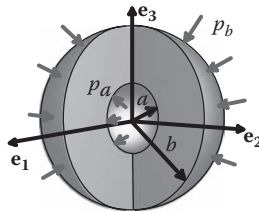


FIGURE 5.2 Spherical shell subjected to internal and external pressure.

The radial stress induced by pressure p_b on the exterior surface with zero pressure on the interior surface is

$$\sigma_{rr} = -\frac{(p_b b^3)}{(b^3 - a^3)} \left(1 - \frac{a^3}{r^3} \right).$$

Note that, in both cases, the stress is directly proportional to the pressure. In addition, to find the radial stress by combined pressures p_a on the interior and p_b on the exterior surface, you can just add these two solutions. Additional examples of superposition and linearity will be given in subsequent sections.

5.1.4 Uniqueness and Existence of Solutions to the Linear Elasticity Equations

The following results are useful:

1. If only displacements are prescribed on the boundary of the solid, the governing equations of linear elasticity always have a solution, and the solution is unique.
2. If mixed boundary conditions are specified, a static solution exists and is unique if the displacements constrain rigid motions. A dynamic solution always exists and is unique, provided the velocity field and displacement field at time $t = 0$ are known.
3. If only tractions are prescribed on the boundary, a static solution exists only if the tractions are in equilibrium. In this case, the stresses and strains are unique, but the displacements are not. A dynamic solution always exists and is unique, again, providing initial conditions are known.

5.1.5 Saint-Venant's Principle

Saint-Venant's principle (SVP) is often invoked to justify approximate solutions to boundary value problems in linear elasticity. For example, when we solve problems involving bending or axial deformation of slender beams and rods in elementary strength of materials courses, we only specify the resultant forces acting on the ends of a rod or the magnitudes of point forces acting on a beam; we don't specify the distribution of

traction in detail. We rely on SVP to justify this approach. In this context, the principle states the following:

The stresses, strains, and displacements far from the ends of a rod or beam subjected to end loading depend only on the resultant forces and moments acting on its ends and do not depend on how the tractions themselves are distributed.

Although SVP is widely used, it turns out to be remarkably difficult to prove mathematically. The difficulty is partly that it is not easy to state the principle itself precisely enough to apply any mathematical machinery to it. A rigorous statement is given by Sternberg [1954], among several other versions. Here, we will just illustrate the most common applications of the principle through specific examples.

One version of SVP can be stated as follows:

Suppose that we calculate the stress, strain, and displacement induced in a solid by two different traction distributions $\mathbf{t}^{(1)}$ and $\mathbf{t}^{(2)}$ that act on some small region of a solid with characteristic size a . If the tractions exert the same resultant force and moment, then the stresses, strains, and displacements induced by the two traction distributions at a distance r from the loaded region are identical for large r/a .

In practice, “large” usually means $r/a > 3$. This principle can be illustrated using a simple example. Consider a large solid with a flat surface, as shown in Figure 5.3. It is possible to calculate formulas for the stresses and displacements induced by various pressure distributions acting on the flat surface; the procedure to do this will be outlined later. For now, we will compare the stresses induced by the following:

1. A *uniform* pressure: $p(r) = P / (\pi a^2)$ $r \leq a$;
2. A *parabolic* pressure: $p(r) = \frac{3P}{2\pi a^2} (1 - r^2 / a^2)^{1/2}$ $r \leq a$.

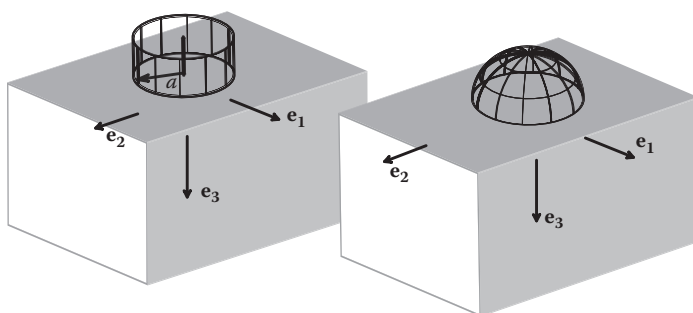


FIGURE 5.3 Surfaces subjected to uniform and parabolic pressure distributions exerting equal resultant forces.

You can verify for yourself that both pressure distributions exert a resultant force P acting in the vertical direction on the surface and exert zero moment about the origin. The variation of stress down the axis of symmetry ($r = \sqrt{x_1^2 + x_2^2} = 0$), expressed in cylindrical-polar coordinates, can be derived as follows:

- Case 1, uniform pressure:

$$\sigma_{zz} = -\frac{P}{\pi a^2} \left(1 - \frac{z^3}{(a^2 + z^2)^{3/2}} \right) \quad \sigma_{rr} = \sigma_{\theta\theta} = -\frac{P}{\pi a^2} \left(\frac{1+2\nu}{2} - \frac{(1+\nu)z}{(a^2 + z^2)^{1/2}} + \frac{z^3}{2(a^2 + z^2)^{3/2}} \right)$$

- Case 2, parabolic pressure:

$$\sigma_{zz} = -\frac{3P}{2\pi a^2} \frac{a^2}{(a^2 + z^2)} \quad \sigma_{rr} = \sigma_{\theta\theta} = -\frac{3P}{2\pi a^2} \left\{ (1+\nu) \left(1 - \frac{z}{a} \tan^{-1} \frac{a}{z} \right) - \frac{1}{2} \frac{a^2}{a^2 + z^2} \right\}.$$

Now, to demonstrate SVP, we want to show that the stresses are equal for large z/a . We can do this graphically. Figure 5.4 compares the variation of vertical and radial stress down the axis of symmetry with z/a .

The stresses induced by the two different pressures are clearly indistinguishable for $z/a > 3$. This example helps to quantify what we mean by a large distance. The second commonly used application of SVP is a rather vague statement:

A localized geometrical feature with characteristic size R in a large solid only influences the stress in a region with size approximately $3R$ surrounding the feature.

This is more a rule of thumb than a precise mathematical statement. It can be illustrated by looking at specific solutions. For example, Figure 5.5 shows the von Mises stress con-

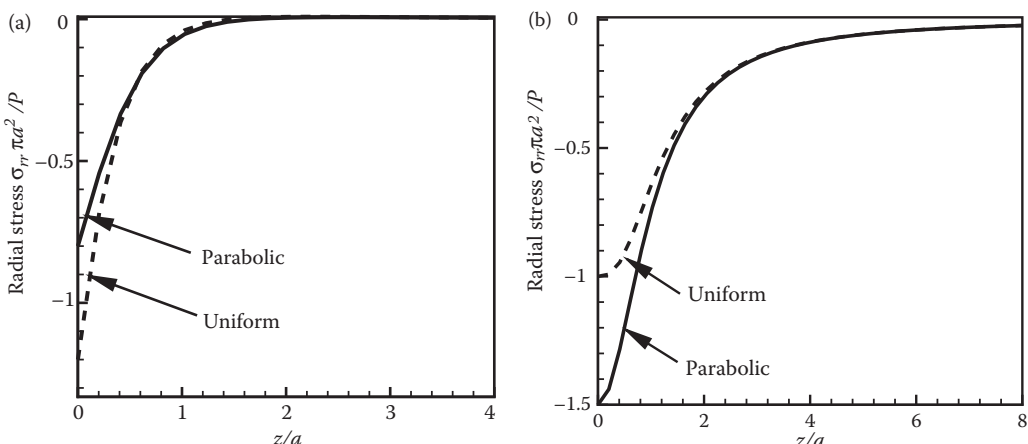


FIGURE 5.4 Variation of stress with depth on the axis of symmetry for the surfaces shown in Figure 5.3. (a) Vertical stress; (b) radial stress.

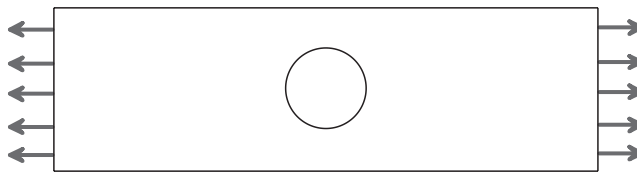


FIGURE 5.5 Contours of horizontal stress near a hole in a strip subjected to uniaxial tension.

tours surrounding a circular hole in a thin rectangular plate that is subjected to extensional loading (calculated using the FEM). Far from the hole, the stress is uniform. The contours deviate from the uniform solution in a region that is about three times the hole radius.

5.2 AIRY FUNCTION SOLUTION TO PLANE STRESS AND STRAIN STATIC LINEAR ELASTIC PROBLEMS

In this section, we outline a general technique for solving 2D static linear elasticity problems. The technique is known as the “Airy stress function” method.

A typical plane elasticity problem is illustrated in Figure 5.6. The solid is two dimensional, which means either of the following:

1. The solid is a thin sheet, with small thickness h , and is loaded only in the $\{e_1, e_2\}$ plane. In this case, the plane stress solution is applicable.
2. The solid is very long in the e_3 direction and is prevented from stretching parallel to the e_3 axis, and every cross-section is loaded identically and only in the $\{e_1, e_2\}$ plane. In this case, the plane strain solution is applicable.

Some additional basic assumptions and restrictions are as follows:

- The Airy stress function is applicable only to isotropic solids. We will assume that the solid has Young's modulus E , Poisson's ratio ν , and mass density ρ_0 .

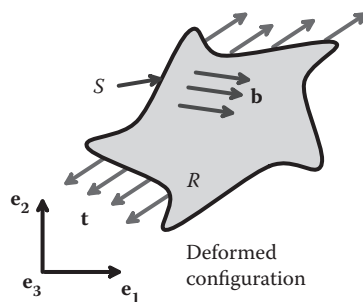


FIGURE 5.6 A 2D elastic solid subjected to external forces.

- The Airy stress function can only be used if the body force has a special form. Specifically, the requirement is

$$\rho_0 b_1 = \frac{\partial \Omega}{\partial x_1} \quad \rho_0 b_2 = \frac{\partial \Omega}{\partial x_2} \quad b_3 = 0,$$

where $\Omega(x_1, x_2)$ is a scalar function of position. Fortunately, most practical body forces can be expressed in this form, including gravity.

- The Airy stress function approach works best for problems in which a solid is subjected to prescribed tractions on its boundary rather than prescribed displacements. Specifically, we will assume that the solid is loaded by boundary tractions $t_1(x_1, x_2)$, $t_2(x_1, x_2)$, $t_3 = 0$.

5.2.1 The Airy Solution in Rectangular Coordinates

The Airy function procedure can then be summarized as follows:

1. Begin by finding a scalar function $\phi(x_1, x_2)$ (known as the Airy potential) that satisfies

$$\nabla^4 \phi \equiv \frac{\partial^4 \phi}{\partial x_1^4} + 2 \frac{\partial^4 \phi}{\partial x_1^2 \partial x_2^2} + \frac{\partial^4 \phi}{\partial x_2^4} = C(\nu) \rho_0 \left(\frac{\partial b_1}{\partial x_1} + \frac{\partial b_2}{\partial x_2} \right)$$

where

$$C(\nu) = \begin{cases} \frac{1-\nu}{1-2\nu} & (\text{Plane Strain}) \\ \frac{1}{1-\nu} & (\text{Plane Stress}). \end{cases}$$

In addition, ϕ must satisfy the following traction boundary conditions on the surface of the solid:

$$\frac{\partial^2 \phi}{\partial x_2^2} n_1 - \frac{\partial^2 \phi}{\partial x_1 \partial x_2} n_2 = t_1 \quad \frac{\partial^2 \phi}{\partial x_1^2} n_2 - \frac{\partial^2 \phi}{\partial x_1 \partial x_2} n_1 = t_2,$$

where (n_1, n_2) are the components of a unit vector normal to the boundary.

2. Given ϕ , the stress field within the region of interest can be calculated from the formulas

$$\begin{aligned} \sigma_{11} &= \frac{\partial^2 \phi}{\partial x_2^2} - \Omega & \sigma_{22} &= \frac{\partial^2 \phi}{\partial x_1^2} - \Omega & \sigma_{12} = \sigma_{21} &= -\frac{\partial^2 \phi}{\partial x_1 \partial x_2} \\ \sigma_{33} &= 0 & & & & (\text{Plane Stress}) \\ \sigma_{33} &= \nu(\sigma_{11} + \sigma_{22}) & & & & (\text{Plane Strain}) \\ \sigma_{23} &= \sigma_{13} = 0. & & & & \end{aligned}$$

3. If the strains are needed, they may be computed from the stresses using the elastic stress-strain relations.
4. If the displacement field is needed, it may be computed by integrating the strains, following the procedure described in Section 2.1.20. An example (in polar coordinates) is given in Section 5.2.4 below.

Although it is easier to solve for ϕ than it is to solve for stress directly, this is still not a trivial exercise. Usually, one guesses a suitable form for ϕ , as illustrated below. This may seem highly unsatisfactory, but remember that we are essentially integrating a system of partial differential equations. The general procedure to evaluate any integral is to guess a solution, differentiate it, and see whether the guess was correct.

5.2.2 Demonstration That the Airy Solution Satisfies the Governing Equations

Recall that, to solve a linear elasticity problem, we need to satisfy the following equations:

- Displacement-strain relation: $\epsilon_{ij} = \frac{1}{2} \left(\frac{\partial u_i}{\partial x_j} + \frac{\partial u_j}{\partial x_i} \right)$
- Stress-strain relation: $\epsilon_{ij} = \frac{1+\nu}{E} \sigma_{ij} - \frac{\nu}{E} \sigma_{kk} \delta_{ij}$
- Equilibrium equation: $\frac{\partial \sigma_{ij}}{\partial x_i} + \rho_0 b_j = 0$

where we have neglected thermal expansion, for simplicity. We proceed to show that these equations are satisfied:

1. We show first that the Airy function satisfies the equilibrium equations automatically. For plane stress or plane strain conditions, the equilibrium equations reduce to

$$\frac{\partial \sigma_{11}}{\partial x_1} + \frac{\partial \sigma_{12}}{\partial x_2} + \rho_0 b_1 = 0 \quad \frac{\partial \sigma_{12}}{\partial x_1} + \frac{\partial \sigma_{22}}{\partial x_2} + \rho_0 b_2 = 0.$$

2. Substitute for the stresses in terms of ϕ to see that

$$\begin{aligned} \frac{\partial}{\partial x_1} \left(\frac{\partial^2 \phi}{\partial x_2^2} - \Omega \right) + \frac{\partial}{\partial x_2} \left(-\frac{\partial^2 \phi}{\partial x_1 \partial x_2} \right) + \rho_0 b_1 &= 0 \\ \frac{\partial}{\partial x_1} \left(\frac{\partial^2 \phi}{\partial x_1 \partial x^2} \right) + \frac{\partial}{\partial x_2} \left(\frac{\partial^2 \phi}{\partial x_1^2} - \Omega \right) + \rho_0 b_2 &= 0, \end{aligned}$$

so that the equilibrium equations are satisfied automatically for any choice of ϕ .

To show that the strain-displacement equation and the strain-displacement equation are satisfied, we first compute the strains using the elastic stress-strain equations. Recall that

$$\sigma_{33} = \beta v(\sigma_{11} + \sigma_{22}),$$

with $\beta = 0$ for plane stress and $\beta = 1$ for plane strain. Hence,

$$\begin{aligned}\epsilon_{ij} &= \frac{1+v}{E} \sigma_{ij} - \frac{v}{E} \sigma_{kk} \delta_{ij} \\ \Rightarrow \epsilon_{11} &= \frac{1+v}{E} \sigma_{11} - \frac{v}{E} (1+\beta v)(\sigma_{11} + \sigma_{22}) \\ \epsilon_{22} &= \frac{1+v}{E} \sigma_{22} - \frac{v}{E} (1+\beta v)(\sigma_{11} + \sigma_{22}) \\ \epsilon_{12} &= \frac{1+v}{E} \sigma_{12}.\end{aligned}$$

Next, recall that the strain-displacement relation is satisfied provided that the strains obey the compatibility conditions

$$\begin{array}{ll}\frac{\partial^2 \epsilon_{11}}{\partial x_2^2} + \frac{\partial^2 \epsilon_{22}}{\partial x_1^2} - 2 \frac{\partial^2 \epsilon_{12}}{\partial x_1 \partial x_2} = 0 & \frac{\partial^2 \epsilon_{11}}{\partial x_2 \partial x_3} - \frac{\partial}{\partial x_1} \left(-\frac{\partial \epsilon_{23}}{\partial x_1} + \frac{\partial \epsilon_{31}}{\partial x_2} + \frac{\partial \epsilon_{12}}{\partial x_3} \right) = 0 \\ \frac{\partial^2 \epsilon_{11}}{\partial x_3^2} + \frac{\partial^2 \epsilon_{33}}{\partial x_1^2} - 2 \frac{\partial^2 \epsilon_{13}}{\partial x_1 \partial x_3} = 0 & \frac{\partial^2 \epsilon_{22}}{\partial x_3 \partial x_1} - \frac{\partial}{\partial x_2} \left(-\frac{\partial \epsilon_{31}}{\partial x_2} + \frac{\partial \epsilon_{12}}{\partial x_3} + \frac{\partial \epsilon_{23}}{\partial x_1} \right) = 0 \\ \frac{\partial^2 \epsilon_{22}}{\partial x_3^2} + \frac{\partial^2 \epsilon_{33}}{\partial x_2^2} - 2 \frac{\partial^2 \epsilon_{23}}{\partial x_2 \partial x_3} = 0 & \frac{\partial^2 \epsilon_{33}}{\partial x_1 \partial x_2} - \frac{\partial}{\partial x_3} \left(-\frac{\partial \epsilon_{12}}{\partial x_3} + \frac{\partial \epsilon_{23}}{\partial x_1} + \frac{\partial \epsilon_{31}}{\partial x_2} \right) = 0.\end{array}$$

All but the first of these equations are satisfied automatically by any plane strain or plane stress field. We therefore need to show that the Airy representation satisfies the first equation. To see this, substitute into the first compatibility equation in terms of stress to see that

$$\frac{1+v}{E} \left(\frac{\partial^2 \sigma_{11}}{\partial x_2^2} + \frac{\partial^2 \sigma_{22}}{\partial x_1^2} \right) - \frac{v}{E} (1+\beta v) \left(\frac{\partial^2}{\partial x_1^2} + \frac{\partial^2}{\partial x_2^2} \right) (\sigma_{11} + \sigma_{22}) - 2 \frac{1+v}{E} \frac{\partial^2 \sigma_{12}}{\partial x_1 \partial x_2} = 0.$$

Finally, substitute into this horrible looking equation for stress in terms of ϕ and rearrange to see that

$$\frac{\partial^4 \phi}{\partial x_2^4} - \frac{\partial^2 \Omega}{\partial x_2^2} + \frac{\partial^4 \phi}{\partial x_1^4} - \frac{\partial^2 \Omega}{\partial x_1^2} - \frac{v(1+\beta v)}{1+v} \left(\frac{\partial^2}{\partial x_1^2} + \frac{\partial^2}{\partial x_2^2} \right) \left(\frac{\partial^2 \phi}{\partial x_1^2} + \frac{\partial^2 \phi}{\partial x_2^2} - 2\Omega \right) + 2 \frac{\partial^4 \phi}{\partial x_1^2 \partial x_2^2} = 0.$$

A few more weeks of algebra reduces this to

$$\frac{\partial^4 \phi}{\partial x_1^4} + 2 \frac{\partial^4 \phi}{\partial x_1^2 \partial x_2^2} + \frac{\partial^4 \phi}{\partial x_2^4} = \frac{1-\beta v^2}{1-v-2\beta v^2} \left(\frac{\partial^2 \Omega}{\partial x_1^2} + \frac{\partial^2 \Omega}{\partial x_2^2} \right).$$

This is the governing equation for the Airy function so, if the governing equation is satisfied, then the compatibility equation is also satisfied.

This proves that the Airy representation satisfies the governing equations. A second important question is this: is it possible to find an Airy function for *all* 2D plane stress and plane strain problems? If not, the method would be useless, because you couldn't tell ahead of time whether ϕ existed for the problem you were trying to solve. Fortunately, it is possible to prove that all properly posed 2D elasticity problems do have an Airy representation.

5.2.3 Airy Solution in Cylindrical-Polar Coordinates

Boundary value problems involving cylindrical regions are best solved using cylindrical-polar coordinates. It is worth recording the Airy function equations for this coordinate system.

In a 2D cylindrical-polar coordinate system, a point in the solid is specified by its radial distance $r = \sqrt{x_1^2 + x_2^2}$ from the origin and the angle $\theta = \tan^{-1}x_2/x_1$. The solution is independent of z . The Airy function is written as a function of the coordinates as $\phi(r, \theta)$. Vector quantities (displacement, body force) and tensor quantities (strain, stress) are expressed as components in the basis $\{\mathbf{e}_r, \mathbf{e}_\theta, \mathbf{e}_z\}$ shown in Figure 5.7.

The governing equation for the Airy function in this coordinate system is

$$\left(\frac{\partial^2}{\partial r^2} + \frac{1}{r} \frac{\partial}{\partial r} + \frac{1}{r^2} \frac{\partial^2}{\partial \theta^2} \right)^2 \phi = C(v) \rho_0 \left(\frac{\partial b_r}{\partial r} + \frac{1}{r} \frac{\partial b_\theta}{\partial \theta} \right)$$

$$C(v) = \begin{cases} \frac{1-v}{1-2v} & (\text{Plane Strain}) \\ \frac{1}{1-v} & (\text{Plane Stress}). \end{cases}$$

The state of stress is related to the Airy function by

$$\sigma_{rr} = \frac{1}{r} \frac{\partial \phi}{\partial r} + \frac{1}{r^2} \frac{\partial^2 \phi}{\partial \theta^2} - \Omega \quad \sigma_{\theta\theta} = \frac{\partial^2 \phi}{\partial r^2} - \Omega \quad \sigma_{r\theta} = -\frac{\partial}{\partial r} \left(\frac{1}{r} \frac{\partial \phi}{\partial \theta} \right).$$

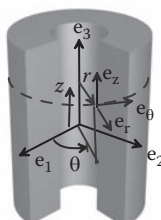


FIGURE 5.7 Cylindrical-polar coordinate system.

In polar coordinates, the strains are related to the stresses by

$$\begin{bmatrix} \varepsilon_{rr} \\ \varepsilon_{\theta\theta} \\ 2\varepsilon_{r\theta} \end{bmatrix} = \frac{(1+\nu)}{E} \begin{bmatrix} 1-\nu & -\nu & 0 \\ -\nu & 1-\nu & 0 \\ 0 & 0 & 2 \end{bmatrix} \begin{bmatrix} \sigma_{rr} \\ \sigma_{\theta\theta} \\ \sigma_{r\theta} \end{bmatrix}$$

for plane strain, whereas

$$\begin{bmatrix} \varepsilon_{rr} \\ \varepsilon_{\theta\theta} \\ 2\varepsilon_{r\theta} \end{bmatrix} = \frac{1}{E} \begin{bmatrix} 1 & -\nu & 0 \\ -\nu & 1 & 0 \\ 0 & 0 & 2(1+\nu) \end{bmatrix} \begin{bmatrix} \sigma_{rr} \\ \sigma_{\theta\theta} \\ \sigma_{r\theta} \end{bmatrix}$$

for plane stress. The displacements must be determined by integrating these strains following the procedure similar to that outlined in Section 2.1.20. To this end, let $\mathbf{u} = u_r \mathbf{e}_r + u_\theta \mathbf{e}_\theta$ denote the displacement vector. The strain-displacement relations in polar coordinates are

$$\varepsilon_{rr} = \frac{\partial u_r}{\partial r} \quad \varepsilon_{\theta\theta} = \frac{u_r}{r} + \frac{1}{r} \frac{\partial u_\theta}{\partial \theta} \quad \varepsilon_{r\theta} = \frac{1}{2} \left(\frac{1}{r} \frac{\partial u_r}{\partial \theta} + \frac{\partial u_\theta}{\partial r} - \frac{u_\theta}{r} \right).$$

These can be integrated using a procedure analogous to that outlined in Section 2.1.20. An example is given in Section 5.2.5.

In the following sections, we give several examples of Airy function solutions to boundary value problems.

5.2.4 Airy Function Solution to the End-Loaded Cantilever

Consider a cantilever beam, with length L , height $2a$, and out-of-plane thickness b , as shown in Figure 5.8. The beam is made from an isotropic linear elastic solid with Young's modulus E and Poisson's ratio ν . The top and bottom of the beam $x_2 = \pm a$ are traction free, the left-hand end is subjected to a resultant force P , and the right-hand end is clamped. Assume that $b \ll a$, so that a state of plane stress is developed in the beam. An approximate solution to the stress in the beam can be calculated from the Airy function

$$\phi = -\frac{3P}{4ab} x_1 x_2 + \frac{P}{4a^3 b} x_1 x_2^3.$$

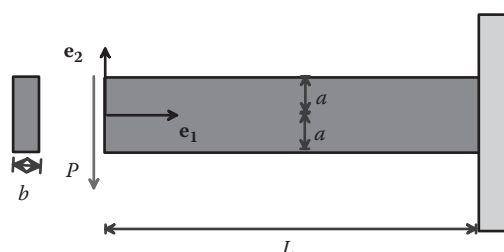


FIGURE 5.8 Cantilever beam subjected to end loading.

You can easily show that this function satisfies the governing equation for the Airy function. The stresses follow as

$$\sigma_{11} = \frac{\partial^2 \phi}{\partial x_2^2} - \Omega = \frac{3P}{2a^3 b} x_1 x_2 \quad \sigma_{22} = \frac{\partial^2 \phi}{\partial x_1^2} - \Omega = 0 \quad \sigma_{12} = \sigma_{21} = -\frac{\partial^2 \phi}{\partial x_1 \partial x_2} = \frac{3P}{4ab} \left(1 - \frac{x_2^2}{a^2}\right).$$

To see that this solution satisfies the boundary conditions, note the following:

1. The top and bottom surfaces of the beam $x_2 = \pm a$ are traction free ($\sigma_{ij} n_i = 0$). Because the normal is in the \mathbf{e}_2 direction on these surfaces, this requires that $\sigma_{22} = \sigma_{21} = 0$. The stress field clearly satisfies this condition.
2. The plane stress assumption automatically satisfies boundary conditions on $x_3 = \pm b/2$.
3. The traction boundary condition on the left-hand end of the beam ($x_1 = 0$) was not specified in detail: instead, we only required that the resultant of the traction acting on the surface is $-P\mathbf{e}_2$. The normal to the surface at the left-hand end of the beam is in the $-\mathbf{e}_1$ direction, so the traction vector is

$$t_i = \sigma_{ij} n_i = -\sigma_{12} \delta_{i2} = -\frac{3P}{4ab} \left(1 - \frac{x_2^2}{a^2}\right) \delta_{i2}.$$

The resultant force can be calculated by integrating the traction over the end of the beam:

$$F_i = b \int_{-a}^a -\frac{3P}{4ab} \left(1 - \frac{x_2^2}{a^2}\right) \delta_{i2} dx_2 = -P \delta_{i2}.$$

The stresses thus satisfy the boundary condition. Note that, by SVP, other distributions of traction with the same resultant will induce the same stresses sufficiently far ($x_1 > 3a$) from the end of the beam.

4. The boundary conditions on the right-hand end of the beam are *not* satisfied exactly. The exact solution should satisfy both $u_1 = 0$ and $u_2 = 0$ on $x_1 = L$. The displacement field corresponding to the stress distribution was calculated in the example problem in Section 2.1.20, where we found that

$$u_1 = \frac{3P}{4Ea^3 b} x_1^2 x_2 - \frac{P}{4Ea^3 b} (2+\nu) x_2^3 + \frac{3P}{2Ea^3 b} (1+\nu) a^2 x_2 - \omega x_2 + c$$

$$u_2 = -\nu \frac{3P}{4Ea^3 b} x_1 x_2^2 - \frac{P}{4Ea^3 b} x_1^3 + \omega x_1 + d,$$

where c, d, ω are constants that may be selected to satisfy the boundary condition as far as possible. We can satisfy $u_1 = 0$ and $u_2 = 0$ at some, but not all, points on $x_1 = L$. The

choice is arbitrary. Usually the boundary condition is approximated by requiring $u_1 = u_2 = \partial u_2 / \partial x_1 = 0$ at $x_1 = L$, $x_1 = 0$. This gives $c = 0$, $d = -PL^3 / 2Ea^3b$ and $\omega = 3PL^2 / 4Ea^3b$. By SVP, applying other boundary conditions (including the *exact* boundary condition) will not influence the stresses and displacements sufficiently far from the end.

5.2.5 2D Line Load Acting Perpendicular to the Surface of an Infinite Solid

As a second example, the stress fields attributable to a line load magnitude P per unit out-of-plane length acting on the surface of a homogeneous, isotropic half-space can be generated from the Airy function

$$\phi = -\frac{P}{\pi} r \theta \sin \theta,$$

where (r, θ) are cylindrical polar coordinates illustrated in Figure 5.9. The formulas in the preceding section yield

$$\sigma_{rr} = -\frac{2P}{\pi} \frac{\cos \theta}{r} \quad \sigma_{\theta\theta} = \sigma_{r\theta} = 0.$$

The stresses in the $\{\mathbf{e}_1, \mathbf{e}_2, \mathbf{e}_3\}$ basis are

$$\sigma_{11} = -\frac{2P}{\pi} \frac{x_1^3}{(x_1^2 + x_2^2)^2} \quad \sigma_{22} = -\frac{2P}{\pi} \frac{x_1 x_2^2}{(x_1^2 + x_2^2)^2} \quad \sigma_{12} = -\frac{2P}{\pi} \frac{x_1^2 x_2}{(x_1^2 + x_2^2)^2}.$$

The method outlined in Section 5.2.3 can be used to calculate the displacements: the procedure is described in detail below to provide a representative example. For plane strain deformation, we find

$$u_r = -\frac{2(1-\nu^2)}{\pi E} P \cos \theta \log r - \frac{(1+\nu)(1-2\nu)}{\pi E} P \theta \sin \theta$$

$$u_\theta = \frac{2(1-\nu^2)}{\pi E} P \sin \theta \log r + \frac{1+\nu}{\pi E} P \sin \theta - \frac{2(1-2\nu)(1+\nu)}{\pi E} P \theta \cos \theta$$

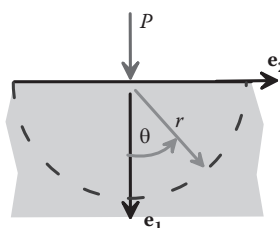


FIGURE 5.9 Line force acting normal to a surface.

to within an arbitrary rigid motion. Note that the displacements vary as $\log(r)$ so they are unbounded at both the origin and infinity. Moreover, the displacements attributable to any *distribution* of traction that exerts a nonzero resultant force on the surface will also be unbounded at infinity.

It is easy to see that this solution satisfies all the relevant boundary conditions. The surface is traction free ($\sigma_{22} = \sigma_{12} = 0$ on $x_1 = 0$) except at $r = 0$. To see that the stresses are consistent with a vertical point force, note that the resultant vertical force exerted by the tractions acting on the dashed curve shown in Figure 5.9 can be calculated as

$$F_1 = \int_{-\pi/2}^{\pi/2} \sigma_{rr} \cos \theta r d\theta = \int_{-\pi/2}^{\pi/2} -\frac{2P}{\pi} \frac{\cos \theta}{r} \cos \theta r d\theta = -P.$$

The expressions for displacement can be derived as follows. Substituting the expression for stress into the stress-strain laws and using the strain-displacement relations yields

$$\varepsilon_{rr} = \frac{\partial u_r}{\partial r} = \frac{(1+\nu)}{E} [(1-\nu)\sigma_{rr} - \nu\sigma_{\theta\theta}] = -\frac{2P(1-\nu^2)}{\pi E} \frac{\cos \theta}{r}.$$

Integrate

$$u_r = -\frac{2P(1-\nu^2)}{\pi E} \cos \theta \log(r) + f_r(\theta),$$

where $f_r(\theta)$ is a function of θ to be determined. Similarly, considering the hoop stresses gives

$$\varepsilon_{\theta\theta} = \frac{u_r}{r} + \frac{1}{r} \frac{\partial u_\theta}{\partial \theta} = \frac{(1+\nu)}{E} [(1-\nu)\sigma_{\theta\theta} - \nu\sigma_{rr}] = \frac{2P\nu(1+\nu)}{\pi E} \frac{\cos \theta}{r}.$$

Rearrange and integrate with respect to θ :

$$u_\theta = \frac{2P(1-\nu)}{\pi E} \sin \theta [\nu + (1-\nu) \log(r)] - \int f_r(\theta) d\theta + f_\theta(r),$$

where $f_\theta(r)$ is a function of r to be determined. Finally, substituting for stresses into the expression for shear strain shows that

$$\varepsilon_{r\theta} = \frac{1}{2} \left(\frac{1}{r} \frac{\partial u_r}{\partial \theta} + \frac{\partial u_\theta}{\partial r} - \frac{u_\theta}{r} \right) = \frac{(1+\nu)}{E} \sigma_{r\theta} = 0.$$

Inserting the expressions for displacement and simplifying gives

$$\frac{1}{r} \left\{ \frac{\partial f_r(\theta)}{\partial \theta} + \int f_r(\theta) d\theta + \frac{2P(1+\nu)(1-2\nu)}{\pi E} \sin \theta \right\} + \left\{ \frac{\partial f_\theta(r)}{\partial r} - \frac{f_\theta(r)}{r} \right\} = 0.$$

The two terms in parentheses are functions of θ and r , respectively, and so must both be separately equal to zero to satisfy this expression for all possible values of θ and r . Therefore,

$$\frac{\partial^2 f_r(\theta)}{\partial \theta^2} + f_r(\theta) = -\frac{2P(1+\nu)(1-2\nu)}{\pi E} \cos \theta.$$

This ordinary differential equation (ODE) has solution

$$f_r(\theta) = -\frac{P(1+\nu)(1-2\nu)}{\pi E} \theta \sin \theta + A \sin \theta + B \cos \theta.$$

The second equation gives

$$\frac{\partial f_\theta(r)}{\partial r} - \frac{f_\theta(r)}{r} = 0,$$

which has solution $f_\theta(r) = Cr$. The constants A , B , and C represent an arbitrary rigid displacement and can be taken to be zero. This gives the required answer.

5.2.6 2D Line Load Acting Parallel to the Surface of an Infinite Solid

Similarly, the stress fields attributable to a line load magnitude P per unit out-of-plane length acting tangent to the surface of a homogeneous, isotropic half-space (Figure 5.10) can be generated from the Airy function

$$\phi = -\frac{P}{\pi} r \theta \cos \theta.$$

The formulas in the preceding section yield

$$\sigma_{rr} = -\frac{2P}{\pi} \frac{\sin \theta}{r} \quad \sigma_{\theta\theta} = \sigma_{r\theta} = 0.$$

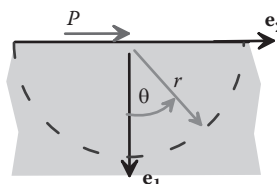


FIGURE 5.10 Line force acting tangent to a surface.

The method outlined in the preceding section can be used to calculate the displacements. The procedure gives

$$u_r = -\frac{2(1-\nu^2)}{\pi E} P \sin \theta \log r - \frac{(1+\nu)(1-2\nu)}{\pi E} P \theta \cos \theta$$

$$u_\theta = \frac{2(1-\nu^2)}{\pi E} P \cos \theta \log r + \frac{1+\nu}{\pi E} P \cos \theta - \frac{2(1-2\nu)(1+\nu)}{\pi E} P \theta \sin \theta$$

to within an arbitrary rigid motion.

The stresses and displacements in the $\{\mathbf{e}_1, \mathbf{e}_2, \mathbf{e}_3\}$ basis are

$$\sigma_{11} = -\frac{2P}{\pi} \frac{x_1^2 x_2}{(x_1^2 + x_2^2)^2} \quad \sigma_{22} = -\frac{2P}{\pi} \frac{x_2^3}{(x_1^2 + x_2^2)^2} \quad \sigma_{12} = -\frac{2P}{\pi} \frac{x_1 x_2^2}{(x_1^2 + x_2^2)^2}.$$

5.2.7 Arbitrary Pressure Acting on a Flat Surface

The principle of superposition can be used to extend the point force solutions to arbitrary pressures acting on a surface. For example, we can find the solution for a uniform pressure acting on the strip of width $2a$ on the surface of a half-space by distributing the point force solution appropriately. Figure 5.11 illustrates the problem to be solved.

Distributing point forces with magnitude $p(s)ds\mathbf{e}_1 + q(s)ds\mathbf{e}_2$ over the loaded region shows that

$$\sigma_{11} = -\frac{2}{\pi} \int_A \frac{x_1^2(x_1 p(s) + (x_2 - s)q(s))}{(x_1^2 + (x_2 - s)^2)^2} ds$$

$$\sigma_{22} = -\frac{2}{\pi} \int_A \frac{(x_2 - s)^2(x_1 p(s) + (x_2 - s)q(s))}{(x_1^2 + (x_2 - s)^2)^2} ds$$

$$\sigma_{12} = -\frac{2}{\pi} \int_A \frac{x_1(x_2 - s)(x_1 p(s) + (x_2 - s)q(s))}{(x_1^2 + (x_2 - s)^2)^2} ds.$$

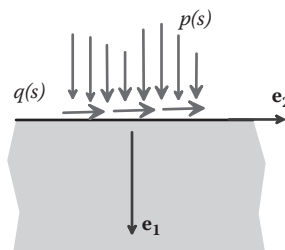


FIGURE 5.11 Pressure and traction acting on a surface.

5.2.8 Uniform Normal Pressure Acting on a Strip

For the particular case of a uniform pressure, the integrals can be evaluated to show that

$$\sigma_{22} = -\frac{p}{2\pi}(2(\theta_1 - \theta_2) + (\sin 2\theta_1 - \sin 2\theta_2))$$

$$\sigma_{11} = -\frac{p}{2\pi}(2(\theta_1 - \theta_2) - (\sin 2\theta_1 - \sin 2\theta_2))$$

$$\sigma_{12} = \frac{p}{2\pi}(\cos 2\theta_1 - \cos 2\theta_2),$$

where $0 \leq \theta_\alpha \leq \pi$ and $\theta_1 = \tan^{-1} x_1/(x_2 - a)$, $\theta_2 = \tan^{-1} x_1/(x_2 + a)$ as shown in Figure 5.12.

5.2.9 Stresses near the Tip of a Crack

Consider an infinite solid that contains a semi-infinite crack on the (x_1, x_3) plane, as illustrated in Figure 5.13. Suppose that the solid deforms in plane strain and is subjected to bounded stress at infinity. The stress field near the tip of the crack can be derived from the Airy function

$$\begin{aligned}\phi &= \frac{K_I}{3\sqrt{2\pi}} r^{3/2} (\cos 3\theta/2 + 3\cos\theta/2) \\ &\quad - \frac{K_{II}}{\sqrt{2\pi}} r^{3/2} (\sin 3\theta/2 + \sin\theta/2).\end{aligned}$$

Here, K_I and K_{II} are two constants, known as *mode I* and *mode II* stress intensity factors, respectively. They quantify the magnitudes of the stresses near the crack tip, as shown below. Their role will be discussed in more detail when we discuss fracture mechanics. The stresses can be calculated as

$$\begin{aligned}\sigma_{rr} &= \frac{K_I}{\sqrt{2\pi}r} \left(\frac{5}{4} \cos \frac{\theta}{2} - \frac{1}{4} \cos \frac{3\theta}{2} \right) + \frac{K_{II}}{\sqrt{2\pi}r} \left(-\frac{5}{4} \sin \frac{\theta}{2} + \frac{3}{4} \sin \frac{3\theta}{2} \right) \\ \sigma_{\theta\theta} &= \frac{K_I}{\sqrt{2\pi}r} \left(\frac{3}{4} \cos \frac{\theta}{2} + \frac{1}{4} \cos \frac{3\theta}{2} \right) - \frac{K_{II}}{\sqrt{2\pi}r} \left(\frac{3}{4} \sin \frac{\theta}{2} + \frac{3}{4} \sin \frac{3\theta}{2} \right) \\ \sigma_{r\theta} &= \frac{K_I}{\sqrt{2\pi}r} \left(\frac{1}{4} \sin \frac{\theta}{2} + \frac{1}{4} \sin \frac{3\theta}{2} \right) + \frac{K_{II}}{\sqrt{2\pi}r} \left(\frac{1}{4} \cos \frac{\theta}{2} + \frac{3}{4} \cos \frac{3\theta}{2} \right).\end{aligned}$$

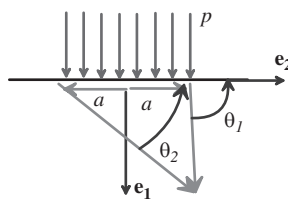


FIGURE 5.12 Uniform pressure acting on a strip.

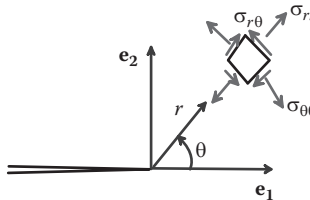


FIGURE 5.13 Coordinate system near the tip of a crack in an infinite solid.

Equivalent expressions in rectangular coordinates are

$$\begin{aligned}\sigma_{11} &= \frac{K_I}{\sqrt{2\pi r}} \cos \frac{\theta}{2} \left(1 - \sin \frac{\theta}{2} \sin \frac{3\theta}{2} \right) - \frac{K_{II}}{\sqrt{2\pi r}} \sin \frac{\theta}{2} \left(2 + \cos \frac{\theta}{2} \cos \frac{3\theta}{2} \right) \\ \sigma_{22} &= \frac{K_I}{\sqrt{2\pi r}} \cos \frac{\theta}{2} \left(1 + \sin \frac{\theta}{2} \sin \frac{3\theta}{2} \right) + \frac{K_{II}}{\sqrt{2\pi r}} \cos \frac{\theta}{2} \sin \frac{\theta}{2} \cos \frac{3\theta}{2} \\ \sigma_{12} &= \frac{K_I}{\sqrt{2\pi r}} \cos \frac{\theta}{2} \sin \frac{\theta}{2} \cos \frac{3\theta}{2} + \frac{K_{II}}{\sqrt{2\pi r}} \cos \frac{\theta}{2} \left(1 - \sin \frac{\theta}{2} \sin \frac{3\theta}{2} \right),\end{aligned}$$

whereas the displacements can be calculated by integrating the strains, with the result

$$\begin{aligned}u_1 &= \frac{K_I}{2\pi} \sqrt{\frac{r}{2\pi}} \left[1 - 2\nu - \sin^2 \frac{\theta}{2} \right] \cos \frac{\theta}{2} + \frac{K_{II}}{\sqrt{2\pi}} \sqrt{\frac{r}{2\pi}} \left[2 - 2\nu + \cos^2 \frac{\theta}{2} \right] \sin \frac{\theta}{2} \\ u_2 &= \frac{K_I}{2\pi} \sqrt{\frac{r}{2\pi}} \left[2 - 2\nu - \cos^2 \frac{\theta}{2} \right] \sin \frac{\theta}{2} + \frac{K_{II}}{\sqrt{2\pi}} \sqrt{\frac{r}{2\pi}} \left[-1 + 2\nu + \sin^2 \frac{\theta}{2} \right] \cos \frac{\theta}{2},\end{aligned}$$

where \$\mu\$ and \$\nu\$ denote the shear modulus and Poisson's ratio of the solid. Note that this displacement field is valid for plane strain deformation only. Observe that the stress intensity factor has the bizarre units of \$Nm^{-3/2}\$.

5.3 COMPLEX VARIABLE SOLUTION TO PLANE STRAIN STATIC LINEAR ELASTIC PROBLEMS

Airy functions have been used to find many useful solutions to plane elastostatic boundary value problems. The method does have some limitations, however. The biharmonic equation is not the easiest field equation to solve, for one thing. Another limitation is that displacement components are difficult to determine from Airy functions, so that the method is not well suited to displacement boundary value problems.

In this section, we outline a more versatile representation for 2D static linear elasticity problems, based on complex potentials. The main goal is to provide you with enough background to be able to interpret solutions that use the complex variable formulation. The techniques to derive the complex potentials are beyond the scope of this book but can be found in most linear elasticity texts.

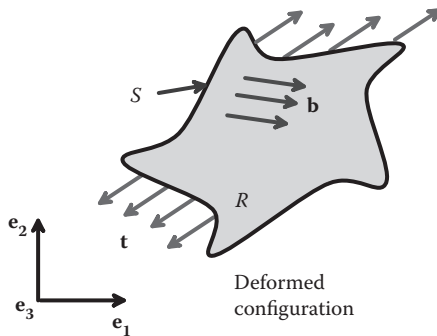


FIGURE 5.14 A representative plane boundary value problem in linear elasticity.

A typical plane elasticity problem is illustrated in Figure 5.14. Just as in the preceding section, the solid is two dimensional, which means that either of the following apply:

1. The solid is a thin sheet, with small thickness h , and is loaded only in the $\{e_1, e_2\}$ plane. In this case, the plane stress solution is applicable.
2. The solid is very long in the e_3 direction and is prevented from stretching parallel to the e_3 axis, and every cross section is loaded identically and only in the $\{e_1, e_2\}$ plane. In this case, the plane strain solution is applicable.

Some additional basic assumptions and restrictions are as follows:

- The complex variable method outlined below is applicable only to isotropic solids. We will assume that the solid has Young's modulus E , Poisson's ratio ν , and mass density ρ_0 .
- We will assume no body forces and constant temperature.

5.3.1 Complex Variable Solutions to Elasticity Problems

Figure 5.15 shows a 2D solid. In the complex variable formalism:

- The position of a point in the solid is specified by a complex number $z = x_1 + ix_2$.
- The position of a point can also be expressed as $z = re^{i\theta}$, where $r = \sqrt{x_1^2 + x_2^2}$ and $\theta = \tan^{-1} x_2 / x_1$.

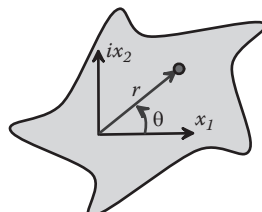


FIGURE 5.15 Coordinate system for the complex plane.

- You can show that these are equivalent using Euler's formula $e^{i\theta} = \cos\theta + i\sin\theta$, which gives

$$\begin{aligned} z &= re^{i\theta} = \sqrt{x_1^2 + x_2^2}(\cos\theta + i\sin\theta) \\ &= \sqrt{x_1^2 + x_2^2} \left(\frac{x_1}{\sqrt{x_1^2 + x_2^2}} + \frac{ix_2}{\sqrt{x_1^2 + x_2^2}} \right) = x_1 + ix_2. \end{aligned}$$

- The displacement of a point is specified using a second complex number $D = u_1 + iu_2$.
- The displacement and stress fields in rectangular coordinates are generated from two *complex potentials* $\Omega(z)$ and $\omega(z)$, which are differentiable (also called “analytic” or “holomorphic”) functions of z (e.g., a polynomial), using the following formulas:

$$\begin{aligned} \frac{E}{(1+\nu)} D &= (3-4\nu)\Omega(z) - z\overline{\Omega'(z)} - \overline{\omega(z)} \\ \sigma_{11} + \sigma_{22} &= 2(\Omega'(z) + \overline{\Omega'(z)}) \\ \sigma_{11} - \sigma_{22} + 2i\sigma_{12} &= -2(z\overline{\Omega''(z)} + \overline{\omega'(z)}). \end{aligned}$$

Here, $\Omega'(z)$ denotes the derivative of $\Omega(z)$ with respect to z , and $\overline{\Omega(z)}$ denotes the complex conjugate of $\Omega(z)$. Recall that, to calculate the complex conjugate of a complex number, you simply change the sign of its imaginary part, i.e., $a + ib = a - ib$.

- The displacement and stress in polar coordinates can be derived as

$$\begin{aligned} \frac{E}{(1+\nu)}(u_r + iu_\theta) &= [(3-4\nu)\Omega(z) - z\overline{\Omega'(z)} - \overline{\omega(z)}]e^{-i\theta} \\ \sigma_{rr} + \sigma_{\theta\theta} &= 2(\Omega'(z) + \overline{\Omega'(z)}) \\ \sigma_{rr} - \sigma_{\theta\theta} + 2i\sigma_{r\theta} &= -2(z\overline{\Omega''(z)} + \overline{\omega'(z)})e^{-2i\theta}. \end{aligned}$$

- The formulas given here for displacements and stresses are the most general representation, but other special formulas are sometimes used for particular problems. For example, if the solid is a half-space in the region $x_2 \geq 0$ with a boundary at $x_2 = 0$, the solution can be generated from a *single* complex potential $\Omega(z)$, using the formulas

$$\begin{aligned} 2 D &= (3-4\nu)\Omega(z) + \Omega(\bar{z}) + (\bar{z} - z)\overline{\Omega'(z)} \\ \sigma_{11} + \sigma_{22} &= 2(\Omega'(z) + \overline{\Omega'(z)}) \\ \sigma_{22} - i\sigma_{12} &= \Omega'(z) - \Omega'(\bar{z}) + (z - \bar{z})\overline{\Omega''(z)}. \end{aligned}$$

For example, you can use these formulas to calculate stresses from the potentials given in Sections 5.3.8 through 5.3.12. The conventional representation gives the same results, of course.

5.3.2 Demonstration That the Complex Variable Solution Satisfies the Governing Equations

We need to show two things:

1. That the displacement field satisfies the equilibrium equation (Section 5.1.2)

$$\frac{1}{1-2\nu} \frac{\partial^2 u_k}{\partial x_k \partial x_i} + \frac{\partial^2 u_i}{\partial x_k \partial x_k} = 0.$$

2. That the stresses are related to the displacements by the elastic stress-strain equations.

To do this, we need to review some basic results from the theory of complex variables. Recall that we have set $z = x_1 + ix_2$, so that a differentiable function $f(z)$ can be decomposed into real and imaginary parts, each of which are functions of x_1, x_2 , as

$$f(z) = v(x_1, x_2) + iw(x_1, x_2) = v\left(\frac{z+\bar{z}}{2}, i\frac{\bar{z}-z}{2}\right) + iw\left(\frac{z+\bar{z}}{2}, i\frac{\bar{z}-z}{2}\right).$$

This shows that

$$\frac{\partial}{\partial z} \equiv \frac{1}{2} \left(\frac{\partial}{\partial x_1} - i \frac{\partial}{\partial x_2} \right) \quad \frac{\partial}{\partial \bar{z}} \equiv \frac{1}{2} \left(\frac{\partial}{\partial x_1} + i \frac{\partial}{\partial x_2} \right).$$

Next, recall that, if $f(z)$ is differentiable with respect to z , its real and imaginary parts must satisfy the Cauchy–Riemann equations

$$\frac{\partial v}{\partial x_1} = \frac{\partial w}{\partial x_2} \quad \frac{\partial w}{\partial x_1} = -\frac{\partial v}{\partial x_2}.$$

We can then show that the derivative of $f(z)$ with respect to \bar{z} is zero, and similarly, the derivative of $\overline{f(z)}$ with respect to z is zero. To see these, use the definitions and the Cauchy–Riemann equations

$$2 \frac{\partial f(z)}{\partial \bar{z}} = \left(\frac{\partial}{\partial x_1} + i \frac{\partial}{\partial x_2} \right) (v + iw) = \frac{\partial v}{\partial x_1} - \frac{\partial w}{\partial x_2} + i \left(\frac{\partial v}{\partial x_2} + \frac{\partial w}{\partial x_1} \right) = 0$$

$$2 \frac{\partial \overline{f(z)}}{\partial z} = \left(\frac{\partial}{\partial x_1} - i \frac{\partial}{\partial x_2} \right) (v - iw) = \frac{\partial v}{\partial x_1} - \frac{\partial w}{\partial x_2} - i \left(\frac{\partial v}{\partial x_2} + \frac{\partial w}{\partial x_1} \right) = 0.$$

We can now proceed with the proof. The equilibrium equations for plane deformation reduce to

$$\begin{aligned} \left(\frac{\partial^2}{\partial x_1^2} + \frac{\partial^2}{\partial x_2^2} \right) u_1 + \frac{1}{1-2\nu} \frac{\partial}{\partial x_1} \left(\frac{\partial u_1}{\partial x_1} + \frac{\partial u_2}{\partial x_2} \right) &= 0 \\ \left(\frac{\partial^2}{\partial x_1^2} + \frac{\partial^2}{\partial x_2^2} \right) u_2 + \frac{1}{1-2\nu} \frac{\partial}{\partial x_2} \left(\frac{\partial u_1}{\partial x_1} + \frac{\partial u_2}{\partial x_2} \right) &= 0. \end{aligned}$$

These equations can be written in a combined, complex, form as

$$\left(\frac{\partial^2}{\partial x_1^2} + \frac{\partial^2}{\partial x_2^2} \right) (u_1 + iu_2) + \frac{1}{1-2\nu} \left(\frac{\partial}{\partial x_1} + i \frac{\partial}{\partial x_2} \right) \left(\frac{\partial u_1}{\partial x_1} + \frac{\partial u_2}{\partial x_2} \right) = 0.$$

It is easy to show (simply substitute $D = u_1 + iu_2$ and use the definitions of differentiation with respect to z and \bar{z}) that this can be rewritten as

$$4 \frac{\partial^2}{\partial z \partial \bar{z}} D + \frac{2}{1-2\nu} \frac{\partial}{\partial \bar{z}} \left(\frac{\partial D}{\partial z} + \frac{\partial \bar{D}}{\partial \bar{z}} \right) = 0.$$

Finally, substituting

$$D = \frac{(1+\nu)}{E} \left\{ (3-4\nu)\Omega(z) - z \overline{\Omega'(z)} - \overline{\omega(z)} \right\}$$

and noting that $\partial\Omega/\partial\bar{z} = 0$ and $\partial\bar{\Omega}/\partial z = \partial\bar{\omega}/\partial z = 0$ shows that this equation is indeed satisfied.

To show that the stress-strain relations are satisfied, note that the stress-strain relations for plane strain deformation (Section 3.1.4) can be written as

$$\begin{aligned} \sigma_{11} + \sigma_{22} &= \frac{E}{(1+\nu)(1-2\nu)} \left(\frac{\partial u_1}{\partial x_1} + \frac{\partial u_2}{\partial x_2} \right) = \frac{E}{(1+\nu)(1-2\nu)} \left(\frac{\partial D}{\partial z} + \frac{\partial \bar{D}}{\partial \bar{z}} \right) \\ \sigma_{11} - \sigma_{22} + 2i\sigma_{12} &= \frac{E}{(1+\nu)} \left(\frac{\partial}{\partial x_1} + i \frac{\partial}{\partial x_2} \right) (u_1 + iu_2) = \frac{2E}{(1+\nu)} \frac{\partial D}{\partial \bar{z}}. \end{aligned}$$

Substituting for D in terms of the complex potentials and evaluating the derivatives gives the required results.

5.3.3 Complex Variable Solution for a Line Force in an Infinite Solid (Plane Strain Deformation)

Figure 5.16 shows a line load with force per unit out-of-plane distance $\mathbf{F} = F_1 \mathbf{e}_1 + F_2 \mathbf{e}_2$ acting at the origin of a large (infinite) solid. The displacements and stresses are calculated from the complex potentials

$$\Omega(z) = -\frac{F_1 + iF_2}{8\pi(1-\nu)} \log(z) \quad \omega(z) = \frac{(3-4\nu)(F_1 + iF_2)}{8\pi(1-\nu)} \log(z).$$

The displacements can be calculated from these potentials as

$$\begin{aligned} u_1 &= -\frac{(1+\nu)F_1}{8\pi E(1-\nu)} \left\{ 2(3-4\nu)\log(r) + \cos 2\theta \right\} - \frac{(1+\nu)F_2}{8\pi E(1-\nu)} \sin 2\theta \\ u_2 &= -\frac{(1+\nu)F_2}{8\pi E(1-\nu)} \left\{ 2(3-4\nu)\log(r) - \sin 2\theta \right\} + \frac{(1+\nu)F_1}{8\pi E(1-\nu)} \cos 2\theta \\ \sigma_{rr} &= -\frac{3-2\nu}{4\pi(1-\nu)r} (F_1 \cos \theta + F_2 \sin \theta) \\ \sigma_{\theta\theta} &= \frac{(1-2\nu)}{4\pi(1-\nu)r} (F_1 \cos \theta + F_2 \sin \theta) \\ \sigma_{r\theta} &= \frac{(1-2\nu)}{4\pi(1-\nu)r} (F_1 \sin \theta - F_2 \cos \theta) \\ \sigma_{11} &= -\frac{F_1 \cos \theta}{4\pi(1-\nu)r} (1-2\nu+2\cos^2 \theta) + \frac{F_2 \sin \theta}{4\pi(1-\nu)r} (1-2\nu-2\cos^2 \theta) \\ \sigma_{22} &= -\frac{F_1 \cos \theta}{4\pi(1-\nu)r} (1+2\nu-2\cos^2 \theta) - \frac{F_2 \sin \theta}{4\pi(1-\nu)r} (3-2\nu-2\cos^2 \theta) \\ \sigma_{12} &= -\frac{F_1 \sin \theta}{4\pi(1-\nu)r} (1-2\nu+2\cos^2 \theta) - \frac{F_2 \cos \theta}{4\pi(1-\nu)r} (3-2\nu-2\cos^2 \theta). \end{aligned}$$

We will work through the algebra required to calculate these formulae for displacement and stress as a representative example. In practice, a symbolic manipulation program makes the calculations painless. To begin, note that

$$\log(z) = \log(re^{i\theta}) = \log(r) + i\theta$$

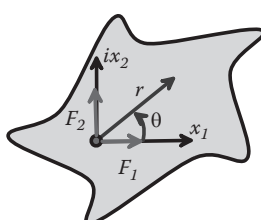


FIGURE 5.16 Line load acting at the origin of an infinite solid.

and

$$\frac{d}{dz}(\log(z)) = \frac{1}{z}.$$

The displacements are thus

$$\begin{aligned} \frac{E}{(1+\nu)} D &= (3-4\nu)\Omega(z) - \overline{\omega(z)} - z\overline{\Omega'(z)} \\ &= -\frac{(3-4\nu)}{8\pi(1-\nu)} \left((F_1+iF_2)\log(z) + \overline{(F_1-iF_2)\log(z)} \right) - \frac{\overline{F_1+iF_2}}{8\pi(1-\nu)} \frac{z}{\bar{z}} \\ &= -\frac{2(3-4\nu)}{8\pi(1-\nu)} (F_1+iF_2)\log(r) - \frac{(F_1-iF_2)}{8\pi(1-\nu)} \frac{re^{i\theta}}{re^{-i\theta}} \\ &= -\frac{2(3-4\nu)}{8\pi(1-\nu)} (F_1+iF_2)\log(r) - \frac{(F_1-iF_2)}{8\pi(1-\nu)} e^{2i\theta}. \end{aligned}$$

Finally, using Euler's formula and taking real and imaginary parts gives the answer listed previously. Similarly, the formulas for stress give

$$\begin{aligned} \sigma_{rr} + \sigma_{\theta\theta} &= 2(\Omega'(z) + \overline{\Omega'(z)}) = -\frac{1}{4\pi(1-\nu)} \left(\frac{F_1+iF_2}{z} + \frac{F_1-iF_2}{\bar{z}} \right) = -\frac{(F_1+iF_2)e^{-i\theta} + (F_1-iF_2)e^{i\theta}}{4\pi(1-\nu)r} \\ \sigma_{rr} - \sigma_{\theta\theta} + 2i\sigma_{r\theta} &= -2(z\overline{\Omega''(z)} + \overline{\omega'(z)})e^{-2i\theta} \\ &= -\frac{e^{-2i\theta}}{4\pi(1-\nu)} \left\{ (F_1-iF_2) \frac{re^{i\theta}}{r^2 e^{-2i\theta}} + (3-4\nu)(F_1+iF_2) \frac{1}{re^{-i\theta}} \right\} \\ &= -\frac{1}{4\pi(1-\nu)r} \left\{ (F_1-iF_2)e^{i\theta} + (3-4\nu)(F_1+iF_2)e^{-i\theta} \right\}. \end{aligned}$$

Adding the two formulas for stress shows that

$$2\sigma_{rr} + 2i\sigma_{r\theta} = -\frac{1}{4\pi(1-\nu)r} \left\{ 2(F_1-iF_2)e^{i\theta} + 4(1-\nu)(F_1+iF_2)e^{-i\theta} \right\}.$$

Using Euler's formula and taking real and imaginary parts of this expression gives the formulas for σ_{rr} and $\sigma_{r\theta}$.

Finally, we need to verify that the stresses are consistent with a point force acting at the origin. To do this, we can evaluate the resultant force exerted by tractions acting on a circle enclosing the point force, as shown in Figure 5.17. Because the solid is in static equilibrium, the *total* force acting on this circular region must sum to zero. Recall that the resultant force exerted by stresses on an internal surface can be calculated as

$$\mathbf{R} = \int_A \mathbf{n} \cdot \boldsymbol{\sigma} dA.$$

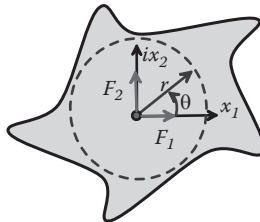


FIGURE 5.17 Circular contour enclosing a line load in an infinite solid.

A unit normal to the circle is $\mathbf{n} = \cos\theta \mathbf{e}_1 + \sin\theta \mathbf{e}_2$; multiplying by the stress tensor (in the $\{\mathbf{e}_1, \mathbf{e}_2, \mathbf{e}_3\}$ basis) gives

$$R_1 = \int_0^{2\pi} (\sigma_{11} \cos\theta + \sigma_{12} \sin\theta) r d\theta \quad R_2 = \int_0^{2\pi} (\sigma_{22} \sin\theta + \sigma_{12} \cos\theta) r d\theta.$$

Evaluating the integrals shows that $R_1 = -F_1$ and $R_2 = -F_2$, so $\mathbf{R} + F_1\mathbf{e}_1 + F_2\mathbf{e}_2 = \mathbf{0}$ as required.

5.3.4 Complex Variable Solution for an Edge Dislocation in an Infinite Solid

A dislocation is an atomic-scale defect in a crystal. The defect can be detected directly in high-resolution transmission electron microscope pictures, which can show the positions of individual atoms in a crystal. Figure 5.18 shows a typical example (an edge dislocation in a step-graded thin film of AlGaAsSb; kindly provided by Prof. David Paine of Brown University, Providence, RI). The dislocation is not easy to see but can be identified by describing a “Burger’s circuit” around the dislocation, as shown by the solid line. Each straight portion of the circuit connects eight atoms. In a perfect crystal, the circuit would start and end at the same atom. (Try this for yourself for any path that does not encircle the

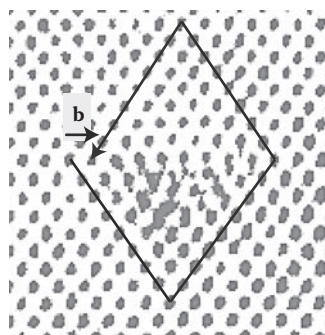


FIGURE 5.18 A Burger’s circuit around a dislocation on the interface between a thin film and a substrate. The transmission electron microscope image was provided by Professor David Paine.

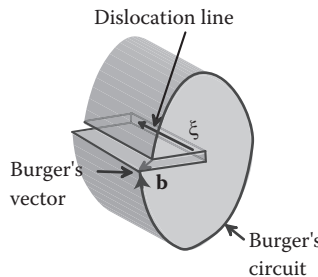


FIGURE 5.19 Burger's circuit convention used to describe displacement discontinuity for a dislocation.

dislocation.) Because the curve encircles the dislocation, it does *not* start and end on the same atom. The “Burger’s vector” for the dislocation is the difference in position vector of the start and end atom, as shown in Figure 5.18.

A continuum model of a dislocation can be created using the procedure illustrated in Figure 5.19. Take an elastic solid and cut partway through it. The edge of the cut defines a dislocation line ξ . Next, displace the two material surfaces created by the cut by the Burger’s vector \mathbf{b} and fill in the (infinitesimal) gap. Note that (by convention) the Burger’s vector specifies the displacement of a point at the end of the Burger’s circuit as seen by an observer who sits on the start of the circuit, as shown in Figure 5.19.

HEALTH WARNING: Some texts define the Burger’s vector to be the negative of the vector defined here, that is to say, the vector pointing from the end of the circuit back to the start.

A general Burger’s vector has three components: the component $b_s = \mathbf{b} \cdot \xi$ parallel to the dislocation line is known as the *screw component* of \mathbf{b} , whereas the two remaining components $\mathbf{b}_e = \mathbf{b} - b_s \xi$ are known as the *edge* components of \mathbf{b} . The stress field induced by the dislocation depends only on ξ and \mathbf{b} and is independent of the cut that created it.

Figure 5.20 illustrates a pure edge dislocation, with line direction parallel to the \mathbf{e}_3 axis and Burger’s vector $\mathbf{b} = b_1 \mathbf{e}_1 + b_2 \mathbf{e}_2$ at the origin of an infinite solid. The displacements and stresses can be derived from the complex potentials

$$\Omega(z) = -i \frac{E(b_1 + ib_2)}{8\pi(1-\nu^2)} \log(z) \quad \omega(z) = i \frac{E(b_1 - ib_2)}{8\pi(1-\nu^2)} \log(z).$$

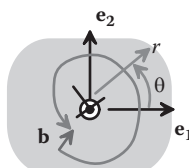


FIGURE 5.20 Burger’s circuit around an edge dislocation in an elastic solid.

The displacement and stresses (in polar coordinates) can be derived from these potentials as

$$\begin{aligned}
 u_1 &= \frac{\theta b_1}{2\pi} + \frac{1-2\nu}{4\pi(1-\nu)} b_2 \log(r) - \frac{1}{8\pi(1-\nu)} (b_2 \cos 2\theta - b_1 \sin 2\theta) \\
 u_2 &= \frac{\theta b_2}{2\pi} - \frac{1-2\nu}{4\pi(1-\nu)} b_1 \log(r) - \frac{1}{8\pi(1-\nu)} (b_1 \cos 2\theta + b_2 \sin 2\theta) \\
 \sigma_{rr} = \sigma_{\theta\theta} &= -\frac{E(b_1 \sin \theta - b_2 \cos \theta)}{4\pi(1-\nu^2)r} \quad \sigma_{r\theta} = \frac{E(b_1 \cos \theta + b_2 \sin \theta)}{4\pi(1-\nu^2)r} \\
 \sigma_{11} &= -\frac{Eb_1(3 \sin \theta + \sin 3\theta)}{8\pi(1-\nu^2)r} + \frac{Eb_2(3 \cos \theta + \cos 3\theta)}{8\pi(1-\nu^2)r} \\
 \sigma_{22} &= -\frac{Eb_1(\sin \theta - \sin 3\theta)}{8\pi(1-\nu^2)r} + \frac{Eb_2(3 \cos \theta - \cos 3\theta)}{8\pi(1-\nu^2)r} \\
 \sigma_{12} &= +\frac{Eb_1(\cos \theta + \cos 3\theta)}{8\pi(1-\nu^2)r} - \frac{Eb_2(\sin \theta - \sin 3\theta)}{8\pi(1-\nu^2)r}
 \end{aligned}$$

The displacement components are plotted in Figure 5.21, for a dislocation with $b_2 = 0$. The contours show a sudden jump in u_1 at $x_2 = 0$, $x_1 > 0$. (This is caused by the term involving θ in the formula for u_1 ; we assumed that $0 < \theta < 2\pi$ when plotting the displacement contours.) Physically, the plane $x_2 = 0$, $x_1 > 0$ corresponds to the “cut” that created the dislocation, and the jump in displacement across the cut is equal to the Burger’s vector.

Contours of stress are plotted in Figure 5.22. The radial and hoop stresses are compressive above the dislocation and tensile below it, as one would expect. Shear stress is positive

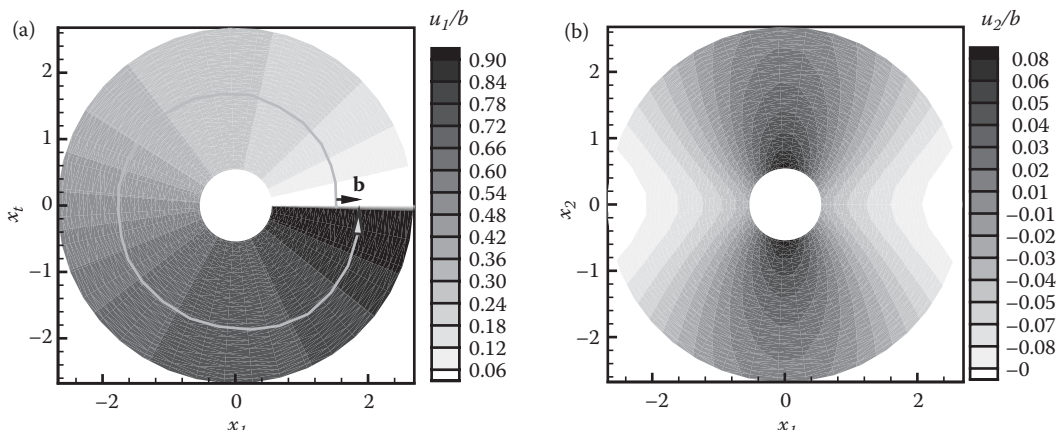


FIGURE 5.21 Displacement fields around an edge dislocation. (a) Horizontal displacements; (b) vertical displacements.

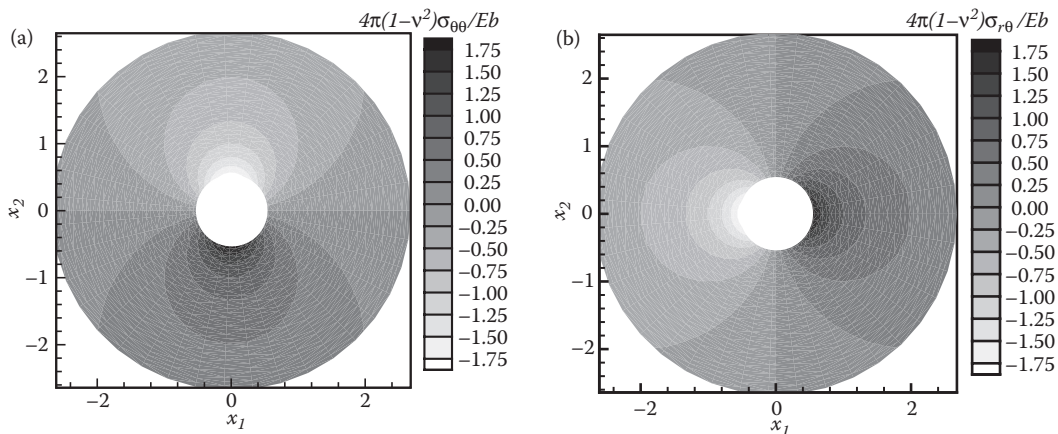


FIGURE 5.22 Stress distribution around a dislocation. (a) Hoop or radial stress; (b) shear stress.

to the right of the dislocation and negative to the left, again, in concord with our physical intuition. The stresses are infinite at the dislocation itself, but of course in this region linear elasticity does not accurately model material behavior, because the atomic bonds are very severely distorted.

5.3.5 Cylindrical Hole in an Infinite Solid under Remote Loading

Figure 5.23 shows a circular cylindrical cavity with radius a in an infinite, isotropic linear elastic solid. Far from the cavity, the solid is subjected to a tensile stress $\sigma_{11} = \sigma_0$, with all other stress components zero.

The solution is generated by complex potentials

$$\Omega(z) = \frac{\sigma_0}{4} \left(z + \frac{2a^2}{z} \right) \quad \omega(z) = \frac{-\sigma_0}{2} \left(z + \frac{a^2}{z} - \frac{a^4}{z^3} \right).$$

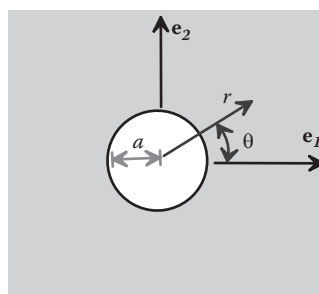


FIGURE 5.23 Cylindrical hole in an elastic solid.

The displacement and stress state is easily calculated as

$$\begin{aligned}
 u_1 &= \frac{\sigma_0(1+\nu)a}{2E} \left\{ 2(1-\nu) \left(\frac{r}{a} + \frac{2a}{r} \right) \cos \theta + \left(\frac{a}{r} - \frac{a^3}{r^3} \right) \cos 3\theta \right\} \\
 u_2 &= \frac{\sigma_0(1+\nu)a}{2E} \left\{ -2(1-2\nu) \frac{a}{r} \sin \theta - 2\nu \frac{r}{a} \sin \theta + \left(\frac{a}{r} - \frac{a^3}{r^3} \right) \sin 3\theta \right\} \\
 \sigma_{11} &= \sigma_0 \left(1 + \left(\frac{3a^4}{2r^4} - \frac{a^2}{r^2} \right) \cos 4\theta - \frac{3a^2}{2r^2} \cos 2\theta \right) \quad \sigma_{22} = \sigma_0 \left(\left(\frac{a^2}{r^2} - \frac{3a^4}{2r^4} \right) \cos 4\theta - \frac{a^2}{2r^2} \cos 2\theta \right) \\
 \sigma_{12} &= \sigma_0 \left(\left(\frac{3a^4}{2r^4} - \frac{a^2}{r^2} \right) \sin 4\theta - \frac{a^2}{2r^2} \sin 2\theta \right).
 \end{aligned}$$

5.3.6 Crack in an Infinite Elastic Solid under Remote Loading

Figure 5.24 shows a 2D crack with length $2a$ in an infinite solid, which is subjected to a uniform state of stress $\sigma_{22}^\infty, \sigma_{12}^\infty$ at infinity. The solution can be generated by complex potentials

$$\begin{aligned}
 \Omega(z) &= \frac{1}{4}(\sigma_{22}^\infty)z + \frac{1}{2}(\sigma_{22}^\infty - i\sigma_{12}^\infty)(\sqrt{z^2 - a^2} - z) \\
 \omega(z) &= \overline{\Omega(\bar{z})} - z\Omega'(z) + \sigma_{22}^\infty z/2 + i\sigma_{12}^\infty z.
 \end{aligned}$$

Here, the notation $\overline{\Omega(\bar{z})}$ indicates that you should substitute \bar{z} into the function Ω and then take the conjugate of the whole function. Because z gets conjugated twice, $\overline{\Omega(\bar{z})}$ is actually a function of z . It is an analytic function, and its derivative with respect to z can be calculated as $\overline{\Omega'(\bar{z})}$.

Some care is required to evaluate the square root in the complex potentials properly (square roots are multiple valued, and you need to know which value, or “branch,” to use.

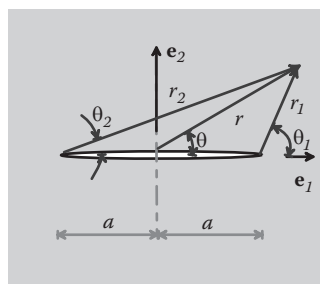


FIGURE 5.24 Slit crack in an elastic solid.

Multiple valued functions are made single valued by introducing a “branch cut” in which the function is discontinuous. In crack problems, the branch cut is always along the line of the crack). For this purpose, it is helpful to note that the appropriate branch can be obtained by setting

$$\sqrt{z^2 - a^2} = \sqrt{(z-a)(z+a)} = \sqrt{r_1} e^{i\theta_1/2} \sqrt{r_2} e^{i\theta_2/2},$$

where the angles and distances r_1 , θ_1 and r_2 , θ_2 are shown in Figure 5.24, and the angles θ_1 and θ_2 must lie in the ranges $-\pi \leq \theta_1 \leq \pi$ $0 \leq \theta_2 \leq 2\pi$, respectively.

The solution is most conveniently expressed in terms of the polar coordinates (r, θ) centered at the origin, together with the auxiliary angles r_1 , θ_1 and r_2 , θ_2 . If the algebra is correct, (which is unlikely because the algebra involved in getting these results from the complex potentials is unbelievably tedious and unfortunately beyond the capabilities of most symbolic manipulation programs), then the displacement and stress fields are

$$u_1 = \frac{(1+\nu)\sigma_{22}^\infty \sqrt{r_1 r_2}}{4E} \left\{ 4(1-2\nu) \cos(\theta_1 + \theta_2)/2 - \frac{4r(1-\nu)}{\sqrt{r_1 r_2}} \cos\theta \right. \\ \left. - \frac{2r^2}{r_1 r_2} (\cos(\theta_1 + \theta_2)/2 - \cos(2\theta - \theta_1/2 - \theta_2/2)) \right\} \\ + \frac{(1+\nu)\sigma_{12}^\infty \sqrt{r_1 r_2}}{E} \left\{ 2(1-2\nu) \sin(\theta_1 + \theta_2)/2 - 2(1-\nu) \frac{r}{\sqrt{r_1 r_2}} \sin\theta \right. \\ \left. + \frac{r^2}{r_1 r_2} \sin\theta \cos(\theta - \theta_1/2 - \theta_2/2) \right\} \\ u_2 = \frac{(1+\nu)\sigma_{22}^\infty \sqrt{r_1 r_2}}{4E} \left\{ 8(1-\nu) \sin(\theta_1 + \theta_2)/2 - \frac{4vr}{\sqrt{r_1 r_2}} \sin\theta \right. \\ \left. - \frac{2r^2}{r_1 r_2} (\sin(\theta_1 + \theta_2)/2 + \sin(2\theta - \theta_1/2 - \theta_2/2)) \right\} \\ + \frac{(1+\nu)\sigma_{12}^\infty \sqrt{r_1 r_2}}{E} \left\{ (1-2\nu) \cos(\theta_1 + \theta_2)/2 + 2(1-\nu) \frac{r}{\sqrt{r_1 r_2}} \cos\theta \right. \\ \left. - \frac{r^2}{r_1 r_2} \sin\theta \sin(\theta - \theta_1/2 - \theta_2/2) \right\} \\ \sigma_{11} = \frac{\sigma_{22}^\infty r}{\sqrt{r_1 r_2}} \left\{ \cos(\theta - \theta_1/2 - \theta_2/2) - 1 - \frac{a^2}{r_1 r_2} \sin\theta \sin 3(\theta_1 + \theta_2)/2 \right\} \\ + \frac{\sigma_{12}^\infty r}{\sqrt{r_1 r_2}} \left\{ 2 \sin(\theta - \theta_1/2 - \theta_2/2) - \frac{a^2}{r_1 r_2} \sin\theta \cos 3(\theta_1 + \theta_2)/2 \right\}$$

$$\sigma_{22} = \frac{\sigma_{22}^{\infty} r}{\sqrt{r_1 r_2}} \left\{ \cos(\theta - \theta_1/2 - \theta_2/2) + \frac{a^2}{r_1 r_2} \sin \theta \sin 3(\theta_1 + \theta_2)/2 \right\}$$

$$+ \frac{\sigma_{12}^{\infty} r}{\sqrt{r_1 r_2}} \frac{a^2}{r_1 r_2} \sin \theta \cos 3(\theta_1 + \theta_2)/2$$

$$\sigma_{12} = \frac{\sigma_{22}^{\infty} r}{\sqrt{r_1 r_2}} \frac{a^2}{r_1 r_2} \sin \theta \cos 3(\theta_1 + \theta_2)/2$$

$$+ \frac{\sigma_{12}^{\infty} r}{\sqrt{r_1 r_2}} \left\{ \cos(\theta - \theta_1/2 - \theta_2/2) + \frac{a^2}{r_1 r_2} \sin \theta \sin 3(\theta_1 + \theta_2)/2 \right\}.$$

5.3.7 Fields near the Tip of a Crack on Bimaterial Interface

Figure 5.25 shows a semi-infinite crack, which lies in the x_1, x_3 plane, with crack tip aligned with the x_3 axis. The material above the crack has shear modulus and Poisson's ratio μ_1, ν_1 ; the material below the crack has shear modulus and Poisson's ratio μ_2, ν_2 . In this section, we give the complex variable solution that governs the variation of stress and displacement near the crack tip. The solution is significant because *all* interface cracks (regardless of their geometry and the way the solid is loaded) have the same stress and displacement distribution near the crack tip.

5.3.7.1 Additional Elastic Constants for Bimaterial Problems

To simplify the solution, we define additional elastic constants as follows:

1. Plane strain moduli: $E'_1 = 2/\nu_1 / (1-\nu_1)$, $E'_2 = 2/\nu_2 / (1-\nu_2)$.

2. Bimaterial modulus: $\frac{1}{E^*} = \left\{ \frac{1}{E'_1} + \frac{1}{E'_2} \right\}$.

3. Dundurs' elastic constants:

$$\alpha = \frac{E'_1 - E'_2}{E'_1 + E'_2} \quad \beta = \frac{(1-2\nu_2)/\nu_2 - (1-2\nu_1)/\nu_1}{2(1-\nu_2)/\nu_2 + 2(1-\nu_1)/\nu_1}.$$

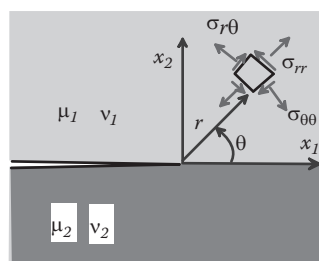


FIGURE 5.25 Crack on a bimaterial interface.

Evidently, α is a measure of the relative stiffness of the two materials. It must lie in the range $-1 < \alpha < 1$ for all possible material combinations, with $\alpha = 1$ signifying that material 1 is rigid, whereas $\alpha = -1$ signifies that material 2 is rigid. The second parameter does not have such a nice physical interpretation: it is a rough measure of the relative compressibilities of the two materials. For Poisson's ratios in the range $0 < \nu < 1/2$, one can show that $-1 < \alpha - 4\beta < 1$.

4. Crack-tip singularity parameter:

$$\varepsilon = \frac{1}{2\pi} \log \left(\frac{1-\beta}{1+\beta} \right).$$

For most material combinations the value of ε is very small—typically of order 0.01 or so.

The full displacement and stress fields in the two materials are calculated from two sets of complex potentials:

$$\begin{aligned}\Omega_1(z) &= \frac{1+\beta}{(1-2i\varepsilon)\sqrt{2\pi}} (K_1 - iK_2) z^{(1-2i\varepsilon)/2} \quad \text{Im}(z) > 0 \\ \Omega_2(z) &= \frac{1-\beta}{(1-2i\varepsilon)\sqrt{2\pi}} (K_1 - iK_2) z^{(1-2i\varepsilon)/2} \quad \text{Im}(z) > 0 \\ \omega_1(z) &= \overline{\Omega_2(\bar{z})} - z\Omega'_1(z) \quad \text{Im}(z) > 0 \\ \omega_2(z) &= \overline{\Omega_1(\bar{z})} - z\Omega'_2(z) \quad \text{Im}(z) < 0,\end{aligned}$$

where K_1 and K_2 are parameters that resemble the mode I and mode II stress intensity factors that characterize the crack-tip stresses in a homogeneous solid. In practice, these parameters are not usually used in fracture criteria for interface cracks; instead, the crack-tip loading is characterized by the magnitude of the stress intensity factor $|K|$, a characteristic length L , and a *phase angle* ψ , defined as

$$|K| = \sqrt{K_1^2 + K_2^2} \quad \psi = \tan^{-1} \frac{\text{Im}[(K_1 + K_2)L^{ie}]}{\text{Re}[(K_1 + iK_2)L^{ie}]}.$$

This means that $(K_1 + iK_2)L^{ie} = |K|e^{i\psi} \Rightarrow (K_1 - iK_2) = |K|e^{-i\psi}L^{ie}$. Complete expressions for the displacement components and stress components at a point r, θ in the solid can be calculated from these potentials. To simplify the results, it is helpful to note that

$$\cosh(\pi\varepsilon) = \frac{1}{2}(e^{\pi\varepsilon} + e^{-\pi\varepsilon}) = \frac{1}{2} \left(\sqrt{\frac{1-\beta}{1+\beta}} + \sqrt{\frac{1+\beta}{1-\beta}} \right) = \frac{1}{\sqrt{(1-\beta)}\sqrt{(1+\beta)}}.$$

Then, in material 1,

$$\begin{aligned}
 2_{-1}(u_1 + iu_2) &= \frac{|K|}{\cosh(\pi\varepsilon)} \sqrt{\frac{r}{2\pi}} \left\{ \frac{1}{1-2i\varepsilon} \left(\frac{r}{L} \right)^{-i\varepsilon} \left[(3-4\nu_1)e^{i(\theta/2-\psi)} e^{\varepsilon(\theta-\pi)} - e^{-i(\theta/2+\psi)} e^{-\varepsilon(\theta-\pi)} \right] \right. \\
 &\quad \left. - \left(\frac{r}{L} \right)^{i\varepsilon} i \sin \theta e^{i(\theta/2+\psi)} e^{\varepsilon(\theta-\pi)} \right\} \\
 \sigma_{11} + \sigma_{22} &= \frac{|K|}{\sqrt{2\pi r}} (1+\beta) e^{\varepsilon\theta} \left\{ \left(\frac{r}{L} \right)^{-i\varepsilon} e^{-i(\theta/2+\psi)} + \left(\frac{r}{L} \right)^{i\varepsilon} e^{i(\theta/2+\psi)} \right\} \\
 \sigma_{11} - \sigma_{22} + 2i\sigma_{12} &= \frac{|K|e^{i\theta}}{\sqrt{2\pi r}} \left\{ \left(\frac{r}{L} \right)^{i\varepsilon} e^{i\psi} e^{\varepsilon\theta} e^{i\theta/2} (1+\beta)(\cos\theta + 2\varepsilon \sin\theta) \right. \\
 &\quad \left. - \left(\frac{r}{L} \right)^{-i\varepsilon} e^{-i\psi} e^{-\varepsilon\theta} e^{-i\theta/2} (1-\beta) \right\},
 \end{aligned}$$

whereas in material 2,

$$\begin{aligned}
 2_{-2}(u_1 + iu_2) &= \frac{|K|}{\cosh(\pi\varepsilon)} \sqrt{\frac{r}{2\pi}} \left\{ \frac{1}{1-2i\varepsilon} \left(\frac{r}{L} \right)^{-i\varepsilon} \left[(3-4\nu_2)e^{i(\theta/2-\psi)} e^{\varepsilon(\theta+\pi)} - e^{-i(\theta/2+\psi)} e^{-\varepsilon(\theta+\pi)} \right] \right. \\
 &\quad \left. - \left(\frac{r}{L} \right)^{i\varepsilon} i \sin \theta e^{i(\theta/2+\psi)} e^{\varepsilon(\theta+\pi)} \right\} \\
 \sigma_{11} + \sigma_{22} &= \frac{|K|}{\sqrt{2\pi r}} (1-\beta) e^{\varepsilon\theta} \left\{ \left(\frac{r}{L} \right)^{-i\varepsilon} e^{-i(\theta/2+\psi)} + \left(\frac{r}{L} \right)^{i\varepsilon} e^{i(\theta/2+\psi)} \right\} \\
 \sigma_{11} - \sigma_{22} + 2i\sigma_{12} &= \frac{|K|e^{i\theta}}{\sqrt{2\pi r}} \left\{ \left(\frac{r}{L} \right)^{i\varepsilon} e^{i\psi} e^{\varepsilon\theta} e^{i\theta/2} (1-\beta)(\cos\theta + 2\varepsilon \sin\theta) \right. \\
 &\quad \left. - \left(\frac{r}{L} \right)^{-i\varepsilon} e^{-i\psi} e^{-\varepsilon\theta} e^{-i\theta/2} (1+\beta) \right\}.
 \end{aligned}$$

The individual stress components can be determined by adding/subtracting the last two equations and taking real and imaginary parts. Note that $(r/L)^{ie} = \exp(i\varepsilon \log(r/L)) = \cos(\varepsilon \log r/L) + i \sin(\varepsilon \log r/L)$. Features of this solution are discussed in more detail in Section 9.6.1.

5.3.8 Frictionless Rigid Flat Indenter in Contact with a Half-Space

Figure 5.26 shows a rigid, flat punch with width $2a$ and infinite length perpendicular to the plane of the figure. It is pushed into an elastic half-space with a force F_2 per unit out-of-plane distance. The half-space is a linear elastic solid with shear modulus μ and Poisson's ratio ν . The interface between the two solids is frictionless.

The solution is generated from the following complex potentials:

$$\Omega(z) = \frac{-iF_2}{2\pi} \log\left(z + \sqrt{z^2 - a^2}\right) + \frac{id_2}{2(1-\nu)} \quad \omega(z) = -\overline{\Omega(\bar{z})} - z\Omega'(z),$$

where d_2 is an arbitrary constant, representing an unknown rigid displacement. Note that the solution is valid only for $\text{Im}(z) > 0$.

Stresses and displacements can be determined by substituting for Ω and ω into the general formulas or, alternatively, by substituting Ω into the simplified representation for half-space problems given in Section 5.3.1. Some care is required to evaluate the square root in the complex potentials, particularly when calculating $\Omega(\bar{z})$ and $\Omega'(\bar{z})$. The solution assumes that

$$\begin{aligned} \sqrt{z^2 - a^2} &= \sqrt{(z-a)(z+a)} = \sqrt{r_1} e^{i\theta_1/2} \sqrt{r_2} e^{i\theta_2/2} \\ \overline{\sqrt{z^2 - a^2}} &= \overline{\sqrt{(z-a)(z+a)}} = \sqrt{r_1} e^{-i\theta_1/2} \sqrt{r_2} e^{-i\theta_2/2} \\ \sqrt{\bar{z}^2 - a^2} &= \sqrt{(\bar{z}-a)(\bar{z}+a)} = \sqrt{r_1} e^{-i\theta_1/2} \sqrt{r_2} e^{-i\theta_2/2}, \end{aligned}$$

where the angles and distances r_1, θ_1 and r_2, θ_2 are shown in Figure 5.26, and θ_1 and θ_2 must lie in the ranges $0 \leq \theta_1 \leq \pi$ $0 \leq \theta_2 \leq \pi$.

The full displacement and stress fields can be determined without difficulty but are too lengthy to write out in full. However, important features of the solution can be extracted, such as the following:

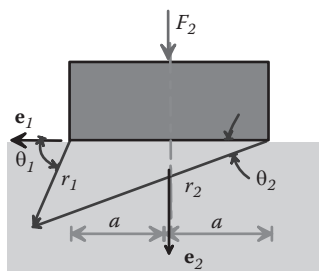


FIGURE 5.26 Rigid flat punch indenting an elastic solid.

1. Contact pressure: The pressure exerted by the indenter on the elastic solid follows as

$$p(x_1) = -\sigma_{22}(x_1, x_2 = 0) = \frac{F_2}{\pi \sqrt{a^2 - x_1^2}}.$$

2. Surface displacement: The displacement of the surface is

$$u_2 = \begin{cases} -\frac{F_2(1-\nu)}{\pi} \log(|x_1| + \sqrt{x_1^2 - a^2}) + d_2 & |x_1| > a \\ -\frac{F_2(1-\nu)}{\pi} \log(a) + d_2 & |x_1| < a. \end{cases}$$

Note that there is no unambiguous way to determine the value of d_2 . It is tempting, for example, to attempt to calculate d_2 by assuming that the surface remains fixed at some point far from the indenter. However, in this case, d_2 increases without limit as the distance of the fixed point from the indenter increases.

3. Contact stiffness: The stiffness of a contact is defined as the ratio of the force acting on the indenter to its displacement $k_c = F_2/u_2(z=0)$ and is of considerable interest in practical applications. Unfortunately, the solution for an infinite solid cannot be used to estimate the stiffness of a 2D contact (the stiffness depends on d_2). Of course, the stiffness of a contact between two finite-sized elastic solids is well defined, but the stiffness depends on the overall geometry of the two contacting solids and varies as $k_c = \mu / [(1 - \nu) \log(R/a)]$, where R is a characteristic length comparable with the specimen size, and a is the contact width.

5.3.9 Frictionless Parabolic (Cylindrical) Indenter in Contact with a Half-Space

Figure 5.27 shows a rigid, parabolic punch with profile

$$f(r) = r^2 / (2R)$$

(and infinite length perpendicular to the plane of the figure), which is pushed into an elastic half-space by a force F_2 . This profile is often used to approximate a cylinder with radius

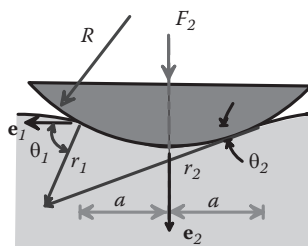


FIGURE 5.27 Rigid cylindrical punch indenting an elastic solid.

R. The interface between the two solids is frictionless and cannot withstand any tensile stress. The indenter sinks into the elastic solid so that the two solids make contact over a finite region $-a < x_1 < a$, where

$$a = \sqrt{4RF_2 / \pi E^*} \quad E^* = E/(1 - \nu^2).$$

The solution is generated from the following complex potentials:

$$\Omega(z) = \frac{iF_2}{2\pi a^2} \left\{ z\sqrt{z^2 - a^2} - z^2 - a^2 \log(z + \sqrt{z^2 - a^2}) \right\} + \frac{Eid_2}{4(1-\nu^2)} \quad \omega(z) = -\overline{\Omega(\bar{z})} - z\Omega'(z),$$

where d_2 is an arbitrary constant, representing an unknown rigid displacement. Note that the solution is valid only for $\text{Im}(z) > 0$. You can use the formulas given at the end of Section 5.3.1 to determine displacements and stress directly from $\Omega(z)$. In addition, the formulas in Section 5.3.8 should be used to determine correct sign for the square root.

Important features of the solution are as follows:

1. Contact pressure: The pressure exerted by the indenter on the elastic solid follows as

$$p(x_1) = -\sigma_{22}(x_1, x_2 = 0) = \frac{2F_2}{\pi a^2} \sqrt{a^2 - x_1^2}.$$

2. Surface displacement: The vertical displacement of the surface is

$$u_2 = \begin{cases} \frac{2F_2}{\pi E^* a^2} \left\{ x_1 \sqrt{x_1^2 - a^2} - x_1^2 - a^2 \log\left(x_1 + \sqrt{x_1^2 - a^2}\right) \right\} + d_2 & |x_1| > a \\ -\frac{2F_2}{\pi E^* a^2} \left(\log(a) + x_1^2 \right) + d_2 & |x_1| < a. \end{cases}$$

As discussed in Section 5.3.8, d_2 or the contact stiffness cannot be determined uniquely.

3. Stress field: The stress field is

$$\begin{aligned} \sigma_{11} &= -\frac{2F_2}{\pi a^2} \left(m \left(1 + \frac{(x_2^2 + n^2)}{(m^2 + n^2)} \right) - 2x_2 \right) \\ \sigma_{22} &= -\frac{2F_2}{\pi a^2} m \left(1 - \frac{(x_2^2 + n^2)}{(m^2 + n^2)} \right) \quad \sigma_{12} = -\frac{2F_2}{\pi a^2} n \frac{(m^2 - x_2^2)}{(m^2 + n^2)} \end{aligned}$$

$$m = \sqrt{(c_1 + c_2)/2} \quad n = x_1 \sqrt{(c_1 - c_2)/(2x_1^2)} \quad c_1 = 1 - x_1^2 - x_2^2 \quad c_2 = \sqrt{c_1^2 + 4x_1^2 x_2^2}.$$

4. Critical load required to cause yield: The elastic limit is best calculated using the Tresca yield criterion, which gives

$$F_2 / a = 2.616Y,$$

where Y is the tensile yield stress of the solid. To derive this result, note that the stresses are proportional to F_2/a . This means we can write

$$\sigma_{ij} = (F_2 / a) \hat{\sigma}_{ij} (x_i / a),$$

where $\hat{\sigma}_{ij}$ is the stress induced at x_i for a contact with $a = 1$ subjected to load $F_2 = 1$. The yield criterion can therefore be expressed as

$$\frac{F_2}{a} \max_{(x_1, x_2)} \left\{ \sqrt{(\hat{\sigma}_{11} - \hat{\sigma}_{22})^2 + 4\hat{\sigma}_{12}^2} \right\} = Y,$$

where $\max_{(x_1, x_2)}$ denotes maximizing with respect to position in the solid. Figure 5.28 shows contours of $\sqrt{(\hat{\sigma}_{11} - \hat{\sigma}_{22})^2 + 4\hat{\sigma}_{12}^2}$: the maximum value is approximately 0.3823 and occurs on the symmetry axis at a depth of about $0.78a$. Substituting this value back into the yield criterion gives the result.

5.3.10 Line Contact between Two Nonconformal Frictionless Elastic Solids

The solution in the preceding section can be generalized to find stress and displacement caused by contact between two elastic solids. The solution assumes the following:

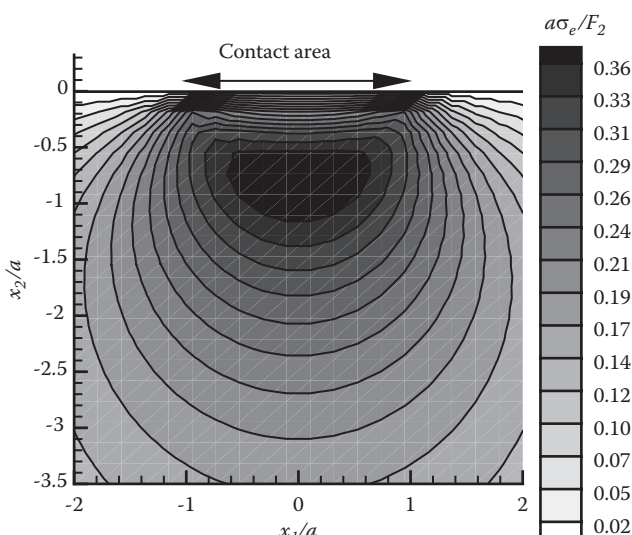


FIGURE 5.28 Contours of von Mises effective stress under a cylindrical contact.

1. The two contacting solids initially meet at along a line perpendicular to the plane of the figure (the line of initial contact lies on the line connecting the centers of curvature of the two solids).
2. The two contacting solids have radii of curvature R_1 and R_2 at the point of initial contact. A convex surface has a positive radius of curvature; a concave surface (like the internal surface of a hole) has a negative radius of curvature.
3. The two solids have Young's modulus and Poisson's ratio E_1, ν_1 and E_2, ν_2 .
4. The two solids are pushed into contact by a force F_2 .

The solution is expressed in terms of an effective contact radius and an effective modulus, defined as

$$R = \frac{R_1 R_2}{R_1 + R_2} \quad E^* = \frac{E_1 E_2}{(1 - \nu_1^2) E_2 + (1 - \nu_2^2) E_1}.$$

The contact width and contact pressure can be determined by substituting these values into the formulas given in the preceding section. The full stress and displacement field in each solid can be calculated from the potential given in the preceding section, by adopting a coordinate system that points into the solid of interest.

5.3.11 Sliding Contact between Two Rough Elastic Cylinders

Figure 5.29 shows two elastic cylinders with elastic constants E_1, ν_1, E_2, ν_2 , radii R_1, R_2 , and infinite length perpendicular to the plane of the figure, which are pushed into contact by a forces F_2 acting perpendicular to the line of contact and F_1 acting parallel to the tangent plane. The interface between the two solids has a coefficient of friction f and cannot withstand any tensile stress. The tangential force is sufficient to cause the two solids to slide

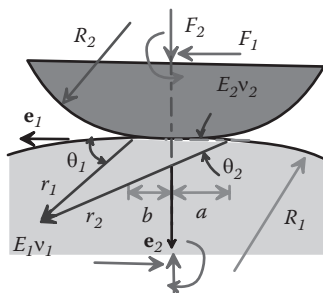


FIGURE 5.29 Sliding contact between two elastic solids.

against each other, so that $F_1 = fF_2$. We give the solution for solid 1 only: the solution for the second solid can be found by exchanging the moduli appropriately.

The coordinate system has origin at the initial point of contact between the two solids. The two solids make contact over a finite region $-a < x_1 < b$, where

$$a = \sqrt{4RF_2(1+2\gamma)/\pi(1-2\gamma)E^*} \quad b = \sqrt{4RF_2(1-2\gamma)/(1+2\gamma)\pi E^*}$$

and

$$\begin{aligned} R &= \frac{R_1 R_2}{R_1 + R_2} \quad E^* = \frac{E_1 E_2}{(1-\nu_1^2)E_2 + (1-\nu_2^2)E_1} \\ \beta &= \frac{(1-2\nu_2)/_2 - (1-2\nu_1)/_1}{2(1-\nu_2)/_2 + 2(1-\nu_1)/_1} \quad \gamma = -\frac{1}{\pi} \tan^{-1}(\beta f). \end{aligned}$$

Only the derivatives of the complex potentials for this solution can be found analytically: they are

$$\Omega'(z) = -\frac{(f+i)F_2}{\pi ab} \left\{ z - (z+a)^{1/2-\gamma} (z-b)^{1/2+\gamma} \right\} \quad \omega'(z) = -\overline{\Omega'(\bar{z})} - z\Omega''(z) - \Omega'(z).$$

Note that the solution is valid only for $\text{Im}(z) > 0$. You can use the formulas given at the end of Section 5.3.1 to determine stresses directly from $\Omega'(z)$. In addition, the branch of $(z+a)^{1/2-\gamma} (z-b)^{1/2+\gamma}$ must be selected so that

$$\begin{aligned} (z-b)^{1/2+\gamma} (z+a)^{1/2-\gamma} &= r_1^{1/2-\gamma} e^{i(1/2-\gamma)\theta_1} r_2^{1/2+\gamma} e^{i(1/2+\gamma)\theta_2} \\ \overline{(z-b)^{1/2+\gamma} (z+a)^{1/2-\gamma}} &= r_1^{1/2-\gamma} e^{-i(1/2-\gamma)\theta_1} r_2^{1/2+\gamma} e^{-i(1/2+\gamma)\theta_2} \\ (\bar{z}-b)^{1/2+\gamma} (\bar{z}+a)^{1/2-\gamma} &= r_1^{1/2-\gamma} e^{-i(1/2-\gamma)\theta_1} r_2^{1/2+\gamma} e^{-i(1/2+\gamma)\theta_2}, \end{aligned}$$

where the angles and distances r_1, θ_1 and r_2, θ_2 are shown in Figure 5.29, and θ_1 and θ_2 must lie in the ranges $0 \leq \theta_1 \leq \pi$, $0 \leq \theta_2 \leq \pi$.

Important features of the solution are as follows:

- 1. Contact pressure:** The tractions exerted by the indenter on the elastic solid follow as

$$p(x_1) = -\sigma_{22}(x_1, x_2 = 0) = \frac{2F_2}{\pi ab\sqrt{1+\beta^2 f^2}} \sqrt{a+x_1} \sqrt{x_1-b} \left(\frac{x_1+a}{x_1-b} \right)^\gamma \quad q(x_1) = \sigma_{12} = fp(x_1).$$

In practice, the value of γ is very small (generally less than 0.05), and you can approximate the solution by assuming that $\gamma = 0$ without significant error.

2. Approximate expressions for stresses: For $\gamma = 0$, the stresses can be written in a simple form. The stresses induced by the vertical force are given in Section 5.3.9. The stresses induced by the friction force are

$$\sigma_{11} = -\frac{2fF_2}{\pi a^2} \left(n \left(2 - \frac{(x_2^2 - m^2)}{(m^2 + n^2)} \right) - 2x_1 \right) \quad \sigma_{22} = -\frac{2fF_2}{\pi a^2} n \frac{(m^2 - x_2^2)}{(m^2 + n^2)}$$

$$\sigma_{12} = -\frac{2fF_2}{\pi a^2} m \left(1 - \frac{(x_2^2 + n^2)}{(m^2 + n^2)} \right)$$

$$m = \sqrt{(c_1 + c_2)/2} \quad n = x_1 \sqrt{(c_1 - c_2)/(2x_1^2)} \quad c_1 = 1 - x_1^2 - x_2^2 \quad c_2 = \sqrt{c_1^2 + 4x_1^2 x_2^2}.$$

5.3.12 Dislocation near the Surface of a Half-Space

Figure 5.30 shows a dislocation with Burger's vector $\mathbf{b} = b_1 \mathbf{e}_1 + b_2 \mathbf{e}_2$ located at a depth h below the surface of an isotropic linear elastic half-space, with Young's modulus E and Poisson's ratio ν . The surface of the half-space is traction free.

The solution is given by the sum of two potentials:

$$\Omega(z) = \Omega_0(z) + \Omega_1(z) \quad \omega(z) = \omega_0(z) + \omega_1(z)$$

where

$$\Omega_0(z) = -i \frac{E(b_1 + ib_2)}{8\pi(1-\nu^2)} \log(z - ih) \quad \omega_0(z) = i \frac{E(b_1 - ib_2)}{8\pi(1-\nu^2)} \log(z - ih) + \frac{E(b_1 + ib_2)}{8\pi(1-\nu^2)} \frac{h}{z - ih}$$

is the solution for a dislocation at position $z_0 = ih$ in an infinite solid and

$$\Omega_1(z) = -z \overline{\Omega'_0(\bar{z})} - \overline{\omega_0(\bar{z})}$$

$$\omega_1(z) = z \overline{\omega'_0(\bar{z})} - \overline{\Omega_0(\bar{z})} + z \overline{\Omega'_0(\bar{z})} + z^2 \overline{\Omega''_0(\bar{z})}$$

corrects the solution to satisfy the traction-free boundary condition at the surface.

The displacement and stress fields can be computed by substituting Ω and ω into the standard formulas given in Section 5.3.1 (do not use the half-space representation). A symbolic manipulation program makes the calculation painless. Most symbolic manipulation programs will not be able to differentiate the complex conjugate of a function, so the

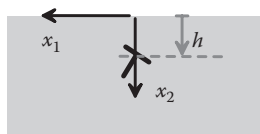


FIGURE 5.30 Edge dislocation near the surface of an elastic solid.

derivatives of Ω_1 and ω_1 should be calculated by substituting appropriate derivatives of Ω_0 and ω_0 into the following formulas:

$$\Omega'_1(z) = -z\overline{\Omega''_0(\bar{z})} - \overline{\Omega'_0(\bar{z})} - \overline{\omega'_0(\bar{z})}$$

$$\Omega''_0(z) = -z\overline{\Omega'''_0(\bar{z})} - 2\overline{\Omega''_0(\bar{z})} - \overline{\omega''_0(\bar{z})}$$

$$\omega'_1(z) = z\overline{\omega''_0(\bar{z})} + \overline{\omega'_0(\bar{z})} + 3z\overline{\Omega''_0(\bar{z})} + z^2\overline{\Omega'''_0(\bar{z})}.$$

As an example, the variation of stress along the line $x_1 = 0$ is given by

$$\sigma_{22} = \frac{Eb_1}{\pi(1-\nu^2)(x_2+h)^3(x_2-h)} \frac{2hx_2^2}{2h^2x_2} \quad \sigma_{11} = \frac{Eb_1}{\pi(1-\nu^2)(x_2+h)^3(x_2-h)} \frac{2h^2x_2}{2h^2x_2}$$

$$\sigma_{12} = \frac{Eb_2}{\pi(1-\nu^2)(x_2+h)^3(x_2-h)} \frac{-2h^2x_2}{-2h^2x_2}.$$

5.4 SOLUTIONS TO 3D STATIC PROBLEMS IN LINEAR ELASTICITY

The field equations of linear elasticity are much more difficult to solve in three dimensions than in two dimensions. Nevertheless, several important problems have been solved. In this section, we outline a common representation for 3D problems and give solutions to selected 3D problems.

5.4.1 Papkovich–Neuber Potential Representations for 3D Solutions for Isotropic Solids

In this section, we outline a general technique for solving 3D static linear elasticity problems. The technique is similar to the 2D Airy function method, in that the solution is derived by differentiating a potential, which is governed by a partial differential equation. Many other potential representations are used in 3D elasticity, but most are simply special cases of the general Papkovich–Neuber representation. Figure 5.31 illustrates a generic linear elasticity problem. Assume the following:

- The solid has Young's modulus E , mass density ρ_0 , and Poisson's ratio ν .
- The solid is subjected to body force distribution $b_i(x_1, x_2, x_3)$ (per unit mass).

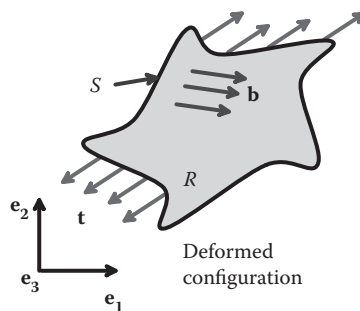


FIGURE 5.31 Representative boundary value problem for an elastic solid.

- Part of the boundary S_1 is subjected to prescribed displacements u_i^* .
- A second part of the boundary S_2 is subjected to prescribed tractions t_i^* .

The Papkovich–Neuber procedure can be summarized as follows:

1. Begin by finding a vector function $\Psi_i(x_1, x_2, x_3)$ and scalar function $\phi(x_1, x_2, x_3)$ that satisfy

$$\frac{\partial^2 \Psi_i}{\partial x_j \partial x_k} = -\rho_0 b_i \quad \frac{\partial^2 \phi}{\partial x_k \partial x_i} = -\rho_0 b_i x_i,$$

as well as boundary conditions

$$\begin{aligned} \frac{2(1+\nu)}{E} \left(\Psi_i + \frac{1}{4(1-\nu)} \frac{\partial}{\partial x_j} (\phi - x_k \Psi_k) \right) &= u_i^* && \text{on } S_1 \\ 2\nu \frac{\partial \Psi_k}{\partial x_k} n_i + (1-2\nu) \left(\frac{\partial \Psi_i}{\partial x_j} + \frac{\partial \Psi_j}{\partial x_i} \right) n_j - x_k \frac{\partial^2 \Psi_k}{\partial x_i \partial x_j} n_j + \frac{\partial^2 \phi}{\partial x_i \partial x_j} n_j &= 2(1-\nu) t_i^* && \text{on } S_2. \end{aligned}$$

2. Calculate displacements from the formula

$$u_i = \frac{2(1+\nu)}{E} \left(\Psi_i + \frac{1}{4(1-\nu)} \frac{\partial}{\partial x_i} (\phi - x_k \Psi_k) \right).$$

3. Calculate stresses from the formula

$$2(1-\nu) \sigma_{ij} = 2\nu \frac{\partial \Psi_k}{\partial x_k} \delta_{ij} + (1-2\nu) \left(\frac{\partial \Psi_i}{\partial x_j} + \frac{\partial \Psi_j}{\partial x_i} \right) - x_k \frac{\partial^2 \Psi_k}{\partial x_i \partial x_j} + \frac{\partial^2 \phi}{\partial x_i \partial x_j}.$$

HEALTH WARNING: Although the displacements and stresses that solve a linear elasticity problem are unique, the Papkovich–Neuber potentials that generate a particular solution are not. Consequently, if you find several different sets of potentials in the literature that claim to solve the same problem, don't panic. It is likely that they really do solve the same problem.

5.4.2 Demonstration That the Papkovich–Neuber Solution Satisfies the Governing Equations

We need to show two things:

1. That the displacement field satisfies the equilibrium equation (Section 5.1.2)

$$\frac{1}{1-2\nu} \frac{\partial^2 u_k}{\partial x_k \partial x_i} + \frac{\partial^2 u_i}{\partial x_k \partial x_k} = -2(1+\nu) \rho_0 \frac{b_i}{E};$$

2. That the stresses are related to the displacements by the elastic stress-strain equations.

To show the first result, differentiate the formula relating potentials to the displacement to see that

$$\frac{\partial^2 u_k}{\partial x_i \partial x_j} = \frac{(1+\nu)}{2E(1-\nu)} \left((3-4\nu) \frac{\partial^2 \Psi_k}{\partial x_i \partial x_j} - \frac{\partial^2 \Psi_j}{\partial x_k \partial x_i} - \frac{\partial^2 \Psi_i}{\partial x_k \partial x_j} - x_m \frac{\partial^2 \Psi_m}{\partial x_k \partial x_i \partial x_j} + \frac{\partial^2 \phi}{\partial x_k \partial x_i \partial x_j} \right).$$

Substitute this result into the governing equation to see that

$$\begin{aligned} \frac{1}{1-2\nu} \frac{\partial^2 u_k}{\partial x_k \partial x_i} + \frac{\partial^2 u_i}{\partial x_k \partial x_k} = \\ \frac{(1+\nu)}{2E(1-\nu)(1-2\nu)} \left(2(1-2\nu) \frac{\partial^2 \Psi_k}{\partial x_i \partial x_k} - \frac{\partial^2 \Psi_i}{\partial x_k \partial x_k} - x_m \frac{\partial^3 \Psi_m}{\partial x_k \partial x_i \partial x_k} + \frac{\partial^3 \phi}{\partial x_k \partial x_i \partial x_k} \right) \\ + \frac{(1+\nu)}{2E(1-\nu)} \left((3-4\nu) \frac{\partial^2 \Psi_i}{\partial x_k \partial x_k} - 2 \frac{\partial^2 \Psi_k}{\partial x_k \partial x_i} - x_m \frac{\partial^3 \Psi_m}{\partial x_k \partial x_i \partial x_k} + \frac{\partial^3 \phi}{\partial x_k \partial x_i \partial x_k} \right). \end{aligned}$$

Finally, substitute the governing equations for the potentials

$$\frac{\partial^2 \Psi_i}{\partial x_j \partial x_j} = -\rho_0 b_i \quad \frac{\partial^2 \phi}{\partial x_k \partial x_k} = -\rho_0 b_i x_i$$

and simplify the result to verify that the governing equation is indeed satisfied. The second result can be derived by substituting the formula for displacement into the elastic stress-strain equations and simplifying.

5.4.3 Point Force in an Infinite Solid

The displacements and stresses induced by a point force $\mathbf{P} = P_1 \mathbf{e}_1 + P_2 \mathbf{e}_2 + P_3 \mathbf{e}_3$ acting at the origin of a large (infinite) elastic solid with Young's modulus E and Poisson's ratio ν are generated by the Papkovich-Neuber potentials

$$\Psi_i = \frac{P_i}{4\pi R} \quad \phi = 0,$$

where $R = \sqrt{x_i x_i}$. The displacements, strains, and stresses follow as

$$\begin{aligned} u_i &= \frac{(1+\nu)}{8\pi E(1-\nu)R} \left\{ \frac{P_k x_k x_i}{R^2} + (3-4\nu)P_i \right\} \\ \varepsilon_{ij} &= \frac{-(1+\nu)}{8\pi E(1-\nu)R^2} \left\{ \frac{3P_k x_k x_i x_j}{R^3} - \frac{P_k x_k \delta_{ij}}{R} + (1-2\nu) \frac{P_i x_j + P_j x_i}{R} \right\} \\ \sigma_{ij} &= \frac{-1}{8\pi(1-\nu)R^2} \left\{ \frac{3P_k x_k x_i x_j}{R^3} + (1-2\nu) \frac{P_i x_j + P_j x_i - \delta_{ij} P_k x_k}{R} \right\}. \end{aligned}$$

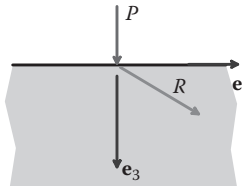


FIGURE 5.32 Point force acting normal to the surface of an elastic solid.

5.4.4 Point Force Normal to the Surface of an Infinite Half-Space

Figure 5.32 shows a point force $\mathbf{P} = Pe_3$ acting normal to the surface of a semi-infinite solid with Young's modulus E and Poisson's ratio ν . The displacements and stresses in the half-space are generated by the Papkovich–Neuber potentials

$$\Psi_i = \frac{(1-\nu)\delta_{i3}}{\pi R} \quad \phi = -\frac{(1-2\nu)(1-\nu)}{\pi} \log(R+x_3),$$

where $R = \sqrt{x_k x_k}$.

The displacements and stresses follow as

$$u_i = \frac{(1+\nu)P}{2\pi E} \left\{ \frac{x_3 x_i}{R^3} + (3-4\nu) \frac{\delta_{i3}}{R} - \frac{(1-2\nu)}{R+x_3} \left(\delta_{3i} + \frac{x_i}{R} \right) \right\}$$

$$\sigma_{ij} = \frac{P}{2\pi R^2} \left\{ -3 \frac{x_i x_j x_3}{R^3} + \frac{(1-2\nu)(2R+x_3)}{R(R+x_3)^2} \left(x_i x_j + \delta_{ij} x_3^2 - x_3 (\delta_{i3} x_j + \delta_{j3} x_i) \right) \right.$$

$$\left. + \frac{(1-2\nu)R^2}{(R+x_3)^2} (\delta_{i3} \delta_{j3} - \delta_{ij}) \right\}.$$

5.4.5 Point Force Tangent to the Surface of an Infinite Half-Space

Figure 5.33 shows a point force $\mathbf{P} = Pe_1$ acting tangent to the surface of a semi-infinite solid with Young's modulus E and Poisson's ratio ν . The stresses and displacements in the solids are generated by the Papkovich–Neuber potentials

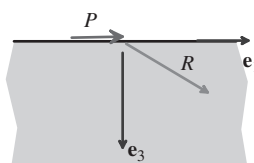


FIGURE 5.33 Point force acting tangent to the surface of an elastic solid.

$$\Psi_i = \frac{P}{2\pi(R+x_3)} \left(\delta_{ii} - \frac{x_2^2 \delta_{ii}}{R(R+x_3)} + \frac{x_1 x_2 \delta_{ij}}{R(R+x_3)} + 2(1-\nu) \frac{x_1 \delta_{ii}}{R} \right)$$

$$\phi = \frac{P}{2\pi} (1+4(1-\nu)^2) \frac{x_1}{R+x_3}.$$

The displacements and stresses can be calculated from these potentials as

$$u_i = \frac{P(1+\nu)}{2\pi E R} \left\{ \delta_{ii} + \frac{x_1 x_2}{R^2} + (1-2\nu) \left(\frac{R \delta_{ii}}{R+x_3} - \frac{R x_1 \delta_{ii}}{(R+x_3)^2} - \frac{x_1 x_i}{(R+x_3)^2} \right) \right\}$$

$$\sigma_{ij} = \frac{P}{2\pi} \left[-\frac{3x_1 x_i x_j}{R^5} + (1-2\nu) \left\{ \frac{x_1 x_i x_j}{R^3 (R+x_3)^2} + \frac{2x_1 x_i x_j}{R^2 (R+x_3)^3} \right\} (1-\delta_{ii})(1-\delta_{jj}) \right. \\ \left. + (1-2\nu) \left\{ \frac{x_1 x_3 (2R+x_3)}{R^3 (R+x_3)^2} (\delta_{ii} \delta_{jj} + \delta_{ij} \delta_{ji}) - \frac{2x_1 \delta_{ii} \delta_{jj}}{R(R+x_3)^2} - \frac{x_2 (\delta_{ii} \delta_{jj} + \delta_{ij} \delta_{ji})}{R(R+x_3)^2} \right\} \right]$$

(no sum on i or j).

5.4.6 The Eshelby Inclusion Problem

The Eshelby problem [Eshelby, 1957] is posed as follows:

1. Consider an infinite, isotropic, linear elastic solid, with (homogeneous) Young's modulus and Poisson's ratio E, ν .
2. The solid is initially stress free, with displacements, strains, and stresses: $u_i = \varepsilon_{ij} = \sigma_{ij} = 0$.
3. Some unspecified external agency then induces a uniform "transformation strain" ε_{ij}^T inside an ellipsoidal region, with semi-axes (a_1, a_2, a_3) centered at the origin (see Figure 5.34). The transformation strain can be visualized as an anisotropic thermal expansion; if the ellipsoidal region were separated from the surrounding elastic solid, it would be stress free and would change its shape according to the strain tensor ε_{ij}^T .
4. Because the ellipsoid is encapsulated within the surrounding elastic solid, stress, strain, and displacement fields are induced throughout the elastic solid. These fields

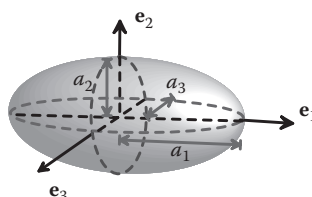


FIGURE 5.34 Ellipsoidal inclusion in an infinite solid.

must be defined carefully because the initial configuration for the solid could be chosen in a number of different ways. In the following, u_i will denote the displacement of a material particle from the initial, unstressed configuration, as the transformation strain is introduced. The total strain is defined as

$$\varepsilon_{ij} = (\partial u_i / \partial x_j + \partial u_j / \partial x_i) / 2.$$

5. Inside the ellipsoid, the total strain consists of the transformation strain (which does not induce stress); together with an additional elastic strain $\varepsilon_{ij} = \varepsilon_{ij}^T + \varepsilon_{ij}^e$. Outside the ellipsoid, $\varepsilon_{ij} = \varepsilon_{ij}^e$. The stress in the solid is related to the elastic part of the strain by the usual linear elastic equations

$$\sigma_{ij} = \frac{E}{1+\nu} \left\{ \varepsilon_{ij}^e + \frac{\nu}{1-2\nu} \varepsilon_{kk}^e \delta_{ij} \right\}.$$

The Eshelby solution gives full expressions for these fields. It has proved to be one of the most important solutions in all of linear elasticity: it is of some interest in its own right, because it provides some insight into the mechanics of phase transformations in crystals. More importantly, a number of very important boundary value problems can be solved by manipulating the Eshelby solution. These include (1) the solution for an ellipsoidal inclusion embedded within an elastically mismatched matrix, (2) the solution for an ellipsoidal cavity in an elastic solid, and (3) solutions for circular and elliptical cracks in an elastic solid. In addition, the Eshelby solution is used extensively in theories that provide estimates of elastic properties of composite materials.

The displacement field is generated by Papkovich–Neuber potentials

$$\Psi_i(x_k) = \int_S \frac{p_{ji}^T n_j(\xi)}{4\pi R(x, \xi)} dA(\xi) \quad \phi(x_k) = \int_S \frac{\xi_i p_{ji}^T n_j(\xi)}{4\pi R(x, \xi)} dA(\xi),$$

where the integral is taken over the surface of the ellipsoid, $n_j(\xi)$ denotes the components of a unit vector perpendicular to the surface of the ellipsoid (pointing outward), $R = \sqrt{(x_k - \xi_k)(x_k - \xi_k)}$, and

$$p_{ij}^T = \frac{E}{1+\nu} \left\{ \varepsilon_{ij}^T + \frac{\nu}{1-2\nu} \varepsilon_{kk}^T \delta_{ij} \right\}$$

is the transformation stress (i.e., the stress that would be induced by applying an elastic strain to the inclusion that is equal to the transformation strain). The stresses outside the inclusion can be calculated using the standard Papkovich–Neuber representation given in

Section 5.4.1. To calculate stresses inside the inclusion, the formula must be modified to account for the transformation strain, which gives

$$2(1-\nu)\sigma_{ij} = -2(1-\nu)p_{ij}^T + 2\nu \frac{\partial \Psi_k}{\partial x_k} \delta_{ij} + (1-2\nu) \left(\frac{\partial \Psi_i}{\partial x_j} + \frac{\partial \Psi_j}{\partial x_i} \right) - x_k \frac{\partial^2 \Psi_k}{\partial x_i \partial x_j} + \frac{\partial^2 \phi}{\partial x_i \partial x_j}.$$

For the general ellipsoid, the expressions for displacement and stress can be reduced to elliptic integrals, with the following results.

Solution inside the ellipsoid: Remarkably, it turns out that the stresses and strains are uniform inside the ellipsoid. The displacements, strains, and stresses can be expressed as follows:

$$1. \text{ Displacement: } u_i = (S_{ijkl}^* + \Pi_{ijkl}) \epsilon_{kl}^T x_j$$

$$2. \text{ Strain: } \epsilon_{ij} = \epsilon_{ij}^e + \epsilon_{ij}^T = S_{ijkl}^* \epsilon_{kl}^T$$

$$3. \text{ Stress: } \sigma_{ij} = \frac{E}{1+\nu} \left(S_{ijkl}^* \epsilon_{kl}^T + \frac{\nu}{1-2\nu} \delta_{ij} S_{ppkl}^* \epsilon_{kl}^T \right) - p_{ij}^T$$

Here, S_{ijkl}^* is a constant called the “Eshelby tensor,” and Π_{ijkl} is a second (anonymous) constant tensor. These tensors can be calculated as follows. Choose the coordinate system so that $a_1 > a_2 > a_3$. Define

$$I_1 = \frac{4\pi a_1 a_2 a_3}{(a_1^2 - a_2^2) \sqrt{(a_1^2 - a_3^2)}} (F(\theta, k) - E(\theta, k)) \quad I_3 = \frac{4\pi a_1 a_2 a_3}{(a_2^2 - a_3^2) \sqrt{(a_1^2 - a_3^2)}} \left\{ \frac{a_2(a_1^2 - a_3^2)^{1/2}}{a_1 a_3} - E(\theta, k) \right\}$$

$$I_2 = 4\pi - I_1 - I_3 \quad I_{ij} = (I_j - I_i) / 3(a_i^2 - a_j^2) \quad (i \neq j, \text{ no sum on } i, j)$$

$$I_{11} = 4\pi / 3a^2 - I_{12} - I_{13} \quad I_{22} = 4\pi / 3a^2 - I_{23} - I_{21} \quad I_{33} = 4\pi / 3a^2 - I_{31} - I_{32},$$

where

$$\theta = \sin^{-1} \sqrt{(1 - a_3^2 / a_1^2)} \quad k^2 = (a_1^2 - a_2^2) / (a_1^2 - a_3^2).$$

and

$$F(\theta, k) = \int_0^\theta \frac{dw}{(1 - k^2 \sin^2 w)^{1/2}} \quad E(\theta, k) = \int_0^\theta (1 - k^2 \sin^2 w)^{1/2} dw$$

are elliptic integrals of the first and second kinds. Then

$$S_{1111}^* = \frac{3}{8\pi(1-\nu)} a_1^2 I_{11} + \frac{1-2\nu}{8\pi(1-\nu)} I_1 \quad S_{1122}^* = \frac{3}{8\pi(1-\nu)} a_2^2 I_{12} - \frac{1-2\nu}{8\pi(1-\nu)} I_1$$

$$S_{1133}^* = \frac{3}{8\pi(1-\nu)} a_3^2 I_{13} - \frac{1-2\nu}{8\pi(1-\nu)} I_1 \quad S_{1212}^* = \frac{a_1^2 + a_2^2}{16\pi(1-\nu)} I_{12} + \frac{1-2\nu}{16\pi(1-\nu)} (I_1 + I_2)$$

$$\Pi_{ijij} = (I_i - I_j) / 8\pi \quad i \neq j.$$

The remaining components of S_{ijkl}^* can be calculated by cyclic permutations of (1,2,3). Any components that cannot be obtained from these formulas are zero: thus, $S_{1112}^* = S_{1223}^* = S_{1232}^* = 0$, $\Pi_{1112} = 0$, etc. Note that S_{ijkl}^* has many of the symmetries of the elastic compliance tensor (e.g., $S_{ijkl}^* = S_{jikl}^*$) but does not have major symmetry $S_{ijkl}^* \neq S_{klji}^*$.

For certain special shapes, the expressions given for I_k break down and simplified formulas must be used:

- Oblate spheroid, $a_1 > a_2 = a_3$:

$$I_1 = I_2 = \frac{2\pi a_1 a_2 a_3}{(a_1^2 - a_3^2)^{3/2}} \left\{ \cos^{-1} \frac{a_3}{a_1} - \frac{a_3}{a_1} \left(1 - \frac{a_3^2}{a_1^2} \right)^{1/2} \right\} \quad I_{12} = I_{21} = \pi / 3a^2 - I_{13} / 4$$

- Prolate spheroid, $a_1 = a_2 > a_3$:

$$I_2 = I_3 = \frac{2\pi a_1 a_2 a_3}{(a_1^2 - a_3^2)^{3/2}} \left\{ \frac{a_1}{a_3} \left(\frac{a_1^2}{a_3^2} - 1 \right)^{1/2} - \cosh^{-1} \frac{a_1}{a_3} \right\} \quad I_{13} = I_{31} = \pi / 3a^2 - I_{12} / 4$$

- Sphere, $a_1 = a_2 = a_3$. In this case, the Eshelby tensor can be calculated analytically:

$$S_{1111}^* = S_{2222}^* = S_{3333}^* = \frac{7 - 5\nu}{15(1-\nu)} \quad S_{1212}^* = S_{2323}^* = S_{3131}^* = \frac{4 - 5\nu}{15(1-\nu)}$$

$$S_{1122}^* = S_{2233}^* = S_{3311}^* = S_{1133}^* = S_{3322}^* = \frac{5\nu - 1}{15(1-\nu)}.$$

Additional terms follow from the symmetry conditions $S_{ijkl} = S_{jikl} = S_{ijlk} = S_{jilk}$. The remaining terms are zero.

- Cylinder, $a_3 \rightarrow \infty$. For this case the Eshelby tensor reduces to

$$S_{1111}^* = \frac{a_2[2(1-\nu)(a_1 + a_2) + a_1]}{2(1-\nu)(a_1 + a_2)^2} \quad S_{2222}^* = \frac{a_1[2(1-\nu)(a_1 + a_2) + a_2]}{2(1-\nu)(a_1 + a_2)^2} \quad S_{3333}^* = 0$$

$$S_{1122}^* = \frac{a_2[(2\nu - 1)a_1 + 2\nu a_2]}{2(1-\nu)(a_1 + a_2)^2} \quad S_{2211}^* = \frac{a_1[(2\nu - 1)a_2 + 2\nu a_1]}{2(1-\nu)(a_1 + a_2)^2} \quad S_{1133}^* = \frac{\nu a_2}{(1-\nu)(a_1 + a_2)}$$

$$S_{3311}^* = 0 \quad S_{2233}^* = \frac{\nu a_1}{(1-\nu)(a_1 + a_2)} \quad S_{3322}^* = 0 \quad S_{1212}^* = \frac{[(1-\nu)(a_1^2 + a_2^2) + (1-2\nu)a_1 a_2]}{2(1-\nu)(a_1 + a_2)^2}$$

$$S_{1313}^* = \frac{a_2(2-\nu)}{2(1-\nu)(a_1 + a_2)} \quad S_{2323}^* = \frac{a_1(2-\nu)}{2(1-\nu)(a_1 + a_2)}.$$

Additional terms follow from the symmetry conditions $S_{ijkl} = S_{jikl} = S_{ijlk} = S_{jilk}$. The remaining terms are zero.

Solution outside the ellipsoid: The solution outside the ellipsoid can also be expressed in simplified form: Eshelby [1959] shows that the displacement can be obtained from a single scalar potential $\omega(x_i)$. For actual calculations, only the derivatives of the potential are required, which can be reduced to

$$\frac{d\omega}{dx_1} = \frac{x_1 a_1 a_2 a_3}{l^3 k^2} \{E(\theta, k) - F(\theta, k)\}$$

$$\frac{d\omega}{dx_2} = \frac{x_2 a_1 a_2 a_3}{l^3 k^2 \hat{k}^2} \{\hat{k}^2 F(\theta, k) - E(\theta, k) + l A_3 k^2 / (A_1 A_2)\}$$

$$\frac{d\omega}{dx_3} = \frac{x_3 a_1 a_2 a_3}{l^3 \hat{k}^2} \{E(\theta, k) - l A_2 / (A_1 A_3)\}$$

$$A_i = \sqrt{a_i^2 + \lambda} \quad l = \sqrt{a_1^2 - a_3^2} \quad k = \sqrt{(a_1^2 - a_2^2) / (a_1^2 - a_3^2)} \quad \hat{k} = \sqrt{(a_2^2 - a_3^2) / (a_1^2 - a_3^2)},$$

where λ is the greatest positive root of $\lambda^3 - L\lambda^2 + M\lambda - N = 0$, with

$$L = r^2 - R^2 \quad M = \sum_{i=1}^3 a_i^2 x_i - a_1^2 a_2^2 - a_2^2 a_3^2 - a_1^2 a_3^2 + r^2 R^2 \quad N = a_1^2 a_2^2 a_3^2 \left(\sum_{i=1}^3 \frac{x_i^2}{a_i^2} - 1 \right)$$

and $r = \sqrt{x_k x_k}$ $R = \sqrt{a_k a_k}$. Additional derivatives can be computed using the relations

$$dF/d\lambda = -l/(2A_1 A_2 A_3) \quad dE/d\lambda = -l A_2 / (A_1^3 A_3) \quad d\lambda/dx_i = 2x_i / (A_i h) \quad h^2 = \sum_{i=1}^3 x_i^2 / A_i^4.$$

The displacements follow as

$$2(1-\nu)u_1 = \frac{\varepsilon_{11}^T - \varepsilon_{22}^T}{a_1^2 - a_2^2} \frac{\partial}{\partial x_2} \left(a_1^2 x_2 \frac{\partial \omega}{\partial x_1} - a_2^2 x_1 \frac{\partial \omega}{\partial x_2} \right) + \frac{\varepsilon_{33}^T - \varepsilon_{11}^T}{a_3^2 - a_1^2} \frac{\partial}{\partial x_3} \left(a_3^2 x_1 \frac{\partial \omega}{\partial x_3} - a_1^2 x_3 \frac{\partial \omega}{\partial x_3} \right) \\ - 2 \left\{ (1-\nu) \varepsilon_{11}^T + \nu (\varepsilon_{11}^T + \varepsilon_{22}^T) \right\} \frac{\partial \omega}{\partial x_1} - 4(1-\nu) \left(\varepsilon_{12}^T \frac{\partial \omega}{\partial x_2} + \varepsilon_{13}^T \frac{\partial \omega}{\partial x_3} \right) + \frac{\partial \beta}{\partial x_1},$$

where

$$\beta = \frac{2\varepsilon_{12}^T}{a_1^2 - a_2^2} \left(a_1^2 x_2 \frac{\partial \omega}{\partial x_1} - a_2^2 x_1 \frac{\partial \omega}{\partial x_2} \right) + \frac{2\varepsilon_{23}^T}{a_2^2 - a_3^2} \left(a_2^2 x_3 \frac{\partial \omega}{\partial x_2} - a_3^2 x_2 \frac{\partial \omega}{\partial x_3} \right) \\ + \frac{2\varepsilon_{31}^T}{a_3^2 - a_1^2} \left(a_3^2 x_1 \frac{\partial \omega}{\partial x_3} - a_1^2 x_3 \frac{\partial \omega}{\partial x_1} \right).$$

The remaining displacement components can be calculated by cyclic permutations of (1,2,3), and strains and stresses can be calculated by differentiating the displacements appropriately. The results are far too complicated to write out in full, and, in practice, the algebra can only be done with the aid of a symbolic manipulation program. However, some special results can be reduced to a tractable form.

Displacements far from the ellipsoid, $R = \sqrt{x_k x_k} \gg a_1$

$$u_i = \frac{a_1 a_2 a_3}{8(1-\nu)R^2} \left\{ \frac{3\varepsilon_{jk}^T x_i x_j x_k}{R^3} + (1-2\nu) \frac{2\varepsilon_{ik}^T x_k - \varepsilon_{kk}^T x_i}{R} \right\}.$$

Solution outside a spherical inclusion: For this case, the Papkovich–Neuber potentials can be reduced to

$$\Psi_i = \frac{a^3 p_{ik}^T x_k}{3R^3} \quad \phi = \frac{a^3 p_{ij}^T}{15R^3} \left((5R^2 - a^2) \delta_{ij} + 3a^2 \frac{x_i x_j}{R^2} \right).$$

The displacements and stresses follow as

$$u_i = \frac{(1+\nu)a^3}{2(1-\nu)E} \left\{ \frac{(2p_{ik}^T x_k + p_{kk}^T x_i)}{15R^2} (3a^2 - 5R^2) + \frac{p_{jk}^T x_j x_k x_i}{R^7} (R^2 - a^2) + \frac{4(1-\nu)p_{ik}^T x_k}{3R^3} \right\}$$

$$\begin{aligned} \sigma_{ij} = & \frac{a^3}{2(1-\nu)R^3} \left\{ \frac{p_{ij}^T}{15} \left((10(1-2\nu) + 6 \frac{a^2}{R^2}) + \frac{p_{ik}^T x_k x_j + p_{jk}^T x_k x_i}{R^2} \left(2\nu - 2 \frac{a^2}{R^2} \right) \right. \right. \\ & \left. \left. + \frac{\delta_{ij} p_{kk}^T}{15} \left(3 \frac{a^2}{R^2} - 5(1-2\nu) \right) \right) \right. \\ & \left. + \frac{\delta_{ij} p_{kl}^T x_k x_l}{R^2} \left((1-2\nu) - \frac{a^2}{R^2} \right) - \frac{x_i x_j p_{kl}^T x_k x_l}{R^4} \left(5 - 7 \frac{a^2}{R^2} \right) + \frac{x_i x_j p_{kk}^T}{R^2} \left(1 - \frac{a^2}{R^2} \right) \right\}, \end{aligned}$$

where $R = \sqrt{x_k x_k}$ and $p_{ij}^T = \{E/(1+\nu)\} \{ \varepsilon_{ij}^T + \nu \varepsilon_{kk}^T \delta_{ij} / (1-2\nu) \}$.

5.4.7 Elastically Mismatched Ellipsoidal Inclusion in an Infinite Solid Subjected to Remote Stress

Figure 5.35 shows an ellipsoidal inclusion, with semi-axes (a_1, a_2, a_3) . The inclusion is made from an isotropic, elastic solid with Young's modulus E^I and Poisson's ratio ν^I . It is embedded in an infinite, isotropic elastic matrix with Young's modulus E^M and Poisson's ratio ν^M . The solid is loaded at infinity by a uniform stress state σ_{ij}^∞ , strains $\varepsilon_{ij}^\infty = ((1+\nu^M) \sigma_{ij}^\infty - \nu^M \sigma_{kk}^\infty \delta_{ij}) / E^M$, and displacements $u_i^\infty = \varepsilon_{ij}^\infty x_j$. The solution is constructed

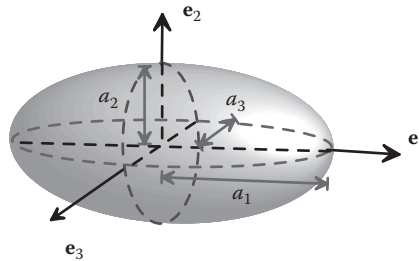


FIGURE 5.35 Elastically mismatched ellipsoidal inclusion in an infinite solid.

by superposing the Eshelby solution to the uniform stress state. To represent the Eshelby solution, we introduce the following:

1. The Eshelby transformation strain: ε_{ij}^T
2. The Eshelby tensor: S_{ijkl}^*
3. The displacement induced by the Eshelby transformation: $u_i = U_{ikl}(x_m) \varepsilon_{kl}^T$
4. The stresses induced by the Eshelby transformation: $\sigma_{ij} = \Sigma_{ijkl}(x_m) \varepsilon_{kl}^T$

The functions S_{ijkl}^* , U_{ikl} and Σ_{ijkl} can be calculated using the results given in Section 5.4.6 (the elastic properties of the matrix should be used when evaluating the formulas). The solution for the solid containing the inclusion follows as

$$u_i = U_{ikl}(x_m) \varepsilon_{kl}^T + u_i^\infty \quad \sigma_{ij} = \Sigma_{ijkl}(x_m) \varepsilon_{kl}^T + \sigma_{ij}^\infty,$$

where the transformation strain is calculated by solving

$$(C_{ijkl}^M - C_{ijkl}^I) \varepsilon_{kl}^T = (C_{ijpq}^M - (C_{ijkl}^M - C_{ijkl}^I) S_{klpq}^*) \varepsilon_{pq}^T$$

for ε_{ij}^T . Here,

$$C_{ijkl}^M = \frac{E^M}{2(1+\nu^M)} (\delta_{il}\delta_{jk} + \delta_{ik}\delta_{jl}) + \frac{E^M \nu^M}{(1+\nu^M)(1-2\nu^M)} \delta_{ij}\delta_{kl}$$

is the stiffness of the matrix, with a similar expression for the stiffness of the inclusion.

5.4.8 Spherical Cavity in an Infinite Solid Subjected to Remote Stress

Figure 5.36 shows a spherical cavity with radius a in an infinite, isotropic linear elastic solid. Far from the cavity, the solid is subjected to a tensile stress $\sigma_{33} = \sigma_0$, with all other stress components zero.

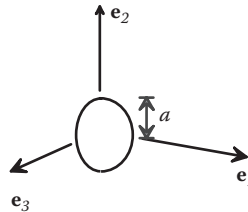


FIGURE 5.36 Spherical hole in an infinite solid.

The solution is generated by potentials

$$\Psi_i = \frac{(1-\nu)\sigma_0}{(1+\nu)}x_3\delta_{i3} + \frac{a^3(1-\nu)\sigma_0}{R^3(7-5\nu)}\left(\frac{(5\nu-1)}{2(1-2\nu)}x_i + 5x_3\delta_{i3}\right)$$

$$\phi = \frac{\nu(1-\nu)\sigma_0}{(1+\nu)}(3x_3^2 - R^2) + \frac{a^3(1-\nu)\sigma_0}{R^3(7-5\nu)}\left(\frac{(7-5\nu)}{2(1-2\nu)}R^2 - a^2 + \frac{3x_3^2a^2}{R^2}\right).$$

The displacements and stresses follow as

$$u_i = \frac{(1+\nu)\sigma_0}{2E}\left[\left[2 + \frac{5(5-4\nu)}{(7-5\nu)}\frac{a^3}{R^3} + \frac{6}{(7-5\nu)}\frac{a^5}{R^5}\right]x_3\delta_{i3} + \left[\frac{-2\nu}{(1+\nu)} + \frac{(5\nu-6)}{(7-5\nu)}\frac{a^3}{R^3} + \frac{3}{(7-5\nu)}\frac{a^5}{R^5}\left(1 - \frac{5x_3^2}{R^2}\right)\right]x_i\right]$$

$$\frac{\sigma_{ij}}{\sigma_0} = \frac{3a^3}{2(7-5\nu)R^3}\left(3 - 5\nu - 4\frac{a^2}{R^2}\right)\delta_{ij} + \frac{3a^3x_i x_j}{2(7-5\nu)R^5}\left(6 - 5\nu - 5\frac{a^2}{R^2} + 10\frac{x_3^2}{R^2}\right)$$

$$+ \frac{\delta_{i3}\delta_{j3}}{(7-5\nu)}\left((7-5\nu) + 5(1-2\nu)\frac{a^3}{R^3} + 3\frac{a^5}{R^5}\right) - \frac{15a^3x_3(x_j\delta_{i3} + x_i\delta_{j3})}{(7-5\nu)R^5}\left(\frac{a^2}{R^2} - \nu\right).$$

Derivation: This solution can be derived by superposing two solutions:

1. A uniform state of stress $\sigma_{ij} = \sigma_0\delta_{i3}\delta_{j3}$, which can be generated from potentials $\Psi_i = (1 - \nu)\sigma_0x_3\delta_{i3}/(1 + \nu)$, $\phi = \nu(1 - \nu)\sigma_0(3x_3^2 - R^2)/(1 + \nu)$.
2. The Eshelby solution for a sphere with transformation stress $p_{ij}^T = A\delta_{ij} + B\delta_{i3}\delta_{j3}$.

The unknown coefficients A and B must be chosen to satisfy the traction-free boundary condition $\sigma_{ij}n_j = 0$ on the surface of the hole $R = a$. Noting that $n_j = -x_j/a$ and working through some tedious algebra shows that

$$A = \frac{3\sigma_0(1-\nu)(5\nu-1)}{2(7-5\nu)(1-2\nu)} \quad B = \frac{15\sigma_0(1-\nu)}{(7-5\nu)}.$$

Substituting back into the Eshelby potentials and simplifying yields the results given. The same approach can be used to derive the solution for a rigid inclusion in an infinite solid subjected to remote stress, as well as the solution to an elastically mismatched spherical inclusion in an infinite solid.

5.4.9 Flat-Ended Cylindrical Indenter in Contact with an Elastic Half-Space

Figure 5.37 shows a rigid, flat-ended, cylindrical punch with radius a , which is pushed into the surface of an elastic half-space with Young's modulus E and Poisson's ratio ν by a force P . The indenter sinks into the surface by a depth h . The interface between the contacting surfaces is frictionless.

The load is related to the displacement of the punch by

$$P = \frac{2Ea}{(1-\nu^2)}h.$$

The solution can be generated from Papkovich–Neuber potentials

$$\Psi_k = \frac{2Eh\delta_{k3}}{(1+\nu)\pi} \operatorname{Im}\{\log(R^* + x_3 + ia)\} \quad \phi = -\frac{2(1-2\nu)Eh}{(1+\nu)\pi} \operatorname{Im}\{(x_3 + ia)\log(R^* + x_3 + ia) - R^*\},$$

where $R^* = \sqrt{x_1^2 + x_2^2 + (x_3 + ia)^2}$, $i = \sqrt{-1}$, and $\operatorname{Im}\{z\}$ denotes the imaginary part of z . The displacements and stresses follow as

$$u_k = \frac{h}{\pi(1-\nu)} \operatorname{Im}\left\{2(1-\nu)\delta_{k3} \log(R^* + x_3 + ia) - \frac{x_3\delta_{k3}}{R^*} + \frac{x_1\delta_{k1} + x_2\delta_{k2}}{R^* + x_3 + ia} \left(1 - 2\nu - \frac{x_3}{R^*}\right)\right\}$$

$$\sigma_{11} = \frac{Eh}{(1-\nu^2)\pi} \operatorname{Im}\left\{\frac{2\nu}{R^*} + \frac{1-2\nu-x_3/R^*}{R^*+x_3+ia} - \frac{x_1^2}{R^*(R^*+x_3+ia)^2} \left(1 + \frac{x_3(1+2R^*+x_3+ia)}{R^{*2}}\right)\right\}$$

$$\sigma_{22} = \frac{Eh}{(1-\nu^2)\pi} \operatorname{Im}\left\{\frac{2\nu}{R^*} + \frac{1-2\nu-x_3/R^*}{R^*+x_3+ia} - \frac{x_2^2}{R^*(R^*+x_3+ia)^2} \left(1 + \frac{x_3(1+2R^*+x_3+ia)}{R^{*2}}\right)\right\}$$

$$\sigma_{33} = \frac{Eh}{(1-\nu^2)\pi} \operatorname{Im}\left\{\frac{1}{R^*} + \frac{(x_3+ia)x_3}{R^{*3}}\right\} \quad \sigma_{13} = \frac{Eh}{(1-\nu^2)\pi} \operatorname{Im}\left\{\frac{x_1x_3}{R^{*3}}\right\} \quad \sigma_{23} = \frac{Eh}{(1-\nu^2)\pi} \operatorname{Im}\left\{\frac{x_2x_3}{R^{*3}}\right\}$$

$$\sigma_{12} = \frac{Eh}{(1-\nu^2)\pi} \operatorname{Im}\left\{\frac{x_1x_2}{R^*(R^*+x_3+ia)} \left(-(1-2\nu) + \frac{x_3(2R^*+x_3+ia)}{R^*(R^*+x_3+ia)}\right)\right\}.$$

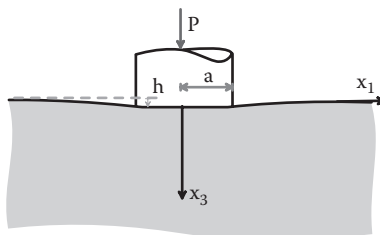


FIGURE 5.37 Flat-ended cylinder indenting the surface of an elastic solid.

A symbolic manipulation program can handle the complex arithmetic in these formulas without difficulty. If you want to find analytical formulas for the displacement or stress, the following expressions are helpful:

$$R^* = \frac{1}{\sqrt{2}} \left(\sqrt{\rho^2 + R^2 - a^2} + i\sqrt{\rho^2 + a^2 - R^2} \right) \quad \text{Im}\{\log(R^* + x_3 + ia)\} = \tan^{-1} \left(\frac{\sqrt{\rho^2 + a^2 - R^2} + a\sqrt{2}}{\sqrt{\rho^2 + R^2 - a^2} + x_3\sqrt{2}} \right),$$

where $R = \sqrt{x_k x_k}$, $\rho = ([R^2 - a^2]^2 + 4x_3^2 a^2)^{1/4}$. Important features of these results include the following:

- 1. Contact pressure:** The pressure exerted by the indenter on the elastic solid follows as

$$p(x_1) = -\sigma_{33}(r, x_3 = 0) = \frac{P}{2\pi a \sqrt{a^2 - r^2}}.$$

- 2. Surface displacement:** The vertical displacement of the surface is

$$u_3 = \begin{cases} \frac{2h}{\pi} \tan^{-1} \frac{a}{\sqrt{r^2 - a^2}} & r > a \\ h & r < a. \end{cases}$$

- 3. Contact stiffness:** The stiffness of a contact is defined as the ratio of the force acting on the indenter to its displacement $k_c = P/h$ and is of interest in practical applications. The stiffness of a 3D contact is well defined (unlike 2D contacts discussed in Section 5.3) and is given by $k_c = 2Ea / (1 - \nu^2)$. This turns out to be a universal relation for any axisymmetric contact with contact radius a .

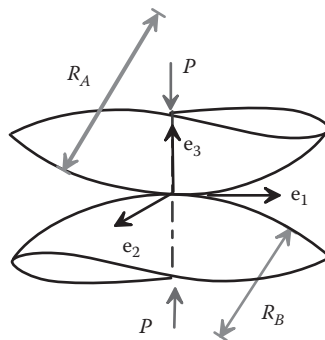


FIGURE 5.38 Contact between two elastic spheres.

5.4.10 Frictionless Contact between Two Elastic Spheres

This solution is known as the “Hertz contact problem” after its author. Figure 5.38 illustrates the problem to be solved. Two elastic spheres, with radii R_A, R_B and elastic constants E_A, v_A, E_B, v_B , initially meet at a point and are pushed into contact by a force P . The two spheres deform so as to make contact over a small circular patch with radius $a \ll R_A, R_B$, and the centers of the two spheres approach one another by a distance h .

The solution is conveniently expressed in terms of an effective modulus and radius for the contact pair:

$$E^* = \frac{E_A E_B}{(1-v_A^2)E_B + (1-v_B^2)E_A} \quad R^* = \frac{R_A R_B}{R_A + R_B}.$$

Relations between P, h, a : The force P , approach of distant points h , and contact area a are related by

$$a = \left(\frac{3PR}{4E^*} \right)^{1/3} \quad h = \frac{a^2}{R} = \left(\frac{9P^2}{16RE^{*2}} \right)^{1/3}.$$

Contact pressure: The two solids are subjected to a repulsive pressure $p(r) = p_0 \sqrt{1 - r^2/a^2}$ within the contact area. The maximum contact pressure is related to the load applied to the spheres by

$$p_0 = \left(\frac{3P}{2\pi a^2} \right) = \left(\frac{6PE^{*2}}{\pi^3 R^2} \right)^{1/3}.$$

Contact stiffness: The stiffness of a contact is defined as the ratio of the force acting on the indenter to its displacement $k_c = dP/dh$ and is of interest in practical applications. The stiffness of a 3D contact is well defined (unlike 2D contacts discussed in Section 5.4) and

is given by $k_c = 2E^*a$. This turns out to be a universal relation for any axisymmetric contact with contact radius a .

Stress field: The two spheres are subjected to the same contact pressure and are both assumed to deform like a half-space (with a flat surface). Consequently, the stress field is identical inside both spheres and can be calculated from formulas derived by Hamilton [1983]:

$$\begin{aligned}\sigma_{11} &= \frac{p_0}{a} \left[\phi + \frac{1}{r^2} \left\{ \frac{x_1^2 - x_2^2}{r^2} \left((1-\nu)N - \frac{1-2\nu}{3}(NS+2AN+a^3) - \nu M x_3 a \right) \right. \right. \\ &\quad \left. \left. - N(x_1^2 + 2\nu x_2^2) - \frac{M x_1^2 x_3 a}{S} \right\} \right] \\ \sigma_{22} &= \frac{p_0}{a} \left[\phi + \frac{1}{r^2} \left\{ \frac{x_2^2 - x_1^2}{r^2} \left((1-\nu)N - \frac{1-2\nu}{3}(NS+2AN+a^3) - \nu M x_3 a \right) \right. \right. \\ &\quad \left. \left. - N(x_2^2 + 2\nu x_1^2) - \frac{M x_2^2 x_3 a}{S} \right\} \right] \\ \sigma_{33} &= \frac{p_0}{a} \left(-N + \frac{ax_3 M}{S} \right) \quad \sigma_{13} = -\frac{x_3 x_1 p_0}{a} \left(\frac{N}{S} - \frac{x_3 H}{G^2 + H^2} \right) \\ \sigma_{23} &= -\frac{x_3 x_2 p_0}{a} \left(\frac{N}{S} - \frac{x_3 H}{G^2 + H^2} \right) \\ \sigma_{12} &= \frac{p_0 x_1 x_2}{ar^4} \left[(1-2\nu) \left\{ -Nr^2 + \frac{2}{3}N(S+2A) - x_3(x_3N+aM) + \frac{2}{3}a^3 \right\} \right. \\ &\quad \left. + x_3 \left\{ -\frac{aMr^2}{S} - x_3N + aM \right\} \right],\end{aligned}$$

where

$$r = \sqrt{x_1^2 + x_2^2} \quad A = r^2 + x_3^2 - a^2 \quad S = \sqrt{A^2 + 4a^2 x_3^2} \quad M = \sqrt{(S+A)/2} \quad N = \sqrt{(S-A)/2}$$

$$G = M^2 - N^2 + x_3 M - aN \quad H = 2MN + aM + x_3 N \quad \phi = (1+\nu)x_3 \tan^{-1}(a/M).$$

The stresses on $r = 0$ must be computed using a limiting process, with the result

$$\sigma_{11} = \sigma_{22} = \frac{p_0}{a} \left[(1+\nu)(x_3 \tan^{-1}(a/x_3) - a) + \frac{a^3}{2(a^2 + x_3^2)} \right] \quad \sigma_{33} = -\frac{p_0 a^2}{a^2 + x_3^2}.$$

Conditions to initiate yield: The material under the contact yields when the maximum von Mises effective stress $\sigma_e = \sqrt{3S_{ij}S_{ij}/2}$ reaches the uniaxial tensile yield stress Y . The

location of the maximum von Mises stress can be found by plotting contours of σ_e / p_0 as a function of $x_1 / a, x_3 / a$. For $\nu = 0.3$, the maximum value occurs at $x_1 = x_2 = 0, x_3 = 0.481a$ and has value $\sigma_e / p_0 = 0.6200$. Yield occurs when $p_0 = 1.61Y$.

5.4.11 Contact Area, Pressure, Stiffness, and Elastic Limit for General Nonconformal Contacts

A nonconformal contact has the following properties: (1) the two contacting solids initially touch at a point or along a line, (2) both contacting solids are smooth in the neighborhood of the contact, so that their local geometry can be approximated as ellipsoids, and (3) the size of the contact patch between the two solids is much smaller than either solid.

Complete solutions for such contacts can be found in the work by Bryant and Keer [1982] or Sackfield and Hills [1983]. These works also account for the effects of friction under sliding contacts. The results are lengthy. Here, we give formulas that predict the most important features of frictionless nonconformal contacts.

Contact geometry: The geometry of the contacting solids is illustrated in Figure 5.39 and is characterized as follows:

1. The principal radii of curvature of the two solids at the point of initial contact are denoted by $\rho_1^A, \rho_2^A, \rho_1^B, \rho_2^B$. The radii of curvature are positive if convex and negative if concave.
2. The angle between the principal directions of curvature of the two solids is denoted by α . Note that, although labels 1 and 2 can be assigned to the radii of curvature of the two surfaces arbitrarily, α must specify the angle between the two planes containing the radii ρ_1^A and ρ_1^B .
3. Define the principal relative contact radii R_1, R_2 as

$$\frac{1}{R_1} = \frac{A+B}{2} \quad \frac{1}{R_2} = \frac{A-B}{2}$$

$$A = \left(\frac{1}{\rho_1^A} + \frac{1}{\rho_2^A} + \frac{1}{\rho_1^B} + \frac{1}{\rho_2^B} \right)$$

$$B = \sqrt{\left(\frac{1}{\rho_1^A} - \frac{1}{\rho_2^A} \right)^2 + \left(\frac{1}{\rho_1^B} - \frac{1}{\rho_2^B} \right)^2 + 2 \left(\frac{1}{\rho_1^A} - \frac{1}{\rho_2^A} \right) \left(\frac{1}{\rho_1^B} - \frac{1}{\rho_2^B} \right) \cos 2\alpha}$$

4. Introduce an effective contact radius $R_e = \sqrt{R_1 R_2}$.

Elastic constants: The two contacting solids are isotropic, with Young's modulus E_A, E_B and Poisson's ratio ν_A, ν_B . Define the effective modulus

$$E^* = \frac{E_A E_B}{(1-\nu_A^2)E_B + (1-\nu_B^2)E_A}.$$

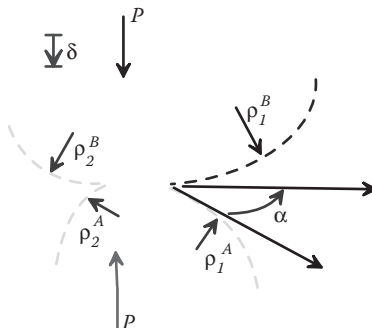


FIGURE 5.39 Contact between two ellipsoidal surfaces.

Contact area: The area of contact between the two solids is elliptical, with semi-axes a, b , as shown in Figure 5.40. The dimensions of the contact area may be calculated as follows:

1. Solve the following equation (numerically) for $e = \sqrt{1 - b^2/a^2}$, with $0 \leq e \leq 1$

$$\frac{R_2}{R_1} = \frac{K(e) - E(e)/(1-e^2)}{E(e) - K(e)},$$

where $K(e)$ and $E(e)$ are complete elliptic integrals of the first and second kind:

$$K(e) = \int_0^{\pi/2} [1 - e^2 \sin^2 \theta]^{-1/2} d\theta \quad E(e) = \int_0^{\pi/2} [1 - e^2 \sin^2 \theta]^{1/2} d\theta.$$

2. Calculate the contact area from

$$A = \pi ab = \pi \left(\frac{3PR_e}{\pi E^*} \right)^{2/3} \left(\frac{R_2}{R_1} \right)^{1/3} \frac{\sqrt{1-e^2}}{e^{4/3}} \{K(e) - E(e)\}^{2/3}$$

(The limit $\lim_{e \rightarrow 0} \{K(e) - E(e)\}^{2/3}/e^{4/3} = (\pi/4)^{2/3}$ is helpful).

3. The dimensions of the contact patch follow as $a = \sqrt{A/\pi}/(1-e^2)^{1/4}$ $b = \sqrt{A/\pi}(1-e^2)^{1/4}$

Contact pressure: The contact pressure distribution is ellipsoidal, with the form

$$p(x_1, x_2) = (3P/2A) \sqrt{1 - x_1^2/a^2 - x_2^2/b^2}.$$

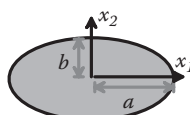


FIGURE 5.40 Area of contact between two elastic solids.

Approach of contacting solids: Points distant from the contact in the two solids approach one another by a displacement

$$\delta = \frac{3P}{2E^* \sqrt{\pi A}} (1 - e^2)^{1/4} K(e).$$

Contact stiffness: The contact stiffness is defined as $k = dP/d\delta$ and is given by

$$k = \left(3\pi^2 E^{*2} R_e P \right)^{1/3} \left(\frac{R_2}{R_1} \right)^{1/6} \frac{\{K(e) - E(e)\}^{1/3}}{e^{2/3} K(e)}.$$

Elastic limit: The stresses in both solids are identical, and therefore yield occurs first in the solid with the lower yield stress. Figure 5.41 shows the critical load required to cause yield in a solid with von Mises yield criterion and uniaxial tensile yield stress Y , based on tabular values in the work of Johnson [1985].

5.4.12 Load Displacement–Contact Area Relations for Arbitrarily Shaped Axisymmetric Contacts

The most important properties of general frictionless axisymmetric contacts can be calculated from simple formulas, even when full expressions for the stress and displacement fields cannot be calculated.

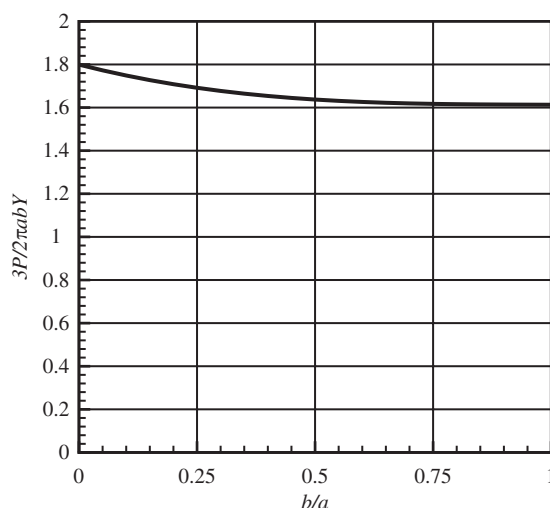


FIGURE 5.41 Critical load required to induce yield under the contact between ellipsoidal solids.

Figure 5.42 illustrates the problem to be solved. Assume the following:

1. The two contacting solids have elastic constants E_1, v_1, E_2, v_2 . Define an effective elastic constant as
$$E^* = \left\{ \frac{1-v_1^2}{E_1} + \frac{1-v_2^2}{E_2} \right\}^{-1}.$$
2. The surfaces of the two solids are axisymmetric near the point of initial contact.
3. When the two solids just touch, the gap between them can be described by a monotonically increasing function $g(r)$, where r is the distance from the point of initial contact. For example, a cone contacting a flat surface would have $g(r) = r/\tan\beta$, where β is the cone angle; a sphere contacting a flat surface could be approximated using $g(r) = r^2/D$, where D is the sphere diameter. In the following, we will use $g'(r) \equiv dg/dr$.
4. The two solids are pushed into contact by a force P . The solids deform so as to make contact over a circular region with radius a and move together by a distance h as the load is applied.
5. The relationship between h and the contact radius a will be specified by a functional relationship of the form $h = H(a)$. The derivative of this function with respect to its argument will be denoted by $H'(a)$.

These quantities are related by the following formulas:

1. Approach as a function of contact radius: $H(a) = a \int_0^a \frac{g'(\xi)}{\sqrt{a^2 - \xi^2}} d\xi$
2. Applied force as a function of contact radius: $P = 2E^* \left(aH(a) - \int_0^a H(\xi) d\xi \right)$

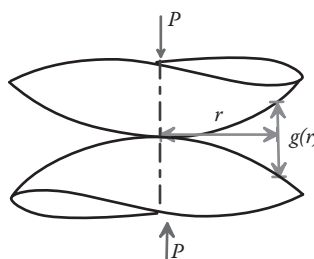


FIGURE 5.42 Contact between two axisymmetric solids.

3. Contact stiffness: $\frac{dP}{dh} = 2E^* a$

4. Contact pressure distribution: $p(r) = \frac{E^*}{\pi} \int_r^a \frac{H'(\xi)}{\sqrt{\xi^2 - r^2}} d\xi$

Once these formulas have been evaluated for a given contact geometry, the results can be combined to determine other relationships, such as contact radius or stiffness as a function of load or approach h .

5.5 SOLUTIONS TO GENERALIZED PLANE PROBLEMS FOR ANISOTROPIC LINEAR ELASTIC SOLIDS

Materials such as wood, laminated composites, and single crystal metals are stiffer when loaded along some material directions than others. Such materials are said to be *anisotropic* and cannot be modeled using the procedures described in the preceding sections. In this chapter, we describe briefly the most widely used method for calculating elastic deformation and stress in 2D anisotropic solids. As you might expect, these calculations are difficult, and, although the solutions can be expressed in a surprisingly compact form, the resulting expressions can usually only be evaluated using a computer. In many practical situations, it is simplest to calculate solutions for anisotropic materials using direct numerical computations (e.g., using the FEM, as discussed in Chapters 7 and 8). Nevertheless, analytical solutions are useful: for example, the FEM cannot easily be applied to problems involving cracks, dislocations, or point forces because they contain singularities; in addition, exact calculations can show how the solutions vary parametrically with elastic constants and material orientation.

5.5.1 Governing Equations of Elasticity for Anisotropic Solids

A typical plane elasticity problem is illustrated in Figure 5.43. The solid is two dimensional: in this case, we are concerned with plane strain solutions, which means that the solid is very long in the e_3 direction, and every cross section is loaded identically and only in the $\{e_1, e_2\}$ plane. The material is an anisotropic, linear elastic solid, whose properties can be characterized by the elasticity tensor C_{ijkl} (or an equivalent matrix) as discussed in Chapter 3.

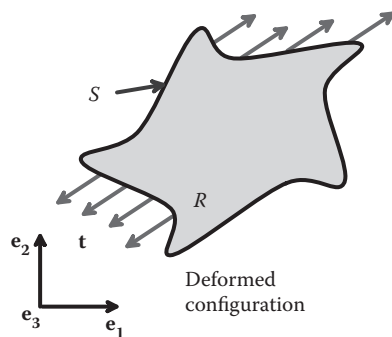


FIGURE 5.43 A representative boundary value problem for an elastic solid.

To simplify calculations, we shall assume that (1) the solid is free of body forces, and (2) thermal strains can be neglected. Under these conditions, the general equations of elasticity listed in Section 5.1.2 reduce to

$$C_{ijkl} \frac{\partial^2 u_k}{\partial x_i \partial x_l} = 0,$$

subject to the usual boundary conditions. In subsequent discussions, it will be convenient to write the equilibrium equations in matrix form as

$$\begin{bmatrix} \frac{\partial}{\partial x_1} & 0 & 0 & \frac{\partial}{\partial x_2} & \frac{\partial}{\partial x_3} & 0 \\ 0 & \frac{\partial}{\partial x_2} & 0 & \frac{\partial}{\partial x_1} & 0 & \frac{\partial}{\partial x_3} \\ 0 & 0 & \frac{\partial}{\partial x_3} & 0 & \frac{\partial}{\partial x_1} & \frac{\partial}{\partial x_2} \end{bmatrix} \begin{bmatrix} c_{11} & c_{12} & c_{13} & c_{14} & c_{15} & c_{16} \\ c_{12} & c_{22} & c_{23} & c_{24} & c_{25} & c_{26} \\ c_{13} & c_{23} & c_{33} & c_{34} & c_{35} & c_{36} \\ c_{14} & c_{24} & c_{34} & c_{44} & c_{45} & c_{46} \\ c_{15} & c_{25} & c_{35} & c_{45} & c_{55} & c_{56} \\ c_{16} & c_{26} & c_{36} & c_{46} & c_{56} & c_{66} \end{bmatrix} = \begin{bmatrix} \frac{\partial u_1}{\partial x_1} \\ \frac{\partial u_2}{\partial x_2} \\ \frac{\partial u_3}{\partial x_3} \\ \frac{\partial u_2}{\partial x_3} + \frac{\partial u_3}{\partial x_2} \\ \frac{\partial u_1}{\partial x_3} + \frac{\partial u_3}{\partial x_1} \\ \frac{\partial u_1}{\partial x_2} + \frac{\partial u_2}{\partial x_1} \end{bmatrix} = 0.$$

5.5.1.1 Conditions Necessary for Strict Plane Strain Deformation of Anisotropic Solids

For plane strain deformations, the displacement field has the form $\mathbf{u} = u_1(x_1, x_2)\mathbf{e}_1 + u_2(x_1, x_2)\mathbf{e}_2$. Under these conditions, the equilibrium equations reduce to

$$\begin{aligned} c_{11} \frac{\partial^2 u_1}{\partial x_1^2} + c_{66} \frac{\partial^2 u_1}{\partial x_2^2} + 2c_{16} \frac{\partial^2 u_1}{\partial x_1 \partial x_2} + c_{16} \frac{\partial^2 u_2}{\partial x_1^2} + c_{26} \frac{\partial^2 u_2}{\partial x_2^2} + (c_{12} + c_{66}) \frac{\partial^2 u_2}{\partial x_1 \partial x_2} &= 0 \\ c_{16} \frac{\partial^2 u_1}{\partial x_1^2} + c_{26} \frac{\partial^2 u_1}{\partial x_2^2} + (c_{66} + c_{12}) \frac{\partial^2 u_1}{\partial x_1 \partial x_2} + c_{66} \frac{\partial^2 u_2}{\partial x_1^2} + c_{22} \frac{\partial^2 u_2}{\partial x_2^2} + 2c_{26} \frac{\partial^2 u_2}{\partial x_1 \partial x_2} &= 0 \\ c_{15} \frac{\partial^2 u_1}{\partial x_1^2} + c_{46} \frac{\partial^2 u_1}{\partial x_2^2} + (c_{56} + c_{14}) \frac{\partial^2 u_1}{\partial x_1 \partial x_2} + c_{56} \frac{\partial^2 u_2}{\partial x_1^2} + c_{24} \frac{\partial^2 u_2}{\partial x_2^2} + (c_{25} + c_{46}) \frac{\partial^2 u_2}{\partial x_1 \partial x_2} &= 0. \end{aligned}$$

In this case, $u_{\alpha\beta}$ can be chosen to satisfy two, but not all three, of the three equations. The elastic constants must satisfy $c_{11} > 0$, $c_{22} > 0$, $c_{66} > 0$. Consequently, the third equation can only be satisfied by setting

$$c_{15} = c_{46} = c_{14} = c_{56} = c_{24} = c_{25} = 0.$$

Strict plane deformations therefore only exist in a material with elastic constants and orientation satisfying

$$\begin{bmatrix} c_{11} & c_{12} & c_{13} & 0 & 0 & c_{16} \\ c_{12} & c_{22} & c_{33} & 0 & 0 & c_{26} \\ c_{13} & c_{23} & c_{23} & c_{34} & c_{35} & c_{36} \\ 0 & 0 & c_{34} & c_{44} & c_{45} & 0 \\ 0 & 0 & c_{35} & c_{45} & c_{55} & 0 \\ c_{16} & c_{26} & c_{36} & 0 & 0 & c_{66} \end{bmatrix}.$$

The most common class of crystals, cubic materials, satisfies these conditions for appropriate orientations.

5.5.1.2 Generalized Plane Strain Deformations

A generalized plane strain displacement field can exist in any general anisotropic crystal. In this case, the displacement field has the form

$$\mathbf{u} = u_1(x_1, x_2)\mathbf{e}_1 + u_2(x_1, x_2)\mathbf{e}_2 + u_3(x_1, x_2)\mathbf{e}_3,$$

i.e., the displacement is independent of position along the length of the cylindrical solid, but points may move out of their original plane when the solid is loaded.

5.5.2 Stroh Representation for Fields in Anisotropic Solids

The Stroh solution is a compact, complex variable, representation for generalized plane strain solutions to elastically anisotropic solids. To write the solution, we need to define several new quantities:

1. We define three new 3×3 matrices of elastic constants, as follows:

$$\mathbf{Q} = \begin{bmatrix} c_{11} & c_{16} & c_{15} \\ c_{16} & c_{66} & c_{56} \\ c_{15} & c_{56} & c_{55} \end{bmatrix} \quad \mathbf{R} = \begin{bmatrix} c_{16} & c_{12} & c_{14} \\ c_{66} & c_{26} & c_{46} \\ c_{56} & c_{25} & c_{45} \end{bmatrix} \quad \mathbf{T} = \begin{bmatrix} c_{66} & c_{26} & c_{46} \\ c_{26} & c_{22} & c_{24} \\ c_{46} & c_{24} & c_{44} \end{bmatrix}.$$

2. We introduce three complex valued eigenvalues p_i ($i=1\dots3$) and eigenvectors $\mathbf{a}^{(i)}$ that satisfy

$$[\mathbf{Q} + p(\mathbf{R} + \mathbf{R}^T) + p^2\mathbf{T}] \mathbf{a}^{(i)} = 0.$$

The eigenvalues can be computed by solving the equation

$$\det [\mathbf{Q} + p(\mathbf{R} + \mathbf{R}^T) + p^2\mathbf{T}] = 0.$$

Because \mathbf{Q} , \mathbf{R} , and \mathbf{T} are 3×3 matrices, this is a sextic equation for p , with six roots. It is possible to show that, for a material with physically admissible elastic constants,

p is always complex, so the six roots are pairs of complex conjugates (p, \bar{p}). Each pair of complex roots has a corresponding pair of complex valued eigenvectors ($\mathbf{a}, \bar{\mathbf{a}}$). We define p_i to be the roots with positive imaginary part and $\mathbf{a}^{(i)}$ to be the corresponding eigenvector.

3. To calculate the stresses, it is helpful to introduce three additional vectors $\mathbf{b}^{(i)}$ defined as

$$[\mathbf{R}^T + p_i \mathbf{T}] \mathbf{a}^{(i)} = \mathbf{b}^{(i)}.$$

4. It is often convenient to collect the eigenvectors $\mathbf{a}^{(i)}$ and $\mathbf{b}^{(i)}$ and the eigenvalues p_i into matrices \mathbf{A} , \mathbf{B} , \mathbf{P} as follows:

$$\mathbf{A} \equiv \begin{bmatrix} a_1^{(1)} & a_1^{(2)} & a_1^{(3)} \\ a_2^{(1)} & a_2^{(2)} & a_2^{(3)} \\ a_3^{(1)} & a_3^{(2)} & a_3^{(3)} \end{bmatrix} \quad \mathbf{B} \equiv \begin{bmatrix} b_1^{(1)} & b_1^{(2)} & b_1^{(3)} \\ b_2^{(1)} & b_2^{(2)} & b_2^{(3)} \\ b_3^{(1)} & b_3^{(2)} & b_3^{(3)} \end{bmatrix} \quad \mathbf{P} \equiv \begin{bmatrix} p_1 & 0 & 0 \\ 0 & p_2 & 0 \\ 0 & 0 & p_3 \end{bmatrix}.$$

Note also that, as always, although the eigenvalues p_i are uniquely defined for a particular set of elastic constants, the eigenvectors $\mathbf{a}^{(i)}$ (and consequently the vectors $\mathbf{b}^{(i)}$) are not unique, because they may be multiplied by any arbitrary complex number and will remain eigenvectors. It is helpful to normalize the eigenvectors so that the matrices \mathbf{A} and \mathbf{B} satisfy

$$\mathbf{B}^T \mathbf{A} + \mathbf{A}^T \mathbf{B} = \mathbf{I} \quad \bar{\mathbf{B}}^T \bar{\mathbf{A}} + \bar{\mathbf{A}}^T \bar{\mathbf{B}} = \mathbf{I},$$

where \mathbf{I} is the identity matrix.

General representation of displacements: The displacement $\mathbf{u} = u_1(x_1, x_2)\mathbf{e}_1 + u_2(x_1, x_2)\mathbf{e}_2 + u_3(x_1, x_2)\mathbf{e}_3$ at a point (x_1, x_2) in the solid is

$$\mathbf{u}(x_1, x_2) = \sum_{i=1}^3 \mathbf{a}^{(i)} f_i(z_i) + \bar{\mathbf{a}}^{(i)} \overline{f_i(z_i)},$$

where p_i, \bar{p}_i are the three pairs of complex roots of the characteristic equation, $\mathbf{a}^{(i)}$ are the corresponding eigenvectors, $z_i = x_1 + p_i x_2$, and $f_i(z_i)$ are analytic functions, which are analogous to the complex potentials $\Omega(z), \omega(z)$ for isotropic solids.

General representation of stresses: The stresses can be expressed in terms of a vector valued stress function φ (you can think of this as a generalized Airy function) defined as

$$\varphi = \sum_{i=1}^3 \mathbf{b}^{(i)} f_i(z_i) + \bar{\mathbf{b}}^{(i)} \overline{f_i(z_i)}.$$

The stresses can be calculated from the three components of ϕ as

$$\sigma_{i1} = \frac{\partial \phi_i}{\partial x_2} \quad \sigma_{i2} = \frac{\partial \phi_i}{\partial x_1}.$$

Combined matrix representation for displacement and stresses: The solution for the displacement field and stress function can be expressed in the form

$$\begin{bmatrix} \mathbf{u} \\ \phi \end{bmatrix} = \begin{bmatrix} \mathbf{A} & \bar{\mathbf{A}} \\ \mathbf{B} & \bar{\mathbf{B}} \end{bmatrix} \begin{bmatrix} \mathbf{f} \\ \bar{\mathbf{f}} \end{bmatrix},$$

where $\mathbf{f} \equiv [f_1(z_1), f_2(z_2), f_3(z_3)]^T$.

Simpler representation for stresses and displacements: The solutions for displacement and stress can also be expressed as

$$\mathbf{u} = 2\operatorname{Re}(\mathbf{Af}) \quad \phi = 2\operatorname{Re}(\mathbf{Bf}) \quad \mathbf{t}_2 = 2\operatorname{Re}(\mathbf{Bf}') \quad \mathbf{t}_1 = -2\operatorname{Re}(\mathbf{B}\mathbf{Pf}'),$$

where $\operatorname{Re}(z)$ denotes the real part of z ,

$$\mathbf{t}_1 = \begin{bmatrix} \sigma_{11} \\ \sigma_{21} \\ \sigma_{31} \end{bmatrix} \quad \mathbf{t}_2 = \begin{bmatrix} \sigma_{12} \\ \sigma_{22} \\ \sigma_{32} \end{bmatrix} \quad \mathbf{f} = \begin{bmatrix} f_1(z_1) \\ f_2(z_2) \\ f_3(z_3) \end{bmatrix} \quad \mathbf{f}' = \begin{bmatrix} f'_1(z_1) \\ f'_2(z_2) \\ f'_3(z_3) \end{bmatrix},$$

and $f'(z) \equiv \partial f / \partial z$.

5.5.3 Demonstration That the Stroh Representation Satisfies the Governing Equations
Our first objective is to show that a displacement field of the form $u_i = a_i f(z)$, with $z = x_1 + px_2$, and (p, a_i) any one of the eigenvalues p_i and eigenvectors $\mathbf{a}^{(i)}$ defined in the preceding section, satisfy the governing equations

$$C_{ijkl} \frac{\partial^2 u_k}{\partial x_i \partial x_l} = 0.$$

To see this,

1. Note that $\partial z / \partial x_i = \delta_{i1} + p\delta_{i2}$, where δ_{ij} is the Kronecker delta. Therefore, it follows that

$$\frac{\partial u_k}{\partial x_l} = a_k (\delta_{l1} + p\delta_{l2}) f'(z) \quad \frac{\partial u_k}{\partial x_{lj}} = a_k (\delta_{l1} + p\delta_{l2}) (\delta_{j1} + p\delta_{j2}) f''(z).$$

2. Substituting this result into the governing equation shows that

$$C_{ijkl}(\delta_{l1} + p\delta_{l2})(\delta_{j1} + p\delta_{j2})a_k f''(z) = 0.$$

3. This can be rewritten as

$$(C_{i1k1} + p(C_{i1k2} + C_{i2k1}) + p^2 C_{i2k2})a_k = 0$$

or in matrix form as

$$[\mathbf{Q} + p(\mathbf{R} + \mathbf{R}^T) + p^2 \mathbf{T}] \mathbf{a} = 0,$$

where \mathbf{Q} , \mathbf{R} , and \mathbf{T} are the matrices defined in Section 5.5.2. The eigenvalue/eigenvector pairs (p, \mathbf{a}) satisfy this equation by definition, which shows that the governing equation is indeed satisfied.

Our next objective is to show that stresses can be computed from the formulas given in Section 5.5.2. To see this,

1. Note that the stresses can be obtained from the constitutive equation $\sigma_{ij} = C_{ijkl} \frac{\partial u_k}{\partial x_l}$.
2. Recall that, for each of the six characteristic solutions, we may obtain displacements as $\partial u_k / \partial x_l = (\delta_{l1} + p\delta_{l2})a_k f'(z)$,

so that

$$\sigma_{i1} = (C_{i1k1} + pC_{i1k2})a_k f'(z) = [Q_{ik} + pR_{ik}]a_k f'(z)$$

$$\sigma_{i2} = (C_{i2k1} + pC_{i2k2})a_k f'(z) = [R_{ki} + pT_{ik}]a_k f'(z),$$

where \mathbf{Q} , \mathbf{R} , and \mathbf{T} are the matrices defined in the preceding section.

3. To simplify this result, define

$$[\mathbf{R}^T + p\mathbf{T}]\mathbf{a} = \mathbf{b} \quad [\mathbf{Q} + p\mathbf{R}]\mathbf{a} = \mathbf{c}$$

and note that the governing equations require that

$$[\mathbf{Q} + p(\mathbf{R} + \mathbf{R}^T) + p^2 \mathbf{T}]\mathbf{a} = \mathbf{c} + p\mathbf{b} = 0.$$

4. Combining the results of steps 2 and 3 shows that stresses can be computed from

$$\sigma_{i1} = -pb_i f'(z) \quad \sigma_{i2} = -b_i f'(z).$$

5. Finally, recall that the stress function ϕ has components $\phi_i = b_i f(z)$ and $\partial z / \partial x_i = \delta_{i1} + p\delta_{i2}$. Consequently, the stresses are related to the stress function by $\sigma_{i1} = -\partial \phi_i / \partial x_2$ $\sigma_{i2} = \partial \phi_i / \partial x_1$ as required.

5.5.4 Stroh Eigenvalues and Anisotropy Matrices for Cubic Materials

Because the eigenvalues p for a general anisotropic material involve the solution to a sextic equation, an explicit general solution cannot be found. Even monoclinic materials (which have a single symmetry plane) give solutions that are so cumbersome that many symbolic manipulation programs cannot handle them. The solution for cubic materials is manageable, as long as one of the coordinate axes is parallel to the x_3 direction. If the cube axes coincide with the coordinate directions, the elasticity matrix reduces to

$$\begin{bmatrix} c_{11} & c_{12} & c_{12} & 0 & 0 & 0 \\ c_{12} & c_{11} & c_{12} & 0 & 0 & 0 \\ c_{12} & c_{12} & c_{11} & 0 & 0 & 0 \\ 0 & 0 & 0 & c_{44} & 0 & 0 \\ 0 & 0 & 0 & 0 & c_{44} & 0 \\ 0 & 0 & 0 & 0 & 0 & c_{44} \end{bmatrix},$$

where

$$\mathbf{Q} = \begin{bmatrix} c_{11} & 0 & 0 \\ 0 & c_{44} & 0 \\ 0 & 0 & c_{44} \end{bmatrix} \quad \mathbf{R} = \begin{bmatrix} 0 & c_{12} & 0 \\ c_{44} & 0 & 0 \\ 0 & 0 & 0 \end{bmatrix} \quad \mathbf{T} = \begin{bmatrix} c_{44} & 0 & 0 \\ 0 & c_{11} & 0 \\ 0 & 0 & c_{44} \end{bmatrix}.$$

The characteristic equation therefore has the form

$$\det \begin{bmatrix} c_{11} + p^2 c_{44} & p(c_{12} + c_{44}) & 0 \\ p(c_{12} + c_{44}) & c_{44} + c_{11} p^2 & 0 \\ 0 & 0 & c_{44}(1 + p^2) \end{bmatrix} = 0,$$

giving

$$(1 + p^2)(p^4 + \eta p^2 + 1) = 0 \quad \eta = \frac{c_{11}^2 - c_{12}^2 - 2c_{12}c_{44}}{c_{11}c_{44}},$$

where

$$p_1 = \frac{1}{2}(\sqrt{2-\eta} + i\sqrt{2+\eta}) \quad p_2 = \frac{1}{2}(-\sqrt{2-\eta} + i\sqrt{2+\eta}) \quad p_3 = i.$$

For $\eta > 2$, the eigenvalues are purely imaginary. The special case $\eta = 2$ corresponds to an isotropic material.

The matrices \mathbf{A} and \mathbf{B} can be expressed as

$$\mathbf{A} = \begin{bmatrix} -p_1(c_{12} + c_{44})/\beta_1 & -p_2(c_{12} + c_{44})/\beta_2 & 0 \\ (c_{11} + p_1^2 c_{44})/\beta_1 & (c_{11} + p_2^2 c_{44})/\beta_2 & 0 \\ 0 & 0 & (1-i)/2 \end{bmatrix}$$

$$\mathbf{B} = \begin{bmatrix} c_{44}(c_{11} - c_{12}p_1^2)/\beta_1 & c_{44}(c_{11} - c_{12}p_2^2)/\beta_2 & 0 \\ p_1(c_{11}c_{44}p_1^2 + c_{11}^2 - c_{12}^2 - c_{12}c_{44})/\beta_1 & p_2(c_{11}c_{44}p_2^2 + c_{11}^2 - c_{12}^2 - c_{12}c_{44})/\beta_2 & 0 \\ 0 & 0 & (1+i)/2 \end{bmatrix}$$

$$\beta_i = \sqrt{2c_{11}p_i((c_{11} + p_i^2c_{44})^2 - (c_{12} + c_{44})^2)}$$

5.5.5 Degenerate Materials

There are some materials for which the general procedure outlined in the preceding sections breaks down. We can illustrate this by attempting to apply it to an isotropic material. In this case, we find that $p_1 = p_2 = p_3 = i$, and there are only two independent eigenvectors \mathbf{a} associated with the repeated eigenvalue p_i . In addition, if you attempt to substitute material constants representing an isotropic material into the formulas for \mathbf{A} and \mathbf{B} given in the preceding section, you will find that the terms in the matrices are infinite.

The physical significance of this degeneracy is not known. Although isotropic materials are degenerate, isotropy does not appear to be a necessary condition for degeneracy, because fully anisotropic materials may exhibit the same degeneracy for appropriate values of their stiffnesses.

Choi, Shin, and Earmme [2003] have found a way to rewrite the complex variable formulation for isotropic materials into a form that is identical in structure to the Stroh formulation. This approach is very useful, because it enables us to solve problems involving interfaces between isotropic and anisotropic materials, but it does not provide any fundamental insight into the cause of degeneracy, nor does it provide a general fix for the problem.

In many practical situations, the problems associated with degeneracy can be avoided by rewriting the solution in terms of special tensors (to be defined below), which can be computed directly from the elastic constants, without needing to determine \mathbf{A} and \mathbf{B} .

5.5.6 Fundamental Elasticity Matrix

The vector $[\mathbf{a}^{(i)}, \mathbf{b}^{(i)}]$ and corresponding eigenvector p_i can be shown to be the right eigenvectors and eigenvalues of a real, unsymmetric matrix known as the *fundamental elasticity matrix*, defined as

$$\mathbf{N} = \begin{bmatrix} \mathbf{N}_1 & \mathbf{N}_2 \\ \mathbf{N}_3 & \mathbf{N}_1^T \end{bmatrix} \quad \mathbf{N}_1 = -\mathbf{T}^{-1}\mathbf{R}^T \quad \mathbf{N}_2 = \mathbf{T}^{-1} \quad \mathbf{N}_3 = \mathbf{R}\mathbf{T}^{-1}\mathbf{R}^T - \mathbf{Q},$$

where the matrices \mathbf{Q} , \mathbf{R} , and \mathbf{T} are the elasticity matrices defined in Section 5.5.2. Similarly, $[\mathbf{b}^{(i)}, \mathbf{a}^{(i)}]$ can be shown to be the left eigenvector of \mathbf{N} .

To see this, note that the expressions relating vectors \mathbf{a} and \mathbf{b}

$$[\mathbf{R}^T + p\mathbf{T}]\mathbf{a} = \mathbf{b} \quad [\mathbf{Q} + p\mathbf{R}]\mathbf{a} = -p\mathbf{b}$$

can be expressed as

$$\begin{bmatrix} -\mathbf{Q} & \mathbf{0} \\ -\mathbf{R}^T & \mathbf{I} \end{bmatrix} \begin{bmatrix} \mathbf{a} \\ \mathbf{b} \end{bmatrix} = p \begin{bmatrix} \mathbf{R} & \mathbf{I} \\ \mathbf{T} & \mathbf{0} \end{bmatrix} \begin{bmatrix} \mathbf{a} \\ \mathbf{b} \end{bmatrix}.$$

Because \mathbf{T} is positive definite and symmetric, its inverse can always be computed. Therefore, we may write

$$\begin{bmatrix} \mathbf{0} & \mathbf{T}^{-1} \\ \mathbf{I} & -\mathbf{R}\mathbf{T}^{-1} \end{bmatrix} \begin{bmatrix} \mathbf{R} & \mathbf{I} \\ \mathbf{T} & \mathbf{0} \end{bmatrix} = \begin{bmatrix} \mathbf{I} & \mathbf{0} \\ \mathbf{0} & \mathbf{I} \end{bmatrix},$$

and therefore

$$\begin{bmatrix} \mathbf{0} & \mathbf{T}^{-1} \\ \mathbf{I} & -\mathbf{R}\mathbf{T}^{-1} \end{bmatrix} \begin{bmatrix} -\mathbf{Q} & \mathbf{0} \\ -\mathbf{R}_T & \mathbf{I} \end{bmatrix} \begin{bmatrix} \mathbf{a} \\ \mathbf{b} \end{bmatrix} = p \begin{bmatrix} \mathbf{a} \\ \mathbf{b} \end{bmatrix}.$$

This is an eigenvalue equation, and multiplying out the matrices gives the required result.

The second identity may be proved in exactly the same way. Note that

$$\begin{aligned} [\mathbf{b} \quad \mathbf{a}] \begin{bmatrix} \mathbf{0} & \mathbf{I} \\ -\mathbf{Q} & -\mathbf{R} \end{bmatrix} &= p [\mathbf{b} \quad \mathbf{a}] \begin{bmatrix} \mathbf{I} & \mathbf{0} \\ \mathbf{R}^T & \mathbf{T} \end{bmatrix} \\ \begin{bmatrix} \mathbf{I} & \mathbf{0} \\ \mathbf{R}^T & \mathbf{T} \end{bmatrix} \begin{bmatrix} \mathbf{I} & \mathbf{0} \\ -\mathbf{T}^{-1}\mathbf{R}^T & \mathbf{T}^{-1} \end{bmatrix} &= \begin{bmatrix} \mathbf{I} & \mathbf{0} \\ \mathbf{0} & \mathbf{I} \end{bmatrix}, \end{aligned}$$

so

$$[\mathbf{b} \quad \mathbf{a}] \begin{bmatrix} \mathbf{0} & \mathbf{I} \\ -\mathbf{Q} & -\mathbf{R} \end{bmatrix} \begin{bmatrix} \mathbf{I} & \mathbf{0} \\ -\mathbf{T}^{-1}\mathbf{R}^T & \mathbf{T}^{-1} \end{bmatrix} = p [\mathbf{b} \quad \mathbf{a}],$$

again, giving the required answer.

For *nondegenerate* materials, \mathbf{N} has six distinct eigenvectors. A matrix of this kind is called *simple*. For some materials, \mathbf{N} has repeated eigenvalues but still has six distinct eigenvectors. A matrix of this kind is called *semi-simple*. For *degenerate* materials, \mathbf{N} does not have six distinct eigenvectors. A matrix of this kind is called *non-semi-simple*.

5.5.7 Orthogonal Properties of Stroh Matrices A and B

The observation that $[\mathbf{a}^{(i)}, \mathbf{b}^{(i)}]$ and $[\mathbf{b}^{(i)}, \mathbf{a}^{(i)}]$ are right and left eigenvectors of \mathbf{N} has an important consequence. If the eigenvalues are distinct (i.e., the material is not degenerate), the left and right eigenvectors of a matrix are orthogonal. This implies that

$$\begin{aligned} [\mathbf{b}^{(i)} \quad \mathbf{a}^{(i)}] \begin{bmatrix} \mathbf{a}^{(j)} \\ \mathbf{b}^{(j)} \end{bmatrix} &= 0 \quad i \neq j \\ [\mathbf{b}^{(i)} \quad \mathbf{a}^{(i)}] \begin{bmatrix} \bar{\mathbf{a}}^{(j)} \\ \bar{\mathbf{b}}^{(j)} \end{bmatrix} &= [\bar{\mathbf{b}}^{(i)} \quad \bar{\mathbf{a}}^{(i)}] \begin{bmatrix} \mathbf{a}^{(j)} \\ \mathbf{b}^{(j)} \end{bmatrix} = 0. \end{aligned}$$

In addition, the vectors can always be normalized so that

$$[\mathbf{b}^{(i)} \quad \mathbf{a}^{(i)}] \begin{bmatrix} \mathbf{a}^{(i)} \\ \mathbf{b}^{(i)} \end{bmatrix} = 1.$$

If this is done, we see that the matrices \mathbf{A} and \mathbf{B} must satisfy

$$\begin{bmatrix} \mathbf{B}^T & \mathbf{A}^T \\ \bar{\mathbf{B}}^T & \bar{\mathbf{A}}^T \end{bmatrix} \begin{bmatrix} \mathbf{A} & \bar{\mathbf{A}} \\ \mathbf{B} & \bar{\mathbf{B}} \end{bmatrix} = \begin{bmatrix} \mathbf{I} & \mathbf{0} \\ \mathbf{0} & \mathbf{I} \end{bmatrix}.$$

Clearly, the two matrices are inverses of each other, and therefore we also have that

$$\begin{bmatrix} \mathbf{A} & \bar{\mathbf{A}} \\ \mathbf{B} & \bar{\mathbf{B}} \end{bmatrix} \begin{bmatrix} \mathbf{B}^T & \mathbf{A}^T \\ \bar{\mathbf{B}}^T & \bar{\mathbf{A}}^T \end{bmatrix} = \begin{bmatrix} \mathbf{I} & \mathbf{0} \\ \mathbf{0} & \mathbf{I} \end{bmatrix}.$$

These results give the following relations between \mathbf{A} and \mathbf{B} :

$$\begin{aligned} \mathbf{B}^T \mathbf{A} + \mathbf{A}^T \mathbf{B} &= \bar{\mathbf{B}}^T \bar{\mathbf{A}} + \bar{\mathbf{A}}^T \bar{\mathbf{B}} = \mathbf{AB}^T + \bar{\mathbf{A}}\bar{\mathbf{B}}^T = \mathbf{BA}^T + \bar{\mathbf{B}}\bar{\mathbf{A}}^T = \mathbf{I} \\ \mathbf{B}^T \bar{\mathbf{A}} + \mathbf{A}^T \bar{\mathbf{B}} &= \bar{\mathbf{B}}^T \mathbf{A} + \bar{\mathbf{A}}^T \mathbf{B} = \mathbf{AA}^T + \bar{\mathbf{A}}\bar{\mathbf{A}}^T = \mathbf{BB}^T + \bar{\mathbf{B}}\bar{\mathbf{B}}^T = \mathbf{0}. \end{aligned}$$

5.5.8 Barnett–Lothe Tensors and the Impedance Tensor

In this section, we define four important tensors that can be calculated from the Stroh matrices \mathbf{A} and \mathbf{B} . Specifically, we introduce the following:

- The Barnett–Lothe tensors: $\mathbf{S} = i(2\mathbf{AB}^T - \mathbf{I}) \quad \mathbf{H} = 2i\mathbf{AA}^T \quad \mathbf{L} = -2i\mathbf{BB}^T$
- The impedance tensor with properties: $\mathbf{M} = -i\mathbf{BA}^{-1} \quad \mathbf{M}^{-1} = i\mathbf{AB}^{-1} \quad \mathbf{B} = i\mathbf{MA}$

The following relations between the Barnett–Lothe tensors and the impedance tensor are also useful:

$$\mathbf{M} = -i\mathbf{BA}^{-1} = \mathbf{H}^{-1} + i\mathbf{H}^{-1}\mathbf{S} \quad \mathbf{M}^{-1} = i\mathbf{AB}^{-1} = \mathbf{L}^{-1} + i\mathbf{SL}^{-1}.$$

Many solutions can be expressed in terms of \mathbf{S} , \mathbf{H} , and \mathbf{L} directly, rather than in terms of \mathbf{A} and \mathbf{B} . In addition, Barnett and Lothe devised a procedure for computing \mathbf{S} , \mathbf{H} , and \mathbf{L}

without needing to calculate \mathbf{A} and \mathbf{B} (see Section 5.5.11). Consequently, these tensors can be calculated even for degenerate materials.

As an example, for cubic materials, with coordinate axes aligned with coordinate directions,

$$\mathbf{M} = \begin{bmatrix} \gamma & \frac{-ic_{44}(c_{11}-c_{12})}{c_{11}+c_{44}} & 0 \\ \frac{ic_{44}(c_{11}-c_{12})}{c_{11}+c_{44}} & \gamma & 0 \\ 0 & 0 & 1 \end{bmatrix} \quad \gamma = \frac{\sqrt{c_{11}c_{44}(c_{11}-c_{12})(c_{11}+2c_{44}+c_{12})}}{c_{11}+c_{44}}.$$

5.5.9 Useful Properties of Matrices in Anisotropic Elasticity

We collect below various useful algebraic relations between the various matrices that were introduced in the preceding sections.

By definition, a matrix \mathbf{M} satisfying $\mathbf{M}^T = \bar{\mathbf{M}}$ is *Hermitian*. A matrix satisfying $\mathbf{M}^T = -\bar{\mathbf{M}}$ is *skew-Hermitian*:

- $\bar{\mathbf{B}}^T \mathbf{A}$ is skew-Hermitian. To see this, note that the orthogonality relations for \mathbf{A} and \mathbf{B} require that $\bar{\mathbf{B}}^T \mathbf{A} + \bar{\mathbf{A}}^T \mathbf{B} = \mathbf{0}$.
- $i\bar{\mathbf{B}}^T \mathbf{A}$ is Hermitian. This follows trivially from the preceding expression.
- \mathbf{M} and \mathbf{M}^{-1} are both Hermitian. To see this, note $\mathbf{M} = \mathbf{B}(-i\bar{\mathbf{B}}^T \mathbf{A})^{-1}\bar{\mathbf{B}}^T \quad \mathbf{M}^{-1} = \mathbf{A}(i\bar{\mathbf{A}}^T \mathbf{B})^{-1}\bar{\mathbf{A}}^T$ and use the preceding result.
- The matrices $i\mathbf{B}^{-1}\bar{\mathbf{B}}$ and $-i\mathbf{A}^{-1}\bar{\mathbf{A}}$ are Hermitian. To show the first expression, note that $i\mathbf{B}^{-1}\bar{\mathbf{B}} = i\mathbf{B}^T(\mathbf{B}\mathbf{B}^T)^{-1}\bar{\mathbf{B}} = 2\mathbf{B}^T\mathbf{L}^{-1}\bar{\mathbf{B}}$ and recall that \mathbf{L} is real. A similar technique shows the second.
- $i\mathbf{B}^{-1}\bar{\mathbf{B}}$ and $-i\mathbf{A}^{-1}\bar{\mathbf{A}}$ are both orthogonal matrices. To see this for the first matrix, note that $i\mathbf{B}^{-1}\bar{\mathbf{B}}(i\mathbf{B}^{-1}\bar{\mathbf{B}})^T = -\mathbf{B}^{-1}\bar{\mathbf{B}}\bar{\mathbf{B}}^T\mathbf{B}^{-T} = \mathbf{B}^{-1}\mathbf{B}\mathbf{B}^T\mathbf{B}^{-T} = \mathbf{I}$, where we have used the orthogonality properties of \mathbf{B} . A similar procedure shows the second result.
- The Barnett–Lothe tensors are real (i.e., they have zero imaginary part). To see this, note that the orthogonality of \mathbf{A} and \mathbf{B} (see Section 5.5.7) implies that

$$\mathbf{AB}^T + \bar{\mathbf{A}}\bar{\mathbf{B}}^T = \mathbf{I} \quad \mathbf{AA}^T + \bar{\mathbf{A}}\bar{\mathbf{A}}^T = \mathbf{BB}^T = \bar{\mathbf{B}}\bar{\mathbf{B}}^T = \mathbf{0}.$$

Therefore, \mathbf{AA}^T and \mathbf{BB}^T are pure imaginary, whereas the real part of $\mathbf{AB}^T = 1/2\mathbf{I}$.

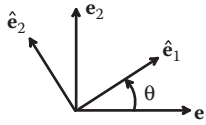


FIGURE 5.44 Coordinate systems for change of basis formulas for elastic constants.

- The impedance tensor can be expressed in terms of the Barnett–Lothe tensors as

$$\mathbf{M} = -i\mathbf{B}\mathbf{A}^{-1} = \mathbf{H}^{-1} + i\mathbf{H}^{-1}\mathbf{S} \quad \mathbf{M}^{-1} = i\mathbf{A}\mathbf{B}^{-1} = \mathbf{L}^{-1} + i\mathbf{S}\mathbf{L}^{-1}.$$

To see the first result, note that $\mathbf{B}\mathbf{A}^{-1} = (\mathbf{AB}^T)^T(\mathbf{AA}^T)^{-1}$ and use the definitions of \mathbf{H} and \mathbf{S} . The second result follows in the same way. Note that \mathbf{H} , \mathbf{L} , and \mathbf{S} are all real, so this gives a decomposition of \mathbf{M} and its inverse into real and imaginary parts. In addition, because we can compute the Barnett–Lothe tensors for degenerate materials, \mathbf{M} can also be determined without needing to compute \mathbf{A} and \mathbf{B} explicitly.

- $\mathbf{H}^{-1}\mathbf{S} + \mathbf{S}^T\mathbf{H}^{-1} = \mathbf{0}$ $\mathbf{S}\mathbf{L}^{-1} + \mathbf{L}^{-1}\mathbf{S}^T = \mathbf{0}$. To see these, note that \mathbf{M} and its inverse are Hermitian and that the imaginary part of a Hermitian matrix is skew symmetric and use the preceding result.
- $\mathbf{BP} = \mathbf{N}_3\mathbf{A} + \mathbf{N}_1^T\mathbf{B}$, where $\mathbf{P} = \text{diag}(p_1, p_2, p_3)$. To see this, recall that the fundamental elasticity tensor satisfies

$$\begin{bmatrix} \mathbf{N}_1 & \mathbf{N}_2 \\ \mathbf{N}_3 & \mathbf{N}_1^T \end{bmatrix} \begin{bmatrix} \mathbf{a}^{(i)} \\ \mathbf{b}^{(i)} \end{bmatrix} = p_i \begin{bmatrix} \mathbf{a}^{(i)} \\ \mathbf{b}^{(i)} \end{bmatrix} \Rightarrow \begin{bmatrix} \mathbf{N}_1 & \mathbf{N}_2 \\ \mathbf{N}_3 & \mathbf{N}_1^T \end{bmatrix} \begin{bmatrix} \mathbf{A} \\ \mathbf{B} \end{bmatrix} = \begin{bmatrix} \mathbf{A} & \mathbf{0} \\ \mathbf{0} & \mathbf{B} \end{bmatrix} \begin{bmatrix} \mathbf{P} \\ \mathbf{P} \end{bmatrix}.$$

The second row of this equation is $\mathbf{N}_3\mathbf{A} + \mathbf{N}_1^T\mathbf{B} = \mathbf{BP}$.

5.5.10 Basis Change Formulas for Matrices Used in Anisotropic Elasticity

The various tensors and matrices defined in the preceding sections are all functions of the elastic constants for the material. Because the elastic constants depend on the orientation of the material with respect to the coordinate axes, the matrices are functions of the direction of the coordinate system.

To this end,

1. Let $\{\mathbf{e}_1, \mathbf{e}_2, \mathbf{e}_3\}$ and $\{\hat{\mathbf{e}}_1, \hat{\mathbf{e}}_2, \hat{\mathbf{e}}_3\}$ be two Cartesian bases, as indicated in the figure.
2. Let n_i, m_i denote the components of $\hat{\mathbf{e}}_1, \hat{\mathbf{e}}_2$ in $\{\mathbf{e}_1, \mathbf{e}_2, \mathbf{e}_3\}$, i.e. $\hat{\mathbf{e}}_1 = n_i \mathbf{e}_i$, $\hat{\mathbf{e}}_2 = m_i \mathbf{e}_i$.
3. Let C_{ijkl} be the components of the elasticity tensor in $\{\mathbf{e}_1, \mathbf{e}_2, \mathbf{e}_3\}$ and let matrices \mathbf{Q}, \mathbf{R} , and \mathbf{T} be matrices of elastic constants defined in Section 5.5.2.

4. Let p , \mathbf{A}, \mathbf{B} denote any one of the three Stroh eigenvalues and the matrices of Stroh eigenvectors, computed for the coordinate system $\{\mathbf{e}_1, \mathbf{e}_2, \mathbf{e}_3\}$.
5. Let $\mathbf{S}, \mathbf{H}, \mathbf{L}$, and \mathbf{M} denote the Barnett–Lothe tensors and impedance tensor in the $\{\mathbf{e}_1, \mathbf{e}_2, \mathbf{e}_3\}$ basis.
6. Similarly, let $\hat{\mathbf{Q}}, \hat{\mathbf{R}}, \hat{\mathbf{T}}, \hat{p}, \hat{\mathbf{A}}, \hat{\mathbf{B}}$, etc. denote the various matrices and tensors in the $\{\hat{\mathbf{e}}_1, \hat{\mathbf{e}}_2, \hat{\mathbf{e}}_3\}$ basis.

In addition, define rotation matrices Ω , $\mathbf{Q}(\theta)$, $\mathbf{R}(\theta)$, $\mathbf{T}(\theta)$ as follows:

$$\Omega \equiv \begin{bmatrix} \cos\theta & \sin\theta & 0 \\ -\sin\theta & \cos\theta & 0 \\ 0 & 0 & 1 \end{bmatrix}$$

$$\begin{bmatrix} \mathbf{Q}(\theta) & \mathbf{R}(\theta) \\ \mathbf{R}^T(\theta) & \mathbf{T}(\theta) \end{bmatrix} = \begin{bmatrix} \cos\theta\mathbf{I} & \sin\theta\mathbf{I} \\ -\sin\theta\mathbf{I} & \cos\theta\mathbf{I} \end{bmatrix} \begin{bmatrix} \mathbf{Q} & \mathbf{R} \\ \mathbf{R}^T & \mathbf{T} \end{bmatrix} \begin{bmatrix} \cos\theta\mathbf{I} & -\sin\theta\mathbf{I} \\ \sin\theta\mathbf{I} & \cos\theta\mathbf{I} \end{bmatrix}.$$

The following alternative expressions for $\mathbf{Q}(\theta)$, $\mathbf{R}(\theta)$, $\mathbf{T}(\theta)$ are also useful:

$$Q_{ij}(\theta) = C_{ikjl}n_k n_l \quad R_{ij}(\theta) = C_{ikjl}n_k m_l \quad T_{ij}(\theta) = C_{ikjl}m_k m_l$$

$$\mathbf{Q}(\theta) = \mathbf{Q}\cos^2\theta + (\mathbf{R} + \mathbf{R}^T)\sin\theta\cos\theta + \mathbf{T}\sin^2\theta$$

$$\mathbf{R}(\theta) = \mathbf{R}\cos^2\theta + (\mathbf{T} - \mathbf{Q})\sin\theta\cos\theta - \mathbf{R}^T\sin^2\theta.$$

$$\mathbf{T}(\theta) = \mathbf{T}\cos^2\theta - (\mathbf{R} + \mathbf{R}^T)\sin\theta\cos\theta + \mathbf{Q}\sin^2\theta$$

The basis change formulas can then be expressed as

$$\hat{p} \equiv p(\theta) = \frac{p\cos\theta - \sin\theta}{p\sin\theta + \cos\theta}$$

$$\hat{\mathbf{A}} = \Omega \mathbf{A} \quad \hat{\mathbf{B}} = \Omega \mathbf{B}$$

$$\hat{\mathbf{Q}} = \Omega \mathbf{Q}(\theta) \Omega^T \quad \hat{\mathbf{R}} = \Omega \mathbf{R}(\theta) \Omega^T \quad \hat{\mathbf{T}} = \Omega \mathbf{T}(\theta) \Omega^T$$

$$\hat{\mathbf{S}} = \Omega \mathbf{S} \Omega^T \quad \hat{\mathbf{H}} = \Omega \mathbf{H} \Omega^T \quad \hat{\mathbf{L}} = \Omega \mathbf{L} \Omega^T \quad \hat{\mathbf{M}} = \Omega \mathbf{M} \Omega^T.$$

Derivation: These results can be derived as follows:

1. Note that the displacements transform as vectors, so that $\hat{\mathbf{u}} = \Omega \mathbf{u}$. Consequently,

$$\hat{\mathbf{u}} = \sum_{i=1}^3 \hat{\mathbf{a}}^{(i)} f_i(z_i) + \bar{\mathbf{a}}^{(i)} \bar{f}_i(z_i) = \Omega \left(\sum_{i=1}^3 \mathbf{a}^{(i)} f_i(z_i) + \bar{\mathbf{a}}^{(i)} \bar{f}_i(z_i) \right),$$

which shows that $\hat{\mathbf{a}}^{(i)} = \Omega \mathbf{a}^{(i)}$ and directly gives the basis change formula for \mathbf{A} .

2. To find the expression for p , we note that

$$\begin{aligned}\hat{z} &= \hat{x}_1 + \hat{p}\hat{x}_2 = x_1 + px_2 = \hat{x}_1 \cos\theta - \hat{x}_2 \sin\theta + p(\hat{x}_1 \sin\theta + \hat{x}_2 \cos\theta) \\ &= (\cos\theta + p \sin\theta) \left\{ \hat{x}_1 + \frac{(p \cos\theta - \sin\theta)}{\cos\theta + p \sin\theta} \hat{x}_2 \right\}.\end{aligned}$$

Therefore, we may write $\hat{f}_i(\hat{z}_i) = f_i([\cos\theta + p_i \sin\theta] \hat{z}_i)$ with $\hat{z}_i = \hat{x}_1 + \hat{p}_i \hat{x}_2$ and

$$\hat{p}_i \equiv p_i(\theta) = \frac{p_i \cos\theta - \sin\theta}{p_i \sin\theta + \cos\theta},$$

as required.

3. The basis change formulas for \mathbf{Q} , \mathbf{R} , and \mathbf{T} follow directly from the definitions of these matrices.
4. The basis change formula for \mathbf{B} is a bit more cumbersome. By definition,

$$\hat{\mathbf{b}} = (\hat{\mathbf{R}}^T + \hat{p}\hat{\mathbf{T}})\hat{\mathbf{a}} = (\mathbf{\Omega}\mathbf{R}(\theta)^T \mathbf{\Omega}^T + \hat{p}\mathbf{\Omega}\mathbf{T}(\theta)\mathbf{\Omega}^T)\mathbf{\Omega}\mathbf{a} = \mathbf{\Omega}(\mathbf{R}(\theta)^T + \hat{p}\mathbf{T}(\theta))\mathbf{a}.$$

Substituting for $\mathbf{R}(\theta), \mathbf{T}(\theta), \hat{p}$ gives

$$\begin{aligned}\hat{\mathbf{b}} &= \mathbf{\Omega} \left(\mathbf{R}^T \cos^2\theta + (\mathbf{T} - \mathbf{Q}) \sin\theta \cos\theta - \mathbf{R} \sin^2\theta \right. \\ &\quad \left. + \frac{p \cos\theta - \sin\theta}{p \sin\theta + \cos\theta} \left[\mathbf{T} \cos^2\theta - (\mathbf{R} + \mathbf{R})^T \sin\theta \cos\theta + \mathbf{Q} \sin^2\theta \right] \right) \mathbf{a} \\ &= \frac{\mathbf{\Omega}}{p \sin\theta + \cos\theta} \left(\mathbf{R}^T \cos\theta + p \mathbf{T} \sin\theta - p \mathbf{R} \sin\theta - \mathbf{Q} \cos\theta \right) \mathbf{a}\end{aligned}$$

and, finally, recalling that $[\mathbf{R}^T + p\mathbf{T}]\mathbf{a} = \mathbf{b}$, $[\mathbf{Q} + p\mathbf{R}]\mathbf{a} = -p\mathbf{b}$, we obtain the required result.

5. The basis change formulas for the Barnett–Lothe tensors and impedance tensor follow trivially from their definitions. The basis change formulas justify our previous assertion that these quantities are tensors.

5.5.11 Barnett–Lothe Integrals

The basis change formulas in the preceding section lead to a remarkable direct procedure for computing the Barnett–Lothe tensors, without needing to calculate \mathbf{A} and \mathbf{B} . The significance of this result is that, whereas \mathbf{A} and \mathbf{B} break down for degenerate materials, \mathbf{S} , \mathbf{H} , and \mathbf{L} are well-behaved. Consequently, if a solution can be expressed in terms of these tensors, it can be computed for any combination of material parameters.

Specifically, we shall show that \mathbf{S} , \mathbf{H} , and \mathbf{L} can be computed by integrating the submatrices of the fundamental elasticity matrix over orientation space, as follows. Let

$$\mathbf{Q}(\theta) = \mathbf{Q} \cos^2 \theta + (\mathbf{R} + \mathbf{R}^T) \sin \theta \cos \theta + \mathbf{T} \sin^2 \theta$$

$$\mathbf{R}(\theta) = \mathbf{R} \cos^2 \theta + (\mathbf{T} - \mathbf{Q}) \sin \theta \cos \theta - \mathbf{R}^T \sin^2 \theta$$

$$\mathbf{T}(\theta) = \mathbf{T} \cos^2 \theta - (\mathbf{R} + \mathbf{R}^T) \sin \theta \cos \theta + \mathbf{Q} \sin^2 \theta$$

and define

$$\mathbf{N}(\theta) = \begin{bmatrix} \mathbf{N}_1(\theta) & \mathbf{N}_2(\theta) \\ \mathbf{N}_3(\theta) & \mathbf{N}_1^T(\theta) \end{bmatrix}$$

$$\mathbf{N}_1(\theta) = -\mathbf{T}^{-1}(\theta)\mathbf{R}^T(\theta) \quad \mathbf{N}_2(\theta) = \mathbf{T}^{-1}(\theta) \quad \mathbf{N}_3(\theta) = \mathbf{R}(\theta)\mathbf{T}^{-1}(\theta)\mathbf{R}^T(\theta) - \mathbf{Q}(\theta).$$

Then,

$$\begin{bmatrix} \mathbf{S} & \mathbf{H} \\ -\mathbf{L} & \mathbf{S}^T \end{bmatrix} = \frac{1}{\pi} \int_0^\pi \mathbf{N}(\theta) d\theta$$

$$\mathbf{S} = -\frac{1}{\pi} \int_0^\pi \mathbf{T}^{-1}(\theta)\mathbf{R}^T(\theta) d\theta \quad \mathbf{H} = \frac{1}{\pi} \int_0^\pi \mathbf{T}^{-1}(\theta) d\theta \quad \mathbf{L} = -\frac{1}{\pi} \int_0^\pi \{\mathbf{R}(\theta)\mathbf{T}^{-1}(\theta)\mathbf{R}^T(\theta) - \mathbf{Q}(\theta)\} d\theta.$$

Derivation: To see this, we show first that $\mathbf{N}(\theta)$ can be diagonalized as

$$\mathbf{N}(\theta) = \begin{bmatrix} \mathbf{A} & \bar{\mathbf{A}} \\ \mathbf{B} & \bar{\mathbf{B}} \end{bmatrix} \begin{bmatrix} \mathbf{P}(\theta) & \mathbf{0} \\ \mathbf{0} & \bar{\mathbf{P}}(\theta) \end{bmatrix} \begin{bmatrix} \mathbf{B}^T & \mathbf{A}^T \\ \bar{\mathbf{B}}^T & \bar{\mathbf{A}}^T \end{bmatrix},$$

where

$$\mathbf{P}(\theta) = \begin{bmatrix} p_1(\theta) & 0 & 0 \\ 0 & p_2(\theta) & 0 \\ 0 & 0 & p_2(\theta) \end{bmatrix}$$

and $p(\theta)$ was defined previously. From the preceding section, we note that

$$\begin{aligned} \mathbf{b} &= (\mathbf{R}(\theta)^T + p(\theta)\mathbf{T}(\theta))\mathbf{a} \\ p(\theta)\mathbf{b} &= -(\mathbf{Q}(\theta) + p(\theta)\mathbf{R}(\theta))\mathbf{a}, \end{aligned}$$

which can be expressed as

$$\begin{bmatrix} -\mathbf{Q}(\theta) & \mathbf{0} \\ -\mathbf{R}^T(\theta) & \mathbf{I} \end{bmatrix} \begin{bmatrix} \mathbf{a} \\ \mathbf{b} \end{bmatrix} = p(\theta) \begin{bmatrix} \mathbf{R}(\theta) & \mathbf{I} \\ \mathbf{T}(\theta) & \mathbf{0} \end{bmatrix} \begin{bmatrix} \mathbf{a} \\ \mathbf{b} \end{bmatrix},$$

and as before, we can arrange this into an Eigenvalue problem by writing

$$\begin{bmatrix} \mathbf{0} & \mathbf{T}^{-1}(\theta) \\ \mathbf{I} & -\mathbf{R}(\theta)\mathbf{T}^{-1}(\theta) \end{bmatrix} \begin{bmatrix} \mathbf{R}(\theta) & \mathbf{I} \\ \mathbf{T}(\theta) & \mathbf{0} \end{bmatrix} = \begin{bmatrix} \mathbf{I} & \mathbf{0} \\ \mathbf{0} & \mathbf{I} \end{bmatrix}$$

where

$$\begin{bmatrix} \mathbf{N}_1(\theta) & \mathbf{N}_2(\theta) \\ \mathbf{N}_3(\theta) & \mathbf{N}_1^T(\theta) \end{bmatrix} \begin{bmatrix} \mathbf{a} \\ \mathbf{b} \end{bmatrix} = p(\theta) \begin{bmatrix} \mathbf{a} \\ \mathbf{b} \end{bmatrix}$$

$$\mathbf{N}_1(\theta) = -\mathbf{T}^{-1}(\theta)\mathbf{R}^T(\theta) \quad \mathbf{N}_2(\theta) = \mathbf{T}^{-1}(\theta) \quad \mathbf{N}_3(\theta) = \mathbf{R}(\theta)\mathbf{T}^{-1}(\theta)\mathbf{R}^T(\theta) - \mathbf{Q}(\theta).$$

This shows that $[\mathbf{a}, \mathbf{b}]$ are eigenvectors of the rotated elasticity matrix. Following standard procedure, we obtain the diagonalization stated.

Now, we examine $p(\theta)$ more closely. Recall that

$$p(\theta) = \frac{p \cos \theta - \sin \theta}{p \sin \theta + \cos \theta} = \frac{1}{p \sin \theta + \cos \theta} \frac{d}{d\theta}(p \sin \theta + \cos \theta).$$

Integrating gives

$$\int_0^\theta p(\theta) d\theta = \ln(\cos \theta + p \sin \theta)$$

$$\int_0^\pi p(\theta) d\theta = \begin{cases} i\pi & \text{Im}(p) > 0 \\ -i\pi & \text{Im}(p) < 0 \end{cases}$$

(the sign of the integral is determined by $\text{Im}(p)$ because the branch cut for $\ln(\cos \theta + p \sin \theta)$ is taken to lie along the negative real axis). Thus,

$$\frac{1}{\pi} \int_0^\pi \mathbf{N}(\theta) d\theta = \begin{bmatrix} \mathbf{A} & \bar{\mathbf{A}} \\ \mathbf{B} & \bar{\mathbf{B}} \end{bmatrix} \begin{bmatrix} i\mathbf{I} & \mathbf{0} \\ \mathbf{0} & -i\mathbf{I} \end{bmatrix} \begin{bmatrix} \mathbf{B}^T & \mathbf{A}^T \\ \bar{\mathbf{B}}^T & \bar{\mathbf{A}}^T \end{bmatrix} =$$

$$\begin{bmatrix} i\mathbf{AB}^T - i\bar{\mathbf{A}}\bar{\mathbf{B}}^T & i\mathbf{AA}^T - i\bar{\mathbf{A}}\bar{\mathbf{A}}^T \\ i\mathbf{BB}^T - i\bar{\mathbf{B}}\bar{\mathbf{B}}^T & i\mathbf{BA}^T - i\bar{\mathbf{B}}\bar{\mathbf{A}}^T \end{bmatrix} = \begin{bmatrix} \mathbf{S} & \mathbf{H} \\ -\mathbf{L} & \mathbf{S}^T \end{bmatrix}.$$

5.5.12 Stroh Representation for a State of Uniform Stress

A uniform state of stress (with generalized plane strain deformation) provides a very simple example of the Stroh representation. The solution can be expressed in several different

forms. Note that, for a uniform state of stress σ_{ij} and corresponding strain ε_{ij} , we may write

$$\mathbf{u} = \boldsymbol{\varepsilon}_1 x_1 + \boldsymbol{\varepsilon}_2 x_2 \quad \boldsymbol{\varphi} = \mathbf{t}_2 x_1 - \mathbf{t}_1 x_2$$

$$\mathbf{u} = \begin{bmatrix} u_1 \\ u_2 \\ u_3 \end{bmatrix} \quad \boldsymbol{\varepsilon}_1 = \begin{bmatrix} \varepsilon_{11} \\ \varepsilon_{12} \\ 2\varepsilon_{31} \end{bmatrix} = \frac{\partial \mathbf{u}}{\partial x_1} \quad \boldsymbol{\varepsilon}_2 = \begin{bmatrix} \varepsilon_{11} \\ \varepsilon_{12} \\ 2\varepsilon_{32} \end{bmatrix} = \frac{\partial \mathbf{u}}{\partial x_2}$$

$$\mathbf{t}_1 = \begin{bmatrix} \sigma_{11} \\ \sigma_{12} \\ \sigma_{31} \end{bmatrix} = -\frac{\partial \boldsymbol{\varphi}}{\partial x_2} \quad \mathbf{t}_2 = \begin{bmatrix} \sigma_{12} \\ \sigma_{22} \\ \sigma_{32} \end{bmatrix} = \frac{\partial \boldsymbol{\varphi}}{\partial x_1}.$$

In terms of these vectors, the Stroh representation is given by

$$\begin{aligned} \mathbf{u} &= 2\operatorname{Re}(\mathbf{A}\mathbf{Z}\mathbf{q}) & \boldsymbol{\varphi} &= 2\operatorname{Re}(\mathbf{B}\bar{\mathbf{Z}}\mathbf{q}) \\ \mathbf{Z} &= \operatorname{diag}(z_1, z_2, z_3) & \mathbf{q} &= \mathbf{A}^T \mathbf{t}_2 + \mathbf{B}^T \boldsymbol{\varepsilon}_1, \\ z_i &= x_1 + p_i x_2 \end{aligned}$$

or, in matrix form,

$$\begin{bmatrix} \mathbf{u} \\ \boldsymbol{\varphi} \end{bmatrix} = \begin{bmatrix} \mathbf{A} & \bar{\mathbf{A}} \\ \mathbf{B} & \bar{\mathbf{B}} \end{bmatrix} \begin{bmatrix} \mathbf{Z} & \mathbf{0} \\ \mathbf{0} & \bar{\mathbf{Z}} \end{bmatrix} \begin{bmatrix} \mathbf{B}^T & \mathbf{A}^T \\ \bar{\mathbf{B}}^T & \bar{\mathbf{A}}^T \end{bmatrix} \begin{bmatrix} \boldsymbol{\varepsilon}_1 \\ \mathbf{t}_2 \end{bmatrix}.$$

Derivation: To see this, recall that \mathbf{a} and \mathbf{b} form eigenvectors of the fundamental elasticity matrix \mathbf{N} as

$$\mathbf{N} \begin{bmatrix} \mathbf{a} \\ \mathbf{b} \end{bmatrix} = p \begin{bmatrix} \mathbf{a} \\ \mathbf{b} \end{bmatrix};$$

therefore, we can write (for each pair of eigenvectors/values)

$$\begin{bmatrix} \mathbf{a} \\ \mathbf{b} \end{bmatrix} (x_1 + p x_2) = \begin{bmatrix} \mathbf{a} \\ \mathbf{b} \end{bmatrix} x_1 + \mathbf{N} \begin{bmatrix} \mathbf{a} \\ \mathbf{b} \end{bmatrix} x_2.$$

Hence,

$$\begin{bmatrix} \mathbf{A}\mathbf{Z} & \bar{\mathbf{A}}\bar{\mathbf{Z}} \\ \mathbf{B}\mathbf{Z} & \bar{\mathbf{B}}\bar{\mathbf{Z}} \end{bmatrix} = x_1 \begin{bmatrix} \mathbf{A} & \bar{\mathbf{A}} \\ \mathbf{B} & \bar{\mathbf{B}} \end{bmatrix} + x_2 \mathbf{N} \begin{bmatrix} \mathbf{A} & \bar{\mathbf{A}} \\ \mathbf{B} & \bar{\mathbf{B}} \end{bmatrix}.$$

Recall that

$$\begin{bmatrix} \mathbf{A} & \bar{\mathbf{A}} \\ \mathbf{B} & \bar{\mathbf{B}} \end{bmatrix} \begin{bmatrix} \mathbf{B}^T & \mathbf{A}^T \\ \bar{\mathbf{B}}^T & \bar{\mathbf{A}}^T \end{bmatrix} = \begin{bmatrix} \mathbf{I} & \mathbf{0} \\ \mathbf{0} & \mathbf{I} \end{bmatrix}$$

so

$$\begin{bmatrix} \mathbf{A}\mathbf{Z} & \bar{\mathbf{A}}\bar{\mathbf{Z}} \\ \mathbf{B}\mathbf{Z} & \bar{\mathbf{B}}\bar{\mathbf{Z}} \end{bmatrix} \begin{bmatrix} \mathbf{B}^T & \mathbf{A}^T \\ \bar{\mathbf{B}}^T & \bar{\mathbf{A}}^T \end{bmatrix} = x_1 \begin{bmatrix} \mathbf{I} & \mathbf{0} \\ \mathbf{0} & \mathbf{I} \end{bmatrix} + x_2 \mathbf{N}$$

$$\begin{bmatrix} \mathbf{A}\mathbf{Z} & \bar{\mathbf{A}}\bar{\mathbf{Z}} \\ \mathbf{B}\mathbf{Z} & \bar{\mathbf{B}}\bar{\mathbf{Z}} \end{bmatrix} \begin{bmatrix} \mathbf{B}^T & \mathbf{A}^T \\ \bar{\mathbf{B}}^T & \bar{\mathbf{A}}^T \end{bmatrix} \begin{bmatrix} \boldsymbol{\epsilon}_1 \\ \mathbf{t}_2 \end{bmatrix} = x_1 \begin{bmatrix} \boldsymbol{\epsilon}_1 \\ \mathbf{t}_2 \end{bmatrix} + x_2 \mathbf{N} \begin{bmatrix} \boldsymbol{\epsilon}_1 \\ \mathbf{t}_2 \end{bmatrix},$$

and finally, defining

$$\mathbf{N} \begin{bmatrix} \boldsymbol{\epsilon}_1 \\ \mathbf{t}_2 \end{bmatrix} = \begin{bmatrix} \boldsymbol{\epsilon}_2 \\ -\mathbf{t}_1 \end{bmatrix}$$

gives the required result.

5.5.13 Line Load and Dislocation in an Infinite Anisotropic Solid

Figure 5.45 illustrates the problem to be solved. We consider an infinite, anisotropic, linear elastic solid, whose elastic properties will be characterized using the Stroh matrices \mathbf{A} and \mathbf{B} .

The solid contains a straight dislocation, with line direction \mathbf{e}_3 , perpendicular to the plane of the figure. The dislocation has Burger's vector $\mathbf{b} = b_i \mathbf{e}_i$.

At the same time, the solid is subjected to a line of force (with line direction extending out of the plane of the figure). The force per unit length acting on the solid will be denoted by $\mathbf{F} = F_i \mathbf{e}_i$.

The displacement and stress function can be expressed in terms of the Stroh matrices as

$$\begin{bmatrix} \mathbf{u} \\ \Phi \end{bmatrix} = \frac{1}{2\pi i} \begin{bmatrix} \mathbf{A} & \bar{\mathbf{A}} \\ \mathbf{B} & \bar{\mathbf{B}} \end{bmatrix} \begin{bmatrix} \boldsymbol{\lambda} & \mathbf{0} \\ \mathbf{0} & \bar{\boldsymbol{\lambda}} \end{bmatrix} \begin{bmatrix} \mathbf{B}^T & \mathbf{A}^T \\ \bar{\mathbf{B}}^T & \bar{\mathbf{A}}^T \end{bmatrix} \begin{bmatrix} \mathbf{b} \\ \mathbf{F} \end{bmatrix},$$

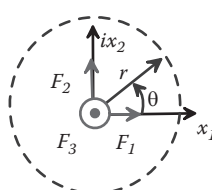


FIGURE 5.45 Line load acting in an infinite anisotropic elastic solid.

where $\boldsymbol{\lambda} = \text{diag}(\ln(z_1), \ln(z_2), \ln(z_3))$, in which diag denotes a diagonal matrix, and

$$\mathbf{b} = [b_1, b_2, b_3]^T \quad \mathbf{F} = [F_1, F_2, F_3]^T.$$

The solution can also be expressed as

$$\mathbf{u} = 2\text{Re}(\mathbf{Af}) \quad \boldsymbol{\varphi} = 2\text{Re}(\mathbf{Bf}) \quad \mathbf{t}_2 = 2\text{Re}(\mathbf{Bf}') \quad \mathbf{t}_1 = -2\text{Re}(\mathbf{BPf}') \quad \mathbf{f} = \boldsymbol{\lambda}(\mathbf{B}^T \mathbf{b} + \mathbf{A}^T \mathbf{F})/(2\pi i).$$

Derivation: We must show that the solution satisfies the following conditions:

1. The displacement field for a dislocation with Burger's vector \mathbf{b} must satisfy $\mathbf{u}(r, \theta = \pi) - \mathbf{u}(r, \theta = -\pi) = \mathbf{b}$ (this corresponds to taking a counterclockwise Burger's circuit around the dislocation, as described in Section 5.3.4).
2. The resultant force exerted by the stresses acting on any contour surrounding the point force must balance the external force \mathbf{F} . For example, taking a circular contour with radius r centered at the origin, we see that

$$\begin{aligned} F_i + \int_{-\pi}^{\pi} \sigma_{ij} n_j r d\theta &= 0 \Rightarrow F_i + \int_{-\pi}^{\pi} \left(-\frac{\partial \phi_i}{\partial x_2} r \cos \theta + \frac{\partial \phi_i}{\partial x_1} r \sin \theta \right) d\theta = 0 \\ &\Rightarrow F_i + \int_{-\pi}^{\pi} \left(-\frac{\partial \phi_i}{\partial x_2} \frac{\partial x_2}{\partial \theta} - \frac{\partial \phi_i}{\partial x_1} \frac{\partial x_1}{\partial \theta} \right) d\theta = 0 \Rightarrow F_i = \phi_i(\theta = \pi) - \phi_i(\theta = -\pi) = 0. \end{aligned}$$

3. We can create the required solution using properties of $\log(z)$. We try a solution of the form

$$\begin{bmatrix} \mathbf{u} \\ \boldsymbol{\varphi} \end{bmatrix} = \begin{bmatrix} \mathbf{A} & \bar{\mathbf{A}} \\ \mathbf{B} & \bar{\mathbf{B}} \end{bmatrix} \begin{bmatrix} \boldsymbol{\lambda} & \mathbf{0} \\ \mathbf{0} & \bar{\boldsymbol{\lambda}} \end{bmatrix} \begin{bmatrix} \mathbf{q} \\ \bar{\mathbf{q}} \end{bmatrix},$$

where $\boldsymbol{\lambda} = \text{diag}(\ln(z_1), \ln(z_2), \ln(z_3))$ and \mathbf{q} is a vector to be determined. Recall that we may write $z = re^{i\theta}$, whence $\log(z) = \log(r) + i\theta$. This, in turn, implies that $\log(z(r, \pi)) - \log(z(r, -\pi)) = 2\pi i$. Therefore,

$$\begin{aligned} \begin{bmatrix} \mathbf{b} \\ \mathbf{F} \end{bmatrix} &= \begin{bmatrix} \mathbf{A} & \bar{\mathbf{A}} \\ \mathbf{B} & \bar{\mathbf{B}} \end{bmatrix} \begin{bmatrix} \boldsymbol{\lambda}(r, \pi) - \boldsymbol{\lambda}(r, -\pi) & \mathbf{0} \\ \mathbf{0} & \bar{\boldsymbol{\lambda}}(r, \pi) - \bar{\boldsymbol{\lambda}}(r, -\pi) \end{bmatrix} \begin{bmatrix} \mathbf{q} \\ \bar{\mathbf{q}} \end{bmatrix} \\ &\Rightarrow \begin{bmatrix} \mathbf{b} \\ \mathbf{F} \end{bmatrix} = \begin{bmatrix} \mathbf{A} & \bar{\mathbf{A}} \\ \mathbf{B} & \bar{\mathbf{B}} \end{bmatrix} \begin{bmatrix} 2\pi i \mathbf{I} & \mathbf{0} \\ \mathbf{0} & -2\pi i \mathbf{I} \end{bmatrix} \begin{bmatrix} \mathbf{q} \\ \bar{\mathbf{q}} \end{bmatrix} \end{aligned}$$

4. Recalling the orthogonality properties of \mathbf{A} and \mathbf{B} ,

$$\begin{bmatrix} \mathbf{B}^T & \mathbf{A}^T \\ \bar{\mathbf{B}}^T & \bar{\mathbf{A}}^T \end{bmatrix} \begin{bmatrix} \mathbf{A} & \bar{\mathbf{A}} \\ \mathbf{B} & \bar{\mathbf{B}} \end{bmatrix} = \begin{bmatrix} \mathbf{I} & \mathbf{0} \\ \mathbf{0} & \mathbf{I} \end{bmatrix},$$

we can solve for \mathbf{q} :

$$\frac{1}{2\pi i} \begin{bmatrix} \mathbf{B}^T & \mathbf{A}^T \\ \bar{\mathbf{B}}^T & \bar{\mathbf{A}}^T \end{bmatrix} \begin{bmatrix} \mathbf{b} \\ \mathbf{F} \end{bmatrix} = \begin{bmatrix} \mathbf{q} \\ \bar{\mathbf{q}} \end{bmatrix},$$

giving

$$\begin{bmatrix} \mathbf{u} \\ \boldsymbol{\varphi} \end{bmatrix} = \frac{1}{2\pi i} \begin{bmatrix} \mathbf{A} & \bar{\mathbf{A}} \\ \mathbf{B} & \bar{\mathbf{B}} \end{bmatrix} \begin{bmatrix} \boldsymbol{\lambda} & \mathbf{0} \\ \mathbf{0} & \bar{\boldsymbol{\lambda}} \end{bmatrix} \begin{bmatrix} \mathbf{B}^T & \mathbf{A}^T \\ \bar{\mathbf{B}}^T & \bar{\mathbf{A}}^T \end{bmatrix} \begin{bmatrix} \mathbf{b} \\ \mathbf{F} \end{bmatrix}.$$

5.5.14 Line Load and Dislocation below the Surface of an Anisotropic Half-Space

Figure 5.46 shows an anisotropic, linear elastic half-space. The elastic properties of the solid are characterized by the Stroh matrices \mathbf{A} , \mathbf{B} , and \mathbf{P} defined in Section 5.5.2. The solid contains a dislocation with Burger's vector \mathbf{b} and is also subjected to a line load with force per unit length \mathbf{F} at a point (d_1, d_2) , whereas the surface of the solid is traction free.

The solution can be computed from the simplified Stroh representation

$$\mathbf{u} = 2\operatorname{Re}(\mathbf{Af}) \quad \boldsymbol{\varphi} = 2\operatorname{Re}(\mathbf{Bf}) \quad \mathbf{t}_2 = 2\operatorname{Re}(\mathbf{Bf}') \quad \mathbf{t}_1 = -2\operatorname{Re}(\mathbf{B}\mathbf{P}\mathbf{f}'),$$

where

$$\mathbf{f} = \boldsymbol{\lambda}(z_i)(\mathbf{B}^T \mathbf{b} + \mathbf{A}^T \mathbf{F}) - \mathbf{B}^{-1} \bar{\mathbf{B}} \overline{\boldsymbol{\lambda}(\bar{z}_i)} (\bar{\mathbf{B}}^T \mathbf{b} + \bar{\mathbf{A}}^T \mathbf{F})$$

and

$$\boldsymbol{\lambda}(z_i) = \frac{1}{2\pi i} \begin{bmatrix} \log(z_1 - (d_1 + p_1 d_2)) & 0 & 0 \\ 0 & \log(z_2 - (d_1 + p_2 d_2)) & 0 \\ 0 & 0 & \log(z_3 - (d_1 + p_3 d_2)) \end{bmatrix}.$$

The first term in the expression for \mathbf{f} will be recognized as the solution for a dislocation and point force in an infinite solid; the second term corrects this solution for the presence of the free surface.

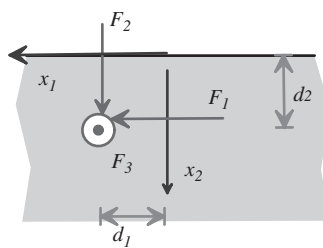


FIGURE 5.46 Line load and dislocation below the surface of an anisotropic elastic solid.

5.6 SOLUTIONS TO DYNAMIC PROBLEMS FOR ISOTROPIC LINEAR ELASTIC SOLIDS

Dynamic problems are even more difficult to solve than static problems. Nevertheless, analytical solutions have been determined for a wide range of important problems. There is not space here to do justice to the subject, but a few solutions will be listed to give a sense of the general features of solutions to dynamic problems.

5.6.1 Love Potentials for Dynamic Solutions for Isotropic Solids

In this section, we outline a general potential representation for 3D dynamic linear elasticity problems. The technique is similar to the 3D Papkovich–Neuber representation for static solutions outlined in Section 5.5.

Figure 5.47 shows a generic problem of interest. Assume the following:

- The solid has Young's modulus E , mass density ρ_0 , and Poisson's ratio ν .
- Define longitudinal and shear wave speeds (see Section 4.4.5)

$$c_L = \sqrt{\frac{E(1-\nu)}{\rho_0(1+\nu)(1-2\nu)}} \quad c_s = \sqrt{\frac{E}{2(1+\nu)\rho_0}}.$$

- Body forces are neglected (a rather convoluted procedure exists for problems involving body force).
- The solid is assumed to be at rest for $t < 0$.
- Part of the boundary S_1 is subjected to time-dependent prescribed displacements u_i^*
- A second part of the boundary S_2 is subjected to prescribed tractions t_i^* .

The procedure can be summarized as follows:

1. Find a vector function $\Psi_i(x_1, x_2, x_3, t)$ and a scalar function $\phi(x_1, x_2, x_3, t)$ that satisfy

$$\frac{\partial \Psi_i}{\partial x_i} = 0 \quad \frac{\partial^2 \Psi_i}{\partial x_j \partial x_j} = \frac{1}{c_s^2} \frac{\partial^2 \Psi_i}{\partial t^2} \quad \frac{\partial^2 \phi}{\partial x_k \partial x_k} = \frac{1}{c_L^2} \frac{\partial^2 \phi}{\partial t^2},$$

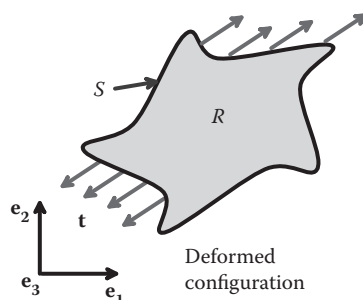


FIGURE 5.47 Representative dynamic problem in linear elasticity.

as well as boundary conditions

$$\frac{\partial \phi}{\partial x_i} + \epsilon_{ijk} \frac{\partial \Psi_k}{\partial x_j} = u_i^* \quad \text{on } S_1$$

$$\frac{\partial^2 \phi}{\partial x_i \partial x_j} n_j + \frac{1}{2} \left(\epsilon_{ilk} \frac{\partial^2 \Psi_k}{\partial x_l \partial x_j} + \epsilon_{jlk} \frac{\partial^2 \Psi_k}{\partial x_l \partial x_i} \right) n_j + \frac{v n_i}{1-2v} \frac{\partial^2 \phi}{\partial x_k \partial x_k} = \frac{(1+v)}{E} t_i^* \quad \text{on } S_2$$

and initial conditions $\Psi_i = \phi = 0$.

2. Calculate displacements from the formula

$$u_i = \frac{\partial \phi}{\partial x_i} + \epsilon_{ijk} \frac{\partial \Psi_k}{\partial x_j}.$$

3. Calculate stresses from the formula

$$\frac{(1+v)}{E} \sigma_{ij} = \frac{\partial^2 \phi}{\partial x_i \partial x_j} + \frac{1}{2} \left(\epsilon_{ilk} \frac{\partial^2 \Psi_k}{\partial x_l \partial x_j} + \epsilon_{jlk} \frac{\partial^2 \Psi_k}{\partial x_l \partial x_i} \right) + \frac{v \delta_{ij}}{1-2v} \frac{\partial^2 \phi}{\partial x_k \partial x_k}.$$

You can easily show that this solution satisfies the equations of motion for an elastic solid, by substituting the formula for displacements into the Cauchy–Navier equation

$$\frac{1}{1-2v} \frac{\partial^2 u_k}{\partial x_k \partial x_i} + \frac{\partial^2 u_i}{\partial x_k \partial x_k} = \rho_0 \frac{\partial^2 u_i}{\partial t^2}.$$

The details are left as an exercise. More importantly, one can also show that the representation is complete, i.e., all dynamic solutions can be derived from some appropriate combination of potentials.

5.6.2 Pressure Suddenly Applied to the Surface of a Spherical Cavity in an Infinite Solid

Figure 5.48 shows a spherical cavity with radius a in an infinite elastic solid with Young's modulus E and Poisson's ratio v . The solid is at rest for $t < 0$. A time $t = 0$, a pressure p is applied to the surface of the hole and thereafter held fixed.

The solution is generated by Love potentials:

$$\Psi_i = 0 \quad \phi = -\frac{(1+v)a^3 p}{2ER} \left\{ 1 - \sqrt{2(1-v)} e^{-\alpha s} \sin(\beta s + \gamma) \right\},$$

where

$$\alpha = \frac{1-2v}{1-v} \quad \beta = \frac{\sqrt{1-2v}}{1-v} \quad \gamma = \cot^{-1} \sqrt{1-2v} \quad R = \sqrt{x_k x_k}$$

$$s = \begin{cases} (c_L t - R + a) / a & R - a < c_L t \\ 0 & R - a > c_L t. \end{cases}$$

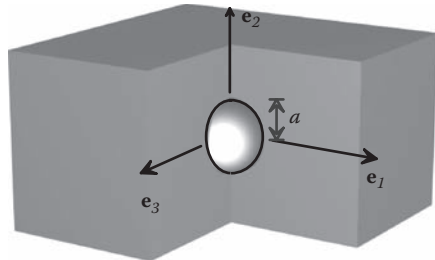


FIGURE 5.48 Cylindrical hole in an infinite solid subjected to a step change in internal pressure.

The displacements and stresses follow as

$$u_i = \frac{(1+\nu)a^3 p x_i}{2ER^3} \left\{ 1 - \sqrt{2(1-\nu)} e^{-\alpha s} \sin(\beta s + \gamma) \left(\frac{\beta R \cot(\beta s + \gamma) - \alpha R}{a} + 1 \right) \right\}$$

$$\sigma_{ij} = -\frac{a^3 p}{2R^3} \left(3 \frac{x_i x_j}{R^2} - \delta_{ij} \right) \left\{ 1 - \sqrt{2(1-\nu)} e^{-\alpha s} \sin(\beta s + \gamma) \left(\frac{\beta R \cot(\beta s + \gamma) - \alpha R}{a} + 1 \right) \right\}$$

$$+ \frac{ap}{2R} \left(\frac{x_i x_j}{R^2} + \frac{\nu \delta_{ij}}{1-2\nu} \right) \sqrt{2(1-\nu)} e^{-\alpha s} \sin(\beta s + \gamma) \{ (\alpha^2 - \beta^2) - 2\beta\alpha \cot(\beta s + \gamma) \}.$$

The radial and hoop stresses at several time intervals are plotted in Figure 5.49. Observe the following:

1. A wave front propagates out from the cavity at the longitudinal wave speed c_L .
2. Unlike the simple 2D wave problems discussed in Section 4.4, the stress is not constant behind the front. Instead, each point in the solid experiences a

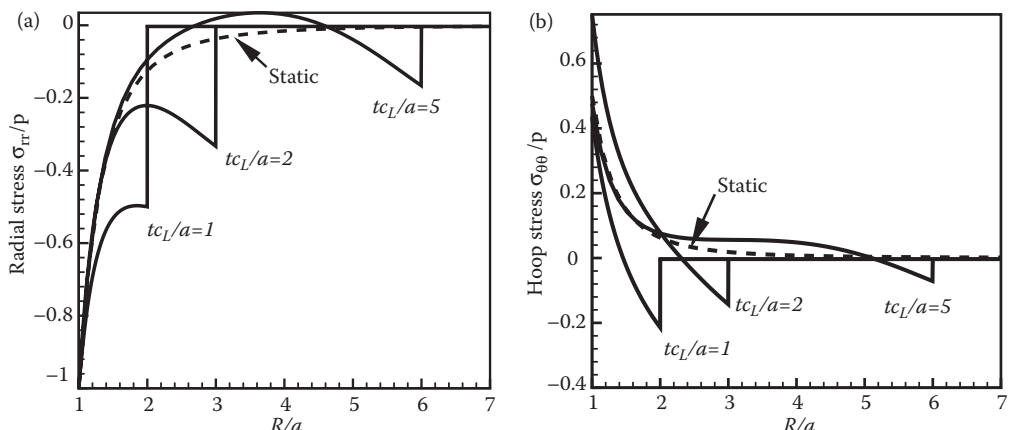


FIGURE 5.49 Variation of stress around a cylindrical hole in an infinite solid at various time intervals. (a) Radial stress; (b) hoop stress.

damped oscillation in displacement and stress that eventually decays to the static solution.

3. Both the radial and hoop stress reverse sign as the wave passes by. For this reason, dynamic loading can cause failures to occur in very unexpected places.
4. The maximum stress induced by dynamic loading substantially exceeds the static solution.

5.6.3 Rayleigh Waves

A Rayleigh wave is a special type of wave that propagates near the surface of an elastic solid. Assume the following:

- The solid is an isotropic, linear elastic material with Young's modulus E , Poisson's ratio ν , and mass density ρ_0 .
- The solid has shear wave speed c_s and longitudinal wave speed c_L .
- The surface is free of tractions.
- A Rayleigh wave with wavelength λ propagates in the x_1 direction, as shown in Figure 5.50.

The displacement and stress attributable can be derived from Love potentials:

$$\phi = \frac{U_0(k^2 + \beta_T^2)}{\beta_L(k^2 - \beta_T^2)} \exp(-\beta_L x_2) \exp(ik(x_1 - c_R t)) \quad \Psi_k = \frac{2ikU_0\delta_{k3}}{(k^2 - \beta_T^2)} \exp(-\beta_T x_2) \exp(ik(x_1 - c_R t)),$$

where $i = \sqrt{-1}$, U_0 is the amplitude of the vertical displacement at the free surface, $k = 2\pi/\lambda$ is the wave number, $\beta_L = k\sqrt{1 - c_R^2/c_L^2}$, $\beta_T = k\sqrt{1 - c_R^2/c_s^2}$, and c_R is the Rayleigh wave speed, which is the positive real root of

$$\left(2 - \frac{c_R^2}{c_s^2}\right)^2 - 4\left(1 - \frac{(1-2\nu)}{2(1-\nu)} \frac{c_R^2}{c_s^2}\right)^{1/2} \left(1 - \frac{c_R^2}{c_s^2}\right)^{1/2} = 0.$$

This equation can easily be solved for c_R/c_s with a symbolic manipulation program, which will most likely return six roots. The root of interest lies in the range $0.65 < c_R/c_s < 1$ for

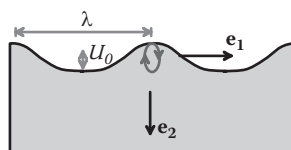


FIGURE 5.50 Rayleigh wave propagating at the surface of an elastic solid.

$-1 < v < 0.5$. The solution can be approximated by $c_R/c_s = 0.875 - 0.2v - 0.05(v + 0.25)^3$ with an error of less than 0.6% over the full range of Poisson's ratio.

The nonzero components of displacement and stress follow as

$$u_1 = \frac{U_0 ik}{(k^2 - \beta_T^2)\beta_L} \exp(ik(x_1 - c_R t)) \left\{ (k^2 + \beta_T^2) \exp(-\beta_L x_2) - 2\beta_L \beta_T \exp(-\beta_T x_2) \right\}$$

$$u_2 = \frac{U_0}{(k^2 - \beta_T^2)} \exp(ik(x_1 - c_R t)) \left\{ 2k^2 \exp(-\beta_T x_2) - (k^2 + \beta_T^2) \exp(-\beta_L x_2) \right\}$$

$$\sigma_{11} = \frac{U_0 E \exp(ik(x_1 - c_R t))}{(k^2 - \beta_T^2)(1+v)(1-2v)\beta_L} \left\{ k^2 [v(\beta_L^2 + \beta_T^2) - (1-v)(k^2 + \beta_T^2)] \exp(-\beta_L x_2) + 2k^2 \beta_T \beta_L (1-2v) \exp(-\beta_T x_2) \right\}$$

$$\sigma_{22} = \frac{U_0 E \exp(ik(x_1 - c_R t))}{(k^2 - \beta_T^2)(1+v)(1-2v)\beta_L} \left\{ (k^2 + \beta_T^2) [(1-v)\beta_L^2 - v k^2] \exp(-\beta_L x_2) - 2k^2 \beta_T \beta_L (1-2v) \exp(-\beta_T x_2) \right\}$$

$$\sigma_{12} = \frac{i U_0 k E (k^2 + \beta_T^2)}{(k^2 - \beta_T^2)(1+v)} \exp(ik(x_1 - c_R t)) \left\{ \exp(-\beta_T x_2) - \exp(-\beta_L x_2) \right\}.$$

You can use either the real or imaginary part of these expressions for the displacement and stress fields (they are identical, except for a phase difference). Of course, if you choose to take the real part of one of the functions, you must take the real part for all the others as well. Note that substituting $x_2 = 0$ in the expression for σ_{22} and setting $\sigma_{22} = 0$ yields the equation for the Rayleigh wave speed, so the boundary condition $\sigma_{22} = 0$ is satisfied. The variations with depth of stress amplitude and displacement amplitude are plotted in Figure 5.51.

Important features of this solution are as follows:

1. The wave is confined to a layer near the surface with thickness about twice the wavelength.
2. The horizontal and vertical components of displacement are 90° out of phase. Material particles therefore describe elliptical orbits as the wave passes by.
3. The speed of the wave is independent of its wavelength, that is to say, the wave is nondispersive.
4. Rayleigh waves are exploited in a range of engineering applications, including surface acoustic wave devices, touch sensors, and miniature linear motors. They are also observed in earthquakes, although these waves are observed to be dispersive, because of density variations of the earth's surface.

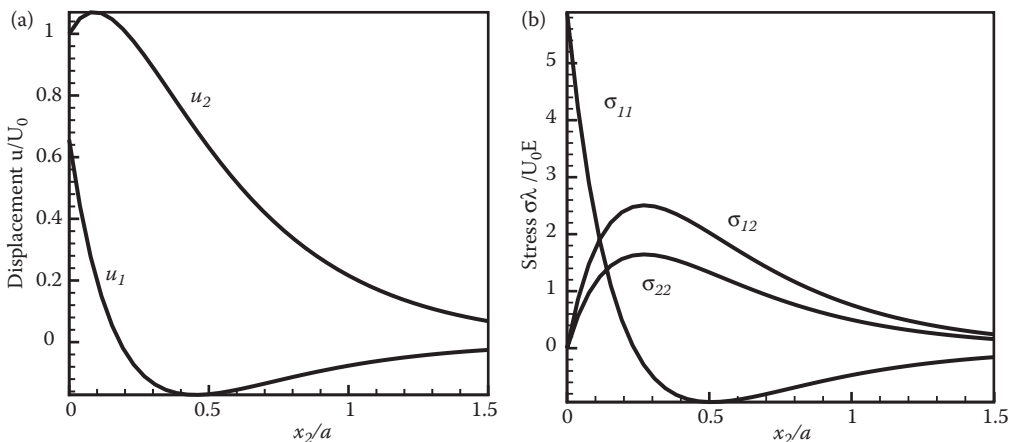


FIGURE 5.51 Variation of displacement and stress below the peak of a Rayleigh wave on an elastic solid. (a) Displacement fields; (b) stress fields.

5.6.4 Love Waves

Love waves are a second form of surface wave, somewhat similar to Rayleigh waves, which propagate through a thin elastic layer bonded to the surface of an elastic half-space (Figure 5.52). Love waves involve motion perpendicular to the plane of the figure. Assume the following:

- The layer has thickness H , shear modulus μ_f , and shear wave speed c_{sf} .
- The substrate has shear modulus μ and shear wave speed c_s .
- The wave speeds satisfy $c_{sf} < c_s$.

The displacement and stress associated with a harmonic Love wave with wavelength λ , which propagates in the x_1 direction can be derived from Love potentials:

$$\Psi_k = \begin{cases} -U_0 \frac{{}_f\gamma \delta_{k1} \exp(-\beta x_2)}{\beta(\beta \sin \gamma H + {}_f\gamma \cos \gamma H)} \exp(ik(x_1 - ct)) & x_2 > 0 \\ \frac{U_0 \delta_{k1} (\beta \cos(\gamma x_2) + {}_f\gamma \sin(\gamma x_2))}{\gamma(\beta \sin \gamma H + {}_f\gamma \cos \gamma H)} \exp(ik(x_1 - ct)) & x_2 < 0, \end{cases}$$

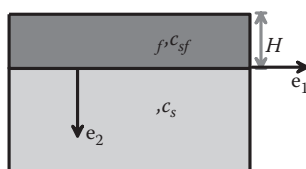


FIGURE 5.52 Elastic layer on the surface of a half-space.

where U_0 is the amplitude of the vertical displacement at the free surface, $k = 2\pi/\lambda$ is the wave number, $\beta = k\sqrt{1 - c^2/c_s^2}$, $\gamma = k\sqrt{c^2/c_{sf}^2 - 1}$, and c is the wave speed (also known as the *phase velocity*) of the wave, which is given by the positive real roots of

$$\tan \left\{ kH \sqrt{\frac{c^2}{c_{sf}^2} - 1} \right\} - \frac{\sqrt{1 - c^2/c_s^2}}{f \sqrt{c^2/c_{sf}^2 - 1}} = 0.$$

This relationship is very unlike the equations for wave speeds in unbounded or semi-infinite solids and leads to a number of counter-intuitive results. Note the following:

1. The wave speed depends on its wavelength. A wave with these properties is said to be *dispersive*, because a pulse consisting of a spectrum of harmonic waves tends to spread out.
2. The wave speed is always faster than the shear wave speed of the layer but less than the wave speed in the substrate.
3. If a wave with wave number k_0 propagates at speed c , then waves with wave number $k_n = k_0 + n\pi/H\sqrt{c^2/c_{sf}^2 - 1}$, where n is any integer, also propagate at the same speed. These waves are associated with different *propagation modes* for the wave. Each propagation mode has a characteristic displacement distribution through the thickness of the layer, as discussed below.
4. A wave with a particular wave number can propagate at several different speeds, depending on the mode. The number of modes that can exist at a particular wave number increases with the wave number. You can see this in the plot of wave speed-versus-wave number in Figure 5.53a.
5. Dispersive wave motion is often characterized by relating the *frequency* of the wave to its wave number rather than by relating wave speed to wave number. The (angular) frequency is related to wave number and wave speed by the usual formula $\omega = ck$. Substituting this result into the equation for wave speed yields the *dispersion relation* for the wave:

$$\tan \left\{ \sqrt{(\omega H/c_{sf})^2 - (kH)^2} \right\} - \frac{\sqrt{(kH)^2 - (\omega H/c_s)^2}}{f \sqrt{(\omega H/c_{sf})^2 - (kH)^2}} = 0.$$

The nonzero displacement component is

$$u_3 = \begin{cases} \frac{-U_0(\beta \sin(\gamma x_2) - f \gamma \cos(\gamma x_2))}{(\beta \sin \gamma H + f \gamma \cos \gamma H)} \exp(ik(x_1 - ct)) & x_2 < 0 \\ \frac{U_0 f \gamma \exp(-\beta x_2)}{(\beta \sin \gamma H + f \gamma \cos \gamma H)} \exp(ik(x_1 - ct)) & x_2 > 0. \end{cases}$$

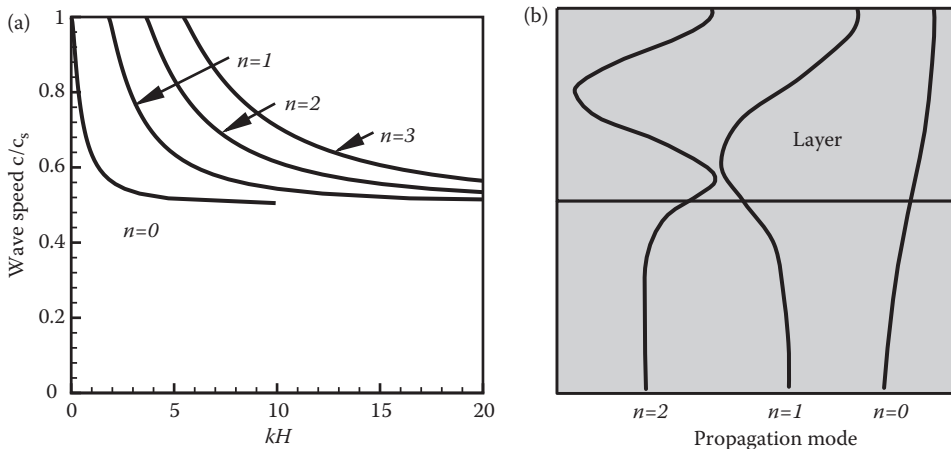


FIGURE 5.53 Propagation modes for a Love wave. (a) Wave speeds; (b) displacement distributions.

The nonzero stresses in the layer can be determined from $\sigma_{3i} = \mu_f \partial u_3 / \partial x_i$, but the calculation is so trivial that the result will not be written out here. The wave speed is plotted as a function of wave number in Figure 5.53a, for the particular case $\mu = \mu_f$, $c_s/c_{sf} = 2$. The displacement amplitude as function of depth is shown for several modes in Figure 5.53b.

5.6.5 Elastic Waves in Waveguides

The surface layer discussed in the preceding section is an example of a wave guide: it is a structure that causes waves to propagate in a particular direction, as a result of the confining effect of its geometry. Figure 5.54 shows a much simpler example of a wave guide: it is a thin sheet of material, with thickness H and infinite length in the x_1 and x_3 directions. The strip can guide three types of wave:

1. Transverse waves, which propagate in the x_1 direction with particle motion in the x_3 direction
2. Flexural waves, which propagate in the x_1 direction with particle motion in the x_2 direction
3. Longitudinal waves, which propagate in the x_1 direction with particle motion in the x_1 direction

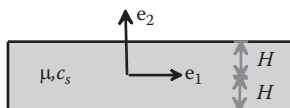


FIGURE 5.54 An elastic strip acting as a wave guide.

The solutions for cases 2 and 3 are lengthy, but the solution for case 1 is simple and can be used to illustrate the general features of waves in wave guides. For transverse waves,

1. The wave can be any member of the following family of possible displacement distributions:

$$u_3 = U_0 \{ \sin^2(\pi n/2) \sin(n\pi x_2/2H) + \cos^2(\pi n/2) \cos(n\pi x_2/2H) \} \exp(ik(x_1 - ct)),$$

where $n = 0, 1, 2 \dots$, and you can use either the real or imaginary part as the solution. This displacement represents a harmonic wave that has wave number $k = 2\pi/\lambda$, where λ is the wavelength in the x_1 direction, which propagates in the x_1 direction with speed c . The variation of displacement with x_2 at any fixed value of x_1 is a standing wave with wavelength H/n and angular frequency $\omega = kc$. Each value of n corresponds to a different propagation mode.

2. The speed of wave propagation (usually referred to as the phase velocity of the wave) satisfies

$$\frac{c^2}{c_s^2} = \left(\frac{n\pi}{2kH} \right)^2 + 1.$$

3. The wave speeds for modes with $n > 0$ depend on the wave number, i.e., the waves are dispersive.
4. There are an infinite number of possible wave speeds for each wave number. Each wave speed is associated with a particular propagation mode n .
5. The formula for wave speed can be rewritten as an equation relating the angular frequency $\omega = kc$ to the wave number k :

$$\left(\frac{\omega H}{c_s} \right)^2 = \left(\frac{n\pi}{2} \right)^2 + (kH)^2.$$

This is called the dispersion relation for the wave.

6. Dispersive waves have a second wave speed associated with them called the *group velocity*. This wave speed is defined as the slope of the dispersion relation $c_g = d\omega/dk$ (in contrast, the phase velocity is $c = \omega/k$). For the wave guide considered here,

$$c_g = \frac{d\omega}{dk} = \frac{c_s k H}{\sqrt{(n\pi/2)^2 + (kH)^2}}.$$

The group velocity, like the phase velocity, depends on the propagation mode and the wave number. The group velocity has two physical interpretations: (1) it is the speed at which the energy in a harmonic wave propagates along the waveguide, and (2) it is the propagation speed of an amplitude modulated wave of the form

$$\begin{aligned} u_3 &= U_0 \cos(\Delta k x_1 - \Delta \omega t) \sin(k x_1 - \omega t) \\ &= U_0 \{ \sin[(k + \Delta k)x_1 - (\omega + \Delta \omega)t] + \sin[(k - \Delta k)x_1 - (\omega - \Delta \omega)t] \} / 2 \end{aligned}$$

where $\Delta k \ll k$ and $\Delta\omega \ll \omega$ are the wave number and frequency of the modulation, and k, ω are the wave number and frequency of the carrier wave. The carrier wave propagates with speed c , whereas the modulation (which can be regarded as a “group” of wavelets) propagates at speed c_g . Note that, for a nondispersive wave, the group and phase velocities are the same.

5.7 ENERGY METHODS FOR SOLVING STATIC LINEAR ELASTICITY PROBLEMS

You may recall that energy methods can often be used to simplify complex problems. For example, to find the equilibrium configuration of a discrete system, you would begin by identifying a suitable set of generalized coordinates q_i and then express the potential energy in terms of these: $V(q_i)$. The equilibrium values of the generalized coordinates could then be determined from the condition that the potential energy is stationary at equilibrium: this gives a set of equations $\partial V / \partial q_i = 0$ that could be solved for q_i .

In this section, we will develop an analogous procedure for solving boundary value problems in linear elasticity. Our generalized coordinates will be the displacement field $u_i(\mathbf{x})$. We will find an expression for the potential energy of an elastic solid in terms of u_i and then show that the potential energy is stationary if the solid is in equilibrium. We will find, furthermore, that the potential energy is not only stationary but is always a minimum, implying that equilibrium configurations in linear elasticity problems are always stable. (This is because the approximations made in setting up the equations of linear elasticity preclude any possibility of buckling.) This principle will be referred to as the *principle of minimum potential energy*.

The main application of the principle is to generate approximate solutions to linear elastic boundary value problems. Indeed, the principle will form the basis of the FEM in linear elasticity.

5.7.1 Definition of the Potential Energy of a Linear Elastic Solid under Static Loading
In the following, we consider a generic static boundary value problem in linear elasticity, as shown in Figure 5.55.

As always, we assume that we are given the following:

1. The shape of the solid in its unloaded condition R
2. The initial stress field in the solid (we will take this to be zero)
3. The elastic constants for the solid C_{ijkl} and its mass density ρ_0
4. The thermal expansion coefficients for the solid and temperature change from the initial configuration ΔT
5. A body force distribution \mathbf{b} (per unit mass) acting on the solid
6. Boundary conditions, specifying displacements $\mathbf{u}^*(\mathbf{x})$ on a portion $\partial_1 R$ or tractions on a portion $\partial_2 R$ of the boundary of R

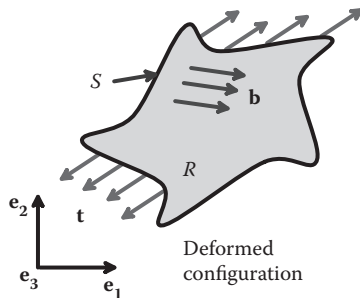


FIGURE 5.55 An elastic solid subjected to external loads.

5.7.1.1 Kinematically Admissible Displacement Fields

A “kinematically admissible displacement field” $v_i(\mathbf{x})$ is any displacement field with the following properties:

1. v_i is continuous everywhere within the solid.
2. v_i is differentiable everywhere within the solid, so that a strain field may be computed as

$$\hat{\varepsilon}_{ij} = \frac{1}{2} \left(\frac{\partial v_i}{\partial x_j} + \frac{\partial v_j}{\partial x_i} \right).$$

3. v_i satisfies boundary conditions anywhere that displacements are prescribed, i.e., $\mathbf{v}(\mathbf{x}) = \mathbf{u}^*(\mathbf{x})$ on the portion $\partial_1 R$ on the boundary.

Note the \mathbf{v} is not necessarily the actual displacement in the solid; it is just an arbitrary displacement field that satisfies the displacement boundary conditions. You can think of it as a possible displacement field that the solid could adopt. Of all these possible displacement fields, it will actually select the one that minimizes the potential energy.

The kinematically admissible displacement field can also be thought of as a system of generalized coordinates in the context of analytical mechanics. Recall that, to use a set of generalized coordinates in Lagrange's equations, you must ensure that the system of coordinates satisfies all the constraints. Similarly, to be admissible, our displacement field must satisfy constraints on the boundary.

5.7.1.2 Definition of Potential Energy of an Elastic Solid

Next, we will define the potential energy of a solid. The definition may look a bit strange, because it seems to give different values for potential energy depending on how the solid is loaded. This is true. But who cares, as long as the definition is useful?

For any kinematically admissible displacement field \mathbf{v} , the potential energy is

$$V(\mathbf{v}) = \int_V U(\mathbf{v}) dV - \int_V \rho_0 b_i v_i dV - \int_{\partial_2 R} t_i v_i dA,$$

where

$$U(\mathbf{v}) = \frac{1}{2} C_{ijkl} (\hat{\epsilon}_{ij} - \alpha_{ij} \Delta T) (\hat{\epsilon}_{kl} - \alpha_{kl} \Delta T)$$

is the strain energy density associated with the kinematically admissible displacement field. You can interpret the three terms in the formula for V as the strain energy stored inside the solid, the work done by body forces, and the work done by surface tractions. For the particular case of an isotropic material, with $\Delta T = 0$, we see that

$$U(\mathbf{v}) = \frac{E}{2(1+\nu)} \left(\hat{\epsilon}_{ij} \hat{\epsilon}_{ij} + \frac{\nu}{1-2\nu} \hat{\epsilon}_{kk} \hat{\epsilon}_{mm} \right).$$

5.7.2 Principle of Stationary and Minimum Potential Energy

Let \mathbf{v} be any kinematically admissible displacement field. Let \mathbf{u} be the actual displacement field, i.e., the one that satisfies the equilibrium equations within the solid as well as all the boundary conditions. We will show the following:

1. $V(\mathbf{v})$ is stationary (i.e., a local minimum, maximum or inflexion point) for $\mathbf{v} = \mathbf{u}$.
2. $V(\mathbf{v})$ is a global minimum for $\mathbf{v} = \mathbf{u}$.

As a preliminary step, recall that the actual displacement field satisfies the following equations:

$$\begin{aligned} \epsilon_{ij} &= \frac{1}{2} \left(\frac{\partial u_i}{\partial x_j} + \frac{\partial u_j}{\partial x_i} \right) & \sigma_{ij} &= C_{ijkl} (\epsilon_{kl} - \alpha_{kl} \Delta T) & \frac{\partial \sigma_{ij}}{\partial x_i} + \rho_0 b_j &= 0 \\ u_i &= u_i^* \quad \text{on } \partial_1 R & \sigma_{ij} n_i &= t_j^* \quad \text{on } \partial_2 R. \end{aligned}$$

Next, rewrite the kinematically admissible displacement field in terms of \mathbf{u} as

$$v_i = u_i + \delta u_i,$$

where δu_i is the difference between the kinematically admissible field and the correct equilibrium field. Observe that

$$\begin{aligned} v_i &= u_i^* & u_i &= u_i^* & \text{on } \partial_1 R \\ \Rightarrow \delta u_i &= 0 & & & \text{on } \partial_1 R, \end{aligned}$$

i.e., the difference between the kinematically admissible field and the actual field is zero wherever displacements are prescribed.

Now, note that $V(\mathbf{v})$ can be expressed in terms of u_i and δu_i as

$$V(\mathbf{u} + \delta\mathbf{u}) = V(\mathbf{u}) + \delta V + \frac{1}{2}\delta^2 V,$$

where

$$\begin{aligned} \delta V &= \int_V C_{ijkl} (\varepsilon_{ij} - \alpha_{ij} \Delta T) \delta \varepsilon_{kl} dV - \int_V b_i \delta u_i dV - \int_{\partial_2 R} t_i \delta u_i dA \quad \delta^2 V = \int_V C_{ijkl} \delta \varepsilon_{ij} \delta \varepsilon_{kl} \\ \varepsilon_{ij} &= \frac{1}{2} \left(\frac{\partial u_i}{\partial x_j} + \frac{\partial u_j}{\partial x_i} \right) \quad \delta \varepsilon_{ij} = \frac{1}{2} \left(\frac{\partial \delta u_i}{\partial x_j} + \frac{\partial \delta u_j}{\partial x_i} \right). \end{aligned}$$

To see this, simply substitute into the definition of the potential energy

$$\begin{aligned} V(\mathbf{v}) &= \int_V U(\mathbf{u} + \delta\mathbf{u}) dV - \int_V b_i (u_i + \delta u_i) dV - \int_{\partial_2 R} t_i (u_i + \delta u_i) dA \\ &= \int_V \frac{1}{2} C_{ijkl} (\varepsilon_{ij} - \alpha_{ij} \Delta T + \delta \varepsilon_{ij}) (\varepsilon_{kl} - \alpha_{kl} \Delta T + \delta \varepsilon_{kl}) dV - \int_V b_i (u_i + \delta u_i) dV - \int_{\partial_2 R} t_i (u_i + \delta u_i) dA. \end{aligned}$$

Multiply everything out and use the condition that $C_{ijkl} = C_{klji}$ to get the result stated.

Now, to show that $V(\mathbf{v})$ is stationary at $\mathbf{v} = \mathbf{u}$, we need to show that $\delta V = 0$. This means that, if we add any small change $\delta\mathbf{u}$ to the actual displacement field \mathbf{u} , the change in potential energy will be zero, to first order in $\delta\mathbf{u}$.

To show this, note that

$$C_{ijkl} (\varepsilon_{ij} - \alpha_{ij} \Delta T) = \sigma_{kl}.$$

Next, note that

$$\sigma_{kl} \delta \varepsilon_{kl} = \sigma_{kl} \frac{1}{2} \left(\frac{\partial \delta u_k}{\partial x_l} + \frac{\partial \delta u_l}{\partial x_k} \right) = \frac{1}{2} \sigma_{lk} \frac{\partial \delta u_k}{\partial x_l} + \frac{1}{2} \sigma_{kl} \frac{\partial \delta u_l}{\partial x_k} = \sigma_{kl} \frac{\partial \delta u_l}{\partial x_k},$$

where we have used the fact that $\sigma_{kl} = \sigma_{lk}$ (angular momentum balance). Rewrite this as

$$\sigma_{ij} \frac{\partial \delta u_j}{\partial x_i} = \frac{\partial}{\partial x_i} (\sigma_{ij} \delta u_j) - \frac{\partial \sigma_{ij}}{\partial x_i} \delta u_j.$$

Substitute back into the expression for δV and rearrange to see that

$$\delta V = \int_V \frac{\partial}{\partial x_i} (\sigma_{ij} \delta u_j) dV - \int_V \left(\frac{\partial \sigma_{ij}}{\partial x_i} + \rho_0 b_j \right) \delta u_j dV - \int_{\partial_2 R} t_i \delta u_i dA.$$

Now, recall the equations of equilibrium

$$\frac{\partial \sigma_{ij}}{\partial x_i} + \rho_0 b_j = 0$$

so that the second term vanishes. Apply the divergence theorem to express the first integral as a surface integral

$$\int_V \frac{\partial}{\partial x_i} (\sigma_{ij} \delta u_j) dV = \int_A \sigma_{ij} \delta u_j n_i dA.$$

Recall that $\delta u_i = 0$ on $\partial_1 R$ and note that

$$\int_A dA = \int_{\partial_1 R} dA + \int_{\partial_2 R} dA$$

because either tractions or displacements (but not both) must be prescribed on every point on the boundary.

Therefore,

$$\int_V \frac{\partial}{\partial x_i} (\sigma_{ij} \delta u_j) dV = \int_A \sigma_{ij} \delta u_j n_i dA = \int_{\partial_1 R} \sigma_{ij} n_i \delta u_j dA + \int_{\partial_2 R} \sigma_{ij} n_i \delta u_j dA = \int_{\partial_2 R} \sigma_{ij} n_i \delta u_j dA.$$

Finally, recall that

$$\sigma_{ij} n_i = t_j \quad \text{on } \partial_2 R$$

and substitute back into the expression for δV to see that

$$\delta V = \int_{\partial_2 R} (\sigma_{ji} n_j - t_i \delta u_i) dA = 0.$$

This proves that $V(\mathbf{v})$ is stationary at $\mathbf{v} = \mathbf{u}$, as stated.

Finally, we want to show that $V(\mathbf{v})$ is a minimum at $\mathbf{v} = \mathbf{u}$. This is easy. Note that we have proved that

$$V(\mathbf{v}) = V(\mathbf{u}) + \frac{1}{2} \delta^2 V$$

$$\delta^2 V = \int_V C_{ijkl} \delta \epsilon_{ij} \delta \epsilon_{kl} .$$

Note that

$$\frac{1}{2} C_{ijkl} \delta \varepsilon_{kl} \delta \varepsilon_{ij}$$

is the strain energy density associated with a strain $\delta \varepsilon_{ij}$. Strain energy density must always be positive or zero, so that

$$V(\mathbf{v}) \geq V(\mathbf{u}).$$

5.7.3 Uniaxial Compression of a Cylinder Solved by Energy Methods

Consider a cylindrical bar subjected to a uniform pressure p on one end and supported on a rigid, frictionless base, as shown in Figure 5.56. Neglect temperature changes. Determine the displacement field in the bar.

We will solve this problem using energy methods. We will guess a displacement field of the form

$$v_1 = \lambda_1 x_1, \quad v_2 = \lambda_2 x_2, \quad v_3 = \lambda_3 x_3.$$

This satisfies the boundary conditions on the bottom face of the cylinder, so it is a kinematically admissible displacement field. The coefficients λ_i are to be determined, by minimizing the potential energy. The strains follow as

$$\varepsilon_{11} = \lambda_1, \quad \varepsilon_{22} = \lambda_2, \quad \varepsilon_{33} = \lambda_3$$

with all other strain components zero. The strain energy density is

$$U = \frac{E}{2(1+\nu)} \left\{ \lambda_1^2 + \lambda_2^2 + \lambda_3^2 + \frac{\nu}{1-2\nu} (\lambda_1 + \lambda_2 + \lambda_3)^2 \right\}.$$

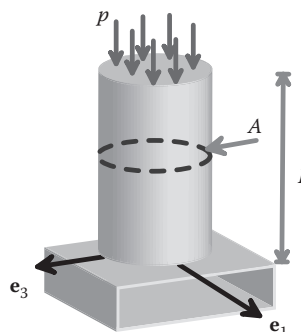


FIGURE 5.56 Elastic cylinder subjected to pressure on one end.

The boundary conditions are as follows:

1. On the bottom of the cylinder, $v_2 = 0, t_1 = t_3 = 0 \Rightarrow v_i t_i = 0$.
2. On the sides of the cylinder, $t_i = 0 \Rightarrow v_i t_i = 0$.
3. On the top of the cylinder, $v_2(L) = \lambda_2 L, t_2 = -p, t_1 = t_3 = 0 \Rightarrow v_i t_i = -p \lambda_2 L$.

Substitute into the expression for strain energy density to see that

$$\begin{aligned} V(\mathbf{v}) &= \int_V \frac{E}{2(1+\nu)} \left\{ \lambda_1^2 + \lambda_2^2 + \lambda_3^2 + \frac{\nu}{1-2\nu} (\lambda_1 + \lambda_2 + \lambda_3)^2 \right\} dV - \int_A \lambda_2 L (-p) \\ &= \frac{ALE}{2(1+\nu)} \left\{ \lambda_1^2 + \lambda_2^2 + \lambda_3^2 + \frac{\nu}{1-2\nu} (\lambda_1 + \lambda_2 + \lambda_3)^2 \right\} + A\lambda_2 L p. \end{aligned}$$

Now, the actual displacement field minimizes V . This requires

$$\frac{\partial V}{\partial \lambda_1} = \frac{\partial V}{\partial \lambda_2} = \frac{\partial V}{\partial \lambda_3} = 0.$$

Evaluate the derivatives to see that

$$\begin{aligned} \frac{ALE}{2(1+\nu)} \left\{ 2\lambda_1 + \frac{2\nu}{1-2\nu} (\lambda_1 + \lambda_2 + \lambda_3) \right\} &= 0 \\ \frac{ALE}{2(1+\nu)} \left\{ 2\lambda_2 + \frac{2\nu}{1-2\nu} (\lambda_1 + \lambda_2 + \lambda_3) \right\} + ALp &= 0 \\ \frac{ALE}{2(1+\nu)} \left\{ 2\lambda_3 + \frac{2\nu}{1-2\nu} (\lambda_1 + \lambda_2 + \lambda_3) \right\} &= 0. \end{aligned}$$

It is easy to solve these equations to see that

$$\lambda_1 = -p/E, \quad \lambda_2 = \lambda_3 = \nu p/E.$$

This is, of course, the exact solution, which is reassuring. Notice that we never had to calculate stresses or worry about equilibrium; the variational principle takes care of all that for us.

Let us solve the same problem, but this time with displacement boundary conditions on the top of the cylinder, as shown in Figure 5.57.

The cylinder has unstretched length L and is stretched between frictionless grips to length $L + h$. This time, the kinematically admissible displacement field must satisfy boundary conditions on both top and bottom surface of the cylinder. Therefore, we choose

$$v_1 = \lambda_1 x_1, \quad v_2 = h x_2/L, \quad v_3 = \lambda_3 x_3.$$

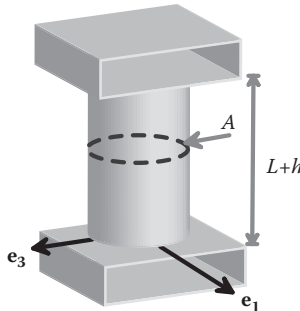


FIGURE 5.57 Elastic cylinder subjected to prescribed axial displacement.

Proceeding as before, we now find that the potential energy is

$$V(\mathbf{v}) = \frac{ALE}{2(1+\nu)} \left\{ \lambda_1^2 + \frac{h^2}{L^2} + \lambda_3^2 + \frac{\nu}{1-2\nu} \left(\lambda_1 + \frac{h}{L} + \lambda_3 \right)^2 \right\}.$$

Note that, this time, there is no contribution to the potential energy from the tractions on the top of the cylinder, because now the displacement is prescribed there instead of the pressure. Minimizing the potential energy as before,

$$\begin{aligned} \frac{ALE}{2(1+\nu)} \left\{ 2\lambda_1 + \frac{2\nu}{1-2\nu} \left(\lambda_1 + \frac{h}{L} + \lambda_3 \right) \right\} &= 0 \\ \frac{ALE}{2(1+\nu)} \left\{ 2\lambda_3 + \frac{2\nu}{1-2\nu} \left(\lambda_1 + \frac{h}{L} + \lambda_3 \right) \right\} &= 0. \end{aligned}$$

Solve these equations to conclude that

$$\lambda_1 = \lambda_3 = -\nu \frac{h}{L}.$$

Again, this is the exact solution.

5.7.4 Variational Derivation of the Beam Equations

Variational methods can be used to solve boundary value problems exactly, as described in the preceding section. The real power of variational methods, however, is to provide a systematic way to find approximate solutions to boundary value problems. We will illustrate this by rederiving the equations governing beam bending theory using the principle of minimum potential energy.

Consider a slender rod with rectangular cross section, subjected to uniform pressure $q(x)$ on its top surface, as shown in Figure 5.58. Assume that the rod is an isotropic, linear elastic solid with Young's modulus E and Poisson's ratio ν . The boundary conditions at the ends of the bar will be left unspecified for the time being.

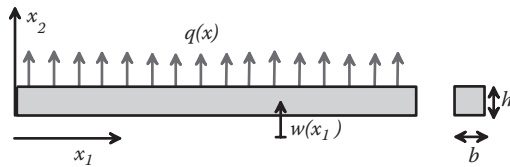


FIGURE 5.58 Beam subjected to transverse loading.

We proceed by approximating the strain field within the bar. Figure 5.59 shows the deflected beam. We will suppose that the strains at any given cross section are completely characterized by the local curvature of the beam so that, at a given cross section x ,

$$\varepsilon_{11} = \frac{-(x_2 - y_0)}{R(x_1)} \quad \varepsilon_{22} = \varepsilon_{33} = -\nu\varepsilon_{11} \quad \varepsilon_{12} = \varepsilon_{13} = \varepsilon_{23} = 0.$$

Here, y_0 is the height of a fiber in the beam whose length is unchanged: y_0 must be determined as part of the solution.

The displacement and strain fields are therefore completely characterized by y_0 and $R(x)$. Rather than solve for R , we will approximate the curvature at x by the second derivative of the vertical deflection w , so that

$$\varepsilon_{11} = \frac{-(x_2 - y_0)}{R(x_1)} \approx -(x_2 - y_0) \frac{d^2 w(x_1)}{dx_1^2}.$$

Now, we want to find $w(x)$ and y_0 that will best approximate the actual displacement field within the bar. We will do this by choosing w and y_0 so as to minimize the potential energy of the solid.

Begin by computing the potential energy. It is straightforward to show that the strain energy density is

$$\phi = \frac{1}{2} E \left\{ (x_2 - y_0) \frac{d^2 w(x_1)}{dx_1^2} \right\}^2.$$

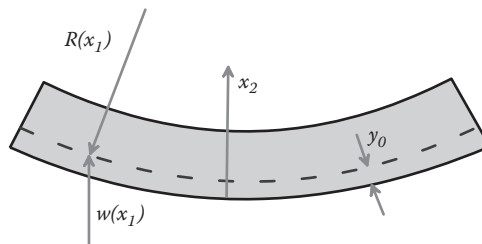


FIGURE 5.59 Bending deformation of a beam.

Hence,

$$V(w, y_0) = \int_0^L \int_A \frac{1}{2} E \left\{ (x_2 - y_0) \frac{d^2 w(x_1)}{dx_1^2} \right\}^2 dA dx_1 - \int_0^L b q(x_1) w(x_1) dx_1.$$

Here, we have neglected the small additional deflection of the beam surface attributable to ε_{22} .

We now want to minimize V with respect to w and y_0 . Do the latter first:

$$\frac{\partial V(w, y_0)}{\partial y_0} = \int_0^L \int_A E \left\{ (x_2 - y_0) \frac{d^2 w(x_1)}{dx_1^2} \right\} dA dx_1 = 0,$$

which is evidently satisfied for any w by choosing

$$y_0 = \frac{1}{A} \int_A x_2 dA.$$

This is the usual expression for the position of the neutral axis of a beam. We can now simplify our expression for potential energy by defining

$$I = \frac{1}{A} \int_A (x_2 - y_0)^2 dA$$

so that

$$V(w) = \int_0^L \frac{1}{2} EI \left\{ \frac{d^2 w(x_1)}{dx_1^2} \right\}^2 dx_1 - \int_0^L b q(x_1) w(x_1) dx_1.$$

Now turn to the more difficult problem of finding w that will minimize V . To do this, let us calculate the change in V when w is changed slightly to $w + \delta w$:

$$\begin{aligned} V(w + \delta w) - V(w) &= \int_0^L \frac{1}{2} EI \left\{ \frac{d^2 w(x_1)}{dx_1^2} + \frac{d^2 \delta w(x_1)}{dx_1^2} \right\}^2 dx_1 - \int_0^L b q(x_1) \{w(x_1) + \delta w(x_1)\} dx_1 \\ &\quad - \int_0^L \frac{1}{2} EI \left\{ \frac{d^2 w(x_1)}{dx_1^2} \right\}^2 dx_1 - \int_0^L b q(x_1) w(x_1) dx_1. \end{aligned}$$

Expand this out to see that

$$\begin{aligned} V(w + \delta w) - V(w) &= \int_0^L EI \frac{d^2 w(x_1)}{dx_1^2} \frac{d^2 \delta w(x_1)}{dx_1^2} dx_1 - \int_0^L b q(x_1) \delta w(x_1) dx_1 \\ &\quad + \int_0^L \frac{1}{2} EI \left\{ \frac{d^2 \delta w(x_1)}{dx_1^2} \right\}^2 dx_1. \end{aligned}$$

Now, if $V(w)$ is a minimum, then

$$\int_0^L EI \frac{d^2 w(x_1)}{dx_1^2} \frac{d^2 \delta w(x_1)}{dx_1^2} dx_1 - \int_0^L b q(x_1) \delta w(x_1) dx_1 = 0.$$

We are none the wiser as a result of this exercise, but if we integrate the first integral by parts twice, we find that

$$\left[EI \frac{d^2 w}{dx_1^2} \frac{d \delta w}{dx_1} \right]_0^L - \left[\frac{d}{dx_1} \left(EI \frac{d^2 w}{dx_1^2} \right) \delta w \right]_0^L + \int_0^L \left(EI \frac{d^4 w(x_1)}{dx_1^4} - b q(x_1) \right) \delta w dx_1 = 0.$$

Because this is zero for any δw , we conclude that

$$EI \frac{d^4 w(x_1)}{dx_1^4} - b q(x_1) = 0$$

to ensure that the third term in this expression vanishes. This gives us the required governing equation for w . However, we still need to deal with the first two boundary terms.

There are several ways to prescribe boundary conditions on the ends of the beam to ensure that V is stationary:

1. We may prescribe w and its first derivative. In this case, the variation in w must satisfy $\delta w = d\delta w/dx = 0$ to ensure that w is a kinematically admissible displacement. The boundary terms are zero under these conditions.
2. Prescribe only the value of w . In this case, we must ensure that $\delta w = 0$ on the end of the beam. The second boundary term is automatically zero. To ensure that the first boundary term is zero, we must set

$$\frac{d^2 w}{dx_1^2} = 0$$

to ensure that V is stationary. We know from elementary strength of materials courses that this is equivalent to the condition that the shear force vanishes on the end of the beam.

3. Prescribe only the value of $d\delta w/dx$. In this case, we must ensure that $d\delta w/dx = 0$ so that $w + \delta w$ is a kinematically admissible displacement. The first boundary term vanishes, whereas the second boundary term is zero if we choose

$$\frac{d}{dx_1} \left(EI \frac{d^2 w}{dx_1^2} \right) = 0.$$

This is equivalent to setting the bending moment to zero at the end of the beam.

Clearly, one could extend this procedure to account for tractions acting on the ends of the beam. The details are left as an exercise. A nice feature of the variational approach that we followed here is that the appropriate boundary conditions follow naturally from the variational principle (indeed, the boundary conditions are called “natural” boundary conditions). This turns out to be particularly helpful in setting up approximate theories of plates and shells, in which the boundary conditions can be very difficult to determine consistently using any other method.

5.7.5 Energy Methods for Calculating Stiffness

Energy methods can also be used to obtain an upper bound to the stiffness of a structure or a component. Begin by reviewing the meaning of stiffness of an elastic solid. A spring is an example of an elastic solid. Recall that, if you apply a force P to a spring, it deflects by an amount Δ , in proportion to P . The stiffness k is defined so that

$$k = P/\Delta.$$

If you apply a load P to any elastic structure (except one that contains two or more contacting surfaces), the point at which you apply the load will deflect by a distance that is proportional to the applied load. For example, for the cantilever beam shown in Figure 5.60, the end deflection is

$$\Delta = \frac{PL^3}{2Ea^3b}.$$

The stiffness of the beam is therefore $k = P/\Delta = 2Ea^3b/L^3$.

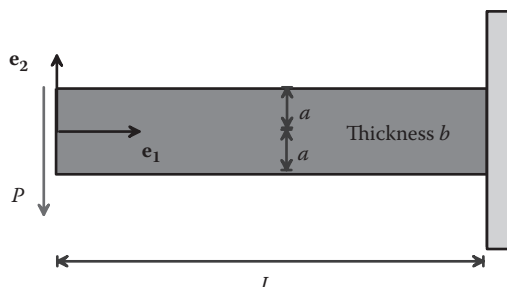


FIGURE 5.60 End-loaded cantilever beam.

To get an upper bound to the stiffness of a structure, one can merely guess its deformed shape and then apply the principle of minimum potential energy. For example, for the beam problem, we might guess that the beam deforms into a circular shape, with unknown radius R , as shown in Figure 5.61. The deflection at the end of the beam is approximately

$$\Delta = R - \sqrt{R^2 - L^2} \approx \frac{L^2}{2R}.$$

From the preceding section, we know that the potential energy of a beam is

$$V(w) = \int_0^L \frac{1}{2} EI \left\{ \frac{d^2 w(x_1)}{dx_1^2} \right\}^2 dx_1 - \int_0^L b q(x_1) w(x_1) dx_1.$$

Here, $q(x_1) = 0$, but we need to account for the potential energy of the load P . Recall that the potential energy of a constant force is $-P\Delta$. Recall also that $d^2w/dx^2 \approx 1/R$. Thus,

$$V(R) = \int_0^L \frac{1}{2} \frac{EI}{R^2} dx_1 - P\Delta = \frac{1}{2} \frac{EI}{R^2} L - P \frac{L^2}{2R}.$$

Choose R to minimize the potential energy

$$\frac{\partial V}{\partial R} = 0 \Rightarrow -\frac{EI}{R^3} L + P \frac{L^2}{2R^2} = 0 \quad \Rightarrow R = \frac{2EI}{PL}.$$

so that

$$\Delta = \frac{L^2}{2R} = \frac{L^3}{4EI} P \quad \Rightarrow k \leq \frac{4EI}{L^3}.$$

For comparison, the exact solution is $k = 3EI/L^3$.

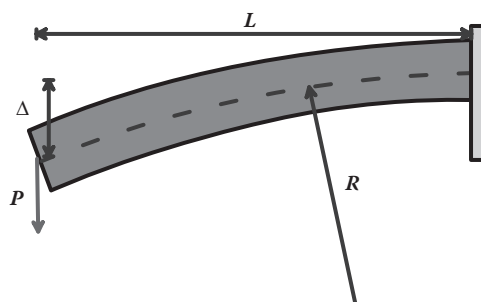


FIGURE 5.61 Deformed shape of an end-loaded beam.

5.8 RECIPROCAL THEOREM AND APPLICATIONS

The reciprocal theorem is a distant cousin of the principle of minimum potential energy and is a particularly useful tool. It is the basis for a computational method in linear elasticity called the boundary element method. It can often be used to extract information concerning solutions to a boundary value problem without having to solve the problem in detail and can occasionally be used to find the full solution; for example, the reciprocal theorem provides a way to compute fields for arbitrarily shaped dislocation loops in an infinite solid.

5.8.1 Statement and Proof of the Reciprocal Theorem

The reciprocal theorem relates two solutions for the same elastic solid, when subjected to different loads. To this end, consider the following scenario:

1. An elastic solid that occupies some region V with boundary S , as shown in Figure 5.62. The outward normal to the boundary is specified by a unit vector \mathbf{n} . The properties of the solid are characterized by the tensor of elastic moduli C_{ijkl} and mass density ρ_0 . The solid is free of stress when unloaded and temperature changes are neglected.
2. When subjected to body forces \mathbf{b}^A (per unit mass) together with prescribed displacements \mathbf{u}^{*A} on portion S_{1A} of its boundary and tractions \mathbf{t}^A on portion S_{2A} , a state of static equilibrium is established in the solid with displacements, strains, and stresses $u_i^A, \varepsilon_{ij}^A, \sigma_{ij}^A$.
3. When subjected to body forces \mathbf{b}^B together with prescribed displacements \mathbf{u}^{*B} on portion S_{1B} of its boundary and tractions \mathbf{t}^B on portion S_{2B} , the solid experiences a static state $u_i^B, \varepsilon_{ij}^B, \sigma_{ij}^B$.

The reciprocal theorem relates the two solutions through

$$\int_S n_i \sigma_{ij}^A u_j^B dA + \int_V \rho_0 b_i^A u_i^B dV = \int_S n_i \sigma_{ij}^B u_j^A dA + \int_V \rho_0 b_i^B u_i^A dV = \int_V \sigma_{ij}^A \varepsilon_{ij}^B dV = \int_V \sigma_{ij}^B \varepsilon_{ij}^A dV.$$

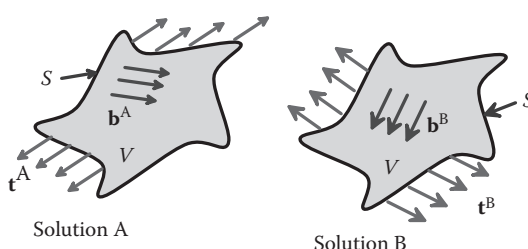


FIGURE 5.62 Elastic solid subjected to two different sets of external forces.

Derivation: Start by showing that $\sigma_{ij}^A \epsilon_{ij}^B = \sigma_{ij}^B \epsilon_{ij}^A$. To see this, note that $\sigma_{ij}^A \epsilon_{ij}^B = C_{ijkl} \epsilon_{ij}^B \epsilon_{ij}^A = C_{klji} \epsilon_{kl}^B \epsilon_{ij}^A = \sigma_{ij}^B \epsilon_{ij}^A$ where we have used the symmetry relation $C_{ijkl} = C_{klji}$. To prove the rest, recall the following:

1. The divergence theorem requires that

$$\int_S n_i \sigma_{ij} u_j dA = \int_V \frac{\partial(\sigma_{ij} u_j)}{\partial x_i} dV = \int_V \left(\frac{\partial \sigma_{ij}}{\partial x_i} u_j + \sigma_{ij} \frac{\partial u_j}{\partial x_i} \right) dV.$$

2. Any pair of strains and displacement are related by $\epsilon_{ij} = (\partial u_i / x_j + \partial u_j / x_i) / 2$.
3. The stress tensor is symmetric, so that $\sigma_{ij} \partial u_j / \partial x_i = \sigma_{ij} (\partial u_j / \partial x_i + \partial u_i / \partial x_j) / 2 = \sigma_{ij} \epsilon_{ij}$.
4. Both stress states satisfy the equilibrium equation $\partial \sigma_{ij} / \partial x_i + \rho_0 b_j = 0$. Consequently, collecting together the volume integrals gives

$$\int_S n_i \sigma_{ij} u_j dA + \int_V \rho_0 b_j u_j dV = \int_V \left(\left[\frac{\partial \sigma_{ij}}{\partial x_i} + \rho_0 b_j \right] u_j + \sigma_{ij} \epsilon_{ij} \right) dV = \int_V \sigma_{ij} \epsilon_{ij} dV.$$

5. Note that this result applies to any equilibrium stress field and pair of compatible strain and displacements; the stresses need not be related to the strains. Consequently, this result can be applied to pairs of stress and displacement:

$$\int_S n_i \sigma_{ij}^A u_j^B dA + \int_V \rho_0 b_i^A u_i^B dA = \int_V \sigma_{ij}^A \epsilon_{ij}^B dA = \int_V \sigma_{ij}^B \epsilon_{ij}^A dA = \int_S n_i \sigma_{ij}^B u_j^A dA + \int_V \rho_0 b_i^B u_i^A dA.$$

5.8.2 Simple Example Using the Reciprocal Theorem

The reciprocal theorem can often be used to extract *average* measures of deformation or stress in an elastic solution. As an example, consider the following problem: an elastic solid with Young's modulus E and Poisson's ratio ν occupies a volume V with surface S , as shown in Figure 5.63. The solid is subjected to a distribution of traction $t_i(x)$ on its surface. The traction exerts zero resultant force and moment on the solid, i.e.,

$$\int_S t_i dA = 0, \quad \int_S \epsilon_{ijk} x_j t_k dA = 0.$$

As a result, a state of static equilibrium with displacement, strain, and stress u_i , ϵ_{ij} , σ_{ij} is developed in the solid. Show that the volume change of the solid can be calculated as

$$\Delta V = \frac{1-2\nu}{E} \int_S x_i t_i dA.$$

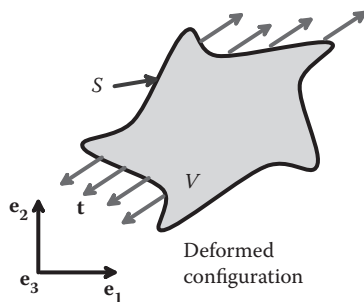


FIGURE 5.63 Elastic solid subjected to external loading.

Derivation

1. Note that, if we were able to determine the full displacement field in the solid, the volume change could be calculated as

$$\Delta V = \int_S u_i n_i dA.$$

If you don't see this result immediately on geometric grounds, it can be derived by first calculating the total volume change by integrating the dilatation over the volume of the solid and then applying the divergence theorem

$$\Delta V = \int_V \varepsilon_{kk} dV = \int_V \partial u_k / \partial x_k dV = \int_S u_k n_k dV.$$

2. Note that we can make one of the terms in the reciprocal theorem reduce to this formula by choosing state \$A\$ to be the actual displacement, stress, and strain in the solid and choosing state \$B\$ to be a uniform stress with unit magnitude \$\sigma_{ij}^B = \delta_{ij}\$. This stress is clearly an equilibrium field, for zero body force. The corresponding strains and displacements follow as

$$\varepsilon_{ij}^B = \frac{1-2\nu}{E} \delta_{ij} \quad u_i^B = \frac{1-2\nu}{E} x_i + c_i + \epsilon_{ijk} \omega_j x_k,$$

where \$c_i\$ and \$\omega_j\$ represent an arbitrary infinitesimal displacement and rotation.

3. Substituting into the reciprocal theorem, recalling that the stresses satisfy the boundary condition \$\sigma_{ij} n_i = t_j\$ and using the equilibrium equations for the traction then yields

$$\begin{aligned} \int_S n_i \sigma_{ij} u_j^B dA &= \int_S n_i \delta_{ij} u_j dA \\ \Rightarrow \Delta V &= \int_S n_i u_i dA = \int_S t_i \left(\frac{1-2\nu}{E} x_i + c_i + \epsilon_{ijk} \omega_j x_k \right) dA = \frac{1-2\nu}{E} \int_S x_i t_i dA. \end{aligned}$$

5.8.3 Formulas Relating Internal and Boundary Values of Field Quantities

The reciprocal theorem also gives a useful relationship between the values of stress and displacement in the interior and on the boundary of the solid, which can be stated as follows. Suppose that a linear elastic solid with Young's modulus E and Poisson's ratio ν is loaded on its boundary (with no body force) so as to induce a static equilibrium displacement, strain, and stress field u_i , ε_{ij} , σ_{ij} in the solid. Define the following functions:

$$U_i^{(k)}(\mathbf{x}) = \frac{(1+\nu)}{8\pi E(\nu)R} \left\{ \frac{x_k x_i}{R^2} + (3-4\nu)\delta_{ik} \right\}$$

$$\Sigma_{ij}^{(k)}(\mathbf{x}) = \frac{-1}{8\pi(1-\nu)R^2} \left\{ \frac{3x_k x_i x_j}{R^3} + (1-2\nu) \frac{\delta_{ik} x_j + \delta_{jk} x_i - \delta_{ij} x_k}{R} \right\}$$

$$\begin{aligned} \Omega_{ij}^{(kq)}(\mathbf{x}) = & \frac{-E}{8\pi(1-\nu^2)R^3} \left\{ \frac{3\delta_{kq} x_i x_j}{R^2} + \frac{3\nu(\delta_{ik} x_q x_j + \delta_{iq} x_k x_j + \delta_{jk} x_i x_q + \delta_{jq} x_i x_k)}{R^2} - 15 \frac{x_i x_j x_k x_q}{R^4} \right. \\ & \left. + (1-2\nu)(\delta_{ik}\delta_{jq} + \delta_{jk}\delta_{iq}) - \frac{1-6\nu+2\nu^2}{1-2\nu} \left(\delta_{ij}\delta_{kq} - \frac{3x_k x_q \delta_{ij}}{R^2} \right) \right\} \end{aligned}$$

You may recognize that the first two of these functions represent the displacements and stresses induced at a point x_i by a point force of unit magnitude acting in the \mathbf{e}_k direction at the origin of an infinite solid.

The displacement and stress at an interior point in the solid can be calculated from the following formulas:

$$\begin{aligned} u_k(\boldsymbol{\xi}) &= \int_S \sigma_{ij} n_i U_j^{(k)}(\mathbf{x}-\boldsymbol{\xi}) dA_{\mathbf{x}} - \int_S n_i \Sigma_{ij}^{(k)}(\mathbf{x}-\boldsymbol{\xi}) u_j dA_{\mathbf{x}} \\ \sigma_{kq}(\boldsymbol{\xi}) &= - \int_S \sigma_{ij} n_i \Sigma_{jq}^{(k)}(\mathbf{x}-\boldsymbol{\xi}) dA_{\mathbf{x}} + \int_S n_i \Omega_{ij}^{(kq)}(\mathbf{x}-\boldsymbol{\xi}) u_j dA_{\mathbf{x}}. \end{aligned}$$

Here, $dA_{\mathbf{x}}$ denotes that the integral is taken with respect to \mathbf{x} , holding $\boldsymbol{\xi}$ fixed.

At first sight, this appears to give an exact formula for the displacement and stress in any 3D solid subjected to prescribed tractions and displacement on its boundary. In fact, this is not the case because you need to know both tractions *and* displacements on the boundary to evaluate the formula, whereas the boundary conditions only specify one or the other. The main application of this formula is a numerical technique for solving elasticity problems known as the *boundary element method*. The idea is simple: the unknown values of traction and displacement on the boundary are first calculated by letting the interior point $\boldsymbol{\xi}$ approach the boundary and solving the resulting integral equation. Then, the formulas are used to calculate field quantities at interior points.

Derivation: These formulas are a consequence of the reciprocal theorem, as follows:

1. Start with the reciprocal theorem:

$$\int_S n_i \sigma_{ij}^A u_j^B dA + \int_V \rho_0 b_i^A u_i^B dA = \int_S n_i \sigma_{ij}^B u_j^A dA + \int_V \rho_0 b_i^B u_i^A dA.$$

2. For state A , we choose the actual stress, strain, and displacement in the solid. For state B , we choose the displacement and stress fields induced by a Dirac delta distribution of body force located at position ξ . The body force vector associated with a force acting in the e_k direction will be denoted by $\rho_0 b_i^{(k)} \delta(\mathbf{x} - \xi)$ and has the property that

$$\int_V \rho_0 b_i^{(k)} \delta(\mathbf{x} - \xi) u_i(\mathbf{x}) dV_x = u_k(\xi).$$

The stress and displacement induced by this body force can be calculated by shifting the origin in the point force solution given in Section 5.4.3. Substituting into the reciprocal theorem immediately yields the formula for displacements.

3. The formula for stress follows by differentiating the displacement with respect to ξ to calculate the strain and then substituting the strain into the elastic stress-strain equation and simplifying the result.

5.8.4 Classical Solutions for Displacement and Stress Induced by a 3D Dislocation Loop in an Infinite Solid

The reciprocal theorem can also be used to calculate the displacement and stress induced by an arbitrarily shaped 3D dislocation loop in an infinite solid. The concept of a dislocation in a crystal was introduced in Section 5.3.4. A 3D dislocation in an elastic solid can be constructed as follows:

1. Consider an infinite solid with Young's modulus E and Poisson's ratio v . Assume that the solid is initially stress free.
2. Introduce a bounded, simply connected surface S inside the solid (Figure 5.64). Denote the edge of this surface by a curve C ; this curve will correspond to the dislocation line. The direction of the line will be denoted by a unit vector τ tangent to the curve. There are, of course, two possible choices for this direction. Either one can be used. The normal to S will be denoted by a unit vector \mathbf{m} , which must be chosen so that the curve C encircles \mathbf{m} in a counterclockwise sense when traveling in direction τ .
3. Create an imaginary cut on S , so that the two sides of the cut are free to move independently. In the derivation below, the two sides of the cut will be denoted by S^+ and S^- , chosen so that the unit vector \mathbf{m} points from S^- to S^+ .

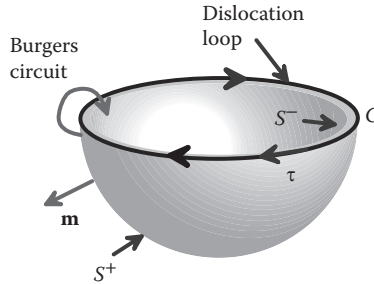


FIGURE 5.64 A 3D dislocation loop in an elastic solid.

4. Hold S^+ fixed, displace S^- by the burgers vector \mathbf{b} , and weld the two sides of the cut back together. Remove the constraint on S^+ .

This procedure creates a displacement field that is consistent with the Burger's circuit convention described in Section 5.3.4. To see this, suppose that a crystal lattice is embedded within the elastic solid. Perform a Burger's circuit around the curve C . Start the circuit on S^+ , encircle the curve according to the right-hand screw convention with respect to the line sense τ , and end at S^- . The end of the circuit is displaced by a distance \mathbf{b} from the start, so that $b_i = u_i^- - u_i^+$.

The displacement and stress induced by the dislocation loop can be calculated from

$$u_k(\mathbf{x}) = \int_S m_i \Sigma_{ij}^{(k)} (\mathbf{x} - \boldsymbol{\xi}) b_j dA_{\boldsymbol{\xi}}$$

$$\sigma_{pq}(\boldsymbol{\xi}) = \frac{E}{2(1+\nu)} \int_C \left(\epsilon_{pij} \Sigma_{im}^{(q)} (\mathbf{x} - \boldsymbol{\xi}) + \epsilon_{qij} \Sigma_{im}^{(q)} (\mathbf{x} - \boldsymbol{\xi}) + \frac{2\nu\delta_{pq}}{1-2\nu} \epsilon_{kij} \Sigma_{im}^{(k)} (\mathbf{x} - \boldsymbol{\xi}) \right) b_m \tau_j ds_{\boldsymbol{\xi}},$$

where $\Sigma_{ij}^{(k)}$ is defined in Section 5.8.3, and ϵ_{ijk} is the permutation symbol. The symbols $dA_{\boldsymbol{\xi}}$ and $ds_{\boldsymbol{\xi}}$ denotes that $\boldsymbol{\xi}$ is varied when evaluating the surface or line integral. These results are also often expressed in the more compact form

$$\begin{aligned} u_k(\mathbf{x}) &= \frac{1}{8\pi} \int_S \left\{ \left[m_k b_j \frac{\partial}{\partial x_j} + m_j b_k \frac{\partial}{\partial x_j} + \frac{\nu b_j m_j}{1-\nu} \frac{\partial}{\partial x_k} \right] \frac{\partial^2 R(\mathbf{x} - \boldsymbol{\xi})}{\partial x_i \partial x_i} - \frac{b_i m_j}{1-\nu} \frac{\partial^3 R(\mathbf{x} - \boldsymbol{\xi})}{\partial x_i \partial x_j \partial x_k} \right\} dA_{\boldsymbol{\xi}} \\ \sigma_{pq}(\mathbf{x}) &= \frac{E}{16\pi(1+\nu)} \int_C \left(\left[\epsilon_{imp} b_m \tau_q + \epsilon_{imq} b_m \tau_p \right] \frac{\partial^3 R(\mathbf{x} - \boldsymbol{\xi})}{\partial x_i \partial x_j \partial x_j} \right) ds_{\boldsymbol{\xi}} \\ &\quad + \frac{E}{8\pi(1-\nu^2)} \int_C \left(b_m \epsilon_{imk} \tau_k \left[\frac{\partial^3 R(\mathbf{x} - \boldsymbol{\xi})}{\partial x_i \partial x_p \partial x_q} - \delta_{pq} \frac{\partial^3 R(\mathbf{x} - \boldsymbol{\xi})}{\partial x_i \partial x_j \partial x_j} \right] \right) ds_{\boldsymbol{\xi}}, \end{aligned}$$

where $R(\mathbf{x} - \boldsymbol{\xi}) = \sqrt{(x_k - \xi_k)(x_k - \xi_k)}$.

Derivation

- Start with the reciprocal theorem

$$\int_S n_i \sigma_{ij}^A u_j^B dA + \int_V \rho_0 b_i^A u_i^B dV = \int_S n_i \sigma_{ij}^B u_j^A dA + \int_V \rho_0 b_i^B u_i^A dV.$$

- For state A , choose the actual stress and displacement in the solid containing the dislocation loop. For state B , choose the stress, strain, and displacement induced by a Dirac delta distribution of body force acting in the \mathbf{e}_k direction at position ξ in the solid. The displacements and stresses attributable to a Dirac delta distribution of body force are denoted by the functions $U_i^{(k)}(\mathbf{x})$ and $\Sigma_{ij}^{(k)}(\mathbf{x})$ defined in the preceding section.
- When evaluating the reciprocal theorem, the two sides of the cut are treated as separate surfaces. Substituting into the reciprocal theorem and using the properties of the delta distribution gives

$$\begin{aligned} \int_{S+} n_i^+ \sigma_{ij} U_j^{(k)}(\mathbf{x} - \xi) dA_x + \int_{S-} n_i^- \sigma_{ij} U_j^{(k)}(\mathbf{x} - \xi) dA_x &= \int_{S+} n_i^+ \Sigma_{ij}^{(k)}(\mathbf{x} - \xi) u_j^+ dA_x \\ &\quad + \int_{S-} n_i^- \Sigma_{ij}^{(k)}(\mathbf{x} - \xi) u_j^- dA_x + u_i(\xi) \end{aligned}$$

where $\mathbf{n}^+ = -\mathbf{m}$ and $\mathbf{n}^- = \mathbf{m}$ denote the outward normals to the two sides of the cut, and u_i^\pm denote the limiting values of the displacement field for the dislocation solution on the two sides of the cut.

- Substituting for \mathbf{n} , collecting together the surface integrals and noting that σ_{ij} and $U_i^{(k)}(\mathbf{x})$ are continuous across S gives

$$0 = \int_S m_j \Sigma_{ij}^{(k)}(\mathbf{x} - \xi) (u_j^- - u_j^+) dA_x + u_k(\xi).$$

Finally, noting that $u_i^- - u_i^+ = b_i$ (the Burger's vector is the displacement of a material point at the end of the Burger's circuit as seen from a point at the start) and that $\Sigma_{ij}^{(k)}(\mathbf{x} - \xi) = -\Sigma_{ij}^{(k)}(\xi - \mathbf{x})$ yields the formula for displacements.

- To calculate the stress, start by differentiating the displacement to see that

$$\frac{\partial u_k}{\partial x_l} = \int_S \frac{\partial}{\partial x_l} m_i \Sigma_{ij}^{(k)}(\mathbf{x} - \xi) b_j dA_\xi.$$

- Next, observe that this can be expressed as an integral around the dislocation line

$$\frac{\partial u_k}{\partial x_l} = \int_C \epsilon_{lij} \Sigma_{im}^{(k)}(\mathbf{x} - \boldsymbol{\xi}) b_m \tau_j dA_{\boldsymbol{\xi}}.$$

To see this, recall Stoke's theorem, which states that

$$\int_S \epsilon_{npj} \frac{\partial F_j}{\partial \xi_p} m_n dA_{\boldsymbol{\xi}} = \int_C F_j \tau_j ds_{\boldsymbol{\xi}}$$

for any differentiable vector field $F_j(\boldsymbol{\xi})$, integrated over a surface S with normal \mathbf{m} that is bounded by curve C . Apply this to the line integral, use $\epsilon_{npj} \epsilon_{lij} = \delta_{nl} \delta_{pi} - \delta_{ni} \delta_{pl}$, note that $\partial \Sigma_{im}^{(k)} / \partial \xi_i = 0$ because $\boldsymbol{\Sigma}$ is a static equilibrium stress field, and finally note that $\partial \Sigma_{ij}^{(k)} / \partial x_l = -\partial \Sigma_{ij}^{(k)} / \partial \xi_l$.

7. Finally, calculate the stress using the elastic stress-strain equation

$$\sigma_{pq} = \frac{E}{2(1+\nu)} (\delta_{pk} \delta_{ql} + \delta_{qk} \delta_{pl}) \frac{\partial u_k}{\partial \xi_l} + \frac{E\nu}{(1+\nu)(1-2\nu)} \delta_{pq} \frac{\partial u_k}{\partial \xi_k}.$$

8. The alternative forms for the displacement and stress follow by noting that

$$U_i^{(k)}(\mathbf{x}) = \frac{(1+\nu)}{4\pi E} \left\{ \delta_{ik} \frac{\partial^2 R}{\partial x_j \partial x_j} - \frac{1}{2(1-\nu)} \frac{\partial^2 R}{\partial x_i \partial x_k} \right\}$$

$$\Sigma_{ij}^{(k)}(\mathbf{x}) = \frac{1}{8\pi} \left\{ \left[\delta_{ik} \frac{\partial}{\partial x_j} + \delta_{jk} \frac{\partial}{\partial x_i} + \frac{\nu \delta_{ij}}{1-\nu} \frac{\partial}{\partial x_k} \right] \frac{\partial^2 R}{\partial x_n \partial x_n} - \frac{1}{1-\nu} \frac{\partial^3 R}{\partial x_i \partial x_j \partial x_k} \right\}.$$

5.9 ENERGETICS OF DISLOCATIONS IN ELASTIC SOLIDS

Dislocations play a crucial role in determining the response of crystalline materials to stress. For example, plastic flow in ductile metals occurs as a result of dislocation motion, dislocation emission from a crack tip can determine whether a material is ductile or brittle, and stress-induced dislocation nucleation plays a critical role in semiconductor devices. Dislocations tend to move through a crystal in response to stress. The goal of this and following sections is to derive some results that can be used to predict this motion.

5.9.1 Classical Solution for Potential Energy of an Isolated Dislocation Loop in an Infinite Solid

In this section, we show that the energy of an isolated dislocation loop with Burger's vector \mathbf{b} in an infinite solid (Figure 5.65) can be calculated using the following expressions:

$$V^{D\infty} = \frac{E}{32\pi(1+\nu)} \oint_C \oint_C \frac{\partial^2 R(\mathbf{x} - \boldsymbol{\xi})}{\partial x_p \partial x_p} b_i b_j \tau_i(\mathbf{x}) \tau_j(\boldsymbol{\xi}) d\mathbf{s}_x d\mathbf{s}_{\boldsymbol{\xi}}$$

$$+ \frac{E}{16\pi(1-\nu^2)} \oint_C \oint_C \epsilon_{ikl} \epsilon_{jmn} b_k b_m \frac{\partial^2 R(\mathbf{x} - \boldsymbol{\xi})}{\partial x_i \partial x_j} \tau_l(\mathbf{x}) \tau_n(\boldsymbol{\xi}) d\mathbf{s}_x d\mathbf{s}_{\boldsymbol{\xi}}.$$

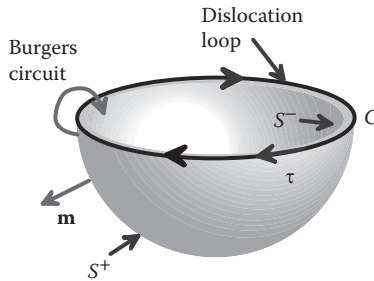


FIGURE 5.65 A 3D dislocation loop in an elastic solid.

Here, $R(\mathbf{x} - \xi) = \sqrt{(x_k - \xi_k)(x_k - \xi_k)}$ and the integral is taken around the dislocation line twice. In the first integral, ξ is held fixed, and \mathbf{x} varies with position around the dislocation line; then \mathbf{x} is varied for the second line integral.

Difficulties with evaluating the potential energy in the classical solution: In practice, this is a purely formal result. In the classical solution, the energy of a dislocation is always infinite. You can see this clearly using the solution for a straight dislocation in an infinite solid given in Section 5.3.4. Consider a pure edge dislocation, with line direction parallel to the \mathbf{e}_3 axis and Burger's vector $\mathbf{b} = b_1\mathbf{e}_1 + b_2\mathbf{e}_2$ at the origin of an infinite solid, as shown in Figure 5.66. The stress field near the dislocation is given (in polar coordinates) by

$$\sigma_{rr} = \sigma_{\theta\theta} = -\frac{E(b_1 \sin \theta - b_2 \cos \theta)}{4\pi(1-\nu^2)r} \quad \sigma_{r\theta} = \frac{E(b_1 \cos \theta + b_2 \sin \theta)}{4\pi(1-\nu^2)r}.$$

The strain energy density distribution around the dislocation follows as

$$U = \frac{1+\nu}{2E} \left\{ (\sigma_{rr}^2 + \sigma_{\theta\theta}^2 + 2\sigma_{r\theta}^2) - \nu(\sigma_{rr} + \sigma_{\theta\theta})^2 \right\}.$$

We can use this to calculate the total strain energy in an annular region around the dislocation, with inner radius a and outer radius b , as shown in Figure 5.67. The result is

$$V = \int_a^b \int_0^{2\pi} U(r, \theta) r d\theta dr = \frac{E(b_1^2 + b_2^2)}{8\pi(1-\nu^2)} \log\left(\frac{b}{a}\right).$$

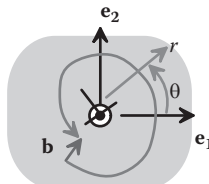


FIGURE 5.66 Burger's circuit around a 2D dislocation line.

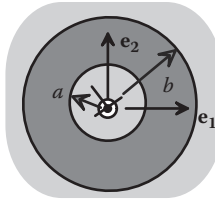


FIGURE 5.67 Cylindrical region around an edge dislocation line.

Taking $a \rightarrow 0$ gives an infinite energy, because the strain energy density varies as $1/r^2$ near the dislocation core.

Various ways to avoid this problem have been proposed. The simplest approach is to neglect the strain energy in a tubular region with small radius $r_0 \approx |\mathbf{b}|/4$ surrounding the dislocation, on the grounds that the elastic solution does not accurately characterize the atomic-scale deformation near the dislocation core. This works for straight dislocations but is not easy to apply to 3D dislocation loops. A more satisfactory approach is described in the next section.

Application to a circular prismatic dislocation loop: As an example, we attempt to apply the general formula to calculate the energy of a circular dislocation loop, with radius a , which lies in the (x_1, x_2) plane, and has a Burger's vector $\mathbf{b} = b\mathbf{e}_3$, that is perpendicular to the plane of the loop. For this case, the contour integral for the potential energy reduces to

$$V^{D_\infty} = \frac{Eab^2}{8(1-\nu^2)} \int_0^{2\pi} \frac{1+\cos\theta}{2\sqrt{2(1-\cos\theta)}} d\theta.$$

(To see this, note that the result of the integral with respect to \mathbf{x} must be independent of ξ by symmetry). As expected, the integral is divergent. In the classical theory, the energy of the loop is estimated by truncating the integral around the singularity, so that

$$V^{D_\infty} = \frac{Eab^2}{8(1-\nu^2)} \int_{r/a}^{2\pi-r/a} \frac{1+\cos\theta}{2\sqrt{2(1-\cos\theta)}} d\theta \approx \frac{Eab^2}{4(1-\nu^2)} \left\{ \log\left(\frac{4a}{r}\right) - 1 \right\} + O(r/a)^2,$$

where r is a small cutoff distance. This is somewhat similar to the core cutoff radius r_0 , but the relationship between r_0 and r is not clear. A circular glide loop, which has Burger's vector \mathbf{b} (with magnitude b) in the plane of the loop, has energy

$$V^{D_\infty} = \frac{Eab^2(2-\nu)}{4(1-\nu^2)} \left\{ \log\left(\frac{4a}{r}\right) - 2 \right\} + O(r/a)^2.$$

Derivation of the solution for the energy of a 3D dislocation loop

- Let $[u_i(\xi), \epsilon_{pq}(\xi), \sigma_{pq}(\xi)]$ denote the displacement, strain, and stress induced by the dislocation loop. The total potential energy of the solid can be calculated by integrating the strain energy density over the volume of the solid

$$V^{D\infty} = \int_V \frac{1}{2} \sigma_{ij} \epsilon_{ij} dV.$$

- The potential energy can also be expressed in terms of the displacement field in the solid, as

$$V^{D\infty} = \int_V \frac{1}{2} \sigma_{ij} \frac{\partial u_i}{\partial x_j} dV = \frac{1}{2} \int_V \frac{\partial(\sigma_{ij} u_i)}{\partial x_j} - u_i \frac{\partial(\sigma_{ij})}{\partial x_j} dV = \frac{1}{2} \int_V \frac{\partial(\sigma_{ij} u_i)}{\partial x_j} dV,$$

where we have used the symmetry of σ_{ij} and recalled that the stress field satisfies the equilibrium equation $\partial \sigma_{ij} / \partial x_j = 0$.

- Applying the divergence theorem and taking into account the discontinuity in u_i across S ,

$$V^{D\infty} = \frac{1}{2} \int_S \sigma_{ij} (-m_j) u_i^+ dA + \frac{1}{2} \int_S \sigma_{ij} m_j u_i^- dA = \frac{1}{2} \int_S \sigma_{ij} m_j b_i dA.$$

- Next, we substitute the expression given in Section 5.8.4 for σ_{ij} and reverse the order of integration

$$\begin{aligned} V^{D\infty} &= \frac{E}{32\pi(1+\nu)} \int_C \int_S \left([\in_{imp} b_m \tau_q + \in_{imp} b_m \tau_p] \frac{\partial^3 R(\mathbf{x}-\xi)}{\partial x_i \partial x_j \partial x_k} \right) m_p b_q dA_x ds_\xi \\ &\quad + \frac{E}{16\pi(1-\nu^2)} \int_C \int_S \left(b_m \in_{imk} \tau_k \left[\frac{\partial^3 R(\mathbf{x}-\xi)}{\partial x_i \partial x_p \partial x_q} - \delta_{pq} \frac{\partial^3 R(\mathbf{x}-\xi)}{\partial x_i \partial x_j \partial x_k} \right] \right) m_p b_q dA_x ds_\xi. \end{aligned}$$

- Finally, the surface integrals in this expression can be transformed into a contour integral around C by means of Stoke's theorem

$$\int_S \in_{npj} \frac{\partial F_j}{\partial x_p} m_n dA_x = \int_C F_j \tau_j ds_x.$$

After some tedious index manipulations, this gives the required result.

5.9.2 Nonsingular Dislocation Theory

The infinite potential energy associated with the classical description of a dislocation is unphysical and highly unsatisfactory. A straightforward approach to avoiding this difficulty was proposed by Cai, Arsenlis, Weinberger, and Bulatov [2006].

In the classical solution, the dislocation core is localized at a single point in space, which leads to an infinite energy. In practice, dislocation cores are distributed over a small, but finite, area as indicated in Figure 5.68. The transmission electron micrograph was kindly provided by Prof. David Paine.

This effect can be modeled approximately by using the classical solution to construct a *distributed* dislocation core. To this end, we suppose that the Burger's vector of the dislocation can be represented by a distribution $\mathbf{b}\beta(\mathbf{x})$, which must be chosen to satisfy

$$\mathbf{b}(\mathbf{x}) = \mathbf{b} \int_V \beta(\xi - \mathbf{x}) dV_\xi,$$

where the volume integral extends over the entire infinite solid. In principle, $\beta(\mathbf{x})$ could be constructed to give an accurate description of the atomic-scale strain field in the immediate neighborhood of the dislocation core, but this is difficult to do and is not the main intent of the theory. Instead, $\beta(\mathbf{x})$ is selected to make the expressions for the energy and stress field of the dislocation as simple as possible. It is particularly convenient to choose $\beta(\mathbf{x})$ to satisfy

$$R_\rho(\mathbf{x} - \xi) = \int_V \int_V R(\mathbf{y} - \mathbf{z}) \beta(\mathbf{z} - \xi) \beta(\mathbf{y} - \mathbf{x}) dV_z dV_y \quad R(\mathbf{x}) = \sqrt{x_k x_k} \quad R_\rho(\mathbf{x}) = \sqrt{x_k x_k + \rho^2},$$

where ρ is a small characteristic length, comparable with the dimensions of the dislocation core. The required distribution cannot be calculated exactly but is closely approximated by

$$\beta(\mathbf{x}) \approx \frac{15}{8\pi} \left\{ \frac{1-m}{\rho_1^3 (x_k x_k / \rho_1^2 + 1)^{7/2}} + \frac{m}{\rho_2^3 (x_k x_k / \rho_2^2 + 1)^{7/2}} \right\},$$

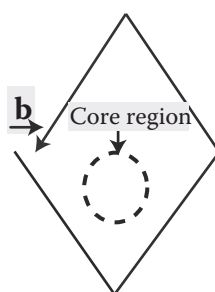


FIGURE 5.68 Burger's circuit and core region for a dislocation on the interface between a thin film and a substrate. The transmission electron microscope image was provided courtesy of Professor David Paine.

with $\rho_1 = 0.9038\rho$, $\rho_2 = 0.5451\rho$, and $m = 0.6575$. The distribution can also be shown to satisfy

$$\int_V \beta(\mathbf{x} - \xi) \beta(\xi) dV = \frac{15}{8\pi} \frac{\rho^3}{(x_k x_k + \rho^2)^{7/2}}.$$

Nonsingular energy: The expression for the energy of a dislocation loop then reduces to

$$V^{D\infty} = \frac{E}{32\pi(1+\nu)} \oint_C \oint_C \frac{\partial^2 R_\rho}{\partial x_p \partial x_p} b_i b_j \tau_i(\mathbf{x}) \tau_j(\xi) ds_x ds_\xi \\ + \frac{E}{16\pi(1-\nu^2)} \oint_C \oint_C \epsilon_{ikl} \epsilon_{jmn} b_k b_m \frac{\partial^2 R_\rho}{\partial x_i \partial x_j} \tau_l(\mathbf{x}) \tau_n(\xi) ds_x ds_\xi.$$

This is virtually identical to the classical singular solution, except that the derivatives of $R_\rho(\mathbf{x}) = \sqrt{x_k x_k + \rho^2}$ are bounded everywhere, so the integral is finite.

Nonsingular stress: The stress induced by the dislocation loop can be expressed in terms of a function $B_\rho(\mathbf{x})$, defined as

$$B_\rho(\mathbf{x}) = \int_V R(\mathbf{y}) \beta(\mathbf{y} - \mathbf{x}) dV_y.$$

This function cannot be calculated exactly but can be estimated using the approximation to $\beta(\mathbf{x})$ as

$$B_\rho(\mathbf{x}) = (1-m)\sqrt{x_k x_k + \rho_1^2} + m\sqrt{x_k x_k + \rho_2^2}.$$

The stress field then becomes

$$\sigma_{pq}(\mathbf{x}) = \frac{E}{16\pi(1-\nu)} \int_C \left([\epsilon_{imp} b_m \tau_q + \epsilon_{imq} b_m \tau_p] \frac{\partial^3 B_\rho(\mathbf{x} - \xi)}{\partial x_i \partial x_p \partial x_j} \right) ds_\xi \\ + \frac{E}{8\pi(1-\nu^2)} \int_C \left(b_m \epsilon_{imk} \tau_k \left[\frac{\partial^3 B_\rho(\mathbf{x} - \xi)}{\partial x_i \partial x_p \partial x_q} - \delta_{pq} \frac{\partial^3 B_\rho(\mathbf{x} - \xi)}{\partial x_i \partial x_j \partial x_j} \right] \right) ds_\xi.$$

Alternatively, one may calculate exactly a modified stress measure, defined as

$$\sigma_{pq}^{(\rho)}(\mathbf{x}) = \int_V \sigma_{pq}(\xi) \beta(\xi - \mathbf{x}) dV_\xi.$$

This stress measure is particularly convenient for calculating the force tending to make a dislocation move, as shown in a subsequent section. In addition, $\sigma_{pq}^{(\rho)}(\mathbf{x}) \approx \sigma_{pq}(\mathbf{x})$ except very close to the core of a dislocation. It is straightforward to show that

$$\begin{aligned}\sigma_{pq}^{(\rho)}(\mathbf{x}) &= \frac{E}{16\pi(1-\nu)} \int_C \left([\epsilon_{imp} b_m \tau_q + \epsilon_{imq} b_m \tau_q] \frac{\partial^3 R_\rho(\mathbf{x}-\xi)}{\partial x_i \partial x_j \partial x_k} \right) ds_\xi \\ &+ \frac{E}{8\pi(1-\nu^2)} \int_C \left(b_m \epsilon_{imk} \tau_k \left[\frac{\partial^3 R_\rho(\mathbf{x}-\xi)}{\partial x_i \partial x_p \partial x_q} - \delta_{pq} \frac{\partial^3 R_\rho(\mathbf{x}-\xi)}{\partial x_i \partial x_j \partial x_k} \right] \right) ds_\xi,\end{aligned}$$

where $R_\rho(\mathbf{x}) = \sqrt{x_k x_k + \rho^2}$, as before.

Nonsingular energy of circular dislocation loops: It is straightforward to calculate the energy of a circular dislocation loop. Cai, Arsenlis, Weinberger, and Bulatov [2006] give the following expression for the energy of a circular loop with radius a :

- Prismatic loop (\mathbf{b} perpendicular to loop):

$$V^{D_\infty} = \frac{Eab^2}{4(1-\nu^2)} \left\{ \log\left(\frac{8a}{\rho}\right) - 1 \right\} + O(\rho/a)^2;$$

- Glide loop (\mathbf{b} in the plane of the loop):

$$V^{D_\infty} \approx \frac{Eab^2}{8(1-\nu)} \left\{ \frac{2-\nu}{1-\nu} \left[\log\left(\frac{8a}{\rho}\right) - 2 \right] - \frac{1}{2} \right\} + O(\rho/a)^2.$$

5.9.3 Energy of a Dislocation Loop in a Stressed, Finite Elastic Solid

Figure 5.69 shows a dislocation loop in an elastic solid. Assume the following:

1. The solid is an isotropic, homogeneous, linear elastic material with Young's modulus E and Poisson's ratio ν .
2. The solid contains a dislocation, which is characterized by the loop C , and the Burger's vector \mathbf{b} for the dislocation, following the conventions described in the preceding section. As before, we can imagine creating the dislocation loop by cutting the crystal over some surface S and displacing the two material surfaces adjacent to the cut by the Burger's vector. Figure 5.69 shows the dislocation loop to be completely contained within the solid, but this is not necessary: the surface S could intersect the exterior boundary of the solid, in which case the dislocation line C would start and end on the solid's surface.

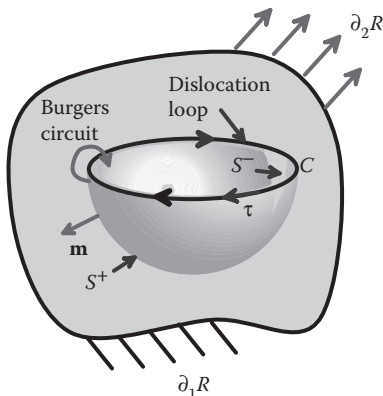


FIGURE 5.69 Dislocation loop inside a finite size elastic solid subjected to external loading.

3. Part of the boundary of the solid $\partial_1 R$ is subjected to a prescribed displacement, whereas the remainder $\partial_2 R$ is subjected to a prescribed traction. Note that there is some ambiguity in specifying the prescribed displacement. In some problems, the solid contains a dislocation before it is loaded: if so, displacements are measured relative to the solid with traction free boundary but containing a dislocation. In other problems, the dislocation may be nucleated during deformation. In this case, displacements are measured with respect to the initial, stress-free and undislocated solid. In the discussion to follow, we consider only the latter case.

To express the potential energy in a useful form, it is helpful to define several measures of stress and strain in the solid, as follows:

1. The actual fields in the loaded solid containing the dislocation will be denoted by $[u_i, \varepsilon_{ij}, \sigma_{ij}]$. Note that u_i is measured with respect to a stress-free solid, which contains no dislocations. The displacement is discontinuous across S .
2. The fields induced by the applied loading in an undislocated solid will be denoted by $[u_i^*, \varepsilon_{ij}^*, \sigma_{ij}^*]$ (Figure 5.70). The displacement field u_i^* is continuous.
3. The fields in a solid containing a dislocation, but with $\partial_2 R$ traction free and with zero displacement on $\partial_1 R$, will be denoted by $[u_i^D, \varepsilon_{ij}^D, \sigma_{ij}^D]$ (Figure 5.70)
4. The fields in an *infinite solid* containing a dislocation with line C and Burger's vector \mathbf{b} will be denoted by $[u_i^{D\infty}, \varepsilon_{ij}^{D\infty}, \sigma_{ij}^{D\infty}]$. If the dislocation line terminates on the solid's surface, any convenient procedure can be used to close the loop when deriving the infinite solid solution, but the fields will depend on this choice.
5. The difference between the fields for a dislocation in a bounded solid and the solution for a dislocation in an infinite solid will be denoted by $[u_i^I = u_i^D - u_i^{D\infty}, \varepsilon_{ij}^I = \varepsilon_{ij}^D - \varepsilon_{ij}^{D\infty}, \sigma_{ij}^I = \sigma_{ij}^D - \sigma_{ij}^{D\infty}]$.

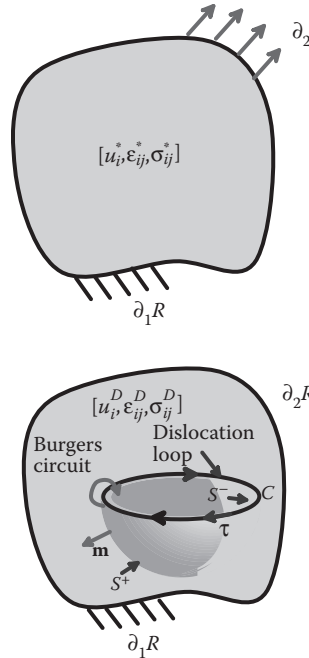


FIGURE 5.70 Decomposition of displacement and stress fields for a dislocation in a bounded solid.

The potential energy of the solid can be expressed as

$$V = V^D + V^{D*} + V^*,$$

where

- $V^D = \int_S \frac{1}{2} \sigma_{ij}^D b_i m_j dA$ is the strain energy of the dislocation itself;
- $V^{D*} = \int_S \sigma_{ij}^* b_i m_j dA$ is the work done to introduce the dislocation into the externally applied stress;
- $V^* = \int_R \frac{1}{2} \sigma_{ij}^* \epsilon_{ij}^* dV - \int_{\partial 2R} t_i u_i^* dA$ is the potential energy of the applied loads.

The strain energy of the dislocation can also be expressed as a sum of two terms:

$$V^D = V^{D\infty} + V^I,$$

where

- $V^{D\infty}$ is the energy of a dislocation with line C in an infinite solid, which can be calculated using the expressions in Section 5.9.2;
- $V^I = \int_S \sigma_{ij}^I b_i m_j dA$ is the change in potential energy resulting from the presence of boundaries in the solid.

If the classical approach is used to represent the Burger's vector of the dislocation, the energy is infinite, because $V^{D\infty}$ contains a contribution from the singular dislocation core. The remaining terms are all bounded. The simplest way to avoid this unsatisfactory behavior is to estimate $V^{D\infty}$ using the nonsingular dislocation theory presented in Section 5.9.2 but use the classical expressions for all the remaining terms. This is not completely consistent because, in a rigorous nonsingular dislocation theory, all the terms should be computed by taking a convolution integral with the Burger's vector distribution. However, provided the solid is large compared with the dislocation core, the error in the approximate result is negligible.

Derivation

1. The potential energy of the solid is given by the usual expression:

$$V = \int_R \frac{1}{2} \sigma_{ij} \epsilon_{ij} dV - \int_{\partial R} t_i u_i dA.$$

2. The total stress consists of the dislocation fields, together with the externally applied fields, so that

$$V = \int_R \frac{1}{2} [\sigma_{ij}^D + \sigma_{ij}^*] [\epsilon_{ij}^D + \epsilon_{ij}^*] dV - \int_{\partial R} t_i (u_i^D + u_i^*) dA.$$

3. This expression can be rewritten as

$$V = \int_R \left(\frac{1}{2} \sigma_{ij}^D \frac{\partial u_i^D}{\partial x_j} + \sigma_{ij}^* \frac{\partial u_i^D}{\partial x_j} + \frac{1}{2} \sigma_{ij}^* \epsilon_{ij}^* \right) dV - \int_{\partial R} t_i (u_i^D + u_i^*) dA.$$

To see this, note that $\sigma_{ij}^D \epsilon_{ij}^D = \sigma_{ij}^D (\partial u_i^D / \partial x_j)$ from the symmetry of σ_{ij}^D and the strain-displacement relations and that $\sigma_{ij}^D \epsilon_{ij}^* = C_{ijkl} \epsilon_{kl}^D \epsilon_{ij}^* = \sigma_{ij}^* \epsilon_{ij}^D$ because of the symmetry of the elasticity tensor C_{ijkl} .

4. The terms involving $(\partial u_i^D / \partial x_j)$ can now be integrated by parts, by writing, for example

$$\sigma_{ij}^D (\partial u_i^D / \partial x_j) = \partial(\sigma_{ij}^D u_i^D) / \partial x_j - u_i (\partial \sigma_{ij}^D / \partial x_j) = \partial(\sigma_{ij}^D u_i^D) / \partial x_j,$$

because σ_{ij}^D is an equilibrium stress field. Using this result, applying the divergence theorem and taking into account the discontinuity in the displacement field across S gives

$$\int_R \frac{1}{2} \sigma_{ij}^D \frac{\partial u_i^D}{\partial x_j} dV = \int_{S+} \frac{1}{2} \sigma_{ij}^D u_i^{D+} (-m_j) dA + \int_{S-} \frac{1}{2} \sigma_{ij}^D u_i^{D-} m_j dA + \int_{\partial R} \frac{1}{2} \sigma_{ij}^D u_i^D n_j dA = \int_S \frac{1}{2} \sigma_{ij}^D b_i m_j dA,$$

where we have noted that $\sigma_{ij}^D n_j u_i^D = 0$ on the exterior boundary of the solid and that $u_i^- - u_i^+ = b_i$. A similar procedure gives

$$\int_R \sigma_{ij}^* \frac{\partial u_i^D}{\partial x_j} dV = \int_S \sigma_{ij}^* b_i m_j dA + \int_{\partial R} \sigma_{ij}^* n_j u_i^D dA.$$

Finally, substituting this result back into the expression for V and noting $\sigma_{ij}^* n_j = t_i$ on $\partial_2 R$ and $u_i^D = 0$ on $\partial_1 R$ gives the required result.

5.9.4 Energy of Two Interacting Dislocation Loops

Consider two dislocation loops in an infinite elastic solid, as shown in Figure 5.71. Assume the following:

1. The solid is an isotropic, homogeneous, linear elastic material with Young's modulus E and Poisson's ratio ν .
2. The dislocations can be characterized by surfaces, contours, and Burger's vectors $[S_1, C_1, \mathbf{b}^{(1)}]$ and $[S_2, C_2, \mathbf{b}^{(2)}]$.

The total potential energy of the solid can be calculated from the following expressions

$$V = V^{D1} + V^{D1D2} + V^{D2},$$

where

- V^{D1} and V^{D2} are the energies of the two dislocation loops in isolation, which can be computed from the formulas in Section 5.9.1 (or Section 5.9.2 if you need a nonsingular expression);
- V^{D1D2} is an “interaction energy,” which can be thought of as the work done to introduce dislocation 2 into the stress field associated with dislocation 1 (or vice versa).

The interaction energy is given by

$$\begin{aligned} V^{D1D2} &= \frac{E}{16\pi(1+\nu)} \oint_{C_2} \oint_{C_1} \frac{\partial^2 R}{\partial x_p \partial x_p} b_i^{(1)} b_j^{(2)} \tau_i^{(1)}(\mathbf{x}) \tau_j^{(2)}(\boldsymbol{\xi}) ds_x ds_{\xi} \\ &\quad - \frac{E}{16\pi(1+\nu)} \oint_{C_2} \oint_{C_1} \epsilon_{ijq} \epsilon_{mnq} b_i^{(1)} b_j^{(2)} \frac{\partial^2 R}{\partial x_k \partial x_k} \tau_m^{(1)}(\mathbf{x}) \tau_n^{(2)}(\boldsymbol{\xi}) ds_x ds_{\xi} \\ &\quad + \frac{E}{8\pi(1-\nu^2)} \oint_{C_2} \oint_{C_1} \epsilon_{ikl} \epsilon_{jmn} b_k^{(1)} b_m^{(2)} \frac{\partial^2 R}{\partial x_i \partial x_j} \tau_l^{(1)}(\mathbf{x}) \tau_n^{(2)}(\boldsymbol{\xi}) ds_x ds_{\xi}. \end{aligned}$$

Although this integral is bounded (provided the dislocation lines only meet at discrete points), it is sometimes convenient to replace $R(\mathbf{x}) = \sqrt{x_k x_k}$ by $R_\rho(\mathbf{x}) = \sqrt{x_k x_k + \rho^2}$ for a nonsingular treatment of dislocations.

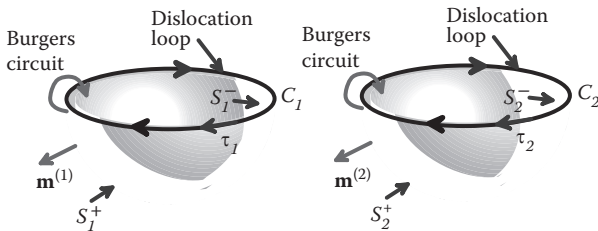


FIGURE 5.71 Interacting dislocation loops in an elastic solid.

HEALTH WARNING: Notice that the expression for the interaction energy is very similar to the formula for the self-energy of a dislocation loop, except that (1) it contains an extra term (that vanishes if $b^{(1)}=b^{(2)}$), and (2) the integrals in the interaction energy are twice those in the self-energy. The latter is an endless source of confusion.

Derivation: We can regard the two interacting dislocations as a special case of a dislocation loop subjected to an applied stress: one dislocation generates the “applied stress,” which influences the second dislocation. The total potential energy follows as $V = V^D + V^{D*} + V^*$, where $V^D = V^{D1}$, $V^* = V^{D2}$ are the potential energies of the two isolated dislocations, and $V^{D*} = V^{D1D2}$ is the interaction energy. We have that

$$V^{D1D2} = \int_{S1} \sigma_{ij}^{D2} b_i^{(1)} m_j^{(1)} dA,$$

where σ_{ij}^{D2} is the stress induced by dislocation 2. We can express this stress in terms of a line integral around dislocation 2. Finally, the surface integral over $S1$ can be reduced to a contour integral around dislocation 1 by applying Stoke's theorem.

5.9.5 Driving Force for Dislocation Motion: Peach–Koehler Formula

If a dislocation is subjected to stress, it tends to move through the crystal. This motion is the mechanism for plastic flow in a crystalline solid, as discussed in Section 3.7.12.

The tendency of a dislocation to move can be quantified by a force. This force needs to be interpreted carefully: it is not a mechanical force (in the sense of Newtonian mechanics) that induces motion of a material particle but rather a *generalized* force (in the sense of Lagrangean mechanics) that causes a rearrangement of atoms around the dislocation core. It is sometimes known as a “configurational force.”

The generalized force for dislocation motion is defined as follows:

1. Consider an elastic solid that contains a dislocation loop. The loop is characterized by a curve C , the tangent vector τ , and the Burger's vector \mathbf{b} . As usual, we can imagine creating the dislocation loop by cutting the crystal over some surface S that is bounded by C and displacing the two material surfaces adjacent to the cut by the Burger's vector.

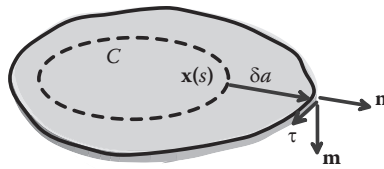


FIGURE 5.72 Motion of a dislocation loop.

2. Suppose that the dislocation moves, so that a point at $\mathbf{x}(s)$ on C advances to a new position $\mathbf{x}(s)+\delta a(s)\mathbf{n}(s)$, where $\mathbf{n}(s)$ is a unit vector normal to C , as shown in Figure 5.72 (in the figure, the dislocation moves in a single plane, but this is not necessary).
3. As the dislocation moves, the potential energy of the solid changes by an amount δV . This change of energy provides the driving force for dislocation motion.
4. The driving force is defined as a vector function of arc length around the dislocation $\mathbf{F}(s)$, whose direction is perpendicular to C and satisfies

$$-\delta V = \int_C \mathbf{F}(s) \cdot \mathbf{n}(s) \delta a(s) ds$$

for all possible choices of $\mathbf{n}(s)$ and $\delta a(s)$ (the change in energy is negative because the displacement is in the same direction as the force).

The Peach–Koehler formula states that the driving force for dislocation motion can be computed from the following formula:

$$F_i(s) = \epsilon_{ijk} \sigma_{jm}(s) b_m \tau_k(s),$$

where σ_{ij} is the total stress acting on the dislocation at a point s along the curve C (the stress includes contributions from the dislocation itself, as well as stresses generated by external loading on the solid).

The Peach–Koehler equation is meaningless without additional discussion, because the classical solution predicts that the stress acting on the dislocation line is *infinite*. To avoid this, we need to partition the stress according to its various origins, as described in Section 5.9.3:

1. We assume that the dislocation loop lies within an elastic solid, which is subjected to some external loading. The external fields subject part of the boundary of the solid $\partial_1 R$ to a prescribed displacement, and the remainder of the boundary $\partial_2 R$ to a prescribed traction, as shown in Figure 5.73.
2. The actual fields in the loaded solid containing the dislocation will be denoted by $[u_i, \epsilon_{ij}, \sigma_{ij}]$.
3. The fields induced by the applied loading in an undislocated solid will be denoted by $[u_i^*, \epsilon_{ij}^*, \sigma_{ij}^*]$

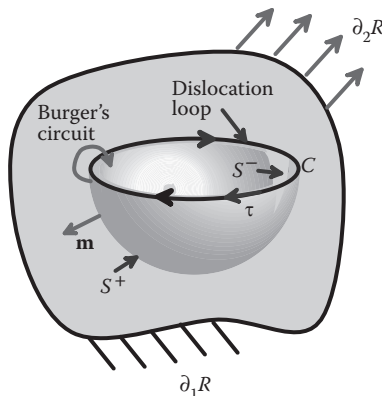


FIGURE 5.73 Dislocation loop in a finite-sized elastic solid.

4. The fields in a solid containing a dislocation, but with $\partial_2 R$ traction free and with zero displacement on $\partial_1 R$, will be denoted by $[u_i^D, \epsilon_{ij}^D, \sigma_{ij}^D]$.
5. The fields in an infinite solid containing a dislocation with line C and Burger's vector \mathbf{b} will be denoted by $[u_i^{D\infty}, \epsilon_{ij}^{D\infty}, \sigma_{ij}^{D\infty}]$. If the dislocation line terminates on the solid's surface, any convenient procedure can be used to close the loop when deriving the infinite solid solution, but the fields will depend on this choice.
6. The difference between the fields for a dislocation in a bounded solid and the solution for a dislocation in an infinite solid will be denoted by $[u_i^I = u_i^D - u_i^{D\infty}, \epsilon_{ij}^I = \epsilon_{ij}^D - \epsilon_{ij}^{D\infty}, \sigma_{ij}^I = \sigma_{ij}^D - \sigma_{ij}^{D\infty}]$.

The Peach–Koehler force can then be divided into contributions from three sources:

$$F_i(s) = F_i^{D\infty}(s) + F_i^I(s) + F_i^*(s),$$

where

1. $F_i^{D\infty}(s) = \epsilon_{ijk} \sigma_{jm}^{D\infty}(s) b_m \tau_k(s)$ is the self-force of the dislocation, i.e., the force exerted by the stresses generated by the dislocation itself. This force always acts so as to reduce the length of the dislocation line. In the classical solution, this force is infinite. The procedure described in Section 5.9.2 can be used to remove the singularity; in this case, the stress in the Peach–Koehler formula should be calculated using the expression

$$\begin{aligned} \sigma_{pq}^{D\infty}(\mathbf{x}) &= \frac{E}{16\pi(1-\nu)} \int_C \left([\epsilon_{imp} b_m \tau_q + \epsilon_{imq} b_m \tau_p] \frac{\partial^3 R_\rho(\mathbf{x}-\boldsymbol{\xi})}{\partial x_i \partial x_j \partial x_j} \right) ds_\xi \\ &+ \frac{E}{8\pi(1-\nu^2)} \int_C \left(b_m \epsilon_{imk} \tau_k \left[\frac{\partial^3 R_\rho(\mathbf{x}-\boldsymbol{\xi})}{\partial x_i \partial x_p \partial x_q} - \delta_{pq} \frac{\partial^3 R_\rho(\mathbf{x}-\boldsymbol{\xi})}{\partial x_i \partial x_j \partial x_j} \right] \right) ds_\xi, \end{aligned}$$

where $R_\rho(\mathbf{x}) = \sqrt{x_k x_k + \rho^2}$. Note that, if the dislocation remains *straight*, the total length of the dislocation line does not change as the dislocation moves. In this case, the self-force is zero. In 2D descriptions of dislocation motion, therefore, the core singularity has no effect; this is why it has been possible to live with the classical dislocation fields for so long.

2. $F_i^I(s) = \epsilon_{ijk} \sigma_{jm}^I(s) b_m \tau_k(s)$ is a force generated by stress associated with the solid's boundaries. These are generally nonsingular. This force is often referred to as the "image force."
3. $F_i^*(s) = \epsilon_{ijk} \sigma_{jm}^*(s) b_m \tau_k(s)$ is the force exerted on the dislocation by externally applied loading. This, too, is generally nonsingular.

Derivation: The following expression for the total energy of a dislocation in an elastic solid was derived in Section 5.9.3:

$$V = V^D + V^{D*} + V^*,$$

where

- $V^D = \int_S \frac{1}{2} \sigma_{ij}^D b_i m_j dA$ is the strain energy of the dislocation itself;
- $V^{D*} = \int_S \sigma_{ij}^* b_i m_j dA$ is the work done to introduce the dislocation into the externally applied stress;
- $V^* = \int_R \frac{1}{2} \sigma_{ij}^* \epsilon_{ij}^* dV - \int_{\partial R} t_i u_i^* dA$ is the potential energy of the applied loads.

We want to calculate the change in potential energy resulting from a small change in area δS as the dislocation line advances by a small distance $\delta a(s)\mathbf{n}(s)$, as shown in Figure 5.74. We consider each term in the potential energy:

1. The last term is independent of S , and therefore $\delta V^* = 0$.
2. The change in V^{D*} follows as $\delta V^{D*} = \int \sigma_{ij}^* b_i m_j dA$, where δS is the increment in area swept by the dislocation. Note that an area element swept by the advancing dislocation line can be expressed as $\mathbf{m}dA = \delta a \mathbf{n} \times \mathbf{t}ds$, so we can write

$$\delta V^{D*} = \int_C \sigma_{ij}^* b_i \epsilon_{jkl} n_k \tau_l \delta a(s) ds.$$

3. The change in V^D can be written as

$$\delta V^D = \int_S \frac{1}{2} \delta \sigma_{ij}^D b_i m_j dA + \int_{\delta S} \frac{1}{2} \sigma_{ij}^D b_i m_j dA.$$

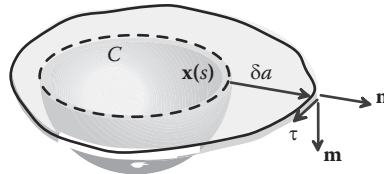


FIGURE 5.74 Motion of a dislocation loop.

To calculate the change in stress $\delta\sigma_{ij}$ arising from the motion of the dislocation line, recall that the displacement and stress induced by the dislocation loop can be calculated from the expression

$$u_k(\mathbf{x}) = \int_S m_i \Sigma_{ij}^{(k)} (\mathbf{x} - \boldsymbol{\xi}) b_j dA_{\xi} \quad \sigma_{pq}^D = C_{pqkl} \int_S m_i \frac{\partial}{\partial x_l} \Sigma_{ij}^{(k)} (\mathbf{x} - \boldsymbol{\xi}) b_j dA_{\xi},$$

where $\Sigma_{ij}^{(k)}$ is the stress induced by a point force in the (bounded) elastic solid. The change in stress therefore follows as

$$\delta\sigma_{pq} = C_{pqkl} \int_C \frac{\partial}{\partial x_l} \Sigma_{ij}^{(k)} (\mathbf{x} - \boldsymbol{\xi}) b_j \in_{jkl} n_k \tau_l \delta a(s) ds_{\xi}.$$

This shows that

$$\delta V^D = \frac{1}{2} \int_S C_{pqkl} \int_C \frac{\partial}{\partial x_l} \Sigma_{ij}^{(k)} (\mathbf{x} - \boldsymbol{\xi}) b_j \in_{jkl} n_k \tau_l \delta a(s) ds_{\xi} dA + \int_{\delta S} \frac{1}{2} \sigma_{ij}^D b_i m_j dA.$$

Reversing the order of integration in the first term, noting that $C_{pqkl} \partial \Sigma_{ij}^k / \partial x_l = C_{ijkl} \partial \Sigma_{pq}^k / \partial x_l$ and using the expression for σ_{pq}^D , then gives

$$\delta V^D = \int_{\delta S} \sigma_{ij}^D b_i m_j dA = \int_C \sigma_{ij}^D b_i \in_{jkl} n_k \tau_l \delta a(s) ds.$$

4. Finally, combining the results of steps 3 and 4 and noting that $\epsilon_{ijk} = -\epsilon_{jik}$ then gives

$$-\delta V = \int_C \epsilon_{jkl} [\sigma_{ij}^D + \sigma_{ij}^*] b_i \tau_l n_k \delta a(s) ds = \int_C \mathbf{F}(s) \cdot \mathbf{n}(s) \delta a(s) ds.$$

This has to hold for all possible $\delta a(s)$, which shows that $F_i(s) = \epsilon_{ijk} \sigma_{jm}(s) b_m \tau_k(s)$ as required.

5.10 RAYLEIGH–RITZ METHOD FOR ESTIMATING NATURAL FREQUENCY OF AN ELASTIC SOLID

We conclude this chapter by describing an energy-based method for estimating the natural frequency of vibration of an elastic solid.

5.10.1 Mode Shapes and Natural Frequencies; Orthogonality of Mode Shapes and Rayleigh's Principle

It is helpful to review the definition of natural frequencies and mode shapes for a vibrating solid. To this end, consider a representative elastic solid, such as a slender beam that is free at both ends, as illustrated in Figure 5.75. The physical significance of the mode shapes and natural frequencies of the vibrating beam can be visualized as follows:

1. Suppose that the beam is made to vibrate by bending it into some (fixed) deformed shape $u_i = u_i^{(0)}(x_1, x_2, x_3)$ and then suddenly releasing it. In general, the resulting motion of the beam will be very complicated and may not even appear to be periodic.
2. However, there exists a set of special initial deflections $u_i^{(0)} = U_i^{(n)}(x_1, x_2, x_3)$, which cause every point on the beam to experience simple harmonic motion at some (angular) frequency ω_n , so that the deflected shape has the form $u_i(x_k, t) = U_i^{(n)}(x_k) \cos \omega_n t$.
3. The special frequencies ω_n are called the *natural frequencies* of the system, and the special initial deflections $U_i^{(n)}(x_1, x_2, x_3)$ are called the *mode shapes*.
4. A continuous system always has an infinite number of mode shapes and natural frequencies. The vibration frequencies and their modes are conventionally ordered as a sequence $\omega_1, \omega_2, \omega_3, \dots$ with $\omega_{n+1} > \omega_n$. The lowest frequency of vibration is denoted ω_1 . The mode shapes for the lowest natural frequencies tend to have a long wavelength; the wavelength decreases for higher-frequency modes. If you are curious, the exact mode shapes and natural frequencies for a vibrating beam are derived in Section 10.4.1.
5. In practice the *lowest* natural frequency of the system is of particular interest, because design specifications often prescribe a minimum allowable limit for the lowest natural frequency.

We will derive two important results below, which give a quick way to estimate the lowest natural frequency:

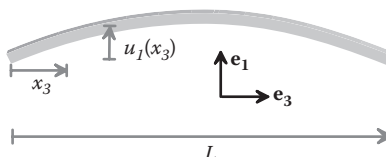


FIGURE 5.75 Deflection of a vibrating beam with free ends.

1. The mode shapes are *orthogonal*, which means that the displacements associated with two different vibration modes $U_i^{(k)}$ and $U_i^{(j)}$ have the property that

$$\int_V U_i^{(k)}(x_n) U_i^{(j)}(x_n) dV = 0 \quad (k \neq j).$$

2. We will prove *Rayleigh's principle*, which can be stated as follows. Let $\hat{U}_i(x_k)$ denote any kinematically admissible displacement field (you can think of this as a guess for the mode shape), which must be differentiable and must satisfy $\hat{U}_i(x_k) = 0$ on S_1 . Define measures of potential energy \hat{V} and kinetic energy \hat{T} associated with $\hat{U}_i(x_k)$ as

$$\hat{V} = \int_V \frac{1}{2} C_{ijkl} \frac{\partial \hat{U}_k}{\partial x_l} \frac{\partial \hat{U}_i}{\partial x_j} dV \quad \omega^2 \hat{T} = \int_V \frac{1}{2} \rho \omega^2 \hat{U}_i \hat{U}_i dV.$$

Then

$$\frac{\hat{V}}{\hat{T}} \geq \omega_i^2, \text{ and } \frac{\hat{V}}{\hat{T}} = \omega_i^2 \text{ if and only if } \hat{U}_i = U_i^{(1)}.$$

The result is useful because the fundamental frequency can be estimated by approximating the mode shape in some convenient way and minimizing \hat{V}/\hat{T} .

5.10.1.1 Orthogonality of Mode Shapes

We consider a generic linear elastic solid, with elastic constants C_{ijkl} and mass density ρ . Note the following:

- External forces do not influence the natural frequencies of a linear elastic solid, so we can assume that the body force acting on the interior of the solid is zero.
- Part of the boundary S_1 may be subjected to prescribed displacements. When estimating vibration frequencies, we can assume that the displacements are zero everywhere on S_1 .
- The remainder of the boundary S_2 can be assumed to be traction free.

By definition, the mode shapes and natural frequencies have the following properties:

- The displacement field associated with this vibration mode is $u_i(x_k, t) = U_i^{(n)}(x_k) \cos \omega_n t$.
- The displacement field must satisfy the equation of motion for a linear elastic solid given in Section 5.1.2, which can be expressed in terms of the mode shape and natural frequency as

$$C_{ijkl} \frac{\partial^2 u_k}{\partial x_i \partial x_l} = \rho \frac{\partial^2 u_j}{\partial t^2} \Rightarrow C_{ijkl} \frac{\partial^2 U_k^{(n)}}{\partial x_i \partial x_l} + \rho \omega_n^2 U_j^{(n)} = 0.$$

3. The mode shapes must satisfy $U_i^{(n)}(x_k)=0$ on S_1 to meet the displacement boundary condition, and $C_{ijkl}(\partial U_k^{(n)} / \partial x_l)n_i = 0$ on S_2 to satisfy the traction-free boundary condition.

Orthogonality of the mode shapes can be seen as follows:

1. Let $U_i^{(m)}$ and $U_i^{(n)}$ be two mode shapes, with corresponding vibration frequencies ω_m and ω_n . Because both mode shapes satisfy the governing equations, it follows that

$$\int_V \left(C_{ijkl} \frac{\partial^2 U_k^{(n)}}{\partial x_i \partial x_l} U_j^{(m)} + \rho \omega_n^2 U_j^{(n)} U_j^{(m)} \right) dV = 0 \quad \int_V \left(C_{ijkl} \frac{\partial^2 U_k^{(m)}}{\partial x_i \partial x_l} U_j^{(n)} + \rho \omega_m^2 U_j^{(m)} U_j^{(n)} \right) dV = 0$$

2. Next we show that

$$\int_V C_{ijkl} \frac{\partial^2 U_k^{(n)}}{\partial x_i \partial x_l} U_j^{(m)} dV = \int_V C_{ijkl} \frac{\partial^2 U_k^{(m)}}{\partial x_i \partial x_l} U_j^{(n)} dV.$$

To see this, integrate both sides of this expression by parts. For example, for the left-hand side,

$$\begin{aligned} \int_V C_{ijkl} \frac{\partial^2 U_k^{(n)}}{\partial x_i \partial x_l} U_j^{(m)} dV &= \int_V \frac{\partial}{\partial x_i} \left(C_{ijkl} \frac{\partial U_k^{(n)}}{\partial x_l} U_j^{(m)} \right) dV - \int_V C_{ijkl} \frac{\partial U_k^{(n)}}{\partial x_l} \frac{\partial U_j^{(m)}}{\partial x_i} dV \\ &= \int_S \left(C_{ijkl} \frac{\partial U_k^{(n)}}{\partial x_l} U_j^{(m)} \right) n_i dA - \int_V C_{ijkl} \frac{\partial U_k^{(n)}}{\partial x_l} \frac{\partial U_j^{(m)}}{\partial x_i} dV \\ &= - \int_V C_{ijkl} \frac{\partial U_k^{(n)}}{\partial x_l} \frac{\partial U_j^{(m)}}{\partial x_i} dV, \end{aligned}$$

where we have used the divergence theorem and noted that the integral over the surface of the solid is zero because of the boundary conditions for $U_i^{(m)}$ and $U_i^{(n)}$. An exactly similar argument shows that

$$\int_V C_{ijkl} \frac{\partial^2 U_k^{(m)}}{\partial x_i \partial x_l} U_j^{(n)} dV = - \int_V C_{ijkl} \frac{\partial U_k^{(m)}}{\partial x_l} \frac{\partial U_j^{(n)}}{\partial x_i} dV.$$

Recalling that $C_{ijkl} = C_{klji}$ shows the result.

3. Finally, orthogonality of the mode shapes follows by subtracting the second equation in step 1 from the first and using step 2 to see that

$$(\omega_n^2 - \omega_m^2) \int_V (U_j^{(n)} U_j^{(m)}) dV = 0.$$

If m and n are two distinct modes with different natural frequencies, the mode shapes must be orthogonal.

5.10.1.2 Proof of Rayleigh's Principle

1. Note first that any kinematically admissible displacement field can be expressed as a linear combination of mode shapes as

$$\hat{U}_i = \sum_{n=1}^{\infty} \alpha_n U_i^{(n)} \quad \alpha_m = \frac{\int_V \hat{U}_i U_i^{(m)} dV}{\int_V U_i^{(m)} U_i^{(m)} dV}.$$

To see the formula for the coefficients α_m , multiply both sides of the first equation by $U_i^{(m)}$, integrate over the volume of the solid, and use the orthogonality of the mode shapes.

2. Second, note that the mode shapes satisfy

$$\int_V C_{ijkl} \frac{\partial U_k^{(m)}}{\partial x_l} \frac{\partial U_j^{(n)}}{\partial x_i} dV = \begin{cases} \omega_m^2 \int_V (U_j^{(m)} U_j^{(m)}) dV & m=n \\ 0 & m \neq n. \end{cases}$$

To see this, note first that because $U_i^{(m)}$ satisfies the equation of motion, it follows that

$$\int_V \left(C_{ijkl} \frac{\partial^2 U_k^{(m)}}{\partial x_i \partial x_l} U_j^{(m)} + \rho \omega_m^2 U_j^{(m)} U_j^{(m)} \right) dV = 0.$$

Next, integrate the first term in this integral by parts (see step 2 in the proof of orthogonality of the mode shapes) and use the orthogonality of the mode shapes to see the result stated.

3. We may now expand the potential and kinetic energy measures \hat{V} and \hat{T} in terms of sums of the mode shapes as follows:

$$\begin{aligned} \hat{V} &= \int_V \frac{1}{2} C_{ijkl} \left(\sum_{n=1}^{\infty} \alpha_n \frac{\partial U_j^{(n)}}{\partial x_i} \right) \left(\sum_{m=1}^{\infty} \alpha_m \frac{\partial U_k^{(m)}}{\partial x_l} \right) dV = \frac{1}{2} \rho \sum_{m=1}^{\infty} \omega_m^2 \alpha_m^2 \int_V (U_j^{(m)} U_j^{(m)}) dV \\ \hat{T} &= \int_V \frac{\rho}{2} \left(\sum_{n=1}^{\infty} \alpha_n U_j^{(n)} \right) \left(\sum_{m=1}^{\infty} \alpha_m U_j^{(m)} \right) dV = \frac{1}{2} \rho \sum_{m=1}^{\infty} \alpha_m^2 \int_V (U_j^{(m)} U_j^{(m)}) dV, \end{aligned}$$

where we have used the result given in step 2 and orthogonality of the mode shapes.

4. Finally, we know that $\omega_m \geq \omega_l$ for $m \geq 1$, which shows that

$$\hat{V} \geq \frac{1}{2} \rho \omega_l^2 \sum_{m=1}^{\infty} \alpha_m^2 \int_V (U_j^{(m)} U_j^{(m)}) dV.$$

We see immediately that $\hat{V}/\hat{T} \geq \omega_l^2$, with equality if and only if $\alpha_m = 0$ for $m > 1$.

5.10.2 Estimate of Natural Frequency of Vibration for a Beam Using Rayleigh–Ritz Method

Figure 5.76 illustrates the problem to be solved: an initially straight beam has Young's modulus E and mass density ρ , and its cross-section has area A and moment of area I . The left-hand end of the beam is clamped, and the right-hand end is free. We want to estimate the lowest natural frequency of vibration.

The deformation of a beam can be characterized by the deflection $w(x)$ of its neutral section. The potential energy of the beam can be calculated from the formula derived in Section 5.7.4, whereas the kinetic energy measure T can be approximated by assuming the entire cross-section displaces with the midplane without rotation, which gives

$$V(w) = \int_0^L \frac{1}{2} EI \left\{ \frac{d^2 w(x_3)}{dx_3^2} \right\}^2 dx_3 \quad T(w) = \int_0^L \frac{1}{2} \rho A \{w(x_3)\}^2 dx_3.$$

The natural frequency can be estimated by selecting a suitable approximation for the mode shape \hat{W} and minimizing the ratio V/T , as follows:

1. Note that the mode shape must satisfy the boundary conditions $\hat{W} = d\hat{W}/dx_3 = 0$. We could try a polynomial $\hat{W} = x_3^2 + Cx_3^3$, where C is a parameter that can be adjusted to get the best estimate for the natural frequency.
2. Substituting this estimate into the definitions of V and T and evaluating the integrals gives

$$\frac{V}{T} = \frac{EI}{\rho AL^4} \frac{420(1+3CL+3C^2L^2)}{(15C^2L^2+35CL+21)}.$$

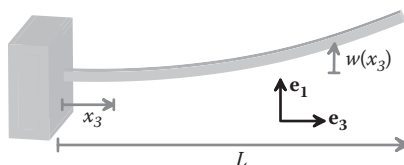


FIGURE 5.76 Deflection of a vibrating cantilever beam.

3. To get the best estimate for the natural frequency, we must minimize this expression with respect to C . It is straightforward to show that the minimum value occurs for $CL = (\sqrt{39} - 12)/15$. Substituting this value back into the results of step 2 gives

$$\frac{V}{T} = 12.48 \frac{EI}{\rho AL^4} \geq \omega^2.$$

4. For comparison, the formula for exact natural frequency of the lowest mode is derived in Section 10.4.1 and gives $\omega^2 = 12.36EI/(\rho AL^4)$.

Solutions for Plastic Solids

Plasticity problems are much more difficult to solve than linear elastic problems. In general, a numerical method must be used, as discussed in Chapters 7 and 8. Nevertheless, several powerful mathematical techniques can be used to find both exact and approximate solutions. In this chapter, we outline two particularly effective methods: *slip-line field theory*, which gives exact solutions for plane strain boundary value problems for rigid plastic solids, and *bounding theorems*, which provide a quick way to estimate collapse loads for plastic solids and structures.

6.1 SLIP-LINE FIELD THEORY

The largest class of solutions to boundary value problems in plasticity exploits a technique known as slip-line field theory. The theory simplifies the governing equations for plastic solids by making several restrictive assumptions:

1. Plane strain deformation, i.e., displacement components in the basis shown in Figure 6.41, satisfy $u_3 = 0$, and u_1, u_2 are functions of x_1 and x_2 only.
2. The loading is quasi-static.
3. Temperature changes are neglected.
4. Body forces are neglected.
5. The solid is idealized as a rigid-perfectly plastic von Mises solid. The uniaxial stress-strain curve for this material is illustrated in Figure 6.1. The material properties are characterized by the yield stress in uniaxial tension Y . Alternatively, the material is sometimes characterized by its yield stress in shear $k = Y / \sqrt{3}$.

Otherwise, the technique can be used to solve any arbitrary 2D boundary value problem for a rigid plastic solid. It is quite difficult to apply in practice, because it is not easy to find the slip-line field that solves a particular problem. Nevertheless, a wide range of important

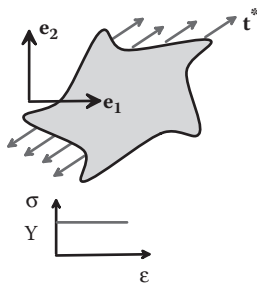


FIGURE 6.1 A rigid-perfectly plastic subjected to external loading.

solutions have been found. The main intent of this section is to illustrate how to interpret these solutions and to outline the basis for slip-line field theory.

6.1.1 Interpreting a Slip-Line Field

An example of a slip-line field solution is shown in Figure 6.2. (This is Hill's solution to a rigid punch indenting a rigid-plastic half-space.)

The slip lines consist of a curvilinear mesh of two families of lines, which always cross each other at right angles. By convention, one set of lines are named α slip lines (shown as dashed lines); the others are called β lines (solid lines). The velocity distribution and stress state in the solid can always be determined from the geometry of these lines.

6.1.1.1 Stress State at a Point in the Slip-Line Field

By definition, the slip lines are always parallel to axes of principal shear stress in the solid. This means that the stress components in a basis oriented with the α, β directions have the form

$$\sigma_{\alpha\alpha} = \bar{\sigma} \quad \sigma_{\beta\beta} = \bar{\sigma} \quad \sigma_{\alpha\beta} = k = Y / \sqrt{3},$$

where $\bar{\sigma} = (\sigma_{\alpha\alpha} + \sigma_{\beta\beta})/2$ is the hydrostatic stress (determined using the equations given below), k is the yield stress of the material in shear, and Y is its yield stress in uniaxial tension. This stress state is sketched in Figure 6.3. Because the shear stress is equal to the shear

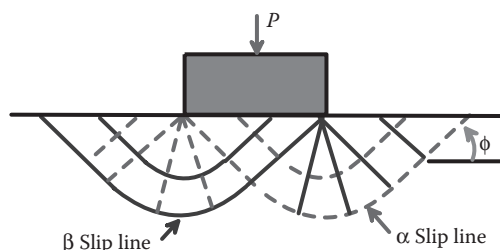


FIGURE 6.2 Slip-line field for indentation of a rigid plastic solid by a flat punch.

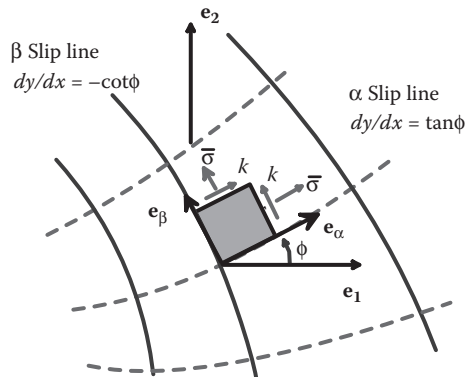


FIGURE 6.3 A typical slip-line field.

yield stress, the material evidently deforms by shearing parallel to the slip lines: this is the reason for their name.

If ϕ denotes the angle between the α slip line and the e_1 direction, the stress components in the $\{e_1, e_2, e_3\}$ basis can be calculated as

$$\sigma_{11} = \bar{\sigma} - k \sin 2\phi$$

$$\sigma_{22} = \bar{\sigma} + k \sin 2\phi$$

$$\sigma_{12} = k \cos 2\phi.$$

The Mohr's circle construction (shown in Figure 6.4) is a convenient way to remember these results.

6.1.1.2 Relations Governing Hydrostatic Stress along Slip Lines (Hencky Equations)

The hydrostatic stress can be shown to satisfy the following relations along slip lines:

$$\bar{\sigma} - 2k\phi = \text{constant} \quad \alpha \text{ slip line}$$

$$\bar{\sigma} + 2k\phi = \text{constant} \quad \beta \text{ slip line.}$$

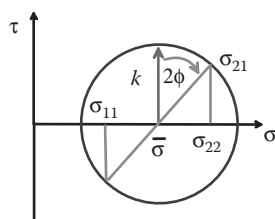


FIGURE 6.4 Mohr's circle of stress for a material element in a rigid plastic solid.

If the hydrostatic stress can be determined at any one point on a slip line (for example, at a boundary), it can be deduced everywhere else. Note that, if there is a region in the field in which both slip lines are straight, the stress is constant.

6.1.1.3 The Velocity Field (Geiringer Equations)

The velocity field can be expressed as components in a fixed $\{\mathbf{e}_1, \mathbf{e}_2\}$ basis or as components parallel and perpendicular to the slip lines, as shown in Figure 6.5. The velocity field satisfies the following equations:

$$\left. \begin{aligned} \frac{dv_1}{ds} + \tan \phi \frac{dv_2}{ds} &= 0 \\ \frac{dv_\alpha}{ds} &= v_\beta \frac{d\phi}{ds} \end{aligned} \right\} \alpha \text{ slip line} \quad \left. \begin{aligned} \frac{dv_1}{ds} - \cot \phi \frac{dv_2}{ds} &= 0 \\ \frac{dv_\beta}{ds} &= -v_\alpha \frac{d\phi}{ds} \end{aligned} \right\} \beta \text{ slip line.}$$

6.1.1.4 Application to the Hill Slip-Line Field

The stress state throughout a slip-line field can be deduced by working step by step along the slip lines. We illustrate the procedure using Hill's indentation solution.

Consider first the state of stress at the point marked a in Figure 6.6. Clearly, $\phi_a = \pi / 4$ at this point. The stress state can be transformed from a basis aligned with the slip lines to the fixed $\{\mathbf{e}_1, \mathbf{e}_2\}$ basis using the Mohr's circle construction shown in the figure. Recall (or use the Mohr's circle to see) that

$$\sigma_{11} = \bar{\sigma} - k \sin 2\phi \quad \sigma_{22} = \bar{\sigma} + k \sin 2\phi \quad \sigma_{12} = k \cos 2\phi,$$

where $\bar{\sigma}$ is the hydrostatic component of stress. The boundary conditions at a require that $\sigma_{12} = \sigma_{22} = 0$. The first condition is clearly satisfied, because the slip lines intersect the boundary at $\phi = \pi / 4$. We can satisfy the second condition by setting $\bar{\sigma} = -k$. Finally, this gives the stress parallel to the surface as $\sigma_{11} = -2k$.

The stress must be constant in the triangular region ABC, because the slip lines in this region are straight.

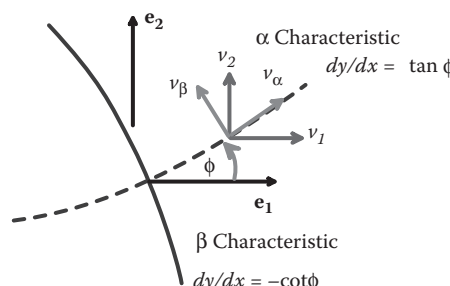


FIGURE 6.5 Coordinate system to define velocity components in a slip-line field.

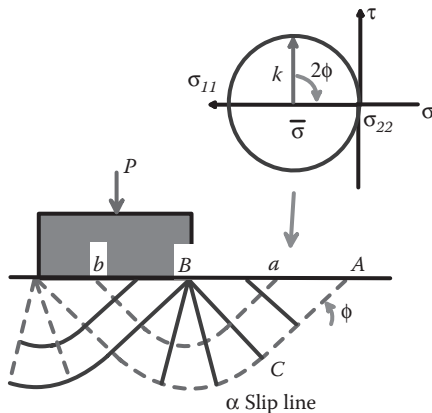


FIGURE 6.6 State of stress at the end of a slip line for the solution shown in Figure 6.2.

Next, consider the stress state at b . Here, we see that $\phi_b = -\pi/4$. We can use the Hencky equation to determine $\bar{\sigma}$ at b . Recall that

$$\bar{\sigma} - 2k\phi = \text{constant} \quad \alpha \text{ slip line}$$

$$\bar{\sigma} + 2k\phi = \text{constant} \quad \beta \text{ slip line}$$

so, following one of the α slip lines, we get

$$\bar{\sigma}_b - 2k\phi_b = \bar{\sigma}_a - 2k\phi_a$$

$$\Rightarrow \bar{\sigma}_b = -k - \pi k.$$

Using the basis-change equation, we then get

$$\sigma_{11} = -\pi k \quad \sigma_{22} = -(\pi + 2)k \quad \sigma_{12} = 0.$$

The pressure under the punch turns out to be uniform (the stress is constant in the triangular region of the slip-line field below the punch), and so the total force (per unit out of plane length) on the punch can be computed as

$$P = w(2+\pi)k,$$

where w is the width of the punch.

6.1.1.5 How to Distinguish the α and β Families of Slip Lines

Usually, slip-line fields are presented without specifying which set of slip lines should be taken as the α and which should be the β set; it is up to you to work out which is which. In fact, the slip lines are interchangeable; switching α and β will simply change the sign of all the stresses.

You can see this clearly using the Hill solution. Figure 6.7 shows the solution with α and β lines switched over. At point a , $\phi = 3\pi/4$, and therefore, to satisfy $\sigma_{22} = 0$, we must now choose $\bar{\sigma} = k$. To find the stress under the contact, we can trace a β slip line to point b . Here, we see that $\phi = \pi/4$, so the Hencky equation

$$\begin{aligned}\bar{\sigma}_b - 2k\phi_b &= \bar{\sigma}_a + 2k\phi_a \\ \Rightarrow \bar{\sigma}_b &= k + \pi k.\end{aligned}$$

Using the basis-change equation, we then get

$$\sigma_{11} = \pi k \quad \sigma_{22} = (\pi + 2)k \quad \sigma_{12} = 0$$

at point b . The normal stress acts upward on the surface, so that this represents the stress induced by a rigid punch that is bonded to the surface and pulled upward.

6.1.2 Derivation of the Slip-Line Field Method

Figure 6.8 shows a rigid-perfectly plastic solid, with a von Mises yield surface. The material is characterized by its yield stress in uniaxial tension Y or its yield stress in shear $k = Y/\sqrt{3}$. Let $u_i, \varepsilon_{ij}, \sigma_{ij}$ denote the components of displacement, strain, and stress in the solid. The solid is assumed to be a long cylinder with its axis parallel to the e_3 direction, which is constrained to deform in plane strain, with $u_3 = 0$ and u_1, u_2 independent of x_3 . It is loaded by subjecting part of its boundary $\partial_1 R$ to a prescribed velocity and the remainder $\partial_2 R$ to a prescribed traction, so that

$$\begin{aligned}\dot{u}_\alpha &= v_\alpha^*(x_1, x_2) && \text{on } \partial_1 R \\ \sigma_{\alpha\beta} n_\alpha &= t_\beta^*(x_1, x_2) && \text{on } \partial_2 R,\end{aligned}$$

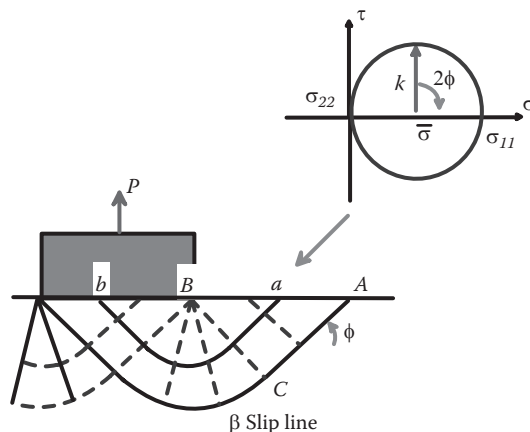


FIGURE 6.7 State of stress if the α and β slip lines are exchanged in the solution shown in Figure 6.2.

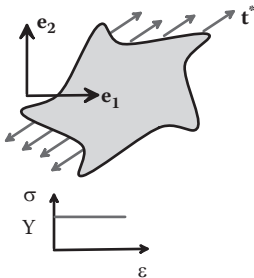


FIGURE 6.8 Rigid plastic solid subjected to external forces.

where the Greek subscripts α, β can have values of 1 or 2. In practice, we will compute the velocity field $v_i = \dot{u}_i$ rather than the displacement field.

6.1.2.1 Summary of Governing Equations

1. Strain rate-velocity relation: $\dot{\epsilon}_{\alpha\beta} = \frac{1}{2}(\partial v_\alpha / \partial x_\beta + \partial v_\beta / \partial x_\alpha)$.
2. The plastic flow rule: $\dot{\epsilon}_{ij} = 3\dot{\bar{\epsilon}}^P S_{ij} / 2Y$. Plane strain deformation then requires

$$\begin{aligned}\dot{\epsilon}_{33} &= 3\dot{\bar{\epsilon}}^P [\sigma_{33} - (\sigma_{11} + \sigma_{22} + \sigma_{33})/3] / 2Y = 0 \\ \Rightarrow \sigma_{33} &= (\sigma_{11} + \sigma_{22})/2,\end{aligned}$$

whereupon the flow rule shows that the remaining components of plastic strain rate satisfy

$$\begin{aligned}\dot{\epsilon}_{11} &= 3\dot{\bar{\epsilon}}^P (\sigma_{11} - (\sigma_{11} + \sigma_{22} + \sigma_{33})/3) / 2Y = 3\dot{\bar{\epsilon}}^P (\sigma_{11} - \sigma_{22}) / 4Y \\ \dot{\epsilon}_{22} &= 3\dot{\bar{\epsilon}}^P (\sigma_{22} - (\sigma_{11} + \sigma_{22} + \sigma_{33})/3) / 2Y = 3\dot{\bar{\epsilon}}^P (\sigma_{22} - \sigma_{11}) / 4Y \\ \dot{\epsilon}_{12} &= 3\dot{\bar{\epsilon}}^P \sigma_{12} / 2Y.\end{aligned}$$

We observe that these conditions imply that

$$\begin{aligned}\dot{\epsilon}_{11} + \dot{\epsilon}_{22} &= 0 \Rightarrow \partial v_1 / \partial x_1 + \partial v_2 / \partial x_2 = 0 \\ \frac{\dot{\epsilon}_{11} - \dot{\epsilon}_{22}}{\sigma_{11} - \sigma_{22}} &= \frac{\dot{\epsilon}_{12}}{\sigma_{12}} \Rightarrow (\dot{\epsilon}_{11} - \dot{\epsilon}_{22})\sigma_{12} = \dot{\epsilon}_{12}(\sigma_{11} - \sigma_{22}) \\ \Rightarrow (\partial v_1 / \partial x_1 - \partial v_2 / \partial x_2)\sigma_{12} &= \frac{1}{2}(\partial v_1 / \partial x_2 + \partial v_2 / \partial x_1)(\sigma_{11} - \sigma_{22}).\end{aligned}$$

3. Yield criterion:

$$\sqrt{\frac{3}{2}S_{ij}S_{ij}} - Y = 0 \Rightarrow \frac{1}{4}(\sigma_{11} - \sigma_{22})^2 + \sigma_{12}^2 = k^2,$$

where $k = Y/\sqrt{3}$ is the shear yield stress of the material, and we have used the condition that $\sigma_{33} = (\sigma_{11} + \sigma_{22})/2$.

4. Equilibrium conditions:

$$\begin{aligned}\partial\sigma_{ij}/\partial x_i &= 0 \quad \Rightarrow \partial\sigma_{11}/\partial x_1 + \partial\sigma_{12}/\partial x_2 = 0 \\ \partial\sigma_{22}/\partial x_2 + \partial\sigma_{21}/\partial x_1 &= 0.\end{aligned}$$

6.1.2.2 Solution of Governing Equations by Method of Characteristics

From the preceding section, we observe that we must calculate a velocity field $v_\alpha(x_\alpha)$ and stress field $\sigma_{\alpha\beta}(x_\alpha)$ satisfying governing equations:

$$\begin{aligned}\frac{1}{4}(\sigma_{11} - \sigma_{22})^2 + \sigma_{12}^2 &= k^2 \\ \partial v_1 / \partial x_1 + \partial v_2 / \partial x_2 &= 0 \\ (\partial v_1 / \partial x_1 - \partial v_2 / \partial x_2)\sigma_{12} &= \frac{1}{2}(\partial v_1 / \partial x_2 + \partial v_2 / \partial x_1)(\sigma_{11} - \sigma_{22}) \\ \partial\sigma_{11}/\partial x_1 + \partial\sigma_{12}/\partial x_2 &= 0 \\ \partial\sigma_{22}/\partial x_2 + \partial\sigma_{21}/\partial x_1 &= 0\end{aligned}$$

together with appropriate boundary conditions.

We focus first on a general solution to the governing equations. It is convenient to start by eliminating some of the stress components using the yield condition. Because the material is at yield, we note that, at each point in the solid, we could find a basis in which the stress state consists of a shear stress of magnitude k (the shear yield stress), together with an unknown component of hydrostatic stress $\bar{\sigma}$. The stress state is sketched in Figure 6.9.

Instead of solving for the stress components $\sigma_{\alpha\beta}$, we will calculate the hydrostatic stress $\bar{\sigma}$ and the angle ϕ between the e_1 direction and the m_1 direction. Recall that we can relate $\sigma_{\alpha\beta}$ to $\bar{\sigma}$, ϕ , and k using Mohr's circle of stress: from Figure 6.10, we see that

$$\sigma_{11} = \bar{\sigma} - k \sin 2\phi \quad \sigma_{22} = \bar{\sigma} + k \sin 2\phi \quad \sigma_{12} = k \cos 2\phi.$$

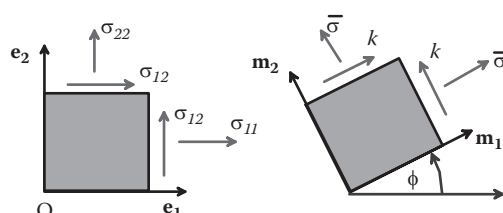


FIGURE 6.9 Stresses acting on a material element with two orientations in a slip-line field.

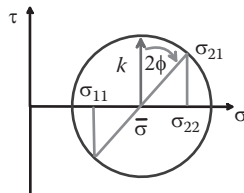


FIGURE 6.10 Mohr's circle relating the stresses on the material elements in Figure 6.9.

We now rewrite the governing equations in terms of $\bar{\sigma}$, ϕ , and k . The yield criterion is satisfied automatically. The remaining four equations are most conveniently expressed in matrix form

$$A_{ij} \frac{\partial q_j}{\partial x_1} + B_{ij} \frac{\partial q_j}{\partial x_2} = 0,$$

where A and B are four-dimensional symmetric matrices, and q is a 1×4 vector, defined as

$$q = \begin{bmatrix} \phi \\ v_1 \\ v_2 \\ \bar{\sigma} \end{bmatrix} \quad A = \begin{bmatrix} 0 & -2k\cos 2\phi & -2k\sin 2\phi & 0 \\ -2k\cos 2\phi & 0 & 0 & 1 \\ -2k\sin 2\phi & 0 & 0 & 0 \\ 0 & 1 & 0 & 0 \end{bmatrix}$$

$$B = \begin{bmatrix} 0 & -2k\sin 2\phi & 2k\cos 2\phi & 0 \\ -2k\sin 2\phi & 0 & 0 & 0 \\ 2k\cos 2\phi & 0 & 0 & 1 \\ 0 & 0 & 1 & 0 \end{bmatrix}.$$

This is a quasi-linear hyperbolic system of partial differential equations, which may be solved by the method of characteristics.

The first step is to find eigenvalues μ and eigenvectors r_i that satisfy

$$r_i A_{ij} = \mu r_i B_{ij}.$$

A straightforward exercise (set $\det(A - \mu B) = 0$ to find the eigenvalues and substitute back to get eigenvectors or, if you're lazy, use a symbolic manipulation program...) shows that there are two repeated eigenvalues, with corresponding eigenvectors:

$$\begin{aligned} \cot \phi & \quad \begin{cases} r = [1, 0, 0, -2k] \\ r = [0, 1, \tan \phi, 0] \end{cases} & -\tan \phi & \quad \begin{cases} r = [1, 0, 0, 2k] \\ r = [0, 1, -\cot \phi, 0] \end{cases}. \end{aligned}$$

We can now eliminate A from the governing matrix equation

$$r_i B_{ij} \left(\frac{\partial q_j}{\partial x_1} + \frac{\partial q_j}{\partial x_2} \right) = 0 \quad \Rightarrow \sqrt{1 + \epsilon^2} r_i B_{ij} \left(\frac{1}{\sqrt{1 + \epsilon^2}} \frac{\partial q_j}{\partial x_1} + \frac{1}{\sqrt{1 + \epsilon^2}} \frac{\partial q_j}{\partial x_2} \right) = 0.$$

Finally, if we set

$$\frac{\partial x_1}{\partial s} = \frac{1}{\sqrt{1 + \epsilon^2}} \quad \frac{\partial x_2}{\partial s} = \frac{1}{\sqrt{1 + \epsilon^2}}$$

and note that

$$\left(\frac{\partial q_j}{\partial x_1} \frac{\partial x_1}{\partial s} + \frac{\partial q_j}{\partial x_2} \frac{\partial x_2}{\partial s} \right) = \frac{dq_j}{ds},$$

we find that

$$r_i B_{ij} \frac{dq_j}{ds} = 0$$

along characteristic lines in the solid that satisfy

$$\frac{\partial x_1}{\partial s} = -\frac{1}{\sqrt{1 + \epsilon^2}} \quad \frac{\partial x_2}{\partial s} = \frac{1}{\sqrt{1 + \epsilon^2}}.$$

The special characteristic lines in the solid can be identified more easily if we note that

$$\frac{dx_2}{dx_1} = \frac{1}{-\frac{1}{\sqrt{1 + \epsilon^2}}} = -\sqrt{1 + \epsilon^2},$$

which shows that the slope of the characteristic lines satisfies

$$\frac{dx_2}{dx_1} = \tan \phi \quad \frac{dx_2}{dx_1} = -\cot \phi$$

for the two possible values of the eigenvalue μ . This shows the following:

1. There are two sets of characteristic lines (one for each eigenvalue).
2. The two sets of characteristics are orthogonal (they therefore define a set of orthogonal curvilinear coordinates in the solid).

3. The characteristic lines are trajectories of maximum shear (to see this, recall the definition of ϕ). For this reason, the characteristics are termed slip lines; the material slips (deforms in shear) along these lines.

Conventionally, the characteristics satisfying $dx_2/dx_1 = \tan\phi$ are designated α slip lines, whereas the orthogonal set are designated β slip lines. A representative set of characteristic lines is sketched in Figure 6.11.

When solving a particular boundary value problem, the central issue will be to identify a set of characteristic lines that will satisfy the boundary conditions. Field equations reduce to simple ODEs that govern variations of hydrostatic pressure and velocity along each slip line.

6.1.2.3 Relations along Slip Lines

To complete the theory, we need to find equations relating the field variables $q = [\phi, \partial v_1 / \partial x_1, \partial v_2 / \partial x_2, \bar{\sigma}]$ along the slip lines. To do so, we return to the governing equation

$$r_i B_{ij} \frac{dq_j}{ds} = 0$$

and substitute for B and r . For the four separate eigenvectors, we find that $r_i B_{ij}$ reduce to

$$\left. \begin{array}{l} [0, -2k \sin 2\phi, 2k(\cos 2\phi - 1), 0] \\ [-2k \sin 2\phi + 2k \tan \phi \cos 2\phi, 0, 0 \tan \phi] \end{array} \right\} = \cot \phi \quad (\alpha \text{ slip line})$$

$$\left. \begin{array}{l} [0, -2k \sin \phi, 2k(\cos \phi + 1), 0] \\ [-2k \sin 2\phi - 2k \cot \phi \cos 2\phi, 0, 0, \tan \phi] \end{array} \right\} = -\tan \phi \quad (\beta \text{ slip line}).$$

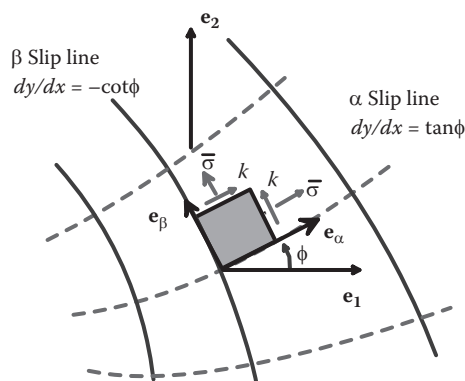


FIGURE 6.11 A representative slip-line field for a rigid plastic solid.

Computing $r_i B_{ij} dq_j / ds$ and simplifying the trig formulas then yields

$$\left. \begin{array}{l} \frac{dv_1}{ds} + \tan \phi \frac{dv_2}{ds} = 0 \\ -2k \frac{d\phi}{ds} + \frac{d\bar{\sigma}}{ds} = 0 \end{array} \right\} \alpha \text{ slip line} \quad \left. \begin{array}{l} \frac{dv_1}{ds} - \cot \phi \frac{dv_2}{ds} = 0 \\ 2k \frac{d\phi}{ds} + \frac{d\bar{\sigma}}{ds} = 0 \end{array} \right\} \beta \text{ slip line.}$$

Conditions relating $\bar{\sigma}$ and ϕ along slip lines are often expressed as

$$\begin{aligned} \bar{\sigma} - 2k\phi &= \text{constant} && \alpha \text{ slip line} \\ \bar{\sigma} + 2k\phi &= \text{constant} && \beta \text{ slip line.} \end{aligned}$$

These are known as the Hencky equations.

One can also obtain simpler expressions relating velocity components along slip lines. It is convenient to express the velocity vector as components in a basis oriented with the slip lines, as shown in Figure 6.12. The necessary basis change is

$$\begin{aligned} v_\alpha &= v_1 \cos \phi + v_2 \sin \phi \\ v_\beta &= -v_1 \sin \phi + v_2 \cos \phi. \end{aligned}$$

A straightforward algebraic exercise then yields

$$\frac{dv_\alpha}{ds} = v_\beta \frac{d\phi}{ds} \quad \frac{dv_\beta}{ds} = -v_\alpha \frac{d\phi}{ds}.$$

These are known as the Geiringer equations.

6.1.3 Examples of Slip-Line Field Solutions to Boundary Value Problems

When using slip-line field theory, the first step is always to find the characteristics (known as the slip-line field). This is usually done by trial and error and can be exceedingly difficult.

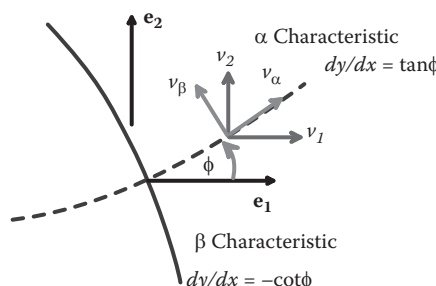


FIGURE 6.12 Coordinate systems used to describe velocity fields in a slip-line field.

These days, we usually hope that some smart person has already been able to find the slip-line field, and, if we cannot find the solution in some ancient book, we give up and clobber the problem with an FEM package. If the slip-line field is known, the stress and velocity everywhere in the solid can be determined using the Hencky and Geiringer equations.

In this section, we give several examples of slip-line field solutions to boundary value problems.

6.1.3.1 Plane Strain Extrusion

A slip-line field solution to plane strain extrusion through a tapered die is shown in Figure 6.13. Friction between the die and work piece is neglected.

It is of particular interest to calculate the force P required to extrude the bar. The easiest way to do this is to consider the forces acting on the region ABCDEF. Note the following:

1. The resultant force on EF is $-P\mathbf{e}_1$.
2. The resultant force on CB is zero (you can see this by noting that no external forces act on the material to the left of CB).
3. The stress state at a point b on the line CD can be calculated by tracing a slip line from a to b . The Mohr's circle construction for this purpose is shown in Figure 6.14. At point a , the slip lines intersect CB at 45° , so that $\phi_a = -45^\circ$; we also know that $\sigma_{11} = 0$ on CB (because the solid to the left of CB has no forces acting on it). These conditions can be satisfied by choosing $\bar{\sigma} = -k$, so that the stress state at a is $\sigma_{11} = 0$ $\sigma_{12} = 0$ $\sigma_{22} = -2k$. Tracing a β slip line from a to b , we see that $\bar{\sigma}_b = \bar{\sigma}_a + 2k(\phi_a - \phi_b) = -\pi k / 3 - k$. Finally, the slip lines intersect CD at 45° , so CD is subjected to a pressure $\sigma_{nn} = \bar{\sigma}_b - k$ acting normal to CD, whereas the component of traction tangent to CD is zero.
4. CD has length H , so the resultant force acting on CD is $H\sigma_{nn} \sin 30^\circ \mathbf{e}_1 - H\sigma_{nn} \cos 30^\circ \mathbf{e}_2$.
5. By symmetry, the resultant force acting on AB is $H\sigma_{nn} \sin 30^\circ \mathbf{e}_1 + H\sigma_{nn} \cos 30^\circ \mathbf{e}_2$.
6. Equilibrium then gives

$$P = kH \left(\frac{\pi}{3} + 2 \right).$$

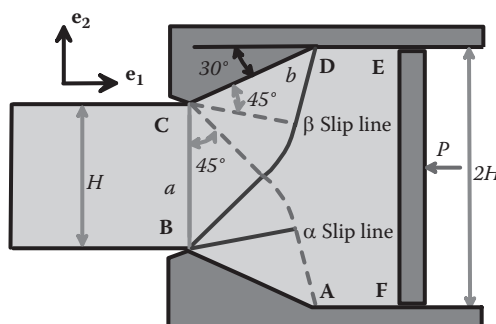


FIGURE 6.13 Slip-line field for plane strain extrusion.

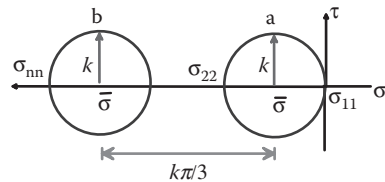


FIGURE 6.14 Mohr's circles of stress for material particles located at *a* and *b* in Figure 6.13.

6.1.3.2 Double-Notched Plate in Tension

A slip-line field solution for a double-notched plate under tensile loading is shown in Figure 6.15. The stress state in the neck and the load *P* are of particular interest. Both can be found by tracing a slip line from either boundary into the constant stress region at the center of the solid.

Consider the slip line starting at *A* and ending at *B*, for example. At *A*, the slip lines meet the free surface at 45° . With α, β designated as shown, $\phi_A = \alpha - \pi/4$ and $\bar{\sigma}_A = k$. Following the slip line to *B*, we see that $\phi_B = \pi/4$, so the Hencky equation gives $\bar{\sigma}_B = k(\pi - 2\alpha)$. The state of stress at *B* follows as

$$\sigma_{11} = (\pi - 2\alpha)k \quad \sigma_{22} = (\pi - 2\alpha + 2)k \quad \sigma_{12} = 0.$$

The state of stress is clearly constant in the region ABCD (and so is constant along the line connecting the two notches). The force required to deform the solid is therefore $P = ak(\pi - 2\alpha + 2)$.

6.1.3.3 Pressurized Cylindrical Cavity

The slip-line field solution to an internally pressurized rigid-plastic cylinder is shown in Figure 6.16. The goal is to determine the stress state everywhere in the cylinder and to calculate the internal pressure necessary to drive the deformation.

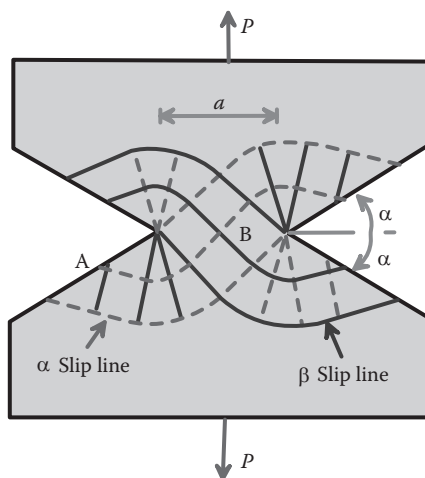


FIGURE 6.15 Slip-line field for a notched tensile specimen under axial loading.

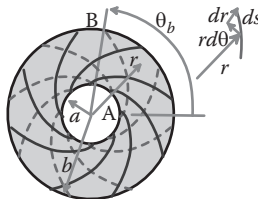


FIGURE 6.16 Slip-line field for an internally pressurized cylinder.

Consider the α slip line, which starts at point A (with cylindrical-polar coordinates $r = a$, $\theta = 0$) and ends at B (with cylindrical-polar coordinates $r = b$, $\theta = \theta_b$).

1. At point B, the surface is traction free, which requires $\sigma_{rr} = \sigma_{r\theta} = 0$. To satisfy $\sigma_{r\theta} = 0$, the slip line must meet the surface at 45° ($\phi_B = \theta_b + \pi/4$). In addition, to satisfy $\sigma_{rr} = 0$, the hydrostatic stress $\bar{\sigma}_B = k$.
2. Note that the shear stress component $\sigma_{r\theta} = 0$ throughout the cylinder. This means that the slip line must cross every radial line at 45° (or, if you prefer, it must cross every circumferential line at 45°).
3. Consider a small segment ds of the slip line. Because the slip line is at 45° to the radial direction, $dr = rd\theta$.
4. Integrating this result from $r = a$, $\theta = 0$ to (r, θ) gives $r = ae^\theta$, i.e., the slip lines are logarithmic spirals.
5. At B, this gives $b = ae^{\theta_B}$ or $\theta_B = \log(b/a)$.
6. Note that $\phi_A = \pi/4$ and apply the Hencky equation from B to A to see that $\bar{\sigma}_A = k - 2k\theta_B = k - 2k\log(b/a)$.
7. Finally, the basis change equation shows that $\sigma_{rr} = -p_A = \bar{\sigma}_A - k = -2k\log(b/a)$.
8. At a generic point (r, θ) , the same procedure gives

$$\sigma_{rr} = -2k\log(b/r) \quad \sigma_{\theta\theta} = -2k\log(b/r) + 2k.$$

This result can be compared with the axisymmetric elastic-plastic solution in Section 4.2.

6.1.3.4 Notched Bar in Bending

Figure 6.17 shows a slip-line field solution for a notched bar subjected to a pure bending moment. The solution is valid for $\omega \geq 1$ (radian). The slip-line field can be used to determine the moment M required to deform the bar as a function of the notch angle ω . To do so, note the following:

1. The stress acting on the line NO is constant, because slip lines are straight.
2. You can determine the stress at a point D between O and N by following the slip-line CD. The stress must satisfy $\sigma_{22} = 0$, $\sigma_{12} = 0$ at C, so the slip lines must meet the surface at 45° ($\phi_C = \pi/4$), and we must choose $\bar{\sigma}_C = -k$. This gives $\sigma_{11} = -2k$, $\sigma_{22} = \sigma_{12} = 0$ at D.

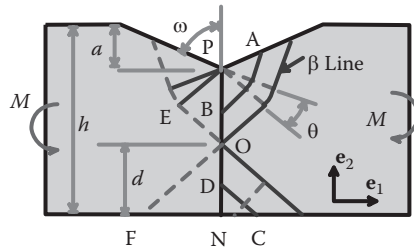


FIGURE 6.17 Shallow notched bar subjected to bending moment.

3. Similarly, the stress acting on the line OP is constant, because slip lines are straight. You can calculate the stress at some point B between P and O by following the slip-line AB. At point A, the surface is free of traction, so the slip line must meet the surface at 45° ($\phi_A = \pi/4 - \omega$), and the hydrostatic stress must satisfy $\bar{\sigma}_A = k$. At B, we see that $\phi_B = -\pi/4$. Using the Hencky equation along the β slip-line AB, we find that $\bar{\sigma}_B = k(1 + \pi - 2\omega)$. Finally $\sigma_{11} = k(2 + \pi - 2\omega)$ $\sigma_{22} = k(\pi - 2\omega)$ $\sigma_{12} = 0$ from the basis change formulas.
4. The height d of point O can be found from the condition that the axial force applied to the bar must vanish. Integrating σ_{11} along the line NOP and setting the result to zero shows that

$$d = \frac{2 + \pi - 2\omega}{4 + \pi - 2\omega} (h - a).$$

5. Finally, taking moments for the region of the bar to the right of NOP about O shows that

$$\frac{d^2}{2}(2k) + \frac{(h-a-d)^2}{2}(2 + \pi - 2\omega)k - M = 0.$$

6. Substituting for d and simplifying shows that

$$M = k(h-a)^2 \frac{2 + \pi - 2\omega}{4 + \pi - 2\omega}.$$

At first sight, this solution is valid for any notch angle ω , but in fact this is not the case. A slip-line field is valid only if the rigid regions in the field do not exceed yield. This means that it must be possible to find a static equilibrium distribution of stress that does not violate the yield criterion anywhere in the rigid part of the solid. If this cannot be done, the solid is said to be *overstressed*.

The slip-line field for a notched bar has a peculiar state of stress at point O; there is a stress discontinuity (and singularity) at the corner, and it turns out that the region that was assumed rigid in this solution is overstressed (the maximum principal shear stress exceeds k) if the notch is too sharp.

To see this, consider the rigid region of the solid just to the left of O, as shown in Figure 6.18. The lines OE and OF are adjacent to α slip lines and so are subjected to a combined shear stress k and normal stresses $\bar{\sigma}_B, \bar{\sigma}_D$ as shown. When the value of $\bar{\sigma}_B - \bar{\sigma}_D$ gets too large, the rigid region OEFO collapses plastically; a possible slip-line field at collapse is shown in Figure 6.18. The slip-line field consists of a 90° fan, centered at O. Applying the Hencky relation along a generic β slip line shows that, at collapse, $\bar{\sigma}_B - \bar{\sigma}_D = k\pi$, and so for the rigid region to remain below yield $\bar{\sigma}_B - \bar{\sigma}_D \leq k\pi$. Substituting the values of $\bar{\sigma}_B, \bar{\sigma}_D$ from parts 2 and 3 then gives $\omega \geq 1$.

A solution for a sharp notch is shown in Figure 6.19. In the modified field, the region PBNFG is rigid. The left-hand part of the bar rotates about point O, shearing along a pair of slip lines formed by the circular arcs AB and GF. To calculate the moment, we need first to calculate the angles θ and ψ , the radius R of the arc BC, the length b of the constant stress regions adjacent to the notch, and the height d of point O above the base of the beam. To this end, note the following:

1. At point A, the surface of the wedge is traction free. The slip lines must intersect the surface at 45° , which shows that $\phi_A = \omega - 3\pi/4$ and that $\bar{\sigma}_A = k$.
2. Tracing the α slip line from A to B and noting $\phi_B = \omega + \theta - 3\pi/4$ gives $\bar{\sigma}_B = k + 2k\theta$.
3. At point D at the base of the beam, the surface is traction free, so the slip lines must meet the surface at 45° . This gives $\phi_D = \pi/4$ and $\bar{\sigma}_D = -k$.
4. The stress is uniform in the region CDEF, so that $\bar{\sigma}_C = -k$.
5. The hydrostatic stresses at B and C must be related by the Hencky equation for a β slip line, which gives $\bar{\sigma}_B = \bar{\sigma}_C + 2k\psi \Rightarrow \psi - \theta = 1$.
6. Finally, elementary geometry shows that $\omega + \theta + \psi = \pi$.
7. Hence, solving items 5 and 6 gives $\theta = (\pi - \omega - 1)/2$ $\psi = (\pi - \omega + 1)/2$.
8. Geometry gives $d + R \sin(\psi - \pi/4) + b \cos(\psi - \pi/4) = h - a$.
9. We obtain two more equations relating the unknown variables from the condition that the resultant force acting on any surface that extends from the top of the beam

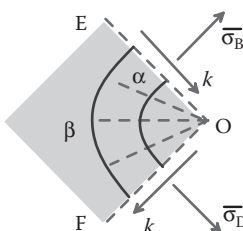


FIGURE 6.18 Slip-line field for a corner of a rigid region bounded by two slip lines.

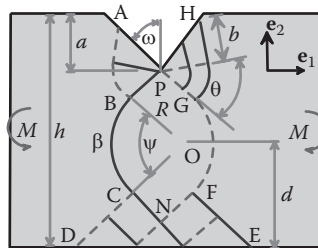


FIGURE 6.19 Deep notched bar subjected to bending moment.

to the bottom must vanish. The resultant force acting on the surface to the right of PBCD can be calculated as

$$\begin{aligned} & \bar{\sigma}_B b (\cos(\psi - \pi/4) \mathbf{e}_1 + \sin(\psi - \pi/4) \mathbf{e}_2) - kb (\sin(\psi - \pi/4) \mathbf{e}_1 + \cos(\psi - \pi/4) \mathbf{e}_2) \\ & + \int_{\pi/4-\psi}^{\pi/4} [k(\sin \lambda \mathbf{e}_1 - \cos \lambda \mathbf{e}_2) - \bar{\sigma}_{BC}(\lambda)(\cos \lambda \mathbf{e}_1 + \sin \lambda \mathbf{e}_2)] R d\lambda \\ & + (d\sqrt{2} - R)[k(\mathbf{e}_1 + \mathbf{e}_2)/\sqrt{2} - \bar{\sigma}_C(\mathbf{e}_1 - \mathbf{e}_2)/\sqrt{2}] = 0, \end{aligned}$$

where $\bar{\sigma}_{BC} = \bar{\sigma}_C + 2k(\pi/4 - \lambda)$ is the hydrostatic stress along the slip-line BC. The results of items 7–9 can be solved for d , R , and b .

10. Finally, taking moments about O gives $M = b^2 \bar{\sigma}_B / 2 + kRb + kR^2 \psi - \bar{\sigma}_C(2d^2 - R^2) / 2$. Thus,

$$M = k(h-a)^2 \{(\omega - \pi)^2 - 1\} / \{(\omega - \pi - 1)^2 - 4\cos^2[(\omega - 1)/2]\}.$$

This result is valid only if $b \geq 0$, which requires $\omega > 0.056$. In addition, the notch angle must satisfy $\omega \leq 1$ to avoid overstressing the rigid corner at P.

6.2 BOUNDING THEOREMS IN PLASTICITY AND THEIR APPLICATIONS

To set the background for plastic limit analysis, it is helpful to review the behavior of an elastic-plastic solid or structure subjected to mechanical loading. The solution to an internally pressurized elastic-perfectly plastic sphere given in Section 4.2 provides a representative example. All elastic-perfectly plastic structures will exhibit similar behavior. In particular,

- An inelastic solid will reach yield at some critical value of applied load.
- If the load exceeds yield, a plastic region starts to spread through the solid. As an increasing area of the solid reaches yield, the displacements in the structure progressively increase.
- At a critical load, the plastic region becomes large enough to allow unconstrained plastic flow in the solid. The load cannot be increased beyond this point. The solid is said to *collapse*.

Strain hardening will influence the results quantitatively, but, if the solid has a limiting yield stress (a stress beyond which it can never harden), its behavior will be qualitatively similar.

In a plasticity calculation, often the two most interesting results are (1) the critical load where the solid starts to yield and (2) the critical load where it collapses. Of course, we don't need to solve a plasticity problem to find the yield point; we only need the elastic fields. In many design problems, this is all we need, because plastic flow must be avoided more often than not. However, there are situations in which some plasticity can be tolerated in a structure or component, and there are even some situations where it is desirable (e.g., in designing crumple zones in cars). In this situation, we usually would like to know the collapse load for the solid. It would be really nice to find some way to get the collapse load without having to solve the full boundary value problem.

This is the motivation for plastic limit analysis. The limit theorems of plasticity provide a quick way to estimate collapse loads, without needing any fancy calculations. In fact, collapse loads are often much easier to find than the yield point!

In this section, we derive several useful theorems of plastic limit analysis and illustrate their applications.

6.2.1 Definition of the Plastic Dissipation

Consider a rigid perfectly plastic solid that has mass density ρ_0 and a von Mises yield surface with yield stress in uniaxial tension Y . By definition, the elastic strains are zero in a rigid plastic material: Figure 6.20 shows the stress-strain curve. The solid is subjected to tractions t^* on its boundary. The solid may also be subjected to a body force b (per unit mass) acting on the interior of the solid. Assume that the loading is sufficient to cause the solid to collapse.

6.2.1.1 Velocity Discontinuities

Note that the velocity and stress fields in a collapsing rigid plastic solid need not necessarily be continuous. The solution often has shear discontinuities, as illustrated in Figure 6.21. In the figure, the top part of the solid slides relative to the bottom part. We need a way to describe this kind of deformation. To do so,

1. We assume that the velocity field $\dot{\mathbf{u}}$ at collapse may have a finite set of such shear discontinuities, which occur over a collection of surfaces S . Let \mathbf{m} be a unit vector normal to the surface at some point and let $\dot{\mathbf{u}}^\pm$, σ_{ij}^\pm denote the limiting values of velocity and stress σ_{ij} on the two sides of the surface.

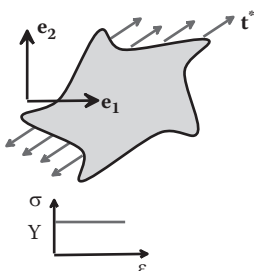


FIGURE 6.20 Rigid plastic solid subjected to external loading.

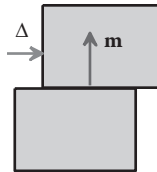


FIGURE 6.21 Velocity discontinuity in a rigid plastic solid.

2. To ensure that no holes open up in the material, the velocity discontinuity must satisfy

$$(\dot{\mathbf{u}}^+ - \dot{\mathbf{u}}^-) \cdot \mathbf{m} = 0.$$

3. The solids immediately adjacent to the discontinuity exert equal and opposite forces on each other. Therefore,

$$\sigma_{ij}^+ m_i = \sigma_{ij}^- m_i.$$

4. We will use the symbol $[[\dot{u}]]$ to denote the relative velocity of sliding across the discontinuity, i.e.,

$$[[\dot{u}]] = |\dot{\mathbf{u}}^+ - \dot{\mathbf{u}}^-| = \sqrt{(\dot{u}_i^+ - \dot{u}_i^-)(\dot{u}_i^+ - \dot{u}_i^-)}.$$

5. The yield criterion and plastic flow rule require that $\sigma_{ij} m_j (\dot{u}_i^+ - \dot{u}_i^-) = Y[[u]] / \sqrt{3}$ on any surfaces of velocity discontinuity.

6.2.1.2 Kinematically Admissible Collapse Mechanism

The kinematically admissible collapse mechanism is analogous to the kinematically admissible displacement field that was introduced to define the potential energy of an elastic solid. By definition, a kinematically admissible collapse mechanism is any velocity field \mathbf{v} satisfying $\partial v_i / \partial x_i = 0$ (i.e., \mathbf{v} is volume preserving).

Like \mathbf{u} , the virtual velocity \mathbf{v} may have a finite set of discontinuities across surfaces \hat{S} with normal $\hat{\mathbf{m}}$ (these are not necessarily the discontinuity surfaces for the actual collapse mechanism). We use

$$[[v]] = |\mathbf{v}^+ - \mathbf{v}^-| = \sqrt{(v_i^+ - v_i^-)(v_i^+ - v_i^-)}$$

to denote the magnitude of the velocity discontinuity. We also define the virtual strain rate

$$\hat{\epsilon}_{ij} = \frac{1}{2} \left(\frac{\partial v_i}{\partial x_j} + \frac{\partial v_j}{\partial x_i} \right)$$

(note that $\hat{\epsilon}_{kk} = 0$) and the effective virtual plastic strain rate

$$\hat{\bar{\epsilon}}^P = \sqrt{2 \hat{\epsilon}_{ij} \hat{\epsilon}_{ij} / 3}.$$

6.2.1.3 Plastic Dissipation

Finally, we define the plastic dissipation associated with the virtual velocity field \mathbf{v} as

$$\Phi(\mathbf{v}) = \int_R Y \dot{\bar{\epsilon}}^p dV + \int_{\hat{S}} \frac{Y}{\sqrt{3}} [[v]] dA - \int_R \rho_0 b_i v_i dA - \int_{\partial R} t_i^* v_i dA.$$

The terms in this expression have the following physical interpretation:

1. The first integral represents the work dissipated in plastically straining the solid.
2. The second integral represents the work dissipated by plastic shearing on the velocity discontinuities.
3. The third integral is the rate of mechanical work done by body forces.
4. The fourth integral is the rate of mechanical work done by the prescribed surface tractions.

6.2.2 Principle of Minimum Plastic Dissipation

Let $\mathbf{\dot{u}}$ denote the actual velocity field that causes a rigid plastic solid to collapse under a prescribed loading. Let \mathbf{v} be any kinematically admissible collapse mechanism. Let $\Phi(\mathbf{v})$ denote the plastic dissipation, as defined in the preceding section. Then,

1. $\Phi(\mathbf{v}) \geq \Phi(\mathbf{\dot{u}})$;
2. $\Phi(\mathbf{\dot{u}}) = 0$.

Thus, Φ is an absolute minimum for $\mathbf{v} = \mathbf{\dot{u}}$; in other words, the actual velocity field at collapse minimizes Φ . Moreover, Φ is zero for the actual collapse mechanism.

Derivation: Begin by summarizing the equations governing the actual collapse solution. Let $[\dot{u}_i, \dot{\epsilon}_{ij}, \sigma_{ij}]$ denote the actual velocity, strain rate, and stress in the solid at collapse. Let $S_{ij} = \sigma_{ij} - \sigma_{kk}\delta_{ij}/3$ denote the deviatoric stress. The fields must satisfy governing equations and boundary conditions:

- Strain-displacement relation: $\epsilon_{ij} = (\partial u_i / \partial x_j + \partial u_j / \partial x_i)/2$.
- Stress equilibrium: $\partial \sigma_{ij} / \partial x_i + \rho_0 b_j = 0$.
- Plastic flow rule and yield criterion:

$$\dot{\epsilon}_{ij} = \begin{cases} \dot{\bar{\epsilon}}^p \frac{3}{2} \frac{S_{ij}}{Y} & \sqrt{\frac{3}{2} S_{ij} S_{ij}} = Y \\ 0 & \sqrt{\frac{3}{2} S_{ij} S_{ij}} < Y \end{cases};$$

On velocity discontinuities, these conditions require that $\sigma_{ij}m_j(\dot{u}_i^+ - \dot{u}_i^-) = Y[[\dot{u}]]/\sqrt{3}$.

- Boundary conditions:

$$\sigma_{ij}n_i = t_j^* \quad x_i \in \partial R.$$

We start by showing that $\Phi(\dot{\mathbf{u}}) = 0$.

1. By definition,

$$\Phi(\dot{\mathbf{u}}) = \int_R Y \dot{\varepsilon}^p dV + \int_S \frac{Y}{\sqrt{3}} [[\dot{u}]] dA - \int_R \rho_0 b_i \dot{u}_i dA - \int_{\partial R} t_i^* \dot{u}_i dA.$$

2. Note that, using (1) the flow rule, (2) the condition that $S_{ii} = 0$, and (3) the yield criterion:

$$\sigma_{ij}\dot{\varepsilon}_{ij}^p = \sigma_{ij}\dot{\varepsilon}^p \frac{3S_{ij}}{2Y} = (S_{ij} + \sigma_{kk}\delta_{ij})\dot{\varepsilon}^p \frac{3S_{ij}}{2Y} = \dot{\varepsilon}^p \frac{3S_{ij}S_{ij}}{2Y} = Y\dot{\varepsilon}^p.$$

3. Note that $\sigma_{ij}\dot{\varepsilon}_{ij} = \sigma_{ij}(\partial u_i / \partial x_j + \partial u_j / \partial x_i) / 2 = \sigma_{ij}\partial u_j / \partial x_i$ from the symmetry of σ_{ij} . Hence,

$$\int_R Y \dot{\varepsilon}^p dV = \int_R \sigma_{ij}\dot{\varepsilon}_{ij} dV = \int_R \sigma_{ij}\partial u_j / \partial x_i dV.$$

4. Note that $\sigma_{ij}\partial u_j / \partial x_i = \partial(\sigma_{ij}u_j) / \partial x_i - (\partial\sigma_{ij} / \partial x_i)\dot{u}_j$. Substitute into the expression for $\Phi(\dot{\mathbf{u}})$, combine the two volume integrals and recall (equilibrium) that $\partial\sigma_{ij} / \partial x_i + \rho_0 b_j = 0$ to see that

$$\Phi(\dot{\mathbf{u}}) = \int_R \partial(\sigma_{ij}\dot{u}_j) / \partial x_i dV + \int_S \frac{Y}{\sqrt{3}} [[\dot{u}]] dA - \int_{\partial R} t_i^* \dot{u}_i dA.$$

5. Apply the divergence theorem to the volume integral in this result. When doing so, note that we must include contributions from the velocity discontinuity across S as follows

$$\Phi(\dot{\mathbf{u}}) = \int_{\partial R} \sigma_{ij}\dot{u}_j n_i dA + \int_S \sigma_{ij}\dot{u}_j^+ n_i^+ dA + \int_S \sigma_{ij}\dot{u}_j^- n_i^- dA + \int_S \frac{Y}{\sqrt{3}} [[\dot{u}]] dA - \int_{\partial R} t_i^* \dot{u}_i dA.$$

6. Finally, recall that $\sigma_{ij}n_i = t_j^*$ on the boundary and note that the outward normals to the solids adjacent to S are related to \mathbf{m} by $n_i^+ = -m_i$, $n_i^- = m_i$ (see Figure 6.22). Thus,

$$\Phi(\dot{\mathbf{u}}) = - \int_S \sigma_{ij}(\dot{u}_i^+ - \dot{u}_i^-) m_i dA + \int_S \frac{Y}{\sqrt{3}} [[\dot{u}]] dA.$$

Because $\sigma_{ij}m_j(\dot{u}_i^+ - \dot{u}_i^-) = Y[[\dot{u}]]/\sqrt{3}$, we find that $\Phi(\dot{\mathbf{u}}) = 0$ as required.

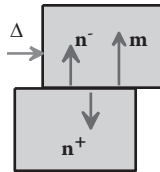


FIGURE 6.22 Vectors normal to a velocity discontinuity in a rigid plastic solid.

Next, we show that $\Phi(\mathbf{v}) \geq 0$. To this end,

1. Let v_i be a kinematically admissible velocity field as defined in the preceding section, with strain rate

$$\hat{\dot{\epsilon}}_{ij} = \frac{1}{2} \left(\frac{\partial v_i}{\partial x_j} + \frac{\partial v_j}{\partial x_i} \right).$$

2. Let \hat{S}_{ij} be the stress necessary to drive the kinematically admissible collapse mechanism, which must satisfy the plastic flow rule and the yield criterion

$$\hat{\dot{\epsilon}}_{ij} = \hat{\bar{\epsilon}} \frac{3 \hat{S}_{ij}}{2 Y} - \sqrt{3 \hat{S}_{ij} \hat{S}_{ij} / 2} = Y.$$

3. Recall that the plastic strains and stresses associated with the kinematically admissible field must satisfy the principle of maximum plastic resistance (Section 3.7.10), which in the present context implies that

$$(\hat{\sigma}_{ij} - \sigma_{ij}) \hat{\dot{\epsilon}}_{ij} \geq 0.$$

To see this, note that $\hat{\sigma}_{ij}$ is the stress required to cause the plastic strain rate $\hat{\dot{\epsilon}}_{ij}$, whereas the actual stress state at collapse σ_{ij} must satisfy $\sqrt{3 S_{ij} S_{ij} / 2} \leq Y$.

4. Note that $\sigma_{ij} \hat{\dot{\epsilon}}_{ij} = (\hat{S}_{ij} + \hat{\sigma}_{kk} \delta_{ij}) d\hat{\bar{\epsilon}}^P 3 \hat{S}_{ij} / 2Y = Y d\hat{\bar{\epsilon}}^P$. Substituting into the principle of maximum plastic resistance and integrating over the volume of the solid shows that

$$\int_R Y \hat{\bar{\epsilon}}^P dV - \int_R \sigma_{ij} \hat{\dot{\epsilon}}_{ij} dV \geq 0.$$

5. Next, note that

$$\sigma_{ij} \hat{\dot{\epsilon}}_{ij} = \sigma_{ij} (\partial v_i / \partial x_j + \partial v_j / \partial x_i) / 2 = \sigma_{ij} \partial v_j / \partial x_i = \partial (\sigma_{ij} v_j) / \partial x_i - (\partial \sigma_{ij} / \partial x_i) v_j.$$

6. The equilibrium equation shows that $\partial \sigma_{ij} / \partial x_i = -\rho_0 b_j$. Substituting this into the result of item 5 and then substituting into the result of item 4 shows that

$$\int_R Y \hat{\bar{\epsilon}}^P dV - \int_R \partial (\sigma_{ij} v_j) / \partial x_i dV - \int_R \rho_0 b_j v_j dV \geq 0.$$

7. Apply the divergence theorem to the second integral. When doing so, note that we must include contributions from the velocity discontinuity across \hat{S} as follows

$$\int_R Y \hat{\bar{\epsilon}}^p dV - \int_{\hat{S}} \sigma_{ij} v_j n_i^+ dA - \int_{\hat{S}} \sigma_{ij} v_j n_i^- dA - \int_{\partial R} \sigma_{ij} v_j n_i dA - \int_R \rho_0 b_j v_j dV \geq 0.$$

8. Recall that $\sigma_{ij} n_i = t_j^*$ on the boundary and note that the outward normals to the solids adjacent to \hat{S} are related to \mathbf{m} by $n_i^+ = -m_i$, $n_i^- = m_i$. Thus,

$$\int_R Y \hat{\bar{\epsilon}}^p dV + \int_{\hat{S}} \sigma_{ij} \hat{m}_j (v_i^+ - v_i^-) dA - \int_R b_i v_i dV - \int_{\partial_2 R} t_i^* v_i dA \geq 0.$$

9. Finally, note that, on \hat{S} ,

$$\sigma_{ij} \hat{m}_j (v_i^+ - v_i^-) \leq Y[[v]] / \sqrt{3}$$

because the shear stress acting on any plane in the solid cannot exceed $Y / \sqrt{3}$. Thus,

$$\int_R Y \hat{\bar{\epsilon}}^p dV + \int_{\hat{S}} Y[[v]] / \sqrt{3} dA - \int_R b_i v_i dV - \int_{\partial_2 R} t_i^* v_i dA \geq 0,$$

proving that $\Phi(\mathbf{v}) \geq 0$ as required.

6.2.3 Upper Bound Plastic Collapse Theorem

Consider a rigid plastic solid, subjected to some distribution of tractions t_i^* and body forces b_i (Figure 6.23). We will attempt to estimate the factor β by which the loading can be increased before the solid collapses (β is effectively the factor of safety). We suppose that the solid will collapse for loading βt_i^* , βb_i .

To estimate β , we guess the mechanism of collapse. The collapse mechanism will be an admissible velocity field, which may have a finite set of discontinuities across surfaces \hat{S} with normal $\hat{\mathbf{m}}$, as discussed in Section 6.2.1.

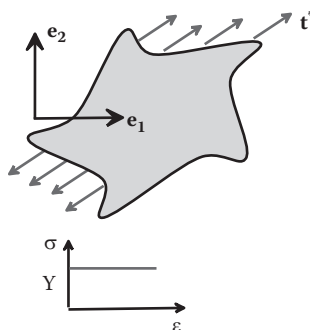


FIGURE 6.23 Rigid plastic solid subjected to external loading.

The principle of minimum plastic dissipation then states that

$$\int_R Y \dot{\varepsilon}^p dV + \int_{\hat{S}} \sigma_{ij} \dot{m}_j (v_i^+ - v_i^-) dA - \int_R \beta b_i v_i dV - \int_{\partial R} \beta t_i^* v_i dA \geq 0$$

for any collapse mechanism, with equality for the true mechanism of collapse. Therefore,

$$\beta \leq \frac{\int_R Y \dot{\varepsilon}^p dV + \int_{\hat{S}} Y[[v]] / \sqrt{3} dA}{\int_R b_i v_i dA + \int_{\partial R} t_i^* v_i dA}.$$

Expressed in words, this equation states that we can obtain an upper bound to the collapse loads by postulating a collapse mechanism, and computing the ratio of the plastic dissipation associated with this mechanism to the work done by the applied loads.

So, we can choose any collapse mechanism and use it to estimate a safety factor. The actual safety factor is likely to be lower than our estimate (it will be equal if we guessed right). This method is evidently inherently unsafe, because it overestimates the safety factor; however, it is usually possible to guess the collapse mechanism quite accurately and so, with practice, you can get excellent estimates.

6.2.4 Examples of Applications of the Upper Bound Theorem

6.2.4.1 Example 1: Collapse Load for a Uniaxial Bar

We will illustrate the bounding theorems using a few examples. First, we will compute bounds to the collapse load for a uniaxial bar. Assume the bar has unit out of plane thickness, for simplicity.

To get an upper bound, we guess a collapse mechanism as shown in Figure 6.24. The top and bottom half of the bar slide past each other as rigid blocks, as shown, with a velocity discontinuity across the line separating the blocks.

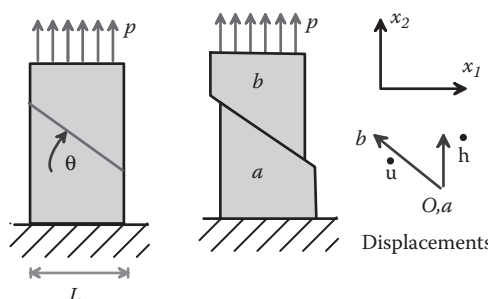


FIGURE 6.24 Collapse mechanism for a bar subjected to uniaxial loading.

The upper bound theorem gives

$$\beta \leq \frac{\int_R Y \dot{\hat{\varepsilon}}^p dV + \int_{\hat{S}} Y[[v]]/\sqrt{3} dA}{\int_R b_i v_i dA + \int_{\partial R} t_i^* v_i dA}.$$

In this problem, the strain rate vanishes, because we assume that the two halves of the bar are rigid. The plastic dissipation is

$$\int_{\hat{S}} Y[[v]]/\sqrt{3} dA = Y(\dot{h}/\sin\theta)(L/\cos\theta)/\sqrt{3}.$$

The body force vanishes and

$$\int_{\partial R} t_i^* u_i dA = p L \dot{h},$$

where \dot{h} is the vertical component of the velocity of the top block. Thus,

$$\beta p \leq 2Y/(\sqrt{3} \sin 2\theta)$$

The best upper bound occurs for $\theta = \pi/4$, giving $\beta p \leq 2Y/\sqrt{3}$ for the collapse load.

6.2.4.2 Example 2: Collapse Load for a Bar Containing a Hole

For a slightly more interesting problem, consider the effect of inserting a hole with radius a in the center of the column, as shown in Figure 6.25. This time we apply a force to the top of the column rather than specify the traction distribution in detail. We will accept any solution that has traction acting on the top surface that is statically equivalent to the applied force.

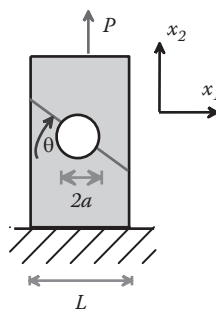


FIGURE 6.25 Collapse mechanism for a plate containing a hole under uniaxial loading.

A possible collapse mechanism is shown. The plastic dissipation is

$$\int_{\hat{S}} Y[[v]]/\sqrt{3} dA = (Y/\sqrt{3})(\dot{h}/\sin\theta)(L/\cos\theta - 2a).$$

The rate of work done by applied loading is

$$\int_{\partial R} t_i \dot{u}_i dA = P \dot{h}.$$

Our upper bound follows as

$$\beta P \leq 2Y(L/\cos\theta - 2a)/(\sqrt{3}\sin\theta),$$

and a simple (but not quite optimal) upper bound solution is $\beta P \leq 2Y(L - 2a)/\sqrt{3}$.

6.2.4.3 Example 3: Force Required to Indent a Rigid Plastic Surface

For our next example, we attempt to find upper and lower bounds to the force required to push a flat plane punch into a rigid plastic solid. This problem is interesting because we have an exact slip-line field solution, so we can assess the accuracy of the bounding calculations.

A possible collapse mechanism is shown in Figure 6.26. In each semicircular region, we assume a constant circumferential velocity $v_\theta = \dot{h}$. To compute the plastic dissipation in one of the regions, adopt a cylindrical-polar coordinate system with origin at the edge of the contact. The strain distribution follows as

$$\begin{aligned} \dot{\epsilon}_{rr} = \dot{\epsilon}_{\theta\theta} = 0 \quad \dot{\epsilon}_{r\theta} &= \frac{1}{2} \frac{v_\theta}{r} = \frac{\dot{h}}{2r} \\ \Rightarrow \hat{\dot{\epsilon}}^P &= \sqrt{\frac{2}{3} \hat{\dot{\epsilon}}_{ij} \hat{\dot{\epsilon}}_{ij}} = \frac{\dot{h}}{r\sqrt{3}}. \end{aligned}$$

Thus, the plastic dissipation is

$$\int_R \hat{\dot{\epsilon}}^P dV + \int_{\hat{S}} Y[[v]]/\sqrt{3} dA = 2 \left\{ \int_0^{\pi/2} \int_0^{a/2} Y \frac{\dot{h}}{r\sqrt{3}} r dr d\theta + \frac{Y}{2\sqrt{3}} \dot{h} \pi a \right\} = \frac{2\pi}{\sqrt{3}} \dot{h} Ya$$

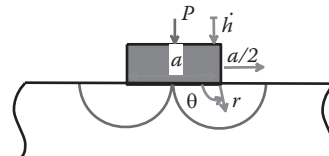


FIGURE 6.26 Collapse mechanism for a rigid plastic solid indented by a flat punch.

(note that there is a velocity discontinuity at $r = a$). The work done by applied loading is just $\dot{h}P$ giving the upper bound

$$\beta P \leq 2\pi Ya / \sqrt{3}.$$

This should be compared with the exact slip-line field solution

$$\beta P = (\pi + 2)Ya / \sqrt{3}.$$

computed in Section 6.1. The error is 17%, close enough for government work.

6.2.4.4 Example 4: Orthogonal Metal Cutting

Figure 6.27 shows a simple model of machining. The objective is to determine the horizontal force P acting on the tool (or work piece) in terms of the depth of cut h , the tool rake angle α , and the yield stress of the material Y .

To perform the calculation, we adopt a reference frame that moves with the tool. Thus, the tool appears stationary, whereas the work piece moves at speed V_w to the right. The collapse mechanism consists of shear across the red line shown in the picture.

Elementary geometry gives the chip thickness d as

$$d = h \frac{\cos(\phi + \alpha)}{\sin \phi}.$$

Mass conservation (material flowing into slip discontinuity = material flowing out of slip discontinuity) gives the velocity of material in the chip V_c as

$$V_c = V_w \frac{h}{d} = V_w \frac{\sin \phi}{\cos(\phi + \alpha)}.$$

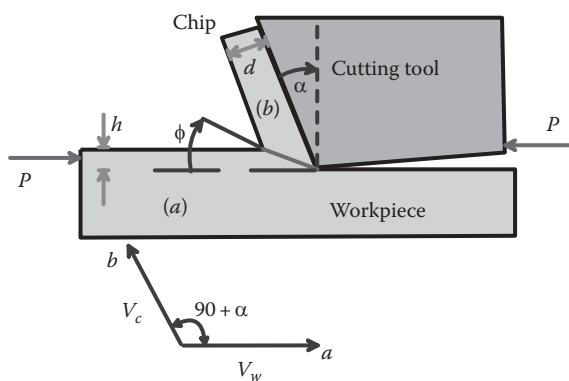


FIGURE 6.27 Collapse mechanism for an orthogonal machining process.

The velocity discontinuity across the shear band is

$$\begin{aligned}|V_{ba}| &= \sqrt{V_w^2 + V_c^2 + 2V_c V_w \sin \alpha} \\&= V_w \sqrt{1 + \frac{\sin^2 \phi}{\cos^2(\phi+\alpha)} + 2 \sin \alpha \frac{\sin \phi}{\cos(\phi+\alpha)}}.\end{aligned}$$

The plastic dissipation follows as

$$\dot{W}^P = \frac{h}{\sin \phi} |V_{ab}| \frac{Y}{\sqrt{3}}.$$

The upper bound theorem gives

$$\begin{aligned}PV_w &\leq \frac{h}{\sin \phi} |V_{ab}| \frac{Y}{\sqrt{3}} \\ \Rightarrow P &\leq \frac{hY}{\sqrt{3} \sin \phi} \sqrt{1 + \frac{\sin^2 \phi}{\cos^2(\phi+\alpha)} + 2 \sin \alpha \frac{\sin \phi}{\cos(\phi+\alpha)}}.\end{aligned}$$

To obtain the best estimate for P , we need to minimize the right-hand side of this expression with respect to ϕ . This gives

$$\phi = \tan^{-1}(1 - \tan(\alpha)).$$

The resulting upper bound to the machining force is plotted in Figure 6.28.

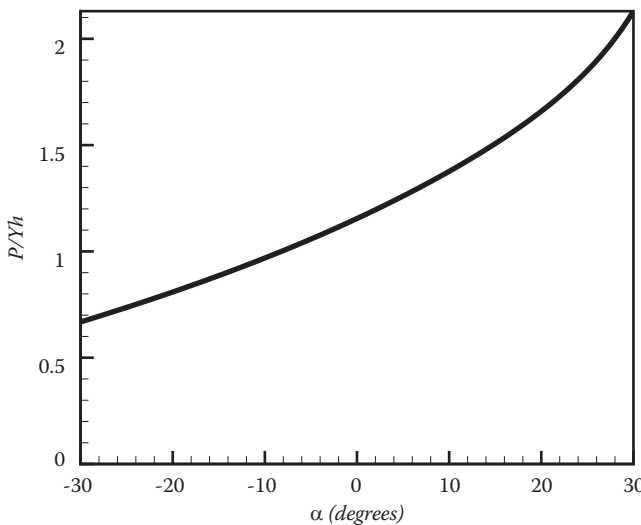


FIGURE 6.28 Cutting force-versus-rake angle predicted by the mechanism shown in Figure 6.27.

6.2.5 Lower Bound Plastic Collapse Theorem

The lower bound theorem provides a safe estimate of the collapse loads for a rigid plastic solid. Consider a rigid plastic solid, subjected to some distribution of tractions t_i^* and body forces b_i , as shown in Figure 6.29. We will attempt to estimate the factor β by which the loading can be increased before the solid collapses (β is effectively the factor of safety). We suppose that the solid will collapse for loading $\beta t_i^*, \beta b_i$.

To estimate β , we guess the distribution of stress in the solid at collapse. We will denote the guess for the stress distribution by $\hat{\sigma}_{ij}$. The stress distribution must do the following:

1. Satisfy the boundary conditions $\hat{\sigma}_{ij}n_j = \beta_L t_i^*$, where β_L is a lower bound to β .
2. Satisfy the equations of equilibrium $\partial\hat{\sigma}_{ij}/\partial x_j + \beta_L b_i = 0$ within the solid.
3. Must not violate the yield criterion anywhere within the solid, $f(\hat{\sigma}_{ij}) \leq 0$.

The lower bound theorem states that if any such stress distribution can be found, the solid will not collapse, i.e., $\beta_L \leq \beta$.

Derivation

1. Let $[\dot{u}_i, \dot{\varepsilon}_{ij}, \sigma_{ij}]$ denote the actual velocity field in the solid at collapse. These must satisfy the field equations and constitutive equations listed in Section 6.4.4.
2. Let $\hat{\sigma}_{ij}$ denote the guess for the stress field.
3. The principle of maximum plastic resistance (see Section 3.7.10) shows that $(\sigma_{ij} - \hat{\sigma}_{ij})\dot{\varepsilon}_{ij} \geq 0$, because $\hat{\sigma}_{ij}$ is at or below yield.
4. Integrating this equation over the volume of the solid and using the principle of virtual work on the two terms shows that

$$\begin{aligned} \int_V (\sigma_{ij} - \hat{\sigma}_{ij})\dot{\varepsilon}_{ij} dV &= \int_{\partial V} \sigma_{ij} n_j \dot{u}_i dA - \int_{\partial V} \hat{\sigma}_{ij} n_j \dot{u}_i dA \geq 0 \\ \Rightarrow \beta \int_{\partial V} t_i \dot{u}_i dA &\geq \beta_L \int_{\partial V} t_i \dot{u}_i dA. \end{aligned}$$

This proves the theorem.

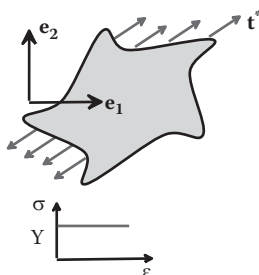


FIGURE 6.29 Rigid plastic solid subjected to external loading.

6.2.6 Examples of Applications of the Lower Bound Plastic Collapse Theorem

6.2.6.1 Example 1: Collapse Load for a Plate Containing a Hole

A plate with width L contains a hole of radius a at its center. The plate is subjected to a tensile force P as shown (the traction distribution is not specified in detail, so we will accept any solution that has traction acting on the top surface that is statically equivalent to the applied force).

For a statically admissible stress distribution, we consider the stress field shown in Figure 6.30, with $\sigma_{22} = 0$ for $|x_1| < a$, $\sigma_{22} = Y$ for $x_1 > a$ and all other stress components zero.

The estimate for the applied load at collapse follows as $\beta_L P = 2Y(L - a)$.

6.2.6.2 Example 2: Rigid Indenter in Contact with a Half-Space

We consider a flat indenter with width a that is pushed into the surface of a half-space by a force P . The stress state illustrated in Figure 6.31 will be used to obtain a lower bound to the collapse load in the solid. Note the following:

1. Regions C, E, and F are stress free.
2. The stress in regions A and D consists of a state of uniaxial stress, with direction parallel to the boundaries between AC (or AE) and CD (or DF), respectively. We will denote this stress by $\sigma^A \mathbf{m} \otimes \mathbf{m}$, where \mathbf{m} is a unit vector parallel to the direction of the uniaxial stress.
3. The stress state in the triangular region B has principal directions of stress parallel to \mathbf{e}_α . We will write this stress state as $\sigma_{11}^B \mathbf{e}_1 \otimes \mathbf{e}_1 + \sigma_{22}^B \mathbf{e}_2 \otimes \mathbf{e}_2$.

The stresses in each region must be chosen to satisfy equilibrium and to ensure that the stress is below yield everywhere. The stress is constant in each region, so equilibrium is satisfied locally. However, the stresses are discontinuous across AC, AB, etc. To satisfy

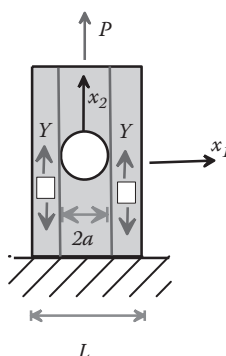


FIGURE 6.30 Statically admissible stress field for a plate containing a hole, subjected to uniaxial tensile loading.

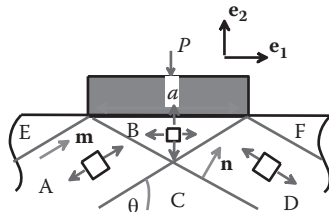


FIGURE 6.31 Statically admissible stress field for a rigid plastic solid indented by a flat punch.

equilibrium, equal and opposite tractions must act on the material surfaces adjacent to the discontinuity, which requires, for example, that $\sigma_{ij}^A n_j = \sigma_{ij}^B n_j$, where \mathbf{n} is a unit vector normal to the boundary between A and B as indicated in Figure 6.31. We enforce this condition as follows:

1. Note that $\mathbf{m} = \cos\theta\mathbf{e}_1 + \sin\theta\mathbf{e}_2$ $\mathbf{n} = \sin\theta\mathbf{e}_1 + \cos\theta\mathbf{e}_2$.
2. Equilibrium across the boundary between A and B requires

$$\begin{aligned}\sigma^A(\mathbf{m} \otimes \mathbf{m}) \cdot \mathbf{n} &= (\sigma_{11}^B \mathbf{e}_1 \otimes \mathbf{e}_1 + \sigma_{22}^B \mathbf{e}_2 \otimes \mathbf{e}_2) \cdot \mathbf{n} \\ &\Rightarrow \sigma^A(\cos\theta\mathbf{e}_1 + \sin\theta\mathbf{e}_2) 2\sin\theta\cos\theta = \sigma_{11}^B \mathbf{e}_1 \sin\theta + \sigma_{22}^B \mathbf{e}_2 \cos\theta \\ &\Rightarrow \sigma_{11}^B = 2\sigma^A \cos^2\theta \quad \sigma_{22}^B = 2\sigma^A \sin^2\theta.\end{aligned}$$

3. We must now choose σ^A and θ to maximize the collapse load but ensure that the stresses do not exceed yield in regions A or B. Clearly, this requires $\sigma^A = -Y$, whereas θ must be chosen to ensure that $|\sigma_{22}^B - \sigma_{11}^B| < Y$. This requires $1/2 < \cos\theta < \sqrt{3}/2$. The largest value for θ maximizes the bound.
4. Finally, substituting for θ gives $\sigma_{22}^B = -3Y/2$. We see that the lower bound is $P = -3Ya/2$.

6.2.7 Lower Bound Shakedown Theorem

In this and the next section, we derive two important theorems that can be used to estimate the maximum cyclic loads that can be imposed on a component without exceeding yield. The concept of shakedown in a solid subjected to cyclic loads was introduced in Section 4.2.4, which discusses the behavior of a spherical shell subjected to cyclic internal pressure. It was shown that, if the first cycle of pressure exceeds yield, residual stresses are introduced into the shell, which may prevent additional plastic deformation under subsequent load cycles. This process is known as shakedown, and the maximum load for which it can occur is known as the shakedown limit.

We proceed to derive a theorem that can be used to obtain a safe estimate to the maximum cyclic load that can be applied to a structure without inducing cyclic plastic deformation.

We consider an elastic-perfectly plastic solid, sketched in Figure 6.32. The solid has Young's modulus E , Poisson's ratio ν , and has a von Mises yield surface with uniaxial tensile yield stress Y and an associated flow law. Assume the following:

1. The displacement $\mathbf{u} = \mathbf{0}$ on part of the boundary of the solid $\partial_1 R$.
2. The remainder of the boundary $\partial_2 R$ is subjected to a prescribed cycle of traction $\mathbf{t}^*(t)$. The history of traction is periodic, with a period T .

Define the following quantities:

1. Let $[u_i, \varepsilon_{ij}, \sigma_{ij}]$ denote the actual history of displacement, strain, and stress induced in the solid by the applied loading. The strain is partitioned into elastic and plastic parts as $\varepsilon_{ij} = \varepsilon_{ij}^e + \varepsilon_{ij}^p$.
2. Let $[u_i^e, \varepsilon_{ij}^e, \sigma_{ij}^e]$ denote the history of displacement, strain, and stress induced by the prescribed traction in a perfectly elastic solid with identical geometry.
3. We introduce (time-dependent) residual stress ρ_{ij} and residual strain γ_{ij} fields, which (by definition) satisfy

$$\sigma_{ij} = \sigma_{ij}^e + \rho_{ij} \quad \varepsilon_{ij} = \varepsilon_{ij}^e + \varepsilon_{ij}^p = \varepsilon_{ij}^e + \gamma_{ij} + \varepsilon_{ij}^p.$$

Note the following: (1) because $\sigma_{ij}^e n_j = \sigma_{ij} n_j = t_i^*$ on $\partial_2 R$, it follows that $\rho_{ij} n_j = 0$ on $\partial_2 R$; and (2) because $\partial \sigma_{ij}^e / \partial x_j = \partial \sigma_{ij} / \partial x_j = 0$, it follows that $\partial \rho_{ij} / \partial x_j = 0$.

The *lower bound shakedown theorem* can be stated as follows. The solid is guaranteed to shake down if any time-independent residual stress field $\bar{\rho}_{ij}$ can be found that satisfies the following:

- The equilibrium equation: $\partial \bar{\rho}_{ij} / \partial x_j = 0$.
- The boundary condition: $\bar{\rho}_{ij} n_j = 0$ on $\partial_2 R$.
- When the residual stress is combined with the elastic solution, the combined stress does not exceed yield $f(\sigma_{ij}^e + \bar{\rho}_{ij}) \leq 0$ at any time during the cycle of load.

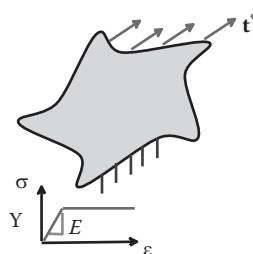


FIGURE 6.32 Elastic-perfectly plastic solid subjected to cyclic external loading.

The theorem is valuable because shakedown limits can be estimated using the elastic solution, which is much easier to calculate than the elastic-plastic solution.

Proof of the lower bound theorem: The proof is one of the most devious in solid mechanics.

1. Consider the strain energy associated with the difference between the actual residual stress field ρ_{ij} and the guess for the residual stress field $\bar{\rho}_{ij}$, which can be calculated as

$$W = \frac{1}{2} \int_R S_{ijkl} (\rho_{ij} - \bar{\rho}_{ij}) (\rho_{kl} - \bar{\rho}_{kl}) dV,$$

where S_{ijkl} is the elastic compliance tensor. For later reference, note that W has to be positive, because strain energy density is always positive or zero.

2. The rate of change of W can be calculated as

$$\frac{dW}{dt} = \int_R S_{ijkl} (\rho_{ij} - \bar{\rho}_{ij}) \frac{d\rho_{kl}}{dt} dV \geq 0$$

(to see this, recall that $S_{ijkl} = S_{klij}$).

3. Note that $S_{ijkl} \rho_{kl} = \gamma_{ij} = \varepsilon_{ij}^e - \dot{\varepsilon}_{ij}^p - \dot{\varepsilon}_{ij}^e$. Consequently, we see that

$$\frac{dW}{dt} = - \int_R (\rho_{ij} - \bar{\rho}_{ij}) \frac{d\varepsilon_{ij}^p}{dt} dV + \int_R (\rho_{ij} - \bar{\rho}_{ij}) \left(\frac{d\varepsilon_{ij}^e}{dt} - \frac{d\varepsilon_{ij}^e}{dt} \right) dV \geq 0.$$

4. Using the principle of virtual work, the second integral can be expressed as an integral over the boundary of the solid

$$\int_S (\rho_{ij} - \bar{\rho}_{ij}) n_j \left(\frac{du_i}{dt} - \frac{du_i^e}{dt} \right) dA = 0.$$

To see this, note that $(\rho_{ij} - \bar{\rho}_{ij}) n_j = 0$ on $\partial_2 R$, whereas $\dot{u}_i - \dot{u}_i^e = 0$ on $\partial_1 R$.

5. The remaining integral in item 3 can be rewritten as

$$\frac{dW}{dt} = - \int_R (\rho_{ij} - \bar{\rho}_{ij}) \frac{d\varepsilon_{ij}^p}{dt} dV = - \int_R [\sigma_{ij} - (\sigma_{ij}^e + \bar{\rho}_{ij})] \frac{d\varepsilon_{ij}^p}{dt} dV \geq 0.$$

6. Finally, recall that $\sigma_{ij}^e + \bar{\rho}_{ij}$ lies at or below yield, whereas σ_{ij} is at yield and is the stress corresponding to the plastic strain rate $\dot{\varepsilon}_{ij}^p$. The principle of maximum plastic resistance therefore shows that $[\sigma_{ij} - (\sigma_{ij}^e + \bar{\rho}_{ij})] \dot{\varepsilon}_{ij}^p \geq 0$. This inequality and $dW / dt \geq 0$

can only be satisfied simultaneously if $[\sigma_{ij} - (\sigma_{ij}^\varepsilon + \bar{\rho}_{ij})] \dot{\epsilon}_{ij}^p = 0$. We conclude that either the plastic strain rate vanishes or $[\sigma_{ij} - (\sigma_{ij}^\varepsilon + \bar{\rho}_{ij})] = 0$. In either case, the solid must shake down to an elastic state.

6.2.8 Examples of Applications of the Lower Bound Shakedown Theorem

6.2.8.1 Example 1: A Simple Three-Bar Problem

It is traditional to illustrate the concept of shakedown using this problem. Consider a structure made of three parallel elastic-plastic bars, with Young's modulus E and cross-sectional area A , as shown in Figure 6.33. The two bars labeled 1 and 2 have yield stress Y ; the central bar (labeled 3) has yield stress $2Y$. The structure is subjected to a cyclic load with mean value \bar{P} and amplitude ΔP . The elastic limit for the structure is $\bar{P} \pm \Delta P = 3AY$; the collapse load is $\bar{P} \pm \Delta P = 4AY$.

To obtain a lower bound to the shakedown limit, we must do the following:

1. Calculate the elastic stresses in the structure; the axial stress in each bar is $\sigma^\varepsilon = P/3A$.
2. Find a residual stress distribution in the structure that satisfies equilibrium and boundary conditions, and that can be added to the elastic stresses to bring them below yield. A suitable residual stress distribution consists of an axial stress $\rho^{(1)} = \rho^{(2)} = \rho_0$, $\rho^{(3)} = -2\rho_0$ in bars 1, 2, and 3. To prevent yield at the maximum and minimum load in all three bars, we require

$$\begin{aligned} -Y &< (\bar{P} - \Delta P)/3A + \rho_0 & (\bar{P} + \Delta P)/3A + \rho_0 &< Y \\ -2Y &< (\bar{P} - \Delta P)/3A - 2\rho_0 & (\bar{P} + \Delta P)/3A - 2\rho_0 &< 2Y. \end{aligned}$$

The first two equations show that $\Delta P < Y$, irrespective of ρ_0 . To avoid yield in all bars at the maximum load, we must choose $\rho_0 = -Y/3$, which gives $P + \Delta P < 4AY$. Similarly, to avoid yield in all bars at the minimum load, we must choose $\rho_0 = Y/3$, showing that $-4AY < (\bar{P} - \Delta P)$.

The various regimes of behavior are summarized in Figure 6.34.

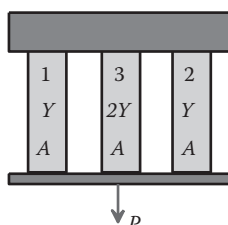


FIGURE 6.33 Parallel bars loaded in tension by a cyclic force.

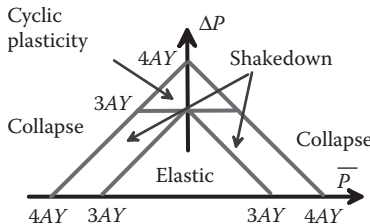


FIGURE 6.34 Map showing regimens of behavior for the three-bar problem shown in Figure 6.33.

6.2.8.2 Example 2: Shakedown Limit for a Pressurized Spherical Shell

We consider an elastic-perfectly plastic thick-walled shell, with inner radius a and outer radius b . The inner wall of the shell is subjected to a cyclic pressure, with minimum value zero and maximum value p_a , as sketched in Figure 6.35.

To estimate the shakedown limit we must do the following:

1. Calculate the stresses induced by the pressure in an elastic shell. The solution can be found in Section 4.1.4:

$$\sigma_{RR} = \frac{p_a a^3}{(b^3 - a^3)} \left(1 - \frac{b^3}{R^3} \right) \quad \sigma_{\theta\theta} = \sigma_{\phi\phi} = \frac{p_a a^3}{(b^3 - a^3)} \left(1 + \frac{b^3}{2R^3} \right).$$

2. Find a self-equilibrating residual stress field, which satisfies traction-free boundary conditions on $R = a$, $R = b$ and which can be added to the elastic stresses to prevent yield in the sphere. The equilibrium equation for the residual stress can be written as

$$\frac{d\rho_{RR}}{dR} + \frac{1}{R}(2\rho_{RR} - \rho_{\theta\theta} - \rho_{\phi\phi}) = 0.$$

We can satisfy this equation by choosing any suitable distribution for ρ_{RR} and calculating the corresponding $\rho_{\theta\theta}$. For example, we can choose $\rho_{RR} = \rho_0(1 - a/R)(1 - b/R)$, which corresponds to $\rho_{\theta\theta} = \rho_0(1 - (b + a)/2R)$. To avoid yield at maximum load, we

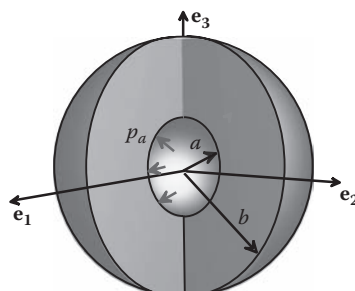


FIGURE 6.35 Thick-walled sphere subjected to cyclic internal pressure.

must ensure that $|\sigma_{RR} - \sigma_{\theta\theta} + \rho_{RR} - \rho_{\theta\theta}| \leq Y$, whereas to avoid yield at zero load, $|\rho_{RR} - \rho_{\theta\theta}| \leq Y$ throughout the shell. The critically stressed material element lies at $R = a$ at both the maximum and zero loads, which shows that

$$\frac{3p_a b^3}{(b^3 - a^3)} + \rho_0 \frac{(b-a)}{2a} < Y \quad -Y < \rho_0 \frac{(b-a)}{2a} < Y.$$

Clearly, the best choice of ρ_0 is $\rho_0 = -2Ya/(b-a)$.

The estimate for the shakedown limit therefore follows as $p_a / Y < 4(1 - a^3 / b^3) / 3$. This is equal to the exact solution derived (with considerably more effort) in Section 4.1.4.

6.2.9 Upper Bound Shakedown Theorem

In this section, we derive a theorem that can be used to obtain an overestimate to the maximum cyclic load that can be applied to a structure without inducing cyclic plastic deformation. Although the estimate is inherently unsafe, the theorem is easier to use than the lower bound theorem.

We consider an elastic-perfectly plastic solid, sketched in Figure 6.36. The solid has Young's modulus E , Poisson's ratio ν , and has a von Mises yield surface with uniaxial tensile yield stress Y and an associated flow law. Assume the following:

1. The displacement $\mathbf{u} = \mathbf{0}$ on part of the boundary of the solid $\partial_1 R$.
2. The remainder of the boundary $\partial_2 R$ is subjected to a prescribed cycle of traction $\mathbf{t}^*(t)$. The history of traction is periodic, with a period T .

Define the following quantities:

1. Let $[u_i, \varepsilon_{ij}, \sigma_{ij}]$ denote the actual history of displacement, strain, and stress induced in the solid by the applied loading. The strain is partitioned into elastic and plastic parts as $\varepsilon_{ij} = \varepsilon_{ij}^e + \varepsilon_{ij}^p$.
2. Let $[u_i^e, \varepsilon_{ij}^e, \sigma_{ij}^e]$ denote the history of displacement, strain, and stress induced by the prescribed traction in a perfectly elastic solid with identical geometry.

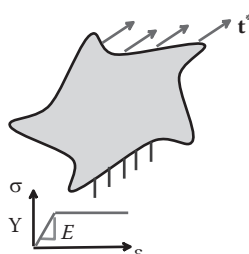


FIGURE 6.36 Elastic-plastic solid subjected to cyclic external loading.

To apply the upper bound theorem, we guess a mechanism of cyclic plasticity that might occur in the structure under the applied loading. We denote the cycle of strain by $\hat{\epsilon}_{ij}^p(t)$ and define the change in strain per cycle as

$$\Delta\hat{\epsilon}_{ij}^p = \int_0^T \hat{\epsilon}_{ij}^p(t) dt.$$

To be a kinematically admissible cycle,

- $\Delta\hat{\epsilon}_{ij}^p$ must be compatible, i.e., $\Delta\hat{\epsilon}_{ij}^p = (\partial\Delta\hat{u}_i / \partial x_j + \partial\Delta\hat{u}_j / \partial x_i) / 2$ for some displacement field $\Delta\hat{u}_i$. Note that only the change in strain per cycle needs to be compatible; the plastic strain rate need not be compatible at every instant during the cycle.
- The compatible displacement field must satisfy $\Delta\hat{u}_i = 0$ on $\partial_1 R$.

The *upper bound shakedown theorem* can then be stated as follows. If there exists any kinematically admissible cycle of strain that satisfies

$$\int_0^T \int_R \sigma_{ij}^\varepsilon(t) \hat{\epsilon}_{ij}^p(t) dV dt \geq \int_0^T \int_R Y \hat{\epsilon}_e^p(t) dV dt \quad \hat{\epsilon}_e^p = \sqrt{2\hat{\epsilon}_{ij}^p \hat{\epsilon}_{ij}^p / 3},$$

the solid will not shake down to an elastic state.

Proof: The upper bound theorem can be proved by contradiction.

1. Suppose that the solid does shake down. Then, from the lower bound shakedown theorem, we know that there exists a time-independent residual stress field $\bar{\rho}_{ij}$, which satisfies equilibrium $\partial\bar{\rho}_{ij} / \partial x_j = 0$; the boundary conditions $\bar{\rho}_{ij} n_j = 0$ on $\partial_2 R$ and is such that $\sigma_{ij}^\varepsilon(t) + \bar{\rho}_{ij}$ lies below yield throughout the cycle.
2. The principle of maximum plastic resistance then shows that

$$(\hat{\sigma}_{ij} - (\sigma_{ij}^\varepsilon + \bar{\rho}_{ij})) \hat{\epsilon}_{ij}^p = Y \hat{\epsilon}_e^p - (\sigma_{ij}^\varepsilon + \bar{\rho}_{ij}) \hat{\epsilon}_{ij}^p \geq 0.$$

Integrating this expression over the volume of the solid and the cycle of loading gives

$$\int_0^T \int_R Y \hat{\epsilon}_e^p(t) dV dt - \int_0^T \int_R \sigma_{ij}^\varepsilon(t) \hat{\epsilon}_{ij}^p(t) dV dt - \int_0^T \int_R \bar{\rho}_{ij}(t) \hat{\epsilon}_{ij}^p(t) dV dt \geq 0.$$

3. Finally, reversing the order of integration in the last integral and using the principle of virtual work, we see that

$$\int_R \int_0^T \bar{\rho}_{ij}(t) \hat{\dot{\epsilon}}_{ij}^P(t) dt dV = \int_R \bar{\rho}_{ij} \Delta \hat{\dot{\epsilon}}_{ij}^P dV = \int_{\partial R} \bar{\rho}_{ij} n_j \Delta u_i^P dA = 0.$$

To see this, note that $\Delta \hat{u}_i = 0$ on $\partial_1 R$ whereas $\bar{\rho}_{ij} n_j = 0$ on $\partial_2 R$.

4. Substituting this result back into item 2 gives a contradiction, so proving the upper bound theorem.

6.2.10 Examples of Applications of the Upper Bound Shakedown Theorem

6.2.10.1 Example 1: A Simple Three-Bar Problem

We revisit the demonstration problem illustrated in Section 6.2.8. Consider a structure made of three parallel elastic-plastic bars, with Young's modulus E , length L , and cross sectional area A , as shown in Figure 6.37. The two bars labeled 1 and 2 have yield stress Y ; the central bar (labeled 3) has yield stress $2Y$. The structure is subjected to a cyclic load with mean value \bar{P} and amplitude ΔP .

To obtain an upper bound to the shakedown limit, we must devise a suitable mechanism of plastic flow in the solid. We could consider three possible mechanisms:

1. An increment of plastic strain $d\epsilon_{22}^P = d\epsilon$ in bars 1 and 2 at the instant of maximum load, followed by $d\epsilon_{22}^P = -d\epsilon$ in bars 1 and 2 at the instant of minimum load. Because the strain at the end of the cycle vanishes, it is automatically compatible.
2. An equal increment of plastic strain $d\epsilon_{22}^P = d\epsilon$ in all three bars at each instant of maximum load.
3. An equal increment of plastic strain $-d\epsilon_{22}^P = d\epsilon$ at each instant of minimum load.

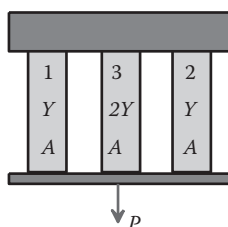


FIGURE 6.37 Parallel bars loaded in tension by a cyclic force.

By finding the combination of loads for which

$$\int_0^T \int_R \sigma_{ij}^\varepsilon(t) \hat{\dot{\epsilon}}_{ij}^p(t) dV dt \geq \int_0^T \int_R Y \hat{\dot{\epsilon}}_e^p(t) dV dt \quad \hat{\dot{\epsilon}}_e^p = \sqrt{2\hat{\dot{\epsilon}}_{ij}^p \hat{\dot{\epsilon}}_{ij}^p / 3},$$

we obtain conditions where shakedown is guaranteed not to occur. Note that the elastic stresses in all three bars are equal and are given by $\sigma_{22} = P(t) / 3A$. Thus,

a. For mechanism 1:

$$2(\bar{P} + \Delta P)Ld\varepsilon / 3 - 2(\bar{P} - \Delta P)Ld\varepsilon / 3 \geq 2YLAde + 2YLAde \Rightarrow \Delta P \geq 3AY.$$

b. For mechanism 2: $(\bar{P} + \Delta P)Ld\varepsilon \geq 4YLAde \Rightarrow \bar{P} + \Delta P \geq 4AY$.

c. For mechanism 3: $-(\bar{P} - \Delta P)Ld\varepsilon \geq 4YLAde \Rightarrow \bar{P} - \Delta P \leq -4AY$.

These agree with the lower bound calculated in Section 6.2.8 and are therefore the exact solution.

6.2.10.2 Example 2: Shakedown Limit for a Pressurized Spherical Shell

We consider an elastic-perfectly plastic thick-walled shell, with inner radius a and outer radius b . The inner wall of the shell is subjected to a cyclic pressure, with minimum value zero and maximum value p_a , as sketched in Figure 6.38.

To estimate the shakedown limit we must do the following:

1. Calculate the stresses induced by the pressure in an elastic shell. The solution can be found in Section 4.1.4:

$$\sigma_{RR} = \frac{p_a a^3}{(b^3 - a^3)} \left(1 - \frac{b^3}{R^3} \right) \quad \sigma_{\theta\theta} = \sigma_{\phi\phi} = \frac{p_a a^3}{(b^3 - a^3)} \left(1 + \frac{b^3}{2R^3} \right).$$

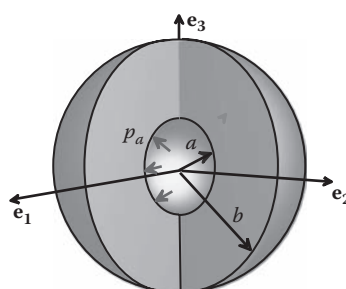


FIGURE 6.38 Spherical thick-walled shell subjected to cyclic internal pressure.

2. Postulate a mechanism of steady-state plastic deformation in the shell. For example, consider a mechanism consisting of a uniform plastic strain increment $d\varepsilon_{rr} = -2d\varepsilon$, $d\varepsilon_{\phi\phi} = d\varepsilon_{\theta\theta} = d\varepsilon$, which occurs in a spherical shell with radius a very small thickness dt at the instant of maximum pressure, followed by a strain $d\varepsilon_{rr} = 2d\varepsilon$, $d\varepsilon_{\phi\phi} = d\varepsilon_{\theta\theta} = -d\varepsilon$ at the instant of minimum load.

The upper bound theorem states that shakedown will not occur if

$$\int_0^T \int_R \sigma_{ij}^e(t) \hat{\dot{\varepsilon}}_{ij}^p(t) dV dt \geq \int_0^T \int_R Y \hat{\dot{\varepsilon}}_e^p(t) dV dt \quad \hat{\dot{\varepsilon}}_e^p = \sqrt{2\hat{\dot{\varepsilon}}_{ij}^p \hat{\dot{\varepsilon}}_{ij}^p / 3}.$$

Substituting the elastic stress field and the strain rate shows that

$$4\pi a^2 t \frac{3p_a b^3}{(b^3 - a^3)} d\varepsilon \geq 4\pi a^2 t Y 2d\varepsilon + 4\pi a^2 t Y 2d\varepsilon.$$

This gives $p_a / Y < 4(1 - a^3 / b^3)/3$ for the shakedown limit. Again, this agrees with the lower bound and is therefore the exact solution.

This page intentionally left blank

Finite Element Analysis: An Introduction

Most practical design calculations involve components with a complicated 3D geometry and may also need to account for inherently nonlinear phenomena, such as contact, large shape changes, or nonlinear material behavior. These problems can only be solved using computer simulations. The FEM is by far the most widely used and versatile technique for simulating deformable solids. This chapter gives a brief overview of the FEM, with a view to providing the background needed to run simple simulations using a commercial finite element program. More advanced analysis requires a deeper understanding of the theory and implementation of finite element codes, which will be addressed in the next chapter.

HEALTH WARNING: It is deceptively easy to use commercial finite element software: most programs come with a nice user interface that allows you to define the geometry of the solid, choose a material model, generate a finite element mesh, and apply loads to the solid with a few mouse clicks. If all goes well, the program will magically turn out animations showing the deformation, contours showing stress distributions, and much more. It is all too easy, however, to produce meaningless results, by attempting to solve a problem that does not have a well-defined solution, by using an inappropriate numerical scheme, or simply using incorrect settings for internal tolerances in the code. In addition, even high-quality software can contain bugs. Always treat the results of a finite element computation with skepticism!

7.1 A GUIDE TO USING FINITE ELEMENT SOFTWARE

FEM is a computer technique for solving partial differential equations. One application is to predict the deformation and stress fields within solid bodies subjected to external forces. However, FEM can also be used to solve problems involving fluid flow, heat transfer, electromagnetic fields, diffusion, and many other phenomena.

The principle objective of the displacement-based FEM is to compute the displacement field within a solid subjected to external forces.

To make this precise, visualize a solid deforming under external loads, as shown in Figure 7.1. Every point in the solid moves as the load is applied. The displacement vector

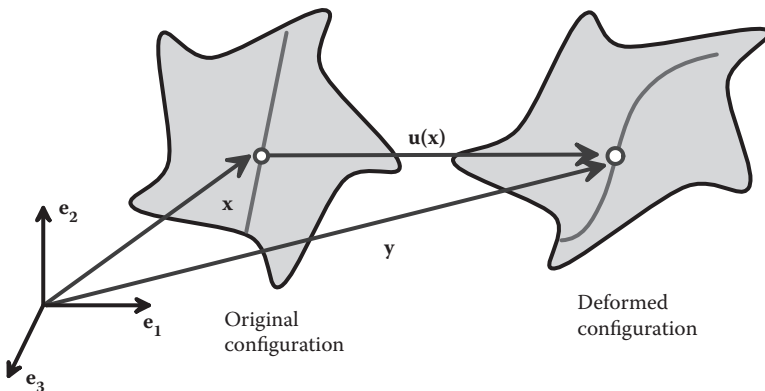


FIGURE 7.1 Displacement vector characterizing deformation of a solid.

$\mathbf{u}(\mathbf{x})$ specifies the motion of the point at position \mathbf{x} in the undeformed solid. Our objective is to determine $\mathbf{u}(\mathbf{x})$. Once $\mathbf{u}(\mathbf{x})$ is known, the strain and stress fields in the solid can be deduced.

There are two general types of finite element analysis (FEA) in solid mechanics. In most cases, we are interested in determining the behavior of a solid body that is in static equilibrium. This means that both external and internal forces acting on the solid sum to zero. In some cases, we may be interested in the dynamic behavior of a solid body. Examples include modeling vibrations in structures, problems involving wave propagation, explosive loading, and crash analysis.

For *dynamic problems*, the FEM solves the equations of motion for a continuum, essentially a more complicated version of $\sum \mathbf{F} = m\mathbf{a}$. Naturally, in this case, it must calculate the motion of the solid as a function of time.

For *static problems*, the FEM solves the equilibrium equations $\sum \mathbf{F} = \mathbf{0}$. In this case, it may not be necessary to calculate the time variation of motion. However, some materials are history dependent (e.g., metals deformed in the plastic regime). In addition, a static equilibrium problem may have more than one solution depending on the load history. In this case, the time variation of the solution must be computed.

For some applications, you may also need to solve additional field equations. For example, you may be interested in calculating the temperature distribution in the solid or calculating electric or magnetic fields. In addition, special finite element procedures are available to calculate buckling loads and their modes, as well as natural frequencies of vibration and the corresponding mode shapes for a deformable solid.

To set up a finite element calculation, you will need to specify the following:

1. The geometry of the solid: This is done by generating a *finite element mesh* for the solid. The mesh can usually be generated automatically from a computer-aided design representation of the solid.
2. The properties of the material: This is done by specifying a *constitutive law* for the solid.
3. The nature of the loading applied to the solid: This is done by specifying the *boundary conditions* for the problem.

4. If your analysis involves contact between two more solids, you will need to specify the surfaces that are likely to come into contact and the properties (e.g., friction coefficient) of the contact.
5. For a dynamic analysis, it is necessary to specify *initial conditions* for the problem. This is not necessary for a static analysis.
6. For problems involving additional fields, you may need to specify initial values for these field variables (e.g., you would need to specify the initial temperature distribution in a thermal analysis).

You will also need to specify some additional aspects of the problem you are solving and the solution procedure to be used:

1. You will need to specify whether the computation should take into account finite changes in the geometry of the solid.
2. For a dynamic analysis, you will need to specify the time period of the analysis (or the number of time increments).
3. For a static analysis, you will need to decide whether the problem is linear or nonlinear. Linear problems are very easy to solve. Nonlinear problems may need special procedures.
4. For a static analysis with history-dependent materials, you will need to specify the time period of the analysis and the time step size (or number of steps).
5. If you are interested in calculating natural frequencies and mode shapes for the system, you must specify how many modes to extract.
6. Finally, you will need to specify what the FEM must compute.

The steps in running a finite element computation are discussed in more detail in the following sections.

7.1.1 Finite Element Mesh for a 2D or 3D Component

The finite element mesh is used to specify the geometry of the solid and is also used to describe the displacement field within the solid. A typical mesh (generated in the commercial FEA code Abaqus) is shown in Figure 7.2.

A finite element mesh may be three dimensional, like the example shown. 2D finite element meshes are also used to model simpler modes of deformation. There are three main types of 2D finite element mesh:

1. Plane stress
2. Plane strain
3. Axisymmetric

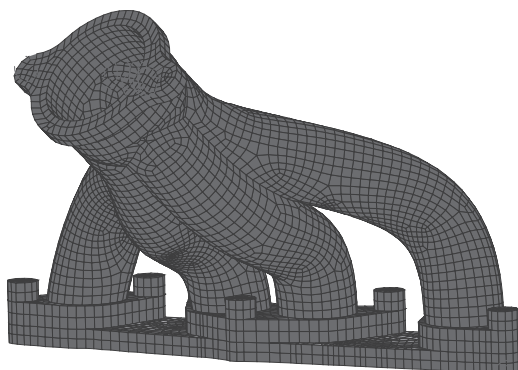


FIGURE 7.2 Typical finite element mesh.

In addition, special types of finite element can be used to model the overall behavior of a 3D solid, without needing to solve for the full 3D fields inside the solid. Examples are shell elements, plate elements, beam elements, and truss elements. These will be discussed in a separate section below.

7.1.1.1 Plane Stress Finite Element Mesh

A plane stress finite element mesh is used to model a plate-like solid that is loaded in its own plane. The solid must have uniform thickness, and the thickness must be much less than any representative cross-sectional dimension. A plane stress finite element mesh for a thin plate containing a hole is shown in Figure 7.3. Only one quadrant of the specimen is modeled, because symmetry boundary conditions will be enforced during the analysis.

7.1.1.2 Plane Strain Finite Element Mesh

A plane strain finite element mesh is used to model a long cylindrical solid that is prevented from stretching parallel to its axis. For example, a plane strain finite element mesh for a

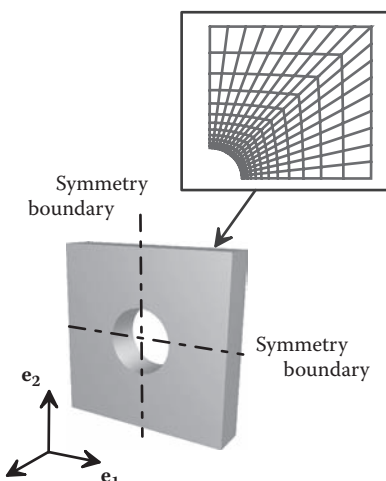


FIGURE 7.3 Typical plane stress finite element mesh.

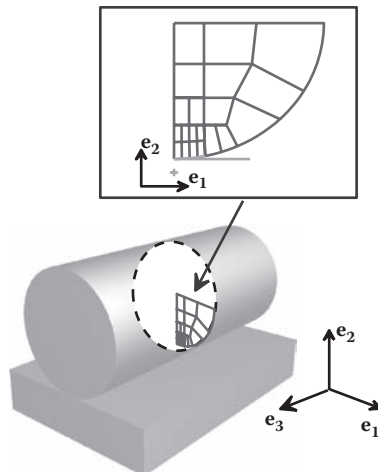


FIGURE 7.4 Typical plane strain finite element mesh.

cylinder that is in contact with a rigid floor is shown in Figure 7.4. Away from the ends of the cylinder, we expect it to deform so that the out-of-plane component of displacement $u_3(x_1, x_2) = 0$. There is no need to solve for u_3 , so a 2D mesh is sufficient to calculate $u_1(x_1, x_2)$ and $u_2(x_1, x_2)$.

As before, only one quadrant of the specimen is meshed: symmetry boundary conditions will be enforced during the analysis.

7.1.1.3 Axisymmetric Finite Element Mesh

An axisymmetric mesh is used to model a solid that has rotational symmetry, which is subjected to axisymmetric loading. An example is in Figure 7.5, which compares a 3D mesh of an axisymmetric bushing to an axisymmetric mesh. Note that half of the bushing has been cut away in the 3D view, to show the geometry more clearly. In an axisymmetric analysis, the origin for the (x, y) coordinate system is always on the axis of rotational

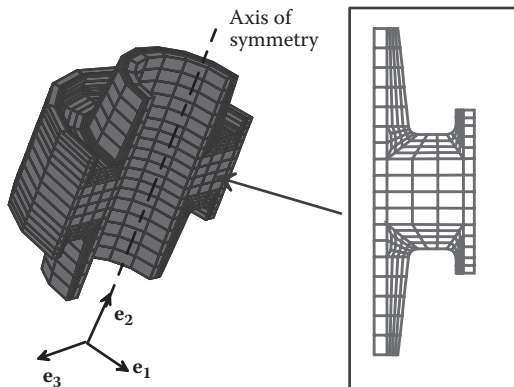


FIGURE 7.5 Typical axisymmetric finite element mesh.

symmetry. Note also that, to run an axisymmetric FEA, both the geometry of the solid and the loading applied to the solid must have rotational symmetry about the y axis.

7.1.2 Nodes and Elements in a Mesh

A finite element mesh is defined by a set of *nodes* together with a set of *finite elements*, as shown in Figure 7.6.

7.1.2.1 Nodes

The nodes are a set of discrete points within the solid body. Nodes have the following properties:

1. A node number: Every node is assigned an integer number, which is used to identify the node. Any convenient numbering scheme may be selected; the nodes do not need to be numbered in order, and numbers may be omitted. For example, one could number a set of n nodes as 100, 200, 300, ... $100n$, instead of 1, 2, 3, ... n .
 2. Nodal coordinates: For a 3D FEA, each node is assigned a set of (x_1, x_2, x_3) coordinates, which specifies the position of the node in the undeformed solid. For a 2D analysis, each node is assigned a pair of (x_1, x_2) coordinates. For an axisymmetric analysis, the x_2 axis must coincide with the axis of rotational symmetry.
 3. Nodal displacements: When the solid deforms, each node moves to a new position. For a 3D FEA, the nodal displacements specify the three components of the displacement field $\mathbf{u}(\mathbf{x})$ at each node: (u_1, u_2, u_3) . For a 2D analysis, each node has two displacement components (u_1, u_2) . The nodal displacements are unknown at the start of the analysis and are computed by the finite element program.

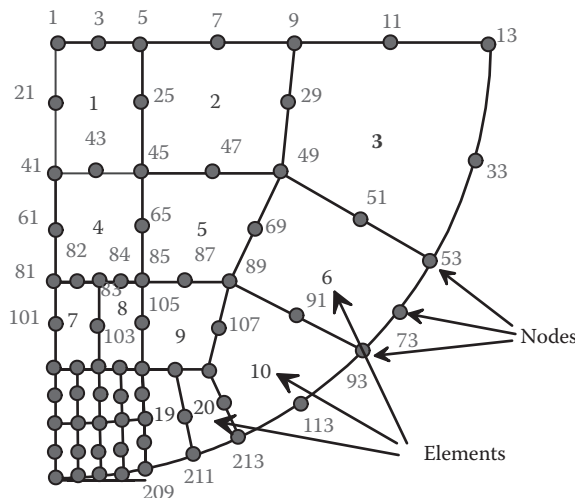


FIGURE 7.6 Nodes and elements in a finite element mesh.

4. Other nodal degrees of freedom: For more complex analyses, we may want to calculate a temperature distribution in the solid, or a voltage distribution, for example. In this case, each node is also assigned a temperature, voltage, or similar quantity of interest. There are also some finite element procedures that use more than just displacements to describe shape changes in a solid. For example, when analyzing 2D beams, we use the displacements and rotations of the beam at each nodal point to describe the deformation. In this case, each node has a rotation, as well as two displacement components. The collection of all unknown quantities (including displacements) at each node are known as *degrees of freedom*. A finite element program will compute values for these unknown degrees of freedom.

7.1.2.2 Elements

Elements are used to partition the solid into discrete regions. Elements have the following properties.

1. An element number: Every element is assigned an integer number, which is used to identify the element. Just as when numbering nodes, any convenient scheme may be selected to number elements.
2. A geometry: There are many possible shapes for an element. A few of the more common element types are shown in Figure 7.7. Nodes attached to the element are shown in red. In two dimensions, elements are generally either triangular or rectangular. In

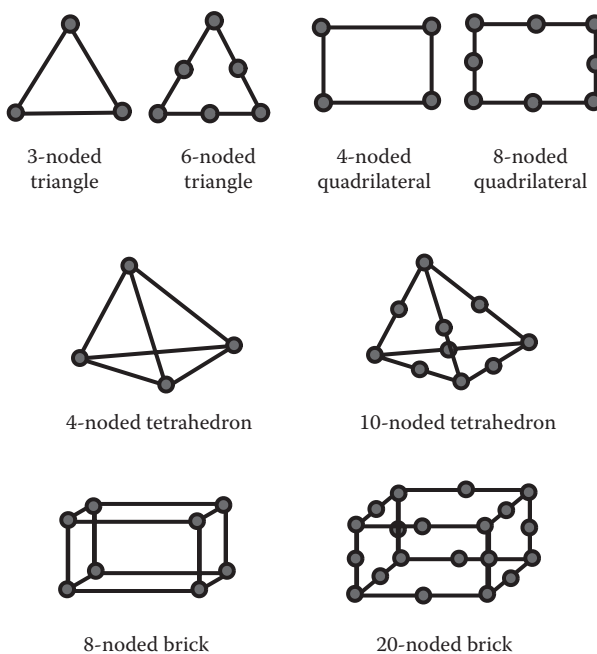


FIGURE 7.7 Common 2D and 3D elements.

three dimensions, the elements are generally tetrahedra, hexahedra, or bricks. There are other types of element that are used for special purposes: examples include truss elements (which are simply axial members), beam elements, and shell elements.

3. A set of faces: these are simply the sides of the element.
4. A set of nodes attached to the element: Figure 7.6 shows a typical finite element mesh. Element numbers are shown in the center of each element; node numbers are shown next to each node (some node and element numbers are omitted for clarity). All the elements are eight-noded quadrilaterals. Note that each element is connected to a set of nodes: element 1 has nodes (41, 45, 5, 1, 43, 25, 3, 21), element 2 has nodes (45, 49, 9, 5, 47, 29, 7, 25), and so on. It is conventional to list the nodes in the order given, with corner nodes first in order going counterclockwise around the element, followed by the midside nodes. The set of nodes attached to the element is known as the *element connectivity*.
5. An element interpolation scheme: The purpose of a finite element is to interpolate the displacement field $\mathbf{u}(\mathbf{x})$ between values defined at the nodes. This is best illustrated using an example. Consider the 2D, rectangular four-noded element shown in Figure 7.8. Let $(u_1^{(a)}, u_2^{(a)}), (u_1^{(b)}, u_2^{(b)}), (u_1^{(c)}, u_2^{(c)}), (u_1^{(d)}, u_2^{(d)})$ denote the components of displacement at nodes a, b, c, d . The displacement at an arbitrary point within the element can be interpolated between values at the corners, as follows:

$$u_1 = (1 - \xi)(1 - \eta)u_1^{(a)} + \xi(1 - \eta)u_1^{(b)} + \xi\eta u_1^{(c)} + (1 - \xi)\eta u_1^{(d)}$$

$$u_2 = (1 - \xi)(1 - \eta)u_2^{(a)} + \xi(1 - \eta)u_2^{(b)} + \xi\eta u_2^{(c)} + (1 - \xi)\eta u_2^{(d)},$$

where

$$\xi = x_1/B, \eta = x_2/H.$$

You can verify for yourself that the displacements have the correct values at the corners of the element, and the displacements evidently vary linearly with position within the element.

Different types of element interpolation scheme exist. The simple example described above is known as a *linear* element. Six-noded triangles and eight-noded triangles are examples of *quadratic* elements: the displacement field varies quadratically with

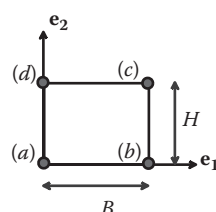


FIGURE 7.8 A rectangular finite element.

position within the element. In three dimensions, the four-noded tetrahedron and the eight-noded brick are linear elements, whereas the 10-noded tet and 20-noded brick are quadratic. Other special elements, such as beam elements or shell elements, use a more complex procedure to interpolate the displacement field.

Some special types of element interpolate both the displacement field and some or all components of the stress field within an element separately. (Usually, the displacement interpolation is sufficient to determine the stress, because one can compute the strains at any point in the element from the displacement and then use the stress-strain relation for the material to find the stress). This type of element is known as a *hybrid* element. Hybrid elements are usually used to model incompressible, or nearly incompressible, materials.

6. Integration points: One objective of FEA is to determine the distribution of stress within a solid. This is done as follows. First, the displacements at each node are computed (the technique used to do this will be discussed in Section 7.2 and Chapter 8). Then, the element interpolation functions are used to determine the displacement at arbitrary points within each element. The displacement field can be differentiated to determine the strains. Once the strains are known, the stress-strain relations for the element are used to compute the stresses.

In principle, this procedure could be used to determine the stress at any point within an element. However, it turns out to work better at some points than others. The special points within an element in which stresses are computed most accurately are known as *integration points*. (Stresses are sampled at these points in the finite element program to evaluate certain volume and area integrals; hence, they are known as integration points.)

For a detailed description of the locations of integration points within an element, you should consult an appropriate user manual. The approximate locations of integration points for a few 2D elements are shown in Figure 7.9.

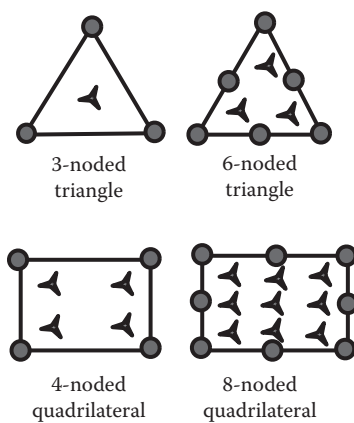


FIGURE 7.9 Integration points in various 2D elements.

There are some special types of element that use fewer integration points than those shown in the figure. These are known as *reduced integration* elements. This type of element must be used to analyze deformation of near-incompressible materials (e.g., rubbers or metals that experience large plastic strains).

7. A stress-strain relation and material properties: Each element is occupied by solid material. The type of material within each element (steel, concrete, soil, rubber, etc.) must be specified, together with values for the appropriate material properties (mass density, Young's modulus, Poisson's ratio, etc.).

7.1.3 Special Elements: Beams, Plates, Shells, and Truss Elements

If you need to analyze a solid with a special geometry (e.g., a simple truss, a structure made of one or more slender beams, or plates), it is not efficient to try to generate a full 3D finite element mesh for each member in the structure. Instead, you can take advantage of the geometry to simplify the analysis.

The idea is quite simple. Instead of trying to calculate the full 3D displacement field in each member, the deformation is characterized by a reduced set of degrees of freedom. Specifically,

1. For a pin jointed truss (Figure 7.10), we simply calculate the *displacement of each joint* in the structure. The members are assumed to be in a state of uniaxial tension or compression, so the full displacement field within each member can be calculated in terms of joint displacements.
2. For a beam (Figure 7.11), we calculate the *displacement and rotation* of the cross section along the beam. These can be used to determine the internal shear forces bending moments and therefore the stresses in the beam. A 3D beam has three displacement and three rotational degrees of freedom at each node.

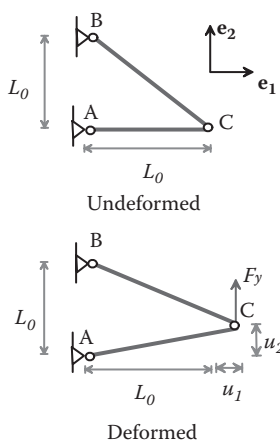


FIGURE 7.10 A typical problem involving deformation in a truss.

3. For a plate, or shell, we again calculate the displacement and rotation of the plate section. A 3D plate or shell has three displacement and two rotational degrees of freedom at each node (these rotations characterize the rotation of a unit vector normal to the plate). In some finite element codes, nodes on plates and shells have a fictitious third rotational degree of freedom that is added for convenience, but you will find that attempting to impose boundary conditions on this fictitious degree of freedom has no effect on the deformation of the structure.

In an analysis using truss, beam, or plate elements, some additional information must be specified to set up the problem:

1. For a truss analysis, each member in the truss is a single element. The area of the member's cross section must be specified.
2. For a beam analysis, the shape and orientation of the cross section must be specified (or, for an elastic analysis, you could specify the area moments of inertia directly). There are also several versions of beam theory that account differently for shape changes within the beam. Euler–Bernoulli beam theory is the simple version covered in introductory courses. Timoshenko beam theory is a more complex version that is more accurate for thicker beams.
3. For plates and shells, the thickness of the plate must be given. In addition, the deformation of the plate can be approximated in various ways: for example, some versions only account for transverse deflections and neglect in-plane shearing and stretching of the plate; more complex theories account for this behavior.

Calculations using beam and plate theory also differ from full 3D or 2D calculations in that both the deflection and rotation of the beam or plate must be calculated. The following then applies:

1. Nodes on beam elements have six degrees of freedom: the three displacement components, together with three angles representing rotation of the cross section about three axes. Nodes on plate or shell elements have five (or, in some FEA codes, six) degrees of freedom. The six degrees of freedom represent three displacement components and two

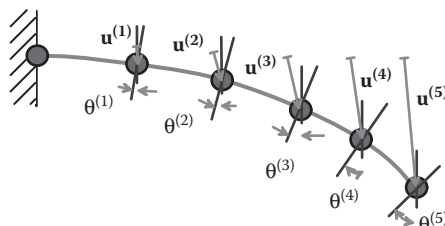


FIGURE 7.11 Displacement and rotational degrees of freedom for nodes in a beam.

angles that characterize rotation of the normal to the plate about two axes (if the nodes have six degrees of freedom, a third, fictitious rotation component has been introduced; you will have to read the manual for the code to see what this rotation represents).

2. Boundary conditions may constrain both displacement and rotational degrees of freedom. For example, to model a fully clamped boundary condition at the end of a beam (or the edge of a plate), you must set all displacements and all rotations to zero.
3. You can apply both forces and moments to nodes in an analysis.

Finally, in an analysis involving several beams connected together, you can connect the beams in two ways:

1. You can connect them with a *pin joint*, which forces the beams to move together at the connection but allows relative rotation.
2. You can connect them with a *clamped joint*, which forces the beams to rotate together at the connection.

In most FEA codes, you can create the joints by adding constraints, as discussed in Section 7.1.6. Occasionally, you may also want to connect beam elements to solid, continuum elements in a model: this can also be done with constraints.

7.1.4 Material Behavior

A good finite element code contains a huge library of different types of material behavior that may be assigned to elements. A few examples are described below.

7.1.4.1 Linear Elasticity

You should already be familiar with the idea of a linear elastic material. It has a uniaxial stress-strain response (valid only for small strains) as shown in Figure 7.12. The stress-strain law for the material may be expressed in matrix form as

$$\begin{bmatrix} \varepsilon_{11} \\ \varepsilon_{22} \\ \varepsilon_{33} \\ \varepsilon_{12} \\ \varepsilon_{13} \\ \varepsilon_{23} \end{bmatrix} = \frac{1}{E} \begin{bmatrix} 1 & -\nu & -\nu & 0 & 0 & 0 \\ -\nu & 1 & -\nu & 0 & 0 & 0 \\ -\nu & -\nu & 1 & 0 & 0 & 0 \\ 0 & 0 & 0 & 1+\nu & 0 & 0 \\ 0 & 0 & 0 & 0 & 1+\nu & 0 \\ 0 & 0 & 0 & 0 & 0 & 1+\nu \end{bmatrix} \begin{bmatrix} \sigma_{11} \\ \sigma_{22} \\ \sigma_{33} \\ \sigma_{12} \\ \sigma_{13} \\ \sigma_{23} \end{bmatrix} + \alpha \Delta T \begin{bmatrix} 1 \\ 1 \\ 1 \\ 0 \\ 0 \\ 0 \end{bmatrix}$$

Here, E and ν are Young's modulus and Poisson's ratio for the material, whereas α denotes the thermal expansion coefficient. Typical values (for steel) are $E = 210 \text{ GN/m}^2$, $\nu = 0.33$, and $\alpha = 5 \times 10^{-6} \text{ K}^{-1}$. More extensive tables of values are given in Section 3.1.5.

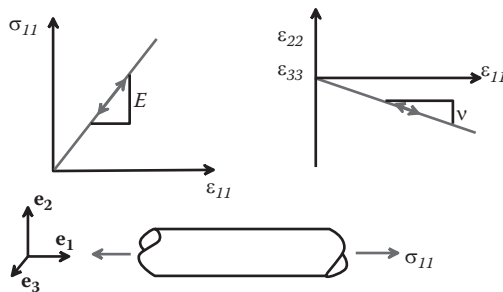


FIGURE 7.12 Linear elastic material behavior.

7.1.4.2 Elastic-Plastic Material Behavior

Recall that the uniaxial stress-strain curve for an elastic-plastic solid looks something like the one shown in Figure 7.13. The material behaves elastically until a critical stress (known as the yield stress) is reached. If yield is exceeded, the material deforms permanently. The yield stress of the material generally increases with plastic strain: this behavior is known as *strain hardening*.

The conditions necessary to initiate yielding under multiaxial loading are specified by a *yield criterion*, such as the von Mises or Tresca criteria. These yield criteria are built into the finite element code.

The strain hardening behavior of a material is approximated by allowing the yield stress to increase with plastic strain. The variation of yield stress with plastic strain for a material is usually specified by representing it as a series of straight lines, as shown in Figure 7.13.

7.1.5 Boundary Conditions

Boundary conditions are used to specify the loading applied to a solid. There are several ways to apply loads to a finite element mesh.

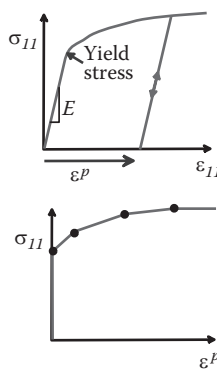


FIGURE 7.13 Elastic-plastic material behavior.

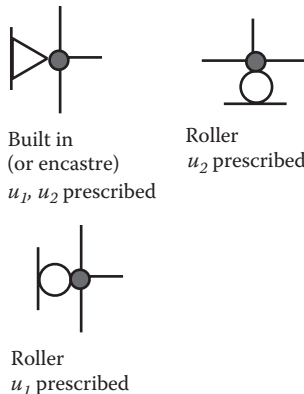


FIGURE 7.14 Constraints that may be applied to nodes.

Displacement boundary conditions: The displacements at any node on the boundary or within the solid can be specified. One may prescribe u_1, u_2, u_3 , or all three. For a 2D analysis, it is only necessary to prescribe u_1 and/or u_2 .

Various symbols are used to denote displacement boundary conditions applied to a finite element mesh: a few of these are illustrated in Figure 7.14. Some user interfaces use small conical arrowheads to indicate constrained displacement components.

For example, to stretch a 2D block of material vertically while allowing it to expand or contract freely horizontally, we would apply boundary constraints to the top and bottom surface as shown in Figure 7.15.

Observe that one of the nodes on the bottom of the block has been prevented from moving horizontally, as well as vertically. It is important to do this: the finite element program will be unable to find a unique solution for the displacement fields if the solid is free to slide horizontally.

During the analysis, the finite element program will apply forces to the nodes with prescribed displacements so as to cause them to move to their required positions. If only the u_1 component of displacement is prescribed, then the force will act in the \mathbf{e}_1 direction. If u_2 is prescribed, the force acts in direction \mathbf{e}_2 and so on. Notice that you cannot directly

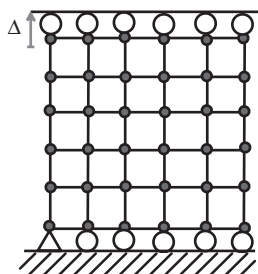


FIGURE 7.15 Mesh subjected to prescribed nodal displacements.

apply a *rotation* to a node attached to a 2D or 3D solid. Rotations can, however, be applied to the nodes attached to certain special types of element, such as beams, plates, and shells, as well as rigid surfaces.

Symmetry conditions: Most finite element codes can automatically enforce symmetry and antisymmetry boundary conditions.

Prescribed forces: Any node in a finite element mesh may be subjected to a prescribed force. The nodal force is a vector and is specified by its three (or two for 2D) components, (F_1, F_2, F_3). Notice that there is no direct way to apply a *moment* to a 3D solid; you would need to do this by applying two point forces a small distance apart or by applying contact loading, as outlined below. Moments can be applied to some special types of element, such as shells, plates, or beams.

Distributed loads: A solid may be subjected to distributed pressure or traction acting on its boundary. Examples include aerodynamic loading, or hydrostatic fluid pressure. Distributed traction is a vector quantity, with physical dimensions of force per unit area in 3D, and force per unit length in 2D. To model this type of loading in a finite element program, distributed loads may be applied to the face of any element.

Default boundary condition at boundary nodes: If no displacements or forces are prescribed at a boundary node and no distributed loads act on any element faces connected to that node, then the node is assumed to be free of external force.

Body forces: External body forces may act on the interior of a solid. Examples of body forces include gravitational loading, or electromagnetic forces. Body force is a vector quantity, with physical dimensions of force per unit volume. To model this type of loading in a finite element program, body forces may be applied to the interior of any element.

Contact: Probably the most common way to load a solid is through contact with another solid. Special procedures are available for modeling contact between solids. These will be discussed in a separate section below.

Load history: In some cases, one may want to apply a cycle of load to a solid. In this case, the prescribed loads and displacements must be specified as a function of time.

General guidelines concerning boundary conditions: When performing a static analysis, it is very important to ensure that boundary conditions are applied properly. A finite element program can only solve a problem if a unique static equilibrium solution to the problem exists.

Difficulties arise if the user does not specify sufficient boundary constraints to prevent rigid body motion of a solid. This is best illustrated by example. Suppose we want to model stretching a 2D solid, as described previously. The examples in Figure 7.16 show two correct ways to do this.

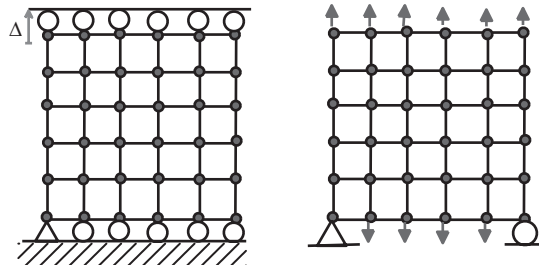


FIGURE 7.16 Examples of properly constrained finite element meshes.

The examples below show various incorrect ways to apply boundary conditions. In each case, one or more rigid body mode is unconstrained (Figure 7.17).

7.1.6 Constraints

You may sometimes need to use more complicated boundary conditions than simply constraining the motion or loads applied to a solid. Some examples might include the following:

1. Connecting different element types, e.g., beam elements to solid elements
2. Enforcing periodic boundary conditions
3. Constraining a boundary to remain flat
4. Approximating the behavior of mechanical components such as welds, bushings, bolted joints, etc.

You can do this by defining *constraints* in an analysis. At the most basic level, constraints can simply be used to enforce prescribed relationships between the displacements or velocities of individual nodes in the mesh. You can also specify relationships between motion of *groups* of nodes.

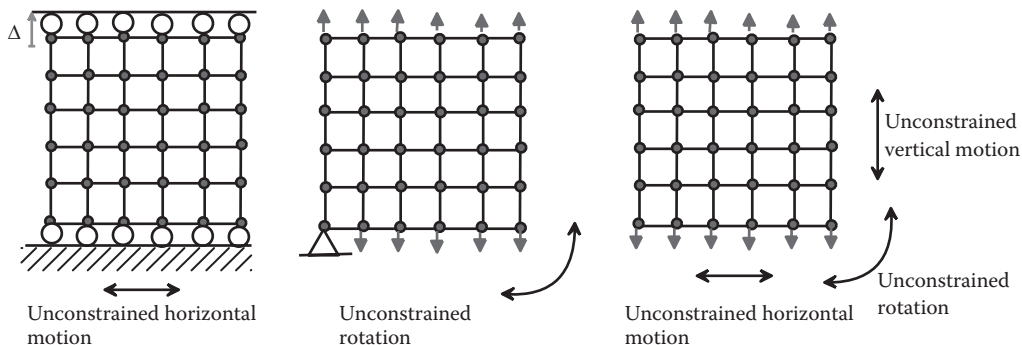


FIGURE 7.17 Examples of improperly constrained finite element meshes.

7.1.7 Contacting Surfaces and Interfaces

In addition to being subject to forces or prescribed displacements, solid objects are often loaded by coming into contact with another solid. An example is shown in Figure 7.18.

Modern finite element codes contain sophisticated capabilities for modeling contact. Unfortunately, contact can make a computation much more difficult, because the region in which the two solids come into contact is generally not known *a priori* and must be determined as part of the solution. This almost always makes the problem *nonlinear*, even if both contacting solids are linear elastic materials. In addition, if there is friction between the contacting solids, the solution is history dependent.

For this reason, many options are available in finite element packages to control the way contacting surfaces behave.

There are three general cases of contact that you may need to deal with:

1. A deformable solid contacts a stiff, hard solid whose deformation may be neglected.
In this case, the hard solid is modeled as a *rigid surface*, as outlined below.
2. You may need to model contact between two deformable solids.
3. The solid comes into contact with itself during the course of deformation (this is common in components made from rubber, for example, and also occurs during some metal forming operations).

Whenever you model contact, you will need to do the following:

1. Specify pairs of surfaces that might come into contact. One of these must be designated as the *master surface* and the other must be designated as the *slave surface*. (If a surface contacts itself, it is both a master and a slave. Kinky!)
2. Define the way the two surfaces interact, for example, by specifying the coefficient of friction between them.

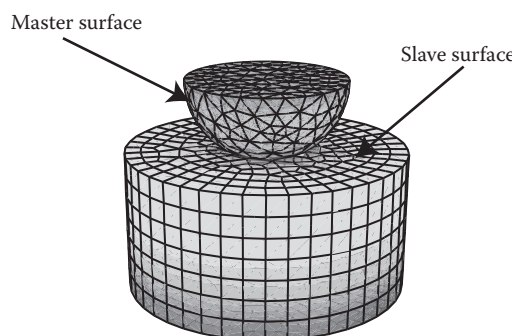


FIGURE 7.18 Contact between two finite element meshes.

7.1.7.1 Modeling a Stiff Solid as a Rigid Surface

In many cases of practical interest, one of the two contacting solids is much more compliant than the other. Examples include a rubber in contact with metal or a metal with low yield stress in contact with a hard material, such as a ceramic. As long as the stresses in the stiff or hard solid are not important, its deformation can be neglected.

In this case, the stiffer of the two solids may be idealized as a *rigid surface*. Both 2D and 3D rigid surfaces can be created, as shown in Figure 7.19.

A rigid surface (obviously) cannot change its shape, but it can move about and rotate. Its motion is defined using a *reference point* on the solid, which behaves like a node. To move the solid around during an analysis, you can define displacement and rotational degrees of freedom at this node. Alternatively, you could apply forces and moments to the reference point. Finally, in a dynamic analysis, you can give the rigid solid appropriate inertial properties (so as to create a rigid projectile, for example).

7.1.7.2 Defining a Contact Pair: Master/Slave Surfaces

Whenever you set up a finite element calculation that involves contact, you need to specify pairs of surfaces that may come into contact during the analysis. One of each pair must be designated the master surface, and the other must be designated the slave surface.

This rather obscure finite element terminology refers to the way that contact constraints are actually applied during a computation. The geometry of the master surface will be interpolated as a smooth curve in some way (usually by interpolating between nodes). The slave surface is not interpolated. Instead, each individual node on the slave surface is constrained so as not to penetrate into the master surface. For example, the nodes on the slave surface shown in Figure 7.20 would be forced to remain outside the boundary of the master surface.

For a sufficiently fine mesh, the results should not be affected by your choice of master and slave surface. However, it improves *convergence* (see below to learn what this means) if you choose the more rigid of the two surfaces to be the master surface. If you do not know which surface is more rigid, just make a random choice. If you run into convergence problems later, try switching them over.

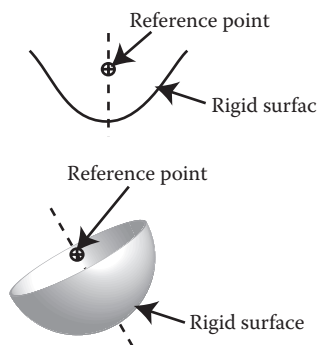


FIGURE 7.19 Reference nodes on rigid surfaces.

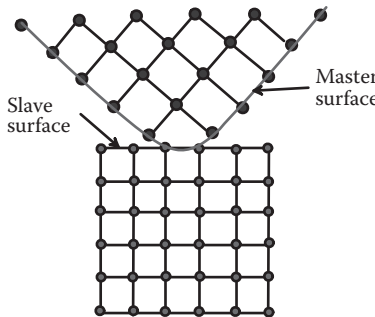


FIGURE 7.20 Contact between master and slave surfaces on two finite element meshes.

7.1.7.3 Contact Parameters

You can define several parameters that control the behavior of two contacting surfaces:

1. The contact formulation, “finite sliding” or “small sliding,” specifies the expected relative tangential displacement of the two surfaces. Finite sliding is the most general but is computationally more demanding. Small sliding should be used if the relative tangential displacement is likely to be less than the distance between two adjacent nodes.
2. You can specify the relationship between the contact pressure and separation between the contacting surfaces. Alternatively, you can assume the contact is “hard”; this means the interface cannot withstand any tension, and the two contacting surfaces cannot interpenetrate.
3. You can specify the tangential behavior of the interface, for example, by giving the friction coefficient.

7.1.8 Initial Conditions and External Fields

For a dynamic analysis, it is necessary to specify the initial velocity and displacement of each node in the solid. The default value is zero velocity and displacement.

In addition, if you are solving a coupled problem, such as one involving coupled deformation and heat flow, you may need to specify initial values for the additional field variables (e.g., the temperature distribution).

7.1.9 Solution Procedures and Time Increments

The FEM calculates the displacement $\mathbf{u}(\mathbf{x}^a)$ at each node in the finite element mesh by solving the equations of static equilibrium or the equations of motion. In this section, we briefly outline some of the solution procedures and the options available to control them.

7.1.9.1 Linear or Nonlinear Geometry

As you know, you can simplify the calculation of internal forces in a structures by neglecting shape changes when solving the equations of equilibrium. For example, when you solve

a truss problem, you usually calculate forces in each member based on the *undeformed* shape of the structure.

You can use the same idea to simplify calculations involving deformable solids. In general, you should do so whenever possible. However, if (1) you anticipate that material might stretch by more than approximately 10%, (2) you expect that some part of the solid might rotate by more than about 10° , or (3) you want to calculate buckling loads for your structure, you should account for finite geometry changes in the computation. This will automatically make your calculation nonlinear (and so more difficult), even if all the materials have linear stress-strain relations.

7.1.9.2 Time Stepping for Dynamic Problems

For a dynamic problem, the nodal displacements $\mathbf{u}(\mathbf{x}^a, t)$ must be calculated as a function of time. The displacements are calculated by solving the equations of motion for the system, which look something like

$$\mathbf{M} \frac{d^2 \mathbf{u}}{dt^2} + \mathbf{Ku} = \mathbf{F}(t),$$

where \mathbf{M} and \mathbf{K} are called mass and stiffness matrices. Both \mathbf{M} and \mathbf{K} can be functions of \mathbf{u} . There are 2.5 ways to integrate this equation.

1. The most direct method is called *explicit time integration* or *explicit dynamics* and works something like this. Remember that, for a dynamic calculation, the values of \mathbf{u} and $\mathbf{v} = d\mathbf{u}/dt$ are known at $t = 0$. We can therefore compute \mathbf{M} and \mathbf{K} at time $t = 0$ and then use them to calculate the acceleration $\mathbf{a} = d^2\mathbf{u}/dt^2$ at $t = 0$, as

$$\mathbf{a} = \mathbf{M}^{-1}(\mathbf{F}(t) - \mathbf{Ku}).$$

The acceleration can then be used to find the velocity $\mathbf{v}(\Delta t)$ and displacement $\mathbf{u}(\Delta t)$ at time Δt as

$$\mathbf{v}(\Delta t) = \mathbf{v}(0) + \mathbf{a}\Delta t \quad \mathbf{u}(\Delta t) = \mathbf{u}(0) + \mathbf{v}(0)\Delta t + \frac{1}{2}\mathbf{a}\Delta t^2.$$

This procedure can then be applied repeatedly to march the solution through time.

2. The second procedure is called *implicit time integration* or *implicit dynamics*. The procedure is very similar to explicit time integration, except that, instead of calculating the mass and stiffness matrices at time $t = 0$ and using them to calculate acceleration at $t = 0$, these quantities are calculated at time Δt instead. This is a bit more time consuming to do, however, because it involves more equation solving.

3. Method 2.5 is called *modal dynamics* and only works if \mathbf{M} and \mathbf{K} are *constant*. In this case, one can take the Fourier transform of the governing equation and integrate it exactly. This method is used to solve linear vibration problems.

The following guidelines will help you to choose the most appropriate method for your application:

1. For explicit dynamics, each time step can be calculated very fast. However, the method is stable only if Δt is very small; specifically, the time interval must be smaller than the time taken for an elastic wave to propagate from one side of an element to the other. This gives $\Delta t < L\sqrt{\rho(1-2\nu)/2(1-\nu)}$, where ρ is the mass density of the solid, μ is its shear modulus, and ν its Poisson's ratio. Explicit dynamics works best for rapid, transient problems, such as crash dynamics or impact. It is not good for modeling processes that take place over a long time. If elastic wave propagation is not the main focus of your computation, you can sometime speed up the calculations by increasing the density ρ (but you have to be careful to ensure this does not affect the results). This is called *mass scaling*.
2. For implicit dynamics, the cost of computing each time step is much greater. The algorithm is unconditionally stable, however, and will always converge even for very large Δt . This is the method of choice for problems in which inertial loading is important, but rapid transients are not the focus of the analysis.
3. Modal dynamics only works for linear elastic problems. It is used for vibration analysis.

7.1.9.3 Nonlinear Solution Procedures for Static Problems

If a problem involves contact, plastically deforming materials, or large geometry changes, it is nonlinear. This means that the equations of static equilibrium for the finite element mesh have the general form

$$\mathbf{F}^{(b)}(\mathbf{u}^{(a)}) = \mathbf{0},$$

where $\mathbf{F}()$ denotes a set of $b = 1, 2 \dots N$ vector functions of the nodal displacements $\mathbf{u}(\mathbf{x}^a)$, $a = 1, 2 \dots N$, and N is the number of nodes in the mesh.

The nonlinear equations are solved using the Newton-Raphson method, which works like this. You first guess the solution to the equations, say $\mathbf{u}^a = \mathbf{w}^{(a)}$. Of course (unless you are a genius), \mathbf{w} will not satisfy the equations, so you try to improve the solution by adding a small correction $d\mathbf{w}$. Ideally, the correction should be chosen so that

$$\mathbf{F}^{(b)}(\mathbf{w}^{(a)} + d\mathbf{w}^a) = \mathbf{0},$$

but of course it is not possible to do this. So instead, we take a Taylor expansion to get

$$\mathbf{F}^{(b)}(\mathbf{w}^{(a)} + d\mathbf{w}^a) \approx \mathbf{F}^{(b)}(\mathbf{w}^{(a)}) + \frac{d\mathbf{F}^{(b)}(\mathbf{u})}{d\mathbf{u}^{(a)}} d\mathbf{w}^{(a)} = 0.$$

The result is a system of linear equations of the form $\mathbf{F}^{(b)} + \mathbf{K}d\mathbf{w}^{(a)} = \mathbf{0}$, where $\mathbf{K} = d\mathbf{F}^{(b)}/d\mathbf{u}^{(a)}$ is a constant matrix called the *stiffness matrix*. The equations can now be solved for $d\mathbf{w}$; the guess for \mathbf{w} can be corrected and the procedure applied again. The iteration is repeated until $|\mathbf{F}^{(b)}(\mathbf{u}^{(a)})| < \varepsilon$, where ε is a small tolerance.

In problems involving *hard contact*, an additional iterative method is used to decide which nodes on the slave surface contact the master surface. This is just a brute-force method; it starts with some guess for contacting nodes, gets a solution, and checks it. If any nodes are found to penetrate the master surface, these are added to the list of nodes in contact. If any nodes are experiencing forces attracting them to the master surface, they are removed from the list of nodes in contact.

The problem with any iterative procedure is that it may not converge; that is, repeated corrections $d\mathbf{w}$ either take the solution farther and farther away from the solution or else just spiral around the solution without ever reaching it.

The solution is (naturally) more likely to converge if the guess $\mathbf{w}^{(a)}$ is close to the correct solution. Consequently, it is best to apply the loads to a nonlinear solid gradually so that, at each load step, the displacements are small. The solution to one load increment can then be used as the initial guess for the next.

Convergence problems are the curse of FEM analysts. They are very common and can be exceedingly difficult to resolve. Here are some suggestions for things to try if you run into convergence problems:

1. Try applying the load in smaller increments. Most commercial codes will do this automatically but will stop the computation if the increment size falls below a minimum value. You can try reducing the minimum step size.
2. Convergence problems are sometimes caused by *ill conditioning* in the stiffness matrix. This means that the equation $\mathbf{F}^{(b)} + \mathbf{K}d\mathbf{w}^{(a)} = \mathbf{0}$ cannot be solved accurately. Ill conditioning can arise because of (1) severely distorted elements in the mesh, (2) material behavior is incompressible or nearly incompressible, and (3) the boundary conditions in the analysis do not properly constrain the solid. You can fix item 1 by modifying the mesh; some FEM codes contain capabilities to automatically remove element distortion during large deformation. You can avoid problems with incompressibility (item 2) by using reduced integration elements or hybrid elements. Problems with boundary conditions (item 3) can usually be corrected by adding more constraints. There is one common problem in which this is hard to do: if the motion of a body in your analysis is constrained only by contacts with other solids (e.g., a roller between two surfaces), the stiffness matrix is always singular at the

start of the analysis. Some finite element codes contain special procedures to deal with this problem.

3. Try to isolate the source of the problem. Convergence issues can often be traced to one or more of the following: (1) severe material nonlinearity, (2) contact, and (3) geometric nonlinearity. Try to change your model to remove as many of these as possible. For example, if you are doing a plasticity computation with contact and geometric nonlinearity, try doing an elastic calculation and see whether it works. If so, the problems are caused by material nonlinearity. Similarly, try analyzing the two contacting solids separately, without the contact, or try the computation without nonlinear geometry. Once you've traced the source of the problem, you might be able to fix it by changing the material properties, contact properties, or loading conditions.
4. Convergence problems are often caused by some kind of mechanical or material failure in the solid that involves a sudden release of energy. In this case, the shape of the solid may suddenly jump from one static equilibrium configuration to another, quite different, equilibrium configuration. There is a special type of loading procedure (called the Riks method) that can be used to stabilize this kind of problem.
5. Some boundary value problems have badly behaved governing equations. For example, the equations governing plane strain deformation of a perfectly plastic solid become hyperbolic for sufficiently large strains. Static FEM simply will not work for these problems. Your best bet is to try an explicit dynamic calculation instead, perhaps using mass scaling to speed up the calculation.

7.1.9.4 Load Steps and Increments

When you set up a finite element model, you usually apply the load in a series of steps. You can define different boundary conditions in each step. Unless you specify otherwise, the loads (or displacements) will vary linearly from their values at the start of the step to their values at the end of the step, as illustrated in Figure 7.21.

In a nonlinear analysis, the solution may not converge if the load is applied in a single increment. If this is the case, the load must be applied gradually, in a series of smaller increments. Many finite element codes will automatically reduce the time step if the solution fails to converge.

7.1.10 Output

The FEM *always* calculates the displacement of each node in the mesh; these are the unknown variables in the computation. However, these may not be the quantities in which you are really interested. A number of quantities can be computed from the displacement fields, including the following:

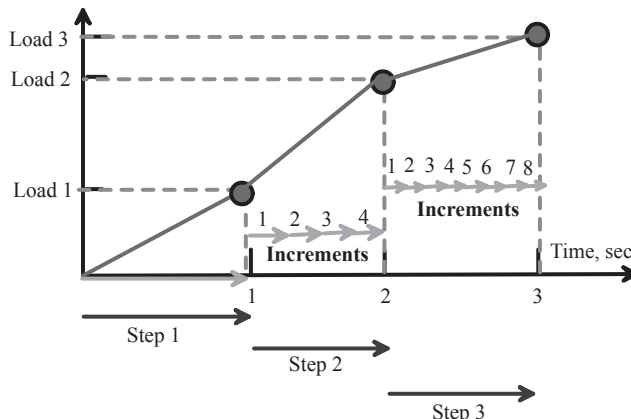


FIGURE 7.21 A load history defined by steps and increments of load.

1. Velocity and acceleration fields
2. Strain components, principal strains, and strain invariants or their rates
3. Elastic and plastic strains or strain rates
4. Stress components, principal stresses, and stress invariants
5. Forces applied to nodes or boundaries
6. Contact pressures
7. Values of material state variables (e.g., yield stresses)
8. Material failure criteria

All these quantities can be computed as functions of time at selected points in the mesh (either at nodes or at element integration points), as functions of position along paths connecting nodes, or as contour plots.

7.1.11 Units in Finite Element Computations

A finite element code merely solves the equations of motion (or equilibrium), together with any equations governing material behavior. Naturally, equations like $\mathbf{F} = m\mathbf{a}$ and $\sigma = E\varepsilon$ do not contain any units a priori. Consequently, when entering geometric dimensions, material data, and loads into an FEA code, you can use any system of units you like, but the units of all quantities must be consistent. You have to be very careful with this. When you sketch the part you are modeling, it is often convenient to enter dimensions in centimeters, inches, or millimeters. This is fine, but then centimeters, inches, or millimeters must be used for any other material or load data that contain length dimensions. For example, if you use centimeters to dimension your part, then you must enter data for Young's modulus and yield stress in Newtons per square centimeter, and you must also specify pressures acting on the system in Newtons per square centimeter. In this case, the FEA code will report stresses in units of Newtons per square centimeter.

7.1.12 Using Dimensional Analysis to Simplify FEA

You may have used dimensional analysis to find relationships between data measured in an experiment (especially in fluid mechanics). The same idea can be used to relate variables you might compute in FEA (e.g., stress), to the material properties of your part (e.g., Young's modulus) and the applied loading.

The basic idea is simple and is best illustrated by example. Suppose we want to use FEA to calculate the deflection of the tip of a cantilever with length L , Young's modulus E , and area moment of inertia I , which is subjected to a force P (Figure 7.22). We would set this up as an FEA problem, entering data for L , E , I , and P in the code and computing δ . We could express the functional relationship as

$$\delta = f(E, I, P, L).$$

If we were asked to calculate the function f numerically, we would have to run simulations in which we vary E , I , L , and P independently. This would be very painful. Fortunately, because the relationship must be independent of the system of units, we know we can rewrite this expression so that both the left- and right-hand side are dimensionless, i.e., as combinations of variables that have *no* units. Noting that δ and L have dimensions of length, I has dimensions of length⁴, P has dimensions mass × length/time², and E has dimensions of mass/(length × time²), we could put

$$\frac{\delta}{L} = g\left(\frac{P}{EL^2}, \frac{L^4}{I}\right).$$

Now, we only need to calculate the function g . We could do this by keeping L and I fixed and varying P to see the results of varying the first group; we could then keep P and L fixed and vary I to see the effect of varying the second group. The results could be displayed graphically as shown in Figure 7.23.

If we had done a linear analysis (no nonlinear geometric effects), the curves would be straight lines.

There is often more than one choice of dimensionless group, and some are better than others. For example, for the beam problem, we could create a new dimensionless group by multiplying together the two groups in the function g ; this gives

$$\frac{\delta}{L} = h\left(\frac{PL^2}{EI}, \frac{L^4}{I}\right).$$

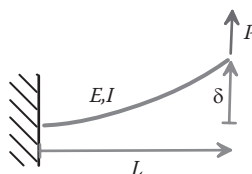


FIGURE 7.22 Cantilever beam subjected to end loading.

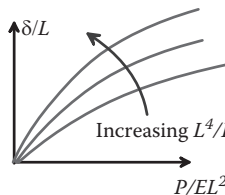


FIGURE 7.23 Deflection-versus-force relation for the beam shown in Figure 7.22.

This turns out to be a much better choice. In fact, if we conducted a linear analysis, we would find that the function h is *independent* of L^4/I . In this case, the data would collapse onto a single master curve as shown in Figure 7.24.

Unfortunately, dimensional analysis alone will not tell you the best dimensionless groups. You have to use your physical intuition to identify them. For the beam example, you might remember that E and I always appear as the product EI in the governing equations, so it makes sense to try to find dimensionless groups that combine them in this way. In other examples, you may see some physical significance of combinations of variables (they might look like a kinetic energy, or a pressure, for example) which might help you to choose the best set.

The beauty of using dimensional analysis to simplify numerical simulations is that, unlike in experiments, you do not need to guess what variables influence the results. You know exactly what they are, because you typed them into the program!

The following steps (known as the Buckingham Pi theorem) will tell you how many dimensionless groups to look for:

1. List the variable you are computing and also the variables you entered into the code to define the problem. Count the total number of variables and call it n .
2. List the dimensions, in terms of fundamental units (i.e., mass, length, time, electric current, and luminous intensity) of all the variables.
3. Count the number of independent fundamental units that appear in the problem (e.g., if mass, length, and time appear independently, then there are three different units) and call the number k . Units are independent if they do not always appear in the same combination. For example, in our beam problem, mass and time are not independent because they appear together as mass/time² in both P and E . The beam problem has length and mass/time² as two independent combinations of fundamental units.

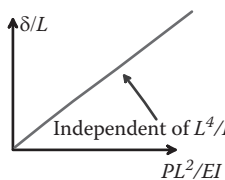


FIGURE 7.24 Unified deflection-versus-force relation for the beam shown in Figure 7.22.

4. A total of $n - k$ independent dimensionless groups must appear in the dimensionless relationship.

For the beam problem, we had five variables, δ , E , I , P , and L , and two independent combinations of fundamental units, so we expect to see three dimensionless groups, which is precisely what we got.

7.1.13 Simplifying FEA by Scaling the Governing Equations

An alternative approach to identifying the dimensionless parameters that control the solution to a problem is to express the governing equations themselves in dimensionless form. This is a much more powerful technique but is also somewhat more difficult to use.

We can illustrate the procedure using our beam problem again. Let x measure distance along the beam and let w denote its vertical deflection, as indicated in Figure 7.25. You may remember that linear Euler–Bernoulli beam theory gives the following governing equation for w :

$$EI \frac{d^4 w}{dx^4} = 0$$

(the right-hand side vanishes because no forces act on $0 < x < L$), whereas the boundary conditions are

$$\left. \begin{array}{l} w = 0 \quad (\text{no deflection at wall}) \\ \frac{dw}{dx} = 0 \quad (\text{no rotation at wall}) \\ EI \frac{d^2 w}{dx^2} = 0 \quad (\text{no moment at free end}) \\ EI \frac{d^3 w}{dx^3} = P \quad (\text{Shear force equal to } P) \end{array} \right\} \begin{array}{l} x=0 \\ x=L. \end{array}$$

(If you don't remember these, it doesn't matter; it is the scaling discussed below that is important).

We now rewrite the equations so that they are dimensionless. We always start by replacing all field variables (in this case, w and x) with dimensionless quantities. In this case, we could use $\xi = x/L$ $\hat{w} = w/L$. Substituting $x = \xi L$ $w = \hat{w}L$ gives

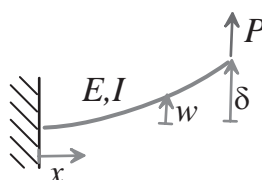


FIGURE 7.25 Deflection of a cantilever beam subjected to end loading.

$$\left. \begin{array}{l} \frac{EI}{L^3} \frac{d^4 \hat{w}}{d\xi^4} = 0 \\ L\hat{w} = 0 \quad (\text{no deflection at wall}) \\ \frac{d\hat{w}}{d\xi} = 0 \quad (\text{no rotation at wall}) \\ \frac{EI}{L} \frac{d^2 \hat{w}}{d\xi^2} = 0 \quad (\text{no moment at free end}) \\ \frac{EI}{L^2} \frac{d^3 \hat{w}}{d\xi^3} = P \quad (\text{shear force equal to } P) \end{array} \right\} \begin{array}{l} \xi = 0 \\ \xi = 1. \end{array}$$

We now look and see whether we can make additional simplifications. Our objective is to remove as many material and geometric parameters from the equations as possible, by defining new dimensionless field variables or introducing dimensionless combinations of material or geometric variables. In this case, we see that, if we define a new dimensionless displacement W so that

$$WPL^2 / (EI) = \hat{w},$$

and substitute and cancel as many terms as possible, the governing equations become

$$\left. \begin{array}{l} \frac{d^4 W}{d\xi^4} = 0 \\ W = 0 \quad (\text{no deflection at wall}) \\ \frac{dW}{dx} = 0 \quad (\text{no rotation at wall}) \\ \frac{d^2 W}{d\xi^2} = 0 \quad (\text{no moment at free end}) \\ \frac{d^3 W}{d\xi^3} = 1 \quad (\text{shear force equal to } P) \end{array} \right\} \begin{array}{l} \xi = 0 \\ \xi = 1. \end{array}$$

In this form, the governing equations contain absolutely no material or geometric parameters. The solution for W must therefore be independent of L , E , I , or P . We can solve the equation just once and then work out the tip deflection from the value of W at $\xi = 1$. Specifically,

$$\delta = w(x = L) = L\hat{w}(\xi = 1) = \frac{PL^3}{EI} W(\xi = 1).$$

This scaling procedure is the best way to simplify numerical computations. It is more difficult to apply than dimensional analysis, however, and it is possible (although perhaps not a good idea) to run an FEA simulation of a problem in which you do not actually know the governing equations! In this case, you should just use standard dimensional analysis to try to simplify the problem.

7.1.14 Dimensional Analysis: Closing Remarks

It is good practice to scale a mechanics problem as outlined in the preceding sections and present results in dimensionless form. Not all practicing engineers and managers are really comfortable with it, however. They don't want to see data presented in dimensionless form; they want to see real numbers.

The best way to deal with this when presenting results in a report is to divide it into two sections: one in which you present master curves in dimensionless form, and another in which the master curves are converted to give real numbers for quantities of interest.

You can make dimensional analysis work in your favor. It is not uncommon for your boss to tell you to run a series of simulations in which you vary a parameter that can be shown on dimensional grounds to have absolutely no effect. Also, dimensional analysis often tells you that varying two parameters are equivalent; for example, if you already had data for deflection as a function of load in the beam problem, you could use that to immediately calculate the deflection as a function of length. Don't tell your bosses this; it will just confuse them. Instead, tell them that you will work night and day to get the simulations done by the end of the week. Then take the week off, and plot up the data 5 mins before your next meeting.

7.2 A SIMPLE FINITE ELEMENT PROGRAM

The goal of this section is to provide some insight into the theory and algorithms that are coded in a finite element program. Here, we will implement only the simplest possible finite element code: specifically, we will develop an FEM to solve a 2D (plane stress or plane strain) static boundary value problem in linear elasticity, as shown in Figure 7.26.

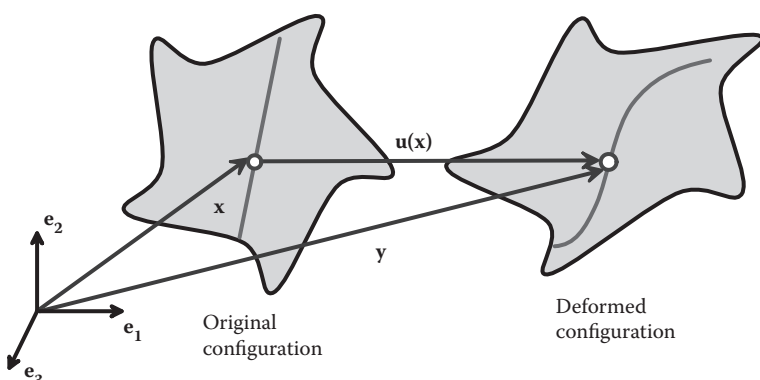


FIGURE 7.26 Displacement vector characterizing deformation in a solid.

We assume that we are given the following:

1. The shape of the solid in its unloaded condition R
2. Boundary conditions, specifying displacements $\mathbf{u}^*(\mathbf{x})$ on a portion $\partial_1 R$ or tractions \mathbf{t}^* on a portion $\partial_2 R$ of the boundary of R

To simplify the problem, we will make the following assumptions:

- The solid is an isotropic, linear elastic solid with Young's modulus E and Poisson's ratio ν .
- Plane strain or plane stress deformation.
- The solid is at constant temperature (no thermal strains).
- We will neglect body forces.

We then want to find a displacement field u_i satisfying the usual field equations and boundary conditions (see Section 5.1.1). The procedure is based on the principle of minimum potential energy discussed in Section 5.7. There are four steps:

1. A finite element mesh is constructed to interpolate the displacement field.
2. The strain energy in each element is calculated in terms of the displacements of each node.
3. The potential energy of tractions acting on the solid's boundary is added.
4. The displacement field is calculated by minimizing the potential energy.

These steps are discussed in more detail in the sections below.

7.2.1 Finite Element Mesh and Element Connectivity

For simplicity, we will assume that the elements are three-noded triangles, as shown in Figure 7.27. The nodes are numbered $1, 2, 3, \dots, N$, whereas the elements are numbered $1, 2, \dots, L$. Element numbers are shown in parentheses.

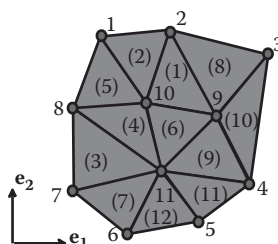


FIGURE 7.27 A typical 2D finite element mesh.

The position of the a th node is specified by its coordinates $x_i^{(a)}$. The *element connectivity* specifies the node numbers attached to each element. For example, in Figure 7.27, the connectivity for element 1 is (10,9,2), for element 2 it is (10,2,1), etc.

7.2.2 Global Displacement Vector

We will approximate the displacement field by interpolating between values at the nodes, as follows. Let $u_i^{(a)}$ denote the unknown displacement vector at nodes $a = 1, 2, \dots, N$. In a finite element code, the displacements for a plane stress or plane strain problem are normally stored as a column vector like the one shown below:

$$\underline{u} = \begin{bmatrix} u_1^{(1)} & u_2^{(1)} & u_1^{(2)} & u_2^{(2)} & u_1^{(3)} & u_2^{(3)} \end{bmatrix}^T.$$

The unknown displacement components will be determined by minimizing the potential energy of the solid.

7.2.3 Element Interpolation Functions

To calculate the potential energy, we need to be able to compute the displacements within each element. This is done by interpolation. Consider a triangular element, with nodes a, b, c at its corners, as shown in Figure 7.28. Let $x_i^{(a)}, x_i^{(b)}, x_i^{(c)}$ denote the coordinates of the corners. Define the element interpolation functions (also known as *shape functions*) as follows:

$$\begin{aligned} N_a(x_1, x_2) &= \frac{(x_2 - x_2^{(b)})(x_1^{(c)} - x_1^{(b)}) - (x_1 - x_1^{(b)})(x_2^{(c)} - x_2^{(b)})}{(x_2^{(a)} - x_2^{(b)})(x_1^{(c)} - x_1^{(b)}) - (x_1^{(a)} - x_1^{(b)})(x_2^{(c)} - x_2^{(b)})} \\ N_b(x_1, x_2) &= \frac{(x_2 - x_2^{(c)})(x_1^{(a)} - x_1^{(c)}) - (x_1 - x_1^{(c)})(x_2^{(a)} - x_2^{(c)})}{(x_2^{(b)} - x_2^{(c)})(x_1^{(a)} - x_1^{(c)}) - (x_1^{(b)} - x_1^{(c)})(x_2^{(a)} - x_2^{(c)})} \\ N_c(x_1, x_2) &= \frac{(x_2 - x_2^{(a)})(x_1^{(b)} - x_1^{(a)}) - (x_1 - x_1^{(a)})(x_2^{(b)} - x_2^{(a)})}{(x_2^{(c)} - x_2^{(a)})(x_1^{(b)} - x_1^{(a)}) - (x_1^{(c)} - x_1^{(a)})(x_2^{(b)} - x_2^{(a)})}. \end{aligned}$$

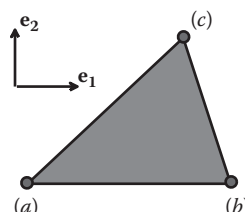


FIGURE 7.28 A triangular finite element.

These shape functions are constructed so that (1) they vary linearly with position within the element, and (2) each shape function has a value of one at one of the nodes and is zero at the other two. We then write

$$u_i(x_1, x_2) = u_i^{(a)} N_a(x_1, x_2) + u_i^{(b)} N_b(x_1, x_2) + u_i^{(c)} N_c(x_1, x_2).$$

One can readily verify that this expression gives the correct values for u_i at each corner of the triangle.

Of course, the shape functions given are valid only for three-noded triangular elements; other elements have more complicated interpolation functions.

7.2.4 Element Strains, Stresses, and Strain Energy Density

We can now compute the strain distribution within the element and hence determine the strain energy density. Because we are solving a plane strain problem, the only non-zero strains are $\epsilon_{11}, \epsilon_{22}, \epsilon_{12}$. It is convenient to express the results in matrix form, as follows:

$$\underline{\epsilon} = [\underline{B}] \underline{u}^{\text{element}} \equiv \begin{bmatrix} \epsilon_{11} \\ \epsilon_{12} \\ 2\epsilon_{12} \end{bmatrix} = \begin{bmatrix} \frac{\partial N_a}{\partial x_1} & 0 & \frac{\partial N_b}{\partial x_1} & 0 & \frac{\partial N_c}{\partial x_1} & 0 \\ 0 & \frac{\partial N_a}{\partial x_2} & 0 & \frac{\partial N_b}{\partial x_2} & 0 & \frac{\partial N_c}{\partial x_2} \\ \frac{\partial N_a}{\partial x_2} & \frac{\partial N_a}{\partial x_1} & \frac{\partial N_b}{\partial x_2} & \frac{\partial N_b}{\partial x_1} & \frac{\partial N_c}{\partial x_2} & \frac{\partial N_c}{\partial x_1} \end{bmatrix} \begin{bmatrix} u_1^{(a)} \\ u_2^{(a)} \\ u_1^{(b)} \\ u_2^{(b)} \\ u_1^{(c)} \\ u_2^{(c)} \end{bmatrix}.$$

The factor of 2 multiplying the shear strains in the strain vector has been introduced for convenience. Note that, for linear triangular elements, the matrix of shape function derivatives $[\underline{B}]$ is constant. It depends only on the coordinates of the corners of the element and does not vary with position within the element. This is not the case for most elements.

Now, we can compute the strain energy density within the element. Begin by computing the stresses within the element. For plane strain deformation, we have that

$$\begin{bmatrix} \sigma_{11} \\ \sigma_{22} \\ \sigma_{22} \end{bmatrix} = \frac{E}{(1+\nu)(1-2\nu)} \begin{bmatrix} 1-\nu & \nu & 0 \\ \nu & 1-\nu & 0 \\ 0 & 0 & \frac{1-2\nu}{2} \end{bmatrix} \begin{bmatrix} \epsilon_{11} \\ \epsilon_{22} \\ 2\epsilon_{12} \end{bmatrix}.$$

For plane stress, the result is

$$\begin{bmatrix} \sigma_{11} \\ \sigma_{22} \\ \sigma_{12} \end{bmatrix} = \frac{E}{(1-\nu^2)} \begin{bmatrix} 1 & \nu & 0 \\ \nu & 1 & 0 \\ 0 & 0 & (1-\nu)/2 \end{bmatrix} \begin{bmatrix} \epsilon_{11} \\ \epsilon_{22} \\ 2\epsilon_{12} \end{bmatrix}.$$

Recall (see Section 3.1.7) that the strain energy density is related to the stresses and strains by $U = \sigma_{ij}\epsilon_{ij}/2$. This can be written in matrix form as

$$U = \frac{1}{2} \underline{\epsilon}^T \underline{\sigma} = \frac{1}{2} \underline{\epsilon}^T [D] \underline{\epsilon},$$

where

$$\underline{\sigma} = \begin{bmatrix} \sigma_{11} \\ \sigma_{22} \\ \sigma_{12} \end{bmatrix} \quad \underline{\epsilon} = \begin{bmatrix} \epsilon_{11} \\ \epsilon_{22} \\ 2\epsilon_{12} \end{bmatrix} \quad [D] = \begin{cases} \frac{E}{(1+\nu)(1-2\nu)} \begin{bmatrix} 1-\nu & \nu & 0 \\ \nu & 1-\nu & 0 \\ 0 & 0 & (1-2\nu)/2 \end{bmatrix} & \text{Plane strain} \\ \frac{E}{(1-\nu^2)} \begin{bmatrix} 1 & \nu & 0 \\ \nu & 1 & 0 \\ 0 & 0 & (1-\nu)/2 \end{bmatrix} & \text{Plane stress.} \end{cases}$$

Now, express these results in terms of the nodal displacements for the element

$$U^{\text{element}} = \frac{1}{2} \underline{u}^{\text{element}T} ([B]^T [D] [B]) \underline{u}^{\text{element}}.$$

We can now compute the total strain energy stored within the element. Because $[B]$ is constant, we merely need to multiply the strain energy density by the area of the element, which can be computed from the coordinates of its corners as follows:

$$A = \frac{1}{2} |(x_1^b - x_1^a)(x_2^c - x_2^a) - (x_1^c - x_1^a)(x_2^b - x_2^a)|$$

Hence, the total strain energy of the element is

$$W^{\text{element}} = \frac{1}{2} \underline{u}^{\text{element}T} (A_{\text{element}} [B]^T [D] [B]) \underline{u}^{\text{element}}.$$

7.2.5 Element Stiffness Matrix

The strain energy can be simplified by defining the *element stiffness matrix*,

$$K^{\text{element}} = A_{\text{element}} [B][D][B],$$

so that

$$W^{\text{element}} = \frac{1}{2} \underline{u}^{\text{element}T} K^{\text{element}} \underline{u}^{\text{element}}.$$

Observe that, because the material property matrix $[D]$ is symmetric, the element stiffness matrix is also symmetric. To see this, note that

$$K^{\text{element}T} = A_{\text{element}}([B]^T [D] [B])^T = A_{\text{element}}[B]^T [D]^T [B] = A_{\text{element}}[B]^T [D] [B] = K^{\text{element}}.$$

7.2.6 Global Stiffness Matrix

The total strain energy of the solid may be computed by adding together the strain energy of each element:

$$W = \sum_{\text{elements}} W^{\text{element}} = \frac{1}{2} \sum_{\text{elements}} \underline{u}^{\text{element}T} K^{\text{element}} \underline{u}^{\text{element}}.$$

It is more convenient to express W in terms of the vector \underline{u} , which contains all the nodal displacements, rather than using $\underline{u}^{\text{element}}$ for each element to describe the displacements. For example, the strain energy for the simple two-element mesh shown in Figure 7.29 is

$$W = \frac{1}{2} \begin{bmatrix} u_1^{(1)} & u_2^{(1)} & u_1^{(2)} & u_2^{(2)} & u_1^{(3)} & u_2^{(3)} \end{bmatrix} \begin{bmatrix} k_{11}^{(1)} & k_{12}^{(1)} & \dots & k_{16}^{(1)} \\ k_{21}^{(1)} & k_{22}^{(1)} & & \\ \vdots & & \ddots & \\ k_{61}^{(1)} & & & k_{66}^{(1)} \end{bmatrix} \begin{bmatrix} u_1^{(1)} \\ u_2^{(1)} \\ u_1^{(2)} \\ u_2^{(2)} \\ u_1^{(3)} \\ u_2^{(3)} \end{bmatrix}$$

$$+ \frac{1}{2} \begin{bmatrix} u_1^{(2)} & u_2^{(2)} & u_1^{(3)} & u_2^{(3)} & u_1^{(4)} & u_2^{(4)} \end{bmatrix} \begin{bmatrix} k_{11}^{(2)} & k_{12}^{(2)} & & k_{16}^{(2)} \\ k_{21}^{(2)} & k_{22}^{(2)} & & \\ \vdots & & \ddots & \\ k_{61}^{(2)} & & & k_{66}^{(2)} \end{bmatrix} \begin{bmatrix} u_1^{(2)} \\ u_2^{(2)} \\ u_1^{(3)} \\ u_2^{(3)} \\ u_1^{(4)} \\ u_2^{(4)} \end{bmatrix}.$$

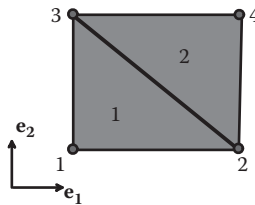


FIGURE 7.29 A mesh with two triangular finite elements.

If we wanted to, we could add the missing terms to each element displacement vector:

$$W = \frac{1}{2}$$

$$\begin{bmatrix} u_1^{(1)} & u_2^{(1)} & u_1^{(2)} & u_2^{(2)} & u_1^{(3)} & u_2^{(3)} & u_1^{(4)} & u_2^{(4)} \end{bmatrix}$$

$$\left[\begin{array}{ccccccc|c} k_{11}^{(1)} & k_{12}^{(1)} & k_{13}^{(1)} & k_{14}^{(1)} & \cdots & 0 & 0 & u_1^{(1)} \\ k_{21}^{(1)} & k_{22}^{(1)} & k_{32}^{(1)} & & & 0 & 0 & u_2^{(1)} \\ & & k_{33}^{(1)} & k_{34}^{(1)} & & 0 & 0 & u_1^{(2)} \\ & & k_{43}^{(1)} & k_{44}^{(1)} & & 0 & 0 & u_2^{(2)} \\ k_{53}^{(1)} & & & & 0 & 0 & 0 & u_1^{(3)} \\ \vdots & & & & \ddots & 0 & 0 & u_2^{(3)} \\ 0 & 0 & 0 & 0 & 0 & 0 & 0 & u_1^{(4)} \\ 0 & 0 & 0 & 0 & 0 & 0 & 0 & u_2^{(4)} \end{array} \right]$$

$$+ \begin{bmatrix} u_1^{(1)} & u_2^{(1)} & u_1^{(2)} & u_2^{(2)} & u_1^{(3)} & u_2^{(3)} & u_1^{(4)} & u_2^{(4)} \end{bmatrix}$$

$$\left[\begin{array}{ccccccccc|c} 0 & 0 & 0 & 0 & 0 & \cdots & 0 & 0 & u_1^{(1)} \\ 0 & 0 & 0 & 0 & 0 & & 0 & 0 & u_2^{(1)} \\ 0 & 0 & k_{11}^{(2)} & k_{12}^{(2)} & & & & & u_1^{(2)} \\ 0 & 0 & k_{21}^{(2)} & k_{22}^{(2)} & & & & & u_2^{(2)} \\ 0 & 0 & k_{31}^{(2)} & & & & & & u_1^{(3)} \\ 0 & 0 & \vdots & & & \ddots & & & u_2^{(3)} \\ 0 & 0 & & & & & k_{56}^{(2)} & & u_1^{(4)} \\ 0 & 0 & & & & & k_{65}^{(2)} & k_{66}^{(2)} & u_2^{(4)} \end{array} \right]$$

We can now collect together corresponding terms in the two element stiffness matrices to express this as

$$W = \frac{1}{2} \begin{bmatrix} u_1^{(1)} & u_2^{(1)} & u_1^{(2)} & u_2^{(2)} & u_1^{(3)} & u_2^{(3)} & u_1^{(4)} & u_2^{(4)} \end{bmatrix} \begin{bmatrix} k_{11}^{(1)} & k_{12}^{(1)} & k_{13}^{(1)} & & k_{11}^{(1)} & \dots & & \\ k_{21}^{(1)} & k_{22}^{(1)} & k_{32}^{(1)} & & & & & \\ & & k_{33}^{(1)} + k_{11}^{(2)} & k_{34}^{(1)} + k_{12}^{(2)} & & & & \\ & & k_{43}^{(1)} + k_{21}^{(2)} & k_{44}^{(1)} + k_{22}^{(2)} & & & & \\ & & k_{53}^{(1)} + k_{31}^{(2)} & & & & & \\ & & \vdots & & & & & \\ & & & & k_{56}^{(2)} & & & \\ & & & & k_{65}^{(2)} & k_{66}^{(2)} & & \end{bmatrix} \begin{bmatrix} u_1^{(1)} \\ u_2^{(1)} \\ u_1^{(2)} \\ u_2^{(2)} \\ u_1^{(3)} \\ u_2^{(3)} \\ u_1^{(4)} \\ u_2^{(4)} \end{bmatrix}.$$

We can therefore write

$$W = \frac{1}{2} \underline{\underline{u}}^T [K] \underline{\underline{u}},$$

where $[K]$ is known as the *global stiffness matrix*. It is the sum of all the element stiffness matrices. Because the element stiffness matrix is symmetric, the global stiffness matrix must also be symmetric. To assemble the global stiffness matrix for a plane strain or plane stress mesh with N nodes, we use the following procedure:

1. Note that, for N nodes, there will be $2N$ unknown displacement components (two at each node). Therefore, we start by setting up storage for a $(2N \times 2N)$ global stiffness matrix and set each term in the matrix to zero.
2. Next, begin a loop over the elements.
3. For the current element, assemble the element stiffness matrix

$$K^{\text{element}} = A_{\text{element}} [B]^T [D][B].$$

4. Add the element stiffness matrix to the global stiffness matrix, using the following procedure. Let a, b, c denote the numbers of the nodes on the three corners of the element.

Let k_{ij}^{element} for $i = 1 \dots 6, j = 1 \dots 6$ denote the terms in the element stiffness matrix. Let K_{nm} for $n = 1 \dots 2N, m = 1 \dots 2N$ denote the terms in the global stiffness matrix. Then,

$$\begin{array}{ll}
K_{2a-1,2a-1} += k_{11}^{\text{element}} & K_{2a-1,2a} += k_{12}^{\text{element}} \\
K_{2a-1,2b-1} += k_{13}^{\text{element}} & K_{2a-1,2b} += k_{14}^{\text{element}} \\
K_{2a-1,2c-1} += k_{15}^{\text{element}} & K_{2a-1,2c} += k_{16}^{\text{element}} \\
\\
K_{2a,2a-1} += k_{21}^{\text{element}} & K_{2a,2a} += k_{22}^{\text{element}} \\
K_{2a,2b-1} += k_{23}^{\text{element}} & K_{2a,2b} += k_{24}^{\text{element}} \\
K_{2a,2c-1} += k_{25}^{\text{element}} & K_{2a,2c} += k_{26}^{\text{element}} \\
\\
K_{2b-1,2a-1} += k_{31}^{\text{element}} & K_{2b-1,2a} += k_{32}^{\text{element}} \\
K_{2b-1,2b-1} += k_{33}^{\text{element}} & K_{2b-1,2b} += k_{34}^{\text{element}} \\
K_{2b-1,2c-1} += k_{35}^{\text{element}} & K_{2b-1,2c} += k_{36}^{\text{element}} \\
& \vdots \\
K_{2c,2a-1} += k_{61}^{\text{element}} & K_{2c,2a} += k_{62}^{\text{element}} \\
K_{2c,2b-1} += k_{63}^{\text{element}} & K_{2c,2b} += k_{64}^{\text{element}} \\
K_{2c,2c-1} += k_{65}^{\text{element}} & K_{2c,2c} += k_{66}^{\text{element}} .
\end{array}$$

Here, the symbol $+=$ means that the term on the left is incremented by the term on the right, following standard C syntax.

5. Proceed to the next element.

7.2.7 Boundary Loading

We have now found a way to compute the strain energy for a finite element mesh. Next, we need to compute the boundary term in the potential energy.

Consider tractions acting on a finite element, as shown in Figure 7.30. Boundary loading will be specified as follows:

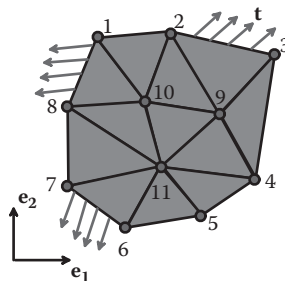


FIGURE 7.30 A finite element mesh subjected to boundary loading.

1. The element on which the loading acts.
2. The face of the element that is loaded.
3. The traction vector \mathbf{t} (force per unit area) that acts on the face of the element. The traction is assumed to be constant on the face of any one element.

Now, we compute the contribution to the potential energy attributable to the traction acting on the face of one element. For the element shown in Figure 7.31, the contribution to the potential energy would be

$$P = - \int_0^L t_i u_i ds.$$

Recall that the displacements vary linearly within a three-noded triangle. Therefore, we can write

$$u_i = u_i^{(a)} \frac{s}{L} + u_i^{(c)} \left(1 - \frac{s}{L}\right).$$

So, because the tractions are uniform,

$$\begin{aligned} P^{\text{element}} &= -t_i u_i^{(a)} \int_0^L \frac{s}{L} ds - t_i u_i^{(c)} \int_0^L \left(1 - \frac{s}{L}\right) ds \\ &= -t_i u_i^{(a)} \frac{L}{2} - t_i u_i^{(c)} \frac{L}{2} \\ &= - \left[t_1 \frac{L}{2} \ t_2 \frac{L}{2} \ t_1 \frac{L}{2} \ t_2 \frac{L}{2} \right] \cdot [u_1^{(a)} \ u_2^{(a)} \ u_1^{(c)} \ u_2^{(c)}]. \end{aligned}$$

Abbreviate this as

$$P^{\text{element}} = -\underline{r}_{\text{face}} \cdot \underline{u}_{\text{face}}.$$

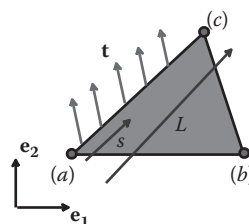


FIGURE 7.31 A finite element subjected to loading on one edge.

7.2.8 Global Residual Force Vector

The total contribution to the potential energy attributable to boundary loading on all element faces is

$$P = - \sum_{\text{faces}} \underline{r}_{\text{faces}} \cdot \underline{u}_{\text{faces}}.$$

It is more convenient to express this in terms of the global displacement vector \underline{u} :

$$P = - \underline{r} \cdot \underline{u},$$

where \underline{r} is the global residual force vector.

The global residual force vector for a mesh with N nodes is assembled as follows:

1. The residual force vector has length $2N$ (two entries per node). Reserve storage for a vector of length $2N$ and initialize to zero.
2. Loop over elements.
3. Determine which face of the element is loaded. Let a, b denote the node numbers attached to this face. Determine the residual force vector for the element face. Let $r_i^{\text{face}}, i = 1 \dots 4$ denote the terms in the element face residual vector. Let $r_n, n = 1 \dots 2N$ denote the terms in the global residual force vector. Then,

$$\begin{aligned} r_{2a-1} &= r_1^{\text{face}} & r_{2a} &= r_2^{\text{face}} \\ r_{2b-1} &= r_3^{\text{face}} & r_{2b} &= r_4^{\text{face}}. \end{aligned}$$

7.2.9 Minimizing the Potential Energy

We have set up the following expression for the potential energy of a finite element mesh:

$$\begin{aligned} V &= \frac{1}{2} \underline{u}^T [K] \underline{u} - \underline{r} \cdot \underline{u} \\ &\equiv \frac{1}{2} \sum_{j=1}^{2N} u_j \sum_{i=1}^{2N} K_{ji} u_i - \sum_{j=1}^{2N} r_j u_j. \end{aligned}$$

Now, minimize V :

$$\frac{\partial V}{\partial u_k} = \frac{1}{2} \sum_{i=1}^{2N} K_{ki} u_i + \frac{1}{2} \sum_{j=1}^{2N} u_j K_{jk} - r_k = 0,$$

where we have noted that

$$\frac{\partial u_j}{\partial u_k} = \begin{cases} 1, & j=k \\ 0, & j \neq k. \end{cases}$$

Simplify this by noting that $[K]$ is symmetric:

$$\begin{aligned} \frac{\partial V}{\partial u_k} &= \frac{1}{2} \sum_{i=1}^{2N} K_{ki} u_i + \frac{1}{2} \sum_{j=1}^{2N} u_j K_{kj} - r_k \\ &= \sum_{i=1}^{2N} K_{ki} u_i - r_k = 0 \\ \Rightarrow [K]u &= r. \end{aligned}$$

This is a system of $2N$ simultaneous linear equations for the $2N$ unknown nodal displacements. Standard computational techniques such as Gaussian elimination, Cholesky factorization, or conjugate gradient methods may be used to solve the system of equations.

7.2.10 Eliminating Prescribed Displacements

So far, we have seen how to calculate displacements in a finite element mesh that is subjected to prescribed loading. What if displacements are prescribed instead?

If this is the case, the stiffness matrix and residual are first assembled exactly as described in the preceding section. They are then modified to enforce the constraint. The procedure is best illustrated using an example. Suppose that the finite element equations after assembly have the form

$$\begin{bmatrix} k_{11} & k_{12} & \cdots & k_{12N} \\ k_{21} & k_{22} & & k_{22N} \\ \vdots & & \ddots & \\ k_{2N1} & k_{2N2} & & k_{2N2N} \end{bmatrix} \begin{bmatrix} u_1^{(1)} \\ u_2^{(1)} \\ \vdots \\ u_2^{(N)} \end{bmatrix} = \begin{bmatrix} r_1 \\ r_2 \\ \vdots \\ r_4 \end{bmatrix}.$$

To prescribe displacements for any node, we simply replace the equation for the appropriate degrees of freedom with the constraint. For example, to force $u_2^{(1)} = \Delta$, we could modify the finite element equations to

$$\begin{bmatrix} k_{11} & k_{12} & \cdots & k_{12N} \\ 0 & 1 & & 0 \\ \vdots & & \ddots & \\ k_{2N1} & k_{2N2} & & k_{2N2N} \end{bmatrix} \begin{bmatrix} u_1^{(1)} \\ u_2^{(1)} \\ \vdots \\ u_2^{(N)} \end{bmatrix} = \begin{bmatrix} r_1 \\ \Delta \\ \vdots \\ r_4 \end{bmatrix}.$$

Thus, the equation for $u_2^{(1)}$ has been replaced with the constraint $u_2^{(1)} = \Delta$.

This procedure works, but it has the disadvantage that the modified stiffness matrix is no longer symmetric. It is preferable to modify the stiffness and residual further, to retain symmetry. To do so, we eliminate the constrained degrees of freedom from all rows of the stiffness matrix. This is best illustrated by example. Suppose our modified stiffness matrix has the form

$$\begin{bmatrix} k_{11} & k_{12} & \cdots & k_{12N} \\ 0 & 1 & & 0 \\ \vdots & & \ddots & \\ k_{2N1} & k_{2N2} & & k_{2N2N} \end{bmatrix} \begin{bmatrix} u_1^{(1)} \\ u_2^{(1)} \\ \vdots \\ u_2^{(N)} \end{bmatrix} = \begin{bmatrix} r_1 \\ \Delta \\ \vdots \\ r_4 \end{bmatrix}.$$

Now, we want to set each entry in the second column (apart from the diagonal) to zero, so that the stiffness is symmetric. Recall that we can add and subtract equations in the system from one another without affecting the solution. Therefore, to symmetrize the stiffness matrix in our example, we can subtract appropriate multiples of the second row so as to set each entry in the second column to zero:

$$\begin{bmatrix} k_{11} & k_{12} & \cdots & k_{12N} \\ 0 & 1 & & 0 \\ \vdots & & \ddots & \\ k_{2N1} & 0 & & k_{2N2N} \end{bmatrix} \begin{bmatrix} u_1^{(1)} \\ u_2^{(1)} \\ \vdots \\ u_2^{(N)} \end{bmatrix} = \begin{bmatrix} r_1 - k_{12}\Delta \\ \Delta \\ \vdots \\ r_4 - k_{2N2}\Delta \end{bmatrix}.$$

7.2.11 Solution

The result of Sections 7.2.1 through 7.2.10 is a set of simultaneous linear equations of the form

$$[K^{\text{mod}}]\underline{u} = \underline{r}.$$

These can be solved for the unknown displacements \underline{u} using standard techniques (e.g., Gaussian elimination or iterative techniques). An important feature of the FEM equations is that the stiffness matrix is *sparse*; that is to say, only a small number of entries in the matrix are nonzero. Consequently, special schemes are used to store and factor the equations, which avoid having to store large numbers of zeros.

7.2.12 Postprocessing

Once the displacements have been computed, the strain in each element can be computed, and so the stress distribution can be deduced. The procedure is as follows:

1. For the element of interest, extract the displacement of each node from the global displacement vector.

2. Calculate the strains using the procedure in Section 7.2.4:

$$\underline{\varepsilon} = [B]\underline{u}^{\text{element}} \equiv \begin{bmatrix} \varepsilon_{11} \\ \varepsilon_{22} \\ 2\varepsilon_{12} \end{bmatrix} = \begin{bmatrix} \frac{\partial N_a}{\partial x_1} & 0 & \frac{\partial N_b}{\partial x_1} & 0 & \frac{\partial N_c}{\partial x_1} & 0 \\ 0 & \frac{\partial N_a}{\partial x_2} & 0 & \frac{\partial N_b}{\partial x_2} & 0 & \frac{\partial N_c}{\partial x_2} \\ \frac{\partial N_a}{\partial x_2} & \frac{\partial N_a}{\partial x_1} & \frac{\partial N_b}{\partial x_2} & \frac{\partial N_b}{\partial x_1} & \frac{\partial N_c}{\partial x_2} & \frac{\partial N_c}{\partial x_1} \end{bmatrix} \begin{bmatrix} u_1^{(a)} \\ u_2^{(a)} \\ u_1^{(b)} \\ u_2^{(b)} \\ u_1^{(c)} \\ u_2^{(c)} \end{bmatrix}.$$

3. The stresses can then be determined from the stress-strain equations:

$$\underline{\sigma} = [D]\underline{\varepsilon},$$

where $[D]$ is defined in Section 7.2.4.

7.2.13 Example FEA Code

MAPLE® and MATLAB® implementations of the procedure are provided in the file FEM_conststrain_mws and FEM_conststrain.m, which can be downloaded from <http://solidmechanics.org/FEA.htm>. Here we will describe only the MAPLE code.

The code reads an input file. A very simple input file (with just two elements) can be found in FEM_conststrain_input.txt.

The data file solves the problem illustrated in Figure 7.32. A rectangular block with Young's modulus 100 and Poisson's ratio 0.3 is meshed with two elements. Node 1 is pinned, node 4 is constrained against horizontal motion, and the right-hand face of element 2 is subjected to a constant horizontal traction with magnitude 10. The input file is shown in Figure 7.33; it should be mostly self-explanatory.

Note the following:

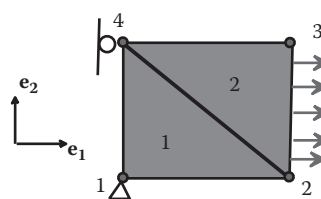


FIGURE 7.32 A simple finite element problem.

```

Material_Props:
  Young's_modulus: 100.
  Poissons_ratio: 0.3
No._nodes:      4
Nodal_coords:
  0.0  0.0
  1.0  0.0
  1.0  1.0
  0.0  1.0
No._elements:      2
Element_connectivity:
  1 2 4
  2 3 4
No._nodes_with_prescribed_DOFs: 3
Node_#, DOF#, Value:
  1 1 0.0
  1 2 0.0
  4 1 0.0
No._elements_with_prescribed_loads: 1
Element_#, Face_#, Traction_components
  2 1 10.0 0.0

```

FIGURE 7.33 Input file for sample finite element program.

1. Nodes are numbered sequentially; thus, node 1 has coordinates (0,0), node 2 has coordinates (1,0), etc.
2. The element connectivity specifies the node numbers attached to each element, using a counterclockwise numbering convention. It doesn't matter which node you use for the first one, as long as all the others are ordered in a counterclockwise sense around the element. For example, you could use (2,4,1) instead of (1,2,4) for the connectivity of the first element.
3. To fix motion of a node, you need to enter the node number, the degree of freedom that is being constrained (1 for horizontal, 2 for vertical), and a value for the prescribed displacement.
4. To specify tractions acting on an element face, you need to enter (1) the element number, (2) the face number of the element, and (3, 4) the horizontal and vertical components of traction acting on the face. The face numbering scheme is determined by the element connectivity, as follows. Face 1 has the first and second nodes as end points, face 2 has the second and third nodes, and face 3 has the third and first nodes as end points. Because connectivity for element 2 was entered as (2,3,4), face 1 of this element has nodes numbered 2 and 3, face 2 connects nodes numbered 3 and 4, whereas face 3 connects nodes numbered 4 and 1.

To run the code, you need to open the .mws file with MAPLE and then follow these steps:

1. Edit the code to insert the full path for the input file in the line near the top of the code that reads

```
# Change the name of the file below to point to your input file
infile:=fopen('insert full path of input file', READ):
```

2. Scroll down near the bottom to the line that reads

```
# Print nodal displacements, element strains, and stresses to a file
outfile:= fopen('insert full path of output file', WRITE):
```

and enter a name for the output file.

3. Return to the top of the file, and press <enter> to execute each MAPLE block. If all goes well, you should see that, after reading the input data, MAPLE plots the mesh (just as a check).
4. If you continue to the end, you should see a plot of the displaced mesh (red) superimposed on the original mesh (green).
5. Finally, open the output file. It should contain the results shown in Figure 7.34.

Nodal displacements: Node u1 u2 1 0.0000 0.0000 2 .0910 .0000 3 .0910 -.0390 4 0.0000 -.0390
Strains and stresses: Element e_11 e_22 e_12 s_11 s_22 s_12 1 .0910 -.0390 .0000 10.0000 -.0000 .0000 2 .0910 -.0390 .0000 10.0000 .0000 .0000

FIGURE 7.34 Output file produced by sample finite element program.

Finite Element Analysis: Theory and Implementation

The derivation and implementation of the FEM outlined in the previous chapter is simple and easy to follow, but it gives the misleading impression that the FEM relies on the principle of minimum potential energy and so is applicable only to linear elastic solids. This is not the case, of course; the FEM can solve problems involving very complex materials and large shape changes.

This chapter contains the following:

1. A more rigorous derivation of the finite element equations, based on the principle of virtual work, which was derived in Section 2.4.
2. A more sophisticated implementation of FEM for static linear elasticity. This includes more accurate element interpolation schemes and also extends the FEM to three dimensions.
3. A discussion of time integration schemes that are used in finite element simulations of dynamic problems and a discussion of modal techniques for dynamic linear elasticity problems.
4. An extension of the FEM to nonlinear materials, using the hypoelastic material model described in Section 3.3 as a representative nonlinear material.
5. An extension of the FEM to account for large shape changes, using finite strain elasticity as a representative example.
6. A discussion of finite element procedures for history-dependent solids, using small strain viscoplasticity as a representative example.
7. A discussion of the phenomenon of “locking” that can cause the standard FEM to fail in certain circumstances. Several techniques for avoiding locking are presented.

In addition, a set of sample finite element codes (implemented in MAPLE and MATLAB) are provided to illustrate how the various finite element procedures are implemented in practice. Sample codes may be downloaded from <http://solidmechanics.org/FEA>.

8.1 GENERALIZED FEM FOR STATIC LINEAR ELASTICITY

This section gives a more general derivation and implementation of the FEM for static linear elastic solids than the energy-based derivation given in Chapter 7.

8.1.1 Review of the Principle of Virtual Work

We begin by summarizing the usual governing equations of linear elasticity, which must be solved by the FEA code. The problem to be solved is illustrated in Figure 8.1. We are given the following:

1. The shape of the solid in its unloaded condition R_0
2. The initial stress field in the solid (we will take this to be zero in setting up our FEM code)
3. The elastic constants for the solid C_{ijkl}
4. The thermal expansion coefficients for the solid and temperature distribution (we will take this to be zero for our FEM code, for simplicity)
5. A body force distribution \mathbf{b} acting on the solid (note that, in this section, we will use \mathbf{b} to denote force per unit volume rather than force per unit mass, to avoid having to write out the mass density all the time)
6. Boundary conditions, specifying displacements $\mathbf{u}^*(\mathbf{x})$ on a portion $\partial_1 R$ or tractions on a portion $\partial_2 R$ of the boundary of R

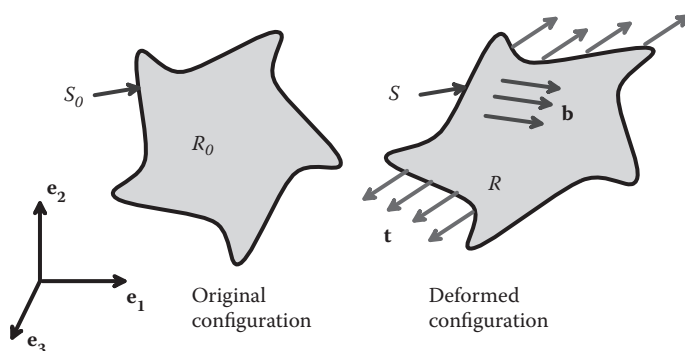


FIGURE 8.1 A representative boundary value problem in solid mechanics.

Calculate displacements, strains, and stresses u_i , ε_{ij} , σ_{ij} , satisfying the governing equations of static linear elasticity:

1. The strain-displacement equation: $\varepsilon_{ij} = \frac{1}{2}(\partial u_i / \partial x_j + \partial u_j / \partial x_i)$
2. The elastic stress-strain law: $\sigma_{ij} = C_{ijkl} \varepsilon_{kl}$
3. The equation of static equilibrium for stresses: $\partial \sigma_{ij} / \partial x_i + b_j = 0$
4. The boundary conditions on displacement and stress: $u_i = u_i^*$ on $\partial_1 R$ $\sigma_{ij} n_i = t_j^*$ on $\partial_2 R$

As we discussed in Section 2.4, the principle of virtual work can be used to replace the stress equilibrium equations. To express the principle, we define a *kinematically admissible virtual displacement field* $\delta \mathbf{v}(\mathbf{x})$, satisfying $\delta \mathbf{v} = 0$ on $\partial_1 R$. You can visualize this field as a small change in the displacement of the solid if you like, but it is really just an arbitrary differentiable vector field. The term “kinematically admissible” is just a complicated way of saying that $\delta \mathbf{v} = 0$ on $\partial_1 R$; that is to say, if you perturb the displacement slightly, the boundary conditions on displacement are still satisfied.

In addition, we define an associated *virtual strain field*:

$$\delta \varepsilon_{ij} = \frac{1}{2} \left(\frac{\partial \delta v_i}{\partial x_j} + \frac{\partial \delta v_j}{\partial x_i} \right)$$

The principle of virtual work states that, if the stress field σ_{ij} satisfies

$$\int_R \sigma_{ij} \delta \varepsilon_{ij} dV_0 - \int_R b_i \delta v_i dV_0 - \int_{\partial_2 R} t_i \delta v_i dA = 0$$

for all possible virtual displacement fields and corresponding virtual strains, it will automatically satisfy the equation of stress equilibrium $\partial \sigma_{ij} / \partial x_i + b_j = 0$ and also the traction boundary condition $\sigma_{ij} n_i = t_j^*$ on $\partial_2 R$.

8.1.2 Integral (Weak) Form of the Governing Equations of Linear Elasticity

The principle of virtual work can be used to write the governing equation for the displacement field in a linear elastic solid in an integral form (called the “weak form”). Instead of solving the governing equations listed in the preceding section, the displacements, strains, and stresses u_i , ε_{ij} , σ_{ij} are calculated as follows:

1. Find a displacement field $u_i(x_j)$ satisfying

$$\int_R C_{ijkl} \frac{\partial u_k}{\partial x_l} \frac{\partial \delta v_i}{\partial x_j} dV - \int_R b_i \delta v_i dV - \int_{\partial_2 R} t_i \delta v_i dA = 0, \quad u_i = u_i^* \text{ on } \partial_1 R$$

- for all virtual velocity fields δv_i satisfying $\delta v_i = 0$ on $\partial_1 R$.
2. Compute the strains from the definition $\epsilon_{ij} = \frac{1}{2}(\partial u_i / \partial x_j + \partial u_j / \partial x_i)$.
 3. Compute the stresses from the stress-strain law $\sigma_{ij} = C_{ijkl} \epsilon_{kl}$. The stress will automatically satisfy the equilibrium equation and boundary conditions, so all the field equations and boundary conditions will be satisfied.

The significance of this result is that it replaces the derivatives in the partial differential equations of equilibrium with an equivalent integral, which is easier to handle numerically. It is essentially equivalent to replacing the equilibrium equation with the principle of minimum potential energy, but the procedure based on the principle of virtual work is very easily extended to dynamic problems, other stress-strain laws, and even to problems involving large shape changes.

Derivation: Start with the virtual work equation

$$\int_R \sigma_{ij} \delta \epsilon_{ij} dV_0 - \int_R b_i \delta v_i dV_0 - \int_{\partial_2 R} t_i \delta v_i dA = 0.$$

Recall that $\sigma_{ij} = \sigma_{ji}$ and that $\delta \epsilon_{ij} = (\partial \delta v_i / \partial x_j + \partial \delta v_j / \partial x_i) / 2$, so that

$$\sigma_{ij} \delta \epsilon_{ij} = (\sigma_{ij} \partial \delta v_i / \partial x_j + \sigma_{ji} \partial \delta v_j / \partial x_i) / 2 = \sigma_{ij} \partial \delta v_i / \partial x_j.$$

Finally, recall that $\sigma_{ij} = C_{ijkl} \epsilon_{kl} = C_{ijkl} (\partial u_k / \partial x_l + \partial u_l / \partial x_k) / 2$ and that the elastic compliances must satisfy $C_{ijkl} = C_{ijlk}$ so that $\sigma_{ij} = C_{ijkl} (\partial u_k / \partial x_l)$. Finally, this shows that

$$\sigma_{ij} \delta \epsilon_{ij} = C_{ijkl} \frac{\partial u_i}{\partial u_j} \frac{\partial \delta v_i}{\partial x_j}.$$

Substituting into the virtual work equation gives the result we need.

8.1.3 Interpolating the Displacement Field and the Virtual Velocity Field

To solve the integral form of the elasticity equations given in Section 8.1.2, we *discretize* the displacement field. A representative finite element mesh is sketched in Figure 8.2. We choose to calculate the displacement field at a set of n discrete points in the solid (called “nodes” in finite element terminology). We will denote the coordinates of these special points by x_i^a , where the superscript a ranges from 1 to n . The unknown displacement vector at each nodal point will be denoted by u_i^a .

The displacement field at an arbitrary point within the solid will be specified by interpolating between nodal values in some convenient way. An efficient and robust implementation

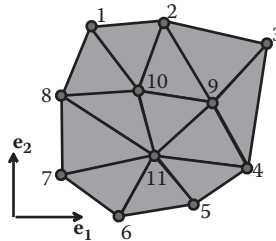


FIGURE 8.2 A typical finite element mesh.

of the FEM requires a careful choice of interpolation scheme, but for now we will denote the interpolation in a general way as

$$u_i(\mathbf{x}) = \sum_{a=1}^n N^a(\mathbf{x}) u_i^a.$$

Here, \mathbf{x} denotes the coordinates of an arbitrary point in the solid. The interpolation functions $N^a(\mathbf{x})$ are functions of position only, which must have the property that

$$u_i^b = \sum_{a=1}^n N^a(\mathbf{x}^b) u_i^a$$

for all $b = 1 \dots n$. (This is to ensure that the displacement field has the correct value at each node). Recently developed meshless FEMs use very complex interpolation functions, but the more traditional approach is to choose them so that

$$N^a(\mathbf{x}^b) = \begin{cases} 1 & a = b \\ 0 & a \neq b. \end{cases}$$

The simple constant strain triangle elements introduced in Section 7.1 are one example of this type of interpolation scheme. We will define more complicated interpolation functions shortly.

We can obviously interpolate the virtual velocity field in exactly the same way (because the principle of virtual work must be satisfied for all virtual velocities, it must certainly be satisfied for an interpolated velocity field) so that

$$\delta v_i(\mathbf{x}) = \sum_{a=1}^n N^a(\mathbf{x}) \delta v_i^a,$$

where δv_i^a are arbitrary nodal values of virtual velocity.

8.1.4 Finite Element Equations

Substituting the interpolated fields into the virtual work equation, we find that

$$\int_R C_{ijkl} \frac{\partial N^b(\mathbf{x})}{\partial x_l} u_k^b \frac{\partial N^a(\mathbf{x})}{\partial x_j} \delta v_i^a dV - \int_R b_i N^a(\mathbf{x}) \delta v_i^a dV - \int_{\partial R} t_i^* N^a(\mathbf{x}) \delta v_i^a dA = 0,$$

where summation on a and b is implied, in addition to the usual summation on i, j, k , and l .

Note that the interpolation functions are *known* functions of position. We can therefore rewrite the virtual work equation in matrix form as

$$(K_{aibk} u_k^b - F_i^a) \delta v_i^a = 0,$$

where

$$K_{aibk} = \int_R C_{ijkl} \frac{\partial N^a(\mathbf{x})}{\partial x_j} \frac{\partial N^b(\mathbf{x})}{\partial x_l} dV \quad F_i^a = \int_R b_i N^a(\mathbf{x}) dV + \int_{\partial R} t_i^* N^a(\mathbf{x}) dA.$$

Here \mathbf{K} is known as the stiffness matrix and \mathbf{F} is known as the force vector. \mathbf{K} is a function only of the elastic properties of the solid, its geometry, and the interpolation functions and nodal positions. It is therefore a known matrix. Similarly, \mathbf{F} is a function only of the known boundary loading and body force field, and the interpolation scheme and nodal positions. Observe that the symmetry of the elasticity tensor implies that \mathbf{K} also has some symmetry, specifically $K_{aibk} = K_{bkai}$.

The virtual work equation must be satisfied for all possible sets of δv_i^a with $\delta v_i^a = 0$ for nodes a that lie on $\partial_1 R$. At these nodes, the displacements must satisfy $u_i^a = u_i^*$. Evidently, this requires

$$\begin{aligned} K_{aibk} u_k^b &= F_i^a & \forall \{a, i\}: x_k^a \text{ not on } \partial_1 R \\ u_i^a &= u_i^*(x_i^a) & \forall \{a, i\}: x_k^a \text{ on } \partial_1 R. \end{aligned}$$

This is a system of n linear equations for the n nodal displacements.

8.1.5 Simple 1D Implementation of the FEM

Before describing a fully general 3D implementation of the FEM, we will illustrate all the key ideas using a simple 1D example. Consider a long linear elastic bar, as shown in Figure 8.3. Assume the following:

1. The bar has shear modulus μ and Poisson's ratio ν .
2. The bar has cross section $h \times h$ and length L .
3. It is constrained on all its sides so that $u_2 = u_3 = 0$.
4. The bar is subjected to body force $\mathbf{b} = b(x_1)\mathbf{e}_1$.

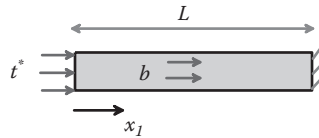


FIGURE 8.3 A 1D bar subjected to end loading and axial body force.

5. The bar is either loaded or constrained at its ends, so that the boundary conditions are either $t_1(0) = t^*(0)$, $t_1(L) = t^*(L)$ or displacement $u_1(0) = u^*(0)$, $u_1(L) = u^*(L)$ at $x = 0$ and $x = L$.

For this 1D example, then, the finite element equations reduce to

$$K_{ab}u_1^b = F^a,$$

where

$$K_{ab} = h^2 \int_0^L \frac{2}{1-2\nu} \frac{\partial N^a(x_1)}{\partial x_1} \frac{\partial N^b(x_1)}{\partial x_1} dx_1$$

$$F^a = h^2 \int_0^L b N^a(x_1) dx_1 + h^2 t_1^*(0) N^a(0) + h^2 t_1^*(L) N^a(L).$$

We could obviously choose any interpolation scheme, evaluate the necessary integrals, and solve the resulting system of equations to compute the solution. It turns out to be particularly convenient, however, to use a piecewise Lagrangian interpolation scheme and to evaluate the integrals numerically using a Gaussian quadrature scheme.

To implement the Lagrangian interpolation scheme, we subdivide the region $0 \leq x_1 \leq L$ into a series of *elements*, as illustrated in Figure 8.4. Each element is bounded by two nodal points and may also contain one or more interior nodes. The displacement field within the element is interpolated between the nodes attached to the element. So, we would use a linear interpolation between the nodes on a two-noded element, a quadratic interpolation between the nodes on a three-noded element, and so on.

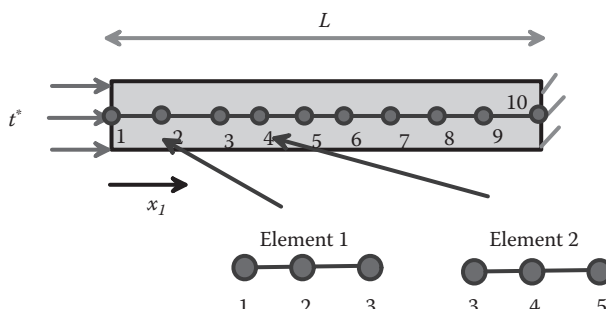


FIGURE 8.4 A 1D finite element mesh for the bar shown in Figure 8.3.

Generic linear and quadrilateral 1D elements are illustrated in Table 8.1. The local nodes on the element are numbered 1 and 2 for the linear element and 1, 2, and 3 for the quadratic element as shown. We suppose that the element lies in the region $-1 \leq \xi_1 \leq 1$. The displacements within the element are then interpolated as

$$u_1(\xi_1) = \sum_{a=1}^{N_e} N^a(\xi_1) u_1^a,$$

where N_e denotes the number of nodes on the element, u_1^a denotes the value of the displacement at each node, and the shape functions are given in the table.

Of course, the actual nodal coordinates do not lie at -1 , $+1$, and 0 for all the elements. For a general element, we *map* this special one to the region of interest. A particularly convenient way to do this is to set

$$x_1(\xi_1) = \sum_{a=1}^{N_e} N^a(\xi_1) x_1^a,$$

where x_1^a denotes the coordinate of each node on the element, and N_e is the number of nodes on the element (2 or 3). Elements that interpolate displacements and position using the same shape functions are called *isoparametric elements*.

Next, we need to devise a way to do the integrals in the expressions for the stiffness matrix and force vector. We can evidently divide up the integral so as to integrate over each element in turn:

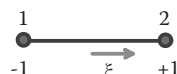
$$\begin{aligned} K_{ab} &= \sum_{l=1}^{N_{lmn}} h^2 \int_{x_0}^{x_1} \frac{2}{1-2\nu} \frac{\partial N^a(x_1)}{\partial x_1} \frac{\partial N^b(x_1)}{\partial x_1} dx_1 \\ F^a &= \sum_{l=1}^{N_{lmn}} h^2 \int_{x_0}^{x_1} b N^a(x_1) dx_1 + h^2 t_i^* N^a(0) + h^2 t_i^* N^a(L), \end{aligned}$$

TABLE 8.1 Shape Functions for 1D Finite Elements

Linear 1D Element

$$N^1(\xi) = 0.5(1 - \xi)$$

$$N^2(\xi) = 0.5(1 + \xi)$$

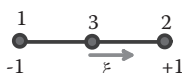


Quadratic 1D Element

$$N^1(\xi) = -0.5\xi(1 - \xi)$$

$$N^2(\xi) = 0.5\xi(1 + \xi)$$

$$N^3(\xi) = (1 - \xi)(1 + \xi)$$



where N_{lmn} is the total number of elements, and x_0 and x_1 denote the coordinates of the ends of the l th element. We now notice an attractive feature of our interpolation scheme. The integral over the l th element depends only on the shape functions associated with the nodes on the l th element, because the displacement in this region is completely determined by its values at these nodes. We can therefore define element stiffness matrix and element force matrix,

$$k_{ab} = h^2 \int_{x_0}^{x_1} \frac{2(1-\nu)}{1-2\nu} \frac{\partial N^a(x_1)}{\partial x_1} \frac{\partial N^b(x_1)}{\partial x_1} dx_1 \quad f^a = h^2 \int_{x_0}^{x_1} b N^a(x_1) dx_1,$$

for each element, which depend on the geometry, interpolation functions, and material properties of the element. The first and last elements have additional contributions to the element force vector from the boundary terms $h^2 t^* N^a(0)$, $h^2 t^* N^a(L)$. The global stiffness matrix is computed by summing all the element stiffness matrices:

$$K_{ab} = \sum_{l=1}^{N_{lmn}} k_{ab} \quad F^a = \sum_{l=1}^{N_{lmn}} f^a + h^2 t^* N^a(0) + h^2 t^* N^a(L).$$

Finally, we need to devise a way to compute the integrals for each element stiffness matrix. It is convenient to map the domain of integration to $[-1, +1]$ and integrate with respect to the normalized coordinate ξ ; thus,

$$k_{ab} = h^2 \int_{-1}^{+1} \frac{2(1-\nu)}{1-2\nu} \frac{\partial N^a(\xi)}{\partial \xi} \frac{\partial N^b(\xi)}{\partial \xi} J d\xi \quad f^a = h^2 \int_{-1}^{+1} b N^a(\xi) J d\xi,$$

where $J = |\partial x / d\xi|$ is the Jacobian associated with the mapping, which may be computed as

$$\frac{\partial x}{\partial \xi} = \frac{\partial}{\partial \xi} \sum_{a=1}^{N_e} N^a(\xi) x^a = \sum_{a=1}^{N_e} \frac{\partial N^a}{\partial \xi} x^a.$$

Note that the mapping also enables us to calculate the shape function derivatives in the element stiffness matrix as

$$\frac{\partial N^a}{\partial x} = \frac{\partial N^a}{\partial \xi} \frac{\partial \xi}{\partial x} = \frac{\partial N^a}{\partial \xi} \left[\frac{\partial x}{\partial \xi} \right]^{-1}.$$

Finally, note that integrals may be computed numerically using a quadrature formula, as follows

$$\int_{-1}^{+1} g(\xi) d\xi \approx \sum_{I=1}^M w_I g(\xi^{(I)}),$$

where $\xi^{(I)} I = 1 \dots M$ denotes a set of *integration points* in the region $[-1, +1]$, and w_I is a set of integration weights, which are chosen so as to make the approximation as accurate as possible. Values are given in Table 8.2 for $M = 1, 2$, and 3 . Higher-order integration schemes exist but are required only for higher-order elements. For the linear 1D element described previously, a single integration point is sufficient to evaluate the stiffness exactly. Similarly, for the quadratic element, two integration points will suffice.

8.1.6 Summary of the 1D Finite Element Procedure

To summarize, then, the finite element solution requires the following steps:

1. For each element, compute the element stiffness matrix as follows:

$$k_{ab} = h^2 \sum_{I=1}^M w_I \frac{2}{1-2\nu} \frac{\partial N^a}{\partial x} \frac{\partial N^b}{\partial x} J(\xi_I),$$

where

$$J = \left| \frac{\partial x}{\partial \xi} \right| = \left| \sum_{a=1}^{N_e} \frac{\partial N^a(\xi_I)}{\partial \xi} x^a \right| \quad \frac{\partial N^a}{\partial x} = \frac{\partial N^a(\xi_I)}{\partial \xi} \frac{\partial \xi}{\partial x} = \frac{\partial N^a(\xi_I)}{\partial \xi} \left[\frac{\partial x}{\partial \xi} \right]^{-1}$$

and the integration points ξ_I , w_I ($I = 1 \dots M$) are tabulated below, and shape functions $N^{(a)}(\xi)$, $a = 1 \dots N_e$ were listed previously.

TABLE 8.2 1D Integration Points and Weights

$M = 1$	
$\xi^{(1)} = 0$	$w_1 = 2$
$M = 2$	
$\xi^{(1)} = -0.5773502691$	$w_1 = 1.0$
$\xi^{(2)} = 0.5773502691$	$w_2 = 1.0$
$M = 3$	
$\xi^{(1)} = -0.7745966692$	$w_1 = 0.555555555555$
$\xi^{(2)} = 0$	$w_2 = 0.888888888888$
$\xi^{(3)} = 0.7745966692$	$w_3 = 0.555555555555$

2. Assemble the contribution from each element to the global stiffness

$$K_{ab} = \sum_{l=1}^{N_{lmn}} k_{ab}.$$

3. Similarly, if there is a nonzero body force, then compute for each element

$$f^a = h^2 \sum_{I=1}^M w_I b N^a(\xi_I) J(\xi_I)$$

and assemble the global force vector

$$F^a = \sum_{l=1}^{N_{lmn}} f^a.$$

4. Add contributions to the force vector from prescribed traction boundary conditions at $x = 0$ and $x = L$

$$F^1 = F^1 + h^2 t^*(0) \quad F^{(L)} = F^{(L)} + h^2 t^*(L),$$

where the (L) superscript denotes the node that lies at $x = L$.

5. Modify the stiffness matrix to enforce the constraints

$$u^1 = u^*(0) \quad u^{(L)} = u^*(L).$$

6. Solve the system of linear equations

$$K_{ab} u_1^b = F^a$$

for the unknown displacements u_1^b .

8.1.7 Example FEM Code and Solution

A simple example MAPLE code for this 1D example can be found in the file FEM_1D_Static.mws at <http://solidmechanics.org/FEA.htm>.

It is set up to solve for displacements for the bar sketched in Figure 8.5, with the following parameters (in arbitrary units):

1. Length $L = 5$ and unit cross-sectional area
2. Shear modulus 50, Poisson's ratio 0.3
3. Uniform body force magnitude 10

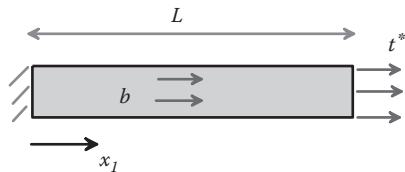


FIGURE 8.5 A 1D bar subjected to body force and end loading.

4. Displacement $u = 0$ at $x = 0$

5. Traction $t^* = 2$ at $x = L$

The code computes the (1D) displacement distribution in the bar. The predicted displacement field is plotted in Figure 8.6.

Of course, in general we want to calculate more than just displacements; usually we want the stress field, too. We can calculate the stress field anywhere within an element by differentiating the displacements to calculate strains and then substituting into the constitutive relation. This gives

$$\sigma_{11} = \frac{2(1-\nu)}{(1-2\nu)} \sum_{a=1}^n \frac{\partial N^a}{\partial x} u^a.$$

This works well for a uniform body force with quadratic (three-noded elements), as Figure 8.7 shows.

However, if we switch to linear elements, the stress results are not so good (displacements are still calculated exactly). In this case, the stress must be uniform in each element (because strains are constant for linear displacement field), so the stress plot looks like Figure 8.8. Notice that the stresses are most accurate near the center of each element (at the integration point). For this reason, FEM codes generally output stress and strain data at integration points.

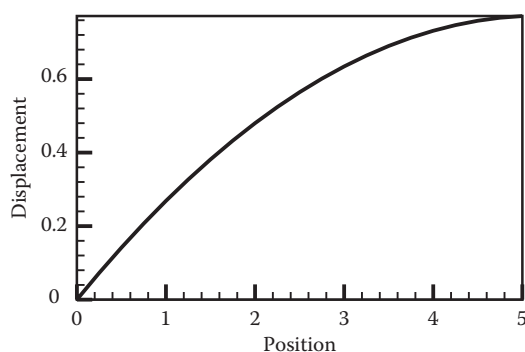


FIGURE 8.6 Displacement-versus-position predicted for the 1D bar shown in Figure 8.5.

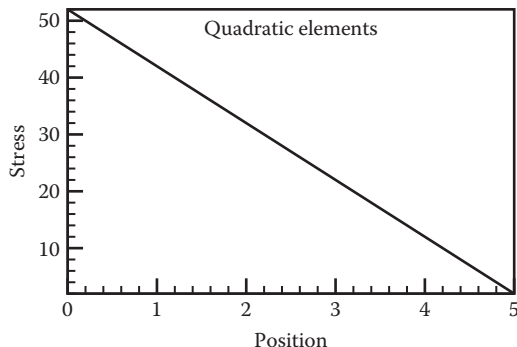


FIGURE 8.7 Stress-versus-position predicted for the 1D bar shown in Figure 8.5.

It is interesting also to examine the stiffness matrix (shown below for three linear elements, before addition of the $u = 0$ constraint for the first node):

$$\begin{bmatrix} 105 & -105 & 0 & 0 \\ -105 & 210 & -105 & 0 \\ 0 & -150 & 210 & -105 \\ 0 & 0 & -105 & 105 \end{bmatrix}.$$

Notice that stiffness is symmetric, as expected, and also *banded*. A large FEM matrix is sparse: most of the elements are zero. This allows the matrix to be stored in compact form: for very large matrices, indexed storage (in which only the nonzero elements together with their indices are stored) is the best approach; for smaller problems skyline storage or band storage (in which only the central, mostly nonzero, band of the matrix is stored) may be preferable. In this case, equation numbers need to be assigned to each degree of freedom so as to minimize the bandwidth of the stiffness matrix.

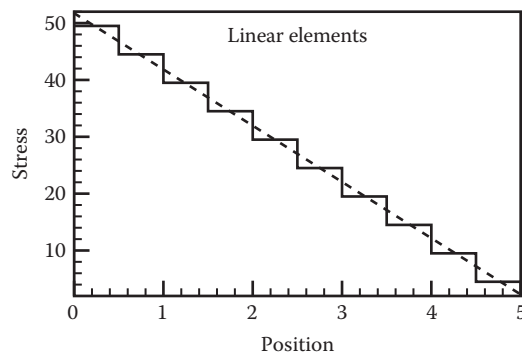


FIGURE 8.8 Stress-versus-position predicted using linear elements for the 1D bar shown in Figure 8.5.

8.1.8 Extending the 1D FEM to 2D and 3D

It is straightforward to extend the 1D case to more general problems. All the basic ideas remain the same. Specifically,

1. In both two and three dimensions, we divide up our solid of interest into a number of elements, shown schematically for a 2D region in Figure 8.9.
2. We define interpolation functions $N^a(\xi_j)$ for each element in terms of a local, dimensionless, coordinate system within the element. The coordinates satisfy $-1 \leq \xi_i \leq +1$. The displacement field and the position of a point inside an element are computed in terms of the interpolation functions as

$$u_i = \sum_{a=1}^{N_e} N^a(\xi_j) u_i^a \quad x_i = \sum_{a=1}^{N_e} N^a(\xi_j) x_i^a,$$

where $N^a(\xi_j)$ denote the shape functions, u_i^a, x_i^a denote the displacement values and coordinates of the nodes on the element, and N_e is the number of nodes on the element.

3. We introduce an element stiffness matrix for each element by defining

$$k_{aibk}^{(l)} = \int_{V_e^{(l)}} C_{ijkl} \frac{\partial N^a(\mathbf{x})}{\partial x_j} \frac{\partial N^b(\mathbf{x})}{\partial x_l} dV \quad f_i^{a(l)} = \int_{V_e^{(l)}} b_i N^a(\mathbf{x}) dV + \int_{\partial_2 V_e^{(l)}} t_i N^a(\mathbf{x}) dA,$$

where $k_{aibk}^{(l)}$ denotes the element stiffness matrix for the (l th) element, and $V_e^{(l)}$ denotes the volume (in three dimensions) or area (in two dimensions) of the (l th) element, whereas $\partial_2 V_e^{(l)}$ denotes the surface of the (l th) element.

4. The volume integrals over each element are calculated by expressing the volume or surface integral in terms of the dimensionless coordinates $-1 \leq \xi_i \leq +1$ and then evaluating the integrals numerically, using a quadrature formula of the form

$$\int_{V_e} f(\xi_i) dV_\xi = \sum_{I=1}^{N_I} w_I f(\xi_i^I).$$

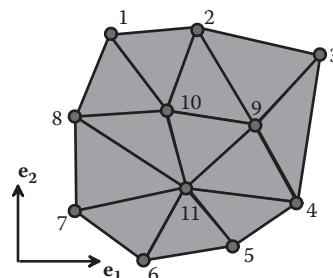


FIGURE 8.9 A typical finite element mesh.

Here, w_I are a set of $I = 1 \dots N_I$ integration weights (just numbers), and $\xi_i^{(I)}$ are a set of coordinates that are selected to make the integration scheme as accurate as possible (also just numbers).

5. The global stiffness matrix

$$K_{aibk} = \int_R C_{ijkl} \frac{\partial N^a(\mathbf{x})}{\partial x_j} \frac{\partial N^b(\mathbf{x})}{\partial x_l} dV \quad F_i^a = \int_R b_i N^a(\mathbf{x}) dV + \int_{\partial R} t_i^* N^a(\mathbf{x}) dA$$

is then computed by summing the contribution from each element as

$$K_{aibk} = \sum_{l=1}^{N_{lmn}} k_{aibk}^{(l)} \quad F_i^a = \sum_{l=1}^{N_{lmn}} f_i^{a(l)}.$$

6. The stiffness matrix is modified to enforce any prescribed displacements.

7. The system of equations

$$K_{aibk} u_k^b = F_i^a \quad \forall \{a,i\}: x_k^a \text{ not on } \partial_i R$$

$$u_i^a = u_i^*(x_i^a) \quad \forall \{a,i\}: x_k^a \text{ on } \partial_i R$$

is solved for the unknown nodal displacements.

8. The stresses and strains within each element are then deduced.

To implement this procedure, we must (1) define the element interpolation functions, (2) express the integrals for the element stiffness matrices and force vectors in terms of normalized coordinates, and (3) formulate a numerical integration scheme to evaluate the element stiffness matrices and force vectors. These details are addressed in the sections to follow.

8.1.9 Interpolation Functions for 2D Elements

The interpolation functions for 2D elements are listed in Table 8.3. They are defined for the region $0 \leq \xi_1 \leq 1 \quad 0 \leq \xi_2 \leq 1$ for triangular elements and $-1 \leq \xi_1 \leq 1 \quad -1 \leq \xi_2 \leq 1$ for quadrilateral elements. The numbers shown inside the element show the convention used to number the element faces.

8.1.10 Interpolation Functions for 3D Elements

Interpolation functions for 3D elements are listed in Table 8.4. The interpolation functions are defined for the region $-1 \leq \xi_i \leq 1$ unless otherwise stated. The element faces are numbered as listed in Table 8.5.

TABLE 8.3 2D Interpolation Functions

$N^1 = \xi_1$	$N^2 = \xi_2$	
$N^3 = 1 - \xi_1 - \xi_2$		
$N^1 = (2\xi_1 - 1)\xi_1$	$N^2 = (2\xi_2 - 1)\xi_2$	
$N^3 = (2(1 - \xi_1 - \xi_2) - 1)(1 - \xi_1 - \xi_2)$		
$N^4 = 4\xi_1\xi_2$	$N^5 = 4\xi_2(1 - \xi_1 - \xi_2)$	
$N^6 = 4\xi_1(1 - \xi_1 - \xi_2)$		
$N^1 = 0.25(1 - \xi_1)(1 - \xi_2)$		
$N^2 = 0.25(1 + \xi_1)(1 - \xi_2)$		
$N^3 = 0.25(1 + \xi_1)(1 + \xi_2)$		
$N^4 = 0.25(1 - \xi_1 - \xi_2)$		
$N^1 = -(1 - \xi_1)(1 - \xi_2)(1 + \xi_1 + \xi_2)/4$		
$N^2 = (1 + \xi_1)(1 - \xi_2)(\xi_1 - \xi_2 - 1)/4$		
$N^3 = (1 + \xi_1)(1 + \xi_2)(\xi_1 + \xi_2 - 1)/4$		
$N^4 = (1 - \xi_1)(1 + \xi_2)(\xi_2 - \xi_1 - 1)/4$		
$N^5 = (1 - \xi_1^2)(1 - \xi_2)/2$	$N^6 = (1 + \xi_1)(1 - \xi_2^2)/2$	
$N^7 = (1 - \xi_1^2)(1 + \xi_2)/2$	$N^8 = (1 - \xi_1)(1 - \xi_2^2)/2$	

8.1.11 Volume Integrals for Stiffness and Force in Terms of Normalized Coordinates

In this section, we outline the procedure that is used to rewrite the integrals for the element stiffness and force in terms of the normalized coordinates ξ_i . The integrals are

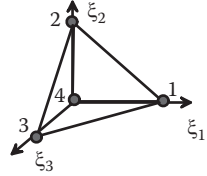
$$K_{aibk}^{(l)} = \int_{V_e^{(l)}} C_{ijkl} \frac{\partial N^a(\mathbf{x})}{\partial x_j} \frac{\partial N^b(\mathbf{x})}{\partial x_l} dV \quad f_i^{a(l)} = \int_{V_e^{(l)}} b_i N^a(\mathbf{x}) dV + \int_{\partial_2 V_e^{(l)}} t_i^* N^a(\mathbf{x}) dA.$$

To evaluate them, we need to (1) find a way to calculate the derivatives of the shape functions in terms of ξ_i , and (2) map the volume (or area) integral to the region $-1 \leq \xi_i \leq +1$.

TABLE 8.4 3D Interpolation Functions

$$N^1 = \xi_1 \quad N^2 = \xi_2$$

$$N^3 = \xi_3 \quad N^4 = 1 - \xi_1 - \xi_2 - \xi_3$$



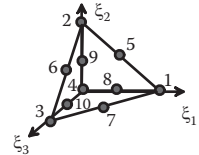
$$N^1 = (2\xi_1 - 1)\xi_1 \quad N^2 = (2\xi_2 - 1)\xi_2$$

$$N^3 = (2\xi_3 - 1)\xi_3 \quad N^4 = (2\xi_4 - 1)\xi_4$$

$$N^5 = 4\xi_1\xi_2 \quad N^6 = 4\xi_2\xi_3$$

$$N^7 = 4\xi_3\xi_1 \quad N^8 = 4\xi_4\xi_1$$

$$\xi_4 = 1 - \xi_1 - \xi_2 - \xi_3$$

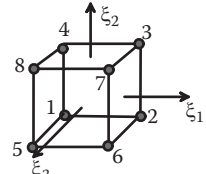


$$N^1 = (1 - \xi_1)(1 - \xi_2)(1 - \xi_3)/8 \quad N^2 = (1 + \xi_1)(1 - \xi_2)(1 - \xi_3)/8$$

$$N^3 = (1 + \xi_1)(1 + \xi_2)(1 - \xi_3)/8 \quad N^4 = (1 - \xi_1)(1 + \xi_2)(1 - \xi_3)/8$$

$$N^5 = (1 - \xi_1)(1 - \xi_2)(1 + \xi_3)/8 \quad N^6 = (1 + \xi_1)(1 - \xi_2)(1 + \xi_3)/8$$

$$N^7 = (1 + \xi_1)(1 + \xi_2)(1 + \xi_3)/8 \quad N^8 = (1 - \xi_1)(1 + \xi_2)(1 + \xi_3)/8$$



$$N^1 = (1 - \xi_1)(1 - \xi_2)(1 - \xi_3)(-\xi_1 - \xi_2 - \xi_3 - 2)/8$$

$$N^2 = (1 + \xi_1)(1 - \xi_2)(1 - \xi_3)(\xi_1 - \xi_2 - \xi_3 - 2)/8$$

$$N^3 = (1 + \xi_1)(1 + \xi_2)(1 - \xi_3)(\xi_1 + \xi_2 - \xi_3 - 2)/8$$

$$N^4 = (1 - \xi_1)(1 + \xi_2)(1 - \xi_3)(-\xi_1 + \xi_2 - \xi_3 - 2)/8$$

$$N^5 = (1 - \xi_1)(1 - \xi_2)(1 + \xi_3)(-\xi_1 - \xi_2 + \xi_3 - 2)/8$$

$$N^6 = (1 + \xi_1)(1 - \xi_2)(1 + \xi_3)(+\xi_1 - \xi_2 + \xi_3 - 2)/8$$

$$N^7 = (1 + \xi_1)(1 + \xi_2)(1 + \xi_3)(+\xi_1 + \xi_2 + \xi_3 - 2)/8$$

$$N^8 = (1 - \xi_1)(1 + \xi_2)(1 + \xi_3)(-\xi_1 + \xi_2 + \xi_3 - 2)/8$$

$$N^9 = (1 - \xi_1^2)(1 - \xi_2)(1 - \xi_3)/4 \quad N^{10} = (1 + \xi_1)(1 - \xi_2^2)(1 - \xi_3)/4$$

$$N^{11} = (1 - \xi_1^2)(1 + \xi_2)(1 - \xi_3)/4 \quad N^{12} = (1 - \xi_1)(1 - \xi_2^2)(1 - \xi_3)/4$$

$$N^{13} = (1 - \xi_1^2)(1 - \xi_2)(1 + \xi_3)/4 \quad N^{14} = (1 + \xi_1)(1 - \xi_2^2)(1 - \xi_3)/4$$

$$N^{15} = (1 - \xi_1^2)(1 + \xi_2)(1 + \xi_3)/4 \quad N^{16} = (1 - \xi_1)(1 - \xi_2^2)(1 + \xi_3)/4$$

$$N^{17} = (1 - \xi_1)(1 - \xi_2)(1 - \xi_3^2)/4 \quad N^{18} = (1 + \xi_1)(1 - \xi_2)(1 - \xi_3^2)/4$$

$$N^{19} = (1 + \xi_1)(1 + \xi_2)(1 - \xi_3^2)/4 \quad N^{20} = (1 - \xi_1)(1 + \xi_2)(1 - \xi_3^2)/4$$

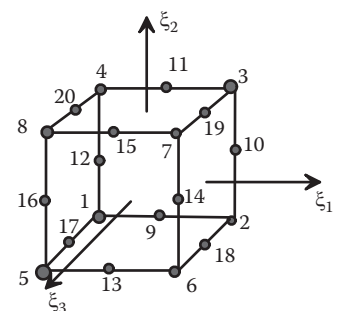


TABLE 8.5 Face Numbering Scheme for 3D Elements

Linear and quadratic tetrahedral:	Linear and quadratic brick elements:
Face 1 has nodes 1, 2, 3	Face 1 has nodes 1, 2, 3, 4
Face 2 has nodes 1, 4, 2	Face 2 has nodes 5, 8, 7, 6
Face 3 has nodes 2, 4, 3	Face 3 has nodes 1, 5, 6, 3
Face 4 has nodes 3, 4, 1	Face 4 has nodes 2, 6, 7, 3
	Face 5 has nodes 3, 7, 8, 4
	Face 6 has nodes 4, 8, 5, 1

Calculating the shape function derivatives: The shape function derivatives can be evaluated by writing

$$\frac{\partial N^a}{\partial x_j} = \frac{\partial N^a}{\partial \xi_i} \frac{\partial \xi_i}{\partial x_j},$$

where the derivatives $\partial N^a / \partial \xi_i$ are easy to compute (just differentiate the expressions given previously). To compute $\partial \xi_i / \partial x_j$, recall that the coordinates of a point at position ξ_j within an element can be determined as

$$x_i = \sum_{a=1}^{N_e} N^a(\xi_j) x_i^a,$$

where N_e denotes the number of nodes on the element. Therefore,

$$\frac{\partial x_i}{\partial \xi_j} = \frac{\partial}{\partial \xi_j} \left(\sum_{a=1}^{N_e} N^a(\xi) x_i^a \right) = \sum_{a=1}^{N_e} \frac{\partial N^a(\xi)}{\partial \xi_j} x_i^a.$$

Note that $\partial x_i / \partial \xi_j$ is a 2×2 matrix (in two dimensions) or a 3×3 matrix (in three dimensions). Finally, $\partial \xi_i / \partial x_j$ follows as the inverse of this matrix

$$\frac{\partial \xi_j}{\partial x_i} = \left(\frac{\partial x_i}{\partial \xi_j} \right)^{-1}_{ji}.$$

Mapping the volume integral: To map the region of integration, we define

$$J = \det \left(\frac{\partial x_i}{\partial \xi_i} \right),$$

where the matrix $\partial x_i / \partial \xi_j$ was defined previously. Then the integral with respect to \mathbf{x} is mapped into an integral with respect to ξ by setting

$$K_{aibk} = \int_{\Omega} C_{ijkl} \frac{\partial N^a(\mathbf{x})}{\partial x_j} \frac{\partial N^b(\mathbf{x})}{\partial x_l} J dV_{\xi} \quad f_i^a = \int_{\Omega} b_i N^a(\mathbf{x}) J dV_{\xi} + \int_{\partial\Omega} t_i^* N^a(\mathbf{x}) \hat{J} dA_{\bar{\xi}}.$$

We note in passing that the boundary integral in the element force vector can be regarded as a 1D line integral for 2D elements and a 2D surface integral for 3D elements. So the procedures we developed in Section 8.1.5 (1D elements) can be used to evaluate the surface integral for a 2D element. Similarly, the procedures we develop to integrate stiffness matrices for 2D elements can be used to evaluate the surface integral for a 3D element.

8.1.12 Numerical Integration Schemes for 2D and 3D Elements

Finally, to evaluate the integrals, we once again adopt a quadrature scheme, so that

$$\int_{\Omega} f(\xi_i) dV_{\xi} = \sum_{I=1}^{N_I} w_I f(\xi_i^I).$$

The integration points ξ_j^I and weights w_I depend on the element geometry and are listed in Tables 8.6 and 8.7 for several element types.

Choosing the number of integration points: There are two considerations. If too many integration points are used, time is wasted without gaining any accuracy. If too few integration points are used, the stiffness matrix may be singular or else the rate of convergence

TABLE 8.6 Integration Points for Triangular Elements

1 point $\xi_1^1 = 1/3 \quad \xi_2^1 = 1/3 \quad w_1 = 1/2$

$\xi_1^1 = 1/2 \quad \xi_2^1 = 0 \quad w_1 = 1/6$

$\xi_1^2 = 0 \quad \xi_2^2 = 1/2 \quad w_2 = 1/6$

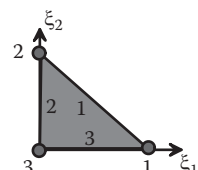
3 point $\xi_1^3 = 1/2 \quad \xi_2^3 = 1/2 \quad w_3 = 1/6$

$\xi_1^1 = 0.6 \quad \xi_2^1 = 0.2 \quad w_1 = 1/6$

or $\xi_1^2 = 0.2 \quad \xi_2^2 = 0.6 \quad w_2 = 1/6$

$\xi_1^3 = 0.2 \quad \xi_2^3 = 0.2 \quad w_3 = 1/6$

(The first scheme here is optimal but has some disadvantages for quadratic elements because the integration points coincide with the midside nodes. The second scheme is less accurate but more robust.)



4 point $\xi_1^1 = 0.6 \quad \xi_2^1 = 0.2 \quad w_1 = 25/96$

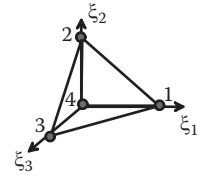
$\xi_1^2 = 0.2 \quad \xi_2^2 = 0.6 \quad w_2 = 25/96$

$\xi_1^3 = 0.2 \quad \xi_2^3 = 0.2 \quad w_3 = 25/96$

$\xi_1^4 = 1/3 \quad \xi_2^4 = 1/3 \quad w_4 = -27/96$

TABLE 8.7 Integration Points for Tetrahedral Elements

1 point	$\xi_1^1 = 1/4$	$\xi_2^1 = 1/4$	$\xi_3^1 = 1/4$	$w_1 = 1/6$
4 point	$\xi_1^1 = \alpha$	$\xi_2^1 = \beta$	$\xi_3^1 = \beta$	$w_1 = 1/24$
	$\xi_1^2 = \beta$	$\xi_2^1 = \alpha$	$\xi_3^2 = \beta$	$w_2 = 1/24$
	$\xi_1^3 = \beta$	$\xi_2^3 = \beta$	$\xi_3^3 = \alpha$	$w_3 = 1/24$
	$\xi_1^4 = \beta$	$\xi_2^4 = \beta$	$\xi_3^4 = \beta$	$w_4 = 1/24$, where $\alpha = 0.58541020, \beta = 0.13819660$



to the exact solution with mesh refinement will be reduced. The schemes listed in Table 8.9 will avoid both.

There are situations in which it is preferable to use fewer integration points and purposely make the stiffness singular. These are discussed in more detail in Section 8.5.

8.1.13 Summary of Formulas for Element Stiffness and Force Matrices

With these definitions, then, we write the element stiffness matrix as

$$k_{aibk} = \sum_{I=1}^{N_I} w_I C_{ijkl} \frac{\partial N^a(\xi_i^I)}{\partial \xi_p} \frac{\partial \xi_p}{\partial x_j} \frac{\partial N^b(\xi_i^I)}{\partial x_q} \frac{\partial \xi_q}{\partial x_l} J(\xi_i^I)$$

$$f_i^a = \sum_{I=1}^N w_I b_i N^a(\xi_i^I) J + \sum_{I=1}^{\hat{N}} w_I t_i^* N^a(\xi_i^I) \bar{J},$$

where

$$\frac{\partial x_i}{\partial \xi_j} = \sum_{a=1}^{N_e} \frac{\partial N^a(\xi)}{\partial \xi_j} x_i^a \quad J = \det \left(\frac{\partial x_i}{\partial \xi_j} \right) \quad \frac{\partial \xi_j}{\partial x_i} = \left(\frac{\partial x}{\partial \xi} \right)_{ji}^{-1}.$$

8.1.14 Sample 2D/3D Linear Elastostatic FEM Code

You can find MAPLE and MATLAB implementations of a simple 2D/3D static linear elasticity code on the web site at <http://solidmechanics.org/FEA.htm>. The code is in the files FEM_2Dor3D_linelast_standard.mws or FEM_2Dor3D_linelast_standard.m.

The code reads an input file. Several examples are provided:

1. Linear_elastic_triangles.txt: Simple 2D plane strain problem with two triangular elements
2. Linear_elastic_quad4.txt: Simple 2D plane strain problem with eight four-noded quadrilateral elements
3. Linear_elastic_quad8.txt: Simple 2D plane strain problem with two eight-noded quadrilateral elements
4. Linear_elastic_brick4.txt: Simple 3D problem with eight-noded brick elements.

TABLE 8.8 Integration Formulas for Quadrilateral and Hexahedral Elements

For quadrilateral elements, we can simply regard the integral over two spatial dimensions as successive 1D integrals

$$\int_{-1}^{+1} \int_{-1}^{+1} f(\xi_1, \xi_2) d\xi_1 d\xi_2 = \sum_{I=1}^N \sum_{J=1}^N w_I w_J f(\xi_1^I, \xi_2^J),$$

which gives rise to the following 2D quadrature scheme. Let η_I and v_I for $I = 1 \dots M$ denote 1D quadrature points and weights listed below. Then, in 2D, an $N=M \times M$ quadrature scheme can be generated as follows:

for $J = 1 \dots M$ and $K = 1 \dots M$, let $\xi_1^I = \eta_J$ $\xi_2^J = \eta_K$ $w_I = v_J v_K$, $I = M(K-1)+J$.

Similarly, in 3D, we generate an $N = M \times M \times M$ scheme as:

for $J = 1 \dots M$, $K = 1 \dots M$, $L = 1 \dots M$, let

$$\xi_1^I = \eta_J \quad \xi_2^J = \eta_K \quad \xi_3^K = \eta_L \quad w_I = v_J v_K v_L, \quad I = M^2(L-1) + M(K-1) + J.$$

$$M = 1 \quad \eta_1 = 0 \quad v_1 = 2$$

$$M = 2 \quad \begin{aligned} \eta_1 &= -0.5773502691 & v_1 &= 1.0 \\ \eta_2 &= 0.5773502691 & v_2 &= 1.0 \end{aligned}$$

$$M = 3 \quad \begin{aligned} \eta_1 &= -0.7745966692 & v_1 &= 0.555555555555 \\ \eta_2 &= 0. & v_2 &= 0.88888888888 \\ \eta_3 &= 0.7745966692 & v_3 &= 0.555555555555 \end{aligned}$$

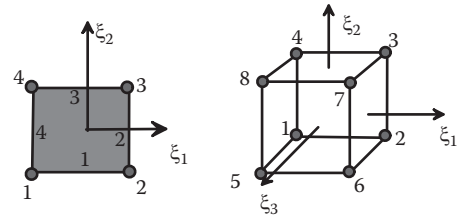


TABLE 8.9 Number of Integration Points for Fully Integrated Elements

Linear triangle (3 nodes): 1 point

Linear tetrahedron (4 nodes): 1 point

Quadratic triangle (6 nodes): 4 points

Quadratic tetrahedron (10 nodes): 4 points

Linear quadrilateral (4 nodes): 4 points

Linear brick (8 nodes): 8 points

Quadratic quadrilateral (8 nodes): 9 points

Quadratic brick (20 nodes): 27 points

As an example, we show how to run the program with the first input file. The file sets up the problem illustrated in Figure 8.10. The elements are linear elastic plane strain with $\mu = 10$, $\nu = 0.3$.

The program input file is listed in Figure 8.11. Here is a brief explanation of the data in the file:

1. The first part of the input file specifies material properties. A number 1 on the plane strain/stress line indicates a plane strain analysis; a number 0 indicates plane stress.
2. The second part specifies properties and coordinates of the nodes. For a 2D problem, each node has two coordinates and two degrees of freedom; for a 3D problem, each node has three coordinates and three degrees of freedom. Then enter nodal coordinates for each node.
3. The third part lists the element properties. Here, you must specify the number of elements and the maximum number of nodes on any one element (you can mix element

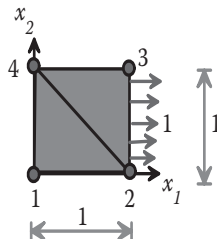


FIGURE 8.10 A simple finite element problem.

```
No._material_props: 3
Shear_modulus: 10.
Poissons_ratio: 0.3
Plane strain/stress: 1
No._coords_per_node: 2
No._DOF_per_node: 2
No._nodes: 4
Nodal_coords:
    0.0 0.0
    1.0 0.0
    1.0 1.0
    0.0 1.0
No._elements: 2
Max_no._nodes_on_any_one_element: 3
element_identifier; no._nodes_on_element;
connectivity:
    1 3 1 2 4
    1 3 2 3 4
No._nodes_with_prescribed_DOFs: 3
Node #, DOF#, Value:
    1 1 0.0
    1 2 0.0
    4 1 0.0
No._elements_with_prescribed_loads: 1
Element #, Face #, Traction_components
    2 1 1.0 0.0
```

FIGURE 8.11 Input file for sample finite element program.

types if you like). Then you must specify the nodes connected to each element (known as element connectivity). For each element, you must specify the number of nodes attached to the element and an identifier that specifies the element type (you can enter any number in this version of the code; the identifier is provided to allow addition of more sophisticated element types such as reduced integration elements) and then enter the nodes on each element following the convention shown previously.

4. The fourth part of the file specifies boundary constraints. For any constrained displacements, enter the node number, the displacement component to be prescribed, and its value.
5. The last part of the file specifies distributed loading acting on the element faces. The loading is assumed to be uniform. For each loaded boundary, you should specify

the element number, the face of the element (the face numbering convention was described in Sections 8.1.9 and 8.1.10; note that you must be consistent in numbering nodes and faces on each element), and the components of traction acting on the element face, as a vector with two or three components.

Note that the program performs absolutely no error checking on the input file. If you put in a typo, you will get some bizarre error message from MAPLE, often during element stiffness assembly.

For the input file shown, the program produces the output file shown in Figure 8.12. The code prints the displacements at each node in the mesh and also the strains and stresses at each integration point (where these quantities are most accurate) for each element.

To run the code, you must complete the following steps:

1. Open the MAPLE executable file.

2. Edit the code to insert the full path for the input file in the line near the top of the code that reads

```
# Change the name of the file below to point to your input file
infile:=fopen('D:/fullpathoffile/Linear_elastic_triangles.txt', READ):
```

3. Scroll down near the bottom to the line that reads

```
# Print nodal displacements, element strains, and stresses to a file
```

```
#
```

```
outfile:= fopen('path/Linear_elastic_triangles.out', WRITE):
```

and enter a name for the output file.

4. Return to the top of the file and press <enter> to execute each MAPLE block. You will see the code plot the undeformed and deformed finite element mesh at the end. The stresses and strains in the elements are printed to the output file.

Nodal displacements:
Node Coords u1 u2
1 0.0000 0.0000 0.0000 0.0000
2 1.0000 0.0000 .0350 .0000
3 1.0000 1.0000 .0350 -.0150
4 0.0000 1.0000 0.0000 -.0150
Strains and stresses:
Element: 1
int pt Coords e_11 e_22 e_12 s_11 s_22 s_12
1 .3333 .3333 .0350 -.0150 0.0000 1.0000 .0000 0.0000
Element: 2
int pt Coords e_11 e_22 e_12 s_11 s_22 s_12
1 .6667 .6667 .0350 -.0150 .0000 1.0000 .0000 .0000

FIGURE 8.12 Output file produced by sample finite element program.

8.2 THE FEM FOR DYNAMIC LINEAR ELASTICITY

In this section, we show how to extend the FEM to solve dynamic problems. Specifically,

1. The principle of virtual work is used to derive a discrete system of equations for the (time varying) nodal displacements.
2. Three methods for integrating the equation of motion with respect to time are presented: (1) explicit time stepping, (2) implicit time stepping, and (3) modal analysis. The properties of each scheme are illustrated by solving simple problems.
3. As always, example codes are provided so you can see how the method is actually implemented and explore its predictions for yourself.

8.2.1 Review of the Governing Equations of Dynamic Linear Elasticity

As before, we begin by summarizing the governing equations for a standard dynamic linear elasticity problem. A generic linear elasticity problem is shown in Figure 8.13. We are given the following:

1. The shape of the solid in its unloaded condition R_0 .
2. The initial stress field in the solid (we will take this to be zero in setting up our FEM code).
3. The mass density ρ and elastic constants for the solid C_{ijkl} .
4. The thermal expansion coefficients for the solid and temperature distribution (we will take this to be zero for our FEM code, for simplicity).
5. The initial displacement field in the solid $\overset{o}{\mathbf{u}}(\mathbf{x})$ and the initial velocity field $\overset{o}{\mathbf{v}}(\mathbf{x})$.
6. A body force distribution $\mathbf{b}(\mathbf{x}, t)$ acting on the solid (note that, in this section, we will use \mathbf{b} to denote force per unit volume rather than force per unit mass, to avoid having to write out the mass density all the time).

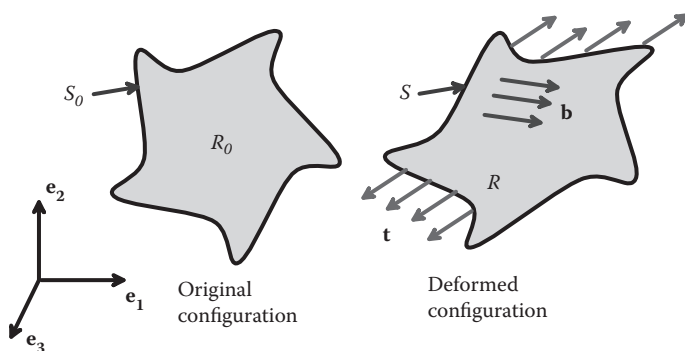


FIGURE 8.13 A typical boundary value problem.

7. Boundary conditions, specifying displacements $\mathbf{u}^*(\mathbf{x}, t)$ on a portion $\partial_1 R$ or tractions $\mathbf{t}^*(\mathbf{x}, t)$ on a portion $\partial_2 R$ of the boundary of R .

Calculate (time-varying) displacements, strains, and stresses u_i , ε_{ij} , σ_{ij} satisfying the governing equations of dynamic linear elasticity:

1. The strain-displacement equation: $\varepsilon_{ij} = \frac{1}{2}(\partial u_i / \partial x_j + \partial u_j / \partial x_i)$
2. The elastic stress-strain law: $\sigma_{ij} = C_{ijkl} \varepsilon_{kl}$
3. The equation of motion for stresses: $\partial \sigma_{ij} / \partial x_i + b_j = \rho \partial^2 u_j / \partial t^2$
4. The boundary conditions on displacement and stress:

$$u_i = u_i^* \text{ on } \partial_1 R \quad \sigma_{ij} n_i = t_j^* \text{ on } \partial_2 R$$

8.2.2 Expressing the Governing Equations Using the Principle of Virtual Work

Just as for static problems, the principle of virtual work can be used to write the governing equation for the displacement field in a linear elastic solid in an integral form (called the weak form). Instead of solving the governing equations listed in the preceding section, the displacements, strains, and stresses u_i , ε_{ij} , σ_{ij} are calculated as follows:

1. Find a displacement field $u_i(x_j)$ satisfying

$$\int_R C_{ijkl} \frac{\partial u_k}{\partial x_l} \frac{\partial \delta v_i}{\partial x_j} dV - \int_R b_i \delta v_i dV + \int_R \rho \frac{\partial^2 u_i}{\partial t^2} \delta v_i dV - \int_{\partial_2 R} t_i^* \delta v_i dA = 0$$

$$u_i = u_i^* \text{ on } \partial_1 R$$

for all virtual velocity fields δv_i satisfying $\delta v_i = 0$ on $\partial_1 R$.

2. Compute the strains from the definition: $\varepsilon_{ij} = \frac{1}{2}(\partial u_i / \partial x_j + \partial u_j / \partial x_i)$.
3. Compute the stresses from the stress-strain law: $\sigma_{ij} = C_{ijkl} \varepsilon_{kl}$. The stress will automatically satisfy the equation of motion and boundary conditions, so all the field equations and boundary conditions will be satisfied.

You can derive this result by following the method outlined in Section 8.1.2.

8.2.3 Finite Element Equations of Motion for Linear Elastic Solids

We now introduce a finite element approximate following exactly the same procedure that we used for static problems. We choose to calculate the displacement field (now a function of time) at a set of n discrete nodes, as sketched in Figure 8.14. We denote the coordinates of these special points by x_i^a , where the superscript a ranges from 1 to n . The unknown

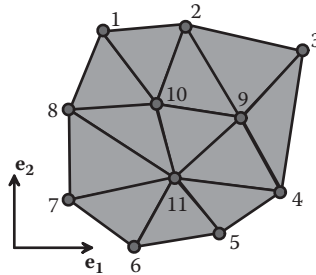


FIGURE 8.14 A typical finite element mesh.

displacement vector at each nodal point will be denoted by u_i^a . We then set up the FEA equations for dynamic problems as follows:

- As before, the displacement and virtual velocity fields are interpolated between nodal values as

$$u_i(\mathbf{x}) = \sum_{a=1}^n N^a(\mathbf{x}) u_i^a \quad \delta v_i(\mathbf{x}) = \sum_{a=1}^n N^a(\mathbf{x}) \delta v_i^a.$$

- Substitute into the virtual work equation to see that

$$\int_R \rho N^b N^a \frac{\partial^2 u_i^b}{\partial t^2} \delta v_i^a dV + \int_R C_{ijkl} \frac{\partial N^b}{\partial x_l} \frac{\partial N^a}{\partial x_j} u_k^b \delta v_i^a dV - \int_R b_i N^a \delta v_i^a dV - \int_{\partial R} t_i^* N^a \delta v_i^a dA = 0.$$

- This is once again a linear system that may be expressed in the form

$$(M_{ab} \ddot{u}_i^b + K_{aibk} u_k^b - F_i^a) \delta v_i^a = 0,$$

where

$$K_{aibk} = \int_R C_{ijkl} \frac{\partial N^a(\mathbf{x})}{\partial x_j} \frac{\partial N^b(\mathbf{x})}{\partial x_l} dV \quad F_i^a = \int_R b_i N^a(\mathbf{x}) dV + \int_{\partial R} t_i^* N^a(\mathbf{x}) dA$$

are the finite element stiffness matrix and force vector introduced in Section 7.2, and

$$M_{ab} = \int_R \rho N^a N^b dV$$

is known as the finite element mass matrix. Procedures for computing the mass matrix are given below.

- Again, because the principle of virtual power holds for all virtual velocity fields such that $\delta v_i^a = 0$ for x_i^a on $\partial_1 R$, we conclude that this requires

$$\left(M_{ab} \frac{\partial^2 u_i^b}{\partial t^2} + K_{aibk} u_k^b - F_i^a \right) = 0 \quad \forall (i, a) : x_k^a \text{ not on } \partial_1 R$$

$$u_i^a = u_i^* \quad \forall (i, a) : x_k^a \text{ on } \partial_1 R.$$

Nodal velocities must also satisfy initial conditions. This is a set of coupled second-order linear differential equations that may be integrated with respect to time to determine u_i^a as a function of time. Observe that M_{ab} and K_{aibk} are constant matrices for linear elastic problems, but F_i^a will in general be a function of time.

To find the solution, we now need to integrate these equations with respect to time. For linear problems, there are two choices:

1. Brute-force time-stepping methods (e.g., Newmark time integration). This technique can be used for both linear and nonlinear problems.
2. Modal methods, which integrate the equations of motion exactly. This method only works for linear problems.

Both methods are described in detail below.

8.2.4 Newmark Time Integration for Elastodynamics

The general idea is simple. Given values of u_i^a and $\partial u_i^a / \partial t$ at some time t , we want to determine values at a slightly later time $t + \Delta t$, using the governing equations of motion. There are of course many ways to do this. Here, we will present the popular Newmark time integration scheme.

8.2.4.1 Newmark Method for a One Degree of Freedom System

It is simplest to illustrate the procedure using a one degree of freedom system (e.g., a forced, undamped spring-mass system) first. For this case, the equation of motion is

$$m\ddot{u} + ku - f = 0,$$

where $f(t)$ and the initial conditions $u(0)$, $\dot{u}(0)$ are given.

Suppose that we are able to get estimates for the acceleration $\ddot{u}(t)$ and $\ddot{u}(t = \Delta t)$ both at the start and end of a general time step Δt . We could then use a Taylor series expansion to obtain estimates of displacement and velocity at time $t + \Delta t$

$$u(t + \Delta t) \approx u(t) + \Delta t \dot{u}(t) + \frac{\Delta t^2}{2} [(1 - \beta_2) \ddot{u}(t) + \beta_2 \ddot{u}(t + \Delta t)]$$

$$\dot{u}(t + \Delta t) \approx \dot{u}(t) + \Delta t [(1 - \beta_1) \ddot{u}(t) + \beta_1 \ddot{u}(t + \Delta t)].$$

Here, β_1 and β_2 are two adjustable parameters that determine the nature of the time integration scheme. If we set $\beta_1 = \beta_2 = 0$, the acceleration is estimated based on its value at time t . This is known as an *explicit* time integration scheme. Alternatively, if we put $\beta_1 = \beta_2 = 1$, the acceleration is estimated from its value at time $t + \Delta t$. This is known as *implicit* time integration.

The acceleration at the start and end of the time step is computed using the equation of motion. At time t , we have

$$\ddot{u}(t) = \frac{1}{m}[-ku(t) + f(t)],$$

whereas, at time $t + \Delta t$,

$$\begin{aligned} m\ddot{u}(t + \Delta t) + ku(t + \Delta t) - f(t + \Delta t) &= 0 \\ \Rightarrow m\ddot{u}(t + \Delta t) + k \left\{ u(t) + \Delta t \dot{u}(t) + \frac{\Delta t^2}{2} [(1 - \beta_2) \ddot{u}(t) + \beta_2 \ddot{u}(t + \Delta t)] \right\} - f(t + \Delta t) &= 0 \\ \Rightarrow \ddot{u}(t + \Delta t) &= \frac{1}{m + k\beta_2 \Delta t^2 / 2} \left\{ -k \left[u(t) + \Delta t \dot{u}(t) + \frac{\Delta t^2}{2} (1 - \beta_2) \ddot{u}(t) \right] + f(t + \Delta t) \right\}. \end{aligned}$$

This then gives us the following time-stepping scheme. Given $k, m, f(t), u(0), \dot{u}(0)$:

1. At $t = 0$, compute $\ddot{u}(0) = \frac{1}{m}[-ku(0) + f(0)]$.
2. Then for successive time steps, compute

$$\begin{aligned} \ddot{u}(t + \Delta t) &= \frac{1}{m + k\beta_2 \Delta t^2 / 2} \left\{ -k \left[u(t) + \Delta t \dot{u}(t) + \frac{\Delta t^2}{2} (1 - \beta_2) \ddot{u}(t) \right] + f(t + \Delta t) \right\} \\ u(t + \Delta t) &\approx u(t) + \Delta t \dot{u}(t) + \frac{\Delta t^2}{2} [(1 - \beta_2) \ddot{u}(t) + \beta_2 \ddot{u}(t + \Delta t)] \\ \dot{u}(t + \Delta t) &\approx \dot{u}(t) + \Delta t [(1 - \beta_1) \ddot{u}(t) + \beta_1 \ddot{u}(t + \Delta t)]. \end{aligned}$$

8.2.4.2 Newmark Applied to FEM Equations

This can immediately be extended to the general n degrees of freedom case as follows. Given $K_{aibk}, M_{ab}, F_i^a(t), u_i^a(0), \dot{u}_i^{a(0)}$:

1. At $t = 0$, compute $\ddot{u}_i^a(0) = M_{ab}^{-1} [-K_{bick} u_k^c(0) + F_i^b(0)]$.
2. Then for successive time steps, solve

$$M_{ab} \ddot{u}_i^b(t + \Delta t) + \frac{\beta_2 \Delta t^2}{2} K_{aibk} \ddot{u}_k^b = -K_{aibk} \left[u_k^b(t) + \Delta t \dot{u}_k^b(t) + \frac{\Delta t^2}{2} (1 - \beta_2) \ddot{u}_k^b(t) \right] + F_i^a(t + \Delta t)$$

for \ddot{u}_i^a .

3. Then compute

$$u_i^a(t + \Delta t) \approx u_i^a(t) + \Delta t \dot{u}_i^a(t) + \frac{\Delta t^2}{2} \left[(1 - \beta_2) \ddot{u}_i^a(t) + \beta_2 \ddot{u}_i^a(t + \Delta t) \right]$$

$$\dot{u}_i^a(t + \Delta t) \approx \dot{u}_i^a(t) + \Delta t \left[(1 - \beta_1) \ddot{u}_i^a(t) + \beta_1 \ddot{u}_i^a(t + \Delta t) \right].$$

8.2.5 1D Implementation of a Newmark Scheme

It is straightforward to extend a static FEM code to dynamics. As before, we illustrate the method in one dimension before developing a 3D code. Consider a long linear elastic bar as shown in Figure 8.15. Assume the following:

1. The bar has shear modulus μ , Poisson's ratio ν , and mass density ρ .
2. The bar has cross-section $h \times h$ and length L .
3. The bar is at rest and strain free at $t = 0$ with $u_1 = du_1 / dt = 0$.
4. It is constrained on all its sides so that $u_2 = u_3 = 0$.
5. The bar is subjected to body force $\mathbf{b} = b(x_1, t)\mathbf{e}_1$.
6. The bar is either loaded or constrained at its ends, so that the boundary conditions are either $t_1 = t^*(0, t)$, $t_1 = t^*(L, t)$ or displacement $u_1(0) = u^*(0)$ $u_1(L) = u^*(L)$ at $x = 0$ and $x = L$.

For this 1D example, then, the finite element equations reduce to

$$M_{ab}u_1^b + K_{ab}u_1^b = F^a,$$

where

$$M_{ab} = h^2 \int_0^L \rho N^a(x_1) N^b(x_1) dx_1 \quad K_{ab} = h^2 \int_0^L \frac{2(1-\nu)}{1-2\nu} \frac{\partial N^a(x_1)}{\partial x_1} \frac{\partial N^b(x_1)}{\partial x_1} dx_1$$

$$F^a = h^2 \int_0^L b N^a(x_1) dx_1 + h^2 t_1^*(0) N^a(0) + h^2 t_1^*(L) N^a(L).$$

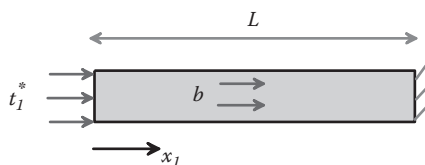


FIGURE 8.15 A 1D bar subjected to time-dependent loading.

We adopt exactly the same interpolation scheme as for the static solution (a 1D finite element mesh is shown in Figure 8.16) and calculate stiffness matrix and force vector accordingly. In addition, we need to determine the mass matrix. This can also be done by evaluating integrals for each element by numerical quadrature and then assembling element mass matrices into a global matrix. Specifically,

- For each element, compute the element mass matrix. The mass matrix can either be evaluated by numerical quadrature, by evaluating the formula

$$m_{ab} = h^2 \sum_{I=1}^{n_I} w_I \rho N^a(\xi_I) N^b(\xi_I) J(\xi_I),$$

where

$$J = \left| \frac{\partial x}{\partial \xi} \right| = \left| \sum_{a=1}^{N_e} \frac{\partial N^a(\xi_I)}{\partial \xi} x^a \right|$$

and the integration points ξ_I , w_I , $I = 1 \dots n_I$, and shape functions $N^{(a)}(\xi)$, $a = 1 \dots N_e$ were listed in Section 7.2.5. Note that a higher-order integration scheme is required to integrate the mass matrix than we needed for the stiffness matrix. Specifically, for quadratic elements, we need a cubic integration scheme (with three integration points), whereas for linear elements, we need a quadratic scheme (two integration points). If the mass matrix is under-integrated, it will be singular (you can check this using the example code provided below). Alternatively, the mass matrix can be integrated analytically, which yields the results in Table 8.10.

- Assemble the contribution from each element to the global mass matrix $M_{ab} = \sum_{l=1}^L m_{ab}$.
- Modify the stiffness and mass matrices to enforce the constraints $\ddot{u}^1 = \ddot{u}^*(0, t)$, $\ddot{u}^{(L)} = \ddot{u}^*(L, t)$.
- Run the Newmark time-stepping scheme outlined above.

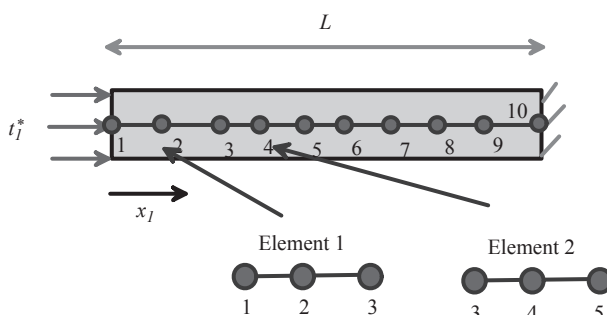
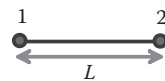


FIGURE 8.16 A 1D mesh for the bar shown in Figure 8.15.

TABLE 8.10 Mass Matrices for 1D Elements

Linear element

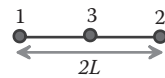
$$[m] = \frac{\rho L}{6} \begin{bmatrix} 2 & 1 \\ 1 & 2 \end{bmatrix}$$



Quadratic element

(midside node must be at center of element)

$$[m] = \frac{\rho L}{15} \begin{bmatrix} 4 & -1 & 2 \\ -1 & 4 & 2 \\ 2 & 2 & 16 \end{bmatrix}$$



8.2.6 Example 1D Dynamic FEM Code and Solution

A simple example MAPLE code for this 1D example is given in the file FEM1D_newmark.mws, which can be downloaded from <http://solidmechanics.org/FEA.htm>. It is set up to solve for displacements for a bar with the following properties:

1. Length 5 and unit cross-sectional area
2. Mass density 100, shear modulus 50, Poisson's ratio 0, (so the wave speed is 1)
3. No body force, displacement $u = 0$ at $x = 0$, and traction $t = 10$ applied at $x = L$ suddenly at $t = 0$ and then held constant for $t > 0$

As an example, we plot the variation of displacement at the end of the bar ($x = L$) with time in Figure 8.17. You should be able to verify for yourself that the exact solution is a sawtooth, amplitude 0.5 and period 20 (the time for a plane wave to make two trips from one end of the bar to the other).

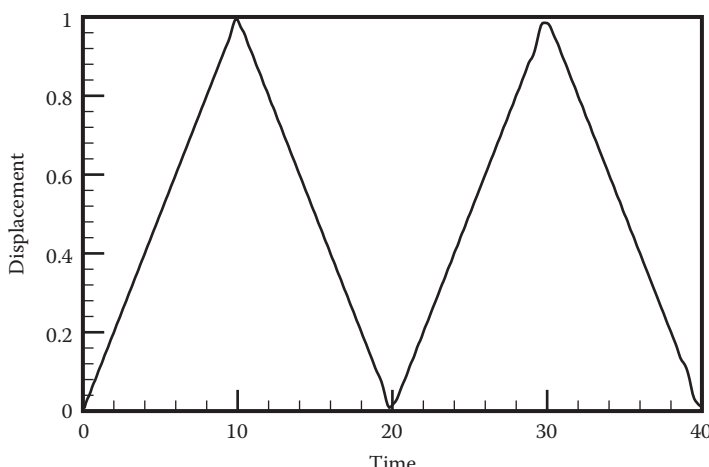


FIGURE 8.17 Time variation of displacement predicted for the bar shown in Figure 8.15.

Notice how the peaks of the sawtooth are blunted; this is because the FEM interpolation functions cannot resolve the velocity discontinuity associated with a propagating plane wave.

The MAPLE file produces animations of the displacement and velocity field in the bar. In the exact solution, a plane wave propagates down the bar and repeatedly reflects off the free and fixed ends of the bar. You can see this quite clearly in the simulation results, but the wave front is not sharp, as it is supposed to be. This gives rise to spurious high-frequency oscillations in the velocity fields.

It is interesting to investigate the effects of the two adjustable parameters in the time integration scheme. First, we look at the solution with $\beta_1 = \beta_2 = 0$ (both velocity and displacement update are fully explicit). Figure 8.18 shows the predicted displacement at the end of the bar for two values of time step Δt .

The result with smaller time step is good, but, with a larger time step, the solution is oscillatory. This is an example of a *numerical instability*, which is a common problem in

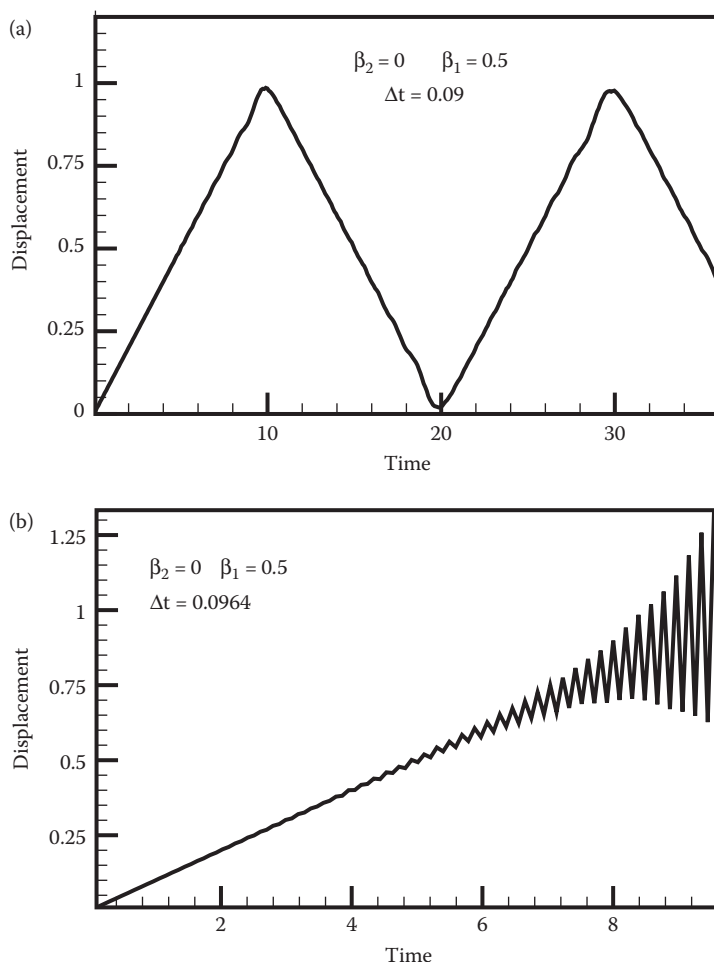


FIGURE 8.18 Time variation of displacement predicted by explicit time integration of the equations of motion for the bar shown in Figure 8.15. (a) Stable solution; (b) unstable solution.

explicit time-stepping schemes. Eventually, the solution blows up completely because the oscillations grow exponentially. With a small enough time step, an explicit scheme will usually work, but the critical time step for stability is proportional to the time required for a wave to propagate through the smallest element in the mesh.

With larger values of β , the problem disappears. In fact, one can show that, for the equation of motion considered here, setting

$$\beta_2 \geq \beta_1 \quad \beta_1 \geq 1/2$$

makes the time-stepping scheme *unconditionally stable*; no oscillations will occur even for very large time steps.

Stability does not necessarily mean accuracy, however. Results with a fully implicit integration scheme ($\beta_1 = \beta_2 = 1$) and a large time step are shown in Figure 8.19. This shows a different problem: energy is dissipated because of the numerical time integration scheme. So, larger values of β buy stability by introducing artificial damping, at the expense of a loss of accuracy. A good compromise is to set $\beta_1 = \beta_2 = 1/2$.

8.2.7 Lumped Mass Matrices

In the Newmark time integration scheme, accelerations are computed by solving a set of linear equations:

$$M_{ab}\ddot{u}_i^b(t + \Delta t) + \frac{\beta_2 \Delta t^2}{2} K_{aibk} \ddot{u}_k^b = -K_{aibk} \left[u_k^b(t) + \Delta t \dot{u}_k^b(t) + \frac{\Delta t^2}{2} (1 - \beta_2) \ddot{u}_k^b(t) \right] + F_i^a(t + \Delta t).$$

This is the most time-consuming part of the procedure. However, notice that, if we set $\beta_2 = 0$ and somehow find a way to make the mass matrix *diagonal*, then equation solution is trivial.

The so-called “lumped” mass matrix is a way to achieve this. Instead of using the correct element mass matrix

$$M_{ab} = \int_R \rho N^a N^b dV,$$

we replace it with a diagonal approximation. Various procedures can be used to do this:

1. Integrate the mass matrix using integration points located at the element nodes.
2. Diagonal scaling procedure: Set $M_{aa} = c M_{aa}$ and $M_{ab} = 0$ $a \neq b$, with the constant c selected to satisfy $\sum_a M_{aa} = \int_{V_e} \rho dV$.
3. Row-sum method: Set $M_{aa} = \sum_b M_{ab}$ and $M_{ab} = 0$ $a \neq b$.

In general, the three approaches give different answers. For some element types, it turns out that some of these procedures give zero or negative masses, which is clearly undesirable. Use whichever method gives the best answers.

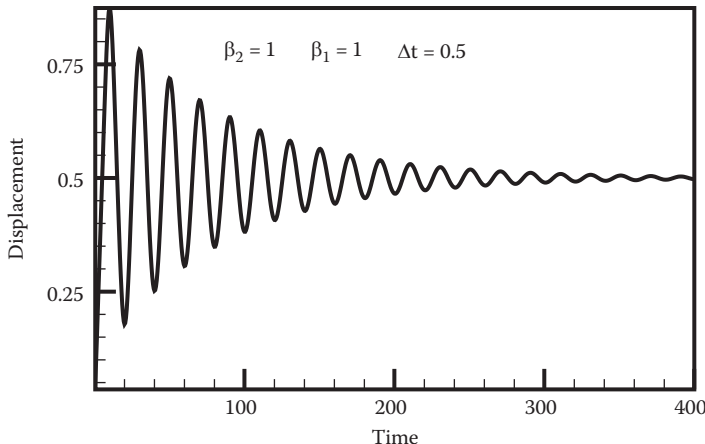


FIGURE 8.19 Time variation of displacement predicted by implicit time integration of the equations of motion for the bar shown in Figure 8.15.

Explicit time integration with a lumped mass matrix has been implemented in the 1D FEM code FEM1D_newmark.mws. To use a lumped mass matrix, find the line in the file that reads

> lumpedmass:= false;

and change it to

> lumpedmass:= true;

As an example, Figure 8.20 shows the predicted displacement at the end of the bar with relatively large time step (set $dt = 0.1$, $\beta_1 = 0$, and $\text{lumpedmass} = \text{true}$ in the code to reproduce the result).

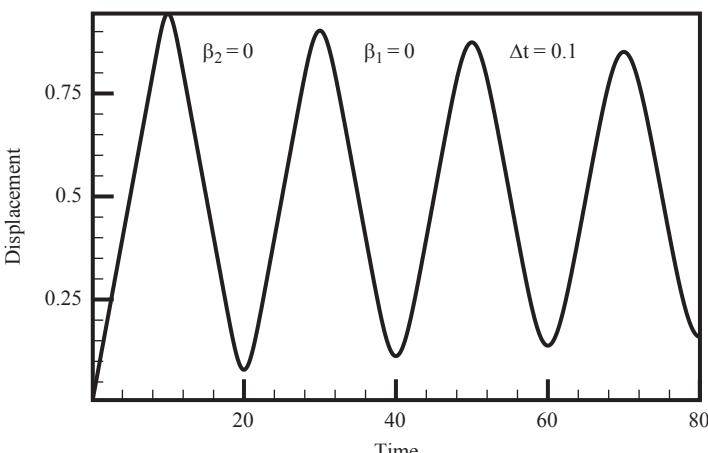


FIGURE 8.20 Time variation of displacement predicted using a lumped mass matrix for the bar shown in Figure 8.15.

In general lumped mass matrices introduce some additional damping that can help stabilize the time-stepping scheme but lead to some accuracy loss. You can see this in the result shown in Figure 8.20. Using a smaller time step reduces the energy loss.

Explicit time integration is cheap, easy to implement, and is therefore a very popular technique. Its disadvantages are that it is conditionally stable and can require very small time steps (the critical step size for stability is proportional to the size of the smallest element in the mesh and inversely proportional to the wave speed).

8.2.8 Example 2D and 3D Dynamic Linear Elastic Code and Solution

It is straightforward to extend a 3D static linear elasticity code to time-domain dynamics. As an example, the MAPLE code outlined in Section 8.1.14 has been extended for this purpose:

1. The code is in a file called FEM_2Dor3D_linelast_dynamic.mws. You will need to modify the line of the code that reads the input file to point to wherever you store the input file, as described in Section 8.1.14.
2. An input file that sets up a simulation of the vibration of a cantilever beam that is subjected to a transverse force at its end is provided in the file Linear_elastic_dynamic_beam.txt.

The format for the input file is described in detail in Section 8.1.14. The mesh is assumed to be at rest at time $t = 0$, and any loads are applied as a step and held constant for $t > 0$. You can always extend the code to do more complex loadings if you need to. The motion of the beam is animated at the end of the file.

8.2.9 Modal Method of Time Integration

The finite element equations

$$(M_{ab}\ddot{u}_i^b + K_{aibk}u_k^b - F_i^a) = 0$$

are a standard set of coupled, second-order linear differential equations such as one would meet in analyzing forced vibrations in discrete systems. They can therefore be solved using the usual modal techniques. The procedure is to rearrange the system of equations to yield n decoupled second-order differential equations, by means of the following substitutions. We will drop index notation in favor of matrix notation:

1. Write the governing equation as $\mathbf{M}\ddot{\mathbf{u}} + \mathbf{K}\mathbf{u} = \mathbf{F}(t)$.
2. Let

$$\mathbf{q} = \mathbf{M}^{1/2}\mathbf{u} \quad \mathbf{H} = \mathbf{M}^{-1/2}\mathbf{K}\mathbf{M}^{-1/2}$$

and substitute for \mathbf{u} ,

$$\ddot{\mathbf{q}} + \mathbf{H}\mathbf{q} = \mathbf{M}^{-1/2}\mathbf{F}.$$

3. Note that \mathbf{H} is a symmetric, positive definite matrix. Consequently, we may perform a spectral decomposition and write

$$\mathbf{H} = \mathbf{Q}\Lambda\mathbf{Q}^T,$$

where \mathbf{Q} is an orthogonal matrix ($\mathbf{Q}^T \mathbf{Q} = \mathbf{I}$) and Λ is diagonal. This spectral decomposition is accomplished as follows: compute the eigenvalues λ_i and corresponding *normalized* eigenvectors $\mathbf{r}^{(i)}$ of \mathbf{H} (normalized to satisfy $\mathbf{r}^{(i)} \cdot \mathbf{r}^{(i)} = 1$), then set

$$\Lambda = \begin{bmatrix} \lambda_1 & & & \\ & \lambda_2 & & \\ & & \ddots & \\ & & & \lambda_n \end{bmatrix} \quad \mathbf{Q} = \begin{bmatrix} \mathbf{r}_1^{(1)} & \mathbf{r}_1^{(2)} & & \\ \mathbf{r}_2^{(1)} & \mathbf{r}_2^{(2)} & & \\ \vdots & & \ddots & \\ \mathbf{r}_n^{(1)} & & & \mathbf{r}_n^{(n)} \end{bmatrix}.$$

4. Next, let $\mathbf{w} = \mathbf{Q}^T \mathbf{q}$ and rearrange the equation of motion a second time to get

$$\ddot{\mathbf{w}} + \Lambda \mathbf{w} = \mathbf{Q}^T \mathbf{M}^{-1/2} \mathbf{F}.$$

Because Λ is diagonal, this is now a set of n uncoupled ODEs for \mathbf{w} .

5. The initial conditions for \mathbf{w} follow as

$$\mathbf{w} = \mathbf{Q}^T \mathbf{M}^{-1/2} \mathbf{u}(t=0) \quad \dot{\mathbf{w}} = \mathbf{Q}^T \mathbf{M}^{-1/2} \dot{\mathbf{u}}(t=0).$$

6. Solve the decoupled ODEs for \mathbf{w} and then recover the displacements through

$$\mathbf{u} = \mathbf{M}^{-1/2} \mathbf{Q} \mathbf{w}.$$

You can use any method you like to solve the ODEs for \mathbf{w} : for harmonic forcing, you could use the exact solution. For general $\mathbf{F}(t)$ you could use Fourier transforms (the fast Fourier transform works for periodic \mathbf{F}). You could even use the Newmark algorithm if you want, although this would be rather perverse!

Effectively, this procedure reduces the general forced FEM problem to an equivalent one that involves solving the equations of motion for n forced, spring-mass systems.

8.2.10 Natural Frequencies and Mode Shapes

The procedure outlined in 8.2.9 can also be used to extract the natural frequencies and mode shapes for a vibrating, linear elastic solid. To see how to do this, note the following:

1. By definition, the natural frequencies and mode shapes of a continuous solid or structure are special deflections and frequencies for which the solid will vibrate harmonically.

2. The governing equations for \mathbf{w} can be regarded as describing the vibration of n uncoupled spring-mass systems.
3. If we solve the problem with $\mathbf{F} = \mathbf{0}$ and excite only the i th spring-mass system (e.g., by choosing appropriate initial conditions), the solution will be a harmonic vibration at the natural frequency of the i th spring-mass system.
4. The natural frequencies of the n decoupled systems are therefore the natural frequencies of vibration of the structure. The corresponding eigenvectors $\mathbf{r}^{(i)}$ are related to the deflections $\mathbf{u}^{(i)}$ associated with the i th vibration mode through $\mathbf{u}^{(i)} = \mathbf{M}^{-1/2}\mathbf{r}^{(i)}$.

The following procedure can be used to determine the natural frequencies and mode shapes of a linear elastic solid:

1. Compute the finite element mass and stiffness matrices \mathbf{M} and \mathbf{K} .
2. Find $\mathbf{H} = \mathbf{M}^{-1/2} \mathbf{K} \mathbf{M}^{-1/2}$.
3. Compute the eigenvalues λ_i and corresponding eigenvectors $\mathbf{r}^{(i)}$ of \mathbf{H} .
4. The natural frequencies ω_i are related to the eigenvalues of \mathbf{H} by $\lambda_i = \omega_i^2$.
5. The deflections $\mathbf{u}^{(i)}$ associated with the i th vibration mode follow as $\mathbf{u}^{(i)} = \mathbf{M}^{-1/2}\mathbf{r}^{(i)}$. The deflections calculated in this way will have some random magnitude; if you like, you can normalize them appropriately.

The procedure is simple on paper (as always), but there are two problems in practice. First, we need to find the square root of the mass matrix. For a general matrix, we would have to compute a spectral decomposition of \mathbf{M} to do this. However, if we use a *lumped* mass matrix, its square root is easily found; just take the square root of all the diagonal elements! Second, computing all the eigenvalues and eigenvectors of a general dynamical matrix \mathbf{H} is an exceedingly time-consuming process. To make this a viable scheme, we normally extract only the lowest few eigenvalues and the corresponding eigenvectors (say 10 to 100) and discard the rest.

8.2.11 Example 1D Code with Modal Dynamics

As an example, a version of the 1D code with modal dynamics is provided in the files FEM_1D_modal.mws (MAPLE) and FEM_1D_modal.m (MATLAB). The codes can be downloaded from <http://solidmechanics.org/FEA>

The code is set up to plot the displacements associated with the fundamental (lowest frequency) vibration mode, as well as to calculate the displacement of the end of the bar as a function of time. The code will handle computations with a full mass matrix as well as a lumped matrix, so you can compare the results with the two cases.

Figure 8.21 shows the mode shape (displacements) for the fundamental vibration mode and the predicted motion at the end of the bar. The code will also animate the displacement in the bar (not shown here).

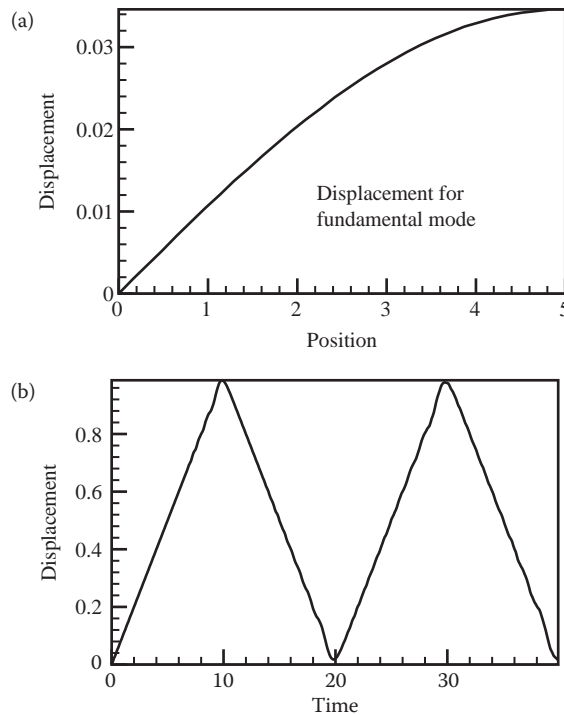


FIGURE 8.21 Modal solution for the 1D bar shown in Figure 8.15. (a) Displacement for the fundamental mode; (b) time variation of displacement at the end of the bar.

Here is a brief comparison of the Newmark and modal time integration schemes:

1. For linear problems, the modal decomposition method usually beats direct time integration in both accuracy and speed.
2. If you are interested in looking in detail at transient wave propagation through the solid, there is not much difference between the two methods; in this case, you need to retain a huge number of terms in the modal expansion for accurate results.
3. For most vibration problems, however, it is generally only necessary to retain a small number of modes in the expansion, in which case the modal decomposition method will be vastly preferable to direct time integration. Moreover, knowledge of the vibration modes can itself be valuable information. You can use also use the modal approach to handle very complex forcing, including random vibrations, directly.
4. The main limitation of the modal decomposition approach is that it can only handle undamped, linear systems (one can introduce *modal damping* for vibration applications, but this does not model any real energy dissipation mechanism). This is, of course, far too restrictive for any real application except the simplest possible problems in vibration analysis.

8.2.12 Example 2D and 3D FEM Code to Compute Mode Shapes and Natural Frequencies

It is straightforward to extend a 3D static linear elasticity code to modal dynamics:

1. An example program is provided in the file FEM_2Dor3D_modeshapes.mws (MAPLE) or FEM_2Dor3D_modeshapes.m (MATLAB).
2. The code can be run with the file Linear_elastic_dynamic_beam.txt; it computes and plots mode shapes for the beam as shown in Figure 8.22 (you need to edit the code to select which mode is displayed).

8.3 FEM FOR NONLINEAR (HYPOELASTIC) MATERIALS

The FEM can also solve boundary value problems for inelastic solids. In this section, we show how to extend the FEM to nonlinear problems. For the time being, we restrict attention to small deformations. Furthermore, before attempting to solve problems involving the rather complex (load history-dependent) plastic stress-strain relations, we begin by setting up the FEM for static, hypoelastic problems. We will idealize the stress-strain behavior of the material using the simple hypoelastic constitutive law described in Section 3.2.

8.3.1 Summary of Governing Equations

We shall solve the following boundary value problem. A generic hypoelastic boundary value problem is illustrated in Figure 8.23. We are given the following:

1. The shape of the solid in its unloaded condition R .

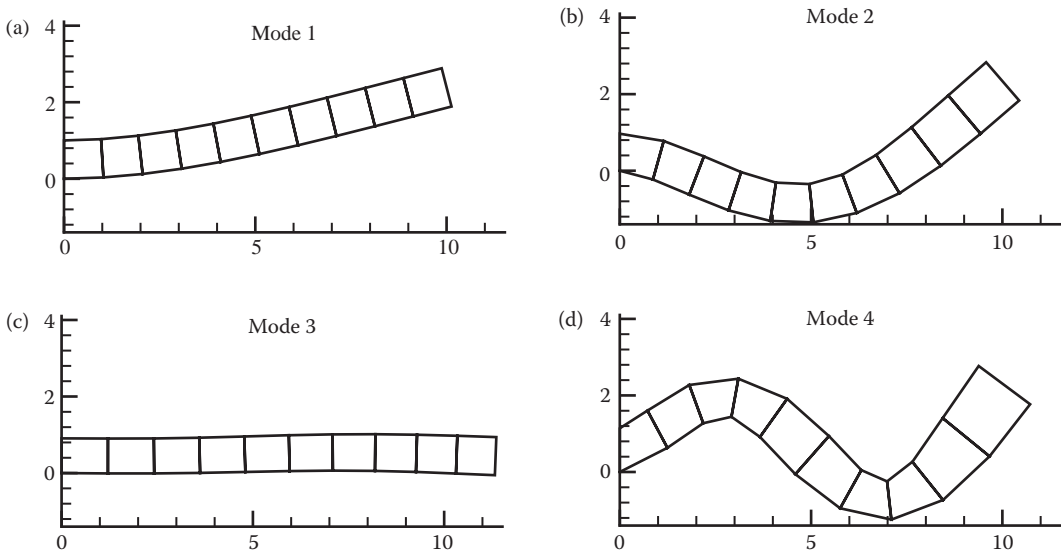


FIGURE 8.22 Predicted mode shapes for a cantilever beam. (a) Mode 1; (b) Mode 2; (c) Mode 3; and (d) Mode 4.

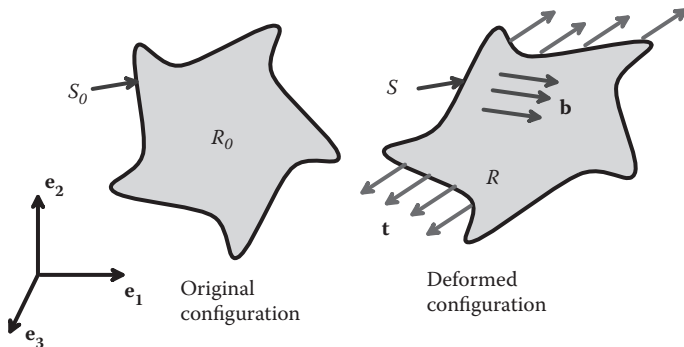


FIGURE 8.23 Representative boundary value problem for a hypoelastic material.

2. A body force distribution \mathbf{b} acting on the solid (note that, in this section, we will use \mathbf{b} to denote force per unit volume rather than force per unit mass, to avoid having to write out the mass density all the time).
3. Boundary conditions, specifying displacements $\mathbf{u}^*(\mathbf{x})$ on a portion $\partial_1 R$ or tractions on a portion $\partial_2 R$ of the boundary of R .
4. The material constants n , σ_0 , and ε_0 for the hypoelastic constitutive law described in Section 3.3.

Calculate displacements, strains, and stresses u_i , ε_{ij} , σ_{ij} satisfying the following equations:

1. Strain-displacement equation: $\varepsilon_{ij} = \frac{1}{2}(\partial u_i / \partial x_j + \partial u_j / \partial x_i)$.
2. The equation of static equilibrium for stresses: $\partial \sigma_{ij} / \partial x_i + b_j = 0$
3. The boundary conditions on displacement and stress:

$$u_i = u_i^* \text{ on } \partial_1 R \quad \sigma_{ij} n_i = t_j^* \text{ on } \partial_2 R$$

4. The hypoelastic constitutive law, which relates stress to strain as follows:

$$\sigma_{ij} = S_{ij} + \sigma_{kk} \delta_{ij} / 3 \quad S_{ij} = \frac{2}{3} \sigma_e \frac{e_{ij}}{\varepsilon_e} \quad \sigma_{kk} = \frac{E}{1-2\nu} \frac{1}{3} \varepsilon_{kk},$$

where

$$e_{ij} = \varepsilon_{ij} - \frac{1}{3} \varepsilon_{kk} \delta_{ij} \quad \varepsilon_e = \sqrt{\frac{2}{3} e_{ij} e_{ij}}$$

$$\frac{\sigma_e}{\sigma_0} = \begin{cases} \sqrt{\frac{1+n^2}{(n-1)^2} - \left(\frac{n}{n-1} - \frac{\varepsilon_e}{\varepsilon_0} \right)^2} - \frac{1}{n-1} & \varepsilon_e \leq \varepsilon_0 \\ \left(\frac{\varepsilon_e}{\varepsilon_0} \right)^{1/n} & \varepsilon_e \geq \varepsilon_0 \end{cases}$$

and $E = n\sigma_0 / \varepsilon_0$ is the slope of the uniaxial stress-strain curve at $\varepsilon_e = 0$.

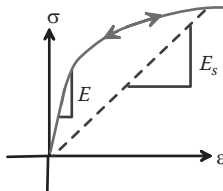


FIGURE 8.24 Stress-strain curve for a hypoelastic material.

The uniaxial stress-strain curve for this material is illustrated in Figure 8.24. The material is elastic, in that it is perfectly reversible, but the stresses are related to strains by a nonlinear function (a power law in this case). This material model does not describe any actual material but is sometimes used to approximate the more complicated stress-strain laws for plastic materials.

8.3.2 Governing Equations in Terms of the Virtual Work Principle

As in all FEM analysis, the stress equilibrium equation is replaced by the equivalent statement of the principle of virtual work. Thus, u_i , ε_{ij} , σ_{ij} are determined as follows:

1. First, calculate a displacement field that satisfies

$$\int_R \sigma_{ij}[u_k] \frac{\partial \delta v_i}{\partial x_j} dV - \int_R b_i \delta v_i dV - \int_{\partial_1 R} t_i^* \delta v_i dA = 0$$

$$u_i = u_i^* \quad \text{on } \partial_1 R$$

for all virtual velocity fields δv_i that satisfy $\delta v_i = 0$ on $\partial_1 R$. Here, the notation $\sigma_{ij}[u_k]$ is used to show that the stress in the solid depends on the displacement field (through the strain-displacement relation and the constitutive equations).

2. Compute the strains from the definition $\varepsilon_{ij} = \frac{1}{2}(\partial u_i / \partial x_j + \partial u_j / \partial x_i)$.
3. Compute the stresses from the stress-strain law. The stress will automatically satisfy the equation of equilibrium, so all the field equations and boundary conditions will be satisfied.

The procedure to solve the equations is conceptually identical to the linear elastic solution found in Sections 8.1.1 and 8.1.2. The only complication is that the stress is now a nonlinear function of the strains, so the virtual work equation is a nonlinear function of the displacement field. It must therefore be solved by iteration.

8.3.3 Finite Element Equations

The finite solution follows almost exactly the same procedure as before. We first discretize the displacement field, by choosing to calculate the displacement field at a set of n nodes, as shown in Figure 8.25. We will denote the coordinates of these special points by x_i^a , where the superscript a ranges from 1 to n . The unknown displacement vector at

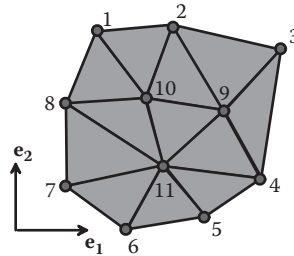


FIGURE 8.25 Simple finite element mesh.

each nodal point will be denoted by u_i^a . The finite element equations are then set up as follows:

1. The displacement field at an arbitrary point within the solid is again specified by interpolating between nodal values in some convenient way:

$$u_i(\mathbf{x}) = \sum_{a=1}^n N^a(\mathbf{x}) u_i^a \quad \delta v_i(\mathbf{x}) = \sum_{a=1}^n N^a(\mathbf{x}) \delta v_i^a.$$

2. Observe that we can compute the stress corresponding to a given displacement field by first computing the strain

$$\varepsilon_{ij} = \frac{1}{2} \left(\frac{\partial u_i}{\partial x_j} + \frac{\partial u_j}{\partial x_i} \right) = \frac{1}{2} \sum_{a=1}^n \left(\frac{\partial N^a}{\partial x_j} u_i^a + \frac{\partial N^a}{\partial x_i} u_j^a \right)$$

and then using the constitutive law to compute the stresses. We write this functional relationship as

$$\sigma_{ij} = \sigma_{ij} [\varepsilon_{kl}(u_i^a)].$$

3. Substituting into the principle of virtual work, we see that

$$\left\{ \int_R \sigma_{ij} [\varepsilon_{kl}(u_i^a)] \frac{\partial N^a}{\partial x_j} dV - \int_R b_i N^a dV - \int_{\partial R} t_i^* N^a dA \right\} \delta v_i^a = 0,$$

and, because this must hold for all δv_i^a , we must ensure that

$$\int_R \sigma_{ij} [\varepsilon_{kl}(u_i^a)] \frac{\partial N^a}{\partial x_j} dV - \int_R b_i N^a dV - \int_{\partial R} t_i^* N^a dA = 0 \quad \forall \{a,i\}: x_k^a \text{ not on } \partial_1 R$$

$$u_i^a = u_i^*(x_i^a) \quad \forall \{a,i\}: x_k^a \text{ on } \partial_1 R.$$

This is a set of $3n$ equations in $3n$ unknowns, very similar to those we obtained for linear elastostatic problems, but now the equations are *nonlinear*, because the stress is a nonlinear function of the unknown nodal displacements u_i^a .

8.3.4 Solving the Finite Element Equations Using Newton–Raphson Iteration

We can solve the nonlinear equations using Newton–Raphson iteration, as follows:

1. We start with some initial guess for u_i^a , say w_i^a (we can start with zero displacements, or, for incremental solutions, we can use the solution at the end of the preceding increment).
2. We then attempt to correct this guess to bring it closer to the proper solution by setting $w_i^a \rightarrow w_i^a + dw_i^a$. Ideally, of course, we would want the correction to satisfy

$$\int_R \sigma_{ij} [\epsilon_{kl}(w_i^a + dw_i^a)] \frac{\partial N^a}{\partial x_j} dV - \int_R b_i N^a dV - \int_{\partial R} t_i^* N^a dA = 0,$$

but because we cannot solve this, we linearize in dw_i^a and set

$$\int_R \left\{ \sigma_{ij} [\epsilon_{kl}(w_i^b)] + \frac{\partial \sigma_{ij}}{\partial \epsilon_{lm}} \frac{\partial \epsilon_{lm}}{\partial u_k^b} dw_k^b \right\} \frac{\partial N^a}{\partial x_j} dV - \int_R b_i N^a dV - \int_{\partial R} t_i^* N^a dA = 0.$$

3. Recall that

$$\begin{aligned} \epsilon_{lm} &= \frac{1}{2} \sum_{a=1}^n \left(\frac{\partial N^a}{\partial x_m} u_l^a + \frac{\partial N^a}{\partial x_l} u_m^a \right) \\ &\Rightarrow \frac{\partial \epsilon_{lm}}{\partial u_k^b} = \frac{1}{2} \sum_{a=1}^n \left(\frac{\partial N^a}{\partial x_m} \delta_{ab} \delta_{lk} + \frac{\partial N^a}{\partial x_l} \delta_{ab} \delta_{mk} \right). \end{aligned}$$

Note also that

$$\frac{\partial \sigma_{ij}}{\partial \epsilon_{ml}} = \frac{\partial \sigma_{ij}}{\partial \epsilon_{lm}}$$

so

$$\frac{\partial \sigma_{ij}}{\partial \epsilon_{lm}} \frac{\partial \epsilon_{lm}}{\partial u_k^b} = \frac{\partial \sigma_{ij}}{\partial \epsilon_{km}} \frac{\partial N^b}{\partial x_m}$$

and finally

$$\int_R \frac{\partial \sigma_{ij}}{\partial \epsilon_{kl}} \frac{\partial N^a}{\partial x_j} \frac{\partial N^b}{\partial x_l} dV dw_k^b + \int_R \sigma_{ij} [\epsilon_{kl}(w_i^b)] \frac{\partial N^a}{\partial x_j} dV - \int_R b_i N^a dV - \int_{\partial R} t_i^* N^a dA = 0.$$

4. This is evidently a system of linear equations for the correction dw_i^a of the form

$$K_{aibk}dw_k^b + R_i^a - F_i^a = 0$$

with

$$K_{aibk} = \int_R \frac{\partial \sigma_{ij}}{\partial \epsilon_{kl}} \frac{\partial N^a}{\partial x_j} \frac{\partial N^b}{\partial x_l} dV \quad R_i^a = \int_R \sigma_{ij} [\epsilon_{kl}(w_i^b)] \frac{\partial N^a}{\partial x_j} dV \quad F_i^a = \int_R b_i N^a dV + \int_{\partial R} t_i^* N^a dA.$$

These expressions are almost identical to the equations we needed to solve for linear elastostatic problems. There are only two differences: the stiffness contains the (strain-dependent) material tangent moduli $\partial \sigma_{ij} / \partial \epsilon_{kl}$ instead of the elastic constants C_{ijkl} , and we need to compute an extra term R_i^a in the residual force vector. This is a straightforward exercise; the integral is divided up into contributions from each element and evaluated numerically using Gaussian quadrature.

8.3.5 Tangent Moduli for the Hypoelastic Solid

One painful aspect of nonlinear FEM is that the material tangent moduli $\partial \sigma_{ij} / \partial \epsilon_{kl}$ must be calculated. This is usually a tedious algebraic exercise. For the hypoelastic constitutive law used in our example, one can show that

$$\frac{d\sigma_{ij}}{d\epsilon_{kl}} = \frac{4}{9}(E_t - E_s) \frac{e_{ij} e_{kl}}{\epsilon_e^2} + \frac{2}{3} E_s \left(\frac{\delta_{ik}\delta_{jl} + \delta_{il}\delta_{jk}}{2} - \frac{\delta_{ij}\delta_{kl}}{3} \right) + \frac{E}{9(1-2\nu)} \delta_{kl} \delta_{ij},$$

where $E_s = \sigma_e / \epsilon_e$ is the secant modulus, and $E_t = d\sigma_e / d\epsilon_e$ is the tangent modulus of the uniaxial stress-strain curve, as shown in Figure 8.26. You can calculate formulas for the tangent and secant moduli using the relationships between σ_e and ϵ_e given in Section 8.3.1.

If you try to re-derive these expressions yourself, you may end up with a different answer for $dS_{ij} / d\epsilon_{kl}$. This is because derivatives of a symmetric tensor with respect to another symmetric tensor are not unique (there is an indeterminate skew part). It is convenient to make the tangent modulus symmetric, so that the element (and global) stiffness matrices are symmetric.

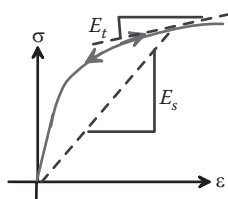


FIGURE 8.26 Tangent and secant moduli for a hypoelastic material.

8.3.6 Summary of the Newton–Raphson Procedure for Hypoelastic Solids

It is evidently quite straightforward to extend a linear elasticity code to nonlinear problems. The Newton–Raphson loop looks like this:

1. Start with an initial guess for the solution w_i^a .
 2. For the current guess, compute K_{aibk} , R_i^a and F_i^a , where
- $$K_{aibk} = \int_R \frac{\partial \sigma_{ij}}{\partial \varepsilon_{kl}} \frac{\partial N^a}{\partial x_j} \frac{\partial N^b}{\partial x_l} dV \quad R_i^a = \int_R \sigma_{ij} [\varepsilon_{kl}(w_i^b)] \frac{\partial N^a}{\partial x_j} dV \quad F_i^a = \int_R b_i N^a dV + \int_{\partial R} t_i^* N^a dA$$
- and formulas for the tangent $\partial \sigma_{ij} / \partial \varepsilon_{kl}$ are given in the preceding section.
3. Modify the system of equations to enforce any displacement boundary constraints.
 4. Solve $K_{aibk} dw_k^b = -R_i^a + F_i^a$.
 5. Let $w_i^a = w_i^a + dw_i^a$.
 6. Check for convergence (more on this below); go to item 2 if the solution has not yet converged.

Two methods may be used to check for convergence:

1. You can check and see whether the residual forces $-R_i^a + F_i^a$ are sufficiently small (they should vanish for an equilibrium stress field). You could find the maximum value at any node and ensure that it falls below a user-defined tolerance, or you could use the root-mean-square error

$$e = \sqrt{\frac{1}{n} \sum_{a=1}^n (R_i^a - F_i^a)(R_i^a - F_i^a)}$$

(where n is the number of nodes in the mesh) as an error measure.

2. Alternatively, you can check the magnitude of the correction dw_i^a and stop iterating when either the maximum correction at any node or the root-mean-square correction falls below some specified tolerance.

In practice *both* criteria are often used.

8.3.7 What to Do if the Newton–Raphson Iterations Do Not Converge

There is no guarantee that the Newton–Raphson method will converge. It will converge quadratically to the exact solution if the initial guess is sufficiently close to the correct answer, but if you are unlucky, it may diverge or spiral hopelessly around forever without finding the correct solution.

The most common way to fix this is to apply the load in a series of *increments* instead of all at once. The solution at the end of the preceding increment is used as the initial guess for the solution at the end of the next. Convergence can sometimes be accelerated by extrapolating the solution from preceding time steps to find a better initial guess for the solution.

The other approach (used in desperation) is to update the approximation to the solution as $w_i^a = w_i^a + \alpha dw_i^a$, where $\alpha < 1$ is a numerical relaxation factor. This slows convergence of the Newton-Raphson iterations but increases the radius of convergence.

8.3.8 Variations on Newton–Raphson Iteration

There are several variants on the fully consistent Newton–Raphson scheme outlined in the preceding section; some are obvious and some are subtle. These techniques are known collectively as “quasi-Newton” methods.

All these variations attempt to address the two major limitations of the fully consistent Newton method, which are (1) that the tangent matrix K_{aibk} must be recomputed during each iteration, and (2) it is necessary to solve the system of equations $K_{aibk}dw_k^b = -R_i^a + F_i^a$ repeatedly to obtain a convergent solution.

A simple fix is not to bother recomputing K_{aibk} or to recompute it occasionally. This gives a quasi-Newton method as follows:

1. Start with an initial guess for the solution w_i^a .
2. Compute K_{aibk} .
3. Compute R_i^a for the current solution.
4. Modify the system of equations to enforce any displacement boundary constraints.
5. Solve $K_{aibk}dw_k^b = -R_i^a + F_i^a$.
6. Let $w_i^a = w_i^a + dw_i^a$.
7. Check for convergence; go to item 3 if the solution has not yet converged, and go to item 2 if you feel like doing some extra work to speed up convergence.

In this method, equation solution can be speeded up further, by computing and storing the LU decomposition of K_{aibk} instead of K_{aibk} itself. Equation solution then just involves back-substitution, which can be accomplished quite quickly.

A more subtle approach is to obtain a succession of improved approximations to K_{aibk}^{-1} directly, from the changes in residual $F_i^a - R_i^a$ and solution increments dw_i^a during successive iterations. A very efficient implementation of the so-called Broyden–Fletcher–Goldfarb–Shanno (BFGS) algorithm is described by Matthies and Strang [1979].

8.3.9 Example Hypoelastic FEM Code

As always, we provide a simple example FEM code to illustrate the actual implementation. The codes can be downloaded from <http://solidmechanics.org/FEA/>

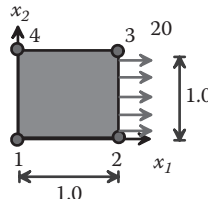


FIGURE 8.27 Simple finite element problem for a hypoelastic material.

1. The code is in the file FEM_2Dor3D_hypoelastic_static.mws (MAPLE) or FEM_2Dor3D_hypoelastic_static.m (MATLAB).
2. An example input file is in Hypoelastic_quad4.txt.

Some notes on the example include the following:

1. The code and sample input file are set up to solve the problem illustrated in Figure 8.27.
2. The element deforms in plane strain and has the hypoelastic constitutive response described previously with $\sigma_0 = 10$, $\varepsilon_0 = 0.001$, $n = 10$, $\nu = 0.3$.
3. The program applies load in a series of five increments and uses consistent Newton–Raphson iteration to solve the nonlinear equations at each step. When you get to the appropriate part of the code, you will see it printing out values for the error measures at each iteration.
4. Element strains and stresses are printed to a file on completion, and the stress-versus-displacement curve for the element is plotted, as shown in Figure 8.28.

HEALTH WARNING: This demonstration code uses fully integrated elements and will in general perform very poorly because of volumetric locking. For details of locking and how to avoid it, see Section 8.6.

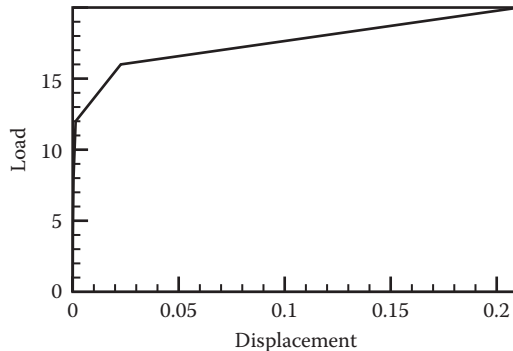


FIGURE 8.28 Predicted load-versus-displacement behavior for the problem illustrated in Figure 8.27.

8.4 FEM FOR LARGE DEFORMATIONS: HYPERELASTIC MATERIALS

The FEM can be used to solve problems involving large shape changes. In this section, we show how to do this, using a solid made from a hyperelastic material as an example.

8.4.1 Summary of Governing Equations

To keep things as simple as possible, we will devise a method to model a hyperelastic solid with a neo-Hookean constitutive law as discussed in Section 3.4. A generic hyperelasticity problem is shown in Figure 8.29. The following are given:

1. The shape of the solid in its unloaded condition R_0 (this will be taken as the stress-free reference configuration).
2. A body force distribution \mathbf{b} acting on the solid (note that, in this section, we return to using \mathbf{b} to denote force per unit mass).
3. Boundary conditions, specifying displacements $\mathbf{u}^*(\mathbf{x})$ on a portion $\partial_1 R$ or tractions $\mathbf{t}^*(\mathbf{x})$ on a portion $\partial_2 R$ of the boundary of the deformed solid (note that tractions are specified as force per unit deformed area, but we could also specify the tractions \mathbf{t}^0 per unit *undeformed* area acting on $\partial_1 R_0$ if this is more convenient).
4. The material constants μ_1, K_1 for the neo-Hookean constitutive law described in Section 3.5.5.
5. The mass density of the solid in its reference configuration ρ_0 .

Calculate displacements u_i , deformation gradient tensor F_{ij} , and Cauchy stresses σ_{ij} satisfying the governing equations and boundary conditions

$$y_i = x_i + u_i(x_k) \quad F_{ij} = \delta_{ij} + \frac{\partial u_i}{\partial x_j} \quad J = \det(\mathbf{F}), \quad B_{ij} = F_{ik} F_{jk}$$

$$\frac{\partial \sigma_{ij}}{\partial y_i} + \rho b_j = 0 \quad u_i = u_i^* \quad \text{on} \quad \partial_1 R \quad \sigma_{ij} n_i = t_j^* \quad \text{on} \quad \partial_2 R$$

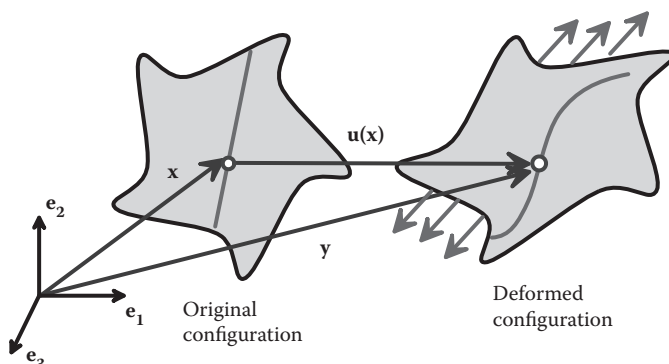


FIGURE 8.29 Representative boundary value problem for a hyperelastic material.

with Cauchy stress related to left Cauchy–Green tensor through the neo-Hookean constitutive law

$$\sigma_{ij} = \frac{1}{J^{5/3}} \left(B_{ij} - \frac{1}{3} B_{kk} \delta_{ij} \right) + K_1 (J-1) \delta_{ij}$$

8.4.2 Governing Equations in Terms of the Principle of Virtual Work

As always, the stress equilibrium equation is replaced by the equivalent principle of virtual work, which now has to be in a form appropriate for finite deformations. The virtual work equation is given in terms of various stress and deformation measures in Section 2.4.5. For our purposes, a slightly modified form of the version in terms of Kirchhoff stress is the most convenient. This states that

$$\int_{R_0} \tau_{ij} \delta L_{ij} dV_0 - \int_{R_0} \rho_0 b_i \delta v_i dV_0 - \int_{\partial R} t_i^* \delta v_i dA = 0$$

for all virtual velocity fields $\delta v_i(x_i)$ and virtual velocity gradients $\delta L_{ij} = \partial v_i / \partial y_j$ that satisfy $\delta v_i = 0$ on $\partial_1 R$. Here $\tau_{ij} = J \sigma_{ij}$ is the Kirchhoff stress. Here are some notes on this equation:

1. The volume integrals in the virtual work equation are taken over the reference configuration. This is convenient, because in a real problem, we can take the given initial shape of the solid as reference, whereas the deformed configuration is unknown.
2. The area integral is taken over the deformed configuration but can be mapped back to the reference configuration by computing the inverse surface Jacobian $\eta = dA / dA_0$. One way (although not the best way in practice) to calculate η would be through the relationship

$$\mathbf{n} dA = J \mathbf{m} \cdot \mathbf{F}^{-1} dA_0$$

where \mathbf{m} is the normal to the surface in the reference configuration, and \mathbf{n} is the normal to the surface in the deformed configuration. Taking the magnitude of both sides gives

$$\eta = J \sqrt{m_i F_{ik}^{-1} F_{jk}^{-1} m_j}.$$

Then the virtual work equation becomes

$$\int_{R_0} \tau_{ij} \delta L_{ij} dV_0 - \int_{R_0} \rho_0 b_i \delta v_i dV_0 - \int_{\partial_2 R_0} t_i^* \delta v_i \eta dA_0 = 0.$$

8.4.3 Finite Element Equations

The finite element solution follows almost exactly the same procedure as before. We first discretize the displacement field, by choosing to calculate the displacement field at a set of n

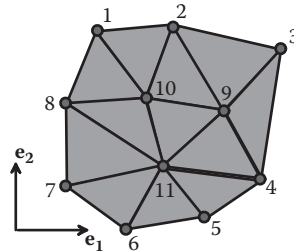


FIGURE 8.30 Example of a finite element mesh.

nodes, as shown in Figure 8.30. We will denote the coordinates of these special points in the reference configuration by x_i^a , where the superscript a ranges from 1 to n . The unknown displacement vector at each nodal point will be denoted by u_i^a :

1. The displacement field and virtual velocity field at an arbitrary point within the solid is again specified by interpolating between nodal values in some convenient way:

$$u_i(\mathbf{x}) = \sum_{a=1}^n N^a(\mathbf{x}) u_i^a \quad \delta v_i(\mathbf{x}) = \sum_{a=1}^n N^a(\mathbf{x}) \delta v_i^a.$$

Here, \mathbf{x} denotes the coordinates of an arbitrary point in the reference configuration. Note that the interpolation gives virtual velocity as a function of position \mathbf{x} in the reference configuration, not \mathbf{y} in the deformed configuration, so we have to be careful when computing the velocity gradient.

2. Observe that we can compute the deformation corresponding to a given displacement field as

$$F_{ij} = \delta_{ij} + \frac{\partial u_i}{\partial x_j} = \delta_{ij} + \sum_{a=1}^n \frac{\partial N^a}{\partial x_j} u_i^a.$$

3. The derivatives of shape functions with respect to reference coordinates are computed exactly as for small strain problems. Let $N^a(\xi)$ denote the shape functions in terms of local element coordinates ξ . Then interpolate position within the element as

$$x_i = \sum_{a=1}^{N_e} N^a(\xi) x_i^a.$$

Define the Jacobian matrix

$$\eta_{ij} = \frac{\partial x_i}{\partial \xi_j} = \sum_{a=1}^{N_e} \frac{\partial N^a}{\partial \xi_j} x_i^a$$

then

$$\frac{\partial N^a}{\partial x_j} = \frac{\partial N^a}{\partial \xi_k} \eta_{kj}^{-1}.$$

4. Given the deformation gradients, we can compute any other deformation measure we need; we don't need to spell out the details for now. By substituting the appropriate deformation measure, we could calculate the Kirchhoff stress. Note that the Kirchhoff stress depends on displacements through the deformation gradient; we will express this functional relationship as $\tau_{ij} [F_{kl}(u_i^a)]$.
5. Note also that the virtual velocity gradient can be calculated as

$$\delta L_{ij} = \frac{\partial \delta v_i}{\partial y_j} = \frac{\partial \delta v_i}{\partial x_k} \frac{\partial x_k}{\partial y_j} = \frac{\partial \delta v_i}{\partial x_k} F_{kj}^{-1} = \sum_{a=1}^n \frac{\partial N^a}{\partial x_k} F_{kj}^{-1} \delta v_i^a.$$

6. We can now substitute everything back into the virtual work equation

$$\left\{ \int_{R_0} \tau_{ij} [F_{pq}(u_k^b)] \frac{\partial N^a}{\partial x_m} F_{mj}^{-1} dV_0 - \int_{V_0} \rho_0 b_i N^a dV_0 - \int_{\partial_2 R_0} t_i^* N^a \eta dA_0 \right\} \delta v_i^a = 0.$$

7. Because this must hold for all δv_i^a , we must ensure that

$$\int_{V_0} \tau_{ij} [F_{pq}(u_k^b)] \frac{\partial N^a}{\partial x_m} F_{mj}^{-1} dV_0 - \int_{V_0} \rho_0 b_i N^a dV_0 - \int_{\partial_2 V_0} t_i^* N^a \eta dA_0 = 0 \quad \forall \{a,i\}: x_k^a \text{ not on } \partial_1 R_0$$

$$u_i^a = u_i^*(x_i^a) \quad \forall \{a,i\}: x_k^a \text{ on } \partial_1 R.$$

This is a set of $3n$ nonlinear equations in $3n$ unknowns, very similar to those we obtained for hypoelastic problems, except that now we have to deal with all the additional geometric terms associated with finite deformations. The procedure for solving these equations is outlined in the following sections.

8.4.4 Solution Using Consistent Newton–Raphson Iteration

As before, we can solve the nonlinear virtual work equation using Newton–Raphson iteration, as follows:

1. Start with some initial guess for u_i^a , say w_i^a (we can start with zero displacements, or, for incremental solutions, we can use the solution at the end of the preceding increment). This solution will not satisfy the governing equation (unless you are very lucky).
2. Next, attempt to correct this guess to bring it closer to the proper solution by setting $w_i^a \rightarrow w_i^a + dw_i^a$. Ideally, we would want the correction to satisfy

$$\int_{R_0} \tau_{ij} [F_{pq}(w_k^b + dw_k^b)] \frac{\partial N^a}{\partial x_m} (F + dF)_{mj}^{-1} dV_0 - \int_{R_0} \rho_0 b_i N^a dV_0 - \int_{\partial_2 R_0} t_i^* N^a (\eta + d\eta) dA_0 = 0$$

where $\mathbf{F} + d\mathbf{F}$ denotes the deformation gradient for the updated solution. This equation cannot be solved for dw_k^b in its present form.

3. To make progress, linearize in dw_k^b , just as for the hypoelastic problem discussed in the preceding section. The linearization (derived in detail below) yields a system of linear equations:

$$K_{aibk} dw_k^b + R_i^a - F_i^a = 0 \quad \forall \{a,i\}: x_k^a \text{ not on } \partial_1 V_0$$

$$u_i^a = u_i^*(x_i^a) \quad \forall \{a,i\}: x_k^a \text{ on } \partial_1 R$$

$$\begin{aligned} K_{aibk} &= \int_{V_0} \frac{\partial \tau_{ij}}{\partial F_{kl}} \frac{\partial N^b}{\partial x_l} \frac{\partial N^a}{\partial x_m} F_{mj}^{-1} dV_0 - \int_{V_0} \tau_{ij} \frac{\partial N^a}{\partial x_m} F_{mk}^{-1} \frac{\partial N^b}{\partial x_p} F_{pj}^{-1} dV_0 - \int_{\partial_2 V_0} t_i^* N^a \frac{\partial \eta}{\partial w_k^b} dA_0 \\ R_i^a &= \int_{V_0} \tau_{ij} \frac{\partial N^a}{\partial x_m} F_{mk}^{-1} dV_0 \quad F_i^a = \int_{V_0} \rho_0 b_i N^a dV_0 + \int_{\partial_2 V_0} t_i^* N^a \eta dA_0 = 0, \end{aligned}$$

which can be solved for dw_k^b .

4. If you prefer, you can use a slightly simpler set of formulas for the stiffness matrix and force vector

$$\begin{aligned} K_{aibk} &= \int_{V_0} C_{ijkl}^e \frac{\partial N^a}{\partial y_j} \frac{\partial N^b}{\partial y_l} dV_0 - \int_{V_0} \tau_{ij} \frac{\partial N^a}{\partial y_k} \frac{\partial N^b}{\partial y_j} dV_0 - \int_{\partial_2 V_0} t_i^* N^a \frac{\partial \eta}{\partial w_k^b} dA_0 \\ R_i^a &= \int_{V_0} \tau_{ij} \frac{\partial N^a}{\partial y_j} dV_0, \end{aligned}$$

where we have defined

$$C_{ijkl}^e = \frac{\partial \tau_{ij}}{\partial F_{km}} F_{lm} = J \sigma_{ij} \delta_{kl} + J \frac{\partial \sigma_{ij}}{\partial F_{km}} F_{lm} \quad \frac{\partial N^a}{\partial y_i} = \frac{\partial N^a}{\partial x_j} F_{ji}^{-1}.$$

Note that the formula for stiffness is very similar to the result for small strain problems, except for two additional terms. These additional terms are called the “geometric stiffness” because they arise as a result of accounting properly for finite geometry changes. In addition, note that, although the first integral in the stiffness is symmetric, the second and third are not. There is therefore some additional computational cost associated with finite strain problems, because it is necessary to store and solve an unsymmetric system of equations.

5. After solving the system of equations in item 3 for dw_k^b , check for convergence (you can use the magnitude of dw_k^b or the magnitude of the force vector $R_i^a - F_i^a$ as a

measure of error). If the solution has not yet converged, go back to item 3 and correct the solution again.

Linearizing the virtual work equation: This is a tedious but straightforward calculation. Start with

$$\int_{V_0} \tau_{ij} [F_{pq}(w_k^b + dw_k^b)] \frac{\partial N^a}{\partial x_m} (F + dF)_{mj}^{-1} dV_0 - \int_{V_0} \rho_0 b_i N^a dV_0 - \int_{\partial V_0} t_i^* N^a (\eta + d\eta) dA_0 = 0.$$

Note that

$$\frac{\partial F_{ij}}{\partial w_k^a} = \frac{\partial N^a}{\partial x_j} \delta_{ik}.$$

We also have that

$$\begin{aligned} F_{ij} F_{jk}^{-1} = \delta_{ik} &\Rightarrow \frac{\partial F_{ij}}{\partial w_n^a} F_{jk}^{-1} + F_{ij} \frac{\partial F_{jk}^{-1}}{\partial w_n^a} = 0 \Rightarrow \frac{\partial F_{pk}^{-1}}{\partial w_n^a} = -F_{pi}^{-1} \frac{\partial F_{ij}}{\partial w_n^a} F_{jk}^{-1} \\ &\Rightarrow (F + dF)_{mn}^{-1} \approx F_{mn}^{-1} - F_{mi}^{-1} \frac{\partial F_{ij}}{\partial w_k^b} F_{jn}^{-1} dw_k^b = F_{mn}^{-1} - F_{mk}^{-1} \frac{\partial N^b}{\partial x_j} F_{jn}^{-1} dw_k^b. \end{aligned}$$

In addition,

$$\tau_{ij} [F_{pq}(w_k^b + dw_k^b)] \approx \tau_{ij} + \frac{\partial \tau_{ij}}{\partial F_{kl}} \frac{\partial F_{kl}}{\partial w_n^b} dw_n^b = \tau_{ij} + \frac{\partial \tau_{ij}}{\partial F_{kl}} \frac{\partial N^b}{\partial x_l} dw_k^b.$$

Substituting these expansions in the virtual work equation and retaining linear terms in dw leads to the results given in step 3 above.

8.4.5 Tangent Stiffness for the Neo-Hookean Material

The tangent stiffness is defined as

$$C_{ijkl}^e = \frac{\partial \tau_{ij}}{\partial F_{km}} F_{lm} = J \sigma_{ij} \delta_{kl} + J \frac{\partial \sigma_{ij}}{\partial F_{km}} F_{lm}.$$

The neo-Hookean solid has a stress-strain relation given by

$$\sigma_{ij} = \frac{1}{J^{5/3}} \left(B_{ij} - \frac{1}{3} B_{kk} \delta_{ij} \right) + K_1 (J-1) \delta_{ij}.$$

Evaluating the derivatives is a tedious but straightforward exercise in index notation. The following identity is helpful:

$$\frac{\partial J}{\partial F_{km}} = J F_{mk}^{-1},$$

giving

$$C^e_{ijkl} = \frac{1}{J^{2/3}} \left(\delta_{ik}B_{jl} + B_{il}\delta_{jk} - \frac{2}{3}\{B_{ij}\delta_{kl} + B_{kl}\delta_{ij}\} + \frac{2}{3}\frac{B_{qq}}{3}\delta_{ij}\delta_{kl} \right) + K_1(2J-1)J\delta_{ij}\delta_{kl}.$$

8.4.6 Evaluating the Boundary Traction Integrals

Finally, we need to address how to calculate the factor η and its derivative in the surface integrals. There are two common cases we need to deal with. In some problems, we find it convenient to specify the *nominal* traction (force per unit undeformed area) acting on part of a solid. For example, if you were to model the behavior of a bar under uniaxial tension, you might know the force you are going to apply to the bar. Because you know the cross-sectional area of the undeformed bar, you could easily calculate nominal traction. However, in this case, you would have no idea what the *true* traction acting on the bar is; to calculate that, you have to know the cross-sectional area of the deformed bar.

In other problems, you need to be able to impose a certain force per unit *deformed* area, i.e., to specify the true traction distribution. This would be the case if you wanted to model fluid or aerodynamic forces acting on part of the solid.

We will deal with both cases. The first case is easy: note that the nominal and true traction are related by $\mathbf{t}^0 = \eta \mathbf{t}^*$. The expression for the external forcing can therefore be written as

$$F_i^a = \int_{V_0} \rho_0 b_i N^a dV_0 + \int_{\partial_2 V_0} t_i^0 N^a dA_0 = 0,$$

and, because this expression does not involve η , the last term in the expression for stiffness vanishes.

The second case is a pain. It is simplest to treat the surface integrals directly. Consider a general 3D element face, with nodal coordinates (in the deformed configuration) $y_i^a = x_i^a + u_i^a$ for $a = 1 \dots n$. Introduce a convenient interpolation scheme to define the shape of the element face in terms of its nodal coordinates

$$x_i(\xi_\alpha) = \sum_{a=1}^n M^a(\xi_\alpha) y_i^a,$$

where $-1 \leq \xi_\alpha \leq 1$ with $\alpha = 1, 2$ denote a suitable set of local coordinates that will specify position within an element face, and M^a are a set of interpolation functions.

We now evaluate the surface integral as

$$\int_{\partial\Omega_e} t_i^* N^a \eta dA_0 = \int_{-1}^{+1} \int_{-1}^{+1} t_i^* N^a(\xi_\alpha) \tilde{\eta}(\xi_\alpha) d\xi_1 d\xi_2,$$

where η must be computed by finding the two natural basis vectors

$$p_i^\alpha = \frac{\partial y_i}{\partial \xi_\alpha} = \sum_a \frac{\partial M^a}{\partial \xi_\alpha} y_i^a$$

and then using $dA = |\mathbf{p}^1 \times \mathbf{p}^2| d\xi_1 d\xi_2 = \tilde{\eta} d\xi_1 d\xi_2$. A straightforward exercise shows that

$$\tilde{\eta} = \sqrt{(p_k^1 p_k^1)(p_m^2 p_m^2) - (p_k^1 p_k^2)^2}.$$

With this in hand, we can calculate

$$\frac{\partial \tilde{\eta}}{\partial u_j^b} = \frac{1}{\tilde{\eta}} \left\{ (p_m^2 p_m^2) p_k^1 \frac{\partial p_k^1}{\partial u_j^b} + (p_m^1 p_m^1) p_k^2 \frac{\partial p_k^2}{\partial u_j^b} - (p_m^1 p_m^2) \left(p_k^2 \frac{\partial p_k^1}{\partial u_j^b} + p_k^1 \frac{\partial p_k^2}{\partial u_j^b} \right) \right\},$$

where

$$\frac{\partial p_i^\alpha}{\partial u_j^b} = \frac{\partial M^b}{\partial \xi_\alpha} \delta_{ij}$$

so that the last term in the stiffness can be evaluated as

$$\int_{\Omega_e} t_i^* N^a \frac{\partial \eta}{\partial w_k^b} dA_0 = \int_{-1}^{+1} \int_{-1}^{+1} t_i^* N^a(\xi_\alpha) \frac{\partial \tilde{\eta}}{\partial u_k^b} d\xi_1 d\xi_2.$$

8.4.7 Example Hyperelastic Finite Element Code

It is evidently quite straightforward to extend a nonlinear small strain finite element code to account for finite strains. The only changes necessary are as follows:

1. The general finite deformation measures must be calculated.
2. The material tangent stiffness is now a function of strain.
3. Two additional geometric terms must be added to the stiffness matrix: one of these is a volume integral over all the elements, and the second is an integral over the boundary.
4. We have to deal with an unsymmetric stiffness matrix.

An example code is provided in the files FEM_2Dor3D_hyperelastic_static.mws (MAPLE) or FEM_2Dor3D_hyperelastic_static.m (MATLAB). For simplicity, the example is coded

to apply a fixed nominal traction to the boundary (the geometric terms in the surface integral outlined above are not included).

An input file Hyperelastic_quad4.txt is also provided: the file sets up a simple plane strain 1 element problem and plots the traction-displacement relation for the element.

8.5 THE FEM FOR VISCOPLASTICITY

We next extend the FEM to treat history- and rate-dependent materials. The main issue to resolve is how to integrate the history-dependent plastic constitutive equations with respect to time. As an example, we will first develop an FEM for a small strain rate-dependent plastic constitutive law.

8.5.1 Summary of Governing Equations

We therefore pose the following boundary value problem, illustrated in Figure 8.31. We are given the following:

1. The shape of the solid in its unloaded condition R_0
2. A body force distribution $\mathbf{b}(t)$ acting on the solid (note that, in this section, we will use \mathbf{b} to denote force per unit volume rather than force per unit mass, to avoid having to write out the mass density all the time)
3. Boundary conditions, specifying displacements $\mathbf{u}^*(\mathbf{x}, t)$ on a portion $\partial_1 R$ or tractions $\mathbf{t}^*(t)$ on a portion $\partial_2 R$ of the boundary of R
4. The material constants $Y, n, m, \dot{\varepsilon}_0, Q$, and ε_0 that characterize the viscoplastic creep law described in Section 3.8.3

Calculate displacements, strains, and stresses $u_i, \varepsilon_{ij}, \sigma_{ij}$ satisfying the following equations:

1. The strain-displacement equation: $\varepsilon_{ij} = \frac{1}{2}(\partial u_i / \partial x_j + \partial u_j / \partial x_i)$

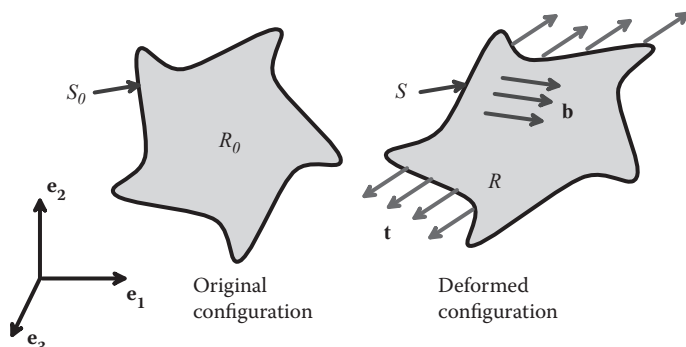


FIGURE 8.31 Representative boundary value problem for a viscoplastic solid.

2. The equation of static equilibrium for stresses: $\partial\sigma_{ij} / \partial x_i + b_j = 0$

3. The boundary conditions on displacement and stress:

$$u_i = u_i^* \quad \text{on } \partial_1 R \quad \sigma_{ij} n_i = t_j^* \quad \text{on } \partial_2 R$$

4. The constitutive equations for small strain, power-law rate-dependent plasticity, with

$$\dot{\epsilon}_{ij} = \dot{\epsilon}_{ij}^e + \dot{\epsilon}_{ij}^p$$

$$\dot{\epsilon}_{ij}^e = \frac{1+\nu}{E} \left(\dot{\sigma}_{ij} - \frac{\nu}{1+\nu} \dot{\sigma}_{kk} \delta_{ij} \right) \quad \dot{\epsilon}_{ij}^p = \dot{\epsilon}_0 \exp(-Q/kT) \left(\frac{\sigma_e}{\sigma_0} \right)^m \frac{3}{2} \frac{S_{ij}}{\sigma_e}$$

$$\sigma_0 = Y \left(1 + \frac{\epsilon_e}{\epsilon_0} \right)^{1/n} \quad S_{ij} = \sigma_{ij} - \sigma_{kk} \delta_{ij} / 3 \quad \sigma_e = \sqrt{\frac{3}{2} S_{ij} S_{ij}} \quad \dot{\epsilon}_e = \sqrt{\frac{2}{3} \dot{\epsilon}_{ij}^p \dot{\epsilon}_{ij}^p}$$

Note that we must now solve a history-dependent problem. We need to specify the time variation of the applied load and boundary conditions, and our objective is to calculate the displacements, strains, and stresses as functions of time.

8.5.2 Governing Equations in Terms of the Virtual Work Principle

As in all FEM analysis, the stress equilibrium equation is replaced by the equivalent statement of the principle of virtual work. Thus, u_i , ϵ_{ij} , σ_{ij} are determined as follows.

1. First, calculate a (time-dependent) displacement field that satisfies

$$\int_R \sigma_{ij}[u_k(t)] \frac{\partial \delta v_i}{\partial x_j} dV - \int_R b_i \delta v_i dV - \int_{\partial_2 R} t_i^* \delta v_i dA = 0$$

$$u_i = u_i^* \quad \text{on } \partial_1 R$$

for all virtual velocity fields δv_i that satisfy $\delta v_i = 0$ on $\partial_1 R$. Here, the notation $\sigma_{ij}[u_k]$ is used to show that the stress in the solid depends on the displacement field (through the strain-displacement relation and the constitutive equations).

2. Compute the strains from the definition $\epsilon_{ij} = \frac{1}{2} (\partial u_i / \partial x_j + \partial u_j / \partial x_i)$.

3. Compute the stresses from the constitutive equations. The stress will automatically satisfy the equation of equilibrium, so all the field equations and boundary conditions will be satisfied.

The procedure to solve the equations is conceptually identical to the hypoelastic solution found in Sections 8.3.1 and 8.3.2. The only complication is that the constitutive equation is time dependent, so the solution must be obtained as a function of time.

8.5.3 Finite Element Equations

The finite solution follows almost exactly the same procedure as before. We first discretize the displacement field, by choosing to calculate the displacement field at a set of n nodes, as shown in Figure 8.32. We will denote the coordinates of these special points by x_i^a , where the superscript a ranges from 1 to n . The unknown displacement vector at each nodal point will be denoted by u_i^a .

Now, however, that the displacements vary as a function of time; we thus need to solve for $u_i^a(t)$. We will do this by applying the load in a series of steps and computing the change in displacement during each step. We assume that the displacements $u_i^a(t)$ are known at the end of a time step. We want to compute $u_i^a(t + \Delta t)$ at the end of the next time step. It is convenient to write

$$u_i^a(t + \Delta t) = u_i^a(t) + \Delta u_i^a$$

and solve for the displacement increment Δu_i^a at each time step. The finite element solutions are then set up as follows:

1. The displacement increment and the virtual displacement are interpolated in the usual way:

$$\Delta u_i(\mathbf{x}) = \sum_{a=1}^n N^a(\mathbf{x}) \Delta u_i^a \quad \delta v_i(\mathbf{x}) = \sum_{a=1}^n N^a(\mathbf{x}) \delta v_i^a.$$

Here, \mathbf{x} denotes the coordinates of an arbitrary point in the solid.

2. The increment in strain during the current load step follows as

$$\Delta \varepsilon_{ij} = \frac{1}{2} \left(\frac{\partial \Delta u_i}{\partial x_j} + \frac{\partial \Delta u_j}{\partial x_i} \right) = \frac{1}{2} \sum_{a=1}^n \left(\frac{\partial N^a}{\partial x_j} \Delta u_i^a + \frac{\partial N^a}{\partial x_i} \Delta u_j^a \right).$$

We now need to find a way to compute the stress field caused by this change in strain during time interval Δt . This issue will be addressed shortly. For now, we just assume that we can do this somehow using the constitutive law (e.g., assign it to a graduate student) and write this functional relationship as

$$\sigma_{ij} = \sigma_{ij} [\Delta \varepsilon_{kl} (\Delta u_i^a), \Delta t],$$

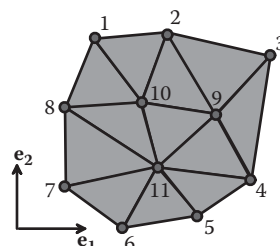


FIGURE 8.32 Example finite element mesh.

where the time interval Δt appears in the equation because the material is rate dependent.

3. Substituting into the principle of virtual work, we see that

$$\left\{ \int_R \sigma_{ij} [\Delta \varepsilon_{kl}(\Delta u_i^a), \Delta t] \frac{\partial N^a}{\partial x_j} dV - \int_R b_i(t + \Delta t) N^a dV - \int_{\partial_2 R} t_i^*(t + \Delta t) N^a dA \right\} \delta v_i^a = 0,$$

and, because this must hold for all δv_i^a , we must ensure that

$$\int_R \sigma_{ij} [\Delta \varepsilon_{kl}(\Delta u_i^a), \Delta t] \frac{\partial N^a}{\partial x_j} dV - \int_R b_i(t + \Delta t) N^a dV - \int_{\partial_2 R} t_i^*(t + \Delta t) N^a dA = 0$$

$$\forall \{a, i\}: x_k^a \text{ not on } \partial_1 R \quad \Delta u_i^a = u_i^*(x_i^a, t, \Delta t) - u_i^*(x_i^a, t) \quad \forall \{a, i\}: x_k^a \text{ on } \partial_1 R$$

This is now a routine set of nonlinear equations to be solved for Δu_i^a .

8.5.4 Integrating the Plastic Stress–Strain Law

The crux of FEM for small strain plasticity problems is to integrate the plastic stress-strain equations to obtain the stress caused by an increment in total strain $\Delta \varepsilon_{ij}$ applied to the specimen during a time interval Δt . There are various ways to do this; here we outline a straightforward and robust technique. The problem we must solve can be posed as follows. Given values of stress $\sigma_{ij}^{(n)}$, accumulated plastic strain $\varepsilon_e^{(n)}$ at time t_n , the total strain increment $\Delta \varepsilon_{ij}$, and time increment Δt , we must compute the values of stress $\sigma_{ij}^{(n+1)}$, accumulated plastic strain $\varepsilon_e^{(n+1)}$ at time $t_{n+1} = t_n + \Delta t$. The following procedure can be used to do this:

1. Calculate the deviatoric strain increment: $\Delta e_{ij} = \Delta \varepsilon_{ij} - \Delta \varepsilon_{kk} \delta_{ij} / 3$.
2. Calculate the “elastic predictor” for the deviatoric and effective stress at the end of the increment

$$S_{ij}^{*(n+1)} = S_{ij}^{(n)} + \frac{E}{1+\nu} \Delta e_{ij} \quad \sigma_e^{*(n+1)} = \sqrt{\frac{3}{2} S_{ij}^{*(n+1)} S_{ij}^{*(n+1)}}.$$

3. Calculate the increment in effective plastic strain $\Delta \varepsilon_e$ by solving (numerically) the following equation:

$$\frac{\sigma_e^{*(n+1)}}{Y} - \frac{3E}{2Y(1+\nu)} \Delta \varepsilon_e - \left(1 + \frac{\varepsilon_e + \Delta \varepsilon_e}{\varepsilon_0} \right)^{1/n} \left(\frac{\Delta \varepsilon_e}{\Delta t \dot{\varepsilon}_0 \exp(-Q/kT)} \right)^{1/m} = 0.$$

4. The stress at the end of the increment then follows as

$$\sigma_{ij}^{(n+1)} = \left(1 - \frac{3E}{2(1+\nu)\sigma_e^{*(n+1)}} \Delta \varepsilon_e \right) \left(S_{ij}^{(n)} + \frac{E}{1+\nu} \Delta e_{ij} \right) + \sigma_{kk}^{(n)} + \frac{E}{3(1-2\nu)} \Delta \varepsilon_{kk}.$$

Derivation: These expressions can be derived as follows:

1. Separate the stress $\sigma_{ij}^{(n+1)}$ into deviatoric and hydrostatic components as follows:

$$p^{(n+1)} = \sigma_{kk}^{(n+1)} / 3 \quad S_{ij}^{(n+1)} = \sigma_{ij}^{(n+1)} - p^{(n+1)} \delta_{ij}.$$

2. The elastic stress-strain equation gives the hydrostatic part of the stress at a time $t_{n+1} = t_n + \Delta t$ as

$$p^{(n+1)} = p^{(n)} + \frac{E}{3(1-2\nu)} \Delta \epsilon_{kk}.$$

3. The deviatoric stress at the end of the increment can be expressed in terms of the total deviatoric strain increment $\Delta \epsilon_{ij} = \Delta \epsilon_{ij} - \Delta \epsilon_{kk} \delta_{ij} / 3$ and the increment in plastic strain $\Delta \epsilon_{ij}^p$ by writing

$$S_{ij}^{(n+1)} = S_{ij}^{(n)} + \frac{E}{1+\nu} \Delta \epsilon_{ij}^e = S_{ij}^{(n)} + \frac{E}{1+\nu} (\Delta \epsilon_{ij} - \Delta \epsilon_{ij}^p).$$

4. To calculate the plastic strain increment $\Delta \epsilon_{ij}^p$, we need to integrate the expression for plastic strain rate with respect to time over the interval Δt . There are many advantages to using an implicit, or backward-Euler, time integration scheme for this purpose, as follows:

$$\Delta \epsilon_{ij}^p = \Delta \epsilon_e \frac{3}{2} \frac{S_{ij}^{(n+1)}}{\sigma_e^{(n+1)}} \quad \Delta \epsilon_e = \Delta t \dot{\epsilon}_0 \exp(-Q/kT) \left(\frac{\sigma_e^{(n+1)}}{\sigma_0^{(n+1)}} \right)^m \quad \sigma_0^{(n+1)} = Y \left(1 + \frac{\epsilon_e^{(n)} + \Delta \epsilon_e}{\epsilon_0} \right)^{1/n}.$$

This is an implicit scheme, because the strain rate is computed based on values of stress and state variables at the *end* of the time interval. It is a bit more cumbersome to deal with than a simple forward-Euler (explicit) scheme, in which the strain rate depends on stresses and state at the start of the increment, but the advantages far outweigh the additional complexity. The implicit scheme can be shown to be unconditionally stable (you can take large time steps without encountering numerical instabilities) and also leads to symmetric material tangents, as shown in the next section.

5. The problem is now algebraic: we need to solve for $S_{ij}^{(n+1)}$ and accumulated plastic strain $\epsilon_e^{(n+1)}$. To this end, define

$$S_{ij}^{*(n+1)} = S_{ij}^{(n)} + \frac{E}{1+\nu} \Delta \epsilon_{ij} \quad \sigma_e^{*(n+1)} = \sqrt{\frac{3}{2} S_{ij}^{*(n+1)} S_{ij}^{*(n+1)}}$$

($S_{ij}^{*(n+1)}$ is the deviatoric stress that you would get in the absence of plasticity).

6. Now assume that the actual stress will be $S_{ij}^{*(n+1)} = \beta S_{ij}^{*(n+1)}$, where β is a numerical factor to be determined. Substitute into the expression for $S_{ij}^{(n+1)}$ and eliminate $\Delta \epsilon_{ij}^p$ to see that

$$\beta S_{ij}^{*(n+1)} = S_{ij}^{*(n+1)} - \Delta \epsilon_e \frac{3E}{2(1+\nu)} \frac{S_{ij}^{*(n+1)}}{\sigma_e^{*(n+1)}}.$$

7. Contracting both sides of this equation with $S_{ij}^{*(n+1)}$ shows that

$$\beta = 1 - \frac{3E}{2(1+\nu)\sigma_e^{*(n+1)}} \Delta \epsilon_e.$$

8. Finally, note that $\beta = \sigma_e^{*(n+1)} / \sigma_e^{(n+1)}$ and eliminate $\sigma_e^{(n+1)}$ and $\sigma_0^{(n+1)}$ from the remaining equations in step 4 to get

$$\frac{\sigma_e^{*(n+1)}}{Y} - \frac{3E}{2Y(1+\nu)} \Delta \epsilon_e - \left(1 + \frac{\epsilon_e + \Delta \epsilon_e}{\epsilon_0}\right)^{1/n} \left(\frac{\Delta \epsilon_e}{\Delta t \dot{\epsilon}_0 \exp(-Q/kT)}\right)^{1/m} = 0.$$

9. The deviatoric stress at the end of the increment follows by substituting the result of step 8 into step 7 and recalling that $S_{ij}^{(n+1)} = \beta S_{ij}^{*(n+1)}$, so

$$S_{ij}^{(n+1)} = \left(1 - \frac{3E}{2(1+\nu)\sigma_e^{*(n+1)}} \Delta \epsilon_e\right) \left(S_{ij}^{(n)} + \frac{E}{1+\nu} \Delta \epsilon_{ij}\right).$$

10. Finally, the formula for stress follows by combining the deviatoric stress in step 9 with the hydrostatic stress in step 2.

8.5.5 Material Tangent

Because the stress-strain relation is nonlinear, the virtual work equation will need to be solved using Newton-Raphson iteration. For this purpose, we must compute the material tangent $\partial \sigma_{ij} / \partial \Delta \epsilon_{kl}$. The result is

$$\frac{\partial \sigma_{ij}}{\partial \Delta \epsilon_{kl}} = C_{ijkl}^{ep} = \frac{\beta E}{1+\nu} \left(\frac{1}{2} (\delta_{ik} \delta_{jl} + \delta_{jk} \delta_{il}) - \frac{1}{3} \delta_{ij} \delta_{kl} + \frac{9E(\Delta \epsilon_e - 1/\gamma)}{4(1+\nu)\sigma_e^{(n+1)}} \frac{S_{ij}^{(n+1)}}{\sigma_e^{(n+1)}} \frac{S_{kl}^{(n+1)}}{\sigma_e^{(n+1)}} \right) + \frac{E}{3(1-2\nu)} \delta_{ij} \delta_{kl},$$

where

$$\beta = \left(1 + \frac{3E\Delta \epsilon_e}{2(1+\nu)\sigma_e^{(n+1)}}\right)^{-1} \quad \gamma = \beta \left\{ \frac{3E}{2(1+\nu)\sigma_e^{(n+1)}} + \left(\frac{1}{n(\epsilon_0 + \epsilon_e + \Delta \epsilon_e)} + \frac{1}{m\Delta \epsilon_e} \right) \right\}.$$

Derivation: As always, calculating the material tangent stiffness is a tiresome algebraic exercise. We have that

$$\sigma_e^{(n+1)} = \beta S_{ij}^{*(n+1)} + \sigma_{kk}^{(n)} + \frac{E}{3(1-2\nu)} \Delta \epsilon_{kk}$$

$$\beta = \left(1 - \frac{3E}{2(1+\nu)\sigma_e^{(n+1)}} \Delta \epsilon_e\right) \quad S_{ij}^{*(n+1)} = \left(S_{ij}^{(n)} + \frac{E}{1+\nu} \Delta \epsilon_{ij}\right) \quad \sigma_e^{*(n+1)} = \sqrt{\frac{3}{2} S_{ij}^{*(n+1)} S_{ij}^{*(n+1)}},$$

Consequently,

$$d\sigma_{ij}^{(n+1)} = \beta \frac{E}{1+\nu} d\Delta e_{ij} - \frac{3E}{2(1+\nu)} \frac{S_{ij}^{*(n+1)}}{\sigma_e^{*(n+1)}} d\Delta \varepsilon_e + \frac{3E\Delta\varepsilon_e}{2(1+\nu)} \frac{S_{ij}^{*(n+1)}}{\sigma_e^{*(n+1)}} \frac{d\sigma_e^{*(n+1)}}{\sigma_e^{*(n+1)}} + \frac{E}{3(1-2\nu)} \delta_{ij} d\Delta \varepsilon_{kk},$$

where

$$d\sigma_e^{*(n+1)} = \frac{\partial \sigma_e^{*(n+1)}}{\partial \varepsilon_{ij}} d\Delta \varepsilon_{ij} = \frac{3E}{2(1+\nu)} \frac{S_{ij}^{*(n+1)} d\Delta \varepsilon_{ij}}{\sigma_e^{*(n+1)}} = \frac{3E}{2(1+\nu)} \frac{S_{ij}^{(n+1)} d\Delta \varepsilon_{ij}}{\sigma_e^{(n+1)}}$$

and $d\Delta \varepsilon_e$ can be computed by differentiating the nonlinear equation for $\Delta \varepsilon_e$ as

$$\frac{d\sigma_e^{*(n+1)}}{Y} - \left\{ \frac{3E}{2(1+\nu)Y} + \left(1 + \frac{\varepsilon_e + \Delta \varepsilon_e}{\varepsilon_0} \right)^{1/n} \left(\frac{\Delta \varepsilon_e}{\Delta t \dot{\varepsilon}_0 \exp(-Q/kT)} \right)^{1/m} \left(\frac{1}{n(\varepsilon_0 + \varepsilon_e + \Delta \varepsilon_e)} + \frac{1}{m \Delta \varepsilon_e} \right) \right\} d\Delta \varepsilon_e = 0.$$

Finally, noting that

$$\frac{d\Delta e_{ij}}{d\Delta \varepsilon_{kl}} = \frac{1}{2} (\delta_{ik} \delta_{jl} + \delta_{jk} \delta_{il}) - \frac{1}{3} \delta_{ij} \delta_{kl},$$

we can collect together all the relevant terms to show that

$$C_{ijkl}^{ep} = \frac{\beta E}{1+\nu} \left(\frac{1}{2} (\delta_{ik} \delta_{jl} + \delta_{jk} \delta_{il}) - \frac{1}{3} \delta_{ij} \delta_{kl} + \frac{9E(\Delta \varepsilon_e - 1/\gamma)}{4(1+\nu)\sigma_e^{(n+1)}} \frac{S_{ij}^{(n+1)}}{\sigma_e^{(n+1)}} \frac{S_{kl}^{(n+1)}}{\sigma_e^{(n+1)}} \right) + \frac{E}{3(1-2\nu)} \delta_{ij} \delta_{kl},$$

where

$$\gamma = \beta \left\{ \frac{3E}{2(1+\nu)\sigma_e^{(n+1)}} + \left(\frac{1}{n(\varepsilon_0 + \varepsilon_e + \Delta \varepsilon_e)} + \frac{1}{m \Delta \varepsilon_e} \right) \right\} \quad \beta = \left(1 + \frac{3E\Delta\varepsilon_e}{2(1+\nu)\sigma_e^{(n+1)}} \right)^{-1}.$$

8.5.6 Solution Using Consistent Newton–Raphson Iteration

At this point, our problem is essentially identical to the hypoelasticity problem we solved previously, except that we have to account for the history dependence of the solid. With this in mind, we apply the loads (or impose displacements) in a series of increments and calculate the change in displacements and stresses during each successive increment. A generic load step is as follows:

- Given are current values for displacement \mathbf{u}_n , accumulated plastic strain ε_e , and stress $\boldsymbol{\sigma}_n$.
- Compute the displacement increment $\Delta \mathbf{u}_n$ and increment in plastic strain $\Delta \varepsilon_e$.
- Update the solution to $\mathbf{u}_n + \Delta \mathbf{u}_n$, $\varepsilon_{en+1} = \varepsilon_{en} + \Delta \varepsilon_e$, $\boldsymbol{\sigma}_{n+1}$.

We start the solution for some generic load step with an initial guess for Δu_i^a , say w_i^a (we can use the solution at the end of the preceding increment). We then attempt to correct this guess to bring it closer to the proper solution by setting $w_i^a \rightarrow w_i^a + dw_i^a$. Ideally, of course, we would want the correction to satisfy

$$\int_R \sigma_{ij} [\epsilon_{kl}(w_i^a + dw_i^a)] \frac{\partial N^a}{\partial x_j} dV - \int_R b_i N^a dV + \int_R t_i^* N^a dA = 0.$$

Just as we did for hypoelastic problems, we linearize in dw_i^a to obtain a system of linear equations

$$K_{aibk} dw_k^b + R_i^a - F_i^a = 0,$$

with

$$K_{aibk} = \int_R C_{ijkl}^{ep} \frac{\partial N^a}{\partial x_j} \frac{\partial N^b}{\partial x_l} dV \quad R_i^a = \int_R \sigma_{ij} [\epsilon_{kl}(w_i^b)] \frac{\partial N^a}{\partial x_j} dV \quad F_i^a = \int_R b_i N^a dV + \int_{\partial R} t_i^* N^a dA.$$

These expressions are essentially identical to those we dealt with in the hypoelasticity problem.

Developing an elastic-plastic FEM code is a chore. It is conceptually no more difficult than the hypoelasticity problem, but there is a lot more bookkeeping to do to keep track of the history dependence of the material. Specifically, it is necessary to store, and to update, the stress and accumulated plastic strain at each integration point of each element and to pass this information to the routines that calculate element residual and element stiffness information. Newton–Raphson solution of the equilibrium equations is standard. Once a convergent solution has been found, the stress and accumulated plastic strain at the element integration points must be updated, before starting the next load step.

8.5.7 Example Small Strain Plastic FEM Code

As always, we provide simple example FEM codes to illustrate actual implementation. The codes can be downloaded from <http://solidmechanics.org/FEA>. The code is in a file FEM_2Dor3D_viscoplastic.mws (MAPLE) or FEM_2Dor3D_viscoplastic.m (MATLAB). An input file is provided in the file Viscoplastic_quad4.txt.

The code and sample input file are set up to solve the problem illustrated in Figure 8.33: the element deforms in plane strain and has the viscoplastic constitutive response described previously with

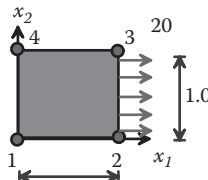


FIGURE 8.33 A simple one-element problem for a viscoplastic solid.

$$E = 1000, \quad \nu = 0.3$$

$$Y = 15, \quad \epsilon_0 = 0.5, \quad n = 10, \quad \dot{\epsilon}_0 = 0.1, \quad m = 10.$$

The program assumes that the load increases from 0 to 20 over a time period of 2. The load is applied in a series of increments and using consistent Newton–Raphson iteration to solve the nonlinear equations at each step. Element strains and stresses are printed to a file at each load step, and the stress-versus-displacement curve for the element is plotted, as shown in Figure 8.34.

8.6 ADVANCED ELEMENT FORMULATIONS: INCOMPATIBLE MODES, REDUCED INTEGRATION, AND HYBRID ELEMENTS

Techniques for interpolating the displacement field within 2D and 3D finite elements were discussed in Sections 8.1.9 and 8.1.10. In addition, methods for evaluating the volume or area integrals in the principle of virtual work were discussed in Section 8.1.11. These procedures work well for most applications, but there are situations in which the simple element formulations can give very inaccurate results. In this section, we illustrate some of the unexpected difficulties that can arise in apparently perfectly well-designed finite element solutions to boundary value problems, and we describe a few more sophisticated elements that have been developed to solve these problems. We focus in particular on “locking” phenomena. Finite elements are said to “lock” if they exhibit an unphysically stiff response to deformation. Locking can occur for many different reasons. The most common causes include the following: (1) the governing equations you are trying to solve are poorly conditioned, which leads to an ill-conditioned system of finite element equations; (2) the element interpolation functions are unable to approximate accurately the strain distribution in the solid, so the solution converges very slowly as the mesh size is reduced; (3) in certain element formulations (especially beam, plate, and shell

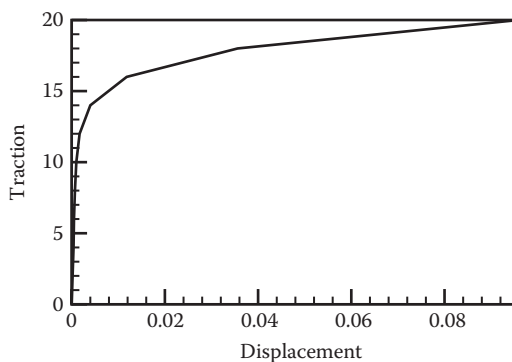


FIGURE 8.34 Traction-displacement relation predicted for the finite element shown in Figure 8.33.

elements), displacements and their derivatives are interpolated separately. Locking can occur in these elements if the interpolation functions for displacements and their derivatives are not consistent.

8.6.1 Shear Locking and Incompatible Mode Elements

Shear locking can be illustrated by attempting to find a finite element solution to the simple boundary value problem illustrated in Figure 8.35. Consider a cantilever beam, with length L , height $2a$, and out-of-plane thickness b , as shown in the figure. The top and bottom of the beam $x_2 = \pm a$ are traction free, the left-hand end is subjected to a resultant force P , and the right-hand end is clamped. Assume that $b \ll a$, so that a state of plane stress is developed in the beam. The analytical solution to this problem is given in Section 5.2.4.

Figure 8.36 compares this result with a finite element solution, obtained with standard four-noded linear quadrilateral plane stress elements. Results are shown for two different ratios of a/L , with $PL^3/Ea^3b = 2.22$ for both cases.

For the thick beam, the finite element and exact solutions agree nearly perfectly. For the thin beam, however, the finite element solution is very poor, although the mesh resolution is unchanged. The error in the finite element solution occurs because the standard four-noded quadrilateral elements cannot accurately approximate the strain distribution associated with bending. The phenomenon is known as “shear locking” because the element interpolation functions give rise to large, unphysical shear strains in bent elements. The solution would eventually converge if a large number of elements were added along the length of the beam. The elements would have to be roughly square, which would require about 133 elements along the length of the beam, giving a total mesh size of about 500 elements.

Shear locking is therefore relatively benign, because it can be detected by refining the mesh and can be avoided by using a sufficiently fine mesh. However, finite element analysts sometimes cannot resist the temptation to reduce computational cost by using elongated elements, which can introduce errors.

Shear locking can also be avoided by using more sophisticated element interpolation functions that can accurately approximate bending. “Incompatible mode” elements do this by adding an additional strain distribution to the element. The elements are called

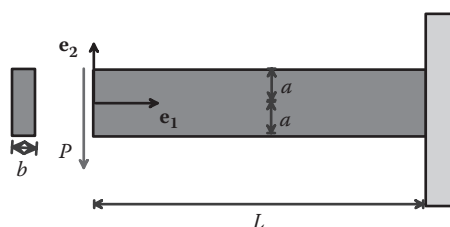


FIGURE 8.35 End-loaded cantilever beam.

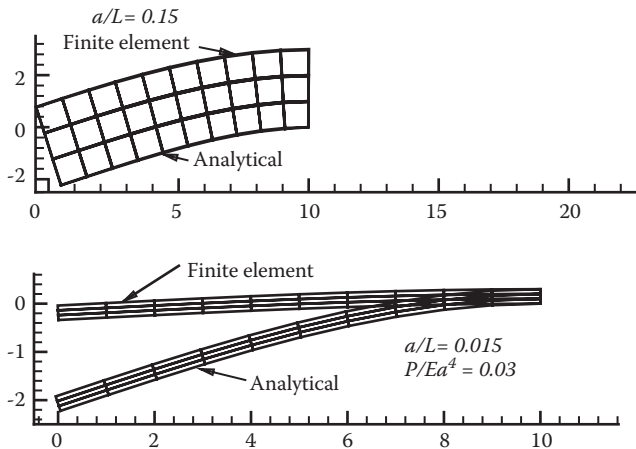


FIGURE 8.36 Comparison of finite element solution for the beam shown in Figure 8.35 with the exact solution. (a) Short beam; (b) long beam.

“incompatible” because the strain is not required to be compatible with the displacement interpolation functions. The approach is conceptually straightforward:

1. The displacement fields in the element are interpolated using the standard scheme, by setting

$$u_i = \sum_{a=1}^{N_e} N^a(\xi_j) u_i^a \quad \delta v_i = \sum_{a=1}^{N_e} N^a(\xi_j) \delta v_i^a \quad x_i = \sum_{a=1}^{N_e} N^a(\xi_j) x_i^a,$$

where $N^a(\xi_j)$ are the shape functions listed in Sections 8.1.9 or 8.1.10, ξ_j are a set of local coordinates in the element, u_i^a , x_i^a denote the displacement values and coordinates of the nodes on the element, and N_e is the number of nodes on the element.

2. The Jacobian matrix for the interpolation functions, its determinant, and its inverse are defined in the usual way:

$$\frac{\partial x_i}{\partial \xi_j} = \sum_{a=1}^{N_e} \frac{\partial N^a(\xi)}{\partial \xi_j} x_i^a \quad J = \det \left(\frac{\partial x_i}{\partial \xi_j} \right) \quad \frac{\partial \xi_j}{\partial x_i} = \left(\frac{\partial x_i}{\partial \xi_j} \right)^{-1}.$$

3. The usual expression for displacement gradient in the element is replaced by

$$\frac{\partial u_i}{\partial x_j} = \left(\sum_{a=1}^{N_e} \frac{\partial N^a(\xi)}{\partial \xi_m} u_i^a + \sum_{k=1}^p \frac{J(0)}{J(\xi)} \alpha_i^{(k)} \delta_{km} \xi_k \right) \frac{\partial \xi_m}{\partial x_j},$$

where $p = 2$ for a 2D problem and $p = 3$ for a 3D problem, $\alpha_i^{(k)}$ are a set of unknown displacement gradients in the element, which must be determined as part of the solution.

4. Similarly, the virtual displacement gradient is written as

$$\frac{\partial \delta v_i}{\partial x_j} = \left(\sum_{a=1}^{N_e} \frac{\partial N^a(\xi)}{\partial \xi_m} \delta v_i^a + \sum_{k=1}^p \frac{J(0)}{J(\xi)} \delta \alpha_i^{(k)} \delta \alpha_{km} \xi_k \right) \frac{\partial \xi_m}{\partial x_j},$$

where $\delta \alpha_i^{(k)}$ is a variation in the internal displacement gradient field for the element.

5. These expressions are then substituted into the virtual work equation, which must now be satisfied for all possible values of virtual nodal displacements δv_i^a and virtual displacement gradients $\delta \alpha_i^{(k)}$. At first sight, this procedure appears to greatly increase the size of the global stiffness matrix, because a set of unknown displacement gradient components must be calculated for each element. However, the unknown $\alpha_i^{(k)}$ are local to each element and can be eliminated while computing the element stiffness matrix. The procedure to do this can be shown most clearly in a sample code.

A sample small strain, linear elastic code with incompatible mode elements can be downloaded from <http://solidmechanics.org/FEA>. The MAPLE code is Femlinelast_incompatible_modes.mws; the MATLAB version is Femlinelast_incompatible_modes.m. When run with the input file shear_locking_demo.txt, the codes produce the results shown in Figure 8.37. The incompatible modes clearly give a spectacular improvement in the performance of the element.

HEALTH WARNINGS: (1) The procedure outlined here only works for small strain problems. Finite strain versions exist but are somewhat more complicated. (2) Adding strain variables to elements can dramatically improve their performance, but this procedure must be used with great care to ensure that the strain and displacement degrees of freedom are independent variables. For additional details, see Simo and Rifai [1990] and Simo and Armero [1992].

8.6.2 Volumetric Locking and Reduced Integration Elements

Volumetric locking can be illustrated using a simple boundary value problem. Consider a long hollow cylinder with internal radius a and external radius b as shown in Figure 8.38. The solid is made from a linear elastic material with Young's modulus E and Poisson's

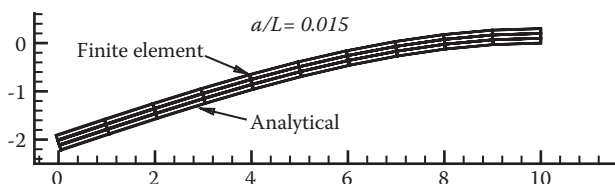


FIGURE 8.37 Comparison of finite element solution to the problem illustrated in Figure 8.34 using incompatible mode elements with the exact solution.



FIGURE 8.38 Internally pressurized thick-walled cylinder.

ratio ν . The cylinder is loaded by an internal pressure p_a and deforms in plane strain. The analytical solution to this problem is given in Section 4.1.9.

Figure 8.39 compares the analytical solution with a finite element solution with standard four-noded plane strain quadrilateral elements. Results are shown for two values of Poisson's ratio ν . The dashed lines show the analytical solution, and the solid line shows the FEA solution.

The two solutions agree well for $\nu = 0.3$, but the finite element solution grossly underestimates the displacements as Poisson's ratio is increased toward 0.5 (recall that the material is incompressible in the limit $\nu = 0.5$). In this limit, the finite element displacements tend to zero; this is known as “volumetric locking.”

The error in the finite element solution occurs because the finite element interpolation functions are unable to properly approximate a volume preserving strain field. In the incompressible limit, a nonzero volumetric strain at any of the integration points gives rise to a very large contribution to the virtual power. The interpolation functions can make the volumetric strain vanish at some, but not all, the integration points in the element.

Volumetric locking is a much more serious problem than shear locking, because it cannot be avoided by refining the mesh. In addition, all the standard fully integrated finite elements will lock in the incompressible limit, and some elements show very poor performance even for Poisson's ratios as small as 0.45. Fortunately, most materials have Poisson's ratios around 0.3 or less, so the standard elements can be used for most linear elasticity and small strain plasticity problems. To model rubbers, or to solve problems involving large plastic strains, the elements must be redesigned to avoid locking.

8.6.2.1 Reduced Integration

Reduced integration is the simplest way to avoid locking. The basic idea is simple: because the fully integrated elements cannot make the strain field volume preserving at all the integration points, it is tempting to reduce the number of integration points so that the constraint can be met. “Reduced integration” usually means that the element stiffness is integrated using an integration scheme that is one order less accurate than the standard scheme. The number of reduced integration points for various element types is listed in Table 8.11. The coordinates of the integration points are listed in the tables in Section 8.1.12.

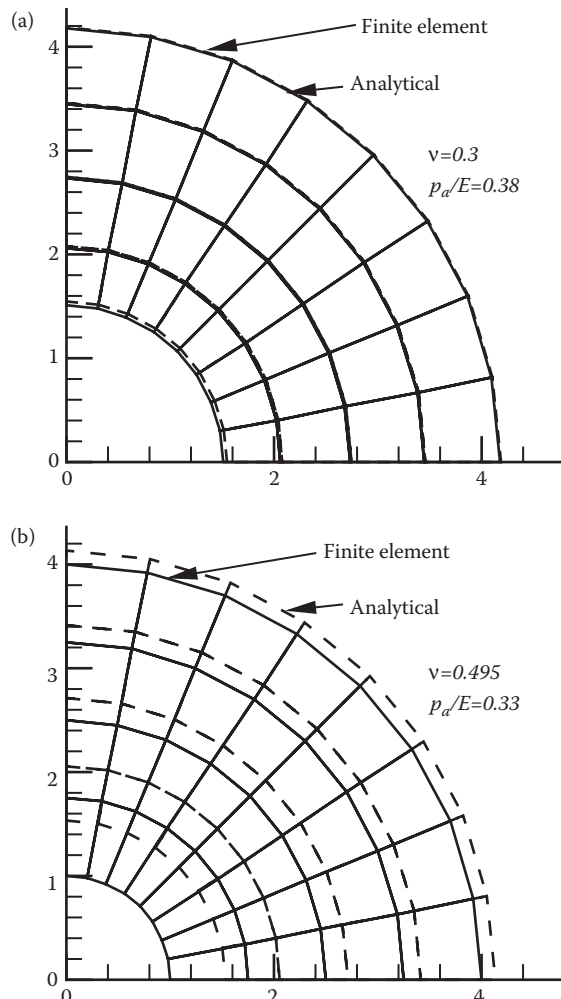


FIGURE 8.39 Comparison of the finite element solution to the problem illustrated in Figure 8.38 with the exact solution. (a) Solution for a compressible solid; (b) solution for a near-incompressible solid.

HEALTH WARNING: Notice that the integration order cannot be reduced for the linear triangular and tetrahedral elements. These elements should not be used to model near incompressible materials, although in desperation you can a few such elements in regions in which the solid cannot be meshed using quadrilaterals.

TABLE 8.11 Number of Integration Points for Reduced Integration Schemes

Linear triangle (3 nodes): 1 point	Linear tetrahedron (4 nodes): 1 point
Quadratic triangle (6 nodes): 3 points	Quadratic tetrahedron (10 nodes): 4 points
Linear quadrilateral (4 nodes): 1 point	Linear brick (8 nodes): 1 point
Quadratic quadrilateral (8 nodes): 4 points	Quadratic brick (20 nodes): 8 points

Remarkably, reduced integration completely resolves locking in some elements (the quadratic quadrilateral and brick) and even improves the accuracy of the element. As an example, Figure 8.40 shows the solution to the pressurized cylinder problem, using both full and reduced integration for eight-noded quadrilaterals. With reduced integration, the analytical and finite element results are indistinguishable.

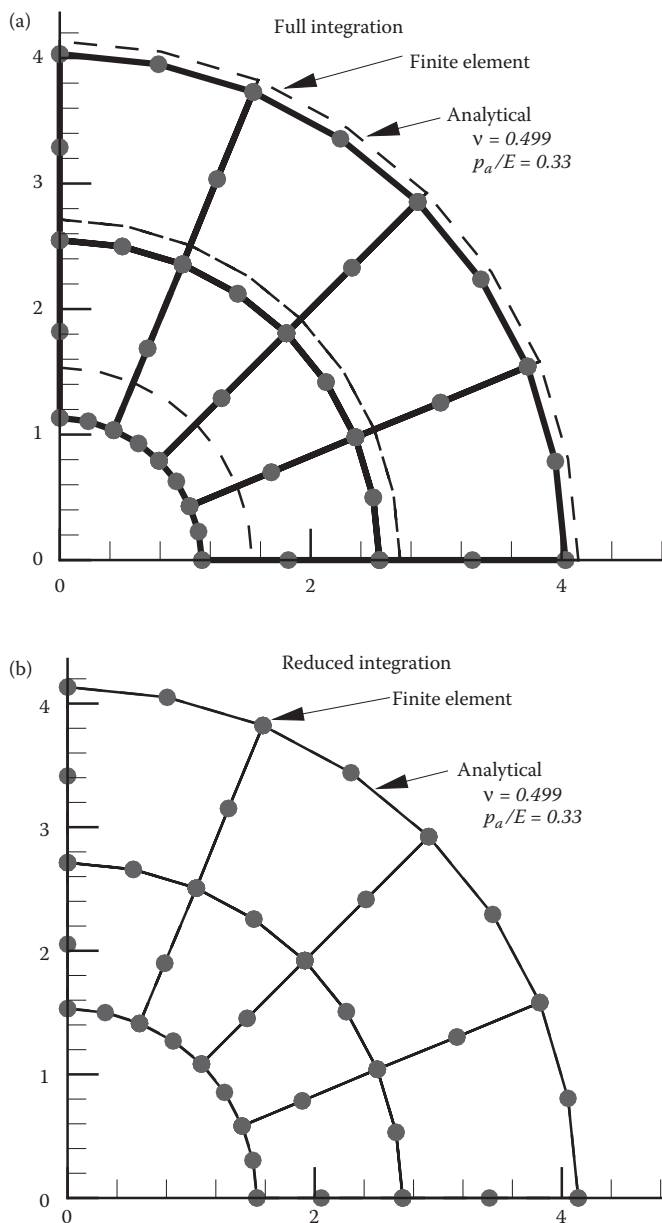


FIGURE 8.40 Comparison of the finite element solution to the problem illustrated in Figure 8.38 with the exact solution. (a) Solution with fully integrated quadratic elements; (b) solution with reduced integration quadratic elements.

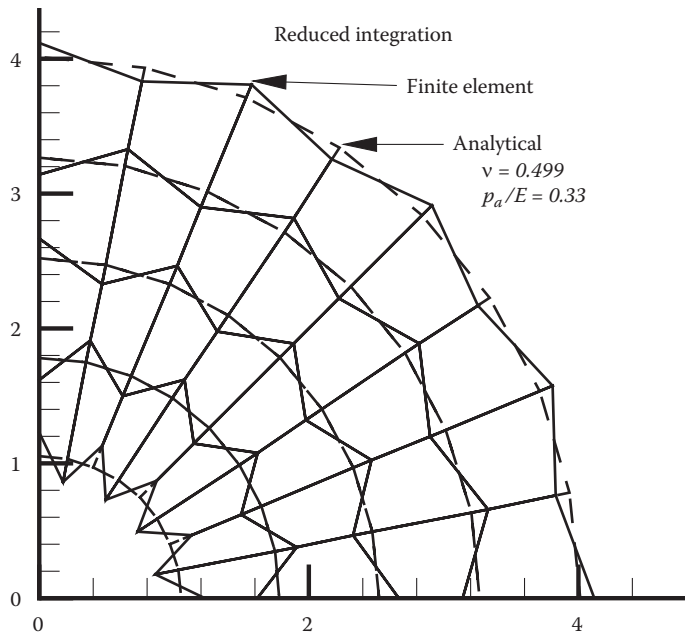


FIGURE 8.41 Comparison of the exact solution to the problem illustrated in Figure 8.38 to the finite element solution obtained linear elements with reduced integration with the exact solution.

Reduced integration does not work in four-noded quadrilateral elements or eight-noded brick elements. For example, Figure 8.41 shows the solution to the pressure vessel problem with linear (four-noded) quadrilateral elements with reduced integration (the displacements have been scaled down to show the hourgassing, plotted to true scale the displacements just look like complete garbage). The solution is clearly a disaster. The error occurs because the stiffness matrix is nearly singular; the system of equations includes a weakly constrained deformation mode. This phenomenon is known as “hourgassing” because of the characteristic shape of the spurious deformation mode.

8.6.2.2 Selectively Reduced Integration

Selectively reduced integration can be used to cure hourgassing. The procedure is illustrated most clearly by modifying the formulation for static linear elasticity. The method is implemented as follows:

1. The volume integral in the virtual work principle is separated into a deviatoric and volumetric part by writing

$$\int_R \sigma_{ij} \delta \epsilon_{ij} dV_0 = \int_R \left(\sigma_{ij} \delta \epsilon_{ij} - \frac{\sigma_{kk}}{3} \delta \epsilon_{qq} \right) dV_0 + \int_R \frac{\sigma_{kk}}{3} \delta \epsilon_{qq} dV_0.$$

Here, the first integral on the right-hand side vanishes for a hydrostatic stress.

2. Substituting the linear elastic constitutive equation and the finite element interpolation functions into the virtual work principle, we find that the element stiffness matrix can be reduced to

$$k_{aibk}^{(l)} = \int_{V_e^{(l)}} \left(C_{ijkl} \frac{\partial N^a(\mathbf{x})}{\partial x_j} \frac{\partial N^b(\mathbf{x})}{\partial x_l} - \frac{1}{3} C_{ppkl} \frac{\partial N^a(\mathbf{x})}{\partial x_i} \frac{\partial N^b(\mathbf{x})}{\partial x_l} \right) dV + \int_{V_e^{(l)}} \frac{1}{3} C_{ppkl} \frac{\partial N^a(\mathbf{x})}{\partial x_i} \frac{\partial N^b(\mathbf{x})}{\partial x_l} dV.$$

3. When selectively reduced integration is used, the first volume integral is evaluated using the full integration scheme; the second integral is evaluated using reduced integration points.

Selective reduced integration has been implemented in the sample programs Fem_selective_reduced_integration.mws (MAPLE) and Fem_selective_reduced_integration.m (MATLAB). Both codes can be downloaded from <http://solidmechanics.org/FEA>. When this code is run with the input file volumetric_locking_demo.txt, it produces the results shown in Figure 8.42. The analytical and finite element solutions agree, and there are no signs of hourgassing.

In many commercial codes, the “fully integrated” elements actually use selective reduced integration.

8.6.2.3 The “B-Bar” Method

Like selective reduced integration, the B-bar method works by treating the volumetric and deviatoric parts of the stiffness matrix separately. Instead of separating the volume integral into two parts, however, the B-bar method modifies the definition of the strain in the element. Its main advantage is that the concept can easily be generalized to finite strain problems. Here, we will illustrate the method by applying it to small strain linear elasticity. The procedure starts with the usual virtual work principle

$$\int_R \sigma_{ij}[\varepsilon_{ij}(u_k)] \delta \varepsilon_{ij} dV - \int_R b_i \delta v_i dV - \int_{\partial_2 R} t_i^* \delta v_i dA = 0.$$

The B-bar method is implemented as follows:

- We introduce a new variable to characterize the volumetric strain in the elements. Define

$$\omega = \frac{1}{3V_e} \int_{V_e} \varepsilon_{kk} dV = B_{bk}^{(vol)} u_k^b \quad B_{bk}^{(vol)} = \frac{1}{3V_e} \int_{V_e} \frac{\partial N^b}{\partial x_k} dV,$$

where the integral is taken over the volume of the element.

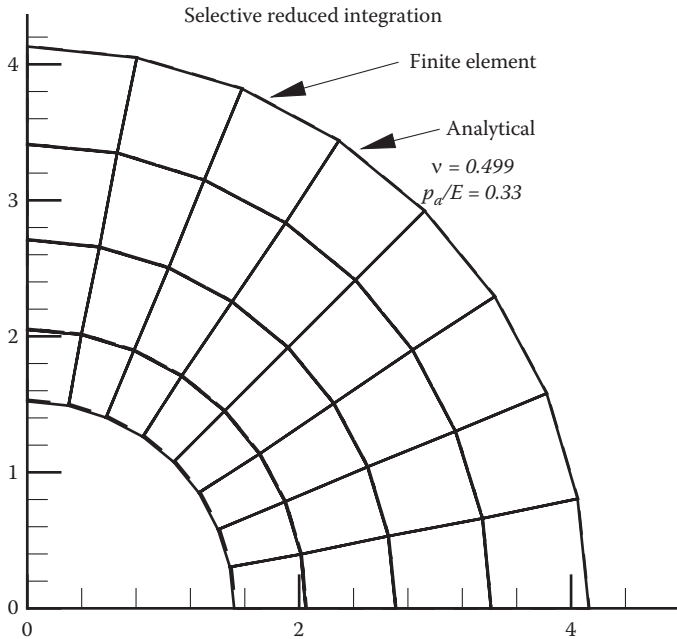


FIGURE 8.42 Comparison of the exact solution to the problem illustrated in Figure 8.38 to the finite element solution obtained using linear elements with selective reduced integration.

2. The strain variation in each element is replaced by the approximation $\bar{\varepsilon}_{ij} = \varepsilon_{ij} + (\omega - \varepsilon_{kk}/3)\delta_{ij}$.
3. Similarly, the virtual strain in each element is replaced by $\delta\bar{\varepsilon}_{ij} = \delta\varepsilon_{ij} + (\delta\omega - \delta\varepsilon_{kk}/3)\delta_{ij}$. This means that the volumetric strain in the element is everywhere equal to its mean value. The virtual work principle is then written in terms of $\bar{\varepsilon}_{ij}$ and $\delta\bar{\varepsilon}_{ij}$ as

$$\int_R \sigma_{ij}[\bar{\varepsilon}_{ij}(u_k)]\delta\bar{\varepsilon}_{ij} dV - \int_R b_i \delta v_i dV - \int_{\partial_2 R} t_i \delta v_i dA = 0.$$

Finally, introducing the finite element interpolation and using the constitutive equation yields the usual system of linear finite element equations but with a modified element stiffness matrix given by

$$k_{aibk}^{(l)} = \int_{V_e^{(l)}} C_{pjql} \bar{B}_{pj}^a \bar{B}_{qlk}^b dV \quad \bar{B}_{pj}^a = \frac{\partial N^a}{\partial x_j} \delta_{ip} + \left(B_{ia}^{(vol)} - \frac{1}{3} \frac{\partial N^a}{\partial x_i} \right) \delta_{pj}.$$

This expression can be integrated using a standard, full integration scheme.

The B-bar method has been implemented in the sample codes FEM_Bbar.mws (MAPLE) or FEM_Bbar.m (MATLAB). The codes can be run with the input file volumetric_locking_demo.txt. Run the codes yourself to verify that the analytical and finite element solutions agree, and there are no signs of hourgassing.

8.6.2.4 Reduced Integration with Hourglass Control

Hourgassing in four-noded quadrilateral and eight-noded brick elements can also be cured by adding an artificial stiffness to the element that acts to constrain the hourglass mode. The stiffness must be carefully chosen so as to influence *only* the hourglass mode. Only the final result will be given here [for details, see Flanagan and Belytschko 1981]. To compute the corrective term, do the following:

1. Define a series of “hourglass base vectors” $\Gamma^{a(i)}$ that specify the displacements of the a th node in the i th hourglass mode. The four-noded quadrilateral element has only one hourglass mode; the eight-noded brick has four modes, listed in Table 8.12.
2. Calculate the “hourglass shape vectors” for each mode as follows:

$$\gamma^{a(i)} = \Gamma^{a(i)} - \frac{\partial N^a(\xi = \mathbf{0})}{\partial x_j} \sum_{b=1}^{N_e} \Gamma^{b(i)} x_j^b,$$

where N_e denotes the number of nodes on the element.

3. The modified stiffness matrix for the element is written as

$$k_{aibk}^{(l)} = \int_{V_e^{(l)}} C_{ijkl} \frac{\partial N^a(\mathbf{x})}{\partial x_j} \frac{\partial N^b(\mathbf{x})}{\partial x_l} dV + \kappa V_e^{(l)} \sum_m \gamma^{a(m)} \gamma^{b(m)},$$

where V_e denotes the volume of the element, and κ is a numerical parameter that controls the stiffness of the hourglass resistance. Taking $\kappa = 0.01 \mu (\partial N^a / \partial x_j)(\partial N^a / \partial x_j)$ where μ is the elastic shear modulus works well for most applications. If κ is too large, it will seriously over-stiffen the solid.

TABLE 8.12 Hourglass Base Vectors

Linear quadrilateral	$\Gamma^{a(1)} = (+1, -1, +1, -1)$
	$\Gamma^{a(1)} = (+1, +1, -1, -1, -1+1, +1)$
Linear brick	$\Gamma^{a(2)} = (+1, -1, -1, +1, -1, +1, +1, -1)$
	$\Gamma^{a(3)} = (+1, -1, +1, -1, +1, -1, +1, -1)$
	$\Gamma^{a(4)} = (-1, +1, -1, +1, +1, -1, +1, -1)$

8.6.2.5 Sample Code

Reduced integration with hourglass control has been implemented in the sample code Fem_hourglasscontrol.mws (MAPLE), and Fem_hourglasscontrol.m (MATLAB). When run with the input file volumetric_locking_demo.txt, it produces the results shown in Figure 8.43. Hourgassing has clearly been satisfactorily eliminated.

HEALTH WARNING: Hourglass control is not completely effective: it can fail for finite strain problems and can also cause problems in a dynamic analysis, in which the low stiffness of the hourglass modes can introduce spurious low-frequency vibration modes and low wave speeds.

8.6.3 Hybrid Elements for Modeling Near-Incompressible Materials

The bulk elastic modulus is infinite for a fully incompressible material, which leads to an infinite stiffness matrix in the standard finite element formulation (even if reduced integration is used to avoid locking). This behavior can cause the stiffness matrix for a nearly incompressible material to become ill conditioned, so that small rounding errors during the computation result in large errors in the solution.

Hybrid elements are designed to avoid this problem. They work by including the hydrostatic stress distribution as an additional unknown variable, which must be computed at the same time as the displacement field. This allows the stiff terms to be removed from the system of finite element equations. The procedure is illustrated most easily using isotropic

Reduced integration with hourglass control

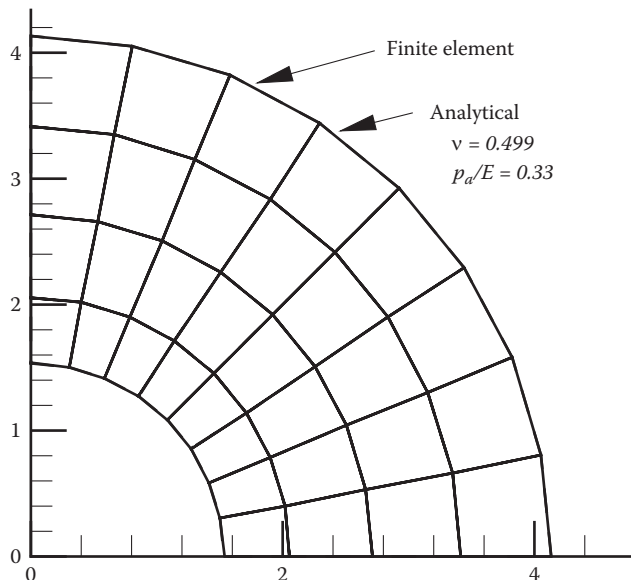


FIGURE 8.43 Comparison of the exact solution to the problem illustrated in Figure 8.38 to the finite element solution obtained using linear elements with reduced integration with hourglass control.

linear elasticity, but, in practice, hybrid elements are usually used to simulate rubbers or metals subjected to large plastic strains.

Hybrid elements are based on a modified version of the principle of virtual work, as follows. The virtual work equation (for small strains) is rewritten as

$$\int_R (S_{ij} \delta \epsilon_{ij}) dV_0 + \int_R p \delta \epsilon_{qq} dV_0 + \int_R \delta p \left(\frac{\sigma_{kk}}{3K} - \frac{p}{K} \right) dV_0 - \int_R b_i \delta v_i dV_0 - \int_{\partial R} t_i^* \delta v_i dA = 0.$$

Here,

1. $S_{ij} = \sigma_{ij} - \sigma_{kk} \delta_{ij} / 3$ is the deviatoric stress, determined from the displacement field.
2. $\sigma_{kk} / 3$ is the hydrostatic stress, again determined from the displacement field.
3. p is an additional degree of freedom that represents the (unknown) hydrostatic stress in the solid.
4. δp is an arbitrary variation in the hydrostatic stress.
5. $K = (1/3) \partial \sigma_{kk} / \partial \epsilon_{pp}$ is the bulk modulus of the solid.

The modified virtual work principle states that, if the virtual work equation is satisfied for all kinematically admissible variations in displacement δv_i and strain $\delta \epsilon_{ij} = (\partial \delta v_i / \partial x_j + \partial \delta v_j / \partial x_i)$ and all possible variations in pressure δp , the stress field will satisfy the equilibrium equations and traction boundary conditions, and the pressure variable p will be equal to the hydrostatic stress in the solid.

The finite element equations are derived in the usual way:

1. The displacement field, virtual displacement field, and position in the each element are interpolated using the standard interpolation functions defined in Sections 8.1.9 and 8.1.10 as

$$u_i = \sum_{a=1}^{N_e} N^a(\xi_j) u_i^a \quad \delta v_i = \sum_{a=1}^{N_e} N^a(\xi_j) \delta v_i^a \quad x_i = \sum_{a=1}^{N_e} N^a(\xi_j) x_i^a.$$

2. Because the pressure is now an independent variable, it must also be interpolated. We write

$$p(\mathbf{x}) = \sum_{a=1}^{N_p} M^a(\xi_j) p^a \quad \delta p(\mathbf{x}) = \sum_{a=1}^{N_p} M^a(\xi_j) \delta p^a \quad x_i = \sum_{a=1}^{N_e} N^a(\xi_j) x_i^a,$$

where p^a are a discrete set of pressure variables, δp^a is an arbitrary change in these pressure variables, M^a are a set of interpolation functions for the pressure, and N_p is the number of pressure variables associated with the element. The pressure need not

be continuous across neighboring elements, so that independent pressure variables can be added to each element. The following schemes are usually used:

- a. In linear elements (the three-noded triangle, four-noded quadrilateral, five-noded tetrahedron, or eight-noded brick) the pressure is constant. The pressure is defined by its value at the centroid of each element, and the interpolation functions are constant.
- b. In quadratic elements (6-noded triangle, 8-noded quadrilateral, 10-noded tetrahedron, or 20-noded brick), the pressure varies linearly in the element. Its value can be defined by the pressure at the corners of each element and interpolated using the standard linear interpolation functions.
3. For an isotropic, linear elastic solid with shear modulus μ and Poisson's ratio ν , the deviatoric stress is related to the displacement field by $S_{ij} = \mu (\delta_{il} \delta_{jk} + \delta_{ik} \delta_{jl} - 2\delta_{ij}\delta_{kl} / 3)$ ($\partial u_k / \partial x_l$), whereas the hydrostatic stress is $\sigma_{kk} / 3 = K(\partial u_k / \partial x_k)$, where $K = E / 3(1 - 2\nu)$ is the bulk modulus.
4. Substituting the linear elastic equations and the finite element interpolation functions into the virtual work principle leads to a system of equations for the unknown displacements u_k^b and pressures p^b of the form

$$\begin{aligned} K_{aibk} u_k^b + Q_{aib} p^b &= F_i^a & \forall \{a, i\}: x_k^a \text{ not on } \partial_1 R \\ Q_{akb} u_k^b - \Pi_{ab} p^b &= 0 \\ u_i^a &= u_i^*(x_i^a) & \forall \{a, i\}: x_k^a \text{ on } \partial_1 R, \end{aligned}$$

where the global stiffness matrices \mathbf{K} , \mathbf{Q} , $\mathbf{\Pi}$ are obtained by summing the following element stiffness matrices

$$\begin{aligned} k_{aibk} &= \int_{V_e} C_{ijkl} \frac{\partial N^a(\mathbf{x})}{\partial x_j} \frac{\partial N^b(\mathbf{x})}{\partial x_l} - K \frac{\partial N^a(\mathbf{x})}{\partial x_i} \frac{\partial N^b(\mathbf{x})}{\partial x_k} dV & q_{aib} &= \int_V \frac{\partial N^a(\mathbf{x})}{\partial x_i} M^b(\mathbf{x}) dV \\ \pi_{ab} &= \int_{V_e} \frac{1}{K} M^a(\mathbf{x}) M^b(\mathbf{x}) dV \end{aligned}$$

and the force \mathbf{F} is defined in the usual way. The integrals defining k_{iakb} may be evaluated using the full integration scheme or reduced integration (hourglass control may be required in this case). The remaining integrals must be evaluated using reduced integration to avoid element locking.

5. Note that, although the pressure variables are local to the elements, they cannot be eliminated from the element stiffness matrix, because doing so would reduce the element stiffness matrix to the usual, nonhybrid form. Consequently, hybrid elements increase the cost of storing and solving the system of equations.

8.7 LIST OF EXAMPLE FEA PROGRAMS AND INPUT FILES

Sample FEA codes, written in MAPLE or MATLAB, can be downloaded from <http://solidmechanics.org/FEA>. MAPLE codes are listed below; in the corresponding MATLAB codes, the extension.mws should be replaced with.m:

1. FEM_1D_Static.mws: Simple static analysis of a 1D bar subjected to axial body force.
2. FEM_1D_newmark.mws: Simple dynamic analysis of a 1D bar subjected to axial body force, using Newmark time integration.
3. FEM_1D_modal.mws: Simple dynamic analysis of a 1D bar subjected to axial body force, using modal time integration.
4. The following files all solve 2D or 3D static linear elastic problems but illustrate various refinements of the FEM:
 - a. FEM_2Dor3D_linelast_standard.mws: 2D(plane strain/stress) or 3D static linear elasticity code with fully integrated elements. The code can be run with the following input files.
 - Linear_elastic_triangles.txt: 2D plane strain problem with two triangular element;
 - Linear_elastic_quad4.txt: 2D plane strain problem with four-noded quadrilateral element;
 - Linear_elastic_quad8.txt: 2D plane strain problem with eight-noded quadrilateral element;
 - Linear_elastic_brick4.txt: 3D problem with four-noded brick element;
 - Linear_elastic_brick20.txt: 3D problem with 20-noded brick element;
 - Linear_elastic_pressurized_cylinder.txt: 2D simulation of a pressurized cylinder;
 - b. FEM_shear_locking_demo.mws: Solves the beam-bending problem discussed in Section 8.6.2 and compares the FEM solution with the exact solution to illustrate shear locking. This version of the code must be run with shear_locking_demo_linear.txt (solution with four-noded quad elements);
 - c. FEM_incompatible_modes.mws: Solves the beam-bending problem discussed in Section 8.6.2 using incompatible mode elements and compares the FEM solution with the exact solution to demonstrate that the elements avoid shear locking. This version of the code must be run with shear_locking_demo_linear.txt (solution with four-noded quad elements);
 - d. FEM_volumetric_locking_demo.mws: Solves the pressurized cylindrical cavity problem discussed in Section 8.6.2 and compares the FEM solution with the exact solution. This version of the code must be run with volumetric_locking_demo_linear.txt (solution with four-noded quad elements) or volumetric_locking_demo_quadratic.txt (solution with eight-noded quadrilateral elements);

- e. FEM_hourglassing_demo.mws: Solves the pressurized cylindrical cavity problem discussed in Section 8.6.2 with reduced integration elements, demonstrating hour-gassing. This version of the code must be run with volumetric_locking_demo_linear.txt (solution with four-noded quad elements);
 - f. FEM_selective_reduced_integration.mws: Solves the pressurized cylindrical cavity problem discussed in Section 8.6.2 using selectively reduced integration and compares the FEM solution with the exact solution. This version of the code must be run with volumetric_locking_demo_quadratic.txt (solution with eight-noded quadrilateral elements);
 - g. FEM_hourglasscontrol.mws: Solves the pressurized cylindrical cavity problem using reduced integration elements with hourglass control and compares the FEM solution with the exact solution. This version of the code must be run with volumetric_locking_demo_linear.txt (solution with four-noded quad elements);
 - h. FEM_Bbar.mws: Solves the pressurized cylinder problem discussed in Section 8.6.2 using the B-bar method and compares the solution with the exact solution. This version of the code must be run with volumetric_locking_demo_linear.txt or volumetric_locking_demo_quadratic.txt;
 - i. FEM_hybrid.mws: Solves the pressurized cylinder problem discussed in Section 8.6.2 using hybrid elements and compares the FEM solution with the exact solution. This version of the code must be run with volumetric_locking_demo_linear.txt or volumetric_locking_demo_quadratic.txt.
5. FEM_2Dor3D_linelast_dynamic.mws: Solves 2D or 3D dynamic linear elasticity problems, using Newmark time integration. The code can be run with the input file Linear_elastic_dynamic_beam.txt.
6. FEM_2Dor3D_modeshapes.mws: Calculates mode shapes and natural frequencies for a linear elastic solid. The code can be run with the input file Linear_elastic_dynamic_beam.txt.
7. FEM_2Dor3D_hypoelastic_static.mws: Solves 2D (plane strain only) or 3D static problems for a hypoelastic material, as discussed in Section 8.3.9. The input file is Hypoelastic_quad4.txt.
8. FEM_2Dor3D_hyperelastic_static.mws: Solves 2D (plane strain only) or 3D static problems for a hyperelastic (neo-Hookean) material. An input file is provided in Hyperelastic_quad4.txt.
9. FEM_2Dor3D_viscoplastic_static.mws: Solves 2D (plane strain only) or 3D static problems for a small strain viscoplastic material. An input file is provided in Viscoplastic_quad4.txt.

This page intentionally left blank

Modeling Material Failure

One of the most important applications of solid mechanics is to design structures, components, or materials that are capable of withstanding cyclic or static service loads. To do this, you need to be able to predict the conditions necessary to cause failure. Materials and structures can fail in many different ways, including by buckling, excessive plastic flow, fatigue and fracture, wear, or corrosion. Calculating the stresses in a structure or component can help to design against these failures but is usually not enough; it is also necessary to understand and to be able to predict the effects of stress.

Fracture mechanics is a subdiscipline of solid mechanics. The goal of the field is to predict the critical loads that will cause catastrophic failure in a material or component. Much of fracture mechanics is based on phenomenological fracture or fatigue criteria, which are calibrated by means of standard tests. The failure criteria are based on current understanding of how materials fail, which is derived from extensive observations of failure mechanisms, together with theoretical models that describe, as far as possible, these mechanisms of failure.

The mechanisms involved in fracture or fatigue failure are complex and are influenced by material and structural features that span 12 orders of magnitude in length scale, as illustrated in Figure 9.1:

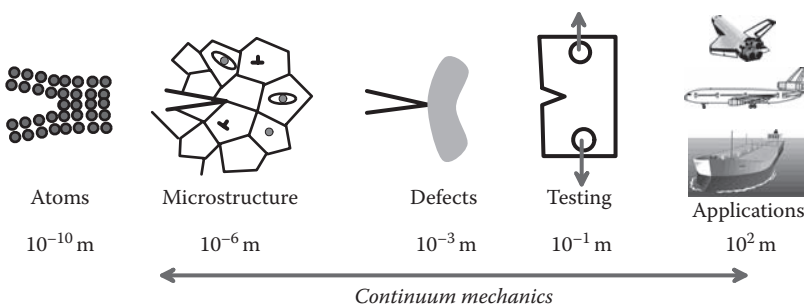


FIGURE 9.1 Length scales of processes involved in fatigue and fracture.

- Most engineering applications involve structures with dimensions of the order of millimeters to kilometers. For many such applications, it is sufficient to measure the maximum cyclic or static stress (or perhaps strain) that the material can withstand and then design the structure to ensure that the stress (or strain) remains below acceptable limits. This involves fairly routine constitutive modeling and numerical or analytical solution of appropriate boundary value problems.
- More critical applications require some kind of *defect tolerance* analysis; perhaps the material or structure is known to contain flaws, and the engineer must decide whether to replace the part, or perhaps it is necessary to specify material quality standards. This kind of decision is usually made using either linear elastic, or plastic, fracture mechanics, which model flaws themselves in detail at length scales of centimeters or below.
- Finally, there is great interest in designing failure resistant materials. In this case, the basic questions are as follows: how does the material fail, and what can be done to the material's microstructure to avoid failure? To answer these questions, we need to understand material behavior at the atomic and microstructural scales. This is a more exploratory field, but solid mechanics has provided insight into a range of issues in this area.

A complete discussion of these issues is beyond the scope of this book. Instead, we will summarize some results in the continuum mechanics of solids that are central to analysis of fracture and fatigue and outline briefly their main applications. Specifically, we will give the following:

1. A brief review of the mechanisms of failure and fatigue
2. An overview of phenomenological stress- or strain-based failure criteria, primarily used in design applications
3. A brief discussion of the mechanics of cracks in solids

9.1 SUMMARY OF MECHANISMS OF FRACTURE AND FATIGUE UNDER STATIC AND CYCLIC LOADING

Before discussing the various approaches to modeling fracture, fatigue, and failure, it is helpful to review briefly the features and mechanisms of failure in solids.

9.1.1 Failure under Monotonic Loading

If you test a sample of any material under uniaxial tension, it will eventually fail. The features of the failure depend on several factors, including the following:

- The materials involved and their microstructure
- The applied stress state (particularly the hydrostatic stress)

- Loading rate
- Temperature
- Ambient environment (water vapor, or presence of corrosive environments)

Materials are normally classified loosely as either “brittle” or “ductile” depending on the characteristic features of the failure. Typical stress-strain curves for brittle and ductile materials are shown in Figure 9.2.

Examples of brittle materials include refractory oxides (ceramics) and intermetallics, as well as BCC metals at low temperature (below about one-quarter of the melting point). Features of a brittle material are as follows:

1. Very little plastic flow occurs in the specimen before failure.
2. The two sides of the fracture surface fit together very well after failure.
3. The fracture surface appears faceted; you can make out individual grains and atomic planes.
4. In many materials, fracture occurs along certain crystallographic planes. In other materials, fracture occurs along grain boundaries.

Examples of ductile materials include FCC metals at all temperatures, BCC metals at high temperatures, and polymers at high temperature. Features of a ductile fracture are as follows:

1. Extensive plastic flow occurs in the material before fracture.
2. There is usually evidence of considerable necking in the specimen.
3. Fracture surfaces do not fit together.
4. The fracture surface has a dimpled appearance; you can see little holes, often with second phase particles inside them.

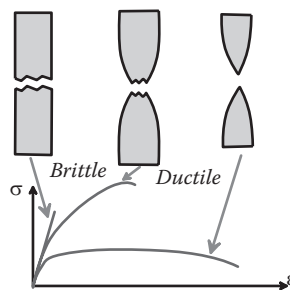


FIGURE 9.2 Typical stress-versus-strain curves during testing to failure under uniaxial tension.

Of course, some materials (especially composites) have such a complex microstructure that it is hard to classify them as entirely brittle or entirely ductile.

Brittle fracture often occurs as a result of a single crack propagating through the specimen. Some materials contain preexisting cracks, in which case fracture is initiated when one of these cracks in a region of high tensile stress starts to grow. In other materials, the origin of the fracture is less clear: various mechanisms for nucleating crack have been suggested, including dislocation pile up at grain boundaries or intersections of dislocations.

Ductile fracture occurs as a result of the nucleation, growth, and coalescence of voids in the material. Failure is controlled by the rate of nucleation of the voids, their rate of growth, and the mechanism of coalescence. High tensile hydrostatic stress promotes rapid void nucleation and growth, but void growth generally also requires significant bulk plastic strain.

A ductile material may also fail as a result of *plastic instability*, such as necking, or the formation of a shear band. This is analogous to buckling: at a critical strain, the component no longer deforms uniformly, and the deformation *localizes* to a small region of the solid. This is normally accompanied by a loss of load-bearing capacity and a large increase in plastic strain rate in the localized region, which eventually causes failure.

Finally, some materials, especially brittle materials such as glasses, and oxide-based ceramics, suffer from a form of time-delayed failure under steady loading, known as *static fatigue*. Automatic coffee-maker jugs are particularly susceptible to static fatigue. You use one for a couple of years, and then one day it shatters if you tap it against the side of the sink. This is because the jug's strength has degraded with time. Static fatigue in brittle materials is a consequence of corrosion crack growth. The highly stressed material near a crack tip is particularly susceptible to chemical attack (the stress increases the rate of chemical reaction). Material near the crack tip may be dissolved altogether, or it may form a reaction product with very low strength. In either event, the crack slowly propagates through the solid, until it becomes long enough to trigger brittle fracture. Glasses and oxide-based ceramics are particularly susceptible to attack by water vapor (and perhaps coffee).

9.1.2 Failure under Cyclic Loading

Mechanical engineers generally have to design components to withstand *cyclic* as opposed to static loading. Under cyclic loading, materials fail by fatigue. Fatigue failure is a familiar phenomenon, but a detailed understanding of the mechanisms involved and the ability to model them quantitatively have only emerged in the past 50 years, driven largely by the demands of the aerospace industry. There are some forms of fatigue failure (contact fatigue is an example) in which the mechanisms involved are still a mystery.

Fatigue life is measured by subjecting the material to cyclic loading. The loading is usually uniaxial tension, but other cycles such as torsion or bending can be used as well. The cycle can be stress controlled (subjecting the material to a prescribed stress) or strain

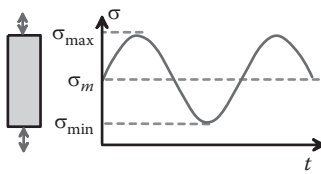


FIGURE 9.3 Cyclic loading used to measure fatigue life.

controlled. A cyclic uniaxial stress-versus-time curve is sketched in Figure 9.3. The cycle is usually characterized by the following:

- The stress amplitude: $(\sigma_{\max} - \sigma_{\min})/2$
- The mean stress: $\sigma_m = (\sigma_{\max} + \sigma_{\min})/2$
- The stress ratio: $R = \sigma_{\min}/\sigma_{\max}$

A rotating bending test is a particularly convenient way to subject a material to a very large number of cycles in a short period of time. The shaft can easily be spun at 2000 rpm, allowing the material to be subjected to 10^7 cycles in less than 100 hours. Pulsating tension is more common in service loading, but a servo-hydraulic tensile testing machine operating at 1 Hz takes nearly 4 months to complete 10^7 cycles.

The resistance of a material to cyclic loading is characterized by plotting an “S-N” curve showing the number of cycles to failure as a function of stress amplitude. The characteristic features of an S-N curve are illustrated in Figure 9.4:

1. The plot normally shows two different regimens of behavior, depending on stress amplitude.
2. At high stress levels, the material deforms plastically and fails rapidly. In this regimen, the life of the specimen depends primarily on the plastic strain amplitude rather than the stress amplitude. This is referred to as “low cycle fatigue” behavior.
3. At lower stress levels, life has a power law dependence on stress. This is referred to as “high cycle” fatigue behavior.
4. In some materials, there is a clear *fatigue limit*. If the stress amplitude lies below a certain limit, the specimen remains intact forever. In other materials, there is no clear fatigue threshold. In this case, the stress amplitude at which the material survives 10^8 cycles is taken as the *endurance limit* of the material. (The term “endurance” appears to refer to the engineer doing the testing rather than the material).

Fatigue life is sensitive to the mean stress, or R ratio, and tends to fall rather rapidly as R increases. It is also influenced by environment, and temperature, and can be very sensitive to details such as the surface finish of the specimen.

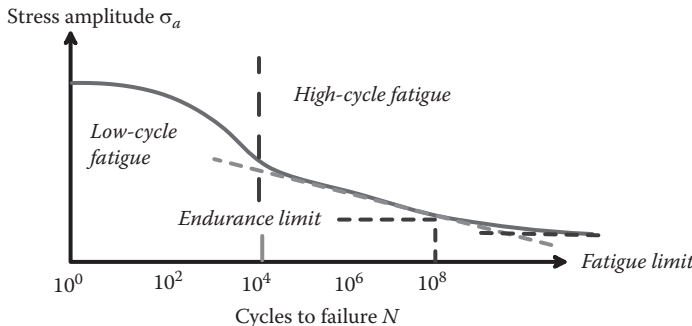


FIGURE 9.4 Typical cycles to failure N as a function of stress amplitude during fatigue failure.

A tensile specimen that has failed by fatigue looks at first sight as though it might have failed by brittle fracture. The fracture surface is flat, and the two sides of the specimen fit together quite well. In fact, for some time, it was thought that some bizarre metallurgical process was responsible for turning a ductile material brittle under cyclic loading. (An engineer named Nevil Norway wrote a successful novel based on this theory [Shute 2000]). A closer examination reveals several differences, however. You usually do not see cleavage planes on a fatigue surface and instead often observe a set of nearly parallel ridges on the surface, spaced at distances between a few 100 Å to a few tenths of micrometers apart. These ridges are known as “striations” and are marks left behind by the tip of a fatigue crack at each cycle of load. In many materials, there is evidence for local areas of cleavage fracture or void coalescence interspersed with the striations.

Fatigue failures are caused by slow crack growth through the material. The failure process involves four stages:

1. Crack initiation
2. Microcrack growth (with crack length less than the materials grain size) (Stage I)
3. Macrocrack growth (crack length between 0.1 and 10 mm) (Stage II)
4. Failure by fast fracture

Cracks will generally only initiate in the presence of cyclic plasticity. However, *bulk* plastic flow in the specimen is not necessary: plastic flow may be caused by local stress concentrations at notches, in part, attributable to geometric defects such as dents or scratches in the surface or even attributable to microstructural features such as large inclusions in the material. In a smooth, clean specimen, the cracks form where “persistent slip bands” reach the surface of the specimen. Plastic flow in a material is generally highly inhomogeneous at the micrometer scale, with the deformation confined to narrow localized bands of slip. Where these bands intersect the surface, intrusions or extrusions form, as sketched in Figure 9.5. Intrusions serve as nucleation sites for cracks.

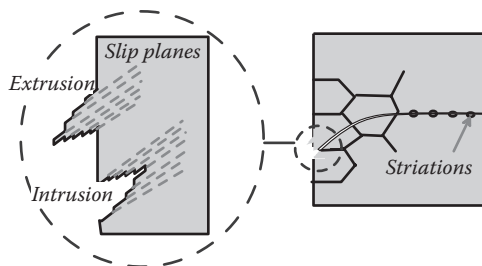


FIGURE 9.5 Mechanism for initiating fatigue cracks.

Cracks initially propagate along the slip bands at around 45° to the principal stress direction—this is known as Stage I fatigue crack growth. When the cracks reach a length comparable with the materials grain size, they change direction and propagate perpendicular to the principal stress. This is known as Stage II fatigue crack growth.

9.2 STRESS- AND STRAIN-BASED FRACTURE AND FATIGUE CRITERIA

Many of the most successful design procedures use simple, experimentally calibrated, functions of stress and strain to assess the likelihood of failure in a component. Some examples of commonly used failure criteria are summarized in this section.

9.2.1 Stress-Based Failure Criteria for Brittle Solids and Composites

Experiments show that brittle solids (such as ceramics, glasses, and fiber-reinforced composites) tend to fail when the stress in the solid reaches a critical magnitude. Materials such as ceramics and glasses can be idealized using an *isotropic* failure criterion. Composite materials are stronger when loaded in some directions than others and must be modeled using an *anisotropic* failure criterion:

- Failure criteria for isotropic materials: The simplest brittle fracture criterion states that fracture is initiated when the greatest tensile principal stress in the solid reaches a critical magnitude, $\sigma_{1\max} = \sigma_{TS}$. (The subscript TS stands for tensile strength). To apply the criterion, you must measure (or look up) σ_{TS} for the material. σ_{TS} can be measured by conducting tensile tests on specimens; it is important to test a large number of specimens because the failure stress is likely to show a great deal of statistical scatter. The tensile strength can also be measured using beam-bending tests. The failure stress measured in a bending test is referred to as the “modulus of rupture” σ_r for the material. It is nominally equivalent to σ_{TS} but in practice usually turns out to be somewhat higher. Next, you must calculate the anticipated stress distribution in your component or structure (e.g., using FEM). Finally, you plot contours of principal stress and find the maximum value $\sigma_{1\max}$. If $\sigma_{1\max} < \sigma_{TS}$, the design is safe (but be sure to use an appropriate factor of safety!).
- Failure criteria for anisotropic materials: More sophisticated criteria must be used to model anisotropic materials (especially composites). The criteria must take account

for the fact that the material is stronger in some directions than others. For example, a fiber-reinforced composite is usually much stronger when loaded parallel to the fiber direction than when loaded transverse to the fibers. There are many different ways to account for this anisotropy. A few approaches are summarized below.

9.2.1.1 Orientation-Dependent Fracture Strength

One approach is to make the tensile strength of the solid orientation dependent. For example, the tensile strength of a brittle, orthotropic solid (with three distinct, mutually perpendicular characteristic material directions) could be characterized by its tensile strengths σ_{TS1} , σ_{TS2} , σ_{TS3} parallel to the three characteristic directions $\{\mathbf{e}_1, \mathbf{e}_2, \mathbf{e}_3\}$ in the solid. The tensile strength when loaded parallel to a general direction $\mathbf{n} = \sin\phi\cos\theta\mathbf{e}_1 + \sin\phi\sin\theta\mathbf{e}_2 + \cos\phi\mathbf{e}_3$ could be interpolated between these values as

$$\sigma_{TS}(\mathbf{n}) = (\sigma_{TS1} \cos^2 \theta + \sigma_{TS2} \sin^2 \theta)\sin^2 \phi + \sigma_{TS3} \cos^2 \phi,$$

where (ϕ, θ) are illustrated in Figure 9.6. The material fails if the stress acting normal to any plane in the solid exceeds the fracture stress for that plane, i.e.,

$$n_i(\theta, \phi)\sigma_{ij}n_j(\theta, \phi) = \sigma_{TS}(\phi, \theta),$$

where σ_{ij} are the stress components in the basis $\{\mathbf{e}_1, \mathbf{e}_2, \mathbf{e}_3\}$. To use this criterion to check for failure at any point in the solid, you must do the following:

1. Find the components of stress in the $\{\mathbf{e}_1, \mathbf{e}_2, \mathbf{e}_3\}$ basis.
2. Maximize the function $n_i(\theta, \phi)\sigma_{ij}n_j(\theta, \phi)/\sigma_{TS}(\phi, \theta)$ with respect to (ϕ, θ) .
3. Check whether the maximum value of $n_i(\theta, \phi)\sigma_{ij}n_j(\theta, \phi)/\sigma_{TS}(\phi, \theta)$ exceeds 1. If so, the material will fail; if not, it is safe.

9.2.1.2 Goldenblat–Kopnov Failure Criterion

A very general phenomenological failure criterion can be constructed by simply combining the stress components in a basis oriented with respect to material axes as polynomial

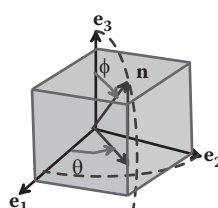


FIGURE 9.6 Coordinate system for characterizing anisotropic fracture strength of a material.

function. The *Goldenblat–Kopnov* criterion is one example, which states that the critical stresses required to cause failure satisfy the equation

$$A_{ij}\sigma_{ij} + B_{ijkl}\sigma_{ij}\sigma_{kl} = 1.$$

Here, \mathbf{A} and \mathbf{B} are material constants: \mathbf{A} is *diagonal* ($A_{ij} = 0$ $i \neq j$) and \mathbf{B} has the same symmetries as the elasticity tensor, i.e., $B_{ijkl} = B_{klji} = B_{jikl} = B_{ijlk}$. The most general anisotropic material would therefore be characterized by 24 independent material constants, but, in practice, simplified versions have far fewer parameters. Most failure criteria for composites are in fact special cases of the Goldenblat–Kopnov criterion, including the Tsai–Hill criterion outlined below.

9.2.1.3 Tsai–Hill Criterion

The Tsai–Hill criterion is used to model damage in brittle laminated fiber-reinforced composites and wood. A specimen of laminated composite subjected to in-plane loading is sketched in Figure 9.7. The Tsai–Hill criterion assumes that a plane stress state exists in the solid. Let σ_{11} , σ_{22} , σ_{12} denote the nonzero components of stress, with basis vectors \mathbf{e}_1 and \mathbf{e}_2 oriented parallel and perpendicular to the fibers in the sheet, as shown. The Tsai–Hill failure criterion is

$$\left(\frac{\sigma_{11}}{\sigma_{TS1}}\right)^2 + \left(\frac{\sigma_{22}}{\sigma_{TS2}}\right)^2 - \frac{\sigma_{11}\sigma_{22}}{\sigma_{TS1}^2} + \frac{\sigma_{12}^2}{\sigma_{SS}^2} = 1$$

at failure, where σ_{TS1} , σ_{TS2} , and σ_{SS} are material properties. They are measured as follows:

1. The laminate is loaded in uniaxial tension parallel to the fibers. The material fails when $\sigma_{11} = \sigma_{TS1}$.
2. The laminate is loaded in uniaxial tension perpendicular to the fibers. The material fails when $\sigma_{22} = \sigma_{TS2}$.
3. In principle, the laminate could be loaded in shear; it would then fail when $\sigma_{12} = \sigma_{SS}$. In practice, it is preferable to pull on the laminate in uniaxial tension with stress σ_0 at 45° to the fibers, which induces stress components $\sigma_{11} = \sigma_{22} = \sigma_{12} = \sigma_0/2$. A simple calculation then shows that $\sigma_{SS} = \sigma_{TS2}\sigma_0 / \sqrt{4\sigma_{TS2}^2 - \sigma_0^2}$.

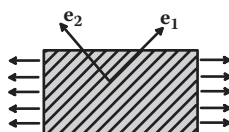


FIGURE 9.7 Basis vectors parallel and perpendicular to fibers in a laminated composite.

9.2.2 Probabilistic Design Methods for Brittle Fracture (Weibull Statistics)

The fracture criterion $\sigma_{1\max} = \sigma_{TS}$ is too crude for many applications. The tensile strength of a brittle solid usually shows considerable statistical scatter, because the likelihood of failure is determined by the probability of finding a large flaw in a highly stressed region of the material. This makes it difficult to determine an unambiguous value for tensile strength: should you use the median value of your experimental data? Pick the stress level where 95% of specimens survive? It is better to deal with this problem using a more rigorous statistical approach.

Weibull statistics refers to a technique used to predict the probability of failure in a brittle material. The following approach is used:

1. Test a large number of samples with identical size and shape under uniform tensile stress and determine their survival probability as a function of stress (survival probability is approximated by the fraction of specimens that survive a given stress level).
2. Fit the survival probability of these specimens. P_s is fit by a Weibull distribution

$$P_s(V_0) = \exp\left\{-\left(\frac{\sigma}{\sigma_0}\right)^m\right\},$$

where σ_0 and m are material constants. The distribution is illustrated in Figure 9.8. The index m is typically of the order 5–10 for ceramics and is independent of specimen volume. The parameter σ_0 is the stress at which the probability of survival is $\exp(-1)$ (about 37%). This critical stress σ_0 depends on the specimen volume V_0 and is smaller for larger specimens.

3. Given m , σ_0 , and the corresponding specimen volume V_0 , the survival probability of a volume V of material subjected to uniform uniaxial stress σ follows as

$$P_s(V) = \exp\left\{-\frac{V}{V_0}\left(\frac{\sigma}{\sigma_0}\right)^m\right\}.$$

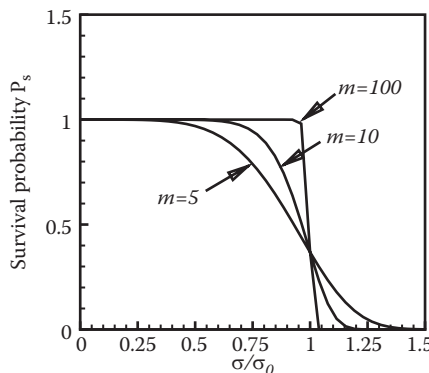


FIGURE 9.8 Examples of Weibull distributions.

To see this, note that the volume V can be thought of as containing $n = V/V_0$ specimens. The probability that they all survive is $\{P_s(V_0)\}^n = \{P_s(V_0)\}^{V/V_0}$.

- More generally, the survival probability of a solid subjected to an arbitrary stress distribution with principal values $\sigma_1, \sigma_2, \sigma_3$ can be computed as

$$\log P_s = -\frac{1}{V_0 \sigma_0^m} \int_V \left(\langle \sigma_1 \rangle^m + \langle \sigma_2 \rangle^m + \langle \sigma_3 \rangle^m \right) dV,$$

where

$$\langle \sigma \rangle = \begin{cases} \sigma & \sigma \geq 0 \\ 0 & \sigma \leq 0. \end{cases}$$

This approach is quite successful in some applications: for example, it explains why brittle materials appear to be stronger in bending than in uniaxial tension. Like many statistical approaches, it has some limitations as a design tool. The method can predict accurately the stress that gives 30% probability of failure. But who wants to buy a product that has a 30% probability of failure? For design applications, we need to predict the probability of one failure in a million or so. It is very difficult to measure the *tail* of a statistical distribution accurately, and a distribution that was fit to predict 63% failure probability may be wildly inaccurate in the region of interest.

9.2.3 Static Fatigue Criterion for Brittle Materials

“Static fatigue” refers to the progressive reduction in tensile strength of a stressed brittle material with time. The simplest way to model static fatigue is to make the tensile strength of the material a function of time and applied stress. The usual approach is to set

$$\sigma_{TS} = \sigma_{TS0} \left(1 - \alpha \int (\sigma / \sigma_{TS0})^m dt \right),$$

where $\sigma(t)$ is the maximum principal stress acting on the solid, which may vary slowly with time t ; σ_{TS0} is the tensile strength of the solid at time $t = 0$, and α, m are two material constants. Typically, m has values between 5 and 10. For the particular case of a *constant* stress, we see that

$$\sigma_{TS} = \sigma_{TS0} (1 - \alpha (\sigma / \sigma_{TS0})^m t).$$

Because failure occurs when $\sigma = \sigma_{TS}$, the time to failure follows as

$$t_f = \frac{1}{\alpha} \left(\frac{\sigma_{TS0}}{\sigma} \right)^m \left(1 - \frac{\sigma}{\sigma_{TS0}} \right) \approx \frac{1}{\alpha} \left(\frac{\sigma_{TS0}}{\sigma} \right)^m$$

so that α and m can easily be determined by measuring the time to failure in uniaxial tension as a function of applied stress.

Under multiaxial loading, the maximum principal tensile stress should be used for σ .

9.2.4 Constitutive Laws for Crushing Failure of Brittle Materials

Brittle materials are generally used in applications in which they are subjected primarily to compressive stress. Brittle materials are very strong in compression, but they will fail if subjected to combined hydrostatic compression and shear (e.g., by loading in uniaxial compression). Failure in compression is a consequence of *distributed microcracking* in the solid: large numbers of small cracks nucleate, propagate for a short while, and then arrest. Failure occurs as a result of coalescence of these cracks. A typical stress-strain curve during compression of a brittle material, such as concrete, is illustrated in Figure 9.9. Failure in compression is less catastrophic than tension and, in some respects, qualitatively resembles metal plasticity. For plastically deforming metals, however, the stress-strain curve is independent of hydrostatic stress. In contrast, the crushing resistance of a brittle material increases with hydrostatic compression.

This type of crushing is often modeled using constitutive equations based on small-strain metal plasticity. The governing equations for a simple, small strain, constitutive model of this form will be summarized briefly here. A more detailed discussion of plasticity theory is given in Section 3.7.

The material is characterized by the following properties:

- The Young's modulus E and Poisson's ratio ν
- The stress-versus-plastic strain curve measured from a uniaxial compression test, which is fit by a functional relation of the form $\sigma = -Y(\bar{\varepsilon}^p)$, where $\bar{\varepsilon}^p$ is the magnitude of the compressive strain. Any of the functions listed in Section 3.7.5 could be used for the function Y
- A material constant c , which controls how rapidly the strength of the material increases with hydrostatic compression

The constitutive equations specify a relationship between an increment in stress $d\sigma_{ij}$ applied to the material and an increment in strain $d\varepsilon_{ij}$, as follows:

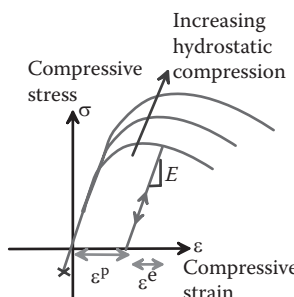


FIGURE 9.9 Typical crushing response of a brittle material.

1. The strain is decomposed into elastic and irreversible (damage) parts as $d\epsilon_{ij} = d\epsilon_{ij}^e + d\epsilon_{ij}^p$.
2. The elastic part of the strain is related to the stress by the linear elastic constitutive equations

$$d\epsilon_{ij}^e = \frac{1+\nu}{E} d\sigma_{ij} - \frac{\nu}{E} d\sigma_{kk} \delta_{ij}.$$

3. The critical stress that initiates crushing damage is given by a failure criterion (analogous to the yield criterion for a metal) of the form

$$f(\sigma_{ij}) = \sqrt{\frac{3}{2} S_{ij} S_{ij}} + 3cp - (1-c)Y(\bar{\epsilon}^p) = 0,$$

where $p = \sigma_{kk}/3$, $S_{ij} = \sigma_{ij} - p\delta_{ij}$, and $\bar{\epsilon}^p = \int \sqrt{2d\epsilon_{ij}^p d\epsilon_{ij}^p / 3}$ is the accumulated irreversible strain. Notice that the failure criterion depends on the hydrostatic part of the stress: unlike yield in metals, the material becomes more resistant to fracture if $p < 0$.

4. The plastic strain components are determined using an associated flow rule

$$d\epsilon_{ij}^p = \frac{d\bar{\epsilon}^p}{\sqrt{1+2c^2}} \frac{df}{d\sigma_{ij}} = \frac{d\bar{\epsilon}^p}{\sqrt{1+2c^2}} \left\{ \frac{3}{2} \frac{S_{ij}}{\sqrt{3S_{kl}S_{kl}/2}} + c\delta_{ij} \right\}.$$

5. The magnitude of the plastic strain increment is related to the stress increment by

$$d\bar{\epsilon}^p = \frac{1}{h(1-c)} \left\langle \frac{3}{2} \frac{S_{ij} d\sigma_{ij}}{\sqrt{3S_{kl}S_{kl}/2}} + cd\sigma_{kk} \right\rangle,$$

where $h = dY/\bar{\epsilon}^p$ is the slope of the uniaxial stress-strain curve, and $\langle x \rangle = x$ for $x > 0$, whereas $\langle x \rangle = 0$ for $x < 0$.

HEALTH WARNING: These constitutive equations should only be used in regions in which the hydrostatic stress is compressive ($p < 0$). In regions of hydrostatic tension, a tensile brittle fracture criterion should be used; for example, the material could be assumed to lose all load-bearing capacity if the principal tensile stress exceeds a critical magnitude.

9.2.5 Ductile Fracture Criteria

9.2.5.1 Strain to Failure Approach

Ductile fracture in tension occurs by the nucleation, growth, and coalescence of voids in the material. A crude criterion for ductile failure could be based on the accumulated plastic strain, for example,

$$\int \sqrt{\frac{2}{3} d\epsilon_{ij}^p d\epsilon_{ij}^p} = \epsilon_f$$

at failure, where ϵ_f is the plastic strain to failure in a uniaxial tensile test.

9.2.5.2 Porous Metal Plasticity

Experiments show that the strain to cause ductile failure in a material depends on the hydrostatic component of tensile stress acting on the specimen, as shown in Figure 9.10. For example, the strain to failure under torsional loading (which subjects the material to shear with no hydrostatic stress) is much greater than under uniaxial tension. The critical strain is influenced by hydrostatic stress because ductile failure occurs as a result of the nucleation and growth of cavities in the solid. A hydrostatic stress greatly increases the rate of growth of the cavities. The simple strain-to-failure approach cannot account for this behavior.

Porous metal plasticity was developed to address this issue. The basic idea is simple: the solid is idealized as a plastic matrix that contains a volume fraction V_f of cavities. To model the solid, the plastic stress-strain laws outlined in Sections 3.7 and 3.8 are extended to calculate the volume fraction of voids in the material as part of the solution and also to account for the weakening effect of the voids. Failure is modeled by constructing the plastic stress-strain law so that the material loses all its strength at a critical void volume fraction.

Both rate independent and viscoplastic versions of porous plasticity exist. The viscoplastic models have some advantages for finite element computations, because the rate dependence can stabilize the effects of strain softening. A simple small strain viscoplastic constitutive law with power-law hardening and power-law rate dependence will be outlined here to illustrate the main features of these models. The constitutive law is known as the “Gurson model.”

The material is characterized by the following properties:

- The Young's modulus E and Poisson's ratio ν
- A characteristic stress Y , a characteristic strain ε_0 and strain hardening exponent n , which govern the strain hardening behavior of the matrix material
- A characteristic strain rate $\dot{\varepsilon}_0$ and strain rate exponent m , which govern the strain rate sensitivity of the solid
- A constant N_v , which controls the rate of void nucleation with plastic straining
- The flow strength of the matrix σ_0 , the void volume fraction, V_f , and the total accumulated effective plastic strain in the matrix material $\bar{\varepsilon}_m$, which all evolve with plastic straining

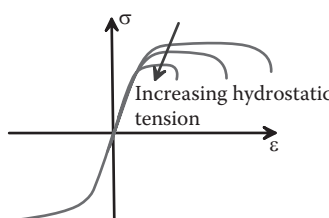


FIGURE 9.10 Typical stress-strain curve for a porous plastic material.

The constitutive equations specify a relationship between the stress σ_{ij} applied to the material and the resulting strain rate $\dot{\epsilon}_{ij}$, as follows:

1. The strain rate is decomposed into elastic and plastic parts as $\dot{\epsilon}_{ij} = \dot{\epsilon}_{ij}^e + \dot{\epsilon}_{ij}^p$.
2. The elastic part of the strain rate is related to the stress rate by the linear elastic constitutive equations

$$\dot{\epsilon}_{ij}^e = \frac{1+\nu}{E} \dot{\sigma}_{ij} - \frac{\nu}{E} \dot{\sigma}_{kk} \delta_{ij}.$$

3. The magnitude of the plastic strain rate is determined by the following plastic flow potential:

$$\dot{\epsilon}_e = g(\sigma_e, p, \sigma_0, V_f) = \dot{\epsilon}_0 \left[\left(\frac{\sigma_e}{\sigma_0} \right)^2 + 2V_f \cosh \left(\frac{3p}{2\sigma_0} \right) - V_f^2 \right]^{m/2},$$

where $\dot{\epsilon}_e = 2\dot{\epsilon}_{ij}^p \dot{\epsilon}_{ij}^p / 3$, $\sigma_e = \sqrt{3S_{ij}S_{ij}/2}$, $p = \sigma_{kk}/3$, and $S_{ij} = \sigma_{ij} - p\delta_{ij}$. Note that for $V_f > 0$ the plastic strain rate increases with hydrostatic stress p .

4. The components of the plastic strain rate tensor are computed from an associated flow law:

$$\begin{aligned} \dot{\epsilon}_{ij}^p &= \sqrt{\frac{3}{2}} \frac{g(\sigma_e, p, \sigma_0, V_f)}{\left[(\partial g / \partial \sigma_{kl})(\partial g / \partial \sigma_{kl}) \right]^{1/2}} \frac{\partial g}{\partial \sigma_{ij}} \\ &= \frac{g(\sigma_e, p, \sigma_0, V_f)}{\sqrt{\sigma_e^2 / \sigma_0^2 + (V_f^2 / 2) \sinh^2(3p / 2\sigma_0)}} \left\{ \frac{3}{2} \frac{S_{ij}}{\sigma_0} + \frac{V_f}{2} \sinh \left(\frac{3p}{2\sigma_0} \right) \delta_{ij} \right\}. \end{aligned}$$

5. Strain hardening in the matrix is modeled by relating its flow stress σ_0 to the accumulated strain in the matrix $\bar{\epsilon}_m$. The following power-law hardening model is often used:

$$\sigma_0 = Y(1 + \bar{\epsilon}_m / \epsilon_0)^{1/n}.$$

6. The effective plastic strain in the matrix is calculated from the condition that the plastic dissipation in the matrix must equal the rate of work done by stresses, which requires that

$$(1 - V_f) \sigma_0 \dot{\bar{\epsilon}}_m = \sigma_{ij} \dot{\epsilon}_{ij}^p \Rightarrow \dot{\bar{\epsilon}}_m = \frac{g(\sigma_e, p, \sigma_0, V_f)}{(1 - V_f)} \left(\frac{\sigma_e^2}{\sigma_0^2} + \frac{3p}{2\sigma_0} V_f \sinh \left(\frac{3p}{2\sigma_0} \right) \right).$$

7. Finally, the model is completed by specifying the void volume fraction as a function of strain. The void volume fraction can increase as a result of growth of existing voids or nucleation of new ones. To account for both effects, one can set

$$\dot{V}_f = (1 - V_f) \dot{\epsilon}_{kk}^p + N_v \dot{\epsilon}_e,$$

where the first term accounts for void growth, and the second accounts for strain controlled void nucleation.

9.2.6 Ductile Failure by Strain Localization

If you test a cylindrical specimen of a very ductile material in uniaxial tension, it will initially deform uniformly and remain cylindrical. At a critical load (or strain), the specimen will start to neck, as shown in Figure 9.11. Necking, once it starts, is usually unstable; there is a concentration in stress near the necked region, increasing the rate of plastic flow near the neck compared with the rest of the specimen, and so increasing the rate of neck formation. The strains in the necked region rapidly become very large and quickly lead to failure.

Neck formation is a consequence of *geometric softening*. A very simple model explains the concept of geometric softening:

1. Consider a cylindrical specimen with initial cross-sectional area A_0 and length L_0 . The specimen is subjected to a load P , which deforms the material plastically. After straining, the length of the specimen increases to L , and its cross-sectional area decreases to A .
2. Assume that the material is perfectly plastic and has a true stress-strain curve (Cauchy stress-versus-logarithmic strain) that can be approximated by a power-law $\sigma = \sigma_0 \varepsilon^n$ with $n < 1$.
3. The true strain in the specimen is related to its length by $\varepsilon = \log \frac{L}{L_0}$.
4. The force on the specimen is related to the Cauchy stress by $P = A\sigma = A\sigma_0\varepsilon^n$.
5. At the point of maximum load, $\frac{dP}{dL} = \frac{dA}{dL}\sigma + A\frac{d\sigma}{dL} = 0$.
6. We can calculate dA/dL by noting that the volume of the specimen is constant during plastic straining, which shows that

$$AL = A_0 L_0 \Rightarrow \frac{dA}{dL}L + A = 0 \Rightarrow \frac{dA}{dL} = -\frac{A}{L}.$$

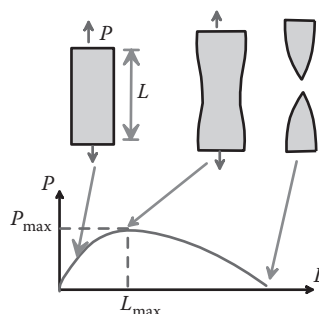


FIGURE 9.11 Load-displacement curve during necking failure.

Notice that dA/dL is negative; this means that the specimen tends to soften as a result of the change in its cross-sectional area. This is what is meant by geometric softening.

7. We can calculate $d\sigma/dL$ from items 2 and 3 as follows:

$$\frac{d\sigma}{dL} = \frac{d\sigma}{d\varepsilon} \frac{d\varepsilon}{dL} = \frac{n\sigma_0 \varepsilon^{n-1}}{L}.$$

Notice that $d\sigma/dL$ is positive; strain hardening in the material tends to compensate for the effects of geometric softening.

8. Finally, substituting the results of items 6 and 7 back into 5 and recalling that $\sigma = \sigma_0 \varepsilon^n$ shows that, at the point of maximum load, the strain and length of the specimen are

$$-\frac{A\sigma}{L} + A \frac{n\sigma_0 \varepsilon^{n-1}}{L} = 0 \Rightarrow \varepsilon_{\max} = n \Rightarrow L_{\max} = L_0 \exp(n).$$

9. Finally, note that, by volume conservation, the cross-sectional area is $A = A_0 L_0 / L$, so the maximum load the specimen can withstand follows as

$$P_{\max} = A\sigma_{\max} = \frac{A_0 L_0}{L} \sigma_0 (\varepsilon_{\max})^n = A_0 \sigma_0 n^n \exp(-n).$$

It turns out that the point of maximum load coincides with the condition for unstable neck formation in the bar. This is plausible: a falling load displacement curve is always a sign that there might be a possibility of non-unique solutions, but a rather sophisticated calculation is required to show this rigorously.

There are two important points to take away from this discussion:

- Plastic localization, as opposed to material failure, may limit load-bearing capacity.
- If you measure the strain to failure of a material in uniaxial tension, it is possible that you have not measured the inherent strength of the material; your specimen may have failed because of a geometric effect. Material behavior does influence the strain to failure, of course: the simple analysis of geometric softening shows that the strain-hardening behavior of the material is critical.

Plastic localization can occur for many reasons. There are two general classes of localization: it may occur as a consequence of changes in specimen geometry (i.e., geometric softening), or it may occur as a result of a natural tendency of the material itself to soften at large strains.

Examples of geometry-induced localization include the following: (1) neck formation in a bar under uniaxial tension, and (2) shear band formation in torsional or shear loading at high strain rate attributable to thermal softening as a result of plastic heat generation.

Examples of material induced localization include the following: (1) localization in a Gurson solid as a result of the softening effect of voids at large strains; (2) localization in a

single crystal as a consequence of the softening effect of lattice rotations; and (3) localization in a brittle microcracking material as a result of the increase in elastic compliance caused by the cracks.

Geometric localization can be modeled quite easily, because it does not rely on any empirical failure criteria. A straightforward FEM computation, with an appropriate constitutive law and proper consideration of finite strains, will predict localization if it is going to occur; the only thing you need to worry about is to be sure you understand what triggered the localization. Localization can start at a geometric imperfection in the model, in which case your prediction is meaningful (but may be sensitive to the nature of the imperfection). It may also be triggered by numerical errors, in which case the predicted failure load is meaningless. It is usually exceedingly difficult to compute what happens *after* localization. Fortunately, it is rather rare to need to do this for design purposes.

9.2.7 Criteria for Failure by High Cycle Fatigue under Constant Amplitude Cyclic Loading

Empirical stress- or strain-based life prediction methods are extensively used in design applications. The approach is straightforward: subject a sample of the material to a cycle of stress (or strain) that resembles service loading, in an environment representative of service conditions, and measure its life as a function of stress (or strain) amplitude, then fit the data with a curve.

Here we will review criteria that are used to predict fatigue life under proportional cyclic loading. A typical stress cycle is parameterized by its amplitude $(\sigma_{\max} - \sigma_{\min})/2$ and the mean stress $\sigma_m = (\sigma_{\max} + \sigma_{\min})/2$, as shown in Figure 9.12.

For tests run in the high cycle fatigue regimen with any fixed value of mean stress, the relationship between stress amplitude σ_a and the number of cycles to failure N is fit well by *Basquin's law*:

$$\sigma_a N^b = C$$

where the exponent b is typically between 0.05 and 0.15. The constant C is a function of mean stress.

There are two ways to account for the effects of mean stress. Both are based on the same idea: we know that, if the mean stress is equal to the tensile strength of the material $\sigma = \sigma_{UTS}$, it will fail in zero cycles of loading. We also know that, for zero mean stress, the fatigue life obeys Basquin's law. We can interpolate between these two points. There are two ways to do this:

- Goodman's rule uses a linear interpolation, giving

$$\sigma_a N^b = C_0 \left(1 - \frac{\sigma_m}{\sigma_{UTS}} \right),$$

where C_0 is the constant in Basquin's law determined by testing at zero mean stress.

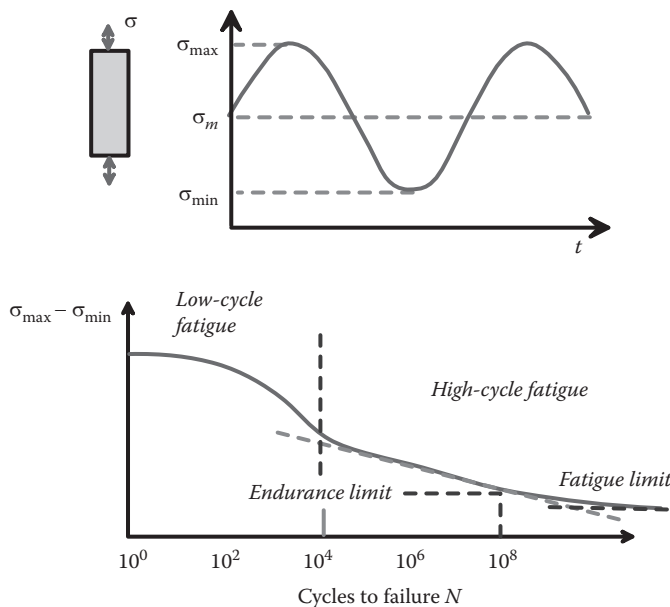


FIGURE 9.12 Typical relationship between stress amplitude and number of cycles to failure during cyclic loading.

- Gerber's rule uses a parabolic fit:

$$\sigma_a N^b = C_0 \left\{ 1 - \left(\frac{\sigma_m}{\sigma_{UTS}} \right)^2 \right\}.$$

In practice, experimental data seem to lie between these two limits. Goodman's rule gives a safe estimate.

These criteria are intended to be used for components that are subjected to uniaxial tensile stress. The criteria can still be used if the loading is *proportional* (i.e., with fixed directions of principal stress). In this case, the maximum principal stress should be used to calculate σ_a and σ_m . They do not work under nonproportional loading. A very large number of fatigue models have been developed for more general loading conditions [for a recent literature review, see Liu and Mahadevan 2005].

9.2.8 Criteria for Failure by Low Cycle Fatigue

If a fatigue test is run with a high stress level (sufficient to cause plastic flow in a large section of the solid), the specimen fails very quickly (less than 10,000 cycles). This regime of behavior is known as low cycle fatigue. The fatigue life correlates best with the plastic strain amplitude rather than stress amplitude, and it is found that the *Coffin–Manson law*

$$\Delta \varepsilon^p N^b = C$$

gives a good fit to empirical data (the constants C and b do not have the same values as for Basquin's law, of course).

9.2.9 Criteria for Failure under Variable Amplitude Cyclic Loading

Fatigue tests are usually done at constant stress (or strain) amplitude. Service loading usually involves cycles with variable (and often random) amplitude. Fortunately, there is a remarkably simple way to estimate fatigue life under variable loading using constant stress data.

Suppose the load history comprises a set of n_1 load cycles at a stress amplitude $\sigma_a^{(1)}$, followed by a set of n_2 cycles at load amplitude $\sigma_a^{(2)}$ and so on (see Figure 9.13). For the i th set of cycles at load amplitude $\sigma_a^{(i)}$, we could compute the number of cycles that would cause the specimen to fail using Basquin's law:

$$\sigma_a^{(i)} N_i^b = C.$$

The *Miner–Palmgren* failure criterion assumes a linear summation of damage attributable to each set of load cycles so that, at failure,

$$\sum_i \frac{n_i}{N_i} = 1.$$

In terms of stress amplitude,

$$\sum_i n_i \left(\frac{\sigma_a^{(i)}}{C} \right)^{1/b} = 1.$$

The same approach works under low cycle fatigue conditions, in which case,

$$\sum_i n_i \left(\frac{\Delta \varepsilon^{p(i)}}{C} \right)^{1/b} = 1.$$

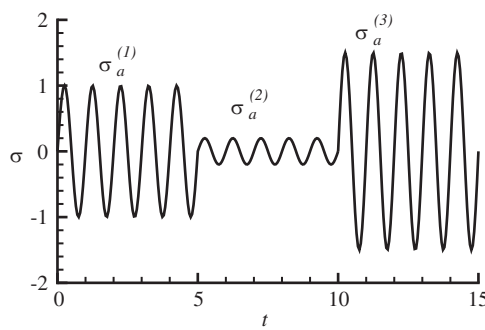


FIGURE 9.13 History of stress during cyclic loading with variable amplitude.

The criterion is often used under random loading. A typical random stress history is illustrated in Figure 9.14. To apply Miner's rule, we need to find a way to estimate the number of cycles of load at a given stress level. There are various ways to do this; one approach is to count the peaks in the load history and compute the probability $P(\sigma)$ of finding a peak at stress level σ . (Of course, this only works if the signal has well-defined peaks; this is not the case for white noise, for example).

Miner's rule then predicts that the number of cycles to failure satisfies

$$N \int_0^{\infty} P(\sigma) \left(\frac{\sigma}{C} \right)^{1/b} d\sigma = 1.$$

9.3 MODELING FAILURE BY CRACK GROWTH: LINEAR ELASTIC FRACTURE MECHANICS

Phenomenological damage models are useful in design applications, but they have many limitations, including the following:

- They require extensive experimental testing to calibrate the model for each application.
- They provide no insight into the relationship between a materials microstructure and its strength.

A more sophisticated approach is to model the mechanisms of failure directly. Crack propagation through the solid, either as a result of fatigue or by brittle or ductile fracture, is by far the most common cause of failure. Consequently, much effort has been devoted to developing techniques to predict the behavior of cracks in solids. Below, we outline some of the most important results.

9.3.1 Crack Tip Fields in an Isotropic, Linear Elastic Solid

Many of the techniques of fracture mechanics rely on the assumption that, if one gets sufficiently close to the tip of the crack, the stress, displacement, and strain fields always have the same distribution, regardless of the geometry of the solid and how it is loaded. The fields near a crack tip are a fundamental result in fracture mechanics.

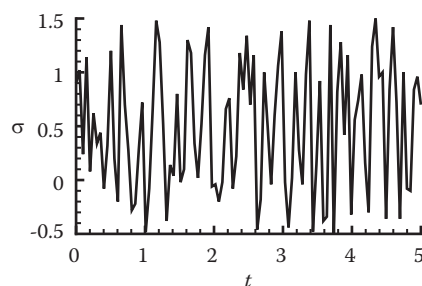


FIGURE 9.14 History of stress during random loading.

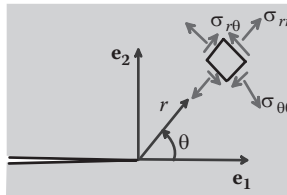


FIGURE 9.15 Coordinate system used to describe stress fields near a crack tip.

Figure 9.15 shows an infinitely large linear elastic solid, with Young's modulus E and Poisson's ratio ν , which contains a crack. The solid is loaded at infinity. Note the following:

- Crack tip fields are most conveniently expressed in terms of cylindrical-polar coordinates (r, θ, z) with origin at the crack tip.
- The displacement and stress near the crack tip can be characterized by three numbers K_I, K_{II}, K_{III} known as *stress intensity factors*. By definition,

$$K_I = \lim_{r \rightarrow 0} \sqrt{2\pi r} \sigma_{22} \quad K_{II} = \lim_{r \rightarrow 0} \sqrt{2\pi r} \sigma_{12} \quad K_{III} = \lim_{r \rightarrow 0} \sqrt{2\pi r} \sigma_{32},$$

with the limit taken along $\theta = 0$.

- The stress intensity factors depend on the detailed shape of the solid and the way that it is loaded. To calculate stress intensity factors, you need to find the full stress field in the solid and then compute the limiting values in the definition. These calculations can be difficult. You can try to find the solution in standard tables of stress intensity factors or, if this fails, use a numerical method (such as FEM). A short table of stress intensity factors for various crack geometries can be found in Section 9.3.3, and FEM techniques are discussed in Section 9.3.4.
- Stress intensity factors have the bizarre units of $Nm^{-3/2}$.
- The physical significance of the three stress intensity factors is illustrated in Figure 9.16. The “mode I” stress intensity factor K_I quantifies the crack opening displacements and stresses, the “mode II” stress intensity factor characterizes in-plane shear displacements and stress, and the “mode III” stress intensity factor quantifies out-of-plane shear displacement of the crack faces and antiplane shear stresses at the crack tip.



FIGURE 9.16 Modes of loading at a crack tip.

The stress field near the crack tip is

$$\begin{aligned}\sigma_{rr} &= \frac{K_I}{\sqrt{2\pi r}} \left(\frac{5}{4} \cos \frac{\theta}{2} - \frac{1}{4} \cos \frac{3\theta}{2} \right) + \frac{K_{II}}{\sqrt{2\pi r}} \left(-\frac{5}{4} \sin \frac{\theta}{2} + \frac{3}{4} \sin \frac{3\theta}{2} \right) \\ \sigma_{\theta\theta} &= \frac{K_I}{\sqrt{2\pi r}} \left(\frac{3}{4} \cos \frac{\theta}{2} + \frac{1}{4} \cos \frac{3\theta}{2} \right) - \frac{K_{II}}{\sqrt{2\pi r}} \left(\frac{3}{4} \sin \frac{\theta}{2} + \frac{1}{4} \sin \frac{3\theta}{2} \right) \\ \sigma_{r\theta} &= \frac{K_I}{\sqrt{2\pi r}} \left(\frac{1}{4} \sin \frac{\theta}{2} + \frac{1}{4} \sin \frac{3\theta}{2} \right) + \frac{K_{II}}{\sqrt{2\pi r}} \left(\frac{1}{4} \cos \frac{\theta}{2} + \frac{3}{4} \cos \frac{3\theta}{2} \right).\end{aligned}$$

Equivalent expressions in rectangular coordinates are

$$\begin{aligned}\sigma_{11} &= \frac{K_I}{\sqrt{2\pi r}} \cos \frac{\theta}{2} \left(1 - \sin \frac{\theta}{2} \sin \frac{3\theta}{2} \right) - \frac{K_{II}}{\sqrt{2\pi r}} \sin \frac{\theta}{2} \left(2 + \cos \frac{\theta}{2} \cos \frac{3\theta}{2} \right) \\ \sigma_{22} &= \frac{K_I}{\sqrt{2\pi r}} \cos \frac{\theta}{2} \left(1 + \sin \frac{\theta}{2} \sin \frac{3\theta}{2} \right) + \frac{K_{II}}{\sqrt{2\pi r}} \cos \frac{\theta}{2} \sin \frac{\theta}{2} \cos \frac{3\theta}{2} \\ \sigma_{12} &= \frac{K_I}{\sqrt{2\pi r}} \cos \frac{\theta}{2} \sin \frac{\theta}{2} \cos \frac{3\theta}{2} + \frac{K_{II}}{\sqrt{2\pi r}} \cos \frac{\theta}{2} \left(1 - \sin \frac{\theta}{2} \sin \frac{3\theta}{2} \right) \\ \sigma_{31} &= -\frac{K_{III}}{\sqrt{2\pi r}} \sin \theta / 2 \quad \sigma_{32} = \frac{K_{III}}{\sqrt{2\pi r}} \cos \theta / 2,\end{aligned}$$

whereas the displacements can be calculated by integrating the strains, with the result

$$\begin{aligned}u_1 &= \frac{K_I}{\sqrt{2\pi}} \sqrt{\frac{r}{2}} \left[1 - 2\nu + \sin^2 \frac{\theta}{2} \right] \cos \frac{\theta}{2} + \frac{K_{II}}{\sqrt{2\pi}} \sqrt{\frac{r}{2}} \left[2 - 2\nu + \cos^2 \frac{\theta}{2} \right] \sin \frac{\theta}{2} \\ u_2 &= \frac{K_I}{\sqrt{2\pi}} \sqrt{\frac{r}{2}} \left[2 - 2\nu + \cos^2 \frac{\theta}{2} \right] \sin \frac{\theta}{2} + \frac{K_{II}}{\sqrt{2\pi}} \sqrt{\frac{r}{2}} \left[-1 + 2\nu + \sin^2 \frac{\theta}{2} \right] \cos \frac{\theta}{2} \\ u_3 &= \frac{K_{III}}{\sqrt{\pi}} \sqrt{\frac{2r}{\pi}} \sin \theta / 2.\end{aligned}$$

Note that the formulas for in-plane displacement components u_1 , u_2 are valid for plane strain deformation only.

9.3.2 Assumptions and Application of Phenomenological Linear Elastic Fracture Mechanics

The objective of linear elastic fracture mechanics is to predict the critical loads that will cause a crack in a solid to grow. For applications involving fatigue or dynamic fracture, the rate and direction of crack growth are also of interest.

The phenomenological theory is based on the following qualitative argument. Consider a crack in a reasonably brittle, isotropic solid. If the solid were ideally elastic, we expect the asymptotic solution listed in the preceding section to become progressively more accurate as we approach the crack tip. Away from the crack tip, the fields are influenced by the geometry of the solid and boundary conditions, and the asymptotic crack tip field is not accurate. In practice, the asymptotic field will also not give an accurate representation of the stress fields very close to the crack tip. The crack may not be perfectly sharp at its tip,

and, if it were, no solid could withstand the infinite stress predicted by the asymptotic linear elastic solution. We therefore anticipate that, in practice, the linear elastic solution will not be accurate very close to the crack tip itself, where material nonlinearity and other effects play an important role. So the actual stress and strain distributions will have three general regions, as shown in Figure 9.17:

1. Close to the crack tip, there will be a process zone, in which the material suffers irreversible damage.
2. A bit further from the crack tip, there will be a region in which the linear elastic asymptotic crack tip field might be expected to be accurate. This is known as the “region of K dominance.”
3. Far from the crack tip, the stress field depends on the geometry of the solid and boundary conditions.

Material failure (crack growth or fatigue) is a consequence of the ugly stuff that goes on in the process zone. Linear elastic fracture mechanics postulates that we don’t need to understand this ugly stuff in detail, because the fields in the process zone are likely to be controlled mainly by the fields in the region of K dominance. The fields in this region depend only on the three stress intensity factors K_I, K_{II}, K_{III} . Therefore, the state in the process zone can be characterized by the three stress intensity factors.

If this is true, the conditions for crack growth, or the rate of crack growth, will be only a function of stress intensity factor and nothing else. We can measure the critical value of K_I, K_{II}, K_{III} required to cause the crack to grow in a standard laboratory test and use this as a measure of the resistance of the solid to crack propagation. For fatigue tests, we can measure crack growth rate as a function of K_I, K_{II}, K_{III} or their history and characterize the relationship using appropriate phenomenological laws.

Having characterized the material, we can then estimate the safety of a structure or component that containing a crack. To do so, calculate the stress intensity factors for the

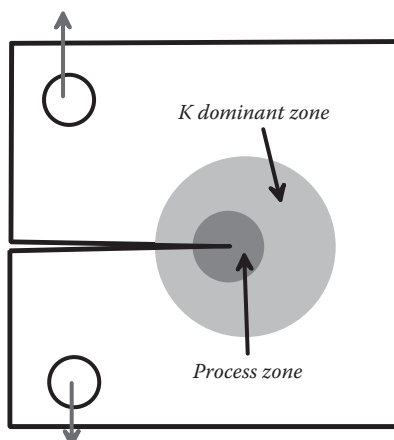


FIGURE 9.17 Characteristic regions of material behavior near a crack tip.

crack in the structure and then use our phenomenological fracture or fatigue laws to decide whether or not the crack will grow.

For example, the fracture criterion under mode I loading is written as

$$K_I \geq K_{IC}$$

for crack growth, where K_{IC} is the critical stress intensity factor for the onset of fracture. The critical stress intensity factor is referred to as the *mode I fracture toughness* of the solid.

Experimentally, it is found that this approach works quite well, provided that the assumptions inherent in linear elastic fracture mechanics are satisfied.

Careful tests and computer simulations have established the following conditions for the applicability of linear elastic fracture mechanics. A representative test specimen is sketched in Figure 9.18. To measure an accurate value of toughness, (1) all characteristic specimen dimensions must exceed 25 times the expected plastic zone size at the crack tip, and (2) for plane strain conditions at the crack tip, the specimen thickness B must exceed at least the plastic zone size. For a material with yield stress Y , loaded in mode I with stress intensity factor K_I , the plastic zone size can be estimated as

$$r_p \sim 2.5 \left(\frac{K_I}{Y} \right)^2.$$

9.3.2.1 Practical Application of Linear Elastic Fracture Mechanics to Design

To apply linear elastic fracture mechanics (LEFM) in a design application, you need to be able to do the following:

1. Design a laboratory specimen that can induce a prescribed stress intensity factor at a crack tip.
2. Measure the critical stress intensity factors that cause fracture in the laboratory specimen, or measure fatigue crack growth rates as a function of static or cyclic stress intensity.
3. Estimate the anticipated size and location of cracks in your structure or component.

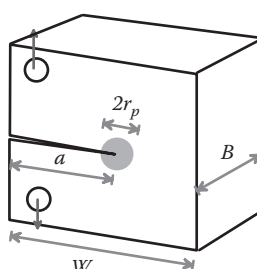


FIGURE 9.18 Plastic zone at a crack tip in a compact tension specimen.

4. Calculate the stress intensity factors for the cracks in your structure or component under anticipated loading conditions.
5. Combine the results of steps 2 and 4 to predict the behavior of the cracks in the structure of interest and make appropriate design recommendations.

These steps are outlined in more detail below.

9.3.3 Calculating Stress Intensity Factors

Calculating stress intensity factors is a critical step in fracture mechanics. Various techniques can be used to do this, including the following:

1. Solve the full linear elastic boundary value problem for the specimen or component containing a crack and deduce stress intensities from the asymptotic behavior of the stress field near the crack tips.
2. Attempt to deduce stress intensity factors directly using energy methods or path-independent integrals, to be discussed in Section 9.4.
3. Look up the solution you need in tables.
4. Use a numerical method; boundary integral equation methods are particularly effective for crack problems, but FEM can be used, too.

9.3.3.1 Analytical Solutions to Some Crack Problems

Calculating stress intensity factors for a crack in a structure or component involves the solution of a standard linear elastic boundary value problem. Once the stresses have been computed, the stress intensity factor is deduced from the definitions given in Section 9.3.1. Exact solutions are known for a few simple geometries. A couple of examples are as follows.

2D slit crack in an infinite solid: Figure 9.19 shows a 2D crack with length $2a$ in an infinite solid, which is subjected to a uniform state of stress $\sigma_{22}^\infty, \sigma_{12}^\infty, \sigma_{32}^\infty$ at infinity. The complex variable solution to this problem can be found in Section 5.3. The solution is

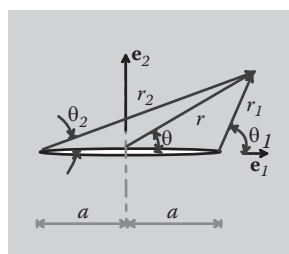


FIGURE 9.19 Coordinate system used to specify stress field near a crack.

most conveniently expressed in terms of the polar coordinates (r, θ) centered at the origin, together with the auxiliary angles and distances r_1, θ_1 and r_2, θ_2 shown in Figure 9.19. When evaluating the formulas, the angles θ_1 and θ_2 must lie in the ranges $-\pi \leq \theta_1 \leq \pi$ and $0 \leq \theta_2 \leq 2\pi$, respectively. The complete displacement and stress fields in the solid are

$$\begin{aligned}
 u_1 &= \frac{(1+\nu)\sigma_{22}^\infty \sqrt{r_1 r_2}}{4E} \left\{ 4(1-2\nu)\cos(\theta_1 + \theta_2)/2 - \frac{4r(1-\nu)}{\sqrt{r_1 r_2}} \cos\theta \right. \\
 &\quad \left. - \frac{2r^2}{r_1 r_2} (\cos(\theta_1 + \theta_2)/2 - \cos(2\theta - \theta_1/2 - \theta_2/2)) \right\} \\
 &+ \frac{(1+\nu)\sigma_{12}^\infty \sqrt{r_1 r_2}}{E} \left\{ 2(1-\nu)\sin(\theta_1 + \theta_2)/2 - 2(1-\nu) \frac{r}{\sqrt{r_1 r_2}} \sin\theta + \frac{r^2}{r_1 r_2} \sin\theta \cos(\theta - \theta_1/2 - \theta_2/2) \right\} \\
 u_2 &= \frac{(1+\nu)\sigma_{22}^\infty \sqrt{r_1 r_2}}{4E} \left\{ 8(1-\nu)\sin(\theta_1 + \theta_2)/2 + \frac{4\nu r}{\sqrt{r_1 r_2}} \sin\theta \right. \\
 &\quad \left. - \frac{2r^2}{r_1 r_2} (\sin(\theta_1 + \theta_2)/2 + \sin(2\theta - \theta_1/2 - \theta_2/2)) \right\} \\
 &+ \frac{(1+\nu)\sigma_{12}^\infty \sqrt{r_1 r_2}}{E} \left\{ (1-2\nu)\cos(\theta_1 + \theta_2)/2 + 2(1-\nu) \frac{r}{\sqrt{r_1 r_2}} \cos\theta - \frac{r^2}{r_1 r_2} \sin\theta \sin(\theta - \theta_1/2 - \theta_2/2) \right\} \\
 \sigma_{11} &= \frac{\sigma_{22}^\infty r}{\sqrt{r_1 r_2}} \left\{ \cos(\theta - \theta_1/2 - \theta_2/2) - 1 - \frac{a^2}{r_1 r_2} \sin\theta \sin 3(\theta_1 + \theta_2)/2 \right\} \\
 &+ \frac{\sigma_{12}^\infty r}{\sqrt{r_1 r_2}} \left\{ 2\sin(\theta - \theta_1/2 - \theta_2/2) - \frac{a^2}{r_1 r_2} \sin\theta \cos 3(\theta_1 + \theta_2)/2 \right\} \\
 \sigma_{22} &= \frac{\sigma_{22}^\infty r}{\sqrt{r_1 r_2}} \left\{ \cos(\theta - \theta_1/2 - \theta_2/2) + \frac{a^2}{r_1 r_2} \sin\theta \sin 3(\theta_1 + \theta_2)/2 \right\} + \frac{\sigma_{12}^\infty r}{\sqrt{r_1 r_2}} \frac{a^2}{r_1 r_2} \sin\theta \cos 3(\theta_1 + \theta_2)/2 \\
 \sigma_{12} &= \frac{\sigma_{22}^\infty r}{\sqrt{r_1 r_2}} \frac{a^2}{r_1 r_2} \sin\theta \cos 3(\theta_1 + \theta_2)/2 + \frac{\sigma_{12}^\infty r}{\sqrt{r_1 r_2}} \left\{ \cos(\theta - \theta_1/2 - \theta_2/2) + \frac{a^2}{r_1 r_2} \sin\theta \sin 3(\theta_1 + \theta_2)/2 \right\} \\
 \sigma_{32} &= \frac{\sigma_{23}^\infty r}{\sqrt{r_1 r_2}} \cos(\theta - \theta_1/2 - \theta_2/2) \quad \sigma_{31} = \frac{\sigma_{23}^\infty r}{\sqrt{r_1 r_2}} \sin(\theta - \theta_1/2 - \theta_2/2).
 \end{aligned}$$

The stress intensity factors are easily computed to be

$$K_I = \sigma_{22}^\infty \sqrt{\pi a} \quad K_{II} = \sigma_{12}^\infty \sqrt{\pi a} \quad K_{III} = \sigma_{32}^\infty \sqrt{\pi a}.$$

Penny-shaped crack in an infinite solid: Figure 9.20 shows a circular crack with radius a in an infinite solid, subjected to uniaxial tension at infinity. The displacement field, in cylindrical-polar coordinates, is

$$u_r = -\frac{\nu \sigma r}{E} + \frac{(1+\nu)\sigma r}{\pi E} \left\{ (1-2\nu) \left(\frac{a\sqrt{\rho_2^2 - a^2}}{\rho_2^2} - \sin^{-1} \frac{a}{\rho_2} \right) + \frac{2a^2 |z| \sqrt{a^2 - \rho_1^2}}{\rho_2^2(\rho_2^2 - \rho_1^2)} \right\}$$

$$u_z = \frac{\sigma z}{E} + \frac{2(1+\nu)}{\pi E} \left\{ 2(1-\nu) \left(\frac{z}{|z|} \sqrt{a^2 - \rho_1^2} - z \sin^{-1} \frac{a}{\rho_2} \right) + z \left(\sin^{-1} \frac{a}{\rho_2} - \frac{\sqrt{\rho_2^2 - a^2}}{\rho_2^2 - \rho_1^2} \right) \right\}$$

$$\rho_1 = \frac{1}{2} \left(\sqrt{(a+r)^2 + z^2} - \sqrt{(a-r)^2 + z^2} \right)$$

$$\rho_2 = \frac{1}{2} \left(\sqrt{(a+r)^2 + z^2} + \sqrt{(a-r)^2 + z^2} \right).$$

The displacement of the upper crack face can be found by setting $r < a$, $z = 0$ in these expressions, which gives

$$u_z = \frac{4(1-\nu^2)\sigma}{\pi E} \sqrt{a^2 - r^2}.$$

The stress intensity factor can be found directly from the displacement of the crack faces. The asymptotic formulas in Section 9.3.1 show that

$$K_I = \lim_{r \rightarrow a} \frac{Eu_z(r)}{4(1-\nu^2)} \sqrt{\frac{2\pi}{(a-r)}},$$

which shows that $K_I = 2\sigma\sqrt{a/\pi}$.

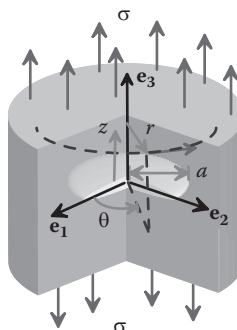
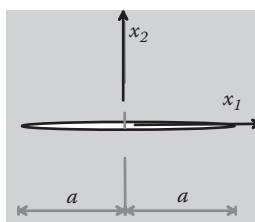


FIGURE 9.20 A penny-shaped crack subjected to uniaxial tensile loading.

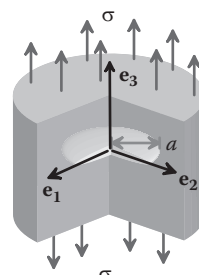
It is not always necessary to solve the full linear elastic boundary value problem to compute stress intensity factors. Energy methods, or the application of path-independent integrals, can sometimes be used to obtain stress intensity factors directly. These techniques will be discussed in more detail in Section 9.4.

Vast numbers of crack problems have been solved to catalog stress intensity factors in various geometries of interest. Two excellent (but expensive) sources of such solutions are Tada, Paris, and Irwin [2000] and Murakami [1987]. A few important (and relatively simple) results are listed in Table 9.1.

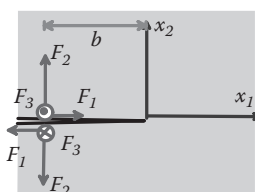
TABLE 9.1 A Short Table of Stress Intensity Factors



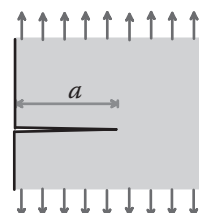
$$K_I = \sigma_{22}^{\infty} \sqrt{\pi a} K_{II} = \sigma_{12}^{\infty} \sqrt{\pi a} K_{III} = \sigma_{32}^{\infty} \sqrt{\pi a}$$



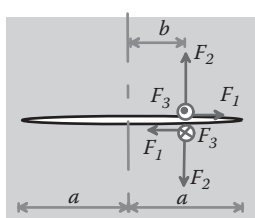
$$K_I = 2\sigma^{\infty} \sqrt{a/\pi}$$



$$K_I = \frac{2F_2}{\sqrt{2\pi b}} \quad K_{II} = \frac{2F_1}{\sqrt{2\pi b}} \quad K_{III} = \frac{2F_3}{\sqrt{2\pi b}}$$

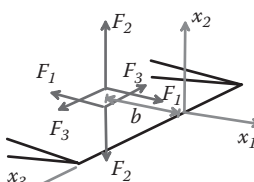


$$K_I = 1.1215\sigma\sqrt{\pi a}$$



$$K_I = \frac{F_2}{\sqrt{\pi a}} f\left(\frac{b}{a}\right) \quad K_{II} = \frac{F_1}{\sqrt{\pi a}} f\left(\frac{b}{a}\right)$$

$$K_{III} = \frac{F_3}{\sqrt{\pi a}} f\left(\frac{b}{a}\right) \quad f(\xi) = \sqrt{(1+\xi)/(1-\xi)}$$



$$K_I = \frac{4F_2}{(2\pi b)^{3/2}} f\left(\frac{x_3}{b}\right)$$

$$K_{II} = \frac{4F_1}{(2\pi b)^{3/2}} f\left(\frac{x_3}{b}\right)$$

$$K_{III} = \frac{4F_3}{(2\pi b)^{3/2}} f\left(\frac{x_3}{b}\right) \quad f(\xi) = 1/(1+\xi^2)$$

9.3.3.2 Calculating Stress Intensity Factors for Cracks in Nonuniform Stress Fields

The solutions for cracks loaded by point forces acting on their faces are particularly useful, because they allow you to calculate stress intensity factors for a crack in an arbitrary stress field using a simple superposition argument. The procedure works like this.

1. We start by computing the stress field in a solid without a crack in it. This solution satisfies all boundary conditions except that the crack faces are subject to tractions.
2. We could correct solution by applying pressure (and shear) to the crack faces that are just sufficient to remove the unwanted tractions.
3. If we know the stress intensity factors induced by point forces acting on the crack faces, we can superpose an appropriate distribution of point forces on the crack faces to calculate stress intensity factors induced by the corrective pressure distribution.

As an example, suppose that we want to calculate stress intensity factors for a crack in a linearly varying stress field (such as would be induced by bending a beam, for example), as illustrated in Figure 9.21:

1. In the uncracked solid, the stress field is $\sigma_{22} = \sigma_0 x_1 / L$.
2. The traction acting along the line of the crack is $p = \sigma_0 x_1 / L$. The sign convention for p is that a positive p acts downward on the upper crack face and upward on the lower crack face.
3. To remove the traction from the crack faces, we must superpose an equal and opposite distribution of point forces on the crack faces. The stress intensity factor induced at the left (L) and right (R) crack tips are

$$K_I^R = \frac{1}{\sqrt{\pi a}} \int_{-a}^a (\sigma_0 x_1 / L) \sqrt{\frac{a+x_1}{a-x_1}} dx_1 \quad K_I^L = \frac{1}{\sqrt{\pi a}} \int_{-a}^a (\sigma_0 x_1 / L) \sqrt{\frac{a-x_1}{a+x_1}} dx_1.$$

Evaluating the integrals gives

$$K_I^R = \frac{1}{2} (\sigma_0 / L) a \sqrt{\pi a} \quad K_I^L = -\frac{1}{2} (\sigma_0 / L) a \sqrt{\pi a}.$$

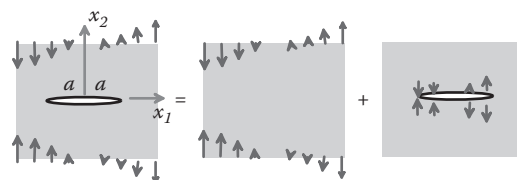


FIGURE 9.21 Superposition method used to calculate stress intensity factors for a crack subjected to a stress gradient.

Actually, this solution is not quite right; note that the stress intensity factor at the left crack tip is predicted to be negative. This cannot be correct. From the asymptotic stress field, we know that, if the stress intensity factor is negative, the crack faces must overlap behind the crack tip (the displacement jump is negative).

With a bit of cunning, we can fix this problem. The cause of the error in the quick estimate is that we removed tractions from the entire crack. This was a mistake; we should only have removed tractions from parts of the crack faces that open up. So let's suppose that the crack closes at $x_1 = -b$ and put the left-hand crack tip there (see Figure 9.22). The stress intensity factors are then

$$K_I^R = \frac{1}{\sqrt{\pi(a+b)/2}} \int_{-b}^a (\sigma_0 x_1 / L) \sqrt{\frac{b+x_1}{a-x_1}} dx_1$$

$$K_I^L = \frac{1}{\sqrt{\pi(a+b)/2}} \int_{-b}^a (\sigma_0 x_1 / L) \sqrt{\frac{a-x_1}{b+x_1}} dx_1.$$

This gives

$$K_I^L = \frac{(\sigma_0 / L) \sqrt{2\pi}}{8\sqrt{(a+b)}} (a^2 - 2ab - 3b^2)$$

for the stress intensity factor at the left-hand crack tip. The stress must be bounded at $x_1 = -b$, where the crack faces touch, so that $K_I^L = 0$. This gives $b = a/3$. The stress intensity factor at the right-hand crack tip then follows as

$$K_I^R = \frac{2(\sigma_0 / L)a\sqrt{6\pi a}}{9}.$$

This is not very different to our previous estimate. This illustrates a general feature of the field of fracture mechanics. There are many opportunities to do clever things, but often the results of all the cleverness are irrelevant.

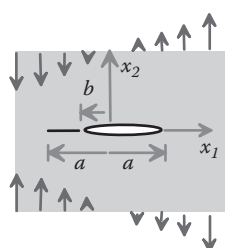


FIGURE 9.22 Closure of a crack in a stress gradient.

9.3.4 Calculating Stress Intensity Factors Using FEA

For solids with a complicated geometry, FEA (or boundary element methods) are the only way to calculate stress intensity factors. It is conceptually very straightforward to calculate stress intensities using finite elements; you just need to solve a routine linear elastic boundary value problem to determine the stress field in the solid and then deduce the stress intensity factors by taking the limits given in Section 9.3.1.

Unfortunately, this is easier said than done. The problem is that the stress and strain fields at a crack tip are *infinite*, and so standard finite element procedures have problems calculating the stresses accurately. Two special procedures have been developed to help deal with this:

1. Special crack tip elements are available to approximate the singular strains at a crack tip.
2. Special techniques are available to calculate stress intensity factors from stresses *far* from the crack tip (where they should be accurate) instead of using the formal definition.

These methods can both give very accurate values for stress intensity factors and can be used together to obtain the best results.

9.3.4.1 Crack Tip Elements

A very simple procedure can be used to approximate the strain singularity at a crack tip:

1. The solid near the crack tip must be meshed with quadratic elements (eight-noded quadrilaterals or six-noded triangles in 2D, or 20-noded bricks/10-noded tetrahedrals in 3D).
2. The elements connected to the crack tip must be quadrilateral or brick elements.
3. One side of each element connected to the crack tip is collapsed to make the three nodes on the side coincident, as shown in Figure 9.23.

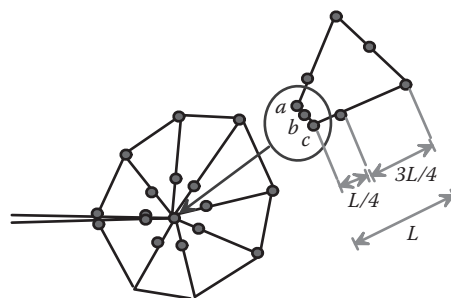


FIGURE 9.23 Finite element mesh near a crack tip.

4. The mid-side nodes on the elements connected to the crack tip are shifted to one-quarter point positions, as shown in the figure.
5. If the coincident nodes a, b, c on each crack-tip element are constrained to move together, this procedure generates an $(r)^{-1/2}$ singularity in strain at the crack tip (good for linear elastic problems). If the nodes are permitted to move independently, an r^{-1} singularity in strain is produced (good for problems involving crack tip plasticity).

9.3.4.2 Calculating Stress Intensity Factors Using Path-Independent Integrals

Energy methods in fracture mechanics are discussed in detail in Section 9.4. Two crucial results emerge from this analysis:

1. The “energy release rate” for a mode I crack in a linear elastic solid with Young’s modulus E and Poisson’s ratio ν is related to the mode I stress intensity factor by

$$G = \frac{1-\nu^2}{E} K_I^2.$$

2. The energy release rate for a crack can be calculated by evaluating the following line integral for *any* contour that starts on one crack face and ends on the other:

$$G = \int_{\Gamma} \left(W \delta_{j1} - \sigma_{ij} \frac{\partial u_i}{\partial x_1} \right) m_j ds,$$

where $W = \sigma_{ij} \varepsilon_{ij}/2$ is the strain energy density, σ_{ij} is the stress field, u_i is the displacement field, m_i is a unit vector normal to Γ , and the e_1 basis vector is parallel to the direction of crack propagation as shown in Figure 9.24.

These results are ideally suited for FEM calculations. The path-independent integral can be calculated for a contour far from the crack tip, in which the stresses are accurate, and then the relationship between G and K_I can be used to deduce the stress intensity factors. Analogous, but rather more complex, procedures exist to extract all three components of stress intensity factor, as well as to compute stress intensity factors for 3D cracks, in which the stress intensity factor is a function of position on the crack front.

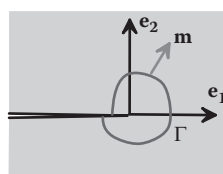


FIGURE 9.24 Contour for a path-independent integral near a crack tip.

9.3.5 Measuring Fracture Toughness

For structural applications, standard testing techniques are available to measure material properties for fracture applications. Two standard test specimen geometries are shown below. Stress intensity factors for these specimens have been carefully computed as a function of crack length and the results fit by curves, as outlined below:

- Compact tension specimen (see Figure 9.25):

$$K_I = \frac{P}{B} \sqrt{\frac{\pi}{W}} \left\{ 16.7 \left(\frac{a}{W} \right)^{1/2} - 104.7 \left(\frac{a}{W} \right)^{3/2} + 369.9 \left(\frac{a}{W} \right)^{5/2} - 573.8 \left(\frac{a}{W} \right)^{7/2} + 360.5 \left(\frac{a}{W} \right)^{9/2} \right\}.$$

- Three-point bend specimen (see Figure 9.26):

$$K_I = \frac{4P}{B} \sqrt{\frac{\pi}{W}} \left\{ 1.6 \left(\frac{a}{W} \right)^{1/2} - 2.6 \left(\frac{a}{W} \right)^{3/2} + 12.3 \left(\frac{a}{W} \right)^{5/2} - 21.2 \left(\frac{a}{W} \right)^{7/2} + 21.8 \left(\frac{a}{W} \right)^{9/2} \right\}.$$

Various other test specimens exist. Conducting a fracture test or fatigue test is (at least conceptually) straightforward: you make a specimen (for fracture tests, a sharp crack is usually created by initiating a fatigue crack at the tip of a notch) and load it in a tensile testing machine.

In principle, the fracture toughness can be determined by measuring the critical load when the crack starts to grow. In practice, it can be difficult to detect the onset of crack growth. For this reason, the usual approach is to monitor the crack opening displacement δ during the test and then plot load as a function of crack opening displacement. A typical result is illustrated in Figure 9.27.

The load-crack tip opening displacement curve ceases to be linear when the crack begins to grow. This point is hard to identify, so instead the convention is to draw a line with slope 5% lower than the initial $P-\delta$ curve (the 5% secant line) and use the point where this line

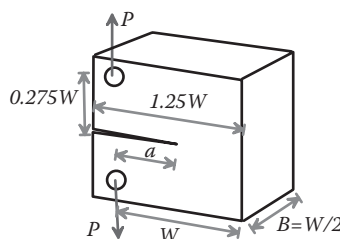


FIGURE 9.25 Compact tension specimen.

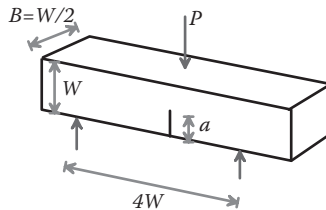


FIGURE 9.26 Three-point bend specimen.

intersects the $P-\delta$ as the fracture load. The plane strain fracture toughness of the material, K_{IC} , is deduced from the fracture load, using the calibration for the specimen.

After measurement, one must check that K_{IC} is within the limits required for K dominance in the specimen, following the rules in the preceding section.

9.3.6 Typical Values for Fracture Toughness

A short table of approximate toughness values is given in Table 9.2 [for a more extensive list, see Ashby and Jones 1997]. The values are highly dependent on material composition and microstructure, however, so if you need accurate data, you will need to measure the toughness of your materials yourself.

9.3.7 Stable Tearing: K_r Curves and Crack Stability

In ideally brittle materials, fracture is usually a catastrophic event. Once the load reaches the level required to trigger crack growth, the crack continues to propagate dynamically through the specimen. In more ductile materials, a period of stable crack growth under steadily increasing load may occur before complete failure. This behavior is particularly common in tearing of thin sheets of metals, but stable crack growth is observed in most materials, even polycrystalline ceramics.

Stable crack growth in metals usually occurs because a zone of plastically deformed material is left in the wake of the crack, as shown in Figure 9.28. This deformed material tends to reduce the stresses at the crack tip. In brittle polycrystalline ceramics, or in fiber-reinforced brittle composites, the stable crack growth is caused by the formation of a “bridging zone” behind the crack tip. Some fibers, or grains, remain intact in the crack wake and tend to hold the crack faces shut, increasing the apparent strength of the solid.

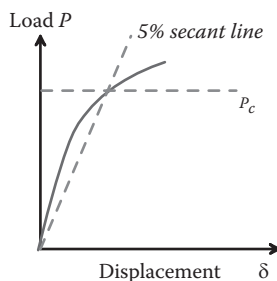


FIGURE 9.27 Procedure used to determine fracture load from a load-displacement curve for a standard specimen.

TABLE 9.2 Representative Values of Fracture Toughness for Materials

Material	Approximate Fracture Toughness ($\text{MNm}^{-3/2}$)
Pressure vessel steel	50–160
Mild steel	140
Titanium alloys	55–120
High carbon steel	30
Nickel, copper	>100
Aluminum and alloys	20–50
Co/WC metal matrix composites	14–16
Woods, perpendicular to grain	11–13
Concrete (steel reinforced)	10–15
Ceramics (alumina, SiC)	3–5
ABS polystyrene	4
Nylon, polypropylene	3
Glasses, rocks	1
Wood, parallel to grain	0.5–1
Concrete (unreinforced)	0.2

In some materials, the increase in load during stable crack growth is so significant that it is worth accounting for the effect in design calculations. The protective effect of the process zone in the crack wake is modeled by making the toughness of the material a function of the increase in crack length. The apparent toughness is measured in the same way as K_{IC} : a precracked specimen is subjected to progressively increasing load, and the crack length is monitored either optically or using compliance methods (more on this later). A value of K_I can be computed for the specimen using the calibrations; during crack growth, it is assumed that K_I is equal to the fracture toughness of the material.

The results are plotted in a “resistance curve” or “R curve” for the material, as shown in Figure 9.29. The fracture toughness K_{IC} is the critical stress intensity factor required to initiate crack growth. The variation of toughness with crack growth is denoted $K_r(\Delta a)$.

The resistance curve is then used to predict the conditions necessary for unstable crack growth through the material. To see how this is done,

1. Consider a large sample of material containing a slit crack of length $2a$, subjected to stress σ , as shown in Figure 9.30. The stress intensity factor for this crack (from the table in Section 9.3.3) is $K_I = \sigma\sqrt{\pi a}$.
2. Crack growth begins when $\sigma\sqrt{\pi a} = K_{IC}$. Thereafter, there will be a period of stable crack growth, during which the applied stress increases. During the period of stable growth, the stress intensity factor must equal the apparent toughness:

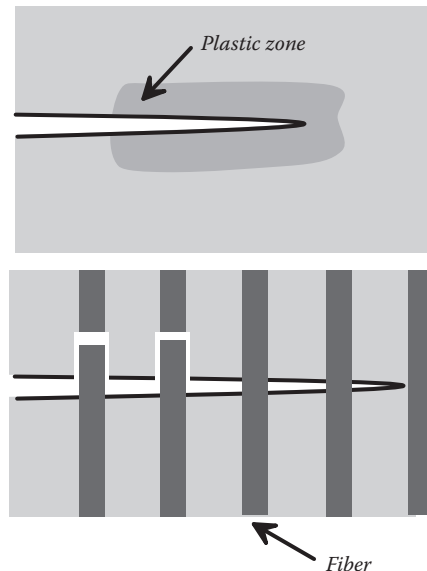


FIGURE 9.28 Process zones in the wake of a crack attributable to plastic flow and fiber bridging.

$$\sigma \sqrt{\pi(a + \Delta a)} = K_r(\Delta a) \Rightarrow \sigma = \frac{K_r(\Delta a)}{\sqrt{\pi(a + \Delta a)}}.$$

3. The stress will continue to increase as long as $K_r(\Delta a)$ increases more rapidly than $\sqrt{\pi(a + \Delta a)}$ with Δa . Catastrophic failure (unstable crack growth) will occur when continued crack growth is possible at constant or decreasing load. The crack length at the point of unstable crack growth follows from the condition that

$$\frac{d\sigma}{d\Delta a} = 0 \Rightarrow a + \Delta a = \frac{K_r}{2(dK_r/d\Delta a)}.$$

4. Substituting the crack length back into the fracture criterion $\sigma \sqrt{\pi(a + \Delta a)} = K_r(\Delta a)$ gives the critical stress at unstable fracture as

$$\sigma = \sqrt{\frac{2}{\pi}} K_r \frac{dK_r}{d\Delta a}.$$

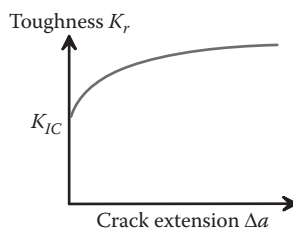


FIGURE 9.29 A typical crack-growth resistance curve.

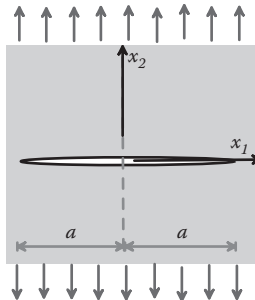


FIGURE 9.30 Slit crack subjected to remote uniaxial stress.

9.3.8 Mixed-Mode Fracture Criteria

Fracture toughness is almost always measured under mode I loading (except when measuring fracture toughness of a bi-material interface). If a crack is subjected to combined mode I and mode II loading, a *mixed mode* fracture criterion is required. There are several ways to construct mixed mode fracture criteria; the issue has been the subject of some quite heated arguments. The *criterion of maximum hoop stress* is one example. Recall that the crack tip hoop and shear stresses are

$$\sigma_{\theta\theta} = \frac{K_I}{\sqrt{2\pi r}} \left(\frac{3}{4} \cos \frac{\theta}{2} + \frac{1}{4} \cos \frac{3\theta}{2} \right) - \frac{K_{II}}{\sqrt{2\pi r}} \left(\frac{3}{4} \sin \frac{\theta}{2} + \frac{1}{4} \sin \frac{3\theta}{2} \right)$$

$$\sigma_{r\theta} = \frac{K_I}{\sqrt{2\pi r}} \left(\frac{1}{4} \sin \frac{\theta}{2} + \frac{1}{4} \sin \frac{3\theta}{2} \right) + \frac{K_{II}}{\sqrt{2\pi r}} \left(\frac{1}{4} \cos \frac{\theta}{2} + \frac{3}{4} \cos \frac{3\theta}{2} \right).$$

The maximum hoop stress criterion postulates that a crack under mixed mode loading starts to propagate when the greatest value of hoop stress $\sigma_{\theta\theta}$ reaches a critical magnitude, at which point the crack will branch at the angle for which $\sigma_{\theta\theta}$ is greatest (or equivalently the angle for which $\sigma_{r\theta} = 0$). The critical angle is plotted as a function of K_{II}/K_I in Figure 9.31. The asymptote for $K_{II}/K_I \rightarrow \infty$ is -70.7° . The resulting failure locus (the critical combination of K_I/K_{IC} and K_{II}/K_{IC} that leads to failure) is also shown.

All available criteria predict that, after branching, a crack will follow a path such that the local mode II stress intensity factor is zero.

9.3.9 Static Fatigue Crack Growth

For a fatigue test, the crack length is measured (optically or using compliance techniques) as a function of time or number of load cycles. Fatigue laws are deduced by plotting crack growth rate as a function of applied stress intensity factor.

Typical static fatigue data (e.g., for corrosion crack growth, or creep crack growth) behavior is shown in Figure 9.32.

Most materials have a *static fatigue threshold*: a value of K_I below which crack growth is undetectable. Then there is a range in which crack growth rate shows a power-law dependence on stress intensity factor of the form

$$\frac{da}{dt} = CK_I^m,$$

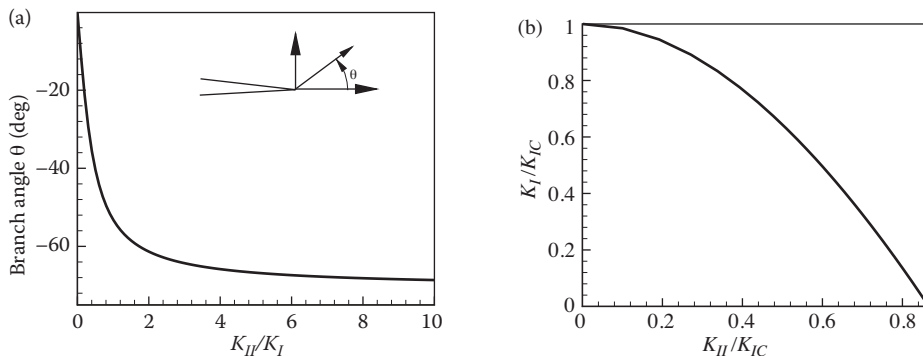


FIGURE 9.31 Predictions of the maximum hoop stress criterion. (a) Branch angle; (b) fracture criterion.

where m is typically of order 5–10. Finally, for values of K_I approaching the fracture toughness, the crack growth rate increases drastically with K_I .

This crack growth law can be used to derive the phenomenological static fatigue criterion outlined in Section 9.2.3. Assume that, at time $t = 0$, the material contains a crack of initial length $2a_0$ and is subjected to a uniaxial stress σ , as shown in Figure 9.33. The stress will cause the crack to increase in length, until it becomes long enough to trigger brittle fracture. The table in Section 9.3.9 shows that a crack of length $2a$ subjected to stress σ has a crack tip stress intensity factor of $K_I = \sigma\sqrt{\pi a}$. Substituting into the static fatigue crack growth law and integrating gives the following expression for crack length as a function of time

$$\frac{2}{m-2} \left(\frac{1}{a_0^{m/2-1}} - \frac{1}{a^{m/2-1}} \right) = C\pi^{m/2} \int \sigma^m dt,$$

where $2a_0$ is the crack length at time $t = 0$. The solid will fracture when the crack tip stress intensity factor reaches the fracture toughness K_{IC} , so that the tensile strength at time $t = 0$ and at time t must satisfy

$$\sigma_{TS0}\sqrt{\pi a_0} = K_{IC} \quad \sigma_{TS}\sqrt{\pi a} = K_{IC}.$$

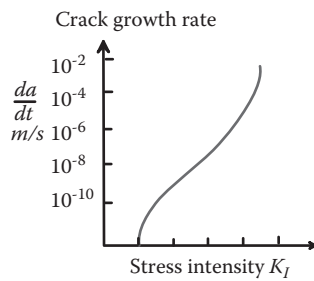


FIGURE 9.32 Typical crack growth rate-versus-stress intensity factor during static fatigue crack growth.

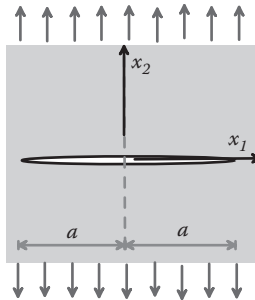


FIGURE 9.33 Slit crack subjected to remote uniaxial stress.

Eliminating the crack length and simplifying gives

$$\sigma_{TS} = \sigma_{TS0} \left(1 - \frac{(m-2)\pi CK_{IC}^{m-2}}{2\sigma_{TS0}^{m-2}} \int \sigma^m dt \right)^{1/(m-2)}.$$

Assuming that the operating stress is well below the fracture stress, we can approximate this by

$$\sigma_{TS} = \sigma_{TS0} \left(1 - \alpha \int (\sigma / \sigma_{TS0})^m dt \right),$$

which is the stress-based static fatigue law of Section 9.2.3.

9.3.10 Cyclic Fatigue Crack Growth

Under cyclic loading, the crack is subjected to a cycle of mode I and mode II stress intensity factor. Most fatigue tests are performed under a steady cycle of pure mode I loading, as sketched in Figure 9.34.

The results are usually displayed by plotting the crack growth per cycle da/dN as a function of the stress intensity factor range

$$\Delta K_I = \begin{cases} K_{\max} - K_{\min} & K_{\min} \geq 0 \\ K_{\max} & K_{\min} < 0 \end{cases}.$$

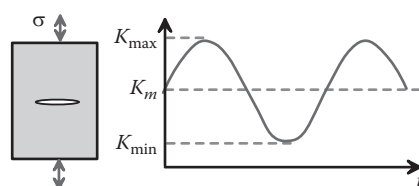


FIGURE 9.34 Cyclic stress intensity factors induced by cyclic loading on a crack.

A typical result shows three regions, as shown in Figure 9.35. There is a fatigue threshold ΔK_{th} below which crack growth is undetectable. For modest loads, the crack growth rate obeys Paris law

$$\frac{da}{dN} = C(\Delta K_I)^n,$$

where the index n is between 2 and 4. As the maximum stress intensity factor approaches the fracture toughness of the material, the crack growth rate accelerates dramatically.

In the Paris law regime, the crack growth rate is only weakly sensitive to the mean value of stress intensity factor K_m . In the other two regimes, K_m has a noticeable effect: the fatigue threshold is reduced as K_m increases, and the crack growth rate in regime III increases with K_m .

9.3.11 Finding Cracks in Structures

Determining the length of preexisting cracks in a component is often the most difficult part of applying fracture mechanics in practice. For most practical applications, you simply don't know if your component will have a crack in it, and it will be expensive if you need to find out. Your options are as follows:

1. Take a wild guess, based on microscopic examinations of representative samples of material. Alternatively, you can specify the biggest flaw you are prepared to tolerate and insist that your material suppliers manufacture appropriately defect-free materials.
2. Conduct a proof test (for example, popular with pressure vessel applications) wherein the structure or component is subjected to a load greatly exceeding the anticipated service load under controlled conditions. If the fracture toughness of the material is known, you can then deduce the largest crack size that could be present in the structure without causing failure during proof testing.
3. Use some kind of nondestructive test technique to attempt to detect cracks in your structure. Examples of such techniques are ultrasound, in which you look for echoes

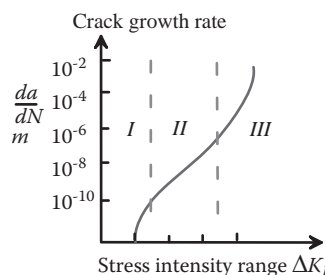


FIGURE 9.35 Typical crack growth rate-versus-stress intensity relation for fatigue crack growth.

off crack surfaces, x-ray techniques, and inspection with optical microscopy. If you detect a crack, most of these techniques will allow you to estimate the crack length. If not, you have to assume for design purposes that your structure is crammed full of cracks that are just too short to be detected.

9.4 ENERGY METHODS IN FRACTURE MECHANICS

Energy methods provide additional insight into fracture and also provide a foundation for a range of analytical and numerical methods in fracture mechanics. In this section, we outline some of the most important results.

9.4.1 Definition of Crack Tip Energy Release Rate for Cracks in Linear Elastic Solids

The crack tip energy release rate quantifies the rate of change of the potential energy of a cracked elastic solid as the crack grows. To make this precise, consider an ideally elastic solid, subjected to some loading (applied tractions, displacements, or body forces). Suppose the solid contains a crack (Figure 9.36 shows a circular crack with radius a as a representative example). Define the potential energy of the solid in the usual way (Section 5.7.1) as

$$V(a) = \int_V U(\mathbf{u}) dV - \int_V \rho_0 b_i u_i dV - \int_{\partial_2 R} t_i u_i dA.$$

Suppose the crack increases in size, so that the crack advances a distance $\alpha\delta a(s)$ with loading kept fixed, where s measures position around the crack front. The principle of minimum potential energy (Section 5.7.2) shows that $V(a + \alpha\delta a) \leq V(a)$, because the displacement field associated with $V(a)$ is a kinematically admissible field for the solid with a longer crack. The *energy release rate* $G(s)$ around the crack front is defined so that

$$\int_C G(s) \delta a(s) ds = -\lim_{\alpha \rightarrow 0} \frac{\partial V(a + \alpha\delta a(s))}{\partial \alpha}.$$

Energy release rate has units of Nm^{-1} (energy per unit area).

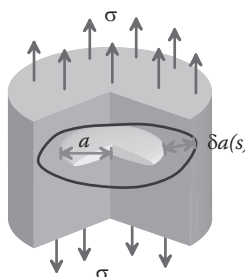


FIGURE 9.36 A penny-shaped crack propagating under remote loading.

For the special case of a 2D slit crack with length a , the energy release rate is

$$G = -\frac{\partial \bar{V}(a)}{\partial a},$$

where \bar{V} is now the potential energy per unit out-of-plane distance.

9.4.2 Energy Release Rate as a Fracture Criterion

Phenomenological fracture (or fatigue) criteria can be based on energy release rate arguments as an alternative to the K -based fracture criteria discussed previously. The argument is as follows. Regardless of the actual mechanisms involved, crack propagation involves dissipation (or conversion) of energy. A small amount of energy is required to create two new free surfaces (twice the surface energy per unit area of crack advance, to be precise). In addition, there may be a complex process zone at the crack tip, in which the material is plastically deformed, voids may be nucleated, there may be chemical reactions, and generally all hell breaks loose. All these processes involve dissipation of energy. We postulate, however, that the process zone remains self-similar during crack growth. If this is the case, energy will be dissipated at a constant rate during crack growth. The crack can only grow if the rate of change of potential energy is sufficient to provide this energy.

This leads to a fracture criterion of the form

$$G \geq G_C$$

for crack growth, where G_C is a property of the material. Unfortunately, G_C is often referred to as the fracture toughness of a solid, just like K_{IC} defined previously. It is usually obvious from dimensional considerations which one is being used, but it is an annoying source of confusion.

9.4.3 Relation between Energy Release Rate and Stress Intensity Factor

The energy release rate G is closely related to the stress intensity factors defined in Section 9.3. Specifically, for an isotropic, linear elastic solid with Young's modulus E and Poisson's ratio ν , the energy release rate is related to stress intensity factors by

$$G = \frac{1-\nu^2}{E} \left(K_I^2 + K_{II}^2 \right) + \frac{1+\nu}{E} K_{III}^2.$$

HEALTH WARNING: The result relating G to K_I and K_{II} is valid only for plane strain deformation at the crack tip.

Derivation: A crack of length a can be regarded as a crack with $a + \delta a$, which is being pinched closed by an appropriate distribution of traction acting on the crack faces between $x_1 = -\delta a$ and $x_1 = 0$. The crack can be made to propagate by applying an equal and opposite distribution of tractions that free the crack faces from stress, as shown in Figure 9.37. We can therefore calculate the change in potential energy as the crack

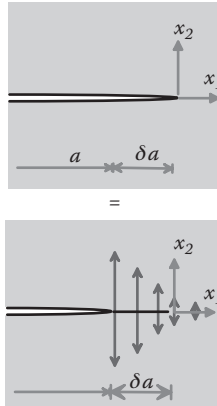


FIGURE 9.37 Superposition method used to relate stress intensity factors to energy release rate.

propagates by distance δa by computing the work done as these tractions are progressively applied to the crack. To this end, note the following:

1. The tractions that pinch the crack tip closed can be calculated from the asymptotic crack tip field (Section 9.3.1):

$$t_1 = \frac{K_{II}}{\sqrt{2\pi(\delta a + x_1)}} \quad t_2 = \frac{K_I}{\sqrt{2\pi(\delta a + x_1)}} \quad t_3 = \frac{K_{III}}{\sqrt{2\pi(\delta a + x_1)}}$$

(equal and opposite tractions must act on the lower crack face).

2. As the crack is allowed to open, the upper crack face displaces by

$$\Delta u_1 = \frac{2(1-\nu^2)}{E} K_{II} \sqrt{\frac{-2x_1}{\pi}} \quad \Delta u_2 = \frac{2(1-\nu^2)}{\pi} K_I \sqrt{\frac{-2x_1}{\pi}} \quad \Delta u_3 = \frac{2(1+\nu)}{E} K_{III} \sqrt{\frac{-2x_1}{\pi}},$$

where we have assumed plane strain deformation.

3. The total work done as the tractions are relaxed quasi-statically to zero is

$$G\delta a = \int_{-\delta a}^0 (t_1 \Delta u_1 + t_2 \Delta u_2 + t_3 \Delta u_3) dx_1$$

(the work done by tractions acting on the upper crack face per unit length is $t_i \Delta u_i / 2$, and there are two crack faces).

4. Evaluating the integrals gives

$$G = \frac{1-\nu^2}{E} (K_I^2 + K_{II}^2) + \frac{1+\nu}{E} K_{III}^2.$$

The same result can be obtained by applying crack tip energy flux integrals, to be discussed below.

9.4.4 Relation between Energy Release Rate and Compliance

Energy release rate is related to the compliance of a structure or specimen, as follows. Consider the compact tension specimen shown in Figure 9.38. Suppose that the specimen is subjected to a load P , which causes the point of application of the load to displace by a distance x_0 in a direction parallel to the load. The compliance of the specimen is defined as

$$C = \frac{x_0}{P}.$$

As the crack grows, the compliance of the specimen always increases, so C is a function of crack length. The energy release rate is related to compliance C by

$$G = \frac{1}{2} \frac{P^2}{B} \frac{dC}{da}.$$

This formula applies to any structure or component, not just to compact tension specimens. The formula is useful for two reasons:

1. It can be used to measure energy release rate in an experiment. All you need to do is measure the crack length as it grows and at the same time measure the compliance of your specimen.
2. It can be used to calculate stress intensity factors, as outlined in the next section.

Derivation: This result can be derived by calculating the change in energy of the system as the crack grows. Note the following:

1. The load P induces a total strain energy $\Phi = \frac{1}{2}x_0P = \frac{1}{2}CP^2$ in the specimen. To see this, note that the solid is elastic and so behaves like a linear spring; this is just the formula for the energy in a spring.
2. Now, suppose that the crack extends by a distance δa . During crack growth, the load increases to $P + \delta P$ and displaces to $x_0 + \delta x$. In addition, the strain energy changes to $\Phi + \delta\Phi$, while the compliance increases to $C + \delta C$.

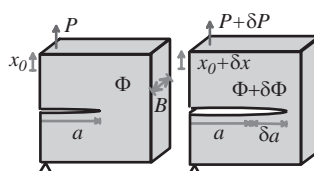


FIGURE 9.38 A cracked specimen containing a propagating crack.

3. The energy released during crack advance is equal to the decrease in potential energy of the system, so that

$$GB\delta a = -\delta V = -[(\Phi + \delta\Phi) - \Phi - P\delta x].$$

4. Note that

$$\begin{aligned}\Phi + \delta\Phi &= \frac{1}{2}(C + \delta C)(P + \delta P)^2 \approx \frac{1}{2}CP^2 + CP\delta P + \frac{1}{2}\delta CP^2 \\ \delta x &= (C + \delta C)(P + \delta P) - CP \approx C\delta P + P\delta C.\end{aligned}$$

5. Substituting these results into the expression in step 3 and simplifying shows that

$$GB\delta a = -\frac{1}{2}P^2\delta C = -\frac{1}{2}P^2 \frac{dC}{da} \delta a.$$

The energy release rate therefore is related to compliance by

$$G = \frac{1}{2} \frac{P^2}{B} \frac{dC}{da}.$$

9.4.5 Calculating Stress Intensity Factors Using Compliance

The relation between compliance and energy release rate can be used to determine energy release rates, and sometimes also stress intensity factors, for structures whose rate of change of compliance with crack length can be easily determined. One example is the cantilever beam specimen shown in Figure 9.39. The mode I stress intensity factor for this specimen can be derived as

$$K_I = \frac{2\sqrt{3}}{\sqrt{1-\nu^2}} \frac{Pa}{Bh^{3/2}}.$$

Derivation: This result is derived by first calculating the compliance of the solid, then using the formula to deduce the energy release rate, and finally using the relationship between stress intensity factor and energy release rate. To proceed,

1. Note that the deflection d of the loaded point can be calculated by visualizing the specimen as two cantilever beams, length a , width B , and height h , clamped on their right-hand end and subjected to a load P at their left-hand ends (see Figure 9.40).

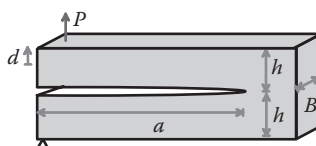


FIGURE 9.39 A double cantilever beam specimen.

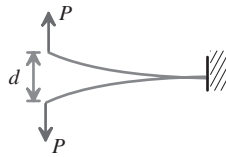


FIGURE 9.40 Idealizing the arms of a double cantilever beam specimen as cantilevers.

From elementary beam theory, the deflection is

$$d = 2 \frac{a^3 P}{3E(Bh^3/12)} = 8 \frac{a^3 P}{EBh^3},$$

where E is the Young's modulus of the specimen.

2. The compliance follows as

$$C = \frac{d}{P} = 8 \frac{a^3}{EBh^3}.$$

3. The energy release rate formula in Section 9.4.4 gives

$$G = \frac{1}{2} \frac{P^2}{B} \frac{dC}{da} = 12 \frac{P^2 a^2}{EB^2 h^3}.$$

4. By symmetry, the crack must be loaded in pure mode I. We can therefore deduce the stress intensity factor using the relation

$$G = \frac{1-\nu^2}{E} K_I^2 \Rightarrow K_I = \frac{2\sqrt{3}}{\sqrt{1-\nu^2}} \frac{Pa}{Bh^{3/2}}.$$

9.4.6 Integral Expressions for Energy Flux to a Crack Tip

In this section, we outline a way to compute the energy release rate for a crack, which applies not only to linear elastic solids under quasi-static loading conditions but is completely independent of the constitutive response of the solid and also applies under dynamic loading (it is restricted to small strains, however). The approach will be to find an expression for the flux of energy through a cylindrical surface Γ enclosing the crack tip, which moves with the crack. We will get the energy release rate by shrinking the surface down onto the crack tip.

Energy flux across a surface in a solid: We first derive a formula that can be used to calculate the flux of kinetic and potential energy across a surface in a deformable solid. To this end,

- Consider an arbitrary surface S , which encloses some volume V in a solid, as shown in Figure 9.41. The surface need not necessarily be a material surface: it could move

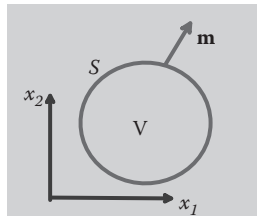


FIGURE 9.41 Surface enclosing a volume within an elastic solid.

with respect to the solid. We will denote the velocity of \$S\$ (with respect to a fixed origin) by \$v_j\$.

- Assume that the solid is free of body forces, for simplicity.
- Let \$[u_i, \varepsilon_{ij}, \sigma_{ij}]\$ denote the displacement, (infinitesimal) strain, and stress field in the solid and let \$\dot{u}_i\$ denote the velocity of a material point with respect to a fixed origin.
- Let \$T = \rho \dot{u}_i \dot{u}_i / 2\$ denote the kinetic energy density of the solid.
- Let \$\dot{W} = \sigma_{ij} \dot{\varepsilon}_{ij} = \sigma_{ij} \frac{\partial \dot{u}_i}{\partial x_j}\$ denote the rate of work done by stresses at a point in the solid.
- Define the rate of change of mechanical energy density at an arbitrary point in the solid as \$\dot{\psi} = \dot{W} + \dot{T}\$ and let \$\psi = \int_{-\infty}^t \dot{\psi} dt\$.
- Denote the total energy within \$V\$ as \$\Psi = \int_V \psi dV\$.
- Define the work flux vector as \$\omega_j = \sigma_{ij} \dot{u}_i\$.

The energy flux across \$S\$ can be calculated in terms of these quantities as follows:

$$\frac{d\Psi}{dt} = \frac{d}{dt} \int_S \psi dA = \int_S (\omega_j + \psi v_j) m_j dA.$$

The right-hand side of this expression denotes the energy flux across the surface; the left-hand side is the rate of change of the total energy within \$V\$. The two are equal by energy conservation, as shown below.

Derivation

1. Begin by showing that the energy flux vector and the rate of change of mechanical energy density are related by

$$\partial \omega_j / \partial x_j = \dot{\psi}.$$

To see this, note that

$$\dot{\psi} = \dot{W} + \dot{T} = \sigma_{ij} \frac{\partial \dot{u}_i}{\partial x_j} + \rho \ddot{u}_i \dot{u}_i = \sigma_{ij} \frac{\partial \dot{u}_i}{\partial x_j} + \frac{\partial \sigma_{ij}}{\partial x_j} \dot{u}_i = \frac{\partial}{\partial x_j} (\sigma_{ij} \dot{u}_i) = \frac{\partial \omega_j}{\partial x_j},$$

where we have used the linear and angular momentum balance equations $\partial \sigma_{ij} / \partial x_j = \rho \ddot{u}_i$ and $\sigma_{ij} = \sigma_{ji}$.

2. Now, integrate both sides of this equation over the volume V and apply the divergence theorem to see that

$$\int_V \frac{\partial \omega_j}{\partial x_j} dV = \int_V \dot{\psi} dV \Rightarrow \int_S \omega_j m_j dA = \int_V \dot{\psi} dV.$$

3. Next note that the total rate of change of ψ within the volume V bounded by S can be expressed as

$$\frac{d}{dt} \int_V \psi dV = \int_V \dot{\psi} dV + \int_S \psi v_j m_j dA.$$

Here, the first term on the right represents the rate of change resulting from the time derivative of ψ within V , whereas the second term represents the flux of energy crossing S as the surface moves with velocity v_j .

4. Combining steps 2 and 3 shows that

$$\int_S \omega_j m_j dA = \frac{d}{dt} \int_V \psi dV - \int_S \psi v_j m_j dA \Rightarrow \int_S (\omega_j + \psi v_j) m_j dA = \frac{d}{dt} \int_V \psi dV.$$

The term on the right-hand side clearly represents the total rate of change of mechanical energy in V . Consequently, the term on the left-hand side must represent the mechanical energy flux across S . This is the result we need.

Energy flux to a crack tip: We can use the energy flux integral to obtain an expression for the energy flux to a crack tip. Suppose the crack tip runs with steady speed v in the x_1 direction. Let Γ denote a cylindrical surface enclosing the crack tip, which moves with the crack tip, as shown in Figure 9.42. The energy flux through Γ follows as

$$\frac{d\Psi}{dt} = \int_{\Gamma} (\omega_j + \psi v \delta_{j1}) m_j dA = \int_{\Gamma} (\omega_j + (T + W)v \delta_{j1}) m_j dA.$$

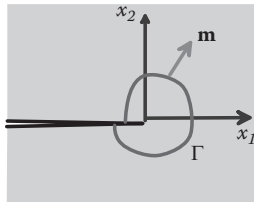


FIGURE 9.42 Contour used to evaluate crack tip integrals.

where

$$W = \int_{-\infty}^t \dot{W} dt = \int_{-\infty}^t \sigma_{ij} \dot{\epsilon}_{ij} dt = \int_0^t \sigma_{ij} d\epsilon_{ij}$$

is the net work done on the solid per unit volume by stresses, and $T = \rho \dot{u}_i \dot{u}_i / 2$ is the kinetic energy density. The energy flux to the crack tip follows by taking the limit as Γ shrinks down onto the crack tip.

Contour integral formula for energy release rate: To obtain an expression for the energy release rate, assume that the crack tip fields remain self-similar (i.e., an observer traveling with the crack tip sees a fixed state of strain and stress). In addition, assume that the crack front is straight and has length L in direction perpendicular to the plane of the figure. Under these conditions, $\dot{u}_i = -v \partial u_i / \partial x_1$, and $d\Psi/dt = GLv$. Consequently,

$$G = \frac{1}{L} \lim_{\Gamma \rightarrow 0} \int_{\Gamma} \left((T + W) \delta_{j1} - \sigma_{ij} \frac{\partial u_i}{\partial x_1} \right) m_j dA = \lim_{C \rightarrow 0} \int_C \left((T + W) \delta_{j1} - \sigma_{ij} \frac{\partial u_i}{\partial x_1} \right) m_j ds,$$

where C is a contour enclosing the crack tip. (Equivalent results can be derived for general 3D cracks, but these details are omitted here.) This result is valid for any material response (including plastic materials) and applies to both static and dynamic conditions.

9.4.7 Rice's J Integral

The result derived in the preceding section becomes particularly useful if we make two further assumptions:

1. Loading is quasi-static.
2. The material is elastic.

In this case, $T = 0$ and W is simply the strain energy density in the solid, e.g., for a linear elastic solid with no thermal stress,

$$W = \frac{E}{2(1+\nu)} \epsilon_{ij} \epsilon_{ij} + \frac{Ev}{2(1+\nu)(1-2\nu)} \epsilon_{jj} \epsilon_{kk}.$$

The expression for energy flux through a surface surrounding the crack tip reduces to

$$J = \int_{\Gamma} \left(W\delta_{j1} - \sigma_{ij} \frac{\partial u_i}{\partial x_1} \right) m_j ds.$$

This is the famous *J integral*. It has the following properties:

1. The crack tip energy integral is *path independent*, as long as the material enclosed by the contour is homogeneous. There is no need then to shrink the contour down onto the crack tip; we get the same answer for *any* contour that encloses the crack tip.
2. $J = G$ for an elastic solid, so the contour integral gives an elegant way to calculate the crack tip energy release rate.

Path independence of J : We first show that, if the J integral is evaluated around any *closed* contour that does not enclose the crack tip, it is zero. To see this, apply the divergence theorem

$$J = \int_{\Gamma} \left(W\delta_{j1} - \sigma_{ij} \frac{\partial u_i}{\partial x_1} \right) m_j ds = \int_A \frac{\partial}{\partial x_j} \left(W\delta_{j1} - \sigma_{ij} \frac{\partial u_i}{\partial x_1} \right) dA = 0,$$

where A is the area enclosed by Γ , as shown in Figure 9.43. To see that the area integral on the right-hand side is zero, note that

$$\begin{aligned} \frac{\partial W}{\partial x_j} \delta_{j1} &= \frac{\partial W}{\partial \varepsilon_{kl}} \frac{\partial \varepsilon_{kl}}{\partial x_1} = \sigma_{kl} \frac{\partial u_k}{\partial x_l \partial x_1} \\ \frac{\partial}{\partial x_j} \left(\sigma_{ij} \frac{\partial u_i}{\partial x_1} \right) &= \frac{\partial \sigma_{ij}}{\partial x_j} \frac{\partial u_i}{\partial x_1} + \sigma_{ij} \frac{\partial u_i}{\partial x_j \partial x_1} = \sigma_{ij} \frac{\partial u_i}{\partial x_j \partial x_1}, \end{aligned}$$

where we have used the equilibrium equation $\partial \sigma_{ij}/\partial x_j = 0$.

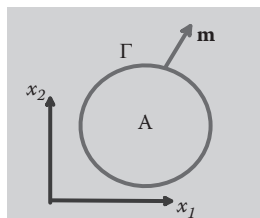


FIGURE 9.43 Contour enclosing an area within a solid.

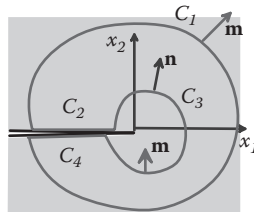


FIGURE 9.44 Contour used to show path independence of the J integral.

Now, evaluate the integral around the closed contour shown in Figure 9.44. Note that the integrand vanishes on C_2 and C_4 so that

$$\int_{C_1} \left(W\delta_{j1} - \sigma_{ij} \frac{\partial u_i}{\partial x_1} \right) m_j ds + \int_{C_3} \left(W\delta_{j1} - \sigma_{ij} \frac{\partial u_i}{\partial x_1} \right) m_j ds = 0.$$

Now reverse the direction of integration around C_3 (note that $\mathbf{m} = -\mathbf{n}$) to get

$$\int_{C_1} \left(W\delta_{j1} - \sigma_{ij} \frac{\partial u_i}{\partial x_1} \right) m_j ds = \int_{C_3} \left(W\delta_{j1} - \sigma_{ij} \frac{\partial u_i}{\partial x_1} \right) n_j ds,$$

showing that the integral is equal for any two contours that start and end on the two crack faces.

9.4.8 Calculating Energy Release Rates Using the J Integral

The J integral has many applications. In some cases, it can be used to compute energy release rates. For example, consider the problem shown in Figure 9.45. A cracked linear elastic cracked sheet is clamped between rigid boundaries. The bottom boundary is held fixed; the top is displaced vertically by a distance Δ . Calculate the energy release rate for the crack.

For this case, $G = J$, and we can easily evaluate the J integral around the contour shown in Figure 9.45. To do so, note the following:

1. Far behind the crack tip ($x_1 \rightarrow -\infty$), the solid is stress free. The J integral vanishes on Γ_1 and Γ_5 .

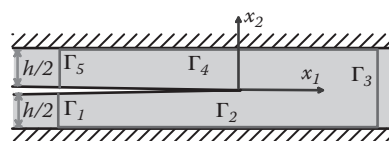


FIGURE 9.45 Contour used to calculate energy release rate for a crack in a strip subjected to prescribed displacements.

2. The displacement field is constant on $x_2 = \pm h/2$ so that $\partial u_i / \partial x_1 = 0$ there. In addition, $m_1 = 0$ on Γ_2 and Γ_4 . The J integral vanishes on Γ_2 and Γ_4 , therefore.
3. Far ahead of the crack tip $x_1 \rightarrow \infty$, the displacement, stress, and strain energy density can easily be calculated as

$$u_2 = x_2 \Delta / h, \quad u_1 = u_3 = 0$$

$$\sigma_{22} = E(1-\nu)\Delta / (1+\nu)(1-2\nu)h \quad \sigma_{11} = \sigma_{33} = Ev\Delta / (1+\nu)(1-2\nu)h.$$

$$W = E(1-\nu)\Delta^2 / 2(1+\nu)(1-2\nu)h^2.$$

The contribution to the J integral from Γ_3 follows as

$$\int_{\Gamma_3} \left(W \delta_{j1} - \sigma_{ij} \frac{\partial u_i}{\partial x_1} \right) n_j ds = \frac{E(1-\nu)\Delta^2}{2(1+\nu)(1-2\nu)h}.$$

4. The energy release rate is therefore

$$G = \frac{E(1-\nu)\Delta^2}{2(1+\nu)(1-2\nu)h}.$$

Symmetry conditions show that the crack must be loaded in pure mode I, so the stress intensity factor can also be computed.

9.5 PLASTIC FRACTURE MECHANICS

Thus far, we have avoided discussing the complicated material behavior in the process zone near the crack tip. This is acceptable as long as the process zone is small compared with the specimen dimensions, and a clear zone of K dominance is established around the crack tip. In some structures, however, the materials are so tough and ductile that the plastic zone near the crack tip is huge and comparable with specimen dimensions. Linear elastic fracture mechanics cannot be used under these conditions. Instead, we adopt a framework based on *plastic* solutions to crack tip fields. In this section, we address three issues:

1. The size of the plastic zone at the crack tip is estimated.
2. The asymptotic fields near the crack tip in a plastic material are calculated.
3. A phenomenological framework for predicting fracture in plastic solids is outlined.

9.5.1 Dugdale–Barenblatt Cohesive Zone Model of Yield at a Crack Tip

The simplest estimate of the size of the plastic zone at a crack tip can be obtained using Dugdale and Barenblatt's cohesive zone model, which gives the plastic zone size at the tip of a crack in a thin sheet (deforming under conditions of plane stress) as

$$r_p \approx \frac{\pi}{8} \left(\frac{K_I}{Y} \right)^2,$$

where K_I is the crack tip stress intensity factor, and Y is the material yield stress.

This estimate is derived as follows. Consider a crack of length $2a$ in an elastic-perfectly plastic material with elastic constants E , v and yield stress Y . We assume that the specimen is a thin sheet, with thickness much less than crack length, so that a state of plane stress is developed in the solid. We anticipate that there will be a region near each crack tip in which the material deforms plastically. The von Mises equivalent stress $\sqrt{3S_{ij}S_{ij}/2}$ should not exceed yield in this region. It is hard to find a solution with stresses at yield everywhere in the plastic zone, but we can easily construct an approximate solution in which the stress along the line of the crack satisfies the yield condition, using the “cohesive zone” model illustrated in Figure 9.46.

Let r_p denote the length of the cohesive zone at each crack tip. To construct an appropriate solution, we extend the crack in both directions to put fictitious crack tips at $x_1 = \pm(a + r_p)$ and distribute tractions of magnitude Y over the crack flanks from $x_1 = a$ to $x_1 = a + r_p$ and similarly at the other crack tip. Evidently, the stress then satisfies $\sigma_{22} = Y$ along the line of the crack just ahead of each crack.

We can use point force solution given in the table in Section 9.3.3 to compute the stress intensity factor at the fictitious crack tip. Omitting the tedious details of evaluating the integral, we find that

$$K_I^* = (\sigma - Y) \sqrt{\pi(a + r_p)} + \frac{2Y}{\pi} \sqrt{\pi(a + r_p)} \sin^{-1} \frac{a}{a + r_p}.$$

The $*$ on the stress intensity factor is introduced to emphasize that this is not the true crack tip stress intensity factor (which is of course $K_I = \sigma \sqrt{\pi a}$) but the stress intensity factor at the fictitious crack tip. The stresses must remain bounded just ahead of the fictitious crack tip, so that r_p must be chosen to satisfy $K_I^* = 0$. This gives

$$r_p = \frac{a}{\sin(\pi[1 - \sigma/Y]/2)} - a \approx \frac{\pi^2}{8} \left(\frac{\sigma}{Y} \right)^2 a.$$

It is more sensible to express this in terms of stress intensity factor

$$r_p \approx \frac{\pi}{8} \left(\frac{K_I}{Y} \right)^2 a.$$

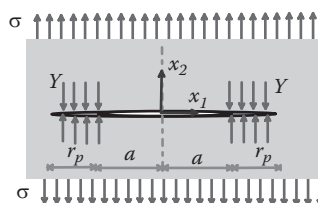


FIGURE 9.46 Superposition method used to estimate the size of a plastic zone at a crack tip.

This estimate turns out to be remarkably accurate for plane stress conditions, in which more detailed calculations give

$$r_p = \frac{1}{\pi} \left(\frac{K_{IC}}{Y} \right)^2.$$

For plane strain, the plastic zone is smaller: detailed calculations show that the plastic zone size is

$$r_p = \frac{1}{3\pi} \left(\frac{K_{IC}}{Y} \right)^2.$$

9.5.2 Hutchinson–Rice–Rosengren Crack Tip Fields for Stationary Crack in a Power Law Hardening Solid

The Hutchinson-Rice-Rosengren (HRR) fields are an exact solution to the stress, strain, and displacement fields near a crack tip in a power-law strain hardening, rigid plastic material, which is subjected to monotonically increasing stress at infinity. The model is based on the following assumptions:

1. The solid is infinitely large and contains an infinitely long crack with its tip at the origin.
2. The material is a rigid plastic, strain hardening solid with uniaxial stress-versus-strain curve

$$\sigma = \sigma_0 (\varepsilon / \varepsilon_0)^{1/n},$$

where σ_0 , ε_0 , n are material properties, with $n > 1$.

The HRR solution shows that the stress, strain, and displacement fields at a point (r, θ) in the solid (see Figure 9.47) can be calculated from functions of the form

$$\begin{aligned} \sigma_{ij} &= \sigma_0 \left(\frac{J}{\sigma_0 \varepsilon_0 r} \right)^{1/(n+1)} \Sigma_{ij}(\theta, n) \\ \varepsilon_{ij} &= \varepsilon_0 \left(\frac{J}{\sigma_0 \varepsilon_0 r} \right)^{n/(n+1)} E_{ij}(\theta, n) \\ u_{ij} &= \frac{J}{\sigma_0} \left(\frac{\sigma_0 \varepsilon_0 r}{J} \right)^{1/(n+1)} U_i(\theta, n), \end{aligned}$$

where Σ_{ij} , E_{ij} , U_i are dimensionless functions of the angle θ and the hardening index n only, and J is the value of the (path independent) J integral

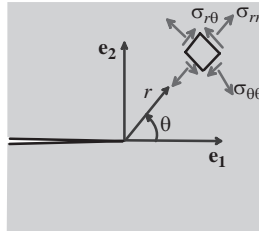


FIGURE 9.47 Coordinate system used to describe crack tip fields.

$$J = \int_C \left(W(\sigma_e) \delta_{j1} - \sigma_{ij} \frac{\partial u_i}{\partial x_1} \right) m_j ds,$$

where

$$W = \frac{n}{n+1} \sigma_0 \varepsilon_0 \left(\frac{3S_{ij}S_{ij}}{2\sigma_0} \right)^{\frac{n+1}{n}},$$

with $S_{ij} = \sigma_{ij} - \sigma_{kk}\delta_{ij}/3$. W can be interpreted as the total work done in loading the material up to a stress σ_{ij} under monotonically increasing, proportional loading.

These results are important for two reasons:

1. They show that the magnitudes of the stress, strain, and displacement near the crack tip are characterized by J . Thus, in highly plastic materials, J can replace K as the fracture criterion.
2. They illustrate the nature of the stress and strain fields near the crack tip. In particular, they show that the stress has a $r^{-(n+1)}$ singularity: for $n = 1$ (a linear stress-strain curve), we recover the square root singularity found in elastic materials, whereas for a perfectly plastic solid ($n \rightarrow \infty$), the stress is constant. In contrast, the strains have a square root singularity for $n = 1$ and an r^{-1} singularity for $n \rightarrow \infty$.

Derivation: The HRR solution is derived by solving the following governing equations for displacements u_i , strains ε_{ij} , and stresses σ_{ij} :

- Strain-displacement relation: $\varepsilon_{ij} = (\partial u_i / \partial x_j + \partial u_j / \partial x_i) / 2$.
- Stress equilibrium: $\partial \sigma_{ij} / \partial x_i = 0$.
- Boundary conditions: $\sigma_{22} = \sigma_{12} = 0$ on $x_2 = 0$ $x_1 < 0$.
- The stress-strain relation for a power-law hardening rigid plastic material subjected to monotonically increasing, proportional loading (this means that material particles

are subjected to stresses and strains whose principal axes do not rotate during loading) can be expressed as

$$\varepsilon_{ij} = \varepsilon_0 \left(\frac{\sigma_e}{\sigma_0} \right)^n \frac{3}{2} \frac{S_{ij}}{\sigma_e} \quad S_{ij} = \sigma_0 \left(\frac{\varepsilon_e}{\varepsilon_0} \right)^{1/n} \frac{2}{3} \frac{\varepsilon_{ij}}{\varepsilon_0},$$

where ε_0 , σ_0 , n are material constants, $S_{ij} = \sigma_{ij} - \sigma_{kk}\delta_{ij}/3$ is the deviatoric stress, and $\sigma_e = \sqrt{3S_{ij}S_{ij}/2}$ is the von Mises effective stress. Of course, we don't know a priori that material elements ahead of a crack tip experience proportional loading, but this can be verified after the solution has been found. It is helpful to note that, under proportional loading, the rigid plastic material is indistinguishable from an elastic material with strain energy potential

$$W = \frac{n}{n+1} \sigma_0 \varepsilon_0 \left(\frac{\sigma_e}{\sigma_0} \right)^{n+1} = \frac{n}{n+1} \sigma_0 \varepsilon_0 \left(\frac{\varepsilon_e}{\varepsilon_0} \right)^{(1+n)/n}.$$

The J integral must then be path independent.

The equilibrium condition may be satisfied through an Airy stress function ϕ , generating stresses in the usual way as

$$\sigma_{rr} = \frac{1}{r} \frac{\partial \phi}{\partial r} + \frac{1}{r^2} \frac{\partial^2 \phi}{\partial \theta^2} \quad \sigma_{\theta\theta} = \frac{\partial^2 \phi}{\partial r^2} \quad \sigma_{r\theta} = -\frac{\partial}{\partial r} \left(\frac{1}{r} \frac{\partial \phi}{\partial \theta} \right).$$

The solution can be derived from an Airy function that has a separable form

$$\phi = r^\alpha f(\theta) + \dots,$$

where the power α and $f(\theta)$ are to be determined. The strength of the singularity α can be determined using the J integral. Evaluating the integral around a circular contour radius r enclosing the crack tip, we obtain

$$J = \int_C \left(W \delta_{j1} - \sigma_{ij} \frac{\partial u_i}{\partial x_1} \right) m_j ds = \int_{-\pi}^{\pi} \left(W \delta_{j1} - \sigma_{ij} \frac{\partial u_i}{\partial x_i} \right) m_j r d\theta.$$

For the J integral to be path independent, it must be independent of r , and therefore W must be of order r^{-1} . The Airy function gives stresses of order $r^{\alpha-2}$, and the corresponding strain energy density would have order $r^{(n+1)(\alpha-2)}$. Consequently, for a path-independent J , we must have $(n + 1)(\alpha - 2) = -1$, so

$$\alpha = \frac{2n+1}{n+1}.$$

Note for a linear material ($n = 1$), we find $\alpha = 3/2$, which corresponds to the expected square-root stress singularity.

We can now scale the governing equations as discussed in Section 7.1.13. To this end, define normalized length, displacement, strain, stress, and Airy function as

$$X_i = \sigma_0 \varepsilon_0 x_i / J \quad R = \sigma_0 \varepsilon_0 r / J \quad U_i = u_i \sigma_0 / J \quad E_{ij} = \varepsilon_{ij} / \varepsilon_0 \quad \Sigma_{ij} = \sigma_{ij} / \sigma_0 \quad \Phi = \phi(\sigma_0 \varepsilon_0 / J)^2.$$

With these definitions, the governing equations reduce to the following:

- Strain-displacement relation: $E_{ij} = (\partial U_i / \partial X_j + \partial U_j / \partial X_i) / 2$.
- Stress equilibrium: $\partial \Sigma_{ij} / \partial X_i = 0$.
- Constitutive equation:

$$E_{ij} = (\Sigma_e)^n \frac{3 \Sigma'_{ij}}{2 \Sigma_e} \quad \Sigma'_{ij} = \Sigma_{ij} - \Sigma_{kk} \delta_{ij} / 3 \quad \Sigma_e = \sqrt{3 \Sigma_{ij} \Sigma_{ij} / 2}.$$

In addition, the stresses are related to the normalized Airy function by

$$\Sigma_{rr} = \frac{1}{R} \frac{\partial \Phi}{\partial R} + \frac{1}{R^2} \frac{\partial^2 \Phi}{\partial \theta^2} \quad \Sigma_{\theta\theta} = \frac{\partial^2 \Phi}{\partial R^2} \quad \Sigma_{r\theta} = -\frac{\partial}{\partial R} \left(\frac{1}{R} \frac{\partial \Phi}{\partial \theta} \right),$$

whereas the expression for the J integral becomes

$$J = \int_{-\pi}^{\pi} \left(\hat{W} \delta_{j1} - \Sigma_{ij} \frac{\partial U_i}{\partial X_1} \right) m_j R d\theta,$$

where $\hat{W} = W / \sigma_0 \varepsilon_0$. The only material parameter appearing in the scaled equations is n . In addition, note that J has been eliminated from the equations, so the solution is independent of J .

The stresses can be derived from an Airy function

$$\Phi = R^{(2n+1)/(n+1)} f(\theta).$$

The scaling of displacements, strain, and stress with load and material properties then follows directly from the definition of the normalized quantities.

To compute the full expression for $f(\theta)$ and hence to determine Σ_{ij} , E_{ij} , U_i is a tedious and not especially straightforward exercise. The governing equation for f is obtained from the condition that the strain field must be compatible. This requires

$$r^{-1} \frac{\partial \epsilon_{rr}}{\partial r} - r^{-2} \frac{\partial^2 \epsilon_{rr}}{\partial \theta^2} - 2r^{-1} \frac{\partial \epsilon_{\theta\theta}}{\partial r} - \frac{\partial^2 \epsilon_{\theta\theta}}{\partial r^2} + r^{-1} \frac{\partial^2 \epsilon_{r\theta}}{\partial r \partial \theta} + r^{-2} \frac{\partial \epsilon_{r\theta}}{\partial \theta} = 0.$$

Computing the stresses from the Airy function, deducing the strains using the constitutive law, and substituting the results into this equation yields a fourth-order nonlinear ODE for f , which must be solved subject to appropriate symmetry and boundary conditions. The solution must be found numerically (details are given by Hutchinson [1968] and Rice and Rosengren [1968]).

9.5.3 Plastic Fracture Mechanics Based on J

There are many situations (e.g., in design of pressure vessels, pipelines, etc.) in which the structure is purposely made from a tough, ductile material. Usually, one cannot apply LEFM to these structures, because a large plastic zone forms at the crack tip (the plastic zone is comparable with specimen dimensions, and there is no K -dominant zone). Some other approach is needed to design against fracture in these applications.

Two related approaches are used: one is based on the HRR crack tip field and uses J as a fracture criterion; the other uses the crack tip opening displacements as a fracture criterion. Only the J based approach will be discussed here.

The most important conclusion from the HRR crack tip field is that the amplitude of stresses, strains, and displacements near a crack tip in a plastically deforming solid scale in a predictable way with J . Just as stress intensity factors quantify the stress and strain magnitudes in a linear elastic solid, J can be used as a parameter to quantify the state of stress near the tip of a crack in a plastic solid.

Phenomenological J -based fracture mechanics is based on the same reasoning that is used to justify K -based LEFM. We postulate that we will find three distinct regions in a plastically deforming specimen containing a crack (see Figure 9.48):

1. A process zone near the crack tip, with finite deformations and extensive material damage, in which the asymptotic HRR field is not accurate.
2. A J dominant zone, which is outside the process zone, but small compared with specimen dimensions. Here, the HRR field accurately describes the deformation.
3. The remainder, in which stress and strain fields are controlled by specimen geometry and loading.

As for LEFM, we hope that the process zone is controlled by the surrounding J -dominant zone, so that crack tip loading conditions can be characterized by J .

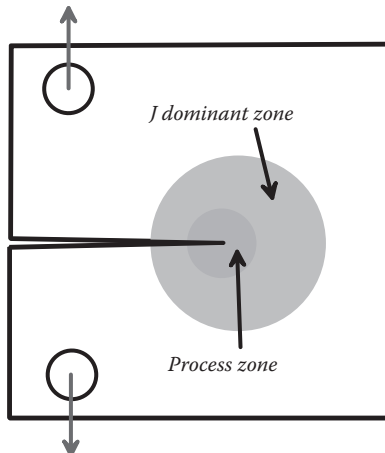


FIGURE 9.48 Regions of behavior near the tip of a crack in a plastically deforming solid.

J -based fracture mechanics is applied in much the same way as LEFM. We assume that crack growth starts when J reaches a critical value (for mode I plane strain loading, this value is denoted J_{IC}). The critical value must be measured experimentally for a given material, using standard test specimens. To assess the safety of a structure or component containing a crack, one must calculate J and compare the predicted value with J_{IC} : if $J < J_{IC}$, the structure is safe.

Practical application of J -based fracture mechanics is somewhat more involved than LEFM. Tests to measure J_{IC} are performed using standard test specimens: deeply cracked three- or four-point bend bars are often used. Calibrations for the three-point bend bar shown in Figure 9.49 are available in the work by Rice, Paris, and Merkle [1973].

Calculating J for a specimen or component usually requires a full-field FEM analysis. Cataloging solutions to standard problems is much more difficult than for LEFM, because the results depend on the stress-strain behavior of the material. Specifically, for a power-law solid containing a crack of length a and subjected to stress σ , we expect that

$$J = \sigma_0 \varepsilon_0 a (\sigma / \sigma_0)^{n+1} f(n, \text{geometry}).$$

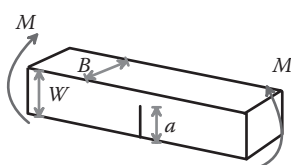


FIGURE 9.49 Four-point bend specimen.

For example, a slit crack of length $2a$ subjected to mode I loading with stress σ has (approximately) [see He and Hutchinson 1981]

$$J = \sigma_0 \varepsilon_0 a \pi \sqrt{n} \left(\frac{\sqrt{3}\sigma}{\sigma_0} \right)^{n+1}.$$

Finally, to apply the theory, it is necessary to ensure that both test specimen and component satisfy conditions necessary for J dominance. As a rough rule of thumb, if all characteristic specimen dimensions (crack length, etc.) exceed $200J/\varepsilon_0\sigma_0$, J dominance is likely to be satisfied.

9.6 LINEAR ELASTIC FRACTURE MECHANICS OF INTERFACES

Many engineering applications require one material to be bonded to another. Examples include adhesive joints, protective coatings, composite materials, and thin films used in the manufacture of microelectronic circuits. In all these applications, techniques are required to predict the strength of the bond. To this end, a great deal of work has been done over the past 20 years to extend linear elastic fracture mechanics to predict the behavior of cracks on, or near, the interface between two dissimilar brittle materials.

9.6.1 Crack Tip Fields for a Crack on an Interface

The foundation for linear elastic interfacial fracture mechanics (LEIFM) is based on an asymptotic analysis of the stress and strain fields near the tip of a crack.

The problem of interest is illustrated in Figure 9.50. A semi-infinite crack with a straight front that coincides with the x_3 axis lies on the interface between two linear elastic solids. The material above the crack has shear modulus and Poisson's ratio μ_1, v_1 ; the material below the crack has shear modulus and Poisson's ratio μ_2, v_2 . In this section, we give the complex variable solution that governs the variation of stress and displacement near the crack tip. The solid is subjected to static remote loading and is assumed to deform in plane strain.

The complete stress and displacement fields for an interface crack are given in Section 5.3.6. The solution is too long to include here. Instead, we summarize the key features.

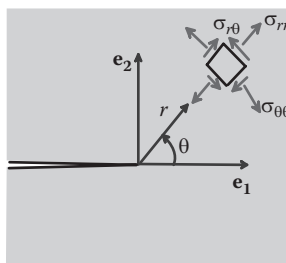


FIGURE 9.50 Crack on the interface between two elastic solids.

9.6.1.1 Material Parameters for an Interface

The solution is expressed in terms of several additional parameters:

1. Plane strain moduli: $E'_1 = 2_{-1}/(1-v_1)$, $E'_2 = 2_{-2}/(1-v_2)$.

2. Bimaterial modulus: $\frac{1}{E^*} = \left\{ \frac{1}{E'} + \frac{1}{E'_2} \right\}$.

3. Dundurs' elastic constants:

$$\alpha = \frac{E'_1 - E'_2}{E'_1 + E'_2} \quad \beta = \frac{(1-2v_2)/_{-2} - (1-2v_1)/_{-1}}{2(1-v_2)/_{-2} + 2(1-v_1)/_{-1}}.$$

Evidently, α is a measure of the relative stiffness of the two materials. It must lie in the range $-1 < \alpha < 1$ for all possible material combinations: $\alpha = 1$ indicates that material 1 is rigid, whereas $\alpha = -1$ signifies that material 2 is rigid. The second parameter does not have such a nice physical interpretation: it is a rough measure of the relative compressibilities of the two materials. For Poisson's ratios in the range $0 < v < 1/2$, one can show that $-1 < \alpha - 4\beta < 1$.

4. Crack tip singularity parameter:

$$\varepsilon = \frac{1}{2\pi} \log \left(\frac{1-\beta}{1+\beta} \right).$$

For most material combinations, the value of ε is very small, typically of order 0.01 or so.

9.6.1.2 Crack Tip Loading Parameters

The state of stress at the crack tip is characterized by three numbers: an arbitrary characteristic length L (a value of $L = 100\mu m$ is often used), the phase angle of the loading ψ , and the magnitude of the stress intensity factor $|K|$. Often, the energy release rate for the crack G is used in place of $|K|$. These quantities are defined as follows:

- Phase angle: $\psi = \tan^{-1} \left(\frac{\sigma_{12}(r=L)}{\sigma_{22}(r=L)} \right)$.
- Stress intensity magnitude: $|K| = e^{-i\psi} \lim_{r \rightarrow 0} (\sigma_{22} + i\sigma_{12})(r/L)^{-i\varepsilon} \sqrt{2\pi r}$.
- Energy release rate: $G = \frac{|K|^2}{2E^* \cosh^2 \pi \varepsilon}$.

- Solutions to interface crack problems are also often expressed in terms of two stress-intensity factor-like parameters K_1 and K_2 . These are related to the crack tip parameters by

$$(K_1 + iK_2) = |K| e^{i\psi} L^{-i\varepsilon}$$

$$|K| = \sqrt{K_1^2 + K_2^2} \quad \psi = \tan^{-1} \left\{ \frac{\text{Im}[(K_1 + iK_2)L^{i\varepsilon}]}{\text{Re}[(K_1 + iK_2)L^{i\varepsilon}]} \right\}.$$

9.6.1.3 Interpreting the Crack Tip Fields

- The values of $|K|$ and ψ are determined by the solid's shape and how it is loaded (the value of ψ also depends on the choice of the characteristic length L). Once $|K|$ and ψ are known, however, the near tip fields always have the form given by the asymptotic solution.
- Because ψ quantifies the ratio of shear to opening stress ahead of the crack tip, it is qualitatively equivalent to the ratio $\tan^{-1}(K_{II}/K_I)$, where K_I and K_{II} are the mode I and mode II stress intensity factors for a crack in a homogeneous solid.
- The opening and shear stresses along $\theta = 0$ ahead of the crack tip can be calculated from

$$\sigma_{22} + i\sigma_{12} = \frac{|K| e^{i\psi}}{\sqrt{2\pi r}} \left(\frac{r}{L} \right)^{i\varepsilon}.$$

- The crack opening displacements behind the crack tip can be calculated from

$$\delta_2 + i\delta_1 = \frac{4|K| e^{i\psi}}{E^*(1+2i\varepsilon)\cosh(\pi\varepsilon)} \sqrt{\frac{r}{2\pi}} \left(\frac{r}{L} \right)^{i\varepsilon}.$$

- The complex exponent appearing in these expressions is scary. To understand what it means, note that

$$r^{i\varepsilon} = \exp(i\varepsilon \log r) = \cos(\varepsilon \log r) + i \sin(\varepsilon \log r),$$

so this term indicates that the stresses *oscillate* near the crack tip. We will discuss this in more detail below.

9.6.1.4 Oscillations in the Stress and Displacement Fields

The asymptotic crack tip field for an interface crack is strikingly different to the corresponding solution for a homogeneous solid. In fact, the results are somewhat disturbing and have been the cause of much anguish in the fracture mechanics community.

We have already noted that the stress fields are oscillatory near the crack tip. The stress distributions are plotted in Figure 9.51 as a function of $\log(\varepsilon r/L)$. Note that the results are

shown for an unphysically large value of ε ; for practical values, the oscillations are so slow that it is hard to see them.

Both normal and shear stresses oscillate with increasing frequency as the crack tip is approached. As a result, it is difficult to unambiguously separate the loading into normal and shear components: an opening stress induces just as much shear near the crack tip as does shear loading and vice versa.

Even more disturbingly, the crack opening displacements show the same oscillatory character. This means that the solution predicts that the crack faces overlap near the crack tip, which is clearly unphysical.

It is possible to find a solution that corrects for the overlapping crack faces [Comninou 1977]. This solution predicts that the crack faces touch just behind the crack tip for all combinations of remote load. There is a square root singularity in shear stress at the crack tip (so it is strictly always loaded in mode II). The zone of contact is extremely small, however, typically of the order of a few nanometers for most practical crack sizes and materials and probably much smaller than the process zone.

The standard procedure in LEIFM is to ignore the overlap between crack faces and accept the asymptotic field described in the beginning of this subsection as characterizing the stress and strain fields for an interface crack. The oscillatory singularity is, after all, no less physical than a square-root singularity. The asymptotic field is expected to represent actual stress and strain fields in an annular region, which is small compared with specimen geometry and large compared with the process zone.

9.6.2 Phenomenological Theory of Interface Fracture

Phenomenological fracture mechanics for interfaces is based on the same reasoning that is used in fracture mechanics of homogeneous solids. We anticipate three distinct regions in a plastically deforming specimen containing a crack, as shown in Figure 9.52. These include the following:

1. A process zone near the crack tip, with finite deformations and extensive material damage, in which the asymptotic field is not accurate

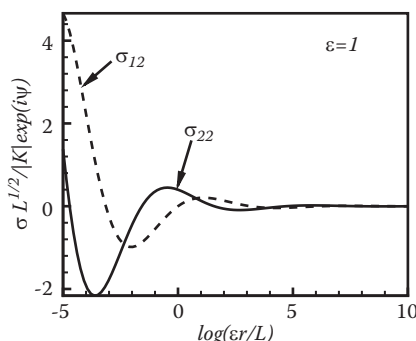


FIGURE 9.51 Stress fields near the tip of an interface crack.

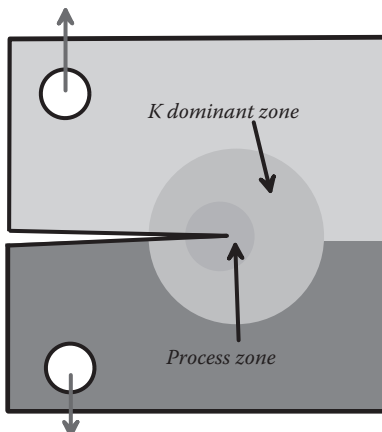


FIGURE 9.52 Regions of behavior near the tip of an interface crack.

2. A K -dominant zone, outside the process zone, but small compared with specimen dimensions, in which the asymptotic linear elastic field accurately describes the deformation
3. The remainder, in which stress and strain fields are controlled by specimen geometry and loading

Material failure (crack growth or fatigue) is a consequence of the failure mechanisms in the process zone. As usual, we do not attempt to model the failure process in detail and instead assume that the fields in the process zone are controlled by the fields in the region of K dominance. In interface fracture, we use the stress state at the reference length L ahead of the crack tip to characterize the loading experienced by the process zone. As we have seen, this stress is characterized by the energy release rate G (or, alternatively, the stress intensity magnitude $|K|$), together with the phase angle ψ .

Fracture criterion: The critical condition for an interface crack to propagate is therefore given by a fracture criterion of the form

$$G = G_i(\psi),$$

where $G_i(\psi)$ is the fracture toughness of the interface and ψ is the phase angle, defined using some appropriate choice of length L . The fracture toughness is a function of phase angle, just as the fracture toughness of a homogeneous solid subjected to mixed mode loading is a function of K_{II}/K_I .

The fracture resistance of the interface $G_i(\psi)$ must be measured experimentally. Several specimens are available for this purpose. Examples include sandwich specimens [Leichti and Knauss 1982; Suo and Hutchinson 1989] and four-point bend specimens [Charalambides, Cao, Lund, and Evans 1990]. Experiments show that G_i increases rapidly with phase angle:

the typical variation of fracture toughness with phase angle is sketched in Figure 9.53. In fact, many experimental data seem to be fit by $G_i = G_0/\cos(\psi)$.

To apply LEIFM, then, it is necessary (1) to measure the fracture resistance of the interface as a function of phase angle, (2) calculate energy release rate and phase angle for the interface crack in the structure or component of interest, and (3) apply the fracture criterion to assess the load bearing capacity of the component.

9.6.3 Stress Intensity Factors for Some Interface Cracks

The solutions to interface crack problems are most conveniently expressed in terms of the stress intensity factors K_1, K_2 , because these are linear in stress and can therefore be superposed. Stress intensity factors have been computed for many standard specimen geometries (usually using a numerical technique). A few examples are shown in Table 9.3.

The point force solutions can be used to calculate stress intensity factors for interface cracks that are subjected to nonuniform stress fields, following the procedure given in Section 9.3.3. The energy release rate and phase angle can be calculated using the formulas given in the preceding section. For example, for the slit crack with length $2a$ subjected to uniform stress far from the crack, the energy release rate and phase angle are

$$\begin{aligned}\psi &= \tan^{-1} \left\{ \frac{\operatorname{Im} \left[(\sigma_{22} + i\sigma_{12})(1+2i\varepsilon)(L/a)^{ie} \right]}{\operatorname{Re} \left[(\sigma_{22} + i\sigma_{12})(1+2i\varepsilon)(L/a)^{ie} \right]} \right\} \\ G &= \frac{(\sigma_{22}^2 + \sigma_{12}^2)(1+4\varepsilon^2)\pi a}{2E^* \cosh^2(\pi\varepsilon)}.\end{aligned}$$

Note that, for a fixed value of L , the phase angle depends on the size of the crack. This is a general feature of interface cracks: the mode mix depends on specimen size. However, the value of ε for most material pairs is very small, so the variation with specimen size is very weak.

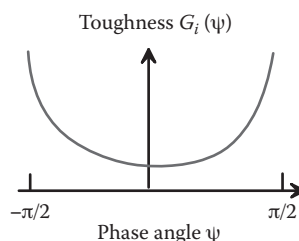
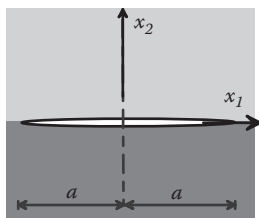
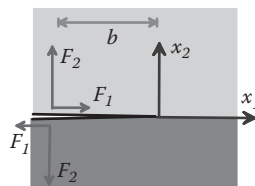


FIGURE 9.53 Typical relation between fracture toughness and crack tip phase angle.

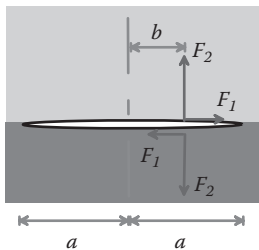
TABLE 9.3 Stress Intensity Factors for Interface Cracks



$$K_1 + iK_2 = (\sigma_{22} + i\sigma_{12})\sqrt{\pi a}(1+2ie)(2a)^{-ie}$$



$$K_1 + iK_2 = \sqrt{\frac{2}{\pi}} \cosh \pi \epsilon \frac{F_2 + iF_1}{b^{1/2+ie}}$$



$$K_1 + iK_2 = \sqrt{\frac{2}{\pi}} \cosh \pi \epsilon \frac{F_2 + iF_1}{(2a)^{1/2+ie}} \left(\frac{a+b}{a-b} \right)^{1/2+ie}$$

9.6.4 Crack Path Selection

A final issue that is of great interest in interfacial fracture is the question of crack path selection. An interface crack can either propagate along the interface or deflect into one of the two materials adjacent to the interface. In addition, a crack approaching transverse to an interface may be deflected along it; this is a mechanism for trapping cracks in composite materials (Figure 9.54).

A rather involved stress analysis is required to predict the path of the crack, but the results are simple. A crack approaching perpendicular to an interface will deflect along the interface as long as

$$G_i(\pi/2) < G_{cm}/4,$$

where \$G_i(\pi/2)\$ is the interface toughness for a phase angle of \$90^\circ\$, and \$G_{cm}\$ is the fracture toughness of the material on the far side of the interface. If this condition is satisfied, the crack remains trapped in the interface and will not kink out of it.

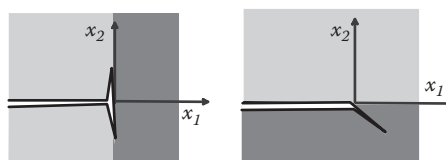


FIGURE 9.54 Crack deflection at a bi-material interface.

This page intentionally left blank

Solutions for Rods, Beams, Membranes, Plates, and Shells

The full-field equations of solid mechanics describe deformation by specifying the motion of every material particle within the solid and describe internal forces by means of the 3D distribution of Cauchy stress within the material. As we have seen, it can be difficult to find solutions to the full 3D equations. For solids with certain special shapes, it is sometimes possible to simplify the governing equations by approximating the variation of strain or stress in the solid. For example, you may be familiar with the Euler–Bernoulli equations governing the elastic deflections of beams. In this theory, the strain and stress distribution in the beam is completely determined by the deflection of the neutral axis of the beam. Consequently, the equations of equilibrium for the solid can be reduced to a system of ODEs for the beam deflections.

Similar approaches may be used to construct approximate solutions to many important problems. In this chapter, we will discuss (1) the deformation of slender rods and the simpler special case of a straight beam, and (2) the deformation of a thin 3D shell and the simpler cases of membranes and flat plates. The theories outlined in this chapter were originally developed in the early part of the past century to help in mechanical vibration and structural design calculations. They are still used for this purpose today but are also used to model biological systems, such as bacterial flagellae or cell walls, and also to model nanoscale structures such as carbon nanotubes.

A number of different approaches are used to derive approximations to the 3D field equations of solid mechanics. Here, we will use a systematic procedure based on the principle of virtual work. In this approach, we begin by approximating the displacement field in the solid in some sensible way. The goal is to describe the 3D displacement field in terms of a reduced set of kinematic variables. The approximate displacement field is then substituted into the virtual work equation, which yields generalized force measures that are conjugate to the kinematic variables, together with a set of equilibrium equations and boundary conditions for these forces.

HEALTH WARNING: In previous chapters, we have been able to express all vector and tensor quantities as Cartesian components in a fixed basis. We can continue to use this notation for some of the simpler problems considered in this chapter, such as modeling the behavior of a straight beam or a flat plate. For more general problems, such as twisted rods, or shells with a complicated geometry, this notation is inadequate. Therefore, most of this chapter uses more generalized notation. The theory of deformable rods describes vectors and tensors as components in a basis consisting of three mutually perpendicular unit vectors that are aligned with the rod and rotate with the rod as it deforms. Shell theory uses a general basis of nonorthogonal unit vectors. It can be a struggle to master the complicated notation associated with curvilinear coordinates, but it is worth making the effort. You may find it helpful to work through rod theory first, which will get you used to expressing vectors and tensor in a position-dependent basis and then move onto shell theory, which adds the additional complexity of nonorthogonal coordinates. If you would prefer to avoid both, simplified theories for straight beams and flat plates are given in Cartesian coordinates.

10.1 PRELIMINARIES: DYADIC NOTATION FOR VECTORS AND TENSORS

All the theories developed in this section involve solids that are subjected to large shape changes. In most cases, the material is only slightly distorted, but, because of the component's geometry, these shape changes can lead to large displacements and rotations in the solid.

When solving problems like this, it is often convenient to express the various vector and tensor measures of deformation and force as components in two different sets of basis vectors, with one set associated with the undeformed solid and the other associated with the deformed solid. In some cases, we even resort to using both bases at the same time. Dyadic notation is a convenient way to express these ideas.

To follow dyadic notation, you need only to understand and remember three basic ideas:

- Dyadic product of vectors: Let \mathbf{a} and \mathbf{b} be two vectors. The dyadic product of \mathbf{a} and \mathbf{b} is a second-order tensor \mathbf{S} denoted by

$$\mathbf{S} = \mathbf{a} \otimes \mathbf{b}$$

with the properties

$$\mathbf{S} \cdot \mathbf{u} = (\mathbf{a} \otimes \mathbf{b}) \cdot \mathbf{u} = \mathbf{a}(\mathbf{b} \cdot \mathbf{u})$$

$$\mathbf{u} \cdot \mathbf{S} = \mathbf{u} \cdot (\mathbf{a} \otimes \mathbf{b}) = (\mathbf{a} \cdot \mathbf{u})\mathbf{b}$$

for all vectors \mathbf{u} .

- Products of dyadic products: Let \mathbf{a} , \mathbf{b} , \mathbf{c} , and \mathbf{d} be four vectors and let $\mathbf{S} = (\mathbf{a} \otimes \mathbf{b})$, $\mathbf{T} = (\mathbf{c} \otimes \mathbf{d})$. The products of \mathbf{S} and \mathbf{T} are expressed in dyadic notation as follows:

$$\mathbf{S} \cdot \mathbf{T} = (\mathbf{a} \otimes \mathbf{b}) \cdot (\mathbf{c} \otimes \mathbf{d}) = (\mathbf{b} \cdot \mathbf{c})\mathbf{a} \otimes \mathbf{d}$$

$$\mathbf{S} : \mathbf{T} = (\mathbf{a} \cdot \mathbf{c})(\mathbf{b} \cdot \mathbf{d})$$

$$\mathbf{S} \cdot \mathbf{T} = (\mathbf{a} \cdot \mathbf{d})(\mathbf{b} \cdot \mathbf{c}).$$

- Representing a general tensor as a sum of dyadic products: Let \mathbf{a}_i (with $i = 1, 2, 3$) be three linearly independent vectors. Then any tensor \mathbf{S} can be expressed as a linear combination of nine dyadic products of these vectors:

$$\mathbf{S} = S_{ij}\mathbf{a}_i \otimes \mathbf{a}_j,$$

where summation on i and j is assumed.

10.2 MOTION AND DEFORMATION OF SLENDER RODS

Figure 10.1 illustrates the problem to be solved. We suppose that a long, initially straight rod is subjected to forces and moments that cause it to stretch, bend, and twist into a complex 3D shape that we want to determine. The initial shape need not necessarily be stress free. Consequently, we can solve problems involving a rod that is bent and twisted in its unloaded configuration (such as a helical spring) by first mapping it onto an intermediate, straight reference configuration and then analyzing the deformation of this shape.

10.2.1 Variables Characterizing the Geometry of a Rod's Cross Section

Figure 10.2 illustrates a generic cross section of the (undeformed) rod. We will characterize the shape of the cross section as follows:

- We introduce three mutually perpendicular, unit basis vectors $\{\mathbf{e}_1, \mathbf{e}_2, \mathbf{e}_3\}$, with \mathbf{e}_3 pointing parallel to the axis of the cylinder and $\mathbf{e}_1, \mathbf{e}_2$ parallel to the principal moments of area of the (undeformed) cross section.
- We introduce a coordinate system (x_1, x_2) within the cross section, with origin at the centroid of the cross section.
- The cross-sectional area of the rod is denoted by $A = \int_A dA$.

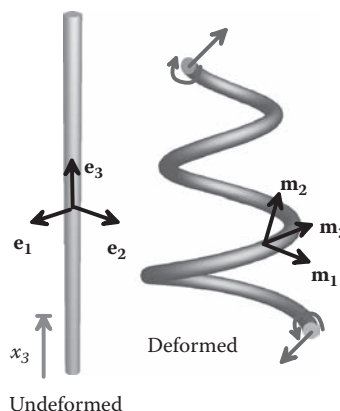


FIGURE 10.1 Deformation of an initially straight rod.

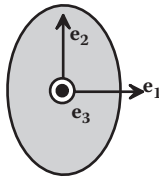


FIGURE 10.2 Cross section of a rod, showing basis used to define vector and tensor components.

4. The principal moments of area of the cross section are defined as

$$I_1 = \int_A x_2^2 dA \quad I_2 = \int_A x_1^2 dA \quad I_3 = \int_A (x_1^2 + x_2^2) dA.$$

5. We define a moment of area tensor \mathbf{H} for the cross section, with components $H_{11} = I_1$, $H_{22} = I_2$, and $H_{33} = I_3$ and all other components zero.

6. In calculations to follow, it will be helpful to note that, because of the choice of origin and coordinate system,

$$\int_A x_1 dA = \int_A x_2 dA = \int_A x_1 x_2 dA = 0.$$

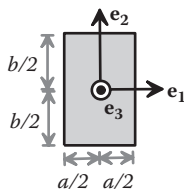
Principal moments of area and their directions are listed for a few simple geometries in Table 10.1. Recall also that area moments of inertia for *hollow* sections can be calculated by subtraction.

10.2.2 Coordinate Systems and Variables Characterizing the Deformation of a Rod

A generic twisted rod is illustrated in Figure 10.3. The deformation of the rod is described as follows:

- The orientation of the straight rod is characterized using the $\{\mathbf{e}_1, \mathbf{e}_2, \mathbf{e}_3\}$ basis described in the preceding section.

TABLE 10.1 Areas and Area Moments of Inertia for Simple Cross Sections

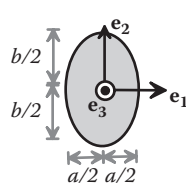


$$A = ab$$

$$I_1 = b^3 a / 12$$

$$I_2 = a^3 b / 12$$

$$I_3 = ab(a^2 + b^2)/12$$

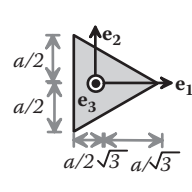


$$A = \pi ab$$

$$I_1 = \pi b^3 a / 4$$

$$I_2 = \pi a^3 b / 4$$

$$I_3 = \pi ab(a^2 + b^2)/4$$



$$A = a^2 \sqrt{3} / 4$$

$$I_1 = I_2 = a^4 \sqrt{3} / 96$$

$$I_3 = a^4 \sqrt{3} / 48$$

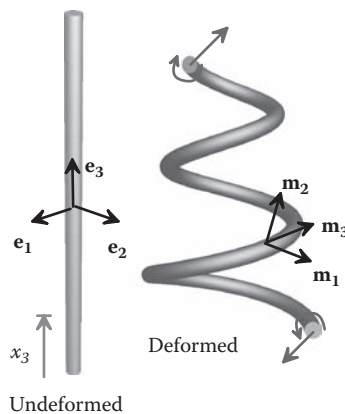


FIGURE 10.3 Deformation of an initially straight rod.

- The position vector of a material particle in the reference configuration is $\mathbf{x} = x_i \mathbf{e}_i$, where $x_1 = x_2 = 0$ corresponds to the centroid of the cross section, and x_3 is the height above the base of the cylinder.
- After deformation, the axis of the cylinder lies on a smooth curve. The point that lies at $\mathbf{x} = x_3 \mathbf{e}_3$ in the undeformed solid moves to a new position $\mathbf{y} = \mathbf{r}(x_3)$ after deformation.
- The orientation of the cross section after deformation will be described by introducing a basis of mutually perpendicular unit vectors $\{\mathbf{m}_1, \mathbf{m}_2, \mathbf{m}_3\}$, chosen so that \mathbf{m}_3 is parallel to the axis of the deformed rod and \mathbf{m}_1 is parallel to the line of material points that lay along \mathbf{e}_1 in the reference configuration (or, more precisely, parallel to the projection of this line perpendicular to \mathbf{m}_3). Note that the three basis vectors $\{\mathbf{m}_1, \mathbf{m}_2, \mathbf{m}_3\}$ are all functions of x_3 , and, if the rod is moving, they are also functions of time.
- The orientation of $\{\mathbf{m}_1, \mathbf{m}_2, \mathbf{m}_3\}$ can be specified by three Euler angles (θ, ϕ, ψ) , which characterize the rigid rotation that maps $\{\mathbf{e}_1, \mathbf{e}_2, \mathbf{e}_3\}$ onto $\{\mathbf{m}_1, \mathbf{m}_2, \mathbf{m}_3\}$. To visualize the significance of the three angles, note that the rotation can be accomplished in three stages, as shown in Figure 10.4. (1) Rotate the basis vectors through an angle ϕ about the \mathbf{e}_3 axis. This results in a new set of vectors $\{\hat{\mathbf{e}}_1, \hat{\mathbf{e}}_2, \mathbf{e}_3\}$. (2) Rotate these new vectors through an angle θ about the $\hat{\mathbf{e}}_2$ axis. This rotates the vectors onto a second

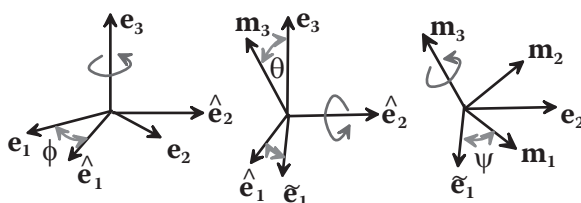


FIGURE 10.4 Visualizing Euler angles as a sequence of three rotations applied to a triad of mutually perpendicular vectors.

configuration $\{\tilde{\mathbf{e}}_1, \hat{\mathbf{e}}_2, \mathbf{m}_3\}$. (3) Finally, rotate these vectors through angle ψ about the \mathbf{m}_3 direction, to create the $\{\mathbf{m}_1, \mathbf{m}_2, \mathbf{m}_3\}$ vectors.

- Relationships between the Euler angles and the curve characterizing the axis of the rod will be given shortly: these results will show that the angles ϕ and θ can be determined from the shape of the axis. The angle ψ is an independent degree of freedom and quantifies the rotation of the rod's cross section about its axis.
- We let s denote the arc length measured along the axis of the rod in the deformed configuration.
- The velocity of the rod is characterized by the velocity vector of its axis, $\mathbf{v} = d\mathbf{r}/dt$.
- The rate of rotation of the rod is characterized by the angular velocity $\boldsymbol{\omega} = \omega_i \mathbf{m}_i$ of the basis vectors $\{\mathbf{m}_1, \mathbf{m}_2, \mathbf{m}_3\}$. It will be shown in Section 10.2.3 that the angular velocity can be related to the velocity \mathbf{v} of the bar's axis and its twist ψ by

$$\boldsymbol{\omega} = \mathbf{m}_3 \times \frac{d\mathbf{v}}{ds} + \dot{\psi} \mathbf{m}_3.$$

- The acceleration of the rod is characterized by the acceleration vector of its axis, $\mathbf{a} = d\mathbf{v}/dt$.
- The angular acceleration of the rod is characterized by the angular acceleration $\boldsymbol{\alpha} = \alpha_i \mathbf{m}_i$ of the basis vectors. It will be shown below that the angular acceleration can be related to the acceleration \mathbf{a} and velocity \mathbf{v} of the bar's axis and its twist ψ by

$$\boldsymbol{\alpha} = \frac{d\boldsymbol{\omega}}{dt} = \mathbf{m}_3 \times \frac{d\mathbf{a}}{ds} - 2 \left(\frac{d\mathbf{v}}{ds} \cdot \mathbf{m}_3 \right) \mathbf{m}_3 \times \frac{d\mathbf{v}}{ds} + \frac{d\psi}{dt} \left\{ \frac{d\mathbf{v}}{ds} - \left(\frac{d\mathbf{v}}{ds} \cdot \mathbf{m}_3 \right) \mathbf{m}_3 \right\} + \frac{d^2\psi}{dt^2} \mathbf{m}_3.$$

10.2.3 Additional Deformation Measures and Useful Kinematic Relations

In this section, we introduce some additional measures of the deformation of the rod, as well as several useful relations between the various deformation measures:

- The curve corresponding to the axis of the deformed rod is often characterized by its *tangent*, *normal*, and *binormal vectors*, together with its *curvature* and its *torsion*. These are defined as follows:

1. The tangent vector is defined as $\mathbf{t} = \frac{d\mathbf{r}}{ds} = \frac{d\mathbf{r}}{dx_3} \frac{dx_3}{ds} = \mathbf{m}_3$.
2. The normal vector and curvature are defined so that $\kappa \mathbf{n} = \frac{d\mathbf{t}}{ds} = \frac{d\mathbf{m}_3}{dx_3} \frac{dx_3}{ds}$, where \mathbf{n} is a unit vector.
3. The binormal vector is defined as $\mathbf{b} = \mathbf{t} \times \mathbf{n}$.
4. The triad of unit vectors $\{\mathbf{t}, \mathbf{n}, \mathbf{b}\}$ defines the *Frenet basis* for the curve.
5. The *torsion* of the curve is defined as $\tau = -\mathbf{n} \cdot \frac{d\mathbf{b}}{ds}$. Note that the torsion is simply a geometric property of the curve; it is not necessarily related to the rod's twist.

These variables are not sufficient to completely describe the deformation, however, because the twist of the rod can vary independently of the shape of its axis.

- The two bases $\{\mathbf{e}_1, \mathbf{e}_2, \mathbf{e}_3\}$, $\{\mathbf{m}_1, \mathbf{m}_2, \mathbf{m}_3\}$ can be related in terms of the Euler angles as follows:

$$\mathbf{m}_1 = (\cos \psi \cos \theta \cos \phi - \sin \psi \sin \phi) \mathbf{e}_1 + (\cos \psi \cos \theta \sin \phi + \sin \psi \cos \phi) \mathbf{e}_2 - \cos \psi \sin \theta \mathbf{e}_3$$

$$\mathbf{m}_2 = -(\cos \psi \sin \phi + \sin \psi \cos \theta \cos \phi) \mathbf{e}_1 + (\cos \psi \cos \phi - \sin \psi \cos \theta \sin \phi) \mathbf{e}_2 + \sin \psi \sin \theta \mathbf{e}_3$$

$$\mathbf{m}_3 = \sin \theta (\cos \phi \mathbf{e}_1 + \sin \phi \mathbf{e}_2) + \cos \theta \mathbf{e}_3.$$

These results can be derived by calculating the effects of the sequence of three rotations. Note also that, because both sets of basis vectors are triads of mutually perpendicular unit vectors, they must be related by

$$\mathbf{m}_i = \mathbf{R} \mathbf{e}_i \quad \mathbf{e}_i = \mathbf{R}^T \mathbf{m}_i = \mathbf{m}_i \mathbf{R},$$

where \mathbf{R} is a proper orthogonal tensor that can be visualized as a rigid rotation. The rotation tensor can be expressed in several different forms:

- It can be expressed as the sum of three dyadic products $\mathbf{R} = \mathbf{m}_i \otimes \mathbf{e}_i$.
- It can be expressed as components in either $\{\mathbf{e}_1, \mathbf{e}_2, \mathbf{e}_3\}$ or $\{\mathbf{m}_1, \mathbf{m}_2, \mathbf{m}_3\}$, which can be written in dyadic notation as $R_{ij}^{ee} \mathbf{e}_i \otimes \mathbf{e}_j$ or $R_{ij}^{mm} \mathbf{m}_i \otimes \mathbf{m}_j$. Surprisingly, the components in both bases are equal and are given by $R_{ij}^{mm} = R_{ij}^{ee} = \mathbf{e}_i \cdot \mathbf{m}_j$. The components can be expressed in terms of the Euler angles as a matrix:

$$R_{ij}^{mm} = R_{ij}^{ee} \equiv \begin{bmatrix} \cos \psi \cos \theta \cos \phi - \sin \psi \sin \phi & -(\cos \psi \sin \phi + \sin \psi \cos \theta \cos \phi) & \sin \phi \sin \theta \\ \cos \psi \cos \theta \sin \phi + \sin \psi \cos \phi & \cos \psi \cos \phi - \sin \psi \cos \theta \sin \phi & \sin \theta \sin \phi \\ -\cos \psi \sin \theta & \sin \psi \sin \theta & \cos \theta \end{bmatrix}.$$

- In additional calculations, the variation of basis vectors \mathbf{m}_i with distance s along the deformed rod will play a central role. To visualize this quantity, imagine that the basis $\{\mathbf{m}_1, \mathbf{m}_2, \mathbf{m}_3\}$ travels up the deformed rod. The basis vectors will then rotate with an angular velocity that depends on the curvature and twist of the deformed rod, suggesting that we can characterize the rate of change of orientation with arc length by a vector $\boldsymbol{\kappa}$, analogous to an angular velocity vector. The curvature vector can be expressed as components in the basis $\{\mathbf{m}_1, \mathbf{m}_2, \mathbf{m}_3\}$ as $\boldsymbol{\kappa} = \kappa_i \mathbf{m}_i$. This vector has the following properties:

- The curvature vector is (by definition) related to the rate of change of \mathbf{m}_i with s by

$$\frac{d\mathbf{m}_i}{ds} = \boldsymbol{\kappa} \times \mathbf{m}_i,$$

which can be expanded out to show that

$$\frac{d\mathbf{m}_1}{ds} = -\kappa_2 \mathbf{m}_3 + \kappa_3 \mathbf{m}_2 \quad \frac{d\mathbf{m}_2}{ds} = \kappa_1 \mathbf{m}_3 - \kappa_3 \mathbf{m}_1 \quad \frac{d\mathbf{m}_3}{ds} = -\kappa_1 \mathbf{m}_2 + \kappa_2 \mathbf{m}_1.$$

2. The components κ_1, κ_2 quantify the bending of the rod and are related to the curvature κ and the binormal vector \mathbf{b} of the curve traced by the axis of the deformed rod by $\kappa_1 \mathbf{m}_1 + \kappa_2 \mathbf{m}_2 = \kappa \mathbf{b}$. You can show this result by comparing the formula for $d\mathbf{m}_3/ds$ with the formula for \mathbf{b} .
3. The curvature vector can also be expressed in terms of the position vector of the rod's centroid as

$$\kappa_i \mathbf{m}_i = \frac{d\mathbf{r}}{ds} \times \frac{d^2\mathbf{r}}{ds^2} + \kappa_3 \frac{d\mathbf{r}}{ds}.$$

The component of curvature κ_3 cannot in general be expressed in terms of \mathbf{r} , because the rotation of the rod's cross section about its centroid axis may provide an additional, independent contribution to κ_3 . For the special case in which \mathbf{m}_1 and \mathbf{m}_2 are everywhere parallel to the normal vector \mathbf{n} and binormal \mathbf{b} , respectively, it follows that $\kappa_3 = \mathbf{b} \cdot d\mathbf{n}/ds = -\mathbf{n} \cdot d\mathbf{b}/ds$. In this case, κ_3 is equal to the torsion of the curve.

- The rate of change of \mathbf{m}_i with distance s can also be expressed in terms of the Euler angles. For example, the derivative of \mathbf{m}_3 can be calculated as follows:

$$\mathbf{m}_3 = \sin\theta(\cos\phi\mathbf{e}_1 + \sin\phi\mathbf{e}_2) + \cos\theta\mathbf{e}_3$$

$$\Rightarrow \frac{d\mathbf{m}_3}{ds} = \cos\theta \frac{d\theta}{ds} (\cos\phi\mathbf{e}_1 + \sin\phi\mathbf{e}_2) + \sin\theta (-\sin\phi\mathbf{e}_1 + \cos\phi\mathbf{e}_2) \frac{d\phi}{ds} - \sin\theta \frac{d\theta}{ds} \mathbf{e}_3.$$

Similar results for \mathbf{m}_1 and \mathbf{m}_2 are left as exercises.

- The bending curvatures κ_1, κ_2 and the twist rate κ_3 are related to the Euler angles by

$$\kappa_1 = \sin\psi \frac{d\theta}{ds} - \cos\psi \sin\theta \frac{d\phi}{ds} \quad \kappa_2 = \cos\psi \frac{d\theta}{ds} + \sin\psi \sin\theta \frac{d\phi}{ds} \quad \kappa_3 = \frac{d\psi}{ds} + \frac{d\phi}{ds} \cos\theta.$$

These results can be derived from the two different formulas for $d\mathbf{m}_i/ds$, together with the equations relating $\{\mathbf{e}_1, \mathbf{e}_2, \mathbf{e}_3\}$ and $\{\mathbf{m}_1, \mathbf{m}_2, \mathbf{m}_3\}$ in terms of the Euler angles.

- The arc length s along the rod's center line is related to the position vector of the rod's axis by

$$\frac{ds}{dx_3} = \sqrt{\frac{d\mathbf{r}}{dx_3} \cdot \frac{d\mathbf{r}}{dx_3}}.$$

- Some relationships between the time derivatives of these various kinematic quantities are also useful in subsequent calculations. The rate of change in shape of the rod can be characterized by the velocity of the axis $\mathbf{v}(s) = d\mathbf{r}/dt$ and the time rate of change of the cross-sectional rotation $d\psi/dt$.

- The time derivative of the tangent vector is a convenient way to characterize the rate of change of bending of the rod. This is related to the velocity of the rod's center line by

$$\frac{d\mathbf{t}}{dt} \equiv \frac{d\mathbf{m}_3}{dt} = \dot{\tau}_1 \mathbf{m}_1 + \dot{\tau}_2 \mathbf{m}_2 = \frac{d}{ds} \left(\frac{d\mathbf{r}}{dt} \right) - \frac{d\mathbf{r}}{ds} \left[\frac{d\mathbf{r}}{ds} \cdot \frac{d}{ds} \left(\frac{d\mathbf{r}}{dt} \right) \right].$$

If we express the velocity in components $d\mathbf{r}/dt = v_i \mathbf{m}_i$ and recall $\mathbf{m}_3 = d\mathbf{r}/ds$, we can write this as

$$\dot{\tau}_1 \mathbf{m}_1 + \dot{\tau}_2 \mathbf{m}_2 = \left(\frac{dv_1}{ds} - v_2 \kappa_3 + v_3 \kappa_2 \right) \mathbf{m}_1 + \left(\frac{dv_2}{ds} + v_1 \kappa_3 - v_3 \kappa_1 \right) \mathbf{m}_2.$$

It is important to note that the components $\dot{\tau}_i$ are not equal to the time derivatives of the components of the tangent vector \mathbf{t} , because the basis $\{\mathbf{m}_1, \mathbf{m}_2, \mathbf{m}_3\}$ varies with time.

- The time derivatives of the basis vectors can also be quantified by an angular velocity vector, $\boldsymbol{\omega}$ which satisfies $\dot{\mathbf{m}}_i = \boldsymbol{\omega} \times \mathbf{m}_i$. The components of $\boldsymbol{\omega}$ are readily shown to be

$$\boldsymbol{\omega} = \mathbf{m}_3 \times \frac{d\mathbf{v}}{ds} + \dot{\psi} \mathbf{m}_3 = -\dot{\tau}_2 \mathbf{m}_1 + \dot{\tau}_1 \mathbf{m}_2 + \dot{\psi} \mathbf{m}_3.$$

- The time derivatives of the remaining basis vectors follow as

$$\frac{d\mathbf{m}_1}{dt} = -\dot{\tau}_1 \mathbf{m}_3 + \dot{\psi} \mathbf{m}_2 \quad \frac{d\mathbf{m}_2}{dt} = -\dot{\tau}_2 \mathbf{m}_3 - \dot{\psi} \mathbf{m}_1.$$

- The time derivative of the arc length of the center line is related to its velocity as follows:

$$\frac{d}{dt} \left(\frac{ds}{dx_3} \right) = \mathbf{m}_3 \cdot \frac{ds}{dx_3} \frac{d}{ds} \left(\frac{d\mathbf{r}}{dt} \right) = \frac{ds}{dx_3} \left(\frac{dv_3}{ds} - v_1 \kappa_2 + v_2 \kappa_1 \right).$$

- We shall also require the gradient of the angular velocity $\boldsymbol{\omega}$, which quantifies the rate of change of bending. We shall give this vector the symbol $\overset{\nabla}{\boldsymbol{\kappa}}$ to denote its physical significance: it can be interpreted (see Appendix E) as the co-rotational time derivative of the curvature vector, as follows:

$$\overset{\nabla}{\boldsymbol{\kappa}} = \overset{\nabla}{\kappa}_i \mathbf{m}_i = \frac{d\boldsymbol{\omega}}{ds} = \frac{d\boldsymbol{\kappa}}{dt} - \boldsymbol{\omega} \times \boldsymbol{\kappa} + \frac{dx_3}{ds} \frac{ds}{dx_3} \boldsymbol{\kappa}.$$

Evaluating the derivatives of $\boldsymbol{\omega}$ shows that

$$\overset{\nabla}{\kappa}_1 = -\frac{d\dot{\tau}_2}{ds} - \dot{\tau}_1 \kappa_3 + \dot{\psi} \kappa_2 \quad \overset{\nabla}{\kappa}_2 = \frac{d\dot{\tau}_1}{ds} - \dot{\tau}_2 \kappa_3 - \dot{\psi} \kappa_1 \quad \overset{\nabla}{\kappa}_3 = \frac{d\dot{\psi}}{ds} + \dot{\tau}_1 \kappa_1 + \dot{\tau}_2 \kappa_2.$$

The co-rotational time derivative of curvature must be used to quantify bending rate (instead of the time derivative $d\boldsymbol{\kappa} / dt$) to correct for the fact that rigid rotations and pure stretching do not change bending.

- Finally, to solve dynamic problems, we will need to be able to describe the linear and angular acceleration of the bar. The linear acceleration is most conveniently characterized by the acceleration of the center line of the bar $\mathbf{a} = d\mathbf{v}/ds = d^2\mathbf{r}/dt^2$.
- The angular acceleration of the bar's cross section can be characterized by the angular acceleration $\boldsymbol{\alpha}$ of the basis vectors $\{\mathbf{m}_1, \mathbf{m}_2, \mathbf{m}_3\}$. A straightforward calculation shows that

$$\boldsymbol{\alpha} = \frac{d\boldsymbol{\omega}}{dt} = \mathbf{m}_3 \times \frac{d\mathbf{a}}{ds} - 2 \left(\frac{d\mathbf{v}}{ds} \cdot \mathbf{m}_3 \right) \mathbf{m}_3 \times \frac{d\mathbf{v}}{ds} + \frac{d\psi}{dt} \left\{ \frac{d\mathbf{v}}{ds} - \left(\frac{d\mathbf{v}}{ds} \cdot \mathbf{m}_3 \right) \mathbf{m}_3 \right\} + \frac{d^2\psi}{dt^2} \mathbf{m}_3.$$

- The second time derivative of the basis vectors can then be calculated as

$$\frac{d^2\mathbf{m}_i}{dt^2} = \frac{d}{dt}(\boldsymbol{\omega} \times \mathbf{m}_i) = \frac{d\boldsymbol{\omega}}{dt} \times \mathbf{m}_i + \boldsymbol{\omega} \times \frac{d\mathbf{m}_i}{dt} = \boldsymbol{\alpha} \times \mathbf{m}_i + \boldsymbol{\omega} \times (\boldsymbol{\omega} \times \mathbf{m}_i).$$

10.2.4 Approximating the Displacement, Velocity, and Acceleration in a Rod

The position vector after deformation of the material point that has coordinates x_k in the undeformed rod can be expressed as

$$\mathbf{y}(x_k) = \mathbf{r}(x_3) + \eta_i(x_k) \mathbf{m}_i(x_3).$$

This is a completely general expression. We now introduce a series of approximations that are based on the following assumptions:

1. The rod is thin compared with its length.
2. The radius of curvature of the rod (attributable to bending) is much larger than the characteristic dimension of its cross section.
3. The rate of change of twist of the rod $d\psi/ds$ has the same order of magnitude as the bending curvature of the rod.
4. The material in the rod experiences small distortions, i.e., the change in length of any infinitesimal material fiber in the rod is much less than its undeformed length.

With this in mind, we assume that $\eta_i(x_j)$ can be approximated by a function of the form

$$\eta_\alpha = x_\alpha + f_{\alpha\beta}(x_3)x_\beta \quad \eta_3 = u_3(x_\beta, x_3),$$

where the Greek indices α, β can have values 1 and 2, and $f_{\alpha\beta}$ can be regarded as the first term in a Taylor expansion of η_α . The definition of \mathbf{m}_1 requires that $f_{21} = 0$. We assume in addition that

$$\frac{df_{\alpha\beta}}{dx_3} x_\beta \approx 0 \quad \frac{du_3}{dx_3} \approx 0$$

for all possible choices of α . The constants $f_{\alpha\beta}$ can be thought of as the components of a homogeneous in-plane deformation applied to the cross section, whereas the function u_3

describes the *warping* of the cross section. To decouple the warping from the axial displacement of the rod, we require that

$$\int_A u_3(x_\alpha, x_3) dA = 0.$$

In addition, for small distortions, the deformation must satisfy $f_{\alpha\beta} \ll 1$ and $du_3 / dx_\gamma \ll 1$, the rod curvatures must satisfy $\kappa_\beta x_\alpha \ll 1$ for all $\alpha, \beta = 1, 2$, and the variation of arc length s along the axis of the deformed rod with x_3 must satisfy $ds/dx_3 - 1 \ll 1$.

The velocity field in the bar can be approximated as

$$\frac{d\mathbf{y}}{dt} = \mathbf{v} + \dot{f}_{\alpha\beta} x_\beta \mathbf{m}_\alpha + x_\alpha \dot{\mathbf{m}}_\alpha + \dot{u}_3 \mathbf{m}_3 = \mathbf{v} + \dot{f}_{\alpha\beta} x_\beta \mathbf{m}_\alpha + x_\alpha \boldsymbol{\omega} \times \mathbf{m}_\alpha + \dot{u}_3 \mathbf{m}_3,$$

where it has been assumed that $u_3 \ll x_\alpha$ and $f_{\alpha\beta} \ll x_\alpha$ for all α, β . Finally, the acceleration field within the bar will be approximated as

$$\frac{d^2\mathbf{y}}{dt^2} = \mathbf{a} + x_\alpha \frac{d^2\mathbf{m}_\alpha}{dt^2} = \mathbf{a} + x_\alpha \{ \boldsymbol{\alpha} \times \mathbf{m}_\alpha + \boldsymbol{\omega} \times (\boldsymbol{\omega} \times \mathbf{m}_\alpha) \}.$$

Here, all time derivatives of u_3 and $f_{\alpha\beta}$ have been neglected. This is not so much because they are small but because they represent a crude approximation to the distortion of the cross section. The time derivatives of these quantities are associated with short wavelength oscillations in the bar, which cannot be modeled accurately using the assumed displacement field.

10.2.5 Approximating the Deformation Gradient

Based on the assumptions listed in Section 10.2.3, the deformation gradient in the rod can be approximated by

$$\begin{aligned} \mathbf{F} \approx & \frac{ds}{dx_3} (1 - \kappa_2 x_1 + \kappa_1 x_2) \mathbf{m}_3 \otimes \mathbf{e}_3 + \frac{ds}{dx_3} x_1 \kappa_3 \mathbf{m}_2 \otimes \mathbf{e}_3 - \frac{ds}{dx_3} x_2 \kappa_3 \mathbf{m}_1 \otimes \mathbf{e}_3 \\ & + (\delta_{\alpha\beta} + f_{\alpha\beta}) \mathbf{m}_\alpha \otimes \mathbf{e}_\beta + \frac{du_3}{dx_\beta} \mathbf{m}_3 \otimes \mathbf{e}_\beta. \end{aligned}$$

The first line of this expression quantifies the effects of axial stretching, bending, and twisting of the rod. The second line approximates the distortion of its cross section.

The deformation gradient can also be decomposed as

$$\mathbf{F} = \mathbf{R}\mathbf{G} = \mathbf{H}\mathbf{R},$$

where \mathbf{R} is the rigid rotation satisfying $\mathbf{m}_i = \mathbf{R}\mathbf{e}_i$, and \mathbf{G} and \mathbf{H} are deformation gradient-like tensors that describe the change in shape of the rod. These tensors are most conveniently expressed as components in $\{\mathbf{e}_1, \mathbf{e}_2, \mathbf{e}_3\}$ and $\{\mathbf{m}_1, \mathbf{m}_2, \mathbf{m}_3\}$, respectively; we can represent this in

diadic notation as $\mathbf{G} = G_{ij}^{\text{ee}} \mathbf{e}_i \otimes \mathbf{e}_j$ or $\mathbf{H} = H_{ij}^{\text{mm}} \mathbf{m}_i \otimes \mathbf{m}_j$. The components can be expressed in matrix form as

$$G_{ij}^{\text{ee}} = H_{ij}^{\text{mm}} \equiv \begin{bmatrix} 1+f_{11} & f_{12} & -\kappa_3 x_2 \frac{ds}{dx_3} \\ 0 & 1+f_{22} & \kappa_3 x_1 \frac{ds}{dx_3} \\ \frac{du_3}{dx_1} & \frac{du_3}{dx_2} & (1+\kappa_1 x_2 - \kappa_2 x_1) \frac{ds}{dx_3} \end{bmatrix}.$$

Derivation: The deformation gradient is, by definition, the derivative of the position vector of material particles with respect to their position in the reference configuration, i.e.,

$$\mathbf{F} = \frac{d\mathbf{y}}{d\mathbf{x}} = \frac{d\mathbf{r}}{dx_3} \otimes \mathbf{e}_3 + \frac{d\eta_i}{dx_j} \mathbf{m}_i \otimes \mathbf{e}_j + \eta_i(x_j) \frac{d\mathbf{m}_i}{dx_3} \otimes \mathbf{e}_3.$$

To reduce this to the expression given,

1. Note that $\frac{d\mathbf{r}}{dx_3} = \frac{d\mathbf{r}}{ds} \frac{ds}{dx_3} = \mathbf{m}_3 \frac{ds}{dx_3}$ $\frac{d\mathbf{m}_i}{dx_3} = \frac{d\mathbf{m}_i}{ds} \frac{ds}{dx_3}$;
2. Recall that $\frac{d\mathbf{m}_1}{ds} = -\kappa_2 \mathbf{m}_3 + \kappa_3 \mathbf{m}_2$ $\frac{d\mathbf{m}_2}{ds} = \kappa_1 \mathbf{m}_3 - \kappa_3 \mathbf{m}_1$ $\frac{d\mathbf{m}_3}{ds} = -\kappa_1 \mathbf{m}_2 + \kappa_2 \mathbf{m}_1$;
3. Substitute $\eta_\alpha = x_\alpha + f_{\alpha\beta}(x_3)x_\beta$, $\eta_3 = u_3(x_\beta, x_3)$ and neglect the derivatives of f and u_3 with respect to x_3 .

The decomposition $\mathbf{F} = \mathbf{RG}$ follows trivially by substituting $\mathbf{m}_i = \mathbf{R}\mathbf{e}_i$ into the dyadic representation of \mathbf{F} and rearranging the result. A similar approach gives $\mathbf{F} = \mathbf{HR}$.

10.2.6 Other Strain Measures

It is straightforward to compute additional strain measures from the deformation gradient. Only a partial list will be given here:

1. The determinant of the deformation gradient follows as

$$J = \det(\mathbf{F}) = \det(\mathbf{G}) = \det(\mathbf{H}) = (1+f_{11})(1+f_{22})(1+\kappa_1 x_2 - \kappa_2 x_1) \frac{ds}{dx_3} \approx \frac{ds}{dx_3}.$$

2. The components of the left and right Cauchy–Green tensors can be computed from $\mathbf{B} = \mathbf{FF}^T = \mathbf{HH}^T$ and $\mathbf{C} = \mathbf{F}^T \mathbf{F} = \mathbf{G}^T \mathbf{G}$, where \mathbf{G} and \mathbf{H} were defined in Section 10.2.5. \mathbf{C} and \mathbf{B} are most conveniently expressed as components in $\{\mathbf{e}_1, \mathbf{e}_2, \mathbf{e}_3\}$ and $\{\mathbf{m}_1, \mathbf{m}_2, \mathbf{m}_3\}$, respectively; we can represent this in diadic notation as $\mathbf{C} = C_{ij}^{\text{ee}} \mathbf{e}_i \otimes \mathbf{e}_j$ or $\mathbf{B} = B_{ij}^{\text{mm}} \mathbf{m}_i \otimes \mathbf{m}_j$. For small distortions, the result can be approximated by

$$C_{ij}^{\text{ee}} = B_{ij}^{\text{mm}} \equiv \begin{bmatrix} 1+2f_{11} & f_{12} & \left(\frac{du_3}{dx_1} - \kappa_3 x_2 \right) \\ \vdots & 1+2f_{22} & \left(\frac{du_3}{dx_2} + \kappa_3 x_1 \right) \\ \text{sym} & \dots & \left(\frac{ds}{dx_3} \right)^2 + 2\kappa_1 x_2 - 2\kappa_2 x_1 \end{bmatrix}.$$

3. The Lagrange strain is defined as $\mathbf{E} = (\mathbf{C} - \mathbf{I})/2$. Its components follow trivially from the preceding formula. Note that the matrix of components for \mathbf{E} resembles the formula for the infinitesimal strain components in a straight bar subjected to axial stretching, bending, and twist deformation. However, if the bent rod does not lie in one plane, the twisting measure κ_3 includes contributions from both the rotation of the rod's cross section about its axis and also from the bending of the rod.
4. The rate of deformation tensor $\mathbf{D} = \dot{\text{sym}}(\mathbf{F}\mathbf{F}^{-1})$ will also be required. It is simplest to calculate the velocity gradient $\mathbf{L} = \dot{\mathbf{F}}\mathbf{F}^{-1}$ by differentiating the expression given for the velocity vector in the preceding section:

$$\begin{aligned} \frac{d\mathbf{y}}{dt} &= \frac{d\mathbf{r}}{dt} + \dot{f}_{\alpha\beta}x_\beta\mathbf{m}_\alpha + x_\alpha\boldsymbol{\omega} \times \mathbf{m}_\alpha + \dot{u}_3\mathbf{m}_3 \\ \Rightarrow \dot{\mathbf{F}} &= \frac{d}{dt} \left(\frac{ds}{dx_3} \frac{d\mathbf{r}}{ds} \right) \otimes \mathbf{e}_3 + \left[\dot{f}_{\alpha\beta}\mathbf{m}_\alpha + \frac{\partial \dot{u}_3}{\partial x_\beta} \mathbf{m}_3 \right] \otimes \mathbf{e}_\beta + \dot{f}_{\alpha\beta}x_\beta \frac{ds}{dx_3} \frac{d\mathbf{m}_\alpha}{ds} \otimes \mathbf{e}_3 \\ &\quad + (\boldsymbol{\omega} \times \mathbf{m}_\alpha) \otimes \mathbf{e}_\alpha + \frac{ds}{dx_3} \frac{d}{ds} (\boldsymbol{\omega} \times \mathbf{m}_\alpha) \otimes \mathbf{e}_3 + \dot{u}_3 \frac{ds}{dx_3} \frac{d\mathbf{m}_3}{ds} \otimes \mathbf{e}_3. \end{aligned}$$

Substitute $d\mathbf{r}/ds = \mathbf{m}_3$, $d\mathbf{m}_i/ds = \boldsymbol{\kappa} \times \mathbf{m}_i$, $d\boldsymbol{\omega}/ds = \nabla \boldsymbol{\kappa}$ and note that

$$\begin{aligned} \mathbf{F}^{-1} &\approx \frac{dx_3}{ds} (1 + \kappa_2 x_1 - \kappa_1 x_2) \mathbf{e}_3 \otimes \mathbf{m}_3 - \frac{ds}{dx_3} x_1 \kappa_3 \mathbf{e}_2 \otimes \mathbf{m}_3 + \frac{ds}{dx_3} x_2 \kappa_3 \mathbf{e}_1 \otimes \mathbf{m}_3 \\ &\quad + (\delta_{\alpha\beta} - f_{\alpha\beta}) \mathbf{e}_\alpha \otimes \mathbf{m}_\beta - \frac{du_3}{dx_\beta} \mathbf{e}_3 \otimes \mathbf{m}_\beta. \end{aligned}$$

Evaluating $\mathbf{D} = \dot{\text{sym}}(\mathbf{F}\mathbf{F}^{-1})$ then shows that the components of \mathbf{D} in $\{\mathbf{m}_1, \mathbf{m}_2, \mathbf{m}_3\}$ are

$$D_{ij}^{\text{mm}} \equiv \begin{bmatrix} \dot{f}_{11} & \frac{1}{2}\dot{f}_{12} & \frac{1}{2} \left(\frac{dx_3}{ds} \frac{du_3}{dx_1} - \kappa_3 x_2 + \kappa_2 \dot{u}_3 \right) \\ \vdots & \dot{f}_{22} & \frac{1}{2} \left(\frac{dx_3}{ds} \frac{du_3}{dx_2} + \kappa_3 x_1 - \kappa_1 \dot{u}_3 \right) \\ \text{sym} & \dots & \left\{ \frac{dx_3}{ds} \frac{ds}{dx_3} + \left(\kappa_1 x_2 - \kappa_2 x_1 \right) \right\} \end{bmatrix}$$

to within second-order terms in curvature, f_{ij} and du_3/dx_α .

10.2.7 Kinematics of Rods That Are Bent and Twisted in the Unstressed State

It is straightforward to generalize the results in Sections 10.2.3 through 10.2.5 to calculate strain measures for rods that are not straight in their initial configuration (Figure 10.5). In this case, we must start by describing the geometry of the undeformed rod. To this end, we do the following:

1. We denote the distance measured along the axis of the initial, unstressed, twisted rod by \bar{s} .
2. At each point \bar{s} on the initial rod, we introduce a set of three mutually perpendicular unit vectors $\{\bar{\mathbf{m}}_1, \bar{\mathbf{m}}_2, \bar{\mathbf{m}}_3\}$, where $\bar{\mathbf{m}}_3$ is chosen to be tangent to the axis of the undeformed rod and $\bar{\mathbf{m}}_1, \bar{\mathbf{m}}_2$ are parallel to the principal moments of inertia of the cross section.
3. We also introduce an arbitrary Cartesian basis $\{\mathbf{e}_1, \mathbf{e}_2, \mathbf{e}_3\}$ where the unit vectors denote three fixed directions in space.
4. The basis vectors $\{\mathbf{e}_1, \mathbf{e}_2, \mathbf{e}_3\}$ and $\{\bar{\mathbf{m}}_1, \bar{\mathbf{m}}_2, \bar{\mathbf{m}}_3\}$ together define a set of three Euler angles $(\bar{\phi}(s), \bar{\theta}(s), \bar{\psi}(s))$, which completely describe the shape of the undeformed rod.
5. We define a rotation tensor $\bar{\mathbf{R}}$ satisfying $\bar{\mathbf{m}}_i = \bar{\mathbf{R}}\mathbf{e}_i$ that characterizes the orientation of $\{\bar{\mathbf{m}}_1, \bar{\mathbf{m}}_2, \bar{\mathbf{m}}_3\}$ with respect to $\{\mathbf{e}_1, \mathbf{e}_2, \mathbf{e}_3\}$. The components of $\bar{\mathbf{R}}$ can be found using the formulas in Section 10.2.3.
6. We define three curvature components $\bar{\kappa}_i$ that characterize the bending and twisting of the initial rod, as follows:

$$\bar{\kappa}_1 = \sin \bar{\psi} \frac{d\bar{\theta}}{ds} - \cos \bar{\psi} \sin \bar{\theta} \frac{d\bar{\phi}}{ds} \quad \bar{\kappa}_2 = \cos \bar{\psi} \frac{d\bar{\theta}}{ds} + \sin \bar{\psi} \sin \bar{\theta} \frac{d\bar{\phi}}{ds} \quad \bar{\kappa}_3 = \frac{d\bar{\psi}}{ds} + \frac{d\bar{\phi}}{ds} \cos \bar{\theta}.$$

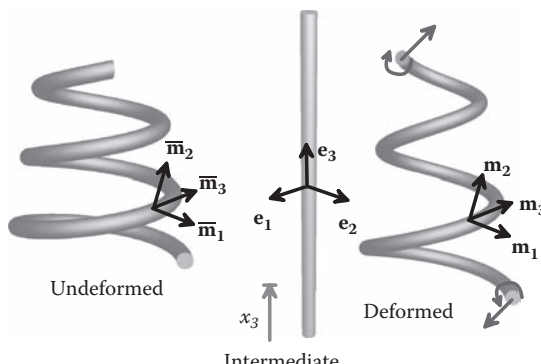


FIGURE 10.5 Deformation of an initially twisted rod onto an intermediate, straight configuration, followed by deformation to a new twisted shape.

The deformed shape of the rod is characterized exactly as described in Section 10.2.1, except that the axial distance x_3 is replaced by the arc length \bar{s} of the undeformed rod.

Assuming small distortions, the deformation gradient can be expressed in dyadic notation as $\mathbf{F} = F_{ij}\mathbf{m}_i \otimes \bar{\mathbf{m}}_j$, where the coefficients F_{ij} are given below. The deformation gradient can also be decomposed into two successive rotations and a small distortion:

$$\mathbf{F} = \mathbf{R}\bar{\mathbf{G}}\bar{\mathbf{R}}^T = \mathbf{H}\mathbf{R}\bar{\mathbf{R}}^T = \mathbf{R}\bar{\mathbf{R}}^T\mathbf{G},$$

where the rotation tensors \mathbf{R} and $\bar{\mathbf{R}}$ satisfy $\bar{\mathbf{m}}_i = \bar{\mathbf{R}}\mathbf{e}_i$, $\mathbf{m}_i = \mathbf{R}\mathbf{e}_i$, $\mathbf{m}_i = \mathbf{R}\bar{\mathbf{R}}^T\bar{\mathbf{m}}_i$, and the tensors $\bar{\mathbf{G}}, \mathbf{H}, \mathbf{G}$ can be expressed in component form as $\bar{\mathbf{G}} = \bar{G}_{ij}^{\text{ee}}\mathbf{e}_i \otimes \mathbf{e}_j$, $H_{ij}^{\text{mm}}\mathbf{m}_i \otimes \mathbf{m}_j$, $G_{ij}^{\bar{\mathbf{m}}\bar{\mathbf{m}}}\bar{\mathbf{m}}_i \otimes \bar{\mathbf{m}}_j$. Their components are given by

$$F_{ij} = \bar{G}_{ij}^{\text{ee}} = H_{ij}^{\text{mm}} = G_{ij}^{\bar{\mathbf{m}}\bar{\mathbf{m}}} = \begin{bmatrix} 1+f_{11} & f_{12} & -\kappa_3 x_2 \frac{ds}{d\bar{s}} + \bar{\kappa}_3 x_2 \\ 0 & 1+f_{22} & \kappa_3 x_1 \frac{ds}{d\bar{s}} - \bar{\kappa}_3 x_1 \\ \frac{du_3}{dx_1} & \frac{du_3}{dx_2} & (1+\kappa_1 x_2 - \kappa_2 x_1) \frac{ds}{d\bar{s}} - \bar{\kappa}_1 x_2 + \bar{\kappa}_2 x_1 \end{bmatrix}.$$

The deformation gradient can be written down immediately, by mapping the initial rod onto a fictitious intermediate configuration in which the rod is straight, chosen as follows:

1. The straight rod has axis parallel to the \mathbf{e}_3 direction.
2. The point at arc length \bar{s} in the unstressed rod has coordinates $\mathbf{x} = \bar{s}\mathbf{e}_3$ in the intermediate configuration.
3. The principal axes of the cross section are parallel to $(\mathbf{e}_1, \mathbf{e}_2)$ in the intermediate configuration.
4. The cross section of the rod has the same shape in the intermediate configuration as in the undeformed configuration.

The deformed state can be reached in two steps:

1. Deform the rod from the unstressed configuration to the intermediate configuration, with a deformation gradient $\bar{\mathbf{F}}$. The components of $\bar{\mathbf{F}}$ can be calculated as the inverse of the deformation gradient that maps the intermediate straight rod onto the undeformed shape.
2. Deform the rod from the straight configuration to the deformed configuration, with a deformation gradient $\hat{\mathbf{F}}$. The total deformation gradient follows as $\mathbf{F} = \hat{\mathbf{F}}\bar{\mathbf{F}}$.

10.2.8 Representation of Forces and Moments in Slender Rods

Figure 10.6 shows a generic cross section of the rod, in the deformed configuration. To describe measures of internal and external force acting on the rod, we first define a basis $\{\mathbf{m}_1, \mathbf{m}_2, \mathbf{m}_3\}$, with the unit vectors chosen using the scheme described in Section 10.2.2. We then define the following vector components in this basis:

- The body force acting on the rod b_i . For simplicity, we shall assume that the body force is uniform within the cross section (but b_i may vary along the length of the rod).
- The tractions acting on the exterior surface of the rod t_i .
- The Cauchy stress within the rod σ_{ij} .

External forces and moments acting on the rod are characterized using the following:

1. The force per unit length acting on the rod, $\mathbf{p} = p_i \mathbf{m}_i$: The force components can be calculated from the tractions and body force acting on the rod as $f_i(x_3) = Ab_i + \int_C t_i ds$.
2. The moment per unit length acting on the rod, $\mathbf{q} = q_i \mathbf{m}_i$: The moment components can be calculated from the tractions acting on the exterior surface of the rod as

$$q_1 = \int_C x_2 t_3 ds \quad q_2 = - \int_C x_1 t_3 ds \quad q_3 = \int_C (x_1 t_2 - x_2 t_1) ds.$$

3. The resultant force acting on each end of the rod: Each force can be expressed as components as $\mathbf{P} = P_i \mathbf{m}_i$. The components are related to the tractions acting on the end of the rod by $P_i = \int_A t_i dA$, where the area integral is taken over the cross section at the appropriate end of the rod.

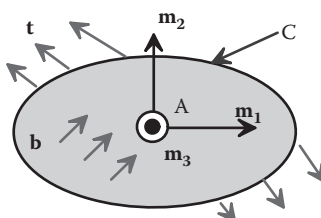


FIGURE 10.6 Forces acting on the interior and exterior of the cross section of a rod.

4. The resultant moment acting on each end of the rod. Each moment can be expressed as components as $\mathbf{Q} = Q_i \mathbf{m}_i$. The components are related to the tractions acting on the end of the rod by

$$Q_1 = \int_A x_2 t_3 dA \quad Q_2 = - \int_A x_1 t_3 dA \quad Q_3 = \int_A (x_1 t_2 - x_2 t_1) dA.$$

Internal forces and moments in the rod are characterized by the following quantities:

1. The variation of internal shear stress in the cross section $\sigma_{\alpha\beta}(x_\beta, x_3)$.
2. The average in-plane stress components

$$S_{\alpha\beta} = \int_A \sigma_{\alpha\beta} dA.$$

3. Three components of a vector bending moment, defined as

$$M_1(x_3) = \int_A \sigma_{33} x_2 dA \quad M_2(x_3) = - \int_A \sigma_{33} x_1 dA \quad M_3(x_3) = \int_A (\sigma_{23} x_1 - \sigma_{13} x_2) dA.$$

4. The axial force on the cross section $T_3(x_3) = \int_A \sigma_{33} dA$.

5. Two additional generalized forces $T_1(x_3), T_2(x_3)$ that represent the transverse shear forces acting on the rod's cross section. Unlike the axial force, however, these forces cannot be directly related to the deformation of the rod. Instead, they are calculated from the bending moments, using the equilibrium equations listed in the next section.

The forces T_i and moments M_i define components of a vector force and moment:

1. $\mathbf{T} = T_i \mathbf{m}_i$ is the resultant force acting on an internal cross section of the rod.
2. $\mathbf{M} = M_i \mathbf{m}_i$ is the resultant moment (about the centroid of the cross section) acting on the cross section.

10.2.9 Equations of Motion and Boundary Conditions

Equations of motion: The internal forces and moments must satisfy the following equations of motion:

$$\frac{\partial \sigma_{\alpha 3}}{\partial x_\alpha} - \sigma_{31} \kappa_2 + \sigma_{32} \kappa_1 = 0 \quad \frac{d\mathbf{T}}{ds} + \mathbf{p} = \rho A \mathbf{a} \quad \frac{d\mathbf{M}}{ds} + \mathbf{m}_3 \times \mathbf{T} + \mathbf{q} = \rho \mathbf{H} \boldsymbol{\alpha} + \boldsymbol{\omega} \times \rho \mathbf{H} \boldsymbol{\omega}.$$

Here, $\sigma_{\alpha 3}$, \mathbf{T} , and \mathbf{M} are the internal forces and moments in the rod, \mathbf{p}, \mathbf{q} are the external force and couple per unit length, ρ is the mass density of the rod, A is its cross-sectional

area, \mathbf{H} is the area moment of inertia tensor defined in Section 10.2.1, and \mathbf{a} , $\boldsymbol{\omega}$, $\boldsymbol{\alpha}$ are the acceleration, angular velocity, and angular acceleration of the rod's center line, respectively. The two equations of motion for \mathbf{T} and \mathbf{M} clearly represent linear and angular momentum balance for an infinitesimal segment of the rod.

The equations of motion for \mathbf{T} and \mathbf{M} are often expressed as components in the $\{\mathbf{m}_1, \mathbf{m}_2, \mathbf{m}_3\}$ basis, as

$$\begin{aligned}\frac{dT_1}{ds} - \kappa_3 T_2 + \kappa_2 T_3 + p_1 &= \rho A a_1 & \frac{dT_2}{ds} + \kappa_3 T_1 - \kappa_1 T_3 + p_2 &= \rho A a_2 & \frac{dT_3}{ds} + \kappa_1 T_2 - \kappa_2 T_1 + p_3 &= \rho A a_3 \\ \frac{dM_1}{ds} - \kappa_3 M_2 + \kappa_2 M_3 - T_2 + q_1 &= \rho I_1 \alpha_1 + \rho (I_3 - I_2) \omega_2 \omega_3 \\ \frac{dM_2}{ds} + \kappa_3 M_1 - \kappa_1 M_3 + T_1 + q_2 &= \rho I_2 \alpha_2 - \rho (I_3 - I_1) \omega_1 \omega_3 \\ \frac{dM_3}{ds} - \kappa_2 M_1 + \kappa_1 M_2 + q_3 &= I_3 \alpha_3 + (I_2 - I_1) \omega_2 \omega_1.\end{aligned}$$

Note the following:

1. If the system is in static equilibrium, the right-hand sides of all the equations of motion are zero.
2. In addition, in many dynamic problems, the right-hand sides of the angular momentum balance equations may be taken to be approximately zero, because the area moments of inertia are small. For example, the rotational inertia may be ignored when modeling the vibration of a beam. The rotational inertia terms can be important if the rod is rotating rapidly: examples include a spinning shaft, or a rotating propeller.

Boundary conditions: The internal stresses, forces, and moments must satisfy the following boundary conditions:

1. $S_{\alpha\beta} = \int_C (x_\beta t_\alpha) d\xi.$
2. $\sigma_{3\alpha} n_\alpha = t_3$ on C .
3. The ends of the rod may be subjected to a prescribed displacement. Alternatively, the transverse or axial tractions may be prescribed on the ends of the bar: in this case, the internal forces must satisfy $\mathbf{T} = \mathbf{P}$ for $s = L$ and $\mathbf{T} = -\mathbf{P}$ for $s = 0$.
4. The ends of the rod may be subjected to a prescribed rotation. Alternatively, if the ends are free to rotate, the internal moments must satisfy $\mathbf{M} = \mathbf{Q}$ for $s = L$ and $\mathbf{M} = -\mathbf{Q}$ for $s = 0$.

Derivation: Measures of internal force and the equilibrium equations emerge naturally from the principle of virtual work, which states that the Cauchy stress distribution must satisfy

$$\int_{V_0} J \sigma_{ij} \delta D_{ij} dV_0 + \int_{V_0} \rho \frac{d^2 y_i}{dt^2} \delta v_i dV_0 - \int_{V_0} b_i \delta v_i dV_0 - \int_{S_2} t_i \delta v_i dA = 0$$

for all virtual velocity fields δv_i and compatible stretch rates δD_{ij} . The virtual velocity field and virtual stretch rates in the bar must have the same general form as the actual velocity and stretch rates, as outlined in Sections 10.2.4 and 10.2.5. The virtual velocity and stretch rate can therefore be characterized by $\dot{\delta f}_{\alpha\beta}, \delta u_3(x_\alpha)$ and compatible sets of $\delta \mathbf{v}, \delta \boldsymbol{\omega}, \delta \dot{s}, \delta \kappa_i^\nabla$. This has two consequences:

- The virtual work principle can be expressed in terms of the generalized deformation measures and forces defined in the preceding sections as

$$\begin{aligned} & \int_0^{L_0} \left\{ \frac{ds}{dx_3} S_{\alpha\beta} \delta \dot{f}_{\alpha\beta} + \int_A \left(\sigma_{\alpha 3} \frac{d\delta \dot{u}_3}{dx_\alpha} + (\sigma_{31}\kappa_2 - \sigma_{32}\kappa_1) \delta \dot{u}_3 - b_3 \delta \dot{u}_3 \right) dA \right\} dx_3 \\ & + \int_0^{L_0} \left\{ \frac{d\delta \dot{s}}{dx_3} T_3 + \delta \kappa_i^\nabla M_i \frac{ds}{dx_3} \right\} dx_3 + \int_0^L \rho A a_i \delta v_i ds \\ & + \int_0^L \rho I_1 (\alpha_1 + \omega_2 \omega_3) \delta \omega_1 ds + \int_0^L \rho I_2 (\alpha_2 - \omega_1 \omega_3) \delta \omega_2 ds \\ & + \int_0^L \rho (I_3 \alpha_3 + (I_1 - I_2) \omega_1 \omega_2) \delta \omega_3 ds \\ & - \int_0^L \left(\int_C (x_\beta t_\alpha \delta \dot{f}_{\alpha\beta} + t_3 \delta u_3) d\xi \right) ds - \int_0^L (p_i \delta v_i + q_i \delta \omega_i) ds - [P_i \delta v_i + Q_i \delta \omega_i]_{x_3=0} \\ & - [P_i \delta v_i + Q_i \delta \omega_i]_{x_3=L_0} \end{aligned}$$

- If the virtual work equation is satisfied for all $\dot{\delta f}_{\alpha\beta}, \delta u_3(x_\alpha)$ and compatible sets of $\delta \mathbf{v}, \delta \boldsymbol{\omega}, \delta \dot{s}, \delta \kappa_i^\nabla$, then the internal forces and moments must satisfy the equilibrium equations and boundary conditions listed above.

It is straightforward to derive the first result. The Jacobian is approximated as $J \approx ds / dx_3$; the components of δD_{ij} follow from the formulas given in Section 10.2.5, and the velocity field is approximated using the formula in Section 10.2.4. Substituting the definitions

given in Section 10.2.8 for generalized internal and external forces immediately gives the required result. The algebra involved is lengthy and tedious and is left as an exercise.

The equilibrium equations and boundary conditions are obtained by substituting various choices of $\delta\dot{f}_{\alpha\beta}$, $\delta u_3(x_\alpha)$ and compatible sets of $\delta\mathbf{v}$, $\delta\omega$, $\delta\psi$, δs , $\delta\kappa_i^\nabla$ into the virtual work equation:

- Choosing $\delta u_3(x_\alpha) = \delta\mathbf{v} = \delta\psi = 0$ reduces the virtual work equation to

$$\int_0^L \left\{ \int_A \sigma_{\alpha\beta} \delta \dot{f}_{\alpha\beta} dA \right\} dx_3 - \int_0^L \left(\int_C (x_\beta t_\alpha \delta \dot{f}_{\alpha\beta}) d\xi \right) ds.$$

The condition $S_{\alpha\beta} = \int_C (x_\beta t_\alpha) d\xi$ follows immediately.

- Choosing $\delta f_{\alpha\beta} = \delta\mathbf{v} = \delta\psi = 0$ reduces the virtual work equation to

$$\int_0^{L_0} \left\{ \int_A \left(\sigma_{\alpha 3} \frac{d\delta u_3}{dx_\alpha} + (\sigma_{31}\kappa_2 - \sigma_{32}\kappa_1) \delta u_3 - b_3 \delta u_3 \right) dA \right\} dx_3 - \int_0^{L_0} \left(\int_C (t_3 \delta u_3) d\xi \right) \frac{ds}{dx_3} dx_3.$$

Recall that (by definition) δu_3 must be chosen to satisfy

$$\int_A \delta u_3 dA = 0.$$

Because the body force is uniform, the term involving b_3 is zero. The first integral can then be integrated by parts as follows

$$\int_A \sigma_{\alpha 3} \frac{\partial \delta u_3}{\partial x_\alpha} dA = \int_A \left(\frac{\partial}{\partial x_\alpha} (\sigma_{\alpha 3} \delta u_3) - \frac{\partial \sigma_{\alpha 3}}{\partial x_\alpha} \delta u_3 \right) dA = \int_C \sigma_{\alpha 3} \delta u_3 n_\alpha - \int_A \delta u_3 \frac{\partial \sigma_{\alpha 3}}{\partial x_\alpha} dA.$$

Choosing δu_3 to vanish on the boundary or the interior yields the equilibrium equation $\partial \sigma_{\alpha 3} / \partial x_\alpha - \sigma_{31}\kappa_2 + \sigma_{32}\kappa_1 = 0$; choosing any other δu_3 gives the boundary condition $\sigma_{3\alpha} n_\alpha = t_3$.

- Choosing $\delta u_3(x_a) = f_{\alpha\beta} = \delta \dot{r} = 0$, using $\delta \kappa_1^\nabla = \delta \dot{\psi} \kappa_2$, $\delta \kappa_2^\nabla = \delta \dot{\psi} \kappa_1$, $\delta \kappa_3^\nabla = d\delta \dot{\psi} / ds$ as well as $\delta \omega_3 = \delta \dot{\psi}$ yields

$$\int_0^L \left\{ (+\kappa_2 M_1 - \kappa_1 M_2) \delta \dot{\psi} + \frac{d\delta \dot{\psi}}{ds} M_3 \right\} dx_3 + \int_0^L \rho (I_3 \alpha_3 + (I_1 - I_2) \omega_1 \omega_2) \delta \dot{\psi} ds$$

$$- \int_0^L (q_3 \delta \dot{\psi}) ds - [Q_3 \delta \dot{\psi}]_{x_3=0} - [Q_3 \delta \dot{\psi}]_{x_3=L} = 0 \Rightarrow$$

$$\int_0^L \left\{ \left(-\frac{dM_3}{ds} + \kappa_2 M_1 - \kappa_1 M_2 - q_3 - \rho(I_3 \alpha_3 + (I_1 - I_2) \omega_1 \omega_2) \right) \delta \dot{\psi} \right\} dx_3 \\ + [(M_3 - Q_3) \delta \dot{\psi}]_{x_3=L} - [(M_3 + Q_3) \delta \dot{\psi}]_{x_3=0} = 0,$$

where we have integrated by parts to obtain the second line. Choosing $\delta \dot{\psi}$ to vanish on the ends of the rod yields the equation of motion $dM_3/ds - \kappa_2 M_1 + \kappa_1 M_2 + q_3 = \rho(I_3 \alpha_3 + (I_1 - I_2) \omega_1 \omega_2)$. Any other choice of $\delta \dot{\psi}$ yields the boundary conditions $M_3 = \pm Q_3$ on the ends of the rod.

4. Choosing $\delta u_3(x_a) = f_{\alpha\beta} = \delta \dot{\psi} = 0$ and substituting $\delta \omega_1 = -\delta \dot{\tau}_2$, $\delta \omega_2 = \delta \dot{\tau}_1$, where $\delta \dot{\tau}_\alpha$ are the components of a virtual rate of change of the tangent vector \mathbf{t} reduces the virtual work equation to

$$\int_0^{L_0} \left\{ \frac{d\delta s}{dx_3} T_3 + \delta \kappa_i M_i \frac{ds}{dx_3} \right\} dx_3 - \int_0^L (P_i \delta v_i - q_2 \delta \dot{\tau}_1 + q_1 \delta \dot{\tau}_2) ds \\ + \int_0^L \rho A a_i \delta v_i ds + \int_0^L \rho I_1 (\alpha_1 + \omega_2 \omega_3) \delta \dot{\tau}_2 ds - \int_0^L \rho I_2 (\alpha_2 - \omega_1 \omega_3) \delta \dot{\tau}_1 ds \\ - [P_i \delta v_i - Q_2 \delta \dot{\tau}_1 + Q_1 \delta \dot{\tau}_2]_{x_3=0} - [P_i \delta v_i - Q_2 \delta \dot{\tau}_1 + Q_1 \delta \dot{\tau}_2]_{x_3=L} = 0.$$

To proceed, it is necessary to express $\delta \kappa_i$, $\delta \dot{\tau}_i$, and δs in terms of the virtual velocity components δv_i . The algebra and the resulting equilibrium equations are greatly simplified if the tangent vector \mathbf{t} is regarded as an independent kinematic variable. The relationship between \mathbf{t} and dr/ds must be enforced by a vector-valued Lagrange multiplier $\mathbf{T}' = T_1 \mathbf{m}_1 + T_2 \mathbf{m}_2$, which must satisfy

$$\int_0^L \left(\frac{d\mathbf{r}}{ds} - \mathbf{t} \right) \cdot \delta \mathbf{T}' ds + \int_0^L \left(\frac{d\delta \mathbf{v}}{ds} - \delta \dot{\mathbf{t}} \right) \cdot \mathbf{T}' ds = 0$$

for all variations $\delta \mathbf{t}$, $\delta \mathbf{v}$, $\delta \mathbf{T}'$. The second integral can be expressed in component form as

$$\int_0^L \left(\frac{d\delta v_\alpha}{ds} T_\alpha + (-\delta v_2 \kappa_3 + \delta v_3 \kappa_2) T_1 + (\delta v_1 \kappa_3 - \delta v_3 \kappa_1) T_2 - \delta \dot{\tau}_\alpha T_\alpha \right) = 0.$$

This equation can simply be added to the virtual work equation to ensure that $\delta \dot{\tau}_\alpha$ and δv_i are consistent. Finally, recall that the curvature rates and stretch rate are related to δv_i by

$$\frac{d\delta s}{dx_3} = \frac{ds}{dx_3} \left(\frac{d\delta v_3}{ds} - \delta v_1 \kappa_2 + \delta v_2 \kappa_1 \right)$$

$$\delta \kappa_1^\nabla = -\frac{d\delta \dot{\tau}_2}{ds} - \delta \dot{\tau}_1 \kappa_3 \quad \delta \kappa_2^\nabla = \frac{d\delta \dot{\tau}_1}{ds} - \delta \dot{\tau}_2 \kappa_3 \quad \delta \kappa_3^\nabla = \delta \dot{\tau}_1 \kappa_1 + \delta \dot{\tau}_2 \kappa_2.$$

Substituting these results into the augmented virtual work equation gives

$$\begin{aligned}
 & \int_0^L \left\{ \left(\frac{d\delta v_\alpha}{ds} T_\alpha + \delta v_1 \kappa_3 T_2 - \delta v_2 \kappa_3 T_1 + \delta v_3 (-\kappa_1 T_2 + \kappa_2 T_1) \right) - \delta \dot{\tau}_\alpha T_\alpha \right\} ds \\
 & + \int_0^L \left\{ \left(\frac{d\delta v_3}{ds} + (-\delta v_1 \kappa_2 + \delta v_2 \kappa_1) \right) T_3 \right\} ds \\
 & + \int_0^L \rho A a_i \delta v_i ds + \int_0^L \rho I_1 (\alpha_1 + \omega_2 \omega_3) \delta \dot{\tau}_2 ds - \int_0^L \rho I_2 (\alpha_2 - \omega_1 \omega_3) \delta \dot{\tau}_1 ds \\
 & + \int_0^L \left\{ \left(-\frac{d\delta \dot{\tau}_2}{ds} - \kappa_3 \delta \dot{\tau}_1 \right) M_1 + \left(\frac{d\delta \dot{\tau}_1}{ds} - \kappa_3 \delta \dot{\tau}_2 \right) M_2 + (\kappa_1 \delta \dot{\tau}_1 + \kappa_2 \delta \dot{\tau}_2) M_3 \right\} ds \\
 & - \int_0^L (P_i \delta v_i + Q_2 \delta \dot{\tau}_1 - Q_1 \delta \dot{\tau}_2) ds - [P_i \delta v_i + Q_2 \delta \dot{\tau}_1 - Q_1 \delta \dot{\tau}_2]_{x_3=0} - [P_i \delta v_i + Q_2 \delta \dot{\tau}_1 - Q_1 \delta \dot{\tau}_2]_{x_3=L} = 0.
 \end{aligned}$$

This equation must be satisfied for all admissible $\delta v_i, \delta \dot{\tau}_\alpha$. Considering each component in turn and integrating by parts appropriately and using $I_3 = I_1 + I_2$ gives the last five equations of motion, as well as the boundary conditions $\mathbf{T} = \pm \mathbf{P}$ and $\mathbf{M} = \pm \mathbf{Q}$ on $s = 0$ and $s = L$.

10.2.10 Constitutive Equations Relating Forces to Deformation Measures in Elastic Rods

Constitutive equations must relate the deformation measures defined in Section 10.2.3 to the forces defined in Section 10.2.8. In this section, we list the relationships between these quantities for an isotropic, elastic rod with Young's modulus E , Poisson's ratio ν , and shear modulus μ that is subjected to small distortions. For simplicity, the sides of the rod are assumed to be traction free.

The results depend on the geometry of the rod's cross section, which is characterized as follows:

1. Introduce a Cartesian coordinate system (x_1, x_2, x_3) as shown in Figure 10.7. The coordinates have origin at the centroid of the cross section, with basis vectors $\mathbf{e}_1, \mathbf{e}_2$ parallel to the principal axes of inertia for the cross section, and \mathbf{e}_3 parallel to the rod's axis.

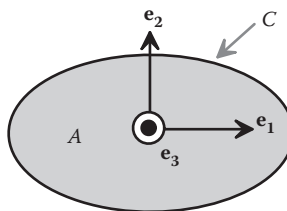


FIGURE 10.7 Cross section of a rod.

2. We denote the cross-sectional area of the rod by A and the curve bounding the cross-section by C and let I_i denote the three principal moments of area of the cross section (see Section 10.2.1).
3. We introduce a warping function $w(x_1, x_2)$ to describe the out-of-plane displacement component u_3 in the cross section of the rod. The warping function is related to the out-of-plane displacement u_3 by

$$u_3(x_1, x_2, x_3) = (\kappa_3(x_3) - \bar{\kappa}_3(x_3))w(x_1, x_2).$$

The warping function depends only on the geometry of the cross section and satisfies the following governing equations and boundary conditions:

$$\frac{\partial^2 w}{\partial x_1^2} + \frac{\partial^2 w}{\partial x_2^2} - \frac{\partial w}{\partial x_1}\kappa_2 + \frac{\partial w}{\partial x_2}\kappa_1 = 0 \text{ in } A \quad \frac{\partial w}{\partial x_\alpha} n_\alpha = x_2 n_1 - x_1 n_2 = x_\alpha \frac{\partial x_\alpha}{\partial s} \text{ on } C.$$

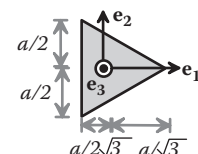
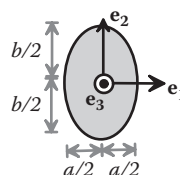
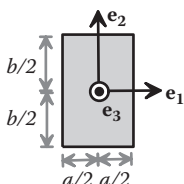
You can easily show that this choice of u_3 will automatically satisfy the shear stress equilibrium equation $\partial\sigma_{\alpha 3}/\partial x_\alpha - \sigma_{31}\kappa_2 + \sigma_{32}\kappa_1 = 0$ as well as the boundary condition $\sigma_{3\alpha}n_\alpha = 0$ on C .

4. Finally, we define a modified polar moment of inertia for the cross section as

$$J_3 = I_3 - \int_A \left(x_2 \frac{\partial w}{\partial x_1} - x_1 \frac{\partial w}{\partial x_2} \right) dA.$$

Calculating the warping function is a nuisance, because it requires the solution to a partial differential equation. In desperation, you can take $w = 0$; this will overestimate the torsional stiffness of the rod, but, in many practical applications, the error is not significant. For a better approximation, warping functions can be estimated by neglecting the terms involving $\kappa_\beta \partial w / \partial x_\alpha$ in the governing equation. A few such approximate warping functions and modified polar moments of area are listed in Table 10.2.

TABLE 10.2 Warping Functions and Modified Polar Moments of Area for Simple Cross Sections



$$w = x_1 x_2 - \sum_{n=0}^{\infty} \frac{4(-1)^n}{ak_n^3 \cosh k_n b} \sin k_n x_1 \sinh k_n x_2$$

$$w = -\frac{x_1 x_2 (a^2 - b^2)}{(a^2 + b^2)}$$

$$w = \frac{x_2 (x_2^2 - 3x_1^2)}{a\sqrt{3}}$$

$$J_3 = 16a^3 b \left\{ \frac{1}{3} - \frac{64}{\pi^3} \frac{a}{b} \sum_{n=0}^{\infty} \frac{\tanh k_n b}{(2n+1)^5} \right\}$$

$$J_3 = \frac{\pi a^3 b^3}{(a^2 + b^2)}$$

$$J_3 = \frac{a^4 \sqrt{3}}{80}$$

$$k_n = \frac{(2n+1)\pi}{2a}$$

The force-deformation relations for the rod are

$$T_3 = \frac{EA}{2} \left(\left(\frac{ds}{d\bar{s}} \right)^2 - 1 \right) \approx EA \left(\frac{ds}{d\bar{s}} - 1 \right) \quad M_\alpha = EI_\alpha (\kappa_\alpha - \bar{\kappa}_\alpha) \quad M_3 = J_3 (\kappa_3 - \bar{\kappa}_3)$$

$$\sigma_{13} = (\kappa_3 - \bar{\kappa}_3) \left(\frac{\partial w}{\partial x_1} - x_2 \right) \quad \sigma_{23} = (\kappa_3 - \bar{\kappa}_3) \left(\frac{\partial w}{\partial x_2} + x_1 \right).$$

The two shear force components T_α cannot be related to the deformation; they are Lagrange multipliers that enforce the condition that the rod does not experience transverse shear, as discussed in the preceding section.

Derivation: These results can be derived as follows:

1. The elastic constitutive equations for materials subjected to small distortions, but arbitrary rotations, are listed in Section 3.4. They have the form

$$\Sigma_{ij} = \frac{E}{(1+\nu)} \left\{ E_{ij} + \frac{\nu}{1-2\nu} (E_{kk}) \delta_{ij} \right\},$$

where Σ_{ij} are the components of the material stress tensor, and E_{ij} are the components of the Lagrange strain tensor. The components of $E_{ij}^{\text{ee}} = (F_{ki}^{\text{ee}} F_{kj}^{\text{ee}} - \delta_{ij})/2$ in the basis $\{\mathbf{e}_1, \mathbf{e}_2, \mathbf{e}_3\}$ can be found using the formulas for \mathbf{F} given in Section 10.2.7 and, when substituted into the constitutive laws, give expressions for the components of material stress Σ_{ij}^{ee} in terms of the deformation measures $f_{\alpha\beta}$, u_3 , κ_i , and $ds/d\bar{s}$.

2. The Cauchy stress is related to the material stress by $\boldsymbol{\sigma} = \mathbf{F} \boldsymbol{\Sigma} \mathbf{F}^T / J$. For small distortions, but arbitrary rotations, we may approximate this by $\boldsymbol{\sigma} \approx \mathbf{R} \boldsymbol{\Sigma} \mathbf{R}^T = \Sigma_{ij}^{\text{ee}} \mathbf{R}_{\mathbf{e}_i} \otimes \mathbf{R}^T \mathbf{e}_j = \Sigma_{ij}^{\text{ee}} \mathbf{m}_i \otimes \mathbf{m}_j$, so the components of the material stress tensor in $\{\mathbf{e}_1, \mathbf{e}_2, \mathbf{e}_3\}$ can be used as an approximation to the components of the Cauchy stress tensor in $\{\mathbf{m}_1, \mathbf{m}_2, \mathbf{m}_3\}$.

3. Because we have assumed that the tractions on the sides of the rod vanish, the in-plane stress components must satisfy $\int_A \sigma_{\alpha\beta} dA = 0$. Substituting the formulas for stresses from step 2 and noting that $\int_A x_\alpha dA = 0$ (because the origin for the coordinate system coincides with the centroid of the cross section) shows that $f_{11} = f_{22} = -\nu \left((ds/d\bar{s})^2 - 1 \right)/2$, $f_{12} = 0$, and $\sigma_{33} = \frac{E}{2} \left(\left(\frac{ds}{d\bar{s}} \right)^2 - 1 + 2(\kappa_1 - \bar{\kappa}_1)x_2 - 2(\kappa_2 - \bar{\kappa}_2)x_1 \right)$.

4. Substituting the formula for σ_{33} into the definitions of T_3 , M_1 , M_2 given in Section 10.2.8 and noting that $\int_A x_1 x_2 dA = 0$ (because the basis vectors coincide with the principal axes of inertia) yields

$$T_3 = \frac{EA}{2} \left(\left(\frac{ds}{d\bar{s}} \right)^2 - 1 \right) \approx EA \left(\frac{ds}{d\bar{s}} - 1 \right) \quad M_\alpha = EI_\alpha (\kappa_\alpha - \bar{\kappa}_\alpha).$$

5. Recall that the shear stress components $\sigma_{\alpha 3}$ must satisfy the equilibrium equation and boundary condition

$$\frac{\partial \sigma_{\alpha 3}}{\partial x_\alpha} - \sigma_{31} \kappa_2 + \sigma_{32} \kappa_1 = 0 \quad \text{in } A \quad \sigma_{\alpha \beta} n_\alpha = 0 \quad \text{on } C.$$

Substituting the shear stress components from step 2 into this equilibrium equation and setting $u_3 = (\kappa_3 - \bar{\kappa}_3)w$ gives the governing equation for w :

$$\frac{\partial^2 w}{\partial x_1^2} + \frac{\partial^2 w}{\partial x_2^2} - \frac{\partial w}{\partial x_1} \kappa_2 + \frac{\partial w}{\partial x_2} \kappa_1 = 0 \quad \text{in } A \quad \frac{\partial w}{\partial x_\alpha} n_\alpha = x_2 n_1 - x_1 n_2 = x_\alpha \frac{\partial x_\alpha}{\partial s} \quad \text{on } C.$$

6. The shear stresses now follow as

$$\sigma_{13} = (\kappa_3 - \bar{\kappa}_3) \left(\frac{\partial w}{\partial x_1} - x_2 \right) \quad \sigma_{23} = (\kappa_3 - \bar{\kappa}_3) \left(\frac{\partial w}{\partial x_2} + x_1 \right).$$

Substituting these results into the equation defining M_3 in Section 10.2.8 gives the last equation:

$$M_3 = J_3 (\kappa_3 - \bar{\kappa}_3).$$

10.2.11 Strain Energy of an Elastic Rod

The total strain energy of an elastic rod can be computed from its curvatures as

$$\Phi = \frac{1}{2} \int_0^L \left\{ EA \left(\frac{ds}{d\bar{s}} - 1 \right)^2 + EI_1 (\kappa_1 - \bar{\kappa}_1)^2 + EI_2 (\kappa_2 - \bar{\kappa}_2)^2 + J_3 (\kappa_3 - \bar{\kappa}_3)^2 \right\} ds.$$

Derivation: The derivation is similar to the procedure used to compute elastic moment-curvature relations:

1. The strain energy density in the rod can be computed from the Lagrange strain E_{ij} and the material stress Σ_{ij} as $U = \sum_{ij} E_{ij}/2$. The material stress can be related to the Lagrange strain using the formulas in Section 10.2.10, whereas the Lagrange strain

can be expressed in terms of the deformation measures $f_{\alpha\beta}$, u_3 , κ_i , and $ds/d\bar{s}$ using the formulas for the deformation gradient listed in Sections 10.2.7.

2. The results can be simplified by recalling that $f_{11} = f_{22} = -v((ds/d\bar{s})^2 - 1)/2$, $f_{12} = 0$, which shows that the strain energy density can be approximated as

$$U = \frac{E}{2} \left[\left(\frac{ds}{d\bar{s}} - 1 \right) + (\kappa_1 - \bar{\kappa}_1)x_2 - (\kappa_2 - \bar{\kappa}_2)x_1 \right]^2 + \frac{1}{2}(\kappa_3 - \bar{\kappa}_3)^2 \left\{ \left(\frac{\partial w}{\partial x_1} - x_2 \right)^2 + \left(\frac{\partial w}{\partial x_2} + x_1 \right)^2 \right\},$$

where w is the warping function defined in Section 10.2.9. The two terms in this expression represent the strain energy density attributable to stretching and bending the rod, and twisting the rod, respectively.

3. The total strain energy follows by integrating U over the volume of the rod. Using the measures of cross-sectional geometry listed in Section 10.2.1, it is straightforward to show that

$$\begin{aligned} & \int_V \frac{E}{2} \left[\left(\frac{ds}{d\bar{s}} - 1 \right) + (\kappa_1 - \bar{\kappa}_1)x_2 - (\kappa_2 - \bar{\kappa}_2)x_1 \right]^2 dV \\ &= \frac{E}{2} \int_0^L \left\{ A \left(\frac{ds}{d\bar{s}} - 1 \right)^2 + I_1 (\kappa_1 - \bar{\kappa}_1)^2 + I_2 (\kappa_2 - \bar{\kappa}_2)^2 \right\} ds \end{aligned}$$

4. Some additional algebra is required to calculate the energy associated with twisting the rod. Begin by noting that

$$\int_A \left\{ \left(\frac{\partial w}{\partial x_1} - x_2 \right)^2 + \left(\frac{\partial w}{\partial x_2} + x_1 \right)^2 \right\} dA = J + \int_A \left(\frac{\partial w}{\partial x_\alpha} \frac{\partial w}{\partial x_\alpha} - x_2 \frac{\partial w}{\partial x_1} + x_1 \frac{\partial w}{\partial x_2} \right) dA.$$

We need to show that the integral on the right-hand side of this expression is zero.

5. To this end, note that

$$\int_A \frac{\partial w}{\partial x_\alpha} \frac{\partial w}{\partial x_\alpha} dA = \int_A \frac{\partial}{\partial x_\alpha} \left(w \frac{\partial w}{\partial x_\alpha} \right) dA = \int_C w \frac{\partial w}{\partial x_\alpha} n_\alpha ds = \int_C w (x_2 n_1 - x_1 n_2) ds,$$

where we have recalled that the warping function w satisfies $\partial^2 w / \partial x_\alpha \partial x_\alpha = 0$ in A as well as $(\partial w / \partial x_\alpha) n_\alpha = x_2 n_1 - x_1 n_2$ on C , and have used the divergence theorem.

6. Second, note that

$$\int_A \left(-x_2 \frac{\partial w}{\partial x_1} + x_1 \frac{\partial w}{\partial x_2} \right) dA = \int_A \left(\frac{\partial}{\partial x_1} (-x_2 w) + \frac{\partial}{\partial x_2} (w x_1) \right) dA = \int_C ((-x_2 w) n_1 + (w x_1) n_2) da.$$

The sum of steps 5 and 6 is zero. Using this result and step 4 gives the expression for the strain energy of the rod.

10.3 SIMPLIFIED VERSIONS OF THE GENERAL THEORY OF DEFORMABLE RODS

In many practical cases of interest, the general equations governing deformation and deformation of generally curved rods can be vastly simplified. In this section, we summarize the governing equations for a number of special solids, including flexible strings, and various forms of beam theory.

10.3.1 Stretched Flexible String with Small Transverse Deflections

This is the simplest possible version of the general theory outlined in Section 10.2. The problem to be solved is illustrated in Figure 10.8. A “string” with Young’s modulus E , mass density ρ , cross-sectional area A , and negligible area moments of inertia $I_1 = I_2 = I_3 = 0$ is initially straight and parallel to the \mathbf{e}_3 direction. The ends of the string are subjected to an axial load T_0 and are prevented from moving transverse to the string. A force per unit length $\mathbf{p} = p_1 \mathbf{e}_1$ acts on the string, inducing a small, time-dependent, transverse deflection $\mathbf{u} = u_1(x_3) \mathbf{e}_1$.

The general governing equations can be simplified to the following form:

1. The curvature of the string can be approximated as $\kappa \approx \frac{d^2 u_1}{dx_3^2} \mathbf{e}_2$.
2. The stretch of the string can be approximated as $\frac{ds}{dx_3} = 1 + T_0 / EA$.
3. The only nonzero internal force is the axial force T_3 (the moment-curvature relations show that the internal moments vanish; the angular momentum balance equations show $T_1 = T_2 = 0$).
4. The equations of motion reduce to $\kappa_2 T_3 + p_1 = \rho A \alpha_1 \frac{dT_3}{ds} = 0$.
5. Combining items 1–4 shows $T_3 = T_0$ and gives the equation of motion for the stretched string

$$T_0 \frac{d^2 u_1}{dx_3^2} + p_1 = \rho A \frac{d^2 u_1}{dt^2}.$$

6. The boundary conditions are $u_1 = 0$ at $x_3 = 0, x_3 = L$.

Large deflection equations for a flexible string can also be found by substituting $M_1 = M_2 = M_3 = T_1 = T_2 = 0$ into the general equations of motion for a rod. The details are left as an exercise.

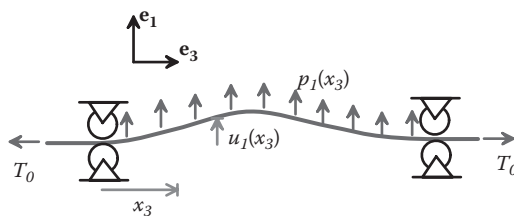


FIGURE 10.8 String subjected to transverse and end loading.

10.3.2 Straight Elastic Beam with Small Deflections and No Axial Force (Euler–Bernoulli Beam Theory)

Figure 10.9 illustrates the problem to be solved: an initially straight beam, with axis parallel to the \mathbf{e}_3 direction and principal axes of inertia parallel to $\mathbf{e}_1, \mathbf{e}_2$, is subjected to a transverse force per unit length $\mathbf{p} = p_1 \mathbf{e}_1$. The beam has Young's modulus E and mass density ρ , and its cross section has area A and principal moments of inertia I_1, I_2, I_3 . Its ends may be constrained in various ways, as described in more detail below. We suppose that the beam experiences a small transverse displacement $\mathbf{u} = u_1 \mathbf{e}_1$ and want to calculate u_1 as a function of time, given appropriate initial conditions.

The general equations of motion for a rod can be used to deduce the following:

1. The stretch of the bar and the curvature vector may be approximated by $\frac{ds}{dx_3} \approx 1$

$$\kappa \approx \frac{d^2 u_1}{dx_3^2} \mathbf{e}_2.$$
2. The internal forces can be characterized by the internal force $\mathbf{T} \approx T_1 \mathbf{e}_1$ and internal moment $\mathbf{M} = M_2 \mathbf{e}_2$. These can be interpreted as the force and moment acting on an internal cross section of the beam that has normal in the \mathbf{e}_3 direction.
3. Moment-curvature relations reduce to $M_2 = EI_2 \frac{d^2 u_1}{dx_3^2}$.
4. Equations of motion can be reduced to $\frac{dT_1}{dx_3} + p_1 = \rho A a_1 \quad \frac{dM_2}{dx_3} + T_1 = \rho I_2 \alpha_2 \approx 0$.
5. Alternatively, the equations in items 3 and 4 can be combined to express the equations of motion in terms of displacement:

$$EI_2 \frac{d^4 u_1}{dx_3^4} + \rho A \frac{d^2 u_1}{dt^2} = p_1.$$

Boundary conditions: Elementary beam theory offers the following boundary conditions:

1. The end of the beam may be *clamped*, i.e., rotations and displacement of the end are completely prevented. The transverse displacement must then satisfy $u_1 = du_1/dx_3 = 0$.

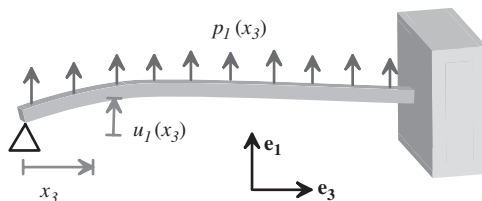


FIGURE 10.9 Beam subjected to transverse loading.

2. The end of the beam may be *simply supported*, i.e., the end cannot move but may rotate freely. In this case, the transverse displacement must satisfy $u_1 = 0$, and the internal moment must satisfy $M_2 = EI_2 d^2 u_1 / dx_3^2 = 0$.
3. The end of the beam may be *free*, i.e., the end can move and rotate freely. In this case, the internal moment and internal force must satisfy $M_2 = EI_2 d^2 u_1 / dx_3^2 = 0$: $T_1 = -EI_2 d^3 u_1 / dx_3^3 = 0$.

10.3.3 Straight Elastic Beam with Small Transverse Deflections and Significant Axial Force

This version of beam theory is used to model beams that are subjected to substantial axial loads (usually caused by forces applied at their ends). The equations can be used to estimate the effects of axial load on the transverse deflection or vibration of a beam. The theory can also be used to calculate buckling loads for beams but does not accurately model their deformation if the buckling loads are exceeded.

The problem to be solved is illustrated in Figure 10.10. An initially straight beam, with axis parallel to the \mathbf{e}_3 direction and principal axes of inertia parallel to $\mathbf{e}_1, \mathbf{e}_2$, is subjected to a force per unit length $\mathbf{p} = p_1 \mathbf{e}_1 + p_3 \mathbf{e}_3$. The beam has Young's modulus E and mass density ρ , and its cross section has area A and principal moments of inertia I_1, I_2, I_3 . Its ends may be constrained in various ways, as described in the preceding section. We assume that a large axial internal force $N\mathbf{m}_3$ is developed in the beam, by either a horizontal force per unit length p_3 or horizontal forces $P_3^{(0)}\mathbf{e}_3, P_3^{(L)}\mathbf{e}_3$ acting at the ends of the beam. We suppose that the beam experiences a small transverse displacement $\mathbf{u} = u_1 \mathbf{e}_1$ and want to calculate u_1 as a function of time, given appropriate initial conditions.

The general equations of motion for a deformable rod can be approximated as follows:

1. The stretch of the bar and the curvature vector may be approximated by $\frac{ds}{dx_3} \approx 1$ $\kappa \approx \frac{d^2 u_1}{dx_3^2} \mathbf{e}_2$.
2. The internal forces can be characterized by the internal force $\mathbf{T} = V\mathbf{m}_1 + N\mathbf{m}_3$ and internal moment $\mathbf{M} = M_2\mathbf{e}_2$. These can be interpreted as the force and moment acting on an internal cross section of the beam that has normal in the \mathbf{m}_3 direction.
3. Moment-curvature relations reduce to $M_2 = EI_2 \frac{d^2 u_1}{dx_3^2}$.

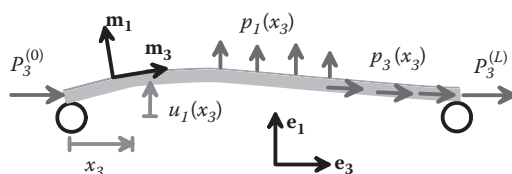


FIGURE 10.10 Beam subjected to transverse and axial loading.

4. Equations of motion may be approximated by

$$\frac{dV}{dx_3} + N \frac{d^2 u_1}{dx_3^2} - p_3 \frac{du_1}{dx_3} + p_1 = \rho A a_1 \quad \frac{dN}{dx_3} + p_3 = 0 \quad \frac{dM_2}{dx_3} + V = 0.$$

5. To interpret these equations, note the following: (1) the axial force N has been assumed to be much larger than the transverse force V , so that nonlinear terms associated with the axial force have been retained when approximating the equations of motion. (2) Although the equations of motion are expressed in terms of components of displacement and external force in the $\{\mathbf{e}_1, \mathbf{e}_2, \mathbf{e}_3\}$ basis, the equations of motion themselves represent an approximation to the components of the full, nonlinear equations of motion in the $\{\mathbf{m}_1, \mathbf{m}_2, \mathbf{m}_3\}$ basis.
6. The results of items 1–4 can be combined to obtain an equation for the transverse deflection of the beam:

$$EI_2 \frac{d^4 u_1}{dx_3^4} + \rho A \frac{d^2 u_1}{dt^2} + p_3 \frac{du_1}{dx_3} = N \frac{d^2 u_1}{dx_3^2} + p_1.$$

Boundary conditions: Elementary beam theory offers the following boundary conditions:

1. The end of the beam may be clamped, i.e., rotations and displacement of the end are completely prevented. The transverse displacement must then satisfy $u_1 = du_1/dx_3 = 0$.
2. The end of the beam may be simply supported, i.e., the end cannot move but may rotate freely. In this case, the transverse displacement must satisfy $u_1 = 0$ and the internal moment must satisfy $M_2 = EI_2 d^2 u_1 / dx_3^2 = 0$.
3. The end of the beam may be free, i.e., the end can move and rotate freely. In this case, the internal moment and internal force must satisfy $M_2 = EI_2 d^2 u_1 / dx_3^2 = 0$, whereas the transverse force must satisfy

$$V = \begin{cases} P_3^{(0)}(du_1/dx_3) & x_3 = 0 \\ -P_3^{(L)}(du_1/dx_3) & x_3 = L. \end{cases}$$

4. In addition, the axial force N must satisfy

$$N = -P_3^{(0)} \quad (x_3 = 0) \quad N = P_3^{(L)} \quad (x_3 = L).$$

10.4 EXACT SOLUTIONS TO SIMPLE PROBLEMS INVOLVING ELASTIC RODS

This section lists solutions to various boundary and initial value problems involving deformable rods, to illustrate representative applications of the equations derived in Sections 10.2 and 10.3. Specifically, we derive solutions for the following:

1. The natural frequencies and mode shapes for an initially straight vibrating beam

2. The buckling load for a vertical rod subjected to gravitational loading
3. The full post-buckled shape for a straight rod compressed by axial loads on its ends
4. Internal forces and moments in an initially straight rod that is bent and twisted into a helix
5. Internal forces, moments, and the deflected shape of a helical spring

10.4.1 Free Vibration of a Straight Beam without Axial Force

Figure 10.11 illustrates the problem to be solved: an initially straight beam, with axis parallel to the \mathbf{e}_3 direction and principal axes of inertia parallel to \mathbf{e}_1 , \mathbf{e}_2 , is free of external force. The beam has Young's modulus E and mass density ρ , and its cross section has area A and principal moments of area I_1 , I_2 , I_3 . Its ends may be constrained in various ways, as described in more detail below. We want to calculate the natural frequencies and mode shapes of vibration for the beam and to use these results to write down the displacement $u_1(x_3, t)$ for a beam that is caused to vibrate with initial conditions $u_1 = u^0(x_3)$, $du_1/dt = v^0(x_3)$ at time $t = 0$.

Mode shapes and natural frequencies: The physical significance of the mode shapes and natural frequencies of a vibrating beam can be visualized as follows:

1. Suppose that the beam is made to vibrate by bending it into some (fixed) deformed shape $u_1 = u^0(x_3)$ and then suddenly releasing it. In general, the resulting motion of the beam will be very complicated and may not even appear to be periodic.
2. However, there exists a set of special initial deflections $u^0 = U_n(k_n x_3)$ that cause every point on the beam to experience simple harmonic motion at some (angular) frequency ω_n , so that the deflected shape has the form $u_1(x, t) = U_n(k_n x_3) \cos(\omega_n t)$.
3. The special frequencies ω_n are called the *natural frequencies* of the beam, and the special initial deflections $U_n(k_n x_3)$ are called the *mode shapes*. Each mode shape has a wave number k_n that characterizes the wavelength of the harmonic vibrations and is related to the natural frequency by

$$\omega_n = k_n^2 \sqrt{\frac{EI_2}{\rho A}}.$$

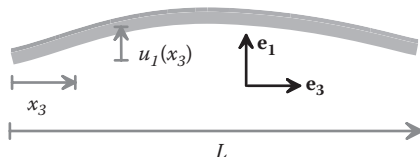


FIGURE 10.11 Vibrating elastic beam.

4. The mode shapes U_n have a very useful property (which is proved in Section 5.9.1):

$$\int_0^L U_i(k_n x_3) U_j(k_n x_3) dx_3 = 0 \quad i \neq j.$$

The mode shapes, wave numbers, and corresponding natural frequencies depend on the way the beam is supported at its ends. A few representative results are listed below.

Beam with free ends: The wave numbers for each mode are given by the roots of the equation

$$\cos(k_n L) \cosh(k_n L) - 1 = 0.$$

The mode shapes are

$$U_n = A_n \left(\sinh(k_n x_3) + \sin(k_n x_3) + \frac{\cosh(k_n L) - \cos(k_n L)}{\sinh(k_n L) + \sin(k_n L)} [\cosh(k_n x_3) + \cos(k_n x_3)] \right),$$

where A_n are arbitrary constants.

Beam with pinned ends: The wave numbers for each mode are $k_n = n\pi/L$. The mode shapes are $U_n = A_n \sin(k_n x_3)$, where A_n are arbitrary constants

Cantilever beam (clamped at $x_3 = 0$, free at $x_3 = L$): The wave numbers for each mode are given by the roots of the equation

$$\cos(k_n L) \cosh(k_n L) + 1 = 0.$$

The mode shapes are

$$U_n = A_n \left(\sinh(k_n x_3) - \sin(k_n x_3) + \frac{\cosh(k_n L) + \cos(k_n L)}{\sin(k_n L) - \sinh(k_n L)} [\cosh(k_n x_3) - \cos(k_n x_3)] \right),$$

where A_n are arbitrary constants.

Vibration of a beam with given initial displacement and velocity: The solution for free vibration of a beam with given initial displacement and velocity can be found by superposing contributions from each mode as follows

$$u_l(x_3, t) = \sum_{n=1}^{\infty} C_n U_n(k_n x_3) \cos(\omega_n t) + \sum_{n=1}^{\infty} D_n U_n(k_n x_3) \sin(\omega_n t),$$

where

$$C_n = \frac{\int_0^L u^0(x_3) U_n(k_n x_3) dx_3}{\int_0^L \{U_n(k_n x_3)\}^2 dx_3} \quad D_n = \frac{\int_0^L v^0(x_3) U_n(k_n x_3) dx_3}{\omega_n \int_0^L \{U_n(k_n x_3)\}^2 dx_3}.$$

Derivation: We will derive the equations for the natural frequencies and mode shapes of a beam with free ends as a representative example. This is a small deflection problem and can be modeled using Euler–Bernoulli beam theory summarized in Section 10.3.2:

1. The deflection of the beam must satisfy the equation of motion given in Section 10.3.2:

$$EI_2 \frac{d^4 u_1}{dx_3^4} + \rho A \frac{d^2 u_1}{dt^2} = 0.$$

2. The general solution to this equation (found, for example, by separation of variables or just direct substitution) is

$$u_1 = \{A_1 \sinh(k_n x_3) + A_2 \cosh(k_n x_3) + A_3 \sin(k_n x_3) + A_4 \cos(k_n x_3)\} \cos(\omega_n t + \phi),$$

where the frequency and wave number must be related by $k_n^4 = \rho A \omega_n^2 / EI_2$ to satisfy the equation of motion.

3. The coefficients $A_1 \dots A_4$ and the wave number k_n must be chosen to satisfy the boundary conditions at the ends of the bar. For a beam with free ends, the boundary conditions reduce to $d^2 u_1 / dx_3^2 = 0$, $d^3 u_1 / dx_3^3 = 0$ at $x_3 = 0$, $x_3 = L$. Substituting the formula from step 2 into the four boundary conditions and writing the resulting equations in matrix form yields

$$\begin{bmatrix} 1 & 0 & -1 & 0 \\ 0 & 1 & 0 & -1 \\ \cosh(k_n L) & \sinh(k_n L) & -\cos(k_n L) & \sin(k_n L) \\ \sinh(k_n L) & \cosh(k_n L) & -\sin(k_n L) & -\cos(k_n L) \end{bmatrix} \begin{bmatrix} A_1 \\ A_2 \\ A_3 \\ A_4 \end{bmatrix} = 0.$$

4. For a nonzero solution, the matrix in this equation must be singular. This implies that the determinant of the matrix is zero, which gives the governing equation for the wave number:

$$\cos(k_n L) \cosh(k_n L) - 1 = 0.$$

5. Because the equation system in step 3 is now singular, we may discard any one of the four equations and use the other three to determine an equation relating A_2 , A_3 , A_4 to A_1 . Choosing to discard the last row of the matrix and taking the first column to the right-hand side shows that

$$\begin{bmatrix} 0 & -1 & 0 \\ 1 & 0 & -1 \\ \sinh(k_n L) & -\cos(k_n L) & \sin(k_n L) \end{bmatrix} \begin{bmatrix} A_2 \\ A_3 \\ A_4 \end{bmatrix} = -A_1 \begin{bmatrix} 1 \\ 0 \\ \cosh(k_n L) \end{bmatrix}.$$

Solving this equation system shows that $A_2 = A_4 = \frac{\cosh(k_n L) - \cos(k_n L)}{\sinh(k_n L) + \sin(k_n L)} A_1$, $A_3 = A_1$.

Substituting these values back into the solution in step 2 gives the mode shape.

6. To understand the formula for the vibration of a beam with given initial conditions, note that the most general solution consists of a linear combination of all possible mode shapes, i.e.,

$$u_1(x_3, t) = \sum_{n=1}^{\infty} C_n U_n(k_n x_3) \cos(\omega_n t) + \sum_{n=1}^{\infty} D_n U_n(k_n x_3) \sin(\omega_n t).$$

Formulas for C_n found by substituting $t = 0$, multiplying both sides of the equation by $U_j(k_n x_3)$, and integrating over the length of the beam. We know that

$$\int_0^L U_n(k_n x_3) U_j(k_j x_3) dx_3 = 0 \quad n \neq j,$$

so the result reduces to

$$\int_0^L u^0(x_3) U_j(k_n x_3) dx_3 = C_j \int_0^L \{U_j(k_n x_3)\}^2 dx_3.$$

The formula for D_n is found by differentiating the general solution with respect to time to find the velocity, substituting $t = 0$, and then proceeding as before to extract each coefficient D_n .

10.4.2 Buckling of a Column Subjected to Gravitational Loading

The problem to be solved is illustrated in Figure 10.12. A straight, vertical elastic cantilever beam with mass density ρ and elastic modulus E is clamped at its base and subjected to gravitational loading. The beam has length L , cross-sectional area A , and principal moments of area I_1, I_2, I_3 . The straight, vertical rod is always an equilibrium configuration, but this configuration is stable only if $L < L_{crit}$. Our objective is to show that the critical buckling length is

$$L_{crit} \approx 2 \left(\frac{EI_2}{\rho Ag} \right)^{1/3}.$$

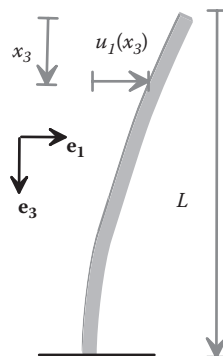


FIGURE 10.12 Rod buckling under gravitational loading.

A number of different techniques can be used to find buckling loads. One of the simplest procedures (which will be adopted here) is to identify the critical conditions in which both the straight configuration (with $u_1 = 0$) and the deflected configuration (with a small transverse deflection $u_1 \neq 0$) are possible equilibrium shapes for the rod.

This problem can be solved using the governing equations for a beam subjected to large axial forces, listed in Section 10.3.3. For the present case, we note the following:

1. The external forces acting on the rod are $p_1 = 0$, $p_3 = \rho g A$, where g is the gravitational acceleration.
2. The acceleration is zero (because the rod is in static equilibrium).
3. The equilibrium equations therefore reduce to

$$EI_2 \frac{d^4 u_1}{dx_3^4} + \rho A g \frac{du_1}{dx_3} = N \frac{d^2 u_1}{dx_3^2} \quad \frac{dN}{dx_3} + \rho A g = 0.$$

4. These equations must be solved subject to the boundary conditions

$$N = 0, \quad \frac{d^2 u_1}{dx_3^2} = 0, \quad \frac{d^3 u_1}{dx_3^3} = 0 \quad x_3 = 0; \quad u_1 = 0, \quad \frac{du_1}{dx_3} = 0 \quad x_3 = L.$$

5. Integrating the second equation of step 3 and using the boundary condition $N = 0$ at $x_3 = 0$ reduces the first equation of step 3 to

$$EI_2 \frac{d^4 u_1}{dx_3^4} + \rho A g \frac{du_1}{dx_3} + \rho A g x_3 \frac{d^2 u_1}{dx_3^2} = 0.$$

6. Integrating this equation with respect to x_3 and imposing the boundary condition $d^3 u_1 / dx_3^3 = 0$ at $x_3 = 0$ shows that

$$EI_2 \frac{d^3 u_1}{dx_3^3} + \rho A g x_3 \frac{du_1}{dx_3} = 0.$$

7. This equation can be solved for du_1/dx_3 using a symbolic manipulation program, which yields

$$\frac{du_1}{dx_3} = C_1 \text{Ai}_0 \left[-x_3 \left(\frac{\rho A g}{EI_2} \right)^{1/3} \right] + C_2 \text{Bi}_0 \left[-x_3 \left(\frac{\rho A g}{EI_2} \right)^{1/3} \right],$$

where $\text{Ai}_0(x)$, $\text{Bi}_0(x)$ are special functions called “Airy wave functions of order zero.”

8. The remaining boundary conditions are $du_1^2/dx_3^2 = 0$ at $x_3 = 0$ and $du_1/dx_3 = 0$ at $x_3 = L$. Substituting step 7 into the boundary conditions and writing the results in matrix form gives

$$\begin{bmatrix} \text{Ai}_1(0) & \text{Bi}_1(0) \\ \text{Ai}_0(-\lambda) & \text{Bi}_0(-\lambda) \end{bmatrix} \begin{bmatrix} C_1 \\ C_2 \end{bmatrix} = 0,$$

where $\lambda = L(\rho Ag/EI_2)^{1/3}$ and $Ai_1(x)$, $Bi_1(x)$ are Airy wave functions of order one.

9. For this system of equations to have a nonzero solution, the determinant of the matrix must vanish, which shows that λ must satisfy $Ai_1(0)Bi_0(-\lambda) - Bi_1(0)Ai_0(-\lambda) = 0$. This equation can easily be solved (numerically) for λ . The smallest value of λ that satisfies the equation is $\lambda \approx 2$.
10. The buckling length follows as

$$L_{crit} \approx 2 \left(\frac{EI_2}{\rho Ag} \right)^{1/3}.$$

10.4.3 Post-Buckled Shape of an Initially Straight Rod Subjected to End Thrust

Figure 10.13 illustrates the problem to be solved. An initially straight, inextensible elastic rod, with Young's modulus E , length L , and principal in-plane moments of area I_1, I_2 (with $I_2 < I_1$) is subjected to end thrust. The ends of the rod are constrained to travel along a line that is parallel to the undeformed rod, but the ends are free to rotate. We want to calculate the deformed shape of the rod. You are probably familiar with the simple Euler buckling analysis that predicts the critical buckling loads. Here, we derive the full post-buckling solution.

The rod is assumed to bow away from its straight configuration as shown: the deflected rod lies in the plane perpendicular to e_2 . The basis $\{\mathbf{m}_1, \mathbf{m}_2, \mathbf{m}_3\}$ and the Euler angle θ that characterize the rotation of the rod's cross sections are shown in the picture; the remaining Euler angles are $\psi = \phi = 0$.

Solution: Several possible equilibrium solutions may exist, depending on the applied load P :

1. The straight rod, with $\theta = y_2 = 0, x_3 = s$ is always an equilibrium solution. It is stable for applied loads $P < \pi^2 EI_2/L^2$.
2. For applied loads $P > n^2 \pi^2 EI_2/L^2$, with n an integer, there are $n + 1$ possible equilibrium solutions. One of these is the straight rod; the rest are possible buckling

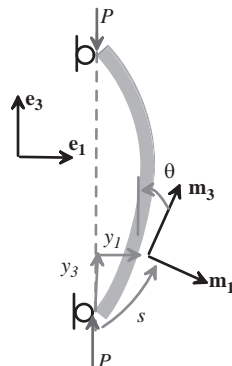


FIGURE 10.13 Rod buckling under axial loading.

modes. The shape of each buckling mode depends on a parameter k_n , which satisfies

$$L\sqrt{P/EI_2} = 2nK(k_n),$$

where K denotes a complete elliptic integral of the first kind

$$K(k) = \int_0^{\pi/2} (1 - k^2 \sin^2 x)^{-1/2} dx.$$

Note that K has a minimum value $K = \pi/2$ at $k = 0$ and increases monotonically to infinity as $k \rightarrow 1$. The equation for k_n has no solutions for $P < \pi^2 EI_2/L^2$ and n solutions for $P > n^2 \pi^2 EI_2/L^2$, as expected. If multiple solutions exist, only the solution with $n = 1$ is stable.

3. The shape of the deformed rod can be characterized by the Euler angle shown in Fig 10.13, which satisfies

$$\theta = 2 \sin^{-1} \left\{ k_n \operatorname{sn}(s\sqrt{P/EI_2} + K(k_n); k_n) \right\},$$

where $\operatorname{sn}(x, k)$ denotes a Jacobi elliptic function called the “sine amplitude”: its second argument k is called the “modulus” of the function.

4. The coordinates of the buckled rod can also be calculated. They are given by

$$y_3 = -s - 2\sqrt{EI_2/P} [\operatorname{E}(\operatorname{am}(s\sqrt{P/EI_2} + K(k_n); k_n); k_n) - \operatorname{E}(\operatorname{am}(K(k_n); k_n); k_n)]$$

$$y_2 = -2k_n \sqrt{EI_2/P} \operatorname{cn}(s\sqrt{P/EI_2} + K(k_n); k_n).$$

Here, $\operatorname{am}(x, k)$ and $\operatorname{cn}(x, k)$ denote Jacobi elliptic functions called the “amplitude” and “cosine amplitude,” and $\operatorname{E}(x, k)$ denotes an incomplete elliptic integral of the second kind: $\operatorname{E}(x, k) = \int_0^x (1 - k^2 \sin^2 t)^{1/2} dt$. The shape of the deflected rod for the stable buckling mode ($n = 1$) is shown in Figure 10.14.

Derivation: This is a large deflection problem and must be treated using the general equations listed in Sections 10.2.7 through 10.2.9:

1. The equilibrium equation $d\mathbf{T}/ds = 0$ immediately shows that $\mathbf{T} = \text{constant}$ along the rod’s length. The boundary conditions at the end of the rod give $\mathbf{T} = -P\mathbf{e}_3$, so that the components of \mathbf{T} in $\{\mathbf{m}_1, \mathbf{m}_2, \mathbf{m}_3\}$ follow as $T_1 = 0$, $T_2 = P \sin \theta$, $T_3 = -P \cos \theta$.
2. Substituting the expressions for T_i into the moment balance equations shows that $M_1 = M_3 = 0$ and $dM_2/ds + P \sin \theta = 0$.

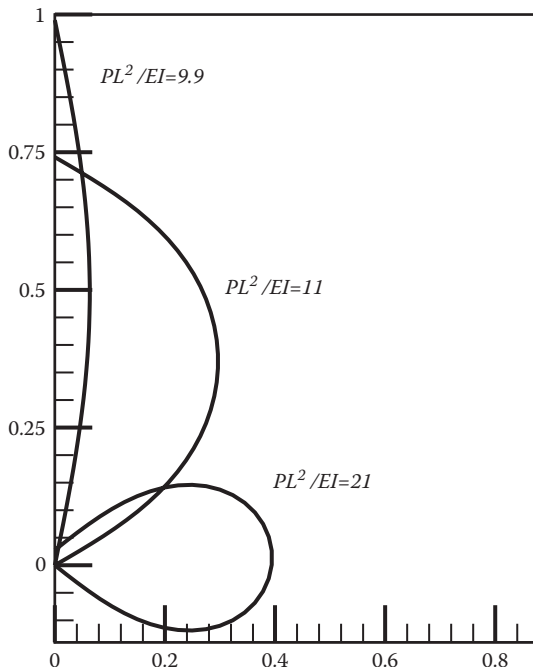


FIGURE 10.14 Post-buckling shape of an axially loaded rod.

3. Finally, note that the curvatures are $\kappa_2 = d\theta/ds$, $\kappa_1 = \kappa_3 = 0$ and recall that $M_2 = EI_2\kappa_2$, so that the angle θ satisfies $EI_2 \frac{d^2\theta}{ds^2} + P \sin\theta = 0$.
4. This is the equation that governs oscillations of a pendulum, and its solution is well known. The equation is satisfied trivially by $\theta = 0$ (this is the straight configuration) and also by two families of functions of the form

$$\theta = 2\sin^{-1}\left\{k \operatorname{sn}\left((s-s_0)\sqrt{(P/EI_2)}; k\right)\right\} \quad \theta = 2\sin^{-1}\left\{\operatorname{sn}\left((s-s_0)\sqrt{(P/k^2EI_2)}; k\right)\right\}.$$

Here, s_0 and $0 < k < 1$ are parameters whose values must be determined from the boundary conditions. The first of these two functions is called an “inflexional” solution because the curve has points where $d\theta/ds = 0$. The second is called “non-inflexional” because it has no such points. For the pendulum, inflexional solutions correspond to periodic swinging motion; the non-inflexional solution corresponds to the pendulum whirling around the pivot.

5. The bending moment must satisfy $M_2 = 0$ at both ends of the rod, which requires that $d\theta/ds = 0$ at $s = 0$ and $s = L$. Only the inflexional solution can satisfy these boundary conditions. For this case, we have

$$\frac{d\theta}{ds} = 2k\sqrt{\frac{I_2}{P}} \operatorname{cn}\left((s-s_0)\sqrt{(P/EI_2)}; k\right).$$

The cosine amplitude cn is a periodic function (it is a generalized cosine) and satisfies $cn(x, k) = 0$ at $x = (2n + 1)K(k)$. We may therefore satisfy the boundary conditions by choosing $-s_0\sqrt{P/EI_2} = K(k)$ and $L\sqrt{P/EI_2} = 2nK(k)$. This leads to the defining equations for k_n .

6. Finally, the formula for the coordinates follows by integrating $dy_3/ds = \cos\theta$ and $dy_2/ds = \sin\theta$ subject to boundary conditions $y_1 = 0$ at $s = 0, L$ and $y_3 = 0$ at $s = 0$.
7. Finally, the (global) stability of the various solutions can be checked by comparing their potential energy.

10.4.4 Rod Bent and Twisted into a Helix

We consider an initially straight rod with Young's modulus E and shear modulus μ . The cross section of the rod has area A , principal in-plane moments of inertia $I_1 = I_2 = I$, and an effective torsional inertia J_3 . The rod is initially straight and unstressed and is then subjected to forces and moments on its ends to bend and twist it into a helical shape, as shown in Figure 10.15. The geometry of the deformed rod can be characterized by the following:

1. The radius r of the cylinder that generates the helix.
2. The number of turns per unit axial length n in the helix.
3. The helix angle α , which is related to n by $\tan\alpha = 1/(2\pi rn)$.
4. The twist curvature κ_3 , which quantifies the distortion induced by twisting the rod about its deformed axis. For the rod to be in equilibrium, κ_3 must be constant.
5. The stretch ratio $\lambda = ds/dx_3$. For the rod to be in equilibrium, λ must be constant.

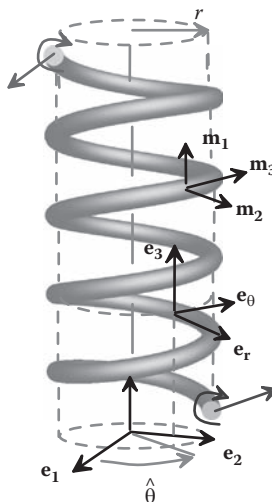


FIGURE 10.15 Rod bent into a helix by terminal couples and forces.

The geometry and forces in the deformed rod are most conveniently described using a cylindrical-polar coordinate system $(r, \hat{\theta}, z)$ and basis $\{\mathbf{e}_r, \mathbf{e}_\theta, \mathbf{e}_3\}$ shown in Figure 10.15. In terms of these basis vectors, we may define:

1. The tangent vector to the rod $\mathbf{t} = \mathbf{m}_3 = \cos\alpha\mathbf{e}_\theta + \sin\alpha\mathbf{e}_3$
2. The binormal vector $\mathbf{b} = -\sin\alpha\mathbf{e}_\theta + \cos\alpha\mathbf{e}_3$

In terms of these variables:

1. The internal moment in the rod is $\mathbf{M} = EI \frac{\cos^2 \alpha}{r} \mathbf{b} + J_3 \kappa_3 \mathbf{m}_3$.
2. The internal force in the rod is $\mathbf{T} = \frac{\cos^2 \alpha}{r} \left(J_3 \kappa_3 - \frac{EI}{r} \cos\alpha \sin\alpha \right) \mathbf{b} + EA(\lambda - 1) \mathbf{m}_3$.

For the limiting case of an inextensible rod, the quantity EA ($\lambda - 1$) should be replaced by an indeterminate axial force T_3 . The forces acting on the ends of the rod must satisfy $\mathbf{P} = \mathbf{T}$ and $\mathbf{Q} = \mathbf{M}$ at $s = L$ and $\mathbf{P} = -\mathbf{T}$, $\mathbf{Q} = -\mathbf{M}$ at $s = 0$.

A variety of force and moment systems may deform the rod into a helical shape, depending on the twist and stretch. An example of particular practical significance consists of a force $\mathbf{P} = F_z \mathbf{e}_3$ and moment $\mathbf{Q} = rF_z \mathbf{e}_\theta + Q_z \mathbf{e}_z$ acting at $s = L$ (with equal and opposite forces at $s = 0$), where

$$F_z = \frac{\cos\alpha}{r} \left(J_3 \kappa_3 - \frac{EI}{r} \cos\alpha \sin\alpha \right) \quad Q_z = J_3 \kappa_3 \sin\alpha + \frac{EI}{r} \cos^3 \alpha.$$

This force system is statically equivalent to a wrench with force $F_z \mathbf{e}_z$ and moment $Q_z \mathbf{e}_z$ acting at $r = 0$. Finally, note that this analysis merely gives conditions for a helical rod to be in static equilibrium. The configuration may not be stable.

Derivation

1. We take $\hat{\theta} = z = 0$ at $s = 0$, so that the cylindrical polar coordinates are related to arc length by $\hat{\theta} = \frac{s}{r} \cos\alpha$, $z = s \sin\alpha$. Note also that the basis vectors satisfy $d\mathbf{e}_r/d\hat{\theta} = \mathbf{e}_\theta$, $d\mathbf{e}_\theta/d\hat{\theta} = -\mathbf{e}_r$, so that

$$\frac{d\mathbf{e}_r}{ds} = \frac{\cos\alpha}{r} \mathbf{e}_\theta \quad \frac{d\mathbf{e}_\theta}{ds} = -\frac{\cos\alpha}{r} \mathbf{e}_r.$$

2. The position vector of a point on the axis of the rod can be expressed as $\mathbf{r} = r\mathbf{e}_r + z\mathbf{e}_3$.
3. The tangent vector follows as $\mathbf{m}_3 = \frac{d\mathbf{r}}{ds} = \cos\alpha\mathbf{e}_\theta + \sin\alpha\mathbf{e}_3$.
4. By definition, the curvature vector is

$$\boldsymbol{\kappa} = \mathbf{m}_3 \times \frac{d\mathbf{m}_3}{ds} + \kappa_3 \mathbf{m}_3 = -\frac{\cos^2 \alpha \sin\alpha}{r} \mathbf{e}_\theta + \frac{\cos^3 \alpha}{r} \mathbf{e}_3 + \kappa_3 \mathbf{m}_3,$$

which can be expressed in terms of the binormal vector as $\boldsymbol{\kappa} = (\cos^2 \alpha/r)\mathbf{b} + \kappa_3 \mathbf{m}_3$.

5. The moment-curvature relations then give the internal moment

$$\mathbf{M} = EI (\cos^2 \alpha / r) \mathbf{b} + \mu J_3 \kappa_3 \mathbf{m}_3.$$

6. The equilibrium equation $d\mathbf{T}/ds + \mathbf{p} = \mathbf{0}$ shows that $\mathbf{T} = \text{constant}$. We may express this constant internal force vector in terms of its components as $T_r \mathbf{e}_r + T_\theta \mathbf{e}_\theta + T_z \mathbf{e}_3$.
7. The internal forces and moments must satisfy the moment equilibrium equation, which shows that

$$\frac{d\mathbf{M}}{ds} + \mathbf{m}_3 \times \mathbf{T} = \frac{\cos^2 \alpha}{r} \left(\frac{EI}{r} \cos \alpha \sin \alpha - J_3 \kappa_3 \right) \mathbf{e}_r + J_3 \frac{d\kappa_3}{ds} (\cos \alpha \mathbf{e}_\theta + \sin \alpha \mathbf{e}_3)$$

$$+ (T_z \cos \alpha - T_\theta \sin \alpha) \mathbf{e}_r + T_r \sin \alpha \mathbf{e}_\theta - T_r \cos \alpha \mathbf{e}_3 = 0.$$

Taking the dot product of both sides of this equation with \mathbf{m}_3 shows that $d\kappa_3/ds = 0$. It then follows that $T_r = 0$ and

$$\frac{\cos^2 \alpha}{r} \left(J_3 \kappa_3 - \frac{EI}{r} \cos \alpha \sin \alpha \right) = (T_z \cos \alpha - T_\theta \sin \alpha).$$

8. Finally, the force-stretch relation requires that $\mathbf{T} \cdot \mathbf{m}_3 = T_\theta \cos \alpha + T_z \sin \alpha = EA(\lambda - 1)$. This equation can be solved together with the final result of step 7 for the components of internal force in the rod.

10.4.5 Helical Spring

The behavior of the helical spring shown in Figure 10.16 can be deduced by means of a simple extension of the results in the preceding section. We assume that the spring is made from a material with Young's modulus E and shear modulus μ . The cross section of the rod has principal in-plane moments of inertia $I_1 = I_2 = I$ and an effective torsional inertia J_3 . The rod is assumed to be inextensible, for simplicity. The geometry of the undeformed spring can be characterized by the following variables:

1. The length of the rod L , the radius \bar{r} of the cylinder that generates the helix, the height \bar{h} of the spring, the number of turns in the coil N , and the helix angle $\bar{\alpha}$.

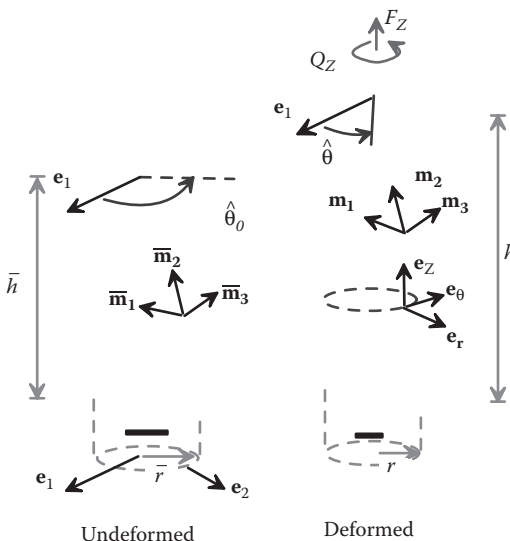


FIGURE 10.16 Deformation of a helical spring.

2. The variables characterizing the undeformed spring are related as follows

$$\tan \bar{\alpha} = \frac{\bar{h}}{2\pi \bar{r}N} \quad \bar{h} = L \sin \bar{\alpha}.$$

3. It is helpful to select a basis $\{\bar{\mathbf{m}}_1, \bar{\mathbf{m}}_2, \bar{\mathbf{m}}_3\}$ to characterize the orientation of the initial spring. Because $I_1 = I_2$, we may select $\bar{\mathbf{m}}_1$ and $\bar{\mathbf{m}}_2$ arbitrarily. It is convenient to choose $\bar{\mathbf{m}}_1$ and $\bar{\mathbf{m}}_2$ to be parallel to the normal vector \mathbf{n} and binormal vector \mathbf{b} of the undeformed spring, respectively, which gives $\bar{\mathbf{m}}_1 = -\mathbf{e}_r$, $\bar{\mathbf{m}}_2 = -\sin \bar{\alpha} \mathbf{e}_\theta + \cos \bar{\alpha} \mathbf{e}_z$.
4. The initial curvature components can be calculated from the condition that $d\mathbf{m}_i/ds = \kappa \times \mathbf{m}_i$ and follow as $\bar{\kappa}_1 = 0$, $\bar{\kappa}_2 = \cos^2 \bar{\alpha} / \bar{r}$, $\bar{\kappa}_3 = \sin \bar{\alpha} \cos \bar{\alpha} / \bar{r}$.

The end of the spring at $s = 0$ is held fixed (so it cannot move or rotate). The end of the spring at $s = L$ is subjected to a combination of a force $F_z \mathbf{e}_z$ and moment $Q_z \mathbf{e}_z$, which act at the axis of the helical coil. The solution can be calculated in exactly the same way as the derivation in Section 10.3.5. The following can be shown:

1. The spring remains helical: its deformed shape can be characterized by new values of r , α , and h after deformation.
2. The spring may tend to twist about the axis of the helix when it is subjected to load. The twisting can be quantified by the change in cylindrical-polar coordinates of the point at $s = L$ on the spring. In the undeformed state, these are $(\bar{r}, \hat{\theta}_0, \bar{h})$; after deformation, they are $(r, \hat{\theta}, h)$. The twisting can be characterized by the rotation $\Delta\omega = \hat{\theta} - \hat{\theta}_0$. The point at which the load is applied therefore displaces through a distance $\Delta h = h - \bar{h}$ and rotates through the angle $\Delta\omega$ about the axis of the cylinder.
3. The displacement and rotation are related to the rod's length L , the coil radius r , and helix angle α by

$$\Delta\omega = L \left(\frac{\cos \alpha}{r} - \frac{\cos \bar{\alpha}}{\bar{r}} \right) \quad \Delta h = L(\sin \alpha - \sin \bar{\alpha}).$$

4. The vectors \mathbf{m}_1 and \mathbf{m}_2 after deformation are given by $\mathbf{m}_1 = -\mathbf{e}_r$, $\mathbf{m}_2 = -\sin \alpha \mathbf{e}_\theta + \cos \alpha \mathbf{e}_z$.
5. The curvatures after deformation follow as $\kappa_1 = 0$, $\kappa_2 = \cos^2 \alpha / r$, $\kappa_3 = \sin \alpha \cos \alpha / r$.
6. The internal moment and force in the spring are related to the curvatures and external force and moment by

$$\begin{aligned} \mathbf{M} &= EI(\kappa_2 - \bar{\kappa}_2) \mathbf{m}_2 + J_3(\kappa_3 - \bar{\kappa}_3) \mathbf{m}_3 = Q_z \mathbf{e}_z + r F_z \mathbf{e}_\theta \\ \mathbf{T} &= \left\{ J_3 \frac{\cos \alpha}{r} (\kappa_3 - \bar{\kappa}_3) - EI \frac{\sin \alpha}{r} (\kappa_2 - \bar{\kappa}_2) \right\} \mathbf{e}_z = F_z \mathbf{e}_z. \end{aligned}$$

7. The external force and moment applied to the axis of the spring are related to the helix angle and coil radius before and after deformation by

$$F_z = J_3 \frac{\cos \alpha}{r} (\kappa_3 - \bar{\kappa}_3) - EI \frac{\sin \alpha}{r} (\kappa_2 - \bar{\kappa}_2) \quad Q_z = J_3 \sin \alpha (\kappa_3 - \bar{\kappa}_3) + EI \cos \alpha (\kappa_2 - \bar{\kappa}_2).$$

8. If the spring is subjected a prescribed force and moment, these equations can be solved for α and r , and the results can be substituted into step 3 to calculate the extension Δh and rotation $\Delta\omega$ of the spring. The results cannot be expressed in closed form for large shape changes. If Δh and $\Delta\omega$ are small, however, the relations can be linearized to yield

$$F_z = k_{FF}\Delta h + k_{FQ}\Delta\omega \quad Q_z = k_{QQ}\Delta\omega + k_{QF}\Delta h,$$

where the spring stiffnesses are

$$k_{FF} = \frac{\sin\bar{\alpha}}{\bar{h}\bar{r}^2} \left(J_3 \cos^2 \bar{\alpha} + EI \sin^2 \bar{\alpha} \right) \quad k_{QQ} = \frac{\sin\bar{\alpha}}{\bar{h}} \left(J_3 \sin^2 \bar{\alpha} + EI \cos^2 \bar{\alpha} \right)$$

$$k_{FQ} = k_{QF} = \frac{\sin^3 \bar{\alpha} \cos \bar{\alpha}}{\bar{h}\bar{r}} (J_3 - EI).$$

10.5 MOTION AND DEFORMATION OF THIN SHELLS: GENERAL THEORY

Figure 10.17 illustrates the problem to be solved. The solid of interest is a shell with uniform thickness h . The shell's thickness is assumed to be much smaller than any relevant in-plane dimension. The exterior surface of the shell is subjected to a prescribed distribution of traction, whereas the edge of the shell may either be supported so as to constrain its motion or be subjected to prescribed forces. Our objective is to calculate the internal forces in the shell and to compute its deformed shape.

10.5.1 Coordinate Systems and Variables Characterizing Deformation of Shells

- To specify the position of a point on the midplane of the undeformed shell, we introduce a convenient curvilinear coordinate system (ξ_1, ξ_2) (examples include cylindrical or spherical polar coordinates). Note that ξ_α need not necessarily be distances along the surface: for example, for a cylindrical shell, we would use the axial distance z and the angle θ as the coordinate system.
- The position vector of a material particle on the midsection of the initial shell is denoted by $\bar{\mathbf{r}}(\xi_1, \xi_2)$.
- To characterize the orientation of an arbitrary point in the undeformed shell, we introduce three basis vectors $(\bar{\mathbf{m}}_1, \bar{\mathbf{m}}_2, \bar{\mathbf{m}}_3)$, with

$$\bar{\mathbf{m}}_\alpha = \frac{\partial \bar{\mathbf{r}}}{\partial \xi_\alpha} \quad \bar{\mathbf{m}}_3 = \frac{\bar{\mathbf{m}}_1 \times \bar{\mathbf{m}}_2}{|\bar{\mathbf{m}}_1 \times \bar{\mathbf{m}}_2|}.$$

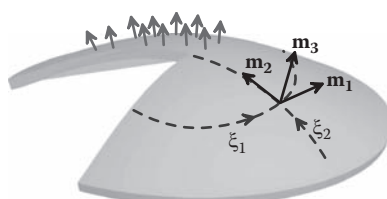


FIGURE 10.17 Thin shell subjected to external loading.

Thus, $\bar{\mathbf{m}}_\alpha$ are tangent to the coordinate lines ξ_α in the undeformed shell, and $\bar{\mathbf{m}}_3$ is a unit vector perpendicular to the midsection of the shell. This basis is called the *covariant basis* or *natural basis* for the coordinate system. Note that the basis vectors $\bar{\mathbf{m}}_\alpha$ are not unit vectors and are not, in general, orthogonal.

- Because $(\bar{\mathbf{m}}_1, \bar{\mathbf{m}}_2, \bar{\mathbf{m}}_3)$ are not orthogonal, it is convenient to introduce a second set of basis vectors $(\bar{\mathbf{m}}^1, \bar{\mathbf{m}}^2, \bar{\mathbf{m}}^3)$ defined so that

$$\bar{\mathbf{m}}^i \cdot \bar{\mathbf{m}}_j = \delta_j^i,$$

where δ_j^i is the Kronecker delta symbol (the index i has been raised to match the indices on the basis vectors), i.e., $\delta_j^i = 1$ for $i = j$ and zero otherwise. This second triad of vectors is called the *contravariant basis* or *reciprocal basis* for the coordinate system. The contravariant basis vectors can be constructed by taking cross products of the covariant basis vectors, as follows:

$$\bar{\mathbf{m}}^1 = \beta \bar{\mathbf{m}}_2 \times \bar{\mathbf{m}}_3 \quad \bar{\mathbf{m}}^2 = \beta \bar{\mathbf{m}}_3 \times \bar{\mathbf{m}}_1 \quad \bar{\mathbf{m}}^3 = \bar{\mathbf{m}}_1,$$

where $\beta = 1/\bar{\mathbf{m}}_1 \cdot (\bar{\mathbf{m}}_2 \times \bar{\mathbf{m}}_3) = 1/|\bar{\mathbf{m}}_1 \times \bar{\mathbf{m}}_2|$. The reciprocal basis is shown in Figure 10.18.

- The position vector of an arbitrary point in the undeformed shell can be expressed as $\mathbf{x} = \bar{\mathbf{r}}(\xi_1, \xi_2) + x_3 \bar{\mathbf{m}}_3$, where x_3 is the perpendicular distance of the material particle from the midsection of the shell.
- After deformation, the midsection of the shell is deformed to another smooth surface. The point that lies at $\mathbf{x} = \bar{\mathbf{r}}(\xi_1, \xi_2)$ on the midsection of the undeformed shell moves to a new position $\mathbf{y} = \mathbf{r}(\xi_1, \xi_2)$ after deformation.
- To characterize the orientation of the deformed shell, we introduce three basis vectors $(\mathbf{m}_1, \mathbf{m}_2, \mathbf{m}_3)$, with

$$\mathbf{m}_\alpha = \frac{\partial \mathbf{r}}{\partial \xi_\alpha} \quad \mathbf{m}_3 = \mathbf{m}_1 \times \mathbf{m}_2 / (|\mathbf{m}_1 \times \mathbf{m}_2|).$$

Now, \mathbf{m}_α are tangent to the coordinate lines ξ_α in the deformed shell, and \mathbf{m}_3 is a unit vector perpendicular to the midsection of the deformed shell. We can introduce a reciprocal basis $(\mathbf{m}^1, \mathbf{m}^2, \mathbf{m}^3)$ in exactly the same way as for the undeformed shell.

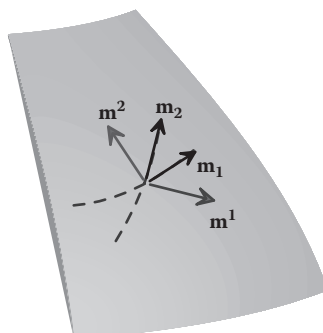


FIGURE 10.18 Natural (covariant) and reciprocal (contravariant) basis vectors.

- A few special vectors and tensors, such as the angular velocity of the shell, and the internal stress couple in the shell are most conveniently expressed in terms of vectors $\mathbf{m}_3 \times \mathbf{m}_\alpha$ or $\mathbf{m}_3 \times \mathbf{m}^\alpha$. Special symbols will not be introduced for these vectors; they will always be written out as a cross product.

10.5.2 Vectors and Tensor Components in Nonorthogonal Bases: Covariant and Contravariant Components

In this section, we introduce some additional notations that help deal with the complicated sets of basis vectors that characterize the deformation of a shell.

- Vectors can be expressed as linear combinations of some subset of the 12 possible basis vectors $(\bar{\mathbf{m}}_1, \bar{\mathbf{m}}_2, \bar{\mathbf{m}}_3)$, $(\bar{\mathbf{m}}^1, \bar{\mathbf{m}}^2, \bar{\mathbf{m}}^3)$, $(\mathbf{m}_1, \mathbf{m}_2, \mathbf{m}_3)$, or $(\mathbf{m}^1, \mathbf{m}^2, \mathbf{m}^3)$. For example, we can write an arbitrary vector \mathbf{a} as

$$\mathbf{a} = \bar{a}^i \bar{\mathbf{m}}_i = \bar{a}_i \bar{\mathbf{m}}^i = a^i \mathbf{m}_i = a_i \mathbf{m}^i.$$

- Here, the coefficients \bar{a}^i are called the *contravariant components* of \mathbf{a} in $(\bar{\mathbf{m}}_1, \bar{\mathbf{m}}_2, \bar{\mathbf{m}}_3)$, and \bar{a}_i are called the *covariant components* of \mathbf{a} . Note that the contravariant components are coefficients of the covariant basis vectors and vice versa. The reason for this confusing terminology is given below. Note also that the components do not in general have the same units as the vector, because the basis vectors may have length dimensions.
- The various components of \mathbf{a} can be expressed as

$$\bar{a}^i = \bar{\mathbf{m}}^i \cdot \mathbf{a} \quad \bar{a}_i = \bar{\mathbf{m}}_i \cdot \mathbf{a} \quad a^i = \mathbf{m}^i \cdot \mathbf{a} \quad a_i = \mathbf{m}_i \cdot \mathbf{a}.$$

To see the first result, take dot products of $\mathbf{a} = \bar{a}^i \bar{\mathbf{m}}_i$ with \mathbf{m}^j and recall that $\bar{\mathbf{m}}^i \cdot \bar{\mathbf{m}}_j = \delta_j^i$. The contravariant and covariant terms assigned to \bar{a}^i and \bar{a}_i refer to the fact that they represent projections of the vector \mathbf{a} onto the contravariant and covariant basis vectors, respectively. The raised and lowered indices for vector components follow the same convention: raised indices indicate contravariant components, whereas lowered indices represent covariant components.

- Tensors can also be expressed as sums of nine dyadic products of various combinations of basis vectors. For example, if \mathbf{S} is a tensor, we could write

$$\mathbf{S} = S^{ij} \mathbf{m}_i \otimes \mathbf{m}_j = S_{.j}^i \mathbf{m}_i \otimes \mathbf{m}^j = S_j^i \mathbf{m}^j \otimes \mathbf{m}_i = S_{ij} \mathbf{m}^i \otimes \mathbf{m}^j$$

or equivalent expressions in terms of $\bar{\mathbf{m}}_i$ and/or $\bar{\mathbf{m}}^j$. Here S^{ij} , S_{ij} are called contravariant and covariant components of \mathbf{S} , respectively, whereas S_j^i , $S_{.j}^i$ are called *mixed* tensor components. The dot that appears before the indices in the mixed tensors is introduced to identify whether the index should be associated with the first or second basis vector in the dyadic product (the dot appears before the index associated with the second basis vector). For symmetric tensors, the dot can be dropped.

- The various components of \mathbf{S} can be regarded as projections of the tensor onto the contravariant or covariant basis vectors, as $S_{ij} = \mathbf{m}_i \cdot \mathbf{S} \cdot \mathbf{m}_j$, $S^{ij} = \mathbf{m}^i \cdot \mathbf{S} \cdot \mathbf{m}^j$, with similar results for the mixed components.
- Once again, it is important to note that the components S_{ij} do not have a convenient physical interpretation. In general, the components do not even have the same units as the tensor itself, because the basis vectors themselves have units.
- The various sets of components can be related by defining the components of the *fundamental tensor* or *metric tensor* \mathbf{g} as follows:

$$g_{ij} = \mathbf{m}_i \cdot \mathbf{m}_j \quad g^{ij} = \mathbf{m}^i \cdot \mathbf{m}^j \quad g_j^i = \mathbf{m}^i \cdot \mathbf{m}_j = \delta_j^i.$$

We can define \bar{g}_{ij} in terms of $\bar{\mathbf{m}}_i$ and/or $\bar{\mathbf{m}}^j$ in the same way. With these definitions, we see that the covariant and contravariant basis vectors are related by

$$\mathbf{m}^i = g^{ij} \mathbf{m}_j \quad \mathbf{m}_i = g_{ij} \mathbf{m}^j.$$

- The metric tensor can be expressed as the sum of three dyadic products $\mathbf{g} = \mathbf{m}_i \otimes \mathbf{m}^i$, with a similar expression for $\bar{\mathbf{g}}$. From this expression, we see that

$$\mathbf{gg} = (\mathbf{m}_i \otimes \mathbf{m}^i)(\mathbf{m}_j \otimes \mathbf{m}^j) = \mathbf{m}_i \otimes \delta_i^j \mathbf{m}^j = \mathbf{m}_i \otimes \mathbf{m}^i = \mathbf{g}.$$

\mathbf{g} is therefore its own inverse. It is a representation of the identity tensor.

10.5.3 Additional Deformation Measures and Kinematic Relations

- An infinitesimal line element $d\bar{\mathbf{r}}$ that lies in the midsection of the undeformed plate can be expressed in terms of infinitesimal changes in the coordinates $d\xi_\alpha$ as

$$d\bar{\mathbf{r}} = \bar{\mathbf{m}}_\alpha d\xi_\alpha.$$

The length $d\bar{s}$ of $d\bar{\mathbf{r}}$ can be computed as

$$d\bar{s}^2 = d\bar{\mathbf{r}} \cdot d\bar{\mathbf{r}} = \bar{\mathbf{m}}_\alpha \cdot \bar{\mathbf{m}}_\beta d\xi_\alpha d\xi_\beta = \bar{g}_{\alpha\beta} d\xi_\alpha d\xi_\beta.$$

This expression is known as the *first fundamental form* for the surface. A similar expression can be constructed for the deformed surface.

- The variation of the normal vectors $\bar{\mathbf{m}}_3$ and \mathbf{m}_3 with position in the midplane of the shell play a particularly important role in describing the shape and deformation of the shell, because they characterize its curvature and bending. To quantify this variation, let $\bar{\mathbf{m}}_3$ and $\bar{\mathbf{m}}_3 + d\bar{\mathbf{m}}_3$ be the vectors normal to the surface at positions $\bar{\mathbf{r}}$ and $\bar{\mathbf{r}} + d\bar{\mathbf{r}}$ in the undeformed shell, with a similar notation for the deformed shell. We introduce symmetric curvature tensors $\bar{\mathbf{k}}$ and \mathbf{k} that satisfy

$$d\bar{\mathbf{m}}_3 = \bar{\mathbf{k}} \cdot d\bar{\mathbf{r}} \quad d\mathbf{m}_3 = \mathbf{k} \cdot d\mathbf{r}.$$

The curvatures $\bar{\mathbf{k}}$ and \mathbf{k} are called *surface tensors*, because they transform like tensors under changes of surface coordinates.

- The curvature components can be expressed in terms of their covariant, contravariant, or mixed components. This can be used to deduce expressions such as

$$d\bar{\mathbf{m}}_3 = (\bar{\kappa}_{\alpha\gamma} \bar{\mathbf{m}}^\alpha \otimes \bar{\mathbf{m}}^\gamma) \cdot (\bar{\mathbf{m}}_\beta d\xi_\beta) = \bar{\kappa}_{\alpha\beta} d\xi_\beta \bar{\mathbf{m}}^\alpha$$

$$d\bar{\mathbf{m}}_3 = (\bar{\kappa}_\gamma^\alpha \bar{\mathbf{m}}_\alpha \otimes \bar{\mathbf{m}}^\gamma) \cdot (\bar{\mathbf{m}}_\beta d\xi_\beta) = \bar{\kappa}_\beta^\alpha d\xi_\beta \bar{\mathbf{m}}_\alpha.$$

- The curvature components can be calculated from the position vector of the mid-plane of the shell, using any of the following expressions:

$$\begin{aligned} \bar{\kappa}_{\alpha\beta} &= \bar{\mathbf{m}}_\alpha \cdot \frac{\partial \bar{\mathbf{m}}_3}{\partial \xi_\beta} = \frac{\partial \bar{\mathbf{r}}}{\partial \xi_\alpha} \cdot \frac{\partial}{\partial \xi_\beta} \left(\frac{1}{\lambda} \frac{\partial \bar{\mathbf{r}}}{\partial \xi_1} \times \frac{\partial \bar{\mathbf{r}}}{\partial \xi_2} \right) = - \left(\frac{1}{\lambda} \frac{\partial \bar{\mathbf{r}}}{\partial \xi_1} \times \frac{\partial \bar{\mathbf{r}}}{\partial \xi_2} \right) \cdot \left(\frac{\partial^2 \bar{\mathbf{r}}}{\partial \xi_\alpha \partial \xi_\beta} \right) \\ &= -\bar{\mathbf{m}}_3 \cdot \frac{\partial \bar{\mathbf{m}}_\alpha}{\partial \xi_\beta} = -\bar{\mathbf{m}}_3 \cdot \frac{\partial \bar{\mathbf{m}}_\beta}{\partial \xi_\alpha} \end{aligned}$$

where $\lambda = |(\partial \bar{\mathbf{r}} / \partial \xi_1) \times (\partial \bar{\mathbf{r}} / \partial \xi_2)|$. The mixed components follow as $\kappa_\beta^\alpha = g^{\alpha\gamma} \kappa_{\gamma\beta}$, where $g^{\alpha\gamma}$ are the components of the metric tensor defined in Section 10.5.2.

- The magnitude of the curvature of a shell is quantified by *principal curvatures* $\bar{\kappa}_1, \bar{\kappa}_2$. These are simply the principal values of \mathbf{k} . The *mean curvature* $(\kappa_1 + \kappa_2)/2$ and *Gaussian curvature* $\kappa_1 \kappa_2$ are also used.
- We will also need to calculate the variation of the remaining basis vectors with position in the surface. These are quantified by *Christoffel symbols of the second kind* $\Gamma_{\alpha\beta}^i$, which satisfy

$$d\mathbf{m}_i = \Gamma_{i\alpha}^k \mathbf{m}_k d\xi_\alpha \quad d\mathbf{m}^i = -\Gamma_{k\alpha}^i \mathbf{m}^k d\xi_\alpha.$$

- The Christoffel symbols are functions of position on the surface and can be related to the position vector of the midplane of the shell and its curvature components as

$$\Gamma_{\beta\gamma}^\alpha = \mathbf{m}^\alpha \cdot \frac{\partial^2 \mathbf{r}}{\partial \xi_\beta \partial \xi_\gamma} \quad \Gamma_{\alpha\beta}^3 = -\kappa_{\alpha\beta} \quad \Gamma_{3\beta}^\alpha = \kappa_\beta^\alpha \quad \Gamma_{3\alpha}^3 = 0.$$

- Some relationships between the time derivatives of these various kinematic quantities are also needed in subsequent calculations. The rate of change in shape of the shell can be characterized by the velocity of its middle surface $\mathbf{v}(\xi_1, \xi_2) = d\mathbf{r}/dt$. The velocity vector can be described as components in any of the various bases: the representation $\mathbf{v} = v_i \mathbf{m}^i$ is particularly useful.

- The time derivatives of the basis vectors \mathbf{m}_α are a convenient way to characterize the rate of change of bending of the shell. These are related to the velocity of the shell's midplane by

$$\begin{aligned}\frac{d\mathbf{m}_\alpha}{dt} &= \frac{d}{dt} \left(\frac{d\mathbf{r}}{d\xi_\alpha} \right) = \frac{d\mathbf{v}}{d\xi_\alpha} = \frac{\partial v^i}{\partial \xi_\alpha} \mathbf{m}_i + v^i \frac{d\mathbf{m}_i}{d\xi_\alpha} = \frac{\partial v^i}{\partial \xi_\alpha} \mathbf{m}_i + v^i \Gamma_{i\alpha}^k \mathbf{m}_k \\ &= \frac{\partial v^\beta}{\partial \xi_\alpha} \mathbf{m}_\beta + v^\beta \Gamma_{\beta\alpha}^\lambda \mathbf{m}_\lambda + v^3 \kappa_{\beta\alpha}^\beta \mathbf{m}_\beta + \left(\frac{\partial v^3}{\partial \xi_\alpha} - v^\beta \kappa_{\beta\alpha} \right) \mathbf{m}_3 \\ \frac{d\mathbf{m}_\alpha}{dt} &= \frac{\partial v_i}{\partial \xi_\alpha} \mathbf{m}^i + v_i \frac{d\mathbf{m}^i}{d\xi_\alpha} = \frac{\partial v_i}{\partial \xi_\alpha} \mathbf{m}^i - v_i \Gamma_{k\alpha}^i \mathbf{m}^k \\ &= \frac{\partial v_\beta}{\partial \xi_\alpha} \mathbf{m}^\beta - v_\beta \Gamma_{\lambda\alpha}^\beta \mathbf{m}^\lambda + v_3 \kappa_{\beta\alpha} \mathbf{m}^\beta + \left(\frac{\partial v_3}{\partial \xi_\alpha} - v_\beta \kappa_\alpha^\beta \right) \mathbf{m}^3.\end{aligned}$$

- We will also need to calculate the time derivative of the vector normal to the mid-plane of the shell \mathbf{m}_3 . Because \mathbf{m}_3 is a unit vector, its time derivative can be quantified by an angular velocity vector $\boldsymbol{\omega}$, defined so that

$$\frac{d\mathbf{m}_3}{dt} = \boldsymbol{\omega} \times \mathbf{m}_3 \quad \boldsymbol{\omega} \cdot \mathbf{m}_3 = 0.$$

The components of $\boldsymbol{\omega}$ can be related to $d\mathbf{m}_\alpha/dt$ as

$$\begin{aligned}\mathbf{m}_3 \times (\boldsymbol{\omega} \times \mathbf{m}_3) &= \boldsymbol{\omega} = \mathbf{m}_3 \times \frac{d\mathbf{m}_3}{dt} = \mathbf{m}_3 \times \frac{(\dot{\mathbf{m}}_1 \times \mathbf{m}_2 + \mathbf{m}_1 \times \dot{\mathbf{m}}_2)}{|\mathbf{m}_1 \times \mathbf{m}_2|} \\ &= \frac{-(\mathbf{m}_3 \cdot \dot{\mathbf{m}}_1) \mathbf{m}_2 + (\mathbf{m}_3 \cdot \dot{\mathbf{m}}_2) \mathbf{m}_1}{|\mathbf{m}_1 \times \mathbf{m}_2|}.\end{aligned}$$

Recalling that $\mathbf{m}_2 \times \mathbf{m}_3/(|\mathbf{m}_1 \times \mathbf{m}_2|) = \mathbf{m}^1$ and $\mathbf{m}_3 \times \mathbf{m}_1/(|\mathbf{m}_1 \times \mathbf{m}_2|) = \mathbf{m}^2$, we see also that

$$\frac{d\mathbf{m}_3}{dt} = \boldsymbol{\omega} \times \mathbf{m}_3 = -(\mathbf{m}_3 \cdot \dot{\mathbf{m}}_1) \mathbf{m}^1 - (\mathbf{m}_3 \cdot \dot{\mathbf{m}}_2) \mathbf{m}^2 = -(\mathbf{m}_3 \cdot \dot{\mathbf{m}}_\alpha) \mathbf{m}^\alpha.$$

Finally we may write this as

$$\frac{d\mathbf{m}_3}{dt} = \dot{\mathbf{m}}_\alpha \mathbf{m}^\alpha \quad \dot{\mathbf{m}}_\alpha = -\mathbf{m}_3 \cdot \dot{\mathbf{m}}_\alpha = -\left(\frac{\partial v_3}{\partial \xi_\alpha} - v_\beta \kappa_\alpha^\beta \right).$$

The components $\dot{\mathbf{m}}_\alpha$ can also be regarded as the components of the angular velocity vector $\boldsymbol{\omega}$ in a basis $\{\mathbf{m}_3 \times \mathbf{m}^1, \mathbf{m}_3 \times \mathbf{m}^2\}$ in the sense that $\boldsymbol{\omega} = \dot{\mathbf{m}}_\alpha \mathbf{m}_3 \times \mathbf{m}^\alpha$.

- The time derivative of the curvature tensor $\dot{\mathbf{k}}$, is related to $\dot{\mathbf{m}}_3$ by $d\dot{\mathbf{m}}_3 = \dot{\mathbf{k}}_\beta^\alpha d\xi_\beta \mathbf{m}_\alpha$. Note that

$$d\dot{\mathbf{m}}_3 = \left(\frac{\partial \dot{\alpha}}{\partial \xi_\beta} \mathbf{m}^\alpha + \dot{\alpha} \frac{\partial \mathbf{m}^\alpha}{\partial \xi_\beta} \right) d\xi_\beta = \left(\frac{\partial \dot{\alpha}}{\partial \xi_\beta} \mathbf{m}^\alpha - \dot{\alpha} \Gamma_{\lambda\beta}^\alpha \mathbf{m}^\lambda \right) d\xi_\beta.$$

The components of the time derivative of curvature can therefore be expressed in terms of $\dot{\alpha}$ as

$$\dot{\kappa}_\beta^\alpha \mathbf{m}_\alpha = \dot{\kappa}_{\alpha\beta} \mathbf{m}^\alpha = \left(\frac{\partial \dot{\alpha}}{\partial \xi_\beta} \mathbf{m}^\alpha - \dot{\alpha} \Gamma_{\lambda\beta}^\lambda \mathbf{m}^\alpha \right).$$

It is important to note that $\dot{\kappa}_{\alpha\beta}$ are not equal to the time derivatives of the curvature components.

- We will also need to characterize the linear and angular acceleration of the shell. The linear acceleration can be quantified by the acceleration of the midplane $\mathbf{a} = d^2\mathbf{r}/dt^2$.
- The angular acceleration of the shell can be characterized by the angular acceleration of the normal to its midplane, $\boldsymbol{\alpha} = d\boldsymbol{\omega}/dt$. The angular acceleration can be related to the acceleration of the midplane of the shell as follows

$$\boldsymbol{\alpha} = \frac{d\boldsymbol{\omega}}{dt} = \mathbf{m}_3 \times \frac{d^2\mathbf{m}_3}{dt^2} = \left[2(\mathbf{m}_3 \cdot \dot{\mathbf{m}}_\alpha)(\mathbf{m}^\alpha \cdot \dot{\mathbf{m}}_\beta) - \mathbf{m}_3 \cdot \frac{d\mathbf{a}}{d\xi_\beta} \right] \mathbf{m}_3 \times \mathbf{m}^\beta,$$

where we have used $\dot{\mathbf{m}}_3 = -(\mathbf{m}_3 \cdot \dot{\mathbf{m}}_\alpha)\mathbf{m}^\alpha$ and noted that $\mathbf{m}^\alpha \cdot \mathbf{m}_\beta = \delta_\beta^\alpha \Rightarrow \dot{\mathbf{m}}^\alpha \cdot \mathbf{m}_\beta + \mathbf{m}^\alpha \cdot \dot{\mathbf{m}}_\beta = 0$ to obtain the final result.

- It is convenient to express $\boldsymbol{\alpha}$ in the form $\boldsymbol{\alpha} = \ddot{\boldsymbol{\alpha}} \mathbf{m}_3 \times \mathbf{m}^\beta = \ddot{\boldsymbol{\alpha}} \mathbf{m}_3 \times \mathbf{m}_\beta$, where $\ddot{\boldsymbol{\alpha}}_\beta = g^{\beta\alpha} \ddot{\boldsymbol{\alpha}}_\alpha$ and the $\ddot{\boldsymbol{\alpha}}^\beta$ can be related to the velocity and acceleration of the midplane of the shell as follows:

$$\begin{aligned} \ddot{\boldsymbol{\alpha}}_\beta &= 2(\mathbf{m}_3 \cdot \dot{\mathbf{m}}_\alpha)(\mathbf{m}^\alpha \cdot \dot{\mathbf{m}}_\beta) - \mathbf{m}_3 \cdot \frac{d\mathbf{a}}{d\xi_\beta} \\ &= 2 \left(\frac{\partial v_3}{\partial \xi_\alpha} - v^\lambda K_{\alpha\lambda} \right) \left(\frac{\partial v^\alpha}{\partial \xi_\beta} + v^\rho \Gamma_{\beta\rho}^\alpha + v_3 K_\beta^\alpha \right) - \left(\frac{\partial a_3}{\partial \xi_\beta} - a^\alpha K_{\alpha\beta} \right). \end{aligned}$$

- These results show that

$$\begin{aligned} \frac{d^2\mathbf{m}_3}{dt^2} &= \frac{d}{dt}(\boldsymbol{\omega} \times \mathbf{m}_3) = \boldsymbol{\alpha} \times \mathbf{m}_3 + \boldsymbol{\omega} \times (\boldsymbol{\omega} \times \mathbf{m}_3) \\ &= \ddot{\boldsymbol{\alpha}} \mathbf{m}_\beta - \dot{\alpha} \dot{\alpha}^\alpha \mathbf{m}_3, \end{aligned}$$

where we have used $\boldsymbol{\omega} \times (\boldsymbol{\omega} \times \mathbf{m}_3) = (\boldsymbol{\omega} \cdot \mathbf{m}_3) \boldsymbol{\omega} - (\boldsymbol{\omega} \cdot \boldsymbol{\omega}) \mathbf{m}_3$ and noted $(\boldsymbol{\omega} \cdot \mathbf{m}_3) = 0$ to obtain the second line.

HEALTH WARNING: The sign convention used to characterize the curvature of a shell can be confusing. In the convention used here, a convex surface has positive curvature. For

example, a spherical shell with coordinate system chosen so that \mathbf{m}_3 points radially out of the sphere would have two equal positive principal curvatures. The mathematical analysis of curved surfaces usually uses the opposite sign convention for curvature, and a few texts on shell theory use curvature measures with the opposite sign to the one used here.

10.5.4 Approximating the Displacement and Velocity Field

The position vector of a material point in the shell before deformation can be expressed as $\mathbf{x} = \bar{\mathbf{r}}(\xi_1, \xi_2) + x_3 \mathbf{m}_3$, where x_3 is the distance of the material particle from the midsection of the shell. After deformation, the material point that has coordinates (ξ_1, ξ_2, x_3) in the undeformed shell moves to a new position, which can be expressed as

$$\mathbf{y}(\xi_\alpha, x_3) = \mathbf{r}(\xi_\alpha) + \eta^i(\xi_\alpha, x_k) \mathbf{m}_i(\xi_\alpha),$$

where $\eta^i(\xi_\alpha, 0) = 0$. This is a completely general expression. We now introduce a series of approximations that are based on the following assumptions:

1. The shell is thin compared with its in-plane dimensions.
2. The principal radii of curvature of the shell (both before and after deformation) are much larger than the characteristic dimension of its cross section.

With this in mind, we assume that $\eta^i(\xi_\alpha, x_3)$ can be approximated by a function of the form

$$\eta^i(\xi_\alpha, x_3) = (\delta_3^i + f_3^i(\xi_\alpha)) x_3,$$

where f_3^i can be regarded as the first term in a Taylor expansion of η^i with respect to x_3 . Note that f_3^α represents transverse shear deformation of the shell, whereas f_3^3 quantifies the through-thickness stretching.

Several versions of plate theory exist that use different approximations for the shear deformation. Here, we will present only simplest approach, known as *Kirchhoff shell theory*, which is to assume that $f_3^i = 0$. This implies that material fibers that are perpendicular to the midplane of the shell remain perpendicular to the midplane of the deformed shell, and the shell does not change its thickness, as shown in Figure 10.19. This reduces the displacement field to $\mathbf{y}(\xi_\alpha, x_3) = \mathbf{r}(\xi_\alpha) + x_3 \mathbf{m}_3(\xi_\alpha)$. The velocity field can be approximated as

$$\frac{d}{dt} \mathbf{y}(\xi_\alpha, x_3) = \mathbf{v} + x_3 \dot{\mathbf{m}}_3,$$

whereas the acceleration is

$$\frac{d^2}{dt^2} \mathbf{y}(\xi_\alpha, x_3) = \mathbf{a} + x_3 \frac{d^2 \mathbf{m}_3}{dt^2} = \mathbf{a} + x_3 [\boldsymbol{\alpha} \times \mathbf{m}_3 + \boldsymbol{\omega} \times (\boldsymbol{\omega} \times \mathbf{m}_3)],$$

where $\boldsymbol{\alpha}$ and $\boldsymbol{\omega}$ denote the angular acceleration and angular velocity of the unit vector normal to the midplane of the plate.

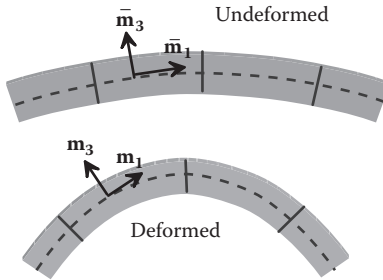


FIGURE 10.9 Deformation of the cross-section of a shell.

HEALTH WARNING: In addition to using this approximation to the displacement and velocity field, Kirchhoff shell theory assumes that the transverse stress σ^{33} vanishes in the shell. Strictly speaking, this is inconsistent with the deformation. A more rigorous approach would be to introduce a uniform transverse strain f_3^3 , which could be calculated as part of the solution. However, this approach yields results that are essentially indistinguishable from the plane-stress approximation.

10.5.5 Approximating the Deformation Gradient

The deformation gradient can be approximated as

$$\begin{aligned} \mathbf{F} &= (\bar{\mathbf{g}} + x_3 \bar{\mathbf{k}}) \cdot (\mathbf{m}_\alpha \otimes \bar{\mathbf{m}}^\alpha) \cdot (\bar{\mathbf{g}} + x_3 \bar{\mathbf{k}})^{-1} \\ &\approx \mathbf{m}_\alpha \otimes \bar{\mathbf{m}}^\alpha + x_3 (\bar{\kappa}_\beta^\alpha - \bar{\kappa}_\beta^\alpha) \mathbf{m}_\alpha \otimes \bar{\mathbf{m}}^\beta + \mathbf{m}_3 \otimes \bar{\mathbf{m}}^3, \end{aligned}$$

where $\bar{\mathbf{g}} = \bar{\mathbf{m}}_i \otimes \bar{\mathbf{m}}^i$ and $\mathbf{g} = \mathbf{m}_i \otimes \mathbf{m}^i$ are the metric tensors for shell before and after deformation, and $\bar{\mathbf{k}} = \bar{\kappa}_\beta^\alpha \bar{\mathbf{m}}_\alpha \otimes \bar{\mathbf{m}}^\beta$ and $\mathbf{k} = \kappa_\beta^\alpha \mathbf{m}_\alpha \otimes \mathbf{m}^\beta$ are the curvature tensors for the midsurface of the shell before and after deformation, respectively. The three terms in the second formula for \mathbf{F} can be interpreted as (1) the effects of in-plane stretching of the shell, (2) the effects of bending, and (3) the effects of a change in the shell's thickness.

Derivation: By definition, the deformation gradient relates infinitesimal line elements in the shell before ($d\mathbf{x}$) and after ($d\mathbf{y}$) deformation by $d\mathbf{y} = \mathbf{F} \cdot d\mathbf{x}$. We construct a tensor with these properties as follows:

1. An infinitesimal line element in the deformed shell can be expressed in terms of a small change in coordinates:

$$d\mathbf{y} = \frac{d\mathbf{r}}{d\xi_\alpha} d\xi_\alpha + x_3 \frac{d\mathbf{m}_3}{d\xi_\alpha} d\xi_\alpha + dx_3 \mathbf{m}_3 = \frac{d\mathbf{r}}{d\xi_\alpha} d\xi_\alpha + x_3 \bar{\kappa}_\beta^\alpha d\xi_\beta \mathbf{m}_\alpha + dx_3 \mathbf{m}_3,$$

where we have used $\frac{\partial \mathbf{m}_3}{\partial \xi_\beta} d\xi_\beta = \kappa_\beta^\alpha d\xi_\beta \mathbf{m}_\alpha$.

2. This expression can be rearranged into the form

$$\begin{aligned} d\mathbf{y} &= (\delta_{\beta}^{\alpha} \mathbf{m}_{\alpha} \otimes \mathbf{m}^{\beta} + \mathbf{m}_3 \otimes \mathbf{m}^3 + x_3 \kappa_{\beta}^{\alpha} \mathbf{m}_{\alpha} \otimes \mathbf{m}^{\beta}) \cdot (\mathbf{m}_{\gamma} d\xi_{\gamma} + \mathbf{m}_3 dx_3) \\ &= (\mathbf{g} + x_3 \bar{\mathbf{k}}) \cdot (\mathbf{m}_{\gamma} d\xi_{\gamma} + \mathbf{m}_3 dx_3). \end{aligned}$$

3. An infinitesimal line element $d\mathbf{x}$ in the undeformed shell can also be related to $d\xi_{\alpha}$, dx_3 as

$$d\mathbf{x} = \frac{d\bar{\mathbf{r}}}{d\xi_{\alpha}} d\xi_{\alpha} + x_3 \frac{\partial \bar{\mathbf{m}}_3}{\partial \xi_{\alpha}} d\xi_{\alpha} + dx_3 \bar{\mathbf{m}}_3.$$

This can be rewritten as

$$\begin{aligned} d\mathbf{x} &= (\delta_{\beta}^{\alpha} \bar{\mathbf{m}}_{\alpha} \otimes \bar{\mathbf{m}}^{\beta} + \bar{\mathbf{m}}_3 \otimes \bar{\mathbf{m}}^3 + x_3 \bar{\kappa}_{\beta}^{\alpha} \bar{\mathbf{m}}_{\alpha} \otimes \bar{\mathbf{m}}^{\beta}) \cdot (\bar{\mathbf{m}}_{\gamma} d\xi_{\gamma} + \bar{\mathbf{m}}_3 dx_3) \\ &= (\bar{\mathbf{g}} + x_3 \bar{\mathbf{k}}) \cdot (\bar{\mathbf{m}}_{\gamma} d\xi_{\gamma} + \bar{\mathbf{m}}_3 dx_3) \end{aligned}$$

so that $(\bar{\mathbf{m}}_{\gamma} d\xi_{\gamma} + \bar{\mathbf{m}}_3 dx_3) = (\bar{\mathbf{g}} + x_3 \bar{\mathbf{k}})^{-1} \cdot d\mathbf{x}$.

4. Finally, note that

$$(\mathbf{m}_{\beta} d\xi_{\beta} + \mathbf{m}_3 dx_3) = (\mathbf{m}_i \otimes \bar{\mathbf{m}}^i) \cdot (\bar{\mathbf{m}}_{\gamma} d\xi_{\gamma} + \bar{\mathbf{m}}_3 dx_3) = (\mathbf{m}_i \otimes \bar{\mathbf{m}}^i) \cdot (\bar{\mathbf{g}} + x_3 \bar{\mathbf{k}})^{-1} \cdot d\mathbf{x}.$$

We can substitute this result into step 2 above to see that

$$d\mathbf{y} = (\mathbf{g} + x_3 \mathbf{k}) \cdot (\mathbf{m}_i \otimes \bar{\mathbf{m}}^i) \cdot (\bar{\mathbf{g}} + x_3 \bar{\mathbf{k}})^{-1} \cdot d\mathbf{x},$$

and the deformation gradient can be read off as the coefficient of $d\mathbf{x}$.

5. The approximate expression for \mathbf{F} is obtained by assuming that, for a thin shell,

$$(\bar{\mathbf{g}} + x_3 \bar{\mathbf{k}})^{-1} \approx (\bar{\mathbf{g}} - x_3 \bar{\mathbf{k}}).$$

To see this, multiply out $(\bar{\mathbf{g}} + x_3 \bar{\mathbf{k}}) \cdot (\bar{\mathbf{g}} - x_3 \bar{\mathbf{k}})$, recall that $\bar{\mathbf{g}}\bar{\mathbf{g}} = \bar{\mathbf{g}}$, $\bar{\mathbf{g}}\bar{\mathbf{k}} = \bar{\mathbf{k}}\bar{\mathbf{g}} = \bar{\mathbf{k}}$, and neglect the term of order x_3^2 . Finally, substitute this approximation into the formula for \mathbf{F} , multiply out the terms, and neglect x_3^2 terms to obtain the approximation for \mathbf{F} .

10.5.6 Other Deformation Measures

It is straightforward to calculate any other deformation of interest from the deformation gradient. A few examples that will be used in calculations to follow are listed below.

The inverse of the deformation gradient can be approximated by

$$\begin{aligned} \mathbf{F}^{-1} &= (\bar{\mathbf{g}} + x_3 \bar{\mathbf{k}}) \cdot (\mathbf{m}_{\alpha} \otimes \bar{\mathbf{m}}^{\alpha})^{-1} \cdot (\mathbf{g} + x_3 \mathbf{k})^{-1} \\ &\approx \bar{\mathbf{m}}_{\alpha} \otimes \mathbf{m}^{\alpha} - x_3 (\kappa_{\alpha}^{\beta} - \bar{\kappa}_{\alpha}^{\beta}) \bar{\mathbf{m}}_{\alpha} \otimes \mathbf{m}^{\beta} + \bar{\mathbf{m}}_3 \otimes \mathbf{m}^3. \end{aligned}$$

The velocity gradient tensor \mathbf{L} , which relates the relative velocity $d\mathbf{\bar{y}}$ of two material particles at positions \mathbf{y} and $\mathbf{y} + d\mathbf{y}$ in the deformed shell as $d\mathbf{\bar{y}} = \mathbf{L}d\mathbf{y}$, can be approximated by

$$\begin{aligned}\mathbf{L} &= (\dot{\mathbf{m}}_i \otimes \mathbf{m}^i + x_3 \dot{\kappa}_{\alpha\beta} \mathbf{m}^\alpha \otimes \mathbf{m}^\beta) \cdot (\mathbf{m}_i \otimes \mathbf{m}^i + x_3 \kappa_{\beta}^{\alpha} \mathbf{m}_\alpha \otimes \mathbf{m}^\beta)^{-1} \\ &\approx (\dot{\mathbf{m}}_i \otimes \mathbf{m}^i + x_3 \dot{\kappa}_{\alpha\beta} \mathbf{m}^\alpha \otimes \mathbf{m}^\beta) \cdot (\mathbf{m}_i \otimes \mathbf{m}^i - x_3 \kappa_{\beta}^{\alpha} \mathbf{m}_\alpha \otimes \mathbf{m}^\beta),\end{aligned}$$

where $\dot{\kappa}_{\alpha\beta}$ are the covariant components of the time derivative of the surface curvature tensor.

The Lagrange strain tensor can be approximated by

$$\mathbf{E} = (\mathbf{F}^T \mathbf{F} - \mathbf{I}) / 2 \approx \frac{1}{2} (g_{\alpha\beta} - \bar{g}_{\alpha\beta}) \bar{\mathbf{m}}^\alpha \otimes \bar{\mathbf{m}}^\beta + x_3 (\kappa_{\beta}^{\alpha} - \bar{\kappa}_{\beta}^{\alpha}) g_{\lambda\alpha} \bar{\mathbf{m}}^\lambda \otimes \bar{\mathbf{m}}^\beta,$$

where terms of order x_3^2 have been neglected; we have used $g_{\alpha\beta} = \mathbf{m}_\alpha \cdot \mathbf{m}_\beta$ and $\mathbf{I} \equiv \bar{g}_{\alpha\beta} \bar{\mathbf{m}}^\alpha \otimes \bar{\mathbf{m}}^\beta$.

When we write constitutive equations relating forces to deformations, it is convenient to introduce two new strain measures defined as follows:

1. The “midplane Lagrange strain tensor”: $\boldsymbol{\gamma} = \gamma_{\alpha\beta} \bar{\mathbf{m}}^\alpha \otimes \bar{\mathbf{m}}^\beta = \frac{1}{2} (g_{\alpha\beta} - \bar{g}_{\alpha\beta}) \bar{\mathbf{m}}^\alpha \otimes \bar{\mathbf{m}}^\beta$,

where $g_{\alpha\beta} = \mathbf{m}_\alpha \cdot \mathbf{m}_\beta$ and $\bar{g}_{\alpha\beta} = \bar{\mathbf{m}}_\alpha \cdot \bar{\mathbf{m}}_\beta$. The tensor quantifies length changes of infinitesimal material elements in the midplane of the shell, in the sense that the lengths $d\bar{s}$ and ds of a line element before and after deformation are related by

$$d\xi_\alpha \bar{\mathbf{m}}_\alpha \cdot \boldsymbol{\gamma} \cdot \bar{\mathbf{m}}_\beta d\xi_\beta = (g_{\alpha\beta} d\xi_\alpha d\xi_\beta - \bar{g}_{\alpha\beta} d\xi_\alpha d\xi_\beta) / 2 = (ds^2 - d\bar{s}^2) / 2.$$

2. The “curvature change tensor”: $\Delta \boldsymbol{\kappa} = \Delta \kappa_{\lambda\beta} \bar{\mathbf{m}}^\lambda \otimes \bar{\mathbf{m}}^\beta = (\kappa_{\beta}^{\alpha} - \bar{\kappa}_{\beta}^{\alpha}) g_{\lambda\alpha} \bar{\mathbf{m}}^\lambda \otimes \bar{\mathbf{m}}^\beta$, which quantifies the additional stretch induced by bending and twisting the shell.

10.5.7 Representation of Forces and Moments in Shells

Figure 10.20 shows a generic cross section of the shell, in the deformed configuration. To define measures of internal and external forces acting on the shell, we define the following variables:

- A basis $\{\mathbf{m}_1, \mathbf{m}_2, \mathbf{m}_3\}$ with vectors chosen following the scheme described in Section 10.5.1. Vector and tensor quantities will be quantified by their contravariant components in this basis.
- The body force acting on the shell \mathbf{b} , or in component form $\mathbf{b} = b^i \mathbf{m}_i$.
- The tractions acting on the exterior surface of the shell $\mathbf{t} = t^i \mathbf{m}_i$. It is convenient to define separate variables to characterize the tractions acting on the various parts of the shell, as indicated in the sketch: the upper surface of the shell (denoted by S_+) is

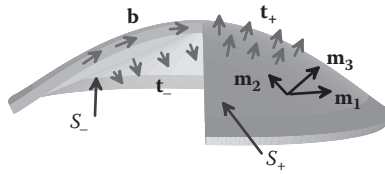


FIGURE 10.20 Shell subjected to external tractions and internal body forces.

subjected to traction t_+^i , the lower surface S_- is subjected to t_-^i , whereas the surface around the edge of the shell S_e is subjected to t_e^i .

- The Cauchy stress within the shell $\sigma = \sigma^{ij} \mathbf{m}_i \otimes \mathbf{m}_j$.

External forces and moments acting on the shell are characterized by the following:

1. The external force per unit area acting on the shell, $\mathbf{p} = p^i \mathbf{m}_i$. The force components can be calculated from the tractions and body force acting on the shell as

$$p^i(\xi_\alpha) = t_+^i(\xi_\alpha) + t_-^i(\xi_\alpha) + h\kappa_\alpha^\alpha (t_+^i(\xi_\alpha) - t_-^i(\xi_\alpha)) / 2 + \int_{-h/2}^{h/2} b^i(\xi_\alpha, x_3) (1 + x_3 \kappa_\alpha^\alpha) dx_3.$$

2. The external moment per unit area \mathbf{q} acting on the shell. It is most convenient to express the external moment as $\mathbf{q} = q^\alpha \mathbf{m}_3 \times \mathbf{m}_\alpha$, where the components q^α can be calculated from the tractions and body force as

$$q^\alpha(\xi_\beta) = [t_+^\alpha(\xi_\beta) - t_-^\alpha(\xi_\beta)] h / 2 + \int_{-h/2}^{h/2} x_3 b^\alpha(\xi_\beta, x_3) dx_3.$$

The vector \mathbf{q} is work conjugate to the angular velocity $\boldsymbol{\omega} = \dot{\alpha} \mathbf{m}_3 \times \mathbf{m}^\alpha$ of the normal to the midplane of the shell, in the sense that $\mathbf{q} \cdot \boldsymbol{\omega} = q^\alpha (\mathbf{m}_3 \times \mathbf{m}_\alpha) \cdot \dot{\alpha} (\mathbf{m}_3 \times \mathbf{m}^\beta) = q^\alpha \dot{\alpha}$ is the rate of work done by the external couple per unit area of the shell's midplane.

3. The resultant force per unit length acting on the external edge of the shell. The force per unit length can be expressed as components as $\mathbf{P} = P^i \mathbf{m}_i$. The components are related to the tractions acting on the external surface at the edge of the shell by

$$P^i = \int_{-h/2}^{h/2} t^i (1 + x_3 \tau^\alpha \tau^\beta \kappa_{\alpha\beta}) dx_3.$$

4. The resultant moment per unit length acting on the external edge of the shell. The moment per unit length can be expressed as components as $\mathbf{Q} = Q^\alpha \mathbf{m}_3 \times \mathbf{m}_\alpha$. The components are related to the tractions acting on external surface at the edge of the shell

$$Q^\alpha = \int_{-h/2}^{h/2} t^\alpha x_3 (1 + x_3 \tau^\alpha \tau^\beta \kappa_{\alpha\beta}) dx_3,$$

where τ^α are the components of a unit vector tangent to the edge of the shell (see Section 10.5.8).

Internal forces and moments within the shell are characterized by three surface tensors \mathbf{T} , \mathbf{V} , and \mathbf{M} . To visualize their physical significance, suppose that the shell is cut through so as to expose an internal surface, which lies perpendicular to the midplane of the shell, as shown in Figure 10.21. Let $\mathbf{n} = n^\alpha \mathbf{m}_\alpha$ denote a unit vector normal to the internal surface and let ds denote an infinitesimal line element that lies in both the exposed surface and the midplane of the shell. The exposed surface is subjected to a distribution of traction, so that a small element of area with dimensions $ds \times h$ is subjected to a resultant force $d\mathbf{f} = df^\beta \mathbf{m}_\beta$ and resultant moment $d\boldsymbol{\eta} = d\eta^\alpha \mathbf{m}_\alpha$. These forces and moments are related to \mathbf{T} , \mathbf{V} , and \mathbf{M} as outlined below:

1. The in-plane stress resultant tensor $\mathbf{T} = T^{\alpha\beta} \mathbf{m}_\alpha \otimes \mathbf{m}_\beta$ quantifies internal forces that tend to stretch and shear the shell in its own plane. It is related to the internal tractions by $df^\alpha \mathbf{m}_\alpha = ds\mathbf{n} \cdot \mathbf{T}$, and its components can be calculated from the stress distribution in the shell as

$$T^{\alpha\beta} = \int_{-h/2}^{h/2} (\sigma^{\alpha\beta} - x_3 \sigma^{\gamma\alpha} \kappa_\gamma^\beta) (1 + x_3 \kappa_\lambda^\lambda) dx_3.$$

2. The transverse shearing stress tensor $\mathbf{V} = V^\beta \mathbf{m}_\beta \otimes \mathbf{m}_3$ quantifies internal forces that act to impose the constraint that material fibers that are perpendicular to the midplane of the shell before deformation remain perpendicular to the midplane after deformation. Strictly speaking, in Kirchhoff shell theory, it is a Lagrange multiplier but can be regarded as quantifying the transverse shear force $df^3 \mathbf{m}_3 = ds\mathbf{n} \cdot \mathbf{V}$. Its value cannot be computed from the deformation of the shell, because the transverse shearing has been neglected; instead, it must be determined by solving the equilibrium equations given in the next section.
3. The internal moment tensor $\mathbf{M} = M^{\alpha\beta} \mathbf{m}_\alpha \otimes (\mathbf{m}_3 \times \mathbf{m}_\beta)$ characterizes internal bending and twisting moments in the shell. It is related to the moment acting on internal through-thickness sections of the shell by $d\boldsymbol{\eta} = \eta^\alpha \mathbf{m}_\alpha = ds\mathbf{n} \cdot \mathbf{M}$. The components $M^{\alpha\beta}$ can be calculated from the internal stresses in the shell as

$$M^{\alpha\beta} = \int_{-h/2}^{h/2} x_3 (\sigma^{\alpha\beta} - x_3 \sigma^{\gamma\alpha} \kappa_\gamma^\beta) (1 + x_3 \kappa_\lambda^\lambda) dx_3.$$

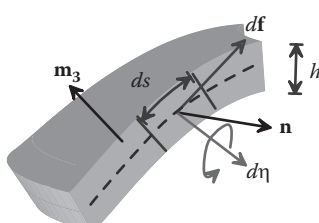


FIGURE 10.21 Internal forces and moments acting on a cross-sectional element within a shell.

The tensor \mathbf{M} is work conjugate to the gradient of the angular velocity of the normal to the midplane of the shell $\boldsymbol{\omega} = \dot{\boldsymbol{\alpha}} \mathbf{m}_3 \times \mathbf{m}^\alpha$ or, alternatively, to the rate of change of curvature in the sense that

$$\begin{aligned}\mathbf{M} : \left(\mathbf{m}^\alpha \otimes \frac{\partial \boldsymbol{\omega}}{\partial \xi_\alpha} \right) &= \left\{ M^{\alpha\beta} \mathbf{m}_\alpha \otimes (\mathbf{m}_3 \times \mathbf{m}_\beta) \right\} : \left\{ \mathbf{m}^\gamma \otimes \frac{\partial}{\partial \xi_\gamma} \left\{ \cdot_\lambda (\mathbf{m}_3 \times \mathbf{m}^\lambda) \right\} \right\} \\ &= M^{\alpha\beta} \left(\frac{\partial \cdot_\beta}{\partial \xi_\alpha} - \cdot_\lambda \Gamma_{\alpha\beta}^\lambda \right) = M^{\alpha\beta} \dot{K}_{\alpha\beta}\end{aligned}$$

is the rate of work done by \mathbf{M} per unit area of the midplane of the shell.

10.5.8 Equations of Motion and Boundary Conditions

We consider a shell with thickness h and mass density ρ . The internal forces and moments must satisfy

$$\mathbf{m}^\alpha \cdot \frac{\partial}{\partial \xi_\alpha} (\mathbf{V} + \mathbf{T}) + \mathbf{p} = \rho h \mathbf{a} \quad \mathbf{m}^\alpha \cdot \frac{\partial \mathbf{M}}{\partial \xi_\alpha} + \mathbf{m}_\alpha \times [\mathbf{m}^\alpha \cdot (\mathbf{V} - \mathbf{T})] + \mathbf{q} = \frac{\rho h^3}{12} \boldsymbol{\alpha} \times \mathbf{m}_3.$$

The operator $\mathbf{m}^\alpha \cdot (\partial / \partial \xi_\alpha)$ represents the surface divergence, \mathbf{T} , \mathbf{V} , and \mathbf{M} are the internal forces defined in Section 10.5.7, \mathbf{p} and \mathbf{q} are the external force and couple per unit area acting on the shell, \mathbf{a} is the acceleration of the midplane, and $\boldsymbol{\alpha}$ is the angular acceleration of the unit vector normal to the midplane of the shell. The two equations can be interpreted as linear and angular momentum balance for an infinitesimal element of the shell. Note the following:

1. If the system is in static equilibrium, the right-hand sides of all the equations of motion are zero.
2. In addition, in many dynamic problems, the right-hand sides of the angular momentum balance equations may be taken to be approximately zero. For example, the rotational inertia may be ignored when modeling the vibration of a shell. The rotational inertia terms can be important if the shell is rotating rapidly: for example, they would influence the out-of-plane vibration of a spinning disk.

The equations of motion can also be expressed in terms of components of the various force and moment tensors by substituting $\mathbf{T} = T^{\alpha\beta} \mathbf{m}_\alpha \otimes \mathbf{m}_\beta$, $\mathbf{V} = V^\beta \mathbf{m}_\beta \otimes \mathbf{m}_3$, $\mathbf{M} = M^{\alpha\beta} \mathbf{m}_\alpha \otimes (\mathbf{m}_3 \times \mathbf{m}_\beta)$, $\mathbf{p} = p^i \mathbf{m}_i$, $\mathbf{q} = q^\alpha \mathbf{m}_3 \times \mathbf{m}_\alpha$, $\mathbf{a} = a^i \mathbf{m}_i$, and $\boldsymbol{\alpha} = \alpha^\beta \mathbf{m}_3 \times \mathbf{m}_\beta + \dot{\alpha}^\beta \mathbf{m}_3$ and recalling that

$$\frac{\partial \mathbf{m}_\alpha}{\partial \xi_\gamma} = \Gamma_{\alpha\gamma}^\lambda \mathbf{m}_\lambda - \kappa_{\alpha\gamma} \mathbf{m}_3 \quad \frac{\partial \mathbf{m}_3}{\partial \xi_\gamma} = \kappa_\gamma^\lambda \mathbf{m}_\lambda.$$

The result is

$$\frac{\partial T^{\alpha\beta}}{\partial \xi_\alpha} + T^{\alpha\beta}\Gamma_{\alpha\gamma}^\gamma + T^{\alpha\gamma}\Gamma_{\gamma\alpha}^\beta + V^\alpha\kappa_\alpha^\beta + p^\beta = \rho ha^\beta$$

$$\frac{\partial V^\alpha}{\partial \xi_\alpha} + V^\alpha\Gamma_{\alpha\beta}^\beta - T^{\alpha\beta}\kappa_{\alpha\beta} + p^3 = \rho ha^3$$

$$\frac{\partial M^{\alpha\beta}}{\partial \xi_\alpha} + M^{\alpha\beta}\Gamma_{\alpha\gamma}^\gamma + M^{\alpha\gamma}\Gamma_{\gamma\alpha}^\beta - V^\beta + q^\beta = \frac{\rho h^3}{12} \cdot \cdot \beta$$

$$T^{12} - T^{21} + M^{\alpha 1}\kappa_\alpha^2 - M^{\alpha 2}\kappa_\alpha^1 = 0.$$

The last equation shows that the stress resultant and moment tensors are not symmetric. The asymmetry is small and is ignored in simplified versions of shell theory. However, there are a few special shell geometries (a cylindrical shell subjected to torsional loading is one example) in which neglecting the asymmetry can lead to substantial errors.

Edge boundary conditions for a shell are complicated and confusing. To understand them, it is helpful to visualize the possible types of motion that can occur at the edge of a shell. The edge of the shell is characterized by a curve C that lies in the midplane of the shell, encircling \mathbf{m}_3 in a counterclockwise sense. We let s denote arc length measured around C from some convenient origin and use $\boldsymbol{\tau} = \tau^\alpha \mathbf{m}_\alpha$ and $\mathbf{n} = \mathbf{m}_3 \times \boldsymbol{\tau}$ to denote unit vectors tangent and normal to C , as shown in Figure 10.22. Elements of the shell that lie on C have four independent degrees of freedom, as follows:

1. The material element can have an arbitrary velocity, with three components $\delta\mathbf{v} = \delta v_i \mathbf{m}^i$.
2. The material element can rotate about the tangent vector $\boldsymbol{\tau}$. To visualize this motion, imagine that the shell is supported around C by a hinge.

The motion of the edge of the shell can be prescribed by constraining one or more of these degrees of freedom. Alternatively, the edge of the shell can be subjected to one or more of *four generalized forces*, which are work conjugate to these degrees of freedom. The generalized

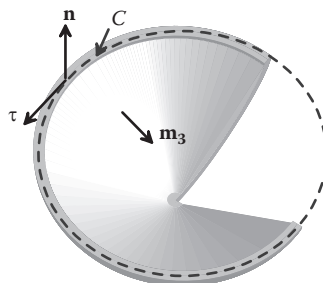


FIGURE 10.22 Contour defining the boundary of a shell.

forces can be expressed in terms of the forces $\mathbf{P} = P^i \mathbf{m}_i$ and couples $\mathbf{Q} = Q^\alpha \mathbf{m}_3 \times \mathbf{m}_\alpha$ acting on the edge of the shell as follows:

1. $P^\beta + Q^\lambda \kappa_\lambda^\beta$ is work conjugate to the in-plane displacement of the shell δv_β .
2. $P^3 - \frac{\partial}{\partial s} [Q^\beta \tau_\beta]$ is work conjugate to the out-of-plane displacement of the edge of the shell δv_3 .
3. $Q^\beta n_\beta$ is work conjugate to the rotation of the shell about its edge.

The four boundary conditions can be expressed in terms of these forces as follows:

$$\begin{aligned} n_\alpha T^{\alpha\beta} + n_\alpha M^{\alpha\lambda} \kappa_\lambda^\beta &= P^\beta + Q^\lambda \kappa_\lambda^\beta \\ n_\alpha V^\alpha + \frac{\partial}{\partial s} [n_\alpha M^{\alpha\beta} \tau_\beta] &= P^3 + \frac{\partial}{\partial s} [Q^\beta \tau_\beta] \\ n_\alpha M^{\alpha\beta} n_\beta &= Q^\beta n_\beta. \end{aligned}$$

Derivation: Measures of internal force, the equilibrium equations, and the boundary conditions emerge naturally from the principle of virtual work. The principle of virtual work states that, for any deformable solid that is in static equilibrium, the Cauchy stress distribution must satisfy

$$\int_V \boldsymbol{\sigma} : \delta \mathbf{L} dV + \int_V \rho \mathbf{a} \cdot \delta \dot{\mathbf{y}} dV - \int_V \mathbf{b} \cdot \delta \dot{\mathbf{y}} dV - \int_S \mathbf{t} \cdot \delta \dot{\mathbf{y}} dA = 0$$

for all virtual velocity fields $\delta \dot{\mathbf{y}}$ and compatible velocity gradients $\delta \mathbf{L}$. The virtual velocity field in the shell must have the same general form as the actual velocity, as outlined in Section 10.2.4. The virtual velocity can therefore be characterized by the virtual velocity of the midplane of the shell $\delta \mathbf{v} = \delta v_i \mathbf{m}^i$. It is convenient to introduce the time derivative of the normal vector to the plate's midplane $\delta \dot{\mathbf{m}}_3 = \delta \dot{\gamma}_\alpha \mathbf{m}^\alpha$ as an additional kinematic variable, which must of course be compatible with $\delta \mathbf{v}$. We will show the following:

- The virtual work principle can be expressed in terms of the generalized deformation measures and forces defined in the preceding sections as

$$\begin{aligned} & \int_A T^{\alpha\beta} \left\{ \frac{\partial \delta v_\beta}{\partial \xi_\alpha} - \delta v_\lambda \Gamma_{\beta\alpha}^\lambda + \delta v_3 \kappa_{\beta\alpha} \right\} dA + \int_A M^{\alpha\beta} \left(\frac{\partial \delta \dot{\gamma}_\alpha}{\partial \xi_\beta} - \delta \dot{\gamma}_\lambda \Gamma_{\alpha\beta}^\lambda \right) dA \\ & + \int_A h \rho a^i \delta v_i dA + \int_A \frac{\rho h^3}{12} \delta \dot{\gamma}_\alpha \delta \dot{\gamma}_\alpha dA - \int_A p^i \delta v_i dA - \int_A q^\alpha \delta \dot{\gamma}_\alpha dA - \int_C P^i \delta v_i ds - \int_C Q^\alpha \delta \dot{\gamma}_\alpha ds = 0. \end{aligned}$$

- If the virtual work equation is satisfied for all δv_i and compatible δ^i_α , then the internal forces and moments must satisfy the following equilibrium equations,

$$\frac{\partial T^{\alpha\beta}}{\partial \xi_\alpha} + T^{\alpha\beta}\Gamma_{\alpha\gamma}^\gamma + T^{\alpha\gamma}\Gamma_{\gamma\beta}^\beta + V^\alpha K_\alpha^\beta + p^\beta = \rho h a^\beta$$

$$\frac{\partial V^\alpha}{\partial \xi_\alpha} + V^\alpha \Gamma_{\alpha\beta}^\beta - T^{\alpha\beta} K_{\alpha\beta} + p^3 = \rho h a^3$$

$$\frac{\partial M^{\alpha\beta}}{\partial \xi_\alpha} + M^{\alpha\beta} \Gamma_{\alpha\gamma}^\gamma + M^{\alpha\gamma} \Gamma_{\gamma\beta}^\beta - V^\beta + q^\beta = \frac{\rho h^3}{12} \cdot \cdot \beta,$$

as well as the boundary conditions listed above.

- The last equilibrium equation $T^{12} - T^{21} + M^{\alpha 1} K_\alpha^2 - M^{\alpha 2} K_\alpha^1 = 0$ does not emerge from the virtual work principle. Instead, this equation is a consequence of the symmetry of the Cauchy stress tensor $\sigma^{\alpha\beta}$, as shown below. It is automatically satisfied if the components $T^{\alpha\beta}$ and $M^{\alpha\beta}$ are calculated by integrating the stresses through the thickness of the shell. However, for some statically determinate shell problems, it is possible to avoid evaluating these integrals explicitly, in which case the equilibrium equation is useful.

Expressing the virtual work equation in terms of generalized force measures is a straightforward but lengthy algebraic exercise:

1. When applying the virtual work principle, we will need to integrate over the volume of the shell. It is convenient to write the volume integral as separate integrals over the midplane of the shell and through its thickness, as follows:

$$\int_V dV = \int_A \int_{-h/2}^{h/2} \left(\frac{\partial \mathbf{y}}{\partial \xi_1} \times \frac{\partial \mathbf{y}}{\partial \xi_2} \right) \cdot \frac{\partial \mathbf{y}}{\partial x_3} dx_3 d\xi_1 d\xi_2.$$

Recall that $\mathbf{y} = \mathbf{r} + x_3 \mathbf{m}_3$, so that

$$\frac{\partial \mathbf{y}}{\partial \xi_\alpha} = \mathbf{m}_\alpha + x_3 K_\alpha^\beta \mathbf{m}_\beta.$$

Therefore, $\left(\frac{\partial \mathbf{y}}{\partial \xi_1} \times \frac{\partial \mathbf{y}}{\partial \xi_2} \right) \cdot \frac{\partial \mathbf{y}}{\partial x_3} \approx (1 + x_3 K_\alpha^\alpha) (\mathbf{m}_1 \times \mathbf{m}_2) \cdot \mathbf{m}_3$, where the term of order x_3^2 has been neglected. Substituting this result into the volume integral yields

$$\int_V dV \approx \int_A \int_{-h/2}^{h/2} (1 + x_3 K_\alpha^\alpha) (\mathbf{m}_1 \times \mathbf{m}_2) \cdot \mathbf{m}_3 d\xi_1 d\xi_2 dx_3 \equiv \int_A \int_{-h/2}^{h/2} (1 + x_3 K_\alpha^\alpha) dx_3 dA,$$

where the area integral is understood to be taken over the midplane of the shell.

2. Similarly, the integrals over the outer surface of the shell can be separated into integrals taken over the upper and lower surfaces of the shell (S_+ and S_-), together with an integral over the surface at the edge of the shell S_e , as follows

$$\int_S dA = \int_{S_+} dA + \int_{S_-} dA + \int_{S_e} dA.$$

Following the procedure in step 1, the integrals over S_+ and S_- can be expressed in terms of integrals taken over the midplane of the shell as

$$\int_{S_+} dA = \int_A (1 + h\kappa_\alpha^\alpha / 2) dA \quad \int_{S_-} dA = \int_A (1 - h\kappa_\alpha^\alpha / 2) dA.$$

The integral over S_e can be reduced to a line integral taken around the curve(s) bounding the edge of the shell, as

$$\int_{S_e} dA = \int_C \int_{-h/2}^{h/2} (1 + x_3 \tau^\alpha \tau^\beta \kappa_{\alpha\beta}) dx_3 ds.$$

The procedure to derive this result is very similar to the steps required to simplify the volume integral and is left as an exercise.

3. Next, consider the integrand

$$\begin{aligned} \boldsymbol{\sigma} : \delta \mathbf{L} &\approx \boldsymbol{\sigma} : \left[(\delta \dot{\mathbf{m}}_i \otimes \mathbf{m}^i + x_3 \delta \dot{\kappa}_{\alpha\beta} \mathbf{m}^\alpha \otimes \mathbf{m}^\beta) \cdot (\mathbf{m}_i \otimes \mathbf{m}^i - x_3 \kappa_\beta^\alpha \mathbf{m}_\alpha \otimes \mathbf{m}^\beta) \right] \\ &= \left[\boldsymbol{\sigma} (\mathbf{m}_i \otimes \mathbf{m}^i - x_3 \kappa_\beta^\alpha \mathbf{m}_\alpha \otimes \mathbf{m}^\beta)^T \right] : (\delta \dot{\mathbf{m}}_i \otimes \mathbf{m}^i + x_3 \delta \dot{\kappa}_{\alpha\beta} \mathbf{m}^\alpha \otimes \mathbf{m}^\beta). \end{aligned}$$

To reduce this to a scalar combination of the components of the various tensors and vectors, substitute $\boldsymbol{\sigma} = \sigma^{ij} \mathbf{m}_i \otimes \mathbf{m}_j$, together with the kinematic formulas:

$$\begin{aligned} \delta \dot{\mathbf{m}}_\alpha &= \frac{\partial \delta v_\beta}{\partial \xi_\alpha} \mathbf{m}^\beta - dv_\beta \Gamma_{\lambda\alpha}^\beta \mathbf{m}^\lambda + \delta v_3 \kappa_{\beta\alpha} \mathbf{m}^\beta + \left(\frac{\partial \delta v_3}{\partial \xi_\alpha} - \delta v_\beta \kappa_\alpha^\beta \right) \mathbf{m}^3 \\ \delta \dot{\mathbf{m}}_3 &= - \left(\frac{\partial \delta v_3}{\partial \xi_\alpha} - v_\beta \kappa_\alpha^\beta \right) \mathbf{m}^\alpha \quad \delta \dot{\kappa}_{\alpha\beta} \mathbf{m}^\alpha = \left(\frac{\partial \delta v_\beta}{\partial \xi_\alpha} \mathbf{m}^\alpha - \delta v_\lambda \Gamma_{\alpha\beta}^\lambda \mathbf{m}^\alpha \right), \end{aligned}$$

with the result

$$\begin{aligned} \boldsymbol{\sigma} : \delta \mathbf{L} &\approx \left(\sigma^{\alpha\beta} - x_3 \sigma^{\alpha\gamma} \kappa_\gamma^\beta \right) \left\{ \frac{\partial \delta v_\beta}{\partial \xi_\alpha} - \delta v_\lambda \Gamma_{\beta\alpha}^\lambda + \delta v_3 \kappa_{\beta\alpha} \right\} \\ &\quad + x_3 \left(\sigma^{\alpha\beta} - x_3 \sigma^{\alpha\gamma} \kappa_\gamma^\beta \right) \left(\frac{\partial \delta v_\beta}{\partial \xi_\beta} - \delta v_\lambda \Gamma_{\alpha\beta}^\lambda \right). \end{aligned}$$

4. Substituting this result into the first integral of the virtual work principle, reducing the volume integral to an integral over the midplane of the shell, and using the definitions of $T^{\alpha\beta}$ and $M^{\alpha\beta}$ gives

$$\int_V \boldsymbol{\sigma} \cdot \delta \mathbf{L} dV = \int_A T^{\alpha\beta} \left\{ \frac{\partial \delta v_\beta}{\partial \xi_\alpha} - \delta v_\lambda \Gamma_{\beta\alpha}^\lambda + \delta v_3 \kappa_{\beta\alpha} \right\} dA + \int_A M^{\alpha\beta} \left(\frac{\partial \dot{v}_\alpha}{\partial \xi_\beta} - \dot{v}_\lambda \Gamma_{\alpha\beta}^\lambda \right) dA.$$

5. Similar manipulations can be used to reduce the remaining terms in the virtual work principle to

$$\begin{aligned} \int_V \rho \mathbf{a} \cdot \delta \ddot{\mathbf{y}} dV &= \int_A h \rho a^i \delta v_i dA + \int_A \frac{\rho h^3}{12} \ddot{v}^\alpha \delta \dot{v}_\alpha dA \\ \int_V \mathbf{b} \cdot \delta \ddot{\mathbf{y}} dV + \int_S \mathbf{t} \cdot \delta \ddot{\mathbf{y}} dA &= \int_A p^i \delta v_i dA + \int_A q^\alpha \delta \dot{v}_\alpha dA + \int_C P^i \delta v_i ds + \int_C Q^\alpha \delta \dot{v}_\alpha ds. \end{aligned}$$

Substituting the equations in steps 4 and 5 into the virtual work equation gives the first result.

Next, we show that the equilibrium equations and boundary conditions follow from the virtual work principle:

1. The virtual work equation must first be augmented by a Lagrange multiplier to enforce compatibility between the velocity field $\delta \mathbf{v} = \delta v_i \mathbf{m}^i$ and the time derivative of the vector normal to the shell's midplane $\delta \dot{\mathbf{m}}_3 = \dot{v}_\alpha \mathbf{m}^\alpha$. To this end, we regard the unit vector \mathbf{m}_3 as an independent degree of freedom and introduce a vector-valued Lagrange multiplier $V^\alpha \mathbf{m}_\alpha$ that must satisfy

$$\int_A \left(\mathbf{m}_3 - \frac{\mathbf{m}_1 \times \mathbf{m}_2}{|\mathbf{m}_1 \times \mathbf{m}_2|} \right) \cdot \delta V^\alpha \mathbf{m}_\alpha dA + \int_A \left\{ \delta \dot{v}_\alpha \mathbf{m}^\alpha + \left(\frac{\partial \delta v_3}{\partial \xi_\alpha} - \delta v_\beta \kappa_\alpha^\beta \right) \mathbf{m}^\alpha \right\} \cdot V^\gamma \mathbf{m}_\gamma dA = 0$$

for all admissible variations $\delta \dot{V}^\alpha \mathbf{m}_\alpha$, $\delta \mathbf{v} = \delta v_i \mathbf{m}^i$, and $\delta \dot{\mathbf{m}}_3 = \dot{v}_\alpha \mathbf{m}^\alpha$. The second integral can simply be added to the virtual work equation to ensure compatibility of $\delta \dot{\mathbf{m}}_3 = \dot{v}_\alpha \mathbf{m}^\alpha$ and $\delta \mathbf{v} = \delta v_i \mathbf{m}^i$.

2. The augmented virtual work equation now reads

$$\begin{aligned} \int_A T^{\alpha\beta} \left\{ \frac{\partial \delta v_\beta}{\partial \xi_\alpha} - \delta v_\lambda \Gamma_{\beta\alpha}^\lambda + \delta v_3 \kappa_{\beta\alpha} \right\} dA + \int_A M^{\alpha\beta} \left(\frac{\partial \dot{v}_\alpha}{\partial \xi_\beta} - \dot{v}_\lambda \Gamma_{\alpha\beta}^\lambda \right) dA + \int_A h \rho a^i \delta v_i dA \\ + \int_A \frac{\rho h^3}{12} \ddot{v}^\alpha \delta \dot{v}_\alpha dA + \int_A \left\{ \delta \dot{v}_\alpha + \left(\frac{\partial \delta v_3}{\partial \xi_\alpha} - \delta v_\beta \kappa_\alpha^\beta \right) \right\} V^\alpha dA \\ - \int_A p^i \delta v_i dA - \int_A q^\alpha \delta \dot{v}_\alpha dA - \int_C P^i \delta v_i ds - \int_C Q^\alpha \delta \dot{v}_\alpha ds = 0. \end{aligned}$$

3. The remaining steps are routine but fiddly. The partial derivatives of δv_α and $\delta \cdot_\alpha$ must be removed by integrating by parts. This is accomplished by applying the surface divergence theorem, which states that, if \mathbf{w} is a differentiable vector field on an area A of the surface and C is the curve bounding A , then

$$\int_A \mathbf{m}^\alpha \cdot \frac{\partial \mathbf{w}}{\partial \xi^\alpha} dA = \int_C \mathbf{n} \cdot \mathbf{w} ds,$$

where \mathbf{n} is the outward normal to C . To see how to use this theorem, consider

$$\int_A T^{\alpha\beta} \left\{ \frac{\partial \delta v_\beta}{\partial \xi^\alpha} - \delta v_\lambda \Gamma_{\beta\alpha}^\lambda \right\} dA \equiv \int_A (T^{\alpha\beta} \mathbf{m}_\alpha \otimes \mathbf{m}_\beta) : \left(\mathbf{m}^\gamma \otimes \frac{\partial \delta v_\lambda \mathbf{m}^\lambda}{\partial \xi_\gamma} \right) dA.$$

The integrand can be rewritten as

$$\mathbf{T} : \left(\mathbf{m}^\gamma \otimes \frac{\partial \delta \mathbf{v}}{\partial \xi_\gamma} \right) = \mathbf{m}^\gamma \cdot \frac{\partial}{\partial \xi_\gamma} (\mathbf{T} \cdot \delta \mathbf{v}) - \mathbf{m}^\gamma \cdot \frac{\partial \mathbf{T}}{\partial \xi_\gamma} \cdot \delta \mathbf{v}.$$

Applying the surface divergence theorem to the first term on the right-hand side of this equation shows that

$$\int_A \mathbf{T} : \left(\mathbf{m}^\gamma \otimes \frac{\partial \delta \mathbf{v}}{\partial \xi_\gamma} \right) dA = \int_C \mathbf{n} \cdot \mathbf{T} \cdot \delta \mathbf{v} ds - \int_A \mathbf{m}^\gamma \cdot \frac{\partial \mathbf{T}}{\partial \xi_\gamma} \cdot \delta \mathbf{v} dA.$$

Finally, substituting $\mathbf{T} = T^{\alpha\beta} \mathbf{m}_\alpha \otimes \mathbf{m}_\beta$ and $\delta \mathbf{v} = \delta v_\alpha \mathbf{m}^\alpha$ and remembering to differentiate the basis vectors gives the component form

$$\int_A T^{\alpha\beta} \left\{ \frac{\partial \delta v_\alpha}{\partial \xi_\beta} - \delta v_\lambda \Gamma_{\alpha\beta}^\lambda \right\} dA = \int_C n_\alpha T^{\alpha\beta} \delta v_\beta ds - \int_A \left(\frac{\partial T^{\alpha\beta}}{\partial \xi_\alpha} + T^{\alpha\beta} \Gamma_{\alpha\gamma}^\gamma + T^{\alpha\gamma} \Gamma_{\gamma\beta}^\beta \right) \delta v_\beta dA.$$

4. Applying the procedure outlined in step 3 to similar terms, the virtual work equation can be rewritten as

$$\begin{aligned} & - \int_A \left\{ \frac{\partial T^{\alpha\beta}}{\partial \xi_\alpha} + T^{\alpha\beta} \Gamma_{\alpha\gamma}^\gamma + T^{\alpha\gamma} \Gamma_{\gamma\beta}^\beta + V^\alpha \kappa_\alpha^\beta + p^\beta - \rho h a^\beta \right\} \delta v_\beta \\ & - \int_A \left\{ \frac{\partial V^\alpha}{\partial \xi_\alpha} + V^\alpha \Gamma_{\alpha\beta}^\beta - T^{\alpha\beta} \kappa_{\alpha\beta} + p^3 - \rho h a^3 \right\} \delta v_3 \\ & - \int_A \left\{ \frac{\partial M^{\alpha\beta}}{\partial \xi_\alpha} + M^{\alpha\beta} \Gamma_{\alpha\gamma}^\gamma + M^{\alpha\gamma} \Gamma_{\gamma\beta}^\beta - V^\beta + q^\beta - \frac{\rho h^3}{12} \ddot{\delta}^\beta \right\} \ddot{\delta}^\alpha \\ & + \int_C n_\alpha T^{\alpha\beta} \delta v_\beta ds + \int_C n_\alpha M^{\alpha\beta} \delta \cdot_\beta ds + \int_C n_\alpha V^\alpha \delta v_3 ds - \int_C P^i \delta v_i ds - \int_C Q^\alpha \delta \cdot_\alpha ds = 0. \end{aligned}$$

This equation must be satisfied for all δv_i and $\delta \dot{v}_\alpha$, which immediately gives the equilibrium equations.

5. Some additional algebra is required to derive the boundary conditions. It is tempting to conclude that coefficients of δv_i and $\delta \dot{v}_\alpha$ in the boundary terms must all vanish, but this is not the case because δv_i and $\delta \dot{v}_\alpha$ are related by compatibility equations. The boundary terms must be expressed in terms of four independent degrees of freedom. To this end, recall that $\dot{v}_\alpha = -(\partial v_3 / \partial \xi_\alpha - v_\beta K_\alpha^\beta)$, so the integral around the boundary can be rewritten as

$$\int_C \left\{ n_\alpha T^{\alpha\beta} - n_\alpha M^{\alpha\lambda} \kappa_\lambda^\beta - P^\beta - Q^\lambda \kappa_\lambda^\beta \right\} \delta v_\beta ds + \int_C (n_\alpha V^\alpha - P^3) \delta v_3 ds \\ - \int_C (n_\alpha M^{\alpha\beta} - Q^\beta) \frac{\partial \delta v_3}{\partial \xi_\beta} ds = 0.$$

6. The vector $\partial \delta v_3 / \partial \xi_\alpha$ can be expressed in terms of components parallel and perpendicular to the boundary of the plate C , as

$$\frac{\partial \delta v_3}{\partial \xi_\alpha} = \frac{\partial \delta v_3}{\partial s} \tau_\alpha + \delta \dot{\theta} n_\alpha.$$

Here, $\tau = \tau_\alpha \mathbf{m}^\alpha$ and $\mathbf{n} = n_\alpha \mathbf{m}^\alpha = \mathbf{m}_3 \times \tau$ represent unit vectors tangent and normal to C , and $\delta \dot{\theta}$ is an independent degree of freedom that represents the rotation of the shell about τ . Finally, we integrate by parts to see that

$$\int_C (n_\alpha M^{\alpha\beta} - Q^\beta) \frac{\partial \delta v_3}{\partial \xi_\beta} ds = \int_C (n_\alpha M^{\alpha\beta} - Q^\beta) \tau_\beta \frac{\partial \delta v_3}{\partial s} ds + \int_C (n_\alpha M^{\alpha\beta} - Q^\beta) n_\beta \delta \dot{\theta} ds \\ = - \int_C \frac{\partial}{\partial s} \left\{ (n_\alpha M^{\alpha\beta} - Q^\beta) \tau_\beta \right\} \delta v_3 ds + \int_C (n_\alpha M^{\alpha\beta} - Q^\beta) n_\beta \delta \dot{\theta} ds.$$

(The terms associated with the ends of C vanish because C is a closed curve.)

7. Substituting the result of step 6 back into step 5 gives

$$\int_C \left\{ n_\alpha T^{\alpha\beta} - n_\alpha M^{\alpha\lambda} \kappa_\lambda^\beta - P^\beta - Q^\lambda \kappa_\lambda^\beta \right\} \delta v_\beta ds \\ + \int_C \left(n_\alpha V^\alpha + \frac{\partial}{\partial s} [n_\alpha M^{\alpha\beta} \tau_\beta] - P^3 - \frac{\partial}{\partial s} [Q^\beta \tau_\beta] \right) \delta v_3 ds - \int_C (n_\alpha M^{\alpha\beta} - Q^\beta) n_\beta \delta \dot{\theta} ds = 0.$$

This condition must be satisfied for all $\delta v_i, \delta \dot{\theta}$, which gives the boundary conditions.

Finally, we must derive the last equilibrium equation $T^{12} - T^{21} + M^{\alpha 1} \kappa_{\alpha}^2 - M^{\alpha 2} \kappa_{\alpha}^1 = 0$. Using the definitions of $T^{\alpha\beta}$, $M^{\alpha\beta}$ and noting that $\sigma^{12} = \sigma^{21}$, it is straightforward to show that

$$\begin{aligned} T^{12} - T^{21} &= \int_{-h/2}^{h/2} x_3 (\sigma^{\gamma 2} \kappa_{\gamma}^1 - \sigma^{\gamma 1} \kappa_{\gamma}^2) (1 + x_3 \kappa_{\lambda}^{\lambda}) dx_3 \\ M^{\alpha 1} \kappa_{\alpha}^2 - M^{\alpha 2} \kappa_{\alpha}^1 &= \int_{-h/2}^{h/2} x_3 (\sigma^{\gamma 1} \kappa_{\gamma}^2 - \sigma^{\gamma 2} \kappa_{\gamma}^1) (1 + x_3 \kappa_{\lambda}^{\lambda}) dx_3. \end{aligned}$$

Adding these two equations gives the last equilibrium equation.

10.5.9 Constitutive Equations Relating Forces to Deformation Measures in Elastic Shells

The internal forces in a shell are related to its deformation by the stress-strain law for the material. Here, we give force-deformation equations for an isotropic elastic shell that experiences small shape changes (but possibly large rotations).

Shape changes are characterized using the following deformation measures, defined in Sections 10.5.6:

1. The in-plane components of the metric tensors for the midplane of the shell before and after deformation are denoted $\bar{g}_{\alpha\beta} = \bar{\mathbf{m}}_{\alpha} \cdot \bar{\mathbf{m}}_{\beta}$, $g_{\alpha\beta} = \mathbf{m}_{\alpha} \cdot \mathbf{m}_{\beta}$.
2. The midplane Lagrange strain tensor is $\boldsymbol{\gamma} = \gamma_{\alpha\beta} \bar{\mathbf{m}}^{\alpha} \otimes \bar{\mathbf{m}}^{\beta} = \frac{1}{2}(g_{\alpha\beta} - \bar{g}_{\alpha\beta}) \bar{\mathbf{m}}^{\alpha} \otimes \bar{\mathbf{m}}^{\beta}$.
3. The curvature change tensor is $\Delta \boldsymbol{\kappa} = \Delta \kappa_{\lambda\beta} \bar{\mathbf{m}}^{\lambda} \otimes \bar{\mathbf{m}}^{\beta} = (\kappa_{\beta}^{\alpha} - \bar{\kappa}_{\beta}^{\alpha}) g_{\lambda\alpha} \bar{\mathbf{m}}^{\lambda} \otimes \bar{\mathbf{m}}^{\beta}$, which quantifies the bending and twisting the shell.

Internal forces are characterized using the stress resultant tensor components $T^{\alpha\beta}$ and internal moment components $M^{\alpha\beta}$ defined in Section 10.5.7. The shell is assumed to have a uniform thickness h and is assumed to be made from an isotropic, linear elastic solid, with Young's modulus E and Poisson's ratio ν . We assume for simplicity that the shell is homogeneous and neglect thermal expansion (the effects of thermal expansion are included in an example problem solved in Section 10.7.4).

It is convenient to introduce a plane stress elasticity tensor with components

$$D^{\alpha\beta\rho} = \frac{E}{2(1-\nu^2)} ((\bar{g}^{\alpha\rho} \bar{g}^{\beta} + \bar{g}^{\alpha} \bar{g}^{\beta\rho}) (1-\nu) + 2\nu \bar{g}^{\alpha\beta} \bar{g}^{\rho}).$$

The force-deformation relations can then be expressed as

$$T^{\alpha\beta} = h D^{\alpha\beta\rho\lambda} \gamma_{\rho\lambda} + \frac{h^3}{12} (\kappa_{\theta}^{\beta} - \kappa_{\theta}^{\beta}) D^{\theta\alpha\rho\lambda} \Delta \kappa_{\rho\lambda} - \frac{h^3}{12} \kappa_{\theta} D^{\theta\alpha\rho\lambda} \kappa_{\theta}^{\beta} \gamma_{\rho\lambda}$$

$$M^{\alpha\beta} = \frac{h^3}{12} D^{\alpha\beta\rho\lambda} \Delta \kappa_{\rho\lambda} + \frac{h^3}{12} (\kappa_\theta^\beta - \kappa_\theta^\alpha) D^{\theta\alpha\rho\lambda} \gamma_{\rho\lambda}.$$

For all but a few very rare shell geometries, these expressions may be approximated by

$$T^{\alpha\beta} \approx h D^{\alpha\beta\rho\lambda} \gamma_{\rho\lambda} \quad M^{\alpha\beta} \approx \frac{h^3}{12} D^{\alpha\beta\rho\lambda} \Delta \kappa_{\rho\lambda}.$$

Derivation

1. We have assumed that the material in the shell experiences small distortions but arbitrary rotations. Material behavior can therefore be modeled using the generalized Hooke's law described in Section 3.4, which relates the material stress to the Lagrange strain using the isotropic linear elastic constitutive equations.
2. We assume that the shell is in a state of plane stress, so that the material stress tensor has the form $\Sigma = \Sigma^{\alpha\beta} \bar{\mathbf{m}}_\alpha \otimes \bar{\mathbf{m}}_\beta$.
3. The Lagrange strain tensor is given in Section 10.5.6 as

$$\mathbf{E} \approx \gamma_{\alpha\beta} \bar{\mathbf{m}}^\alpha \otimes \bar{\mathbf{m}}^\beta + x_3 (\kappa_\beta^\alpha - \bar{\kappa}_\beta^\alpha) g_{\lambda\alpha} \bar{\mathbf{m}}^\lambda \otimes \bar{\mathbf{m}}^\beta.$$

4. The material stress is related to the Lagrange strain by the plane stress version of the linear elastic constitutive equations, which can be expressed as

$$\Sigma = \frac{E}{(1+\nu)} \left\{ \mathbf{E} + \frac{\nu}{1-\nu} (\bar{\mathbf{g}} : \mathbf{E}) \bar{\mathbf{g}} \right\},$$

where $\bar{\mathbf{g}} = \bar{g}^{\alpha\beta} \bar{\mathbf{m}}_\alpha \otimes \bar{\mathbf{m}}_\beta$ is the in-plane component of the metric tensor associated with the undeformed shell (this replaces the identity tensor in the Cartesian version of the constitutive equations).

5. The Cauchy stress is related to the material stress by $\sigma = \mathbf{F} \Sigma \mathbf{F}^T / J \approx \mathbf{F} \Sigma \mathbf{F}^T$. Substituting the formulas for Σ from step 4 and approximating \mathbf{F} as $\mathbf{F} \approx \mathbf{m}_i \otimes \bar{\mathbf{m}}^i$, we find after some algebra that

$$\sigma = \sigma^{\alpha\beta} \mathbf{m}_\alpha \otimes \mathbf{m}_\beta \approx D^{\alpha\beta\lambda\rho} (\gamma_{\lambda\rho} + x_3 (\kappa_\rho^\alpha - \bar{\kappa}_\rho^\alpha) g_{\lambda\rho}) \mathbf{m}_\alpha \otimes \mathbf{m}_\beta,$$

where

$$D^{\alpha\beta\rho} = \frac{E}{2(1-\nu^2)} ((\bar{g}^{\alpha\rho} \bar{g}^\beta + \bar{g}^\alpha \bar{g}^{\beta\rho}) (1-\nu) + 2\nu \bar{g}^{\alpha\beta} \bar{g}^\rho).$$

6. The components of the stress-resultant tensor are given by

$$T^{\alpha\beta} = \int_{-h/2}^{h/2} (\sigma^{\alpha\beta} - x_3 \sigma^{\gamma\alpha} \kappa_\gamma^\beta) (1 + x_3 \kappa_\lambda^\lambda) dx_3.$$

Substituting the formula for stress components into this expression and integrating through the thickness of the shell gives

$$T^{\alpha\beta} = h D^{\alpha\beta\rho\lambda} \gamma_{\rho\lambda} + \frac{h^3}{12} (\kappa \delta_\theta^\beta - \kappa_\theta^\beta) D^{\theta\alpha\rho\lambda} \Delta \kappa_{\rho\lambda} - \frac{h^3}{12} \kappa D^{\theta\alpha\rho\lambda} \kappa_\theta^\beta \gamma_{\rho\lambda}.$$

Here, terms of order h^4 have been neglected.

7. The components of the internal moment tensor are

$$M^{\alpha\beta} = \int_{-h/2}^{h/2} x_3 (\sigma^{\alpha\beta} - x_3 \sigma^{\gamma\alpha} \kappa_\gamma^\beta) (1 + x_3 \kappa_\lambda^\lambda) dx_3.$$

Substituting the formula for stress components into this expression and integrating through the thickness of the shell gives

$$M^{\alpha\beta} = \frac{h^3}{12} D^{\alpha\beta\rho\lambda} \Delta \kappa_{\rho\lambda} + \frac{h^3}{12} (\kappa \delta_\theta^\beta - \kappa_\theta^\beta) D^{\theta\alpha\rho\lambda} \gamma_{\rho\lambda},$$

where terms of order h^5 and higher have been neglected.

10.5.10 Strain Energy and Kinetic Energy of an Elastic Shell

It is useful to express the strain energy and kinetic energy of a deformed shell in terms of the motion and deformation of its midplane. To this end, do the following:

1. Consider an isotropic, linear elastic shell, with Young's modulus E , Poisson's ratio ν , mass density ρ , and thickness h . Denote the contravariant components of the tensor of elastic constants by

$$D^{\alpha\beta\rho} = \frac{E}{2(1-\nu^2)} ((\bar{g}^{\alpha\rho} \bar{g}^\beta + \bar{g}^\alpha \bar{g}^{\beta\rho}) (1-\nu) + 2\nu \bar{g}^{\alpha\beta} \bar{g}^\rho).$$

2. Let $\gamma_{\alpha\beta}$ and $\Delta \kappa_{\alpha\beta}$ denote the covariant components of the midplane Lagrange strain tensor, defined in the preceding section,

3. Let $\mathbf{v} = v_i \mathbf{m}_i = v_i \mathbf{m}^i$ and $\boldsymbol{\omega} = \dot{\gamma}_\alpha \mathbf{m}_3 \times \mathbf{m}^\alpha = \dot{\gamma}^\alpha \mathbf{m}_3 \times \mathbf{m}_\alpha$ denote the linear and angular velocity of the midplane of the shell.

The total strain energy of the shell can be calculated as

$$\Phi = \frac{h}{2} D^{\alpha\beta\rho} \int_A \left(\gamma_{\alpha\beta} \gamma_\rho + \frac{h^2}{12} (\Delta \kappa_{\alpha\beta} \Delta \kappa_\rho + 2\kappa_\lambda^\lambda \Delta \kappa_{\alpha\beta} \gamma_\rho) \right) dA.$$

For all but a very few special shell geometries, this result may be approximated by

$$\Phi \approx \frac{h}{2} D^{\alpha\beta\rho} \int_A \left(\gamma_{\alpha\beta} \gamma_\rho + \frac{h^2}{12} \Delta \kappa_{\alpha\beta} \Delta \kappa_\rho \right) dA.$$

The kinetic energy K can be calculated using the formula

$$K = \int_A \left(\frac{h}{2} \rho v^i v_i + \frac{h^3}{24} \rho \cdot \alpha \cdot \alpha \right) dA.$$

The second term in the expression for the kinetic energy represents the rotational energy. In many practical problems, such as vibration of a shell, the rotational energy can be neglected.

Derivation: The strain energy density in the shell is given by $\Sigma : E / 2$, where Σ is the material stress tensor, and E is the Lagrange strain tensor, defined in the preceding section. The stress can be expressed in terms of the strain using the constitutive equation, whereas the strain can be expressed in terms of $\gamma_{\alpha\beta}$ and $\Delta\kappa_{\lambda\beta}$ using step 3 in Section 10.5.9. Integrating over the volume of material in the shell and evaluating the integral through the shell's thickness explicitly gives the result stated. The kinetic energy is calculated using the formula for the velocity field in Section 10.5.4.

10.6 SIMPLIFIED VERSIONS OF GENERAL SHELL THEORY: FLAT PLATES AND MEMBRANES

In many practical cases of interest, the general equations of shell theory can be vastly simplified. In this section, we summarize the governing equations for a number of special solids, including equations governing behavior of flat plates and membranes.

10.6.1 Flat Plates with Small Out-of-Plane Deflections and Negligible In-Plane Loading

This is the simplest version of plate theory and is used in most practical applications. Figure 10.23 illustrates the problem to be solved. An initially flat plate, which has uniform (small) thickness h , Young's modulus E , Poisson's ratio ν , and mass density ρ , is subjected to a distributed force p per unit area (acting vertically upward). The edge of the plate can be constrained in various ways, as discussed in more detail below. We want to determine its deformed shape, as well as the internal forces and moments in the plate.

All vector and tensor quantities can be expressed in a fixed Cartesian basis $\{\mathbf{e}_1, \mathbf{e}_2, \mathbf{e}_3\}$ illustrated in Figure 10.23. The covariant and reciprocal basis vectors are identical so there is no need to use the system of raised and lowered indices that was needed in general shell theory. In addition, because the basis vectors are independent of position, the Christoffel

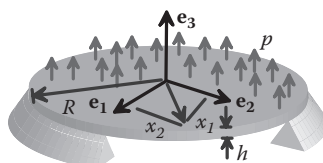


FIGURE 10.23 Flat plate subjected to transverse loading.

symbols are all zero. We continue to use the convention that Greek subscripts can have values 1 or 2, whereas Latin subscripts may have values 1, 2, or 3.

We make the following assumptions:

1. The variation of displacements within the plate conforms to the usual approximations of Kirchhoff plate theory, i.e., material fibers that are perpendicular to the midplane of the undeformed plate remain perpendicular to the midplane of the deformed plate and stretching transverse to the midplane is neglected.
2. The displacement of the midplane of the plate has the form $\mathbf{u} = u_3(x_1, x_2)\mathbf{e}_3$, i.e., material points on the midplane of the plate deflect only transverse to the plate.
3. The midplane deflection is small compared with the dimensions of the plate, and the slope of the deflected plate is small, so that $\partial u_3 / \partial x_\alpha \ll 1$ for all α ; second-order terms in displacement are ignored in all the strain definitions and also the equilibrium equations.

The following (approximate) results can then be extracted from the general shell equations.

Kinematics

- The curvature change tensor is $\Delta\kappa_{\alpha\beta} = -\frac{\partial^2 u_3}{\partial x_\alpha \partial x_\beta}$, whereas the in-plane strain tensor is $\gamma_{\alpha\beta} = 0$.
- The normal vector to the deformed plate can be approximated as $\mathbf{m}_3 = \mathbf{e}_3 - \frac{\partial u_3}{\partial \xi_\alpha} \mathbf{e}_\alpha$.
- The displacement field in the plate is approximated as $\mathbf{u} = u_3 \mathbf{e}_3 - x_3 \frac{\partial u_3}{\partial x_\alpha} \mathbf{e}_\alpha$.
- The (infinitesimal) strain field in the plate is approximated as $\varepsilon_{\alpha\beta} = x_3 \Delta\kappa_{\alpha\beta}$.

Kinetics

- The external force is characterized by the force per unit area $p\mathbf{e}_3$ acting on the surface of the plate.
- The in-plane stress tensor is $T_{\alpha\beta} = 0$, so the internal forces are completely characterized by the internal moment tensor $\mathbf{M} = M_{\alpha\beta} \mathbf{e}_\alpha \otimes (\mathbf{m}_3 \times \mathbf{e}_\beta)$ and transverse force tensor $\mathbf{V} = V_\alpha \mathbf{e}_\alpha$.
- The components V_α represent the vertical force per unit length acting on an internal plane perpendicular to the \mathbf{e}_α direction.
- The physical significance of $M_{\alpha\beta}$ is illustrated in Figure 10.24: $M_{1\alpha}$ characterizes the moment per unit length acting on planes inside the shell that are normal to the \mathbf{e}_1 direction, whereas $M_{2\alpha}$ characterizes the moment per unit length acting on planes that are normal to \mathbf{e}_2 . Note that $M_{\alpha 1}$ represents a moment about the \mathbf{e}_2 axis, whereas $M_{\alpha 2}$ is a moment acting about the $-\mathbf{e}_1$ axis.

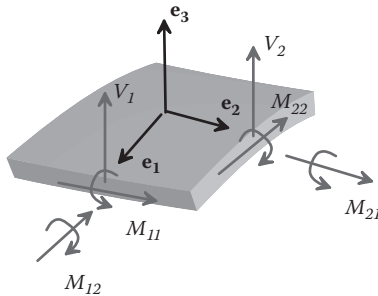


FIGURE 10.24 Internal shear forces and bending and twisting moments inside a shell.

Moment-curvature relation: Moment-curvature relation reduces to

$$M_{\alpha\beta} = \frac{Eh^3}{12(1-\nu^2)} ((1-\nu)\Delta\kappa_{\alpha\beta} + \nu\Delta\kappa_{\lambda\lambda}\delta_{\alpha\beta}).$$

Equations of motion: Equations of motion are approximated by

$$\frac{\partial V_\alpha}{\partial x_\alpha} + p = \rho h \frac{\partial^2 u_3}{\partial t^2} \quad \frac{\partial M_{\alpha\beta}}{\partial x_\alpha} - V_\beta \approx 0$$

(rotational inertia has been neglected). These equations can be combined to eliminate V ,

$$\frac{\partial^2 M_{\alpha\beta}}{\partial x_\alpha \partial x_\beta} + p = \rho h \frac{\partial^2 u_3}{\partial t^2} \equiv \frac{\partial^2 M_{11}}{\partial x_1^2} + 2 \frac{\partial^2 M_{12}}{\partial x_1 \partial x_2} + \frac{\partial^2 M_{22}}{\partial x_2^2} + p = \rho h \frac{\partial^2 u_3}{\partial t^2},$$

and can also be expressed in terms of the displacements as

$$\begin{aligned} & \frac{Eh^3}{12(1-\nu^2)} \frac{\partial^4 u_3}{\partial x_\alpha \partial x_\alpha \partial x_\beta \partial x_\beta} + \rho h \frac{\partial^2 u_3}{\partial t^2} = p \\ & \equiv \frac{Eh^3}{12(1-\nu^2)} \left\{ \frac{\partial^4 u_3}{\partial x_1^4} + 2 \frac{\partial^4 u_3}{\partial x_1^2 \partial x_2^2} + \frac{\partial^4 u_3}{\partial x_2^4} \right\} + \rho h \frac{\partial^2 u_3}{\partial t^2} = p. \end{aligned}$$

Edge boundary conditions: The edge of the plate is characterized by a curve C that lies in the midplane of the shell, encircling \mathbf{e}_3 in a counterclockwise sense. We let s denote arc length measured around C from some convenient origin and use $\tau = \tau_\alpha \mathbf{e}_\alpha$ and $\mathbf{n} = \mathbf{e}_3 \times \tau$ to denote unit vectors tangent and normal to C . Elementary plate theory offers the following choices of boundary condition for each point on C :

1. Part of the boundary of the plate C_1 may be clamped, i.e., rotations and displacement of the boundary are completely prevented. The transverse displacement must then satisfy $u_3 = n_\alpha \partial u_3 / \partial x_\alpha = 0$ on C_1 .

2. Part of the boundary C_2 may be simply supported, i.e., the boundary of the plate is prevented from moving but is permitted to rotate freely about the tangent vector τ . In this case, the transverse displacement and internal moment must satisfy

$$u_3 = 0 \quad n_\alpha M_{\alpha\beta} n_\beta = 0.$$

3. Part of the boundary C_3 may be free, i.e., the boundary is free to both translate and rotate. In this case, the transverse shear force and internal moment must satisfy

$$n_\alpha V_\alpha + \frac{\partial}{\partial s} [n_\alpha M_{\alpha\beta} \tau_\beta] = 0 \quad n_\alpha M_{\alpha\beta} n_\beta = 0.$$

More general boundary conditions, in which the edge of the plate is subjected to prescribed forces and moments, can also be derived from the results given in Section 10.5.8 if this is of interest.

Strain energy and kinetic energy of a flat plate: The formula for the strain energy and kinetic energy of the plate can be expressed in terms of displacements as

$$\Phi = \frac{Eh^3}{24(1-\nu^2)} \int_A \left((1-\nu) \frac{\partial^2 u_3}{\partial x_\alpha \partial x_\beta} \frac{\partial^2 u_3}{\partial x_\alpha \partial x_\beta} + \nu \left(\frac{\partial^2 u_3}{\partial x_\alpha \partial x_\alpha} \right)^2 \right) dA$$

$$K = \int_A \left(\frac{h}{2} \rho v_i v_i + \frac{h^3}{24} \rho \frac{\partial v_3}{\partial x_\alpha} \frac{\partial v_3}{\partial x_\alpha} \right) dA.$$

The second term in the integral for the kinetic energy represents the energy associated with the plate's out-of-plane rotation and can be ignored in most practical applications.

10.6.2 Flat Plates with Small Out-of-Plane Deflections and Significant In-Plane Loading

This version of plate theory is used to model plates that are subjected to substantial loading parallel to the plane of the plate (usually attributable to loads applied at its boundaries, as shown in Figure 10.25). The theory assumes that displacements are small enough to use linearized measures of strain but includes nonlinear terms associated with the in-plane loading in the equilibrium equations. The theory can be used to calculate buckling loads for plates but does not accurately model their deformation if the buckling loads are exceeded.

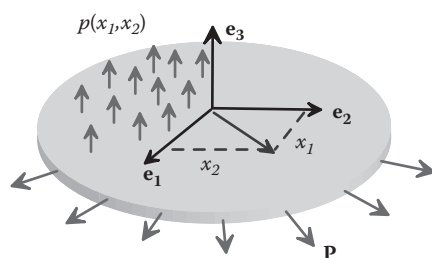


FIGURE 10.25 Flat plate subjected to transverse and in-plane loading.

The problem to be solved is stated in Section 10.6.1. The majority of the governing equations are identical to those of standard plate theory, given in Section 10.6.1. The equations that need to be modified to account for transverse forces are listed below.

Kinematics

- The in-plane strain tensor is approximated as $\gamma_{\alpha\beta} = (\partial u_\alpha / \partial u_\beta + \partial u_\beta / \partial u_\alpha) / 2$.
- The displacement field in the plate is approximated as $\mathbf{u} = u_i \mathbf{e}_i - x_3 \frac{\partial u_3}{\partial x_\alpha} \mathbf{e}_\alpha$.
- The (infinitesimal) strain field in the plate is approximated as $\varepsilon_{\alpha\beta} = \gamma_{\alpha\beta} + x_3 \Delta \kappa_{\alpha\beta}$, where the components of the curvature change tensor are given in Section 10.6.1.

Kinetics

- The external force consists of a force per unit area $p_i \mathbf{e}_i$ acting on the surface of the plate.
- The internal forces are characterized as described in Section 10.6.1, except that the stress resultant tensor $T_{\alpha\beta}$ is nonzero. The components of the stress resultant tensor can be interpreted as illustrated in Figure 10.26: $T_{\alpha\beta}$ represents the force per unit length, acting in the \mathbf{e}_β direction, on an internal plane perpendicular to the \mathbf{e}_α direction within the plate.

Stress resultant-strain and moment-curvature relations: Stress resultant-strain and moment-curvature relations are expressed as

$$T_{\alpha\beta} = \frac{Eh}{(1-\nu^2)} ((1-\nu)\gamma_{\alpha\beta} + \nu\gamma_{\lambda\lambda}\delta_{\alpha\beta}) \quad M_{\alpha\beta} = \frac{Eh^3}{12(1-\nu^2)} ((1-\nu)\Delta\kappa_{\alpha\beta} + \nu\Delta\kappa_{\lambda\lambda}\delta_{\alpha\beta}).$$

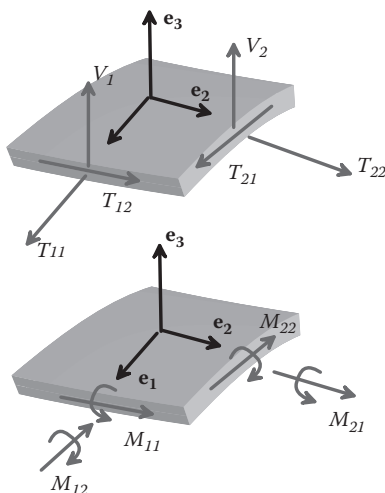


FIGURE 10.26 Internal shear forces and bending and twisting moments inside a shell.

Equations of motion: Equations of motion reduce to

$$\frac{\partial T_{\alpha\beta}}{\partial x_\alpha} + p_\beta = \rho h \frac{\partial^2 u_\beta}{\partial t^2} \quad \frac{\partial V_\alpha}{\partial x_\alpha} - T_{\alpha\beta} \Delta \kappa_{\alpha\beta} - p_\alpha \frac{\partial u_3}{\partial x_\alpha} + p_3 = \rho h \frac{\partial^2 u_3}{\partial t^2} \quad \frac{\partial M_{\alpha\beta}}{\partial x_\alpha} - V_\beta \approx 0.$$

The second two equations can be combined to eliminate V :

$$\frac{\partial M_{\alpha\beta}}{\partial x_\alpha \partial x_\beta} - T_{\alpha\beta} \kappa_{\alpha\beta} - p_\alpha \frac{\partial u_3}{\partial x_\alpha} + p_3 = \rho h \frac{\partial^2 u_3}{\partial t^2}.$$

This result can also be expressed in terms of displacement as

$$\frac{Eh^3}{12(1-v^2)} \frac{\partial^4 u_3}{\partial x_\alpha \partial x_\alpha \partial x_\beta \partial x_\beta} - T_{\alpha\beta} \frac{\partial^2 u_3}{\partial x_\alpha \partial x_\beta} + p_\alpha \frac{\partial u_3}{\partial x_\alpha} + \rho h \frac{\partial^2 u_3}{\partial t^2} = p_3.$$

Edge boundary conditions: The edge of the plate is characterized as described in Section 10.6.1. Boundary conditions for the transverse displacement u_3 , transverse force V_α , and internal moment $M_{\alpha\beta}$ are identical to those listed in Section 10.6.1. In addition, the in-plane displacements or forces must satisfy the following boundary conditions:

1. On part of the boundary of the plate C_1 , one or more components of the in-plane displacement may be prescribed $u_\beta = u_\beta^*$.
2. Portions of the boundary of the plate C_2 may be subjected to a prescribed in-plane force per unit length P^β . The in-plane forces must then satisfy $n_\alpha T^{\alpha\beta} = P^\beta$.

10.6.3 Flat Plates with Small In-Plane and Large Transverse Deflections (von Karman Theory)

This version of plate theory is used to model plates that are subjected to substantial loading parallel to the plane of the plate (usually caused by loads applied at its boundaries) and also experience substantial out-of-plane displacement. The theory uses a nonlinear strain measure to account for the in-plane stretching that results from finite transverse displacement and rotation and includes nonlinear terms associated with the in-plane loading in the equilibrium equations. The theory can be used to estimate the shape of a buckled plate if the buckling loads are exceeded.

We make the following assumptions:

1. The variation of displacements within the plate conforms to the usual approximations of Kirchhoff plate theory.
2. The displacement of the midplane of the plate has the form $\mathbf{u} = u_i(x_1, x_2)\mathbf{e}_i$; all three displacement components are considered.

3. The in-plane deflections are small and satisfy $\partial u_\beta / \partial x_\alpha \ll 1$ for all α, β ; second-order terms in these displacement components are ignored in all the strain definitions and also the equilibrium equations. The out-of-plane displacement is assumed to be small enough to use a linearized measure of curvature. However, the terms involving products of $\partial u_3 / \partial x_\alpha$ are retained when computing the strain of the midplane of the plate, so that the stretching attributable to transverse deflection is considered approximately.
4. The in-plane forces are assumed to be much larger than transverse forces. Nonlinear terms in the equilibrium equations involving in-plane forces are retained; those associated with transverse loading are neglected.

Most of the governing equations of von Karman plate theory are identical to those listed in the preceding section. Nevertheless, the full set of governing equations is given below for convenience.

Kinematics

- The in-plane strain tensor is approximated by $\gamma_{\alpha\beta} = \frac{1}{2} \left(\frac{\partial u_\alpha}{\partial x_\beta} + \frac{\partial u_\beta}{\partial x_\alpha} + \frac{\partial u_3}{\partial x_\alpha} \frac{\partial u_3}{\partial x_\beta} \right)$. The additional, nonlinear, term in this expression is the main feature of von Karman theory.
- The curvature change tensor has components $\Delta \kappa_{\alpha\beta} = -\frac{\partial^2 u_3}{\partial x_\alpha \partial x_\beta}$.
- The normal vector to the deformed plate can be approximated as $\mathbf{m}_3 = \mathbf{e}_3 - \frac{\partial u_3}{\partial x_\alpha} \mathbf{e}_\alpha$.
- The displacement field in the plate is approximated as $\mathbf{u} = u_3 \mathbf{e}_3 - x_3 \frac{\partial u_3}{\partial x_\alpha} \mathbf{e}_\alpha$.
- The (infinitesimal) strain field in the plate is approximated as $\varepsilon_{\alpha\beta} = \gamma_{\alpha\beta} + x_3 \Delta \kappa_{\alpha\beta}$.

Kinetics

- The external force is characterized by the force per unit area $p \mathbf{e}_3$ acting on the surface of the plate.
- The transverse stress tensor $T_{\alpha\beta} = 0$, so the internal forces are characterized by the in-plane stress resultant tensor $T_{\alpha\beta}$, the transverse force tensor V_α , and internal moment tensor $M_{\alpha\beta}$. The physical significance of the components of these tensors is discussed in Sections 10.6.1 and 10.6.2.

Stress resultant-strain and moment-curvature relations: Stress resultant-strain and moment-curvature relations are expressed as

$$T_{\alpha\beta} = \frac{Eh}{(1-\nu^2)} ((1-\nu)\gamma_{\alpha\beta} + \nu\gamma_{\lambda\lambda}\delta_{\alpha\beta}) \quad M_{\alpha\beta} = \frac{Eh^3}{12(1-\nu^2)} ((1-\nu)\Delta\kappa_{\alpha\beta} + \nu\Delta\kappa_{\lambda\lambda}\delta_{\alpha\beta}).$$

Equations of motion: Equations of motion reduce to

$$\frac{\partial T_{\alpha\beta}}{\partial x_\alpha} + p_\beta = \rho h \frac{\partial^2 u_\beta}{\partial t^2} \quad \frac{\partial V_\alpha}{\partial x_\alpha} - T_{\alpha\beta} \Delta \kappa_{\alpha\beta} - p_\alpha \frac{\partial u_3}{\partial x_\alpha} + p_3 = \rho h \frac{\partial^2 u_3}{\partial t^2} \quad \frac{\partial M_{\alpha\beta}}{\partial x_\alpha} - V_\beta \approx 0,$$

where the rotational inertia term has been neglected in the last equation.

Edge boundary conditions

1. The boundary conditions for transverse displacement u_3 and/or the internal moment $M_{\alpha\beta}$ and transverse force V_α are identical to those listed in Section 10.6.1.
2. The boundary conditions for in-plane displacements u_α and/or in-plane forces $T_{\alpha\beta}$ are identical to those listed in Section 10.6.2.

Alternative forms for the von Karman equations: If the plate is in static equilibrium (so the velocity and acceleration of the plate is zero), the von Karman equations can be written in a compact form by expressing the in-plane forces $T_{\alpha\beta}$ in terms of an Airy stress function ϕ , following the procedure outlined for plane elasticity problems in Section 5.2. As a result, the governing equations can be reduced to a pair of coupled, nonlinear partial differential equations for ϕ and u_3 . These formulas will not be given here but can be found in Timoshenko and Woinowsky-Krieger [1959].

10.6.4 Stretched, Flat Membrane with Small Out-of-Plane Deflections

This is a simplified version of the stretched plate theory outlined in Section 10.6.2, which can be used if the plate is so thin that internal bending moments can be neglected. The problem to be solved is illustrated in Figure 10.27. A “membrane” with Young’s modulus E , Poisson’s ratio ν , mass density ρ , and thickness h is initially planar and lies in the plane perpendicular to the e_3 direction. The edge of the membrane is subjected to a load per unit length $P = P_\alpha e_\alpha$ and prevented from moving transverse to the membrane. A force per unit area $p = p_3 e_3$ acts on the membrane, inducing a small, time-dependent, transverse deflection $u = u_3(x_3)e_3$.

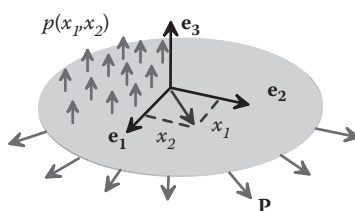


FIGURE 10.27 Membrane subjected to transverse loading and in-plane forces.

Kinematics

- The in-plane strain tensor is approximated as $\gamma_{\alpha\beta} = (\partial u_\alpha / \partial x_\beta + \partial u_\beta / \partial x_\alpha) / 2$.
- The displacement field in the plate is approximated as $\mathbf{u} = u_i \mathbf{e}_i$. We assume that $u_3 \gg u_\alpha$.
- The curvature of the membrane has components $\Delta \kappa_{\alpha\beta} = -\frac{\partial^2 u_3}{\partial x_\alpha \partial x_\beta}$.
- The (infinitesimal) strain field in the membrane is approximated as $\varepsilon_{\alpha\beta} = \gamma_{\alpha\beta}$.

Kinetics

- The external force consists of a force per unit area $p_i \mathbf{e}_i$ acting on the surface of the plate.
- The internal forces are characterized by the stress resultant tensor $T_{\alpha\beta}$ (the internal moments are neglected).

Stress resultant-strain relations: Stress resultant-strain relations are expressed as

$$T_{\alpha\beta} = \frac{Eh}{(1-\nu^2)} ((1-\nu)\gamma_{\alpha\beta} + \nu\gamma_{\lambda\lambda}\delta_{\alpha\beta}).$$

Equations of motion: Equations of motion are approximated as

$$\frac{\partial T_{\alpha\beta}}{\partial x_\alpha} \approx 0 \quad -T_{\alpha\beta}\Delta\kappa_{\alpha\beta} + p_3 = \rho h \frac{\partial^2 u_3}{\partial t^2}.$$

The second equation can also be expressed in terms of displacement as

$$T_{\alpha\beta} \frac{\partial^2 u_3}{\partial x_\alpha \partial x_\beta} + p_3 = \rho h \frac{\partial^2 u_3}{\partial t^2}.$$

Edge boundary conditions: On the edge of the membrane, the following applies:

1. The transverse displacement must satisfy $u_3 = 0$.
2. The in-plane forces must satisfy $n_\alpha T_{\alpha\beta} = P_\beta$, where \mathbf{n} is a unit vector in the $(\mathbf{e}_1, \mathbf{e}_2)$ plane perpendicular to the edge of the membrane.

10.6.5 Membrane Equations in Cylindrical-Polar Coordinates

In this section, we rewrite the governing equations for a stretched membrane in a cylindrical-polar coordinate system to provide a simple example of the use of general curvilinear coordinates. We reconsider the membrane described in the preceding section but now assume that the membrane is circular, with radius R .

HEALTH WARNING: We use polar coordinates $r \equiv \xi_1$, $\theta \equiv \xi_2$ illustrated in Figure 10.28 as the choice of curvilinear coordinates. However, all vector and tensor quantities will be expressed as covariant or contravariant components in the natural basis for this coordinate system, *not* as components in a cylindrical-polar basis of unit vectors $\{\mathbf{e}_r, \mathbf{e}_\theta, \mathbf{e}_3\}$.

Coordinate system and kinematic relations

- Let $\{\mathbf{e}_1, \mathbf{e}_2, \mathbf{e}_3\}$ be a fixed Cartesian basis of mutually perpendicular unit vectors, with \mathbf{e}_3 normal to the plane of the undeformed membrane.
- The position vector of a point in the membrane can be expressed as

$$\bar{\mathbf{r}} = r \cos \theta \mathbf{e}_1 + r \sin \theta \mathbf{e}_2.$$

- The natural basis vectors and the reciprocal basis (for the undeformed membrane) follow as

$$\bar{\mathbf{m}}_1 = \frac{\partial \bar{\mathbf{r}}}{\partial r} = \cos \theta \mathbf{e}_1 + \sin \theta \mathbf{e}_2 \quad \bar{\mathbf{m}}_2 = \frac{\partial \bar{\mathbf{r}}}{\partial \theta} = -r \sin \theta \mathbf{e}_1 + r \cos \theta \mathbf{e}_2 \quad \bar{\mathbf{m}}_3 = \mathbf{e}_3$$

$$\bar{\mathbf{m}}^1 = \cos \theta \mathbf{e}_1 + \sin \theta \mathbf{e}_2 \quad \bar{\mathbf{m}}^2 = -\frac{1}{r} \sin \theta \mathbf{e}_1 + \frac{1}{r} \cos \theta \mathbf{e}_2 \quad \bar{\mathbf{m}}^3 = \mathbf{e}_3.$$

Here the reciprocal basis has simply been written down by inspection; you can readily verify that $\bar{\mathbf{m}}_i \cdot \bar{\mathbf{m}}^j = \delta_i^j$. Note that neither the natural basis vectors nor the reciprocal basis vectors are unit vectors.

- The Christoffel symbols for the coordinate system and the curvature tensor for the undeformed membrane follow as

$$\bar{\Gamma}_{\beta\gamma}^\alpha = \bar{\mathbf{m}}^\alpha \cdot \frac{\partial^2 \bar{\mathbf{r}}}{\partial \xi_\alpha \partial \xi_\beta} \Rightarrow \bar{\Gamma}_{11}^1 = \bar{\Gamma}_{12}^1 = \bar{\Gamma}_{21}^1 = 0 \quad \bar{\Gamma}_{22}^1 = -r \quad \bar{\Gamma}_{11}^2 = \bar{\Gamma}_{22}^2 = 0 \quad \bar{\Gamma}_{12}^2 = \bar{\Gamma}_{21}^2 = \frac{1}{r}$$

$$\bar{\kappa}_{\alpha\beta} = -\bar{\mathbf{m}}_3 \cdot \frac{\partial \bar{\mathbf{m}}_\alpha}{\partial \xi_\beta} = 0.$$

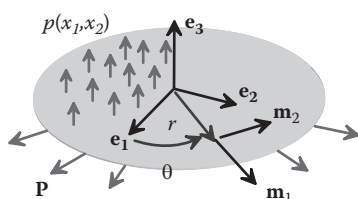


FIGURE 10.28 Polar coordinate system used to describe deformation of a membrane.

5. The position vector of a point in the deformed membrane is

$$\mathbf{r} = r \cos \theta \mathbf{e}_1 + r \sin \theta \mathbf{e}_2 + u_3 \mathbf{e}_3.$$

6. The natural basis vectors and reciprocal basis for the deformed membrane follow as

$$\mathbf{m}_1 = \frac{\partial \mathbf{r}}{\partial r} = \cos \theta \mathbf{e}_1 + \sin \theta \mathbf{e}_2 + \frac{\partial u_3}{\partial r} \mathbf{e}_3 \quad \mathbf{m}_2 = \frac{\partial \mathbf{r}}{\partial \theta} = -r \sin \theta \mathbf{e}_1 + r \cos \theta \mathbf{e}_2 + \frac{\partial u_3}{\partial \theta} \mathbf{e}_3$$

$$\mathbf{m}_3 = \mathbf{m}_1 \times \mathbf{m}_2 / |\mathbf{m}_1 \times \mathbf{m}_2| \approx -\left(\cos \theta \frac{\partial u_3}{\partial r} - \sin \theta \frac{1}{r} \frac{\partial u_3}{\partial \theta} \right) \mathbf{e}_1 - \left(\sin \theta \frac{\partial u_3}{\partial r} + \cos \theta \frac{1}{r} \frac{\partial u_3}{\partial \theta} \right) \mathbf{e}_2 + \mathbf{e}_3,$$

where terms of order $(\partial u_3 / \partial r)^2$, $(\partial u_3 / \partial \theta)^2$, etc. have been neglected in the expression for \mathbf{m}_3 . The reciprocal basis vectors can also be calculated but are not required in the analysis to follow.

7. For small transverse deflections, the Christoffel symbols associated with the deformed membrane can be approximated using those for the undeformed membrane. The curvature tensor for the deformed membrane has covariant components

$$\kappa_{11} = -\frac{\partial^2 u_3}{\partial r^2} \quad \kappa_{12} = \kappa_{21} = \frac{1}{r} \frac{\partial u_3}{\partial \theta} - \frac{\partial^2 u_3}{\partial r \partial \theta} \quad \kappa_{22} = -r \frac{\partial u_3}{\partial r} - \frac{\partial^2 u_3}{\partial \theta^2}.$$

Notice that the curvature components all have different units. This is because the basis vectors themselves have units. It is easy to check that the terms in the dyadic product $\kappa_{\alpha\beta} \mathbf{m}^\alpha \otimes \mathbf{m}^\beta$ all have correct units.

Equations of motion: The general equations of motion for a shell are

$$\frac{\partial T^{\alpha\beta}}{\partial \xi_\alpha} + T^{\alpha\beta} \Gamma_{\alpha\gamma}^\gamma + T^{\alpha\gamma} \Gamma_{\gamma\alpha}^\beta + V^\alpha \kappa_\alpha^\beta + p^\beta = \rho h a^\beta$$

$$\frac{\partial V^\alpha}{\partial \xi_\alpha} + V^\alpha \Gamma_{\alpha\beta}^\beta - T^{\alpha\beta} \kappa_{\alpha\beta} + p^3 = \rho h a^3.$$

$$\frac{\partial M^{\alpha\beta}}{\partial \xi_\alpha} + M^{\alpha\beta} \Gamma_{\alpha\gamma}^\gamma + M^{\alpha\gamma} \Gamma_{\gamma\alpha}^\beta - V^\beta + q^\beta = \frac{\rho h^3}{12} \ddot{a}^\beta$$

$$T^{12} - T^{21} + M^{\alpha 1} \kappa_\alpha^2 - M^{\alpha 2} \kappa_\alpha^1 = 0.$$

We proceed to simplify these for a flat membrane:

1. No external moments q^β act on the membrane, and the membrane thickness is assumed to be so small that the internal moments $M^{\alpha\beta}$ can be neglected. We may also assume $\rho h^3 \approx 0$. The equations of motion in the right-hand column then show that transverse forces V^α must vanish and that the in-plane forces $T^{\alpha\beta}$ are symmetric $T^{12} = T^{21}$.

2. Substituting for the Christoffel symbols and curvature components into the remaining equations of motion and recalling that in-plane forces $p^\beta = 0$, we find that the three remaining equilibrium equations reduce to

$$\begin{aligned} \frac{\partial T^{11}}{\partial r} + \frac{\partial T^{21}}{\partial \theta} + \frac{T^{11}}{r} - T^{22}r &= 0 & \frac{\partial T^{22}}{\partial \theta} + \frac{\partial T^{12}}{\partial r} + 3\frac{T^{12}}{r} &= 0 \\ T^{11}\frac{\partial^2 u_3}{\partial r^2} + 2T^{12}\left(\frac{\partial^2 u_3}{\partial r \partial \theta} - \frac{1}{r}\frac{\partial u_3}{\partial \theta}\right) + T^{22}\left(r\frac{\partial u_3}{\partial r} + \frac{\partial^2 u_3}{\partial \theta^2}\right) + p^3 &= \rho h \frac{\partial^2 u_3}{\partial t^2}. \end{aligned}$$

Boundary conditions

1. The transverse displacement must satisfy $u_3 = 0$ on the edge of the membrane at $r = R$.
2. The in-plane forces must satisfy $T^{1\beta} = P^\beta$, where $\mathbf{P} = P^\beta \bar{\mathbf{m}}_\beta$ is the force per unit length acting on the edge of the membrane at $r = R$.

Special case: Membrane subjected to uniform biaxial in-plane loading: If the membrane is subjected to a uniform radial force per unit length $\mathbf{P} = T_0 \bar{\mathbf{m}}_1$ acting on its edge at $r = R$, the first two equations of motion and the boundary conditions are satisfied by $T^{11} = T_0$, $T^{22} = T_0 / r^2$, $T^{12} = 0$. This corresponds to a state of uniform biaxial tension in the membrane. The equation of motion for the transverse deflection reduces to

$$T_0\left(\frac{\partial^2 u_3}{\partial r^2} + \frac{1}{r}\frac{\partial u_3}{\partial r} + \frac{1}{r^2}\frac{\partial^2 u_3}{\partial \theta^2}\right) + p^3 = \rho h \frac{\partial^2 u_3}{\partial t^2}.$$

10.7 SOLUTIONS TO SIMPLE PROBLEMS INVOLVING MEMBRANES, PLATES, AND SHELLS

In this section, we derive solutions to several initial and boundary value problems for plates and shells to illustrate applications of the general theories derived in the preceding sections.

10.7.1 Thin Circular Plate Bent by Pressure Applied to One Face

A thin circular plate, with radius R and thickness h , is made from a linear elastic solid with Young's modulus E and Poisson's ratio ν , as shown in Figure 10.29. It is subjected to a pressure $\mathbf{p} = p_3 \mathbf{e}_3$ acting perpendicular to the plate and is simply supported at its edge. The solution can be derived using the simplified version of plate theory described in Section 10.6.1. Although the plate is circular, the problem can be solved by expressing all vector and tensor quantities as components in a Cartesian basis $\{\mathbf{e}_1, \mathbf{e}_2, \mathbf{e}_3\}$ shown in the figure.

The deflection of the plate is given by

$$u_3 = \frac{3(1-\nu^2)p}{16Eh^3}(R^2 - r^2)\left(\frac{5+\nu}{1+\nu}R^2 - r^2\right),$$

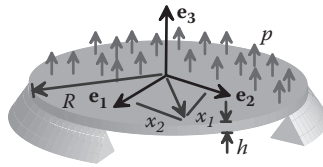


FIGURE 10.29 Circular plate subjected to transverse loading.

where $r = \sqrt{x_\alpha x_\alpha}$. The internal force and moment in the plate are

$$M_{\alpha\beta} = -\frac{1}{8}(1-\nu)px_\alpha x_\beta - \frac{1}{16}p(r^2(1+3\nu) - R^2(3+\nu))\delta_{\alpha\beta}$$

$$V_\beta = \frac{\partial M_{\alpha\beta}}{\partial x_\alpha} = -\frac{1}{2}px_\beta$$

Derivation

1. The transverse deflection must satisfy the static equilibrium equation

$$\frac{Eh^3}{12(1-\nu^2)} \frac{\partial^4 u_3}{\partial x_\alpha \partial x_\alpha \partial x_\beta \partial x_\beta} = p.$$

2. The solution must be axially symmetric, so that $u_3 = w(r)$ where $r = \sqrt{x_\alpha x_\alpha}$.

Substituting this expression into the equilibrium equation and using $\partial r / \partial x_\alpha = x_\alpha / r$ reduces the governing equation to

$$\frac{Eh^3}{12(1-\nu^2)} \left(\frac{d^4 w}{dr^4} + \frac{2}{r} \frac{d^3 w}{dr^3} - \frac{1}{r^2} \frac{d^2 w}{dr^2} + \frac{1}{r^3} \frac{dw}{dr} \right) = \frac{Eh^3}{12(1+\nu^2)} r \frac{d}{dr} \left(r \frac{d}{dr} \left(\frac{1}{r} \frac{d}{dr} \left(r \frac{dw}{dr} \right) \right) \right) = p.$$

3. This equation can be integrated repeatedly to give

$$w = \frac{1-\nu^2}{Eh^2} \left(\frac{3}{16} pr^4 + Ar^2 \log r + B \log r + Cr^2 + D \right),$$

where A, B, C , and D are constants of integration.

4. The curvature is related to w by

$$\kappa_{\alpha\beta} = -\frac{\partial^2 u_3}{\partial x_\alpha \partial x_\beta} = -\left(\frac{d^2 w}{dr^2} - \frac{1}{r} \frac{dw}{dr} \right) \frac{x_\alpha x_\beta}{r^2} - \frac{dw}{dr} \frac{\delta_{\alpha\beta}}{r}.$$

5. Substituting this result into the curvature-moment equations gives the following equation for the internal moment distribution:

$$M_{\alpha\beta} = \frac{-Eh^3}{12(1-\nu^2)} \left((1-\nu) \left(\frac{d^2 w}{dr^2} - \frac{1}{r} \frac{dw}{dr} \right) \frac{x_\alpha x_\beta}{r^2} + \left(\nu \frac{d^2 w}{dr^2} + \frac{1}{r} \frac{dw}{dr} \right) \delta_{\alpha\beta} \right).$$

6. The displacement and curvature of the plate must be finite at $r = 0$, which is only possible if $A = B = 0$. To see this, note that the $B \log(r)$ term in the formula for w is infinite at $r = 0$; similarly, substituting the expression for w into the curvature formula produces a term involving $A \log(r)$ that is also infinite at $r = 0$. The remaining constants must be determined from the boundary conditions at the edge of the plate. For a simply supported plate, the boundary conditions are $w = 0$ and $M_{\alpha\beta}n_\alpha n_\beta = 0$ on $r = R$, where $n_\alpha = x_\alpha/r$ is a unit vector normal to the edge of the plate. This yields two equations that can be solved for C and D . Substituting the results back into the formulas in steps 3 and 5 then gives the solution.

10.7.2 Vibration Modes and Natural Frequencies for a Circular Membrane

A thin circular membrane with thickness h , radius R , and mass density ρ is subjected to a uniform radial force per unit length T_0 acting on its edge, as shown in Figure 10.30. Our goal is to calculate the mode shapes and natural frequencies of vibration of the membrane (the physical significance of natural frequencies and mode shapes for a continuous system are described in more detail in Section 10.4.1).

The natural frequencies of vibration and mode shapes are identified by two integers (m, n) that characterize the mode shape. The index $m = 1, 2, 3 \dots$ corresponds to the number of circumferential lines (with $r = \text{constant}$) on the membrane that have zero displacement, whereas $n = 0, 1, 2 \dots$ corresponds to the number of diametral lines (with $\theta = \text{constant}$) that have zero displacement.

The natural frequencies of vibration are given by the solutions to the equation $J_n(\omega_{(m,n)}R\sqrt{\rho h/T_0})=0$, where $J_n(x)$ is a Bessel function of the first kind of order n (this sounds scary, but symbolic manipulation programs have predefined functions that compute roots of Bessel functions). A few zeros for Bessel functions of order $n = 0, 1, 2$ are listed in Table 10.3.

The first few natural frequencies are $\omega_{(1,0)} = 2.4048\sqrt{\rho h/R^2 T_0}$, $\omega_{(1,1)} = 3.8317\sqrt{\rho h/R^2 T_0}$, $\omega_{(1,2)} = 5.1356\sqrt{\rho h/R^2 T_0}$, and so on.

The mode shapes are $U_{(m,n)}(r,\theta) = AJ_n(r\omega_{(m,n)}\sqrt{\rho h/T_0})\sin(n\theta + \theta_0)$. Contour plots of the displacements for the first few vibration modes are shown in Figure 10.31.

Derivation

1. The equation that governs transverse motion of a membrane under equibiaxial tension was derived in Section 10.6.5 as

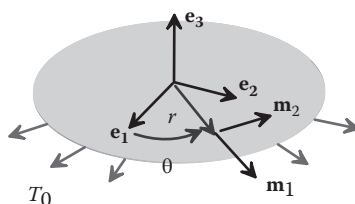


FIGURE 10.30 Vibrating stretched membrane.

TABLE 10.3 Roots of Bessel Functions of the First Kind

	J_0	J_1	J_2
$m = 1$	2.4048	3.8317	5.1356
$m = 2$	5.5201	7.0155	8.4172
$m = 3$	8.6537	10.1735	11.620

$$T_0 \left(\frac{\partial^2 u_3}{\partial r^2} + \frac{1}{r} \frac{\partial u_3}{\partial r} + \frac{1}{r^2} \frac{\partial^2 u_3}{\partial \theta^2} \right) = \rho h \frac{\partial^2 u_3}{\partial t^2}.$$

2. The general solution to this equation (which can be found by separation of variables or, if you are lazy, using a symbolic manipulation program) is

$$u_3(r, \theta) = (A J_n(k_{(m,n)} r) \sin(n\theta + \theta_0) + B Y_n(k_{(m,n)} r) \sin(n\theta + \theta_1)) \cos(\omega_{(m,n)} t + \phi),$$

where $k_{(m,n)} = \omega_{(m,n)} \sqrt{\rho h / T_0}$, $A, B, n, \theta_0, \theta_1, \phi$ are arbitrary constants, and J_n, Y_n are Bessel functions of the first and second kinds, with order n , respectively.

3. The solution must satisfy $u_3(\theta) = u_3(2\pi + \theta)$, which is only possible if n is an integer.
 4. The Bessel function of the second kind is infinite at $r = 0$, so $B = 0$.
 5. The transverse displacement must satisfy the boundary condition $u_3 = 0$ on the edge of the membrane, which leads to the condition $J_n(\omega_{(m,n)} R \sqrt{\rho h / T_0}) = 0$.

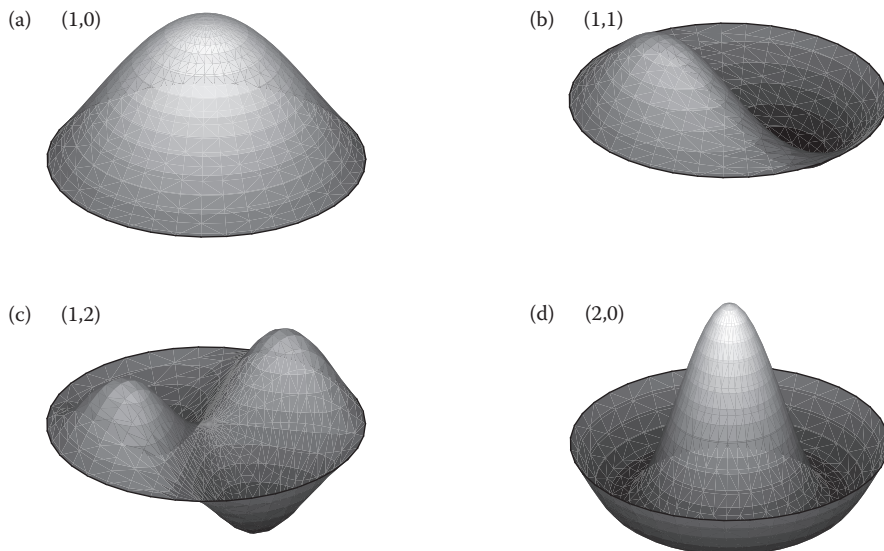


FIGURE 10.31 Mode shapes for a vibrating membrane: (a) Mode (1,0); (b) Mode (1,1); (c) Mode (1,2); and (d) Mode (2,0).

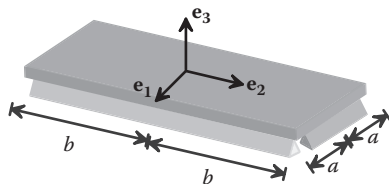


FIGURE 10.32 Vibrating flat rectangular plate.

10.7.3 Estimate for the Fundamental Frequency of Vibration of a Simply Supported Rectangular Flat Plate

Figure 10.32 shows an initially flat plate, which lies in the e_1, e_2 plane and is free of external force. The plate has Young's modulus E , mass density ρ , and thickness h . Its edges are simply supported. We want to calculate the lowest natural frequency of vibration for the plate.

The exact natural frequencies and modes of vibration for a rectangular plate are best calculated using a numerical method (e.g., finite elements). However, it is very straightforward to estimate the lowest natural frequency of vibration using the Rayleigh–Ritz method described in Section 5.9. The Rayleigh–Ritz method proceeds as follows:

1. Select a suitable estimate for the lowest-frequency mode of vibration, which must satisfy all displacement boundary conditions. For present purposes, the following mode shape is reasonable:

$$\hat{U}_3(x_1, x_2) = (x_1 - a)(x_1 + a)(x_2 - b)(x_2 + b) + C(x_1 - a)^2(x_1 + a)^2(x_2 - b)^2(x_2 + b)^2,$$

where C is a parameter that can be adjusted to obtain the best estimate for the natural frequency. More terms could be added to obtain a more accurate solution.

2. Calculate the kinetic energy measures

$$\hat{V} = \frac{Eh^3}{24(1-\nu^2)} \int_A \left((1-\nu) \frac{\partial^2 U_3}{\partial x_\alpha \partial x_\beta} \frac{\partial^2 U_3}{\partial x_\alpha \partial x_\beta} + \nu \left(\frac{\partial^2 U_3}{\partial x_\alpha \partial x_\alpha} \right)^2 \right) dA \quad \hat{T} = \int_A \left(\frac{h}{2} \rho U_3 \dot{U}_3 \right) dA.$$

3. The frequency is estimated as $\omega^2 \leq \hat{V} / \hat{T}$; we therefore need to choose C to minimize \hat{V} / \hat{T} . Although an exact formula can be calculated for the resulting upper bound to the natural frequency, the expression is very long and is best displayed graphically. Figure 10.33 shows the variation of normalized natural frequency as a function of the aspect ratio of the plate b/a . As a guide to the accuracy of the solution, an exact solution can be calculated for the natural frequency in the limit $b/a \rightarrow \infty$ (in this limit, the plate is a beam), following the procedure described in Section 10.4.1. The result is $12(1-\nu^2)\omega^2\rho a^4/Eh^2 = (\pi/2)^4$. It is clear that the Rayleigh–Ritz method gives an excellent estimate of the natural frequency in this limit.

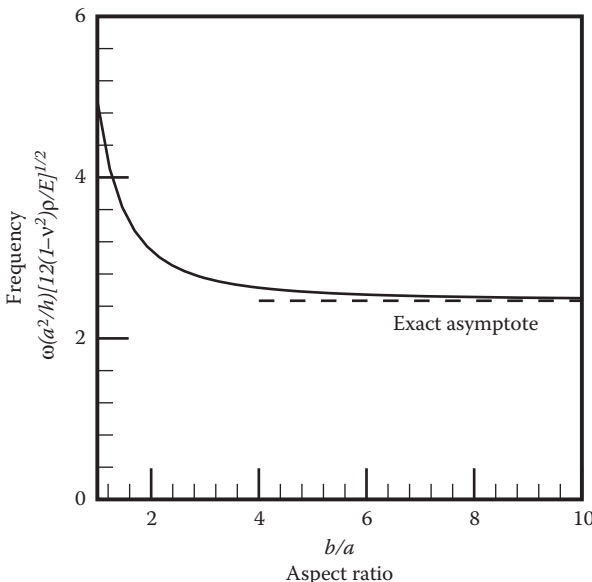


FIGURE 10.33 Estimated natural frequency of the plate shown in Figure 10.32 as a function of aspect ratio.

10.7.4 Bending Induced by Inelastic Strain in a Thin Film on a Substrate

Figure 10.34 illustrates the problem to be solved. A thin film, with Young's modulus E_f , Poisson's ratio ν_f , and thickness h_f , is deposited onto the surface of an initially flat, circular wafer, which has Young's modulus E_s , Poisson's ratio ν_s , radius R , and thickness h_s . An inelastic strain $\varepsilon_{11}^P = \varepsilon_{22}^P = \varepsilon_0$ is introduced into the film by some external process, which generates stresses in the film and also causes the substrate to bend. Provided the inelastic strain is not too large, the plate adopts a state of uniform curvature κ (its deformed shape can be visualized as a spherical cap, with large radius of curvature $1/\kappa$). Our goal is to relate the curvature κ to the inelastic strain ε_0 and to calculate the stress in the film. The results are important because stresses in thin films are often determined by measuring the curvature of the substrate.

The inelastic strain may be caused by a number of different processes, including the following:

1. A mismatch in thermal expansion between the film and the substrate. In this case, the inelastic strain is related to the thermal expansion coefficients α_f , α_s of the film and

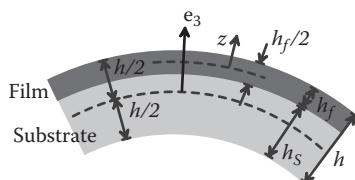


FIGURE 10.34 Thin film on a substrate.

substrate and the temperature T by $\varepsilon_0 = (\alpha_f - \alpha_s)(T - T_0)$, where T_0 is the temperature at which the system is stress free (many films are approximately free of stress at deposition temperature).

2. The film may grow epitaxially on the substrate, so that the spacing between atoms in the film is forced to match that of the substrate. In this case, the inelastic strain can be calculated as follows. Suppose that, in their stress-free states, the film and substrate have lattice spacing a_f and a_s , respectively. Then $\varepsilon_0 = (a_f - a_s)/a_s$.
3. Mismatch strain may develop in the film as a result of the deposition process.
4. Mismatch strain may be developed as a result of interdiffusion and possibly chemical reactions between the film and substrate.

Solution: The inelastic strain in the film is related to the curvature of the substrate by

$$\varepsilon_0 = \frac{\kappa h_s (1 + \rho^4 \eta^2 + 4\rho\eta + 4\rho\eta^3 + 6\rho^2\eta)}{6\rho\eta(1 + \rho)},$$

where $\rho = h_f/h_s$, and $\eta = E_f(1 - \nu_s)/(E_s(1 - \nu_f))$. Note that, with the sign convention adopted here, the substrate has a positive curvature if the film is on the convex side of the bent plate. The stress in the film is related to the curvature by

$$\sigma_{11} = \sigma_{22} = \frac{-\kappa E_s}{(1 - \nu_s)} \frac{[(1 + \rho^3\eta)h_s - 6\eta\rho z(1 + \rho)]}{6\rho(1 + \rho)},$$

where z is the distance above the midplane of the film. In most practical situations, the thickness of the substrate greatly exceeds the thickness of the film, in which case these results can be approximated by

$$\varepsilon_0 \approx \frac{\kappa h_s^2 E_s (1 - \nu_f)}{6h_f E_f (1 - \nu_s)} \quad \sigma_{11} = \sigma_{22} \approx \frac{-\kappa h_s^2 E_s}{6h_f (1 - \nu_s)}.$$

These are known as the *Stoney equations*.

Derivation: It is simplest to derive these results by using the general equations of shell theory to write down the potential energy of the bent plate and then calculating the values of midplane strain and curvature that minimize the potential energy. To this end, we do the following:

1. We consider the plate to consist of the film and substrate together, with combined thickness $h = h_f + h_s$. The midplane of the plate is at height $h/2$ above the base of the substrate.

2. We assume that the deformed plate has a small, uniform curvature $\kappa_{11} = \kappa_{22} = \kappa$, $\kappa_{12} = 0$ and midplane strain $\gamma_{11} = \gamma_{22} = \gamma$, $\gamma_{12} = 0$. As long as the curvature of the plate is small, the in-plane strain is a function only of the in-plane displacement components of the plate, whereas the curvature is a function only of the out-of-plane displacement (see Section 10.6.2). This means that γ and κ can be taken as independent variables that describe the deformed shape of the plate.
3. The total strain in the substrate follows as $\epsilon_{11} = \epsilon_{22} = \gamma + x_3 \kappa$, where x_3 is the distance from the midplane of the plate.
4. The stress in the substrate is proportional to the total strain. We assume that the plate is in a state of plane stress, so that the stress components in the substrate are

$$\sigma_{11} = \sigma_{22} = \frac{E_s}{(1-\nu_s)}(\gamma + x_3 \kappa).$$

The strain energy density in the substrate can then be calculated as

$$U_s = \frac{1}{2} \sigma_{ij} \epsilon_{ij} = \frac{E_s}{(1-\nu_s)} (\gamma + x_3 \kappa)^2.$$

5. In the film, the total strain includes contributions from an elastic distortion of the lattice, together with the inelastic strain, so $\epsilon_{ij} = \epsilon_{ij}^e + \epsilon_{ij}^p$. The stress in the film is proportional to the elastic strain $\epsilon_{ij}^e = \epsilon_{ij} - \epsilon_{ij}^p$. The nonzero components of elastic strain follow as $\epsilon_{11}^e = \epsilon_{22}^e = \gamma + x_3 \kappa - \epsilon_0$ and the stress in the film is $\sigma_{11} = \sigma_{22} = \frac{E_f}{(1-\nu_f)}(\gamma + x_3 \kappa - \epsilon_0)$. The strain energy density in the film is

$$U_f = \frac{1}{2} \sigma_{ij} \epsilon_{ij}^e = \frac{E_f}{(1-\nu_f)} (\gamma + x_3 \kappa - \epsilon_0)^2.$$

6. The total potential energy of the system is the integral of the strain energy density

$$V = \int_0^R \int_{-h/2}^{h/2-h_f} 2\pi r U_s dx_3 dr + \int_0^R \int_{h/2-h_f}^{h/2} 2\pi r U_f dx_3 dr.$$

The resulting expression is lengthy and will not be written out here.

7. Finally, the equilibrium values of γ and κ can be calculated from the condition that the potential energy must be a minimum, which requires that

$$\frac{\partial V}{\partial \kappa} = 0 \quad \frac{\partial V}{\partial \gamma} = 0.$$

Solving the resulting linear equations for γ and ϵ_0 in terms of κ gives the formula relating ϵ_0 and κ ; substituting the results into the formula for stress in step 5 and setting $x_3 = (h - h_f)/2 + z$ gives the formula for stress.

10.7.5 Bending of a Circular Plate Caused by a Through-Thickness Temperature Gradient

Figure 10.35 illustrates the problem to be solved. An initially flat, circular plate, which lies in the e_1, e_2 plane, is free of external force. The plate has Young's modulus E , thermal expansion coefficient α , radius R , and thickness h . Its edges are free. The plate is heated on one face and cooled on the other, so as to establish a temperature distribution $T = T_0 + \Delta T x_3/h$ through the thickness of the plate. Here, T_0 is the temperature of the midplane of the plate, whereas ΔT is the drop in temperature across the plate. The thermal expansion of the plate causes it to bend: our objective is to estimate the curvature of the plate as a function of the temperature gradient $\Delta T/h$. The solution will account for large out-of-plane deflections and will predict that the plate buckles when the temperature gradient reaches a critical value.

We will derive an approximate solution, by assuming that the curvature of the plate is uniform. Because we are interested in calculating the plate's shape after buckling, the solution is obtained by means of the von Karman theory described in Section 10.6.3. We denote the two principal curvatures of the deformed plate by κ_1, κ_2 . There are three possible equilibrium configurations, as follows:

1. For temperature gradients satisfying

$$\frac{\alpha \Delta T R^2 (1+\nu)^{3/2}}{4h^2} < 2,$$

the plate bends into a spherical cap shape, with two equal principal curvatures. The curvatures are related to the temperature gradient by

$$\frac{\alpha \Delta T R^2 (1+\nu)^{3/2}}{4h^2} = \bar{\kappa} (\bar{\kappa}^2 (1-\nu) + (1+\nu)) \quad \kappa_1 = \kappa_2 = \frac{4h\bar{\kappa}}{R^2\sqrt{1+\nu}}.$$

2. For temperature gradients

$$\frac{\alpha \Delta T R^2 (1+\nu)^{3/2}}{4h^2} > 2,$$

the solution 1 is still a possible equilibrium configuration but is unstable. There are infinitely many additional stable configurations, which have two unequal principal curvatures. One of these solutions can be related to the temperature gradient by

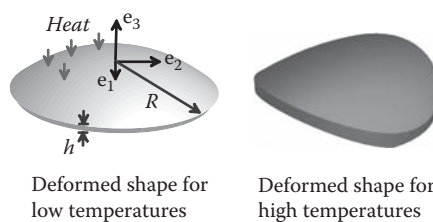


FIGURE 10.35 Pre-buckled and post-buckled shapes of a plate heated on one side.

$$\frac{\alpha\Delta TR^2(1+\nu)^{3/2}}{4h^2} = \frac{\hat{\kappa}^2 + 1}{\hat{\kappa}} \quad \kappa_1 = \frac{4h}{\hat{\kappa}R^2\sqrt{1+\nu}} \quad \kappa_2 = \frac{4h\hat{\kappa}}{R^2\sqrt{1+\nu}}.$$

The other solutions have the same principal curvatures, but the principal directions are different.

These results are displayed by plotting the normalized curvature $\kappa_1 R^2 \sqrt{1+\nu} / (4h)$ as a function of the dimensionless temperature gradient $\alpha\Delta TR^2(1+\nu)^{3/2} / (4h^2)$ in Figure 10.36, for a Poisson's ratio $\nu = 0.3$ (the graph is virtually identical for other values of ν). To visualize the significance of the graph, suppose that the temperature drop across the plate is gradually increased from zero. The plate will first deform with two equal principal curvatures, which are related to the temperature by the formula given in step 1. At the critical temperature, the plate will buckle and assume one of the two possible equilibrium configurations, with two unequal principal curvatures.

Derivation: The solution is derived by approximating the shape of the plate and selecting the deformed shape that minimizes the potential energy:

1. The displacement of the midplane of the plate will be approximated as

$$u_3 = \kappa_1 x_1^2/2 + \kappa_2 x_2^2/2 \quad u_1 = A_1 x_1 + A_2 x_1^3 + A_3 x_1 x_2^2 \quad u_2 = B_1 x_2 + B_2 x_2^3 + B_3 x_2 x_1^2,$$

where κ_1 and κ_2 are the two principal curvatures of the plate, and A_i, B_i are six adjustable parameters that must be selected to minimize the potential energy of the plate.

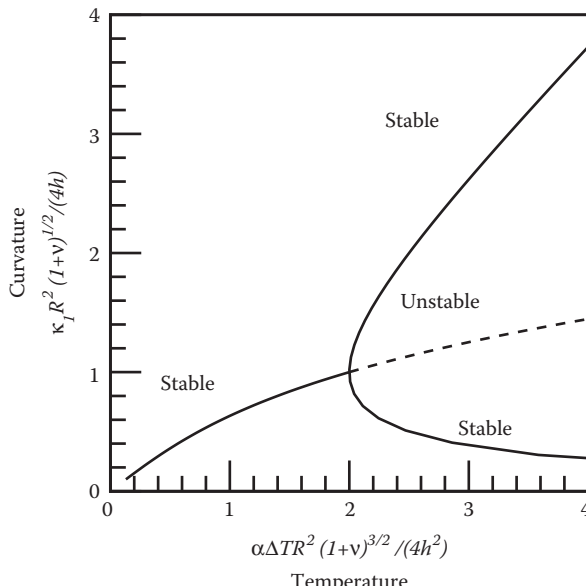


FIGURE 10.36 Curvature of the plate shown in Section 10.25 as a function of temperature gradient.

2. The total strain in the plate must be calculated using the von Karman formulas in Section 10.6.3, which yield

$$\varepsilon_{\alpha\beta} = \frac{1}{2} \left(\frac{\partial u_\alpha}{\partial x_\beta} + \frac{\partial u_\beta}{\partial x_\alpha} + \frac{\partial u_3}{\partial x_\alpha} \frac{\partial u_3}{\partial x_\beta} \right) + x_3 \kappa_{\alpha\beta} \Rightarrow \begin{cases} \varepsilon_{11} = A_1 + 3A_2x_1^2 + A_3x_2^2 + \kappa_1^2x_1^2/2 + x_3\kappa_1 \\ \varepsilon_{22} = B_1 + 3B_2x_2^2 + B_3x_1^2 + \kappa_2^2x_2^2/2 + x_3\kappa_2 \\ \varepsilon_{12} = (A_3 + B_3)x_1x_2 + \kappa_1\kappa_2x_1x_2/2. \end{cases}$$

3. The plate is assumed to be in a state of plane stress: the stress components can be calculated using the plane stress version of the linear elastic constitutive equations

$$\sigma_{\alpha\beta} = \frac{E}{1+\nu} \left\{ \varepsilon_{\alpha\beta} + \frac{\nu}{1-\nu} \varepsilon_{\gamma\gamma} \delta_{\alpha\beta} \right\} - \frac{E\alpha(T_0 + \Delta T x_3/h)}{1-\nu} \delta_{\alpha\beta}.$$

4. The strain energy density in the plate can be calculated using the formulas given in Section 3.1.7 as $U = ((1+\nu)\sigma_{\alpha\beta}\sigma_{\alpha\beta} - \nu\sigma_{\gamma\gamma}\sigma_{\alpha\alpha})/2E$. The result is lengthy and is best calculated using a symbolic manipulation program.
5. The total strain energy of the plate follows by integrating the strain energy density over the volume of the plate as

$$\Phi = \int_0^R \int_0^{2\pi} \int_{-h/2}^{h/2} U(r, \theta, x_3) dx_3 d\theta dr.$$

To evaluate the integral, the strain energy density can be expressed in polar coordinates by substituting $x_1 = r\cos\theta$, $x_2 = r\sin\theta$ into the results of step 4. Again, a symbolic manipulation program makes the algebra painless.

6. The coefficients A_i, B_i and the curvatures must now be determined by minimizing the potential energy Φ . To proceed, we first calculate the coefficients A_i, B_i in terms of the temperature gradient and curvature by solving the six simultaneous equations $\partial\Phi/\partial A_i = 0$ $\partial\Phi/\partial B_i = 0$. Substituting the resulting formulas for A_i, B_i back into the results of step 5 and using the two remaining conditions $\partial\Phi/\partial\kappa_1 = 0$ $\partial\Phi/\partial\kappa_2 = 0$ yields two equations for κ_1 and κ_2 :

$$\kappa_1\kappa_2^2(1-\nu^2)R^4 + 16h^2\kappa_1 + 16h^2\nu\kappa_2 - 16(1+\nu)\alpha\Delta Th = 0$$

$$\kappa_2\kappa_1^2(1-\nu^2)R^4 + 16h^2\kappa_2 + 16h^2\nu\kappa_1 - 16(1+\nu)\alpha\Delta Th = 0.$$

7. Eliminating the temperature from these equations and simplifying the result gives the expression

$$(\kappa_1 - \kappa_2)(\kappa_1\kappa_2 R^4(1 + \nu) - 16h^2) = 0.$$

This shows that there are two possible equilibrium configurations: in the first, $\kappa_1 = \kappa_2$; in the second, the two curvatures are related by $\kappa_1 R^4(1 + \nu) = 16h^2/\kappa_2$. Finally, these two possible relationships can be substituted back into either of the two equations in step 6 to relate the temperature gradient to the curvatures.

10.7.6 Buckling of a Cylindrical Shell Subjected to Axial Loading

Figure 10.37 illustrates a thin-walled cylinder, with radius a , height L , and wall thickness h . The shell is made from a linear elastic solid with Young's modulus E and Poisson's ratio ν . It is loaded in compression by subjecting its ends to a prescribed axial displacement Δ . We want to estimate the critical axial strain Δ/L or axial force P that will cause the cylinder to buckle.

We will derive an approximate solution, by assuming a shape for the buckled cylinder and calculating the shape that minimizes the potential energy of the system. Specifically, we assume that the radial displacement of the surface of the cylinder at the instant of buckling has the form $u_r = C + A \sin(\lambda \pi z/L)$. The solution shows the following:

1. Buckling occurs at a critical axial strain $\Delta/L = h/\left(\sqrt{3}a(1-\nu^2)\right)$.
2. The corresponding axial load is $P = 2\pi Eh^2/\left((1-\nu^2)\sqrt{3}\right)$.
3. The wavelength of the buckling mode is $L/\lambda = \pi\sqrt{ah}/(12)^{1/4}$. Note that the buckling mode describes the shape of the cylinder at the instant when buckling begins; it does not correspond to the shape of the cylinder after buckling.

The exact buckling strain and load are a factor $\sqrt{1-\nu^2}$ smaller than this approximate result.

Derivation: We must calculate, and then minimize, the potential energy of the cylinder. It is convenient to work through this problem using curvilinear coordinates. We shall use cylindrical-polar coordinates $\xi_1 \equiv z$, $\xi_2 \equiv \theta$ to identify a point on the midplane of the shell:

1. The position vector of a point in the undeformed shell is $\bar{\mathbf{r}} = a \cos \theta \mathbf{e}_1 + a \sin \theta \mathbf{e}_2 + z \mathbf{e}_3$.
2. The natural basis vectors for the undeformed shell are therefore

$$\bar{\mathbf{m}}_1 = \frac{\partial \bar{\mathbf{r}}}{\partial z} = \mathbf{e}_3 \quad \bar{\mathbf{m}}_2 = \frac{\partial \bar{\mathbf{r}}}{\partial \theta} = -a \sin \theta \mathbf{e}_1 + a \cos \theta \mathbf{e}_2 \quad \bar{\mathbf{m}}_3 = -(\cos \theta \mathbf{e}_1 + \sin \theta \mathbf{e}_2),$$

and the reciprocal basis vectors are $\bar{\mathbf{m}}^1 = \mathbf{e}_3$, $\bar{\mathbf{m}}^2 = (-\sin \theta \mathbf{e}_1 + \cos \theta \mathbf{e}_2)/a$, $\bar{\mathbf{m}}^3 = \bar{\mathbf{m}}_3$.

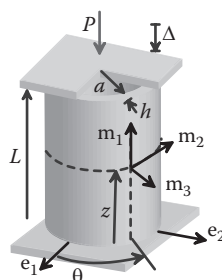


FIGURE 10.37 Cylindrical shell subjected to axial displacement.

3. The components of the metric tensor are $\bar{g}^{\alpha\beta} = \bar{\mathbf{m}}^\alpha \cdot \bar{\mathbf{m}}^\beta \Rightarrow \bar{g}^{11} = 1, \bar{g}^{12} = 0, \bar{g}^{22} = 1/a^2$.
 $\bar{g}_{\alpha\beta} = \bar{\mathbf{m}}_\alpha \cdot \bar{\mathbf{m}}_\beta \Rightarrow \bar{g}_{11} = 1, \bar{g}_{12} = 0, \bar{g}_{22} = a^2$.

4. The covariant components of the curvature tensor for the undeformed shell are

$$\bar{\kappa}_{\alpha\beta} = -\bar{\mathbf{m}}_3 \cdot \frac{\partial \bar{\mathbf{m}}_\alpha}{\partial \xi_\beta} \Rightarrow \bar{\kappa}_{11} = \bar{\kappa}_{12} = 0 \quad \bar{\kappa}_{22} = -a.$$

5. The position vector of the midplane of the deformed shell is approximated as

$$\mathbf{r} = (a + C + A \sin \lambda \pi z/L)(\cos \theta \mathbf{e}_1 + \sin \theta \mathbf{e}_2) + (1 - \Delta/L)z \mathbf{e}_3.$$

It will greatly simplify subsequent calculations to assume a priori that $\lambda \gg 1$.

6. The natural basis vectors for the deformed shell are therefore

$$\mathbf{m}_1 = \frac{\partial \mathbf{r}}{\partial z} = (A \lambda \pi / L) \sin \lambda \pi z / L (\cos \theta \mathbf{e}_1 + \sin \theta \mathbf{e}_2) + (1 - \Delta / L) \mathbf{e}_3$$

$$\mathbf{m}_2 = \frac{\partial \mathbf{r}}{\partial \theta} = (a + C + A \sin \lambda \pi z / L) (-\sin \theta \mathbf{e}_1 + \cos \theta \mathbf{e}_2)$$

$$\mathbf{m}_3 \approx (A \lambda \pi / L) \cos(\lambda \pi z / L) \mathbf{e}_3 - (\cos \theta \mathbf{e}_1 + \sin \theta \mathbf{e}_2).$$

7. The covariant components of the metric tensor and curvature for the deformed shell follow as

$$g_{\alpha\beta} = \mathbf{m}_\alpha \cdot \mathbf{m}_\beta \Rightarrow g_{11} = (\lambda \pi A / L)^2 \cos^2(\lambda \pi z / L) + (1 - \Delta / L)^2$$

$$g_{12} = 0 \quad g_{22} = (a + C + A \sin(\lambda \pi z / L))^2$$

$$\kappa_{\alpha\beta} = -\mathbf{m}_3 \cdot \frac{\partial \mathbf{m}_\alpha}{\partial \xi_\beta} \Rightarrow \kappa_{11} \approx (\lambda \pi / L)^2 A \sin(\lambda \pi z / L) \quad \kappa_{12} = 0$$

$$\kappa_{22} \approx -(a + C + A \sin(\lambda \pi z / L)).$$

8. The in-plane strain tensor and curvature change tensor may be approximated as

$$\gamma_{\alpha\beta} = (g_{\alpha\beta} - \bar{g}_{\alpha\beta})/2 \Rightarrow \gamma_{11} = -\Delta / L + (\lambda \pi A / L)^2 \cos^2(\lambda \pi z / L) / 2$$

$$\gamma_{12} = 0 \quad \gamma_{22} \approx aC + A \cos(\lambda \pi z / L)$$

$$\Delta \kappa_{\alpha\beta} = \kappa_{\alpha\beta} - \bar{\kappa}_{\alpha\beta} \bar{g}^\lambda g_\beta \Rightarrow \Delta \kappa_{11} \approx (\lambda \pi / L)^2 A \sin(\lambda \pi z / L) \quad \Delta \kappa_{12} = 0 \quad \Delta \kappa_{22} \approx 0.$$

9. The strain energy of the deformed shell can be calculated from

$$\Phi = \left(\int_A \frac{h}{2} D^{\alpha\beta\rho} \gamma_{\alpha\rho} \gamma_\beta + \frac{h^3}{24} D^{\alpha\beta\rho} \Delta \kappa_{\alpha\beta} \Delta \kappa_\rho \right) dA,$$

with

$$D^{\alpha\beta\rho} = \frac{E}{2(1-\nu^2)} \left((\bar{g}^{\alpha\rho} \bar{g}^\beta + \bar{g}^\alpha \bar{g}^{\beta\rho}) (1-\nu) + 2\nu \bar{g}^{\alpha\beta} \bar{g}^\rho \right).$$

Substituting for $\bar{g}^{\alpha\beta}$ and noting that $\gamma_{12} = \Delta\kappa_{12} = 0$ reduces this result to

$$\Phi = \frac{\pi a h E}{(1-\nu^2)} \int_0^L \left(\gamma_{11}^2 + \gamma_{22}^2/a^4 + 2\nu \gamma_{11} \gamma_{22}/a^2 \right) + \frac{h^2}{12} \left(\Delta\kappa_{11}^2 + \Delta\kappa_{22}^2/a^4 + 2\nu \Delta\kappa_{11} \Delta\kappa_{22}/a^2 \right).$$

10. The potential energy can be evaluated exactly, but the resulting expression is too long to write out in full. To proceed, we eliminate C by finding the value of C that minimizes the potential energy (set $\partial\Phi/\partial C=0$ and solve for C , then substitute the result back into Φ). For $\lambda \gg 1$, the resulting expression for Φ may be simplified to

$$\Phi \approx E\pi a h L \left(\frac{\Delta}{L} \right)^2 + \frac{\pi^2 E h a \lambda A^2}{4(1-\nu^2)L} \left(\phi_1 - \phi_2 \left(\frac{\Delta}{L} \right) \right) + O(A^4)$$

$$\phi_1 = \frac{\pi^3 \lambda^3 h^2}{6L^2} + \frac{2L^2}{\pi \lambda a^2} \quad \phi_2 = (1-\nu^2) 2\pi \lambda.$$

11. The buckling load can now be deduced from this result. Note that both $\phi_1 > 0$, $\phi_2 > 0$, so the potential energy is minimized with $A = 0$ (no buckling) if $\Delta/L < \phi_1/\phi_2$ and with $A > 0$ if $\Delta/L > \phi_1/\phi_2$. The critical axial strain for which buckling is first possible corresponds to the minimum value of ϕ_1/ϕ_2 with respect to λ . The minimum occurs for $\lambda = (12)^{1/4} L / (\pi \sqrt{ah})$, which gives a critical axial strain of $\Delta/L = h/(a(1-\nu^2)\sqrt{3})$.
12. The axial force at buckling can be computed trivially by noting that the cylinder is in a state of uniaxial axial stress. The axial force is therefore $2\pi a h E \Delta/L = 2\pi E h^2 / ((1-\nu^2)\sqrt{3})$.

10.7.7 Torsion of an Open-Walled Circular Cylinder

Figure 10.38 shows a thin-walled tube, with radius a and wall thickness h , which has been slit along a line parallel to its axis. The tube is made from a linear elastic solid with Young's modulus E and Poisson's ratio ν and is subjected to a twisting moment $\Lambda = \Lambda e_z$ parallel to its axis. The moment causes the end of the tube at $z = L$ to twist through an angle ϕ relative to the end at $z = 0$.

The displacement field and the internal forces in the shell can be expressed as components in a cylindrical-polar basis $\{e_r, e_\theta, e_z\}$ as follows:

$$\mathbf{u} = \frac{3\Lambda(1+\nu)}{\pi h^3 a E} (a\theta e_z + e_\theta) \quad \mathbf{T} = \frac{\Lambda}{4\pi a^2} e_z \otimes e_\theta \quad \mathbf{M} = \frac{\Lambda}{4\pi a} (e_z \otimes e_\theta + e_\theta \otimes e_z).$$

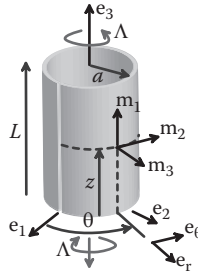


FIGURE 10.38 Open-walled circular cylinder subjected to torsional loading.

Note that this is one of the rare shell geometries for which the internal force tensor \mathbf{T} is not symmetric.

Derivation: We choose the cylindrical-polar coordinates $\xi_1 \equiv z$, $\xi_2 \equiv \theta$ as our coordinate system:

1. The position vector of a point in the undeformed shell is $\bar{\mathbf{r}} = a\cos\theta\mathbf{e}_1 + a\sin\theta\mathbf{e}_2 + z\mathbf{e}_3$.
2. The natural basis vectors for the undeformed shell are therefore

$$\bar{\mathbf{m}}_1 = \frac{\partial \bar{\mathbf{r}}}{\partial z} = \mathbf{e}_3 \quad \bar{\mathbf{m}}_2 = \frac{\partial \bar{\mathbf{r}}}{\partial \theta} = -a\sin\theta\mathbf{e}_1 + a\cos\theta\mathbf{e}_2 \quad \bar{\mathbf{m}}_3 = -(\cos\theta\mathbf{e}_1 + \sin\theta\mathbf{e}_2),$$

and the reciprocal basis vectors are $\bar{\mathbf{m}}^1 = \mathbf{e}_3$ $\bar{\mathbf{m}}^2 = (-\sin\theta\mathbf{e}_1 + \cos\theta\mathbf{e}_2)/a$ $\bar{\mathbf{m}}^3 = \bar{\mathbf{m}}_3$.

3. The components of the metric tensor are $\bar{g}^{\alpha\beta} = \bar{\mathbf{m}}^\alpha \cdot \bar{\mathbf{m}}^\beta$. $\bar{\mathbf{m}}^\beta \Rightarrow \bar{g}^{11} = 1$, $\bar{g}^{12} = 0$, $\bar{g}^{22} = 1/a^2$, $\bar{g}_{\alpha\beta} = \bar{\mathbf{m}}_\alpha \cdot \bar{\mathbf{m}}_\beta \Rightarrow \bar{g}_{11} = 1$, $\bar{g}_{12} = 0$, $\bar{g}_{22} = a^2$.
4. The covariant components of the curvature tensor for the undeformed shell are

$$\bar{\kappa}_{\alpha\beta} = -\bar{\mathbf{m}}_3 \cdot \frac{\partial \bar{\mathbf{m}}_\alpha}{\partial \xi_\beta} \Rightarrow \bar{\kappa}_{11} = \bar{\kappa}_{12} = 0 \quad \bar{\kappa}_{22} = -a$$

$$\bar{\kappa}_\beta^\alpha = \bar{\kappa}_{\beta\lambda} \bar{g}^{\alpha\lambda} \Rightarrow \bar{\kappa}_1^1 = \bar{\kappa}_1^2 = 0 \quad \bar{\kappa}_2^2 = -1/a.$$

5. The Christoffel symbols for the undeformed shell are $\bar{\Gamma}_{\beta\alpha}^\lambda = 0$.
6. To proceed, we assume that the internal stresses and moments in the cylinder are uniform; in addition, we assume small strains, so that the geometric terms in the equilibrium equations can be approximated using the geometry of the undeformed shell. The equilibrium equations therefore reduce to

$$V^2 = 0 \quad T^{22}a = 0 \quad -V^\beta = 0 \quad T^{12} - T^{21} + M^{21}/a = 0.$$

7. The boundary conditions on $\theta = 0$, $\theta = 2\pi$ are $T^{21} = 0$ $T^{22} - M^{22}/a = 0$ $M^{22} = 0$.

8. The boundary conditions on $z = 0, z = L$ are $T^{11} = 0 \quad T^{12} - M^{12}/a = P^2 \quad M^{11} = 0$.
9. The only nonzero components of internal force are the in-plane shear forces T^{12}, T^{21} and the twisting moments M^{12}, M^{21} . We therefore assume that the shell deforms in shear, so that the position vector of a point in the deformed shell is

$$\mathbf{r} = a\cos\theta\mathbf{e}_1 + a\sin\theta\mathbf{e}_2 + z\mathbf{e}_3 + Ca\theta\mathbf{e}_3 + (az\phi/L)(-\sin\theta\mathbf{e}_1 + \cos\theta\mathbf{e}_2).$$

10. The natural basis vectors for the deformed shell are

$$\begin{aligned}\mathbf{m}_1 &= \mathbf{e}_3 + (a\phi/L)(-\sin\theta\mathbf{e}_1 + \cos\theta\mathbf{e}_2) \\ \mathbf{m}_2 &= -a\sin\theta\mathbf{e}_1 + a\cos\theta\mathbf{e}_2 + Ca\mathbf{e}_3 - (z\phi a/L)(\cos\theta\mathbf{e}_1 + \sin\theta\mathbf{e}_2) \\ \mathbf{m}_3 &\approx -(\cos\theta\mathbf{e}_1 + \sin\theta\mathbf{e}_2) + (z\phi/L)(\sin\theta\mathbf{e}_1 - \cos\theta\mathbf{e}_2).\end{aligned}$$

11. The metric tensor for the deformed shell can be approximated by

$$g_{\alpha\beta} = \mathbf{m}_\alpha \cdot \mathbf{m}_\beta \Rightarrow g_{11} \approx 1 \quad g_{12} = Ca - (a^2\phi/L) \quad g_{22} \approx a^2.$$

12. The strain and curvature components follow as

$$\gamma_{11} = \gamma_{22} = 0, \quad \gamma_{12} = (Ca - (a^2\phi/L)/2, \quad \Delta\kappa_{11} = 0, \quad \Delta\kappa_{12} = (a\phi/L), \quad \Delta\kappa_{22} \approx 0.$$

13. The constitutive equations can be reduced to

$$\begin{aligned}T^{12} &= \frac{Eh}{(1+\nu)a^2} \gamma_{12} - \frac{Eh^3}{12(1+\nu)a^4} \gamma_{12} \quad T^{21} = \frac{Eh}{(1+\nu)a^2} \left(\gamma_{12} - \frac{h^2}{12a} \Delta\kappa_{12} \right) \\ M^{12} &= \frac{Eh^3}{12(1+\nu)a^2} \Delta\kappa_{12} \quad M^{21} = \frac{Eh^3}{12(1+\nu)a^2} (\Delta\kappa_{12} - \gamma_{12}/a).\end{aligned}$$

Note that this is one of the rare shell geometries for which the full coupled constitutive equations must be used.

14. The equations listed in steps 6–8, 12, and 13 can be solved to show that

$$C = (a\phi/L)(1 + h^2/12a^2),$$

$$T^{12} = \frac{Eh^3}{12(1+\nu)a^3} \frac{a\phi}{L} \left(1 - \frac{h^2}{12a^2} \right) \quad M^{12} = \frac{Eh^3}{12(1+\nu)a^2} \frac{a\phi}{L} \quad M^{21} = \frac{Eh^3}{12(1+\nu)a^2} \frac{a\phi}{L} \left(1 - \frac{h^2}{12a^2} \right).$$

15. The components of internal force and moment may be expressed in terms of cylindrical-polar coordinates by noting that $\mathbf{m}_1 = \mathbf{e}_z \quad \mathbf{m}_2 = a\mathbf{e}_\theta$, hence

$$\mathbf{T} = T^{\alpha\beta} \mathbf{m}_\alpha \otimes \mathbf{m}_\beta = aT^{12} \mathbf{e}_z \otimes \mathbf{e}_\theta$$

$$\mathbf{M} = M^{\alpha\beta} \mathbf{m}_\alpha \otimes \mathbf{m}_\beta = aM^{12} \mathbf{e}_z \otimes \mathbf{e}_\theta + aM^{21} \mathbf{e}_\theta \otimes \mathbf{e}_z.$$

16. Finally, external force and couple per unit length acting on the end of the cylinder at $z = L$ are $\mathbf{P} = \mathbf{e}_z \cdot \mathbf{T}$ $\mathbf{Q} = \mathbf{e}_z \cdot \mathbf{M}$. The resultant moment about the axis of the cylinder induced by these tractions is

$$\Lambda = \Lambda \mathbf{e}_z = \int_0^{2\pi} (\mathbf{a} \mathbf{e}_r \times \mathbf{P} + \mathbf{Q}) ad\theta = \frac{2\pi Eh^3}{12(1+\nu)} \frac{a\phi}{L} \left(2 - \frac{h^2}{12a^2} \right) \approx \frac{\pi Eh^3}{3(1+\nu)} \frac{a\phi}{L}.$$

It follows that the twist per unit length is related to the twisting moment by $\phi / L = 3\Lambda(1 + \nu) / (\pi ah^3 E)$. Substituting this result back into the formulas for \mathbf{T} and \mathbf{M} and neglecting the terms of order h^2/a^2 gives the result stated.

10.7.8 Membrane Shell Theory Analysis of a Spherical Dome under Gravitational Loading

Figure 10.39 shows a thin-walled, spherical dome with radius R , thickness h , and mass density ρ . We want to calculate the internal forces induced by gravitational loading of the structure. Shells that are used for structural applications are usually modeled using a simplified version of general shell theory, known as “membrane shell theory.” The theory simplifies the governing equations by neglecting internal moments, so that the structure is supported entirely by in-plane forces $T^{\alpha\beta}$. The theory is intended to be applied to masonry or concrete structures, which can generally support substantial (compressive) in-plane forces but are weak in bending. Of course, some bending resistance is critical to ensure stability against buckling; in addition, significant bending moments may develop near the edges of the structure if the boundary conditions constrain the rotation or transverse motion of the shell. So membrane theory must be used with caution.

The internal forces are best expressed as components in a spherical-polar basis of *unit vectors* $\{\mathbf{e}_R, \mathbf{e}_\phi, \mathbf{e}_\theta\}$ shown in Figure 10.39. The solution shows that the in-plane membrane forces are

$$\mathbf{T} = \rho gh \left(\frac{1}{(1+\cos\theta)} - \cos\theta \right) \mathbf{e}_\phi \otimes \mathbf{e}_\phi - \frac{\rho g h R}{(1+\cos\theta)} \mathbf{e}_\theta \otimes \mathbf{e}_\theta,$$

where g is the gravitational acceleration.

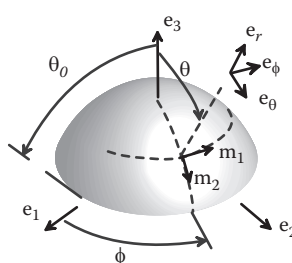


FIGURE 10.39 Spherical dome under gravitational loading.

A concrete dome should be designed so that the membrane forces are compressive everywhere. The solution shows that the hoop forces $T_{\theta\theta}$ are always compressive, but the circumferential forces $T_{\phi\phi}$ are compressive only if $\cos\theta > 1 / (1 + \cos\theta)$. The dome should therefore be designed with $\theta_0 < 51.8^\circ$.

Derivation: We adopt as curvilinear coordinates the spherical-polar coordinates (ϕ, θ) shown in Figure 10.39. Let $\{\mathbf{e}_1, \mathbf{e}_2, \mathbf{e}_3\}$ be the Cartesian basis that is used to provide reference directions for (ϕ, θ) as indicated in the figure:

1. The position vector of a point in the undeformed shell can be expressed as

$$\bar{\mathbf{r}} = R\cos\phi\sin\theta\mathbf{e}_1 + R\sin\phi\sin\theta\mathbf{e}_2 + R\cos\theta\mathbf{e}_3.$$
2. The natural basis vectors follow as

$$\bar{\mathbf{m}}_1 = \frac{\partial \bar{\mathbf{r}}}{\partial \phi} = -R\sin\phi\sin\theta\mathbf{e}_1 + R\cos\phi\sin\theta\mathbf{e}_2$$

$$\bar{\mathbf{m}}_2 = \frac{\partial \bar{\mathbf{r}}}{\partial \theta} = R\cos\phi\cos\theta\mathbf{e}_1 + R\sin\phi\cos\theta\mathbf{e}_2 - R\sin\theta\mathbf{e}_3$$

$$\bar{\mathbf{m}}_3 = -(\cos\phi\sin\theta\mathbf{e}_1 + \sin\phi\sin\theta\mathbf{e}_2 + \cos\theta\mathbf{e}_3).$$

3. The reciprocal base vectors are

$$\bar{\mathbf{m}}^1 = (-\sin\phi\mathbf{e}_1 + \cos\phi\mathbf{e}_2)/R\sin\theta$$

$$\bar{\mathbf{m}}^2 = (\cos\phi\cos\theta\mathbf{e}_1 + \sin\phi\cos\theta\mathbf{e}_2 - \sin\theta\mathbf{e}_3)/R$$

$$\bar{\mathbf{m}}^3 = -(\cos\phi\sin\theta\mathbf{e}_1 + \sin\phi\sin\theta\mathbf{e}_2 + \cos\theta\mathbf{e}_3)$$

4. The Christoffel symbols for the undeformed shell and its curvature components can be calculated as

$$\Gamma_{\beta\gamma}^\alpha = \bar{\mathbf{m}}^\alpha \cdot \frac{\partial^2 \bar{\mathbf{r}}}{\partial \xi_\beta \partial \xi_\gamma} \Rightarrow \bar{\Gamma}_{11}^1 = \bar{\Gamma}_{22}^1 = 0 \quad \bar{\Gamma}_{12}^1 = \bar{\Gamma}_{21}^1 = \frac{\cos\theta}{\sin\theta}$$

$$\bar{\Gamma}_{11}^2 = -\sin\theta\cos\theta \quad \bar{\Gamma}_{12}^2 = \bar{\Gamma}_{21}^2 = \bar{\Gamma}_{22}^2 = 0$$

$$\bar{\kappa}_{\alpha\beta} = -\bar{\mathbf{m}}^\alpha \cdot \frac{\partial \bar{\mathbf{m}}_\beta}{\partial \xi_\gamma} \Rightarrow \bar{\kappa}_{11} = -R\sin^2\theta \quad \bar{\kappa}_{12} = 0 \quad \bar{\kappa}_{22} = -R.$$

5. We now introduce two assumptions: (1) the bending resistance of the shell is zero, so that the internal moment components $M^{\alpha\beta} = 0$; (2) the deformations are small enough so that the Christoffel symbols and curvature terms in the equilibrium equations can be approximated using the values for the undeformed shell (this amounts to enforcing equilibrium in the undeformed configuration of the shell). In addition,

the shell is in static equilibrium, and the external couples are zero. The equations of motion of Section 10.5.8 can therefore be reduced to

$$\begin{aligned}\frac{\partial T^{\alpha\beta}}{\partial \xi_\alpha} + T^{\alpha\beta} \Gamma_{\alpha\gamma}^\gamma + T^{\alpha\gamma} \Gamma_{\gamma\alpha}^\beta + V^\alpha \kappa_\alpha^\beta + p^\beta &= 0 \\ \frac{\partial V^\alpha}{\partial \xi_\alpha} + V^\alpha \Gamma_{\alpha\beta}^\beta - T^{\alpha\beta} \kappa_{\alpha\beta} + p^3 &= 0 \quad V^\beta = 0 \quad T^{12} - T^{21} = 0.\end{aligned}$$

6. We note that $T^{12} = 0$ by symmetry, and the external force acting on unit area of the shell is $\mathbf{p} = -\rho g h \mathbf{e}_3 = p^i \mathbf{m}_i$. The contravariant components of \mathbf{p} can therefore be computed as $p^i = -\rho g h \mathbf{m}^i \cdot \mathbf{e}_3$. Substituting these, as well as the Christoffel symbols and curvature components reduces the equilibrium equations to

$$\begin{aligned}\frac{\partial T^{11}}{\partial \phi} &= 0 \quad \frac{\partial T^{22}}{\partial \theta} + T^{22} \frac{\cos \theta}{\sin \theta} - T^{11} \sin \theta \cos \theta + \frac{\rho g h}{R} \sin \theta &= 0 \\ T^{11} R \sin^2 \theta + T^{22} R + \rho g h \cos \theta &= 0.\end{aligned}$$

7. Eliminating T^{11} from the second and third equations gives

$$\frac{\partial T^{22}}{\partial \theta} + 2T^{22} \frac{\cos \theta}{\sin \theta} = \frac{\rho g h}{R \sin \theta}.$$

8. This equation can be integrated directly by substituting $T^{22} = \Psi / \sin^2 \theta$, with the solution

$$T^{22} = \frac{\rho g h}{R \sin^2 \theta} (\cos \theta - 1) + C = \frac{-\rho g h}{R(1 + \cos \theta)} + C,$$

where C is a constant of integration.

9. The constant of integration can be found using the boundary condition at the edge of the shell at $\theta = \theta_0$. The reaction force must act in the plane of the shell, and the vertical component of the force must balance the shell's weight so that the force per unit length is $\mathbf{P} = \rho g h R(1 - \cos \theta_0) \mathbf{e}_\theta / \sin^2 \theta_0$. The boundary condition requires that $\mathbf{e}_\theta \cdot \mathbf{T} = \mathbf{P}$ at $\theta = \theta_0$, which shows that $C = 0$.

10. T^{11} can be calculated from the third equation in step 6, giving

$$T^{11} = \frac{\rho g h (1 + \cos \theta)^{-1} - \cos \theta}{R \sin^2 \theta}.$$

11. Finally, the components of \mathbf{T} in the cylindrical-polar basis can be calculated by noting that $\mathbf{m}_1 = R \sin \theta \mathbf{e}_\phi$ $\mathbf{m}_2 = R \mathbf{e}_\theta$, whence

$$\mathbf{T} = T^{11} \mathbf{m}_1 \otimes \mathbf{m}_1 + T^{22} \mathbf{m}_2 \otimes \mathbf{m}_2 = T^{11} R^2 \sin^2 \theta \mathbf{e}_\phi \otimes \mathbf{e}_\phi + T^{22} R^2 \mathbf{e}_\theta \otimes \mathbf{e}_\theta.$$

Appendix A: Review of Vectors and Matrices

A.1 VECTORS

A.1.1 Definition

For the purposes of this text, a vector is an object that has magnitude and direction. Examples include forces, electric fields, and the normal to a surface. A vector is often represented pictorially as an arrow and symbolically by an underlined letter \underline{a} or using bold type \mathbf{a} . Its magnitude is denoted $|\underline{a}|$ or $|\mathbf{a}|$. There are two special cases of vectors: the *unit vector* \mathbf{n} has $|\mathbf{n}| = 1$, and the *null vector* $\mathbf{0}$ has $|\mathbf{0}| = 0$.

A.1.2 Vector Operations

Addition: Let \mathbf{a} and \mathbf{b} be vectors. Then $\mathbf{c} = \mathbf{a} + \mathbf{b}$ is also a vector. The vector \mathbf{c} may be shown diagrammatically by placing arrows representing \mathbf{a} and \mathbf{b} head to tail, as shown in Figure A.1.

Multiplication

1. Multiplication by a scalar: Let \mathbf{a} be a vector, and α a scalar. Then $\mathbf{b} = \alpha \mathbf{a}$ is a vector.

The direction of \mathbf{b} is parallel to \mathbf{a} , and its magnitude is given by $|\mathbf{b}| = |\alpha| |\mathbf{a}|$. Note that you can form a unit vector \mathbf{n} that is parallel to \mathbf{a} by setting $\mathbf{n} = \frac{\mathbf{a}}{|\mathbf{a}|}$.

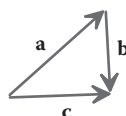


FIGURE A.1 Vector addition.

2. **Dot product (also called the scalar product):** Let \mathbf{a} and \mathbf{b} be two vectors. The dot product of \mathbf{a} and \mathbf{b} is a scalar denoted by $\alpha = \mathbf{a} \cdot \mathbf{b}$ and is defined by

$$\mathbf{a} \cdot \mathbf{b} = |\mathbf{a}| |\mathbf{b}| \cos \theta(\mathbf{a}, \mathbf{b}),$$

where $\theta(\mathbf{a}, \mathbf{b})$ is the angle subtended by \mathbf{a} and \mathbf{b} , as shown in Figure A.2. Note that $\mathbf{a} \cdot \mathbf{b} = \mathbf{b} \cdot \mathbf{a}$, and $\mathbf{a} \cdot \mathbf{a} = |\mathbf{a}|^2$. If $|\mathbf{a}| \neq 0$ and $|\mathbf{b}| \neq 0$, then $\mathbf{a} \cdot \mathbf{b} = 0$ if and only if $\cos \theta(\mathbf{a}, \mathbf{b}) = 0$, i.e. \mathbf{a} and \mathbf{b} are perpendicular.

3. **Cross product (also called the vector product):** Let \mathbf{a} and \mathbf{b} be two vectors. The cross product of \mathbf{a} and \mathbf{b} is a vector denoted by $\mathbf{c} = \mathbf{a} \times \mathbf{b}$. The direction of \mathbf{c} is perpendicular to \mathbf{a} and \mathbf{b} and is chosen so that $(\mathbf{a}, \mathbf{b}, \mathbf{c})$ form a right-handed triad (Figure A.3). The magnitude of \mathbf{c} is given by

$$|\mathbf{c}| = |\mathbf{a} \times \mathbf{b}| = |\mathbf{a}| |\mathbf{b}| \sin \theta(\mathbf{a}, \mathbf{b}).$$

Note that $\mathbf{a} \times \mathbf{b} = -\mathbf{b} \times \mathbf{a}$ and $\mathbf{a} \cdot (\mathbf{a} \times \mathbf{b}) = \mathbf{b} \cdot (\mathbf{a} \times \mathbf{b}) = 0$.

Some useful vector identities: Some useful vector identities include the following:

$$\begin{aligned}\mathbf{a} \cdot (\mathbf{b} \times \mathbf{c}) &= \mathbf{b} \cdot (\mathbf{c} \times \mathbf{a}) = \mathbf{c} \cdot (\mathbf{a} \times \mathbf{b}) \\ \mathbf{a} \times (\mathbf{b} \times \mathbf{c}) &= (\mathbf{a} \cdot \mathbf{c})\mathbf{b} - (\mathbf{a} \cdot \mathbf{b})\mathbf{c} \\ (\mathbf{a} \times \mathbf{b}) \times (\mathbf{c} \times \mathbf{d}) &= (\mathbf{a} \cdot \mathbf{c})(\mathbf{b} \cdot \mathbf{d}) - (\mathbf{b} \cdot \mathbf{c})(\mathbf{a} \cdot \mathbf{d}).\end{aligned}$$

A.1.3 Cartesian Components of Vectors

Let $(\mathbf{e}_1, \mathbf{e}_2, \mathbf{e}_3)$ be three mutually perpendicular unit vectors that form a right-handed triad (Figure A.4). Then $\{\mathbf{e}_1, \mathbf{e}_2, \mathbf{e}_3\}$ are said to form an *orthonormal basis*. The vectors satisfy

$$|\mathbf{e}_1| = |\mathbf{e}_2| = |\mathbf{e}_3| = 1 \quad \mathbf{e}_1 \times \mathbf{e}_2 = \mathbf{e}_3, \quad \mathbf{e}_1 \times \mathbf{e}_3 = -\mathbf{e}_2, \quad \mathbf{e}_2 \times \mathbf{e}_3 = \mathbf{e}_1.$$

We may express any vector \mathbf{a} as a suitable combination of the unit vectors \mathbf{e}_1 , \mathbf{e}_2 , and \mathbf{e}_3 . For example, we may write

$$\mathbf{a} = a_1 \mathbf{e}_1 + a_2 \mathbf{e}_2 + a_3 \mathbf{e}_3 = \sum_{i=1}^3 a_i \mathbf{e}_i,$$

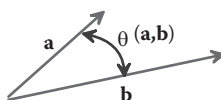


FIGURE A.2 Angle between two vectors.

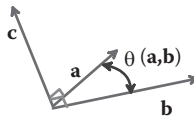


FIGURE A.3 Vector formed by the cross product of two vectors.

where (a_1, a_2, a_3) are scalars, called the *components* of \mathbf{a} in the basis $\{\mathbf{e}_1, \mathbf{e}_2, \mathbf{e}_3\}$. The components of \mathbf{a} have a simple physical interpretation. For example, if we evaluate the dot product $\mathbf{a} \cdot \mathbf{e}_1$, we find that

$$\mathbf{a} \cdot \mathbf{e}_1 = (a_1 \mathbf{e}_1 + a_2 \mathbf{e}_2 + a_3 \mathbf{e}_3) \cdot \mathbf{e}_1 = a_1$$

in view of the properties of the three vectors \mathbf{e}_1 , \mathbf{e}_2 , and \mathbf{e}_3 . Recall that

$$\mathbf{a} \cdot \mathbf{e}_1 = |\mathbf{a}| |\mathbf{e}_1| \cos \theta(\mathbf{a}, \mathbf{e}_1).$$

Then, noting that $|\mathbf{e}_1| = 1$, we have

$$a_1 = \mathbf{a} \cdot \mathbf{e}_1 = |\mathbf{a}| \cos \theta(\mathbf{a}, \mathbf{e}_1).$$

Thus, a_1 represents the projected length of the vector \mathbf{a} in the direction of \mathbf{e}_1 , as illustrated in Figure A.4. Similarly, a_2 and a_3 may be shown to represent the projection of \mathbf{a} in the directions \mathbf{e}_2 and \mathbf{e}_3 , respectively.

The advantage of representing vectors in a Cartesian basis is that vector addition and multiplication can be expressed as simple operations on the components of the vectors. For example, let \mathbf{a} , \mathbf{b} , and \mathbf{c} be vectors, with components (a_1, a_2, a_3) , (b_1, b_2, b_3) , and (c_1, c_2, c_3) , respectively. Then, it is straightforward to show that

$$\mathbf{c} = \mathbf{a} + \mathbf{b} \Leftrightarrow c_1 = a_1 + b_1; \quad c_2 = a_2 + b_2; \quad c_3 = a_3 + b_3$$

$$\mathbf{a} \cdot \mathbf{b} = \sum_{i=1}^3 a_i b_i$$

$$\mathbf{c} = \mathbf{a} \times \mathbf{b} \Leftrightarrow c_1 = a_2 b_3 - a_3 b_2; \quad c_2 = a_3 b_1 - a_1 b_3; \quad c_3 = a_1 b_2 - a_2 b_1.$$

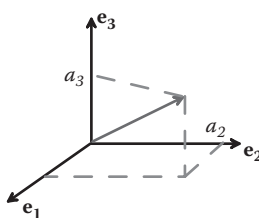


FIGURE A.4 Graphical interpretation of the components of a vector.

A.1.4 Change of Basis

Let \mathbf{a} be a vector, and let $\{\mathbf{e}_1, \mathbf{e}_2, \mathbf{e}_3\}$ be a Cartesian basis. Suppose that the components of \mathbf{a} in the basis $\{\mathbf{e}_1, \mathbf{e}_2, \mathbf{e}_3\}$ are known to be (a_1, a_2, a_3) . Now, suppose that we want to compute the components of \mathbf{a} in a second Cartesian basis, $\{\mathbf{m}_1, \mathbf{m}_2, \mathbf{m}_3\}$. This means that we want to find components $(\alpha_1, \alpha_2, \alpha_3)$, such that

$$\mathbf{a} = \alpha_1 \mathbf{m}_1 + \alpha_2 \mathbf{m}_2 + \alpha_3 \mathbf{m}_3.$$

To do so, note that

$$\begin{aligned}\alpha_1 &= \mathbf{a} \cdot \mathbf{m}_1 = a_1 \mathbf{e}_1 \cdot \mathbf{m}_1 + a_2 \mathbf{e}_2 \cdot \mathbf{m}_1 + a_3 \mathbf{e}_3 \cdot \mathbf{m}_1 \\ \alpha_2 &= \mathbf{a} \cdot \mathbf{m}_2 = a_1 \mathbf{e}_1 \cdot \mathbf{m}_2 + a_2 \mathbf{e}_2 \cdot \mathbf{m}_2 + a_3 \mathbf{e}_3 \cdot \mathbf{m}_2 \\ \alpha_3 &= \mathbf{a} \cdot \mathbf{m}_3 = a_1 \mathbf{e}_1 \cdot \mathbf{m}_3 + a_2 \mathbf{e}_2 \cdot \mathbf{m}_3 + a_3 \mathbf{e}_3 \cdot \mathbf{m}_3.\end{aligned}$$

This transformation is conveniently written as a matrix operation

$$[\alpha] = [Q][a],$$

where $[\alpha]$ is a matrix consisting of the components of \mathbf{a} in the basis $\{\mathbf{m}_1, \mathbf{m}_2, \mathbf{m}_3\}$, $[a]$ is a matrix consisting of the components of \mathbf{a} in the basis $\{\mathbf{e}_1, \mathbf{e}_2, \mathbf{e}_3\}$, and $[Q]$ is a “rotation matrix” as follows:

$$[\alpha] = \begin{bmatrix} \alpha_1 \\ \alpha_2 \\ \alpha_3 \end{bmatrix} \quad [a] = \begin{bmatrix} a_1 \\ a_2 \\ a_3 \end{bmatrix} \quad [Q] = \begin{bmatrix} \mathbf{m}_1 \cdot \mathbf{e}_1 & \mathbf{m}_1 \cdot \mathbf{e}_2 & \mathbf{m}_1 \cdot \mathbf{e}_3 \\ \mathbf{m}_2 \cdot \mathbf{e}_1 & \mathbf{m}_2 \cdot \mathbf{e}_2 & \mathbf{m}_2 \cdot \mathbf{e}_3 \\ \mathbf{m}_3 \cdot \mathbf{e}_1 & \mathbf{m}_3 \cdot \mathbf{e}_2 & \mathbf{m}_3 \cdot \mathbf{e}_3 \end{bmatrix}.$$

Note that the elements of $[Q]$ have a simple physical interpretation. For example, $\mathbf{m}_1 \cdot \mathbf{e}_1 = \cos \theta(\mathbf{m}_1, \mathbf{e}_1)$, where $\theta(\mathbf{m}_1, \mathbf{e}_1)$ is the angle between the \mathbf{m}_1 and \mathbf{e}_1 axes. Similarly $\mathbf{m}_1 \cdot \mathbf{e}_2 = \cos \theta(\mathbf{m}_1, \mathbf{e}_2)$, where $\theta(\mathbf{m}_1, \mathbf{e}_2)$ is the angle between the \mathbf{m}_1 and \mathbf{e}_2 axes. In practice, we usually know the angles between the axes that make up the two bases, so it is simplest to assemble the elements of $[Q]$ by putting the cosines of the known angles in the appropriate places.

Index notation provides another convenient way to write this transformation:

$$\alpha_i = Q_{ij} a_j, \quad Q_{ij} = \mathbf{m}_i \cdot \mathbf{e}_j.$$

You don't need to know index notation in detail to understand this; all you need to know is that

$$Q_{ij} a_j \equiv \sum_{j=1}^3 Q_{ij} a_j.$$

The same approach may be used to find an expression for a_i in terms of α_i . If you work through the details, you will find that

$$\begin{bmatrix} a_1 \\ a_2 \\ a_3 \end{bmatrix} = \begin{bmatrix} \mathbf{m}_1 \cdot \mathbf{e}_1 & \mathbf{m}_2 \cdot \mathbf{e}_1 & \mathbf{m}_3 \cdot \mathbf{e}_1 \\ \mathbf{m}_1 \cdot \mathbf{e}_2 & \mathbf{m}_2 \cdot \mathbf{e}_2 & \mathbf{m}_3 \cdot \mathbf{e}_2 \\ \mathbf{m}_1 \cdot \mathbf{e}_3 & \mathbf{m}_2 \cdot \mathbf{e}_3 & \mathbf{m}_3 \cdot \mathbf{e}_3 \end{bmatrix} \begin{bmatrix} \alpha_1 \\ \alpha_2 \\ \alpha_3 \end{bmatrix}.$$

Comparing this result with the formula for α_i in terms of a_i , we see that

$$[a] = [Q]^T [\alpha],$$

where the superscript T denotes the transpose (rows and columns interchanged). The transformation matrix $[Q]$ is therefore *orthogonal* and satisfies

$$[Q]^{-1} = [Q]^T \quad [Q][Q]^T = [Q]^T [Q] = [I],$$

where $[I]$ is the identity matrix.

A.1.5 Useful Vector Operations

Calculating areas: The area of a triangle bounded by vectors \mathbf{a} , \mathbf{b} , and $\mathbf{b} - \mathbf{a}$ is

$$A = \frac{1}{2} |\mathbf{a} \times \mathbf{b}|.$$

The area of the parallelogram shown in Figure A.5 is $2A$.

Calculating angles: The angle between two vectors \mathbf{a} and \mathbf{b} is

$$\theta = \cos^{-1}(\mathbf{a} \cdot \mathbf{b} / |\mathbf{a}| |\mathbf{b}|).$$

Calculating the normal to a surface: If two vectors \mathbf{a} and \mathbf{b} can be found that are known to lie in the surface, then the unit normal to the surface is

$$\mathbf{n} = \pm \frac{\mathbf{a} \times \mathbf{b}}{|\mathbf{a} \times \mathbf{b}|}.$$

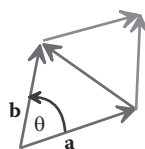


FIGURE A.5 Triangle and parallelogram formed by two vectors.

If the surface is specified by a parametric equation of the form $\mathbf{r} = \mathbf{r}(s, t)$, where s and t are two parameters and \mathbf{r} is the position vector of a point on the surface, then two vectors that lie in the plane may be computed from

$$\mathbf{a} = \frac{\partial \mathbf{r}}{\partial s}, \quad \mathbf{b} = \frac{\partial \mathbf{r}}{\partial t}.$$

Calculating volumes: The volume of the parallelopiped defined by three vectors \mathbf{a} , \mathbf{b} , and \mathbf{c} as shown in Figure A.6 is

$$V = |\mathbf{c} \cdot (\mathbf{a} \times \mathbf{b})|.$$

The volume of the tetrahedron is $V/6$.

A.2 VECTOR FIELDS AND VECTOR CALCULUS

A.2.1 Scalar Field

Let $\{\mathbf{e}_1, \mathbf{e}_2, \mathbf{e}_3\}$ be a Cartesian basis with origin O in 3D space. Let

$$\mathbf{r} = x_1 \mathbf{e}_1 + x_2 \mathbf{e}_2 + x_3 \mathbf{e}_3$$

denote the position vector of a point in space. A *scalar field* is a scalar-valued function of position in space. A scalar field is a function of the components of the position vector and so may be expressed as $\phi(x_1, x_2, x_3)$. The value of ϕ at a particular point in space must be independent of the choice of basis vectors. A scalar field may be a function of time (and possibly other parameters) as well as position in space.

A.2.2 Vector Field

Let $\{\mathbf{e}_1, \mathbf{e}_2, \mathbf{e}_3\}$ be a Cartesian basis with origin O in 3D space. Let

$$\mathbf{r} = x_1 \mathbf{e}_1 + x_2 \mathbf{e}_2 + x_3 \mathbf{e}_3$$

denote the position vector of a point in space. A *vector field* is a vector-valued function of position in space. A vector field is a function of the components of the position vector and

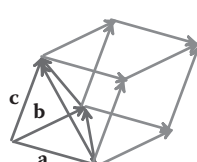


FIGURE A.6 Tetrahedron and parallelopiped formed by three vectors.

so may be expressed as $\mathbf{v}(x_1, x_2, x_3)$. The vector may also be expressed as components in the basis $\{\mathbf{e}_1, \mathbf{e}_2, \mathbf{e}_3\}$:

$$\mathbf{v}(x_1, x_2, x_3) = v_1(x_1, x_2, x_3)\mathbf{e}_1 + v_2(x_1, x_2, x_3)\mathbf{e}_2 + v_3(x_1, x_2, x_3)\mathbf{e}_3.$$

The magnitude and direction of \mathbf{v} at a particular point in space is independent of the choice of basis vectors. A vector field may be a function of time (and possibly other parameters) as well as position in space.

A.2.3 Change of Basis for Scalar Fields

Let $\{\mathbf{e}_1, \mathbf{e}_2, \mathbf{e}_3\}$ be a Cartesian basis with origin O in 3D space (Figure A.7). Express the position vector of a point relative to O in $\{\mathbf{e}_1, \mathbf{e}_2, \mathbf{e}_3\}$ as

$$\mathbf{r} = x_1\mathbf{e}_1 + x_2\mathbf{e}_2 + x_3\mathbf{e}_3$$

and let $\phi(x_1, x_2, x_3)$ be a scalar field.

Let $\{\mathbf{m}_1, \mathbf{m}_2, \mathbf{m}_3\}$ be a second Cartesian basis, with origin P. Let $\mathbf{c} \equiv \overrightarrow{OP}$ denote the position vector of P relative to O. Express the position vector of a point relative to P in $\{\mathbf{m}_1, \mathbf{m}_2, \mathbf{m}_3\}$ as

$$\mathbf{p} = \xi_1\mathbf{m}_1 + \xi_2\mathbf{m}_2 + \xi_3\mathbf{m}_3.$$

To find $\phi(\xi_1, \xi_2, \xi_3)$, use the following procedure. First, express \mathbf{p} as components in the basis $\{\mathbf{e}_1, \mathbf{e}_2, \mathbf{e}_3\}$, using the procedure outlined in Section 1.4:

$$\mathbf{p} = p_1\mathbf{e}_1 + p_2\mathbf{e}_2 + p_3\mathbf{e}_3,$$

where

$$\begin{aligned} p_1 &= \xi_1\mathbf{e}_1 \cdot \mathbf{m}_1 + \xi_2\mathbf{e}_1 \cdot \mathbf{m}_2 + \xi_3\mathbf{e}_1 \cdot \mathbf{m}_3 \\ p_2 &= \xi_1\mathbf{e}_2 \cdot \mathbf{m}_1 + \xi_2\mathbf{e}_2 \cdot \mathbf{m}_2 + \xi_3\mathbf{e}_2 \cdot \mathbf{m}_3 \\ p_3 &= \xi_1\mathbf{e}_3 \cdot \mathbf{m}_1 + \xi_2\mathbf{e}_3 \cdot \mathbf{m}_2 + \xi_3\mathbf{e}_3 \cdot \mathbf{m}_3 \end{aligned}$$

or, using index notation,

$$p_i = Q_{ji} \xi_j,$$

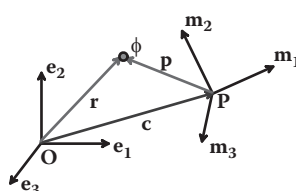


FIGURE A.7 Two Cartesian bases with different origin and orientation.

where the transformation matrix Q_{ij} is defined in Section 1.4. Now, express \mathbf{c} as components in $\{\mathbf{e}_1, \mathbf{e}_2, \mathbf{e}_3\}$ and note that

$$\begin{aligned}\mathbf{r} &= \mathbf{p} + \mathbf{c} \\ \Rightarrow x_1\mathbf{e}_1 + x_2\mathbf{e}_2 + x_3\mathbf{e}_3 &= p_1\mathbf{e}_1 + p_2\mathbf{e}_2 + p_3\mathbf{e}_3 + c_1\mathbf{e}_1 + c_2\mathbf{e}_2 + c_3\mathbf{e}_3 \\ \Rightarrow x_1 = p_1 + c_1, \quad x_2 = p_2 + c_2, \quad x_3 = p_3 + c_3 \\ \Rightarrow x_i &= Q_{ji}\xi_j + c_i\end{aligned}$$

so that

$$\begin{aligned}\phi(x_1, x_2, x_3) &= \phi(p_1 + c_1, p_2 + c_2, p_3 + c_3) \\ &= \phi(Q_{j1}\xi_j + c_1, Q_{j2}\xi_j + c_2, Q_{j3}\xi_j + c_3).\end{aligned}$$

A.2.4 Change of Basis for Vector Fields

Let $\{\mathbf{e}_1, \mathbf{e}_2, \mathbf{e}_3\}$ be a Cartesian basis with origin O in 3D space (Figure A.7). Express the position vector of a point relative to O in $\{\mathbf{e}_1, \mathbf{e}_2, \mathbf{e}_3\}$ as

$$\mathbf{r} = x_1\mathbf{e}_1 + x_2\mathbf{e}_2 + x_3\mathbf{e}_3$$

and let $\mathbf{v}(x_1, x_2, x_3)$ be a vector field, with components

$$\mathbf{v}(x_1, x_2, x_3) = v_1(x_1, x_2, x_3)\mathbf{e}_1 + v_2(x_1, x_2, x_3)\mathbf{e}_2 + v_3(x_1, x_2, x_3)\mathbf{e}_3.$$

Let $\{\mathbf{m}_1, \mathbf{m}_2, \mathbf{m}_3\}$ be a second Cartesian basis, with origin P. Let $\mathbf{c} \equiv \overline{OP}$ denote the position vector of P relative to O. Express the position vector of a point relative to P in $\{\mathbf{m}_1, \mathbf{m}_2, \mathbf{m}_3\}$ as

$$\mathbf{p} = \xi_1\mathbf{m}_1 + \xi_2\mathbf{m}_2 + \xi_3\mathbf{m}_3.$$

To express the vector field as components in $\{\mathbf{m}_1, \mathbf{m}_2, \mathbf{m}_3\}$ and as a function of the components of \mathbf{p} , use the following procedure. First, express (v_1, v_2, v_3) in terms of (ξ_1, ξ_2, ξ_3) using the procedure outlined for scalar fields in the preceding section:

$$\begin{aligned}v_k(x_1, x_2, x_3) &= v_k(p_1 + c_1, p_2 + c_2, p_3 + c_3) \\ &= v_k(Q_{j1}\xi_j + c_1, Q_{j2}\xi_j + c_2, Q_{j3}\xi_j + c_3)\end{aligned}$$

for $k = 1, 2, 3$. Now, find the components of \mathbf{v} in $\{\mathbf{m}_1, \mathbf{m}_2, \mathbf{m}_3\}$ using the procedure outlined in Section A.1.4. Using index notation, the result is

$$\begin{aligned}\mathbf{v} &= Q_{1i}v_i(Q_{j1}\xi_j + c_1, Q_{j2}\xi_j + c_2, Q_{j3}\xi_j + c_3)\mathbf{e}_1 \\ &\quad + Q_{2i}v_i(Q_{j1}\xi_j + c_1, Q_{j2}\xi_j + c_2, Q_{j3}\xi_j + c_3)\mathbf{e}_2 \\ &\quad + Q_{3i}v_i(Q_{j1}\xi_j + c_1, Q_{j2}\xi_j + c_2, Q_{j3}\xi_j + c_3)\mathbf{e}_3.\end{aligned}$$

A.2.5 Time Derivatives of Vectors

Let $\mathbf{a}(t)$ be a vector whose magnitude and direction vary with time, t . Suppose that $\{\mathbf{i}, \mathbf{j}, \mathbf{k}\}$ is a *fixed* basis, i.e. independent of time. We may express $\mathbf{a}(t)$ in terms of components (a_x, a_y, a_z) in the basis $\{\mathbf{i}, \mathbf{j}, \mathbf{k}\}$ as

$$\mathbf{a}(t) = a_x \mathbf{i} + a_y \mathbf{j} + a_z \mathbf{k}.$$

The *time derivative* of \mathbf{a} is defined using the usual rules of calculus

$$\dot{\mathbf{a}}(t) = \frac{d}{dt} \mathbf{a}(t) = \lim_{\epsilon \rightarrow 0} \frac{\mathbf{a}(t + \epsilon) - \mathbf{a}(t)}{\epsilon},$$

or in component form as

$$\dot{\mathbf{a}}(t) = \dot{a}_x \mathbf{i} + \dot{a}_y \mathbf{j} + \dot{a}_z \mathbf{k}.$$

The definition of the time derivative of a vector may be used to show the following rules

$$\begin{aligned} \frac{d}{dt} [\alpha(t) \mathbf{a}(t)] &= \dot{\alpha}(t) \mathbf{a}(t) + \alpha(t) \dot{\mathbf{a}}(t) \\ \frac{d}{dt} [\mathbf{a}(t) \cdot \mathbf{b}(t)] &= \dot{\mathbf{a}}(t) \cdot \mathbf{b}(t) + \mathbf{a}(t) \cdot \dot{\mathbf{b}}(t) \\ \frac{d}{dt} [\mathbf{a}(t) \times \mathbf{b}(t)] &= \dot{\mathbf{a}}(t) \times \mathbf{b}(t) + \mathbf{a}(t) \times \dot{\mathbf{b}}(t). \end{aligned}$$

A.2.6 Using a Rotating Basis

It is often convenient to express position vectors as components in a basis that rotates with time. To write equations of motion, one must evaluate time derivatives of rotating vectors. Let $\{\mathbf{e}_1, \mathbf{e}_2, \mathbf{e}_3\}$ be a basis that rotates with instantaneous angular velocity $\boldsymbol{\Omega}$. Then,

$$\frac{d\mathbf{e}_1}{dt} = \boldsymbol{\Omega} \times \mathbf{e}_1, \quad \frac{d\mathbf{e}_2}{dt} = \boldsymbol{\Omega} \times \mathbf{e}_2, \quad \frac{d\mathbf{e}_3}{dt} = \boldsymbol{\Omega} \times \mathbf{e}_3.$$

A.2.7 Gradient of a Scalar Field

Let ϕ be a scalar field in 3D space. The gradient of ϕ is a vector field denoted by $\text{grad } (\phi)$ or $\phi \nabla$ and is defined so that

$$(\phi \nabla) \cdot \mathbf{a} = \lim_{\epsilon \rightarrow 0} \frac{\phi(\mathbf{r} + \epsilon \mathbf{a}) - \phi(\mathbf{r})}{\epsilon}$$

for every position \mathbf{r} in space and for every vector \mathbf{a} . Let $\{\mathbf{e}_1, \mathbf{e}_2, \mathbf{e}_3\}$ be a Cartesian basis with origin O in 3D space. Let

$$\mathbf{r} = x_1 \mathbf{e}_1 + x_2 \mathbf{e}_2 + x_3 \mathbf{e}_3$$

denote the position vector of a point in space. Express ϕ as a function of the components of \mathbf{r} as $\phi = \phi(x_1, x_2, x_3)$. The gradient of ϕ in this basis is then given by

$$\phi \nabla = \frac{\partial \phi}{\partial x_1} \mathbf{e}_1 + \frac{\partial \phi}{\partial x_2} \mathbf{e}_2 + \frac{\partial \phi}{\partial x_3} \mathbf{e}_3.$$

A.2.8 Gradient of a Vector Field

Let \mathbf{v} be a vector field in 3D space. The gradient of \mathbf{v} is a tensor field denoted by $\text{grad}(\mathbf{v})$ or $\mathbf{v} \otimes \nabla$ and is defined so that

$$(\mathbf{v} \otimes \nabla) \cdot \mathbf{a} = \lim_{\epsilon \rightarrow 0} \frac{\mathbf{v}(\mathbf{r} + \epsilon \mathbf{a}) - \mathbf{v}(\mathbf{r})}{\epsilon}$$

for every position \mathbf{r} in space and for every vector \mathbf{a} . Let $\{\mathbf{e}_1, \mathbf{e}_2, \mathbf{e}_3\}$ be a Cartesian basis with origin O in 3D space. Let

$$\mathbf{r} = x_1 \mathbf{e}_1 + x_2 \mathbf{e}_2 + x_3 \mathbf{e}_3$$

denote the position vector of a point in space. Express \mathbf{v} as a function of the components of \mathbf{r} , so that $\mathbf{v} = \mathbf{v}(x_1, x_2, x_3)$. The gradient of \mathbf{v} in this basis is then given by

$$\mathbf{v} \otimes \nabla = \begin{bmatrix} \frac{\partial v_1}{\partial x_1} & \frac{\partial v_1}{\partial x_2} & \frac{\partial v_1}{\partial x_3} \\ \frac{\partial v_2}{\partial x_1} & \frac{\partial v_2}{\partial x_2} & \frac{\partial v_2}{\partial x_3} \\ \frac{\partial v_3}{\partial x_1} & \frac{\partial v_3}{\partial x_2} & \frac{\partial v_3}{\partial x_3} \end{bmatrix}.$$

Alternatively, in index notation,

$$[\mathbf{v} \otimes \nabla]_{ij} \equiv \frac{\partial v_i}{\partial x_j}.$$

A.2.9 Divergence of a Vector Field

Let \mathbf{v} be a vector field in 3D space. The divergence of \mathbf{v} is a scalar field denoted by $\text{div}(\mathbf{v})$ or $\nabla \cdot \mathbf{v}$. Formally, it is defined as $\text{trace}(\text{grad}(\mathbf{v}))$ (the trace of a tensor is the sum of its diagonal terms). Let $\{\mathbf{e}_1, \mathbf{e}_2, \mathbf{e}_3\}$ be a Cartesian basis with origin O in 3D space. Let

$$\mathbf{r} = x_1 \mathbf{e}_1 + x_2 \mathbf{e}_2 + x_3 \mathbf{e}_3$$

denote the position vector of a point in space. Express \mathbf{v} as a function of the components of \mathbf{r} as $\mathbf{v} = \mathbf{v}(x_1, x_2, x_3)$. The divergence of \mathbf{v} is then

$$\operatorname{div}(\mathbf{v}) = \frac{\partial v_1}{\partial x_1} + \frac{\partial v_2}{\partial x_2} + \frac{\partial v_3}{\partial x_3}.$$

A.2.10 Curl of a Vector Field

Let \mathbf{v} be a vector field in 3D space. The curl of \mathbf{v} is a vector field denoted by $\operatorname{curl}(\mathbf{v})$ or $\nabla \times \mathbf{v}$. It is best defined in terms of its components in a given basis, although its magnitude and direction are not dependent on the choice of basis.

Let $\{\mathbf{e}_1, \mathbf{e}_2, \mathbf{e}_3\}$ be a Cartesian basis with origin O in 3D space. Let

$$\mathbf{r} = x_1 \mathbf{e}_1 + x_2 \mathbf{e}_2 + x_3 \mathbf{e}_3$$

denote the position vector of a point in space. Express \mathbf{v} as a function of the components of \mathbf{r} as $\mathbf{v} = \mathbf{v}(x_1, x_2, x_3)$. The curl of \mathbf{v} in this basis is then given by

$$\nabla \times \mathbf{v} = \begin{vmatrix} \mathbf{e}_1 & \mathbf{e}_2 & \mathbf{e}_3 \\ \frac{\partial}{\partial x_1} & \frac{\partial}{\partial x_2} & \frac{\partial}{\partial x_3} \\ v_1 & v_2 & v_3 \end{vmatrix} = \left(\frac{\partial v_3}{\partial x_2} - \frac{\partial v_2}{\partial x_3} \right) \mathbf{e}_1 + \left(\frac{\partial v_1}{\partial x_3} - \frac{\partial v_3}{\partial x_1} \right) \mathbf{e}_2 + \left(\frac{\partial v_2}{\partial x_1} - \frac{\partial v_1}{\partial x_2} \right) \mathbf{e}_3$$

Using index notation, this may be expressed as

$$[\nabla \times \mathbf{v}]_i = \epsilon_{ijk} \frac{\partial v_j}{\partial x_k}.$$

A.2.11 The Divergence Theorem

Let V be a closed region in 3D space, bounded by an orientable surface S . Let \mathbf{n} denote the unit vector normal to S , taken so that \mathbf{n} points out of V as shown in Figure A.8. Let \mathbf{u} be a vector field that is continuous and has continuous first partial derivatives in some domain containing V . Then

$$\int_V \operatorname{div}(\mathbf{u}) dV = \int_S \mathbf{u} \cdot \mathbf{n} dA,$$

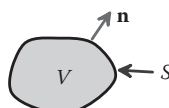


FIGURE A.8 Volume bounded by a surface.

or alternatively, expressed in index notation

$$\int_V \frac{\partial u_i}{\partial x_i} dV = \int_S u_i n_i dA.$$

For a proof of this extremely useful theorem consult, see Kreyzig [1998].

A.3 MATRICES

A.3.1 Definition

An $(n \times m)$ matrix $[A]$ is a set of numbers, arranged in m rows and n columns

$$[A] = \begin{bmatrix} a_{11} & a_{12} & a_{13} & \cdots & a_{1n} \\ a_{21} & a_{22} & a_{23} & \cdots & a_{2n} \\ \vdots & \vdots & \vdots & \ddots & \vdots \\ a_{m1} & a_{m2} & a_{m3} & \cdots & a_{mn} \end{bmatrix}$$

- A *square matrix* has equal numbers of rows and columns.
- A *diagonal matrix* is a square matrix with elements such that $a_{ij} = 0$ for $i \neq j$.
- The *identity matrix* $[I]$ is a diagonal matrix for which all diagonal elements $a_{ii} = 1$.
- A *symmetric matrix* is a square matrix with elements such that $a_{ij} = a_{ji}$.
- A *skew symmetric matrix* is a square matrix with elements such that $a_{ij} = -a_{ji}$.

A.3.2 Matrix Operations

Addition: Let $[A]$ and $[B]$ be two matrices of order $(m \times n)$ with elements a_{ij} and b_{ij} . Then

$$[C] = [A] + [B] \Leftrightarrow c_{ij} = a_{ij} + b_{ij}.$$

Multiplication by a scalar: Let $[A]$ be a matrix with elements a_{ij} , and let k be a scalar. Then

$$[B] = k[A] \Leftrightarrow b_{ij} = ka_{ij}$$

Multiplication by a matrix: Let $[A]$ be a matrix of order $(m \times n)$ with elements a_{ij} , and let $[B]$ be a matrix of order $(p \times q)$ with elements b_{ij} . The product $[C] = [A][B]$ is defined only if $n = p$, and is an $(m \times q)$ matrix such that

$$[C] = [A][B] \Leftrightarrow c_{ij} = \sum_{k=1}^n a_{ik} b_{kj}$$

Note that multiplication is distributive and associative, but not commutative, i.e.,

$$[A]([B] + [C]) = [A][B] + [A][C] \quad [A]([B][C]) = ([A][B])[C] \quad [A][B] \neq [B][A]$$

The multiplication of a vector by a matrix is a particularly important operation. Let \mathbf{b} and \mathbf{c} be two vectors with n components, which we think of as $(1 \times n)$ matrices. Let $[A]$ be an $(m \times n)$ matrix. Thus

$$\mathbf{b} = \begin{bmatrix} b_1 \\ b_2 \\ b_3 \\ \vdots \\ b_n \end{bmatrix} \quad \mathbf{c} = \begin{bmatrix} c_1 \\ c_2 \\ c_3 \\ \vdots \\ c_n \end{bmatrix} \quad [A] = \begin{bmatrix} a_{11} & a_{12} & a_{13} & \cdots & a_{1n} \\ a_{21} & a_{22} & a_{23} & \cdots & a_{2n} \\ \vdots & \vdots & \vdots & \ddots & \vdots \\ a_{m1} & a_{m2} & a_{m3} & \cdots & a_{mn} \end{bmatrix}$$

Now,

$$\mathbf{c} = [A]\mathbf{b} \Leftrightarrow c_i = \sum_{j=1}^n a_{ij} b_j$$

i.e.,

$$\begin{aligned} c_1 &= a_{11}b_1 + a_{12}b_2 + a_{13}b_3 + \cdots + a_{1n}b_n \\ c_2 &= a_{21}b_1 + a_{22}b_2 + a_{23}b_3 + \cdots + a_{2n}b_n \\ &\vdots \\ c_m &= a_{m1}b_1 + a_{m2}b_2 + a_{m3}b_3 + \cdots + a_{mn}b_n \end{aligned}$$

Transpose: Let $[A]$ be a matrix of order $(m \times n)$ with elements a_{ij} . The transpose of $[A]$ is denoted $[A]^T$. If $[B]$ is an $(n \times m)$ matrix such that $[B] = [A]^T$, then $b_{ij} = a_{ji}$, i.e.,

$$[A]^T = \begin{bmatrix} a_{11} & a_{12} & a_{13} & \cdots & a_{1n} \\ a_{21} & a_{22} & a_{23} & \cdots & a_{2n} \\ \vdots & \vdots & \vdots & \ddots & \vdots \\ a_{m1} & a_{m2} & a_{m3} & \cdots & a_{mn} \end{bmatrix}^T = \begin{bmatrix} a_{11} & a_{21} & a_{31} & \cdots & a_{n1} \\ a_{12} & a_{22} & a_{32} & \cdots & a_{n2} \\ \vdots & \vdots & \vdots & \ddots & \vdots \\ a_{1m} & a_{2m} & a_{3m} & \cdots & a_{nm} \end{bmatrix}$$

Note that

$$([A][B])^T = [B]^T[A]^T$$

Determinant: The determinant is defined only for a square matrix. Let $[A]$ be a (2×2) matrix with components a_{ij} . The determinant of $[A]$ is denoted by $\det[A]$ or $|A|$ and is given by

$$|A| = \begin{vmatrix} a_{11} & a_{12} \\ a_{21} & a_{22} \end{vmatrix} = a_{11}a_{22} - a_{12}a_{21}$$

Now, let $[A]$ be an $(n \times n)$ matrix. Define the *minors* M_{ij} of $[A]$ as the determinant formed by omitting the i th row and j th column of $[A]$. For example, the minors M_{11} and M_{12} for a (3×3) matrix are computed as follows. Let

$$[A] = \begin{bmatrix} a_{11} & a_{12} & a_{13} \\ a_{21} & a_{22} & a_{23} \\ a_{31} & a_{32} & a_{33} \end{bmatrix}$$

Then

$$M_{11} = \begin{vmatrix} a_{22} & a_{23} \\ a_{32} & a_{33} \end{vmatrix} = a_{22}a_{33} - a_{32}a_{23} \quad M_{12} = \begin{vmatrix} a_{21} & a_{23} \\ a_{31} & a_{33} \end{vmatrix} = a_{21}a_{33} - a_{31}a_{23}$$

Define the *cofactors* C_{ij} of $[A]$ as

$$C_{ij} = (-1)^{i+j} M_{ij}$$

Then, the determinant of the $(n \times n)$ matrix $[A]$ is computed as follows

$$|A| = \sum_{j=1}^n a_{ij} C_{ij}$$

The result is the same whichever row i is chosen for the expansion. For the particular case of a (3×3) matrix

$$\det[A] = \det \begin{bmatrix} a_{11} & a_{12} & a_{13} \\ a_{21} & a_{22} & a_{23} \\ a_{31} & a_{32} & a_{33} \end{bmatrix} = a_{11}(a_{22}a_{33} - a_{23}a_{32}) + a_{12}(a_{23}a_{31} - a_{21}a_{33}) + a_{13}(a_{21}a_{32} - a_{22}a_{31})$$

The determinant may also be evaluated by summing over rows, i.e.,

$$|A| = \sum_{i=1}^n a_{ij} C_{ij}$$

and as before the result is the same for each choice of column j . Finally, note that

$$\det[A]^T = \det[A] \quad \det([A][B]) = \det[A]\det[B]$$

Inversion: Let $[A]$ be an $(n \times n)$ matrix. The inverse of $[A]$ is denoted by $[A]^{-1}$ and is defined such that

$$[A]^{-1} [A] = [I]$$

The inverse of $[A]$ exists if and only if $\det[A] \neq 0$. A matrix which has no inverse is said to be *singular*. The inverse of a matrix may be computed explicitly, by forming the *cofactor matrix* $[C]$ with components c_{ij} as defined in the preceding section. Then

$$[A]^{-1} = \frac{1}{\det[A]} [C]^T$$

In practice, it is faster to compute the inverse of a matrix using methods such as Gaussian elimination. Note that

$$([A][B])^{-1} = [B]^{-1}[A]^{-1}$$

For a *diagonal matrix*, the inverse is

$$[A] = \begin{bmatrix} a_{11} & 0 & 0 & \cdots & 0 \\ 0 & a_{22} & 0 & \cdots & 0 \\ \vdots & \vdots & \vdots & \ddots & \vdots \\ 0 & 0 & 0 & \cdots & a_{nn} \end{bmatrix} = \begin{bmatrix} 1/a_{11} & 0 & 0 & \cdots & 0 \\ 0 & 1/a_{22} & 0 & \cdots & 0 \\ \vdots & \vdots & \vdots & \ddots & \vdots \\ 0 & 0 & 0 & \cdots & 1/a_{nn} \end{bmatrix}$$

For a (2×2) matrix, the inverse is

$$\begin{bmatrix} a_{11} & a_{12} \\ a_{21} & a_{22} \end{bmatrix} = \frac{1}{a_{11}a_{22} - a_{12}a_{21}} \begin{bmatrix} a_{22} & -a_{12} \\ -a_{21} & a_{11} \end{bmatrix}$$

Eigenvalues and eigenvectors: Let $[A]$ be an $(n \times n)$ matrix, with coefficients a_{ij} . Consider the vector equation

$$[A]\mathbf{x} = \lambda\mathbf{x}$$

where \mathbf{x} is a vector with n components, and λ is a scalar (which may be complex).

The n nonzero vectors \mathbf{x} and corresponding scalars λ that satisfy this equation are the eigenvectors and eigenvalues of $[A]$.

Formally, eigenvalues and eigenvectors may be computed as follows. Rearrange the preceding equation to

$$([A] - \lambda[I])\mathbf{x} = 0.$$

This has nontrivial solutions for \mathbf{x} only if the determinant of the matrix $([A] - \lambda[I])$ vanishes. The equation

$$\det([A] - \lambda[I]) = 0$$

is an n th order polynomial that may be solved for λ . In general, the polynomial will have n roots, which may be complex. The eigenvectors may then be computed by finding \mathbf{x} satisfying $([A] - \lambda[I])\mathbf{x} = 0$. For example, a (2×2) matrix generally has two eigenvectors, which satisfies

$$|[A] - \lambda[I]| = \begin{vmatrix} a_{11} - \lambda & a_{12} \\ a_{21} & a_{22} - \lambda \end{vmatrix} = (a_{11} - \lambda)(a_{22} - \lambda) - a_{12}a_{21} = 0.$$

Solve the quadratic equation to see that

$$\begin{aligned}\lambda_1 &= \frac{1}{2}(a_{11} + a_{22}) - \frac{1}{2}\left\{(a_{11} + a_{22})^2 - 4(a_{11}a_{22} - a_{12}a_{21})\right\}^{1/2} \\ \lambda_2 &= \frac{1}{2}(a_{11} + a_{22}) + \frac{1}{2}\left\{(a_{11} + a_{22})^2 - 4(a_{11}a_{22} - a_{12}a_{21})\right\}^{1/2}\end{aligned}$$

The two corresponding eigenvectors may be computed from (2), which shows that

$$\begin{bmatrix} a_{11} - \lambda_i & a_{12} \\ a_{21} & a_{22} - \lambda_i \end{bmatrix} \begin{bmatrix} x_1^{(i)} \\ x_2^{(i)} \end{bmatrix} = 0,$$

so that multiplying out the first row of the matrix (You can use the second row, too, if you want; because we chose λ to make the determinant of the matrix vanish, the two equations have the same solutions. In fact, if $a_{12} = 0$, you will need to do this, because the first equation will simply give $0 = 0$ when trying to solve for one of the eigenvectors.):

$$\begin{aligned}\left(\frac{1}{2}(a_{11} - a_{22}) + \frac{1}{2}\left\{(a_{11} + a_{22})^2 - 4(a_{11}a_{22} - a_{12}a_{21})\right\}^{1/2}\right)x_1^{(1)} + a_{12}x_2^{(1)} &= 0 \\ \left(\frac{1}{2}(a_{11} - a_{22}) - \frac{1}{2}\left\{(a_{11} + a_{22})^2 - 4(a_{11}a_{22} - a_{12}a_{21})\right\}^{1/2}\right)x_1^{(2)} + a_{12}x_2^{(2)} &= 0,\end{aligned}$$

which are satisfied by any vector of the form

$$\mathbf{x}^{(2)} = \begin{bmatrix} 2a_{12} \\ (a_{11} - a_{22}) + \left\{ (a_{11} + a_{22})^2 - 4(a_{11}a_{22} - a_{12}a_{21}) \right\}^{1/2} \end{bmatrix} p$$

$$\mathbf{x}^{(2)} = \begin{bmatrix} 2a_{12} \\ (a_{11} - a_{22}) - \left\{ (a_{11} + a_{22})^2 - 4(a_{11}a_{22} - a_{12}a_{21}) \right\}^{1/2} \end{bmatrix} q$$

where p and q are arbitrary real numbers.

It is often convenient to *normalize* eigenvectors so that they have unit “length.” For this purpose, choose p and q so that $\sum_n x_i x_i = 1$. (For vectors of dimension n , the generalized dot product is defined such that $\mathbf{x} \cdot \mathbf{x} = \sum_{i=1}^n x_i x_i$.)

You can calculate explicit expressions for eigenvalues and eigenvectors for any matrix up to order (4×4) , but the results are so cumbersome that, except for the (2×2) results, they are virtually useless. In practice, numerical values may be computed using several iterative techniques. Symbolic manipulation programs make calculations like this easy.

The eigenvalues of a real symmetric matrix are always real, and its eigenvectors are *orthogonal*, i.e. the i th and j th eigenvectors (with $i \neq j$) satisfy $\mathbf{x}^{(i)} \cdot \mathbf{x}^{(j)} = 0$. The eigenvalues of a skew symmetric matrix are pure imaginary.

Spectral and singular value decomposition: Let $[A]$ be a real symmetric $(n \times n)$ matrix. Denote the n (real) eigenvalues of $[A]$ by λ_i , and let $\mathbf{w}^{(i)}$ be the corresponding *normalized* eigenvectors, such that $\mathbf{w}^{(i)} \cdot \mathbf{w}^{(i)} = 1$. Then, for any arbitrary vector \mathbf{b} ,

$$[A]\mathbf{b} = \sum_{i=1}^n \lambda_i (\mathbf{w}^{(i)} \cdot \mathbf{b}) \mathbf{w}^{(i)}.$$

Let $[\Lambda]$ be a diagonal matrix that contains the n eigenvalues of $[A]$ as elements of the diagonal, and let $[Q]$ be a matrix consisting of the n eigenvectors as columns, i.e.,

$$[\Lambda] = \begin{bmatrix} \lambda_1 & 0 & 0 & \cdots & 0 \\ 0 & \lambda_2 & 0 & \cdots & 0 \\ \vdots & \vdots & \vdots & \ddots & \vdots \\ 0 & 0 & 0 & \cdots & \lambda_n \end{bmatrix} \quad [Q] = \begin{bmatrix} \mathbf{w}_1^{(1)} & \mathbf{w}_1^{(2)} & \mathbf{w}_1^{(3)} & \cdots & \mathbf{w}_1^{(n)} \\ \mathbf{w}_2^{(1)} & \mathbf{w}_2^{(2)} & \mathbf{w}_2^{(3)} & \cdots & \mathbf{w}_2^{(n)} \\ \vdots & \vdots & \vdots & \ddots & \vdots \\ \mathbf{w}_n^{(1)} & \mathbf{w}_n^{(2)} & \mathbf{w}_n^{(3)} & \cdots & \mathbf{w}_n^{(n)} \end{bmatrix}.$$

Then,

$$[A] = [Q][\Lambda][Q]^T \quad [Q]^T[Q] = [Q][Q]^T = [I] \quad [Q]^T[A][Q] = [\Lambda].$$

Note that this gives another (generally quite useless) way to invert $[A]$:

$$[A]^{-1} = [Q][\Lambda]^{-1}[Q]^T,$$

where $[\Lambda]^{-1}$ is easy to compute because $[\Lambda]$ is diagonal.

Square root of a matrix: Let $[A]$ be a real symmetric $(n \times n)$ matrix. Denote the singular value decomposition of $[A]$ by $[A] = [Q][\Lambda][Q]^T$ as defined above. Suppose that $[S] = [A]^{1/2}$ denotes the square root of $[A]$, defined so that

$$[S][S] = [A].$$

One way to compute $[S]$ is through the singular value decomposition of $[A]$

$$[S] = [Q][\Lambda]^{1/2}[Q]^T,$$

where

$$[\Lambda]^{1/2} = \begin{bmatrix} \sqrt{\lambda_1} & 0 & 0 & \cdots & 0 \\ 0 & \sqrt{\lambda_2} & 0 & \cdots & 0 \\ \vdots & \vdots & \vdots & \ddots & \vdots \\ 0 & 0 & 0 & \cdots & \sqrt{\lambda_n} \end{bmatrix}.$$

Appendix B: Introduction to Tensors and Their Properties

B.1 BASIC PROPERTIES OF TENSORS

B.1.1 Examples of Tensors

The gradient of a vector field is a good example of a tensor. Visualize a vector field: at every point in space, the field has a vector value $\mathbf{u}(x_1, x_2, x_3)$. Let $\mathbf{G} = \mathbf{u} \otimes \nabla$ represent the gradient of \mathbf{u} . By definition, \mathbf{G} enables you to calculate the change in \mathbf{u} when you move from a point \mathbf{x} in space to a nearby point at $\mathbf{x} + d\mathbf{x}$:

$$d\mathbf{u} = \mathbf{G} \cdot d\mathbf{x},$$

where \mathbf{G} is a second-order tensor. From this example, we see that, when you multiply a vector by a tensor, the result is another vector. This is a general property of all second-order tensors. A tensor is a linear mapping of a vector onto another vector. Two examples, together with the vectors on which they operate, are as follows.

The stress tensor: In

$$\mathbf{t} = \mathbf{n} \cdot \boldsymbol{\sigma},$$

\mathbf{n} is a unit vector normal to a surface, $\boldsymbol{\sigma}$ is the stress tensor, and \mathbf{t} is the traction vector acting on the surface.

The deformation gradient tensor: In

$$d\mathbf{w} = \mathbf{F} \cdot d\mathbf{x},$$

$d\mathbf{x}$ is an infinitesimal line element in an undeformed solid, and $d\mathbf{w}$ is the vector representing the deformed line element.

B.1.2 Matrix Representation of a Tensor

To evaluate and manipulate tensors, we express them as *components in a basis*, just as for vectors. We can use the displacement gradient to illustrate how this is done. Let $\mathbf{u}(x_1, x_2, x_3)$ be a vector field and let $\mathbf{G} = \mathbf{u} \otimes \nabla$ represent the gradient of \mathbf{u} . Recall the definition of \mathbf{G}

$$d\mathbf{u} = \mathbf{G} \cdot d\mathbf{x}.$$

Now, let $\{\mathbf{e}_1, \mathbf{e}_2, \mathbf{e}_3\}$ be a Cartesian basis and express both $d\mathbf{u}$ and $d\mathbf{x}$ as components. Then, calculate the components of $d\mathbf{u}$ in terms of $d\mathbf{x}$ using the usual rules of calculus:

$$\begin{aligned} du_1 &= \frac{\partial u_1}{\partial x_1} dx_1 + \frac{\partial u_1}{\partial x_2} dx_2 + \frac{\partial u_1}{\partial x_3} dx_3 \\ du_2 &= \frac{\partial u_2}{\partial x_1} dx_1 + \frac{\partial u_2}{\partial x_2} dx_2 + \frac{\partial u_2}{\partial x_3} dx_3. \\ du_3 &= \frac{\partial u_3}{\partial x_1} dx_1 + \frac{\partial u_3}{\partial x_2} dx_2 + \frac{\partial u_3}{\partial x_3} dx_3 \end{aligned}$$

We could represent this as a matrix product:

$$\begin{bmatrix} du_1 \\ du_2 \\ du_3 \end{bmatrix} = \begin{bmatrix} \frac{\partial u_1}{\partial x_1} & \frac{\partial u_1}{\partial x_2} & \frac{\partial u_1}{\partial x_3} \\ \frac{\partial u_2}{\partial x_1} & \frac{\partial u_2}{\partial x_2} & \frac{\partial u_2}{\partial x_3} \\ \frac{\partial u_3}{\partial x_1} & \frac{\partial u_3}{\partial x_2} & \frac{\partial u_3}{\partial x_3} \end{bmatrix} \begin{bmatrix} dx_1 \\ dx_2 \\ dx_3 \end{bmatrix}.$$

From this, we see that \mathbf{G} can be represented as a 3×3 matrix. The elements of the matrix are known as the components of \mathbf{G} in the basis $\{\mathbf{e}_1, \mathbf{e}_2, \mathbf{e}_3\}$. All second-order tensors can be represented in this form. For example, a general second-order tensor \mathbf{S} could be written as

$$\mathbf{S} \equiv \begin{bmatrix} S_{11} & S_{12} & S_{13} \\ S_{21} & S_{22} & S_{23} \\ S_{31} & S_{32} & S_{33} \end{bmatrix}.$$

You have probably already seen the matrix representation of stress and strain components in introductory courses.

Because \mathbf{S} can be represented as a matrix, all operations that can be performed on a 3×3 matrix can also be performed on \mathbf{S} . Examples include sums and products, the transpose, inverse, and determinant. One can also compute eigenvalues and eigenvectors for tensors and thus define the log of a tensor, the square root of a tensor, etc. These tensor operations are summarized below.

Note that the numbers $S_{11}, S_{12}, \dots, S_{33}$ depend on the basis $\{\mathbf{e}_1, \mathbf{e}_2, \mathbf{e}_3\}$, just as the components of a vector depend on the basis used to represent the vector. However, just as the magnitude and direction of a vector are independent of the basis, so the properties of a tensor are independent of the basis. That is to say, if \mathbf{S} is a tensor and \mathbf{u} is a vector, then the vector $\mathbf{v} = \mathbf{S} \cdot \mathbf{u}$ has the same magnitude and direction, irrespective of the basis used to represent \mathbf{u} , \mathbf{v} , and \mathbf{S} .

B.1.3 The Difference between a Matrix and a Tensor

If a tensor is a matrix, why is a matrix not the same thing as a tensor? Well, although you can multiply the three components of a vector \mathbf{u} by any 3×3 matrix,

$$\begin{bmatrix} b_1 \\ b_2 \\ b_3 \end{bmatrix} = \begin{bmatrix} a_{11} & a_{12} & a_{13} \\ a_{21} & a_{22} & a_{23} \\ a_{31} & a_{32} & a_{33} \end{bmatrix} \begin{bmatrix} u_1 \\ u_2 \\ u_3 \end{bmatrix},$$

the resulting three numbers (b_1, b_2, b_3) may or may not represent the components of a vector. If they are the components of a vector, then the matrix represents the components of a tensor \mathbf{A} ; if not, then the matrix is just an ordinary old matrix.

To check whether (b_1, b_2, b_3) are the components of a vector, you need to check how (b_1, b_2, b_3) change as a result of a change of basis. That is to say, choose a new basis, calculate the new components of \mathbf{u} in this basis, and calculate the new matrix in this basis. (The new elements of the matrix will depend on how the matrix was defined. The elements may or may not change; if they don't, then the matrix cannot be the components of a tensor.) Then, evaluate the matrix product to find a new left-hand side, say $(\beta_1, \beta_2, \beta_3)$. If $(\beta_1, \beta_2, \beta_3)$ are related to (b_1, b_2, b_3) by the same transformation that was used to calculate the new components of \mathbf{u} , then (b_1, b_2, b_3) are the components of a vector, and, therefore, the matrix represents the components of a tensor.

B.1.4 Creating a Tensor using a Dyadic Product of Two Vectors

Let \mathbf{a} and \mathbf{b} be two vectors. The dyadic product of \mathbf{a} and \mathbf{b} is a second-order tensor \mathbf{S} denoted by

$$\mathbf{S} = \mathbf{a} \otimes \mathbf{b}$$

with the property

$$\mathbf{S} \cdot \mathbf{u} = (\mathbf{a} \otimes \mathbf{b}) \cdot \mathbf{u} = \mathbf{a}(\mathbf{b} \cdot \mathbf{u})$$

for all vectors \mathbf{u} . (Clearly, this maps \mathbf{u} onto a vector parallel to \mathbf{a} with magnitude $|\mathbf{a}|(\mathbf{b} \cdot \mathbf{u})$.) The components of $\mathbf{a} \otimes \mathbf{b}$ in a basis $\{\mathbf{e}_1, \mathbf{e}_2, \mathbf{e}_3\}$ are

$$\begin{bmatrix} a_1 b_1 & a_1 b_2 & a_1 b_3 \\ a_2 b_1 & a_2 b_2 & a_2 b_3 \\ a_3 b_1 & a_3 b_2 & a_3 b_3 \end{bmatrix}.$$

Note that not all tensors can be constructed using a dyadic product of only two vectors (this is because $(\mathbf{a} \otimes \mathbf{b}) \cdot \mathbf{u}$ always has to be parallel to \mathbf{a} , and therefore the representation cannot map a vector onto an arbitrary vector). However, if \mathbf{a} , \mathbf{b} , and \mathbf{c} are three independent vectors (i.e., no two of them are parallel), then all second-order tensors can be constructed as a sum of scalar multiples of the nine possible dyadic products of these vectors.

B.2 OPERATIONS ON SECOND-ORDER TENSORS

B.2.1 Tensor Components

Let $\{\mathbf{e}_1, \mathbf{e}_2, \mathbf{e}_3\}$ be a Cartesian basis and let \mathbf{S} be a second-order tensor. The components of \mathbf{S} in $\{\mathbf{e}_1, \mathbf{e}_2, \mathbf{e}_3\}$ may be represented as a matrix

$$\begin{bmatrix} S_{11} & S_{12} & S_{13} \\ S_{21} & S_{22} & S_{23} \\ S_{31} & S_{32} & S_{33} \end{bmatrix},$$

where

$$\begin{aligned} S_{11} &= \mathbf{e}_1 \cdot (\mathbf{S} \cdot \mathbf{e}_1), & S_{12} &= \mathbf{e}_1 \cdot (\mathbf{S} \cdot \mathbf{e}_2), & S_{13} &= \mathbf{e}_1 \cdot (\mathbf{S} \cdot \mathbf{e}_3), \\ S_{21} &= \mathbf{e}_2 \cdot (\mathbf{S} \cdot \mathbf{e}_1), & S_{22} &= \mathbf{e}_2 \cdot (\mathbf{S} \cdot \mathbf{e}_2), & S_{23} &= \mathbf{e}_2 \cdot (\mathbf{S} \cdot \mathbf{e}_3), \\ S_{31} &= \mathbf{e}_3 \cdot (\mathbf{S} \cdot \mathbf{e}_1), & S_{32} &= \mathbf{e}_3 \cdot (\mathbf{S} \cdot \mathbf{e}_2), & S_{33} &= \mathbf{e}_3 \cdot (\mathbf{S} \cdot \mathbf{e}_3). \end{aligned}$$

The representation of a tensor in terms of its components can also be expressed in dyadic form as

$$\mathbf{S} = \sum_{j=1}^3 \sum_{i=1}^3 S_{ij} \mathbf{e}_i \otimes \mathbf{e}_j.$$

This representation is particularly convenient when using polar coordinates, as described in Appendix E.

Addition: Let \mathbf{S} and \mathbf{T} be two tensors. Then $\mathbf{U} = \mathbf{S} + \mathbf{T}$ is also a tensor.

Denote the Cartesian components of \mathbf{U} , \mathbf{S} , and \mathbf{T} by matrices as defined above. The components of \mathbf{U} are then related to the components of \mathbf{S} and \mathbf{T} by

$$\begin{bmatrix} U_{11} & U_{12} & U_{13} \\ U_{21} & U_{22} & U_{23} \\ U_{31} & U_{32} & U_{33} \end{bmatrix} = \begin{bmatrix} S_{11} + T_{11} & S_{12} + T_{12} & S_{13} + T_{13} \\ S_{21} + T_{21} & S_{22} + T_{22} & S_{23} + T_{23} \\ S_{31} + T_{31} & S_{32} + T_{32} & S_{33} + T_{33} \end{bmatrix}.$$

Product of a tensor and a vector: Let \mathbf{u} be a vector and \mathbf{S} a second-order tensor. Then

$$\mathbf{v} = \mathbf{S} \cdot \mathbf{u}$$

is a vector.

Let (u_1, u_2, u_3) and (v_1, v_2, v_3) denote the components of vectors \mathbf{u} and \mathbf{v} in a Cartesian basis $\{\mathbf{e}_1, \mathbf{e}_2, \mathbf{e}_3\}$, and denote the Cartesian components of \mathbf{S} as described above. Then,

$$\begin{bmatrix} v_1 \\ v_2 \\ v_3 \end{bmatrix} = \begin{bmatrix} S_{11} & S_{12} & S_{13} \\ S_{21} & S_{22} & S_{23} \\ S_{31} & S_{32} & S_{33} \end{bmatrix} \begin{bmatrix} u_1 \\ u_2 \\ u_3 \end{bmatrix} = \begin{bmatrix} S_{11}u_1 + S_{12}u_2 + S_{13}u_3 \\ S_{21}u_1 + S_{22}u_2 + S_{23}u_3 \\ S_{31}u_1 + S_{32}u_2 + S_{33}u_3 \end{bmatrix}.$$

The product

$$\mathbf{v} = \mathbf{u} \cdot \mathbf{S}$$

is also a vector. In component form,

$$\begin{bmatrix} v_1 & v_2 & v_3 \end{bmatrix} = \begin{bmatrix} u_1 & u_2 & u_3 \end{bmatrix} \begin{bmatrix} S_{11} & S_{12} & S_{13} \\ S_{21} & S_{22} & S_{23} \\ S_{31} & S_{32} & S_{33} \end{bmatrix} = \begin{bmatrix} u_1S_{11} + u_2S_{21} + u_3S_{31} \\ u_1S_{12} + u_2S_{22} + u_3S_{32} \\ u_1S_{13} + u_2S_{23} + u_3S_{33} \end{bmatrix}.$$

Observe that $\mathbf{u} \cdot \mathbf{S} \neq \mathbf{S} \cdot \mathbf{u}$ (unless \mathbf{S} is symmetric).

Product of two tensors: Let \mathbf{T} and \mathbf{S} be two second-order tensors. Then $\mathbf{U} = \mathbf{TS}$ is also a tensor. Denote the components of \mathbf{U} , \mathbf{S} , and \mathbf{T} by 3×3 matrices. Then,

$$\begin{aligned} \begin{bmatrix} U_{11} & U_{12} & U_{13} \\ U_{21} & U_{22} & U_{23} \\ U_{31} & U_{32} & U_{33} \end{bmatrix} &= \begin{bmatrix} T_{11} & T_{12} & T_{13} \\ T_{21} & T_{22} & T_{23} \\ T_{31} & T_{32} & T_{33} \end{bmatrix} \begin{bmatrix} S_{11} & S_{12} & S_{13} \\ S_{21} & S_{22} & S_{23} \\ S_{31} & S_{32} & S_{33} \end{bmatrix} \\ &= \begin{bmatrix} T_{11}S_{11} + T_{12}S_{21} + T_{13}S_{31} & T_{11}S_{12} + T_{12}S_{22} + T_{13}S_{32} & T_{11}S_{13} + T_{12}S_{23} + T_{13}S_{33} \\ T_{21}S_{11} + T_{22}S_{21} + T_{23}S_{31} & T_{21}S_{12} + T_{22}S_{22} + T_{23}S_{32} & T_{21}S_{13} + T_{22}S_{23} + T_{23}S_{33} \\ T_{31}S_{11} + T_{32}S_{21} + T_{33}S_{31} & T_{31}S_{12} + T_{32}S_{22} + T_{33}S_{32} & T_{31}S_{13} + T_{32}S_{23} + T_{33}S_{33} \end{bmatrix}. \end{aligned}$$

Note that tensor products, like matrix products, are not commutative, i.e., $\mathbf{TS} \neq \mathbf{ST}$.

Transpose: Let \mathbf{S} be a tensor. The transpose of \mathbf{S} is denoted by \mathbf{S}^T and is defined so that $\mathbf{u} \cdot \mathbf{S}^T = \mathbf{S} \cdot \mathbf{u}$. Denote the components of \mathbf{S} by a 3×3 matrix. The components of \mathbf{S}^T are then

$$\mathbf{S}^T \equiv \begin{bmatrix} S_{11} & S_{21} & S_{31} \\ S_{12} & S_{22} & S_{32} \\ S_{13} & S_{23} & S_{33} \end{bmatrix},$$

i.e., the rows and columns of the matrix are switched. Note that, if \mathbf{A} and \mathbf{B} are two tensors, then

$$(\mathbf{AB})^T = \mathbf{B}^T \mathbf{A}^T.$$

Trace: Let \mathbf{S} be a tensor and denote the components of \mathbf{S} by a 3×3 matrix. The trace of \mathbf{S} is denoted by $\text{tr}(\mathbf{S})$ or $\text{trace}(\mathbf{S})$ and can be computed by summing the diagonals of the matrix of components:

$$\text{trace}(\mathbf{S}) = S_{11} + S_{22} + S_{33}.$$

More formally, let $\{\mathbf{e}_1, \mathbf{e}_2, \mathbf{e}_3\}$ be any Cartesian basis. Then,

$$\text{trace}(\mathbf{S}) = \mathbf{e}_1 \cdot \mathbf{S} \cdot \mathbf{e}_1 + \mathbf{e}_2 \cdot \mathbf{S} \cdot \mathbf{e}_2 + \mathbf{e}_3 \cdot \mathbf{S} \cdot \mathbf{e}_3.$$

The trace of a tensor is an example of an *invariant* of the tensor; you get the same value for $\text{trace}(\mathbf{S})$ whatever basis you use to define the matrix of components of \mathbf{S} .

Contraction

Inner product: Let \mathbf{S} and \mathbf{T} be two second-order tensors. The inner product of \mathbf{S} and \mathbf{T} is a scalar, denoted by $\mathbf{S} : \mathbf{T}$. Represent \mathbf{S} and \mathbf{T} by their components in a basis. Then,

$$\begin{aligned} \mathbf{S} : \mathbf{T} &= S_{11}T_{11} + S_{12}T_{12} + S_{13}T_{13} \\ &\quad + S_{21}T_{21} + S_{22}T_{22} + S_{23}T_{23} \\ &\quad + S_{31}T_{31} + S_{32}T_{32} + S_{33}T_{33}. \end{aligned}$$

Observe that $\mathbf{S} : \mathbf{T} = \mathbf{T} : \mathbf{S}$ and also that $\mathbf{S} : \mathbf{I} = \text{trace}(\mathbf{S})$, where \mathbf{I} is the identity tensor.

Outer product: Let \mathbf{S} and \mathbf{T} be two second-order tensors. The outer product of \mathbf{S} and \mathbf{T} is a scalar, denoted by $\mathbf{S} \cdot \mathbf{T}$. Represent \mathbf{S} and \mathbf{T} by their components in a basis. Then,

$$\begin{aligned}\mathbf{S} \cdot \mathbf{T} &= S_{11}T_{11} + S_{21}T_{12} + S_{31}T_{13} \\ &\quad + S_{12}T_{21} + S_{22}T_{22} + S_{32}T_{23} \\ &\quad + S_{13}T_{31} + S_{23}T_{32} + S_{33}T_{33}\end{aligned}$$

Observe that $\mathbf{S} \cdot \mathbf{T} = \mathbf{S}^T : \mathbf{T}$.

Determinant: The determinant of a tensor is defined as the determinant of the matrix of its components in a basis. For a second-order tensor

$$\begin{aligned}\det \mathbf{S} &= \det \begin{bmatrix} S_{11} & S_{12} & S_{13} \\ S_{21} & S_{22} & S_{23} \\ S_{31} & S_{32} & S_{33} \end{bmatrix} \\ &= S_{11}(S_{22}S_{33} - S_{23}S_{32}) + S_{12}(S_{23}S_{31} - S_{21}S_{33}) + S_{13}(S_{21}S_{32} - S_{23}S_{31}).\end{aligned}$$

Note that, if \mathbf{S} and \mathbf{T} are two tensors, then

$$\det(\mathbf{S}) = \det(\mathbf{S}^T) \quad \det(\mathbf{ST}) = \det(\mathbf{S}) \det(\mathbf{T}).$$

Inverse: Let \mathbf{S} be a second-order tensor. The inverse of \mathbf{S} exists if and only if $\det(\mathbf{S}) \neq 0$ and is defined by

$$\mathbf{S}^{-1} \mathbf{S} = \mathbf{I},$$

where \mathbf{S}^{-1} denotes the inverse of \mathbf{S} and \mathbf{I} is the identity tensor. The inverse of a tensor may be computed by calculating the inverse of the matrix of its components. The result cannot be expressed in a compact form for a general 3D second-order tensor and is best computed by methods such as Gaussian elimination.

Eigenvalues and eigenvectors (principal values and direction): Let \mathbf{S} be a second-order tensor. The scalars λ and unit vectors \mathbf{m} that satisfy

$$\mathbf{S} \cdot \mathbf{m} = \lambda \mathbf{m}$$

are known as the eigenvalues and eigenvectors of \mathbf{S} or the principal values and principal directions of \mathbf{S} . Note that λ may be complex. For a second-order tensor in three dimensions, there are generally three values of λ and three unique unit vectors \mathbf{m} that satisfy this equation. Occasionally, there may be only two or one value of λ . If this is the case, there are infinitely many possible vectors \mathbf{m} that satisfy the equation. The eigenvalues of a tensor, and the components of the eigenvectors, may be computed by finding the eigenvalues and eigenvectors of the matrix of components (see Section A.3.2)

The eigenvalues of a symmetric tensor are always real. The eigenvalues of a skew tensor are always pure imaginary or zero.

Change of basis: Let \mathbf{S} be a tensor and let $\{\mathbf{e}_1, \mathbf{e}_2, \mathbf{e}_3\}$ be a Cartesian basis. Suppose that the components of \mathbf{S} in the basis $\{\mathbf{e}_1, \mathbf{e}_2, \mathbf{e}_3\}$ are known to be

$$\left[S^{(\mathbf{e})} \right] = \begin{bmatrix} S_{11}^{(\mathbf{e})} & S_{12}^{(\mathbf{e})} & S_{13}^{(\mathbf{e})} \\ S_{21}^{(\mathbf{e})} & S_{22}^{(\mathbf{e})} & S_{23}^{(\mathbf{e})} \\ S_{31}^{(\mathbf{e})} & S_{32}^{(\mathbf{e})} & S_{33}^{(\mathbf{e})} \end{bmatrix}.$$

Now, suppose that we want to compute the components of \mathbf{S} in a second Cartesian basis, $\{\mathbf{m}_1, \mathbf{m}_2, \mathbf{m}_3\}$. Denote these components by

$$\left[S^{(\mathbf{m})} \right] = \begin{bmatrix} S_{11}^{(\mathbf{m})} & S_{12}^{(\mathbf{m})} & S_{13}^{(\mathbf{m})} \\ S_{21}^{(\mathbf{m})} & S_{22}^{(\mathbf{m})} & S_{23}^{(\mathbf{m})} \\ S_{31}^{(\mathbf{m})} & S_{32}^{(\mathbf{m})} & S_{33}^{(\mathbf{m})} \end{bmatrix}.$$

To do so, first compute the components of the transformation matrix $[Q]$

$$[Q] = \begin{bmatrix} \mathbf{m}_1 \cdot \mathbf{e}_1 & \mathbf{m}_1 \cdot \mathbf{e}_2 & \mathbf{m}_1 \cdot \mathbf{e}_3 \\ \mathbf{m}_2 \cdot \mathbf{e}_1 & \mathbf{m}_2 \cdot \mathbf{e}_2 & \mathbf{m}_2 \cdot \mathbf{e}_3 \\ \mathbf{m}_3 \cdot \mathbf{e}_1 & \mathbf{m}_3 \cdot \mathbf{e}_2 & \mathbf{m}_3 \cdot \mathbf{e}_3 \end{bmatrix}$$

(this is the same matrix you would use to transform vector components from $\{\mathbf{e}_1, \mathbf{e}_2, \mathbf{e}_3\}$ to $\{\mathbf{m}_1, \mathbf{m}_2, \mathbf{m}_3\}$). Then,

$$[S^{(\mathbf{m})}] = [Q][S^{(\mathbf{e})}][Q]^T,$$

or, written out in full,

$$\begin{aligned} \begin{bmatrix} S_{11}^{(\mathbf{m})} & S_{12}^{(\mathbf{m})} & S_{13}^{(\mathbf{m})} \\ S_{21}^{(\mathbf{m})} & S_{22}^{(\mathbf{m})} & S_{23}^{(\mathbf{m})} \\ S_{31}^{(\mathbf{m})} & S_{32}^{(\mathbf{m})} & S_{33}^{(\mathbf{m})} \end{bmatrix} &= \\ \begin{bmatrix} \mathbf{m}_1 \cdot \mathbf{e}_1 & \mathbf{m}_1 \cdot \mathbf{e}_2 & \mathbf{m}_1 \cdot \mathbf{e}_3 \\ \mathbf{m}_2 \cdot \mathbf{e}_1 & \mathbf{m}_2 \cdot \mathbf{e}_2 & \mathbf{m}_2 \cdot \mathbf{e}_3 \\ \mathbf{m}_3 \cdot \mathbf{e}_1 & \mathbf{m}_3 \cdot \mathbf{e}_2 & \mathbf{m}_3 \cdot \mathbf{e}_3 \end{bmatrix} \begin{bmatrix} S_{11}^{(\mathbf{e})} & S_{12}^{(\mathbf{e})} & S_{13}^{(\mathbf{e})} \\ S_{21}^{(\mathbf{e})} & S_{22}^{(\mathbf{e})} & S_{23}^{(\mathbf{e})} \\ S_{31}^{(\mathbf{e})} & S_{32}^{(\mathbf{e})} & S_{33}^{(\mathbf{e})} \end{bmatrix} \begin{bmatrix} \mathbf{m}_1 \cdot \mathbf{e}_1 & \mathbf{m}_2 \cdot \mathbf{e}_1 & \mathbf{m}_3 \cdot \mathbf{e}_1 \\ \mathbf{m}_1 \cdot \mathbf{e}_2 & \mathbf{m}_2 \cdot \mathbf{e}_2 & \mathbf{m}_3 \cdot \mathbf{e}_2 \\ \mathbf{m}_1 \cdot \mathbf{e}_3 & \mathbf{m}_2 \cdot \mathbf{e}_3 & \mathbf{m}_3 \cdot \mathbf{e}_3 \end{bmatrix}. \end{aligned}$$

To prove this result, let \mathbf{u} and \mathbf{v} be vectors satisfying

$$\mathbf{v} = \mathbf{S} \cdot \mathbf{u}.$$

Denote the components of \mathbf{u} and \mathbf{v} in the two bases by $\underline{u}^{(\mathbf{e})}$, $\underline{u}^{(\mathbf{m})}$ and $\underline{v}^{(\mathbf{e})}$, $\underline{v}^{(\mathbf{m})}$, respectively. Recall that the vector components are related by

$$\begin{aligned}\underline{u}^{(\mathbf{m})} &= [Q] \underline{u}^{(\mathbf{e})} & \underline{u}^{(\mathbf{e})} &= [Q]^T \underline{u}^{(\mathbf{m})} \\ \underline{v}^{(\mathbf{m})} &= [Q] \underline{v}^{(\mathbf{e})} & \underline{v}^{(\mathbf{e})} &= [Q]^T \underline{v}^{(\mathbf{m})}.\end{aligned}$$

Now, we could express the tensor-vector product in either basis

$$\underline{v}^{(\mathbf{m})} = [S^{(\mathbf{m})}] \underline{u}^{(\mathbf{m})} \quad \underline{v}^{(\mathbf{e})} = [S^{(\mathbf{e})}] \underline{u}^{(\mathbf{e})}.$$

Substitute for $\underline{u}^{(\mathbf{e})}$, $\underline{v}^{(\mathbf{e})}$ from above into the second of these two relations; we see that

$$[Q]^T \underline{v}^{(\mathbf{m})} = [S^{(\mathbf{e})}] [Q]^T \underline{u}^{(\mathbf{m})}.$$

Recall that

$$[Q][Q]^T = [I] \quad [I] \underline{v}^{(\mathbf{m})} = \underline{v}^{(\mathbf{m})},$$

so multiplying both sides by $[Q]$ shows that

$$\underline{v}^{(\mathbf{m})} = [Q] [S^{(\mathbf{e})}] [Q]^T \underline{u}^{(\mathbf{m})},$$

so, comparing with the tensor-vector product in $\{\mathbf{m}_1, \mathbf{m}_2, \mathbf{m}_3\}$,

$$[S^{(\mathbf{m})}] = [Q] [S^{(\mathbf{e})}] [Q]^T$$

as stated.

Invariants: *Invariants* of a tensor are functions of the tensor components that remain constant under a basis change. That is to say, the invariant has the same value when computed in two arbitrary bases $\{\mathbf{e}_1, \mathbf{e}_2, \mathbf{e}_3\}$ and $\{\mathbf{m}_1, \mathbf{m}_2, \mathbf{m}_3\}$. A symmetric second-order tensor always has three independent invariants. Examples of invariants include the following:

1. The three eigenvalues
2. The determinant

3. The trace
4. The inner and outer products.

These are not all independent: for example, any of 2–4 can be calculated in terms of 1.

B.3 SPECIAL TENSORS

B.3.1 Identity Tensor

The identity tensor \mathbf{I} is the tensor such that, for any tensor \mathbf{S} or vector \mathbf{v} ,

$$\begin{aligned}\mathbf{I} \cdot \mathbf{v} &= \mathbf{v} \cdot \mathbf{I} = \mathbf{v} \\ \mathbf{S}\mathbf{I} &= \mathbf{IS} = \mathbf{S}.\end{aligned}$$

In any basis, the identity tensor has components

$$\begin{bmatrix} 1 & 0 & 0 \\ 0 & 1 & 0 \\ 0 & 0 & 1 \end{bmatrix}.$$

B.3.2 Symmetric Tensor

A symmetric tensor \mathbf{S} has the property

$$\mathbf{S} = \mathbf{S}^T.$$

The components of a symmetric tensor have the form

$$\begin{bmatrix} S_{11} & S_{12} & S_{13} \\ S_{12} & S_{22} & S_{23} \\ S_{13} & S_{23} & S_{33} \end{bmatrix},$$

so that there are only six independent components of the tensor, instead of nine.

B.3.3 Skew Tensor

A skew tensor \mathbf{S} has the property

$$\mathbf{S}^T = -\mathbf{S}.$$

The components of a skew tensor have the form

$$\begin{bmatrix} 0 & S_{12} & S_{13} \\ -S_{12} & 0 & S_{23} \\ -S_{13} & -S_{23} & 0 \end{bmatrix}.$$

B.3.4 Orthogonal Tensors

An orthogonal tensor \mathbf{S} has the property

$$\begin{aligned}\mathbf{SS}^T &= \mathbf{S}^T\mathbf{S} = \mathbf{I} \\ \mathbf{S}^{-1} &= \mathbf{S}^T.\end{aligned}$$

An orthogonal tensor must have $\det(\mathbf{S}) = \pm 1$; a tensor with $\det(\mathbf{S}) = +1$ is known as a *proper orthogonal tensor*.

This page intentionally left blank

Appendix C: Index Notation for Vector and Tensor Operations

Operations on Cartesian components of vectors and tensors may be expressed very efficiently and clearly using *index notation*.

C.1 VECTOR AND TENSOR COMPONENTS

Let \mathbf{x} be a (3D) vector and let \mathbf{S} be a second-order tensor. Let $\{\mathbf{e}_1, \mathbf{e}_2, \mathbf{e}_3\}$ be a Cartesian basis. Denote the components of \mathbf{x} in this basis by (x_1, x_2, x_3) and denote the components of \mathbf{S} by

$$\begin{bmatrix} S_{11} & S_{12} & S_{13} \\ S_{21} & S_{22} & S_{23} \\ S_{31} & S_{32} & S_{33} \end{bmatrix}.$$

Using index notation, we would express \mathbf{x} and \mathbf{S} as

$$\mathbf{x} \equiv x_i \quad \mathbf{S} \equiv S_{ij}.$$

C.2 CONVENTIONS AND SPECIAL SYMBOLS FOR INDEX NOTATION

Range convention: Lowercase Latin subscripts ($i, j, k \dots$) have the range (1, 2, 3). The symbol x_i denotes three components of a vector x_1, x_2 , and x_3 . The symbol S_{ij} denotes nine components of a second-order tensor, $S_{11}, S_{12}, S_{13}, S_{21} \dots S_{33}$.

Summation convention (Einstein convention): If an index is repeated in a product of vectors or tensors, summation is implied over the repeated index. Thus,

$$\lambda = a_i b_i \equiv \lambda = \sum_{i=1}^3 a_i b_i \equiv \lambda = a_1 b_1 + a_2 b_2 + a_3 b_3$$

$$c_i = S_{ik} x_k \equiv c_i = \sum_{k=1}^3 S_{ik} x_k \equiv \begin{cases} c_1 = S_{11}x_1 + S_{12}x_2 + S_{13}x_3 \\ c_2 = S_{21}x_1 + S_{22}x_2 + S_{23}x_3 \\ c_3 = S_{31}x_1 + S_{32}x_2 + S_{33}x_3 \end{cases}$$

$$\lambda = S_{ij} S_{ij} \equiv \lambda = \sum_{i=1}^3 \sum_{j=1}^3 S_{ij} S_{ij} \equiv \lambda = S_{11}S_{11} + S_{12}S_{12} + \dots + S_{31}S_{31} + S_{32}S_{32} + S_{33}S_{33}.$$

$$C_{ij} = A_{ik} B_{kj} \equiv C_{ij} = \sum_{k=1}^3 A_{ik} B_{kj} \equiv [C] = [A][B]$$

$$C_{ij} = A_{kj} B_{kj} \equiv C_{ij} = \sum_{k=1}^3 A_{ki} B_{kj} \equiv [C] = [A]^T [B]$$

In the last two equations, $[A]$, $[B]$, and $[C]$ denote the (3×3) component matrices of \mathbf{A} , \mathbf{B} , and \mathbf{C} .

The Kronecker delta: The symbol δ_{ij} is known as the Kronecker delta and has the properties

$$\delta_{ij} = \begin{cases} 1 & i=j \\ 0 & i \neq j; \end{cases}$$

thus,

$$\delta_{11} = \delta_{22} = \delta_{33} = 1 \quad \delta_{12} = \delta_{21} = \delta_{13} = \delta_{31} = \delta_{23} = \delta_{32} = 0.$$

You can also think of δ_{ij} as the components of the identity tensor or a (3×3) identity matrix. Observe the following useful results:

$$\delta_{ij} = \delta_{ji}$$

$$\delta_{kk} = 3$$

$$a_i = \delta_{ik} a_k$$

$$A_{ij} = \delta_{ik} A_{kj}.$$

The permutation symbol: The symbol ϵ_{ijk} has properties

$$\epsilon_{ijk} = \begin{cases} 1 & i,j,k = 1,2,3, \quad 2,3,1 \quad \text{or} \quad 3,1,2 \\ -1 & i,j,k = 3,2,1, \quad 2,1,3 \quad \text{or} \quad 1,3,2; \\ 0 & \text{otherwise} \end{cases}$$

thus,

$$\begin{aligned} \epsilon_{123} &= \epsilon_{231} = \epsilon_{312} = 1 \\ \epsilon_{321} &= \epsilon_{213} = \epsilon_{132} = -1 \\ \epsilon_{111} &= \epsilon_{112} = \epsilon_{113} = \epsilon_{121} = \epsilon_{122} = \epsilon_{131} = \epsilon_{133} = 0 \\ \epsilon_{211} &= \epsilon_{212} = \epsilon_{221} = \epsilon_{222} = \epsilon_{223} = \epsilon_{232} = \epsilon_{233} = 0 \\ \epsilon_{311} &= \epsilon_{313} = \epsilon_{322} = \epsilon_{323} = \epsilon_{321} = \epsilon_{332} = \epsilon_{333} = 0. \end{aligned}$$

Note that

$$\begin{aligned} \epsilon_{ijk} &= \epsilon_{kij} = \epsilon_{jki} = -\epsilon_{jik} = -\epsilon_{kji} = -\epsilon_{kji} \\ \epsilon_{kki} &= 0 \\ \epsilon_{ijk}\epsilon_{imn} &= \delta_{jm}\delta_{kn} - \delta_{jn}\delta_{mk} \\ \epsilon_{ijk}\epsilon_{lmn} &= \delta_{il}(\delta_{jm}\delta_{kn} - \delta_{jn}\delta_{km}) - \delta_{im}(\delta_{jl}\delta_{kn} - \delta_{jn}\delta_{kl}) + \delta_{in}(\delta_{jl}\delta_{km} - \delta_{jm}\delta_{kl}). \end{aligned}$$

C.3 RULES OF INDEX NOTATION

The rules of index notation are as follows:

1. The same index (subscript) may not appear more than twice in a product of two (or more) vectors or tensors. Thus,

$$A_{ik}x_k, \quad A_{ik}B_{kj}, \quad A_{ij}B_{ik}C_{nk}$$

are valid, but

$$A_{kk}x_k, \quad A_{ik}B_{kk}, \quad A_{ij}B_{ik}C_{ik}$$

are meaningless.

2. Free indices on each term of an equation must agree. Thus,

$$\begin{aligned} x_i &= u_i + c_i \quad \equiv \quad \mathbf{x} = \mathbf{u} + \mathbf{c} \\ a_i &= A_{ki}B_{kj}x_j + C_{ik}u_k \quad \equiv \quad \mathbf{a} = \mathbf{A}^T\mathbf{Bx} + \mathbf{Cu} \end{aligned}$$

are valid, but

$$\begin{aligned} x_i &= A_{ij} \\ x_j &= A_{ik}u_k \\ x_i &= A_{ik}u_k + c_j \end{aligned}$$

are meaningless.

3. Free and dummy indices may be changed without altering the meaning of an expression, provided that rules 1 and 2 are not violated. Thus,

$$x_i = A_{ik} x_k \Leftrightarrow x_j = A_{jk} x_k \Leftrightarrow x_j = A_{ji} x_i.$$

C.4 VECTOR OPERATIONS EXPRESSED USING INDEX NOTATION

Addition: For addition,

$$\mathbf{c} = \mathbf{a} + \mathbf{b} \quad \equiv \quad c_i = a_i + b_i.$$

Dot product: For the dot product,

$$\lambda = \mathbf{a} \cdot \mathbf{b} \quad \equiv \quad \lambda = a_i b_i.$$

Vector product: For the vector product,

$$\mathbf{c} = \mathbf{a} \times \mathbf{b} \quad \equiv \quad c_i = \epsilon_{ijk} a_j b_k.$$

Dyadic product: For the dyadic product,

$$\mathbf{S} = \mathbf{a} \otimes \mathbf{b} \quad \equiv \quad S_{ij} = a_i b_j.$$

Change of basis: Let \mathbf{a} be a vector. Let $\{\mathbf{e}_1, \mathbf{e}_2, \mathbf{e}_3\}$ be a Cartesian basis and denote the components of \mathbf{a} in this basis by a_i . Let $\{\mathbf{m}_1, \mathbf{m}_2, \mathbf{m}_3\}$ be a second basis and denote the components of \mathbf{a} in this basis by α_i . Then, define

$$Q_{ij} = \mathbf{m}_i \cdot \mathbf{e}_j = \cos \theta(\mathbf{m}_i, \mathbf{e}_j),$$

where $\theta(\mathbf{m}_i, \mathbf{e}_j)$ denotes the angle between the unit vectors \mathbf{m}_i and \mathbf{e}_j . Then,

$$\alpha_i = Q_{ij} a_j.$$

C.5 TENSOR OPERATIONS EXPRESSED USING INDEX NOTATION

Addition: For addition,

$$\mathbf{C} = \mathbf{A} + \mathbf{B} \quad \equiv \quad C_{ij} = A_{ij} + B_{ij}.$$

Transpose: For the transpose,

$$\mathbf{A} = \mathbf{B}^T \quad \equiv \quad A_{ij} = B_{ji}.$$

Scalar products: For the scalar products,

$$\lambda = \mathbf{A} : \mathbf{B} \quad \equiv \quad \lambda = A_{ij} B_{ij}$$

$$\lambda = \mathbf{A} \cdot \mathbf{B} \quad \equiv \quad \lambda = A_{ji} B_{ij}.$$

Product of a tensor and a vector: For the products of a tensor and a vector,

$$\begin{aligned}\mathbf{c} = \mathbf{A} \cdot \mathbf{b} &\equiv c_i = A_{ij} b_j \\ \mathbf{c} = \mathbf{A}^T \cdot \mathbf{b} &\equiv c_i = A_{ji} b_j.\end{aligned}$$

Product of two tensors: For the product of two tensors,

$$\begin{aligned}\mathbf{C} = \mathbf{AB} &\equiv C_{ij} = A_{ik} B_{kj} \\ \mathbf{C} = \mathbf{A}^T \mathbf{B} &\equiv C_{ij} = A_{ki} B_{kj}.\end{aligned}$$

Determinant: For the determinant,

$$\begin{aligned}\lambda = \det \mathbf{A} \equiv \lambda &= \frac{1}{6} \epsilon_{ijk} \epsilon_{lmn} A_{li} A_{mj} A_{nk} \\ &\Leftrightarrow \epsilon_{lmn} \lambda = \epsilon_{ijk} A_{li} A_{mj} A_{nk}.\end{aligned}$$

Change of basis: Let \mathbf{A} be a second-order tensor. Let $\{\mathbf{e}_1, \mathbf{e}_2, \mathbf{e}_3\}$ be a Cartesian basis and denote the components of \mathbf{A} in this basis by A_{ij} . Let $\{\mathbf{m}_1, \mathbf{m}_2, \mathbf{m}_3\}$ be a second basis and denote the components of \mathbf{A} in this basis by Λ_{ij} . Then, define

$$Q_{ij} = \mathbf{m}_j \cdot \mathbf{e}_i = \cos \theta(\mathbf{m}_i, \mathbf{e}_j),$$

where $\theta(\mathbf{m}_i, \mathbf{e}_j)$ denotes the angle between the unit vectors \mathbf{m}_i and \mathbf{e}_j . Then,

$$\Lambda_{ij} = Q_{ik} A_{km} Q_{jm}.$$

C.6 CALCULUS USING INDEX NOTATION

The derivative $\partial x_i / \partial x_j$ can be deduced by noting that $\partial x_i / \partial x_j = 1$ if $i = j$ and $\partial x_i / \partial x_j = 0$ if $i \neq j$. Therefore,

$$\frac{\partial x_i}{\partial x_j} = \delta_{ij}.$$

The same argument can be used for higher-order tensors

$$\frac{\partial A_{ij}}{\partial A_{kl}} = \delta_{ik} \delta_{jl}.$$

C.7 EXAMPLES OF ALGEBRAIC MANIPULATIONS USING INDEX NOTATION

1. Let \mathbf{a} , \mathbf{b} , \mathbf{c} , and \mathbf{d} be vectors. Prove that

$$(\mathbf{a} \times \mathbf{b}) \cdot (\mathbf{c} \times \mathbf{d}) = (\mathbf{a} \cdot \mathbf{c})(\mathbf{b} \cdot \mathbf{d}) - (\mathbf{a} \cdot \mathbf{d})(\mathbf{b} \cdot \mathbf{c}).$$

Express the left-hand side of the equation using index notation (check the rules for cross products and dot products of vectors to see how this is done):

$$(\mathbf{a} \times \mathbf{b}) \cdot (\mathbf{c} \times \mathbf{d}) \equiv \epsilon_{ijk} a_j b_k \epsilon_{imn} c_m d_n.$$

Recall the identity

$$\epsilon_{ijk} \epsilon_{imn} = \delta_{jm} \delta_{kn} - \delta_{jn} \delta_{mk}$$

so

$$\epsilon_{ijk} a_j b_k \epsilon_{imn} c_m d_n = (\delta_{jm} \delta_{kn} - \delta_{jn} \delta_{mk}) a_j b_k c_m d_n.$$

Multiply out and note that

$$\delta_{jm} a_j = a_m \quad \delta_{kn} b_k = b_n$$

(multiplying by a Kronecker delta has the effect of switching indices) so,

$$(\delta_{jm} \delta_{kn} - \delta_{jn} \delta_{mk}) a_j b_k c_m d_n = a_m b_n c_m d_n - a_n b_m c_m d_n.$$

Finally, note that

$$a_m c_m \equiv \mathbf{a} \cdot \mathbf{c}$$

and similarly for other products with the same index, so that

$$a_m b_n c_m d_n - a_n b_m c_m d_n = a_m c_m b_n d_n - b_m c_m a_n d_n \equiv (\mathbf{a} \cdot \mathbf{c})(\mathbf{b} \cdot \mathbf{d}) - (\mathbf{b} \cdot \mathbf{c})(\mathbf{a} \cdot \mathbf{d}).$$

2. The stress-strain relation for linear elasticity may be expressed as

$$\sigma_{ij} = \frac{E}{1+\nu} \left(\epsilon_{ij} + \frac{\nu}{1-2\nu} \epsilon_{kk} \delta_{ij} \right),$$

where σ_{ij} and ϵ_{ij} are the components of the stress and strain tensor, and E and ν denote Young's modulus and Poisson's ratio. Find an expression for strain in terms of stress.

Set $i = j$ to see that

$$\sigma_{ii} = \frac{E}{1+\nu} \left(\epsilon_{ii} + \frac{\nu}{1-2\nu} \epsilon_{kk} \delta_{ii} \right).$$

Recall that $\delta_{ii} = 3$ and notice that we can replace the remaining ii by kk

$$\begin{aligned} \sigma_{kk} &= \frac{E}{1+\nu} \left(\epsilon_{kk} + \frac{\nu}{1-2\nu} 3 \epsilon_{kk} \right) = \frac{E}{1-2\nu} \epsilon_{kk} \\ \Leftrightarrow \epsilon_{kk} &= \frac{1-2\nu}{E} \sigma_{kk}. \end{aligned}$$

Now, substitute for ε_{kk} in the given stress-strain relation

$$\begin{aligned}\sigma_{ij} &= \frac{E}{1+\nu} \left(\varepsilon_{ij} + \frac{\nu}{E} \sigma_{kk} \delta_{ij} \right) \\ \Leftrightarrow \varepsilon_{ij} &= \frac{1+\nu}{E} \left(\sigma_{ij} - \frac{\nu}{1+\nu} \sigma_{kk} \delta_{ij} \right).\end{aligned}$$

3. Solve the equation

$$\left\{ \delta_{kj} a_i a_i + \frac{1}{1-2\nu} a_k a_j \right\} U_k = P_j$$

for U_k in terms of P_j and a_i .

Multiply both sides by a_j to see that

$$\begin{aligned}&\left\{ a_j \delta_{kj} a_i a_i + \frac{1}{1-2\nu} a_k a_j a_j \right\} U_k = P_j a_j \\ \Leftrightarrow &\left\{ a_k a_i a_i + \frac{1}{1-2\nu} a_k a_j a_j \right\} U_k = P_j a_j \\ \Leftrightarrow &U_k a_k \frac{2(1-\nu)}{1-2\nu} a_i a_i = P_j a_j \Leftrightarrow U_k a_k = \frac{(1-2\nu)P_j a_j}{2(1-\nu)a_i a_i}.\end{aligned}$$

Substitute back into the equation given for $U_k a_k$ to see that

$$U_j a_i a_i + \frac{P_k a_k}{2(1-\nu)a_i a_i} a_j = P_j \Rightarrow U_j = \frac{1}{a_i a_i} \left(P_j - \frac{P_k a_k}{2(1-\nu)a_n a_n} a_j \right).$$

4. Let $r = \sqrt{x_k x_k}$. Calculate $\frac{\partial r}{\partial x_i}$.

We can just apply the usual chain and product rules of differentiation:

$$\frac{\partial r}{\partial x_i} = \frac{1}{2} \frac{1}{\sqrt{x_k x_k}} \left(x_k \frac{\partial x_k}{\partial x_i} + \frac{\partial x_k}{\partial x_i} x_k \right) = \frac{1}{\sqrt{x_k x_k}} x_k \delta_{ik} = \frac{x_i}{\sqrt{x_k x_k}} = \frac{x_i}{r}.$$

5. Let $\lambda = A_{ij} A_{ij}$. Calculate $\partial \lambda / \partial A_{kl}$.

Use the product rule

$$\frac{\partial \lambda}{\partial A_{kl}} = A_{ij} \delta_{ik} \delta_{jl} + \delta_{ik} \delta_{jl} A_{ij} = 2A_{kl}.$$

This page intentionally left blank

Appendix D: Vectors and Tensor Operations in Polar Coordinates

Many simple boundary value problems in solid mechanics (such as those that tend to appear in homework assignments or examinations!) are most conveniently solved using spherical or cylindrical-polar coordinate systems. This appendix reviews the main ideas and procedures associated with polar coordinate systems. A more sophisticated discussion of general nonorthogonal coordinate systems is given in Chapter 10.

The main drawback of using a polar coordinate system is that there is no convenient way to express the various vector and tensor operations using index notation; everything has to be written out in longhand. In this appendix, therefore, we completely abandon index notation; vector and tensor components are always expressed as matrices.

D.1 SPHERICAL-POLAR COORDINATES

D.1.1 Specifying Points in Spherical-Polar Coordinates

To specify points in space using spherical-polar coordinates, we first choose two convenient, mutually perpendicular reference directions (\mathbf{i} and \mathbf{k} in Figure D.1). For example, to

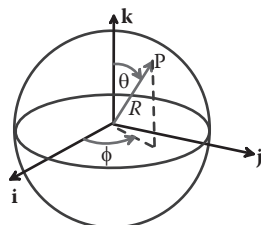


FIGURE D.1 Spherical-polar coordinates.

specify position on the Earth's surface, we might choose \mathbf{k} to point from the center of the earth toward the North Pole and choose \mathbf{i} to point from the center of the earth toward the intersection of the equator (which has 0° latitude) and the Greenwich Meridian (which has 0° longitude, by definition). Then, each point P in space is identified by three numbers, R , θ , ϕ shown in Figure D.1. These are not components of a vector. In words,

- R is the distance of P from the origin.
- θ is the angle between the \mathbf{k} direction and OP .
- ϕ is the angle between the \mathbf{i} direction and the projection of OP onto a plane through O normal to \mathbf{k} .

By convention, we choose $R \geq 0$, $0 \leq \theta \leq 180^\circ$, and $0 \leq \phi \leq 360^\circ$.

D.1.2 Converting between Cartesian and Spherical-Polar Representations of Points

When we use a Cartesian basis, we identify points in space by specifying the components of their position vector relative to the origin (x, y, z) , such that $\mathbf{r} = x\mathbf{i} + y\mathbf{j} + z\mathbf{k}$. When we use a spherical-polar coordinate system, we locate points by specifying their spherical-polar coordinates R, θ, ϕ (Figure D.1). The formulas below relate the two representations. They are derived using basic trigonometry:

$$\begin{aligned} x &= R \sin \theta \cos \phi & R &= \sqrt{x^2 + y^2 + z^2} \\ y &= R \sin \theta \sin \phi & \theta &= \cos^{-1} z/R \\ z &= R \cos \theta & \phi &= \tan^{-1} y/x. \end{aligned}$$

D.1.3 Spherical-Polar Representation of Vectors

When we work with vectors in spherical-polar coordinates, we abandon the $\{\mathbf{i}, \mathbf{j}, \mathbf{k}\}$ basis. Instead, we specify vectors as components in the $\{\mathbf{e}_R, \mathbf{e}_\theta, \mathbf{e}_\phi\}$ basis shown in Figure D.2. For example, an arbitrary vector \mathbf{a} is written as $\mathbf{a} = a_R \mathbf{e}_R + a_\theta \mathbf{e}_\theta + a_\phi \mathbf{e}_\phi$, where (a_R, a_θ, a_ϕ) denote the components of \mathbf{a} . The basis is different for each point P . In words,

- \mathbf{e}_R points along OP .
- \mathbf{e}_θ is tangent to a line of constant longitude through P .
- \mathbf{e}_ϕ is tangent to a line of constant latitude through P .

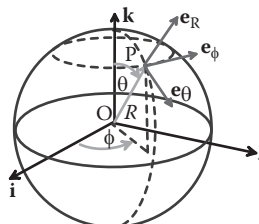


FIGURE D.2 Basis vectors for spherical-polar coordinates.

For example, if polar-coordinates are used to specify points on the Earth's surface, you can visualize the basis vectors like this. Suppose you stand at a point P on the Earth's surface. Relative to you, \mathbf{e}_R points vertically upward, \mathbf{e}_θ points due south, and \mathbf{e}_ϕ points due east. Notice that the basis vectors depend on where you are standing.

You can also visualize the directions as follows:

1. To see the direction of \mathbf{e}_R , keep θ and ϕ fixed and increase R . P is moving parallel to \mathbf{e}_R .
2. To see the direction of \mathbf{e}_θ , keep R and ϕ fixed and increase θ . P now moves parallel to \mathbf{e}_θ .
3. To see the direction of \mathbf{e}_ϕ , keep R and θ fixed and increase ϕ . P now moves parallel to \mathbf{e}_ϕ .

Mathematically, this concept can be expressed as follows. Let \mathbf{r} be the position vector of P. Then,

$$\mathbf{e}_R = \frac{1}{|\partial \mathbf{r} / \partial R|} \frac{\partial \mathbf{r}}{\partial R}, \quad \mathbf{e}_\theta = \frac{1}{|\partial \mathbf{r} / \partial \theta|} \frac{\partial \mathbf{r}}{\partial \theta}, \quad \mathbf{e}_\phi = \frac{1}{|\partial \mathbf{r} / \partial \phi|} \frac{\partial \mathbf{r}}{\partial \phi}.$$

By definition, the “natural basis” for a coordinate system is the derivative of the position vector with respect to the three scalar coordinates that are used to characterize position in space (for a more detailed discussion, see Chapter 10). The basis vectors for a polar coordinate system are parallel to the natural basis vectors but are normalized to have unit length. In addition, the natural basis for a polar coordinate system happens to be orthogonal. Consequently, $\{\mathbf{e}_R, \mathbf{e}_\theta, \mathbf{e}_\phi\}$ is an orthonormal basis (basis vectors have unit length, are mutually perpendicular, and form a right-handed triad).

D.1.4 Converting Vectors between Cartesian and Spherical-Polar Bases

Let $\mathbf{a} = a_R \mathbf{e}_R + a_\theta \mathbf{e}_\theta + a_\phi \mathbf{e}_\phi$ be a vector, with components (a_R, a_θ, a_ϕ) in the spherical-polar basis $\{\mathbf{e}_R, \mathbf{e}_\theta, \mathbf{e}_\phi\}$. Let a_x, a_y, a_z denote the components of \mathbf{a} in the basis $\{\mathbf{i}, \mathbf{j}, \mathbf{k}\}$. The two sets of components are related by

$$\begin{bmatrix} a_x \\ a_y \\ a_z \end{bmatrix} = \begin{bmatrix} \sin\theta\cos\phi & \cos\theta\cos\phi & -\sin\phi \\ \sin\theta\sin\phi & \cos\theta\sin\phi & \cos\phi \\ \cos\theta & -\sin\theta & 0 \end{bmatrix} \begin{bmatrix} a_R \\ a_\theta \\ a_\phi \end{bmatrix},$$

whereas the inverse relationship is

$$\begin{bmatrix} a_R \\ a_\theta \\ a_\phi \end{bmatrix} = \begin{bmatrix} \sin\theta\cos\phi & \sin\theta\sin\phi & \cos\theta \\ \cos\theta\cos\phi & \cos\theta\sin\phi & -\sin\theta \\ -\sin\phi & \cos\phi & 0 \end{bmatrix} \begin{bmatrix} a_x \\ a_y \\ a_z \end{bmatrix}.$$

Observe that the two 3×3 matrices involved in this transformation are transposes (and inverses) of one another. The transformation matrix is therefore orthogonal, satisfying $[Q][Q]^T = [I]$, where $[I]$ denotes the 3×3 identity matrix.

Derivation: It is easiest to do the transformation by expressing each basis vector $\{\mathbf{e}_R, \mathbf{e}_\theta, \mathbf{e}_\phi\}$ as components in $\{\mathbf{i}, \mathbf{j}, \mathbf{k}\}$ and then substituting. To do this, recall that $\mathbf{r} = x\mathbf{i} + y\mathbf{j} + z\mathbf{k}$, recall also the conversion

$$x = R\sin\theta \cos\phi \quad y = R\sin\theta \sin\phi \quad z = R\cos\theta,$$

and finally recall that, by definition,

$$\mathbf{e}_R = \frac{1}{|\frac{\partial \mathbf{r}}{\partial R}|} \frac{\partial \mathbf{r}}{\partial R} \quad \mathbf{e}_\theta = \frac{1}{|\frac{\partial \mathbf{r}}{\partial \theta}|} \frac{\partial \mathbf{r}}{\partial \theta} \quad \mathbf{e}_\phi = \frac{1}{|\frac{\partial \mathbf{r}}{\partial \phi}|} \frac{\partial \mathbf{r}}{\partial \phi}.$$

Hence, substituting for x, y, z and differentiating

$$\begin{aligned} \mathbf{r} &= R\sin\theta \cos\phi \mathbf{i} + R\sin\theta \sin\phi \mathbf{j} + R\cos\theta \mathbf{k} \\ \Rightarrow \frac{\partial \mathbf{r}}{\partial R} &= \sin\theta \cos\phi \mathbf{i} + \sin\theta \sin\phi \mathbf{j} + \cos\theta \mathbf{k}. \end{aligned}$$

Conveniently, we find that $\left| \frac{\partial \mathbf{r}}{\partial R} \right| = 1$. Therefore,

$$\mathbf{e}_R = \sin\theta \cos\phi \mathbf{i} + \sin\theta \sin\phi \mathbf{j} + \cos\theta \mathbf{k}.$$

Similarly,

$$\begin{aligned} \frac{\partial \mathbf{r}}{\partial \theta} &= R\cos\theta \cos\phi \mathbf{i} + R\cos\theta \sin\phi \mathbf{j} - R\sin\theta \mathbf{k} \\ \frac{\partial \mathbf{r}}{\partial \phi} &= -R\sin\theta \sin\phi \mathbf{i} + R\sin\theta \cos\phi \mathbf{j}, \end{aligned}$$

whereas $\left| \frac{\partial \mathbf{r}}{\partial \theta} \right| = R$, $\left| \frac{\partial \mathbf{r}}{\partial \phi} \right| = R\sin\theta$, so that

$$\mathbf{e}_\theta = \cos\theta \cos\phi \mathbf{i} + \cos\theta \sin\phi \mathbf{j} - \sin\theta \mathbf{k} \quad \mathbf{e}_\phi = -\sin\phi \mathbf{i} + \cos\phi \mathbf{j}.$$

Finally, substituting

$$\begin{aligned} \mathbf{a} &= a_R [\sin\theta \cos\phi \mathbf{i} + \sin\theta \sin\phi \mathbf{j} + \cos\theta \mathbf{k}] \\ &\quad + a_\theta [\cos\theta \cos\phi \mathbf{i} + \cos\theta \sin\phi \mathbf{j} - \sin\theta \mathbf{k}] \\ &\quad + a_\phi [-\sin\phi \mathbf{i} + \cos\phi \mathbf{j}]. \end{aligned}$$

Collecting terms in \mathbf{i} , \mathbf{j} , and \mathbf{k} , we see that

$$\begin{aligned} a_x &= \sin\theta \cos\phi a_R + \cos\theta \cos\phi a_\theta - \sin\phi a_\phi \\ a_y &= \sin\theta \sin\phi a_R + \cos\theta \sin\phi a_\theta + \cos\phi a_\phi \\ a_z &= \cos\theta a_R - \sin\theta a_\theta. \end{aligned}$$

This is the result stated.

To show the inverse result, start by noting that

$$\begin{aligned}\mathbf{a} &= a_R \mathbf{e}_R + a_\theta \mathbf{e}_\theta + a_\phi \mathbf{e}_\phi = a_x \mathbf{i} + a_y \mathbf{j} + a_z \mathbf{k} \\ \Rightarrow \mathbf{a} \cdot \mathbf{e}_R &= a_R = a_x \mathbf{i} \cdot \mathbf{e}_R + a_y \mathbf{j} \cdot \mathbf{e}_R + a_z \mathbf{k} \cdot \mathbf{e}_R\end{aligned}$$

(where we have used $\mathbf{e}_\theta \cdot \mathbf{e}_R = \mathbf{e}_\phi \cdot \mathbf{e}_R = 0$). Recall that

$$\begin{aligned}\mathbf{e}_R &= \sin\theta \cos\phi \mathbf{i} + \sin\theta \sin\phi \mathbf{j} + \cos\theta \mathbf{k} \\ \Rightarrow \mathbf{i} \cdot \mathbf{e}_R &= \sin\theta \cos\phi \quad \mathbf{j} \cdot \mathbf{e}_R = \sin\theta \sin\phi \quad \mathbf{k} \cdot \mathbf{e}_R = \cos\theta.\end{aligned}$$

Substituting, we get

$$a_R = \sin\theta \cos\phi a_x + \sin\theta \sin\phi a_y + \cos\theta a_z.$$

Proceeding in exactly the same way for the other two components gives the remaining expressions

$$a_\theta = \cos\theta \cos\phi a_x + \cos\theta \sin\phi a_y - \sin\theta a_z$$

$$a_\phi = -\sin\phi a_x + \cos\phi a_y.$$

Rewriting the last three equations in matrix form gives the result stated.

D.1.5 Spherical-Polar Representation of Tensors

The triad of vectors $\{\mathbf{e}_R, \mathbf{e}_\theta, \mathbf{e}_\phi\}$ is an orthonormal basis (i.e., the three basis vectors have unit length and are mutually perpendicular). Consequently, tensors can be represented as components in this basis in exactly the same way as for a fixed Cartesian basis $\{\mathbf{e}_1, \mathbf{e}_2, \mathbf{e}_3\}$. In particular, a general second-order tensor \mathbf{S} can be represented as a 3×3 matrix:

$$\mathbf{S} \equiv \begin{bmatrix} S_{RR} & S_{R\theta} & S_{R\phi} \\ S_{\theta R} & S_{\theta\theta} & S_{\theta\phi} \\ S_{\phi R} & S_{\phi\theta} & S_{\phi\phi} \end{bmatrix}.$$

You can think of S_{RR} as being equivalent to S_{11} , $S_{R\theta}$ as S_{12} , and so on. All tensor operations such as addition, multiplication by a vector, tensor products, etc., can be expressed in terms of the corresponding operations on this matrix, as discussed in Section B.2 of Appendix B. The component representation of a tensor can also be expressed in dyadic form as

$$\begin{aligned}\mathbf{S} &= S_{RR} \mathbf{e}_R \otimes \mathbf{e}_R + S_{R\theta} \mathbf{e}_R \otimes \mathbf{e}_\theta + S_{R\phi} \mathbf{e}_R \otimes \mathbf{e}_\phi \\ &\quad + S_{\theta R} \mathbf{e}_\theta \otimes \mathbf{e}_R + S_{\theta\theta} \mathbf{e}_\theta \otimes \mathbf{e}_\theta + S_{\theta\phi} \mathbf{e}_\theta \otimes \mathbf{e}_\phi \\ &\quad + S_{\phi R} \mathbf{e}_\phi \otimes \mathbf{e}_R + S_{\phi\theta} \mathbf{e}_\phi \otimes \mathbf{e}_\theta + S_{\phi\phi} \mathbf{e}_\phi \otimes \mathbf{e}_\phi.\end{aligned}$$

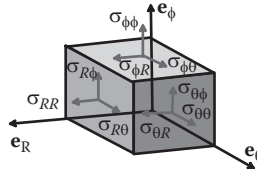


FIGURE D.3 Physical interpretation of stress components in spherical-polar coordinates.

Furthermore, the physical significance of the components can be interpreted in exactly the same way as for tensor components in a Cartesian basis. For example, the spherical-polar coordinate representation for the Cauchy stress tensor has the form

$$\boldsymbol{\sigma} \equiv \begin{bmatrix} \sigma_{RR} & \sigma_{R\theta} & \sigma_{R\phi} \\ \sigma_{\theta R} & \sigma_{\theta\theta} & \sigma_{\theta\phi} \\ \sigma_{\phi R} & \sigma_{\phi\theta} & \sigma_{\phi\phi} \end{bmatrix}.$$

The component $\sigma_{\theta R}$ represents the traction component in direction e_R acting on an internal material plane with normal e_θ and so on (Figure D.3). Of course, the Cauchy stress tensor is symmetric, with $\sigma_{\theta R} = \sigma_{R\theta}$.

D.1.6 Constitutive Equations in Spherical-Polar Coordinates

The constitutive equations listed in Chapter 3 all relate some measure of stress in the solid (expressed as a tensor) to some measure of local internal deformation (deformation gradient, Eulerian strain, rate of deformation tensor, etc.), also expressed as a tensor. The constitutive equations can be used without modification in spherical-polar coordinates, as long as the matrices of Cartesian components of the various tensors are replaced by their equivalent matrices in spherical-polar coordinates.

For example, the stress-strain relations for an isotropic, linear elastic material in spherical-polar coordinates read

$$\begin{bmatrix} \varepsilon_{RR} \\ \varepsilon_{\theta\theta} \\ \varepsilon_{\phi\phi} \\ 2\varepsilon_{\theta\phi} \\ 2\varepsilon_{R\phi} \\ 2\varepsilon_{R\theta} \end{bmatrix} = \frac{1}{E} \begin{bmatrix} 1 & -\nu & -\nu & 0 & 0 & 0 \\ -\nu & 1 & -\nu & 0 & 0 & 0 \\ -\nu & -\nu & 1 & 0 & 0 & 0 \\ 0 & 0 & 0 & 2(1+\nu) & 0 & 0 \\ 0 & 0 & 0 & 0 & 2(1+\nu) & 0 \\ 0 & 0 & 0 & 0 & 0 & 2(1+\nu) \end{bmatrix} \begin{bmatrix} \sigma_{RR} \\ \sigma_{\theta\theta} \\ \sigma_{\phi\phi} \\ \sigma_{\theta\phi} \\ \sigma_{R\phi} \\ \sigma_{R\theta} \end{bmatrix} + \alpha \Delta T \begin{bmatrix} 1 \\ 1 \\ 1 \\ 0 \\ 0 \\ 0 \end{bmatrix}.$$

HEALTH WARNING: If you are solving a problem involving *anisotropic* materials using spherical-polar coordinates, it is important to remember that the orientation of the basis

vectors $\{\mathbf{e}_R, \mathbf{e}_\theta, \mathbf{e}_\phi\}$ vary with position. For example, for an anisotropic, linear elastic solid, you could write the constitutive equation as

$$\boldsymbol{\sigma} = \mathbf{C}(\boldsymbol{\epsilon} - \boldsymbol{\alpha}\Delta T)$$

$$\boldsymbol{\sigma} = \begin{bmatrix} \sigma_{RR} \\ \sigma_{\theta\theta} \\ \sigma_{\phi\phi} \\ \sigma_{\theta\phi} \\ \sigma_{R\phi} \\ \sigma_{R\theta} \end{bmatrix} \quad \mathbf{C} = \begin{bmatrix} c_{11} & c_{12} & c_{13} & c_{14} & c_{15} & c_{16} \\ c_{12} & c_{22} & c_{23} & c_{24} & c_{25} & c_{26} \\ c_{13} & c_{23} & c_{33} & c_{34} & c_{35} & c_{36} \\ c_{14} & c_{24} & c_{34} & c_{44} & c_{45} & c_{46} \\ c_{15} & c_{25} & c_{35} & c_{45} & c_{55} & c_{56} \\ c_{16} & c_{26} & c_{36} & c_{46} & c_{56} & c_{66} \end{bmatrix} \quad \boldsymbol{\epsilon} = \begin{bmatrix} \epsilon_{RR} \\ \epsilon_{\theta\theta} \\ \epsilon_{\phi\phi} \\ 2\epsilon_{\theta\phi} \\ 2\epsilon_{R\phi} \\ 2\epsilon_{R\theta} \end{bmatrix} \quad \boldsymbol{\alpha} = \begin{bmatrix} \alpha_{RR} \\ \alpha_{\theta\theta} \\ \alpha_{\phi\phi} \\ 2\alpha_{\theta\phi} \\ 2\alpha_{R\phi} \\ 2\alpha_{R\theta} \end{bmatrix}.$$

However, the elastic constants c_{11}, c_{12}, \dots would need to represent the material properties in the basis $\{\mathbf{e}_R, \mathbf{e}_\theta, \mathbf{e}_\phi\}$ and would therefore be functions of position (you would have to calculate them using the lengthy basis change formulas listed in Section 3.2.11). In practice, the results are so complicated that there would be very little advantage in working with a spherical-polar coordinate system in this situation.

D.1.7 Converting Tensors between Cartesian and Spherical-Polar Bases

Let \mathbf{S} be a tensor, with components

$$\mathbf{S} \equiv \begin{bmatrix} S_{RR} & S_{R\theta} & S_{R\phi} \\ S_{\theta R} & S_{\theta\theta} & S_{\theta\phi} \\ S_{\phi R} & S_{\phi\theta} & S_{\phi\phi} \end{bmatrix}, \quad \begin{bmatrix} S_{xx} & S_{xy} & S_{xz} \\ S_{yx} & S_{yy} & S_{yz} \\ S_{zx} & S_{xy} & S_{zz} \end{bmatrix}$$

in the spherical-polar basis $\{\mathbf{e}_R, \mathbf{e}_\theta, \mathbf{e}_\phi\}$ and the Cartesian basis $\{\mathbf{i}, \mathbf{j}, \mathbf{k}\}$, respectively. The two sets of components are related by

$$\begin{bmatrix} S_{xx} & S_{xy} & S_{xz} \\ S_{yx} & S_{yy} & S_{yz} \\ S_{zx} & S_{xy} & S_{zz} \end{bmatrix} = \begin{bmatrix} \sin\theta\cos\phi & \cos\theta\cos\phi & -\sin\phi \\ \sin\theta\sin\phi & \cos\theta\sin\phi & \cos\phi \\ \cos\theta & -\sin\theta & 0 \end{bmatrix} \begin{bmatrix} S_{RR} & S_{R\theta} & S_{R\phi} \\ S_{\theta R} & S_{\theta\theta} & S_{\theta\phi} \\ S_{\phi R} & S_{\phi\theta} & S_{\phi\phi} \end{bmatrix} \begin{bmatrix} \sin\theta\cos\phi & \sin\theta\sin\phi & \cos\theta \\ \cos\theta\cos\phi & \cos\theta\sin\phi & -\sin\theta \\ -\sin\phi & \cos\phi & 0 \end{bmatrix}$$

$$\begin{bmatrix} S_{RR} & S_{R\theta} & S_{R\phi} \\ S_{\theta R} & S_{\theta\theta} & S_{\theta\phi} \\ S_{\phi R} & S_{\phi\theta} & S_{\phi\phi} \end{bmatrix} = \begin{bmatrix} \sin\theta\cos\phi & \sin\theta\sin\phi & \cos\theta \\ \cos\theta\cos\phi & \cos\theta\sin\phi & -\sin\theta \\ -\sin\phi & \cos\phi & 0 \end{bmatrix} \begin{bmatrix} S_{xx} & S_{xy} & S_{xz} \\ S_{yx} & S_{yy} & S_{yz} \\ S_{zx} & S_{xy} & S_{zz} \end{bmatrix} \begin{bmatrix} \sin\theta\cos\phi & \cos\theta\cos\phi & -\sin\phi \\ \sin\theta\sin\phi & \cos\theta\sin\phi & \cos\phi \\ \cos\theta & -\sin\theta & 0 \end{bmatrix}.$$

These results follow immediately from the general basis change formulas for tensors given in Appendix B.

D.1.8 Vector Calculus Using Spherical-Polar Coordinates

Calculating derivatives of scalar, vector, and tensor functions of position in spherical-polar coordinates is complicated by the fact that the basis vectors are functions of position. The

results can be expressed in a compact form by defining the *gradient operator*, which, in spherical-polar coordinates, has the representation

$$\nabla \equiv \left(\mathbf{e}_R \frac{\partial}{\partial R} + \mathbf{e}_\theta \frac{1}{R} \frac{\partial}{\partial \theta} + \mathbf{e}_\phi \frac{1}{R \sin \theta} \frac{\partial}{\partial \phi} \right).$$

In addition, the derivatives of the basis vectors are

$$\begin{aligned} \frac{\partial \mathbf{e}_R}{\partial R} &= \frac{\partial \mathbf{e}_\theta}{\partial R} = \frac{\partial \mathbf{e}_\phi}{\partial R} = 0 & \frac{\partial \mathbf{e}_R}{\partial \theta} &= \mathbf{e}_\theta & \frac{\partial \mathbf{e}_\theta}{\partial \theta} &= -\mathbf{e}_R & \frac{\partial \mathbf{e}_\phi}{\partial \theta} &= 0 \\ \frac{\partial \mathbf{e}_R}{\partial \phi} &= \sin \theta \mathbf{e}_\phi & \frac{\partial \mathbf{e}_\theta}{\partial \phi} &= \cos \theta \mathbf{e}_\phi & \frac{\partial \mathbf{e}_\phi}{\partial \phi} &= \sin \theta \mathbf{e}_R - \cos \theta \mathbf{e}_\theta. \end{aligned}$$

You can derive these formulas by differentiating the expressions for the basis vectors in terms of $\{\mathbf{i}, \mathbf{j}, \mathbf{k}\}$,

$$\mathbf{e}_R = \sin \theta \cos \phi \mathbf{i} + \sin \theta \sin \phi \mathbf{j} + \cos \theta \mathbf{k} \quad \mathbf{e}_\theta = \cos \theta \cos \phi \mathbf{i} + \cos \theta \sin \phi \mathbf{j} - \sin \theta \mathbf{k} \quad \mathbf{e}_\phi = -\sin \phi \mathbf{i} + \cos \phi \mathbf{j},$$

and evaluating the various derivatives. When differentiating, note that $\{\mathbf{i}, \mathbf{j}, \mathbf{k}\}$ are fixed, so their derivatives are zero. The details are left as an exercise. The various derivatives of scalars, vectors, and tensors can be expressed using operator notation as follows.

Gradient of a scalar function: Let $f(R, \theta, \phi)$ denote a scalar function of position. The gradient of f is denoted by

$$\nabla f = f \left(\mathbf{e}_R \frac{\partial}{\partial R} + \mathbf{e}_\theta \frac{1}{R} \frac{\partial}{\partial \theta} + \mathbf{e}_\phi \frac{1}{R \sin \theta} \frac{\partial}{\partial \phi} \right) = \mathbf{e}_R \frac{\partial f}{\partial R} + \mathbf{e}_\theta \frac{1}{R} \frac{\partial f}{\partial \theta} + \mathbf{e}_\phi \frac{1}{R \sin \theta} \frac{\partial f}{\partial \phi}.$$

Alternatively, in matrix form,

$$\nabla f = \left[\frac{\partial f}{\partial R}, \frac{1}{R} \frac{\partial f}{\partial \theta}, \frac{1}{R \sin \theta} \frac{\partial f}{\partial \phi} \right]^T.$$

Gradient of a vector function: Let $\mathbf{v} = v_R \mathbf{e}_R + v_\theta \mathbf{e}_\theta + v_\phi \mathbf{e}_\phi$ be a vector function of position. The gradient of \mathbf{v} is a tensor, which can be represented as a dyadic product of the vector with the gradient operator as

$$\mathbf{v} \otimes \nabla = (v_R \mathbf{e}_R + v_\theta \mathbf{e}_\theta + v_\phi \mathbf{e}_\phi) \otimes \left(\mathbf{e}_R \frac{\partial}{\partial R} + \mathbf{e}_\theta \frac{1}{R} \frac{\partial}{\partial \theta} + \mathbf{e}_\phi \frac{1}{R \sin \theta} \frac{\partial}{\partial \phi} \right).$$

The dyadic product can be expanded. However, when evaluating the derivatives, it is important to recall that the basis vectors are functions of the coordinates (R, θ, ϕ) , and consequently their derivatives do not vanish. For example,

$$\frac{1}{R} \frac{\partial}{\partial \theta} (\nu_R \mathbf{e}_R) \otimes \mathbf{e}_\theta = \frac{1}{R} \frac{\partial \nu_R}{\partial \theta} \mathbf{e}_R \otimes \mathbf{e}_\theta + \frac{\nu_R}{R} \frac{\partial \mathbf{e}_R}{\partial \theta} \otimes \mathbf{e}_\theta = \frac{1}{R} \frac{\partial \nu_R}{\partial \theta} \mathbf{e}_R \otimes \mathbf{e}_\theta + \frac{\nu_R}{R} \mathbf{e}_\theta \otimes \mathbf{e}_\theta.$$

Verify for yourself that the matrix representing the components of the gradient of a vector is

$$\mathbf{v} \otimes \nabla \equiv \begin{bmatrix} \frac{\partial \nu_R}{\partial R} & \frac{1}{R} \frac{\partial \nu_R}{\partial \theta} - \frac{\nu_\theta}{R} & \frac{1}{R \sin \theta} \frac{\partial \nu_R}{\partial \phi} - \frac{\nu_\phi}{R} \\ \frac{\partial \nu_\theta}{\partial R} & \frac{1}{R} \frac{\partial \nu_\theta}{\partial \theta} + \frac{\nu_R}{R} & \frac{1}{R \sin \theta} \frac{\partial \nu_\theta}{\partial \phi} - \cot \theta \frac{\nu_\phi}{R} \\ \frac{\partial \nu_\phi}{\partial R} & \frac{1}{R} \frac{\partial \nu_\phi}{\partial \theta} & \frac{1}{R \sin \theta} \frac{\partial \nu_\phi}{\partial \phi} + \cot \theta \frac{\nu_\theta}{R} + \frac{\nu_R}{R} \end{bmatrix}.$$

Divergence of a vector function: Let $\mathbf{v} = \nu_R \mathbf{e}_R + \nu_\theta \mathbf{e}_\theta + \nu_\phi \mathbf{e}_\phi$ be a vector function of position. The divergence of \mathbf{v} is a scalar, which can be represented as a dot product of the vector with the gradient operator as

$$\nabla \cdot \mathbf{v} = \left(\mathbf{e}_R \frac{\partial}{\partial R} + \mathbf{e}_\theta \frac{1}{R} \frac{\partial}{\partial \theta} + \mathbf{e}_\phi \frac{1}{R \sin \theta} \frac{\partial}{\partial \phi} \right) \cdot (\nu_R \mathbf{e}_R + \nu_\theta \mathbf{e}_\theta + \nu_\phi \mathbf{e}_\phi).$$

Again, when expanding the dot product, it is important to remember to differentiate the basis vectors. Alternatively, the divergence can be expressed as trace $(\mathbf{v} \otimes \nabla)$, which immediately gives

$$\nabla \cdot \mathbf{v} \equiv \frac{\partial \nu_R}{\partial R} + 2 \frac{\nu_R}{R} + \frac{1}{R} \frac{\partial \nu_\theta}{\partial \theta} + \frac{1}{R \sin \theta} \frac{\partial \nu_\phi}{\partial \phi} + \cot \theta \frac{\nu_\theta}{R}.$$

Curl of a vector function: Let $\mathbf{v} = \nu_R \mathbf{e}_R + \nu_\theta \mathbf{e}_\theta + \nu_\phi \mathbf{e}_\phi$ be a vector function of position. The curl of \mathbf{v} is a vector, which can be represented as a cross product of the vector with the gradient operator as

$$\nabla \times \mathbf{v} = \left(\mathbf{e}_R \frac{\partial}{\partial R} + \mathbf{e}_\theta \frac{1}{R} \frac{\partial}{\partial \theta} + \mathbf{e}_\phi \frac{1}{R \sin \theta} \frac{\partial}{\partial \phi} \right) \times (\nu_R \mathbf{e}_R + \nu_\theta \mathbf{e}_\theta + \nu_\phi \mathbf{e}_\phi).$$

The curl rarely appears in solid mechanics so the components will not be expanded in full.

Divergence of a tensor function: Let \mathbf{S} be a tensor, with dyadic representation

$$\begin{aligned}\mathbf{S} = & S_{RR}\mathbf{e}_R \otimes \mathbf{e}_R + S_{R\theta}\mathbf{e}_R \otimes \mathbf{e}_\theta + S_{R\phi}\mathbf{e}_R \otimes \mathbf{e}_\phi \\ & + S_{\theta R}\mathbf{e}_\theta \otimes \mathbf{e}_R + S_{\theta\theta}\mathbf{e}_\theta \otimes \mathbf{e}_\theta + S_{\theta\phi}\mathbf{e}_\theta \otimes \mathbf{e}_\phi \\ & + S_{\phi R}\mathbf{e}_\phi \otimes \mathbf{e}_R + S_{\phi\theta}\mathbf{e}_\phi \otimes \mathbf{e}_\theta + S_{\phi\phi}\mathbf{e}_\phi \otimes \mathbf{e}_\phi.\end{aligned}$$

The divergence of \mathbf{S} is a vector, which can be represented as

$$\nabla \cdot \mathbf{S} = \left(\mathbf{e}_R \frac{\partial}{\partial R} + \mathbf{e}_\theta \frac{1}{R} \frac{\partial}{\partial \theta} + \mathbf{e}_\phi \frac{1}{R \sin \theta} \frac{\partial}{\partial \phi} \right) \cdot \begin{pmatrix} S_{RR}\mathbf{e}_R \otimes \mathbf{e}_R + S_{R\theta}\mathbf{e}_R \otimes \mathbf{e}_\theta + S_{R\phi}\mathbf{e}_R \otimes \mathbf{e}_\phi \\ + S_{\theta R}\mathbf{e}_\theta \otimes \mathbf{e}_R + S_{\theta\theta}\mathbf{e}_\theta \otimes \mathbf{e}_\theta + S_{\theta\phi}\mathbf{e}_\theta \otimes \mathbf{e}_\phi \\ + S_{\phi R}\mathbf{e}_\phi \otimes \mathbf{e}_R + S_{\phi\theta}\mathbf{e}_\phi \otimes \mathbf{e}_\theta + S_{\phi\phi}\mathbf{e}_\phi \otimes \mathbf{e}_\phi \end{pmatrix}.$$

Evaluating the components of the divergence is an extremely tedious operation, because each of the basis vectors in the dyadic representation of \mathbf{S} must be differentiated, in addition to the components themselves. The final result (expressed as a column vector) is

$$\nabla \cdot \mathbf{S} = \begin{bmatrix} \frac{\partial S_{RR}}{\partial R} + 2 \frac{S_{RR}}{R} + \frac{1}{R} \frac{\partial S_{\theta R}}{\partial \theta} + \cot \theta \frac{S_{\theta R}}{R} + \frac{1}{R \sin \theta} \frac{\partial S_{\phi R}}{\partial \phi} - \frac{1}{R} (S_{\theta\theta} + S_{\phi\phi}) \\ \frac{\partial S_{R\theta}}{\partial R} + 2 \frac{S_{R\theta}}{R} + \frac{1}{R} \frac{\partial S_{\theta\theta}}{\partial \theta} + \cot \theta \frac{S_{\theta\theta}}{R} + \frac{1}{R \sin \theta} \frac{\partial S_{\phi\theta}}{\partial \phi} + \frac{S_{\theta R}}{R} - \cot \theta \frac{S_{\phi\theta}}{R} \\ \frac{\partial S_{R\phi}}{\partial R} + 2 \frac{S_{R\phi}}{R} + \frac{\sin \theta}{R} \frac{\partial S_{\theta\phi}}{\partial \theta} + \cos \theta \frac{S_{\theta\phi}}{R} + \frac{1}{R \sin \theta} \frac{\partial S_{\phi\phi}}{\partial \phi} + \frac{1}{R} (S_{\phi R} + S_{\phi\theta}) \end{bmatrix}.$$

D.2 CYLINDRICAL-POLAR COORDINATES

D.2.1 Specifying Points in Space Using Cylindrical-Polar Coordinates

To specify the location of a point in cylindrical-polar coordinates, we choose an origin at some point on the axis of the cylinder, select a unit vector \mathbf{k} to be parallel to the axis of the cylinder, and choose a convenient direction for the basis vector \mathbf{i} , as shown in Figure D.4. We then use the three numbers r, θ, z to locate a point inside the cylinder, as shown in the figure. These are not components of a vector. In words,

- r is the radial distance of P from the axis of the cylinder.
- θ is the angle between the \mathbf{i} direction and the projection of OP onto the \mathbf{i}, \mathbf{j} plane.
- z is the length of the projection of OP on the axis of the cylinder.

By convention $r > 0$ and $0 \leq \theta \leq 360^\circ$.

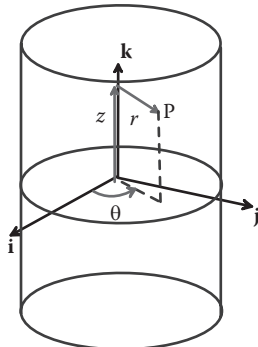


FIGURE D.4 Cylindrical-polar coordinates.

D.2.2 Converting between Cylindrical Polar and Rectangular Cartesian Coordinates

When we use a Cartesian basis, we identify points in space by specifying the components of their position vector relative to the origin (x, y, z), such that $\mathbf{r} = xi + yj + zk$. When we use a spherical-polar coordinate system, we locate points by specifying their spherical-polar coordinates r, θ, z .

The formulas below relate the two representations. They are derived using basic trigonometry:

$$x = r \cos \theta \quad r = \sqrt{x^2 + y^2}$$

$$y = r \sin \theta \quad \theta = \tan^{-1} y/x$$

$$z = z. \quad z = z.$$

D.2.3 Cylindrical-Polar Representation of Vectors

When we work with vectors in spherical-polar coordinates, we specify vectors as components in the $\{\mathbf{e}_r, \mathbf{e}_\theta, \mathbf{e}_z\}$ basis shown in Figure D.5. For example, an arbitrary vector \mathbf{a} is

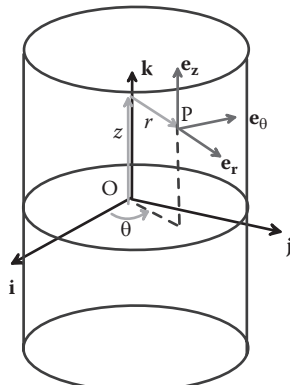


FIGURE D.5 Basis vectors for cylindrical-polar coordinates.

written as $\mathbf{a} = a_r \mathbf{e}_r + a_\theta \mathbf{e}_\theta + a_z \mathbf{e}_z$, where (a_r, a_θ, a_z) denote the components of \mathbf{a} . The basis vectors are selected as follows:

- \mathbf{e}_r is a unit vector normal to the cylinder at P.
- \mathbf{e}_θ is a unit vector circumferential to the cylinder at P, chosen to make $\{\mathbf{e}_r, \mathbf{e}_\theta, \mathbf{e}_z\}$ a right-handed triad.
- \mathbf{e}_z is parallel to the \mathbf{k} vector.

You will see that the position vector of point P would be expressed as

$$\mathbf{r} = r \mathbf{e}_r + z \mathbf{e}_z = r \cos \theta \mathbf{i} + r \sin \theta \mathbf{j} + z \mathbf{k}.$$

Note also that the basis vectors are intentionally chosen to satisfy

$$\mathbf{e}_r = \frac{1}{|\partial \mathbf{r}|} \frac{\partial \mathbf{r}}{\partial r}, \quad \mathbf{e}_\theta = \frac{1}{|\partial \mathbf{r}|} \frac{\partial \mathbf{r}}{\partial \theta}, \quad \mathbf{e}_z = \frac{1}{|\partial \mathbf{r}|} \frac{\partial \mathbf{r}}{\partial z}.$$

The basis vectors have unit length, are mutually perpendicular, and form a right-handed triad, and therefore $\{\mathbf{e}_r, \mathbf{e}_\theta, \mathbf{e}_z\}$ is an orthonormal basis. The basis vectors are parallel to (but not equivalent to) the natural basis vectors for a cylindrical polar coordinate system (for a more detailed discussion, see Chapter 10).

D.2.4 Converting Vectors between Cylindrical and Cartesian Bases

Let $\mathbf{a} = a_r \mathbf{e}_r + a_\theta \mathbf{e}_\theta + a_z \mathbf{e}_z$ be a vector, with components (a_r, a_θ, a_z) in the spherical-polar basis $\{\mathbf{e}_r, \mathbf{e}_\theta, \mathbf{e}_z\}$. Let a_x, a_y, a_z denote the components of \mathbf{a} in the basis $\{\mathbf{i}, \mathbf{j}, \mathbf{k}\}$.

The two sets of components are related by

$$\begin{bmatrix} a_x \\ a_y \\ a_z \end{bmatrix} = \begin{bmatrix} \cos \theta & -\sin \theta & 0 \\ \sin \theta & \cos \theta & 0 \\ 0 & 0 & 1 \end{bmatrix} \begin{bmatrix} a_r \\ a_\theta \\ a_z \end{bmatrix} = \begin{bmatrix} a_r \\ a_\theta \\ a_z \end{bmatrix} = \begin{bmatrix} \cos \theta & \sin \theta & 0 \\ -\sin \theta & \cos \theta & 0 \\ 0 & 0 & 1 \end{bmatrix} \begin{bmatrix} a_x \\ a_y \\ a_z \end{bmatrix}.$$

Observe that the two 3×3 matrices involved in this transformation are transposes (and inverses) of one another. The transformation matrix is therefore orthogonal, satisfying $[Q][Q]^T = [I]$, where $[I]$ denotes the 3×3 identity matrix. The derivation of these results follows the procedure outlined in D.1.4 exactly and is left as an exercise.

D.2.5 Cylindrical-Polar Representation of Tensors

The triad of vectors $\{\mathbf{e}_r, \mathbf{e}_\theta, \mathbf{e}_z\}$ is an orthonormal basis (i.e., the three basis vectors have unit length and are mutually perpendicular). Consequently, tensors can be

represented as components in this basis in exactly the same way as for a fixed Cartesian basis $\{\mathbf{e}_1, \mathbf{e}_2, \mathbf{e}_3\}$. In particular, a general second-order tensor \mathbf{S} can be represented as a 3×3 matrix:

$$\mathbf{S} \equiv \begin{bmatrix} S_{rr} & S_{r\theta} & S_{rz} \\ S_{\theta r} & S_{\theta\theta} & S_{\theta z} \\ S_{zr} & S_{z\theta} & S_{zz} \end{bmatrix}.$$

You can think of S_{rr} as being equivalent to S_{11} , $S_{r\theta}$ as S_{12} , and so on. All tensor operations, such as addition, multiplication by a vector, tensor products, etc., can be expressed in terms of the corresponding operations on this matrix, as discussed in Section B.2 of Appendix B. The component representation of a tensor can also be expressed in dyadic form as

$$\begin{aligned} \mathbf{S} = & S_{rr}\mathbf{e}_r \otimes \mathbf{e}_r + S_{r\theta}\mathbf{e}_r \otimes \mathbf{e}_\theta + S_{rz}\mathbf{e}_r \otimes \mathbf{e}_z \\ & + S_{\theta r}\mathbf{e}_\theta \otimes \mathbf{e}_r + S_{\theta\theta}\mathbf{e}_\theta \otimes \mathbf{e}_\theta + S_{\theta z}\mathbf{e}_\theta \otimes \mathbf{e}_z \\ & + S_{zr}\mathbf{e}_z \otimes \mathbf{e}_r + S_{z\theta}\mathbf{e}_z \otimes \mathbf{e}_\theta + S_{zz}\mathbf{e}_z \otimes \mathbf{e}_z. \end{aligned}$$

The remarks in Section D.1.5 regarding the physical significance of tensor components also applies to tensor components in cylindrical-polar coordinates.

D.2.6 Constitutive Equations in Cylindrical-Polar Coordinates

The constitutive equations listed in Chapter 3 all relate some measure of stress in the solid (expressed as a tensor) to some measure of local internal deformation (deformation gradient, Eulerian strain, rate of deformation tensor, etc.), also expressed as a tensor. The constitutive equations can be used without modification in cylindrical-polar coordinates, as long as the matrices of Cartesian components of the various tensors are replaced by their equivalent matrices in spherical-polar coordinates.

For example, the stress-strain relations for an isotropic, linear elastic material in cylindrical-polar coordinates read

$$\begin{bmatrix} \varepsilon_r \\ \varepsilon_{\theta\theta} \\ \varepsilon_{zz} \\ 2\varepsilon_{rz} \\ 2\varepsilon_{r\theta} \\ 2\varepsilon_{\theta z} \end{bmatrix} = \frac{1}{E} \begin{bmatrix} 1 & -\nu & -\nu & 0 & 0 & 0 \\ -\nu & 1 & -\nu & 0 & 0 & 0 \\ -\nu & -\nu & 1 & 0 & 0 & 0 \\ 0 & 0 & 0 & 2(1+\nu) & 0 & 0 \\ 0 & 0 & 0 & 0 & 2(1+\nu) & 0 \\ 0 & 0 & 0 & 0 & 0 & 2(1+\nu) \end{bmatrix} \begin{bmatrix} \sigma_{rr} \\ \sigma_{\theta\theta} \\ \sigma_{zz} \\ \sigma_{\theta z} \\ \sigma_{rz} \\ \sigma_{r\theta} \end{bmatrix} + \alpha \Delta T \begin{bmatrix} 1 \\ 1 \\ 1 \\ 0 \\ 0 \\ 0 \end{bmatrix}.$$

The cautionary remarks regarding anisotropic materials in Appendix D.1.6 also applies to cylindrical-polar coordinate systems.

D.2.7 Converting Tensors between Cartesian and Spherical-Polar Bases

Let \mathbf{S} be a tensor, with components

$$\mathbf{S} \equiv \begin{bmatrix} S_{rr} & S_{r\theta} & S_{rz} \\ S_{\theta r} & S_{\theta\theta} & S_{\theta z} \\ S_{zr} & S_{z\theta} & S_{zz} \end{bmatrix} \equiv \begin{bmatrix} S_{xx} & S_{xy} & S_{xz} \\ S_{yx} & S_{yy} & S_{yz} \\ S_{zx} & S_{xy} & S_{zz} \end{bmatrix}$$

in the cylindrical-polar basis $\{\mathbf{e}_r, \mathbf{e}_\theta, \mathbf{e}_z\}$ and the Cartesian basis $\{\mathbf{i}, \mathbf{j}, \mathbf{k}\}$, respectively. The two sets of components are related by

$$\begin{aligned} \begin{bmatrix} S_{xx} & S_{xy} & S_{xz} \\ S_{yx} & S_{yy} & S_{yz} \\ S_{zx} & S_{xy} & S_{zz} \end{bmatrix} &= \begin{bmatrix} \cos\theta & -\sin\theta & 0 \\ \sin\theta & \cos\theta & 0 \\ 0 & 0 & 1 \end{bmatrix} \begin{bmatrix} S_{rr} & S_{r\theta} & S_{rz} \\ S_{\theta r} & S_{\theta\theta} & S_{\theta z} \\ S_{zr} & S_{z\theta} & S_{zz} \end{bmatrix} \begin{bmatrix} \cos\theta & \sin\theta & 0 \\ -\sin\theta & \cos\theta & 0 \\ 0 & 0 & 1 \end{bmatrix} \\ \begin{bmatrix} S_{rr} & S_{r\theta} & S_{rz} \\ S_{\theta r} & S_{\theta\theta} & S_{\theta z} \\ S_{zr} & S_{z\theta} & S_{zz} \end{bmatrix} &= \begin{bmatrix} \cos\theta & \sin\theta & 0 \\ -\sin\theta & \cos\theta & 0 \\ 0 & 0 & 1 \end{bmatrix} \begin{bmatrix} S_{xx} & S_{xy} & S_{xz} \\ S_{yx} & S_{yy} & S_{yz} \\ S_{zx} & S_{xy} & S_{zz} \end{bmatrix} \begin{bmatrix} \cos\theta & -\sin\theta & 0 \\ \sin\theta & \cos\theta & 0 \\ 0 & 0 & 1 \end{bmatrix}. \end{aligned}$$

D.2.8 Vector Calculus Using Cylindrical-Polar Coordinates

Calculating derivatives of scalar, vector, and tensor functions of position in cylindrical-polar coordinates is complicated by the fact that the basis vectors are functions of position. The results can be expressed in a compact form by defining the *gradient operator*, which, in spherical-polar coordinates, has the representation

$$\nabla \equiv \left(\mathbf{e}_r \frac{\partial}{\partial r} + \mathbf{e}_\theta \frac{1}{r} \frac{\partial}{\partial \theta} + \mathbf{e}_z \frac{\partial}{\partial z} \right).$$

In addition, the nonzero derivatives of the basis vectors are

$$\frac{\partial \mathbf{e}_r}{\partial \theta} = \mathbf{e}_\theta \quad \frac{\partial \mathbf{e}_\theta}{\partial \theta} = -\mathbf{e}_r \quad (\text{all other derivatives are zero}).$$

The various derivatives of scalars, vectors, and tensors can be expressed using operator notation as follows.

Gradient of a scalar function: Let $f(r, \theta, z)$ denote a scalar function of position. The gradient of f is denoted by

$$\nabla f = \left(\mathbf{e}_r \frac{\partial}{\partial r} + \mathbf{e}_\theta \frac{1}{r} \frac{\partial}{\partial \theta} + \mathbf{e}_z \frac{\partial}{\partial z} \right) f = \mathbf{e}_r \frac{\partial f}{\partial r} + \mathbf{e}_\theta \frac{1}{r} \frac{\partial f}{\partial \theta} + \mathbf{e}_z \frac{\partial f}{\partial z}.$$

Alternatively, in matrix form,

$$\nabla f = \left[\frac{\partial f}{\partial r}, \frac{1}{r} \frac{\partial f}{\partial \theta}, \frac{\partial f}{\partial z} \right]^T.$$

Gradient of a vector function: Let $\mathbf{v} = v_r \mathbf{e}_r + v_\theta \mathbf{e}_\theta + v_z \mathbf{e}_z$ be a vector function of position. The gradient of \mathbf{v} is a tensor, which can be represented as a dyadic product of the vector with the gradient operator as

$$\mathbf{v} \otimes \nabla = (v_r \mathbf{e}_r + v_\theta \mathbf{e}_\theta + v_z \mathbf{e}_z) \otimes \left(\mathbf{e}_r \frac{\partial}{\partial r} + \mathbf{e}_\theta \frac{1}{r} \frac{\partial}{\partial \theta} + \mathbf{e}_z \frac{\partial}{\partial z} \right).$$

The dyadic product can be expanded; however, when evaluating the derivatives, it is important to recall that the basis vectors are functions of the coordinate θ and consequently their derivatives may not vanish. For example,

$$\frac{1}{r} \frac{\partial}{\partial \theta} (v_r \mathbf{e}_r) \otimes \mathbf{e}_\theta = \frac{1}{r} \frac{\partial v_r}{\partial \theta} \mathbf{e}_r \otimes \mathbf{e}_\theta + \frac{v_r}{r} \frac{\partial \mathbf{e}_r}{\partial \theta} \otimes \mathbf{e}_\theta = \frac{1}{r} \frac{\partial v_r}{\partial \theta} \mathbf{e}_r \otimes \mathbf{e}_\theta + \frac{v_r}{r} \mathbf{e}_\theta \otimes \mathbf{e}_\theta.$$

Verify for yourself that the matrix representing the components of the gradient of a vector is

$$\mathbf{v} \otimes \nabla \equiv \begin{bmatrix} \frac{\partial v_r}{\partial r} & \frac{1}{r} \frac{\partial v_r}{\partial \theta} - \frac{v_\theta}{r} & \frac{\partial v_r}{\partial z} \\ \frac{\partial v_\theta}{\partial r} & \frac{1}{r} \frac{\partial v_\theta}{\partial \theta} + \frac{v_r}{r} & \frac{\partial v_\theta}{\partial z} \\ \frac{\partial v_z}{\partial r} & \frac{1}{r} \frac{\partial v_z}{\partial \theta} & \frac{\partial v_z}{\partial z} \end{bmatrix}.$$

Divergence of a vector function: Let $\mathbf{v} = v_r \mathbf{e}_r + v_\theta \mathbf{e}_\theta + v_z \mathbf{e}_z$ be a vector function of position. The divergence of \mathbf{v} is a scalar, which can be represented as a dot product of the vector with the gradient operator as

$$\nabla \cdot \mathbf{v} = \left(\mathbf{e}_r \frac{\partial}{\partial r} + \mathbf{e}_\theta \frac{1}{r} \frac{\partial}{\partial \theta} + \mathbf{e}_z \frac{\partial}{\partial z} \right) \cdot (v_r \mathbf{e}_r + v_\theta \mathbf{e}_\theta + v_z \mathbf{e}_z).$$

Again, when expanding the dot product, it is important to remember to differentiate the basis vectors. Alternatively, the divergence can be expressed as trace $(\mathbf{v} \otimes \nabla)$, which immediately gives

$$\nabla \cdot \mathbf{v} \equiv \frac{\partial v_r}{\partial r} + \frac{v_r}{r} + \frac{1}{r} \frac{\partial v_\theta}{\partial \theta} + \frac{\partial v_z}{\partial z}.$$

Curl of a vector function: Let $\mathbf{v} = v_r \mathbf{e}_r + v_\theta \mathbf{e}_\theta + v_z \mathbf{e}_z$ be a vector function of position. The curl of \mathbf{v} is a vector, which can be represented as a cross product of the vector with the gradient operator as

$$\nabla \times \mathbf{v} = \left(\mathbf{e}_r \frac{\partial}{\partial r} + \mathbf{e}_\theta \frac{1}{r} \frac{\partial}{\partial \theta} + \mathbf{e}_z \frac{\partial}{\partial z} \right) \times (v_r \mathbf{e}_r + v_\theta \mathbf{e}_\theta + v_z \mathbf{e}_z).$$

The curl rarely appears in solid mechanics so the components will not be expanded in full.

Divergence of a tensor function: Let \mathbf{S} be a tensor, with dyadic representation

$$\begin{aligned} \mathbf{S} = & S_{rr} \mathbf{e}_r \otimes \mathbf{e}_r + S_{r\theta} \mathbf{e}_r \otimes \mathbf{e}_\theta + S_{rz} \mathbf{e}_r \otimes \mathbf{e}_z \\ & + S_{\theta r} \mathbf{e}_\theta \otimes \mathbf{e}_r + S_{\theta\theta} \mathbf{e}_\theta \otimes \mathbf{e}_\theta + S_{\theta z} \mathbf{e}_\theta \otimes \mathbf{e}_z \\ & + S_{zr} \mathbf{e}_z \otimes \mathbf{e}_r + S_{z\theta} \mathbf{e}_z \otimes \mathbf{e}_\theta + S_{zz} \mathbf{e}_z \otimes \mathbf{e}_z. \end{aligned}$$

The divergence of \mathbf{S} is a vector, which can be represented as

$$\nabla \cdot \mathbf{S} = \left(\mathbf{e}_r \frac{\partial}{\partial r} + \mathbf{e}_\theta \frac{1}{r} \frac{\partial}{\partial \theta} + \mathbf{e}_z \frac{\partial}{\partial z} \right) \cdot \begin{pmatrix} S_{rr} \mathbf{e}_r \otimes \mathbf{e}_r + S_{r\theta} \mathbf{e}_r \otimes \mathbf{e}_\theta + S_{rz} \mathbf{e}_r \otimes \mathbf{e}_z \\ + S_{\theta r} \mathbf{e}_\theta \otimes \mathbf{e}_r + S_{\theta\theta} \mathbf{e}_\theta \otimes \mathbf{e}_\theta + S_{\theta z} \mathbf{e}_\theta \otimes \mathbf{e}_z \\ + S_{zr} \mathbf{e}_z \otimes \mathbf{e}_r + S_{z\theta} \mathbf{e}_z \otimes \mathbf{e}_\theta + S_{zz} \mathbf{e}_z \otimes \mathbf{e}_z \end{pmatrix}.$$

Evaluating the components of the divergence is an extremely tedious operation, because each of the basis vectors in the dyadic representation of \mathbf{S} must be differentiated, in addition to the components themselves. The final result (expressed as a column vector) is

$$\nabla \cdot \mathbf{S} \equiv \begin{bmatrix} \frac{\partial S_{rr}}{\partial r} + \frac{S_{rr}}{r} - \frac{1}{r} \frac{\partial S_{\theta r}}{\partial \theta} + \frac{\partial S_{zr}}{\partial z} - \frac{S_{\theta\theta}}{r} \\ \frac{1}{r} \frac{\partial S_{\theta\theta}}{\partial \theta} + \frac{\partial S_{r\theta}}{\partial r} + \frac{S_{r\theta}}{r} + \frac{S_{\theta r}}{r} + \frac{\partial S_{z\theta}}{\partial z} \\ \frac{\partial S_{zz}}{\partial z} + \frac{\partial S_{rz}}{\partial r} + \frac{S_{rz}}{r} + \frac{1}{r} \frac{\partial S_{\theta z}}{\partial \theta} \end{bmatrix}.$$

Appendix E: Miscellaneous Derivations

E.1 RELATION BETWEEN THE AREAS OF THE FACES OF A TETRAHEDRON

For the tetrahedron shown in Figure E.1, we prove that:

$$\frac{dA_1}{dA_{(n)}} = n_1 \quad \frac{dA_2}{dA_{(n)}} = n_2 \quad \frac{dA_3}{dA_{(n)}} = n_3,$$

where $dA_{(n)}$ is the area of the face with normal \mathbf{n} , and dA_i is the face with normal $-\mathbf{e}_i$. Note that

$$dA_1 = \frac{1}{2}bc \quad dA_2 = \frac{1}{2}ac \quad dA_3 = \frac{1}{2}ab.$$

Note also that we can compute the area of the face with normal \mathbf{n} by taking cross products of the vectors defining the sides of the face:

$$\begin{aligned} dA_{(n)}\mathbf{n} &= \frac{1}{2}(c\mathbf{e}_3 - b\mathbf{e}_2) \times (a\mathbf{e}_1 - b\mathbf{e}_2) = \frac{1}{2}(bce_1 + ace_2 + abe_3) \\ \Rightarrow dA_{(n)}\mathbf{n} &= dA_1\mathbf{e}_1 + dA_2\mathbf{e}_2 + dA_3\mathbf{e}_3 \\ \Rightarrow \mathbf{n} &= \frac{dA_1}{dA_{(n)}}\mathbf{e}_1 + \frac{dA_2}{dA_{(n)}}\mathbf{e}_2 + \frac{dA_3}{dA_{(n)}}\mathbf{e}_3 \end{aligned}$$

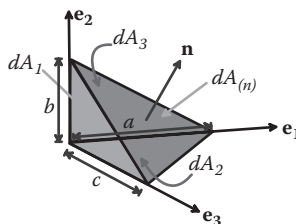


FIGURE E.1 Tetrahedron with three faces perpendicular to basis vectors.

so that

$$\frac{dA_1}{dA_{(n)}} = n_1 \quad \frac{dA_2}{dA_{(n)}} = n_2 \quad \frac{dA_3}{dA_{(n)}} = n_3,$$

as required.

E.2 RELATION BETWEEN AREA ELEMENTS BEFORE AND AFTER DEFORMATION

Consider an element of area dA_0 with normal \mathbf{n}^0 in a deformable solid (Figure E.2). Suppose the solid is deformed by subjecting it to some loading and let F_{ij} denote the components of the deformation gradient tensor field in the solid. The area element deforms with the solid and has a new area dA and normal \mathbf{n} , as shown in Figure E.2. We plan to prove that the deformed area element is related to its undeformed area through

$$dAn_i = JF_{ki}^{-1}n_k^0dA_0,$$

where $J = \det(F_{ij})$.

Start by noting that the area dA_0 before deformation can be computed by taking the cross product of two infinitesimal vectors dv_i , dw_i bounding the area element in the undeformed configuration

$$dA_0 n_i^0 = \epsilon_{ijk} dv_j dw_k.$$

Note that the infinitesimal vectors map to $F_{ij}dw_j$, $F_{ij}dv_j$ in the deformed configuration. Therefore, the area after deformation is given by

$$dAn_i = \epsilon_{ijk} F_{jm} dv_m F_{kn} dw_n.$$

Let F_{ij}^{-1} denote the inverse of the deformation gradient tensor, i.e., $F_{ik}F_{kj}^{-1} = \delta_{ij}$. Then, we could write

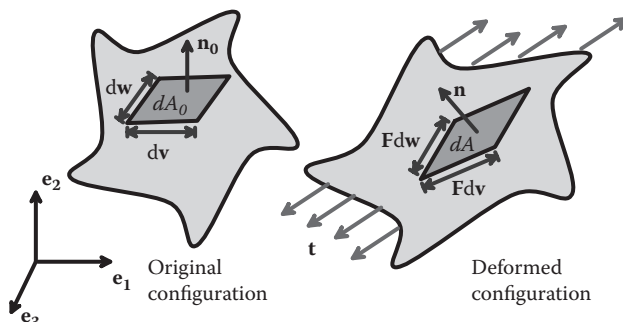


FIGURE E.2 Deformation of an area element within a solid.

$$dAn_i = F_{pl}F_{li}^{-1} \epsilon_{pjk} F_{jm}F_{kn} dv_m dw_n.$$

Now, recall the identity

$$\begin{aligned} \lambda &= \det \mathbf{A} \equiv \lambda = \frac{1}{6} \epsilon_{ijk} \epsilon_{lmn} A_{li} A_{mj} A_{nk} \\ &\Leftrightarrow \epsilon_{lmn} \lambda = \epsilon_{ijk} A_{il} A_{jm} A_{kn} \end{aligned}$$

so that

$$dAn_i = F_{li}^{-1} J \epsilon_{lmn} dv_m dw_n = F_{li}^{-1} J dA_0 n_l^0,$$

where $J = \det(F_{ij})$, giving the required result.

E.3 TIME DERIVATIVES OF INTEGRALS OVER VOLUMES WITHIN A DEFORMING SOLID

Consider the deformable solid sketched in Figure E.3. Let ρ_0 denote the mass density of the solid in the original configuration and let ρ denote the mass density in the deformed configuration (both ρ_0 and ρ can vary with position in the solid). Let V_0 denote a closed region within the undeformed solid and let V be the same region of the solid in the deformed configuration. Suppose that

$$v_i = \frac{\partial u_i}{\partial t}$$

denotes the velocity field within the body. We shall show that

$$\frac{d}{dt} \left\{ \int_V \rho v_i dV \right\} = \int_V \rho \frac{dv_i}{dt} dV$$

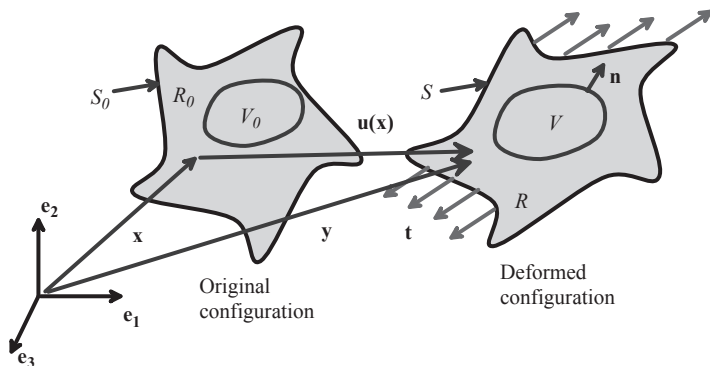


FIGURE E.3 Internal volume within a deformable solid.

and also that

$$\frac{d}{dt} \left\{ \int_V \epsilon_{ijk} y_j \rho v_k dV \right\} = \int_V \rho \epsilon_{ijk} y_j \frac{dv_k}{dt} dV.$$

At first glance, this looks obvious: why not just take the derivative under the integral sign? You can't do this, however, because the volume V changes with time, as the solid is deforming. In addition, the mass density varies with time, because of the deformation, so even if we could take the time derivative under the integral, we would end up with an additional term. To do the derivative properly, we first need to change variables so the integral is evaluated over the undeformed volume (which is independent of time). Thus,

$$\int_V \rho v_i dV = \int_{V_0} \rho v_i J dV_0 = \int_{V_0} \rho_0 v_i dV_0,$$

where

$$J = \det(F_{ij}) = \frac{dV}{dV_0},$$

and we have recalled a result from Section 2.1.4:

$$J\rho = \rho_0.$$

Now, we can happily differentiate. The mass density in the undeformed configuration does not vary with time, so that

$$\frac{d}{dt} \left\{ \int_{V_0} \rho_0 v_i dV_0 \right\} = \int_{V_0} \rho_0 \frac{dv_i}{dt} dV_0 = \int_V \rho \frac{dv_i}{dt} dV.$$

The last expression was obtained by changing variables in the integral back to the deformed configuration. This is the first result we wanted.

To show the second result, follow exactly the same procedure, until you obtain

$$\frac{d}{dt} \left\{ \int_{V_0} \epsilon_{ijk} y_j v_k \rho_0 dV_0 \right\} = \int_{V_0} \rho_0 \epsilon_{ijk} \left(\frac{dy_j}{dt} v_k + y_j \frac{dv_k}{dt} \right) dV_0.$$

Now, observe that

$$\epsilon_{ijk} \frac{dy_j}{dt} v_k = \epsilon_{ijk} v_j v_k = 0,$$

(the cross product of two parallel vectors is zero), so substituting this into the preceding equation and changing variables in the integral as before gives the required result.

E.4 TIME DERIVATIVES OF THE CURVATURE VECTOR FOR A DEFORMING ROD

Consider a deforming rod, as shown in Figure E.4:

- Let x_3 denote arc-length coordinate of a material particle on the axis of the undeformed rod.
- Let s denote the arc-length coordinate of this particle after deformation.
- Define basis vectors $\{\mathbf{m}_1, \mathbf{m}_2, \mathbf{m}_3\}$ attached to the deformed rod, following the convention described in Section 10.2.
- Define an angular velocity vector $\boldsymbol{\omega}$ and curvature vector $\boldsymbol{\kappa}$ through

$$\frac{d\mathbf{m}_i}{dt} = \boldsymbol{\omega} \times \mathbf{m}_i \quad \frac{d\mathbf{m}_i}{ds} = \boldsymbol{\kappa} \times \mathbf{m}_i.$$

We shall show that the gradient of the angular velocity vector characterizing the rotation of the rod's cross-section is related to the time derivative of the curvature vector by

$$\frac{d\boldsymbol{\omega}}{ds} = \nabla \boldsymbol{\kappa} = \frac{d\boldsymbol{\kappa}}{dt} - \boldsymbol{\omega} \times \boldsymbol{\kappa} + \frac{dx_3}{ds} \frac{ds}{dx_3} \boldsymbol{\kappa}.$$

To see this, start by differentiating the definition of the angular velocity vector with respect to arc length,

$$\frac{d^2\mathbf{m}_i}{dsdt} = \frac{d\boldsymbol{\omega}}{ds} \times \mathbf{m}_i + \boldsymbol{\omega} \times \frac{d\mathbf{m}_i}{ds} = \frac{d\boldsymbol{\omega}}{ds} \times \mathbf{m}_i + \boldsymbol{\omega} \times (\boldsymbol{\kappa} \times \mathbf{m}_i),$$

and, similarly, differentiating the definition of the curvature vector with respect to time,

$$\frac{d}{dt} \frac{d\mathbf{m}_i}{ds} = \frac{d}{dt} \left(\frac{dx_3}{ds} \frac{d\mathbf{m}_i}{dx_3} \right) = -\frac{ds}{dx_3} \frac{dx_3}{ds} \frac{d\mathbf{m}_i}{ds} + \frac{d^2\mathbf{m}_i}{dsdt} = \frac{d\boldsymbol{\kappa}}{dt} \times \mathbf{m}_i + \boldsymbol{\kappa} \times (\boldsymbol{\omega} \times \mathbf{m}_i),$$

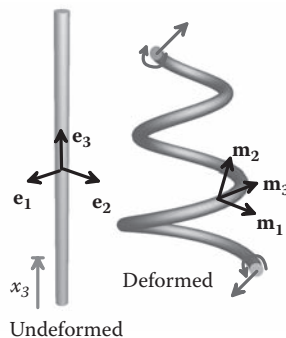


FIGURE E.4. Bending and twisting of an initially straight rod.

where $\dot{s} = (ds/dt)$ with x_3 held fixed. The preceding two results show that

$$\frac{d\omega}{ds} \times \mathbf{m}_i + \omega \times (\kappa \times \mathbf{m}_i) = \frac{d\kappa}{dt} \times \mathbf{m}_i + \kappa \times (\omega \times \mathbf{m}_i) + \frac{d\dot{s}}{dx_3} \frac{dx_3}{ds} \kappa \times \mathbf{m}_i.$$

Next, note that we can expand the triple cross products (see Appendix A) as

$$\begin{aligned}\kappa \times (\omega \times \mathbf{m}_i) - \omega \times (\kappa \times \mathbf{m}_i) &= (\kappa \cdot \mathbf{m}_i)\omega - (\omega \cdot \kappa)\mathbf{m}_i - [(\omega \cdot \mathbf{m}_i)\kappa - (\omega \cdot \kappa)\mathbf{m}_i] \\ &= (\kappa \cdot \mathbf{m}_i)\omega - (\omega \cdot \mathbf{m}_i)\kappa = -\mathbf{m}_i \times (\kappa \times \omega).\end{aligned}$$

Hence, we conclude that

$$\frac{d\omega}{ds} \times \mathbf{m}_i = \frac{d\kappa}{dt} \times \mathbf{m}_i + (\kappa \times \omega) \times \mathbf{m}_i + \frac{d\dot{s}}{dx_3} \frac{dx_3}{ds} \kappa \times \mathbf{m}_i.$$

This result must hold for all three vectors $\{\mathbf{m}_1, \mathbf{m}_2, \mathbf{m}_3\}$ and therefore

$$\frac{d\omega}{ds} = \frac{d\kappa}{dt} - (\omega \times \kappa) + \frac{d\dot{s}}{dx_3} \frac{dx_3}{ds} \kappa,$$

as stated.

References

- Arruda, E., and Boyce, M.C. 1992. "A three-dimensional constitutive model for the large stretch behavior of rubber elastic materials." *J. Mech. Phys. Solids* 41:389.
- Ashby, M.F., and Jones, D.R.H. 1997. *Engineering Materials I*. London: Butterworth-Heinemann.
- Bergstrom, J.S., and Boyce, M.C. 1998. "Constitutive modeling of the large strain time-dependent behavior of elastomers." *J. Mech. Phys. Solids* 46:931.
- Blatz, P.J., and Ko, W.L. 1962. "Application of finite elastic theory to the deformation of rubbery materials." *Trans. Soc. Rheol.* 6:224.
- Bryant, M.D., and Keer, L.M. 1982. "Rough contact between elastically and geometrically identical curved bodies." *J. Appl. Mech.* 49:345.
- Cai, W., Arsenlis, A., Weinberger, C.R., and Bulatov, V.V. 2006. "A non-singular continuum theory of dislocations." *J. Mech. Phys. Solids* 54:561.
- Charalambides, P.G., Cao, H.C., Lund, J., and Evans, A.G. 1990. "Development of a test-method for measuring the mixed mode fracture resistance of bimaterial interfaces." *Mech. Mater.* 8:269.
- Choi, S.T., Shin, H., and Earmme, Y.Y. 2003. "On the unifield approach to anisotropic elasticity, interface and crack in dissimilar media." *Int. J. Solids Struct* 40:1411.
- Clifton, R.J. 1990. "High strain rate behavior of metals." *Appl Mech Rev* 43:S9–S22.
- Coker, D., Lykotrafitis, G., Needleman, A., and Rosakis, A. 2005. "Frictional sliding modes along an interface between identical elastic plates subject to shear impact loading." *J. Mech. Phys. Solids* 53:884.
- Comninou, M. 1977. "Interface crack with friction in the contact zone." *J. Appl. Mech.* 44:631.
- Dieterich, J.H. 1979. "Modeling of rock friction. 1. Experimental results and constitutive equations." *J. Geophys. Res.* 84:2161.
- Eshelby, J.D. 1957. "The determination of the elastic field of an ellipsoidal inclusion and related problems." *Proc. R. Soc. Lond. B. Biol. Sci.* A241:376.
- Eshelby, J.D. 1959. "The elastic field outside an ellipsoidal inclusion." *Proc. R. Soc. Lond. B. Biol. Sci.* A252:561.
- Flanagan, D.P., and Belytschko, T. 1981. "A uniform strain hexahedron and quadrilateral with orthogonal hourglass control." *Int. J. Num. Methods Eng.* 17:679.
- Freund, L.B., and Suresh, S. 2003. *Thin Film Materials*. Cambridge, UK: Cambridge University Press.
- Frost, H.J., and Ashby, M.F. 1982. *Deformation Mechanism Maps*. New York: Pergamon Press.
- Gearing, B.P., Moon, H.S., and Anand, L. 2001. "A plasticity model for interface friction: application to sheet metal forming." *Int. J. Plasticity* 17:237.

- Hamilton, G.M. 1983. "Explicit equations for stresses beneath a sliding spherical contact." *Proc. I. Mech. E.* 197C:53.
- He, M., and Hutchinson, J.W. 1981. "The penny-shaped crack and the plane strain crack in an infinite body of power-law material." *J. Appl. Mech.* 48:830.
- Hutchinson, J.W. 1968. "Singular behavior at the end of a tensile crack in a hardening material." *J. Mech. Phys. Solids* 16:13.
- Johnson, K.L. 1985. *Contact Mechanics*. Cambridge, UK: Cambridge University Press.
- Kreyszig, E. 1998. *Advanced Engineering Mathematics*. New York: Wiley.
- Leichti, K.M., and Knauss, W. 1982. "Crack propagation at material interfaces. I. Experimental technique to determine crack profiles." *Exp. Mech.* 22:383.
- Liu, Y., and Mahadevan, S. 2005. "Multiaxial high-cycle fatigue criterion and life prediction for metals." *Int. J. Fatigue* 27:790.
- Malvern, L.E. 1969. *Introduction to the Mechanics of a Continuous Medium*. Upper Saddle River, NJ: Prentice Hall.
- Matthies, G., Strang, H. 1979. "The solution of nonlinear finite equations." *Int. J. Num. Methods Eng.* 14:1613.
- McCrumb, N.G., Buckley, C.P., and Bucknall, C.B. 1996. *Principles of Polymer Engineering*. New York: Oxford University Press, p. 112.
- Mooney, M. 1940. "A theory of large elastic deformation." *J. Appl. Phys.* 11:582.
- Murakami, Y. 1987. *Stress intensity factors handbook*. New York: Pergamon Press.
- Ogden, R. 1972a. "Large deformation isotropic elasticity: on the correlation of theory and experiment for incompressible rubberlike solids." *Proc. R. Soc. Lond.* A326:565.
- Ogden, R. 1972b. "Large deformation isotropic elasticity: on the correlation of theory and experiment for compressible rubberlike solids." *Proc. R. Soc. A*328:567.
- Ortiz, M., and Pandolfi, A. 1999. "Finite-deformation irreversible cohesive element for three-dimensional crack-propagation analysis." *Int. J. Num. Methods Eng.* 44:1276.
- Pierce, D., Asaro, R.J., and Needleman, A. 1983. "Material rate dependence and localized deformation in crystalline solids." *Acta Metall.* 31:1951.
- Prakash, V. 1998. "Frictional response of sliding interfaces subjected to time varying normal pressures." *J. Tribol.* 120:27.
- Quested, D.L., Pae, K.D., Sheinbein, J.L., and Newman, B.A. 1981. "Viscoplastic behavior of a rubber at high pressures." *J. Appl. Phys.* 52:5977.
- Rice, J.R., and Rosengren, G.F. 1968. "Plane strain deformation near a crack tip in a power-law hardening material." *J. Mech. Phys. Solids* 16:31.
- Rice, J.R., Paris, P.C., and Merkle, J.G. 1973. "Progress in flaw growth and fracture toughness testing." *ASTM STP 536*:231.
- Ruina, A.L. 1983. "Slip instability and state variable friction laws." *J. Geophys. Res.* 88:10359.
- Sackfield, A., and Hills, D.A. 1983. "A note on the Hertz contact problem: a correlation of standard formulae." *J. Strain Anal.* 18:105.
- Shute, N. 1948. *No Highway*. London: Heinemann.
- Simmons, G., and Wang, H. 1970. *Single Crystal Elastic Constants and Calculated Aggregate Properties*. Cambridge, MA: MIT Press.
- Simo, J.C., and Rifai, M.S. 1990. "Class of mixed assumed strain methods and the method of incompatible modes." *Int. J. Num. Methods Eng.* 29:1595.
- Simo, J.C., and Armero, F. 1992. "Geometrically nonlinear enhanced strain mixed methods and the method of incompatible modes." *Int. J. Num. Methods Eng.* 33:1413.
- Sternberg, E. 1954. "On Saint-Venant's principle." *Q. J. Appl. Mech.* 11:393.
- Storakers, B. 1986. "On material representation and constitutive branching in finite compressible elasticity." *J. Mech. Phys. Solids* 34:125.
- Suo, Z., and Hutchinson, J.W. 1989. "Sandwich test specimens for measuring interface crack toughness." *Mat. Sci. Eng.* A107:135.

- Tada, H., Paris, P.C., and Irwin, G.R. 2000. *The Stress Analysis of Cracks Handbook*, 3rd Edition. New York: ASME.
- Timoshenko, S.P., and Woinowsky-Krieger, S. 1959. *Theory of Plates and Shells*. New York: McGraw-Hill.
- Ting, T.C.T. 1996. *Anisotropic Elasticity: Theory and Applications*. New York: Oxford University Press.
- Treloar, L.R.G. 1944. "Stress-strain data for vulcanized rubber under various states of deformation." *Trans. Faraday Soc.* 40:59.
- Treloar, L.R.G. 1948. "Stresses and birefringence in rubber subjected to general homogeneous strain." *Proc. Phys. Soc.* 60:135.
- Wood, D.M. 1990. *Soil Behavior and Critical State Soil Mechanics*. Cambridge, UK: Cambridge University Press.
- Wu, P.D., Neale, K., and Van der Giessen, E. 1996. "Simulation of the behaviour of FCC polycrystals during reversed torsion." *Int. J. Plasticity* 12:1199.
- Xu, X.P., and Needleman, A. 1995. "Numerical simulations of fast crack growth in brittle solids." *J. Mech. Phys. Solids* 42:1397.

This page intentionally left blank

Index

1D FEM, extending to 2D and 3D, 480–481
1D finite element procedure, 476–477
2D analysis, boundary conditions, 5
2D line load
 parallel to infinite solid surface, 264–265
 perpendicular to infinite solid surface, 262–264
2D strain fields, displacement computation, given strain, 35–37
2D/3D linear elastostatic code, sample, 486–489
3D analysis, boundary conditions, 5
3D dislocation loop, 362
 in infinite solid, displacement and stress induced by, 356–359
3D strain fields, displacement computation, given strain, 37–38
3D static linear elasticity problems, solutions to axisymmetric contacts, load displacement-contact area relations for, 308–310
ellipsoidal inclusion in infinite solid subjected to remote stress, elastically mismatched, 299–300
Eshelby inclusion problem, 294–299
flat-ended cylindrical indenter in contact with elastic half-space, 302–303
frictionless contact between two elastic spheres, 304–306
infinite solid subject to remote stress, spherical cavity in, 300–302
nonconformal contacts, frictionless, 306–308
Papkovich–Neuber potential representations, for isotropic solids, 290–291
Papkovich–Neuber solution satisfying governing equations, demonstration of, 291–292
point force in infinite solid, 292
point force normal to infinite half-space surface, 293
point force tangent to infinite half-space surface, 293–294

A

Acoustic tensor, 240
Advanced element formulations, FEM, 530–531
 hybrid elements for modeling near-incompressible materials, 541–543
shear locking and incompatible mode elements, 531–533
volumetric locking and reduced integration elements, 533–534
“B-bar” method, 538–540
reduced integration, 534–537
reduced integration with hourglass control, 540
sample code, 541
selectively reduced integration, 537–538
Aeroelasticity, 7
Airy stress function and solutions, 255
2D line load
 parallel to infinite solid surface, 264–265
 perpendicular to infinite solid surface, 262–264
arbitrary pressure on flat surface, 265
in cylindrical-polar coordinates, 259–260
to end-loaded cantilever, 260–262
in rectangular coordinates, 256–257
satisfying governing equations, demonstration of, 257–259
stress near crack tip, 266–267
uniform normal pressure, on strip, 266
Analysis method
 exact solution, 11–12
 numerical solution, 12
Angular momentum balance, in terms of Cauchy stress, 51–52
Anisotropic linear elastic materials, 310
 Barnett–Lothe integrals, 323–325
 Barnett–Lothe tensors and impedance tensor, 319–320

- basis change formulas for, 79–81
 basis change formulas for matrices in anisotropic elasticity, 321–323
 degenerate materials, 317
 fundamental elasticity matrix, 317–318
 governing equations, 310–312
 line load and dislocation
 below anisotropic half-space surface, 329
 in infinite anisotropic solid, 327–329
 matrices properties in anisotropic elasticity, 320–321
 orthogonal properties of Stroh matrices A and B, 318–319
 physical interpretation of, 78–79
 strain energy density for, 79
 stress-strain relations for, 76–78
 material symmetry effect on, 81–82
 Stroh eigenvalues and anisotropy matrices for cubic materials, 316–317
 Stroh representation
 for fields in, 312–315
 for uniform stress state, 325–327
- Anisotropic linear elasticity, 7
 Anisotropic materials, failure criteria for, 553–554
 Armstrong–Frederick hardening law, 122, 123
 Arruda–Boyce eight-chain model, 101
 Atomistic models, 10, 12
 Axially symmetric problems
 general solutions to boundary value problem, 205–206
 and linear elasticity problems, simplified equations for, 202–205
 simplified equations for plane strain elastic–perfectly plastic solids, 223–225
-
- B**
- Barnett–Lothe integrals, 323–325
 Barnett–Lothe tensors and impedance tensor, 319–320
 “B-bar” method, 538–540
 Blatz–Ko foam rubber, 102
 Body-centered cubic (BCC) crystal
 atoms in, 87
 crystal structures for, 163
 slip directions and planes for, 167
 Body force vector, 39
 Boundary and initial value problems, 193
 simple dynamic solutions for linear elastic materials
 one-dimensional bar subjected to end loading, 239–240
 plane waves in infinite solid, 240–241
- plate impact experiment, 245–248
 reflection and transmission of waves normal to interface, 243–245
 reflection of waves traveling normal to free surface, 242–243
 surface subjected to time-varying normal pressure, 236–238
 surface subjected to time-varying shear traction, 239
 wave speeds in isotropic elastic solids, 241–242
- symmetric solution to quasi-static large strain elasticity problems
 governing equations of finite elasticity in Cartesian components, 229–230
 pressurized hollow sphere, from
 incompressible rubber, 232–236
 simplified equations for incompressible spherically symmetric solids, 230–232
- symmetric solutions to quasi-static elastic–plastic problems, 211
 governing equations, 212–213
 hollow sphere subjected to cyclic internal pressure, 219–223
 hollow sphere subjected to monotonically increasing internal pressure, 215–219
 long cylinder subjected to internal pressure, 226–229
 simplified equations
 for plane strain axially symmetric elastic–perfectly plastic solids, 223–225
 for spherical problems, 213–215
- symmetric solutions to quasi-static linear elastic problems
 general solution
 to axisymmetric boundary value problem, 205–206
 to spherical problems, 197
 gravitating sphere, 199–200
 linear elasticity in Cartesian components, governing equations of, 193–194
 long cylinder subjected to internal and external pressure, 206–208
 pressurized hollow sphere, 197–198
 simplified equations
 for axially symmetric linear elasticity problems, 202–205
 for spherical problems, 194–196
 sphere with steady-state heat flow, 200–202
 spinning circular plate, 208–209
 stresses induced by interference fit between two cylinders, 209–211

- Boundary conditions, 5, 49
 Boundary element methods, *see* Boundary integral equation methods
 Boundary integral equation methods, 12, 355
 Boundary traction integrals evaluations, in large deformations, 520–521
 Boundary value problem, 10; *see also* Boundary and initial value problems
 slip-line field theory solutions to, 392–398
 double-notched plate in tensile loading, 394
 notched bar in bending, 395–398
 plane strain extrusion, 393–394
 pressurized cylindrical cavity, 394–395
 Bounding theorems, 12
 in plasticity, 398–421
 lower bound plastic collapse theorem, 410–412
 lower bound shakedown theorem, 412–417
 minimum plastic dissipation principle, 401–404
 plastic dissipation, 399–401
 upper bound plastic collapse theorem, 404–409
 upper bound shakedown theorem, 417–421
 Brittle fracture
 probabilistic design methods, 556
 static fatigue criterion, 557–558
 Buckingham Pi theorem, 448–449
 Bulk modulus, 74, 75
 Burger's circuit, 274–275, 360, 363
 Burger's vector, 275, 359
-
- C
- Cam-clay, 9
 constitutive equations for, 153–160
 critical state surfaces, 156–157
 elastic constitutive equations, 156
 flow law, 157–158
 hardening law, 158
 plastic stress-strain relation, calculation of, 158–160
 pressure decomposition, 154–156
 strain rate decomposition, 154
 yield criterion, 156–157
 Cartesian components
 finite elasticity in, governing equations of, 229–230
 linear elasticity in, governing equations of, 193–194
 Cauchy–Green tensors, 27, 626
 Cauchy–Navier equation of motion, 240
 Cauchy stress tensor, 43–44, 46, 69, 70, 89, 145
 and angular momentum balance, 51–52
 and linear momentum balance, 49–51
 work done by, 54–56
 Circular cylinder, torsion of, 705–708
 Circular dislocation loop
 nonsingular energy of, 365
 prismatic, 361
 Circular plate, spinning, 208–209
 Cohesive zone models, for interfaces, 176–182
 representative values for properties of, 181–182
 separation of interfaces, 176–177
 irreversible separation, constitutive equations of, 179–181
 reversible separation, constitutive equations of, 178–179
 Cohesive zone law, 177
 Collapse, 398
 Compatibility conditions, 34–35
 Complex variable solution, 267
 crack in infinite elastic solid, under remote loading, 278–280
 cylindrical hole in infinite solid, under remote loading, 277–278
 dislocation near half-space surface, 289–290
 for edge dislocation in infinite solid, 274–277
 to elasticity problems, 268–270
 fields near crack tip, on bimaterial interface, 280–282
 frictionless parabolic indenter, in contact with half-space, 284–286
 frictionless rigid indenter, in contact with half-space, 283–284
 line contact, between two nonconformal frictionless elastic solids, 286–287
 for line force in infinite solid (plane strain deformation), 272–274
 satisfying governing solutions, demonstration of, 270–271
 sliding contact between two rough elastic cylinders, 287–289
 Computer simulations, 12
 Concrete models, 9
 Configurational force, 370
 Constitutive models, 65
 for anisotropic linear elastic materials, 76–82
 basis change formulas for, 79–81
 physical interpretation of, 78–79
 strain energy density for, 79
 stress-strain relations for, 76–78
 material symmetry effect on, 81–82
 for Cam-clay, 153–160
 critical state surfaces, 156–157
 elastic constitutive equations, 156

- flow law, 157–158
- hardening law, 158
- plastic stress-strain relation, calculation of, 158–160
- pressure decomposition, 154–156
- strain rate decomposition, 154
- yield criterion, 156–157
- cubic crystals and compounds, representative values for, 87
- for cubic materials, linear elastic stress-strain relations for, 85–87
- generalized Hooke's law, 91–93
- general requirements for
 - Drucker stability criterion, 67–69
 - objectivity, 66–67
 - thermodynamic restrictions, 66
- hyperelasticity, 93–103
 - deformation measures used in finite elasticity, 95–96
 - nonlinear elasticity models, calibrating, 102
 - perfectly incompressible materials, 99–100
 - rubbers, representative values of material properties for, 103
 - strain energy density, forms of, 100–102
 - stress measures used in finite elasticity, 96–97
 - stress-strain relations, 97–99
- hypoelasticity, 87–91
- for isotropic, linear elastic materials, 69–76
 - behavior, 69–70
 - elastic constants
 - physical interpretation of, 75
 - representative values for, 73
 - mass density, representative values for, 73
 - plane deformation of
 - reduced stress-strain behavior for, 72
 - strain energy density for, 75–76
 - stress-strain relations for, 70–71
 - large strain, rate-dependent plasticity, 143–148
 - large strain viscoelasticity, 148–152
- for linear elastic orthotropic materials, 82–83
 - stress-strain relations for, 82–83
- for linear elastic transversely isotropic material, 83–85
- linear viscoelastic materials, 103–113
 - polymers
 - small strain rate-dependent response of, 104–109
 - viscoelastic properties, representative values for, 113
 - constitutive equations for, 109–110
 - constitutive laws for, 112–113
- Prony series representation for relaxation
 - modulus, 112
- spring-damper approximations to relaxation
 - modulus, 110–111
- for metal single crystals, 161–176
 - elastic stress-strain relation, 174
 - kinematic descriptions, 171–173
 - planes and directions, representing
 - inverse pole figures, 165
 - Miller index notation for, 162–166
 - pole figures, 166
 - using stereographic projections, 164
 - plastic flow in, 166–171
 - plastic properties, representative values for, 176
 - plastic stress-strain relation in, 174–176
 - stress measures, 173–174
- plastic constitutive equations, perspectives on, 129–132
- small strain rate-independent plasticity, 113
 - decomposition of strain into elastic and plastic parts, 118
 - Drucker's postulate, 131–132
 - elastic unloading condition, 126
 - inelastic response of metals, features of, 115–117
 - isotropically conditioning elastic-plastic solid, 126–128
 - linear kinematically hardening solid, 128
 - plastic flow in metals, microscopic perspectives on, 132–135
 - plastic flow law, 122–126
 - polycrystalline metals, typical values for yield stress of, 129
 - strain hardening laws, 120–122
 - yield criteria, 118–119
 - yield surface, graphical representation of, 119–120
- small strain, viscoplastic constitutive equations, 137–141
 - elastic constitutive equations, 138
 - plastic flow potential, 139–140
 - power-law rate sensitivity, 140
 - strain rate decomposition, 138
 - von Mises flow potential, 140
- small strain viscoplasticity, 135–142
- solids, constitutive models
 - for contacting interfaces in, 176–182
 - for contacting surfaces in, 176–182
- transversely isotropic hexagonal close-packed crystals
 - elastic constants, representative values for, 85, 86

- Contact, in two solids, 308
 Contact area, 307
 Contact pressure, 284, 285, 288, 303, 304, 307
 Contact stiffness, 284, 303, 304–305, 308
 Contact yield, 305–306
 Copper crystal, properties of, 176
 Coulomb friction, 186
 with shear cutoff, 187
 Coupled atomistic-discrete dislocation
 method, 10
 Coupled problems, 7
 Crack path selection, 613
 Crack tip energy release rate, 588; *see also* Energy
 release rate
 Crack tip field
 Dugdale–Barenblatt cohesive zone model,
 599–601
 elements, 578
 energy flux, 593–596
 integral expressions, 593
 Hutchinson–Rice–Rosengren crack tip fields, 601
 interface, 607
 material parameters, 608
 interpretation, 609
 loading parameters, 608–609
 Creep, 9
 features of behavior, 135–137
 Critical state plasticity, 9
 Crystallography, *see* Body-centered cubic (BCC)
 crystal; Copper crystal, properties of;
 Face-centered cubic (FCC) crystal;
 Hexagonal close-packed (HCP) crystal;
 Metal single crystals, constitutive
 models for
 Crystal plasticity, 9
 Cubic crystals and compounds, representative
 values for, 87
 Cubic materials, linear elastic stress-strain relations
 for, 85–87
 Cyclic fatigue, crack growth, 586
 Cylinder, long (plane strain)
 subjected to internal and external pressure,
 206–208, 226–229
-
- D
- Deformable rods, simplified versions of general
 theory
 straight elastic beam
 with small deflections and no axial force,
 642–643
 with small transverse deflections and
 significant axial force, 643–644
 stretched flexible string with small transverse
 deflections, 641
 Deformation gradient tensor, 14–18
 inverse of, 17–18
 Jacobian of, 19–20
 resulting from two successive deformations, 18
 Deformations
 examples, 15
 relation between area elements before and after,
 766–767
 Degeneracy, 317
 Degrees of freedom, 429
 Deviatoric infinitesimal strain, 24, 25
 Deviatoric stress tensor, 48
 Direct strains, 24
 Discrete dislocation plasticity, 9
 Dislocation motion and Peach–Kohler formula,
 370–374
 Dispersion relation for wave, 336, 338
 Dispersive wave, 336
 Displacement field, 13–14, 470–471
 Displacement gradient tensor, 14–18
 and Lagrange strain tensor, 20–21
 Displacement vector, 14
 Divergence theorem, 353, 721–722
 Drucker stability, 67–69
 Ductile fracture criteria, 559
 Dugdale–Barenblatt cohesive zone model,
 599–601
 Dynamic analysis, 7
 Dynamic linear elasticity, FEM for, 490
 1D code with modal dynamics, example,
 503–504
 1D dynamic code and solution, example,
 497–499
 1D implementation, of Newmark scheme,
 495–497
 2D and 3D code to compute mode shapes and
 natural frequencies, example, 505
 2D and 3D dynamic linear elastic code and
 solution, example, 501
 finite element equations of motion, for linear
 elastic solids, 491–493
 governing equations, 490–491
 expressing using the principle of virtual
 work, 491
 lumped mass matrices, 499–501
 modal method of time integration, 501–502
 natural frequencies and mode shapes, 502–503
 Newmark time integration for elastodynamics,
 493
 Newmark applied to FEM equations,
 494–495

- Newmark method for a one degree of freedom system, 493–494
-
- E**
- Edge components, 275
- Eigenvectors, of symmetric tensor, 47
- Elastic beam
- with small deflections and no axial force, 642–643
 - with small transverse deflections and significant axial force, 643–644
- Elastic compliance tensor, 71, 77–78
- Elastic constants, 306–307
- Elastic limit, 308
- Elastic modulus tensor, 71
- Elastic perfectly plastic solid model, 8
- Elastic-plastic material behavior, 435
- Elastic rods
- constitutive equations relating to deformation measures, 636–639
 - cross section of rod, 636
 - force-deformation relations, 638
 - warping functions and modified polar moments, 637
- solutions to simple problems, 644
- buckling of column, 648–650
 - helical spring, 655–657
 - post-buckled shape of rods, 650–653
 - rod bent and twisted into helix, 653–655
 - vibration of straight beam without axial force, 645–648
 - strain energy, 639–640
- Elastic stiffness tensor, 77–78
- Elastic strain, 76
- Elastic unloading condition, 126
- Element connectivity, 430
- Element stiffness and force matrices formulas, static linear elasticity, 486
- Ellipsoid, 294–296
- displacements far from, 299
 - solution inside the, 296–297
 - solution outside the, 298–299
- Ellipsoidal inclusion
- in infinite solid subjected to remote stress, elastically mismatched, 299–300
- Energetics of dislocations in elastic solids
- dislocation motion and Peach-Koehler formula, 370–374
 - energy of two interacting dislocation loops, 369–370
 - nonsingular dislocation theory, 362–365
- potential energy of isolated dislocation loop in infinite solid, classical solution for, 359–362
- application to circular prismatic dislocation loop, 361
- derivation of solution for 3D dislocation loop energy, 362
- difficulties in evaluation, 360–361
- stressed, finite elastic solid, 365–369
- Energy methods, *see* Static linear elasticity problems, energy methods to solve
- Energy release rate
- and compliance, 591
 - calculating stress intensity factors, 592–593
 - contour integral formula for, 596
 - as fracture criterion, 589
 - J integral, calculation, 598–599
 - in linear elastic solids, 588–589
 - and stress intensity factor, 589–591
- Engineering shear strains, 24
- Equations of motion, 53–54
- Eshelby inclusion problem, 294–299
- Eshelby tensor, 297
- Euler–Bernoulli beam theory, 449, 642–643
- Eulerian logarithmic strain, 30
- Eulerian nominal strain, 30
- Eulerian strain tensor, 22
- Exaction solution, in method of analysis, 11–12
- Explicit dynamics, 442–443
- Explicit time integration, *see* Explicit dynamics
-
- F**
- Face-centered cubic (FCC) crystal
- atoms in, 87
 - crystal structures for, 163
 - inverse pole figure during uniaxial tensile loading, 170
 - slip directions and planes for, 167
 - slip systems for, 168
 - during uniaxial tensile loading, 169–170
 - typical stress-strain curves during uniaxial tensile loading, 171
- Failure prediction, 3
- Finite deformation plasticity, stress measures for, 145
- Finite difference methods, 12
- Finite element analysis (FEA), 467
- advanced element formulations, 530–531
 - “B-bar” method, 538–540
 - hybrid elements for modeling near-incompressible materials, 541–543
 - reduced integration, 534–537

- reduced integration with hourglass control, 540
- sample code, 541
- selectively reduced integration, 537–538
- shear locking and incompatible mode elements, 531–533
- volumetric locking and reduced integration elements, 533–534
- application of, 423
- boundary conditions in, 435–438
 - body forces, 437
 - contact, 437
 - default, at boundary nodes, 437
 - displacement, 436–437
 - distributed loads, 437
 - guidelines, 437
 - load history, 437
 - prescribed forces, 437
 - symmetry, 437
- constraints in, 438–439
- convergence problems in, 444–445
- displacement-based, 423–424
- for dynamic linear elasticity, *see* Dynamic linear elasticity, FEM for
- governing equations, scaling, 449–451
- initial conditions and external fields, 441
- for large deformations (hyperelastic materials), *see* Large deformations (hyperelastic materials), FEM for
- material behavior in, 434–435
 - elastic-plastic, 435
 - linear elastic, 434–435
- for nonlinear (hypoelastic) materials, *see* Nonlinear (hypoelastic) materials, FEM for
- output, 445–446
- program
 - boundary loading, 459–460
 - element interpolation functions, 453–454
 - element stiffness matrix, 455–456
 - example, 464–466
 - finite element mesh and element connectivity, 452–453
 - global displacement vector, 453
 - global residual force vector, 461
 - global stiffness matrix, 456–459
 - postprocessing, 463–464
 - potential energy, minimizing, 461–462
 - prescribed displacements, eliminating, 462–463
 - solution, 463
 - strain energy calculation, 454–455
- programs and input files, examples, 544–545
- solution procedures in, 442–445
 - linear or nonlinear geometry, 442
 - load steps and increments, 445
 - nonlinear, for static problems, 443–445
 - time stepping, for dynamic problems, 442–443
- of special elements, 432–434
- specifications of, 424–425
- for static linear elasticity, *see* Static linear elasticity, FEM for
- surfaces and interfaces, contacting, 439–441
 - master/slave surfaces, contacting, 440–441
 - parameters, 441
 - stiff solid as rigid surface, modeling, 440
- types of, 424
- units in, 446
- using dimensional analysis, 447–449
- for viscoplasticity, *see* Viscoplasticity, FEM for
- Finite element mesh
 - for 2D component
 - axisymmetric, 427–428
 - plane strain, 426–427
 - plane stress, 426
 - for 3D component, 426
 - axisymmetric, 427
 - beams, 432, 433–434
 - plates, 433
 - shells, 433
 - truss, 432, 433
 - elements in, 429–432
 - nodes in, 428–429
- Finite element method (FEM), 12; *see also* Finite element analysis and principle of virtual work, 58
- Finite strain plasticity
 - elastic stress-strain relation for, 146–147
 - kinematics of, 143–144
- Finite strain viscoelasticity
 - kinematics for, 148–150
 - representative values for material parameters in, 152
 - stress measures for, 150
- Finite strain viscoplasticity, plastic constitutive law for, 147–148
- First Piola–Kirchhoff stress, *see* Nominal stress
- Flat membrane
 - equations in cylindrical-polar coordinates, 689–692
 - boundary conditions, 692
 - coordinate systems and kinetic relations, 690–691
 - equations of motion, 691–692
 - subject to uniform biaxial in-plane loading, 692

- with small out-of-plane deflections, 688–689
 edge boundary conditions, 689
 equation of motion, 689
 kinematics, 689
 kinetics, 689
 stress-resultant strain relations, 689
 solutions to simple problems
 vibration modes and natural frequencies for
 circular membrane, 694–696
 Flexural waves, 337
 Flow rule, 175
 Flow stress, 9
 Forces, 38–39
 Fracture mechanics
 crack growth, 567
 analytical solution, 572–575
 cyclic fatigue, 586–587
 linear elastic solid, 567–569
 phenomenological theory, 569–572
 static fatigue, 584–586
 energy release rate
 and compliance, 591–593
 contour integral formula for, 596
 as fracture criterion, 589
 J integral, calculation, 598–599
 in linear elastic solids, 588–589
 and stress intensity factor, 589–591
 failures
 stress-based criteria for brittle solids and
 composites, 553–563
 under cyclic loading, 550–553, 564–567
 under monotonic loading, 548–550
 fracture toughness
 measurements, 580
 values, 581
 interface fracture, 610–611
 mixed-mode, 584
 plastic fracture mechanics, 599
 stress intensity factors, calculation, 572
 nonuniform stress fields, 576–577
 using FEA, 578–579
 Fracture toughness
 measurement, 580–581
 mixed mode fracture criterion, 584
 values, 581
 Free volume methods, 12
 Friction, 182–191
 coefficients
 for materials, 187
 transient variation
 after changes in contact pressure, 184
 after changes in sliding velocity,
 183–184
 Coulomb, 186
 with shear cutoff, 187
 laws, 189–191
 rate and state variable models of, 187–189
 material properties, representative values of,
 189, 190
 Fundamental elasticity matrix, 317–318
-
- G
- Geiringer equations, 384, 392
 Generalized forces, 46
 Generalized Hooke's law, 91–93, 146
 Generalized Mooney–Rivlin solid,
 100–101
 Generalized neo-Hookean solid, 100
 Generalized plane strain, 203, 206–208
 Generalized polynomial rubber elasticity potential,
 101
 Generalized strain measures, 30–31
 Geometric hardening, 170; *see also* Hardening
 Geometry of solid, 4–5
 Glass transition temperature, 93
 Goldenblat–Kopnov failure criterion, 554–555
 Governing equations, 10–11, 468–469
 angular momentum balance, in terms of Cauchy
 stress, 51–52
 for dynamic linear elasticity, 490–491
 equations of motion, 53–54
 internal forces in solids, mathematical
 descriptions, *see* Internal forces in
 solids, mathematical descriptions
 for large deformations, 514–515
 of linear elasticity, integral (weak) form of,
 469–470
 linear momentum balance, in terms of Cauchy
 stress, 49–51
 for nonlinear (hypoelastic) materials,
 505–507
 principle of virtual work, 58–63
 shape changes in solids, mathematical
 description, *see* Shape changes in
 solids, mathematical description
 for viscoplasticity, 522–523
 work done
 by Cauchy stresses, 54–56
 by Kirchhoff stress, 56, 57
 by material stress, 56, 57
 by nominal stress, 56, 57
 by stresses per unit volume (infinitesimal
 deformations), 57
 Gradient of vector field, 16
 Gravitating sphere, 199–200

Green's strain, 31
 Group velocity, 338–339
 Gurson plasticity law, 8

H

Hardening, 141; *see also* Hardening rule
 geometric, 170
 isotropic, 120–121, 123
 kinematic, 122, 124, 128
 latent, 170
 linear kinematically, 128
 self, 170
 strain, 435
 Hardening rule, 158, 175–176; *see also* Hardening
 Armstrong–Frederick, 122, 123
 strain, 120–122
 Heat generated by plastic flow, 6
 Helical spring, 655–657
 Hencky equations, 383–384, 392
 Hermitian matrix, 320
 Hertz contact problem, 304
 Hexagonal close-packed (HCP) crystal
 atoms in, 87
 crystal structures for, 163
 slip directions and planes for, 167
 Hollow sphere
 pressurized, 197–198
 from incompressible rubber, 232–236
 subjected to cyclic internal pressure, 219–223
 subjected to monotonically increasing internal
 pressure, 215–219
 Hutchinson–Rice–Rosengren crack tip fields, 601
 Hybrid element, 431
 for modeling near-incompressible materials,
 541–543
 Hydrostatic stress, 48, 49, 383–384
 Hyperelasticity, 8, 93–103
 deformation measures used in finite elasticity,
 95–96
 nonlinear elasticity models, calibrating, 102
 perfectly incompressible materials, 99–100
 rubbers, representative values of material
 properties for, 103
 strain energy density, forms of
 Arruda–Boyce eight-chain model, 101
 Blatz–Ko foam rubber, 102
 generalized Mooney–Rivlin solid, 100–101
 generalized neo-Hookean solid, 100
 generalized polynomial rubber elasticity
 potential, 101
 Ogden model, 101
 Ogden–Storakers hyperelastic foam, 101

stress measures used in finite elasticity,
 96–97
 stress-strain relations, 97–99
 Hypoelasticity, 87–91

I

Impedance tensors and Barnett–Lothe tensors,
 319–320
 Implicit dynamics, 443
 Implicit time integration, 443
 Index notation, 14, 741
 algebraic manipulation using, 746–748
 calculus using, 746
 Kronecker delta, 742
 permutation symbol, 743
 range convention, 741
 rules of, 743–744
 summation convention, 742
 for tensor operations, 744–745
 for vector operations, 744
 Infinite solid subject to remote stress
 elastically mismatched, 299–300
 spherical cavity in, 300–302
 Infinitesimal deformations
 rate of mechanical work for, 57
 stress measures for, 47
 virtual work equation, 62–63
 Infinitesimal rotation tensor, 25–26
 Infinitesimal strain tensor, 22, 24–25, 69, 70, 89
 directions, 26–27
 principal values, 26
 Initial value problem, 10–11; *see also* Boundary and
 initial value problems
 Integration points, 431
 Interface crack
 crack path selection, 613
 fracture resistance, 611–612
 stress intensity factors, 612–613
 Internal body force, 39–40
 Internal forces in solids, mathematical descriptions
 Cauchy stress tensor, 43–44
 deviatoric stress tensor, 48
 hydrostatic stress, 48, 49
 internal body forces, 38–40
 Kirchhoff stress, 44, 45
 principal directions, 47
 principal stresses, 47–48
 stresses near external surface, 49
 stress measures for infinitesimal deformations,
 47
 stress state at edges, 49
 surface traction, 38, 39

traction acting on planes within a solid, 40–43
von Mises effective stress, 48, 49
Internal traction vector, 40
Interpolation functions
 for 2D elements, 481
 for 3D elements, 481, 483, 484
Invariants, 49
Inverse pole figures, 165, 170; *see also* Pole figures
Isotropic elastic solids, wave speeds in, 241–242
Isotropic hardening, 120–121, 123
Isotropic linear elasticity, 7
Isotropic linear elastic materials, *see also* Linear elastic material behavior
 behavior, 69–70
 elastic constants
 physical interpretation of, 75
 representative values for, 73
 mass density, representative values for, 73
 plane deformation of
 reduced stress-strain behavior for, 72
 solutions to dynamic problems for
 elastic waves in waveguides, 337–339
 infinite solid, pressure suddenly applied to
 spherical cavity surface in, 331–333
 Love potentials for, 330–331
 Love waves, 335–337
 Rayleigh waves, 333–335
 strain energy density for, 75–76
 stress-strain relations for, 70–71
Isotropic materials
 crack tip field, 567–569
 failure criteria for, 553
Isotropically conditioning elastic-plastic solid, 126–128

J

Jacobian of deformation gradient, 19–20

K

Kinematically admissible collapse mechanism, 400–401
Kinematically admissible displacement fields, 340
Kinematically admissible virtual velocity field, 58
Kinematic hardening, 121–122
Kinematics, 177–178
Kinetics, 178
Kirchhoff shell theory, 664
Kirchhoff stress, 145
 virtual work equation, 61–62
 work done by, 56, 57
Kronecker delta symbol, 16

L

Lagrange strain tensor, 20–21, 69, 70, 89, 627
 time derivative of, 33
Lagrangian logarithmic strain, 30
Lagrangian nominal strain, 30
Lame modulus, 74
Large deformations (hyperelastic materials), FEM
 for, 514
 boundary traction integrals evaluations, 520–521
 code, example, 521–522
 finite element equations, 515–517
 solution using consistent Newton-Raphson iteration, 517–519
 governing equations, 514–515
 expressing using principle of virtual work, 515
 tangent stiffness for the neo-Hookean material, 519–520
Large strain, rate-dependent plasticity
 finite deformation plasticity, stress measures for, 145
 finite strain plasticity
 elastic stress-strain relation for, 146–147
 kinematics of, 143–144
 finite strain viscoplasticity, plastic constitutive law for, 147–148
Large strain viscoelasticity, 148
 finite strain viscoelasticity
 kinematics for, 148–150
 representative values for material parameters in, 152
 stress measures for, 150
 strain relaxation, 151–152
 stress, deformation measures, and strain energy density, relation between, 150–151
Laser interferometer, 245
Latent hardening, 170; *see also* Hardening ratio, 170
Laws of thermodynamics, 66
Left stretch tensor, 27, 28
Linear elastic fracture mechanics, 567
 crack tip energy release rate, 588–589
 design application, 571–572
 phenomenological theory, 569–571
Linear elasticity, 434–435
 in Cartesian components, governing equations of, 193–194
Linear elastic material behavior, 69–87
 anisotropic, 76–82
 isotropic, 69–76
 orthotropic, 82–83

- transversely isotropic, 83–85
- Linear elastic materials, simple dynamic solutions
 - for
 - one-dimensional bar subjected to end loading, 239–240
 - plane waves in infinite solid, 240–241
 - plate impact experiment, 245–248
 - reflection and transmission of waves normal to interface, 243–245
 - reflection of waves traveling normal to free surface, 242–243
 - surface subjected to time-varying normal pressure, 236–238
 - surface subjected to time-varying shear traction, 239
 - wave speeds in isotropic elastic solids, 241–242
- Linear elastic orthotropic materials
 - stress-strain relations for, 82–83
- Linear elastic solids, solutions for, 249
 - 2D line load, parallel to infinite solid surface, 264–265
 - 2D line load, perpendicular to infinite solid surface, 262–264
 - airy stress function and solutions, 255
 - arbitrary pressure on flat surface, 265
 - in cylindrical-polar coordinates, 259–260
 - to end-loaded cantilever, 260–262
 - in rectangular coordinates, 256–257
 - satisfying governing equations, demonstration of, 257–259
 - stress near crack tip, 266–267
 - uniform normal pressure, on strip, 266
- anisotropic solids, 310
 - Barnett–Lothe integrals, 323–325
 - Barnett–Lothe tensors and impedance tensor, 319–320
 - basis change formulas for matrices in anisotropic elasticity, 321–323
 - degenerate materials, 317
 - fundamental elasticity matrix, 317–318
 - governing equations of elasticity for, 310–312
 - line load and dislocation
 - below anisotropic half-space surface, 329
 - in infinite anisotropic solid, 327–329
 - matrices properties in anisotropic elasticity, 320–321
 - orthogonal properties of Stroh matrices A and B, 318–319
 - Stroh eigenvalues and anisotropy matrices for cubic materials, 316–317
 - Stroh representation
 - for fields in, 312–315
 - for uniform stress state, 325–327
- complex variable solution, 267
- crack in infinite elastic solid, under remote loading, 278–280
- cylindrical hole in infinite solid, under remote loading, 277–278
- dislocation near half-space surface, 289–290
- for edge dislocation in infinite solid, 274–277
- to elasticity problems, 268–270
- fields near crack tip, on bimaterial interface, 280–282
- frictionless parabolic indenter, in contact with half-space, 284–286
- frictionless rigid indenter, in contact with half-space, 283–284
- line contact, between two nonconformal frictionless elastic solids, 286–287
- for line force in infinite solid (plane strain deformation), 272–274
- satisfying governing solutions, demonstration of, 270–271
- sliding contact between two rough elastic cylinders, 287–289
- energetics of dislocations in elastic solids
 - dislocation motion and Peach–Koehler formula, 370–374
- energy of two interacting dislocation loops, 369–370
- nonsingular dislocation theory, 362–365
- potential energy of isolated dislocation loop in infinite solid, 359–362
- stressed, finite elastic solid, 365–369
- governing equations, of linear elasticity
 - dynamic problems, 251
 - static problems, 250
- isotropic linear elastic solids, solutions to dynamic problems for
 - elastic waves in waveguides, 337–339
 - infinite solid, pressure suddenly applied to spherical cavity surface in, 331–333
 - Love potentials for, 330–331
 - Love waves, 335–337
 - Rayleigh waves, 333–335
- linear elasticity equations, uniqueness and existence of solutions to, 252
- Navier equation, 251
- Rayleigh–Ritz method, for natural frequency of elastic solid estimation
 - mode shapes, 375–378
 - vibration for beam, 379–380
- reciprocal theorem and applications
 - displacement and stress induced by 3D dislocation loop in infinite solid, 278–279
 - classical solutions for, 356–359

- example, 353–354
 internal and boundary values of field quantities,
 formulas relating, 355–356
 statement and proof, 352–353
 Saint-Venant's principle (SVP), 252–255
 static linear elasticity problems, energy methods to
 solve, 339
 3D static problems, solutions to
 axisymmetric contacts, load displacement-
 contact area relations for, 308–310
 ellipsoidal inclusion in infinite solid
 subjected to remote stress, elastically
 mismatched, 299–300
 Eshelby inclusion problem, 294–299
 flat-ended cylindrical indenter in contact
 with elastic half-space, 302–303
 frictionless contact between two elastic
 spheres, 304–306
 infinite solid subject to remote stress,
 spherical cavity in, 300–302
 nonconformal contacts, frictionless, 306–308
 Papkovich–Neuber potential representations,
 for isotropic solids, 290–291
 Papkovich–Neuber solution satisfying
 governing equations, demonstration
 of, 291–292
 point force in an infinite solid, 292
 point force normal to infinite half-space
 surface, 293
 point force tangent to infinite half-space
 surface, 293–294
 potential energy definition
 of elastic solid, 340–341
 of linear elastic solid under static loading,
 339–340
 principle of stationary and minimum potential
 energy, 341–344
 stiffness, energy methods to calculate, 350–351
 uniaxial compression of cylinder solved by
 energy methods, 344–346
 variation derivation of beam equations, 346–350
 superposition and linearity of solutions, 251–252
 Linear elastic transversely isotropic material
 stress-strain relations for, 83–85
 Linear element, 430
 Linear kinematically hardening solid, 128
 Linear kinematic hardening, 122, 124, 128; *see also*
 Kinematic hardening
 Linear momentum balance, in terms of Cauchy
 stress, 49–51
 Linear viscoelastic materials, 103–113
 constitutive equations for, 109–110
 constitutive laws for, 112–113
- polymers
 small strain rate-dependent response of,
 104–109
 viscoelastic properties, representative values
 for, 113, 114
 Prony series representation for relaxation
 modulus, 112
 spring-damper approximations to relaxation
 modulus, 110–111
 Line load and dislocation
 below anisotropic half-space surface, 329
 in infinite anisotropic solid, 327–329
 Loading, 5–6
 boundary conditions, 5
 Longitudinal waves, 337
 Love potentials, 330–331
 Love waves, 335–337
 Lower bound plastic collapse theorem, 410–412
 examples of applications of
 collapse load for a plate containing a hole, 411
 rigid indenter in contact with half-space,
 411–412
 Lower bound shakedown theorem, 412–417
 examples of applications of
 pressurized spherical shell, shakedown limit
 for, 416–417
 three-bar problem, 415–416
 proof of, 414–415
 Lumped mass matrices, 499–501
-
- M
- Mass scaling, 443
 Material behavior
 anisotropic linear elasticity, 7
 atomistic models, 9–10
 concrete models, 9
 critical state plasticity, 9
 crystal plasticity, 9
 discrete dislocation plasticity, 9
 hyperelasticity, 8
 isotropic linear elasticity, 7
 rate-independent metal plasticity, 8
 strain gradient plasticity, 9
 viscoelasticity, 8
 viscoplasticity, 8–9
 Material frame independence, 66–67
 Material stress, 46, 145
 virtual work equation, 61–62
 Material tangent, 527–528
 Materuak stress, work done by, 56, 57
 Matrices
 addition, 722

- definition, 722
 determinant, 724–725
 eigenvalues and eigenvectors, 725–727
 inversion, 725
 multiplication
 by scalar, 722
 by matrix, 722–723
 spectral and singular value decomposition, 727–728
 square root of, 26–27, 728
 transpose, 723–724
- Maximum plastic resistance principle, 129–131
 interpretation, 129–130
 proof of, 130–131
 statement, 129
- Membrane shell theory, 708–710
- Metals
 crystal structures for, 163
 inelastic response of, 115–117
 plastic flow in
 microscopic perspectives on, 132–135
 polycrystalline
 typical values for yield stress of, 129
- Metal single crystals, constitutive models for, 161–176
 elastic stress-strain relation in, 174
 kinematic descriptions, 171–173
 planes and directions, representing
 inverse pole figures, 165
 Miller index notation for, 162–164
 pole figures, 166
 using stereographic projections, 164
 plastic flow in, 166–171
 plastic properties, representative values for, 176
 plastic stress-strain relation in, 174–176
 stress measures, 173–174
- Minimum plastic dissipation principle, 401–404; *see also* Plastic dissipation
- Modal dynamics, 443
- Modal method of time integration, dynamic linear elasticity, 501–502
- Models, for failure mechanism, 3
- Mode shapes, 375
 orthogonality of, 376–378
- Mohr's circle, 389
 construction of, 383
- Molecular dynamic techniques, 12
- Molecular statics technique, 12
-
- N
- Natural frequencies, 375
 and mode shapes, 502–503
- Navier equation, 251
- Neo-Hookean material, 8
 tangent stiffness for, 519–520
- Newmark time integration for elastodynamics, 493
 Newmark applied to FEM equations, 494–495
 Newmark method for a one degree of freedom system, 493–494
- Newton–Raphson iteration, 509–510, 511, 517–519, 528–529
 nonconvergence, 511–512
 variations on, 512
- Newton's laws, 41, 49
- Nominal stress, 44, 45, 46, 69, 70, 89, 145
 virtual work equation, 61
 work done by, 56, 57
- Nonlinear (hypoelastic) materials, FEM for
 code, example, 512–513
 finite element equations, 507–509
 solution using Newton–Raphson iteration, 509–510
 governing equations, 505–507
 expressing using virtual work principle, 507
- Newton–Raphson iteration, 511
 nonconvergence, 511–512
 variations on, 512
 tangent moduli, 510
- Nonlinear elasticity models, calibrating, 102
- Non-semi-simple matrix, 318
- Nonsingular dislocation theory, 362–365
 nonsingular energy, 364
 of circular dislocation loop, 365
 nonsingular stress, 364–365
- Normal traction, 39
- Numerical integration schemes for 2D and 3D elements, 485
 number of integration points, choosing, 485–486
- Numerical solution, in method of analysis, 12
-
- O
- Objectivity, 66–67
- Oblate spheroid, 297
- Ogden model, 101
- Ogden–Storakers hyperelastic foam, 101
- Orientation-dependent fracture strength, 554
- Overstressed, 396
-
- P
- Papkovich–Neuber potential
 representations, for isotropic solids, 290–291
 solution satisfying governing equations,
 demonstration of, 291–292

- Peach–Koehler formula, 370–374
 Perfectly incompressible materials, 99–100
 Phase angle, 281
 Phase velocity, *see* Wave speed
 Plane strain deformations
 generalized, 312
 strict, 311–312
 Plane strain extrusion, slip-line field for, 393–394
 Plane waves in infinite solid, 240–241
 Plastic dissipation, 399–401; *see also* Minimum plastic dissipation principle
 kinematically admissible collapse mechanism, 400–401
 velocity discontinuities, 399–400
 Plastic flow
 in metals, microscopic perspectives on, 132–135
 in single crystals, 166–171
 Plastic flow law, 122–126, 140–141
 isotropic hardening, 123
 and Levy–Mises flow rule, comparison between, 124–125
 linear kinematic hardening, 124
 yield criterion, differentiating, 125–126
 Plastic fracture mechanics, 599; *see also* Fracture mechanics
 crack tip
 Dugdale–Barenblatt cohesive zone model, 599–601
 Hutchinson–Rice–Rosengren, 601–605
 Rice's J Integral, 605–607
 Plastic solids, solutions for, 381
 bounding theorems, 398–421
 slip-line field theory, 381–398
 Plastic stress-strain law, integrating, 525–527
 Plate impact experiment, 245–248
 Plate theory
 with small in-plane and large transverse deflections, 686–688
 alternative forms of von Karman equations, 688
 edge boundary conditions, 688
 equation of motion, 688
 kinematics, 687
 kinetics, 687
 stress-resultant strain and moment-curvature relation, 687
 with small out-of-plane deflections and negligible in-plane loading, 681–684
 edge boundary conditions, 683–684
 equation of motion, 683
 kinematics, 682
 kinetics, 682
 moment-curvature relation, 683
 strain energy and kinetic energy, 684
 with small out-of-plane deflections and significant in-plane loading, 684–686
 edge boundary conditions, 686
 equation of motion, 686
 kinematics, 685
 kinetics, 685
 stress-resultant strain and moment-curvature relation, 685
 solutions to simple problems
 bending caused by through-thickness temperature gradient, 700–702
 fundamental frequency of vibration of rectangular flat plate, 696–697
 plate bent by pressure applied to one face, 692–694
 Point force
 in infinite solid, 292
 normal to infinite half-space surface, 293
 tangent to infinite half-space surface, 293–294
 Poisson's ratio, 70–71, 73, 74, 75
 Polar decompositions, 30
 Pole figures, 166; *see also* Inverse pole figures
 Polycrystalline metals
 typical values for yield stress of, 129
 Polyisobutylene
 relaxation behavior of, 114
 viscoelastic properties of, 114
 Polymeric foams
 hyperelasticity of, 94
 Polymers
 small strain rate-dependent response of, 104–109
 viscoelastic properties, representative values for, 113, 114
 Porous metal plasticity, 560–562
 Power-law rate sensitivity, 140
 Pressure-dependent viscoplasticity, 9
 Principal directions, 47
 Principal stresses, 47–48
 Principal stretches, 29–30
 in deformed solids, 29
 in undeformed solids, 29
 Principle of minimum potential energy, 339, 343–344
 Principle of stationary potential energy, 341–343
 Principle of virtual work, 58–63, 469, 491, 515; *see also* Work done
 first version, 59
 for infinitesimal deformations, 62–63
 second version, 59–61
 virtual work equations, 61–62
 Prolate spheroid, 297
 Propagation modes and waves, 336

Q

- Quadratic element, 430
 Quasi-continuum method, 10
 Quasi-static elastic-plastic problems, symmetric solutions to, 211
 governing equations, 212–213
 hollow sphere subjected to cyclic internal pressure, 219–223
 hollow sphere subjected to monotonically increasing internal pressure, 215–219
 long cylinder subjected to internal pressure, 226–229
 simplified equations for plane strain axially symmetric elastic-perfectly plastic solids, 223–225
 simplified equations for spherical problems, 213–215
 Quasi-static large strain elasticity problems, symmetric solution to
 governing equations of finite elasticity in Cartesian components, 229–230
 pressurized hollow sphere, from incompressible rubber, 232–236
 simplified equations for incompressible spherically symmetric solids, 230–232
 Quasi-static linear elastic problems, symmetric solutions to
 general solution
 to axisymmetric boundary value problem, 205–206
 to spherical problems, 197
 gravitating sphere, 199–200
 linear elasticity in Cartesian components, governing equations of, 193–194
 long cylinder subjected to internal and external pressure, 206–208
 pressurized hollow sphere, 197–198
 simplified equations
 for axially symmetric linear elasticity problems, 202–205
 for spherical problems, 194–196
 sphere with steady-state heat flow, 200–202
 spinning circular plate, 208–209
 stresses induced by interference fit between two cylinders, 209–211

R

- Radial stress, 252
 Rate-independent metal plasticity, 8
 Rate of deformation
 infinitesimal strain rate, 33

- rotation rate, 33
 spin tensor, 31–32
 stretch rate, 32
 and time derivatives of strain measures, 33
 velocity gradient, 30
 Rate of work, 46
 Rayleigh's principle, 376
 proof of, 378–379
 Rayleigh–Ritz method, for natural frequency of elastic solid estimation
 mode shapes, 375, 376–378
 vibration for beam, 379–380
 Rayleigh waves, 333–335
 Reciprocal theorem and applications
 displacement and stress induced by 3D dislocation loop in infinite solid, classical solutions for, 356–359
 example, 353–354
 internal and boundary values of field quantities, formulas relating, 355–356
 statement and proof, 352–353
 Reduced integration, 534–537
 with hourglass control, 540
 Reduced integration element, 432
 Relaxation modulus
 Prony series representation for, 112
 spring-damper approximations to, 110–111
 Remote stress
 infinite solid subject to, 299–302
 Residual stress, 220
 Resultant force, acting on internal volume, 41
 Reynold's number, 7
 Rice's *J* integral, 596
 energy release rate, calculation, 598–599
 plastic fracture mechanics, 605–607
 Right stretch tensor, 27, 28
 Rigid perfectly plastic solid model, 8
 Rotation rate, 33
 Rotation tensor, 27, 28
 Rubbers, *see also* Solid rubber
 material properties, representative values of, 103

S

-
- Saint-Venant's principle (SVP), 252–255
 Screw component, 275
 Second Piola–Kirchhoff stress, *see* Material stress
 Selectively reduced integration, 537–538
 Self-hardening, 170; *see also* Hardening
 Shakedown, 412
 Shakedown limit, 220
 Shape changes in solids, mathematical description, 13–38

- Cauchy–Green deformation tensors, 27
 deformation gradient resulting from two successive deformations, 18
 deformation gradient tensor, 14–18
 displacement field, 13–14
 displacement gradient tensor, 14–18
 engineering shear strains, 24
 Eulerian strain tensor, 22
 generalized strain measures, 30–31
 infinitesimal rotation tensor, 25–26
 infinitesimal strain rate, 33
 infinitesimal strain tensor, 22–27
 Jacobian of deformation gradient, 19–20
 Lagrange strain tensor, 20–21
 left stretch tensor, 27, 28
 principal stretches, 29–30
 right stretch tensor, 27, 28
 rotation rate, 33
 rotation tensor, 27, 28
 spin tensor, 32–33
 strain equations of compatibility for infinitesimal strains, 34–38
 stretch rate tensor, 32
 time derivatives of Lagrange strain tensor, 33
 velocity field, 14
 velocity gradient, 31
 Shear locking and incompatible mode elements, 531–533
 Shear modulus, 74, 75
 Shear strains, 24
 Shear traction, 39
 Shear wave propagating through an elastic solid, speed of, 7
 Shells, motion and deformation
 additional deformation measures and kinematic relations, 660–664
 angular acceleration of shell, 663
 Christoffel symbols of second kind, 661
 fundamental form for the surface, 660
 Gaussian curvature, 661
 linear acceleration of shell, 663
 mean curvature, 661
 principal curvature, 661
 time derivative
 of basis vectors, 662
 of curvature tensors, 662–663
 velocity and acceleration of midplane, 663
 approximation
 of deformation gradient, 665–666
 of displacement and velocity field, 664–665
 constitutive equations
 relating to deformation measures, 678–680
 in elastic shells, 678–680
- coordinate systems and variables
 characterization, 657–659
 contravariant basis vectors, 658
 covariant basis vectors, 658
 curvature change tensor, 667
 Elastic shells
 equation of motion and boundary conditions, 670–678
 edge boundary conditions, 671
 equilibrium equations, 675–678
 generalized forces, 671–672
 virtual work principle, 672–675
 flat membrane
 equations in cylindrical-polar coordinates, 689–692
 with small out-of-plane deflections, 688–689
- flat plates
 with small in-plane and large transverse deflections, 686–688
 with small out-of-plane deflections and negligible in-plane loading, 681–684
 with small out-of-plane deflections and significant in-plane loading, 684–686
 inverse of deformation gradient, 666
 Lagrange strain tensor, 667
 midplane Lagrange strain tensor, 667
 representation of forces and moments, 667–670
 external forces and moments, 668
 internal forces and moments, 669–670
 solutions to simple problems
 buckling of cylindrical shell, 703–705
 strain energy and kinetic energy, 680–681
 vectors and tensors components in nonorthogonal bases, 659–660
 velocity gradient tensor, 667
- Skew–Hermitian, 320
 Skew tensor, 25
 Slender rods, motion and deformation
 additional deformation measures and kinematic relations, 620–624
 approximation
 of deformation gradient, 625–626
 of displacement, velocity and acceleration, 624–625
 Cauchy–Green tensors, 626
 constitutive equations relating to deformation measures in elastic rods, 636–639
 cross section of rod, 636
 force-deformation relations, 638
 warping functions and modified polar moments, 637
 coordinate systems and variables
 characterization, 618–620

- equation of motion and boundary conditions, 631–636
- geometry of the cross section, characterization, 617–618
- kinematics of bent and twisted rods, 628–629
- Lagrange strain, 627
- representation of forces and moments, 630–631
- strain energy of elastic rod, 639–640
- Sliding contact**
 - finite, 441
 - small, 441
- Slip-line field theory**, 381–398
 - application to, 384–385
 - assumptions, 381
 - derivation of, 386–392
 - interpretation of, 382–386
 - α and β families, distinction between, 385–386
 - hydrostatic stress, 383–384
 - stress state at a point in slip-line field, 382–383
 - velocity field, 384
 - solutions to boundary value problems, 392–398
 - double-notched plate in tensile loading, 394
 - notched bar in bending, 395–398
 - plane strain extrusion, 393–394
 - pressurized cylindrical cavity, 394–395
- Small strain plastic code, example, 529–530
- Small strain rate-dependent response, of polymers, 104–109
- Small strain rate-independent plasticity, 113
 - decomposition of strain into elastic and plastic parts, 118
- Drucker's postulate, 131–132
- elastic unloading condition, 126
- inelastic response of metals, features of, 115–117
- isotropically conditioning elastic-plastic solid, 126–128
- linear kinematically hardening solid, 128
- plastic flow in metals, microscopic perspectives on, 132–135
- plastic flow law, 122–126
- polycrystalline metals, typical values for yield stress of, 129
- strain hardening laws, 120–122
- yield criteria, 118–119
- yield surface, graphical representation of, 119–120
- Small strain viscoplasticity**
 - constitutive equations, 137–141
 - creep behavior, features of, 135–137
 - high strain rate behavior
 - features of, 137
- representative values of parameters for, 142–143
- models of creeping solids**
 - representative values of parameters for, 142
- Soils, critical state models for**
 - behavior of, 152–153
 - Cam-clay, constitutive equations for, 153–160
 - critical state applications to simple 2D loading, 160–161
 - material properties, typical values of, 161
- Solid mechanics**
 - applications, 1, 3–4
 - defining a problem
 - problem goal, 3–4
 - geometry of the solid, defining, 4–5
 - loading, defining, 5–6
 - physics factors, deciding, 6–7
 - material behavior, defining, 7–10
 - initial value problem, 10–11
 - method of analysis, 11–12
 - definition, 1
 - Solid rubber, *see also* Rubbers**
 - hyperelasticity of, 94
 - Solids, contacting interfaces in**
 - constitutive models for
 - Cohesive zone models, 176–182
 - Solids, contacting surfaces in**
 - constitutive models for, 182–191
 - sliding contact**
 - kinematics of surfaces in, 185–186
 - kinetics of surfaces in, 186
 - Sphere, 297**
 - outside the inclusion of, 299
 - Spherical problems**
 - general solution to, 197
 - simplified equations for, 194–196, 213–215
 - incompressible symmetric solids, 230–232
 - steady-state heat flow, 200–202
 - Spin tensor, 31–32**
 - Stability**
 - Drucker stability, 67–69
 - Stable crack growth, 581–582**
 - Static analysis, 7**
 - Static fatigue, 557**
 - for Brittle materials, 557–558
 - crack growth, 584–586
 - Static linear elasticity, FEM for, 468**
 - 1D FEM, extending to 2D and 3D, 480–481
 - 1D finite element procedure, 476–477
 - 2D/3D linear elastostatic code, sample, 486–489
 - code and solution, examples, 477–479
 - displacement field and virtual velocity field, 470–471

- element stiffness and force matrices formulas, 486
finite element equations, 472
governing equations, 468–469
of linear elasticity, integral (weak) form of, 469–470
interpolation functions
for 2D elements, 481
for 3D elements, 481, 483, 484
numerical integration schemes for 2D and 3D elements, 485
number of integration points, choosing, 485–486
principle of virtual work, 469
simple 1D implementation of, 472–476
volume integrals for stiffness and force in terms of normalized coordinates, 482–484
shape function derivatives calculation, 484
volume integral mapping, 484–485
- Static linear elasticity problems, energy methods to solve, 339
potential energy definition
of elastic solid, 340–341
of linear elastic solid under static loading, 339–340
principle of stationary and minimum potential energy, 341–344
stiffness, energy methods to calculate, 350–351
uniaxial compression of cylinder solved by energy methods, 344–346
variation derivation of beam equations, 346–350
- Static problems, boundary conditions for, 5
Steady-state temperature, 6
Stiffness matrix, 444
element, 455–456
global, 456–459
Strain, 20–21
Strain-displacement relationship, 34–38
Strain energy density, 90–91
for anisotropic, linear elastic solids, 79
forms of
Arruda–Boyce eight-chain model, 101
Blatz–Ko foam rubber, 102
generalized Mooney–Rivlin solid, 100–101
generalized neo-Hookean solid, 100
generalized polynomial rubber elasticity potential, 101
Ogden model, 101
Ogden–Storakers hyperelastic foam, 101
for isotropic solids, 75–76
Strain equations of compatibility for infinitesimal strains, 34–38
2D strain fields, 35–37
- 3D strain fields, 37–38
Strain gradient plasticity, 9
Strain hardening laws, 120–122
isotropic hardening, 120–121
kinematic hardening, 121–122
Strain hardening, 8, 435
Strain relaxation, 151–152
Stress, *see also* specific stresses
approximate expressions for, 289
induced
by acceleration, 7
by interference fit between two cylinders, 209–211
by temperature variation, 6
in stress gradient, 577
Stress field, 285, 305
Stress intensity factors, 575
calculation, 572
compliance, 592–593
FEA, 578–579
path-independent integrals, 579
cracks, 572–575
nonuniform stress fields, 576–577
and energy release rate, 589
interface cracks, 612–613
Stress measure
for infinitesimal deformations, 47
modified, 364–365
Stretch rate, 32
Stroh eigenvalues and anisotropy matrices, for cubic materials, 316–317
Stroh matrices, orthogonal properties of, 318–319
Stroh representation
for fields, in anisotropic solids, 312–314
satisfying governing equations, 314–315
for uniform stress state, 325–327
Superposition principle, 265
and linearity of solutions, 251–252
Surface displacement, 284, 285, 303
Surface traction, 38
Surface traction vector, 39
-
- T
- Tangent moduli, 510
Tangent stiffness, for neo-Hookean material, 519–520
Tasi–Hill Criterion, 555
Temperature, 6
Tensors
addition, 732
change of basis, 736–737
components, 732

contraction
 inner product, 734
 outer product, 734–735
 determinant, 735
 of dyadic product of two vectors, 731–732
 eigenvalues and eigenvectors, 735–736
 examples, 729
 stress tensors, 729
 deformation gradient tensors, 729–730
 identity tensor, 738
 index notation for, 744–745
 invariants, 737–738
 inverse, 735
 and matrix, differences between, 731
 matrix representation of, 730–731
 multiplication
 with a vector, 733
 with a tensor, 733
 operations
 cylindrical-polar coordinates, 758–764
 spherical-polar coordinates, 749–758
 orthogonal tensor, 739
 skew tensor, 738
 symmetric tensor, 738
 trace, 734
 transpose, 734
 Tetrahedron, areas of faces, 765–766
 Thermal expansion coefficient, 70–71, 73, 75, 77
 Thermal strain, 76
 Thin film on a substrate
 bending induced by inelastic strain, 697–699
 Time derivatives
 of curvature vector for deforming rod, 769–770
 of integrals over volumes within deforming
 solid, 767–768
 Total strain, 295
 Traction, acting on planes within solid, 40–43
 Traction vector, 39
 Transformation strain, 294
 Transient heat conduction analysis, 6
 Transversely isotropic hexagonal close-packed
 crystals
 elastic constants, representative values for, 85, 86
 Transverse waves, 337, 338
 Tresca yield criterion, 119, 120, 286
 True stress tensor, *see* Cauchy stress tensor

U

Upper bound plastic collapse theorem, 404–409
 examples of applications of
 collapse load for a bar containing a hole,
 406–407

collapse load for uniaxial bar, 405–406
 orthogonal metal cutting, 408–409
 rigid plastic solid indented by flat punch,
 407–408
 Upper bound shakedown theorem, 417–421
 examples of applications of
 pressurized spherical shell, shakedown limit
 for, 420–421
 three-bar problem, 419–420
 proof of, 418–419

V

Vectors
 addition, 711
 Cartesian components of, 712–713
 change of basis, 714–715
 definition, 711
 divergence theorem, 721–722
 dyadic notation, 616–617
 fields and calculus, 716–722
 identities, 712
 index notation for, 744
 multiplication
 cross product (vector product), 712
 dot product (scalar product), 712
 multiplication by scalar, 711
 operations, 715–716
 cylindrical-polar coordinates, 758–764
 spherical-polar coordinates, 749–758
 rotating basis, 719
 scalar field, 716
 change of basis for, 717–718
 gradient of, 719–720
 time derivatives of, 719
 vector field, 716–717
 change of basis for, 718
 curl of, 721
 divergence of, 720–721
 gradient of, 720
 Velocity discontinuity, in rigid plastic solid,
 399–400, 403
 Velocity field, 14
 Velocity gradient, 31
 Virtual stretch rate, 58
 Virtual velocity field, static linear elasticity,
 470–471
 Virtual velocity gradient, 58
 Virtual work equation
 for infinitesimal deformations, 62–63
 in terms of Kirchhoff stress, 61–62
 in terms of material stress, 61–62
 in terms of nominal stress, 61–62

Viscoelasticity, 8
 large strain, 148
 finite strain viscoelasticity
 kinematics for, 148–150
 representative values for material
 parameters in, 152
 stress measures for, 150
 strain relaxation, 151–152
 stress, deformation measures, and strain energy
 density, relation between, 150–151

Viscoplasticity, 8–9
 pressure-dependent, 9
 small strain, 135–142
 constitutive equations, 137–141
 creep behavior, features of, 135–137
 high strain rate behavior
 features of, 137
 representative values of parameters for,
 142–143
 models of creeping solids
 representative values of parameters for,
 142
 Viscoplasticity, FEM for, 522
 finite element equations, 524–525
 solution using consistent Newton-Raphson
 iteration, 528–529
 governing equations, 522–523
 expressing using virtual work principle, 523
 material tangent, 527–528
 plastic stress-strain law, integrating, 525–527
 small strain plastic code, example, 529–530

Volume integrals
 for stiffness and force in terms of normalized
 coordinates, 482–484
 shape function derivatives calculation, 484
 volume integral mapping, 484–485

Volumetric infinitesimal strain, 24
 Volumetric locking and reduced integration
 elements, 533–534
 “B-bar” method, 538–540
 reduced integration, 534–537
 reduced integration with hourglass control,
 540
 sample code, 541
 selectively reduced integration, 537–538
 von Karman theory, 686–688
 Von Mises effective stress, 48, 49
 Von Mises flow potential, 140
 Von Mises yield criterion, 118, 119–120, 123–124

W

Wave speed, 336
 Weibull statistics, 556–557
 Work done, *see also* Principle of virtual work
 by Cauchy stress, 54–56
 by Kirchhoff stress, 56, 57
 by material stress, 56, 57
 by nominal stress, 56, 57
 by stresses per unit volume (infinitesimal
 deformations), 57

Y

Yield criterion, 118–119, 435
 Yield stress, 8
 Yield surface, graphical representation of,
 119–120
 Tresca, 120
 von Mises, 118, 119–120
 Young’s modulus, 70–71, 73, 74, 75